ASSL ASTROPHYSICS AND SPACE SCIENCE LIBRARY

COSMIC RAYS IN THE EARTH'S ATMOSPHERE AND UNDERGROUND

LEV I. DORMAN

SPRINGER SCIENCE+BUSINESS MEDIA, LLC

COSMIC RAYS IN THE EARTH'S ATMOSPHERE AND UNDERGROUND

ASTROPHYSICS AND SPACE SCIENCE LIBRARY

VOLUME 303

COSMIC RAYS IN THE EARTH'S ATMOSPHERE AND UNDERGROUND

by

LEV I. DORMAN

Israel Cosmic Ray Center, Space Weather Center, and Emilio Segrè Observatory, affiliated to Tel Aviv University, Israel Space Agency, and Technion, Qazrin, Israel; and Cosmic Ray Department of IZMIRAN, Russian Academy of Science, Troitsk, Russia

SPRINGER SCIENCE+BUSINESS MEDIA, LLC

A C.I.P. Catalogue record for this book is available from the Library of Congress.

Cover picture courtesy of the Jungfrau Railways, Switzerland.
View of the Observatory on Mt. Jungfraujoch in the Swiss Alps equipped with NM-IQSY, NM-IGY, and with NST (for measurements of solar neutrons; developed in Japan, see Section 4.10).

Printed on acid-free paper

ISBN 978-94-015-6987-3 ISBN 978-1-4020-2113-8 (eBook)
DOI 10.1007/978-1-4020-2113-8

Originally published by Kluwer Academic Publisher in 2004
Softcover reprint of the hardcover 1st edition 2004

Dedicated to the memory of my late brother Zuss
(1916-1958),
Captain in the Second World War,
then a hydro-meteorologist,
Head of Department in the Moscow
Meteorological Prognosis Institute,
who was the first to interest me in geophysics

CONTENTS

Preface

The present monograph as well as the next one (Dorman, M2005) is a result of more than 50 years working in cosmic ray (CR) research. After graduation in December 1950 Moscow Lomonosov State University (Nuclear and Elementary Particle Physics Division, the Team of Theoretical Physics), my supervisor Professor D.I. Blokhintsev planned for me, as a winner of a Red Diploma, to continue my education as an aspirant (a graduate student) to prepare for Ph.D. in his very secret Object in the framework of what was in those time called the Atomic Problem. To my regret the KGB withheld permission, and I, together with other Jewish students who had graduated Nuclear Divisions of Moscow and Leningrad Universities and Institutes, were faced with a real prospect of being without any work. It was our good fortune that at that time there was being brought into being the new Cosmic Ray Project (what at that time was also very secret, but not as secret as the Atomic Problem), and after some time we were directed to work on this Project. It was organized and headed by Prof. S.N. Vernov (President of All-Union Section of Cosmic Rays) and Prof. N.V. Pushkov (Director of IZMIRAN); Prof. E.L. Feinberg headed the theoretical part of the Project. Within the framework of this Project there was organized in former Soviet Union in 1951–1952 a wide network of CR stations equipped with a Compton type of large ASC-1 and ASC-2 ionization chambers developed in USSR (see Sections 1.2.7 and 4.2).

At that time many experimental results on CR time variations were obtained, but they were very considerably affected by meteorological effects and by meson-nuclear cascade in the atmosphere. Therefore it was not possible to make reasonable transformation from observed CR time variations in the atmosphere and underground to the variations expected in space. To solve this problem, it became necessary to develop a full theory of cosmic ray meteorological effects and a special method of coupling functions between primary and secondary CR variations (this work was finished at the end of 1951 and was described in the IZMIRAN's *Instructions on CR Data Processing*, see References to Chapter 1: Dorman, 1951a,b). Only from 1954 it becomes possible for our work on CR variations to appear in the open scientific literature, and from 1955 – to take part (by presentation of papers) in International Cosmic Ray Conferences. Mainly our results of that time were described in my first book (Dorman, M1957, which was translated very soon into English in the USA, thanks to the help of Professor John Simpson, President of International CR Commission). Soon after this under the auspices of the International CR Commission the Committee of CR Meteorological Effects was organized, and I became its Chairman. Under the auspices of this Committee a special Instruction for CR Data Processing was developed which took into account meteorological effects.

In 1957 I was invited to work on special problems in Magnetic Laboratory of the Academy of Sciences of USSR as a Head of Department (in 1962 this Laboratory was taken into the I.V. Kurchatov Institute of Atomic Energy). In parallel I also worked at Moscow State University as Professor in the CR and Space Research Team (I also gave lectures in Irkutsk, Alma-Ata, Nalchik, Tbilisi, Erevan, Samarkand, and others places; over about 40 years of teaching under my supervision more than hundred graduate students and scientists who became experts in CR research in many countries gained their Ph.D.). As my hobby I continued to work in CR research, and as Vice-President of All-Union Section of Cosmic Rays and Radiation Belts, took an active part in preparing

the Soviet net of CR stations to the IGY (International Geophysical Year, 1957-1958): we equipped all soviet stations in USSR and in Antarctica with standard cubic and semi-cubic muon telescopes and with neutron monitors of IGY (or Simpson's) type. In 1957 regular CR measurements in troposphere and stratosphere by radio-balloons at several sites of USSR and in Antarctica, were organized by Professors S.N. Vernov and A.N. Charakhchyan as well as several latitude surveys on ships along the route Leningrad – Antarctica – Leningrad (see Sections 2.13 and 4.6). In connection with preparing for the IQSY (the International Quiet Sun Year, 1964-1965), the soviet net of CR stations was extended about two fold and they were equipped with neutron super-monitors of IQSY type (with an effective surface about 10 times bigger than the previous monitor of IGY type).

In 1965 I returned to IZMIRAN, and founded the Cosmic Ray Department (thanks to help of Professor N.V. Pushkov and Academicians M.D. Millionshchikov, L.A. Artsimovich, and V.I. Veksler). For the next 30 years, I was a Head of this Department, which became the center in the Soviet Union of scientific CR research in geophysical and astrophysical aspects. Our Department supported the work of all Soviet CR stations in the USSR and undertook the entire work of Soviet CR stations in Antarctica. We organized many CR expeditions inside USSR and in the Arctic Ocean, as well as in Pacific, Atlantic, Indian, and Southern Oceans on the ships "Academician Kurchatov", "Kislovodsk" and others (expeditions were equipped with a neutron super-monitor of IQSY type, with a multi-directional muon telescope, with radio-balloon CR measurements in the troposphere and stratosphere). Much very important data were obtained about coupling functions, integral multiplicities, and on the planetary distribution of cut-off rigidities.

At the end of the 1960s, in cooperation with V. Yanke, the theory of CR meteorological effects was generalized to take into account the spectrum and angular distribution of muons at the decay of charged pions, and Coulomb scattering of muons during their propagation in the atmosphere (see review in Dorman, M1972). We proposed and developed the spectrographic method of separation of observed CR variations (corrected on meteorological effects) in variations of geomagnetic and extra-terrestrial origin (see Chapter 3). It became possible based on CR data determine the change of cut-off rigidity and from this the structure of magnetospheric currents and their time variation during large geomagnetic storms (these results will be reviewed in detail in Dorman, M2005). Simultaneously it became possible, based on CR data, to investigate in detail the variation of the CR spectrum in space outside the Earth's magnetosphere. This method was then generalized and developed in two directions. The first - by also considering CR meteorological effects as being unknown (the so called generalized spectrographic method), allowed, based only on CR data, to determine simultaneously and separately of each class of CR variations: atmospheric, geomagnetic, and extra-terrestrial. The second, by taking into account CR anisotropy (the so called global spectrographic method), allowed, based only on the CR data of many CR stations (about 40–50) corrected for meteorological effects, to determine simultaneously of the change of cut-off rigidities on our planet and the CR distribution function in space. These methods we consider in details in Chapter 3, and their applications to CR data will be considered in the next book (Dorman, M2005).

From 1955 I took part in all International Cosmic Ray Conferences by presenting of original papers, as well as Invited Papers (in 1959 and 1965), Rapporteur Papers (in 1969 and 1987), Highlight Paper (in 1999), but I was able to go abroad only in 1966-

1969 (thanks to N.V. Pushkov and M.D. Millionshchikov) and then from 1988, after "perestroika". The first country I traveled to was Bulgaria (the International School on Space Physics, 1966), then Yugoslavia (the International Symposium on Solar-Terrestrial Relations). In 1967-1968 I headed the CR expedition to South America on the ship "Kislovodsk", went to Czechoslovakia in 1968, and to the International CR Conference in Budapest in 1969. After 'perestroika', thanks to invitations, from K. Nagashima I went to Japan, from C.J. Cesarsky to France, from A.W. Wolfendale and J.J. Quenby to England, from K. Otaola and J.F. Valdes-Galicia to Mexico, from D. Venkatesan to Canada, from J.A. Simpson and H. Ahluwalia to the USA, from W.I. Axford and H.J. Völk to Germany, from A. Bishara to Egypt, from L.O'C. Drury to Ireland, from N. Iucci, G. Villoresi, and M. Parisi to Italy, from P.J. Tanskanen to Finland, from M. Duldig to Australia.

In 1991 I was invited by the Israeli Minister of Science, Professor Yuval Ne'eman, to visit Israel (the Institute of Advance Study at Tel Aviv University) to give lectures and organize a Cosmic Ray Research Center. Step by step, thanks to great help of Prof. Yuval Ne'eman, Dr. Abraham Sternlieb, Mr. Abi Har-Even, and of three Italian colleagues, N. Iucci, G. Villoresi, and M. Parisi, there was founded the Israel Cosmic Ray Center with National Space Weather Center and Israel-Italian Emilio Segre' Observatory on Mt. Hermon (2200 m, cut-off rigidity 10.8 GV; see description in Section 4.8), and I became a Head of this Center and Observatory (to this day I continue also to work as a volunteer at IZMIRAN as Chief Scientist of the Cosmic Ray Department, which has been headed since 1995 by Dr. V.G. Yanke).

About two years ago I was invited by Dr. Harry Blom to prepare monographs on geophysical and space aspects of CR research and possible applications of them. As a result of our discussions it was decided to prepare two books: *Cosmic Rays in the Earth's Atmosphere and Underground*, and *Cosmic Rays in the Magnetosphere and in Space*. The first book is now ready, and the second will be in about a year's time, in 2004. The present book consists of four Parts, and each Part of four or five Chapters. To each Part we have given a short Preface, explaining the main aims of the Part and of the Chapters in it. Here we will give only very short survey of the book's structure (it is described in detail in the Contents).

In **Part 1** (Chapters 1–4) we consider CR as an object of research and as a research tool. The main notions and the nature on CR, a short historical survey of the discovery of CR and the development of research, and the main properties of primary CR we consider in Chapter 1; in Chapter 2 the properties of secondary CR; in Chapter 3 how, from ground CR observations, to obtain information about the situation in the magnetosphere and in space; and in Chapter 4 the experimental basis of CR research. So, in Chapters 1 and 2 we consider CR mainly as a subject of research, and in Chapters 3 and 4 mainly as a research tool.

Part 2 (Chapters 5–9) is devoted to the problem of the influence of changes in the atmosphere on the intensity of primary and different secondary components of CR in atmosphere and underground, so called meteorological effects of CR: barometric (containing negative absorption and decay effects, and the positive generation effect); temperature and humidity (contains positive pion and negative muon effects); snow, wind, gravitational, and atmospheric electric field effects. In Chapter 5 we consider the full theory of CR meteorological effects in the one-dimensional approximation; in Chapter 6 data on CR snow, wind, and barometric effects, in Chapter 7 data on CR

temperature and humidity effects; in Chapter 8 – data and detail theory of CR atmospheric electric field effects on muon and neutron components, and in different multiplicities; and in Chapter 9 the development of the full theory of CR meteorological effects with account experimental data described in Chapters 6–8 and results of their comparison with theory in the one-dimensional approximation (Chapter 5).

In the **Part 3** (Chapters 10–14) we consider the inverse problem, that of how CR influences the atmosphere and atmosphere processes: through nuclear reactions of primary and secondary CR with air and aerosol matter accompanied by the formation of many unstable and stable cosmogenic nuclides (Chapter 10); through the generation in the atmosphere of secondary relativistic electrons and EAS (Extensive Atmospheric Showers) playing a crucial role in atmospheric electric field phenomena (Chapter 11); through air ionization influences on the low ionosphere and radio wave propagation (Chapter 12); through induced chemical reactions, influences on the chemistry of the atmosphere and the ozone layer (Chapter 13) as well as on the formation of clouds and influence on long-term global climate change (Chapter 14).

In the last **Part 4** (Chapters 15–18) we consider realized and potential applications of CR research for many different branches of Science and Technology. Chapters 15–17 described the applications in detail: the solution of the inverse problem of determining from CR data the vertical distribution of air temperature, applications to CR latitude data processing, and applications of the radiocarbon method, respectively. In Chapter 18 we consider many possible applications of CR research in different branches of Science (Meteorology, Geology, Atmospheric Electricity, Hydrology, Archaeology, Ecology, Physics of Magnetosphere, Physics of Heliosphere, CR interactions with the atmospheres of the Sun and other planets and their satellites, with the Moon, asteroids, and meteorites) and Technology (the Meteorological Service of Large Airports, for Geophysical Prospecting, in Agriculture, the Security Service, Environment Monitoring of Radioactive Clouds, for Space Weather Monitoring and Forecasting by using on-line data from many CR Observatories, for Large Earthquake Forecasting by using on-line data on thermal neutrons and participating energetic particles from radiation belts, using CR research for Medical problems and the problem of road accidents). Many of these applications we consider in detail, and others – very briefly, we only formulate the principal meaning of any application (some of them need additional checking and development, and some, concerned with problems of CR in Magnetosphere and in Space, will be considered in detail in Dorman, M2005).

At the end of book, in the **Conclusion** we consider some unsolved problems and prospect for the development of CR research in the atmosphere and underground. In the **References** there are separately references for Monographs and Books as well as for each Chapter. For the convenience of the reader, at the end of book we also put a **Subject Index** and an **Author Index.**

We shall be grateful for any comments, suggestions, preprints and reprints which can be useful in our future research, and can make the next Edition of the book better and clearer; they may be sent directly to me by e-mail (lid@physics.technion.ac.il, lid1@post.tau.ac.il), by fax [+972] 4 696 4952, and by surface or air-mail to the address: Prof. Lev I. Dorman, Head of ICRC and ESO, P.O. Box 2217, QAZRIN 12900, Israel.

Lev I. Dorman
27 June, 2003 – 27 January 2004, Qazrin; Moscow; Princeton

Acknowledgements

It is my great pleasure to thank cordially:

my Teacher in Science and in Life – Evgeny Lvovich Feinberg;

for many years support of our research – A.E. Chudakov, A. Har-Even, G.B. Khristiansen, V.V. Migulin, M.D. Millionshikov, Yu. Ne'eman, V.N. Oraevsky, L.P. Pitaevsky, N.V. Pushkov, I.V. Rakobolskaya, A. Sternlieb, S.N. Vernov, G.T. Zatsepin;

my former students who became colleagues and friends, – for many years of collaboration and interesting discussions – M.V. Alania, R.G. Aslamazashvili, V.Kh. Babayan, M. Bagdasariyan, L. Baisultanova, V. Bednaghevsky, A.V. Belov, A. Bishara, D. Blenaru, Ya.L. Blokh, A.M. Chkhetia, L. Churunova, T.V. Dzhapiashvili, E.A. Eroshenko, S. Fisher, E.T. Franzus, L. Granitskij, R.T. Gushchina, O.I. Inozemtseva, K. Iskra, N.S. Kaminer, V.L. Karpov, M.E. Kats, T.V. Kebuladse, Kh. Khamirzov, Z. Kobilinsky, V.K. Koiava, E.V. Kolomeets, V.G. Koridse, V. Korotkov, V.A. Kovalenko, Yu.Ya. Krestyannikov, T.M. Krupitskaja, A.E. Kuzmicheva, A.I. Kuzmin, I.Ya. Libin, A.A. Luzov, N.P. Milovidova, L.I. Miroshnichenko, Yu.I. Okulov, I.A. Pimenov, L.V. Raichenko, L.E. Rishe, A.B. Rodionov, O.G. Rogava, A. Samir Debish, V.S. Satsuk, A.V. Sergeev, A.A. Shadov, B. Shakhov, L.Kh. Shatashvili, G.Sh. Shkhalakhov, V.Kh. Shogenov, V.S. Smirnov, M.A. Soliman, F.A. Starkov, M.I. Tyasto, V.V. Viskov, V.G. Yanke, K.F. Yudakhin, A.G. Zusmanovich;

for interesting discussions and fruitful collaboration – H.S. Ahluwalia, T.M. Aleksanyan, V.V. Alexeenko, H. Alfven, W.I. Axford, J.H. Allen, G.A. Bazilevskaja, G. Bella, M. Bercovitch, E.G. Berezhko, V.S. Berezinsky, J.W. Bieber, R.C. Binford, S.P. Burlatskaya, G. Cini Castagnoli, A.N. Charakhchyan, T.N. Charakhchyan, A. Chilingarian, J. Clem, E. Cliver, H. Coffey, J.W. Cronin, I. Daglis, E. Daibog, A. Dar, R.Jr. Davis, H. Debrunner, V.A. Dergachev, V.A. Dogiel, I.V. Dorman, L.O.C. Drury, M. Duldig, V.M. Dvornikov, D. Eichler, E. Etzion, Yu.I. Fedorov, E.O. Fluckiger, V. Fomichev, M. Galli, A.M. Galper, Yu.I. Galperin, V.L. Ginzburg, E.S. Glokova, N.L. Grigorov, O.V. Gulinsky, A.V. Gurevich, S.R. Habbal, J.E. Humble, N. Iucci, R. Kallenbach, G.S. Ivanov-Kholodny, G.E. Kocharov, I.D. Kozin, O.N. Kryakunova, G.F. Krymsky, K. Kudela, L.V. Kurnosova, V. Kuznezov, A. Laor, A.K. Lavrukhina, Yu.I. Logachev, C. Lopate, H. Mavromichalaki, K.G. McCracken, B. Mendoza, I. Moskalenko, Y. Muraki, M. Murat, K. Mursula, V.S. Murzin, N. Nachkebia, K. Nagashima, G.M. Nikolsky, S.I. Nikolsky, V. Obridko, J. Pap, E.N. Parker, M. Parisi, B.S. Pikelner, L.P. Pitaevsky, M.K.W. Pohl, A. Polyakov, M.S. Potgieter, C. Price, N.G. Ptitsyna, V.S. Ptuskin, L.A. Pustil'nik, R. Pyle, A.I. Rez, S.I. Rogovaya, I.L. Rosental, S. Sakakibara, N. Sanchez, V. Sarabhai, I.A. Savenko, K. Scherer, V. Sdobnov, V.B. Semikoz, V.P. Shabansky, Yu.G. Shafer, G.V. Shafer, M.A. Shapiro, P.I. Shavrin, M.A. Shea, I.S. Shklovsky, Ya. Shwarzman, B.I. Silkin, J.A. Simpson, G.V. Skripin, D.F. Smart, A. Somogyi, T. Stanev, M. Stehlic, A. Sternlieb, P.H. Stoker, M. Storini, Yu.I. Stozhkov, A. Struminsky, A.K. Svirzhevskaya, S.I. Syrovatsky, P.J. Tanskanen, A.G. Tarkhov, I. Transky, V.A. Troitskaya, B.A. Tverskoy, I.G. Usoskin, J.F. Valdes-Galicia, E.V. Vashenyuk, P. Velinov, D. Venkatesan, S.N. Vernov, E.S. Vernova, G. Villoresi, T. Watanabe, J.P. Wefel, G. Wibberenz, A.W. Wolfendale, V. Yakhot, G. Yom Din, A.K. Yukhimuk, N.L. Zangrilli, G.T. Zatsepin, G.B. Zhdanov, I.G. Zukerman;

for constant support and kind-hearted atmosphere during my education and long way in CR research – parents Isaac (1887-1954) and Eva (1894-1958), wife Irena, daughters Maria and Victoria, sisters Maria Tiraspolskaya (Dorman) and Mara Pustil'nik (Dorman), brothers Abraham Argov (Dorman) and Zuss (1916-1958), parents-in-law Olga Ivanovna Zamsha and Vitaly Lazarevich Ginzburg, son-in-law Michael Petrov;

for great help and collaboration in the period of my work in Israel which made possible to continue the research in CR – Yuval Ne'eman, Abraham Sternlieb, Aby Har-Even, Lev Pustil'nik, Igor Zukerman, Michael Murat, Alexei Zusmanovich, Lev Pitaevsky, David Eichler, Matilda Elron, Ronit Nevo, Shushana Shalom, Sami Bar-Lev, Avi Gurevich, Nunzio Iucci, Giorgio Villoresi, Mario Parisi, Marisa Storini, John A. Simpson, W.I. Axford, Arnold W. Wolfendale, Victor Yakhot, Alexander Polyakov, Doraswamy Venkatesan, Harjit Ahluwalia, Jose F. Valdes-Galicia, Yasushi Muraki, Marc Duldig, Heleni Mavromichalaki, Anatoly Belov, Victor Yanke, Eugenia Eroshenko, Natalie Ptitsyna, Marta Tyasto, Olga Kryakunova;

for great help in preparing many figures – Igor Zukerman;

for big help in preparing full references – I.G. Zukerman, L.A. Pustil'nik, M.I. Tyasto, M. Parisi, E.A. Eroshenko, O.N. Krjakunova;

for great help in correction English in all book – Michael Murat;

for many fruitful advices and help in preparing manuscript – Harry Blom, Sonja Japenga, and Language Editor Michael Cole.

The Israel Cosmic Ray Center (from 2003 – Israel Cosmic Ray & Space Weather Center) is supported by Tel Aviv University, Technion and Israel Space Agency (Ministry of Science and Technology of Israel). The Israeli-Italian Emilio Segre' Observatory is supported by the Collaboration of Tel Aviv University (ISRAEL) and "Uniroma Tre" University and IFSN/CNR (ITALY). We are grateful also to all authors of articles from which we used figures and tables, and to all scientists of many CR Observatories in the World whose data were used in our research.

FREQUENTLY USED ABBREVIATIONS AND NOTATIONS

AEF — Atmospheric Electric Field
ASC-1 and ASC-2 — Ionization Chambers, developed in USSR, volume 950 and 50 *l*
BMA — Brazilian Magnetic Anomaly
CR — cosmic rays
CRA — cosmic ray activity indices
E — intensity of AEF (in kV/m)
E — energy of CR particles
E_o — energy of primary CR particle
EAS — External Atmospheric Showers of CR
EFS-1000 — Electric Field Sensor
$e(h)$ — vertical air humidity distribution
EPE — electron precipitation event
ESA — European Space Agency
ESO — Israel-Italian Emilio Segre' Observatory (Mt. Hermon, Israel)
FEP — Flare Energetic Particles
FIP — First Ionization Potential
g — gravitational acceleration (in cm/sec^2)
GCR — galactic cosmic rays
GLE — Ground Level Enhancement of solar CR increasing
H — altitude
h — atmospheric pressure
h_o — pressure on the level of observations
IC — ionization chamber, shielded by 10 cm Pb
ICRC — International Cosmic Ray Conference
ICRC — Israel Cosmic Ray Center (from 1992)
ICR-SWC — Israel Cosmic Ray – Space Weather Center (from 2003)
ICRS — International Cosmic Ray Service (proposed in 1991)
IGY — International Geophysical Year (July 1957-December 1958)
IMF — interplanetary magnetic field
IQSY — International Quiet Sun Year (1964-1965)
ISS — International Space Station
L — transport path for primary CR absorption
l — transport path for absorption of pions
LDB — Long Duration Balloon
m = 1, 2, 3 , … — neutron multiplicities: number of pulses in NM from one neutron, proton, pion or muon in dependence of their energy during the time-gate (~ 10^{-3} sec)
m w.e. — meters of water equivalent
$m_i(R, h)$ — integral multiplicity: number of secondary CR particles of type i on level h from one primary CR particle with rigidity R on the top of atmosphere
m_π , m_μ — rest mass of pions, muons
MT — muon or meson telescope

$N(R_c, h)$ or $I(R_c, h)$ — CR intensity
NM — neutron monitor or super-monitor
NM-64 or NM-IQSY — neutron super-monitor of IQSY type
NM-IGY — neutron monitor of IGY or Simpson's type
$R = pc/Ze$ — particle rigidity
R_c — geomagnetic cutoff rigidity
$R(h)$ – gas constant of air
R_o – gas constant of dry air at normal conditions
SA — solar activity
SCR — solar cosmic rays
SDE — strong destructive earthquakes
SEP — solar energetic particles
SNE — solar neutron events
SNT — solar neutron telescope
SSM — Standard Solar Model
SW — Space Weather
$T(h)$ — vertical air temperature distribution
$W(R, h)$ — coupling function
$W_{Ei}(h, h_o)$ — total atmospheric electric field coefficient
$W_{ei}(h, h_o)$ — total humidity coefficient
$W_{gi}(h_o)$ — total gravitational coefficient
$W_{hi}(h_o)$ or $\beta(h_o)$ — total barometric coefficient
$W_{Ti}(h, h_o) = W_{Ti}^{\mu}(h, h_o) + W_{Ti}^{\pi}(h, h_o)$ — total temperature coefficient
$W_{Ti}^{\mu}(h, h_o)$ — muon's part of total temperature coefficient
$W_{Ti}^{\pi}(h, h_o)$ — pion's part of total temperature coefficient
$Y(R, h_o)$ or $Y(E, h_o)$ — yield function (characterized the dependence of CR detector counting rate per one primary proton from particle rigidity or energy)
Z or θ — zenith angle
λ — latitude
φ — longitude
π^+, π^-, π^o — positive, negative and neutral pions
μ^+, μ^- — positive and negative muons
τ_π, τ_μ — life-time of rest pions and muons
$\Omega_{Ei}(R, h, h_o)$ — partial atmospheric electric field coefficient
$\Omega_{ei}(R, h, h_o)$ — partial humidity coefficient
$\Omega_{gi}(R, h_o)$ — partial gravitational coefficient
$\Omega_{hi}(R, h_o)$ — partial barometric coefficient
$\Omega_{Ti}(R, h, h_o)$ — partial temperature coefficient

Part 1

COSMIC RAYS AS AN OBJECT OF RESEARCH AND AS A RESEARCH INSTRUMENT

Preface of Part 1

Part 1 contains four Chapters. In **Chapter 1** we consider the main information about CR as a universal phenomenon in the Universe, the development of CR research starting from its discovery at the beginning of the 20th Century, the main aspects of CR research and their inter-relations. In this chapter we also consider the main properties of primary CR (energy spectrum, chemical and isotopic composition, the main properties of protons and α–particles, electrons, positrons, antiprotons in primary CR, as well as the search for anti-helium). The main properties of secondary CR generated and propagated in the atmosphere and underground we consider in **Chapter 2**. In both Chapters 1 and 2 CR are considered mainly as an object of research, but in many cases CR are considered as an effective instrument of research. Namely, CR for a long time had been widely used as a natural source of high energy particles for discovering new particles (positrons, muons, pions, kaons, hyperons, and others) as well as for investigations of nuclear interactions and the formation of meson–nuclear and electromagnetic cascades at high energies (see Section 1.2 in Chapter 1, and in more detail in I.V. Dorman, M1981, M1989). Up to now CR continue to be used in this way: the CR particle energies still several orders higher than can be obtained on accelerators. The first time estimation of space magnetic fields was made by CR: in the interstellar space (Fermi, 1949), and in the interplanetary space (Dorman, 1955; Dorman and Feinberg, 1955; Dorman, 1957, 1957M). Namely, before direct measurements of magnetic fields in the interplanetary space, it was determined by CR that this field has a significant part as a disordered, turbulent field and roughly estimated the spectrum of turbulence (Dorman, 1959b). Let us note that CR are also used widely as a research instrument also for discovering and investigating such an important phenomenon as particle acceleration by shock waves, for research of modes of particle propagation and acceleration in magnetized space plasma, for discovering and investigation of convection–diffusion and drift mechanisms of CR modulation in the Heliosphere. As will be considered in detail in Dorman (M2005), by investigation of the CR – solar activity hysteresis phenomenon, it was determined 35 years ago for the first time that the dimension of the Heliosphere is about 100 AU (Dorman and Dorman, 1967a,b).

For effective use of CR as a research instrument for many phenomena in the atmosphere and underground, in the magnetosphere, and in space, there were developed special methods of integral multiplicity and coupling functions, the spectrographic method, the method of variational coefficients and global–spectrographic method (acceptance vectors and spherical analyses). These methods described in **Chapter 3** allow us to transform CR data observations in atmosphere and underground to the top of the atmosphere, and then to space (outside the magnetosphere), and to determine the energy–space distribution function of CR and its time variations caused by many different phenomena on the Sun, in the Heliosphere, in the Galaxy. So the worldwide network of CR continue observations underground and in the atmosphere can be considered as giant multi-directional and energy multi-channel space CR detector rotated and moved with the Earth.

The experimental basis of this planetary detector (worldwide networks of ionization chambers, muon ground and underground telescopes, neutron monitors and neutron telescopes, arrays of EAS) as well as experimental methods of CR direct investigations on balloons, satellites and space–probes we consider in **Chapter 4**.

Chapter 1

Cosmic Rays as an Object of Research

1.1. CR as an universal phenomenon in the Universe

1.1.1. What are CR? Internal and external CR; multiple origin of CR

It is natural to define cosmic rays (CR) as particles and photons with energies at least several orders of magnitude higher than the average energy of thermal particles of background plasma. There is internal CR, generated inside the background plasma of object considered, and external CR generated in other objects and propagated to the object considered. We are now aware of CR of different origin:

Extragalactic CR of very high energy (up to 10^{21} eV), are generated in radio-galaxies, quasars, and other powerful objects in the Universe, and come through intergalactic space to our Galaxy, to the Heliosphere, and into the Earth's atmosphere. Therefore, they are external CR relative to our Galaxy.

Galactic CR, with energy at least up to $10^{15}-10^{16}$ eV, are generated mainly in supernova explosions and supernova remnants, in magnetospheres of pulsars and double stars, by shock waves in interstellar space and other possible objects in the Galaxy. These CR are internal relative to our Galaxy and external to our Heliosphere and the Earth's magnetosphere.

Solar CR, with energy up to $15-30$ GeV, generated in the solar corona in periods of powerful solar flares, are internal CR for the Sun's corona and external for interplanetary space and the Earth's magnetosphere.

Interplanetary CR, with energy up to $10-100$ MeV, are generated by a terminal shock wave at the boundary of the Heliosphere and by powerful interplanetary shock waves. They are internal to our Heliosphere and external to the Earth's magnetosphere.

Magnetospheric (or planetary) CR, with energy up to 10 MeV for Jupiter and Saturn, and up to 30 keV for the Earth, are generated inside the magnetospheres of rotating magnetic planets.

1.1.2. Two maxima in particle energy distribution in magnetized space plasma

Now, we know very well from observations of CR, radio-waves, X-rays, and gamma-rays that practically any astrophysical object with a magnetized dynamic space plasma generates and contains CR. Why? What is the main cause of this universal phenomenon in the Universe?

Let us consider the particle energy distribution in any magnetized dynamic space plasma. We can see that there are always two maxima in this distribution, with a great difference in average energies (many orders of magnitude). Examples are numerous: the magnetospheres of the Earth and other rotating planets with magnetic fields, interplanetary space and the Heliosphere with outgoing solar wind with frozen-in magnetic fields and a lot of moving disturbances, solar and stellar hot coronas of rotating

stars with magnetic field, inter-stellar and inter-galactic space with background plasma and frozen-in magnetic fields, supernova explosions and supernova remnants from massive magnetic rotating stars, very fast rotating pulsars with giant magnetic fields and many other objects in the Galaxy, galaxies of different types, quasars, clusters and super-clusters of galaxies, and so on; both in the modern stage of the Universe's evolution and in the earlier stages. The first maximum is usual; it corresponds to the well known thermal Maxwell function

$$D_M(E_k) \propto E_k \exp(-E_k/kT), \tag{1.1.1}$$

where E_k is the kinetic energy of electrons or ions of background plasma with temperature T (and with average energy $\langle E_k \rangle_M = (3/2)kT \approx 1 \div 100\ eV$ in different astrophysical objects). The second maximum corresponds to CR of different origin, containing much smaller numbers of particles, but with much higher energy (a factor of $10^3 - 10^6$ higher than $\langle E_k \rangle_M$ of the background plasma), and is characterized in a broad energetic interval by the quasi-power spectrum:

$$D_{CR}(E_k) \propto E_k^{-\gamma(E_k)}, \tag{1.1.2}$$

where the power index is function on E_k: at some energy $E_{k\max}$, $\gamma(E_{k\max}) = 0$ and $D_{CR}(E_k)$ reaches its maximum value; for $E_k < E_{k\max}$, $\gamma(E_k) < 0$, and $D_{CR}(E_k)$ increases with increasing E_k; for $E_k > E_{k\max}$, $\gamma(E_k) > 0$ and $D_{CR}(E_k)$ decreases with increasing E_k. Let us note that for galactic CR the average energy $\langle E_k \rangle_{GCR} \approx 10^{10}$ eV and density $N_{GCR} \approx 10^{-10}\,\mathrm{cm}^{-3}$, so that the energy density $\langle E_k \rangle_{GCR} N_{GCR}$ is about the same order as the energy density of interstellar matter with $\langle E_k \rangle_M \approx 1$eV, $N_I \approx 1\,\mathrm{cm}^{-3}$ and interstellar magnetic field with $H_I \approx 3 \times 10^{-6}$ Oe:

$$\langle E_k \rangle_{GCR} N_{GCR} \approx \langle E_k \rangle_M N_I \approx H_I^2/8\pi \approx 1\mathrm{eV.cm}^{-3}. \tag{1.1.3}$$

1.1.3. The main cause of the CR phenomenon

What is the main cause of the second maximum in the particle energy distribution? It is very easy to see that in any magnetized dynamic space plasma there is a macroscopic motion of magnetic disturbances and magnetic clouds, shock waves and other types of magneto-hydrodynamics waves, which interact through the magnetic field with charged particles. The effective temperature of the macroscopic motion is extremely high: for example, a magnetic cloud (or the shock wave connected with this cloud) in the interplanetary space with velocity $u \approx 500\,\mathrm{km/s} = 5 \times 10^7$ cm/s with dimension $L \approx 0.1\,\mathrm{AU} = 1.5 \times 10^{12}$ cm and density $\rho \approx 5\,\mathrm{cm}^{-3}$ (near the Earth's orbit) has kinetic energy

$$W_k = L^3 \rho u^2 / 2 \approx 10^{28} \text{ erg} \approx 10^{40} \text{ eV} ; \quad (1.1.4)$$

magnetic clouds in the interstellar space with dimension $L \approx 1\text{pc} = 3 \times 10^{18}$ cm, chaotic velocities $u \approx 10\text{km/s} = 10^6$ cm/s and density $\rho \approx 1 \text{ cm}^{-3}$ have kinetic energy

$$W_k = L^3 \rho u^2 / 2 \approx 10^{43} \text{ erg} \approx 10^{55} \text{ eV} . \quad (1.1.5)$$

This means that charged particles that interact with these magnetic clouds can increase their energy in thermodynamic equilibrium up to giant energies, much higher than really observed.

1.1.4. Formation of CR spectrum and upper energy limit

In practice the thermodynamic equilibrium between macroscopic magnetized plasma motion and CR charged particles can not be reached, since the energy increase is hardly limited and the formation of energy spectrum is determined by the following three important factors (Dorman, 1979a,b; in more details see Dorman, M2005):

1. The rate of energy increase during the acceleration process (as determined by the details of the acceleration mechanism, e.g. according to Fermi, 1949).

2. The energy loss of accelerating particles by ionization and nuclear interactions (important for small and middle energy), on interactions with magnetic field (synchrotron radiation; important for electrons), interactions with photons (especially with relict photons at $2.7\,^{o}\text{K}$, important for very high energy particles with $E > 10^{19} - 10^{20}$ eV).

3. Particle escape from the acceleration region: for the energy interval in which the escape probability is proportional to the time of a particle's acceleration and does not depend on the energy of particles E_k, the power index γ in Eq. 1.1.2 is constant (for galactic CR, the range is $10^{10} - 10^{15}$ eV); when the probability of escape starts to increase with increasing particle energy, the power index γ starts to increase with increasing E_k. This gives a gradual upper cut off for the energy spectrum: for galactic CR generated in supernova remnants it is expected to be about $10^{14} - 10^{15}$ eV and for CR generated in magnetospheres of pulsars is expected about 10^{20} eV; for solar CR generated in solar flare events it was observed from 100 MeV up to about 20-30 GeV (in different cases) and for stellar CR generated in much greater stellar flare events upper energy limit expected to be several order higher. For interplanetary CR generated by terminal shock wave and interplanetary shock waves the observations give a cut off energy of about 10–100 MeV, for planetary CR generated in planetary magnetospheres direct measurements gave for upper energy limit from 30–50 keV for the Earth up to 10–20 MeV for Jupiter and Saturn.

1.2. Main steps of CR discovery and research development

Detailed description of the history of the discovery of CR and development of many aspects of CR research up to the middle of the 20th century was given in the monographs of Irena Dorman (M1981, M1989), and is reflected in a collection of original papers edited by Sekido and Elliot (M1985). Here we will give a very short description of the main milestones of the discovery of CR and the development of CR research in many aspects.

1.2.1. Air conductivity and CR discovery (1900–1912)

Geophysical investigations of air conductivity, which was started by Coulomb (1785) and continued up to the beginning of 20th century by Elster and Geitel (1900), Wilson (1900, 1901) and others, led to the discovery of some additional to the radioactive emanations some unknown source of air ionization. Detailed research of this unknown source led finally to the discovery of CR. After seven flights on balloons by Victor Hess in 1911–1912, and especially after the famous seventh flight to the height 5350 m on 7th August, 1912 (Hess, 1912), it was shown that the intensity of this source does not decrease with increasing altitude (as was expected if the source is radioactive emanation from the ground, as was assumed by many scientists before), but increases by several times on height about 5 km. Kolhörster (1913) continued balloon measurements and showed that at the height of about 9 km the intensity of air ionization reaches 80 $\text{ion.cm}^{-3}.\text{sec}^{-1}$, about 40 times higher than the ionization near sea level (only $\approx 2\ \text{ion.cm}^{-3}.\text{sec}^{-1}$; this value is in good agreement with modern measurements of Kyker and Liboff (1978) by a 900–liter ionization chamber, who obtained the value $2.15\pm0.05\ \text{ion.cm}^{-3}.\text{sec}^{-1}$). The radiation discovered was called 'penetrating radiation' or 'ultra-gamma radiation' by V. Hess. For this discovery Victor Hess received the Nobel Prize in 1936.

1.2.2. Investigations of the origin of 'penetrating radiation'; establishment of extra-terrestrial origin of CR (1913–1926)

Many years after V. Hess seminal observations in 1912 scientists discussed the problem of the origin of 'penetrating radiation': Is it of terrestrial or extra-terrestrial origin? That is, is it from radioactive emanations in the atmosphere or it is coming from the space? Only in the middle of the 1920s was the problem of the origin of this previously unknown radiation solved: the answer to this fundamental problem was obtained on the basis of many experiments. It was shown finally that this radiation is not produced by radioactive emanations in the atmosphere but comes from space and, according to suggestion of Millikan and Cameron (1926), this radiation was named cosmic rays (CR).

1.2.3. Investigations of the nature of CR: charged particles or gamma rays (1927–1939)

The second main problem was the nature of CR: at the end of 1920s the common opinion was that CR are high-energy gamma rays (concepts developed by Millikan and Cameron, 1928a,b). As became clear later in the 1930s, this opinion was wrong.

However, it generated a lot of attempts to determine the directions to the sources of CR and gave the impulse to develop the astrophysical aspect of CR research. The CR latitude survey of Millikan (1930), obtained a negative result (no latitude effect), which was considered as an important support of the Millikan and Cameron (1928a,b) concept. But other direct measurements of CR intensity *vs* latitude made mostly in connection with the First Geophysical Year (Clay, 1930, 1932; Compton, 1932, 1933) indicated that a small latitude geomagnetic effect at sea level exists (about 10–15%), and at least some part of primary CR are charged particles. The problem of the nature of the CR was a subject of a great famous public discussion between the Nobel Laureates Robert Millikan and Arthur Compton in December 1932 in Atlantic City during the winter meeting of American Physical Society (see Fig. 1.2.1); this discussion prolonged several years.

Nobel Prizewinners In Historic Debate Over Cosmic-Ray Origins

MEET IN FRIENDLY RIVALRY

Robert A. Millikan, Pasadena (Left), and Arthur H. Compton, Chicago, Who Today Discussed Physical Research Findings

COSMIC RADIATION FOES BATTLE OVER THEORIES OF ORIGIN

P. S-N. Dec. 30 '32

Dr. Robert A. Millikan, Dr. Arthur H. Compton Present Opposing Ideas on Whether Cosmos Being Recreated or Disintegrated

What most of the 2000 or more physical scientists gathered at Atlantic City for the winter meet- siders them the original rays. Dr. Millikan advanced evidence that they are secondary radiation pro-

Fig. 1.2.1. The page of newspaper *The Pasadena Star News* of December 30, 1932 on the discussion about the origin of CR. From I.V. Dorman (M1981).

To obtain more exact results, latitude CR surveys were continued by Clay (1933), Compton (1936), Compton and Turner (1937), Johnson and Read (1937). In particular, Compton and Turner (1937), during their 12 CR latitude surveys throughout the Pacific Ocean, found that the measured latitude effect changed with the seasons; they came to the conclusion that about 2/3 of the latitude effect is caused by the influence of the geomagnetic field on the primary CR, and about 1/3 by CR meteorological effects (difference in air temperature between the equatorial region and the mid-latitude region). The common opinion in those times was that primary CR are mostly charged particles. But experimental evidence of this was obtained only later, when the CR latitude effect was measured on balloons in the stratosphere by Bowen et al. (1937, 1938), Vernov (1938, 1939). In particular, Vernov (1939) found that the CR intensity in the stratosphere is about four times smaller at latitude 5° than at 56°. From this he came to the conclusion that at least 90% of the primaries CR are charged particles.

1.2.4. Discovery in secondary CR positrons, muons, pions, and other new elementary particles (1932–1950)

The multitude of observations of secondary CR particles near the ground with a Wilson chamber in a strong magnetic field carried out at the beginning of the 1930s gave the possibility of observing not only the tracks of CR particles, but also of determining their energy and rest mass. Use of some absorber (*e.g.*, Pb or Al plates) inside the chamber made it possible to determine the direction of the particle's velocity and the sign of its charge. The first person who observed by this method the positive electron – positron, predicted by relativistic quantum electrodynamics developed by Dirac (1930, 1931), – was Anderson (1932, 1933a,b). Fig. 1.2.2 depicts the first famous photograph of the positron's track, obtained by Anderson on August 2, 1932 (for the discovery of positrons in CR C.D. Anderson received the Nobel Prize in 1936, together with V. Hess, who discovered CR in 1912).

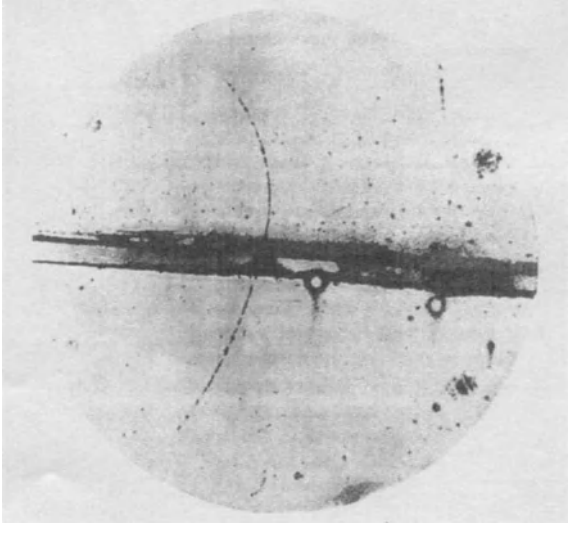

Fig. 1.2.2. The first famous photograph of a positron track, obtained by Anderson (1932).

It was the first antiparticle predicted by the new relativistic quantum theory and its discovery was very important for the development of the fundamental basis of elementary particle theory. After this muons, pions and various strange particles were discovered in the secondary CR during 1937–1950 (see in detail in I.V. Dorman, M1981, M1989).

1.2.5. Investigations of the sign of primary CR charged particles (1933–1950)

Let us note that as a result of detailed investigations of the CR latitude effect, many scientists came to the conclusion that primary CR can be high energy electrons or positrons (positrons were discovered in CR in 1932, see above, Section 1.2.4). Determination of the sign of the primary CR particles can be achieved using the azimuthally geomagnetic effect: if the sign of primary CR particles is positive the flux of particles from the West will be bigger than from the East. The West–East geomagnetic effect was discovered in 1933 on the basis of measurements by CR telescopes at sea level and at mountain altitudes. According to Johnson (1933) the CR flux from the West was bigger than from the East in Peru (near the equator) by about 7% at sea level and 16% at 4200 m above sea level. Johnson (1933) came to the conclusion that about all primary particles must be positive. In the middle of the 1930s were made a lot of investigations of geomagnetic effects at different altitudes and latitudes on balloons. In the review of these results Johnson (1938) came to the preliminary conclusion that primary CR are very probably mostly protons rather than positrons. But finally this problem was solved by the experiments carried by Schein et al. (1941) on balloons which reached the altitudes up to 20,000 m. To the end of the 1940s direct measurements of primary CR contents at high altitudes by different apparatus (mostly on balloons) finally established that primary CR are not gamma rays and not electrons or positrons, but positively charged particles such as protons, alpha–particles, and heavier nuclei (total about 99%), and only about 1% are high energy primary electrons, positrons, and gamma rays. Secondary CR are mainly composed of pions, kaons, muons, protons, neutrons, electrons, positrons, photons, neutrinos, and a lot of very short lived strange particles. At this time CR were beginning to be widely used as an important natural source of energetic particles for research in nuclear and elementary particle physics.

1.2.6. The first attempts to measure CR time variations (1923–1935)

As mentioned above, at the beginning of the 1920s the main opinion was that CR are high energy gamma rays, and many scientists tried to discover the object where CR were generated, and to determine the direction to this object. If the main source is the Sun, CR intensity must have a solar-daily variation but if the source is out of the Solar system the CR intensity should exhibit a daily variation in stellar time (stellar-daily variation). The first researcher who reported the discovery of big CR stellar-daily variation, was Kolhörster (1923), relying on observations at altitudes from 2,900 m up to 4,100 m and in tunnels of railway to Mt. Jungfraujoch in Switzerland. The measurements were made using 5 different ionization chambers (including measurements under 4.5 m ice to exclude the influence of radioactivity). Kolhörster (1923) came to the conclusion that there is no CR solar-daily variation, but rather CR stellar-daily variations with an amplitude of about 15% with the maximum occurring at time of Milky Way culmination.

Many scientists tried to repeat and test this result. During the investigations of CR time variations, Myssowsky and Tuwim (1926) discovered the existence of a CR time variation connected with the change of air pressure (barometric effect); the existence of this effect was confirmed with much higher accuracy by Steinke (1929). Moreover, Steinke (1929), after correcting the observed data for the barometric effect, did not find any periodic daily CR variations in stellar or solar time above the errors bars. Millikan and Cameron (1928a) according to measurements on the altitude 4,700 m also did not find any effect of Milky Way culmination, and they came to the conclusion that CR sources are distributed approximately homogeneously in the interstellar space. Hoffman (1932) reviewed all experimental results obtained before 1932 and came to the conclusion that within the experimental error bars (about 1%) there is no observed evidence of a CR stellar-daily variation.

The interest in CR stellar-daily variation reappeared in connection with the hypothesis of Baade and Zwicky (1934a,b) that the main sources of CR are supernovae explosions with a giant realization of total energy. To test this hypothesis, Kolhörster (1935) measured by counter telescope the possible effect on CR of the Nova explosion in 1934 in Hercules: he found this effect to be about 1.7%. Messerschmidt (1935) found for this Nova explosion 2.5% effect (on the basis of measurements by ionization chamber). But the observations carried out at the same time with much higher accuracy by Hess and Steinmaurer (1935), and Barnothy and Forro (1935a,b) showed that within the error bars there is no significant effect.

The first results on the CR solar-daily variation was obtained with a good accuracy on the basis of CR measurements using ionization chambers by Lindholm and Hoffmann (1928): it was found that the amplitude is 0.4–0.5%, and the maximum CR intensity occurred in few hours after noon, and minimum intensity at mid-night. These results were confirmed by Compton et al. (1932) on the basis of CR measurements using ionization chamber on Mt. Evans.

1.2.7. The 1st worldwide network of CR observatories equipped by ionization chambers; main results on CR variations (1934–1952)

The important step in CR time variation research was made in the 1930s: Compton et al. (1934) constructed a special precision ionization chamber with compensation, shielded by 10.7 cm Pb. The spherical main chamber with volume 19.3 liters was filled with argon at a pressure of 50 atm. Ionization current generated in the main chamber by CR was mainly compensated by a constant current from a small subsidiary chamber with an uranium radioactive source. The value of the resulting current was recorded continuously on a moving tape by Lindemann's electrometer. As part of the first worldwide network of CR stations such chambers were installed in Resolute (Canada), Godhavn (Greenland), Ottawa (Canada), Cheltenham and Climax (U.S.A.), Teoloukan (Mexico), Huancayo (Peru) and Christchurch (New Zealand). One hour and two hour data of CR intensity observed on these stations were published by Forbush and Lange (M1948, M1957). In 1949–1951 this net of ionization chambers was significantly extended: in former USSR this type of chamber was developed and contained automatically working chambers with a volume of 950 liters and 50 liters (ASC-1 and ASC-2). Seven new CR Observatories were equipped with these chambers at Heiss Island and Cape Schmidt at high North latitudes, in Moscow, Sverdlovsk (Yekaterinburg), Irkutsk, and Yakutsk at middle latitudes, and in Tbilisi of low latitude.

One hour data of CR intensity obtained at these stations for many years were published by Shafer and Shafer (M1985).

The worldwide network of ionization chambers worked continuously for more than three solar cycles (see description on this network below, in Section 4.2).

On the basis of this continuous record of many types of CR effects and time variations in the intensity of CR hard (muon) component there were discovered: temperature effect and effect of CR intensity increase caused by energetic particles from great solar flares (solar CR ground level effects in February–March 1942, in July 1946, and in November 1949), effect of CR decrease during great geomagnetic storms (Forbush effect), solar daily, 27–days, seasonal, and 11–year variations. These data and others obtained later will be considered in detail in the present book, and in the next one (Dorman, M2005).

On the basis of measurements made by Shonland et al. (1937) in 1933–1935 in Capetown (35° S) it was found that the amplitude of the solar daily CR variation is not constant: in summer it is much higher than in winter (as became clear later, it was caused by the influence of CR solar-daily temperature effect). As a result of detailed analysis of CR data for the period 1936–1946 on stations of the Carnegie Institute equipped with ionization chambers of Compton's type (Compton et al., 1934), Elliot (1952) found (by averaging data of 11 years) a regular solar-daily CR variation with amplitude 0.15% and time of maximum at about 3 p.m. in Cheltenham and Christchurch, and at about noon at Mt. Huancayo.

Analysis of the data from these stations carried out by Monk and Compton (1939) and Forbush (1940), allowed the observation of systematic changes in CR intensity with a period of about 27 days that corresponds to the period (relative to the Earth) of the Sun's rotation about its axis. The first results on CR 27–day variation were obtained by Hess and Graziadei (1936) on the basis of CR observations by ionization chamber on Mt. Hafelekar.

By analysis of the Carnegie Institute stations CR data, Roka (1950) found the connection between the annual Wolf sunspot numbers and annual average of CR intensity (11–year variation): with increasing solar activity, CR intensity decreases (correlation coefficient –0.8). More detailed data on CR 11–year variation was obtained by Forbush (1957).

At the beginning of 1930s Messerschmidt (1933) reported on CR intensity decrease during some geomagnetic storms by about 1%; according to Steinmaurer and Graziadei (1933), the average decrease during 17 storms was 0.3%. These measurements were made by ionization chambers at one individual station, and it was not clear if this effect is of local or planetary character. Only after establishing the first network of Carnegie Institute CR stations did it become possible to investigate this problem. The phenomenon of planetary CR intensity decrease was first observed by Hess and Demmelmair (1937) during the great magnetic storm started on April 24, 1937. Later this phenomenon was investigated in detail by Forbush (1938), and in the 1950s it came to be called the Forbush–decrease or Forbush–effect. The first attempt to explain CR effects during geomagnetic storms was made by Chapman (1937): he assumed that the magnetic field of the equatorial ring current (formed during the main phase of a magnetic storm) shields the Earth from the approaching CR, so that the CR flux on Earth decreases. But more detailed calculations of Johnson (1938) and Treiman (1953) showed that the decrease in CR intensity can be realized only if the radius of the equatorial ring current is smaller

than 1.3 $R_{\oplus}$ ($R_{\oplus}$ is the radius of the Earth). Since the radius of the equatorial ring current is in fact much larger, it was expected that the influence of the ring current's magnetic field will cause the CR intensity to increase, rather than to decrease (after this the effect of increase of CR intensity during main phase of magnetic storm was first observed by Yoshida and Wada, 1959; see review in Dorman, M1963a,b, M1974, and in more detail about main causes of this effect and Forbush decrease – in Dorman, M2005).

The first explanation of the temperature effect was given by Blackett (1938) taking into account the decay of muons: during the heating and expanding of the atmosphere (e.g., from winter to summer, or from night to day) the path of muons from the higher atmospheric level (where they are generated) to the ground becomes longer, and more muons decay, leading to decreasing of the muon intensity (negative temperature effect). Later it became clear that this effect is much more complicated: 1) it is necessary to account for the mass distribution in the atmosphere (Feinberg, 1946), 2) the discovery of the positive temperature effect led to the explanation of muon generation through decay of charged pions (Forro, 1947; Duperier, 1949, 1951); and 3) it is necessary to account for the distribution function of pion generation in the atmosphere and develop an integral method that includes all these effects (Dorman, 1951, 1952, 1954a,b, M1957; Olbert, 1953; Maeda and Wada, 1954). Much more complicated is also the barometric effect: in Chapter 2 it will be shown that it actually consists of three effects: absorption, decay and generation effects (the relative role of these effects depends on the altitude of observations and the value of total detector shielding (including the underground depth in the case of underground observations). During the preparations for the IGY, the theory of meteorological effects for neutron and general components was also developed (Dorman, 1958a,b; M1957).

Let us note that the discovery of solar CR generation in periods of great solar flares, and solar-daily CR variation with its maximum near noon, led to the development of a wrong theory of the origin of CR in the Sun and in the solar system (CR observed up to very high energies are considered as a local phenomenon, they are to be confined only to thesolar system): Richtmyer and Teller (1948), Alfven (1949, 1950). But later (Dorman, M1957) it was shown (by determining the energy spectrum of the solar-daily variation and taking into account the influence of geomagnetic field on trajectories of CR particles) that the real maximum of flux caused by solar-daily variation is directed in the interplanetary space not from the Sun, but from a perpendicular direction. Modern data in gamma ray astronomy also show that CR observed in the solar system have about the same intensity as in the Galaxy. The contribution of solar CR is negligible; only during some short time periods of great GLE the part of solar CR became significant and even can be much bigger than part from galactic CR.

1.2.8. Construction of neutron monitors and the greatest GLE of February 23, 1956; the IGY and the 2nd CR wide network (1952-1959)

During the great GLE of November 19, 1949, secondary neutrons were registered by a detector in Manchester (Adams, 1950). The detector was based on two proportional counters filled with $B^{10}F_3$ gas, surrounded by thick graphite blocks for braking high energy CR neutrons to thermal neutrons. This detector registered about 500% increase, much higher than the increase in the hard component of CR (about 11%). This result showed that the neutron component is much more sensitive to small energies of primary CR than the hard component. However, this detector has a big deficiency: it is very

sensitive to the changes in the surrounding matter, where a sufficient number of secondary small energy neutrons also are generated by CR neutrons. This deficiency made it impossible to use Adams's (1950) detector for registration of the usual time variations with much smaller amplitudes. To surmount this deficiency, Simpson et al. (1953), Simpson (M1955) developed this detector to add blocks of lead (Pb) as a generator of secondary small energy neutrons and replaced graphite by paraffin blocks with a big content of hydrogen which slows the neutrons much more effectively to thermal energies. During 1952–1954 Simpson's detectors equipped CR Observatories in Chicago, on Mt. Huancayo, Mt. Climax, and Mt. Washington. This detector with an effective area 2 m^2 (consisting of 12 proportional $B^{10}F_3$ counters with 6 cm diameter and 100 cm length), called a neutron monitor (NM) was recommended in 1954–1955 to be used as one of the main detectors during International Geophysical Year (IGY, July 1957–December 1958). This type of neutron monitors is now called NM IGY type (see detailed description in Simpson, M1955 and in Dorman, M1957; on the worldwide network of these detectors – below, in Section 4.4).

For measuring the charged CR components (muons and electron-photons) it was recommended to use telescopes of cubic or semi-cubic geometry as well as multi directional telescopes on Geiger-Muller gas filled counters and on scintillators based on the ground at different altitudes and latitudes, and underground at different depths (see detail description in Dorman, M1957, M1974, M1975a; on the worldwide network of these detectors – see below, in Section 4.3).

At the beginning of 1956 many CR observatories were equipped by NM and muon telescopes. This was very important, since the biggest GLE of the last 70 years occurred on February 23, 1956. A lot of data from continuously operating ionization chambers, muon telescopes, neutron monitors were obtained for this GLE, as well as results from balloon measurements. On the basis of these observations acceleration mechanisms in the solar atmosphere during the dissipation of magnetic energy in a solar flare and the main characteristics of solar CR propagation in the interplanetary space were developed (see review and analysis in Dorman, M1957, 1958c, M1963a,b, Dorman and Miroshnichenko, M1968). At the beginning of the IGY (July 1957) there were more than 50 continuously operating CR observatories equipped with ionization chambers, muon telescopes, and NM IGY. Creation of a large network of CR observatories made possible to investigate in detail many types of CR variations. For example, during a great geomagnetic storm at August 29, 1957 a big Forbush decrease was observed, and, for the first time, a very clear CR intensity increase before sudden commencement of magnetic storm. This type of increase was very anisotropic and its detailed analyses brings forward the discovery of high energy CR acceleration by reflecting from the interplanetary shock wave moving from the Sun (Blokh et al., 1959). On the basis of these data a drift mechanism of charged particle acceleration by shock wave was developed (single acceleration, Dorman, 1959a, Dorman and Freidman, 1959), which after about 20 years was extended to include multiple acceleration (shock wave diffusion acceleration, Krymsky, 1977; Axford et al., 1977; Bell, 1978a,b; Blanford and Ostriker, 1978).

This period is characterized by a wide use of airplanes and balloons for CR research. During this period many important results in investigations of CR meteorological and geomagnetic effects, solar-daily, semi-solar-daily, stellar-daily, 27-day, seasonal, and 11–year variations were obtained. The main part of the results obtained during IGY was

reported at the 6-th International Cosmic Ray Conference (Moscow, 1959). In particular, before direct measurements of the interplanetary magnetic field (IMF), the strength of this field in corpuscular streams of the first type (solar wind) was estimated by cosmic rays: near the Earth's orbit about several 10^{-5} Gs . For corpuscular streams of the second type responsible for great geomagnetic storms with sudden commencement (interplanetary shock waves) was obtained the strength of IMF about one order of magnitude bigger (Dorman, 1957, M1957). Moreover, from analysis of the energy spectrum of 11-year variation it was shown that in interplanetary space there is a resonance scattering of CR particles (on magnetic inhomogeneities with dimension of about the Larmor radius of particles), and that magnetic inhomogeneities have a broad spectrum (Dorman, 1959b). Also this result was obtained a long time before direct measurements of the magnetic field in space.

Let us note that in this period the modern theory of CR origin based on radio-astronomy data was founded, from which direct information on space distribution of primary CR relativistic electrons can be obtained (Ginzburg, 1953a,b).

1.2.9. Construction of super NM, the IQSY and the 3rd CR network, wide use satellites and space probes for CR research (1960–1992)

Investigations carried out with the NM IGY show that for many investigations of CR variations the statistical errors are too big. In order to decrease the statistical errors significantly, and in connection with preparing for the new International Quiet Sun Year (IQSY, 1964–1965) project, neutron super-monitors of the same geometry consisting of 18 neutron $B^{10}F_3$ counters with 15 cm diameter and 200 cm length with total effective area 18 m^2 (about one order bigger than area of NM IGY) were constructed in Canada and in USSR. The detector was divided into three independently working sections (each section with an effective area 2×3 m^2 with 6 counters). Instead of Pb blocks, Pb rings were used, and instead of paraffin polyethylene was used. The neutron super-monitor was recommended to use as one of main detectors during and after IQSY (for some time they were called NM IQSY or are shown the number of counters used and year of the starts IQSY: 18NM-64, 6NM-64, 3NM-64, and so on). In Fig. 1.2.3 are shown how the total numbers of NM IGY and NM IQSY in the World changed during the last 50 years.

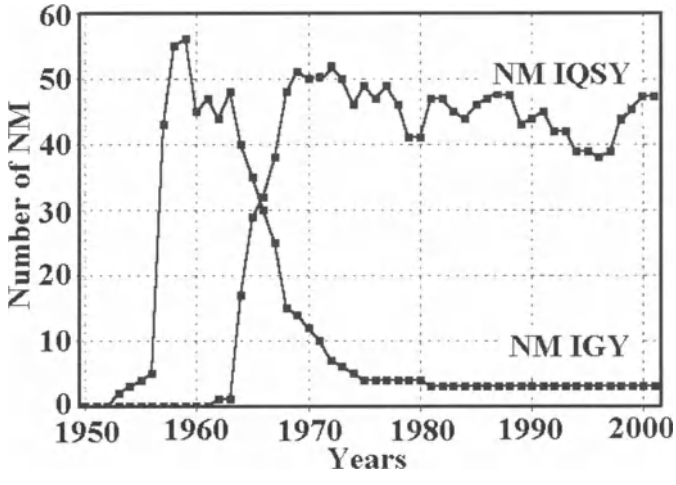

Fig. 1.2.3. Dynamics of total number in the World of NM IGY and NM IQSY. Prepared by E.A. Eroshenko.

It can be seen that there is a big increase of the number of NM IGY before 1957 and then they are replaced by NM IQSY after 1962–1963. Now only five NM IGY continue to work in Potchefstrum (South Africa), and on the mountains: Haleakala (Hawaii, USA), Huancayo (Peru), Climax (USA), and Jungfraujoch (Switzerland). NM IGY on mountains has about the same statistical errors as NM IQSY at sea level. Most of the CR observatories are now equipped with NM IQSY (for more details see in Dorman, M1974, M1975a; the description of the 3rd worldwide network equipped with NM IQSY – see below, in Section 4.4). The data (one hour values of intensity) of this network of CR Observatories are collected in the World Data Centers, and can be used freely by any scientist. On the basis of these data a lot of very important investigations of different types of CR time variations of meteorological and magnetospheric origin, interplanetary modulation, and solar origin were made: many results were reflected in books by Parker (M1963), Dorman (M1963a,b), Kuzmin (M1964, M1968), Dorman and Miroshnichenko (M1968, translation to English, M1976), Dorman and Kolomeets (M1968), Krymsky (M1969), Dorman et al. (M1971), Dorman (M1972a,b), Dorman et al. (M1972), Velinov et al. (M1974), Dorman (M1974, M1975a,b, M1978), Dorman et al. (M1978, M1979), Alania and Dorman (M1981), Dorman and Kozin (M1983), Alania et al. (M1987). Results obtained in this period will be considered also below in this book as well as in the next book (Dorman, M2005).

The period considered (1960–1992) is also characterized by a wide use of balloons, satellites, and space probes for investigations in all aspects of CR research: the Earth's radiation belts; CR albedo; measured radial and transverse gradients of CR in the interplanetary space; and other phenomena were investigated in detail. These results will be partly considered here, but mostly in the next book (Dorman, M2005). In this period was developed the modern theory of CR origin mostly reflected in books Ginzburg and Syrovatsky (M1963), Berezinsky et al. (M1990); it was started to investigate in detail the chemical and isotopic contents of primary CR which are very important for development of CR origin theory. In this period gamma ray astronomy was developed by measurements on balloons and satellites: it was shown that not only relativistic electrons, but also the nuclear component of primary CR are distributed in the disc and halo of our Galaxy (in contradiction with the theory of solar origin of CR mentioned in Section 1.2.7).

1.2.10. Development of fundamental and applied CR research: step by step formation of International Cosmic Ray Service, wide use of Internet for real time data exchange, combining of ground and satellite CR data (after 1992)

All hourly CR data from worldwide network of CR Observatories are sent each month to the World Data Centers (WDC) in Boulder (Colorado, USA), Moscow (Russia), and Nagoya (Japan), and any scientist can use these data. The problem is that these data are not in real time scale. In 1991 was prepared the Project (Dorman, M1991) on the foundation of the Israel Cosmic Ray Center, and on the step by step formation of International Cosmic Ray Service (ICRS) on the basis of wide Collaboration of all CR Observatories and on real-time scale exchange of one hour and one minute data. It was shown by Dorman (1993), Dorman et al. (1993a,b,c), that in this case there could be realized very important applications of CR research: using CR data for continue

monitoring space weather and forecasting of space phenomena dangerous for people health and technology in space near the Earth's orbit and at different distances from the Sun (important for space probes and spaceships with astronauts in interplanetary space), in the magnetosphere (important for satellites and spaceships in different orbits), and in the atmosphere at different altitudes and at different cut-off rigidities (important for balloons, commercial jets, and in some periods for people and technology on the ground). In Fig. 1.2.4 and 1.2.5 is shown the scheme of ICRS working and connection with other organizations.

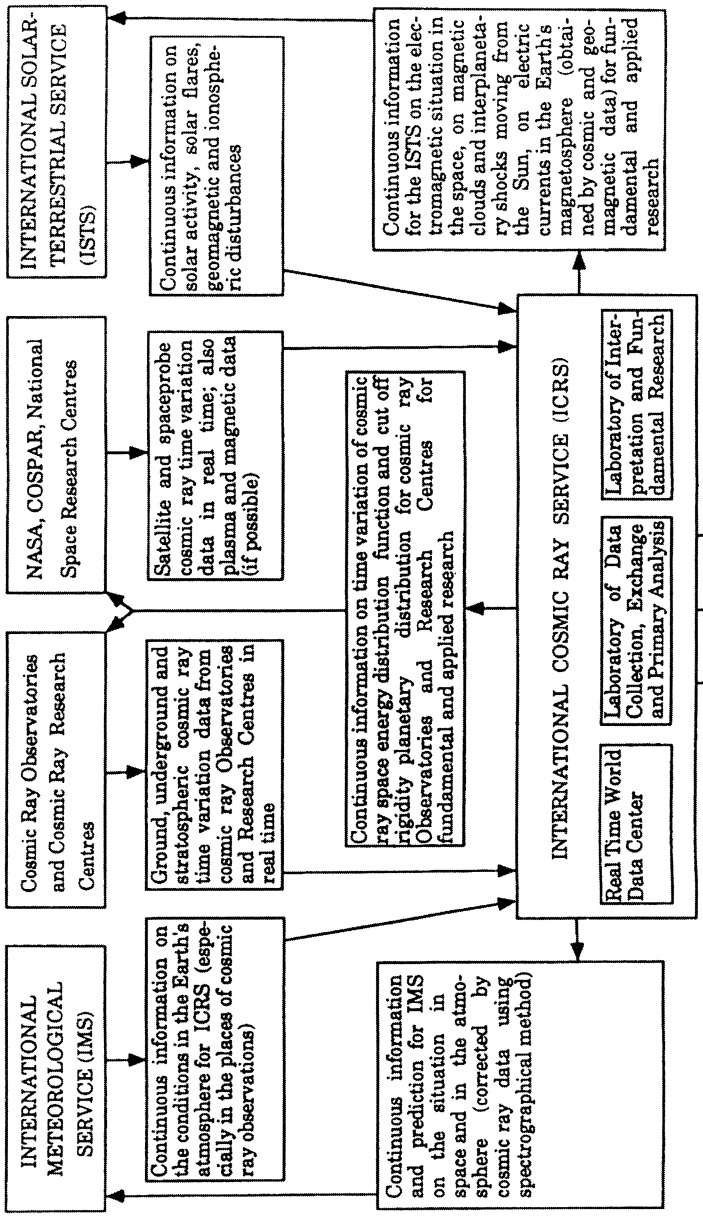

Fig. 1.2.4. Supposed scheme of exchange data between collaborated CR Observatories and other organizations in the farmework of the ICRS.

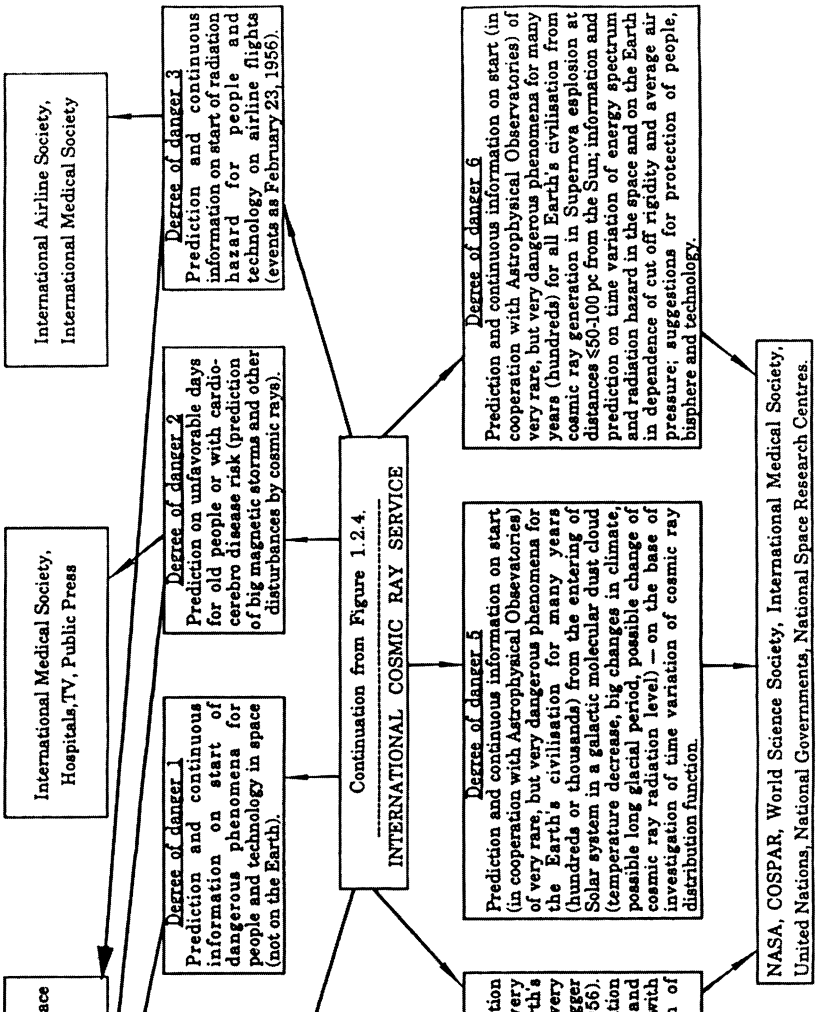

Fig. 1.2.5. Output information on spase weather and dengerous situations at different levels from ICRS to collaborating organizations.

In Fig. 1.2.4 are shown information of the planned input from collaborating CR Observatories, as well as meteorological, solar activity, geomagnetic field, and other data. On the basis of these data ICRS will realize continuous monitoring of space weather and determination of the level of hazards and send alarms to different organizations if the level is expected to be dangerous (it will be considered in more detail in our next book Dorman, M2005).

In those times it was a great problem how to realize the real-time exchange of data. Now it is becoming much easier: many CR Observatories put their observational data in corresponding websites, updated each one minute (as in our Emilio Segre' Observatory on Mt. Hermon in Israel; see description in Section 4.8), each 5 min (as Apatity in Russia, and some other), or each hour (as Moscow, Athens, Kiel, and some other). The total number of CR Observatories which give their data in real time through the Internet increases each year, and we hope that in few years it will become large enough (more than 35–40; such number of observatories are needed to use the automatic global spectrographic method, see Section 3.9), that ICRS can start to work continuously according to the scheme was shown in Fig. 1.2.4 and 1.2.5. As a some steps of organizing of ICRS can be considered the tendency in the last time to use CR ground data in combination of many Observatories, as networks (Bieber and Evenson, 1995; Moraal et al., 2000; Dorman et al., 2004).

This period is characterized also by wide combining of ground and satellite data in many branches of CR research (see review in Simpson, 1997; McDonald, 2000; and in more detail in Dorman, M2005).

In this period was investigated in details that the Sun is a source of high energy particles with energy up to about 15–20 GeV in a periods of great solar flare events, it was started to investigate many types of CR meteorological effects, CR behavior underground, influence of solar activity and geomagnetic storms on CR intensity, founded the basis of modern theory of CR origin, it was started to investigate in detail the chemical and isotopic contents of primary CR, founded the basis of modern theory of CR modulation in the Heliosphere, the basis of the theory of CR propagation in the Earth's magnetosphere and formation of meson–nucleonic and electron–photon cascades in the atmosphere, formation of EAS (external atmospheric showers) generated by primary particles with very high energy up to 10^{21} eV. As a result, now are formatted all five main aspects of CR research: a very short description of them is given below, in Section 1.3. Let us classify and number the aspects from ground, atmosphere, magnetosphere, space (interplanetary space and the Heliosphere), Galaxy and Universe.

1.3. Main aspects of CR research and their interconnections

1.3.1. The first aspect: CR underground and in the atmosphere

The main subjects of this aspect are: CR interaction with the Earth's ground and atmosphere, generation of secondary particles (different types of 'strange' particles, pions, kaons, muons, neutrons, neutrinos, gamma rays, positrons and electrons) and formation of meson–nuclear and electron–photon cascades (reflected in CR integral multiplicities, coupling and response functions), air ionization and influence on ionosphere and radio wave propagation (the last is especially important in periods of great solar CR events), possible influence of CR on chemical processes and formation of

ozone layer, generation of radioactive and stable cosmogenic isotopes, CR meteorological effects (influence of variations of air pressure, air temperature and humidity vertical distribution on CR intensity), Earth's gravitational effects (influence of variations of the value of gravitational acceleration on CR intensity), atmospheric electric field effects (acceleration and deceleration of CR particles by atmospheric electric field, especially important before and during thunderstorms), using CR data for continuous determination of air temperature and electric field vertical distributions, for determination parameters of ring current in the magnetosphere (especially in periods of great magnetic storms), in problems of long term change of climate, of geomagnetic field and solar activity, in the problem of elements exchange between atmosphere, biosphere and ocean, possible applications of CR research in CR Solar and Heliospheric Physics, in CR Astrophysics, in Meteorology, Archeology, for Police, in Geology and Geophysical Prospecting, Technology, Agriculture, Communications, Navigations, Ecology, and others. This subject was partly reflected in Dorman (M1957, M1963a,b, M1972, M1974); Velinov et al. (M1974); Dorman et al. (M1978, M1979); Dorman and Kozin (M1983); Grieder (M2001), and will be a matter of the present book.

1.3.2. The second aspect: CR in the magnetosphere and in space

The main subjects of this aspect are: influence of the Earth's magnetic field (main field and caused by magnetosphere's processes) on CR trajectories and formation of CR penumbra and cut off rigidities; use of the Earth as giant magnetic spectrograph for investigations of the dependence of different phenomena and processes caused or connected with CR from the energy of primary particles (in particular, development of spectrographic and global–spectrographic methods); transport of galactic CR in the Heliosphere, and modulation by solar wind, CME (coronal mass ejections) and shock waves; formation of convection–diffusion and drift CR anisotropies and gradients in the interplanetary space, CR nonlinear effects – influence of CR pressure and kinetic stream instability on the plasma processes in the Heliosphere. One of the important applications of this research is the Monitoring of Space Weather by CR and Forecasting of Space Dangerous Phenomena as Great Radiation and Magnetic Storms. This subject was reflected in monographs Dorman (M1957, M1963a,b, M1974, M1975a,b), Parker (M1963), Kuzmin (M1964, M1968), Krymsky (M1969), Dorman et al. (M1971), Alania and Dorman (M1981), Alania et al. (M1987), and will be a matter of our second book (Dorman, M2005).

1.3.3. The third aspect: CR of solar, planetary, and interplanetary origin

The main subjects of this aspect are: particle acceleration in processes connected with solar flares (solar charged CR particles with energy up to 15–20 GeV, and secondary neutrons generated in solar atmosphere with energy up to few GeV), in rotating magnetospheres of planets (magnetospheric energetic particles with energy up to about 30 keV in the Earth's magnetosphere, and up to about 10 MeV in the magnetospheres of Jupiter and Saturn), in interplanetary space connected with interstellar ions acceleration by terminal shock wave (anomaly CR with an energy up to about 50 MeV/nucleon), and with ions acceleration by interplanetary shock waves (with an energy up to about 10 MeV); propagation of these particles and their nonlinear effects. This research was partly reflected in books Dorman (M1957, M1963a,b), Dorman and Miroshnichenko (M1968),

Dorman (M1972b, M1978), Miroshnichenko (M2001), and will be partly a subject of our next book Dorman (M2005)

1.3.4. The forth aspect: CR astrophysics

The main subjects of this aspect are: the problem of CR origin in our Galaxy and in the Universe; primary CR energy spectrum, anisotropy, elemental and isotopic contents; electrons, positrons and antiprotons in CR; connection with radio astronomy, gamma ray astronomy and neutrino astronomy; sources of CR in the Galaxy and in the Universe, acceleration and propagation processes, CR nonlinear effects – influence of CR pressure and kinetic stream instability on the formation of galactic wind, on acceleration and propagation processes; this was the subject of monographs Ginzburg and Syrovatsky (M1963), Berezinsky at al. (M1990), Dorman (M1972b, M1975a), Schlikeizer (M2001). The history outlook of this research in the first half of 20-th century is given in monograph of I.V. Dorman (M1981), and is reflected in collection of original papers ed. by Sekido and Elliot (M1985).

1.3.5. The fifth aspect: CR elementary particles and high energy physics

The main subjects of this aspect are: investigation of high energy particles in CR by EAS installations and other methods, search for new elementary particles, investigation of elementary particle interaction at extremely high energy, research on the generation by CR of high and very high energies meson–nuclear and electromagnetic cascades and generation of secondary particles (which is especially important also for CR Geophysics), and determination of energy spectrum, anisotropy and contents at high and very high energies (which is especially important also for CR Astrophysics). The historical outlook of development of this research in connection also with experiments on accelerators can be found in the monograph of I.V. Dorman (M1989). This research was mainly reflected in books Dobrotin (M1954), Rossi (M1966), Hayakawa (M1969), Khristiansen (M1975), Murzin (M1988), Gaisser (M1990).

1.3.6. Interconnections between different aspects of CR research

All these five aspects of CR research are closely interconnected. Results of CR research underground and in the atmosphere (1st aspect) are used in the 2nd aspect (meteorological corrections for solar-daily variations, annual variations, modulation effects), in the 3rd aspect (GLE data corrections on meteorological effects, using coupling coefficients method for determining of solar CR spectrum out of the atmosphere), in 4th aspect (meteorological corrections for stellar-daily variations), and in the 5-th aspect (meteorological corrections of EAS data). Results on geomagnetic effects and cut-off rigidities (2nd aspect) are used in the 1st aspect for determining coupling functions and integral multiplicities of different secondary CR components, and in other aspects for determining dependencies from primary particle energy of CR anisotropies and intensity variations as well as nuclear interactions in atmosphere. Results on cosmogenic nuclides and nitrates (1st aspect) are used in the 2nd aspect to obtain information on very long-term CR modulation by solar activity (on the scale of many thousand years), in the 3rd aspect for determining great GLE in the past, and in the 4th aspect for determining possible local Supernova explosion in the past (within about hundred pc from the Sun). Results of the 2nd aspect on CR modulation in the

Heliosphere are used in the 4th aspect for determining of CR demodulated energy spectrum and stellar anisotropy in the Galaxy, and so on.

1.4. Primary CR: energy spectrum, chemical and isotopic contents, antimatter

1.4.1. Primary CR of extragalactic, galactic, and solar origin

Primary CR observed outside the Earth's magnetosphere are mostly galactic CR generated in supernova explosions, in supernova remnants and in other acceleration processes in our Galaxy; it is not excluded that CR of very high energy up to $10^{20}-10^{21}$ eV are of extragalactic origin (Ginzburg and Syrovatsky, M1964; Dorman, M1972b; Berezinsky et al., M1990; Schlickeiser, M2001).

In some short periods are also solar CR, generated in acceleration processes in the solar corona connected with great chromospheric flares (Dorman, M1957, M1963a,b; Dorman and Miroshnichenko, M1968; Dorman, M1972b, M1978; Miroshnichenko, M2001). The differential energy spectrum of solar CR is usually softer than galactic CR, differs very much from one event to another, and is not constant in time (in the beginning of an event it is very hard, and then became more and more soft owing to diffusion process in the interplanetary space). The chemical and isotopic contents of solar CR varied very much from one event to another (see mentioned above monographs and review papers in Dorman and Venkatesan, 1993; Stoker, 1994).

1.4.2. Energy spectrum and chemical composition of galactic CR; main sources of CR in the Galaxy

Here we will give some brief information about galactic CR changing with solar activity. In the Table 1.4.1 are given particle fluxes with total energy $E \geq 2.5$ GeV/nucleon in the space, outside the Earth's magnetosphere (this flux varies by about 30% in the course of a solar cycle, and reaches the maximum value near the minimum of solar activity). The integral spectrum of galactic CR can be described by

$$I_A(>E) = K_A E^{-(\gamma-1)} \text{ particles.m}^{-2}\text{.ster}^{-1}, \qquad (1.4.1)$$

where the parameters K_A and γ for protons, $\alpha-$particles and different groups of nuclei are given in Table 1.4.1. Besides nucleons galactic CR also contain primary electrons, positrons, and gamma rays (about 1%), and a very small flux of neutrinos from CR interactions with matter in the Galaxy (see below, Chapter 2).

Table 1.4.1. Particle fluxes of galactic CR with total energy $E \geq 2.5$ GeV/nucleon in the space, out of the Earth's magnetosphere near the minimum of solar activity, and parameters K_A and γ for protons, α – particles and different groups of nuclei in Eq. 1.4.1.

particles	Z	Flux for $E \geq 2.5$ GeV/nucleon, in $m^{-2}.ster^{-1}.sec^{-1}$	γ	K_A	Interval of E GeV/nucleon
p	1	1300	2.4±0.1	4800	4.7 – 16
α	2	88	2.5±0.2	360	2.5 – 800
L	3-5	1.9			
M	6-9	5.6	2.6±0.1	25±5	2.4 – 8
H	≥10	2.5	2.6±0.15	12±2	2.4 – 8
VH	≥20	0.7			

The observed chemical composition of galactic CR (see Fig. 1.4.1) is determined by chemical composition of CR sources in the Galaxy, by peculiarities of acceleration mechanisms, and by nuclear interactions of CR with interstellar matter during the propagation in the Galaxy.

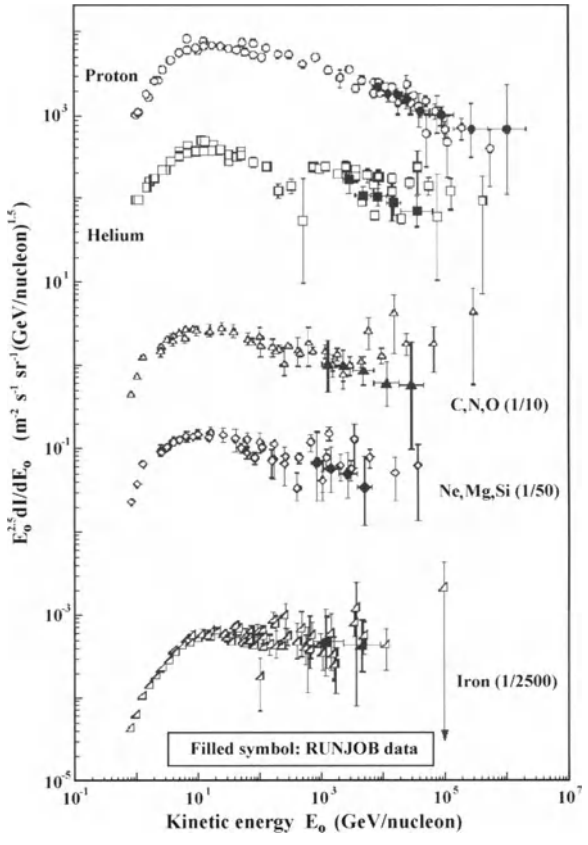

Fig. 1.4.1. Energy spectra for various components of the cosmic radiation: proton, helium, CNO group, NeMgSi group and iron. RUNJOB data are denoted by filled symbols. According to Apanasenko et al. (2001).

Important data on the secondary nuclei generated during CR propagation in the Galaxy (mainly Li, Be and B, and their isotopes) in the energy interval 30–500 MeV/nucleon were obtained in De Nolfo et al. (2003) by the CR Isotopic Spectrometer on ACE satellite in operation from 1997.

After CR data correction on nuclear interactions during propagation can be obtained information on expected CR chemical composition formatted by the acceleration processes in CR sources (in more details see in Ginzburg and Syrovatsky, M1964; Dorman, M1972b; Berezinsky et al., M1990; Schlickeiser, M2001). Some recent results of Waddington (2001) are shown in Fig. 1.4.2; this Figure reflects an important influence of the first ionization potential (FIP) on particle injection in the acceleration process in CR sources in the Galaxy.

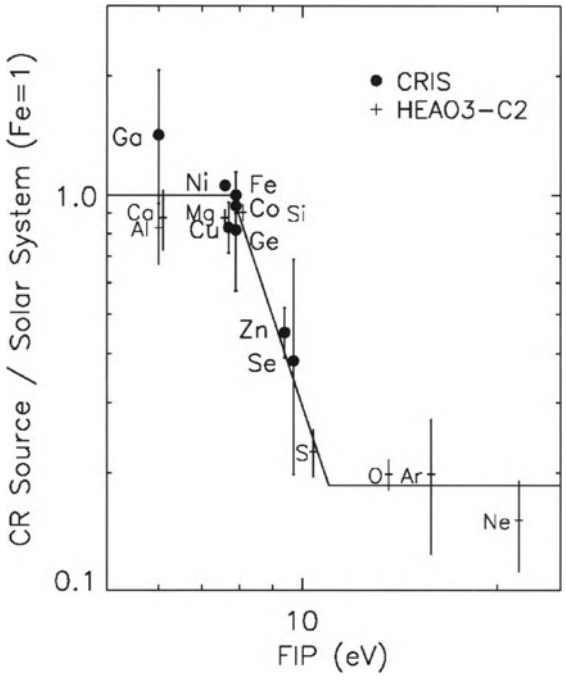

Fig. 1.4.2. The ratio of the Cosmic Ray Source (CRS) abundance to the Solar System (SS) abundance organized as a function of the First Ionization Potential (FIP). According to Waddington (2001).

Now it is generally accepted that supernova shocks are the main acceleration source for CR whose energy per nucleon is less than about 10^{14}–10^{15} eV. The exact source materials from which CR are accelerated is still uncertain. Results presented in Fig. 1.4.2 show that the galactic CR abundances are remarkably similar to the abundance of elements in the solar system with some differences determined with FIP: elements with FIP less than about 10 eV are more abundant in the CR source. This has led to the idea that galactic CR may originate in stellar atmospheres in regions with temperatures at about 10^4 K; elements with a low FIP are more likely to be ionized and injected into the acceleration process than elements with high FIP (Meyer, 1985; Binns et al., 1989).

However, it has also been observed that the GCR elemental abundances can be ordered by their 'volatility' (Meyer et al., 1997). In this model, the CR source is

interstellar gas enriched by atoms sputtered off from accelerated interstellar dust grains. The dust grains will have a higher rigidity at a given velocity than atoms and thus are more easily accelerated by supernova shocks. The elements that form these grains will therefore be enriched in CR. According to Link et al. (2003), since most low-FIP elements are refractory and most high-FIP elements are volatile, it is difficult to differentiate between these two models. There are a few elements that are both low-FIP and volatile or semi-volatile that break this degeneracy and can enable to distinguish between FIP and volatile models: several of these are ultra-heavy galactic CR including Zn (Z = 30), Ga (Z = 31), Ge (Z = 32), Rb (Z = 37), and some other.

Recently important results are obtained in Link et al. (2003) by the TIGER (Trans-Iron Galactic Element Recorder, is a balloon borne CR telescope consisting of four plastic scintillation detectors, two Cherenkov detectors and a scintillating fiber hodoscope; see description of TIGER in Chapter 4, Section 4.6.4). TIGER was launched on a long duration balloon (LDB) from McMurdo, Antarctica in December 2001, and the flight lasted for a record 31.8 days at an average altitude of 118,000 feet; during the flight approximately 360,000 iron nuclei and 300 nuclei with $30 \leq Z \leq 40$ were measured. The abundances of the elements for $30 \leq Z \leq 40$ were determined using a maximum likelihood fitting routine and were corrected for interactions in the instrument and in 5 g/cm^2 of residual atmosphere, and are compared in Fig. 1.4.3 with expected abundances using Solar System source abundances (according to Anders and Grevesse, 1989) fractionated by FIP (according to Binns et al., 1989) and volatility (according to Meyer et al., 1997). As a mode of CR propagation in the interstellar space was used a weighted-slab leaky-box model according to Waddington (2000).

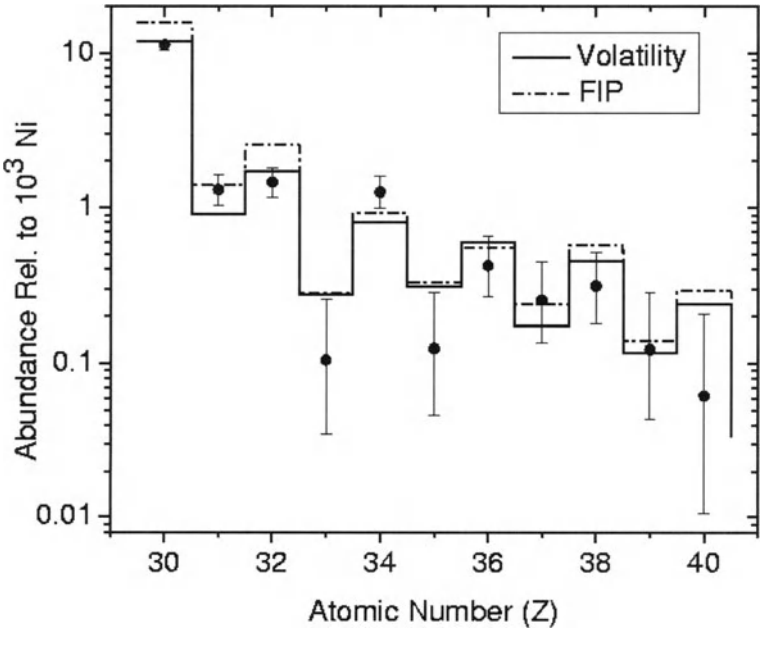

Fig. 1.4.3. Comparison of TIGER data to FIP and Volatility models. According to Link et al. (2003).

From Fig. 1.4.3 can be seen that the measured elemental abundances are in good agreement with the solar system abundances modified by propagation and by FIP or volatility. In more detail, we see that the Z=30 and Z=32 abundances measured by TIGER are in good agreement with the volatility model; Z=31 agrees better with the FIP model, but is only ≈1.5 sigma from the volatility model. Overall those elements that distinguish between FIP and volatility models appear to favor volatility. However additional data are required to improve the statistical significance of measured abundances.

1.4.3. Protons and α–particles in primary galactic CR

In Fig. 1.4.4 are shown differential energy spectra of protons and α–particles in the kinetic energy interval 10–2000 MeV/nucleon in 1965 (near the minimum of solar activity) and in 1967–1968 (near the maximum of solar activity). At energies smaller than 20–30 MeV/nucleon it can be seen that the flux increases with decreasing particle energy; it is caused by an anomaly CR – atoms of interstellar matter penetrating the Heliosphere and accelerating in it. In Fig. 1.4.5 are shown recent data on proton and He spectrum in the high energy region up to 10^6 GeV/nucleon .

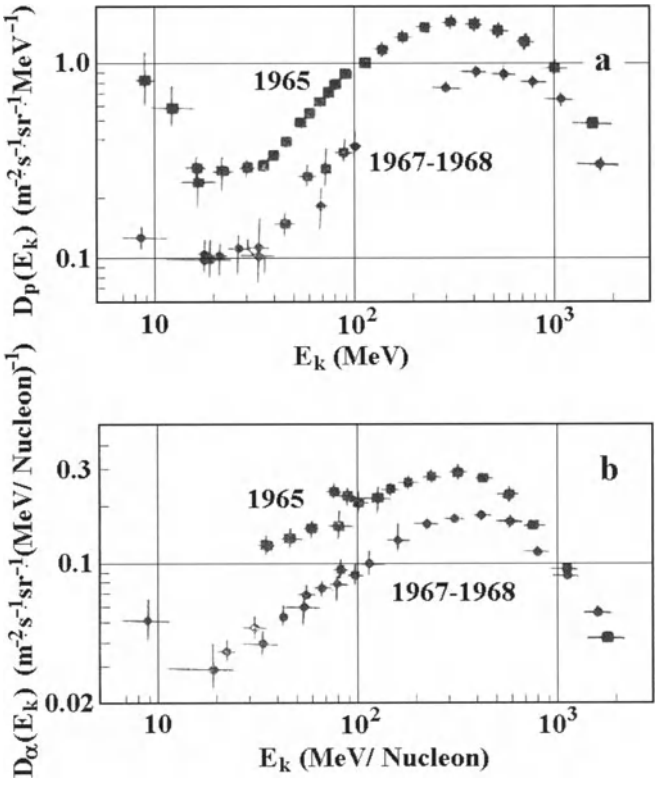

Fig. 1.4.4. Differential energy spectra of protons (a) and alpha-particles (b) according to measurements on space probes OGO-A, IMP-3 and IMP-4, Pioneer-8, and on balloons near minimum of solar activity in 1965 (squares) and near maximum of solar activity in 1967-1968 (circles). Compiled in Dorman (M1975a).

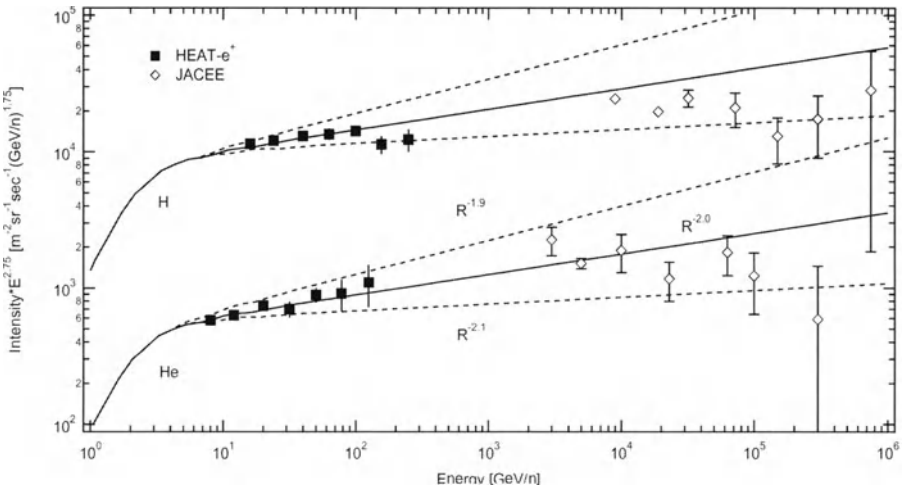

Fig. 1.4.5. Differential energy spectra of protons and α – particles in the high energy region up to 10^6 GeV/nucleon according to measurements in HEAT experiment (DuVernois et al., 2001; interval of energy 16-250 GeV/nucleon) and JACEE experiment (Asakimori et al., 1998; interval of energy $3\times10^3 \div 10^6$ GeV/nucleon).

A lot of data on primary protons and He was analyzed by Gaisser et al. (2001). Results for protons are shown in Fig. 1.4.6.

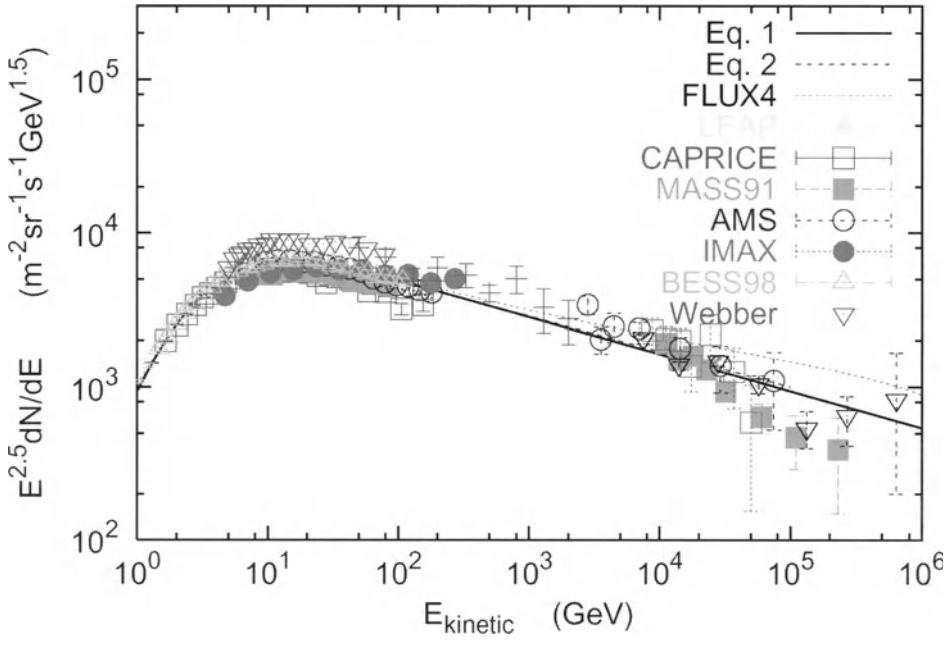

Fig. 1.4.6. Differential flux of protons compared to fits of Eq. 1.4.2 and Eq. 1.4.3 (in Figure Eq. 1 and Eq. 2, correspondingly), which are nearly indistinguishable on these plots. Also plotted is the proton spectrum of Agrawal *et al.* (1996). According to Gaisser et al. (2001).

Gaisser et al. (2001) used two forms to fit a differential spectrum in kinetic energy per nucleon E_k to the data on the various mass groups:

$$D_1(E_k) = K\left(E_k + a\exp\left(-b\sqrt{E_k}\right)\right)^{-\alpha}, \tag{1.4.2}$$

$$D_2(E_k) = K\left(E_k + m_p c^2\right)^{-\alpha} \exp\left(-\frac{b}{\varepsilon + p}\right), \tag{1.4.3}$$

where π is momentum per nucleon, ε = 0.25 GeV is a constant and all energy units are expressed in GeV.

In Fig. 1.4.7 are shown results for α–particles in the broad interval of energies from 0.3 GeV up to 100,000 GeV, obtained in experiments BESS, AMS, RICH, SOKOL and others on long duration balloons and satellites (see description of these experiments below, in Chapter 4).

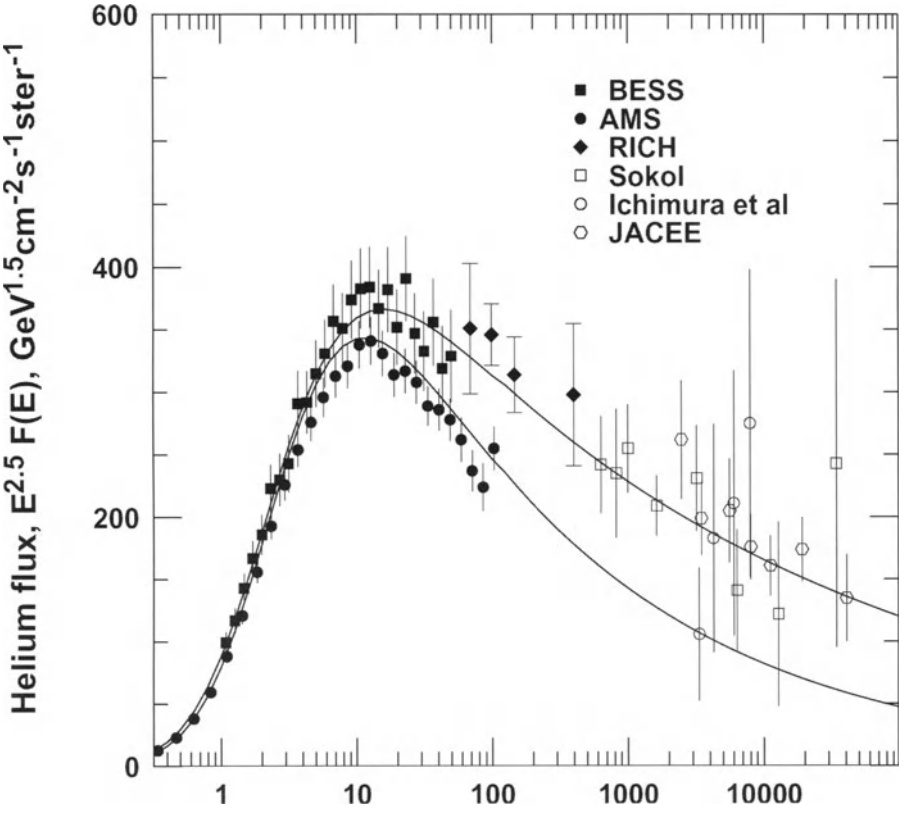

Fig. 1.4.7. Differential flux of helium compared to the 'high' and 'low' fits of Eq. 1.4.2. According to Gaisser et al. (2001).

1.4.4. Isotopic contents of primary galactic CR

Data on the isotopic contents of primary galactic CR are very important, especially for determining of the mode of CR propagation in the Galaxy.

The isotopes of hydrogen and helium provide a probe that allows propagation models to be tested and the effects of solar modulation to be investigated. For example, deuterons are primarily produced in the interactions of CR with the interstellar medium during propagation, predominantly from the spallation of ^{4}He. Deuterons are interesting because they have an interaction mean free path that is considerably larger than the escape mean free path for CR from the galaxy. This makes deuterons an effective probe to test propagation models. In Fig. 1.4.8 are shown results of Lamanna et al. (2001) on a high statistics measurements of the deuteron spectrum by the Alpha Magnetic Spectrometer (AMS) experiment during the Shuttle flight STS-91.

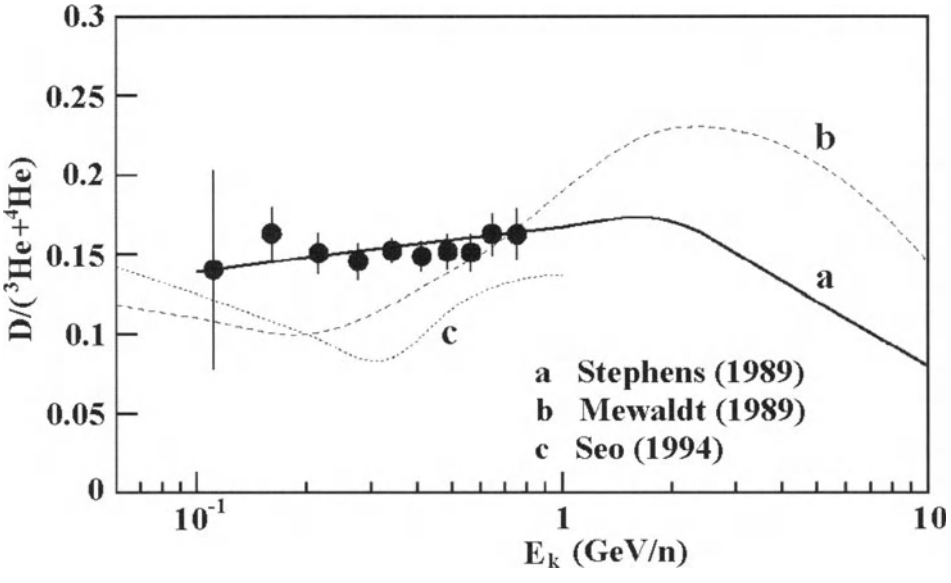

Fig. 1.4.8. Measurements of CR deuterons obtained with the AMS instrument aboard STS-91 and comparison with three models of CR propagation: **a** – according to Stephens (1989), ***b*** – according to Mewaldt (1989), and ***c*** – according to Seo and Ptuskin (1994), Seo et al. (1994). According to Lamanna et al. (2001).

Fig. 1.4.8 shows the deuteron/He ratio in the energy range from 90 to 850 MeV/nucleon in comparison with the predictions of several models. The statistics of these measurements are good enough for some models or sets of parameters for models to be able to be excluded.

In Fig. 1.4.9 are shown the ratio of deuterium to protons in dependence of particle energy and the comparison with different propagation models. From Fig. 1.4.9 can be seen that rather good agreement is found with the Standard Leaky Box Model, while the Stochastic Reacceleration Model seems to be excluded.

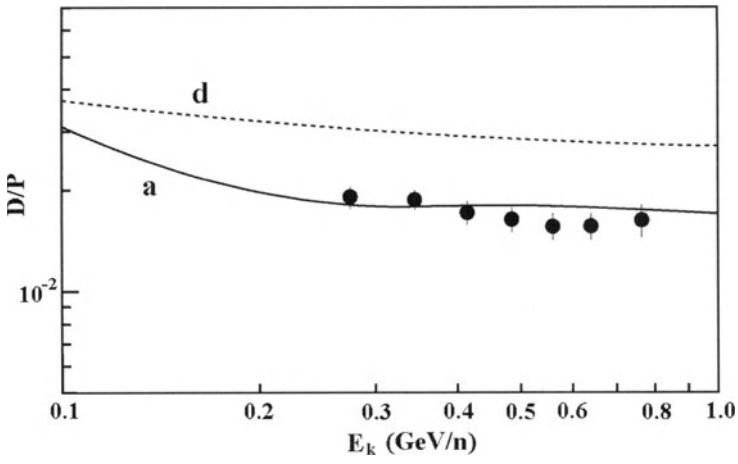

Fig. 1.4.9. Deuteron to proton ratio as measured from AMS compared with model predictions: **a** – Standard Leaky Box Model prediction according to Stephens (1989) and Seo et al. (1994); **d** – Stochastic Reacceleration Model prediction according to Seo and Ptuskin. (1994). According to Lamanna et al. (2001).

Results for primary deuterium flux were obtained in CAPRICE98 experiment (Vannuccini et al., 2003). The balloon-borne CAPRICE98 instrument was flown on 28-29 May 1998 from Fort Sumner, New Mexico, USA. The detector configuration included the NMSU-WiZard/CAPRICE magnetic spectrometer equipped with a gas ring imaging Cherenkov detector, a silicon-tungsten calorimeter and a time-of-flight system (see description in Section 4.6.4). Obtained results in the interval between 12 GeV/n and 22 GeV/n. for spectrum are shown in Fig. 1.4.10 and on the deuteron to helium ratio in Fig. 1.4.11 in comparison with other results.

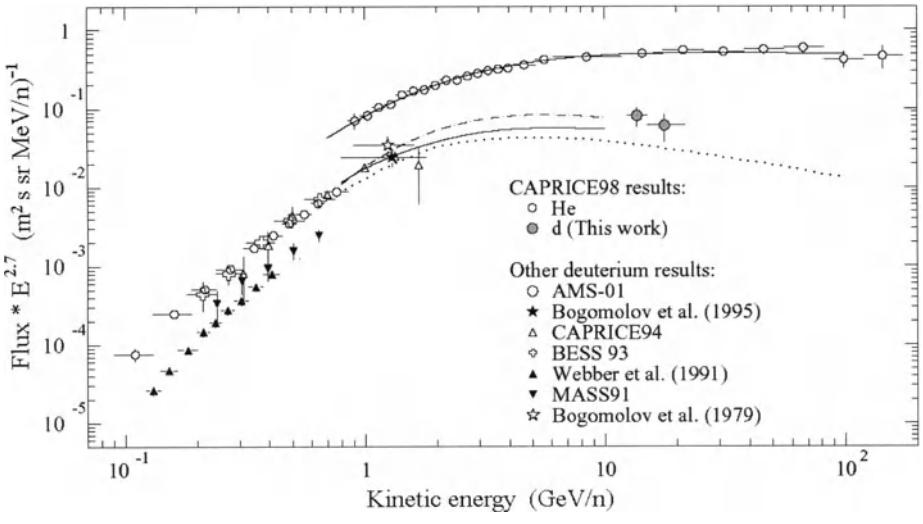

Fig. 1.4.10. Deuterium flux. Symbols: experimental results from CAPRICE98 (filled circles) and from other experiments. Curves: theoretical prediction (see Fig. 1.4.11). According to Vannuccini et al. (2003).

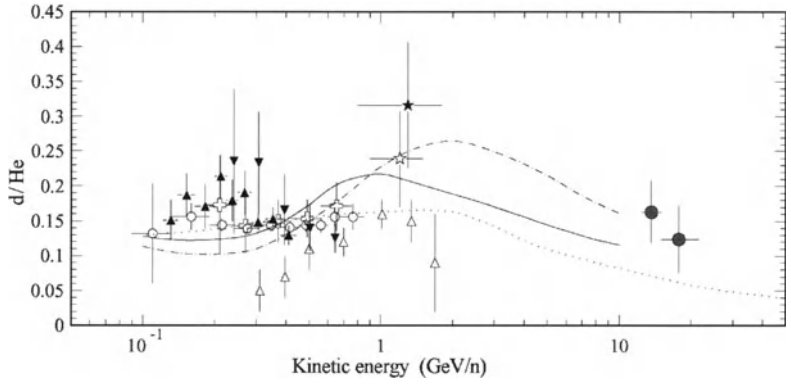

Fig. 1.4.11. Results of d/He ratio measurements and comparison with models. Symbols: experimental results from CAPRICE98 (filled circles) and from other experiments. Curves: theoretical prediction from Mewaldt, 1989 (dot-dashed curve), Stephens, 1989 (dotted curve) and Wang et al., 2002 (solid curve). According to Vannuccini et al. (2003).

For determining of the amount of matter which CR passed during their propagation in the Galaxy are very important data on contents of Li, Be and B, and their isotopes (about fully produced in nuclear interactions of heavier nuclei of galactic CR with interstellar medium). As an example, in Fig. 1.4.12 are shown different results of measurements of ratio $^{10}\mathrm{Be}/^{9}\mathrm{Be}$ in comparison with predictions by different models of propagation.

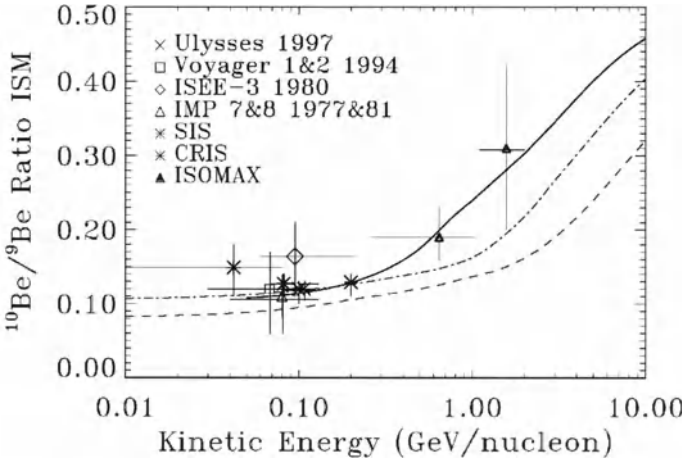

Fig. 1.4.12. $^{10}\mathrm{Be}/^{9}\mathrm{Be}$ ratio according to measurements in experiments: Ulysses (Connell et al., 1998), Voyager 1 and 2 (Lukasiak et al., 1997), ISEE-3 (Wiedenbeck and Greiner, 1980), IMP 7 and 8 (Garcia-Munoz et al., 1977, 1981), ACE (Yanasak et al., 1999), ISCMAX (De Nolfo et al., 2001). The solid curve is the prediction of a Leaky Box model by Yanasak et al. (2001) assuming an average interstellar density of 0.34 atoms.cm^{-3}. The dashed-dot curve is the prediction of a Leaky Box model by Molnar and Simon (2001) assuming an ISM density of 0.23 atoms.cm^{-3}. The dashed curve represents the predictions of a diffusion model by Moskalenko and Strong (2000) for a galactic halo size of 4 kpc and takes into account the local galactic structure and results from other spectroscopic observations. According to De Nolfo et al. (2001).

From Fig. 1.4.12 it can be seen that the accuracy of experimental data up to now is not enough to determine the correct theoretical model from different models of CR propagation in the Galaxy, but there seems to be tendency to a better fit of experimental data to the Leaky Box model of Yanasak et al. (2001), presented in Fig. 1.4.12 by the solid curve.

1.4.5. Primary electrons and positrons in galactic CR

In Fig. 1.4.13 are shown differential energy spectra of primary electrons in the kinetic energy interval 10–10,000 MeV in 1965–1966 (near the minimum of solar activity) and in 1967–1968 (near maximum of solar activity).

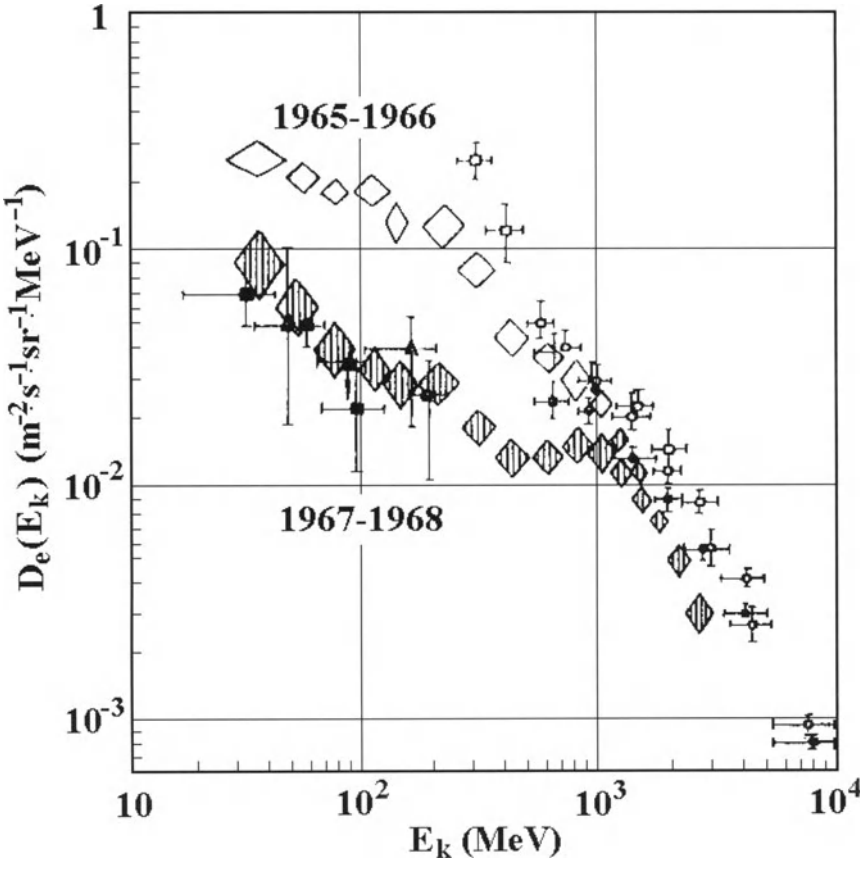

Fig. 1.4.13. Differential energy spectrum of electrons according to different measurements on space probes and on balloons near minimum of solar activity in 1965–1966 and near maximum of solar activity in 1967–1968. Compiled in Dorman (M1975a).

In Fig. 1.4.14 are shown results of Hams et al. (2003) obtained in the BESS-1999 experiment in comparison with other results on the galactic electron energy spectrum (the description on the experiment BESS on the long duration balloons see below in the Chapter 4, Section 4.6.4).

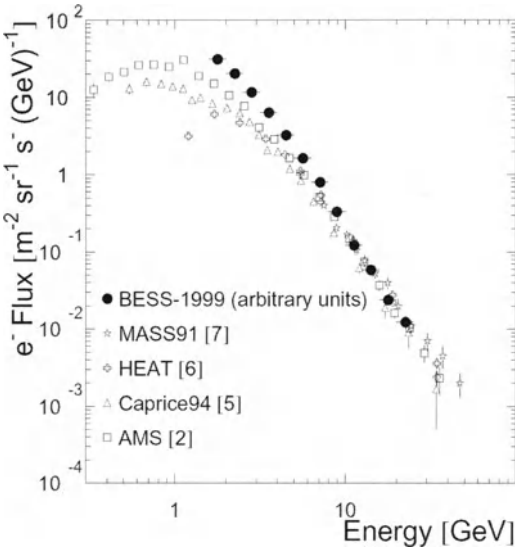

Fig. 1.4.14. Preliminary BESS-1999 electrons spectra in arbitrary units compared with other magnet spectrometers data. According to Hams et al. (2003).

Results of the recent measurements of the fraction of positrons are shown in Fig. 1.4.15. It can be seen that the solar modulation of electrons at the same energy as protons is much smaller in comparison with modulation of nucleons (the main cause of this is that electrons at few MeV energy have their velocity near the velocity of light and diffusion coefficient much bigger than for nucleons; see in details in Dorman, M2005).

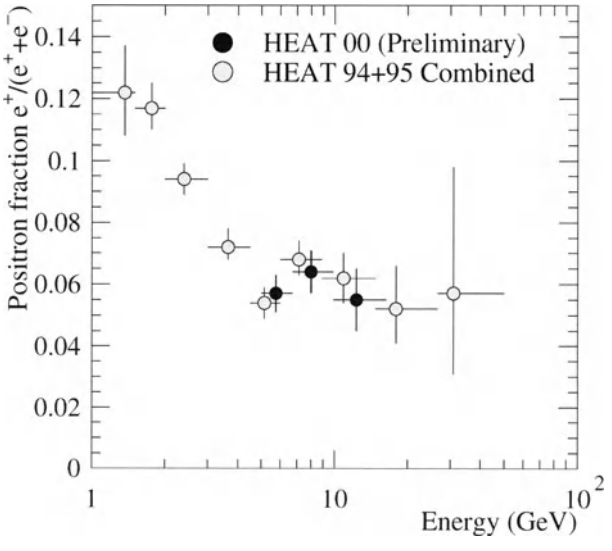

Fig. 1.4.15. Positron fraction as a function of energy measured in 2000 with the HEAT-pbar instrument, compared to previous HEAT-$e^{\pm}$ measurements in 1994–1995 (description of HEAT experiment on long duration balloons see below in Chapter 4, Section 4.6.4). According to Coutu et al. (2001).

1.4.6. Antimatter in galactic CR; the problem of asymmetry of the Galaxy and the Universe

Antiparticles are produced during the propagation phase as secondaries via the interaction of galactic CR with the interstellar matter. Excesses in the abundances of these particles over those predicted by propagation models may indicate a non-standard source, some exotic processes. In their most mundane form antiprotons and positrons (see Section 1.4.4) serve as a probe of both the propagation phase of galactic CR and the charge–sign dependence of solar modulation (Stochaj, 2001; see in detail in Dorman, M2005). Alternatively, they might hold the keys to larger questions such as the nature of dark matter or the physics that may exist beyond the standard model. To date, all results are consistent with secondary production, but the energy regime over 50 GeV has just begun to be explored and better statistics at lower energies are needed to preclude the existence of structure in the spectra of antiprotons and positrons. Recently very important results on antiprotons were obtained by Asaoka et al. (2001) on the basis of BESS experiment (the details on this experiment see in Section 4.6.4) taken in 2000, just after the general solar field reversal. The BESS collaboration has collected a huge data base, with balloon flights in 1993, 1995, 1997, 1998, 1999 and 2000. This data base is an excellent tool for the study of antiproton spectrum and solar modulation. Fig. 1.4.16 and Fig. 1.4.17 show the collection of BESS antiproton results in comparison with the prediction of Bieber et al. (1999a,b) on the basis of modern theory of CR modulation in the Heliosphere.

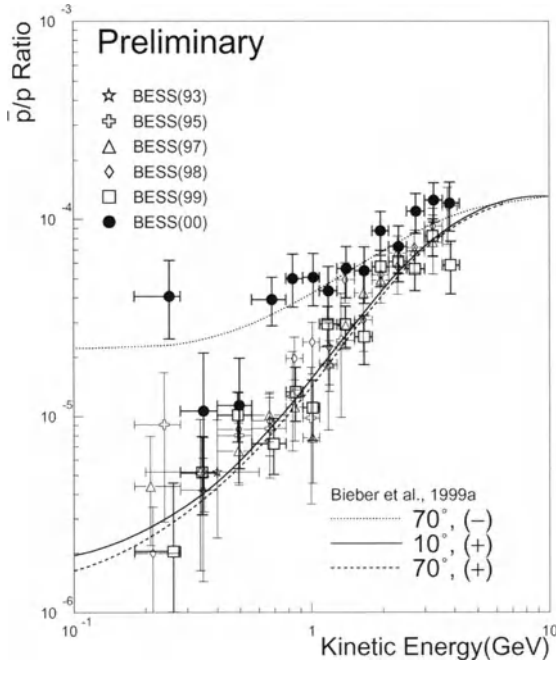

Fig. 1.4.16. Comparison of the BESS 1993, 1995, 1997, 1998, 1999 and 2000 $\bar{p}/p$ ratios with the calculation (Bieber et al., 1999a) taking the charge sign dependence of the solar modulation into account. The solid and dashed curves represent the calculated $\bar{p}/p$ ratios at a solar minimum and at a solar maximum in the positive Sun's polarity. On the other hand, the dotted curve represents the calculated $\bar{p}/p$ ratios at a solar maximum in the negative Sun's polarity. According to Asaoka et al. (2001).

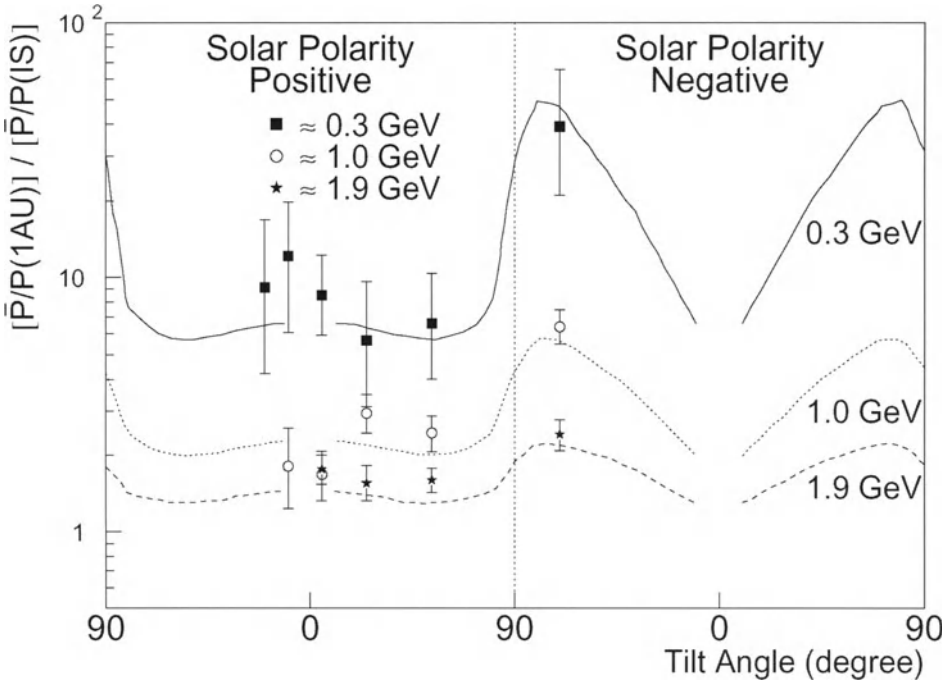

Fig. 1.4.17. The tilt angle dependence of $\bar{p}/p$ ratio at 0.3 GeV (closed squares), 1.0 GeV (open circles) and 1.9 GeV (closed stars) kinetic energy measured by BESS (1993–2000, from left to right), in comparison with the variation predicted by Bieber et al. (1999b). According to Asaoka et al. (2001).

The BESS experiment measures the rigidity and velocity of incident particles which, when combined with charge measurements, allow the identity of the particles to be determined. Combining a time of flight system with Cherenkov counter, antiprotons can be distinguished from the background events (e^- and μ^-) up to a kinetic energy of 4 GeV. The BESS program demonstrates that, given stable long term funding, balloon instruments can perform world class observations.

The collaborations associated with two other experiments, CAPRICE and HEAT, made their observations of antiprotons over a much higher energy regime. According to Boezio et al. (2001), the CAPRICE experiment uses a suite of detectors, most notably a ring imaging Cherenkov system, to identify antiprotons on an event by event basis (observations were performed by the balloon borne experiment CAPRICE98 that was flown on 28–29 May 1998 from Fort Sumner, New Mexico, USA; the experiment used the NMSU-WIZARD/CAPRICE98 balloon borne magnet spectrometer equipped with a gas Ring Imaging Cherenkov detector, a time of flight system, a tracking device consisting of drift chambers and a superconducting magnet and a silicon–tungsten calorimeter; the short description of this experiment see below, in Chapter 4, Section 4.6.4).

The paper of Boezio et al. (2001) reports the absolute flux of antiprotons over the energy range from 3.2 GeV to 49.1 GeV. These measurements are consistent with the

theoretical predictions by Simon et al. (1998) and Bergström et al. (1999a,b), which assume a purely secondary origin for the cosmic ray antiprotons (see Fig. 1.4.18).

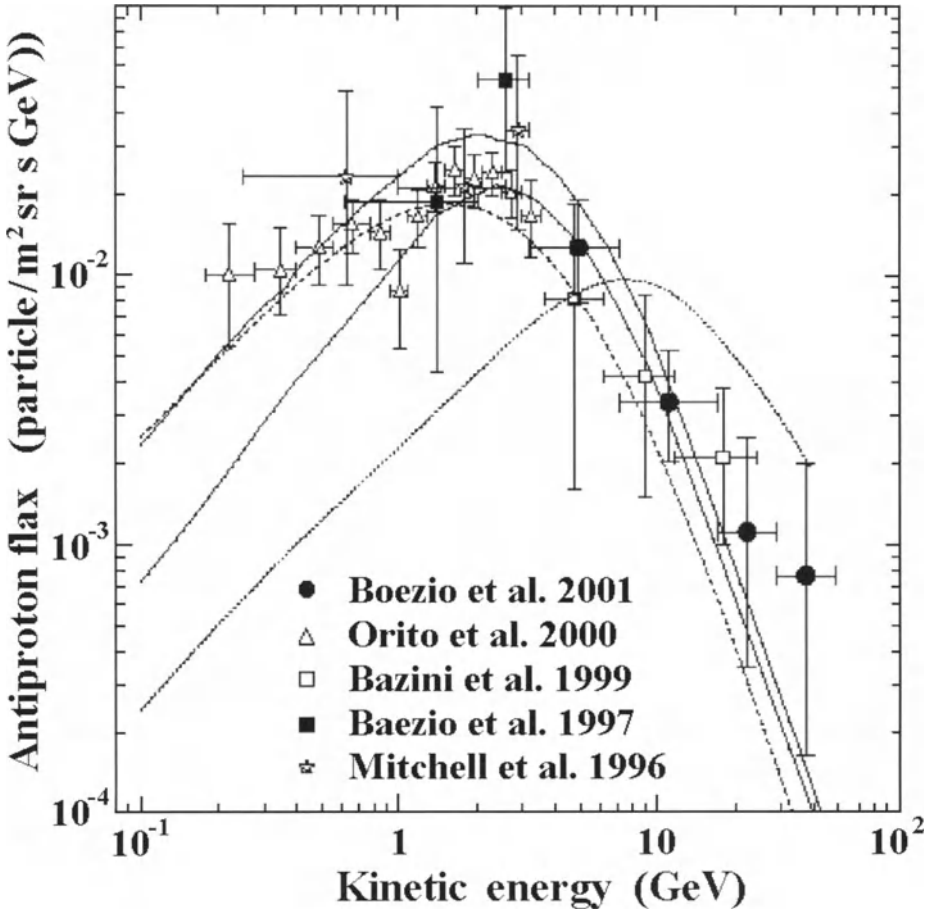

Fig. 1.4.18. Results of measurements of the antiproton flux in comparison with the predictions of several models. The two solid lines show the upper and lower limit of a calculated flux of interstellar antiprotons by Simon et al. (1998) assuming a pure secondary production during the propagation of cosmic rays in the Galaxy and using a recently measured proton and helium spectra (Menn et al., 1997). The dashed line shows the interstellar secondary antiproton flux calculated by Bergström et al. (1999a,b). The dotted line shows the primary antiproton flux by Ullio (1999), which includes a Minimal Supersymmetric Standard Model with a contribution from an assumed Higgsino-like neutralino, with a mass of 964 GeV. According to Boezio et al. (2001).

Fig. 1.4.19 shows the antiproton to proton ratio measured by CAPRICE98 along with other experimental data (Buffington et al., 1981; Golden et al., 1984; Bogomolov et al., 1987, 1990; Mitchell et al., 1996; Boezio et al., 1997; Basini et al., 1999; Orito et al., 2000) and with theoretical calculations. The two solid lines show the upper and lower limit of the calculated fraction of interstellar antiprotons by Simon et al. (1998). The dashed line shows the similar calculation by Bergström et al. (1999a,b).

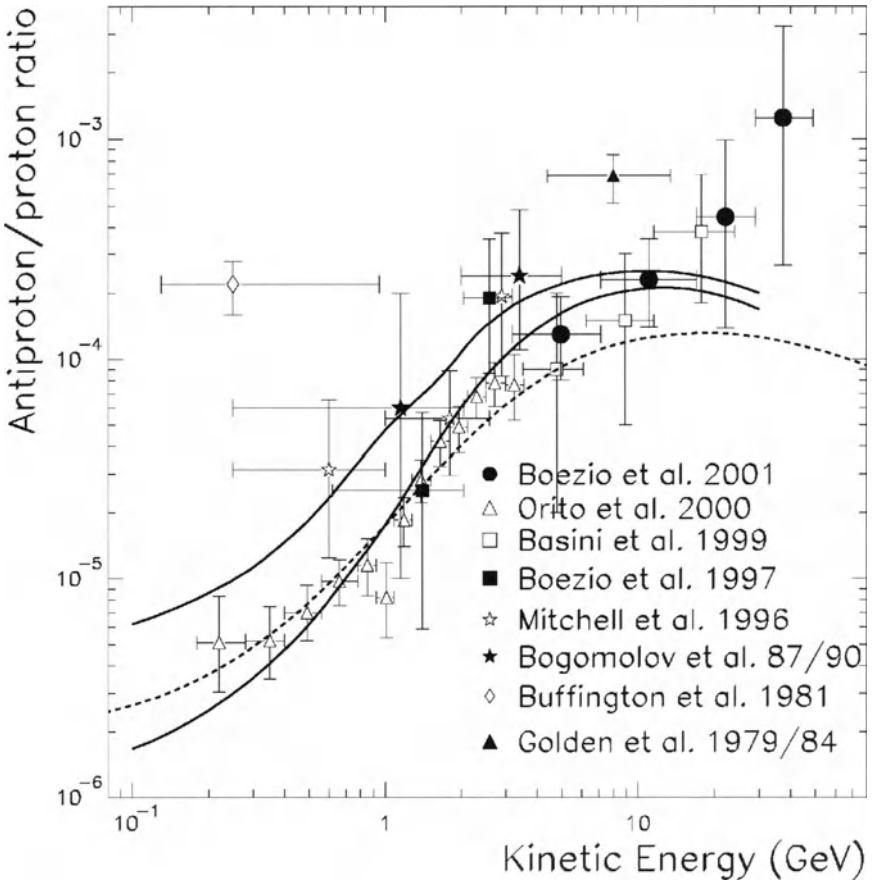

Fig. 1.4.19. The $\bar{p}/p$ ratio at the top of the atmosphere obtained in the CAPRICE98 experiment in comparison with other experiments and with theoretical calculations (full and dash curves are explained in the text). According to Boezio et al. (2001).

Up to now there is no evidence that antimatter in the form of antinuclear (antideuterium $\bar{D}$, antihelium $\bar{He}$, and others) exists in CR (Ormes et al., 1997; Saeki et al., 1998; Alcaraz et al., 1999; Sasaki et al., 2001; Fuke et al., 2003). This is a direct demonstration that our Galaxy is made of matter and a baryon asymmetry is maximal. The question is whether this asymmetry is global or local in the Universe. The absence of annihilation gamma ray peaks shows that little antimatter is to be found within ~ 20 Mpc, however, the possibility of existence of antimatter clusters in the Universe is not completely precluded. If $\bar{D}$ or $\bar{He}$ were observed in CR it would be a strong indication of the existence of antimatter clusters because the probability to produce $\bar{D}$ or $\bar{He}$ in collisions of CR with the interstellar medium is too small.

Fuke et al. (2003) performed a search for low-energy $\bar{D}$ with the BESS superconducting spectrometer on long duration balloons (see description of the BASS

instrument below in Chapter 4, Section 4.6.4). Results are shown in Fig. 1.4.20 in comparison with other results and with expected for $\overline{D}$ as possible product of nuclear interactions of primary CR with interstellar matter). No candidate was found in the data obtained from four balloon flights at Lynn Lake, Canada during 1997 to 2000. It was obtained, for the first time, at the 95% confidence level an upper limit of 1.9×10^{-4} $(m^2 s\ sr\ GeV/n)^{-1}$ for the differential flux of $\overline{D}$ in the energy region between 0.17 and 1.15 GeV/n.

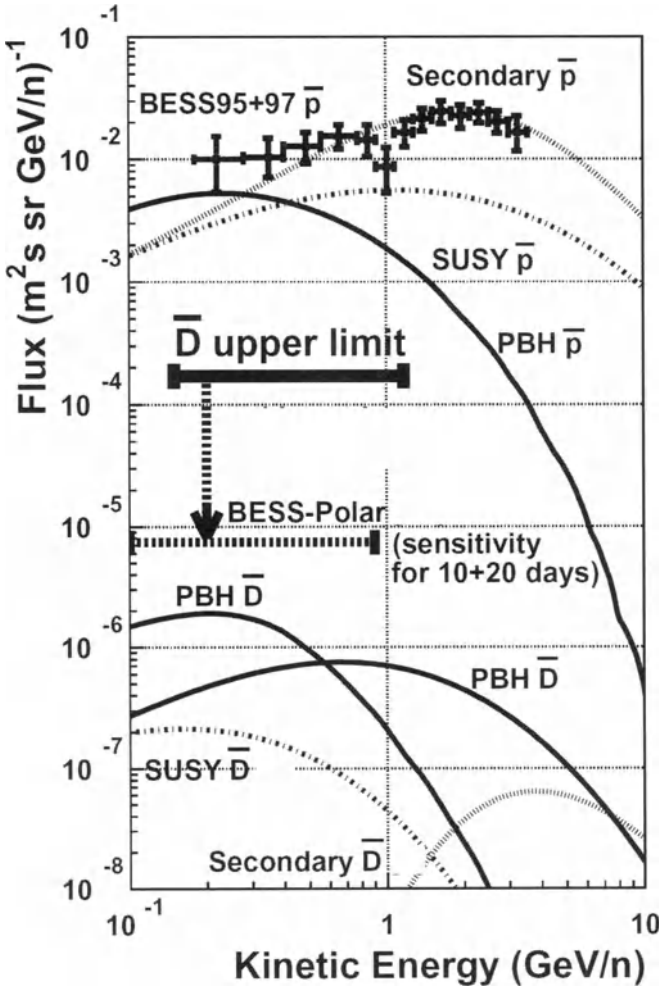

Fig. 1.4.20. Obtained upper limit on the differential CR antideuterium $\overline{D}$ flux according to measurements by the BESS instrument in 1997-2000 (Fuke et al., 2003) and the expected $\overline{D}$ sensitivity for BESS-Polar (according to Yamamoto et al., 2002) in comparison with expected secondary $\overline{D}$ (according to Chardonnet et al., 1997). For comparison are shown also results for antiprotons (observed fluxes and expected for secondary antiprotons). According to Fuke et al. (2003).

Sasaki et al. (2001) searched for $\overline{\text{He}}$ in CR using also the BESS detector (see description of this detector in Section 4.6.4) in every summer since 1993 (the last balloon flights of the BESS magnetic spectrometer were in 1999 and 2000 at Lynn Lake, Canada). The search was mainly based on track quality selection and rigidity analysis and on the time of flight and dE/dx measurements of the scintillation counter hodoscope. Sasaki et al. (2001) re-analyzed all the data collected during 1993–2000 with a common analysis procedure. The total number of helium nuclei observed by BESS in 1993–2000 was $> 6.6\times10^{6}$ in the rigidity region from 1 GV to 14 GV. No $\overline{\text{He}}$ candidate was found in the corresponding rigidity region. The resulting 95 % confidence level upper limit on the $\overline{\text{He}}/\text{He}$ flux ratio at the top of the atmosphere is 7×10^{-7} in the rigidity range from 1 to 14 GV with the model dependent assumption that the $\overline{\text{He}}$ energy spectrum coincides with the He spectrum. This result is shown in Fig. 1.4.21 in comparison with previous limits: Smoot et al. (1975), Evenson et al. (1972), Aizu et al. (1961), Badhwar et al. (1978), Golden et al. (1997), Buffington et al. (1981), Ormes et al. (1997), Saeki et al. (1998), Alcaraz et al. (1999).

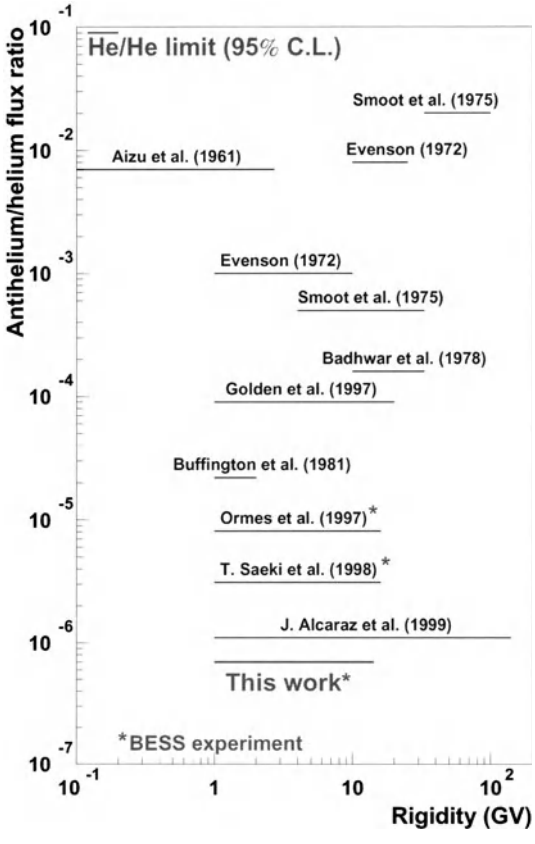

Fig. 1.4.21. The upper limit of $\overline{\text{He}}/\text{He}$ obtained by Sasaki et al., 2001 ('This work' – in Figure) in comparison with previous BESS results and results of other experiments. According to Sasaki et al. (2001).

Chapter 2

Secondary Cosmic Rays Underground and in the Atmosphere

2.1. CR interactions with air and ground atoms

Primary CR of galactic and solar origin (mostly protons and nuclei of different Z) undergo nuclear interactions with air atoms and generate a lot of secondary particles (secondary CR). As will be shown in Chapter 11, secondary relativistic positrons and electrons are responsible for lightning between clouds and ground, and between two clouds, as well as for discharges at great altitudes between clouds and the ionosphere (sprites). Primary CR (mostly protons, alpha–particles and heavier nuclei) and some part of secondary CR (nuclear active particles, mostly protons and neutrons) are important for the generation of stable and unstable cosmogenic nuclides in the atmosphere, in the oceans and underground (Chapters 10 and 17). Charged secondary particles such as protons, positive and negative pions, positive and negative muons, positrons and electrons (including re-entrant and splash albedo particles, see below Section 2.12) are important for the ionization of air and chemical processes in the atmosphere (particularly, formation of nitrates and influence on ozone layer – see Chapter 13). Ionization of air by primary and secondary charged CR particles is responsible for the effects of CR on ionosphere and radio wave propagation, for disruptions in radio communications during great solar flare events (Chapter 12). The ionization of air at altitudes higher than a few km caused by primary and secondary charged CR particles affects cloud formation as well, leading to long-term variation in global cloudiness, and consequently to global climate changes (Chapter 14).

2.2. Meson nuclear cascade and generation of pions

The kinetics of the meson nuclear cascade is determined by the generation of nucleons by nucleons, as well as by the generation of pions by nucleons and by pions (see, for example, in Murzin, M1988):

$$\partial I_n(E,x)/\partial x = -\lambda_n^{-1} I_n(E,x) + \lambda_n^{-1} \int_E^\infty I_n(E',x) D_{nn}(E',E) dE', \tag{2.2.1}$$

$$\partial I_\pi(E,x)/\partial x = -\lambda_\pi^{-1} I_\pi(E,x) + \lambda_n^{-1} \int_E^\infty I_n(E',x) D_{\pi n}(E',E) dE' +$$

$$+ \lambda_\pi^{-1} \int_E^\infty I_\pi(E',x) D_{\pi\pi}(E',E) dE' - \frac{C_\pi}{Ex} I_\pi(E,x), \tag{2.2.2}$$

where $I_n(E,x)$ and $I_\pi(E,x)$ are the differential energy spectra of nucleons and pions at a depth of x (in g/cm^2); λ_n and λ_π are respectively the transport paths for nuclear

interaction of nucleons and pions; $D_{nn}(E',E)$ is the spectrum of nucleons generated by nucleons with energy E'; $D_{\pi n}(E',E)$ is the spectrum of pions generated by nucleons with energy E', and $D_{\pi\pi}(E',E)$ is the spectrum of pions generated by pions with energy E'.

2.3. Meson-nuclear and electromagnetic cascades in the atmosphere; Geant4 simulation Monte Carlo code

The main components of secondary CR, important for the initiation of meson-nuclear and electromagnetic cascades are secondary neutrons and protons, and π^+,π^-,π^o pions directly generated in nuclear interactions. Decay of charged pions

$$\pi^+ \rightarrow \mu^+ + \nu_\mu,\ \pi^- \rightarrow \mu^- + \tilde{\nu}_\mu \tag{2.3.1}$$

generates muon (μ^+,μ^-) secondary component, while decay of neutral pions

$$\pi^o \rightarrow \gamma + \gamma \tag{2.3.2}$$

generates the non-equilibrium (relative to muon component) electron–photon component. Generation of electron–positron pairs by gamma rays from neutral pion decay, as described by Eq. 1.5.4, leads to the development of an electromagnetic cascade – electrons and positrons generate gamma rays, which in turn generate electron-positron pairs and so on). The decay

$$\mu^+ \rightarrow e^+ + \nu_e + \tilde{\nu}_\mu,\ \mu^- \rightarrow e^- + \tilde{\nu}_e + \nu_\mu \tag{2.3.3}$$

leads to equilibration of the muonic part of the electron–photon component.

In Fig. 2.3.1 are shown vertical fluxes in the atmosphere of protons + neutrons, pions, muons, electrons and neutrinos with energy more than 1 GeV, calculated from flux of primary CR. In the first approximation the flux of secondary particles generated by primary CR on the small values of depth $x << \lambda_n$ will be

$$N_i(E_i)dE_i = K_i x E_i^{-2.64} \times 10^{-4} dE_i \ \ \mathrm{cm}^{-2}.\mathrm{sr}^{-1}.\mathrm{sec}^{-1}, \tag{2.3.4}$$

where x is in g/cm^2, and coefficient $K_i = 3.27, 3.05,$ and 1.11 correspondingly for generation gamma rays $(i=\gamma)$, neutrino $(i=\nu)$, and electrons $(i=e)$. Here the energy E_i is measured in GeV. For our Galaxy the expected flux of secondary CR is very small: the maximum is expected from the center of Galaxy ($x \approx 0.1$ g/cm^2) about 2×10^{-5} cm^{-2}.sr^{-1}.sec^{-1} for gamma-rays and neutrino with energy more than 1 GeV (significantly lower than the flux generated in the Earth's atmosphere). For secondary electrons with $E_e \geq 1$ GeV the generation rate in the halo of our Galaxy (concentration

of matter $\approx 10^{-2}$ atoms.cm^{-3}) is expected to be $\approx 2\times10^{-29}$ electron.cm^{-3}.sec^{-1}, smaller by about two order of magnitude than the flux needed for the explanation of the observed synchrotron radiation and galactic CR electron fluxes. This means that the observed electrons in galactic CR are mostly primary; see Ginzburg and Syrovatsky, M1964; Berezinsky et al., M1990. For the Earth's atmosphere, where the depth of matter x is much bigger than in the Galaxy, the role of secondary CR is significant.

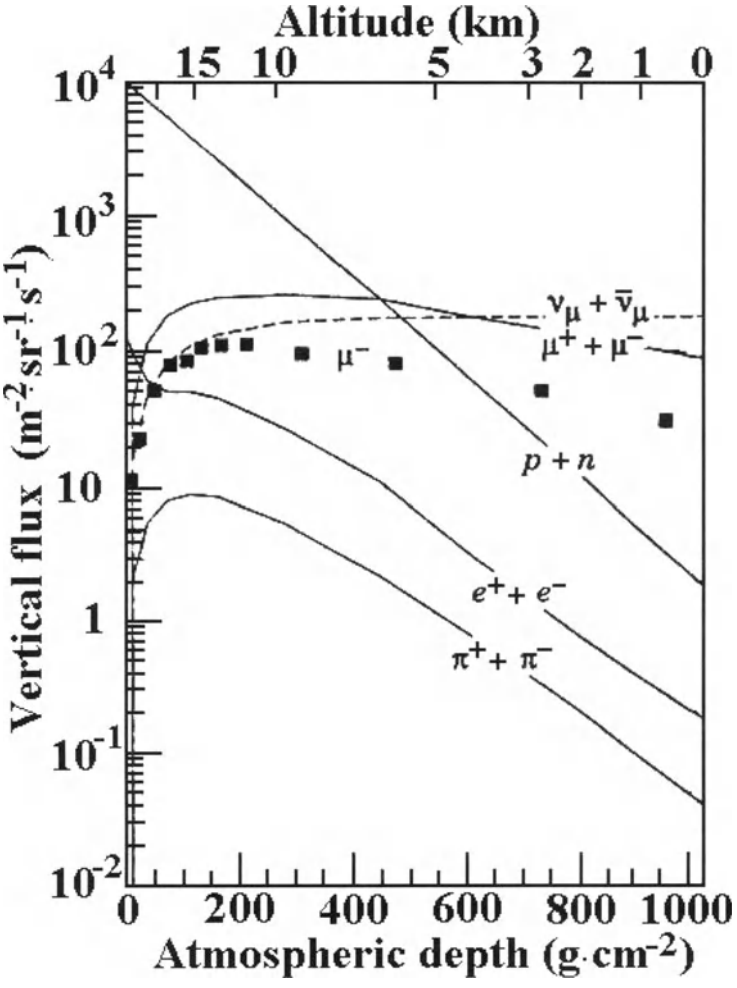

Fig. 2.3.1. Vertical fluxes of CR (protons + neutrons, pions, muons, electrons and neutrinos) in the atmosphere with energy more than 1 GeV *vs*. the atmospheric depth. The black squares show measurements of negative muons (Bellotti et al., 1996). According to Gaisser and Stanev (1996).

The precise knowledge of the flux of atmospheric cascade particles induced by galactic and solar CR is of utmost importance for a large field of applications. Complex Monte Carlo codes that can simulate the transport of CR through the atmosphere allow bettering quantifying these fluxes. The Geant4 Monte Carlo toolkit offers all the libraries

needed to build such codes (Geant4 Collaboration, M2003; see in website: Geant4 collaboration, the Geant4 toolkit, http://geant4.web.cern.ch). This Code allows simulating the propagation of primary and secondary particles through matter in the energy range 250 eV–10 TeV. First developed for the accelerator community, it has been sponsored by European Space Agency for extending its capabilities for the space and astrophysics community. Desorgher et al. (2003) have developed a Monte Carlo code based on Geant4 that simulates the interaction of CR with energy < 100 GeV with the Earth's atmosphere. The code allows computing the fluxes of secondary particles at user-defined altitudes. Possible applications include e.g. neutron albedo estimations, solar particle flux studies, and cosmogenic nuclide production. In this Monte Carlo code the atmosphere is represented by the superposition of several homogeneous horizontal layers with the same atmospheric depth. The density, pressure and temperature are taken as a function of altitude according to the 1976 U.S. standard atmospheric model (see in Grieder, M2001). The atmosphere is considered as composed by 78.1% of N_2 and 21.9% of O_2. The electromagnetic shower is simulated by the standard electromagnetic package available in Geant4. For the simulation of hadronic interactions, different models of Geant4 are used, depending on the energy range (Geant4 Collaboration, M2003). For high energies (more than 10 GeV), a quark gluon string model has been selected. For nucleons at energies lower than 10 GeV the binary intranuclear cascade model has been chosen (in this model the cascade phase is followed by a pre-equilibrium phase at intermediate energy, and then by an evaporation regime at lower energy). For neutrons with energy lower than 20 MeV the G4NeutronHP model based on the ENDF database is used. In a first application, Desorgher et al. (2003) have simulated the interaction of a CR proton population with a geomagnetic cutoff energy 2.7 GeV, and have only considered primary protons of vertical incidence. The resulting albedo neutron flux at the top of the atmosphere and the resulting flux of secondary particles at sea level are plotted in Fig. 2.3.2 and Fig. 2.3.3, respectively. These fluxes were obtained by simulating 3×10^5 cascades.

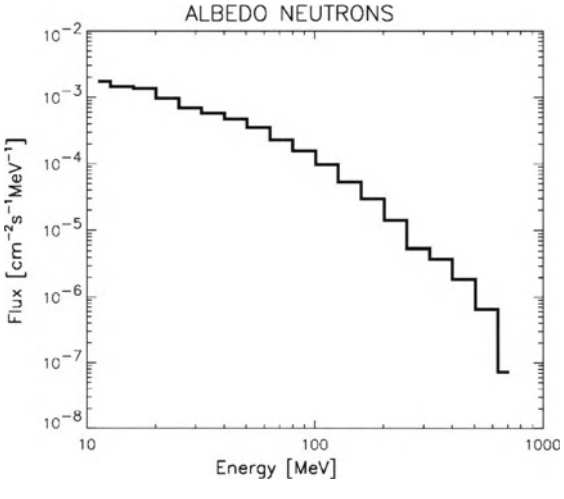

Fig. 2.3.2. Albedo neutron flux at the top of the atmosphere computed by using a vertically incident flux of CR protons. According to Desorgher et al. (2003).

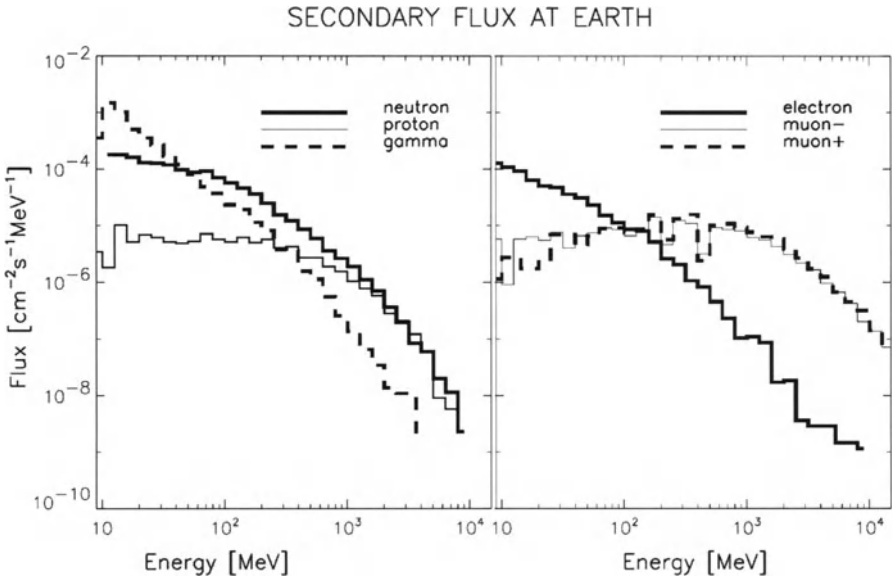

Fig. 2.3.3. The same as in Fig. 2.3.2, but for different secondary CR components near the Earth's surface. According to Desorgher et al. (2003).

According to Desorgher et al. (2003), a rapid comparison with former Monte Carlo simulation results and measurements shows that results shown in Fig. 2.3.2 and Fig. 2.3.3 are realistic; however to validate the code, more simulations with varying input parameters are needed.

2.4. Secondary CR underwater and underground

2.4.1. Origin and nature of CR underwater and underground

Primary CR (mostly protons and nuclei of different Z) are absorbed very quickly in the atmosphere, so that near sea level their flux is negligible in comparison with a hard secondary CR component (relativistic muons), secondary soft equilibrium and non-equilibrium components (soft muons, electrons, positrons, gamma quanta), and even in comparison with secondary nuclear active particles (mostly neutrons and protons). Most of our present knowledge on CR underwater and underground was obtained about 50 years ago (see review in George, 1952). Underwater and underground secondary nuclear active particles very quickly are absorbed in nuclear interactions with atoms of water and ground. This is also the fate of the non-equilibrium soft secondary CR component (electrons, positrons, and photons generated by decay of neutral pions on two gamma quanta). Thus there are only three secondary CR components underground and in the oceans: 1) hard component (relativistic muons); 2) soft equilibrium component (soft muons, electrons, positrons, and photons which are in equilibrium with hard component); 3) secondary neutrinos, generated in the atmosphere, in water, and in the ground by the decay of charged pions and muons (intensity of these neutrinos is practically independent of the depth, see Section 2.6 for more details).

2.4.2. CR measurements underwater and underground

The first attempts to measure CR intensity by electroscopes underwater on depths 4.5–5.0 m at sea level and on mountains on altitude about 3 km were made by Kolhörster (1923). In the summer of 1925 these investigations were continued by Myssowsky and Tuwim (1925) using electroscopes at different depths (up to 10 m) in Lake Onega.

From 1925 a lot of systematical measurements of CR intensity underwater up to 15 m depth were made in experiments of Millikan (1925) and Millikan and Cameron (1926) by special water resistant electroscopes in two mountain lakes: Muir at an altitude of 3595 m above sea level and Arrowhead at 1555 m. It was found that the results on CR intensity obtained underwater in lake Arrowhead are identical to the intensity in lake Muir, but at depths larger than 1.8 m (corresponding to a depth of 2040 m in air, which is the difference in altitudes of the two lakes). These measurements were continued by Millikan and Cameron (1928, 1931) up to an underwater depth 80 m (for these experiments ionization chambers of high pressure were used).

Regener (1931) extended these measurements up to a depth of 236.5 m. Let us note that the use of ionization chambers of high pressure and special water resistant electroscopes at great depths met with a major difficulties, caused by the radioactive background of the detector materials and the surrounding matter. These difficulties limited the depth where these instruments can be used to only by few hundred m w. e. (water equivalent). To overcome this limitation, Regener (1931) used also Geiger–Muller counters. Later these measurements were continued up to more than 10 km w. e. (Crouch, 1987; Andreev et al., 1987; Berger et al., 1989; Aglietta et al., 1995; Ambrosio et al., 1995)

2.4.3. The CR intensity dependence on depth of water and ground

Use of a vertical telescope from two Geiger–Muller counters connected by an electronic scheme for coincidences reduces significantly the influence of radioactivity. This type of a detector was first used by Kolhörster for underwater measurements (1933) at different depths down to 1000 m w. e.. During 1937-1939 many CR intensity measurements with high accuracy were carried out down to depths of 1,400 m w. e. by Ehmert (1937), Clay et al. (1937), Wilson (1938a,b) and Clay and Ehmert (1939). These measurements were later extended to depths of about 3,000 *m* w. e. (see review in George, 1952 and Fig. 2.4.1 below).

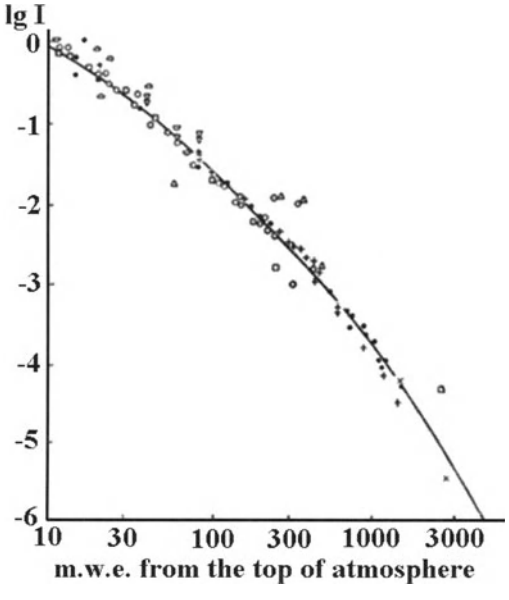

Fig. 2.4.1. CR intensity change underwater and underground, measured in different experiments.

To the beginning of 1960s the maximum depth where CR intensity was measured was 6,400 m w. e. (Menon et al., 1963). The measurements were made by telescope of scintillation counters with an effective surface of 1.5 m^2 with 5 cm lead between counters (so that only the hard muon component was detected). The vertical CR intensity at this depth was found to be

$$I_v(6{,}400\,\text{m w.e.}) = (1.92 \pm 0.47) \times 10^{-10}\,\text{particles.cm}^{-2}.\text{sec}^{-1}.\text{ster}^{-1}. \qquad (2.4.1)$$

As we mentioned above, now the underground CR measurements are continued up to depths much more than 10 km w. e. (see Fig. 2.4.2; the flat portion of the curve is owed to muons produced locally by charged–current interactions of ν_μ).

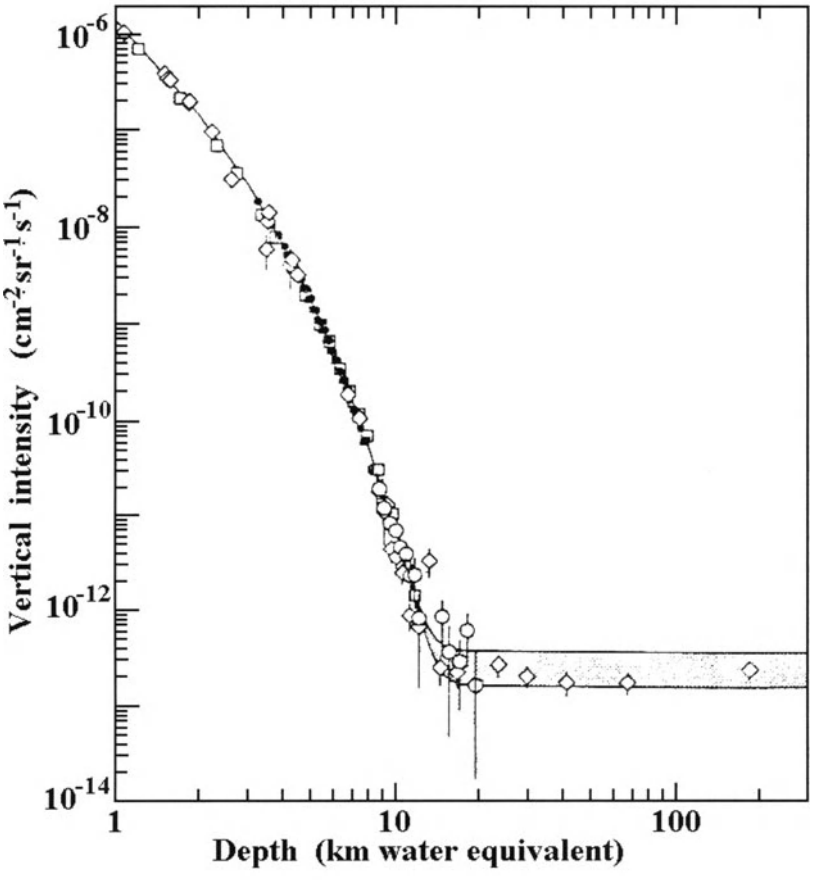

Fig. 2.4.2. Vertical muon intensity *vs.* depth (1 km w. e. = 10^5 $g.cm^{-2}$ of standard rock). The experimental data are from: light rhombs – the compilations of Crouch (1987); light squares – from Baksan experiment (Andreev et al., 1987); light circles – from LVD experiment (Aglietta et al., 1995); black circles – from MACRO experiment (Ambrosio et al., 1995), and black squares – from Frejus experiment (Berger et al., 1987). The shaded area at large depths represents neutrino induced muons of energy above 2 GeV (the upper line is for horizontal neutrino-induced muons, the lower one for vertically upward muons). According to Gaisser and Stanev (1996).

2.4.4. Energy dependence of muon absorption path

From the dependence of CR muon intensity on underwater or underground depth one can derive the dependence of the absorption path of muons on their energy. The latter is shown in Fig. 2.4.3.

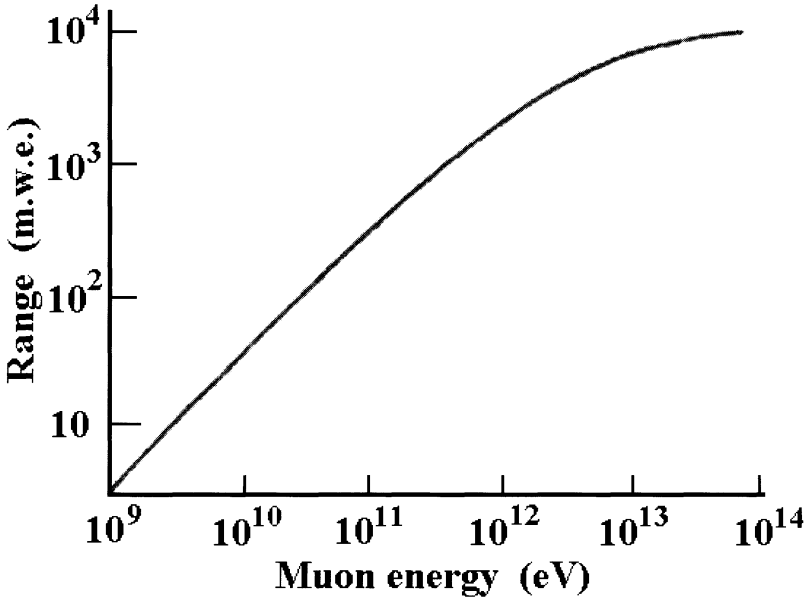

Fig. 2.4.3. The dependence of muon absorption path underwater and underground (in m w. e., vertical axes) on muon energy. According to George (1952).

The muon absorption path underwater and underground is determined by the energy losses owed to the following processes: ionization, bremsstrahlung, generation of electron-positron pairs, generation of Cherenkov radiation, formation of 'stars' and generation of secondary light absorbing particles (including neutrinos):

$$-dE_\mu/dx = a(E_\mu) + \sum b_i(E_\mu) E_\mu , \qquad (2.4.2)$$

where the coefficients $a(E_\mu)$, $b_i(E_\mu)$, $\sum b_i(E_\mu)$ are shown in Table 2.4.1.

Table 2.4.1. Average muon range R_μ and energy loss parameters in Eq. 2.4.2 calculated for standard rock ($A = 22$, $Z = 11$, $\rho = 2.65\,\mathrm{g.cm^{-3}}$). According to Gaisser and Stanev (1996).

E_μ, GeV	R_μ, km w. e.	$a(E_\mu)$, MeV.g^{-1}cm^2	$b_{\mathrm{pair}}(E_\mu)$, 10^{-6}g^{-1}cm^2	$b_{\mathrm{brems}}(E_\mu)$ 10^{-6}g^{-1}cm^2	$b_{\mathrm{nucl}}(E_\mu)$ 10^{-6}g^{-1}cm^2	$\sum b_i(E_\mu)$ 10^{-6}g^{-1}cm^2
10	0.05	2.15	0.73	0.74	0.45	1.91
100	0.41	2.40	1.15	1.56	0.41	3.12
1000	2.42	2.58	1.47	2.10	0.44	4.01
10000	6.30	2.76	1.64	2.27	0.50	4.40

From Fig. 2.4.3 it can be seen that at $E_\mu \le 10^{11}$ eV the absorption path increases linearly with the muon energy, since at these energies the main losses are caused by ionization processes that are about constant per 1 g.cm^{-2}. At higher muon energies the energy losses per 1 g.cm^{-2} increase with muon energy due to the other processes mentioned above. The dependence of the absorption path on muon energy becomes non-linear with visible signs of saturation at absorption path about 10 km w. e. The dependence of R_μ from E_μ for $E_\mu \ge 100$ GeV can be approximated with high accuracy (correlation coefficient 0.999) as

$$R_\mu(E_\mu) = 0.9025(\lg(E_\mu/\text{GeV}))^2 - 2.4095\times\lg(E_\mu/\text{GeV}) + 1.5725 \text{ km w.e.} \quad (2.4.3)$$

The dependences of $a(E_\mu)$ and $\sum b_i(E_\mu)$ from E_μ for $E_\mu \ge 10$ GeV can be approximated with high accuracy (correlation coefficients 0.996 and 0.999) as

$$a(E_\mu) = 0.201\times\lg(E_\mu/\text{GeV}) + 1.97 \text{ MeV.g}^{-1}\text{.cm}^2, \quad (2.4.4)$$

$$\sum b_i(E_\mu) = \left[-0.205\times(\lg(E_\mu/\text{GeV}))^2 + 1.861\times\lg(E_\mu/\text{GeV}) + 0.245\right]\times 10^{-6}\text{g}^{-1}\text{cm}^2. \quad (2.4.5)$$

2.4.5. Angular distribution of muons underwater and underground

According to Cousins et al. (1957) the angular distribution of muon intensity underwater and underground can be described by

$$I_\mu(Z,h) \approx I_{\mu v}(h)\times(\cos Z)^{\gamma(h)}, \quad (2.4.6)$$

where Z is the angle from the zenith, h is the depth in m w. e., $I_{\mu v}(h)$ is the muon intensity in vertical direction, and $\gamma(h)$ = 2.0 at 60 m w. e. (Follet and Crawskaw, 1936), $\gamma(h)$ = 1.92±0.08 at 103 m w. e. (Sreekantan et al. 1956), $\gamma(h)$ = 2.8±0.1 at 850 *m* w. e. (Randell and Hazen, 1951), and $\gamma(h)$ = 3.0 at 1,700 m w. e. (Bollinger, 1950). So, as the depth h increases, the secondary CR (mostly muons) becomes more concentrated near the vertical direction.

2.5. Negative and positive muons in the atmosphere

CR muons in the atmosphere and at ground level have recently been measured in several experiments: BESS (Motoki et al., 2001; Sanuki et al., 2001), CAPRICE (Hansen et al., 2001; Tsuji et al., 2001), MASS, HEAT and others (see description of these experiments below, in Chapter 4, Section 4.6.4). In order to select muons with a high purity, these experiments comprised a variety of particle identification techniques. For example, Fig. 2.5.1 shows the results of measurements of μ^+ and μ^- fluxes on balloons in BESS-98 and CAPRICE-98 experiments, compared with the theoretical

calculations made by Honda et al. (2001) and Engel et al. (2001) for muons with momentums of 1.0, 1.5, 2.5, 3.9 and 6.3 GeV/c.

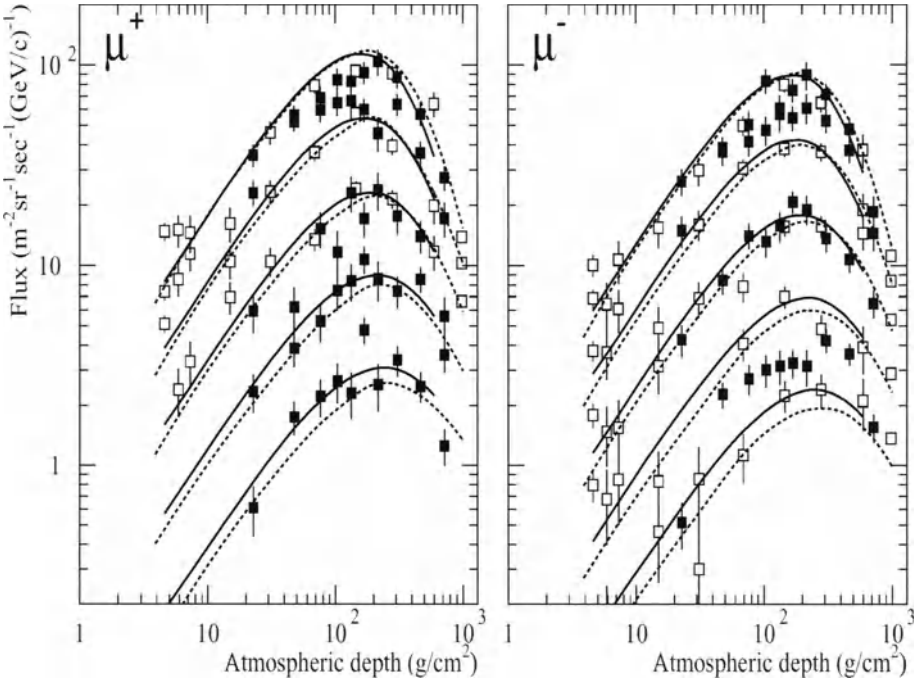

Fig. 2.5.1. Measured muon fluxes during the ascend of balloon experiments. Blank and black squares show data from BESS-98 and CAPRICE-98 experiments, respectively. Dotted and solid lines show predictions by Honda et al. (2001) and Engel et al. (2001), respectively. The mean momentums are 1.0, 1.5, 2.5, 3.9 and 6.3 GeV/c from the top to the bottom. According to Kajita (2001).

The measurements μ^+ and μ^- fluxes at very high altitudes are difficult owing to higher proton flux. Especially in the high momentum range, the separation of muons and protons is very difficult. Only recently have these fluxes been separately measured in the CAPRICE experiment in the atmosphere up to 18 GeV/c (Hansen et al., 2001). However, the high altitude muon data are still limited in statistics and in the momentum range, as seen in Figs. 2.5.1 and 2.5.2. The latter figure also shows results of μ^+ and μ^- momentum spectra measurements of at depths of $3-5$ g/cm^2, in comparison with the theoretical results obtained by Honda et al. (1995).

Momentum spectra of total muon fluxes ($\mu^+ + \mu^-$) at different altitudes and at different cutoff rigidities are shown in Fig. 2.5.3. From Fig. 2.5.3 it can be seen that the data from BESS and CAPRICE experiments taken at Lynn Lake in Canada agree within 5%. Altitude and geomagnetic cut off dependences of the measured fluxes are also clearly seen.

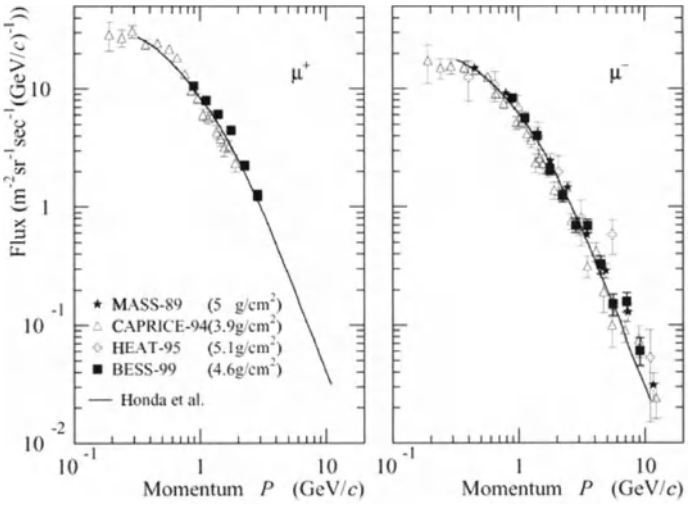

Fig. 2.5.2. Measured muon fluxes at 3 – 5 g/cm^2 altitude. Also shown are the calculated muon fluxes by Honda et al. (1995). According to Kajita (2001).

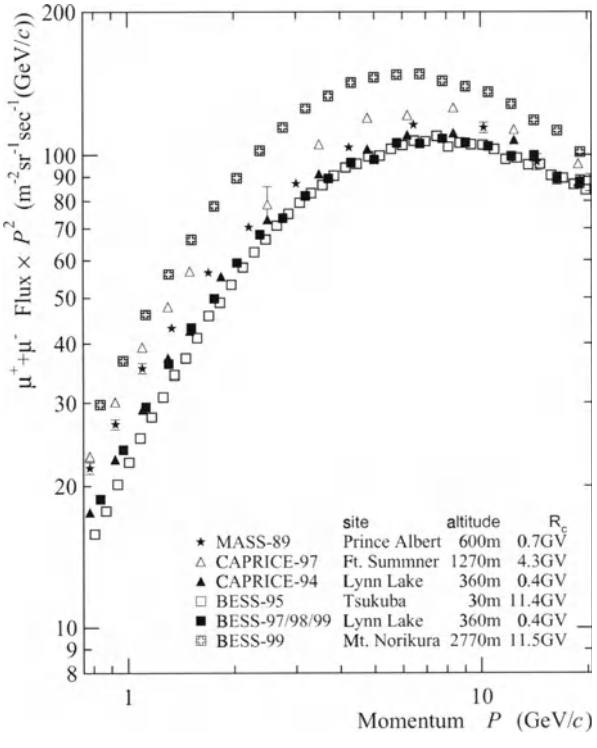

Fig. 2.5.3. Momentum spectra of total muon fluxes ($\mu^+ + \mu^-$) at different altitudes and at different cut off rigidities. According to Kajita (2001).

Results shown in Fig. 2.5.4 are in good agreement with calculations of Hebbeker and Timmermans (2001) for the ratio μ^+/μ^- in the momentum range 10 to 300 GeV/c:

$$\mu^+/\mu^- = 1.268 \pm (0.008 + 0.0002\,p), \tag{2.5.1}$$

where p is the muon momentum in GeV/c.

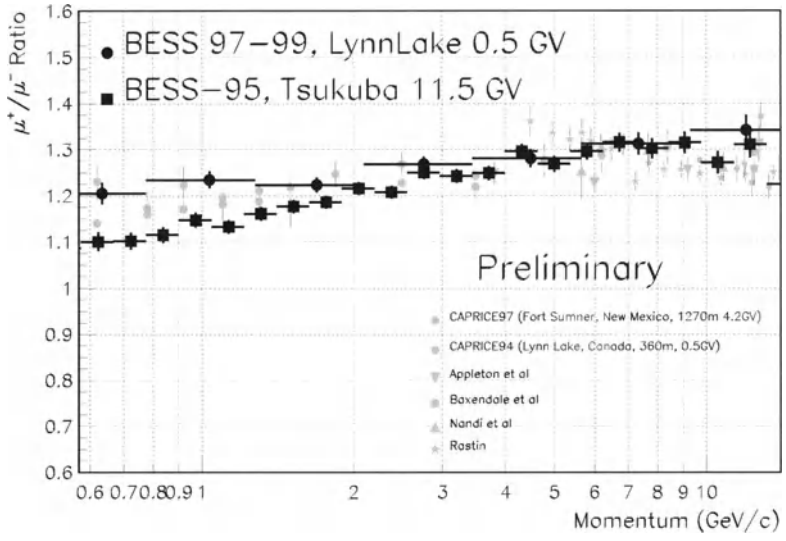

Fig. 2.5.4. Results of recent measurements of μ^+/μ^- ratio in the BESS experiment near Lynn Lake in Canada at $R_C = 0.5$ GV and near Tsukuba in Japan at $R_C = 11.5$ GV in comparison with previous measurements in different experiments: Appleton et al. (1971), Baxendale et al. (1975), Nandi and Sinha (1972), Rastin (1984). According to Motoki et al. (2001).

Let us note that in the GeV energy range, most of the muons decay before reaching to the ground, may accelerate and decelerate by atmospheric electric field. Therefore the comparison of the measured data and calculations of the ground muon flux is sensitive to experimental conditions such as the vertical temperature distribution over the point of observations, humidity, atmospheric pressure, gravitational acceleration, atmospheric electric field (meteorological effects of muon component, see below, Part 2).

2.6. Secondary neutrino fluxes in the atmosphere and underground

The flux (in units of $\mathrm{cm}^{-2}.\mathrm{sec}^{-1}.\mathrm{sr}^{-1}.\mathrm{GeV}^{-1}$) of muon neutrinos ($\nu_\mu$, $\widetilde{\nu}_\mu$) at the bottom of the atmosphere and underground, generated by the decay of charged pions (Eq. 2.3.1) is approximately given by (Murzin, M1988):

$$I_{\pi\nu}(E_\nu) = \begin{cases} 1.85\times10^{-2}(0.08 + E_\nu)^{-2.8}, \text{ if } 1\ \text{GeV} \le E_\nu \le 10\ \text{GeV} \\ 6.65\times10^{-2}(1.1 + E_\nu)^{-3.2}, \text{ if } 10\ \text{GeV} \le E_\nu \le 100\ \text{GeV} \end{cases}. \tag{2.6.1}$$

Neutrino flux (ν_μ, $\tilde{\nu}_\mu$, ν_e, $\tilde{\nu}_e$) from the decay of muons (Eq. 2.3.2) in the atmosphere is approximately (Murzin, M1988):

$$I_{\mu\nu}(E_\nu)=\begin{cases}7.65\times10^{-2}(0.37+E_\nu)^{-3.75}, & \text{if } 1\text{ GeV}\le E_\nu\le 10\text{ GeV},\\ 1.48\times10^{-2}(3.5+E_\nu)^{-4.5}, & \text{if } 10\text{ GeV}\le E_\nu\le 100\text{ GeV}.\end{cases} \tag{2.6.2}$$

This flux of CR secondary neutrino generated in the atmosphere is several orders of magnitude higher than the flux generated in the Galaxy. It can be seen from Fig. 2.6.1 that the flux of muon neutrinos is higher than that of electron neutrinos, and this difference increases with increasing neutrino energy E_ν.

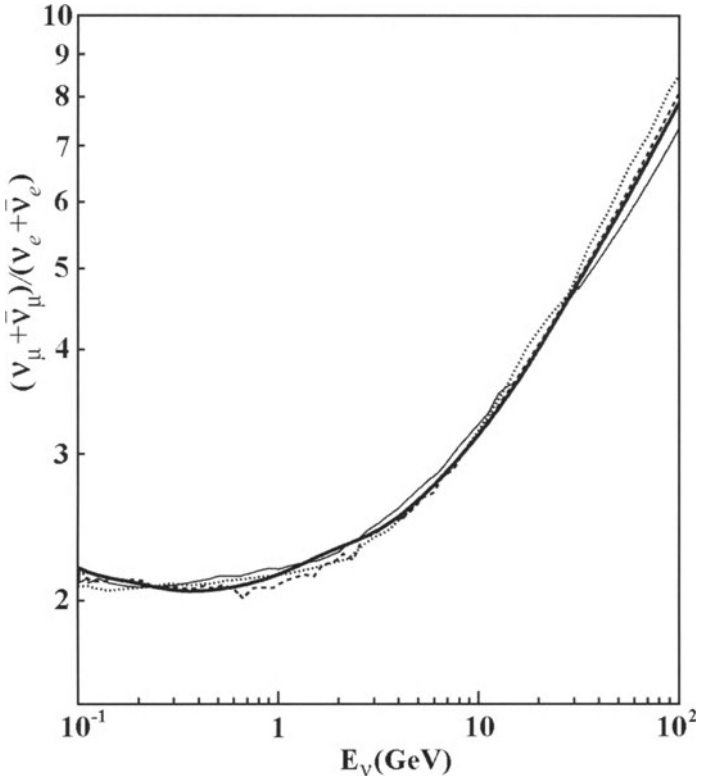

Fig. 2.6.1. Calculated ratio of muon neutrinos to electron neutrinos as a function of neutrino energy, integrated over the solid angle. Results from one-dimensional calculations are shown by a dotted line (Agrawal et al., 1996) and a thin-solid line (Honda et al., 1995). Results from three-dimensional calculations are shown by a dashed line (Battistoni, 2000; Battistoni et al., 2001) and a thick-solid line (Honda et al., 2001). According to Kajita (2001).

Differential energy spectra (multiplied by E_ν^2) expected for muon and electron neutrino in the range from 0.1 to 10^2 GeV are depicted in Fig. 2.6.2..

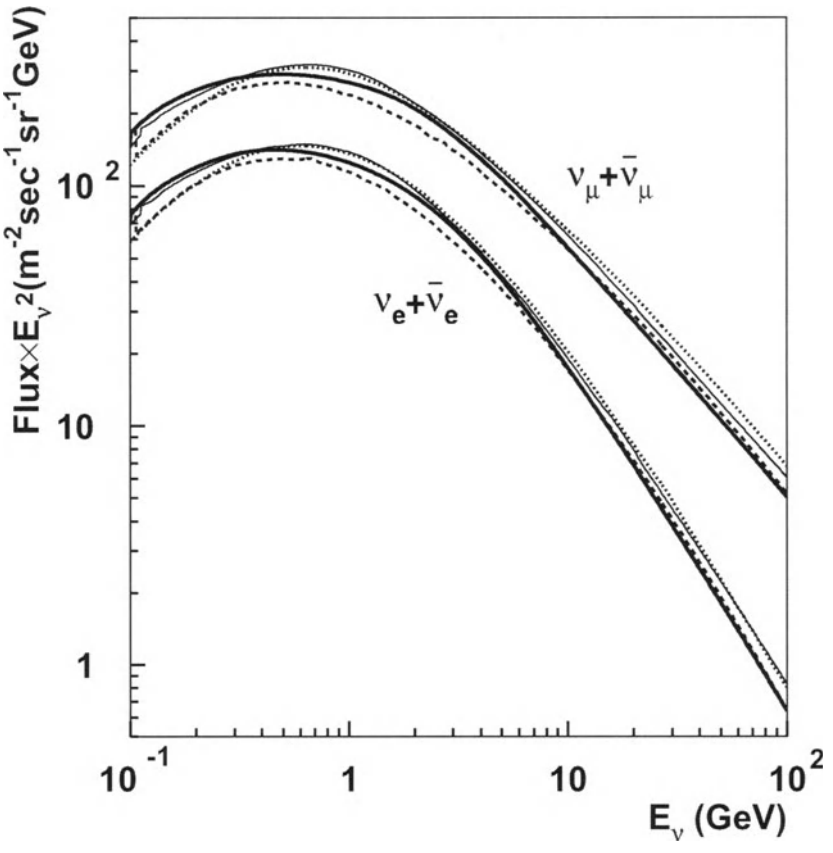

Fig. 2.6.2. Calculated differential energy spectra (multiplied by E_ν^2), of muon and electron neutrinos in the E_ν range from 0.1 to 10^2 GeV. Calculations made using one-dimensional approximation are shown by the dotted line (Agrawal et al., 1996), and the thin-solid line (Honda et al., 1995). Recent calculations using a three-dimensional approximation are given by the dashed line (Battistoni, 2000; Battistoni et al., 2001) and the thick solid line (Honda et al., 2001). From Kajita (2001).

Calculations of secondary neutrino fluxes generated by galactic CR in the atmosphere are widely used in underground neutrino experiments: Kamiokande and Super-Kamiokande (with water as the target), Homestake (^{37}Cl as target), SAGE and Gallex+GNO (^{71}Ga as target), and SNO (heavy water D_2O as target).

2.7. Underground measurements of solar and cosmic neutrinos

2.7.1. Importance of solar and cosmic neutrinos measurements for Astrophysics and Elementary Particle Physics

Underground measurements of solar and cosmic neutrinos are very important not only for Astrophysics (thermonuclear reactions inside the Sun and inside stars, physics of the Sun interior, physics of Supernova explosions, and so on) but also for Elementary

Particle Physics (neutrino propagation, neutrino non-zero mass and oscillations, possible magnetic moment and spin-flavor precession). Let us note, that for "pioneering contributions to neutrino astrophysics, in particular for the detection of solar and cosmic neutrinos" (was detected from Supernova explosion in Magellan Clouds at February 23, 1987 in Kamiokande experiment, see Section 2.7.4 below) Prof. Raymond Davis, Jr. (USA) and Prof. Masatoshi Koshiba (Japan) received Nobel Prize in Physics for 2002.

2.7.2. Solar neutrinos deficit and oscillations; non zero neutrino mass

The problem of solar neutrinos generated in thermonuclear reactions in the center of the Sun at a temperature of about $1.5\times10^7\ ^{o}\mathrm{C}$, is very closely related to the field covered by CR research underground (see review in Bahcall, M1990). These experiments were stimulated by the first results of Prof. Raymond Davis and his group on the solar neutrino deficit obtained in Homestake ($^{37}\mathrm{Cl}$) experiment (using the reaction $\nu_e + {}^{37}\mathrm{Cl} \rightarrow e + {}^{37}\mathrm{Ar}$) many years ago (see review and short historical outline in Davis, 2002). Fig. 2.7.1 shows the ratio of the measured solar neutrino flux relative to the flux expected from the Standard Solar Model (SSM), as obtained in Kamiokande and Super-Kamiokande (used water as a target), Homestake ($^{37}\mathrm{Cl}$), SAGE and Gallex + GNO ($^{71}\mathrm{Ga}$), and SNO (heavy water D_2O) experiments.

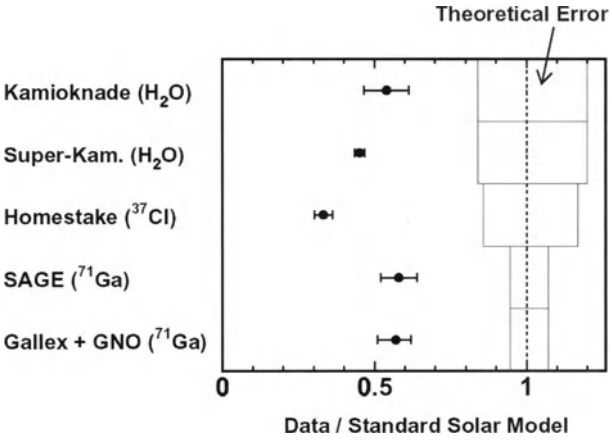

Fig. 2.7.1. Summary of the observed solar neutrino flux by various experiments (before SNO). The uncertainties in the SSM prediction are also shown. From Kajita (2001).

The result shown in Fig. 2.7.1 can be explained by neutrino oscillations in the Sun or on the way from the Sun to the Earth (Mikheyev and Smirnov, 1985, 1986; Wolfenstein, 1978; see also review in Berezinsky, 1997); i.e., transformation of the electron neutrinos generated inside the Sun to muon and tau neutrinos, which can not be detected with the abovementioned underground neutrino detectors. This means that in contradiction to the standard elementary particles theory, neutrinos must have a non-zero mass, and that the masses of tau, muon, and electron neutrinos must be different.

On the other hand, the recent measurements of the solar neutrino flux (ν_e from ^{8}B decay) made in SNO (using heavy water as target so that other types of neutrinos can also be detected) show that total flux of all types of neutrino is

$$I_\nu(SNO) = (5.44 \pm 0.99) \times 10^6 \text{ cm}^{-2}.\text{sec}^{-1} , \qquad (2.7.1)$$

in good agreement with the SMM prediction (Bahcall et al., 2001):

$$I_\nu(SMM) = 5.05 \times 10^6 \text{ cm}^{-2}.\text{sec}^{-1} . \qquad (2.7.2)$$

The last available results on observed solar neutrino fluxes to the end of 2002 (including very important results of SNO) are shown in Fig. 2.7.2.

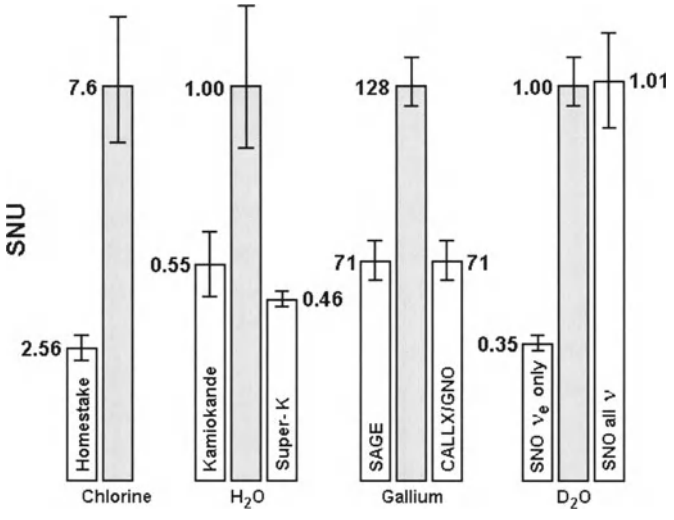

Fig. 2.7.2. The same as in Fig. 2.7.1, but to the end of 2002 and including data of SNO. According to Davis (2002).

2.7.3. Possible anomalous magnetic moment and spin-flavor neutrino precession

If the neutrino has a non-zero mass it is not excluded that it can have an anomalous magnetic moment. In this case, on the way from the central region of the Sun where neutrinos are generated (with a radius about 0.05 of the Sun's radius) to the Sun's surface, neutrinos will interact with the strong interior solar magnetic field, leading to spin-flavor neutrino precession (Akhmedov and Bychuk, 1989) with the changing of neutrino type (from electron neutrino to electron or muon anti-neutrino). This change will be in addition to the change caused by oscillations (from the difference in neutrino masses and discussed above in Section 2.7.1). The oscillation effect does not depend on solar interior magnetic field and its possible variations during solar cycle. In contrast, spin-flavor neutrino precession effects are totally determined by interactions with the strong solar interior magnetic field, which can vary with the solar cycle.

On the basis of the Homestake experimental data many authors investigated the solar neutrino time variability connected with solar activity and galactic CR intensity variations (Bazilevskaya et al., 1984; Davis et al., 1989; Bahcall, M1989; Akhmedov and Bychuk, 1989; Dorman and Wolfendale, 1991a,b,c; Bahcall and Press, 1991; Gavryusev et al., 1991; Dorman et al., 1993, 1995; Rivin, 1993; Rivin and Obridko, 1997; Massetti, 1995; Massetti et al., 1995; Oakley et al., 1994; Oakley and Snodgrass, 1995, 1996, 1997; Bykov et al., 1998; Sturrock et al., 1998; Snodgrass and Oakley, 1999). Let us note that up to now, not many scientists have believed in the reliability of solar neutrino time variations. A possible cause can be found in the large fluctuations of Homestake data which decrease the reliability of the obtained correlation coefficients. A second cause is that, in contradiction with the Homestake experiment, Kamiokande data do not show any significant time variations (Raychaudhuri, 1991). Recently the reliability of solar neutrino flux time variations and their connection with solar activity appeared to be even lower after obtaining the Homestake data for the period 1990–1994, during which the correlation with solar activity changed its sign (became positive) and the total correlation for 1970–1994 became very weak (Walther, 1999).

To make the analysis more reliable, Dorman (2000a) used the weight–time function by taking into account ^{37}Ar decay, and determined for each solar neutrino run n the following parameters: the effective heliolatitude of the Earth $L_{\text{eff}}(n)$, the effective Zurich sunspots number $Z_{\text{eff}}(n)$, the effective latitude of sunspots distribution $\Lambda_{\text{eff}}(n)$, and the effective surfaces of sunspots in different intervals of heliolatitudes $\Sigma 50_{\text{eff}}$ (covered from +52.5° to −52.5°), and so on. Then it was considered the correlation of solar electron neutrino fluxes $F(T_{\text{eff}})$ determined on the basis of all Homestake experimental data (Cleveland et al., 1998) with these parameters for different periods of solar activity. Results are shown in Table 2.7.1 and Table 2.7.2.

Table 2.7.1. Correlation coefficients of solar neutrino flux $F(T_{\text{eff}})$ with solar activity parameters in different time periods.

Period	Z_{eff}	$Z_{\text{eff}}/\Lambda_{\text{eff}}$	$\Sigma 50_{\text{eff}}$	$\Sigma 20_{\text{eff}}$	$\Sigma 15_{\text{eff}}$	$\Sigma 10_{\text{eff}}$	$\Sigma 5_{\text{eff}}$
1970–1994	−0.11 ± 0.06	−0.06 ± 0.06	−0.05 ± 0.06	−0.03 ± 0.06	−0.05 ± 0.06	0.08 ± 0.06	0.12 ± 0.06
1970–1979	−0.14 ± 0.10	−0.18 ± 0.10	−0.18 ± 0.10	0.23 ± 0.10	−0.29 ± 0.10	−0.18 ± 0.10	0.03 ± 0.11
1980–1989	−0.33 ± 0.09	−0.26 ± 0.09	−0.22 ± 0.09	−0.15 ± 0.10	−0.16 ± 0.10	0.01 ± 0.10	−0.02 ± 0.10
1970–1974	0.23 ± 0.17	0.26 ± 0.16	0.15 ± 0.17	0.16 ± 0.17	0.13 ± 0.18	0.12 ± 0.18	0.06 ± 0.18
1975–1979	−0.23 ± 0.12	−0.25 ± 0.12	−0.27 ± 0.12	−0.30 ± 0.12	−0.38 ± 0.11	−0.20 ± 0.13	−0.02 ± 0.13
1980–1984	−0.21 ± 0.13	0.05 ± 0.13	−0.01 ± 0.13	0.19 ± 0.13	0.24 ± 0.12	0.30 ± 0.12	0.15 ± 0.13
1985–1989	−0.41 ± 0.13	−0.43 ± 0.13	−0.35 ± 0.13	−0.34 ± 0.14	−0.48 ± 0.12	0.29 ± 0.14	0.16 ± 0.15
1990–1994	0.24 ± 0.13	0.18 ± 0.13	0.25 ± 0.13	0.20 ± 0.13	0.14 ± 0.14	0.21 ± 0.13	0.29 ± 0.13

Table 2.7.2. Correlation coefficients of 3-run moving averages of neutrino flux $F3(T_{\text{eff3}})$ and corresponding 3-run averages of effective solar activity parameters

Period	$Z_{\text{eff}}3$	$Z_{\text{eff}}3/\Lambda_{\text{eff}}3$	$\Sigma 50_{\text{eff}}3$	$\Sigma 20_{\text{eff}}3$	$\Sigma 15_{\text{eff}}3$	$\Sigma 10_{\text{eff}}3$	$\Sigma 5_{\text{eff}}3$
1970–1994	−0.16 ± 0.06	−0.15 ± 0.06	−0.10 ± 0.06	−0.10 ± 0.06	−0.10 ± 0.06	0.04 ± 0.06	0.06 ± 0.06
1970–1979	−0.18 ± 0.10	−0.29 ± 0.09	−0.21 ± 0.10	−0.32 ± 0.09	−0.44 ± 0.08	−0.38 ± 0.09	−0.34 ± 0.09
1980–1989	−0.51 ± 0.07	−0.49 ± 0.08	−0.48 ± 0.08	−0.42 ± 0.08	−0.37 ± 0.09	−0.15 ± 0.10	−0.13 ± 0.10
1970–1974	0.08 ± 0.18	0.08 ± 0.18	0.02 ± 0.18	0.01 ± 0.18	0.05 ± 0.18	0.00 ± 0.18	−0.18 ± 0.17
1975–1979	−0.26 ± 0.12	−0.32 ± 0.12	−0.29 ± 0.12	−0.35 ± 0.11	−0.49 ± 0.10	−0.41 ± 0.11	−0.34 ± 0.12
1980–1984	−0.47 ± 0.10	−0.23 ± 0.12	−0.43 ± 0.11	−0.14 ± 0.13	0.04 ± 0.13	0.34 ± 0.12	0.27 ± 0.12
1985–1989	−0.49 ± 0.12	−0.51 ± 0.11	−0.48 ± 0.12	−0.48 ± 0.12	−0.48 ± 0.12	−0.38 ± 0.13	0.12 ± 0.15
1990–1994	0.39 ± 0.12	0.28 ± 0.13	0.45 ± 0.11	0.37 ± 0.12	0.34 ± 0.12	0.42 ± 0.11	0.44 ± 0.11

From Tables 2.7.1 and 2.7.2 it can be seen that the connection between solar activity parameters and solar neutrino flux, according to Homestake measurements in 1980–1989, was more evident than in 1970–1979. This difference can be understood if we consider the correlations separately for 1970–1974, 1975–1979, 1980–1984, and 1985–1989. Correlation in 1970–1974 was positive, but in 1975–1979 it was negative; therefore, in the total period 1970–1979 correlation became very weak. In both periods 1980–1984 and 1985–1989 correlation was negative; as a result this gives in 1980–1989, much better negative correlation than in 1970–1979. It is important to note that in 1990–1994 (after about two solar cycles) correlation again becomes positive. These two periods with positive correlation (1970–1974 and 1990–1994) decrease very much the total negative correlation coefficient for 1970–1994 and make it very small. This could be the reason why many people do not believe in the reality of the existence of solar neutrino time variations and in their connection with solar activity. In both parts of the odd solar cycle 21 we have a negative correlation of solar activity with solar electron neutrino flux. This means that in the odd cycle the correlation between the magnetic field in convection zone (in which a fraction of the electron neutrinos are transformed in other types of neutrinos, an effect that was not detected in the Homestake experiment, leading to a decrease in the observed neutrino counting rate) and the solar activity is positive: increase of solar activity reflects an increase of internal magnetic field in the convection zone and a decrease of electron neutrino flux. A more complicated situation is observed in the even solar cycles 20 and 22: in periods of increasing solar activity the character of correlation between solar activity and electron neutrino flux is the same as in the odd cycle (negative correlation), but in periods of decreasing solar activity the character of this correlation is opposite to that of the odd cycle (positive correlation). It means that in even solar cycles there is positive correlation between magnetic field in convection zone and solar activity on the Sun's surface in periods of increasing solar activity and negative correlation in periods of decreasing solar activity: solar activity decreases after reaching the maximum, but the magnetic field in the convection zone continues to increase in the region around the equatorial plane where neutrinos, detected on the Earth, cross the convection zone. The results obtained can be considered as a peculiar feature of 22-year variations in convection zone, which can be connected to 22-year variations of solar activity on the Sun's surface, as well as to the observed time lag between changes of magnetic fields in the convection zone and solar activity variations. On the other hand, the connection of solar neutrino time variations with solar activity and variable magnetic fields in the convection zone can be considered as a manifestation of non zero neutrino mass and nonzero magnetic moment in the frame of the theory of magnetic neutrino resonant spin-flavor precession (Akhmedov and Bychuk, 1989; Bykov et al., 1998).

This analysis was continued by Dorman (2000b), where all data are separated on three groups NORTH, EQUATOR and SOUTH, corresponding to the effective heliolatitude for each run (see Fig. 2.7.3).

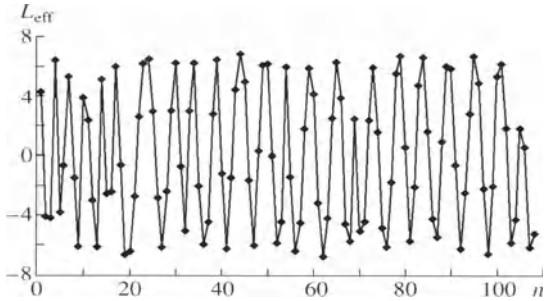

Fig. 2.7.3. L_{eff} *vs* the run's number n.

The data were also separated in three groups in dependence of the level of solar activity (SA): Low SA, Medium SA and High SA. Results are shown in Table 2.7.3.

Table 2.7.3. Average values of solar neutrino flux $\langle F \rangle$, effective helio-latitude $\langle L_{\text{eff}} \rangle$, and effective sunspots number $\langle Z_{\text{eff}} \rangle$ in different latitudinal zones and different groups of solar activity (SA) levels.

Zone	Parameter	Low SA	Medium SA	High SA
SOUTH	$\langle F \rangle$, SNU	2.9 ± 0.4	2.4 ± 0.3	2.5 ± 0.6
	$\langle L_{\text{eff}} \rangle$, deg	−5.5 ± 0.3	−4.9 ± 0.3	−5.5 ± 0.2
	$\langle Z_{\text{eff}} \rangle$	23.9 ± 3.3	67.8 ± 3.6	138.6 ± 6.1
EQUATOR	$\langle F \rangle$, SNU	3.6 ± 0.5	2.5 ± 0.4	2.1 ± 0.4
	$\langle L_{\text{eff}} \rangle$, deg	−0.2 ± 0.7	0.0 ± 0.5	−0.6 ± 0.5
	$\langle Z_{\text{eff}} \rangle$	21.7 ± 3.5	80.8 ± 8.5	156.3 ± 3.5
NORTH	$\langle F \rangle$, SNU	2.1 ± 0.6	2.8 ± 0.5	2.7 ± 0.6
	$\langle L_{\text{eff}} \rangle$, deg	5.0 ± 0.4	5.4 ± 0.3	5.5 ± 0.3
	$\langle Z_{\text{eff}} \rangle$	29.4 ± 3.7	91.7 ± 7.5	154.7 ± 3.1

From Table 2.7.3 it follows that: 1. In the SOUTH zone there is a tendency of decreasing solar-neutrino flux with increasing solar activity, but in the NORTH zone the tendency is opposite. 2. The biggest decrease of solar neutrino flux with increasing solar activity from LOW ($Z_{\text{eff}} \approx 22$) to HIGH ($Z_{\text{eff}} \approx 156$) is observed in the EQUATOR zone: from 3.6 ± 0.5 SNU to 2.1 ± 0.4 SNU. 3. The biggest NEAR–FAR effect (the difference between NEAR = EQUATOR zone and FAR zone = (SOUTH + NORTH)/2) is observed in periods of LOW solar activity: 3.6 ± 0.5 SNU in NEAR zone and 2.5 ± 0.5 SNU in FAR zone; this effect decreases with increasing solar activity and disappears in periods of MEDIUM and HIGH solar activity. 4. The biggest NORTH–SOUTH asymmetry also is observed in periods of LOW solar activity: 2.1 ± 0.6 SNU in NORTH zone and 2.9 ± 0.4 SNU in SOUTH zone.

The connection between $F(T_{\text{eff}})$ and Z_{eff} (T_{eff}) for SOUTH zone is characterized by correlation coefficient $R_S = -0.14 \pm 0.11$, for EQUATOR zone by $R_E = -0.35 \pm 0.10$, and for NORTH zone by $R_N = +0.12 \pm 0.11$. Therefore, in correlation coefficients there are a significant NEAR–FAR effect and a great NORTH–SOUTH asymmetry (with opposite signs in the correlation coefficients). For EQUATOR zone, characterized by the highest correlation coefficient, the regression equation will be

$$F(Z_{\text{eff}}) \approx 3.52 - 0.0094 Z_{\text{eff}} \ (SNU), \tag{2.7.3}$$

what gives for $Z_{\text{eff}} \to 0$ an expected flux $F_{\max} = 3.52$ SNU, in good agreement with Table 2.7.3.

The main results that characterize the latitudinal dependences of solar-neutrino fluxes and their correlation with parameters of solar activity, can be summarized as follows:

1. Homestake experimental data of solar-neutrino fluxes for about 24 years show the existence of NEAR–FAR effect; this effect increases significantly in periods of LOW solar activity, when a significant NORTH–SOUTH asymmetry is also observed.

2. The biggest decrease of solar-neutrino flux with increasing solar activity was observed in EQUATOR zone; in this zone the maximum solar-neutrino flux at zero solar activity is expected to be 3.5 SNU.

3. Correlation coefficients of solar-neutrino flux with solar activity for SOUTH and NORTH zones have opposite signs for sunspots numbers, as well as for sunspots surfaces, taken in symmetrical latitudinal belts.

4. We show that there are reliable NORTH – SOUTH asymmetry in fluxes and correlation coefficients and that neutrino flux in SOUTH zone F_S better correlates with sunspots surfaces ΣS than with ΣN, and neutrino flux in NORTH zone F_N better correlates with sunspots surfaces ΣN than with ΣS. Neutrino fluxes in SOUTH zone are controlled mainly by solar activity in south latitude belts (correlation coefficients for south latitude belts are in 2–4 times bigger than for north latitude belts), and fluxes in NORTH zone are controlled by solar activity in north latitude belts.

5. Neutrino fluxes in EQUATOR zone are controlled mainly by solar activity in symmetrical latitudinal belts.

6. In our opinion, the much smaller 11–year solar cycle variation in Kamiokande and Super-Kamiokande experiments in comparison with Homestake experiment can be understood if we take into account that this variation really has only EQUATOR zone, and that about 1/3 part of transformed neutrino will be detected in Kamiokande experiment and not detected in Homestake experiment. This problem is very important and let us consider it in more detail. From Table 2.7.3 and mentioned above values on the correlation coefficients between $F(T_{eff})$ and Z_{eff} (T_{eff}) for SOUTH, EQUATOR, and NORTH zones (by $R_S = -0.14 \pm 0.11$, $R_E = -0.35 \pm 0.10$, and $R_N = +0.12 \pm 0.11$, correspondingly) follows that solar activity influenced mostly only on the electron neutrino flux passed the Sun's surface in the EQUATOR zone. In this zone the expected 11-year variation according to Eq. 2.7.3 will have amplitude about 30%. For SOUTH and NORTH zones we have very small correlation coefficients with opposite signs so expected 11–year variation for SOUTH + NORTH is about zero. Because each zone contained the same number of runs (27 runs), the expected 11–year variation for all runs will be about 10%. Let us suppose that neutrino flux detected in Kamiokande experiment has the same amplitude for 11–year variation – about 10%. But because about 1/3 part of transformed neutrino will be detected in Kamiokande experiment, that this amplitude will be reduced to about 7% what is in the frame of statistical errors (if it will be possible in the near future to separate Kamiokande data on the 3 zones mentioned above, the expected 11–year variation for EQUATOR zone will be about 20%).

Dependences of solar neutrino fluxes and of correlation coefficients on the position of the region where neutrino crosses the solar surface give additional arguments to support the conclusion made above: the interpretation of obtained results can be based on the standard solar model of electron neutrino generation in thermonuclear processes, their propagation through 22–year variable strong magnetic fields in the convection zone (connected with solar activity magnetic cycle) – in the frame of the theory of magnetic neutrino resonant spin-flavor precession (Akhmedov and Bychuk, 1989; Bykov et al., 1998). It gives additional argument that neutrino must have non-zero mass and anomaly magnetic moment. From this follows that by an underground solar neutrino experiment important information can be obtained not only on the thermonuclear processes in the central region of the Sun, but also on the variable strong magnetic fields in the solar interior caused the solar activity phenomenon: the intensity of these fields can be measured if in some independent experiment the value of neutrino anomaly magnetic

moment will be measured (which is hoped to be done in the near future by using a large flux of very small energy neutrinos from ^{3}H decay).

Let us note that described above results of Dorman (2000a,b) are in good accordance with obtained by Snodgrass and Oakley (1999) on the basis of Homestake neutrino data and solar photospheric magnetic flux data (Fig. 2.7.4).

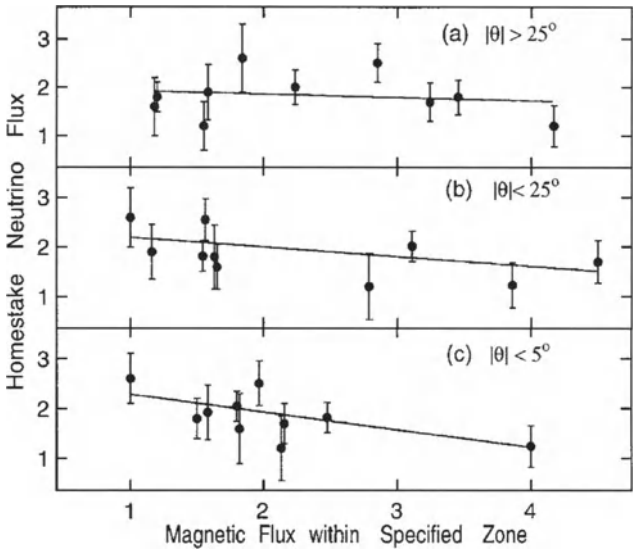

Fig. 2.7.4. Regression of neutrino flux vs photospheric magnetic flux, in arbitrary units. The lines show χ^2 best linear fits to 2–year mean values. Zero slope indicates no correlation and a negative slope indicates anti-correlation. According to Snodgrass and Oakley (1999).

From Fig. 2.7.4 can be seen that for a zone outside of the equatorial zone there are no significant connections, but for the equatorial zone it may be that, and with decreasing of central equatorial zone (panel *c*), the connection looks more reliable.

2.7.4. Main results obtained in KamiokaNDE and Super-KamiokaNDE; detection of solar, atmospheric, and cosmic neutrinos from Supernova; neutrino oscillations, the problem of proton decay

According to Koshiba (1992, 2002), the first KamiokaNDE, which might be called an Imaging Water Cherenkov detector had a surface coverage of 20% by photomultipliers and the total mass of the water inside this detector is 3,000 tons (it costs about 3 million U.S. dollars). The second experiment called Super-KamiokaNDE, is the same type of detector but with 40% of the entire surface covered by photomultipliers and the total mass of the water 50,000 tons (it costs about 100 million U.S. dollars). Both experiments are situated about 1,000 meters underground in Kamioka Mine (Japan). The capital letters NDE at the end of the two experiments means originally 'Nucleon Decay Experiment' (the search of reaction $p \to e^+ + \pi^o$). However, now NDE more often means as 'Neutrino Detection Experiment'. According to Koshiba (2002), in KamiokaNDE and Super-KamiokaNDE where obtained following main results.

The first main result is the observation of solar neutrinos by electron neutrino scattering on electrons in the water ($\nu_e + e \to \nu_e' + e'$); it was first independent support of famous Davis's result on solar electron neutrino deficit (Hirata et al., 1989; see in more detail Section 3.7.2 above).

The second main result is the first observation of anti-electron neutrino from SN1987A explosion in Magellan Clouds at February 23, 1987 (Hirata et al., 1987) by anti-electron neutrino interactions in water ($\bar{\nu}_e + p \rightarrow e^+ + n$). The result is shown in Fig. 2.7.5.

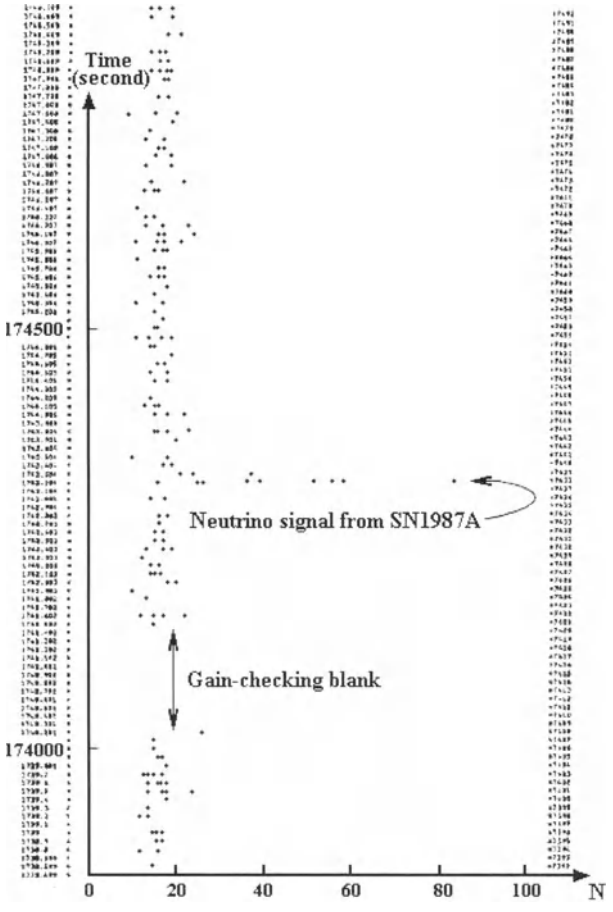

Fig. 2.7.5. The famous result on the detection of SN1987A neutrino 'signal' at February 23, 1987 in the computer print-out. According to Koshiba (2002).

From Fig. 2.7.5 can be clearly seen the supernova neutrino signal above the background level. This observation gave the confirmation of theoretical ideas on the supernova explosion triggered by a gravitational collapse (not only the average energy and the total number of detected neutrinos agreed with the theoretical expectations, but also the time duration of about ten seconds implies that those neutrinos are emitted from a very dense matter, like in a nucleus, probably a neutron star is responsible).

The third result is the discovery of what is called 'Atmospheric Neutrino Anomaly'(Hirata et al., 1988): when CR particles enter the atmosphere, they interact with the N and O nuclei of air to produce $\pi^{\pm}$-mesons and K-mesons; these mesons decay into $\mu^{\pm}$-mesons and ν_{μ}, and then $\mu^{\pm}$-mesons decay on $\nu_{\mu} + \nu_e + e^{\pm}$ (so it is expected that ν_{μ} will be two times more than ν_e, but really with increasing of energy it was observed bigger ratio $N(\nu_{\mu})/N(\nu_e)$ because some part of muons are not decayed and ν_e are not formatted).

The forth result is the neutrino oscillations problem: transformation of neutrino during propagation and interaction with matter from one type to another; the existent of the neutrino oscillations was confirmed by observations of solar and atmospheric neutrino as well as neutrino from distant nuclear reactors.

The fifth main result obtained in KamiokaNDE regards to the problem of proton decay ($p \rightarrow e^{+} + \pi^{o}$): Hirata et al (1989), Koshiba (2002) came to conclusion that the non-observation of proton decay by the KamiokaNDE is a serious argument against of the well known Grand Unified Theory based on SU.

2.8. Secondary neutrons and protons in the atmosphere

Secondary neutrons and protons are very important for generation cosmogenic nuclides in the Earth's atmosphere (see Chapters 10 and 17), and secondary protons – for ionization and chemical processes (see Chapters 11 – 14). Lingenfelter (1963) calculated the expected altitude-latitude distribution of neutron production rate from galactic CR in minimum and maximum of solar activity. Results are shown in Fig. 2.8.1 for the minimum of solar activity, and in Fig. 2.8.2 for the maximum of solar activity.

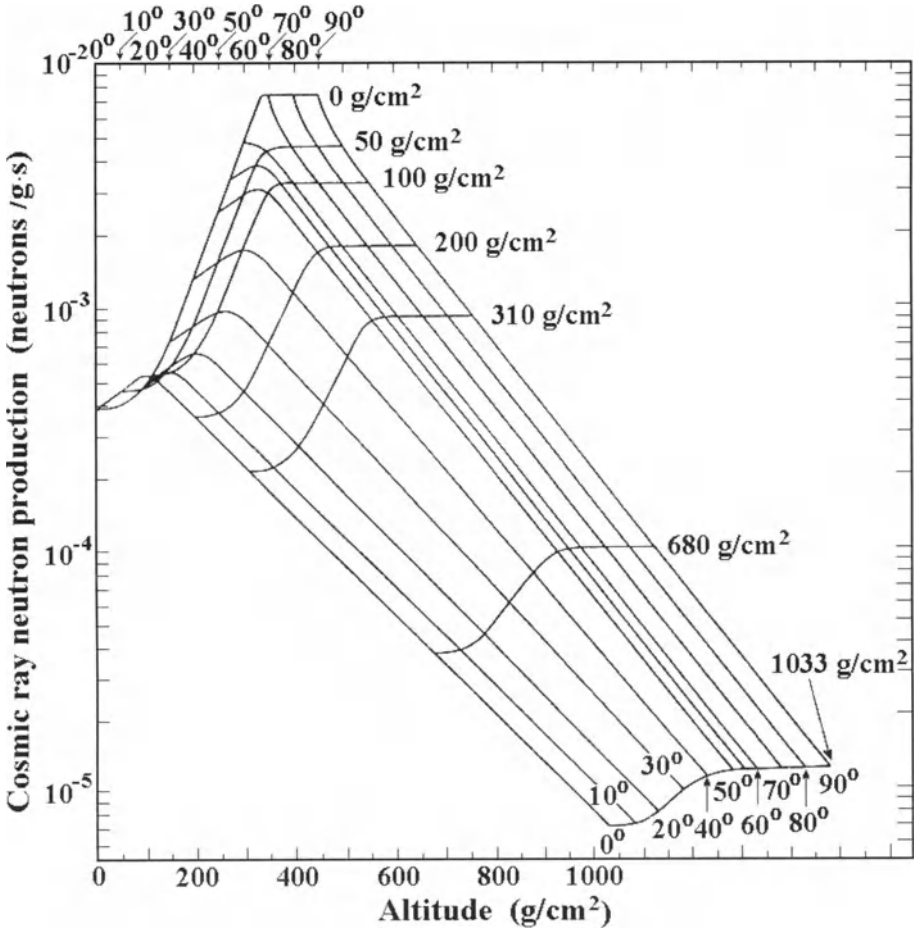

Fig. 2.8.1. Production rate of neutrons in the atmosphere by primary and secondary CR (in units of neutron.g^{-1}.sec^{-1}), as a function of altitude in g/cm^{2} and geomagnetic latitude in the period of solar minimum activity. According to Lingenfelter (1963).

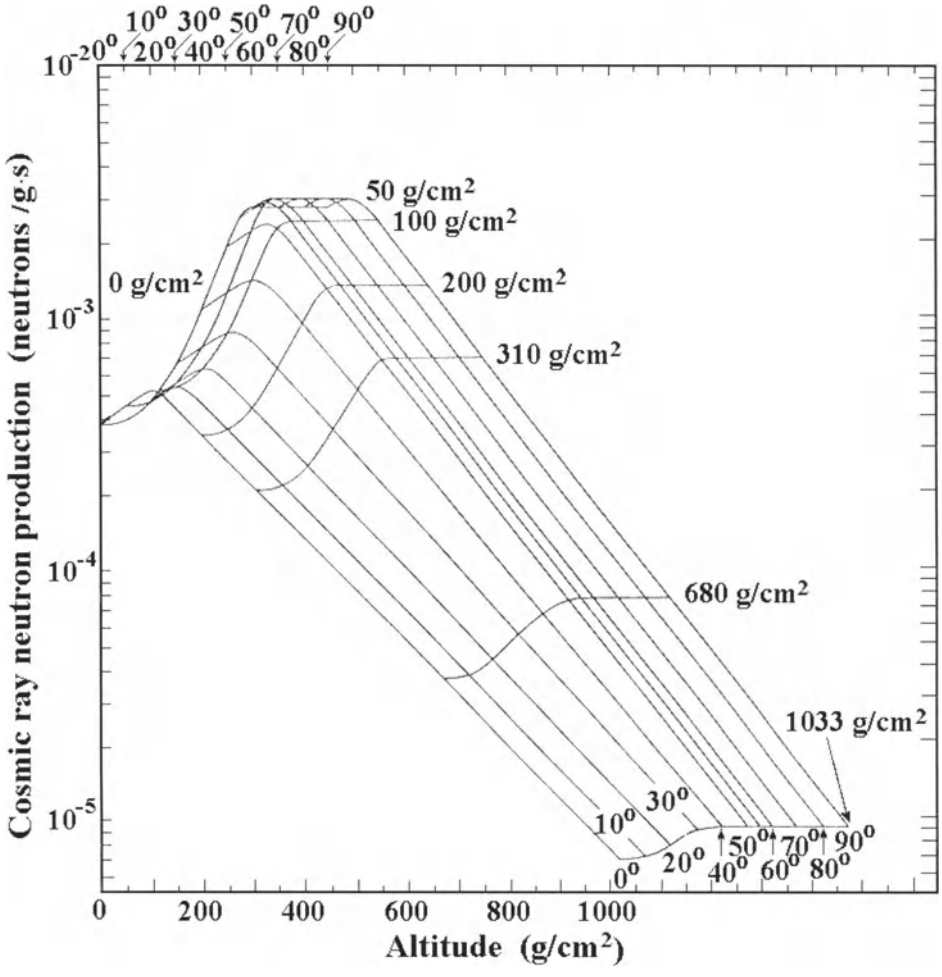

Fig. 2.8.2. The same as in Fig. 2.8.1, but for the period of solar maximum activity. According to Lingenfelter (1963).

More detailed results on the generation of neutrons and protons were obtained recently by Masarik and Beer (1999). To simulate in detail the development of the CR cascade and to calculate the expected production rates of cosmogenic nuclides in the atmosphere, Masarik and Beer (1999) used the GEANT (Brun et al., 1987) and MCNP (Briesmeister, 1993) code systems.

The solid Earth in the calculations of Masarik and Beer (1999) was considered as a sphere with a radius 6,378 km, a surface density of $g.cm^{-3}$ with an average chemical composition as shown in Table 2.8.1. The Earth's atmosphere was modeled as a spherical shell with inner radius of 6,378 km and a thickness of 100 km; it was divided into 34 concentric sub-shells of equal thickness (in $g.cm^{-2}$) with an average chemical composition as shown also in Table 2.8.1.

Table 2.8.1. Chemical composition (in weight fractions) adopted for calculations in Masarik and Beer (1999).

region	elements									
	H	N	O	Na	Mg	Al	Si	Ar	Ca	Fe
soil	0.002		0.473	0.025	0.040	0.060	0.290		0.050	0.060
atmosphere		0.755	0.232					0.013		

The Earth and atmospheric shells were divided into 9 latitudinal sections corresponding to steps of 10° in magnetic latitude. The atmospheric density was approximated by

$$\rho(H)=\begin{cases}1.27\times10^{-3}\exp(-0.1091H)\,\mathrm{g/cm^3} \text{ if } H<9.73 \text{ km},\\ 2.03\times10^{-3}\exp(-0.1573H)\,\mathrm{g/cm^3} \text{ if } H>9.73 \text{ km},\end{cases} \quad (2.8.1)$$

where H is the altitude above sea level in km.

To take into account the change of galactic CR with solar activity, an analytical approximation of Castagnoli and Lal (1980) was used:

$$D(E_p,\Phi)=C_p\frac{E_p\left(E_p+m_pc^2\right)\left(E_p+x+\Phi\right)^{-2.5}}{\left(E_p+\Phi\right)\left(E_p+2m_pc^2+\Phi\right)}, \quad (2.8.2)$$

where $x=780\exp\left(-2.5\times10^{-4}E_p\right)$, E_p is the proton kinetic energy (in MeV), Φ is the modulation parameter (varying from 0 to 1,000 MeV), $m_pc^2=938$ MeV is the proton rest energy, and normalization factor $C_p=1.244\times10^6\ \mathrm{cm^{-2}sec^{-1}MeV^{-1}}$. From the fitting of lunar experimental data (Reedy and Masarik, 1994), the average flux of protons with energy above 10 MeV was determined to be $4.56\ \mathrm{proton.cm^{-2}sec^{-1}}$, corresponding to Eq. 2.8.2 with $\Phi=550$ MeV, which is about the same as the long–term average value (Reedy, 1987).

For each latitudinal section interaction of 5,000,000 primary protons in the energy range from 10 MeV up to 1000 GeV was simulated; the expected statistical errors for neutron flux near the Earth's surface are 4–5%, and in the upper atmosphere 3–4% (for proton flux statistical errors in stratosphere are 4–5%, and near sea level about 10%). Big errors for proton fluxes in the low atmosphere are not important because the proton flux here is about one to two orders of magnitude smaller than neutron flux. For production of cosmogenic nuclides the most important quantities are the neutron and proton fluxes and the energy spectrum in different latitudinal zones at different depths in the atmosphere. Results of the expected integral fluxes of neutrons and protons with energy $E_k\geq1$ MeV in dependence from depth (in the interval from 0 to 1033 g/cm^2) in near equatorial (0–10°) and polar (80–90°) latitudinal zones are shown in Fig. 2.8.3.

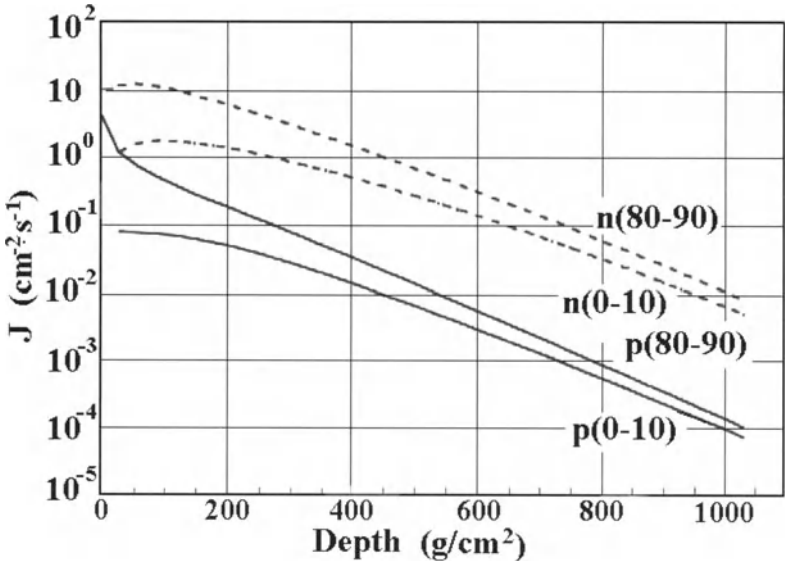

Fig. 2.8.3. Integral fluxes of neutrons and protons with energy $E_k \geq 1$ MeV in the Earth's atmosphere as a function of the depth (in the interval from 0 to 1033 g/cm^2) in near equatorial (0-10°) and polar (80-90°) latitudinal zones for the average modulation parameter $\Phi = 550$ MeV. According to Masarik and Beer (1999).

Fig. 2.8.4 shows the expected differential energy spectra of neutrons and protons (in kinetic energy range from 1 MeV up to 1000 GeV) on the depths in the atmosphere 30, 150, 420, and 990 g/cm^2 in 0–10° and 80–90° latitudinal zones.

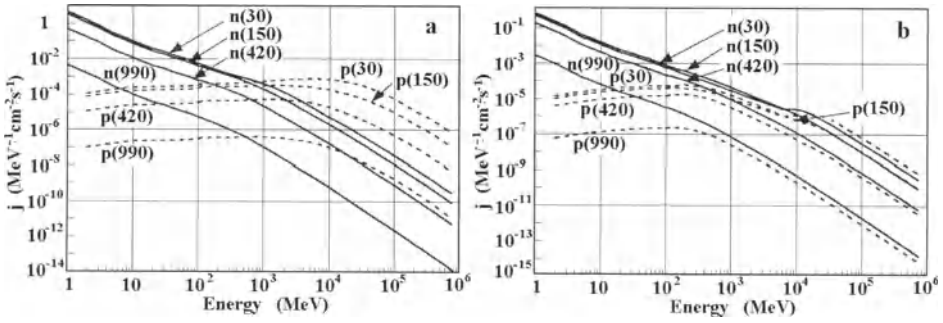

Fig. 2.8.4. Differential energy spectrums of neutrons and protons (in kinetic energy range from 1 MeV up to 1000 GeV) on the depths in the atmosphere 30, 150, 420 and 990 g/cm^2 in 0–10° (*a*) and 80–90° (*b*) latitudinal zones for the average modulation parameter $\Phi = 550$ MeV. According to Masarik and Beer (1999).

The calculated fluxes of neutrons are compared with observations made by neutron monitors on depths 1033 g/cm^2 (sea level), 843 g/cm^2 (1.68 km) and 680 g/cm^2 (3.4 km) at different cut off rigidities from 1 to 14 GV. The differences obtained are within a few

percent, which are about the same as the accuracy of the calculations. The changes of the modulation parameter during the period 1953–1995, determined in Masarik and Beer (1999) from comparison with Deep River NM, are shown in Fig. 2.8.5.

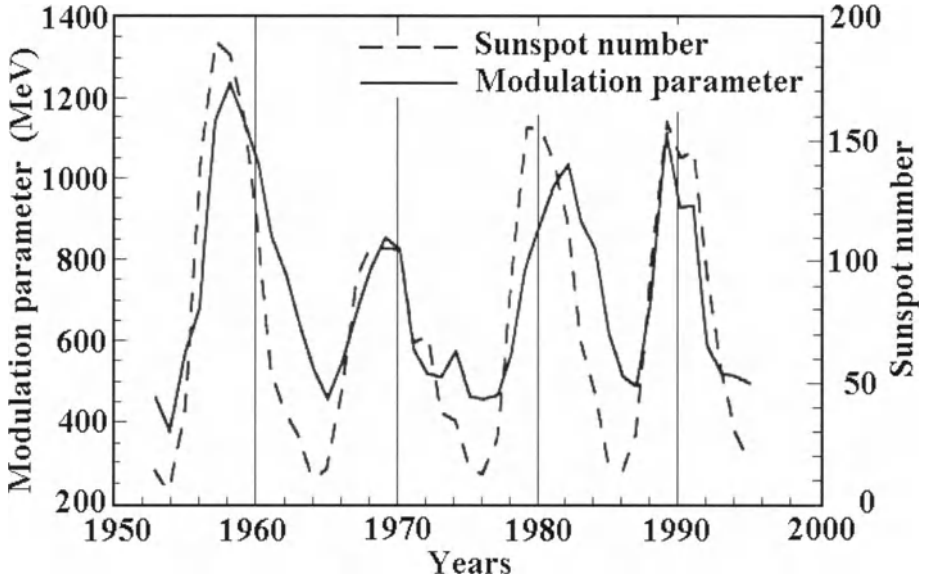

Fig. 2.8.5. The changes of modulation parameter during the period 1953–1995, determined in Masarik and Beer (1999) from comparison with Deep River NM counting rate long-term variations.

In Vannuccini et al. (2003) by analyzing the available experimental data on light fragments produced in nucleus-nucleus collisions, a new parameterization has been developed for the energy and angular distributions of these fragments from 10 MeV/n to 1 GeV/n; using this parameterization, it was determined the energy spectra of secondary protons from 100 MeV to 100 GeV, as a function of the depth and zenith angle in the upper atmosphere (at the level about 5 g/cm^2).

A lot of measurements of secondary neutrons at different altitudes and latitudes were made by Zanini et al (2003): on Mt. Matterhorn (46 °N, 3480 m above sea level), Mt. Chacaltaya (16 °S, 5230 m), on airplanes of Alitalia Flights at altitude about 10500m, on Trans-Mediterranean balloon flights at altitudes 15000, 28000, and 30000 m. These measurements were made in energy ranges 100 keV–100 GeV and 10 keV–20 MeV. For the energy range 100 keV–100 GeV were used following experimental systems: Bubble Dosimeter BD100R (100keV–20MeV), Polycarbonate detector foils (1MeV–150MeV), Polycarbonate detector bottles (1MeV–150MeV), and Fission detector 209Bi layers (100MeV–hundreds of GeV). For the energy range 10 keV–20 MeV an adapted version of the BUNTO unfolding code was used like limited energy range detector system; it is constituted by six types of bubble detectors, which differ in energy thresholds and responses. Two Monte Carlo codes (GEANT 3.2 and FLUKA) have been used to simulate the hadronic cascade and the interaction between primary protons and atmosphere at various altitudes and latitudes. Obtained results on the

neutron energy spectrum at Mt. Matterhorn (46 °N, 3480 m above sea level) in comparison with obtained at other mountains are shown in Fig. 2.8.6.

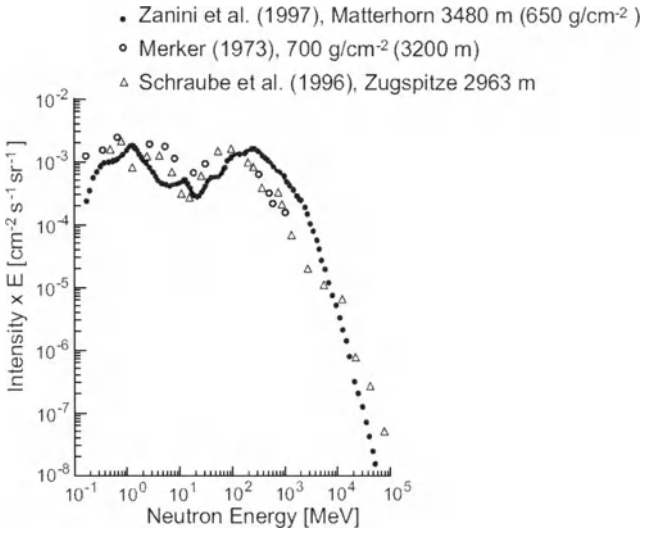

Fig. 2.8.6. Measured neutron energy spectrum at different mountains. According to Zanini et al. (2003).

Results of determining of vertical profile of integral neutron flux by measurements on high mountains, intercontinental airplane flights, and on balloons in comparison with results of Monte Carlo simulation on the basis of GEANT code are shown in Fig. 2.8.7.

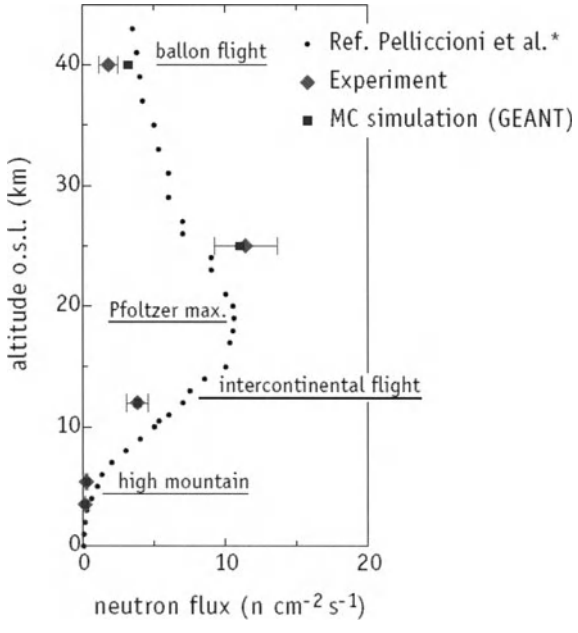

Fig. 2.8.7. Vertical profile of integral neutron flux: comparison of measurements with simulation. According to Zanini et al. (2003).

Secondary neutrons gave important contribution in the radiation doze, especially on altitudes of transcontinental airplane flights. In Fig. 2.8.8 are shown calculated vertical profiles of radiation dozes caused by different secondary particles (γ, μ, n, p, e) as well as total doze (from sea level up to altitude of 60 km).

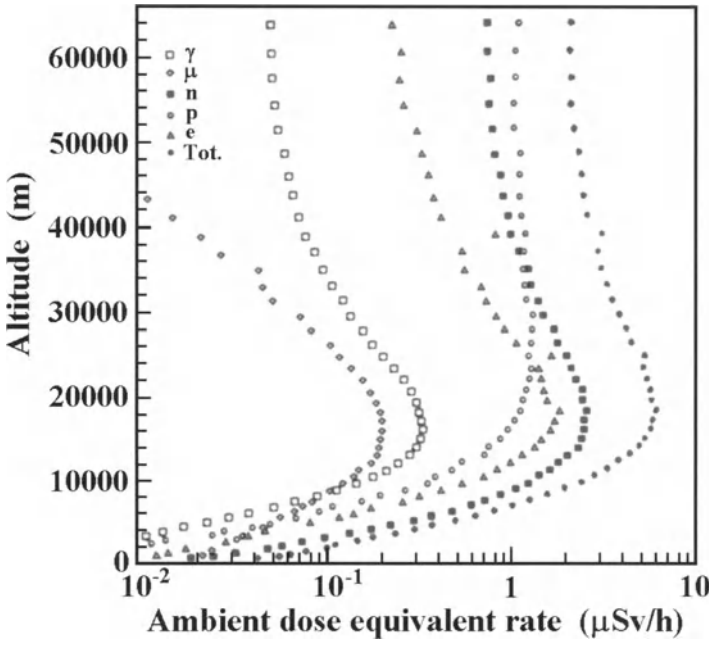

Fig. 2.8.8. Vertical profiles of radiation dozes caused by neutrons and other secondary particles (γ, μ, p, e) as well as profile of total doze. According to Zanini et al. (2003).

The radiation dozes shown in Fig. 2.8.8 are calculated as generated by galactic CR near minimum of solar activity (interplanetary modulation potential Φ = 465 MV) for the point on the Earth characterized by cutoff rigidity R_c = 6.1 GV (these dozes decrease with increasing of solar activity and increasing R_c). Let us note that in periods of great solar flares the radiation dozes may increase many times and it became dangerous for people health and apparatus (see in more details below, in Chapter 18, Section 18.12, and in Dorman, M2005).

2.9. Secondary gamma rays in the atmosphere from galactic and solar CR

Share et al. (1999) investigated atmospheric gamma ray lines produced by galactic and solar CR. The Earth's atmosphere is the most intense source of gamma radiation observed by satellite–borne spectrometers. Energetic protons in the galactic and solar CR interact with nuclei in the atmosphere to directly excite nuclear states, create spallation products in excited states, and produce secondary neutrons. These neutrons also excite nuclear states and produce spallation products. Letaw et al. (1989) listed the most intense gamma ray lines from these processes based on earlier compilations by

Ling (1975), Ramaty et al. (1979), and nuclear data tables. Comprehensive nuclear–line observations of atmospheric gamma rays produced by CR interactions have been conducted using NASA's HEAO 3 high resolution (Mahoney et al., 1981; Willett and Mahoney, 1992) and SMM moderate resolution (Letaw et al. 1989; Share et al., 1999) spectrometer experiments. The spectrum of atmospheric gamma rays was derived by using data accumulated in 10.4×10^6 sec over a 9-year period with the SMM instrument's axis pointed to within 72° of the center of the Earth (see Fig. 2.9.1).

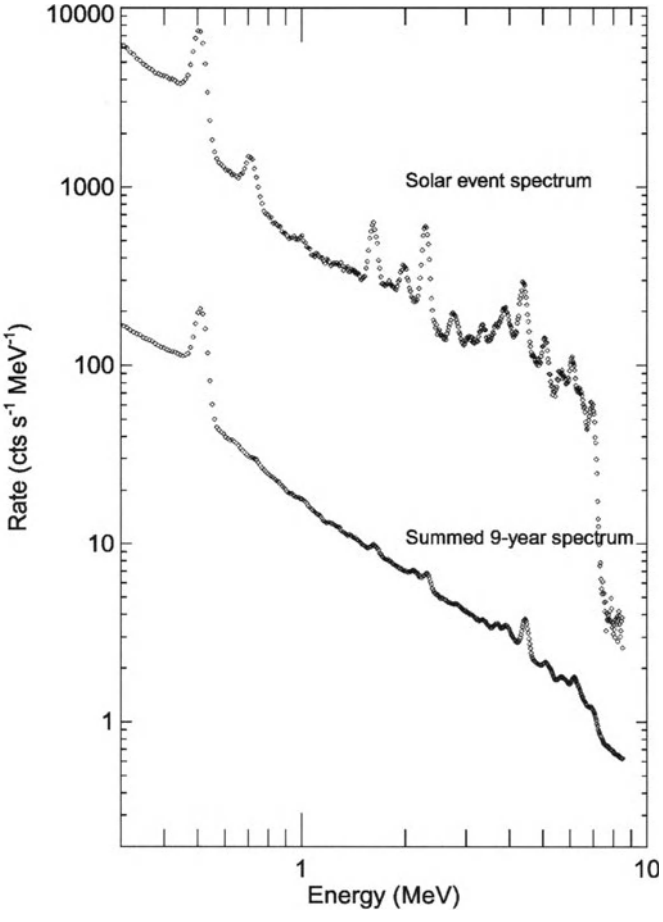

Fig. 2.9.1. Comparison of the atmospheric gamma ray spectrum, produced by galactic CR observed by SMM over 9 years, with the spectrum excited by the 1989 October solar energetic particle event. According to Share et al. (1999)

In Fig. 2.9.1 is also shown the spectrum observed from 15.50.52 to 16.05.04 UT on October 20, 1989 during the period of high geomagnetic disturbance that followed an intense class X13 X-ray flare and coronal mass ejection on the previous day. The atmospheric gamma-ray emission increased by more than a hundred times during this period and was dominated by annihilation and nuclear gamma ray lines emission. It can

be seen from Fig. 2.9.1, that the positron annihilation line at 0.511 MeV and its atmospherically scattered Compton continuum dominate the spectrum between 0.3 and 0.55 MeV. A bremsstrahlung continuum and various nuclear line features dominate the spectrum at higher energies. Table 2.9.1 gives a comparison between SMM and HEAO-3 measurements of atmospheric gamma ray lines generated by galactic CR.

Table 2.9.1. Comparison between SMM and HEAO-3 measurements of atmospheric gamma ray lines generated by galactic CR. According to Share et al. (1999)

	Energy, keV		Width, keV		Flux, $10^{-4}\gamma/cm^2$-s-sr	
Lab	SMM	HEAO-3	SMM	HEAO-3	SMM	HEAO-3
511	513.4 ± 3.0	511.07 ± 0.1	13.0 ± 7.3	2.29 ± 0.3	87.3 ± 0.5	110.6 ± 2.2
1635	1636.1 ± 3.5	1634.8 ± 1.4	34.9 ± 16.7	20.2 ± 5.7	2.8 ± 0.2	3.4 ± 0.8
2313	2311.2 ± 3.5	2309.4 ± 1.9	40.2 ± 20.5	24.0 ± 5.4	5.3 ± 0.5	5.4 ± 0.8
3684	3688.8 ± 22.6	3673.0 ± 4.7	196.2 ± 81.7	70 ± 15	12.7 ± 6.7	4.0 ± 1.0
4444	4451.2 ± 3.0	4428.5 ± 7.5	163.3 ± 7.4	135 ± 12	22.8 ± 0.1	19.6 ± 2.1
5105, 5180	5134.7 ± 4.3	5090.2 ± 10.4	253.4 ± 9.2	95 ± 26	5.3 ± 0.1	3.4 ± 1.2
6129, 6170	6150.9 ± 3.8	6137.2 ± 10.2	96.6 ± 22.0	98 ± 27	4.0 ± 0.1	5.4 ± 1.5

2.10. Secondary gamma rays from precipitating radiation belts electrons

Bucik et al. (1999) analyzed data received by the SONG instrument in the experiment onboard CORONAS-I satellite (nearly circular polar orbit with height about 500 km).

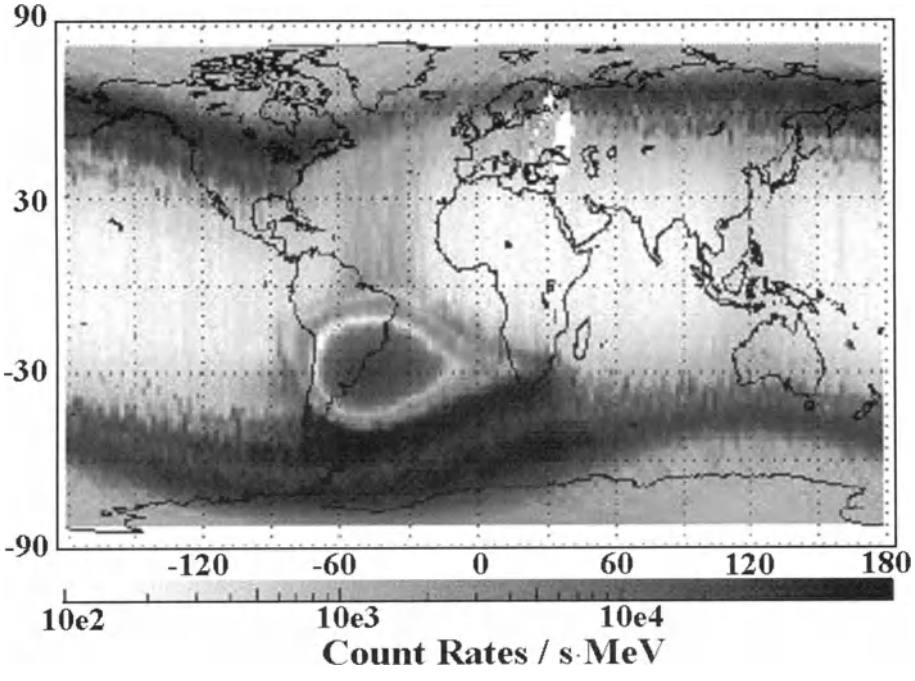

Fig. 2.10.1. Planetary distribution of gamma ray flux of 0.12–0.32 MeV. According to Bucik et al. (1999).

Gamma rays with energies 0.12–0.32 MeV, 0.32–1 MeV, 1–3 MeV and 3–8.3 MeV were detected by a CsI(Tl) crystal with a diameter of 200 mm and a height of 100 mm in active 4π anti-coincidence shielding of plastic scintillator with thickness 20 mm. CORONAS-I satellite was oriented with its longitudinal axis directed toward the Sun. The SONG instrument observed the Sun in the day side of the orbit and the Earth on the night side. Results are shown in Fig. 2.10.1 and Fig. 2.10.2, which display geographical maps of 0.12–0.32 MeV and 3.0–8.3 MeV gamma ray fluxes, correspondingly. In both figures data from 5 March to 14 June 1994 were used. The values of gamma ray fluxes obtained from measurements have been corrected for the induced background caused by decay of the long living radioisotopes induced due to the interactions of CR and protons of inner radiation belt with the detector material. The correction of gamma ray fluxes on time dependence of primary CR was done by using data of NM on Mt. Haleakala.

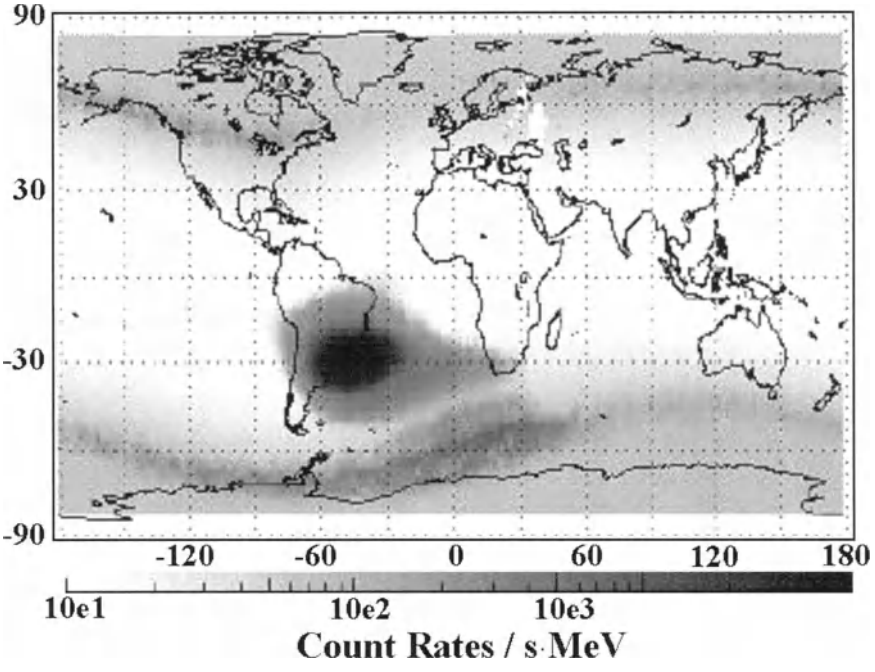

Fig. 2.10.2. Planetary distribution of gamma ray flux of 3.0–8.3 MeV. According to Bucik et al. (1999).

Fig. 2.10.3 shows the dependence of 3.0–8.3 MeV gamma-ray fluxes for local day (10.00–14.00) and local night (22.00–02.00) on vertical cut off rigidity

$$R_c = 14.9L^{-2}\ \text{GV}, \tag{2.10.1}$$

where L is the McIlwain's parameter (according to Shea et al, 1987). The data shown in Fig. 2.10.1 can be fitted to the power law

$$I_\gamma(3.0-8.3\ \text{MeV}) \propto R_c^{-\beta}, \tag{2.10.2}$$

in the cut off rigidity interval 2–15 GV, where for the local night the spectral index β = 0.936 ± 0.001 and for the local day β=0.924±0.001 (for equal cut off rigidities measured gamma ray flux on the night side is larger than on the day side).

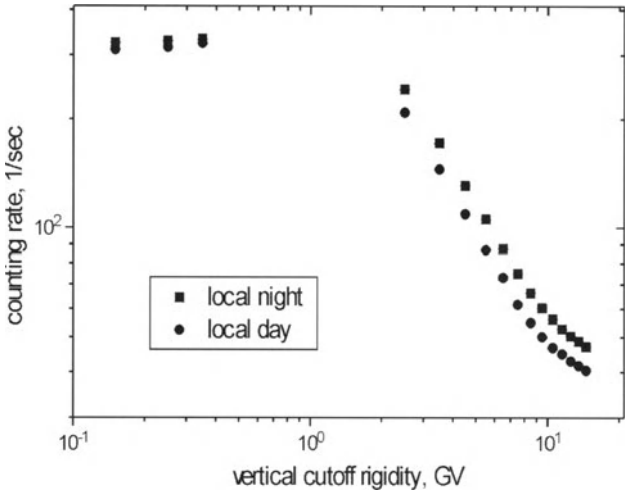

Fig. 2.10.3. Dependences of gamma ray 3.0–8.3 MeV fluxes for local night (22.00–02.00) and local day (10.00–14.00) from vertical cut off rigidity. According to Bucik et al. (1999).

2.11. Secondary electrons, positrons, and photons generated by CR in the atmosphere

Secondary electrons and positrons generated by CR in the atmosphere play an important role in the following phenomena:

- formation of thunderstorms, with relativistic secondary electrons playing a key role in discharges, see Chapter 11;
- air ionization, which is important for formation and developing of atmospheric electric fields, see also Chapter 11;
- ionosphere and radio wave propagation (Chapter 12);
- many chemical processes in the atmosphere, formation of nitrates, and effects in the ozone layer (Chapter 13);
- cloud formation, mainly by affecting global cloudiness, and consequently global climate change (Chapter 14).

Extended review on observations and calculations of fluxes and energy spectrum of secondary electrons, positrons, and photons generated by CR in the atmosphere was given by Daniel and Stephens (1974). Figs. 2.11.1–2.11.6 show results of their calculations for energies from 1 MeV up to 10 GeV. These theoretical results were checked against a great number of observations. In Figs. 2.11.1–2.11.6 differential atmospheric growth curves from 0.1 $g.cm^{-2}$ up to 1000 $g.cm^{-2}$ for electrons (solid curves), positrons (dot–dashed curves), and gamma rays (dashed curves) are shown. All fluxes (in units $m^{-2}.sec^{-1}.sr^{-1}.GeV^{-1}$) are calculated for different vertical cut-off rigidities: 0, 2, 4.5, 10 and 17 GV for the period of minimum solar activity (only for cut

off rigidity of 0 GV, the expected fluxes for the period of maximum solar activity were also calculated).

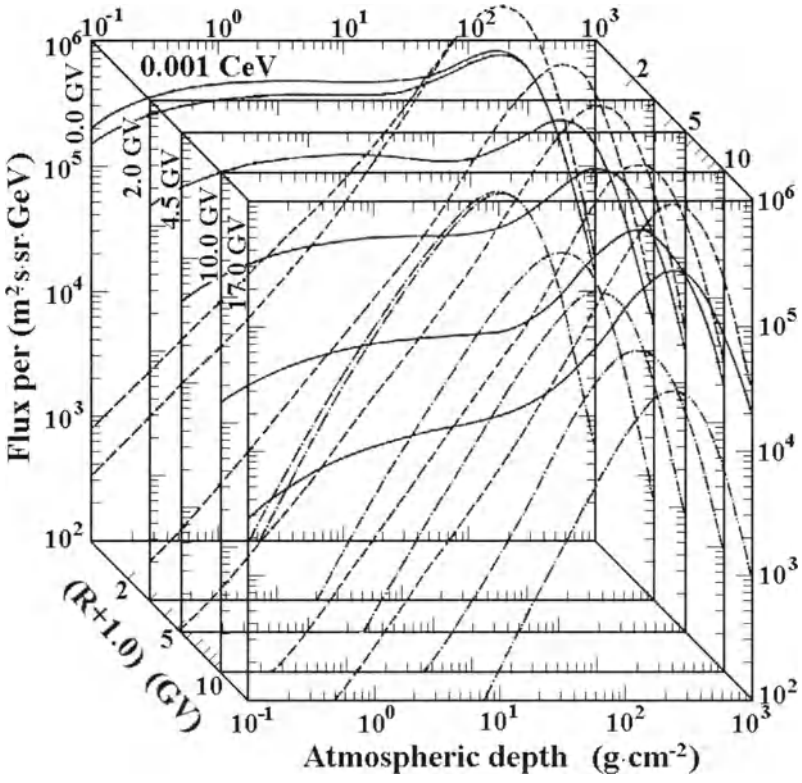

Fig. 2.11.1. Expected differential atmospheric growth curves of secondary electrons (solid curves), positrons (dot–dashed curves), and gamma rays (dashed curves) with energy 1 MeV for cut off rigidities: 0, 2, 4.5, 10 and 17 GV. According to Daniel and Stephens (1974).

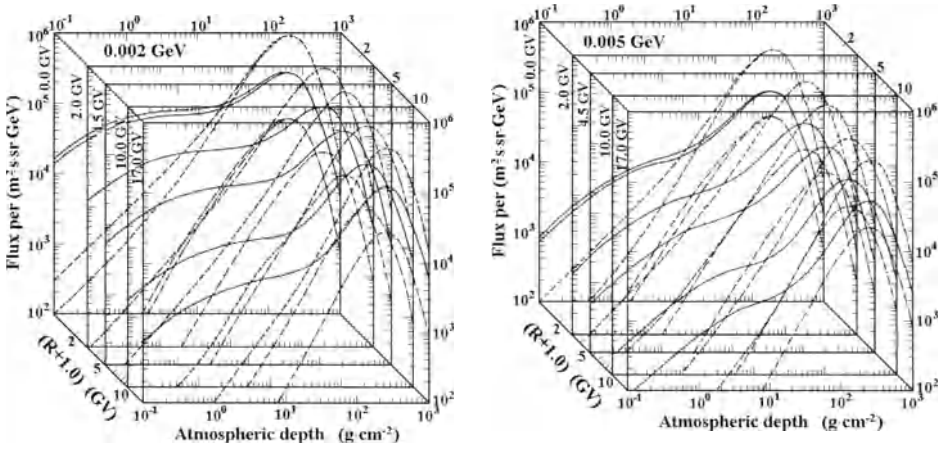

Fig. 2.11.2. The same as in Fig. 2.11.1, but for energies 2 and 5 MeV (Daniel and Stephens, 1974).

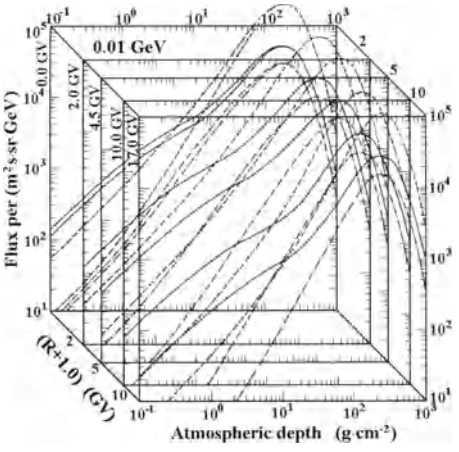

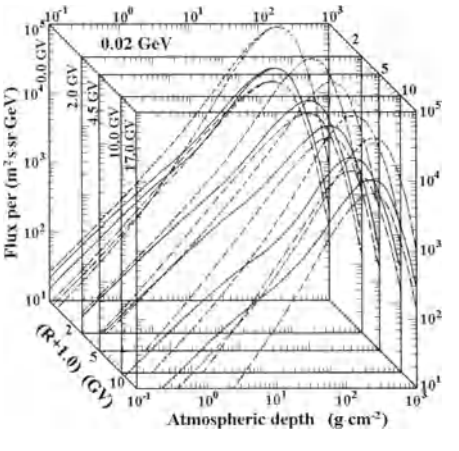

Fig. 2.11.3. The same as in Fig. 2.11.1, but for energies 10 and 20 MeV (Daniel and Stephens, 1974).

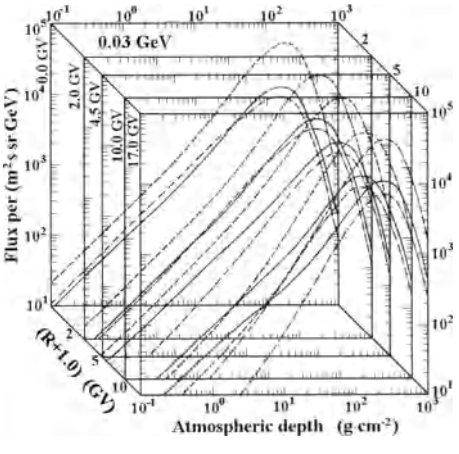

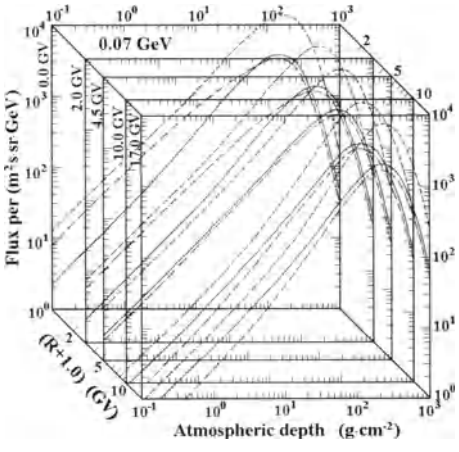

Fig. 2.11.4. The same as in Fig. 2.11.1, but for energies 30 and 70 MeV (Daniel and Stephens, 1974).

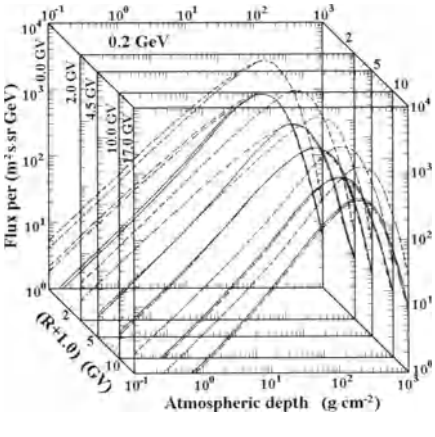

Fig. 2.11.5. The same as in Fig. 2.11.1, but for energies 200 MeV (Daniel and Stephens, 1974).

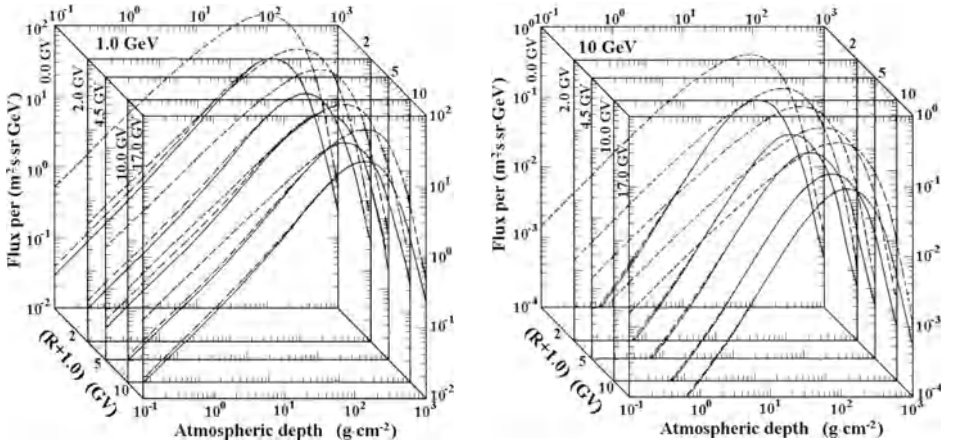

Fig. 2.11.6. The same as in Fig. 2.11.1, but for energies 1 and 10 GeV. According to Daniel and Stephens (1974).

In Fig. 2.11.7 are shown integral atmospheric growth curves for energies > 10 MeV and > 100 MeV for minimum and maximum of solar activity at different cut off rigidities.

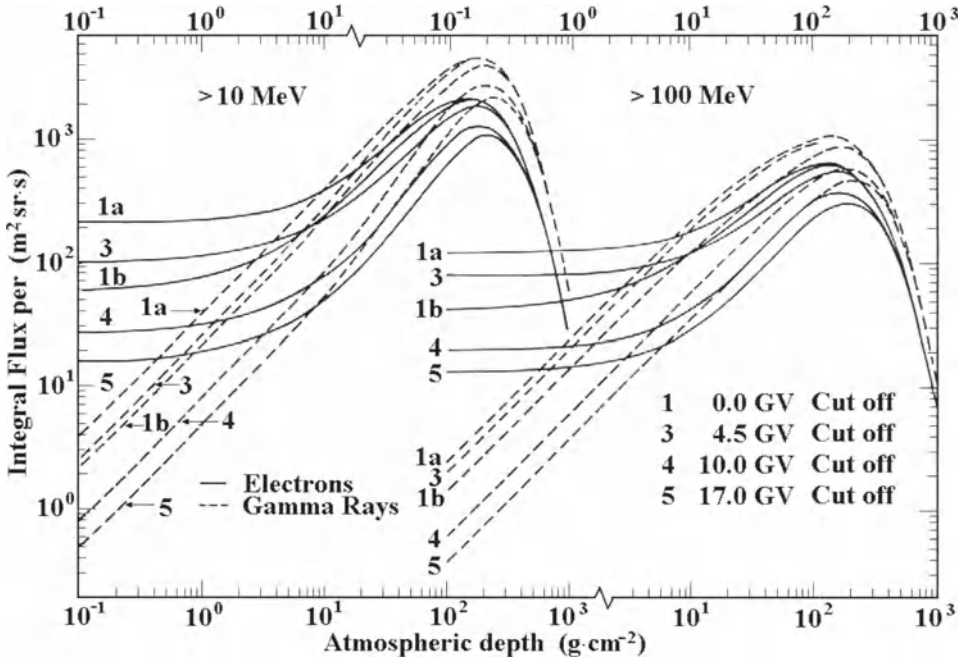

Fig. 2.11.7. Integral atmospheric growth curves for electrons (solid curves) and gamma-rays (dashed curves) for energies > 10 MeV (left) and > 100 MeV (right) at cut off rigidities 0 GV (curves *1a* for minimum of solar activity and curves *1b* for maximum of solar activity), 4.5 GV (curves *3* for minimum of solar activity), 10 GV (curves *4* for minimum of solar activity), and 17 GV (curves *5* for minimum of solar activity). According to Daniel and Stephens (1974).

2.12. CR albedo radiation directed down and up

Primary protons and heavy nuclei interact in the atmosphere to produce short-lived pions and kaons. Electrons (both positrons and electrons) are among the decay products of the short-lived species. Secondary electrons and positrons are produced in roughly equal numbers through decay chains such as the reactions:

$$\pi^{\pm} \rightarrow \mu^{\pm} \rightarrow e^{\pm} \ . \qquad (2.12.1)$$

Below local geomagnetic cutoff, the electrons at balloon altitudes include an upward-going particle population (the splash albedo) and a downward-traveling particle population (the re-entrant albedo). The splash electron albedo particles are produced largely by incident protons at large zenith angles. The re-entrant electron albedo then consists of the splash albedo population after propagation back to the top of the atmosphere and along the trapping magnetic field lines to the field-conjugate location on the opposite side of the Earth. Simulations and balloon measurements have both been performed to track the production and propagation processes of the albedo populations.

CR albedo radiation is significant for ionization and chemical processes in the upper atmosphere (see below, Chapters 11–14). Here we shall briefly describe only some recent results. Important measurements of electron-positron albedo were made in De Nolfo et al. (1997; on long duration balloons which was flown from Fort Sumner, New Mexico, in 1994 at the atmosphere depth between 3.8 and 7.4 g/cm^2) and DuVernois et al. (2001a,b; the same but were flown in 1999 and 2000) by the High Energy Antimatter Telescope (HEAT). The HEAT was designed to measure antiprotons up to 50 GeV. Although the instrument was optimized for antiprotons, a significant sample of albedo electrons and positrons was also measured (see the short description of HEAT in Chapter 4, Section 4.6.4). The splash albedo, in contrast to the re-entrant albedo, is straightforward to measure with no significant backgrounds. All upward-moving electrons are included in splash electron albedo measurement.

The results of measurements of re-entrant albedo flux of electrons (e^++e^-) in De Nolfo et al. (1997) between 1.0–2.4 GV in dependence of atmospheric depth are shown in Table 2.12.1.

Table 2.12.1. HEAT growth curve for electron re-entrant albedo in 1.0–2.4 GV range. According to De Nolfo et al. (1997)

Mean depth (g/cm^2)	Number of electrons	Number of positrons	Live-time (seconds)	Integral Flux (m^2 s sr)$^{-1}$
3.98	131 ± 11	128 ± 11	7841	4.59 ± 0.22
4.18	50 ± 7	40 ± 6	2671	4.69 ± 0.38
4.30	124 ± 11	91 ± 10	5726	5.22 ± 0.28
4.78	143 ± 12	106 ± 10	7110	4.87 ± 0.24
5.50	173 ± 13	114 ± 11	7441	5.36 ± 0.25
6.80	319 ± 18	315 ± 18	12000	7.35 ± 0.24
7.22	242 ± 16	188 ± 14	7848	7.62 ± 0.30

De Nolfo et al. (1997) come to conclusion that between 1.0–2.4 GV re-entrant albedo component amounts to 40% of total electron flux. In Fig. 2.12.1 is shown energy spectrum of re-entrant albedo flux.

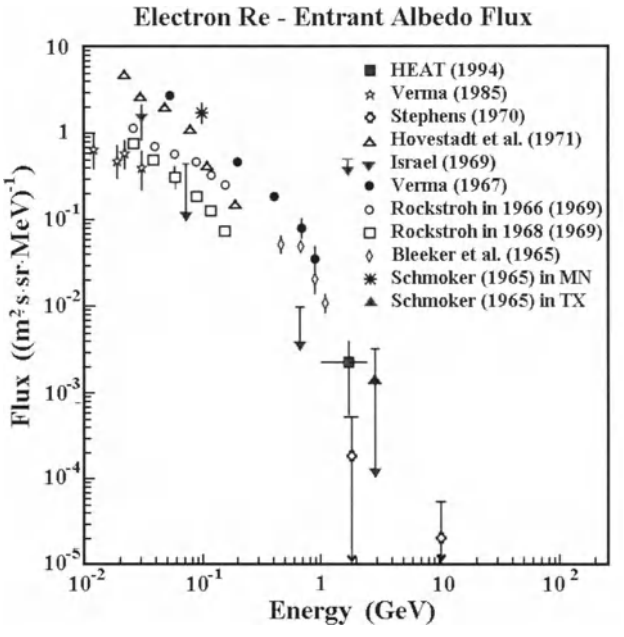

Fig. 2.12.1. Energy spectrum of re-entrant electron albedo flux measured by HEAT in 1994 in comparison with other measurements. According to De Nolfo et al. (1997).

The results of DuVernois et al. (2001a,b) in comparison with other measurements are shown in Fig. 2.12.2.

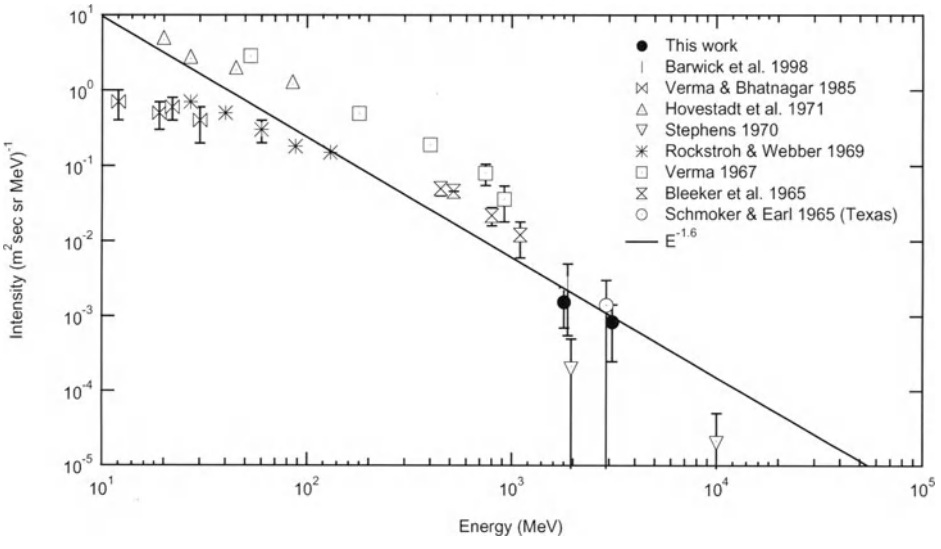

Fig. 2.12.2. Re-entrant electron albedo fluxes from a variety of different experiments from the mid 1960s through the HEAT experiment (black circles – this work is DuVernois et al., 2001a,b). The $E^{-1.6}$ spectrum is theoretical modeling for the re-entrant electron albedo flux. According to DuVernois et al. (2001a,b).

The HEAT instrument is symmetric from top to bottom with paddles of time of flight scintillators at the extremes, 140 layers of multiple δE–δξ wire chambers split equally above and below the 1 Tesla superconducting magnets with a 479 channel drift–tube–hodoscope for tracking in the central field. During the 2000 New Mexico flight analyzed in DuVernois et al. (2001a,b), the instrument flew at a nearly constant 4.2 GV vertical geomagnetic cut off rigidity, allowing measurements significantly below cut off. The secondary nature of both albedo populations is clear in Fig. 2.12.3, with the combined splash and re-entrant electron albedo population being approximately half positrons. Both splash and re-entrant albedo populations individually are consistent with a positron fraction of 0.5. Secondary production processes in the atmosphere give a positron fraction also of close to 0.5. Propagation through the magnetosphere and corresponding energy losses should not change this.

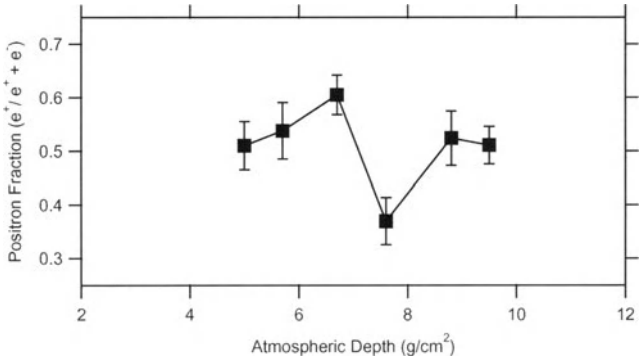

Fig. 2.12.3. Positron fraction $e^+/\left(e^+ + e^-\right)$ in the splash + re-entrant albedo (DuVernois et al., 2001a).

The number of splash electrons at all atmospheric depths (see Fig. 2.12.4) is greater than the number of re-entrant electrons at the same depth. In essence this is owing to the relatively local origin of the splash population and the much more significant propagation losses for the re-entrant particles.

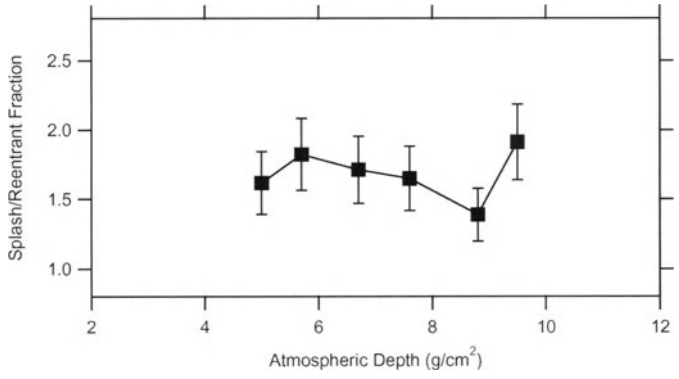

Fig. 2.12.4. The ratio of splash to reentrant albedo as a function of depth in the atmosphere. Splash albedo particles are expected to outnumber the downward-going counterparts simply because of propagation losses for the reentrant albedo. According to DuVernois et al. (2001a).

2.13. Secondary CR in the troposphere and stratosphere according to routine measurements on radio balloons

2.13.1. Regular radio balloon CR measurements and comparison with ground measurements by NM and MT

As we mentioned in Chapter 1 in connection with the IGY in 1957, regular (daily or several times per week) measurements of CR intensity in the troposphere and stratosphere by radio balloons were organized under supervision of Prof. S. N Vernov and Prof. A. N. Charakhchyan in former USSR. The count rates of single counter and of telescope from two counters were monitored (see the description of the detector in Section 4.6.3). These measurements were organized at several sites with different cutoff rigidities and during many latitude survey expeditions (see Table 2.13.1).

Table 2.13.1. The sites and periods of CR regular measurements in the troposphere and stratosphere by radio balloons. According to Stozhkov et al. (2001).

Site of observations	Geographic coordinates	R_c, GV	Period of observations
Mirny, Antarctica	66°33′ S; 93°00′	0.04	03.1963 - present time
Tixie	71°33′ N; 128°54′	0.4	02.1978 – 09.1987
Murmansk region	68°59′ N; 33°05′	0.6	07.1957 - present time
Norilsk	69°00′ N; 88°00′	0.6	11.1974 – 06.1982
Moscow region	55°28′ N; 37°19′	2.4	07.1957 - present time
Alma-Ata	43°12′ N; 76°56′	6.7	03.1962 – 02.1992
Erevan	40°10′ N; 44°30′	7.6	01.1976 – 06.1989
Sea expeditions	60° N - 60° S	0.1-17	1963-65; 1968-72; 1975-76; 1986-87

The CR measurements in the troposphere and stratosphere by radio balloons are very important because they are sensitive to primary CR with energy about 10 times smaller than ground neutron monitors (NM), and about 100 times smaller than ground muon telescopes (MT) and ionization chambers shielded by 10 cm Pb (IC): see illustration in Fig. 2.13.1.

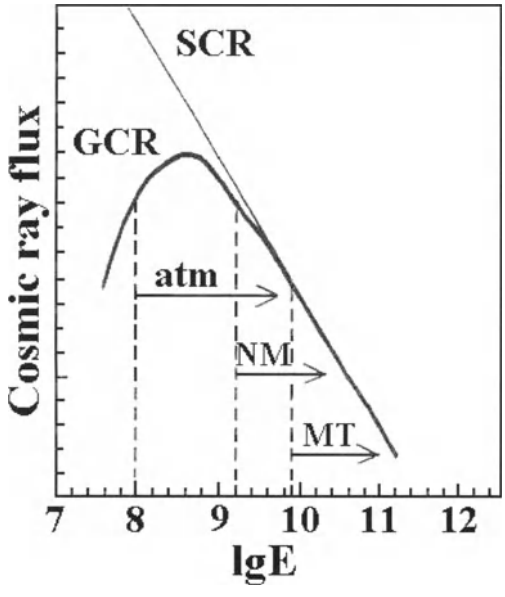

Fig. 2.13.1. Schematic view of galactic and solar CR spectra (GCR, SCR, thick and thin curves accordingly). The dotted vertical lines show the minimal energy of primary particles, which are detected by radio balloons in the atmosphere ($E > 10^8$ eV, upper arrow labeled atm) and by neutron monitors on the ground level ($E > 1.5\times10^9$ eV, arrow with NM). The ground–based ionization chambers and meson telescopes record the primary particles with $E > 9\ 10^9$ eV (arrow with MT). According to Stozhkov et al. (2001).

2.13.2. Altitude and angular distributions of secondary CR intensity at different cut off rigidities

Since 1957 more than 70,000 balloon flights have been performed from the sites listed in Table 2.13.1 and during many expeditions to Antarctica. In Fig. 2.13.2 and 2.13.3 are shown the samples of data obtained at the northern and southern latitudes with the different values of R_c during the Antarctic sea expedition of 1986–1987.

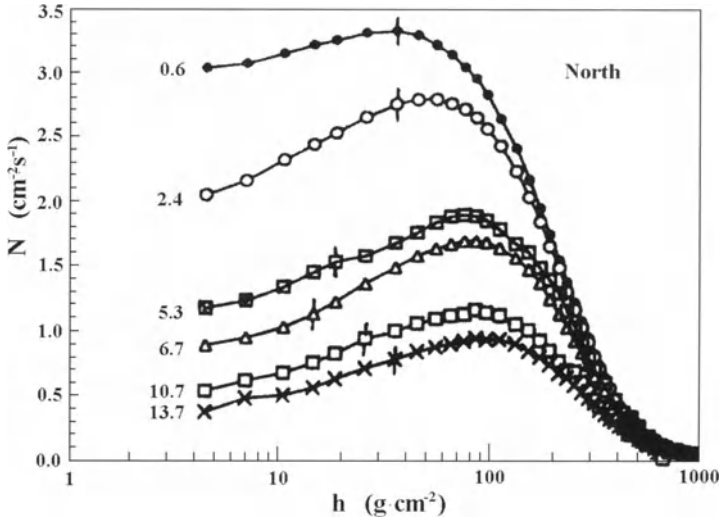

Fig. 2.13.2. The CR fluxes vs. atmospheric pressure h measured at different latitudes of the Northern hemisphere during the sea expedition of 1986–1987. The values of R_c in GV are shown for each curve. The vertical bars show standard errors. According to Golenkov et al. (1990).

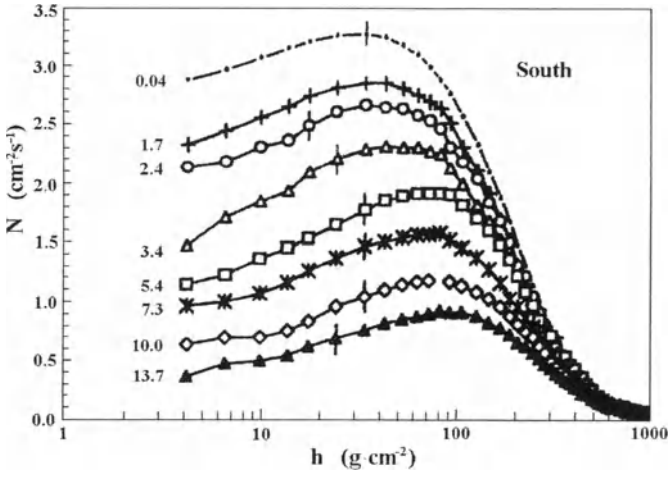

Fig. 2.13.3. The same as in Fig. 2.13.2, but for the Southern hemisphere.

The angular distribution of CR intensity in the Earth's atmosphere was determined according to Bazilevskaya et al. (1997) on the basis of routine CR measurements on radio-balloons with the standard device (see description in Chapter 4, Section 4.6.3) in combination with measurements by rotated special multidirectional telescopes characterized by 5 zenith angles 0°, 22.5°, 45°, 67.5°, and 90° (near the minimum of solar activity in 1975–1976 where made 22 successful flights at different cutoff rigidities R_c). The measured galactic CR intensity by each telescope can be considered as a sum of spherical harmonics:

$$N(\theta,x,R_c)=\sum_{m=0}^{m=2}\int_0^{2\pi} J^{2m}(x,R_c)Y_{2m}^0(\theta,\varphi)d\varphi, \tag{2.13.1}$$

where θ and φ are zenith and azimuthally angles, x is the atmosphere depth in g/cm^2, and Y are spherical harmonics (in Eq. 2.13.1 is taken into account the rotation of telescopes around vertical axis with period much smaller than the data collecting time). The results of determining coefficients $J^{2m}(x,R_c)$ for m = 0, 1 and 2 in four regions of cutoff rigidities (0.4–0.6, 2.35, 8.8–9.5, and 12.6–14.1 GV) by the method of the least square fit are shown in Fig. 2.13.4 for telescopes with filter about 2 g/cm^2 Al, and without filter.

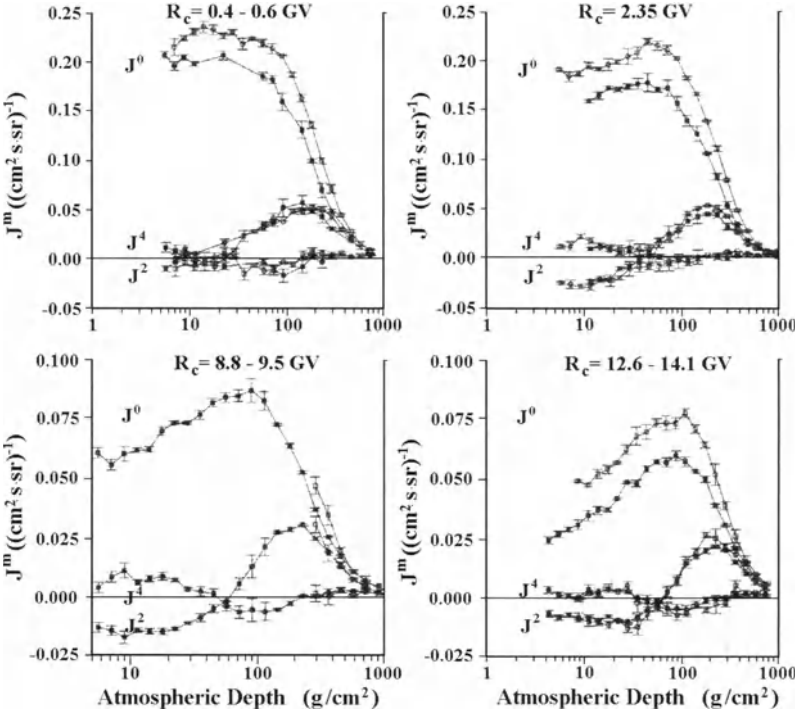

Fig. 2.13.4. Results of determining coefficients $J^{2m}(x,R_c)$ for galactic CR in Eq. 2.13.1 for four regions of cutoff rigidities for telescopes with filter about 2 g/cm^2 Al, and without filter (open and filled squares, respectively). According to Bazilevskaya et al. (1997).

On the basis of obtained results was determined the effective geometrical factor of standard device used in routine radio-balloon flights. Results are shown in Fig. 2.13.5.

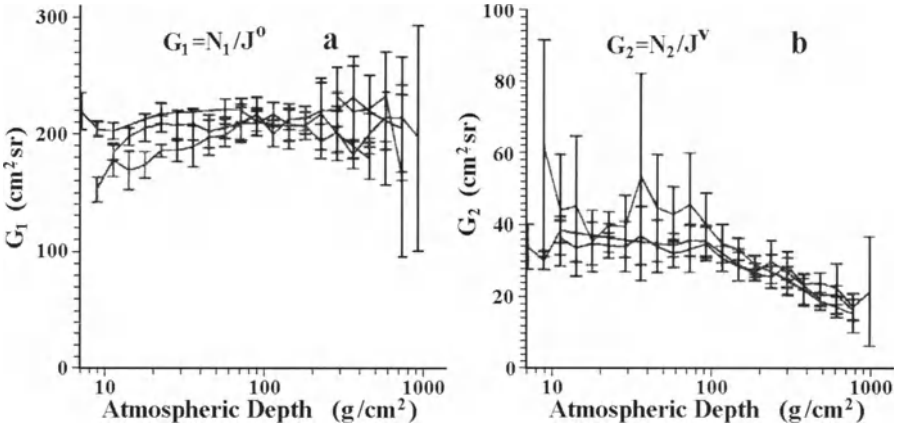

Fig. 2.13.5. The effective geometrical factor of standard device used in routine radio-balloon flights: **a** – for single counter, **b** – for double coincidence telescope (data for all cutoff rigidity regions are superposed). According to Bazilevskaya et al. (1997).

From Fig. 2.13.5 can be seen that for single counter the geometrical factor is about const in the interval of depths 10-1000 g/cm^2, but for the double coincidence telescope geometrical factor is about const in the interval 10-100 g/cm^2, and then with increasing the atmosphere depth up to 1000 g/cm^2, decreases about two times. The latter can be understand if the fact that angle distribution of secondary galactic CR in the atmosphere became more sharp with increasing of the atmosphere depth will be taken into account.

For solar CR events, characterized by a spectral index γ in the solar CR energy spectrum ($D_S(E_k) \propto E_k^{-\gamma}$), the depth-angular CR distribution according to Bazilevskaya (1985), Bazilevskaya et al. (1997) can be presented in the form

$$N(x,\theta,R_c) \approx Ax^{-\beta(\gamma,R_c)}(\cos\theta)^{\beta(\gamma,R_c)}, \qquad (2.13.2)$$

where index $\beta(\gamma,R_c)$ depends also from the cutoff rigidity R_c.

2.13.3. Time variations of secondary CR intensity at different depths in troposphere and stratosphere

The examples of the time dependences of charged particle fluxes (monthly averaged values) measured at the polar (northern and southern) and middle latitudes in the stratosphere and troposphere are given in Fig. 2.13.6 and 2.13.7. The period of observations covers 19–23 solar activity cycles. It is important that the amplitude of these variations, as well as variations in periods of great solar CR events are much bigger than observed by muon detectors on the ground and underground, and even sufficiently bigger than observed by neutron monitors (in more details see in Dorman, M2005).

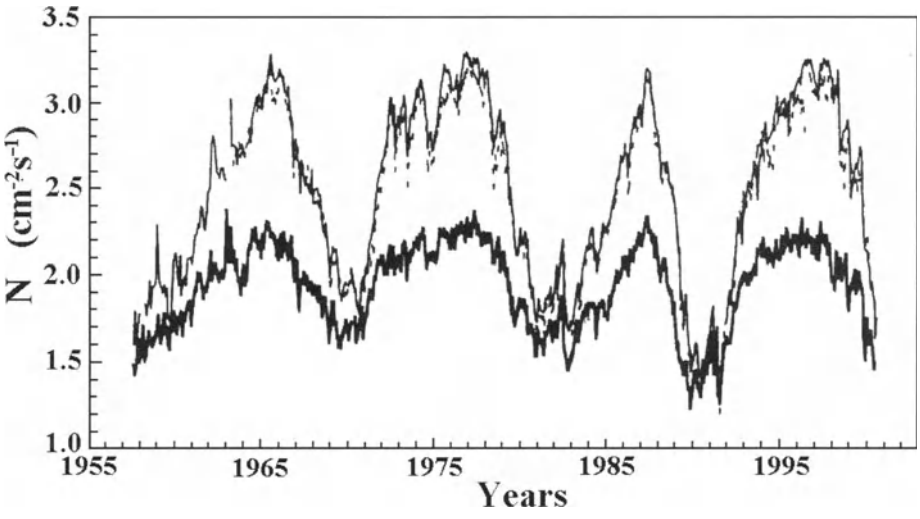

Fig. 2.13.6. Time dependence of monthly averaged CR fluxes in the stratosphere at H = 31 km (h = 10 g/cm^2) measured at the northern and southern polar latitudes (R_c = 0.6 and 0.04 GV, upper solid and dotted curves, accordingly) and at the middle latitude (bottom gray curve, R_c = 2.4 GV). According to Stozhkov et al. (2001).

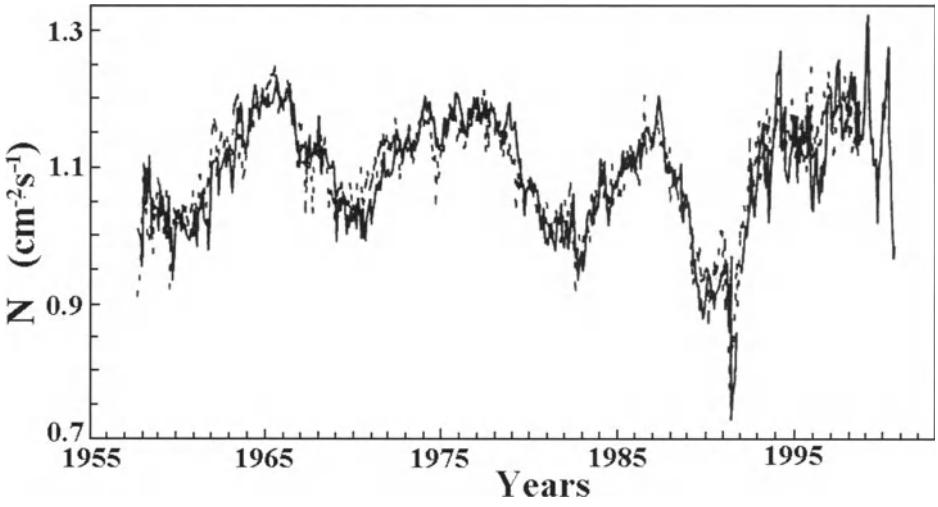

Fig. 2.13.7. Time dependence of CR fluxes averaged per month in the troposphere at H = 10.5 km (h = 250 g/cm^2) measured at the northern polar latitudes (R_c = 0.6 GV, solid curve) and at the middle latitude (dotted curve, R_c = 2.4 GV). According to Stozhkov et al. (2001).

2.13.4. The atmospheric cut off energy for radio balloon measurements vs. atmospheric depth

At each atmospheric pressure level h, only particles with energy $E > E_a$ (or rigidity $R > R_a$), where E_a is the atmospheric cut off energy, can contribute to the counting rate of CR detectors on radio balloons. The atmospheric cut off E_a and R_a are defined by the

characteristics of nuclear interactions of the primary CR with air atoms. From the latitude expedition radio balloon measurements at different h and at different geomagnetic cut off rigidities R_c, Stozhkov et al. (2001) determined experimentally values of R_a as a function of h. Results are shown in Fig. 2.13.8. The experimentally observed dependence can be approximated by the function

$$R_a \approx 0.04h^{0.8}\ GV\,, \tag{2.13.3}$$

where h is in g/cm^2.

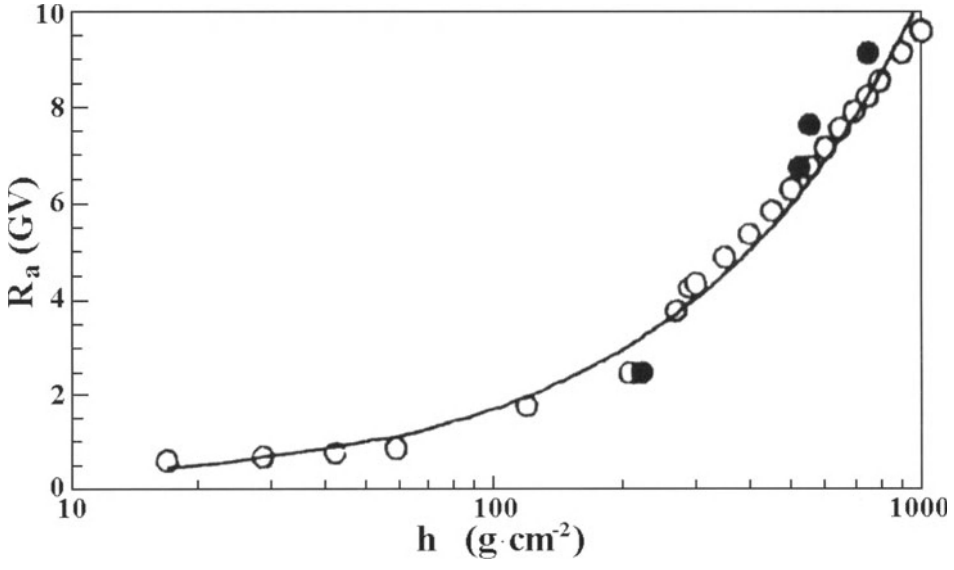

Fig. 2.13.8. Results of determination the atmospheric cut off R_a vs. atmospheric pressure h (in g/cm^2). Open points were obtained from the sea expedition data and black points – from the long term data obtained at the stationary sites (see Table 2.13.1). The solid curve is the approximation described by Eq. 2.13.1. According to Stozhkov et al. (2001).

2.13.5. Precipitation of high-energy electrons from the Earth's radiation belts

In Section 2.10 we considered satellite data on precipitation of high energy electrons from the Earth's radiation belts (with generation of gamma rays). This phenomenon can be investigated also by radio balloon measurements. During the geomagnetic disturbed periods in the polar atmosphere near Murmansk at high altitudes relativistic electron precipitation events are detected by radio balloons (Makhmutov et al., 1995; Bazilevskaya and Makhmutov, 1999; Makhmutov et al., 2001a,b). In Fig. 2.13.9 an example of precipitation phenomenon detected in May 2000 is shown.

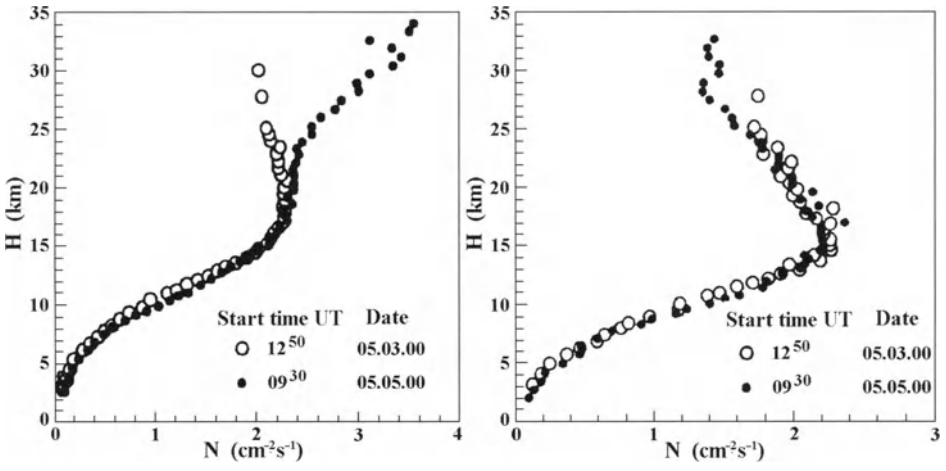

Fig. 2.13.9. Precipitation of relativistic electrons into the northern polar atmosphere near Murmansk recorded by a single counter on 5 the March, 2000 (left panel, black points). The background from galactic CR is shown by open points. The telescope recorded galactic CR background only (right panel). The inserts show the dates of radio balloon flights and launching times. According to Makhmutov et al. (2001a).

From Fig. 2.13.9 can be seen that the single counter records secondary γ-rays produced by precipitating electrons in the atmosphere (at the same time the telescope records only the background from galactic CR; it allows to separate precipitation phenomena from solar proton events). It is significant that gamma rays recorded in the atmosphere at H of about 25–35 km are produced by the precipitating electrons with energy more than several MeV. The time dependence of yearly precipitation number and sunspot number are given in Fig. 2.13.10.

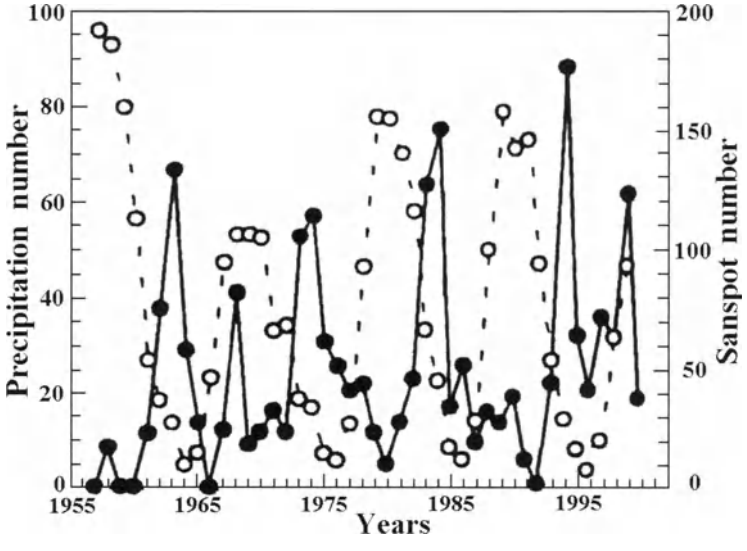

Fig. 2.13.10. The time variations of the yearly number of precipitation (black points) and sunspot number (open points). The observations were made on radio-balloons at the northern polar station in Murmansk region (see Table 2.13.1) during the time interval of (6–12) UT. According to Stozhkov et al. (2001).

The data in Fig. 2.13.10 show that precipitations take place most often during the descending phase of solar activity, supporting the results obtained by Reeves (1998). The total number of precipitations recorded by radio-balloons in Murmansk region during 1957-2000 equals 549 events. In Table 2.13.2 the yearly precipitation numbers during 20 – 23 solar cycles are given.

Table 2.13.2. The number of precipitations in different solar cycles. According to Stozhkov et al. (2001)

Solar cycle	Period	Average sunspot number	Total number of precipitations	Number of precipitations per year
20	1964–1975	58.8	144	12
21	1976–1985	82.9	140	14
22	1986–1995	78.5	118	12
23	from 1996	46.9	85 (for 5 years)	17

2.13.6. Bremsstrahlung photons from precipitating high energy electrons

As we mentioned above, the regular radio balloon measurements were carried out with a standard detector consisting of two Geiger counters and an Al filter inserted between the counters (see for details Section 4.6.3). A single counter records the omni-directional flux of charged particles: electrons with energy $E_e > 0.2$ MeV, protons with energy $E_p > 5$ MeV, and is also sensitive to X-rays ($E_{ph} > 20$ keV). During precipitation events omni-directional counter records the penetrated into the atmosphere bremsstrahlung photons, generated by the precipitating electrons at atmospheric altitudes 70–100 km. In Fig. 2.13.9 are given examples of observations of bremsstrahlung photons in the atmosphere at Olenya on 28 and 29 September, 1999, and 5 May 2000.

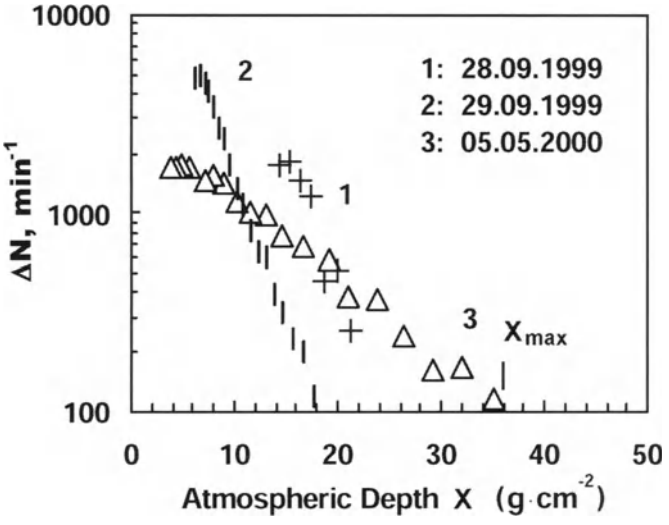

Fig. 2.13.11. The bremsstrahlung photon absorption spectra: counting rate of the omni-directional counter vs. atmospheric depth x during the electron precipitation events. **1** - on 28 September (08.14 – 08.32 UT) 1999; **2** - 29 September (08.19 – 09.10 UT) 1999; and **3** - 5 May (08.32 – 09.29 UT) 2000 as observed in Murmansk region, at Olenya (68°57' N, 33°03' E). The pre-precipitation event quiet time background counting rate is eliminated. According to Makhmutov et al. (2001b).

Fig. 2.13.11 displays the bremsstrahlung photon absorption spectra, i.e., the counting rates of the omni-directional counter owed to the X–rays, vs. atmospheric depth x. To evaluate these spectra a pre-precipitation event quiet time background caused by galactic CR is eliminated. The enhanced counting rate up to a few thousand per minute at atmospheric depths x below 10 g.cm^{-2} corresponds to the electron flux at the top of the atmosphere of $J(E_e > 300$ keV$)$ above 104 cm^{-2}·s^{-1}·sr^{-1}. For each bremsstrahlung photons event the dependence of roentgen flux $D(x)$ was approximated as

$$D(x) = ax^{-m} \tag{2.13.4}$$

For each individual event, the parameters a and m, as well as the maximum atmospheric depth (X_{max}, in g/cm^2) down to which the X-rays were observed, were determined. The results for all events during 1965–2000 are shown in Fig. 2.13.12.

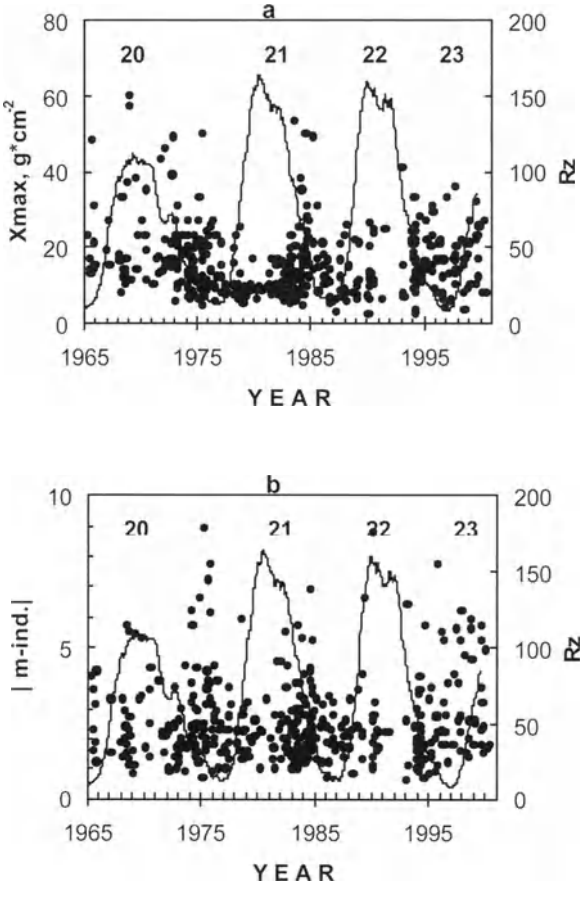

Fig. 2.13.12. Yearly sunspot numbers (Rz, solid line, both panels), X_{max} (panel **a**) and absolute values of individual indexes |m-ind| (panel **b**), characterizing bremsstrahlung photon events from precipitating electrons observed by regular radio balloon measurements during solar cycles 20–23. According to Makhmutov et al. (2001b).

The data presented in Fig. 2.13.12 are characterized according to Makhmutov et al. (2001b) by the following features:

(A) A very wide distributions of X_{max} and |m-ind| values during the descending phases and years close to the minimum of solar activity during cycles 20 to 22. It means that primary energy of incident electrons from radiation belts varied from a few tens of keV up to (or more) 6–10 MeV during these precipitation events at L=5.6; it was suggested that these events were mainly originated from geomagnetic disturbances caused by interaction of the high speed solar wind streams from solar coronal holes with the Earth's magnetosphere;

(B) an extended distribution of X_{max} is a peculiarity of the solar cycle 20 in comparison with that in cycles 21 and 22. This fact is in accordance with the distributions of geomagnetic storms with *Dst* more than 50 *nT* in solar cycles 20 and 21 (Gonzales et al., 1996).

Mean values of X_{max} and *m*-indices for each solar cycle are given in Table 2.13.3.

Table 2.13.3. Mean values (**Mean**) and standard deviations (**STD**) of interplanetary medium parameters, geomagnetic indices and characteristics of bremsstrahlung photon events from precipitating electrons observed in the atmosphere for each of the solar cycles 20–23 (N: number of selected events). According to Makhmutov et al. (2001b).

Solar Cycle	Parameter	Mean	STD
SC 20	*B, nT*	6.6	2.2
	Bz, nT	-1.6	3.1
N=89	*V, km/s*	559	124
	Dst, nT	-33	21
	AE, nT	510	201
	Xmax, g cm^{-2}	18.4	10.2
	m-ind.	-2.6	1.5
SC 21	*B, nT*	8.9	3.5
	Bz, nT	-1.5	4.8
N=68	*V, km/s*	508	97
	Dst, nT	-44	29
	AE, nT	518	222
	Xmax, g cm^{-2}	14.1	8.2
	m-ind.	-2.4	1.1
SC 22	*B, nT*	6.6	2.6
	Bz, nT	-1.2	2.4
N=47	*V, km/s*	564	130
	Dst, nT	-46	26
	Xmax, g cm^{-2}	15.4	7.8
	m-ind.	-2.4	1.6
SC 23	*B, nT*	8.6	4.1
(incl. 2000)	*Bz, nT*	-1.6	5.2
N=36	*V, km/s*	472	84
	Dst, nT	-39	24
	Xmax, g cm^{-2}	17.4	8.0
	m-ind.	-3.6	2.2

Makhmutov et al. (2001b) come to following conclusions:

(1) there is a very wide distribution of bremsstrahlung photons from precipitating electrons events parameters (X_{max} = 10–60 g.cm^{-2} and $|m\text{-}ind|$ = 1.5–8) during the descending phases and years close to the minimum of solar activity cycles 20–22;

(2) there is no a simple correlation between the sets of the considered parameters: interplanetary/geomagnetic and characteristics of the electron precipitation events observed in the atmosphere;

(3) the events with X_{max} = 10–30 g.cm^{-2} were observed during small, moderate and intense geomagnetic storms (*Dst* up to 200 *nT*);

(4) bremsstrahlung photons penetrate down to atmospheric depth X_{max} = 40–60 g.cm^{-2} only during moderate and small storms (*Dst* up to 100 nT). Such photons could be generated by precipitating electrons with energy more than 6–10 MeV (during these events the hard photons absorption spectra characterized by $\langle m \rangle \approx -2$ were recorded in the atmosphere).

2.14. Perspectives of secondary CR research development

In the last years the interest in more detailed investigations of secondary CR generated in the atmosphere, underwater and underground increased sufficiently and a lot of very important results were obtained. In this Chapter we have tried to reflect this progress. In our opinion this progress is caused by the understanding of the important role played by secondary CR in many large underground neutrino experiments, and in existing and planned experiments for investigations of CR very high energies (up to $10^{20} - 10^{21}$ eV). From this point of view it is very important to investigate the influence of atmospheric change on the contents and intensity of secondary CR (see Part 2 of the present book), as well as the influence of the Earth's magnetic field changes on secondary CR, the influence of solar activity and other space processes on the intensity of secondary CR (these problems will be considered in the next book Dorman, M2005). On other hand, as it will be shown below, in Part 3, secondary CR play a key role in many atmospheric processes such as thunderstorms and lightnings, sprites, air ionization, formation of the lower ionosphere, generation of cosmogenic nuclides, all of which play an important role in some atmospheric chemical processes (formation of nitrates and ozone layer). There are evidences of secondary CR influence on cloudiness, and through cloudiness on long–term climate change. Secondary CR are also very important for many CR research applications in Meteorology, Archeology, Geology and Geophysical Prospecting, in Space Weather monitoring and forecasting, in Environment monitoring, and many others (see below, Part 4). There is no doubt that the effects mentioned above will further stimulate secondary CR research.

Chapter 3

Coupling Functions, Integral Multiplicities, and Inverse Transformations

3.1. Integral multiplicities, coupling functions, and CR time variations

The intensity of any CR component of type *i* (e.g. total neutron counting rate and different neutron multiplicities, muon component on the ground and underground at different depths and different directions, electron-photon component, frequency of External Atmospheric Showers (EAS), and others), observed at cut off rigidity $R_C(t)$ at the level $h_O(t)$ in the atmosphere at some moment of time *t* can be determined from

$$N_i(R_C(t),h_O(t),t)=\int_{R_C(t)}^{\infty} D(R,t)m_i(R,h_O(t),g(t),T(h,t),E(h,t))dR\,. \qquad (3.1.1)$$

Here $D(R,t)$ is the primary CR spectrum out of the atmosphere, and $m_i(R,h_O(t),T(h,t),E(h,t))$ is the integral multiplicity (number of total secondary CR particles of type *i* generated from one primary particle with rigidity *R*), which depends on the mass of air $h_O(t)$ in the vertical column under the point of observations. (Note that atmospheric pressure is usually used instead of vertical column mass. This is correct only if the velocity of the wind is zero or very small. Otherwise it is necessary to take into account the Bernoulli effect; see Chapter 6 for details). The integral multiplicity depends also on the value $g(t)$ of gravitational acceleration which is a function of the latitude and varies with time because of the gravitational influence of the Moon and the Sun, and on the vertical distribution of air temperature $T(h,t)$ and atmospheric electric field $E(h,t)$.

Possible time variation of observed CR intensity can be caused by any of three variables on the right hand side of Eq. 3.1.1:

$$\delta N_i(R_C(t),h_O(t),t)=\int_{R_{CO}}^{\infty} D_O(R)\delta m_i(R,h_O(t),g(t),T(h,t),E(h,t))dR-\delta R_C(t)D_O(R_{CO})$$

$$\times m_{iO}(R_{CO},h_O,g_O,T_O(h),E_O(h))+\int_{R_{CO}}^{\infty}\delta D(R,t)m_{iO}(R,h_O,g_O,T_O(h),E_O(h))dR, \qquad (3.1.2)$$

where we denote by the index *o* values at $t=0$ (it can be some average values or choused at special conditions, e.g. at minimum of solar activity and considered as standard). It is assumed that the relative variations are very small, so that we can neglect the interference of different CR variation classes. For the relative CR time variation we obtain (by dividing Eq. 3.1.2 on N_{iO}):

$$\delta N_i(R_c(t),h_o(t),t)/N_{io} = \int_{R_{co}}^{\infty} \frac{\delta m_i(R,h_o(t),g(t),T(h,t),E(h,t))}{m_{io}} W_i(R_{co},R)dR$$

$$-\delta R_c(t) W_i(R_{co},R_{co}) + \int_{R_{co}}^{\infty} \frac{\delta D(R,t)}{D_o(R)} W_i(R_{co},R)dR, \quad (3.1.3)$$

where

$$W_i(R_{co},R) = D_o(R) m_{io}(R,h_{oo},g_o,T_o(h),E_o(h))/N_{io} \quad (3.1.4)$$

is the coupling function between secondary CR of type i and primary CR. Coupling functions were introduced by Dorman, M1957. (The difference coupling functions for couple detectors with different cut off rigidities were introduced in Dorman, 1976a,b,c and Dorman 1977a,b; see below Sections 3.9 and 3.10). It is easy to see on the basis of Eq. 3.1.1 that

$$\int_{R_{co}}^{\infty} W_i(R_{co},R)dR = 1. \quad (3.1.5)$$

The first term on the right hand side of Eq. 3.1.3 reflects CR time variations of atmospheric origin (meteorological effects). The second term is of geomagnetic origin, caused by secular variations of the main geomagnetic field connected with processes in the earth's core, as well as with changes of great electric currents in the Earth's magnetosphere, especially in periods of geomagnetic storms. The third term reflects CR variations of extra-terrestrial origin, such as the generation of CR in the Sun, interplanetary modulation of galactic CR, and interstellar CR variations. The atmospheric CR variations are considered in detail below, in Part 2 (Chapters 5–9). Geomagnetic and extra-terrestrial CR variations are considered in detail in Dorman (M2005).

Let us consider the coupling function at $R_{co} = 0$, the so called polar coupling function (Dorman, M1957):

$$W_i(0,R) = D_o(R) m_{io}(R,h_{oo},g_o,T_o(h),E_o(h))/N_{io}(0,h_{oo}) \quad (3.1.6)$$

The coupling function at any value of $R_{co} > 0$ can be determined through polar coupling function:

$$W_i(R_{co},R) = \begin{cases} 0 & \text{if } R \le R_{co} \\ W_i(0,R)\left(\int_{R_{co}}^{\infty} W_i(0,R)dR\right)^{-1} & \text{if } R > R_{co}, \end{cases} \quad (3.1.7)$$

where R_{co} is the effective cut off rigidity for some chosen moment of time $t = 0$ (note that the effective cut off rigidity varies with time due to the changes in the main Earth's magnetic field and changes of the magnetosphere).

3.2. The interference between different CR variation classes

In Section 3.1 was assumed that variations of the three parameters which determine the observed change of CR intensity are very small. But in reality in many cases these variations can be relatively big (great GLE – Ground Level Events – caused by solar CR increases, great Forbush decreases, 11 year CR variations, and so on). In these cases Eq. 3.1.2 will be transformed to the following:

$$\frac{\Delta N_i}{N_{io}} = \int_{R_{co}}^{\infty} \frac{\Delta m_i}{m_{io}} W_{io}(R_{co},R)\left\{1+\delta(R-\overline{R}_{co})\Delta R_{co}\left(1+\frac{\Delta D(R)}{D_o(R)}\right)+\frac{\Delta D(R)}{D_o(R)}\right\}dR$$

$$-\Delta R_{co} W_{io}(R_{co},\overline{R}_{co})\left[1+\frac{\Delta D(\overline{R}_{co})}{D_o(\overline{R}_{co})}\right]+\int_{R_{co}}^{\infty}\frac{\Delta D(R)}{D_o(R)}W_{io}(R_{co},R)dR, \qquad (3.2.1)$$

where $R_{co} < \overline{R}_{co} < R_{co}+\Delta R_{co}$, $\delta(x)$ is the δ–function, and we denote

$$\Delta N_i = N_i(R_c(t),h_o(t),t)-N_{io},\ \Delta R_{co} = R_c(t)-R_{co},\ \Delta D(R)=D(R,t)-D_o(R),$$
$$\Delta m_i = m_i(R,h_o(t),g(t),T(h,t),E(h,t))-m_{io} \qquad (3.2.2)$$

From Eq. 3.2.1 it can be seen that the more complicated term is the first one, denoted as the meteorological effect: it is influenced by both the geomagnetic and extra-terrestrial effects (i.e., the change of cut off rigidity and the change of primary CR rigidity spectrum). The geomagnetic variations (the second term in the right hand side of Eq. 3.2.1) is influenced only by CR variations of extra-terrestrial origin (the change of primary CR rigidity spectrum that will be consider in detail in Dorman, M2005). The variations of extra-terrestrial origin (the third term on the right hand side of Eq. 3.2.1) are not affected by the other CR variation classes.

3.3. CR in the geomagnetic field: asymptotic directions, penumbra and cut off rigidities

In the first approximation the magnetic field of the Earth can be considered as a dipole field of with a moment 8.1×10^{25} Gs.cm^3 and inclined to the Earth's axis of rotation at the angle 11.5°. All primary CR charged particles with rigidity $R < R_1(\lambda,Z,\varphi)$, where

$$R_1(\lambda,Z,\varphi) = 59.6\cos^4\lambda\left[1+\left(1-\sin Z\cos\varphi\cos^3\lambda\right)^{1/2}\right]^{-2}\ \text{GV}, \qquad (3.3.1)$$

cannot arrive at the Earth's surface (here λ is the geomagnetic latitude of the point of observations, Z and φ are the zenith and azimuth angles of the incident particle. Eq. 3.3.1 describes in the dipole approximation latitude and East–West geomagnetic CR effects. All particles with $R > R_2(\lambda,Z,\varphi)$ will reach the Earth's surface, but in the region of penumbra

$$R_1(\lambda,Z,\varphi) < R < R_2(\lambda,Z,\varphi) \tag{3.3.2}$$

only part of the particles can arrive the Earth's surface. Fig. 3.3.1 shows examples of penumbra function f(R) = 0 (trajectories are forbidden) or f(R) = 1 (trajectories are allowed) for vertical arrival in the dipole approximation for geomagnetic latitudes λ = 30, 40, and 50°.

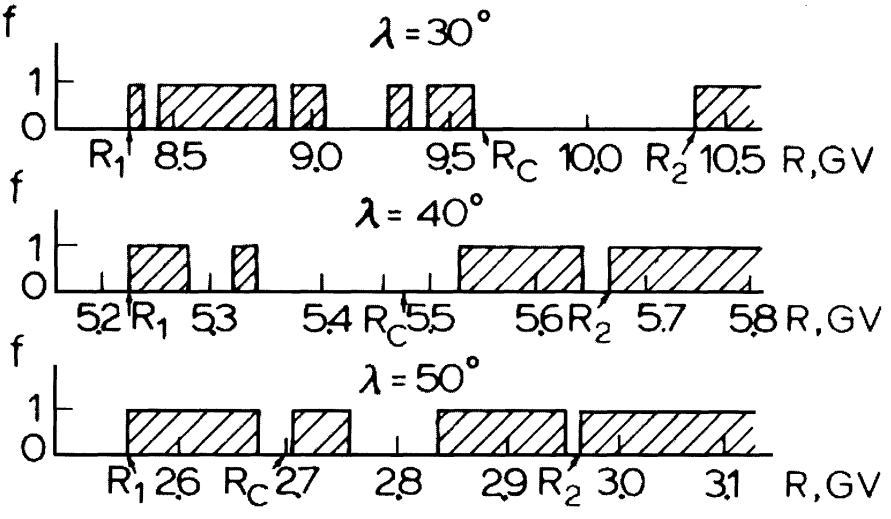

Fig. 3.3.1. Penumbra in the dipole approximation at the Earth's surface.

The effective cut off rigidity $R_{ci}(\lambda,Z,\varphi,H)$ for the CR component of type i can be determined from the following equation:

$$\int_0^\infty f(\lambda,Z,\varphi,H)D(R)m_i(R,h_o,g,T(h),E(h)) = \int_{R_{ci}(\lambda,Z,\varphi,H)}^\infty D(R)m_i(R,h_o,g,T(h),E(h)). \tag{3.3.3}$$

The penumbra is much more complicated in the actual geomagnetic field; trajectory calculations of the penumbra function f in the real geomagnetic field for many CR Observatories were made in the monograph Dorman et al. (M1972), where results of calculations of effective cut off rigidities as a function of the solar activity for different types of primary CR variations are also given (see in detail in Dorman, M2005).

In order to use CR data from the worldwide network of CR Observatories it is very important to perform trajectory calculations of incident CR particles with a given rigidity, zenith and azimuthally angles. For CR Observatories of the former USSR these calculations were made by Dorman and Smirnov (1967), and for many Observatories in the World – by McCracken et al. (1965). Let us note that the asymptotic directions are not constant; they are changed sufficiently with time caused by changing of main magnetic field and magnetosphere (see in detail in Dorman et al., M1971, and in Dorman, M2005).

3.4. Determination of coupling functions and integral multiplicities by geomagnetic effects; extrapolation to higher energies and estimations for underground detectors and EAS installations

3.4.1. Using geomagnetic effects for determining coupling functions and integral multiplicities

Let us rewrite Eq. 3.1.1 for $t = 0$:

$$N_{io}(R_{co}, h_{oo}) = \int_{R_{co}}^{\infty} D_o(R) m_{io}(R, h_{oo}, g_o, T_o(h), E_o(h)) dR . \qquad (3.4.1)$$

By differentiating Eq. 3.4.1 with respect to R_{co}, we obtain

$$dN_{io}(R_{co}, h_{oo})/d\,R_{co} = -D_o(R_{co}) m_{io}(R_{co}, h_{oo}, g_o, T_o(h), E_o(h)) . \qquad (3.4.2)$$

By comparing Eq. 3.4.2 with Eq. 3.1.4 we obtain

$$W_i(R_{co}, R) = D_o(R) m_{io}(R, h_{oo}, g_o, T_o(h), E_o(h)) / N_{io}(R_{co}, h_{oo})$$

$$= -(dN_{io}(R_{co}, h_{oo})/d\,R_{co}) / N_{io}(R_{co}, h_{oo}). \qquad (3.4.3)$$

From Eq. 3.4.3 it follows that

$$m_{io}(R, h_{oo}, g_o, T_o(h), E_o(h)) = -(dN_{io}(R_{co}, h_{oo})/d\,R_{co}) / D_o(R) . \qquad (3.4.4)$$

Let us note that in Eq. 3.4.3 and 3.4.4 it is supposed that all CR latitude survey data are corrected by extra-terrestrial CR time variations as well as by meteorological effects and by possible time-variations of cut off rigidities (if a big geomagnetic storm occurred during the survey). The methods of CR latitude survey data correction were developed in Villoresi et al. (2000), Iucci et al (2000), Dorman et al. (2000), and are described in detail below, in Chapter 16. Eq. 3.4.3 and Eq. 3.4.4 are the basis for the determination of coupling functions and integral multiplicities for different CR components using data from latitude surveys and from measurements of the East–West effect (in detail this problem will be considered in Dorman, M2005).

3.4.2. Extrapolation to higher energies or rigidities

Let us assume that coupling functions are determined on the basis of data on geomagnetic effects up to $R_{c\max}$ or $E_{c\max}$, and near these values

$$W(R_c, R)_{R \to R_{c\max}} = m(R/R_{c\max})^l , \qquad (3.4.5)$$

where $m = W(R_c, R_{c\max})$. Let us take into account that primary spectrum of galactic CR in high energy region is power function from energy or rigidity with little changing of

the slope γ ($D_o(R) \propto R^{-\gamma}$ or $D_o(E) \propto E^{-\gamma}$); integral multiplicity is also power function from energy or rigidity with possible small changing of slope (according to EAS data, see review in Khristiansen, M1975; Murzin, M1988). Because the coupling function is proportional to the product of differential primary CR spectrum and integral multiplicity, it must be also power function from energy or rigidity with possible small changing of the slope; so we assume that

$$W(R_c,R)_{R>R_{c\max}} = k(R/R_{c\max})^{-a+b/(R/R_{c\max})}, \tag{3.4.6}$$

where coefficients k, a, and b can be determined from condition of normalization (see Eq. 3.1.5) as well as conditions of equality in the point $R = R_{c\max}$ values coupling function and their first derivatives:

$$k = m, \quad l = -a + b, \quad \int_{R_{c\max}}^{\infty} W(R_c,R)dr = 1 - \int_{0}^{R_{c\max}} W(R_c,R)dR = 1 - B(R_{c\max}), \tag{3.4.7}$$

where

$$B(R_{c\max}) = \int_{0}^{R_{c\max}} W(R_c,R)dR\,. \tag{3.4.8}$$

is the observed value of the total CR geomagnetic effect (i.e. the ratio of observed CR intensity at $R_c = R_{c\max}$ to the polar CR intensity at $R_c = 0$). By introducing Eq. 3.4.6 in the third equation of Eq. 3.4.7 and using substitution $R/R_{c\max} = \exp(t)$ we obtain

$$m\int_{R_{c\max}}^{\infty} (R/R_{c\max})^{-a+b/(R/R_{c\max})}dR = mR_{c\max}\int_{0}^{\infty}\exp(t(1-a)+tb\exp(-t))dt = mR_{c\max}$$
$$\times\int_{0}^{\infty}\exp(t(1-a))\left[1+\frac{bt\exp(-t)}{1!}+\frac{(bt\exp(-t))^2}{2!}+\ldots\right]dt = mR_{c\max}\sum_{n=0}^{\infty}\frac{b^n}{(a+n-1)^{n+1}}, \tag{3.4.9}$$

and then by using $k = m$ and $b = l + a$, we obtain equation for determining parameter a:

$$\sum_{n=0}^{\infty}\frac{(l+a)^n}{(a+n-1)^{n+1}} = \frac{1-B(R_{c\max})}{mR_{c\max}}\,. \tag{3.4.10}$$

Eq. 3.4.10 can be very easy solved by iteration method:

$$a_1 = 1 + \left(\frac{1-B(R_{c\max})}{mR_{c\max}}\right)^{-1};\; a_2 = 1 + \left(\frac{1-B(R_{c\max})}{mR_{c\max}} - \frac{l+a_1}{a_1^2}\right)^{-1}; \tag{3.4.11}$$

$$a_3 = 1 + \left(\frac{1-B(R_{c\max})}{mR_{c\max}} - \frac{l+a_2}{a_2^2} - \frac{(l+a_2)^2}{(a_2+1)^3}\right)^{-1}; \tag{3.4.12}$$

and so on. As example, in Fig. 3.4.1 are shown results of determining coupling functions for different CR components on the basis of geomagnetic effects and by described above extrapolation to higher energies.

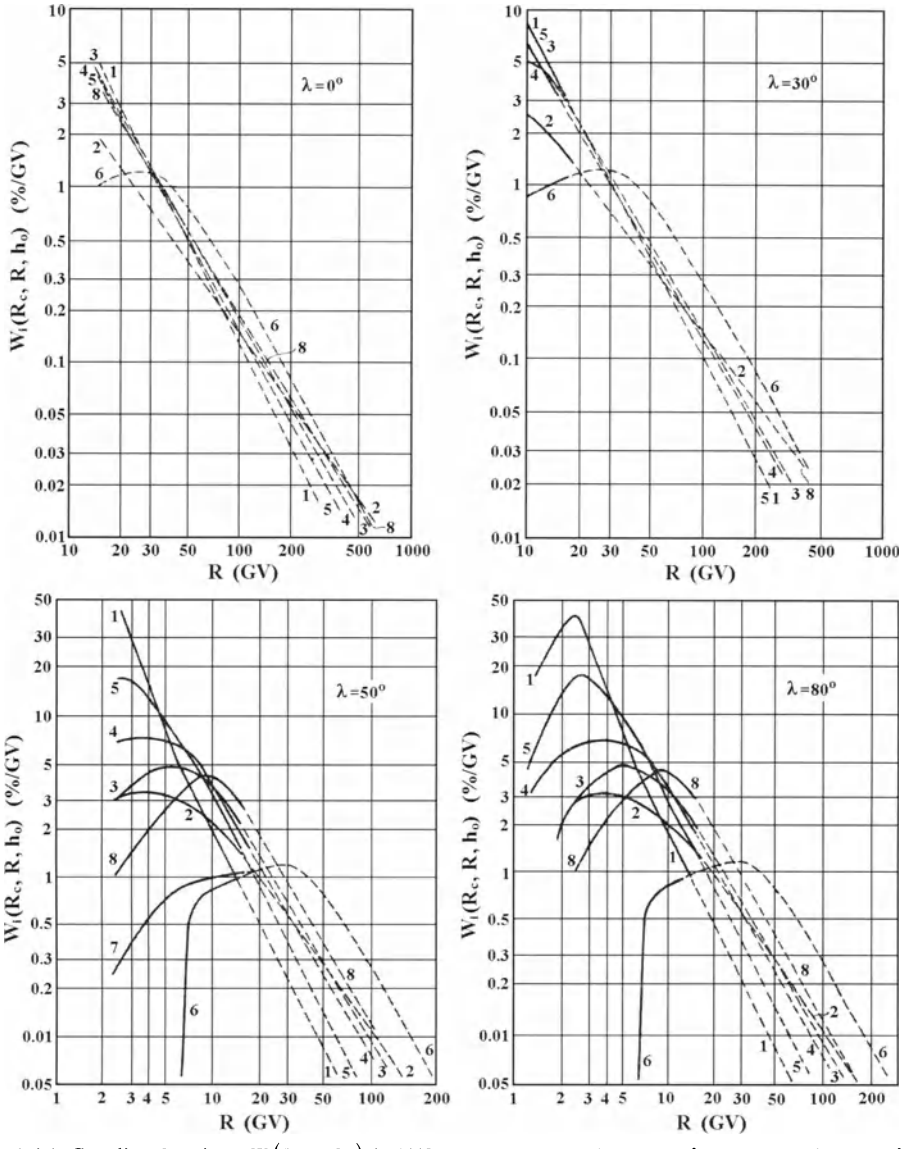

Fig. 3.4.1. Coupling functions $W_i(R_c, R, h_o)$ in %/GV near geomagnetic equator λ = 0° ($R_c \approx 15$ GV), λ = 30° ($R_c \approx 10$ GV), λ = 50° ($R_c \approx 2.5$ GV), and λ = 80° ($R_c \approx 0$ GV). Full lines – derived from latitude surveys, dashed – obtained by extrapolation to higher energies. Curves: 1 and 2 for total charged CR component near boundary of atmosphere and on altitude 4300 m; 3, 4, and 5 for neutron component at sea level, on mountains ($h_o \approx 700$ g.cm^{-2}), and at altitude 10 km ($h_o \approx 300$ g.cm^{-2}); 6 and 7 for muon component at sea level corrected and not corrected on temperature effect; and 8 for total charged CR component at altitude 10 km. According to Dorman (M1957).

In Fig. 3.4.2 are shown coupling functions for muon telescopes in Ahmadabad (India) directed to West and East at zenith angle 45° (obtained by the same way: from geomagnetic effects and by described above extrapolation).

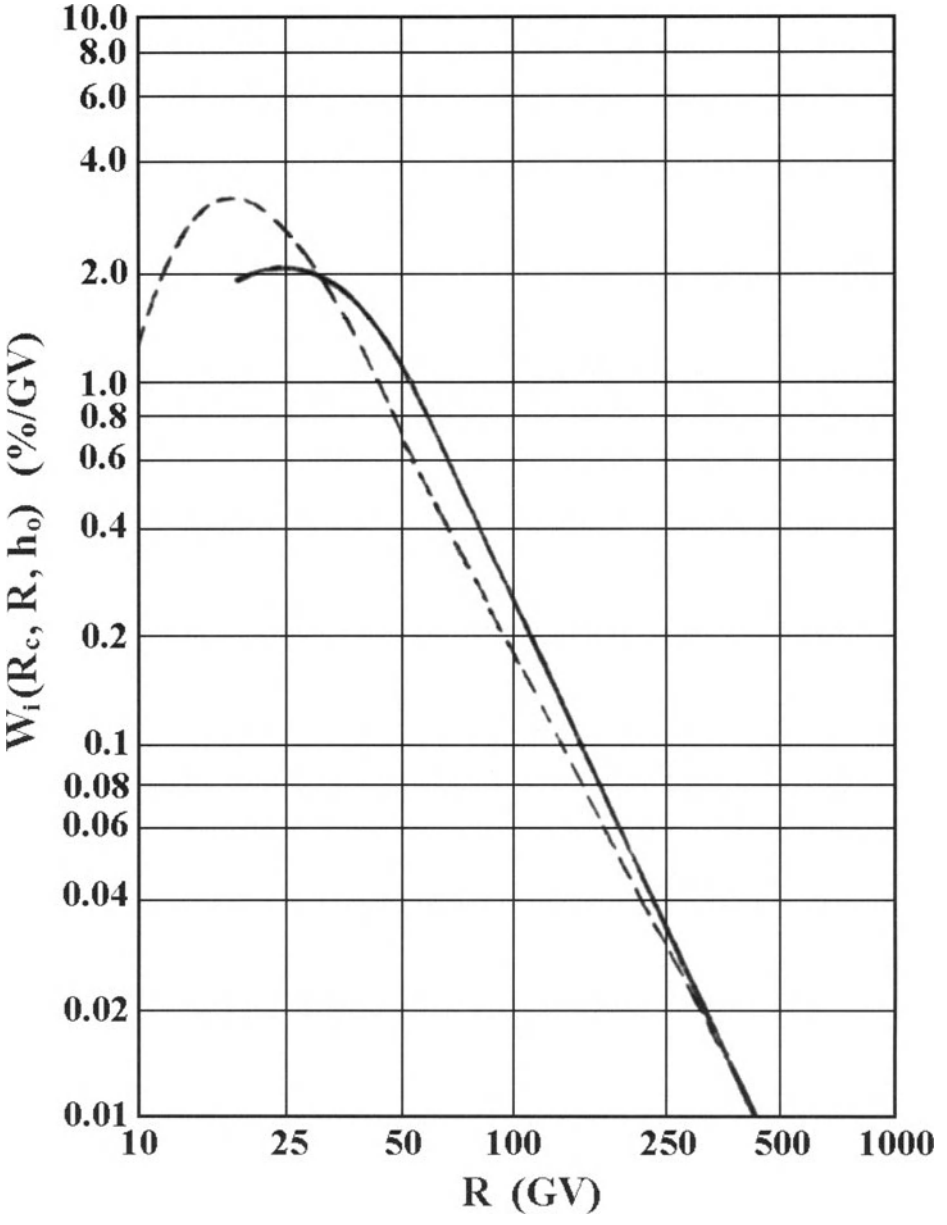

Fig. 3.4.2. Coupling functions for muon component in Ahmadabad near sea level for CR particles arriving from West (dashed curve) and East (full curve) at zenith angle 45°. Calculated by Rao and Sarabhai (1961) accordon the basis of latitude survey data of Johnson and Read (1937), and extrapolated by described above method to higher energies. According to Rao and Sarabhai (1961).

In Fig. 3.4.3 are shown found by Webber and Quenby (1959) on the basis of geomagnetic effects differential sensitivities $dN_i(R_c,h_o)/dR_c$ at $R_c \to R$ (are proportional to coupling functions but not normalized) and yield functions $S_i(R,h_o)$ (have the same meaning as integral multiplicities) for primary protons, and secondary neutron and muon components at different altitudes.

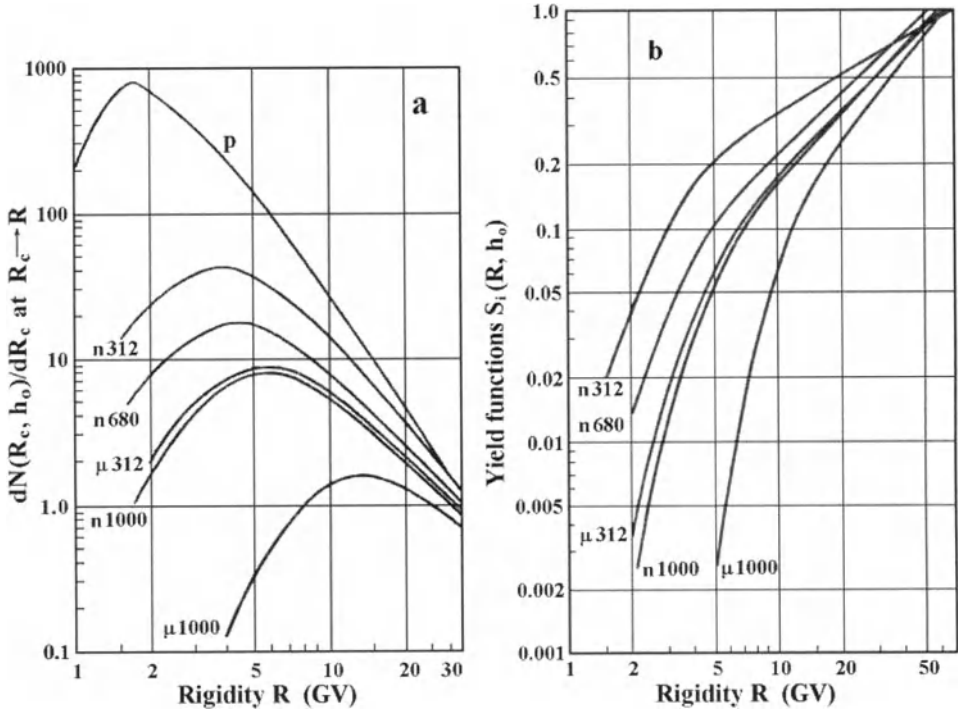

Fig. 3.4.3. Differential sensitivities $dN_i(R_c,h_o)/dR_c$ at $R_c \to R$ (are proportional to coupling functions but not normalized, see left panel **a**) and yield functions $S_i(R,h_o)$ (have the same meaning as integral multiplicities, right panel **b**) for primary protons (denote as **p**), secondary neutrons (**n**) and muons (**μ**) at different altitudes (numbers near curves denote atmospheric depth in g.cm^{-2}). According to Webber and Quenby (1959).

3.4.3. Coupling functions for underground CR measurements

For underground CR measurements at different depths it is not possible to apply described above method of the using of geomagnetic effects because the minimal detected energy is higher than geomagnetic cutoff energy. For determining the coupling functions $W(E,\alpha_{ef}\Delta E_\mu)$ for underground observations of muon intensity in vertical direction with muon energy more than ΔE_μ (including atmospheric depth), we assume that they are generated by primary CR particles with energy $E \geq \alpha_{ef}\Delta E_\mu$, where $\alpha_{ef} \approx 10$. The choose of the factor α_{ef} is very important for this problem. Let us note that the

choice of the value $\alpha_{ef} \approx 10$ is to some extent justified by the results of a paper Vernov et al. (1955) in which it was shown that, in the region of primary particle energies $E \leq 10^{12}$ eV just as in the region of relatively low energies ($E \approx 10^{10}$ eV , see Grigorov and Murzin, 1953), in the primary event of interaction with the nucleus of any atom of air, on the average about 10% of the energy of the primary particle is expended on the formation of a pion, and at the maximum about 15% (Grigorov, 1955). If we take into account the fact that the energy of a decay muon amounts to about two thirds of the energy of a pion, we get the result $\alpha_{ef} \approx 10$). The coupling functions $W(E,\alpha_{ef}\Delta E_\mu)$ for underground observations we will estimate in the first approximation through multiplicity for the muon component at sea level in the high energy region $E \geq \alpha_{ef}\Delta E_\mu$. It means that

$$W(E,\alpha_{ef}\Delta E_\mu) \approx \begin{cases} 0 & \text{if } E < \alpha_{ef}\Delta E_\mu, \\ \beta W_\mu(E,h_o) & \text{if } E \geq \alpha_{ef}\Delta E_\mu, \end{cases} \tag{3.4.13}$$

where $W_\mu(E,h_o)$ is the coupling function for the muon component at sea level, and constant β is determined by the condition of coupling function normalization:

$$\int_{\alpha_{ef}\Delta E_\mu}^{\infty} W(E,\alpha_{ef}\Delta E_\mu)dE = \int_{\alpha_{ef}\Delta E_\mu}^{\infty} \beta W_\mu(E,h_o)dE = 1. \tag{3.4.14}$$

The coupling functions for any desired depth may be calculated by means of Eq. (3.4.13) and (3.4.14). As an example, we give, in Fig. 3.4.4, $W(E,\alpha_{ef}\Delta E_\mu)$ for four values of $\alpha_{ef}\Delta E_\mu$ corresponding at α_{ef} = 10 to depths of penetration of 30, 60, 100, and 1000 m of water equivalent (the relation between the minimum muon energy $\alpha_{ef}\Delta E_\mu$ and the depth of their penetration see in Fig. 2.4.3 in Section 2.4.4, Chapter 2).

Let us note that the coupling functions for underground observations are defined very approximately by Eq. 3.4.13 and 3.4.14. This is primarily due to the following facts: a) the coupling function for muons $W_\mu(R,h_o)$ is used in the field of extrapolation, where its values are not sufficiently reliable; b) it is considered that muons of energy ΔE_μ may be formed only by primary particles of energy over $\alpha_{ef}\Delta E_\mu$, but this boundary in reality it is somewhat blurred; c) the value of α_{ef} is not known exactly.

Another method of finding coupling functions for CR underground research (discussed in Dorman, M1957), is based on the using data of underground CR intensity measurements (described in Chapter 2, Section 2.4) and the fact that in the expressions for both coupling functions at sea level and underground are used the same primary differential rigidity spectrum and the same integral multiplicity function, and the difference is determined only by the difference of muon intensities at sea level and at different depths underground. As it was shown in Dorman (M1957) this method give about the same results which obtained by using $\alpha_{ef} \approx 10$ and presented in Fig. 3.4.4.

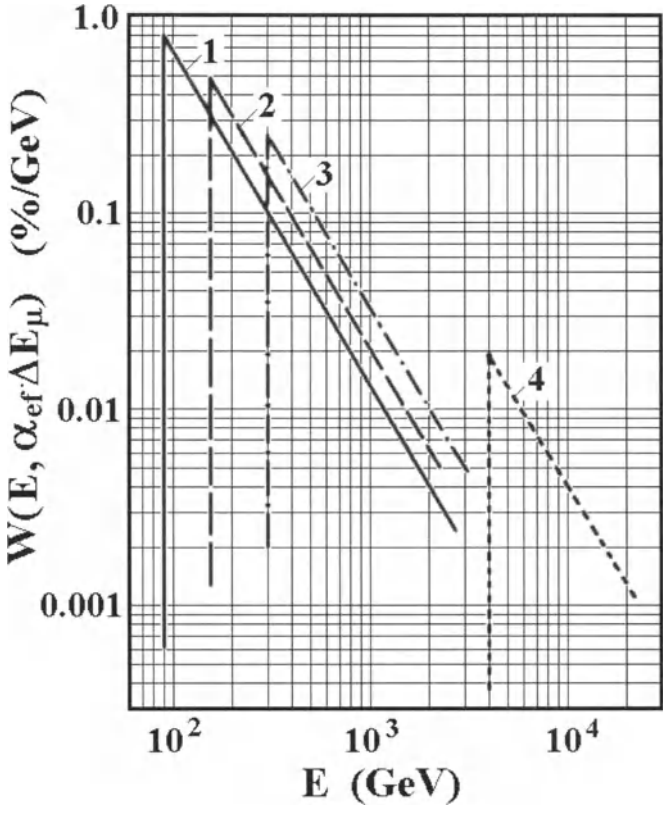

Fig. 3.4.4. The approximate coupling functions $W(E,\alpha_{ef}\Delta E_\mu)$ for underground measurements in vertical direction at different depths: **1** for $\alpha_{ef}\Delta E_\mu$ = 90 GeV (about 30 m w.e.), **2** for $\alpha_{ef}\Delta E_\mu$ = 150 GeV (about 60 m w.e.), **3** for $\alpha_{ef}\Delta E_\mu$ = 300 GeV (about 100 m w.e.), **4** for $\alpha_{ef}\Delta E_\mu$ = 4000 GeV (about 1000 m w.e.). According to Dorman (M1957).

The next approximation was made in Dorman (M1963b). On the basis of scaling theorem for high energy particle interactions it was assumed that

$$W(R,\Delta E_{\mu 2})=\frac{\Delta E_{\mu 1}}{\Delta E_{\mu 2}}W\left(\frac{\Delta E_{\mu 2}}{\Delta E_{\mu 1}}\times R,\Delta E_{\mu 1}\right), \qquad (3.4.15)$$

where $\Delta E_{\mu 1}$ and $\Delta E_{\mu 2}$ are minimal energies of muon detection with accounting the atmospheric depth. It is easy to see that if for some $\Delta E_{\mu 1}$ coupling function $W(R,\Delta E_{\mu 1})$ is normalized, that for any other $\Delta E_{\mu 2}$ coupling function $W(R,\Delta E_{\mu 2})$ will be also normalized. Let us use as a basis coupling function $W(R,\Delta E_{\mu 1})$ for sea level ($\Delta E_{\mu 1}$ = 2.3 GeV) which was presented in Fig. 3.4.1 by curve 6. The obtained results on the basis of Eq. 3.4.15 and curve 6 of Fig. 3.4.1 are shown in Fig. 3.4.5.

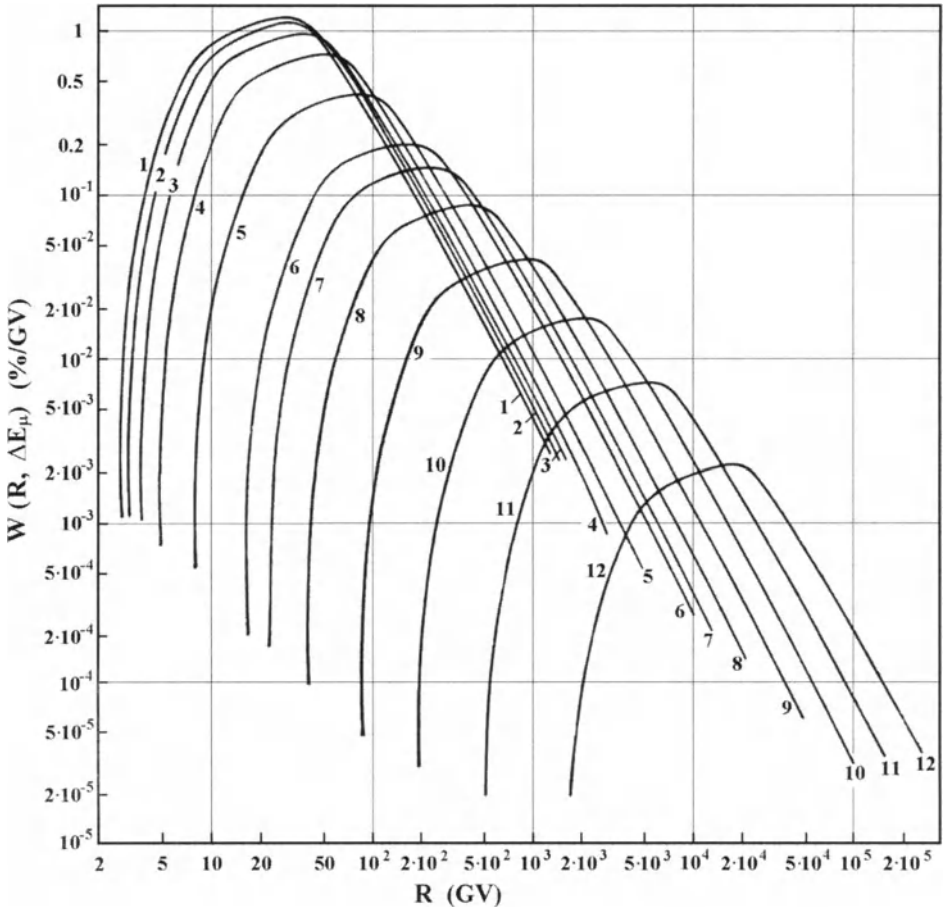

Fig. 3.4.5. Expected coupling functions for underground measurements in the vertical direction derived by scaling from curve 1 by Eq. 3.4.15. Curve **1** for sea level (ΔE_μ = 2.3 GeV) is the same as curve 6 in Fig. 3.4.1; curve **2** for the depth 1 m w.e. (ΔE_μ = 2.5 GeV), **3** for 3 m w.e. (ΔE_μ = 3.0 GeV), **4** for 7 m w.e. (ΔE_μ = 4.0 GeV), **5** for 20 m w.e. (ΔE_μ = 8.5 GeV), **6** for 40 m w.e. (ΔE_μ = 13 GeV), **7** for 60 m w.e. (ΔE_μ = 18 GeV), **8** for 100 m w.e. (ΔE_μ = 32 GeV), **9** for 200 m w.e. (ΔE_μ = 70 GeV), **10** for 500 m w.e. (ΔE_μ = 160 GeV), **11** for 1000 m w.e. (ΔE_μ = 400 GeV), **12** for the depth 2000 m w.e. (ΔE_μ = 1300 GeV). According to Dorman (M1963b).

The considered above coupling functions are for underground vertical muon intensity. Underground muon telescope inclined to the some zenith angle θ at the depth characterized by minimal detected muon energy ΔE_μ in vertical direction (including atmospheric absorption) will have the coupling function $W(R,\Delta E_\mu,\theta)$ which can be approximately derived from coupling function for vertical direction:

$$W(R,\Delta E_\mu,\theta)=W(R,\Delta E_\mu/\cos\theta). \qquad (3.4.16)$$

3.4.4. Coupling functions for EAS

The method considered in Sections 3.4.1 and 3.4.2 is inapplicable in this case, since extensive air showers (EAS) are due to primary particles of such high energies that the Earth's magnetic field exerts no substantial influence on them. We must find, in essence, the probability of recording, by a given EAS installation, of showers formed by primary particles of energy E, and its dependence on E. The wanted coupling functions will then be given by the normalization of this probability.

Here we will consider two cases, detectors located close together (the distance between them being $d \le 10$ m) and detectors spaced at considerable distances D (some tens, or hundreds, or thousands of meters). In the former case, we may neglect the dependence of the probability of recording of the shower on the value of d, but in the latter case the dependence on the distance between the detectors D will be substantial.

Closely spaced detectors ($d \le 10$ m). If the spatial divergence of the electrons of one pair in the electron-nuclear cascade is much more than the mean distance between the particles in the shower (which is always the case, except for showers of very low density), then we may consider that the trajectories of the particles are distributed independently in space. In this case, on passage of a shower of density ρ (mean number of particles per m^2) the probability that not a single particle will pass through detector with effective surface σ (in m^2) will be $\exp(-\rho\sigma)$. The probability of at least one particle impinging will be

$$\omega(r, N, h_o, \sigma) = 1 - \exp(-\rho(r, N, h_o)\sigma), \tag{3.4.17}$$

where r is the distance from the EAS axis, N is the total number of particles in EAS, and h_o is the level of observations.

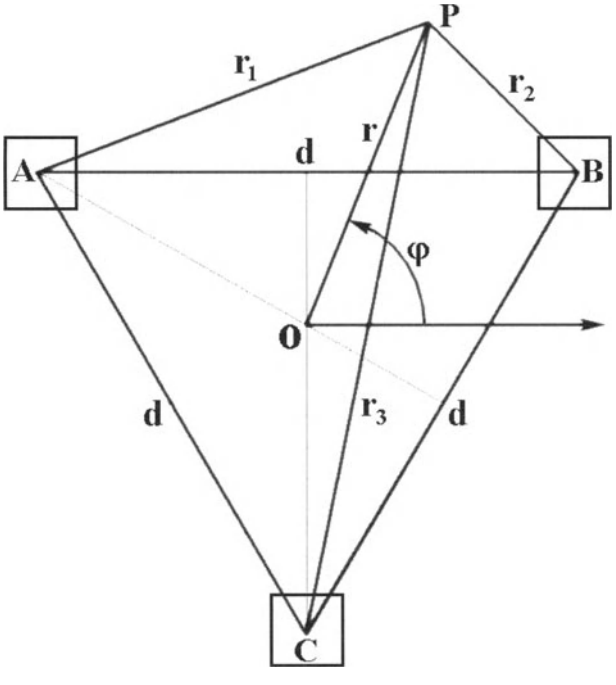

Consider a local installation consisting of, e.g., three detectors 1 at point A, 2 at point B, and 3 at point C with the equal effective surfaces σ on the equal distances d one from other (Fig. 3.4.6).

Fig. 3.4.6. Local elementary installation for recording EAS: A, B and C – detectors. By point P is shown some axis of EAS.

Let the axis of the shower pass through the point P (characterized by the polar coordinates r and φ; for center of the system of coordinates we choose the center of triangle ABC and φ is calculated from the line parallel AB in counterclockwise direction). It is easy to see that the point P of the EAS axis will be located at the following distances from the respective detectors:

$$r_1 = PA = \left[\left(r\cos\varphi + \frac{d}{2}\right)^2 + \left(r\sin\varphi - \frac{d}{2\sqrt{3}}\right)^2\right]^{1/2}, \tag{3.4.18}$$

$$r_2 = PB = \left[\left(\frac{d}{2} - r\cos\varphi\right)^2 + \left(r\sin\varphi - \frac{d}{2\sqrt{3}}\right)^2\right]^{1/2}, \tag{3.4.19}$$

$$r_3 = PC = \left[(r\cos\varphi)^2 + \left(r\sin\varphi + \frac{d}{\sqrt{3}}\right)^2\right]^{1/2}. \tag{3.4.20}$$

The density at points A, B, and C will be $\rho(r_1, N, h_o)$, $\rho(r_2, N, h_o)$, and $\rho(r_3, N, h_o)$, respectively. According to Dobrotin (M1954), Zatsepin (1954), Khristiansen (M1975), Murzin (M1988), $\rho(r, N, h_o)$ may be represented in the form

$$\rho(r, N, h_o) = u(r, h_o)N, \tag{3.4.21}$$

where N is the total number of particles in the shower at a given level, and the function $u(r, h_o)$, satisfying the normalization condition

$$2\pi \int_0^\infty u(r, h_o) r dr = 1, \tag{3.4.22}$$

has the form

$$u(r, h_o) = \begin{cases} a(h_o) r^{-1} \exp(-r/r_o(h_o)) & \text{if} \quad r < r_o(h_o), \\ b(h_o) r^{-2.6} & \text{if} \quad r \geq r_o(h_o). \end{cases} \tag{3.4.23}$$

Here $r_o(h_o)$ is the effective radius of the shower, depending on the pressure at the level of observation. Thus, at the level of the mountains ($h_o \approx 700$ mb), $r_o \approx 80$ m while at sea level ($h_o \approx 1000$ mb), $r_o \approx 55$ m. The coefficients $a(h_o)$ and $b(h_o)$ are determined from the condition of normalizing Eq. 3.4.22 and of tie-in of the function $u(r, h_o)$ at the point $r = r_o$:

$$a(h_o)=e(2\pi(e-1+1/0.6))^{-1}(r_o(h_o))^{-1}=0.1278\times(r_o(h_o))^{-1};$$
$$b(h_o)=(2\pi(e-1+1/0.6))^{-1}(r_o(h_o))^{0.6}=0.04702\times(r_o(h_o))^{0.6}. \quad (3.4.24)$$

From Eq. 3.4.24 for the level of the mountains ($h_o \approx 700$ mb, $r_o \approx 80$ m) we obtain $a(h_o)=1.60\times10^{-3}$ m^{-1}, $b(h_o)=0.652$ m$^{0.6}$, and for sea level ($h_o \approx 1000$ mb, $r_o \approx 55$ m) $a(h_o)=2.32\times10^{-3}$ m^{-1}, $b(h_o)=0.521$ m$^{0.6}$.

The probability that all three detectors *A*, *B* and *C* will be actuated by such a shower with axis at point *r*,φ, taking Eq. 3.4.17–3.4.24 will be (it is here assumed that the efficiency of the detectors is equal to 1, i.e., that detector is actuated on the passage of as little as one particle through it),

$$\Omega(r,\varphi,N,h_o,\sigma)=\omega(r_1,N,h_o,\sigma)\omega(r_2,N,h_o,\sigma)\omega(r_3,N,h_o,\sigma)$$
$$=(1-\exp(-u(r_1,h_o)N\sigma))(1-\exp(-u(r_2,h_o)N\sigma))(1-\exp(-u(r_3,h_o)N\sigma)), \quad (3.4.25)$$

where r_1, r_2, r_3 are determined by Eq. 3.4.18–3.4.20, and $u(r,h_o)$ is determined by Eq. 3.4.23–3.4.24. The integral multiplicity $m_{\text{loc}}(N,h_o,\sigma)$ for the EAS installation shown in Fig. 3.4.6 will be determined by the probability that the installation will record a shower with a number of particles *N*, whose axis may pass in any point of the plane. It will be found by integration of Eq. 3.4.24 over the entire plane:

$$m_{\text{loc}}(N,h_o,\sigma)=\int_0^{2\pi}d\varphi\int_0^{\infty}\Omega(r,\varphi,N,h_o,\sigma)rdr=\int_0^{2\pi}d\varphi\int_0^{\infty}\prod_{i=1}^{3}(1-\exp(-u(r_i,h_o)N\sigma))rdr$$
$$=\int_0^{2\pi}d\varphi\int_0^{10d}\prod_{i=1}^{3}(1-\exp(-u(r_i,h_o)N\sigma))rdr+2\pi\int_{10d}^{\infty}(1-\exp(-u(r,h_o)N\sigma))^3rdr, \quad (3.4.26)$$

where we take into account that for $r \geq 10d$ with a good accuracy $r_1 \approx r_2 \approx r_3 \approx r$.

The differential particle-number spectrum of the showers may be represented in the form:

$$D(N)\propto N^{-(\kappa+1)}, \quad (3.4.27)$$

where κ is a constant varying extremely little with variations in *E* (as *E* varies from 10^5 GeV to 10^9 GeV, κ varies only from 1.4 to 2.1). Taking into account of Eq. 3.4.26 and Eq. 3.4.27 we obtain the following expression for the coupling function of EAS local installation (in dependence on $x=N\sigma$):

$$W_{\mathrm{loc}}(x,h_o)=Bx^{-(\kappa+1)}m_{\mathrm{loc}}(x,h_o)=Bx^{-(\kappa+1)}$$

$$\times\left\{\int_0^{2\pi}d\varphi\int_0^{10d}\prod_{i=1}^{3}(1-\exp(-u(r_i,h_o)x))rdr+2\pi\int_{10d}^{\infty}(1-\exp(-u(r,h_o)x))^3rdr\right\},\quad(3.4.28)$$

where B is a certain coefficient determined from the normalizing condition:

$$\int_0^{\infty}W_{\mathrm{loc}}(x,h_o)dx=1\,.\quad(3.4.29)$$

The function $W_{\mathrm{loc}}(N\sigma,h_o)$, found by numerical integration according Eq. (3.4.28) with counting Eq. 3.4.29 for a distances between detectors d = 3 m, is shown in Fig. 3.4.7.

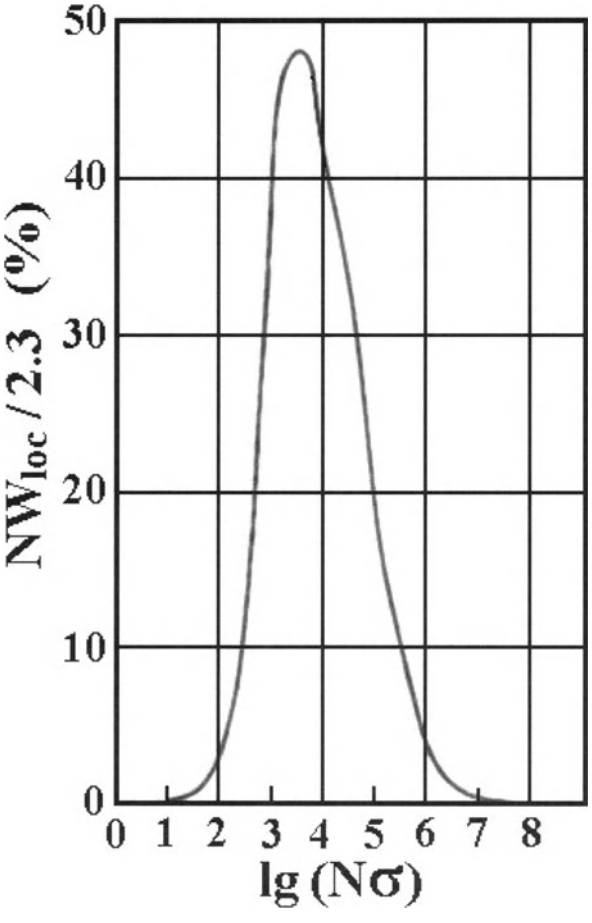

Fig. 3.4.7. Coupling function $W_{\mathrm{loc}}(N\sigma,h_o)$ for observations at sea level at κ = 1.4.

The dependence of the integral multiplicity $m_{\mathrm{loc}}(N,h_o,\sigma)$ on N may be easily converted into its dependence on primary particle energy E, if we bear in mind that, according to Dobrotin (M1954), Zatsepin (1954), Khristiansen (M1975), Murzin (M1988),

$$N = AE^s\,, \tag{3.4.30}$$

where the quantity $A \approx 0.3$ (if E is measured in GeV) is a constant coefficient, and s is a weakly varying parameter characterizing the degree of development of the shower (up to maximum of the shower $s < 1$, at the maximum $s = 1$, after the maximum $s > 1$; at sea level $s \approx 1.2$). By means of Eq. (3.4.30), the coupling function $W_{\mathrm{loc}}(N\sigma,h_o)$ can easily be converted into a dependence on primary particle energy E. Figure 3.4.8 represents the coupling function $W_{\mathrm{loc}}(E\sigma,h_o)$ for the same EAS installation at sea level, which was shown in Fig. 3.4.6.

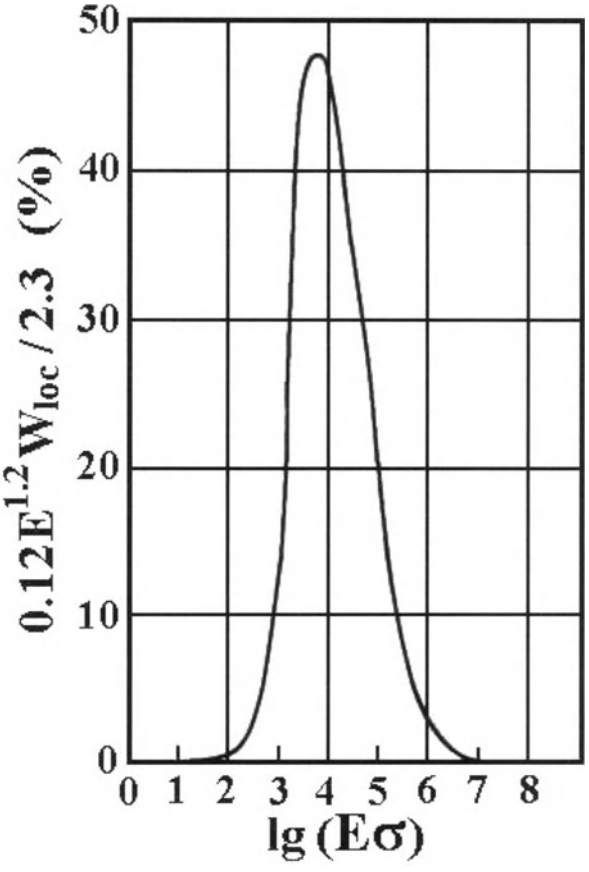

Fig.3.4.8. The coupling function $W_{\mathrm{loc}}(E\sigma,h_o)$ for sea level at $\kappa = 1.4$ and $s = 1.2$; primary particle energy E in GeV (in the abscissa axis values E must be multiplied on factor 0.3), effective surface of each detector σ in m^2. According to Dorman (M1957).

Installation with detectors spaced at considerable distances. The coupling functions for any desired geometry of the installation can be found in an entirely analogous way. In particular, for the installation shown in Fig.3.4.9, coincidences were selected between two local installations, separated from each other by a distance of D meters ($D >> r_o >> d$), where d is the distance between detectors in each local installation.

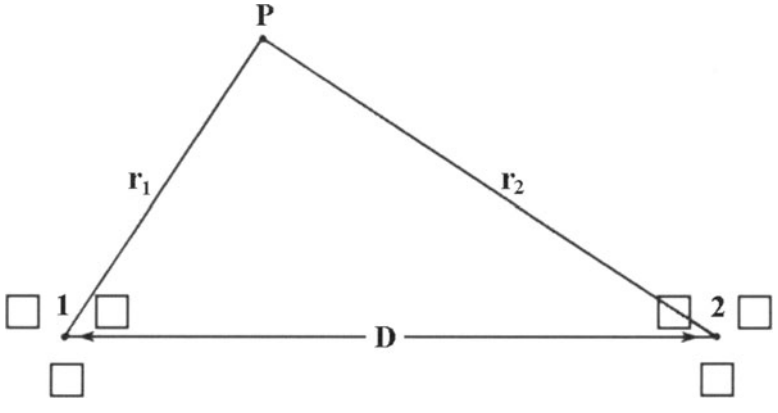

Fig.3.4.9. Installation with detectors spaced at considerable distances. Point P shows the axis of EAS.

In this case instead of Eq. 3.4.28 we obtain

$$W_{\mathrm{EAS}}(D,N\sigma,h_o)=2\pi B(N\sigma)^{-(\kappa+1)}\int_0^{\infty}\prod_{i=1}^{2}(1-\exp(-u(r_i,h_o)N\sigma))^3 r dr\,, \tag{3.4.31}$$

where $x=N\sigma$, r_1 and r_2 are distances from the EAS axis P to the centers of local installations 1 and 2 (see Fig. 3.4.9); constant B is determined by normalization condition

$$\int_0^{\infty} W_{\mathrm{EAS}}(D,x,h_o)dx=1\,. \tag{3.4.32}$$

where $x=N\sigma$. The dependence of the integral multiplicity $W_{\mathrm{EAS}}(D,N\sigma,h_o)$ on $N\sigma$ may be easily converted into its dependence on $E\sigma$ by using Eq. 3.4.30. The coupling functions $W_{\mathrm{EAS}}(D,E\sigma,h_o)$ for various values of D are given in Fig. 3.4.10.

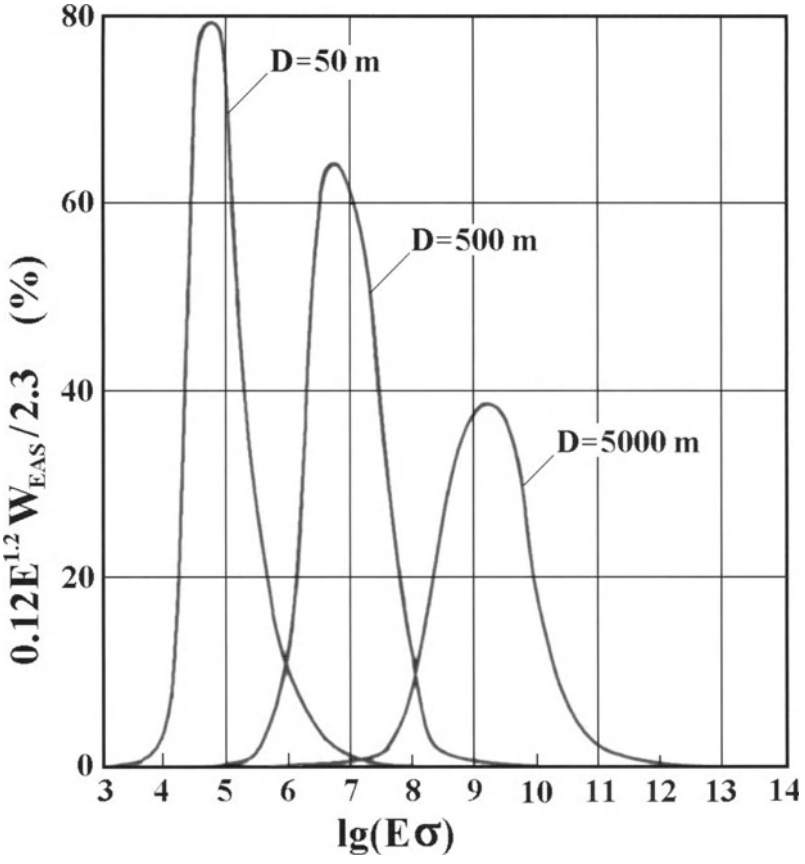

Fig. 3.4.10. Coupling functions $W_{\mathrm{EAS}}(D, E\sigma, h_o)$ for observations at sea level by installation shown in Fig. 3.4.9 at different values of D (primary particle energy in GeV, effective surface of detectors σ in m^2). According to Dorman (M1957).

3.5. Analytical calculations of integral multiplicities and coupling functions for CR total neutron component

3.5.1. Calculations of integral multiplicities and coupling functions for neutron component using the method of discontinuous Markov processes

The great difficulties encountered in the determination of the integral multiplicity for the neutron component by directly solving the equations of the hadronic cascade in the Earth's atmosphere stimulated searches for another method that leads to the final result without having to go through the intermediate details of cascade development. This can be realized by using the formalism of discontinuous Markov processes including non-ordinariness of random events in the hadronic cascades. In this case the numerical integral characteristics of the process are determined from the comparison with the data on the altitude dependence, latitudinal distribution, energy spectrum, and

other integral effects of the neutron component. A portion of the results obtained which can be compared with available experimental data shows a good agreement with experiment. It is well known that the data on the spatial and energy distributions of secondary neutrons can be obtained from solving the transport equation. This equation may be accurately solved only in a few simple cases, sometimes involving considerable mathematical difficulties. In weakly absorbing media neutron transport can be described by the diffusion approximation (Hess et al., 1961; Newkirk, 1963; Lingenfelter, 1963a,b). This theory gives accurate results in the extreme case when $\sigma_a/\sigma_t \to 0$, where σ_a is the absorption cross section, and σ_t is the total interaction cross-section. For the atmospheric neutrons this relation is invalid, and therefore various approximations are usually used when solving the transfer equation (Bekurz and Wirtz, M1968).

To solve the problem of neutrons transfer in the atmosphere the work of Dorman and Rishe (1973) employs the ideas about the collective behavior of multiple neutrons in the generalized state determined by the energy range $(E_o, \Delta E)$ where E_o is the kinetic energy of a primary proton, and ΔE is the lower energy limit of secondary neutrons. Introduction of the generalized states including the neutron component energy portion permits multiple neutrons to be considered as a single ensemble irrespective of the generation number, the number of multiple neutrons (generated in an elementary interaction event) and their angular distribution. This significantly simplifies the solution of the problem as a whole. The problems associated with the random character of the neutron distribution over the generalized state range determined by its limits and atmospheric depth are solved in terms of the non-ordinary Markov processes of the type of production (for the system state continuum).

The equation for the intensity of neutrons with energies $>\Delta E$ (in GeV) at an atmospheric depth h (g/cm^2) at the observation point with the geomagnetic cut off energy for primary protons E_C was derived on the assumption that: (1) the primary CR are isotropic over the upper hemisphere; (2) the upper atmospheric surface is flat; and (3) the geomagnetic threshold gradient is zero within the nucleon cascade section by a plane parallel to the atmospheric boundary. The last assumption is equivalent to the statement that within the above mentioned limits the primary CR flux is homogeneous and isotropic throughout the radiating surface located at the upper atmospheric boundary. In this case we get for the particle flux of the i type with energy $>\Delta E$ at altitude h with geomagnetic threshold E_C produced by the j type of primaries:

$$N_i(E_c,\Delta E,h)=\int_{E_c}^{\infty} D(E_o)\left[\exp\left(-\frac{h}{l_i(E_o)}\right)\right]dE_o+\sum_j\left\{\int_{E_c}^{\infty} D_j(E_o)\left[\exp\left(-\frac{h}{L^*_{ij}(E_o,\Delta E)}\right)\right.\right.$$
$$\left.+\frac{h}{L^*_{ij}(E_o,\Delta E)}E_i\left(-\frac{h}{L^*_{ij}(E_o,\Delta E)}\right)-\exp\left(-\frac{h}{l_j(E_o)}\right)-\frac{h}{l_j(E_o)}E_i\left(-\frac{h}{l_j(E_o)}\right)\right]$$
$$\left.\times\left[L_i\left(\frac{eE_o}{\Delta E}\right)-C\right]\times\frac{h}{el_j(E_o)}\times\frac{S_{ij}(h,E_o)}{1+(n_i/n_j)}\times\frac{n_i}{n_j}dE_o\right\}. \qquad (3.5.1)$$

Examined below will be the secondary neutrons associated genetically with the primary CR protons. Therefore the Eq. 3.5.1 for a single primary component is to be rewritten in the form

$$N(E_c,\Delta E,h)=\times\int_{E_c}^{\infty}\frac{S_{np}(h,E_o)}{1+(n/p)}\times\frac{h}{el(E_o)}\times\left[L_i\left(\frac{eE_o}{\Delta E}\right)-C\right]\times P(E_o,\Delta E,h)D(E_o)dE_o \ , \quad (3.5.2)$$

where

$$P(E_o,\Delta E,h)=\exp\left(-\frac{h}{L^*(E_o,\Delta E)}\right)+\frac{h}{L^*(E_o,\Delta E)}E_i\left(-\frac{h}{L^*(E_o,\Delta E)}\right)$$
$$-\exp\left(-\frac{h}{l(E_o)}\right)-\frac{h}{l(E_o)}E_i\left(-\frac{h}{l(E_o)}\right) \quad (3.5.3)$$

determines the probability that at a depth h the energies of the multiple neutrons will be within the range $(E_o,\Delta E)$. In Eq. 3.5.3 $l(E_o)$ is the pre-interaction mean path of a primary proton in air, the value $L^*(E_o,\Delta E)$ is the mean path of a generalized-state proton in the direction of the primary proton motion:

$$L^*(E_o,\Delta E)=l_o\sqrt{\frac{E_o}{E_o-\Delta E}\ln\left(\frac{E_o}{\Delta E}\right)} \ , \quad (3.5.4)$$

where $l_o=l(\Delta E)$ determines the mean free path of a neutron with energy ΔE in air:

$$l_o=\frac{mA}{\pi(r_o+\lambda)^2} \ , \quad (3.5.5)$$

A is the mean atomic weight of air ($A\approx 14.4$), m is the neutron rest mass,

$$r_o=\left(1.37A^{1/3}+0.5\right)\left[1-\exp\left(-0.49A^{1/2}\right)\right]\times 10^{-13} \text{ cm} \quad (3.5.6)$$

is the radius of the light atom nuclei according to Mukhin (M1963), and

$$\lambda=4.5\times 10^{-13}\Delta E^{-1/2} \text{ cm} \quad (3.5.7)$$

is the Broglie length of neutron wave (in Eq. 3.5.7 ΔE is in MeV). Inclusion of ionization loss of primary protons is of significance at $E\le 10$ GeV. For direct calculations of Dorman and Rishe (1973), a graphical representation of the specific ionization loss of protons in the air calculated by the Bethe formula was used. The function n/p determines the neutron to proton number ratio:

$$\frac{n(E_o,h)}{p(E_o,h)}=\frac{1+\rho_o+(\rho_o-1)\exp\left(-\frac{2h}{l(E_o)}\left\langle\eta\beta^{\gamma-1}\right\rangle\right)}{1+\rho_o-(\rho_o-1)\exp\left(-\frac{2h}{l(E_o)}\left\langle\eta\beta^{\gamma-1}\right\rangle\right)}, \tag{3.5.8}$$

where $\rho_o = n/p$ for the primary CR (in quiet conditions $\rho_o = 0$, but during large solar flares when solar neutrons can be generated, $\rho_o > 0$), γ is the exponent of the primary differential energy spectrum, $l(E_o)$ is the nucleon interaction path, β is the coefficient of elasticity, η is the charge exchange coefficient. The primary proton energy portion lost for the nuclear-active component is determined by the function $S_{np}(h,E_o)$ according to Grigorov et al. (1959).

The latitudinal effect, altitude dependence, and neutron spectrum at the various altitudes were preliminarily calculated. Then the constants forming part of Eq. 3.5.2 were determined by comparing with the experimental data. After that Eq. 3.5.2 was used to calculate the integral multiplicities and the coupling coefficients for the neutron component. The results are shown in Fig. 3.5.1 and Fig. 3.5.2.

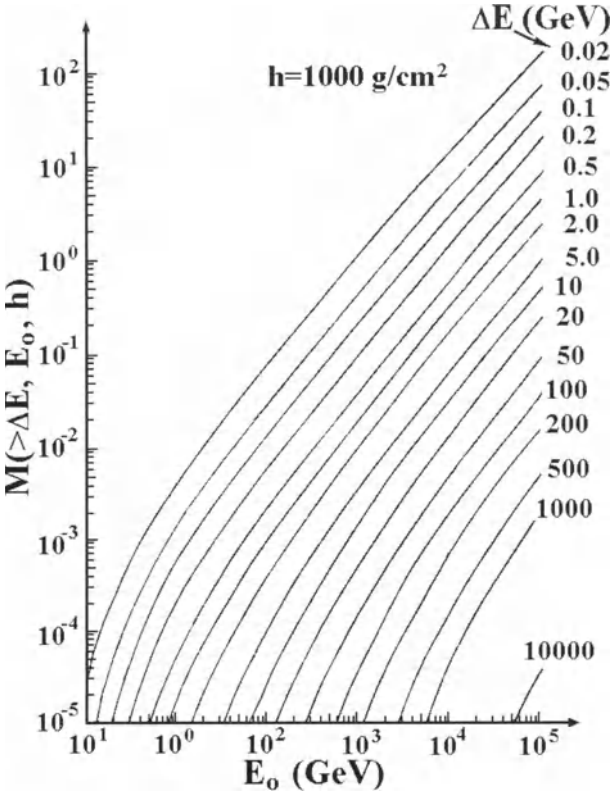

Fig. 3.5.1. Integral multiplicities for neutron component at sea level for the various ΔE (in GeV). According to Dorman and Rishe (1973).

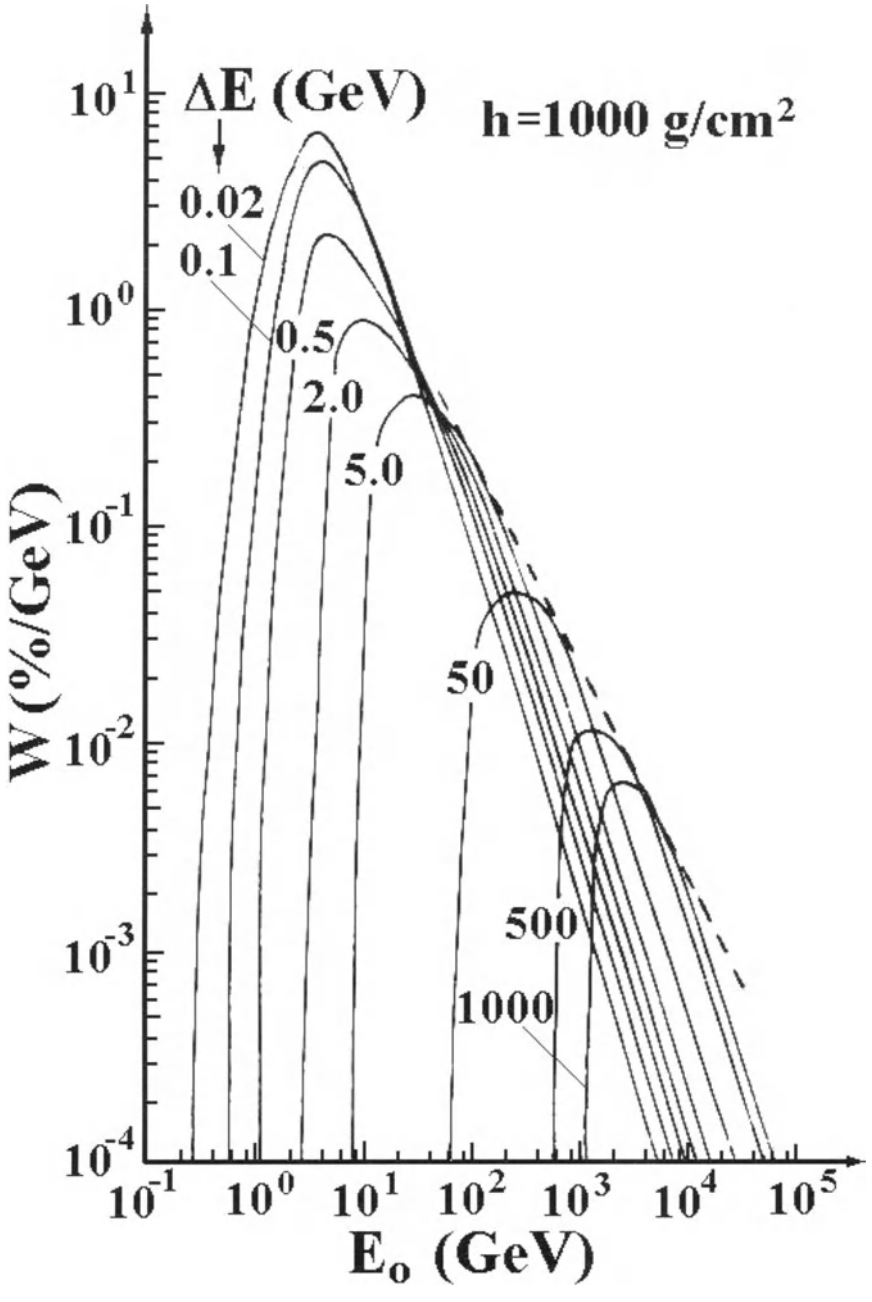

Fig.3.5.2. Coupling coefficients for the neutron component at sea level for various values of ΔE (in GeV). According to Dorman and Rishe (1973).

Comparison between the coupling coefficients thus obtained and those found on the basis of latitudinal effects has shown a good agreement, substantiating the reliability of the results presented in Fig. 3.5.1 and Fig. 3.5.2.

3.5.2. Calculations of integral multiplicity, coupling and response functions for total neutron component by consideration of hadronic cascade in the atmosphere

According to Dorman and Yanke (1981), the differential spectrum of the neutron component $N(E_o,E,h,\theta_o)$ at altitude h from one primary particle with energy E_o arriving at the atmosphere boundary at zenith angle θ_o will be determined by 'high-energy nucleons' $N_n(E_o,E,h,\theta_o)$ and by δ–nucleons $N_\delta(E_o,E,h,\theta_o)$ in elementary act:

$$N(E_o,E,h,\theta_o)=N_n(E_o,E,h,\theta_o)+N_\delta(E_o,E,h,\theta_o), \tag{3.5.9}$$

where $N_n(E_o,E,h,\theta_o)$ and $N_\delta(E_o,E,h,\theta_o)$ can be determined by the system of equations:

$$\frac{\partial N_n(E_o,E,h,\theta_o)}{\partial h}=-\frac{N_n(E_o,E,h,\theta_o)}{\Lambda_n(E)\cos\theta_o}+\frac{\partial}{\partial E}\left(\frac{\beta(E)}{\cos\theta_o}N_n(E_o,E,h,\theta_o)\right)$$
$$+\int_E^{E_o}\frac{N_n(E_o,E',h,\theta_o)}{\Lambda_n(E')\cos\theta_o}f_{nn}(E',E)\,dE', \tag{3.5.10}$$

$$\frac{\partial N_\delta(E_o,E,h,\theta_o)}{\partial h}=-\frac{N_\delta(E_o,E,h,\theta_o)}{\Lambda_\delta(E)\cos\theta_o}+\frac{\partial}{\partial E}\left(\frac{\beta(E)}{\cos\theta_o}N_\delta(E_o,E,h,\theta_o)\right)$$
$$+\int_E^{E_o}\frac{N_n(E_o,E',h,\theta_o)}{\Lambda_n(E')\cos\theta_o}f_{n\delta}(E',E)\,dE'. \tag{3.5.11}$$

Here $f_{nn}(E',E)$ is the secondary nucleon spectrum resultant from nuclear–atom interaction of nucleon with energy E' (in accordance with Gaisser (1976), the inelastic coefficient is about 0.5), $f_{n\delta}(E',E)$ is the same for δ–nucleons, and $\beta(E)$ is the energy loss. After determining $N(E_o,E,h,\theta_o)$ according to Eq. 3.5.9 it is easy to calculate integral multiplicity for neutron monitor according to expression:

$$M_n(E_o,\theta_o,h)=\int N(E_o,E,\theta_o,h)P(E)dE\ , \tag{3.5.12}$$

where $P(E)$ is the differential sensitivity of the detector (the probability of detecting neutron of energy E). The results of calculations of $M_n(E_o,\theta_o,h)$ with $P(E)$ according to Dorman et al., 1981 (see below, Section 3.6), are shown in Figure 3.5.3 for levels of observation 1030, 760, 490 and 40 g/cm^2 and for zenith angle θ_o = 0° as a function of the primary particle energy of E_o from 1 GeV up to 10^4 GeV. For sea level 'high

energy nucleons' $N_n(E_o,E,h,\theta_o)$ and δ–nucleons $N_\delta(E_o,E,h,\theta_o)$ are also separately shown.

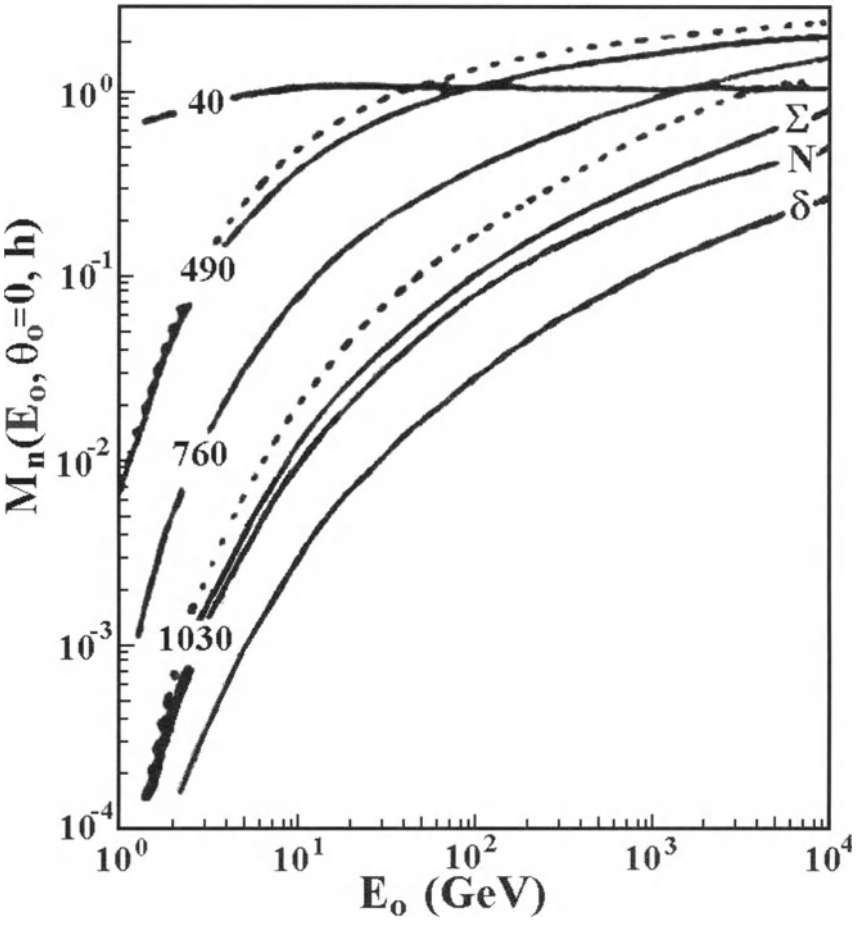

Fig. 3.5.3. Results of calculations of integral multiplicities for NM-IQSY total neutron component for levels of observation 1030, 760, 490 and 40 g/cm^2 for vertical arrival primary CR as a function of primary particle energy E_o from 1 GeV up to 10^4 GeV at inelastic coefficient 0.5 dashed curves correspond to results at inelastic coefficient 0.45). For sea level 'high energy nucleons' and δ–nucleons are shown separately: the curves with *N* and δ, respectively. According to Dorman and Yanke (1981).

Fig. 3.5.4 shows the dependence of $M_n(E_o,\theta_o,h)$ on *h* in the interval from 0 (boundary of the atmosphere) up to sea level 1030 g.cm^{-2} for different primary particle energy E_o from E_o = 1 GeV up to $E_o = 10^4$ GeV; for E_o = 10 GeV are shown also the 'high energy nucleons' $N_n(E_o,E,h,\theta_o)$ and δ–nucleons $N_\delta(E_o,E,h,\theta_o)$ components separately.

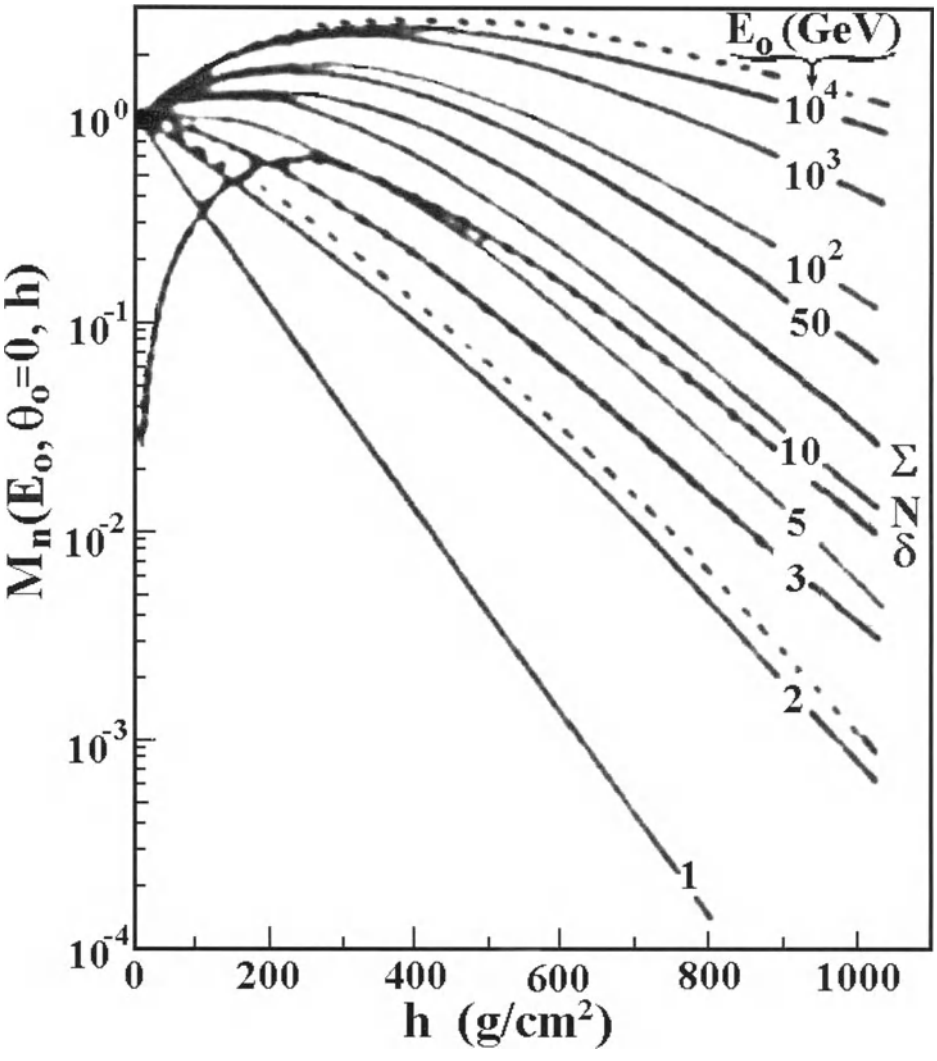

Fig. 3.5.4. The dependence of integral multiplicities for NM-IQSY total neutron component from h in the interval from 0 (boundary of the atmosphere) up to the sea level 1030 g/cm^2 for different primary energy E_o from E_o = 1 GeV up to E_o = 10^4 GeV. For E_o = 10 GeV are shown also 'high energy nucleons' $N_n(E_o,E,h,\theta_o)$ and δ–nucleons $N_\delta(E_o,E,h,\theta_o)$ separately: curves N and δ, respectively. According to Dorman and Yanke (1981).

In Fig. 3.5.5 are shown values $M_n(E_o,\theta_o,h)$ for sea level in dependence of zenith angle θ_o for different primary energy E_o from E_o = 1 GeV up to E_o = 10^4 GeV.

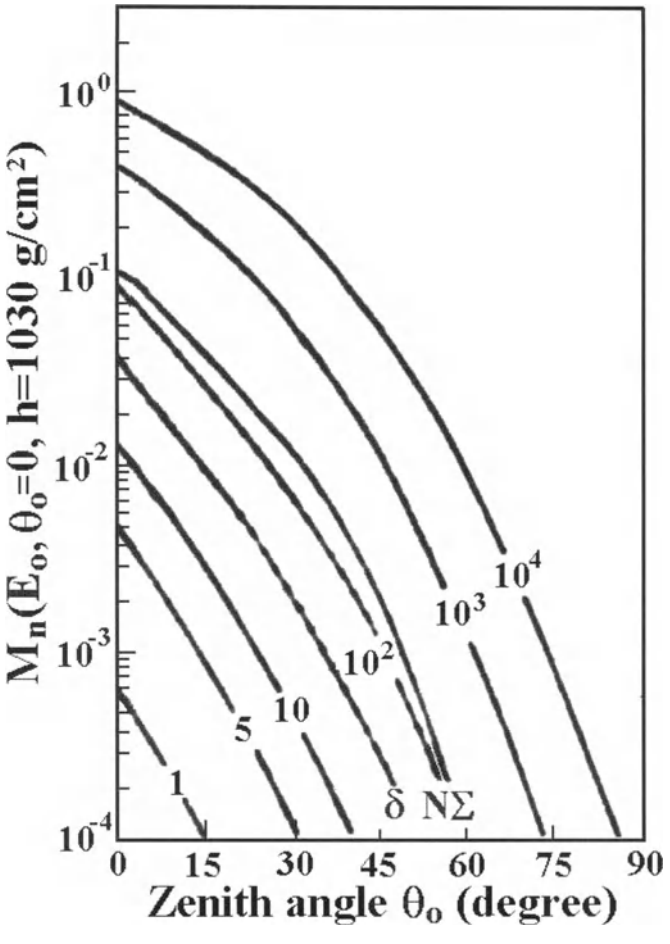

Fig. 3.5.5. The dependence of integral multiplicities for NM-IQSY total neutron component for sea level from zenith angle θ_o for different primary energy E_o from E_o = 1 GeV up to $E_o = 10^4$ GeV. According to Dorman and Yanke (1981).

From the calculated integral multiplicities we can determine the expected NM counting rate $I_n(h,R_c)$, the coupling function $W(h,R,R_c)$, the relative response function $F(h,R,R_c)$, and the zenith distribution of neutron component $D_n(\theta)$:

$$I_n(h,R_c) = \int_{R_{\min}}^{\infty} dR \int_0^{\pi/2} S(\theta) G(R,\theta) \sum_Z M_Z(R,h,\theta) D_Z(R) \sin\theta d\theta, \qquad (3.5.12)$$

$$W(h,R,R_c) = \int_0^{\pi/2} S(\theta) G(R,\theta) \sum_Z \frac{M_Z(R,h,\theta) D_Z(R)}{I_n(h,R_c)} \sin\theta d\theta, \qquad (3.5.13)$$

$$F(h,R,R_c)=\int_0^R W(h,R,R_c)dR \Big/ \int_{R_c}^{\infty} W(h,R,R_c)dR\,, \tag{3.5.14}$$

$$D_n(\theta)=\int_{R_{\min}}^{\infty} S(\theta)G(R,\theta)\sum_Z M_Z(R,h,\theta)D_Z(R)\sin\theta dR\,, \tag{3.5.15}$$

where $S(\theta)$ is the effective surface of NM in direction θ, $G(R,\theta)$ is the penumbra function (see Section 3.3). For differential energy spectra of primary CR it is supposed that at high rigidities $D_Z(R)\propto R^{-2.7}$.

The coupling functions found for different NM-IQSY stations are given in Table 3.5.1 for low latitude stations and in Table 3.5.2 for high and middle latitude stations. The penumbra function was accounted for (started from $R_{\min}$; see above, Section 3.3). Calculations were made for minimum and maximum solar activity (upper and low lines, correspondingly).

Table 3.5.1. Coupling functions for low latitude mountain NM (in %/GV) for periods minimum and maximum of solar activity. According to Dorman and Yanke (1981).

Station	h, mb	R_c, GV	$R_{\min}$, GV	SA	R, GV						
					9	10	11	13	15	20	50
Mt. Norikura	720	11.4	8.51	min	0.02	0.86	2.56	4.30	4.12	2.80	0.569
				max	0.01	0.74	2.23	3.86	3.82	2.76	0.601
Chacaltaya	541	13.1	9.54	min		0.01	0.73	3.25	4.22	3.38	0.591
				max		0.01	0.63	2.90	3.86	3.32	0.622
Huancayo	690	13.5	9.77	min			0.26	2.50	3.82	3.34	0.666
				max			0.22	2.23	3.50	3.26	0.656

Table 3.5.2. Coupling functions for high and middle latitude NM (in %/GV) for periods minimum and maximum of solar activity. In the second row are shown results of calculation polar coupling function for observations at sea level. According to Dorman and Yanke (1981).

Station	h, mb	R_c, GV	$R_{\min}$, GV	SA	R, GV						
					1	2	3	4	5	7	10
Polar coup. f.	1030	0	0	min	1.42	3.96	4.73	5.12	4.90	3.89	3.04
				max	0.87	2.88	3.55	4.00	4.06	3.44	2.89
Vostok	620	0	0	min	4.14	8.12	8.42	8.13	7.05	4.88	3.32
				max	2.73	6.32	6.73	6.79	6.35	4.63	3.39
South Pole	680	0.11	0	min	3.55	7.44	7.90	7.79	6.86	4.86	3.38
				max	2.32	5.75	6.28	6.45	6.04	4.57	3.43
Calgary	883	1.09	1.03	min		5.16	5.90	6.17	5.73	4.36	3.26
				max		3.81	4.49	4.09	4.82	3.91	3.15
Climax	672	3.03	2.78	min			3.82	9.11	8.02	5.69	3.95
				max			2.91	7.24	6.77	5.13	3.85
Jungfraujoch	642	4.48	3.82	min				0.09	9.02	6.55	4.48
				max				0.07	7.38	5.72	4.23
Zugspitze	706	4.24	3.71	min				1.31	8.39	6.02	4.23
				max				1.01	6.86	5.26	3.99
Pic-du-Midi	720	5.36	4.48	min					1.30	6.78	4.77
				max					1.04	5.78	4.38

Fig. 3.5.6 shows the coupling and response functions (calculated according to Eq. 3.5.13 and Eq. 3.5.14, respectively) for observations by NM-IQSY at sea level in comparison with the functions obtained from latitude surveys.

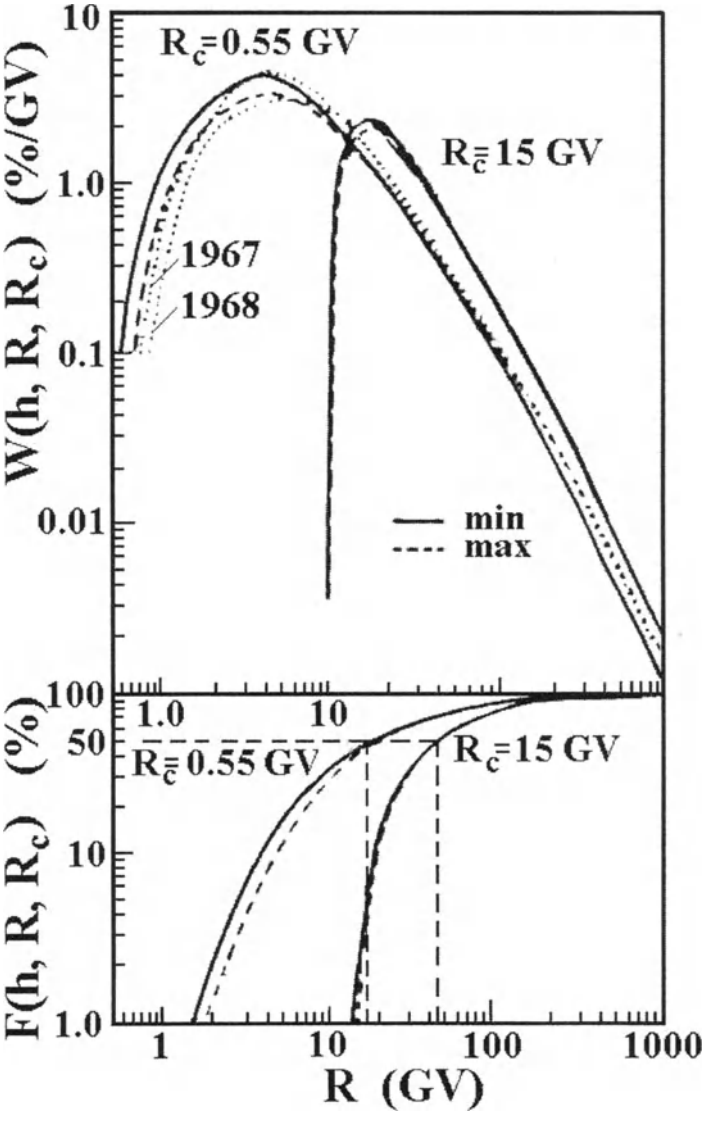

Fig. 3.5.6. The expected coupling functions (the top panel) and the response functions (bottom panel) for NM-IQSY total neutron component at sea level for minimum and maximum of solar activity (full and dash curves, respectively). Also shown are coupling functions determined from latitude surveys in 1967 and 1968 according to Aleksanyan et al. (1979). The bottom panel demonstrates the determination of median rigidities. The coupling and response functions are shown for high latitude NM (R_C = 0.55 GV) and near equatorial NM (R_C = 14.98 GV). According to Dorman and Yanke (1981).

Results of calculations of the zenith angle sensitivity of NM-IQSY according to Eq. 3.5.15 in comparison with the zenith sensitivity of muon telescopes that are vertical cubic, semi-cubic, and inclined at 45° are shown in Fig. 3.5.7.

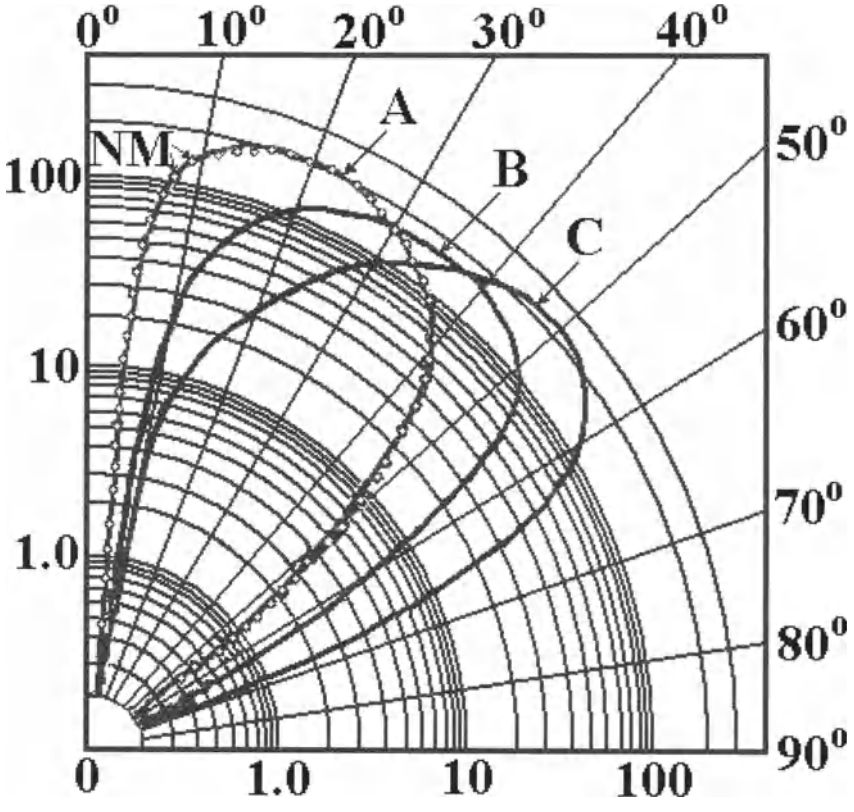

Fig. 3.5.7. Zenith angle sensitivity diagram of a sea level NM-IQSY (dotted curve) in comparison with the zenith directivity diagrams of muon telescopes (full curves: *A* – vertical cubic, *B* – vertical semi-cubic, **C** - inclined at 45°). According to Dorman and Yanke (1981).

Dorman and Yanke (1981) estimated the accuracy of the results obtained for integral multiplicities by the calculation accuracy (about 1%) and by the errors owed to uncertainties in some parameters (6–8%); the errors may also be owed to the choice of the energy sensitivity function $P(E)$ and to the selection of the particular model of CR interactions and propagation in the atmosphere. Therefore in order to check the results, Dorman and Yanke (1981) calculated the expected partial and total barometric coefficients: Chapter 9 describes the partial barometric coefficient as well as total barometric coefficients for minimum and maximum of solar activity as a function of the cut off rigidity, on the basis of results described here. It is shown that they are in good agreement with obtained from observations (see Section 9.10.3 for details). Let us note that the inclusion of the chemical composition of primary CR in calculations gives rise to a 18% shift of the coupling function maximum towards higher rigidities in comparison with calculations including only primary protons.

3.6. Calculations of integral multiplicities and coupling functions for multiple neutrons in NM-IQSY

According to Dorman et al. (1981) the integral multiplicity $M_{nm}(E_O,\theta_O,h)$ for m multiple neutrons in the NM-IQSY will be determined by the same Eq. 3.5.12, but instead of the function $P(E)$, one has to use $P_m(E)$, which denotes the probability that the incident neutron with energy E will be detected as m multiple neutron:

$$M_{nm}(E_O,\theta_O,h)=\int N(E_O,E,\theta_O,h)P_m(E)dE \quad , \tag{3.6.1}$$

where $N(E_o,E,h,\theta_o)$ was determined in Dorman and Yanke (1981) and is the same as in Section 3.5.2, Eq. 3.5.9–3.5.11. The function $P_m(E)$ according to Dorman et al. (1981) is determined by the expression:

$$P_m(E)=\sum_{k=m}^{\infty}\int_0^E dE'\int_0^{E'}d\varepsilon H_k(E')D(E',\varepsilon)G(E,E')B_k^m(\varepsilon) \ . \tag{3.6.2}$$

Here E' is the excitation energy of the residual nucleus in NM from interaction with incident neutron with energy E; the distribution of E' *vs* E is described according to Metropolis et al. (1958) and Hayakawa (M1973) by the function

$$G(E,E')=(2\pi)^{-1/2}\overline{E'}(E)\exp\left(-\frac{1}{2}\cdot\left(\frac{E'}{\overline{E'}(E)}-1\right)^2\right) , \tag{3.6.3}$$

where

$$\overline{E'}(E)=a\lg E-b \ . \tag{3.6.4}$$

In Eq. 3.6.4 $\overline{E'}(E)$ and E are in MeV, coefficients a and b are as following:

$$a=\begin{cases}69 \text{ MeV for } E\le 350 \text{ MeV}\\ 350 \text{ MeV for } 350\le E\le 1000 \text{ MeV};\\ 580 \text{ MeV for } E\ge 1000 \text{ MeV}\end{cases} \quad b=\begin{cases}61 \text{ MeV for } E\le 350 \text{ MeV}\\ 770 \text{ MeV for } 350\le E\le 1000 \text{ MeV}\\ 1460 \text{ MeV for } E\ge 1000 \text{ MeV}\end{cases} \ . \tag{3.6.5}$$

The function $H_k(E')$ determines the probability that k neutrons will evaporate from the residual nucleus excited to the energy E'. According to Dostrovsky et al. (1958) and Hayakawa (M1973), $H_k(E')$ can be approximated by the expression (E' in MeV):

$$H_k(E')=\frac{10}{k\sqrt{2\pi}}\exp\left(-50\left(\frac{k}{\bar{k}}-1\right)^2\right); \quad \bar{k}=0.6\,E' \quad \text{for Pb} \ . \tag{3.6.6}$$

The function $D(E',\varepsilon)$ determines the differential energy spectrum of evaporated neutrons with energy ε as a function of the nucleus excitation energy E'. According to Dostrovsky et al. (1958) and Hayakawa (M1973) the spectrum of evaporated neutrons is sufficiently close to the Maxwellian form:

$$D(E',\varepsilon) = 23(\varepsilon/E')\exp\left(-5\varepsilon/\sqrt{E'}\right) . \tag{3.6.7}$$

The last function in Eq. 3.6.2 $B_k^m(\varepsilon)$ determines the probability that m neutrons will be detected from k evaporated neutrons with energy ε. If the neutron deceleration in neutron monitor between evaporation and detection is disregarded, then according to Dorman et al. (1981) this function will be:

$$B_k^m(\varepsilon) = C_k^m(\Phi(\varepsilon))^m(1-\Phi(\varepsilon))^{k-m} , \tag{3.6.8}$$

where $\Phi(\varepsilon)$ determines the effectiveness of NM-IQSY to detect an evaporated neutron with energy ε (in MeV). According to Pearce and Fowler (1964), this can be approximated by expression:

$$\Phi(\varepsilon) \approx 0.079 - 0.031\times\lg\varepsilon - 0.01\times(\lg\varepsilon)^2 . \tag{3.6.9}$$

On the basis of the evaluated $P_m(E)$ for multiple neutrons it is possible to determine also $P(E)$ for the total neutron component:

$$P(E) = \sum_{m=1}^{\infty} A_m P_m(E) , \tag{3.6.10}$$

where A_m depends on the relation between dead time τ of NM electronic scheme and the lifetime T_l of neutrons in the monitor: $A_m \approx m$ for very small dead time τ and $A_m \approx 1$ for large τ. According to Carmichael (1964), for the standard NM-IQSY τ = 10 mks and T_l = 329 mks. For these parameters A_m = 1.0, 1.97, 2.91 and 3.83 for m = 1, 2, 3 and 4, respectively (Dorman et al, 1981). If, for example, τ = 100 mks, then A_m = 1.0, 1.74, 2.35 and 2.84 for m = 1, 2, 3 and 4. Results for $P_m(E)$ and $P(E)$ are shown in Fig. 3.6.1 in comparison with the results of Pakhomov and Sdobnov (1977), where the process of neutron deceleration in the monitor was taken into account. Fig. 3.6.1 shows that the neutron deceleration in the monitor is especially important at calculations of differential sensitivity $P(E)$ for small energy neutrons arriving at the monitor.

Eq. 3.6.1, together with Eq. 3.6.2–3.6.10 and $N(E_o,E,h,\theta_o)$ from Dorman and Yanke (1981) (see Section 3.5) determines the integral multiplicity $M_{nm}(E_O,\theta_O,h)$ for

m-multiple neutrons in the NM-IQSY as well as $M_n(E_O,\theta_O,h)$ for total neutron intensity. Fig. 3.6.2 shows the results of calculations of $M_{nm}(E_O,\theta_O,h)$ as well as $M_n(E_O,\theta_O,h)$ for observations at sea level, comparison with $M_{nm}(E_O,\theta_O,h)$ determined by Debrunner and Fluckiger (1971) for multiple neutrons and with $M_n(E_O,\theta_O,h)$ for total neutron component determined in Pakhomov and Sdobnov (1977). In Fig. 3.6.3 are shown obtained results for observations at level 541 *mb*. In bottoms of Figs. 3.6.2 and 3.6.3 are shown also corresponding polar coupling functions for multiple neutrons $W_{om}(h,R)$ calculated on the basis of $M_{nm}(E_O,\theta_O,h)$ at m = 1, 2, 3, 4 by Eq. 3.1.4 at $R_c = 0$ as well as polar coupling functions for total neutron intensity $W_o(h,R)$ calculated on the basis of $M_n(E_O,\theta_O,h)$.

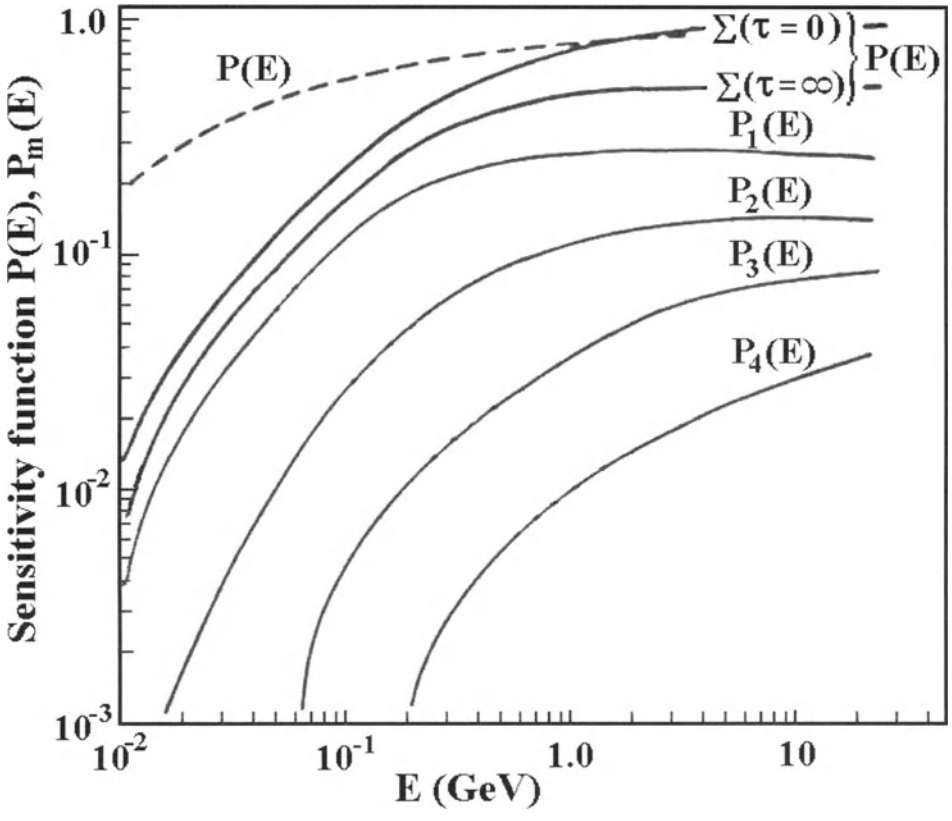

Fig. 3.6.1. Sensitivity functions $P_m(E)$ for multiplicities m = 1, 2, 3, and 4, and $P(E)$ for total neutron intensity: curves Σ for very small dead time (τ = 0) and very large dead time (τ = ∞). Full curves – calculated in Dorman et al. (1981); dashed curve shows the $P(E)$ according to Pakhomov and Sdobnov (1977), where the process of neutron deceleration in the monitor was taken into account.

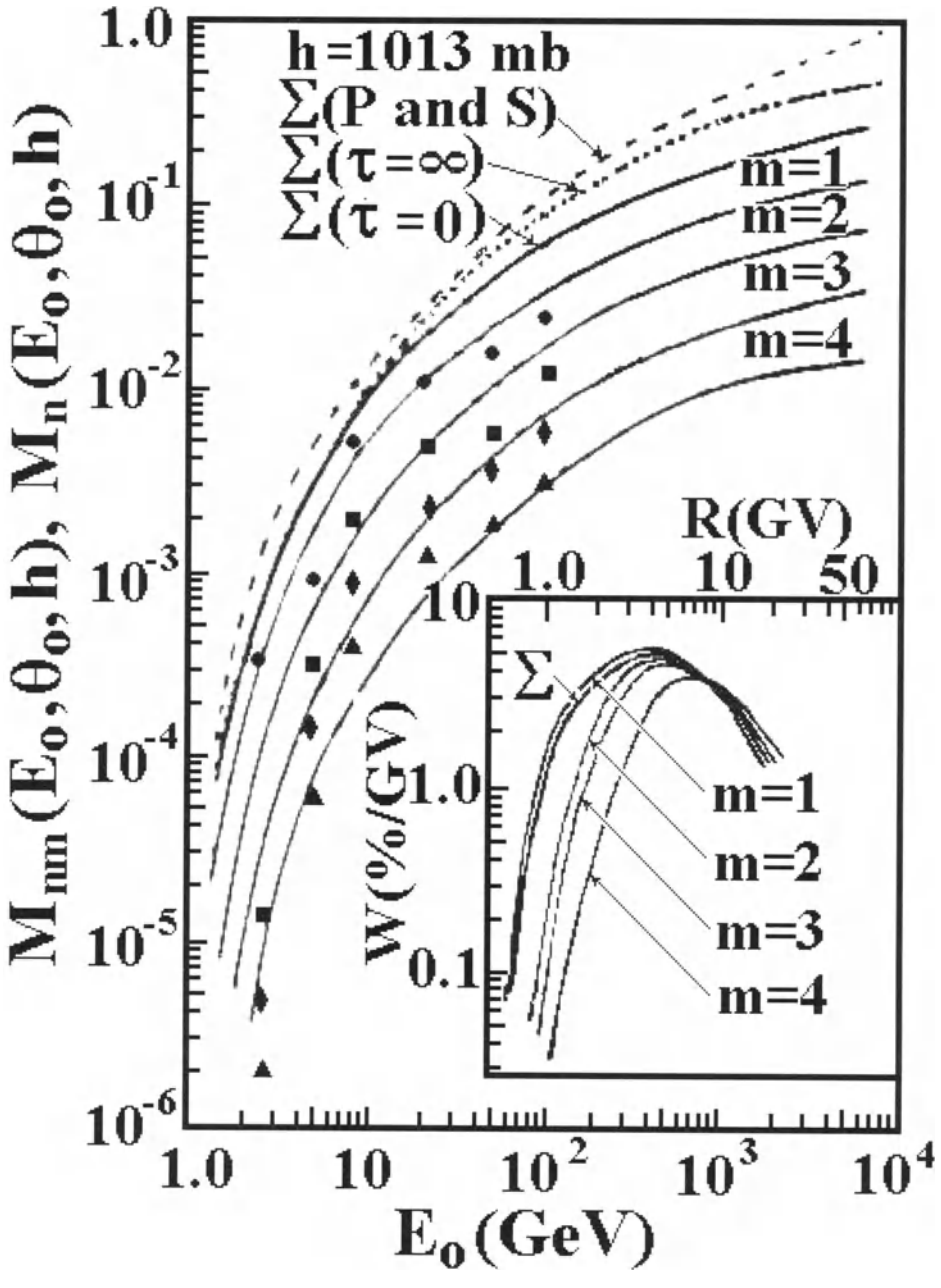

Fig. 3.6.2. Results of calculations of $M_{nm}(E_O,\theta_O,h)$ as well as $M_n(E_O,\theta_O,h)$ for sea level. At the bottom are also shown the corresponding polar coupling functions. For comparison the results of calculations of $M_{nm}(E_O,\theta_O,h)$ by Debrunner and Flückiger (1971) are also shown : full circles for m = 1, quadrants for m = 2, rhombs for m = 3, and triangles for m = 4. According to Dorman et al. (1981).

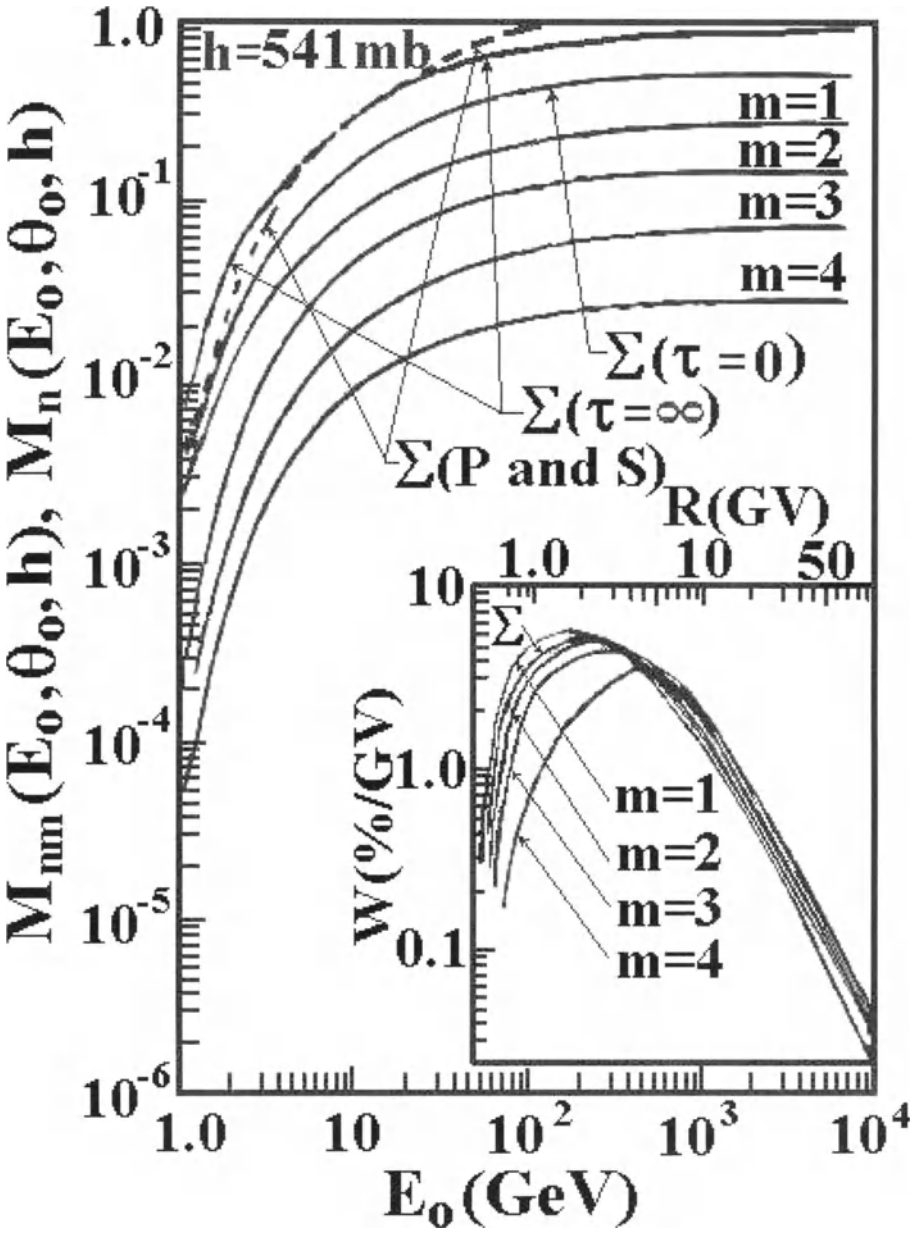

Fig. 3.6.3. Results of calculations of $M_{nm}(E_o,\theta_o,h)$ as well as $M_n(E_o,\theta_o,h)$ for level 541 mb. At the bottom are shown also corresponding polar coupling functions. According to Dorman et al. (1981).

The evaluated polar coupling functions $W_{om}(h,R)$ for multiple neutrons are presented in Table 3.6.1 for observations at sea level (h = 1013 mb), and in Table 3.6.2 for observations at level h = 541 mb.

Table 3.6.1. The polar coupling functions (at R_c = 0) for multiple neutrons $W_{om}(h,R)$ in %/GV for observations at sea level (h = 1013 mb) in periods of minimum and maximum solar activity. According to Dorman et al. (1981).

m	Solar activity	R, GV										
		1	2	3	4	5	6	7	10	20	50	100
1	min	1.82	4.45	5.17	5.48	5.18	4.53	4.05	3.12	1.38	0.348	0.108
	max	1.12	3.25	3.90	4.32	4.33	3.92	3.61	2.99	1.52	0.408	0.128
2	min	0.145	2.34	3.85	4.93	4.84	4.32	3.92	3.14	1.46	0.388	0.134
	max	0.091	1.73	2.96	3.82	3.93	3.66	3.42	2.94	1.66	0.442	0.154
3	min	0.125	1.69	3.20	4.13	4.26	3.89	3.61	3.04	1.50	0.424	0.139
	max	0.077	1.43	2.42	3.18	3.47	3.28	3.12	2.82	1.59	0.476	0.157
4	min	0.037	0.569	1.38	2.55	3.87	3.59	3.44	3.40	1.64	0.457	0.149
	max	0.011	0.464	1.05	2.05	3.26	3.08	3.07	3.06	1.68	0.500	0.165

Table 3.6.2. The polar coupling functions (at R_c = 0) for multiple neutrons $W_{om}(h,R)$ in %/GV for observations at level h = 541 *mb* in periods of minimum and maximum solar activity. According to Dorman et al. (1981).

m	Solar activity	R, GV										
		1	2	3	4	5	6	7	10	20	50	100
1	min	7.79	10.7	9.94	8.82	7.22	5.73	4.74	3.51	1.16	0.154	0.0345
	max	5.25	8.47	8.14	7.58	6.61	5.44	4.66	1.79	1.42	0.214	0.0461
2	min	4.43	8.09	8.50	8.07	7.45	6.10	5.17	3.34	1.17	0.195	0.044
	max	2.96	6.28	6.87	7.07	6.70	5.67	4.95	3.63	1.39	0.248	0.0572
3	min	5.74	8.25	8.34	7.96	7.08	5.84	4.97	3.43	1.19	0.206	0.0476
	max	3.73	6.33	6.70	6.73	6.36	5.42	4.75	3.53	1.41	0.262	0.0614
4	min	1.10	3.70	5.32	6.80	7.62	6.38	5.59	4.39	1.42	0.242	0.0555
	max	0.70	2.82	4.27	5.74	6.80	5.80	5.17	4.25	1.60	0.291	0.0677

These results for polar coupling functions can be compared with those obtained from latitude surveys according to Aleksanyan et al. (1979). Table 3.6.3 lists R_{max} and W_{max} derived from latitude surveys on the ship 'Academician Kurchatov' by the method described in Section 3.3, and those calculated in Dorman et al. (1981).

Table 3.6.3. Comparison of R_{max} (in GV) and W_{max} (in %/GV) derived from latitude surveys in 1975–1977 by Aleksanyan et al (1979) with found in Dorman et al. (1981).

m	Theory, Dorman et al. (1981)				Latitude surveys, Aleksanyan et al. (1979)					
	minimum solar activity		maximum solar activity		1975		1976		1977	
	R_{max}	W_{max}	R_{max}	W_{max}	R_{max}	W_{max}	R_{max}	W_{max}	R_{max}	W_{max}
1	4.01	5.48	4.53	4.38	3.90	5.21	4.30	4.76	4.30	5.05
2	4.43	5.04	4.83	3.96	4.30	5.28	4.80	5.58	4.60	5.00
3	4.76	4.27	5.09	3.48	4.60	4.34	5.40	4.96	5.30	4.27
4	5.33	3.95	5.37	3.35	4.0	3.3	6.0	4.1	5.0	3.2
total	4.20	5.12	4.71	4.11	4.27	4.91	4.48	4.86	4.55	4.88

From Table 3.6.3 it can be seen that the experimental results obtained on the basis of CR latitude surveys are within the theoretical values for minimum and maximum solar activity calculated in Dorman et al. (1981).

3.7. Monte Carlo simulations of NM sensitivity (integral multiplicity) to primary protons arriving at different zenith angles

3.7.1. Calculations of integral multiplicity for primary protons with energy 3 and 10 GeV.

The integral multiplicities of neutron component at atmosphere depths 710, 806, 965 and 1033 g/cm^2 from 3 GeV and 10 GeV protons incident on the atmospheric boundary at zenith angles 0°, 15°, 30°, 45°, 60° and 75° have been calculated by Dorman and Pakhomov (1979). To obtain the integral multiplicities, the Monte Carlo method was used in simulating a pion–nucleon cascade in the atmosphere (the cascade evaporation model was used as the basis of simulation of inelastic pion–nucleus interactions according to Barashenkov and Tokayev, M1972). Small energy neutron propagation was described in terms of transport approximation according to Abagyan et al. (M1964). The ionization energy loss in propagation of charged particles was calculated by using the phenomenological expressions from Vzorov (1969). The standard atmospheric model was used to simulate the conditions in the Earth's atmosphere. As result of these calculations, the differential multiplicity $N(E_o,E,h,\theta_o)$ that describes the differential energy spectrum of secondary neutrons on the pressure level h, generated by one primary particle with energy E_o and incident on the atmospheric boundary at zenith angle θ_0 was evaluated. The integral multiplicity for NM-IQSY neutron supermonitor $M_n(E_o,\theta_o,h)$ will be determined using Eq. 3.5.12 in Section 3.5, but with $P(E)$ according to Luzov et al. (1971) and Pakhomov and Sdobnov (1977). The results of calculation $M_n(E_o,\theta_o,h)$ according to Eq. 3.5.12 are listed in Table 3.7.1 for E_o=3 GeV and in Table 3.7.2 for E_o=10 GeV. The last column shows the parameter γ that characterizes the zenith dependencies of integral multiplicities (see below, Section 3.7.3).

Table 3.7.1. Integral multiplicity for NM-IQSY neutron supermonitor for E_o = 3 GeV in dependence of h and θ_0 according to Dorman and Pakhomov (1979).

h, g/cm^2	0°	15°	30°	45°	60°	75°	γ
710	0.095	0.082	0.056	0.026	0.010	0.0026	**2.8**
806	0.056	0.044	0.024	0.011	0.0035	0.00082	**3.4**
965	0.023	0.019	0.0079	0.0019	0.0011	0.000054	**4.6**
1033	0.013	0.012	0.0052	0.0015	0.00052	0.0000016	**5.0**

Table 3.7.2. The same as in Table 3.7.1, but for E_o = 10 GeV.

h, g/cm^2	0°	15°	30°	45°	60°	75°	γ
710	0.27	0.25	0.17	0.061	0.017	0.0051	**3.2**
806	0.16	0.14	0.084	0.026	0.0080	0.0017	**3.7**
965	0.068	0.058	0.025	0.0061	0.0024	0.00011	**4.9**
1033	0.049	0.039	0.015	0.0031	0.0014	0.000039	**5.4**

3.7.2. Dependence of integral multiplicities on atmospheric depth

The dependence of integral multiplicities on the atmospheric depth h for primary protons with energy E_o = 3 and 10 GeV and θ_o = 0°, 15°, 30°, 45°, 60° and 75° is shown in Figure 3.7.1.

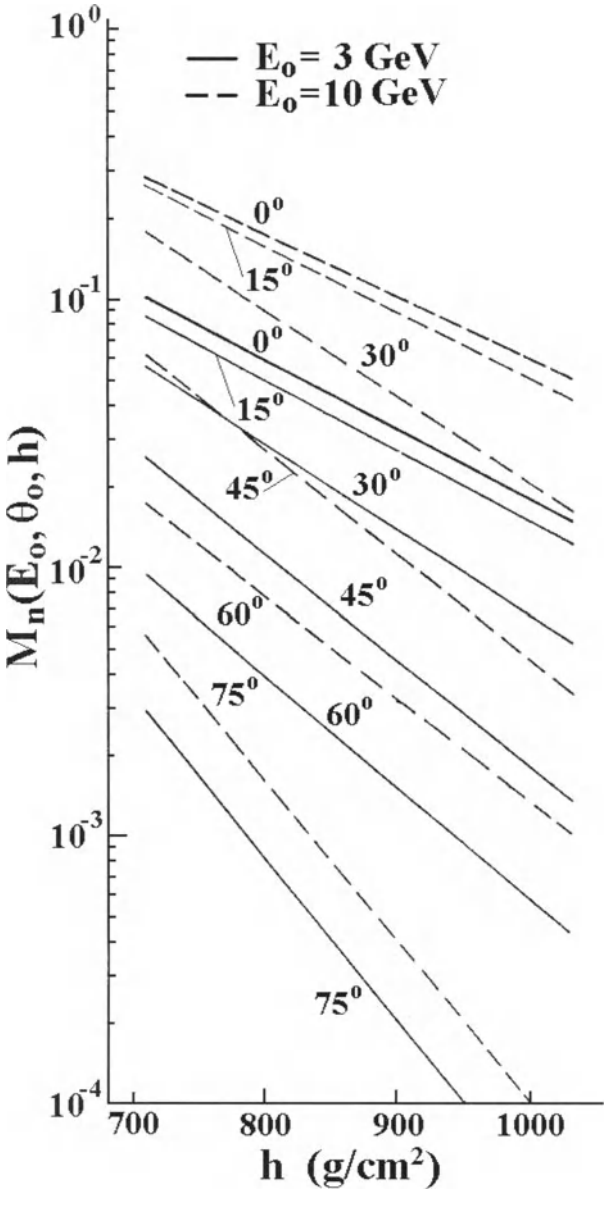

Fig. 3.7.1. Results of Monte Carlo simulations for integral multiplicities of NM-IQSY $M_n(E_o,\theta_o,h)$ from incident primary protons with energies E_o = 3 and 10 GeV at different zenith angles as a function of h. According to Dorman and Pakhomov (1979).

From Fig. 3.7.1 it can be seen that for each θ_o and E_o the dependence of $M_n(E_o,\theta_o,h)$ on h in the interval from 710 to 1033 g/cm^2 is approximately exponential:

$$M_n(E_o,\theta_o,h) \propto \exp(-h/\Lambda(E_o,\theta_o)) , \qquad (3.7.1)$$

where the values of the attenuation coefficient $\Lambda(E_o,\theta_o)$ for the integral multiplicities are listed in the Table 3.7.3. In this Table there are four types of $\Lambda(E_o,\theta_o)$: (1) obtained

from Eq. 3.7.1 by comparison with values of $M_n(E_O,\theta_O,h)$ at levels 710 and 1033 g/cm^2 in Tables 3.7.1 and 3.7.2; (2) obtained by multiplying $\Lambda(E_O,\theta_O=0^o)$, determined in (1), by $\cos\theta_O$; (3) obtained by averaging $\Lambda(E_O,\theta_O)$ determined from Eq. 3.7.1 by comparison values of $M_n(E_O,\theta_O,h)$ at each level of observation (710, 806, 965 and 1033 g/cm^2) with all other (on the basis of data listed in Tables 3.7.1 and 3.7.2); (4) obtained by multiplying $\Lambda(E_O,\theta_O=0^o)$, determined in (3), by $\cos\theta_O$.

Table 3.7.3. The values of attenuation coefficient $\Lambda(E_O,\theta_O)$ in g/cm^2 for E_O = 3 and 10 GeV in dependence on θ_O.

E_O, GeV	Type	0°	15°	30°	45°	60°	75°
3	(1)	162.4	168.1	135.9	113.2	109.2	43.7
	(2)	162.4	156.9	140.6	114.8	81.2	42.0
	(3)	162.8	168.1	138.9	135.7	110.6	51.1
	(4)	162.8	157.2	141.0	115.1	81.4	42.1
10	(1)	189.3	173.9	133.0	108.4	67.3	66.3
	(2)	189.3	182.8	163.9	133.8	94.6	49.0
	(3)	190.5	173.9	133.1	108.1	89.5	67.3
	(4)	190.5	184.0	165.0	134.7	95.2	49.3

3.7.3. Dependence of integral multiplicities on the zenith angle

As shown in Dorman and Pakhomov (1979), the dependence of the neutron monitor integral multiplicities $M_n(E_O,\theta_O,h)$ on zenith angle θ_O for each level of observation h and each primary energy E_O can be approximated by

$$M_n(E_O,\theta_O,h)=M_n\left(E_O,\theta_O=0^o,h\right)\cdot(\cos\theta_O)^{\gamma(E_O,h)}\ . \qquad (3.7.2)$$

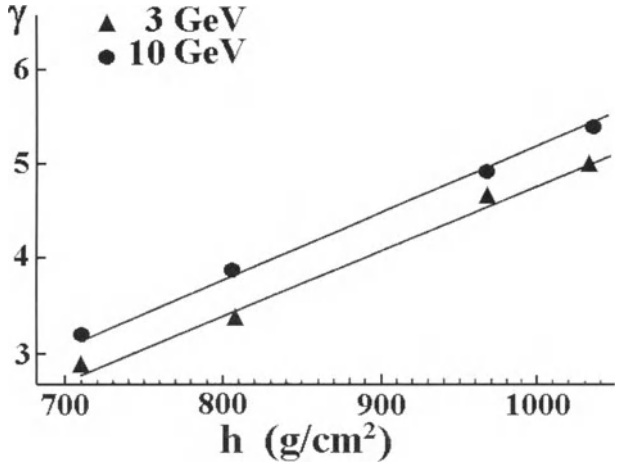

Fig. 3.7.2. The dependences of $\gamma(E_O,h)$ in Eq. 3.7.2 from h.

The values of $\gamma(E_O,h)$ are listed in the last columns in Tables 3.7.1 and 3.7.2 for E_O = 3 and 10 GeV. The dependencies of $\gamma(E_O,h)$ on h are shown in Fig. 3.7.2.

According to Fig. 3.7.2 the dependences of $\gamma(E_o,h)$ from h can be approximated by a linear function:

$$\gamma(E_o,h)= A(E_o)+ B(E_o)h \ , \tag{3.7.3}$$

where for E_o = 3 GeV:

$$A(3\ \text{GeV}) = -\ 2.15, \quad B(3\ \text{GeV}) = 0.00690\ (\text{g/cm}^2)^{-1} \tag{3.7.4}$$

and for E_o = 10 GeV:

$$A(10\ \text{GeV}) = -\ 1.93, \quad B(10\ \text{GeV}) = 0.00717\ (\text{g/cm}^2)^{-1} \ . \tag{3.7.5}$$

3.7.4. Dependence of integral multiplicities on atmospheric depth and zenith angle

We can combine Eq. 3.7.1–3.7.5 and determine approximately the dependence of integral multiplicities $M_n(E_o,\theta_o,h)$ on atmospheric depth h and zenith angle θ_o simultaneously:

$$M_n(E_o,\theta_o,h)= M_n(E_o,\theta_o = 0,h=h_o)(\cos\theta_o)^{\gamma(E_o,h)}\exp(-(h-h_o)/\Lambda(E_o,\theta_o)), \tag{3.7.6}$$

where $M_n(E_o,\ \theta_o = 0,\ h=h_o)$ is the integral multiplicity for neutron component observed at $h=h_o$ from vertically arriving primary particles..

3.7.5. Test of Dorman and Pakhomov (1979) calculations of the integral multiplicities by solar neutron observation data

Efimov et al. (1993) tested the calculations of Dorman and Pakhomov (1979) of the integral multiplicities $M_n(E_o,\theta_o,h)$ for primary protons with energies 3 GeV and 10 GeV, using solar neutron data obtained for the events of June 3, 1982 and May 24, 1990. These events were observed by many ground based neutron monitors, characterized with different levels of observation h and different zenith angles θ_o at the time of event. From Table 3.7.1 and Table 3.7.2 as well as from Figure 3.7.2 it is possible to see that the average $\gamma(E_o,h)$ for levels of 700–1030 g/cm^2 and for particle energies 3–10 GeV is about 4. Efimov et al. (1993) showed that the dependence of the observed solar neutron flux N divided by $(\cos\theta_o)^{\gamma(E_o,h)}$ (where $\gamma(E_o,h)$ = 4) on the zenith angle is described exactly by Eq. 3.7.1, and that the average Λ was about ≈ 96 g/cm^2 and 111 g/cm^2 for the events of June 3, 1982 and May 24, 1990 respectively. The test made by Efimov et al. (1993) of Dorman and Pakhomov (1979) calculations showed that in the first approximation we can use the results on the $M_n(E_o,\theta_o,h)$ obtained for protons also for research of high energy solar neutrons detected by neutron monitors and other ground based detectors.

3.8. Analytical presentation of coupling functions

3.8.1. The form of analytical approximation for coupling functions

According to Dorman (1969), the polar normalized coupling function for any secondary component of type i ($i = h\mu$ – for hard muons, $i = s\mu$ – for soft muons, $i = ep$ – for electron-photon component, $i = n$ – for total neutron component, $i = m$ – for neutron multiplicities $m = 1,2,3,...$, and so on) can be approximated by the special function (in scientific literature it is called as Dorman function):

$$W_{oi}(R,h_o) = a_i(h_o)k_i(h_o)R^{-(k_i(h_o)+1)}\exp\left(-a_i(h_o)R^{-k_i(h_o)}\right). \tag{3.8.1}$$

It is easy to see that for any values of $a_i(h_o)$, $k_i(h_o)$

$$\int_0^\infty W_{oi}(R,h_o)dR = \int_0^\infty a_i k_i R^{-(k_i+1)}\exp\left(-a_i R^{-k_i}\right)dR = 1. \tag{3.8.2}$$

The normalized coupling functions at any point on Earth with cut off rigidity R_c will be

$$W_i(R_c,R,h_o) = \begin{cases} 0 & \text{if } R < R_c \\ a_i k_i R^{-(k_i+1)}\left(1-a_i R_c^{-k_i}\right)^{-1}\exp\left(-a_i R^{-k_i}\right) & \text{if } R \geq R_c. \end{cases} \tag{3.8.3}$$

The coupling functions in the analytical approximation described by Eq. 3.8.1 and 3.8.3, have the following important properties: 1) at large values of R, when $a_i R^{-k_i} << 1$, we obtain $W_i(R_c,R) \propto R^{-(k_i+1)}$, in good agreement with the observed data on the power law differential rigidity spectrum of primary CR and power law increase of integral multiplicity with R (let us remember that according to Eq. 3.1.5 the coupling function is proportional to the product of the primary CR spectrum and integral multiplicity), 2) at very small values of R, when $a_i R^{-k_i} >> 1$, we obtain a rapid decrease of $W_i(R_c,R)$ with decreasing R, what is in a good agreement with observed data from CR latitude surveys (plateau at small R_c).

3.8.2. Analytical approximation for CR intensity dependence on cut off rigidity

The expected dependence of CR intensity on the cut off rigidity R_c can be determined from Eqs. 3.1.1 and 3.8.1:

$$N_i(R_c,h_o)/N_i(0,h_o) = \int_{R_c}^\infty W_{oi}(R,h_o)dR = 1 - a_i R_c^{-k_i}, \tag{3.8.4}$$

where $N_i(0,h_o)$ is the CR intensity on the pole at $R_c = 0$. From Eq. 3.8.4 follows that coefficients a_i and k_i can be determined by fitting to a linear regression relation

$$\ln(1 - N_i(R_c,h_o)/N_i(0,h_o)) = \ln a_i(h_o) - k_i(h_o)\ln R_c, \tag{3.8.5}$$

3.8.3. Analytical presentation of coupling functions for NM–IQSY (total intensity and different multiplicities); their dependencies from solar activity

The coefficients a_i and k_i for neutron supermonitors (Eq. 3.8.5) for different multiplicities m (coefficients a_m and k_m, where m = 1, 2, 3, ...) and total neutron component (coefficients a_n and k_n) were determined from a latitude surveys by Aleksanyan et al. (1985), Moraal et al., 1989, and they are in good agreement with theoretical calculations of Dorman and Yanke (1981), Dorman et al. (1981). Improved coefficients were determined on the basis of recent Italian expedition to Antarctica (Dorman et al., 2000). The dependence of a_m and k_m on the average station pressure h (in atm = 1000 g/cm^2) and solar activity level characterized by the logarithm of CR intensity (we used here monthly averaged of Climax NM $\ln(N_{\mathrm{Cl}})$, available starting from 1952) can be approximated by the functions:

$$a_n = \left(-2.915h^2 - 2.237h - 8.654\right)\ln(N_{\mathrm{Cl}}) + \left(24.584h^2 + 19.460h + 81.230\right), \tag{3.8.6}$$

$$k_n = \left(0.180h^2 - 0.849h + 0.750\right)\ln(N_{\mathrm{Cl}}) + \left(-1.440h^2 + 6.403h - 3.698\right), \tag{3.8.7}$$

$$a_m = \left[\left(-2.915h^2 - 2.237h - 8.638\right)\ln(N_{\mathrm{Cl}}) + \left(24.584h^2 + 19.46h + 81.23\right)\right]\times \\ \times\left(0.987m^2 + 0.225m + 6.913\right)/9.781, \tag{3.8.8}$$

$$k_m = \left[\left(0.180h^2 - 0.849h + 0.750\right)\ln(N_{\mathrm{Cl}}) + \left(-1.440h^2 + 6.403h - 3.698\right)\right]\times \\ \times\left(0.081m + 1.819\right)/1.940, \tag{3.8.9}$$

where m = 1, 2, 3, ... Instead of Climax NM, one can also use monthly averages of any other CR Observatory with appropriate recalculation of the coefficients determined by correlation between monthly data N_{Cl} of Climax NM and this Observatory for several years. For example, the recalculated coefficients for ESO 6NM–64 are

$$\ln(N_{\mathrm{Cl}}) = 2.161\times\ln(N_{\mathrm{ESO}}) - 9.665 \tag{3.8.10}$$

(the correlation coefficient 0.899 based on comparison of $\ln(N_{\mathrm{Cl}})$ and $\ln(N_{\mathrm{ESO}})$ for about two years). For Rome 17NM-64 these recalculation coefficients are

$$\ln(N_{\mathrm{Cl}}) = 1.767\times\ln(N_{\mathrm{Rome}}) - 3.857 \tag{3.8.11}$$

with correlation coefficient 0.949 (from comparison of $\ln(N_{\mathrm{Cl}})$ and $\ln(N_{\mathrm{Rome}})$ for about two solar cycles). Substituting Eq. 3.8.10 or 3.8.11 in Eq. 3.8.6–3.8.9, we obtain the coupling functions as a function of the level of solar activity on the basis of monthly data of ESO NM or Rome NM, correspondingly.

3.8.4. Analytical representation of polar coupling functions for different CR secondary components

According to Dorman et al. (M1972), the coefficients a_i, k_i in the analytical form described by Eq. 3.8.1 for different CR secondary components will be as following: 1) for neutron component at $h_o = 312$ mb, $a_n = 8.30$, $k_n = 1.45$; 2) for neutron component at $h_o = 680$ mb, $a_n = 13.62$, $k_n = 1.26$; 3) for hard muon component at sea level $h_o = 1030$ mb $a_{h\mu} = 35.3$, $k_{h\mu} = 0.95$; and 4) for hard muon component underground at the depth 7 m w.e., $a_{h\mu} = 58.5$, $k_{h\mu} = 0.94$.

3.9. Difference coupling functions for CR observations in the atmosphere and their analytical representation

3.9.1. The problem of narrowing the energy sensitivity of CR instruments

The coupling functions for individual instruments considered above reflect a broad rigidity sensitivity to primary CR (usually they have a broad maximum covering about tens of GV). To obtain more exact information it will be important to narrow the energy sensitivity of CR instruments. The polar coupling function for individual instrument increases relatively rapidly (almost exponentially) from zero at zero rigidity and, after reaching its maximum, decreases as $R^{-\gamma}$, where $\gamma \approx 1.5 - 2.0$ depending on the type of secondary components. This kind of dependence of the coupling functions W on R makes it difficult and somewhat uncertain to determine the primary variations $\delta D(R)/D_o(R)$ on the basis of the secondary variations $\delta I_i(R,t)/I_{io}(R)$, by solving the appropriate set of integral equations with kernels $W_i(R)$ (see Sections 3.11–3.12 below). The uncertainty is associated with an appreciable contribution of a broad range of high rigidities where the coupling functions and the secondary variations are insufficiently known. The selectivity and effectiveness of the method may be improved pronouncedly if the range of the energy sensitivity of the instruments is significantly narrowed. It will be shown below that installation of similar equipments at the worldwide network of stations makes it possible to successfully solve this problem by introducing some complex 'difference instrument' which is a combination of two identical instruments at different stations with different cut off rigidities (Dorman, 1977a).

3.9.2. The main equation for the difference intensities for the two identical CR instruments at different cut off rigidities

Let the equipment detecting the secondary component of type *i* be installed at some point *k* with an effective geomagnetic cut off rigidity R_k (the directional diagram of the

instrument and the penumbra effect are included when the effective geomagnetic cut off rigidity R_k is determined). Let us suppose that at the point l with the cut off rigidity R_l there is the same type of equipment (with the same integral multiplicity). Assume without loss of generality, that $R_k < R_l$. In this case

$$I_{ki}(t) = \int_{R_k}^{\infty} D(R,t) m_i(R) dR, \quad I_{li}(t) = \int_{R_l}^{\infty} D(R,t) m_i(R) dR, \tag{3.9.1}$$

and for the difference of intensities of these two instruments we obtain

$$I_{kli}(t) = I_{ki}(t) - I_{li}(t) = \int_{R_k}^{R_l} D(R,t) m_i(R) dR. \tag{3.9.2}$$

At $t = 0$ it will be

$$I_{kli}(0) = I_{ki}(0) - I_{li}(0) = \int_{R_k}^{R_l} D(R,0) m_i(R) dR. \tag{3.9.3}$$

For the time variation of intensity difference we obtain

$$\Delta I_{kli}(t) = \int_{R_k}^{R_l} \Delta D(R,t) m_i(R) dR, \tag{3.9.4}$$

where

$$\Delta I_{kli}(t) = I_{kli}(t) - I_{kli}(0), \quad \Delta D(R,t) = D(R,t) - D(R,0). \tag{3.9.5}$$

Dividing both parts of Eq. 3.9.5 by $I_{kli}(0)$ we obtain

$$\Delta I_{kli}(t)/I_{kli}(0) = \int_{R_k}^{R_l} (\Delta D(R,t)/D(R,0)) \Omega_{kli}(R) dR, \tag{3.9.6}$$

where

$$\Omega_{kli}(R) = \begin{cases} D(R,0) m_i(R)/I_{kli}(0) & \text{if } R_k \le R \le R_l, \\ 0 & \text{if } R < R_k,\ R > R_l, \end{cases} \tag{3.9.7}$$

is the difference coupling function, introduced by Dorman (1977a). This function determines the relation between the extraterrestrial variations in the primary CR $\Delta D(R,t)/D(R,0)$ and the variations of the intensity difference between the readings of two identical (or appropriately calibrated instruments) at different stations $\Delta I_{kli}(t)/I_{kli}(0)$. It can easily be seen that the normalization condition for the difference coupling function is satisfied: in fact, it follows from Eq. 3.9.3 and Eq. 3.9.7 that

$$\int_0^\infty \Omega_{kli}(R)dR = 1. \tag{3.9.8}$$

3.9.3. Representation of the differential coupling functions through polar coupling functions

The polar coupling functions were determined above, in the Section 3.1. For the component of type i it will be

$$W_{oi}(R) = D(R,0)m_i(R)/I_{oi}(0), \tag{3.9.9}$$

where $I_{oi}(0)$ is the intensity of the i-th CR component at a point with zero geomagnetic cut off rigidity). From comparison Eq. 3.9.7 and Eq. 3.9.9 we obtain

$$\Omega_{kli}(R) = \begin{cases} (I_{oi}(0)/I_{kli}(0))W_{oi}(R) & \text{if } R_k \le R \le R_l, \\ 0 & \text{if } R < R_k,\ R > R_l. \end{cases} \tag{3.9.10}$$

Bearing in mind the properties of the polar coupling function, Eq. 3.9.10 may be rewritten as

$$\Omega_{kli}(R) = \begin{cases} W_{oi}(R)\left(\int_{R_k}^{R_l} W_{oi}(R)dR\right)^{-1} & \text{if } R_k \le R \le R_l, \\ 0 & \text{if } R < R_k,\ R > R_l. \end{cases} \tag{3.9.11}$$

Since in all cases $\int_{R_k}^{R_l} W_{oi}(R)dR < 1$ then $\Omega_{kli}(R) > W_{oi}(R)$. Let us note that if the interval (R_k, R_l) is sufficiently narrow, the difference coupling function may be many times bigger than the coupling function for individual instrument.

3.9.4. Analytical approximation for the difference coupling function

Such an approximation is of importance for the study of the CR variations of various types and makes it possible to significantly simplify the calculations and the use of computers in analyzing the experimental data. As was shown in Section 3.8, the optimal analytical approximation of the polar coupling functions is the form proposed in Dorman (1969) and described by Eq. 3.8.1. Substituting Eq. 3.8.1 in Eq. 3.9.11 we obtain

$$\Omega_{kli}(R) = \begin{cases} \omega_i(R_k, R_l)R^{-(k_i+1)}\exp\left(-a_i R^{-k_i}\right) & \text{if } R_k \le R \le R_l, \\ 0 & \text{if } R < R_k,\ R > R_l, \end{cases} \tag{3.9.12}$$

where the normalizing factor

$$\omega_i(R_k,R_l)=a_i k_i\left[\exp\left(-a_i R_l^{-k_i}\right)-\exp\left(-a_i R_k^{-k_i}\right)\right]^{-1}. \qquad (3.9.13)$$

3.9.5. The difference coupling functions for inclined muon telescopes

An extensive network of cubic and crossed muon telescopes is in operation at present. The method of the difference coupling functions in case of the cubic telescopes and shielded ionization chambers may be used for the difference in the counting rates at two stations with different geomagnetic cut off rigidities as was described above. In case of the inclined telescopes with the same zenith angle θ and different azimuthally angles Φ_1 and Φ_2 with different cut off rigidities R_1 and R_2, this method may be applied to a single instrument (for the case of so called crossed muon telescopes $|\Phi_1-\Phi_2|=\pi$). In fact, let $I_1(\theta,t)$ and $I_2(\theta,t)$ be the counting rates of the telescopes with azimuthally angles Φ_1 and Φ_2 with cut off rigidities R_1 and R_2 (the latter are determined by the coordinates of the observation point, the zenith angle θ and the azimuthally angles Φ_1 and Φ_2). Then applying a procedure similar to that used in Section 3.9.2 we obtain (assume for the sake of determinacy that $R_1 < R_2$)

$$\Delta I_{12}(\theta,t)/I_{12}(\theta,0)=\int_{R_1}^{R_2}(\Delta D(R,t)/D(R,0))\Omega_{12}(R,\theta)dR, \qquad (3.9.14)$$

where

$$\Delta I_{12}(\theta,t)=I_{12}(\theta,t)-I_{12}(\theta,0),\ I_{12}(\theta,t)=I_1(\theta,t)-I_2(\theta,t),$$

$$I_{12}(\theta,0)=I_1(\theta,0)-I_2(\theta,0),\ \Delta D(R,t)=D(R,t)-D(R,0), \qquad (3.9.15)$$

and the difference coupling function for the pair of inclined telescopes

$$\Omega_{12}(R,\theta)=\begin{cases}D(R,0)m(R,\theta)/I_{12}(\theta,0) & \text{if } R_1\le R\le R_2\\ 0 & \text{if } R<R_1,\ R>R_2.\end{cases} \qquad (3.9.16)$$

In Eq. 3.9.16 $m(R,\theta)$ is the integral multiplicity for zenith angle θ. It can easily be seen that the normalization condition

$$\int_0^\infty \Omega_{12}(R,\theta)dR=1 \qquad (3.9.17)$$

is satisfied since

$$I_{12}(\theta,0)=\int_{R_1}^{R_2} D(R,0)m(R,\theta)dR. \qquad (3.9.18)$$

The difference coupling function $\Omega_{12}(R,\theta)$ can be expressed through the polar coupling function $W_o(R,\theta)$ using the relation (similar to Eq. 3.9.10),

$$\Omega_{12}(R,\theta)=\begin{cases}(I_o(\theta,0)/I_{12}(\theta,0))W_o(R,\theta) & \text{if } R_1 \le R \le R_2 \\ 0 & \text{if } R<R_1,\ R>R_2,\end{cases} \tag{3.9.19}$$

where $I_o(\theta,0)$ is the intensity at an zenith angle θ on the pole at moment $t = 0$, and

$$W_o(R,\theta)=D(R,0)m(R,\theta)/I_o(\theta,0) \tag{3.9.20}$$

is the polar coupling function for the zenith angle θ. Since $I_o(\theta,0)/I_{12}(\theta,0)\approx 10-20$, the difference coupling function for a pair of directed measurements is correspondingly many times larger than the coupling function for a single instrument. Another important circumstance should be emphasized, namely, that the meteorological effects are automatically excluded in the variation of the difference between the readings of two inclined telescopes $\Delta I_{12}(\theta,t)$ for the same zenith angle θ (if the weak dependence of the meteorological functions on geomagnetic cut off rigidity is neglected).

3.9.6. Main equation for determination of CR variations of magnetospheric and extraterrestrial origin using the difference coupling functions for observations in atmosphere

Assume that the same component of type *i* is measured at points *k* and *l* and that the observation data from the two stations are corrected for meteorological effects. After this we shall vary the resultant Eq. 3.9.2 for $I_{kli}(t)$ over the possible changes of the geomagnetic thresholds and extraterrestrial CR rigidity spectrum, and divide the variation by $I_{kli}(0)$:

$$\Delta I_{kli}(t)/I_{kli}(0)=\delta R_l\Omega_{kli}(R_l)-\delta R_k\Omega_{kli}(R_k)+\int_{R_k}^{R_l}(\Delta D(R,t)/D(R,0))\Omega_{kli}(R)dR, \tag{3.9.21}$$

where the difference coupling function $\Omega_{kli}(R)$ is determined by Eq. 3.9.10 or Eq. 3.9.11. The first two terms in Eq. 3.9.21 determine the variations of magnetospheric origin, the third term define the variations of extraterrestrial origin (modulation, generation on the Sun, extra-solar variations). Thus Eq. 3.9.21 is the fundamental equation of CR variations in the difference between the readings at two stations.

A similar equation will be for observations in the one point by azimuthally muon telescope (denotations see in Section 3.9.5):

$$\Delta I_{12}(\theta,t)/I_{12}(\theta,0)=\delta R_2\Omega_{12}(R_2,\theta)-\delta R_1\Omega_{12}(R_1,\theta)+\int_{R_1}^{R_2}(\Delta D(R,t)/D(R,0))\Omega_{12}(R,\theta)dR. \tag{3.9.22}$$

3.10. Difference coupling functions and difference meteorological coefficients for underground CR observations

The method of difference coupling functions for muon CR component developed in Dorman (1977a) and considered above in Section 3.9 for inclined muon telescopes, was generalized by Dorman (1977b) for studies of CR variations on the basis of underground measurements data at a single point at various depths and at the same depth but at various zenith angles (Dorman, M1963a,b; Kuzmin, M1964, M1968; Bishara and Dorman, 1973a-c, 1974a,b, 1975).

3.10.1. The difference coupling functions for underground observations by identical muon telescopes relevant to the coupling functions for single instruments

The CR muon intensity detected by muon telescope on the depth d (in m w. e.) can be described as

$$I_{\mu d}(R_c,t)=\int_{R_c}^{\infty} D(R,t)m_{\mu d}(R)dR, \qquad (3.10.1)$$

where R_c is the cut off geomagnetic rigidity at the point of observation, $D(R,t)$ is the differential energy spectrum of primary CR; and $m_{\mu d}(R)$ is the integral multiplicity of muon generation. It is assumed that the observationed data are preliminarily corrected for meteorological effects (see Part 2 of this monograph). The minimal energy of detected muons $E_{\mu\min}(d)$ is determined by the underground depth d (see Fig. 2.4.2 in Section 2.4.4). Generated muons with energy $E_{\mu\min}(d)$ will have energy at 5–7 times bigger (see the discussion of this problem and corresponding references in Chapter 5). Let us denote by R_d the minimal effective rigidity of primary CR particles that generate muons with energy $E_{\mu\min}(d)$. If $R_d < R_c$ geomagnetic effects and CR geomagnetic variations must be accounted for. In the inverse situation, when $R_d > R_c$, the underground CR detector will not be influenced by geomagnetic effects and CR geomagnetic variations; this means that the variations of $I_{\mu d}(R_c,t)$ in Eq. 3.10.1 are completely determined by the variations of only the primary spectrum (let us mention that it was supposed that all corrections on meteorological effects were introduced). Let us assume that at the same point (with the same R_c) there are CR observations on some other depth q (with the muon cut off energy $E_{\mu\min}(q)$ and minimal effective rigidity of primary CR particles R_q). Assume for the sake of definiteness that $q > d$ (it means $E_{\mu\min}(q) > E_{\mu\min}(d)$ and $R_q > R_d$). The expression for CR intensity underground at a depth q will be

$$I_{\mu q}(R_c,t)=\int_{R_c}^{\infty} D(R,t)m_{\mu q}(R)dR\,. \qquad (3.10.2)$$

The difference of intensities described by Eq. 3.10.1 and Eq. 3.10.2 will be

$$I_{\mu dq}(R_c,t)=I_{\mu d}(R_c,t)-I_{\mu q}(R_c,t)=\int_{R_d}^{R_q}D(R,t)\left[m_{\mu d}(R)-m_{\mu q}(R)\right]dR. \qquad (3.10.3)$$

The same difference for the moment $t = 0$ will be

$$I_{\mu dq}(R_c,0)=I_{\mu d}(R_c,0)-I_{\mu q}(R_c,0)=\int_{R_d}^{R_q}D(R,0)\left[m_{\mu d}(R)-m_{\mu q}(R)\right]dR. \qquad (3.10.4)$$

Let us very Eq. 3.10.3 on R_c (geomagnetic variations) and on $D(R,t)$ (extra-terrestrial variations), and then let us divide the result by $I_{\mu dq}(R_c,0)$ (to obtain relative variations); we obtain:

$$\frac{\Delta I_{\mu dq}(R_c,t)}{I_{\mu dq}(R_c,0)}=-\Delta R_c\Omega_{\mu dq}(R_c,R_c)+\int_{R_d}^{R_q}\frac{\Delta D(R,t)}{D(R,0)}\Omega_{\mu dq}(R_c,R)dR, \qquad (3.10.5)$$

where

$$\Delta I_{\mu dq}(R_c,t)=I_{\mu dq}(R_c,t)-I_{\mu dq}(R_c,0);\ \Delta D(R,t)=D(R,t)-D(R,0). \qquad (3.10.6)$$

In Eq. 3.10.5 the function

$$\Omega_{\mu dq}(R_c,R)=\begin{cases}\left[D(R,0)\left(m_{\mu d}(R)-m_{\mu q}(R)\right)\right]/I_{\mu dq}(R_c,0) & \text{if } R_d<R<R_q,\\ 0 & \text{if } R<\max(R_c,R_d),\ R>R_q.\end{cases} \qquad (3.10.7)$$

determines the relationship between the relative variations of the intensity difference at various levels underground $\Delta I_{\mu dq}(R_c,t)/I_{\mu dq}(R_c,0)$ and the relative variations of the differential spectrum of primary CR $\Delta D(R,t)/D(R,0)$, as well as variation of cut off rigidity ΔR_c. This function was introduced in Dorman (1977b) and was called the difference coupling function for underground observations. This function can be calculated through coupling functions for underground individual instruments:

$$W_{\mu d}(R_c,R)=\begin{cases}D(R,0)m_{\mu d}(R)/I_{\mu d}(R_c,0) & \text{if } R>\max(R_c,R_d),\\ 0 & \text{if } R<\max(R_c,R_d),\end{cases}$$

$$W_{\mu q}(R_c,R)=\begin{cases}D(R,0)m_{\mu q}(R)/I_{\mu q}(R_c,0) & \text{if } R>\max(R_c,R_q),\\ 0 & \text{if } R<\max(R_c,R_q).\end{cases} \qquad (3.10.8)$$

From Eq. 3.10.7 and Eq. 3.10.8 follows

$$\Omega_{\mu dq}(R_c,R)=\begin{cases}\dfrac{I_{\mu d}(R_c,0)W_{\mu d}(R_c,R)-I_{\mu q}(R_c,0)W_{\mu q}(R_c,R)}{I_{\mu d}(R_c,0)-I_{\mu q}(R_c,0)} & \text{if } \max(R_c,R_d)\le R\le R_q,\\ 0 & \text{if } R<\max(R_c,R_d),\ R>R_q.\end{cases} \quad (3.10.9)$$

It can be easily seen that the normalization condition

$$\int_{R_c}^{\infty}\Omega_{\mu dq}(R_c,R)dR=1 \quad (3.10.10)$$

for the difference coupling function is automatically satisfied; this follows from Eq. 3.10.9 since coupling functions for individual instruments are normalized:

$$\int_{R_c}^{\infty}W_{\mu d}(R_c,R)dR=\int_{R_c}^{\infty}W_{\mu q}(R_c,R)dR=1. \quad (3.10.11)$$

Let us note that if $R_c > R_d$ the difference underground CR coupling function may be used to investigate both geomagnetic and extra-terrestrial CR variations according to Eq. 3.10.5. But if $R_c < R_d$ we obtain according to Eq. 3.10.9 that $\Omega_{\mu dq}(R_c,R_c)=0$, and instead of Eq. 3.10.5, we obtain

$$\frac{\Delta I_{\mu dq}(R_c,t)}{I_{\mu dq}(R_c,0)}=\int_{R_c}^{\infty}\frac{\Delta D(R,t)}{D(R,0)}\Omega_{\mu dq}(R_c,R)dR. \quad (3.10.12)$$

This means that at $R_c < R_d$ the difference underground CR coupling function may be used to investigate only extra-terrestrial CR variations according to Eq. 3.10.12.

3.10.2. Difference coupling functions for underground measurements on the same depth but at different zenith angles

It will be noted that the relations presented above are also valid for CR measurements at the same level but at different zenith angles θ_1 and θ_2. If l is the underground depth in the vertical direction (in m w.e.), the effective depths d and q for these two muon telescopes in Eq. 3.10.1–3.10.12 will be

$$d=l/\cos\theta_1,\quad q=l/\cos\theta_2. \quad (3.10.13)$$

In this case Eq. 3.10.5 and Eq. 3.10.12 will describe CR variations and Eq. 3.10.9 the difference underground coupling functions for two muon telescopes on the same depth but at different zenith angles.

3.10.3. The difference meteorological coefficients for pair of underground observations and their relation to the meteorological coefficients for single instruments

In Sections 3.10.1 and 3.10.2 above we have considered underground observation data corrected for meteorological effects according to procedure described in Part 2 of this monograph. Let us note that in the difference of CR intensities measured underground at different depths (or on the same depth in vertical direction, but at different zenith angles), meteorological effects are mostly compensated. So it will be more appropriate to introduce meteorological corrections not in data of single detectors but directly in the difference of CR intensities. But in this case we need to determine the difference meteorological coefficients for a pair of underground observations.

The atmospheric variations in CR intensity data obtained by underground observations at the depth d (in m w.e.) will be written in the form (see Chapters 5–9):

$$\left(\Delta I_{\mu d}(R_c,t)/I_{\mu d}(R_c,0)\right)_{atm} = \beta_{\mu d}\Delta h_o + \int_0^{h_o}\alpha_{\mu d}(h)\Delta T(h)dh\,, \tag{3.10.14}$$

where h_o is the atmospheric pressure at the observation point, $\beta_{\mu d}$ is the barometric coefficient, $\alpha_{\mu d}(h)$ is the temperature coefficient as function of isobaric level h over the observation point, and $\Delta T(h)$ is the air temperature variation. For underground observations at the depth q we obtain similar expression:

$$\left(\Delta I_{\mu q}(R_c,t)/I_{\mu q}(R_c,0)\right)_{atm} = \beta_{\mu q}\Delta h_o + \int_0^{h_o}\alpha_{\mu q}(h)\Delta T(h)dh. \tag{3.10.15}$$

Let us consider atmospheric variations in the difference $\Delta I_{\mu dq}(R_c,t)/I_{\mu dq}(R_c,0)$ of CR intensities measured underground at different depths (or on the same depth in the vertical direction, but at different zenith angles). From Eq. 3.10.14 and Eq. 3.10.15 follows

$$\left(\Delta I_{\mu dq}(R_c,t)/I_{\mu dq}(R_c,0)\right)_{atm} = \beta_{\mu dq}\Delta h_o + \int_0^{h_o}\alpha_{\mu dq}(h)\Delta T(h)dh, \tag{3.10.16}$$

where

$$\beta_{\mu dq} = \frac{I_{\mu d}(R_c,0)\beta_{\mu d} - I_{\mu q}(R_c,0)\beta_{\mu q}}{I_{\mu d}(R_c,0) - I_{\mu q}(R_c,0)} \tag{3.10.17}$$

is the difference barometric coefficient, and

$$\alpha_{\mu dq}(h) = \frac{I_{\mu d}(R_c,0)\alpha_{\mu d}(h) - I_{\mu q}(R_c,0)\alpha_{\mu q}(h)}{I_{\mu d}(R_c,0) - I_{\mu q}(R_c,0)} \tag{3.10.18}$$

is the difference temperature coefficient.

3.10.4. General equation of the variations for the relative difference in the CR intensities from underground observations

The general equation of the CR variations for the relative difference in the intensities at two underground observation levels (or at a single level for telescopes at different zenith angles) including all three groups of variations will be written in the form

$$\frac{\Delta I_{\mu dq}(R_c,t)}{I_{\mu dq}(R_c,0)} = \beta_{\mu dq}\Delta h_o + \int_0^{h_o} \alpha_{\mu dq}(h)\Delta T(h)dh$$

$$-\Delta R_c \Omega_{\mu dq}(R_c,R_c) + \int_{R_d}^{R_q} \frac{\Delta D(R,t)}{D(R,0)} \Omega_{\mu dq}(R_c,R)dR. \qquad (3.10.19)$$

The first two terms of Eq. 3.10.19 describe the atmospheric variations, with the difference temperature and barometric coefficients $\beta_{\mu dq}$ and $\alpha_{\mu dq}(h)$ determined by Eq. 3.10.17 and Eq. 3.10.17. The third term defines the geomagnetic variations, where $\Omega_{\mu dq}(R_c,R_c)$ is determined by Eq. 3.10.9 at $R = R_c$. The fourth term describes the extra-terrestrial variations determined by the relative variations of primary CR rigidity spectrum in interval (R_d,R_q) out of the magnetosphere and by the difference coupling function $\Omega_{\mu dq}(R_c,R)$ for the pair of underground measurements on the depths d and q.

3.11. Spectrographic method for determining rigidity spectrum of primary CR variation on the basis of single Observatory data

3.11.1. Two approximations for rigidity spectrum of primary CR variation

In the first approximation the spectrum of primary CR variation can be described as

$$\Delta D(R,t)/D_o(R) = b(t)R^{-\gamma(t)}, \qquad (3.11.1)$$

where $\Delta D(R,t) = D(R,t) - D_o(R)$, and $D_o(R)$ is the differential spectrum of galactic CR at $t = 0$ (for which coupling functions are defined). In Eq. 3.11.1 the parameters $b(t)$ and $\gamma(t)$ depend on t. The approximation described by Eq. 3.11.1 can be used for describing a limited interval of rigidities in the sensitivity range corresponding to different CR secondary components (determined by coupling function). On the other hand, many historical GLE (Ground Level Event from solar CR) data show that, in the broad energy interval, the rigidity spectrum for this type of CR primary variation has a maximum, and the parameter $\gamma(t)$ in Eq. 3.11.1 depends also on particle rigidity R (usually $\gamma(t)$ increases with increasing R). This dependence can be described by the second approximation:

$$\Delta D(R,t)/D_o(R) = b(t)R^{-\gamma_o(t)-\gamma_1(t)\ln(R/R_o(t))}, \qquad (3.11.2)$$

with 4 unknown parameters $b(t)$, $\gamma_o(t), \gamma_1(t)$, and $R_o(t)$. The position of the maximum in the FEP spectrum will be at

$$R_{\max}(t) = R_o(t)\exp(-\gamma_o(t)/\gamma_1(t)), \tag{3.11.3}$$

which varies significantly from one event to another and changes very much with time: in the beginning of the GLE event it is great (many GV), but, with time during the development of the event, $R_{\max}(t)$ decreases very significantly.

3.11.2. Determination of the rigidity spectrum of primary CR variation in the magnetically quiet period

In this case, for rigidity spectrum described by Eq. 3.11.1, the observed variation $\delta N_i(R_c,t) \equiv \Delta N_i(R_c,t)/N_{io}(R_c)$ in some component i can be described in the first approximation by the function $F_i(R_c,\gamma(t))$:

$$\delta N_i(R_c,t) = b(t)F_i(R_c,\gamma(t)), \tag{3.11.4}$$

where

$$F_i(R_c,\gamma) = a_i k_i \left(1-\exp\left(-a_i R_c^{-k_i}\right)\right)^{-1} \int_{R_c}^{\infty} R^{-(k_i+1+\gamma)} \exp\left(-a_i R^{-k_i}\right) dR \tag{3.11.5}$$

is a known function. Let us compare the data for two components m and n. According to Eq. 3.11.5 we obtain

$$\delta N_m(R_c,t)/\delta N_n(R_c,t) = \Psi_{mn}(R_c,\gamma(t)), \tag{3.11.6}$$

where

$$\Psi_{mn}(R_c,\gamma) = F_m(R_c,\gamma)/F_n(R_c,\gamma) \tag{3.11.7}$$

can be calculated using Eq. 3.11.5. Comparison of experimental results with function $\Psi_{mn}(R_c,\gamma)$ according to Eq. 3.11.7 gives the value $\gamma(t)$, and then from Eq. 3.11.4 the value of the parameter $b(t)$. Eq. 3.11.7 shows that on the basis of CR observation data in atmosphere and underground one can determine the parameters $b(t)$ and $\gamma(t)$ of the rigidity spectrum of primary CR variation in the quiet period at the top of atmosphere.

Let us suppose now that from some single CR Observatory at least 4 components $i = k,l,m,n$ with different coupling functions are available. Then for the spectrum describing by Eq. 3.11.2, we obtain

$$\delta N_i(R_c,t) = b(t)\Phi_i(R_c,\gamma_o(t),\gamma_1(t),R_o(t)), \tag{3.11.8}$$

where *i=k, l, m, n*, and

$$\Phi_i(R_c,\gamma_o,\gamma_1,R_o)$$
$$= a_i k_i\left(1-\exp\left(-a_i R_c^{-k_i}\right)\right)^{-1}\int_{R_c}^{\infty} R^{-(k_i+1+\gamma_o+\gamma_1\ln(R/R_o))}\exp\left(-a_i R^{-k_i}\right)dR. \quad (3.11.9)$$

By comparing data for the different components, we obtain three equations from which one can determine the three unknown parameters $\gamma_o(t)$, $\gamma_1(t)$, and $R_o(t)$:

$$\frac{\delta N_k(R_c,t)}{\delta N_l(R_c,t)} = Y_{kl}(R_c,\gamma_o(t),\gamma_1(t),R_o(t)), \quad \frac{\delta N_l(R_c,t)}{\delta N_m(R_c,t)} = Y_{lm}(R_c,\gamma_o(t),\gamma_1(t),R_o(t)),$$
$$\frac{\delta N_m(R_c,t)}{\delta N_n(R_c,t)} = Y_{mn}(R_c,\gamma_o(t),\gamma_1(t),R_o(t)), \quad (3.11.10)$$

where ($i, j=k, l, m, n$) and

$$Y_{ij}(R_c,\gamma_o,\gamma_1,R_o) = \Phi_i(R_c,\gamma_o,\gamma_1,R_o)/\Phi_j(R_c,\gamma_o,\gamma_1,R_o) \quad (3.11.11)$$

can be calculated using Eq. 3.11.9. Solution of the system of Eq. 3.11.10 gives the values of $\gamma_o(t), \gamma_1(t), R_o(t)$, and from these one can determine the parameter $b(t)$ by Eq. 3.11.8:

$$b(t) = \delta N_i(R_c,t)/\Phi_i(R_c,\gamma_o(t),\gamma_1(t),R_o(t)) \quad (3.11.12)$$

for any $i=k, l, m, n$ (and the final result must be the same).

3.11.3. Determination of the rigidity spectrum of primary CR variation and cut off rigidity change in magnetically disturbed periods

For magnetically disturbed periods the observed CR variation will be described by

$$\delta N_k(R_c,t) = -\Delta R_c(t) W_k(R_c,R_c) + b(t) F_k(R_c,\gamma(t)) \quad (3.11.13)$$

(instead of Eq. 3.11.4). Here ΔR_c is the change of cut off rigidity owed to the change of the Earth's magnetic field, and $W_k(R_c,R_c)$ is determined by Eq. 3.8.3 at $R = R_c$.

Now for the first approximation of the rigidity spectrum of primary CR variation we have three unknown variables $\gamma(t)$, $b(t)$, and $\Delta R_c(t)$, and for their determination we need data from at least 3 different components $k = l, m, n$ in Eq. 3.11.13. In accordance with the spectrographic method (Dorman, M1975b) let us introduce the function

$$\Psi_{lmn}(R_c,\gamma) = \frac{W_l F_m(R_c,\gamma) - W_m F_l(R_c,\gamma)}{W_m F_n(R_c,\gamma) - W_n F_m(R_c,\gamma)}, \quad (3.11.14)$$

where

$$W_l \equiv W_l(R_c,R_c), \quad W_m \equiv W_m(R_c,R_c), \quad W_n \equiv W_n(R_c,R_c). \quad (3.11.15)$$

Then from

$$\Psi_{lmn}(R_c,\gamma)=\frac{W_l\delta N_m(R_c,t)-W_m\delta N_l(R_c,t)}{W_m\delta N_n(R_c,t)-W_n\delta N_m(R_c,t)} \tag{3.11.16}$$

the value of $\gamma(t)$ can be determined. Using this value of $\gamma(t)$ for time t, we determine

$$\Delta R_c(t)=\frac{F_l(R_c,\gamma(t))\delta N_m(R_c,t)-F_m(R_c,\gamma(t))\delta N_l(R_c,t)}{F_m(R_c,\gamma(t))\delta N_n(R_c,t)-F_n(R_c,\gamma(t))\delta N_m(R_c,t)}, \tag{3.11.17}$$

$$b(t)=\frac{W_l\delta N_m(R_c,t)-W_m\delta N_l(R_c,t)}{W_lF_m(R_c,\gamma(t))-W_mF_l(R_c,\gamma(t))}. \tag{3.11.18}$$

So in magnetically disturbed periods the rigidity spectrum of primary CR variation at the top of the atmosphere and cut off rigidity change can be determined.

Let us consider now the rigidity spectrum of primary CR variation described by Eq. 3.11.2. In this case (for magnetically disturbed periods) we need at least 5 different components, and the observed CR variation will be described by

$$\delta N_i(R_c,t)=-\Delta R_c(t)W_i(R_c,R_c)+b(t)\Phi_i(R_c,\gamma_o(t),\gamma_1(t),R_o(t)) \tag{3.11.19}$$

(instead of Eq. 3.11.8), where $i = j, k, l, m, n$. Here $W_i(R_c,R_c)$ are determined by Eq. 3.5.3 at $R=R_c$ and $\Phi_i(R_c,\gamma_o,\gamma_1,R_o)$ are determined by Eq. 3.11.9. By excluding from the system of Eq. 3.11.19 the linear unknown variables $\Delta R_c(t)$ and $b(t)$, we obtain three equations for determining the three unknown parameters $\gamma_o(t)$, $\gamma_1(t)$, and $R_o(t)$ of the rigidity spectrum of primary CR variation:

$$\frac{W_l\delta N_m(R_c,t)-W_m\delta N_l(R_c,t)}{W_m\delta N_n(R_c,t)-W_n\delta N_m(R_c,t)}=Y_{lmn}(R_c,\gamma_o,\gamma_1,R_o), \tag{3.11.20}$$

where

$$Y_{lmn}(R_c,\gamma_o,\gamma_1,R_o)=\frac{W_l\Phi_m(R_c,\gamma_o,\gamma_1,R_o)-W_m\Phi_l(R_c,\gamma_o,\gamma_1,R_o)}{W_m\Phi_n(R_c,\gamma_o,\gamma_1,R_o)-W_n\Phi_m(R_c,\gamma_o,\gamma_1,R_o)}. \tag{3.11.21}$$

In Eq. 3.11.20 the left hand side is known from experimental data for each moment of time t, and the right hand side contains known functions of γ_o,γ_1,R_o, calculated by taking into account Eq. 3.11.9 and Eq. 3.11.15 (at $R=R_c$). From the system of three equations of the type of Eq. 3.11.20 one can determine $\gamma_o(t)$, $\gamma_1(t)$, $R_o(t)$, and then the parameters $b(t)$ and $\Delta R_c(t)$ by:

$$b(t)=\frac{W_l\delta N_m(R_c,t)-W_m\delta N_l(R_c,t)}{W_l\Phi_m(R_c,\gamma_o(t),\gamma_1(t),R_o(t))-W_m\Phi_l(R_c,\gamma_o(t),\gamma_1(t),R_o(t))}, \tag{3.11.22}$$

$$\Delta R_c(t)=\frac{\Phi_l(R_c,\gamma_o(t),\gamma_1(t),R_o(t))\delta N_m(R_c,t)-\Phi_m(R_c,\gamma_o(t),\gamma_1(t),R_o(t))\delta N_l(R_c,t)}{\Phi_m(R_c,\gamma_o(t),\gamma_1(t),R_o(t))\delta N_n(R_c,t)-\Phi_n(R_c,\gamma_o(t),\gamma_1(t),R_o(t))\delta N_m(R_c,t)} \tag{3.11.23}$$

3.11.4. Special program for on-line determination of the energy or rigidity spectrum of CR primary variation

Let us consider data from a neutron monitor with independent registration of total neutron intensity and intensities of different multiplicities, as well as intensities of other CR components as input vector $I_m(i)$ at some moment of time i (here m is the order number of channel, e.g., $m=0-$ for total neutron intensity, $m=1-7$ for intensities of different neutron multiplicities from 1 to 7, $m \geq 8$ for intensities of muons from different directions, and so on). For estimation of the statistical properties of the input vector $I_m(i)$ we calculate the average values and standard deviations for each channel $\langle I_m(i)\rangle$ and $\sigma_m(i)$ on the basis of 60 one-minute values that precede the investigated time moment i. During the next step we calculate a vector of relative deviations:

$$\delta I_m(i) = \left(I_m(i)-\langle I_m(i)\rangle\right)/\langle I_m(i)\rangle \tag{3.11.24}$$

and the corresponding standard deviations $\sigma(\delta I_m(i))$. On the basis of the deviation vector $\delta I_m(i)$ we calculate the matrix

$$R_{mn}(i)=\delta I_m(i)/\delta I_n(i) \tag{3.11.25}$$

of ratios of deviations for different channels of registration m and n at the time moment i and their standard deviations $\sigma(R_{mn}(i))$. On the basis of Eq. 3.11.6 and Eq. 3.11.7, and by using Eq. 3.11.24 we calculate the matrix of the spectral slope $\gamma_{mn}(i)$, and then by Eq. 3.11.4 the matrix $b_{mn}(i)$ of the amplitude and estimations of corresponding standard deviations $\sigma(\gamma_{mn}(i))$ and $\sigma(b_{mn}(i))$.

In order to convert the matrix output of estimated spectral slope $\gamma_{mn}(i)$ to the scalar form $\gamma(i)$, we use the estimation of the average values, taking into account the correspondent weights W of the individual values $\gamma_{mn}(i)$ determined by the corresponding standard deviations

$$W(\gamma_{mn}(i))=(\sigma(\gamma_{mn}(i)))^{-2}\left(\sum_{m,n}(\sigma(\gamma_{mn}(i)))^{-2}\right)^{-1}, \tag{3.11.26}$$

and obtain

$$\gamma(i) = \sum_{m,n} \gamma_{mn}(i) \times W(\gamma_{mn}(i)). \tag{3.11.27}$$

We do the same for the parameter $b(i)$:

$$b(i) = \sum_{m,n} b_{mn}(i) \times W(b_{mn}(i)), \tag{3.11.28}$$

where

$$W(b_{mn}(i)) = (\sigma(b_{mn}(i)))^{-2} \left(\sum_{m,n} (\sigma(b_{mn}(i)))^{-2} \right)^{-1}. \tag{3.11.29}$$

From the evaluated values of $\gamma(i)$ and $b(i)$ we then determine the rigidity spectrum of the primary CR variation by using Eq. 3.11.4 for each moment of time:

$$\Delta D(R,i) = b(i) R^{-\gamma(i)} \times D_o(R). \tag{3.11.30}$$

3.12. Spectrographic method on the basis of two CR Observatories data

3.12.1. Determination of the rigidity spectrum of primary CR variation in the magnetically quiet period

For determining the rigidity spectrum of primary CR variation according to Eq. 3.9.1 and 3.9.2, one can use data from pairs of CR Observatories with different cut off rigidities R_{c1} and R_{c2}. If the same component m is used from both Observatories (e.g., total neutron component on about the same level of average air pressure h_o), the energy spectrum in the interval $R_{c1} - R_{c2}$ can be determined approximately for any moment of time t (here $W_{om}(R)$ is determined by Eq. 3.5.1):

$$\frac{\Delta D}{D_o}(R_{c1} - R_{c2}) = \left[\delta N_m(R_{c1}) \left(1 - a_m R_{c1}^{-k_m}\right) - \delta N_m(R_{c2}) \left(1 - a_m R_{c2}^{-k_m}\right) \right] \left(\int_{R_{c1}}^{R_{c2}} W_{om}(R) dR \right)^{-1} \tag{3.12.1}$$

More precisely, the rigidity spectrum of primary CR variation can be determined by the spectrographic method. In this case for determining $b(t)$ and $\gamma(t)$ in Eq. 3.9.1 we need to have data at least of one component on each Observatory. If it is the same component m at both Observatories, parameter $\gamma(t)$ will be evaluated from the equation

$$\delta N_m(R_{c1},t) / \delta N_m(R_{c2},t) = \Psi_{mm}(R_{c1}, R_{c2}, \gamma), \tag{3.12.2}$$

where

$$\Psi_{mm}(R_{c1},R_{c2},\gamma)=F_m(R_{c1},\gamma)/F_m(R_{c2},\gamma), \tag{3.12.3}$$

and then one can determine

$$b(t)=\delta N_m(R_{c1},t)/F_m(R_{c1},\gamma(t))=\delta N_m(R_{c2},t)/F_m(R_{c2},\gamma(t)). \tag{3.12.4}$$

If two different components m and n are used, the solution for γ will be determined by equation:

$$\delta N_m(R_{c1},t)/\delta N_n(R_{c2},t)=\Psi_{mn}(R_{c1},R_{c2},\gamma), \tag{3.12.5}$$

where

$$\Psi_{mn}(R_{c1},R_{c2},\gamma)=F_m(R_{c1},\gamma)/F_n(R_{c2},\gamma), \tag{3.12.6}$$

and then $b(t)$ can be determined from:

$$b(t)=\delta N_m(R_{c1},t)/F_m(R_{c1},\gamma(t))=\delta N_n(R_{c2},t)/F_n(R_{c2},\gamma(t)). \tag{3.12.7}$$

In the case of the rigidity spectrum of primary CR variation determined by Eq. 3.9.2, we need at least 4 components: it can be 1 component from one Observatory and 3 components from the other, or 2 components from each observatory with cut off rigidities R_{c1} and R_{c2}. In the former case the parameters γ_o, γ_1, R_o will be determined by the solution of the system of following three equations

$$\frac{\delta N_k(R_{c1},t)}{\delta N_l(R_{c2},t)}=\frac{\Phi_k(R_{c1},\gamma_o,\gamma_1,R_o)}{\Phi_l(R_{c2},\gamma_o,\gamma_1,R_o)},\ \frac{\delta N_l(R_{c2},t)}{\delta N_m(R_{c2},t)}=Y_{lm}(R_{c2},\gamma_o,\gamma_1,R_o),$$
$$\frac{\delta N_m(R_{c2},t)}{\delta N_n(R_{c2},t)}=Y_{mn}(R_{c2},\gamma_o,\gamma_1,R_o), \tag{3.12.8}$$

and then we determine

$$b(t)=\delta N_k(R_{c1},t)/\Phi_k(R_{c1},\gamma_o(t),\gamma_1(t),R_o(t))=\delta N_l(R_{c2},t)/\Phi_l(R_{c2},\gamma_o(t),\gamma_1(t),R_o(t))$$
$$=\delta N_m(R_{c2},t)/\Phi_m(R_{c2},\gamma_o(t),\gamma_1(t),R_o(t))=\delta N_n(R_{c2},t)/\Phi_n(R_{c2},\gamma_o(t),\gamma_1(t),R_o(t)). \tag{3.12.9}$$

For the latter case, the system of equations for determining parameters γ_o,γ_1,R_o will be

$$\frac{\delta N_k(R_{c1},t)}{\delta N_l(R_{c1},t)}=Y_{kl}(R_{c1},\gamma_o,\gamma_1,R_o),\quad \frac{\delta N_l(R_{c1},t)}{\delta N_m(R_{c2},t)}=\frac{\Phi_l(R_{c1},\gamma_o,\gamma_1,R_o)}{\Phi_m(R_{c2},\gamma_o,\gamma_1,R_o)},$$

$$\frac{\delta N_m(R_{c2},t)}{\delta N_n(R_{c2},t)}=Y_{mn}(R_{c2},\gamma_o,\gamma_1,R_o), \tag{3.12.10}$$

and then we determine

$$b(t)=\delta N_k(R_{c1},t)/\Phi_k(R_{c1},\gamma_o(t),\gamma_1(t),R_o(t))=\delta N_l(R_{c1},t)/\Phi_l(R_{c1},\gamma_o(t),\gamma_1(t),R_o(t))$$

$$=\delta N_m(R_{c2},t)/\Phi_m(R_{c2},\gamma_o(t),\gamma_1(t),R_o(t))=\delta N_n(R_{c2},t)/\Phi_n(R_{c2},\gamma_o(t),\gamma_1(t),R_o(t)).(3.12.11)$$

3.12.2. Determination of the rigidity spectrum of primary CR variation and cut off rigidity change in the magnetically disturbed periods

For the spectrum described by Eq. 3.9.1 we have 4 unknown variables (instead of two for the quiet period): $\Delta R_{c1}(t)$, $\Delta R_{c2}(t)$, $b(t)$, $\gamma(t)$.

If there are 1 and 3 components in both observatories with cut off rigidities R_{c1} and R_{c2}, the system of equations for determining $\Delta R_{c1}(t)$, $\Delta R_{c2}(t)$, $b(t)$, $\gamma(t)$ is

$$\delta N_k(R_{c1},t)=-\Delta R_{c1}(t)W_k(R_{c1},R_{c1})+b(t)F_k(R_{c1},\gamma(t)), \tag{3.12.12}$$

$$\delta N_l(R_{c2},t)=-\Delta R_{c2}(t)W_l(R_{c2},R_{c2})+b(t)F_l(R_{c2},\gamma(t)), \tag{3.12.13}$$

$$\delta N_m(R_{c2},t)=-\Delta R_{c2}(t)W_m(R_{c2},R_{c2})+b(t)F_m(R_{c2},\gamma(t)), \tag{3.12.14}$$

$$\delta N_n(R_{c2},t)=-\Delta R_{c2}(t)W_n(R_{c2},R_{c2})+b(t)F_n(R_{c2},\gamma(t)). \tag{3.12.15}$$

In this case we determine from Eq. 3.12.13–3.12.15 $\gamma(t)$, $b(t)$, and $\Delta R_{c2}(t)$ as follows:

1. We determine the function

$$\Psi_{lmn}(R_{c2},\gamma)=\frac{W_lF_m(R_{c2},\gamma)-W_mF_l(R_{c2},\gamma)}{W_mF_n(R_{c2},\gamma)-W_nF_m(R_{c2},\gamma)}, \tag{3.12.16}$$

where

$$W_l\equiv W_l(R_{c2},R_{c2}),\ W_m\equiv W_m(R_{c2},R_{c2}),\ W_n\equiv W_n(R_{c2},R_{c2}). \tag{3.12.17}$$

2. Then from

$$\Psi_{lmn}(R_{c2},\gamma)=\frac{W_l\delta N_m(R_{c2},t)-W_m\delta N_l(R_{c2},t)}{W_m\delta N_n(R_{c2},t)-W_n\delta N_m(R_{c2},t)}, \tag{3.12.18}$$

the value of $\gamma(t)$ can be determined.

3. Using this value of $\gamma(t)$, for each time t, we determine

$$\Delta R_{c2}(t)=\frac{F_l(R_{c2},\gamma(t))\delta N_m(R_{c2},t)-F_m(R_{c2},\gamma(t))\delta N_l(R_{c2},t)}{F_m(R_{c2},\gamma(t))\delta N_n(R_{c2},t)-F_n(R_{c2},\gamma(t))\delta N_m(R_{c2},t)}, \tag{3.12.19}$$

$$b(t)=\frac{W_l\delta N_m(R_{c2},t)-W_m\delta N_l(R_{c2},t)}{W_lF_m(R_{c2},\gamma(t))-W_mF_l(R_{c2},\gamma(t))}. \tag{3.12.20}$$

4. From Eq. 3.12.12 we then determine

$$\Delta R_{c1}(t)=[b(t)F_k(R_{c1},\gamma(t))-\delta N_k(R_{c1},t)]/W_k(R_{c1},R_{c1}). \tag{3.12.21}$$

If there are 2 and 2 components in both CR Observatories, instead of system Eq. 3.12.12–3.12.15 we will have

$$\delta N_k(R_{c1},t)=-\Delta R_{c1}(t)W_k(R_{c1},R_{c1})+b(t)F_k(R_{c1},\gamma(t)), \tag{3.12.22}$$

$$\delta I_l(R_{c1},t)=-\Delta R_{c1}(t)W_l(R_{c1},R_{c1})+b(t)F_l(R_{c1},\gamma(t)). \tag{3.12.23}$$

$$\delta N_m(R_{c2},t)=-\Delta R_{c2}(t)W_m(R_{c2},R_{c2})+b(t)F_m(R_{c2},\gamma(t)), \tag{3.12.24}$$

$$\delta N_n(R_{c2},t)=-\Delta R_{c2}(t)W_n(R_{c2},R_{c2})+b(t)F_n(R_{c2},\gamma(t)). \tag{3.12.25}$$

From the system of Eq. 3.12.22–3.12.25 we exclude the linear unknowns b, $b(t)$, $\Delta R_{c1}(t)$, $\Delta R_{c2}(t)$ and finally obtain a non-linear equation for determining $\gamma(t)$:

$$\frac{W_k\delta N_l(R_{c1},t)-W_l\delta N_k(R_{c1},t)}{W_m\delta N_n(R_{c2},t)-W_n\delta N_m(R_{c2},t)}=\Psi_{klmn}(R_{c1},R_{c2},\gamma(t)), \tag{3.12.26}$$

where the special function for combination of two Observatories is determined by

$$\Psi_{klmn}(R_{c1},R_{c2},\gamma)=\frac{W_k(R_{c1},R_{c1})F_l(R_{c1},\gamma)-W_l(R_{c1},R_{c1})F_k(R_{c1},\gamma)}{W_m(R_{c2},R_{c2})F_n(R_{c2},\gamma)-W_n(R_{c2},R_{c2})F_m(R_{c2},\gamma)} \tag{3.12.27}$$

which can be calculated for any pair of Observatories by using the known functions $F_k(R_{c1},\gamma)$, $F_l(R_{c1},\gamma)$, $F_m(R_{c2},\gamma)$, $F_n(R_{c2},\gamma)$, and known values $W_k(R_{c1},R_{c1})$, $W_l(R_{c1},R_{c1})$, $W_m(R_{c2},R_{c2})$, and $W_n(R_{c2},R_{c2})$. After determining $\gamma(t)$ we can determine the other 3 unknown variables:

$$\Delta R_{c1}(t)=\frac{F_k(R_{c1},\gamma(t))\delta N_l(R_{c1},t)-F_l(R_{c1},\gamma(t))\delta N_k(R_{c1},t)}{W_kF_l(R_{c1},\gamma(t))-W_lF_k(R_{c1},\gamma(t))}, \tag{3.12.28}$$

$$\Delta R_{c2}(t)=\frac{F_m(R_{c2},\gamma(t))\delta N_n(R_{c2},t)-F_n(R_{c2},\gamma(t))\delta N_m(R_{c2},t)}{W_mF_n(R_{c2},\gamma(t))-W_nF_m(R_{c2},\gamma(t))}, \tag{3.12.29}$$

$$b(t)=\frac{W_k\delta N_l(R_{c1},t)-W_l\delta N_k(R_{c1},t)}{W_kF_l(R_{c1},\gamma(t))-W_lF_k(R_{c1},\gamma(t))}=\frac{W_m\delta N_n(R_{c2},t)-W_n\delta N_m(R_{c2},t)}{W_mF_n(R_{c2},\gamma(t))-W_nF_m(R_{c2},\gamma(t))}. \tag{3.12.30}$$

Let us consider again magnetically disturbed periods, but the rigidity spectrum of primary CR variations in the form described by Eq. 3.9.2. In this case we have 6 unknown variables $\Delta R_{c1}(t)$, $\Delta R_{c2}(t)$, $b(t)$, $\gamma_o(t)$, $\gamma_1(t)$, $R_o(t)$, thus from both observatories we need total at least 6 components (they can be in different combinations). For example, if there are 1 and 5 components from the two observatories, we first solve the set of 5 equations for the second observatory as described in Section 3.9.3 for determining $\Delta R_{c2}(t)$, $b(t)$, $\gamma_o(t)$, $\gamma_1(t)$, $R_o(t)$, and then by using one equation for the first Observatory determine $\Delta R_{c1}(t)$. Let us note that a set from 6 equations for both CR Observatories can be solved also for any other combination of registered components: 2 and 4, or 3 and 3. In all cases the method is as follows: first we exclude the linear unknown variables $\Delta R_{c1}(t)$, $\Delta R_{c2}(t)$, $b(t)$, and then, on the basis of the remaining 3 equations, determine $\gamma_o(t)$, $\gamma_1(t)$, $R_o(t)$; after this it is easy to determine $\Delta R_{c1}(t)$, $\Delta R_{c2}(t)$, $b(t)$. In the solution the functions Φ and Y will be used, instead of the functions F and Ψ that were used above for spectrum described by Eq. 3.9.1.

3.12.3. Spectrographic method for pairs of CR Observatories with about the same asymptotic directions

If the primary CR variation is isotropic, use of the spectrographic method described above will give about the same result for the rigidity spectrum of primary CR variation at the top of atmosphere for any pair of CR Observatories. But for cases in which the primary CR variation is sufficiently anisotropic it is better to apply the spectrographic method to pairs of CR Observatories with about the same asymptotic directions. Comparison of the results from different pairs will then allow determine approximately the CR primary variation distribution out of the atmosphere and out of the magnetosphere. Using the International CR Service (ICRS) proposed by Dorman et al. (1993) and the above technique, the information on the primary CR variation distribution can be obtained in real time scale.

More detailed information on the primary CR variation distribution function over the atmosphere and magnetosphere can be obtained by using the method of ring CR Observatories with about the same asymptotic latitudes (see below, Section 3.13) and global spectrographic method (acceptance vectors and spherical analyses), as described in Section 3.14.

3.13. Ring CR Observatories with about the same asymptotic latitudes (method of variational coefficients).

3.13.1. The basis of the variational coefficients method

McCracken et al. (1962, 1965) developed, for the study of CR anisotropy, the method of variational coefficients, which is a generalization of the method of coupling coefficients to the case where an anisotropic CR flux is recorded. Its main point is the following. Generally CR anisotropy can be characterized by the differential rigidity spectrum $D_k(R)$ in a small solid angle of asymptotic directions Ω_k, as a sub-division

of the entire 4π of the celestial sphere. Then the counting rate ΔN_i of a detector, recording the secondary component of type i owed to the flux of primary particles from the solid angle Ω_k in the rigidity interval R, $R+dR$ and generating secondary particles in solid angle $d\omega$ near zenith angle Z and azimuth φ, will be:

$$\Delta N_i(\Omega_k,R,Z,\varphi)=D_k(R)F_i(R,Z,\varphi)d\omega dR\,. \tag{3.13.1}$$

Let us assume that $F_i(R,Z,\varphi)$ can be written as a product

$$F_i(R,Z,\varphi)=X_i(R)\Phi_i(Z,\varphi)\,. \tag{3.13.2}$$

Then by integrating over Z and φ we shall find

$$\Delta N_i(\Omega_k,R)=D_k(R)X_i(R)Y_i(\Omega_k,R)dR\,. \tag{3.13.3}$$

where $Y_i(\Omega_k,R)$ is the result of integrating $\Phi_i(Z,\varphi)$ over all Z and φ for primary particles with rigidity R coming from the solid angle of asymptotic directions Ω_k.

For an isotropic flux $\Omega_k=4\pi$, $D_k(R)=D_o(R)$ and

$$\Delta N_i(4\pi,R)=D_o(R)X_i(R)Y_i(4\pi,R)dR\,. \tag{3.13.4}$$

On the other hand, from the determination of the coupling coefficients $W_i(R)$ in Section 3.2 (according to Dorman, M1957) it follows that

$$W_i(R)=-dN_i/N_i dR\,, \tag{3.13.5}$$

Comparison of Eq. 3.13.4 and Eq. 3.13.5 gives

$$X_i(R)=\frac{N_i W_i(R)}{D_o(R)Y_i(4\pi,R)}, \tag{3.13.6}$$

and substitution in Eq. 3.13.3 gives

$$\Delta N_i(\Omega_k,R)=N_i W_i(R)\frac{D_k(R)}{D_o(R)}\frac{Y_i(\Omega_k,R)}{Y_i(4\pi,R)}dR\,. \tag{3.13.7}$$

In Eq. 3.13.7 $D_o(R)$ is a certain average CR energy spectrum, N_i and $W_i(R)$ are respectively the mean counting rate for the given instrument and the coupling coefficient for the given isotropic energy spectrum $D_o(R)$. Let $D_k(R)=D_o(R)+\Delta D_k(R)$. Then integration with respect to R gives

$$\frac{\Delta N_i(\Omega_k,R)}{N_i}=\int_0^{\infty}W_i(R)\frac{\Delta D_k(R)}{D_o(R)}\frac{Y_i(\Omega_k,R)}{Y_i(4\pi,R)}dR\,. \tag{3.13.8}$$

We assume that

$$\Delta D_k(R)/D_o(R)=AR^{\beta}, \tag{3.13.9}$$

where A is, in general, a function of the asymptotic direction, R is measured in GV and β is the exponent in the anisotropy spectrum. Substitution of Eq. 3.13.9 in Eq. 3.13.8 gives

$$\Delta N_i(\Omega_k,R)/N_i=AV_i(\Omega_k,\beta), \tag{3.13.10}$$

where

$$V_i(\Omega_k,\beta)=\int_0^{\infty}W_i(R)R^{\beta}\frac{Y_i(\Omega_k,R)}{Y_i(4\pi,R)}dR\,. \tag{3.13.11}$$

is the so called partial variational coefficient of the detector of type *i,* corresponding to the solid angle Ω_k and the exponent β in the anisotropy spectrum.

3.13.2. Determination of the longitude variational coefficients if the anisotropy follows a cosine law in latitude

In the coefficients $V_i(\Omega_k,\beta)$ the ratio $Y_i(\Omega_k,R)/Y_i(4\pi,R)$ appears, which in turn contains the asymptotic directions for various zenith and azimuth angles. Considering that the main contribution to the counting rate of a neutron monitor is owed to primary particles reaching the Earth's atmosphere under zenith angles $Z < 40°$, this ratio was computed in McCracken et al. (1962, 1965) using the results of trajectory computations for Z = 0°, 16° and 32° and directions of incidence from north, south, east, and west. Further it was assumed that the quantity A may be written as the product of two functions of asymptotic longitude Ψ and asymptotic latitude Λ, the latter being simply $\cos\Lambda$, i.e.,

$$A(\Psi,\Lambda)=f(\Psi)\cos\Lambda\,. \tag{3.13.12}$$

This assumption evidently restricts the possible forms of anisotropy but the actual solar-daily anisotropy does not differ much from Eq. 3.13.12. Therefore one may write for each interval of asymptotic longitudes $\Psi_j \pm 2.5^o$:

$$\Delta N_i(\Psi_j)/N_i=f(\Psi_j)V_i(\Psi_j,\beta), \tag{3.13.13}$$

where

$$V_i(\Psi_j,\beta)=\sum_k V_i(\Omega_{jk}(\Psi_j,\Lambda_k),\beta)\cos\Lambda_k \tag{3.13.14}$$

are the longitude variational coefficients. We shall distinguish in terminology the differential variational coefficient $V_i(\Omega_k,\beta)$ and the longitude variational coefficient

$V_i(\Psi_j, \beta)$. The first coefficient describes a detailed picture of the anisotropy (valid for any type of its space distribution), and the second only the longitude dependence of the anisotropy.

Longitude variational coefficients have been computed by McCracken et al. (1965) for 79 neutron monitors of the world-wide network of stations for 10 values of β from +0.6 to −1.5 (with the step 0.2), and values of Ψ_j in 5° intervals of longitude. As an example, Table 3.13.1 shows the results of McCracken et al. (1965) for β equal to 0 and −1 for four stations: high-latitude (Thule, Greenland), intermediate latitude (Chicago, USA), low-latitude (Alma-Ata, Kazakhstan) and equatorial (Huancayo, Peru).

Table 3.13.1. Longitude variational coefficients (according to McCracken et al., 1965).

Station	Thule		Chicago		Alma-Ata		Huancayo	
Coordinates	76°.55 N		41°.83 N		43°.20 N		12°.03 S	
	68°.84 W		87°.67 W		76°.94 E		76°.88 W	
Spectrum slope	$\beta = 0$	$\beta = -1$	$\beta = 0$	$\beta = -1$	$\beta = 0$	$\beta = -1$	$\beta = 0$	$\beta = -1$
Asymptotic longitude								
0° –5°	0.75	0.01	0.75	0.21	0.72	0.10	1.51	0.06
5 –10	0.18	0.00	0.38	0.11	0	0	1.45	0.06
10 –15	0.06	0.00	0	0	0.64	0.10	3.02	0.15
15 –20	0.53	0.02	0	0	0	0	1.52	0.06
20 –25	0	0	0.45	0.18	0	0	2.32	0.12
25 –30	0.08	0.00	0.23	0.09	0	0	1.16	0.06
30 –35	0	0	0.69	0.28	0	0	2.22	0.13
35 –40	0.05	0.00	0.46	0.19	0	0	1.16	0.06
40 –45	0.29	0.01	0	0	0.67	0.00	2.69	0.18
45 –50	0.09	0.00	0.23	0.09	0.52	0.00	2.28	0.11
50 –55	0.01	0.00	0	0	0.41	0.00	0.74	0.04
55 –60	0.20	0	0	0	0.45	0.00	1.14	0.06
60 –65	0	0.00	0	0	0.71	0.01	0	0
65 –70	0.11	0	0	0	0.49	0.00	0.77	0.05
70 –75	0	0.00	0	0	0.27	0.00	0	0
75 –80	0.09	0.00	0	0	0.91	0.01	2.05	0.14
80 –85	0.07	0.00	0	0	2.81	0.01	1.12	0.09
85 –90	0.08	0	0	0	2.32	0.02	0	0
90 –95	0.15	0	0	0	3.00	0.04	1.81	0.11
95 –100	0	0	0	0	1.88	0.03	0	0
100 –105	0.17	0	0	0	2.13	0.04	0.98	0.07
105 –110	0	0	0	0	3.01	0.06	0	0
110 –115	0.12	0	0	0	2.89	0.07	0	0
115 –120	0.11	0	0	0	2.34	0.07	0	0
120 –125	0	0.00	0	0	3.59	0.10	0	0
125 –130	0.01	0	0	0	4.39	0.15	0	0
130 –135	0	0.00	0	0	5.33	0.20	0	0
135 –140	0.11	0.00	0	0	5.29	0.24	0	0
140 –145	0.11	0.00	0	0	2.79	0.11	0	0
145 –150	0	0	0	0	4.28	0.22	0	0
150 –155	0	0	0	0	5.00	0.30	0	0
155 –160	0	0	0	0	1.17	0.08	0	0
160 –165	0	0	0	0	2.39	0.23	1.06	0.07
165 –170	0	0	0	0	2.55	0.20	0	0
170 –175	0	0	0	0	2.18	0.16	0	0
175 –180	0	0	0	0	1.92	0.15	1.16	0.06
180 –185	0.17	0.00	0	0	2.90	0.26	0	0
185 –190	0		0	0	2.02	0.18	0	0
190 –195	0.15	0.00	0	0	1.94	0.21	0	0

Table 3.13.1. (continued).

Station Coordinates	Thule 76°.55 N 68°.84 W		Chicago 41°.83 N 87°.67 W		Alma-Ata 43°.20 N 76°.94 E		Huancayo 12°.03 S 76°.88 W	
Spectrum slope	$\beta = 0$	$\beta = -1$	$\beta = 0$	$\beta = -1$	$\beta = 0$	$\beta = -1$	$\beta = 0$	$\beta = -1$
Asymptotic longitude								
195 –200	0		0	0	3.47	0.34	0	0
200 –205	0.24	0.00	0	0	0.68	0.007	0	0
205 –210	0.09	0.00	0	0	1.40	0.14	0	0
210 –215	0.30	0.00	0	0	2.05	0.24	0	0
215 –220	0.29	0.00	0	0	0.61	0.07	0	0
220 –225	0.29	0.00	0	0	1.89	0.21	0	0
225 –230	0.23	0.00	0	0	0	0	0	0
230 –235	0.23	0.00	0.50	0.00	1.52	0.20	0	0
235 –240	0.31	0.00	0.38	0.00	0.60	0.07	0	0
240 –245	0.23	0.00	0.30	0.00	0.76	0.10	0	0
245 –250	0	0	0.23	0.00	0	0	0	0
250 –255	0	0	0.40	0.00	0	0	0.24	0.00
255 –260	0.58	0.03	0.43	0.00	1.24	0.17	0.93	0.00
260 –265	0.10	0.01	0.38	0.00	0.76	0.10	0.96	0.01
265 –270	0.35	0.01	1.01	0.01	0	0	0.81	0.01
270 –275	0.26	0.01	3.09	0.03	0	0	1.81	0.01
275 –280	0.80	0.03	2.94	0.04	0	0	1.40	0.01
280 –285	0.87	0.02	3.00	0.07	0.76	0.10	1.38	0.02
285 –290	0.93	0.02	2.01	0.06	0	0	5.19	0.04
290 –295	1.92	0.07	2.88	0.11	0	0	4.81	0.03
295 –300	0.50	0.02	3.31	0.12	0.76	0.10	3.35	0.05
300 –305	1.00	0.08	6.42	0.38	0	0	5.69	0.07
305 –310	1.50	0.19	24.48	1.93	0	0	3.60	0.04
310 –315	2.28	0.22	11.64	1.00	0	0	4.38	0.08
315 –320	4.52	0.67	6.76	0.55	0	0	4.25	0.10
320 –325	5.01	0.92	4.84	0.66	0	0	3.98	0.07
325 –330	1.74	0.31	3.77	0.52	0	0	2.17	0.03
330 –335	1.61	0.14	5.70	0.99	0	0	5.85	0.16
335 –340	1.08	0.07	1.01	0.22	0	0	3.66	0.09
340 –345	1.40	0.08	0	0	0	0	2.60	0.10
345 –350	0.83	0.03	0.76	0.22	0	0	0.58	0.01
350 –355	0.63	0.03	1.13	0.32	0	0	3.45	0.14
355 –360	0.57	0.02	0.38	0.11	0	0	4.93	0.20
1st harmonic								
amplitude	26.41	2.90	83.62	7.59	60.17	3.44	63.56	1.85
phase shift (hrs)	1.70	1.97	2.52	3.64	4.54	6.86	3.56	5.97
2nd harmonic								
amplitude	18.73	2.63	68.06	5.66	23.32	1.49	27.82	0.62
phase shift (hrs)	1.88	2.00	2.48	3.38	3.98	6.50	2.52	5.41

3.13.3. Ways of using the longitude variational coefficients in studying the anisotropy of primary variations out of the magnetosphere

When the longitude variational coefficients are known, the distribution over the surface of the Earth of amplitude and phase of the anisotropy can be found. Let the longitude distribution of the intensity outside the Earth's magnetosphere be characterized by the function $f(\Psi)$, the latitude distribution being taken in the form $\cos\Lambda$. Let χ be the angle between the asymptotic direction for the given station and the direction

towards the Sun (counted to the west from the line Earth-Sun, see Fig. 3.13.1) and T the local time for the given station in hours. Then

$$\chi = \Psi + 15^o \times T - 180^o . \tag{3.13.15}$$

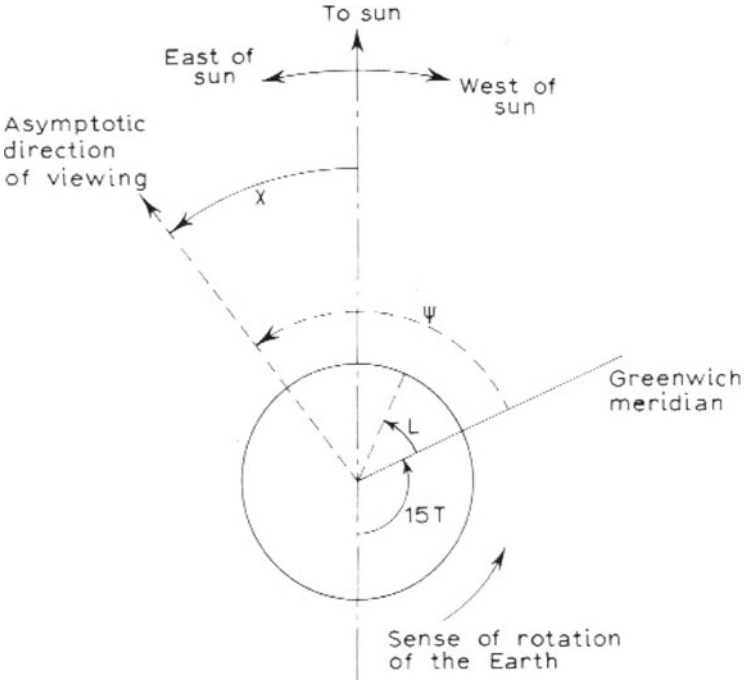

Fig. 3.13.1. Angles employed to specify the asymptotic direction of viewing of an arbitrary CR Observatory.

Let us develop the distribution $f(\chi)$ in the series

$$f(\chi) = \sum_{n=1}^{\infty} \alpha_n \cos n(\chi - \chi_n), \tag{3.13.16}$$

where χ_n is the direction on the maximum of the n-th harmonic, and α_n its amplitude (all harmonics are assumed to have the same spectrum). Substituting Eq. 3.13.16 in Eq. 3.13.13 and adding over all intervals of longitudes from 0 to 360° one finds

$$\frac{\Delta N_i(T)}{N_i} = \sum_{j=0}^{71} V_i\left(5^o j + 2.5^o, \beta\right) \sum_{n=1}^{\infty} \alpha_n \cos n\left(5^o j + 15^o T + 2.5^o - 180^o - \chi_n\right). \tag{3.13.17}$$

Eq. 3.13.17 can be transformed into

$$\frac{\Delta N_i(T)}{N_i} = \sum_{n=1}^{\infty} \alpha_n B_{in} \cos\left[n\left(15^o T - 180^o - \chi_n\right) + \gamma_{in}\right], \tag{3.13.18}$$

where

$$B_{in} = \left\{ \left[\sum_{j=0}^{71} V_i\left(5^o j + 2.5^o, \beta\right) \sin n\left(5^o j + 2.5^o\right) \right]^2 + \left[\sum_{j=0}^{71} V_i\left(5^o j + 2.5^o, \beta\right) \cos n\left(5^o j + 2.5^o\right) \right]^2 \right\}^{1/2}, \tag{3.13.19}$$

and

$$\gamma_{in} = \operatorname{arctg} \frac{\sum_{j=0}^{71} V_i\left(5^o j + 2.5^o, \beta\right) \sin n\left(5^o j + 2.5^o\right)}{\sum_{j=0}^{71} V_i\left(5^o j + 2.5^o, \beta\right) \cos n\left(5^o j + 2.5^o\right)} . \tag{3.13.20}$$

It is easily seen that the local time of maximum for the n-th harmonic $T_{\max,in}$ at a station with geographic longitude L will be

$$T_{\max,in} = \frac{180^o n + n\chi_n - (\gamma_{in} - nL)}{15^o n} \text{ hours.} \tag{3.13.21}$$

This means that the maximum is shifted owing to the influence of the geomagnetic field by $(\gamma_{in} - nL)/(15^o n)$ hours. These shifts and the relative amplitudes B_{in} for $n = 1$ and 2 (i.e. for the first and second harmonics of the CR diurnal variation) were computed by McCracken et al. (1965) for the same 79 neutron monitors and the same 10 values of β from +0.6 to −1.5 by the longitudinal variation coefficients. Table 3.13.1 gives in the bottom lines, again as an example, the values for the four stations mentioned above.

3.13.4. Limitations of the method of variational coefficients

The method of variational coefficients discussed above has played an important role in investigations of CR anisotropy (see in detail in Dorman, M2005). However, in many cases it cannot be used on account of the following limitations:

1. It is assumed that $\Delta D(R)/D_o(R) \propto R^{\beta}$ in the whole range of R with constant β.
2. It is assumed that for all harmonics and all asymptotic directions $\Delta D(R)/D_o(R)$ depends on R in the same way.
3. It is assumed that for all R and all harmonics the amplitude of the anisotropy depends on the asymptotic latitude Λ by the same $\cos\Lambda$ law.

3.14. Global spectrographic method (acceptance vectors and spherical analyses)

Kryrnsky et al. (1966, 1967a,b,c), Chirkov et al. (1967), and Nagashima (1971) have developed the method of investigating the space distribution of primary CR intensity variation out of the magnetosphere, in the interplanetary space by means of the acceptance vectors of detectors. This is a further development of the method of integral multiplicities and coupling coefficients or functions (Sections 3.2–3.10) and of the method of variational coefficients (Section 3.11). The simplest version of the global spectrographic method was developed in Belov et al. (1983).

3.14.1. Representation of primary CR intensity variation distribution function by spherical harmonics

The CR intensity depends on their direction of motion and may be represented by a scalar on the celestial sphere. This function $I(\theta,\varphi)$, where θ,φ are the latitude and longitude angles, may be developed in a series of spherical harmonic functions as:

$$I(\theta,\varphi)=\sum_{n=0}^{\infty}\sum_{m=0}^{n}\left(a_n^m\cos m\varphi+b_n^m\sin m\varphi\right)P_n^m(\sin\theta), \tag{3.14.1}$$

where $P_n^m(\sin\theta)$ are the associated Legendre functions. The intensity distribution can be measured in absolute or in relative units. Since the coefficient a_o^o, determining the isotropic intensity, is 2–3 orders larger than the other coefficients, it is more convenient to use relative units. We subtract from a_o^o the constant part $\bar{a}_o^o$, close to the time average of a_o^o, and refer all coefficients of the series determined by the Eq. 3.14.1 to $\bar{a}_o^o$. Then the values

$$I'(\theta,\varphi)=\frac{I(\theta,\varphi)-\bar{a}_o^o}{\bar{a}_o^o},\quad \bar{a'}_o^o=\frac{a_o^o-\bar{a}_o^o}{\bar{a}_o^o},\quad \bar{a'}_n^m=\frac{a_n^m}{\bar{a}_o^o} \tag{3.14.2}$$

form a new series differing from Eq. 3.14.1 only by the primes. In the following this series described by Eq. 3.14.1 with variables of Eq. 3.14.2 will be used but the primes are omitted. The intensity distribution described by Eq. 3.14.1 can be thought of as a vector $\mathbf{A}=\left\{a_n^m,b_n^m\right\}$, in which the infinite number of components ($0\le m\le n<\infty$) has been arranged in a definite order. Then for each point-like instrument the acceptance vector **K**, also with an infinite number of dimensions, may be defined so that the intensity recorded by the instrument is the scalar product

$$I=\mathbf{A}\bullet\mathbf{K}, \tag{3.14.3}$$

where

$$\mathbf{K} = \left\{P_n^m(\sin\theta)\cos m\varphi,\ P_n^m(\sin\theta)\sin m\varphi\right\}. \tag{3.14.4}$$

The vectors **A** and **K** may also be written with complex components:

$$\mathbf{A}=\{r_n^m\},\ r_n^m = a_n^m + i b_n^m;\ \mathbf{K}=\{Z_n^m\},\ Z_n^m = x_n^m + i y_n^m = e^{im\varphi}P_n^m(\sin\theta). \tag{3.14.5}$$

The components of these vectors will be displayed in order of increasing values of the indices n, m: $r_0^0, r_1^0, r_1^1, r_2^0, r_2^1, r_2^2, r_3^0, ...; Z_0^0, Z_1^0, Z_1^1, Z_2^0, Z_2^1, ...$ With Eq. 3.14.5 the Eq. 3.14.3 becomes

$$I = (\mathbf{A}\bullet\mathbf{K} + \mathbf{A}^*\bullet\mathbf{K}^*)/2\,, \tag{3.14.6}$$

where **A*** and **K*** are the conjugate complex vectors of **A** and **K**.

3.14.2. The CR space distribution and the diurnal variation

We shall express the CR distribution vector **A** in an immobile geographic coordinate system (θ',φ'), and the acceptance vector **K** in the geographic system rotating with the Earth (θ'',φ''). With this choice of coordinates **A** and **K** can be taken to be independent of time.

At the moment t in 'universal' time (local time at the zero meridian) the instrument will be directed towards the point $\theta'=\theta$, $\varphi'=\varphi''+\omega t$ and will record the intensity

$$I(t)=\sum_{n=0}^{\infty}\sum_{m=0}^{n}\left[a_n^m\cos m(\varphi''+\omega t)+b_n^m\sin m(\varphi''+\omega t)\right]P_n^m(\sin\theta), \tag{3.14.7}$$

Hence owing to the Earth's rotation a diurnal variation will be recorded, and which can be expressed in a Fourier series:

$$I(t)=\sum_{m=0}^{\infty}(A_m\cos m\omega t + B_m\sin m\omega t), \tag{3.14.8}$$

where

$$A_m = \sum_{n=m}^{\infty}\left(a_n^m x_n^m + b_n^m y_n^m\right),\ B_m = \sum_{n=m}^{\infty}\left(-a_n^m y_n^m + b_n^m x_n^m\right). \tag{3.14.9}$$

Here $a_n^m, b_n^m, x_n^m, y_n^m$ are the components of the vectors **A** and **K** in the coordinate systems chosen above and t in Eq. 3.14.8 is local time. The harmonics of the series described by Eq. 3.13.9 can be represented by vectors with periods of 24, 12, 8, 6, ... hours. In the complex plane, where the real axis passes through 0 hours, each harmonic can be expressed by the corresponding complex number

$$\Theta_m = \sum_{n=m}^{\infty} r_n^m \left(Z_n^m\right)^* . \tag{3.14.10}$$

It is seen from Eq. 3.14.10 that the component r_n^m of vector **A** determines the contribution of the n-th spherical harmonic of the CR distribution to the m-th harmonic of the diurnal variation. Evidently this contribution is also proportional to the modulus $\left|Z_n^m\right|$. The amplitude of the diurnal variations therefore varies with the angle θ between the direction of incidence of the particles and the plane of the geographic equator as the function $Z_n^m(\theta) = P_n^m(\sin\theta)$ shown in Fig. 3.14.1. Negative values indicate that the phase of the diurnal variations is reversed. This diagram shows that the variations with periods of 24 h and 12 h, arising from the first and second spherical harmonics, are largest at the equator. The second 24 h variation, arising from the presence of the second spherical harmonic, has its maximum at latitudes +45° and becomes zero at the poles and at the equator. In the northern and southern hemispheres its phase is the opposite. Variations with a period of 8 hours must be even more concentrated towards the equator, and evidently, can hardly be observed at intermediate and high latitudes.

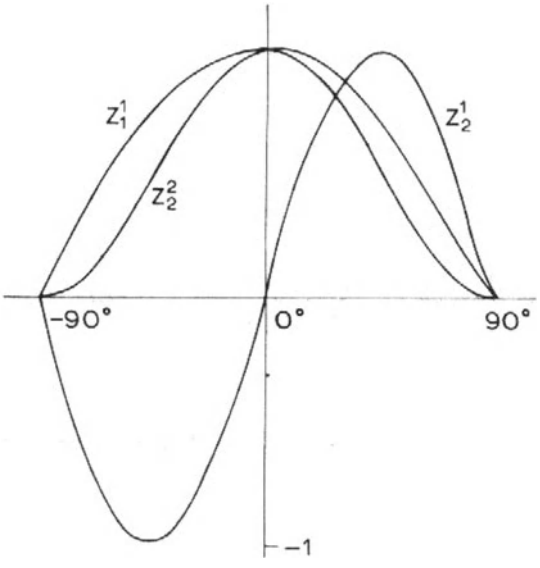

Fig. 3.14.1. Latitude dependence of the function Z_n^m of low order. The vertical scale is different for each curve.

3.14.3. Determination of acceptance vectors of actual instruments

The notion acceptance vector, defined above for an ideal point-like instrument can be generalized to the case of actual instruments. First, the instrument covers a certain region of the sky defined by its directional diagram

$$N(\alpha,\beta)d\omega = N(\alpha,\beta)\sin\beta\, d\alpha\, d\beta, \tag{3.14.11}$$

where α,β are the azimuth and zenith angles and $N(\alpha,\beta)$ is normalized by

$$\int_0^{2\pi}\int_0^{\pi/2} N(\alpha,\beta)\sin\beta\, d\alpha\, d\beta = 1. \tag{3.14.12}$$

Further, as in Eq. 3.14.2, we assume that the isotropic background $\bar{I}_O(R)$ near the mean intensity level over a sufficiently long period, has been subtracted from the distribution $I(\theta,\varphi,R)$ and that the intensity distribution itself is measured in relative units in fractions of the isotropic background $\bar{I}_O(R)$. Moreover, we assume that each component can be represented in the form:

$$r_n^m(R) = r_n^m(R_O) f_n(R), \tag{3.14.13}$$

where R_O is a certain constant rigidity. The function $f_n(R)$ is the rigidity spectrum of the *n*-th spherical harmonic and the restricting assumption is made that it is independent of *m*. Each instrument records the integral intensity averaged over the primary rigidities *R* with weight determined by the coupling coefficient *W*(*R*) (Dorman, M1957) normalized to

$$\int_{R_c}^{\infty} W(R)dR = 1, \tag{3.14.14}$$

where R_c is the geomagnetic cut off rigidity. The coupling coefficients also depend on the zenith angle of observation β, i.e. $W(R,\beta)$, with the normalizing condition analogous to Eq. 3.14.14: $\int_{R_c}^{\infty} W(R,\beta)dR = 1$. The coupling coefficients $W(R)$ and $W(R,\beta)$ are connected by the directional diagram:

$$W(R) = \int_0^{2\pi}\int_0^{\pi/2} W(R,\beta)N(\alpha,\beta)\sin\beta\, d\alpha\, d\beta. \tag{3.14.15}$$

Hence the integral distribution becomes

$$I(\theta,\varphi) = \int_{R_c}^{\infty} W(R)I(\theta,\varphi,R)dR, \tag{3.14.16}$$

or

$$A = \int_{R_c}^{\infty} W(R)A(R)dR \,. \tag{3.14.17}$$

We define the vector **K** for the actual instrument so that the Eq. 3.14.3 holds, but now **A** is given by Eq. 3.14.17. We remember that in Eq. 3.14.3 **A** and **K** must be defined in one coordinate system; it is convenient to choose for this system the geomagnetic system. Particles incident under angles α,β arrive from the direction $\theta(R,\alpha,\beta)$, $\varphi(R,\alpha,\beta)$. The angles θ (asymptotic latitude) and φ (offset angle in longitude) take into account the influence of the geomagnetic field. They also depend on the geographic position of the instrument. However, if the geomagnetic field is taken to be a dipole the angles θ and φ will not depend on the geomagnetic longitude of the instrument; later a correction will be applied to take account of the real geomagnetic field.

The intensity owed to particles incident under angles α,β (in the interval $d\alpha,d\beta$) and connected with rigidity R (interval dR) in the primary spectrum is

$$dI = W(R,\beta)\sin\beta \sum_{n=0}^{\infty}\sum_{m=0}^{n}\left[a_{nm}(R)x_n^m(R,\alpha,\beta)+b_{nm}(R)y_n^m(R,\alpha,\beta)\right]dRd\alpha d\beta$$

$$=\frac{1}{2}W(R,\beta)\sin\beta \sum_{n=0}^{\infty}\sum_{m=0}^{n}\left[r_{nm}(R)Z_n^{m*}(R,\alpha,\beta)+r_n^{m*}(R)Z_n^m(R,\alpha,\beta)\right]dRd\alpha d\beta, \tag{3.14.18}$$

where

$$Z_n^m(R,\alpha,\beta)=x_n^m(R,\alpha,\beta)+iy_n^m(R,\alpha,\beta)=\exp(im\varphi(R,\alpha,\beta))P_n^m(\sin\theta(R,\alpha,\beta)). \tag{3.14.19}$$

The total intensity I is obtained by threefold integration with respect to rigidity R and the angles α,β. The double sum (over n and m) thus contains integrals of the type

$$\int_{R_c}^{\infty}\int_0^{2\pi}\int_0^{\pi/2} W(R,\beta)N(\alpha,\beta)r_n^m(R)Z_n^m(R,\alpha,\beta)dRd\alpha\sin\beta d\beta \,. \tag{3.14.20}$$

With Eq. 3.14.13 we find I in the form described by Eq. 3.14.6, but now the vector **A** is determined by Eq. 3.14.17 and the acceptance vector **K** has components

$$Z_n^m = \frac{\int_{R_c}^{\infty}\int_0^{2\pi}\int_0^{\pi/2} W(R,\beta)f_n(R)N(\alpha,\beta)e^{im\varphi(R,\alpha,\beta)}P_n^m(\sin\theta(R,\alpha,\beta))dRd\alpha\sin\beta d\beta}{\int_{R_c}^{\infty}\int_0^{2\pi}\int_0^{\pi/2} W(R,\beta)f_n(R)N(\alpha,\beta)dRd\alpha\sin\beta d\beta} \,. \tag{3.14.21}$$

Eq. 3.14.21 represents the averaging of the components of **K** over the coupling coefficients and the directional diagram. Here the role of the coupling coefficients for the anisotropic intensity is performed by the products $W(R)f_n(R)$. If these functions are normalized analogously to Eq. 3.14.14 the denominator in Eq. 3.14.21 can be omitted. The spectra $f_n(R)$ must, in general, be determined. However, since the components of the acceptance vector depend relatively little on the form of the spectra, they may be computed from spectra, in zero approximation, say $f_n(R)$ = const. After the vector **A** has been found for the different components with different $W(R)$, one can estimate the functions **A**(R) by means of Eq. 3.14.17, one can find the spectrum $f_n(R)$ in the first approximation, according to Eq. 3.14.13 and then iterate the procedure.

3.14.4. Acceptance vectors for neutron monitors

Acceptance vectors, computed by Eq. 3.14.21 for 73 neutron monitors of the world-wide net, are given in Table 3.14.1. In these computations the real magnetic field, asymptotic directions, and cut off rigidities of McCracken et al. (1965) were used. It was assumed that the counting rate in the neutron monitor is due only to vertically incident particles. Estimates Chirkov et al. (1967) based on directional diagrams of a neutron monitor in the form

$$N(\alpha,\beta)=\left(1+\frac{h}{L\cos\beta}\right)\exp\left(-\frac{h}{L\cos\beta\sin\beta}\right) \tag{3.14.22}$$

and in the form

$$N(\alpha,\beta)=\cos^6\beta\sin\beta \tag{3.14.23}$$

showed that numerically the acceptance vectors for $n \leq 2$ did not differ from those for vertically incident particles. Also the variation of the coupling coefficients from maximum to minimum solar activity was taken into account. The computations were made for two forms of the anisotropy spectrum:

$$f_n(R)=aR^{-\gamma}, \tag{3.14.24}$$

where $\gamma = 0$, 0.5, and 1.0, and

$$f_n(R)=\frac{0.006b}{b+R}, \tag{3.14.25}$$

where b = 10, 30, and 100 GV.

Table 3.14.1. Acceptance vectors computed for NM of the worldwide net.

Name of station	Φ						$\lvert Z_1^1 \rvert$					
	γ			b			γ			b		
	0	−0.5	−1.0	10	30	100	0	−0.5	−1.0	10	30	100
	1	2	3	4	5	6	7	8	9	10	11	12
1. Thule	74.0	74.0	72.0	74.0	74.0	74.0	.27	.30	.31	.30	.29	.28
2. Resolute	72.0	70.0	67.0	68.5	70.0	70.0	.32	.36	.40	.37	.36	.34
3. Alert	84.5	84.5	84.5	84.5	84.5	84.5	.10	.10	.10	.10	.10	.10
4. Murchison Bay	72.0	68.0	65.0	68.0	70.0	71.0	.32	.39	.45	.40	.37	.35
5. Heiss Is.	70.0	70.0	61.0	65.0	65.5	67.0	.34	.42	.49	.44	.40	.39
6. Inuvik	49.0	41.5	36.5	41.5	43.5	46.2	.62	.71	.77	.73	.70	.66
7. Churchill	41.5	33.5	28.5	33.0	35.5	38.5	.70	.80	.85	.81	.77	.74
8. Reykjavik	46.5	38.0	31.0	37.0	39.5	42.5	.63	.74	.82	.76	.72	.68
9. Goose Bay	34.5	24.0	16.5	23.0	26.5	30.0	.74	.84	.90	.86	.82	.79
10. Tixie	48.5	39.0	31.0	37.0	40.5	45.0	.61	.73	.81	.75	.71	.66
11. College	38.0	27.0	19.0	26.5	29.5	33.5	.72	.83	.89	.85	.81	.77
12. Kiruna	48.0	38.0	31.0	37.5	40.5	44.0	.62	.73	.81	.75	.71	.68
13. Cape Schmidt	40.5	30.0	22.5	28.5	30.5	36.5	.68	.80	.87	.82	.79	.74
14. Apatity	40.0	37.0	29.0	35.5	39.5	42.0	.63	.73	.81	.76	.72	.68
15. Oulu	40.5	32.0	24.0	31.0	34.0	38.0	.67	.77	.84	.80	.76	.72
16. Deep-River	20.5	2.5	0	0.5	10.5	15.5	.82	.88	.90	.91	.88	.85
17. Ottawa	19.5	7.5	1.0	6.0	10.0	14.0	.82	.88	.89	.90	.88	.86
18. Lervik	35.0	24.0	16.0	23.0	27.0	31.0	.71	.80	.85	.83	.80	.76
19. Sulphur	19.5	6.0	−4.0	5.0	9.0	13.5	.82	.86	.85	.88	.86	.85
20. Washington	18.0	6.5	1.0	5.0	8.5	13.0	.81	.85	.84	.87	.86	.84
21. Durham	16.5	4.0	−4.0	22.5	6.0	10.5	.81	.85	.85	.88	.86	.84
22. Upsala	32.0	21.0	13.0	19.5	24.0	27.5	.72	.82	.85	.84	.80	.77
23. Cambridge	18.0	8.0	1.0	6.5	10.0	13.5	.72	.79	.80	.82	.81	.80
24. Yakutsk	29.0	14.5	4.5	12.0	16.5	22.5	.73	.81	.84	.84	.82	.78
25. Chicago	10.5	−2.0	−11.0	−4.5	0	5.0	.82	.84	.85	.86	.85	.85
26. Swarthmore	10.5	−1.0	−7.5	−2.5	−1.5	6.0	.82	.81	.81	.84	.84	.82
27. Leeds	27.5	18.0	7.0	12.0	16.0	21.0	.71	.76	.76	.80	.78	.76
28. Kiel	29.5	18.0	8.5	15.0	19.5	24.5	.70	.76	.77	.79	.77	.74
29. Sverdlovsk	27.5	15.0	6.5	12.5	17.0	21.5	.71	.75	.73	.77	.77	.75
30. Moscow	25.5	13.0	5.0	10.5	15.0	20.0	.71	.75	.76	.78	.77	.76
31. London	24.5	11.0	4.0	9.0	13.5	18.0	.70	.74	.75	.78	.76	.74
32. Denver	3.0	−10.0	−18.0	−13.0	−8.0	3.0	.80	.74	.71	.76	.76	.76
33. Lindau	24.5	19.0	5.0	9.0	13.0	18.0	.70	.74	.73	.76	.76	.73
34. Climax	3.0	−10.0	−17.0	−13.5	−8.5	−4.0	.74	.73	.69	.73	.75	.76
35. Orsay	22.0	10.0	4.0	7.0	11.0	16.0	.66	.70	.71	.73	.72	.70
36. Irkutsk	20.5	6.0	−3.0	2.5	5.0	13.5	.65	.66	.62	.68	.68	.68
37. Lomnicky Stit	16.0	11.0	4.0	8.0	10.5	17.0	.66	.68	.66	.71	.71	.70
38. München	23.0	10.5	2.0	6.5	10.5	16.0	.62	.62	.58	.63	.64	.63
39. Zugspitze	15.0	9.0	2.0	5.0	9.5	14.5	.66	.70	.71	.73	.72	.70
40. Dallas	0	−10.5	−19.0	−18.0	−12.0	−7.0	.69	.65	.62	.66	.68	.68

Table 3.14.1. Acceptance vectors computed for NM of the worldwide net (continued).

Name of station	Φ						$\lvert Z_1^1 \rvert$					
	γ			b			γ			b		
	0	−0.5	−1.0	10	30	100	0	−0.5	−1.0	10	30	100
	1	2	3	4	5	6	7	8	9	10	11	12
41. Hafelekar	29.0	17.0	7.0	13.5	18.0	23.0	.60	.60	.57	.62	.63	.62
42. Berkeley	0	−13.5	−13.5	−17.0	−13.0	−7.5	.69	.68	.66	.69	.70	.71
43. Pic-du-Midi	22.5	11.0	5.0	7.0	10.5	16.0	.61	.62	.64	.67	.64	.63
44. Rome	23.0	12.5	5.0	8.5	12.0	17.0	.58	.60	.62	.63	.72	.60
45. Tbilisi	24.0	13.0	5.0	8.5	12.5	17.0	.57	.57	.58	.60	.60	.59
46. Alma-Ata	20.0	7.5	1.0	3.5	8.0	13.0	.58	.60	.60	.62	.62	.61
47. Mexico	3.0	−5.0	−10.0	−8.5	−5.9	−2.0	.59	.52	.48	.50	.53	.56
48. Teheran	22.0	13.0	4.0	9.0	11.5	16.5	.57	.53	.52	.54	.55	.56
49. Mt. Norikura	12.5	9.0	−2.5	2.5	7.5	12.5	.57	.50	.45	.49	.51	.54
50. Mt. Haleakala	3.5	−4.0	−12.0	−7.5	−6.0	−2.0	.66	.59	.55	.58	.60	.62
51. Ahmedabad	16.5	13.5	9.0	10.5	12.0	13.5	.64	.60	.58	.59	.60	.62
52. Trivandrum	10.0	9.0	8.0	9.0	10.0	10.0	.69	.66	.64	.66	.66	.66
53. Lae	−7.0	−5.0	−5.0	−5.0	−5.0	−5.0	.68	.64	.62	.63	.64	.65
54. Huancayo	−9.5	−6.5	−4.5	−6.0	−6.5	−8.5	.65	.61	.58	.60	.61	.62
55. Makerere	−11.0	−7.0	−2.5	−4.0	−6.0	−8.0	.68	.65	.64	.66	.66	.66
56. Mina Aguilar	−14.0	−9.0	−3.0	−5.0	−7.5	−10.0	.65	.59	.55	.57	.60	.62
57. Rio de Janeiro	−9.0	−2.0	5.0	2.0	−1.0	−4.5	.66	.61	.62	.62	.63	.65
58. Buenos Aires	−22.5	−14.5	−3.0	−8.5	−13.0	−18.5	.56	.48	.40	.45	.49	.53
59. Ushuaia	−22.5	−7.5	−6.5	0	−6.5	−15.0	.56	.59	.63	.62	.61	.59
60. Hermanus	−5.0	8.5	15.0	12.0	8.5	2.5	.64	.61	.62	.62	.63	.63
61. Mt. Wellington	−18.0	−7.0	0	−5.0	−8.5	−13.0	.78	.81	.81	.84	.83	.81
62. Invercargill	−25.0	−12.5	−6.0	−11.0	−14.5	−18.5	.72	.79	.82	.82	.80	.77
63. Kerguelen	−16.5	−4.5	4.5	−2.0	−6.5	−10.5	.83	.87	.86	.89	.89	.86
64. Sanae	−32.5	−19.5	−10.0	−18.0	−21.5	−26.5	.73	.84	.88	.86	.83	.79
65. Ellsworth	−39.0	−29.5	−20.0	−28.5	−32.5	−37.0	.65	.79	.86	.81	.76	.71
66. Macquarie Is.	−39.0	−31.0	−29.0	−29.0	−32.0	−35.5	.71	.81	.87	.83	.79	.76
67. Mawson	−44.0	−36.5	−31.5	−36.5	−38.0	−40.5	.67	.76	.83	.78	.78	.72
68. Dumont	−65.5	−66.0	−62.0	−63.0	−65.0	−66.0	.41	.45	.48	.46	.45	.42
69. Mc Murdo	−84.5	−81.0	−78.0	−79.5	−81.5	−82.5	.10	.17	.22	.28	.15	.14
70. Mirny	−52.5	−49.5	−46.0	−49.0	−51.0	−52.0	.58	.64	.69	.74	.65	.62
71. Wilkes	−58.5	−58.5	−59.0	−59.5	−58.5	−57.5	.48	.49	.50	.49	.49	.49
72. Vostok	−74.0	−74.0	−72.0	−74.0	−74.0	−74.0	.24	.28	.32	.30	.28	.26

Table 3.14.1. Acceptance vectors computed for NM of the worldwide net (continued).

	Ψ_1^1						$\lvert Z_2^1\rvert$						Ψ_2^1		
	γ			b			γ			b			γ		
	0	−0.5	−1.0	10	30	100	0	−0.5	−1.0	10	30	100	0	−0.5	−1.0
	13	14	15	16	17	18	19	20	21	22	23	24	25	26	27
1.	1.3	1.6	1.8	1.7	1.6	1.5	.49	.55	.59	.55	.53	.52	1.4	1.7	1.8
2.	0.7	0.7	0.7	0.8	0.7	0.7	.58	.65	.70	.65	.63	.61	0.7	0.8	0.8
3.	1.9	2.4	3.2	2.7	2.4	2.4	.17	.19	.21	.21	.20	.19	2.1	2.7	3.0
4.	2.7	3.1	3.2	3.0	2.9	2.9	.54	.68	.76	.69	.66	.60	2.8	3.0	3.1
5.	2.3	2.5	2.6	2.5	2.5	2.4	.49	.72	.81	.74	.69	.65	2.4	2.5	2.6
6.	0.6	0.5	0.5	0.5	0.5	0.6	.80	.85	.85	.87	.86	.83	0.6	0.6	0.5
7.	1.2	1.3	1.4	1.3	1.3	1.2	.78	.77	.72	.78	.79	.79	1.1	1.3	1.4
8.	2.6	3.0	3.3	3.0	2.8	2.7	.73	.76	.73	.78	.78	.76	2.4	2.8	3.0
9.	2.2	2.6	2.9	2.6	2.5	2.4	.64	.55	.43	.55	.59	.62	1.8	2.2	2.3
10.	2.0	2.1	2.2	2.1	2.1	2.1	.72	.75	.71	.78	.78	.76	1.9	2.0	2.1
11.	1.0	1.0	1.1	1.0	1.0	1.0	.68	.61	.49	.62	.65	.67	0.9	0.9	0.9
12.	2.4	2.8	3.0	2.8	2.7	2.5	.74	.76	.73	.79	.78	.77	2.3	2.5	2.7
13.	1.4	1.4	1.5	1.5	1.4	1.4	.67	.63	.53	.65	.67	.69	1.4	1.3	1.3
14.	3.5	3.8	4.0	3.8	3.7	3.6	.74	.74	.67	.76	.76	.76	3.3	3.6	3.7
15.	2.5	2.9	3.2	2.9	2.8	2.7	.69	.66	.57	.67	.69	.70	2.2	2.5	2.6
16.	2.1	2.5	2.9	2.6	2.4	2.3	.39	.19	.09	.17	.25	.31	1.0	0.4	−4.2
17.	2.6	2.9	3.3	2.9	2.8	2.7	.36	.16	.10	.13	.21	.28	2.0	1.0	−5.2
18.	2.9	3.4	3.8	3.4	3.2	3.1	.59	.49	.39	.51	.54	.58	2.3	2.7	2.8
19.	1.6	1.9	2.2	1.8	1.7	1.6	.36	.13	.12	.20	.19	.27	0.8	−0.4	−5.0
20.	2.5	3.0	3.5	3.1	2.9	2.7	.35	.15	.14	.12	.19	.27	0.9	−0.5	−6.0
21.	2.5	3.2	3.6	3.2	3.0	2.8	.33	.14	.18	.12	.17	.24	0.6	−1.7	−5.6
22.	2.9	3.4	3.8	3.4	3.2	3.0	.55	.44	.31	.44	.48	.51	2.1	2.3	2.2
23.	2.7	3.4	4.0	3.4	3.2	3.0	.29	.14	.14	.11	.15	.22	0.7	−1.1	−5.5
24.	2.7	3.2	3.6	3.2	3.0	2.9	.45	.27	.17	.27	.34	.39	1.6	1.2	−0.7
25.	2.3	3.0	3.6	3.0	2.8	2.6	.22	.18	.31	.19	.14	.14	−0.6	−5.6	−7.3
26.	2.7	3.6	4.3	3.6	3.3	3.1	.24	.17	.27	.18	.15	.17	−0.4	−4.8	−6.8
27.	3.4	4.1	4.8	4.2	3.9	3.7	.41	.33	.10	.21	.29	.34	1.9	1.7	0.4
28.	3.3	4.0	4.6	4.1	3.8	3.6	.48	.34	.21	.32	.38	.43	2.0	2.3	2.1
29.	2.8	3.4	3.8	3.4	3.2	3.1	.43	.28	.15	.25	.32	.38	1.7	1.5	0.7
30.	3.0	3.8	4.4	3.8	3.6	3.4	.41	.25	.14	.23	.29	.35	1.4	1.2	0
31.	3.5	4.4	5.1	4.5	4.2	3.9	.37	.20	.08	.17	.22	.29	1.5	1.2	0.9
32.	2.6	3.4	4.3	3.5	3.2	2.9	.19	.31	.42	.35	.28	.21	3.4	6.9	7.5
33.	3.6	4.5	5.3	4.6	4.3	4.0	.35	.18	.06	.14	.20	.27	1.4	0.9	1.8
34.	2.6	3.5	4.4	3.6	3.3	3.0	.20	.32	.45	.38	.30	.23	−3.9	−7.0	−7.6
35.	3.7	4.7	5.5	4.9	4.5	4.2	.31	.14	.06	.11	.16	.23	1.0	0.2	−3.0
36.	3.7	4.6	5.4	4.7	4.4	4.0	.29	.18	.16	.16	.18	.23	0.7	1.3	3.8
37.	3.6	4.6	5.4	4.8	4.4	4.0	.31	.13	.07	.10	.15	.22	0.9	0.3	4.9
38.	3.1	4.1	5.0	4.3	3.9	3.5	.32	.15	.06	.11	.16	.24	1.0	1.2	−3.3
39.	3.8	4.8	5.6	5.0	4.7	4.3	.32	.15	.08	.11	.17	.23	0.8	0.3	3.3
40.	3.1	4.2	5.2	4.5	4.0	3.6	.25	.34	.43	.39	.34	.40	4.1	6.4	7.0

Table 3.14.1. Acceptance vectors computed for NM of the worldwide net (continued).

	Ψ_1^1						$\lvert Z_2^1\rvert$						Ψ_2^1		
	γ			b			γ			b			γ		
	0	−0.5	−1.0	10	30	100	0	−0.5	−1.0	10	30	100	0	−0.5	−1.0
	13	14	15	16	17	18	19	20	21	22	23	24	25	26	27
41.	3.7	4.8	5.6	5.0	4.6	4.2	.42	.26	.16	.23	.29	.35	1.7	1.6	1.5
42.	3.0	3.9	4.6	4.1	3.8	3.4	.24	.36	.44	.40	.34	.28	−4.2	−6.4	−7.1
43.	4.2	5.5	6.4	5.7	5.3	4.8	.32	.17	.09	.13	.18	.24	0.7	−0.3	−2.7
44.	4.2	5.6	6.7	6.0	5.4	4.9	.32	.15	.05	.10	.16	.22	0.8	0.3	−2.5
45.	4.0	5.4	5.5	5.8	5.3	4.7	.33	.16	.06	.11	.16	.24	1.0	0.7	0.7
46.	4.2	5.5	6.6	5.9	5.4	4 8	.29	.17	.12	.13	.17	.22	0.5	−0.9	−3.2
47.	3.0	4.6	5.9	5.1	4.6	4.0	.19	.22	.25	.24	.22	.20	−3.1	−5.1	−5.8
48.	3.4	4.7	5.9	5.3	4.7	4.1	.37	.24	.15	.19	.23	.29	0.7	0.5	0.3
49.	3.0	4.1	5.3	4.7	4.2	3.7	.39	.30	.25	.27	.29	.32	0.1	0.9	2.1
50.	2.7	3.7	4.7	4.2	3.9	3.3	.26	.27	.32	.30	.27	.25	−2.0	−3.4	−4.3
51.	3.0	4.0	5.0	4.6	4.2	3.7	.34	.27	.21	.22	.25	.29	0.9	0.1	0
52.	2.7	3.5	4.2	3.9	3.7	3.2	.19	.18	.16	.17	.17	.15	2.1	2.6	2.9
53.	2.8	4.0	4.9	4.6	4.1	3.6	.11	.07	.03	.04	.06	.08	12.4	12.0	10.7
54.	2.9	4.0	5.1	4.6	4.2	3.6	.26	.24	.22	.22	.23	.24	13.2	13.1	13.1
55.	2.9	4.0	5.0	4.6	4.1	3.6	.29	.24	.22	.22	.24	.25	12.7	12.5	12.0
56.	2.8	3.7	4.7	4.3	3.8	3.3	.31	.25	.20	.22	.24	.27	12.5	12.1	11.2
57.	2.8	4.0	5.1	4.6	4.1	3.5	.29	.26	.26	.24	.25	.25	11 5	10.3	9.2
58.	2.9	3.5	3.9	3.8	3.7	3.3	.42	.31	.23	.28	.31	.35	13.7	13.9	14.5
59	4.4	5.8	6.7	6.0	5.5	5.3	.37	.27	.28	.26	.27	.30	12.0	10.0	8.4
60.	3.1	4.6	5.7	4.9	4.3	3.8	.27	.30	.35	.33	.29	.29	9.3	6.8	6.0
61.	2.8	3.6	4.4	3.7	3.4	3.1	.34	.16	.10	.13	.19	.26	12.8	12.5	7.5
62.	3.2	4.0	4.7	4.1	3.8	3.6	.38	.23	.10	.22	.28	.33	13.7	13.8	13.2
63.	1.1	1.4	1.7	1.3	1.2	1.2	30	.10	.16	.08	.14	.22	12.0	9.6	3.7
64.	1.2	1.3	1.4	1.2	1.2	1.2	50	.38	.24	.40	.44	.48	13.2	13.0	12.4
65.	2.2	2.3	2.3	2.2	2.2	2.3	59	.57	.47	.59	.61	.61	14.1	14.1	13.9
66.	2.2	2.7	3.0	2.7	2.5	2.4	72	.68	.59	.69	.72	.72	14.0	14.3	14.5
67.	−0.3	−0.5	−0.6	−0.5	−0.5	−0.4	79	.81	.79	.83	.83	.82	11.8	11.5	11.5
68.	0.9	1.3	1.5	1.3	1.2	1.0	69	.76	.82	.78	.75	.72	13.0	13.0	13.5
69.	5.6	6.7	6.9	6.7	6.5	6.0	20	.31	.42	.33	.29	.24	17.7	18.6	18.9
70.	−0.4	−0.6	−0.7	−0.6	−0.6	−0.6	84	.91	.94	.92	.90	.88	11.6	11.4	11.3
71.	−0.4	−0.4	−0.4	−0.4	−0.4	−0.4	71	.76	.77	.75	.74	.75	11.9	11.8	11.7
72.	−3.4	−3.9	−4.2	−4.0	−3.8	−3.6	46	.53	.62	.54	.51	.49	8.6	8.0	7.7

Table 3.14.1. Acceptance vectors computed for NM of the world-wide net (continued).

	Ψ_2^1			$\lvert Z_2^2\rvert$						Ψ_2^2					
	b			γ			b			γ			b		
	10	30	100	0	−0.5	−1.0	10	30	100	0	−0.5	−1.0	10	30	100
	28	29	30	31	32	33	34	35	36	37	38	39	40	41	42
1.	1.7	1.6	1.5	.08	.08	.08	.08	.08	.08	1.7	1.8	2.0	2.0	1.8	1.7
2.	0.8	0.8	0.8	.10	.14	.16	.14	.13	.12	0.6	0.6	0.6	0.6	0.6	0.6
3.	2.6	2.5	2.3	0	.01	.01	.01	.01	.01	3.0	3.0	3.0	3.0	3.0	3.0
4.	3.0	3.0	2.9	.11	.16	.21	.17	.15	.33	3.0	3.1	3.2	3.2	3.2	3.0
5.	2.6	2.5	2.5	.14	.21	.36	.21	.19	.17	2.6	2.6	2.6	2.6	2.6	2.6
6.	0.5	0.5	0.6	.41	.53	.62	.55	.50	.46	0.6	0.5	0.5	0.5	0.6	0.6
7.	.13	1.3	1.2	.51	.64	.74	.67	.62	.57	1.2	1.3	1.4	1.4	1.4	1.3
8.	2.8	2.7	2.6	.43	.58	.69	.60	.55	.50	2.8	3.0	3.2	3.0	3.0	2.9
9.	2.3	2.2	2.1	.55	.71	.80	.74	.69	.63	2.4	2.8	3.0	2.8	2.6	2.6
10.	2.0	2.0	2.0	.42	.57	.68	.59	.53	.48	2.1	2.2	2.2	2.2	2.2	2.2
11.	0.9	0.9	1.0	.64	.71	.79	.73	.68	.62	1.0	1.0	1.0	1.0	1.0	1.0
12.	2.6	2.4	2.5	.42	.56	.66	.59	.54	.49	2.6	2.8	3.0	2.8	2.8	2.7
13.	1.4	1.4	1.4	.51	.67	.78	.69	.64	.58	1.4	1.5	1.5	1.4	1.4	1.4
14.	3.7	3.6	3.5	.43	.56	.64	.58	.53	.48	3.6	3.8	4.0	3.8	3.8	3.8
15.	2.6	2.5	2.4	.48	.61	.69	.64	.61	.55	2.8	3.0	3.2	3.0	2.8	2.8
16.	0.5	0.9	1.1	.64	.76	.80	.79	.76	.70	2.2	2.6	2.8	2.6	2.5	2.4
17.	0.9	1.7	1.8	.63	.74	.73	.78	.75	.69	2.6	2.8	3.1	2.8	2.8	2.7
18.	2.8	2.7	2.6	.50	.64	.68	.69	.64	.59	3.1	3.4	3.6	3.4	3.3	3.2
19.	−3.8	0.4	0.7	.67	.74	.73	.78	.76	.72	1.6	1.7	1.9	1.8	.16	1.6
20.	−0.9	0.4	0.9	.61	.71	.73	.75	.72	.69	2.6	3.1	3.4	3.0	2.9	2.8
21.	−2.3	0.4	0.3	.60	.68	.67	.72	.70	.66	2.8	3.2	3.6	3.2	3.0	2.9
22.	3.4	3.4	2.3	.52	.65	.71	.69	.65	.61	3.1	3.4	3.8	3.4	3.3	3.2
23.	−1.7	0	0.5	.54	.58	.56	.62	.62	.59	2.8	3.4	3.8	3.5	3.2	3.0
24.	1.3	1.6	1.7	.54	.66	.67	.69	.66	.61	2.8	3.2	3.4	3.1	3.0	3.0
25.	−6.4	−4.6	−2.6	.60	.63	.60	.67	.67	.66	2.4	2.8	3.3	2.0	2.7	2.6
26.	−5.8	−3.8	−1.9	.56	.58	.53	.62	.63	.60	2.8	3.4	3.9	3.4	3.2	3.0
27.	1.8	1.9	2.0	.50	.59	.59	.63	.61	.57	3.6	4.0	4.3	4.0	3.8	3.8
28.	2.4	2.3	2.3	.45	.54	.57	.58	.56	.51	3.5	3.9	4.5	4.1	3.8	3.7
29.	1.7	1.7	1.8	.48	.54	.54	.59	.58	.55	3.1	3.6	4.0	3.6	3.4	3.2
30.	1.4	1.5	1.6	.48	.53	.51	.57	.56	.53	3.2	3.6	4.2	3.8	3.6	3.4
31.	0.9	1.4	1.6	.45	.51	.50	.55	.52	.51	3.6	4.3	4.8	4.4	4.2	4.0
32.	7.4	6.8	5.6	.50	.46	.38	.48	.51	.52	2.4	3.0	3.6	3.2	2.9	2.6
33.	0.7	1.0	1.5	.43	.48	.45	.52	.52	.49	3.6	4.2	4.6	4.2	4.0	3.8
34.	−7.5	−7.1	−6.0	.49	.46	.38	.48	.51	.52	2.4	3.0	3.6	3.0	2.9	2.6
35.	−0.4	0.4	0.9	.38	.43	.41	.47	.47	.44	3.8	4.4	4.8	4.5	4.1	4.1
36.	2.2	1.0	0	.39	.43	.32	.43	.44	.44	3.4	3.8	4.2	4.0	3.8	3.6
37.	1.2	0.3	0.7	.40	.43	.41	.46	.47	.45	3.6	4.2	4.8	4.4	4.2	4.0
38.	0	0.7	1.0	.31	.35	.36	.38	.37	.34	3.5	4.3	4.8	4.5	4.2	3.8
39.	1.0	0	0.7	.37	.43	.44	.47	.45	.42	4.0	4.8	5.3	4.8	4.6	4.4
40.	6.8	6.4	2.9	.39	.39	.39	.41	.42	.41	3.0	4.0	4.6	4.0	3.8	3.4

Table 3.14.1. Acceptance vectors computed for NM of the worldwide net (continued)

	Ψ_2^1			$\lvert Z_2^2\rvert$						Ψ_2^2					
	b			γ			b			γ			b		
	10	30	100	0	−0.5	−1.0	10	30	100	0	−0.5	−1.0	10	30	100
	28	29	30	31	32	33	34	35	36	37	38	39	40	41	42
41.	1.7	1.9	1.8	.31	.38	.42	.43	.41	.37	4.1	5.0	5.5	5.1	4.8	4.5
42.	−6.7	−6.4	−5.7	.40	.36	.31	.37	.40	.41	2.6	3.4	4.1	3.6	3.4	3.0
43.	−0.9	0	0.5	.23	.33	.40	.44	.34	.29	4.6	5.7	6.4	4.9	5.5	5.2
44.	−0.4	0.2	0.7	.18	.21	.24	.24	.23	.21	4.0	5.6	6.6	5.8	5.4	4.8
45.	0.3	0.7	1.0	.19	.21	.26	.25	.24	.22	3.8	5.3	6.3	5.8	5.2	4.6
46.	−1.8	−0.9	0	.21	.22	.27	.25	.25	.23	3.8	5.4	6.5	5.7	5.2	4.6
47.	−5.8	−5.3	−4.5	.28	.15	.07	.12	.16	.22	2.0	2.8	5.0	3.6	2.9	2.6
48.	0	0.3	0.7	.22	.18	.19	.20	.21	.21	2.8	4.2	5.2	4.8	4.2	3.6
49.	1.5	0.9	0.3	.30	.26	.24	.27	.27	.29	2.6	3.5	4.1	3.8	3.6	3.2
50.	−4.0	−3.6	−3.0	.35	.26	.21	.24	.27	.30	2.1	2.9	4.0	3.5	3.2	2.7
51.	0	0	0	.31	.24	.19	.22	.24	.26	2.2	3.0	3.8	3.6	3.2	2.8
52.	2.7	2.7	2.6	.29	.21	.18	.20	.21	.25	2.0	2.9	4.0	3.6	3.2	2.7
53.	11.2	12.0	12.0	.31	.21	.13	.16	.20	.24	2.8	2.6	3.9	3.3	3.0	2.4
54.	13.2	13.1	13.0	.31	.22	.18	.20	.22	.25	2.1	3.0	4.2	3.8	3.5	2.8
55.	12.0	12.4	12.9	.31	.22	.19	.18	.22	.26	2.1	3.2	4.4	3.1	3.5	2.8
56.	11.9	12.2	12.4	.34	.25	.24	.27	.29	.32	2.2	3.1	3.8	3.5	3.2	3.0
57.	9.7	10.2	10.8	.34	.25	.18	.29	.26	.30	2.0	2.7	3.5	4.4	2.8	2.5
58.	14.1	14.1	14.0	.18	.08	.06	.09	.11	.13	2.4	3.8	6.4	5.2	4.1	3.3
59.	9.4	10.4	11.1	.22	.23	.21	.25	.26	.26	4.3	5.2	6.2	5.5	5.0	4.7
60.	6.4	6.9	7.9	.27	.18	.17	.19	.29	.25	2.4	3.6	5.4	4.2	3.4	2.9
61.	11.4	12.4	12.8	.54	.59	.54	.63	.63	.60	2.8	3.5	4.0	3.5	3.4	3.2
62.	13.8	14.0	13.9	.50	.57	.57	.62	.60	.56	3.3	3.8	4.4	3.9	3.7	3.5
63.	15.0	12.8	11.9	.70	.75	.73	.79	.77	.74	1.1	1.3	1.4	1.3	1.2	1.2
64.	13.0	13.1	13.2	.57	.71	.76	.74	.70	.64	1.2	1.2	1.3	1.2	1.2	1.2
65.	14.0	14.2	14.2	.48	.65	.75	.68	.62	.56	2.2	2.2	2.4	2.2	2.5	3.2
66.	14.5	14.4	14.2	.51	.65	.74	.68	.63	.57	2.4	2.8	3.0	2.8	2.7	2.6
67.	11.5	11.5	11.7	.47	.60	.69	.61	.58	.53	0.4	−0.5	−0.6	−0.6	−0.5	−0.4
68.	13.3	13.2	13.1	.16	.20	.23	.21	.19	.18	1.3	1.4	1.6	1.4	1.3	1.2
69.	18.8	18.7	18.3	.01	.03	.06	.04	.03	.03	7.5	7.1	7.0	7.2	7.2	7.5
70.	11.3	11.4	11.5	.34	.41	.46	.42	.40	.36	0.5	0.6	0.7	0.6	0.6	0.6
71.	11.7	11.8	11.8	.23	.26	.29	.27	.25	.24	0.6	0.5	0.4	0.5	0.6	0.6
72.	8.0	8.1	8.3	.05	.07	.09	.08	.07	.06	8.2	7.8	7.6	7.7	7.8	8.0

The Fig. 3.14.2 shows the asymptotic latitude $\Phi = \arcsin x_1^0$ as a function of longitude and latitude of the point of observation for maximum and minimum solar activity and for the values γ = 0, 0.5 and 1 in the energy spectrum of the anisotropy described by Eq. 3.14.24. Evidently, the asymptotic latitude Φ depends strongly on the geographic longitude φ of the station and varies by as much as 20° for $\gamma = 0$. The values

of Φ decrease with increasing solar activity and for a steeper variation spectrum. In diagram (*b*) of the Fig. 3.14.2 curves are computed for a dipole field, the dots for the real magnetic field. It is seen that stations at geomagnetic latitudes 45° gather radiation chiefly from the plane of the geographic equator; and only high latitude stations receive radiation under considerable angles with the plane of the ecliptic. The values of the component x_1^0 depend in the same way on latitude as Φ. The x_1^0 component characterizes the sensitivity of the detector to the Z component of the anisotropic stream in the isotropic variations. The component x_2^0 has about the same latitude dependence as x_1^0 only it is still more concentrated to high latitudes. Thus if any anomalies exist in the latitude run in the isotropic variations, they can be expected at the high latitude stations only.

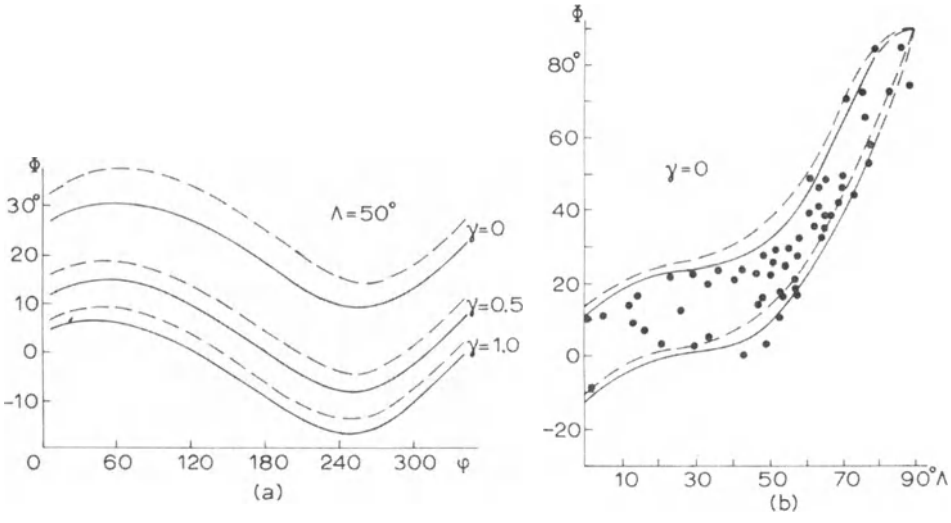

Fig. 3.14.2. Dependence of the asymptotic latitude Φ at the geomagnetic latitude and longitude of the point of observation. Full curves solar minimum, dashed curves solar maximum: (a) Fixed geomagnetic latitude 50° *vs* longitude φ for different values of γ; (b) individual stations in longitudes φ = 40° – 90° (Eastern Europe, upper curves) and longitudes φ = 230° – 280° (America, lower curves) *vs* geomagnetic latitude Λ.

Fig. 3.14.3 gives $\Psi_1 = \mathrm{arctg}\left(y_1^1 / x_1^1\right)$ and $\left|Z_1^1\right| = \left(\left(x_1^1\right)^2 + \left(y_1^1\right)^2\right)^{1/2}$ as functions of geographic longitude for geomagnetic latitude Λ = 50° and the dipole representation of the geomagnetic field. A strong longitude dependence of Ψ_1^1 is seen; for γ = 0 it varies by 23°, for γ = 2 by 30°. Hence at the same geomagnetic latitude the times of maximum of the first harmonic of the diurnal variation may differ by 1 hour and more. With increasing solar activity the values of Ψ_1^1 decrease by 3° – 6°, i.e. by 0.2–0.4 hours for γ = 0. The largest values of Ψ_1^1 are observed at longitudes 30° – 60° (Europe), the smallest at longitudes 190° – 220° (Western America).

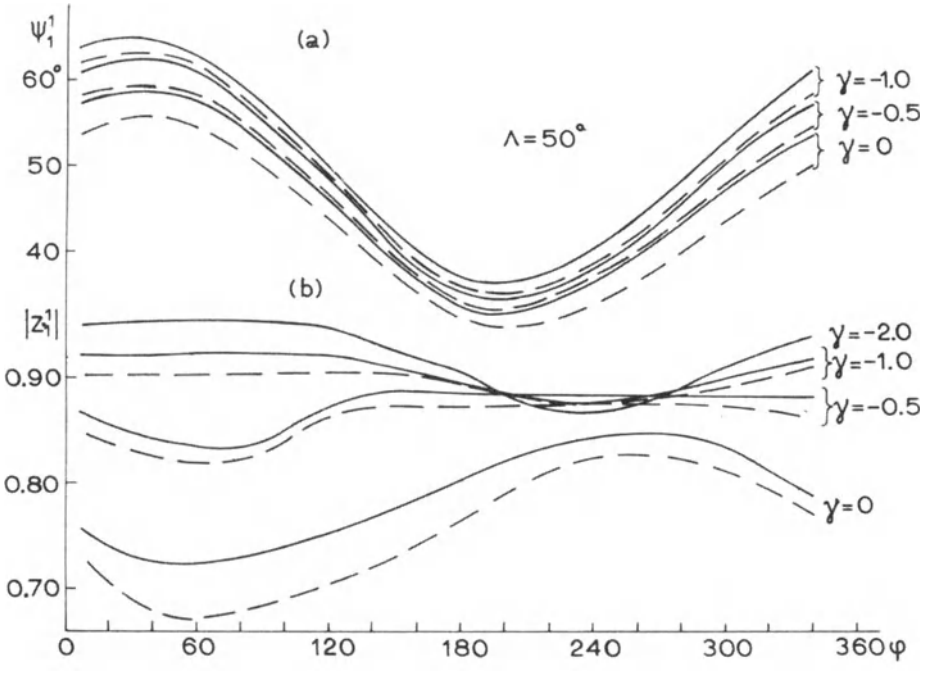

Fig. 3.14.3. Dependence of Ψ_1^1 (a) and $\left|Z_1^1\right|$ (b) on longitude φ for geomagnetic latitude Λ = 50° and dipole representation of the geomagnetic field. Full curves solar minimum, broken curves solar maximum.

The modulus $\left|Z_1^1\right|$ shown in Fig. 3.14.3 also depends on longitude and on solar activity. Evidently in the observations the amplitude of the primary anisotropy will drop for higher solar activity. The first harmonic of the solar-daily variation will be lowered most at longitudes 40-70°, and least at longitudes 250 - 280°, for $\gamma = 0$. For $\gamma = -2$ this longitude dependence will be reversed at latitudes < 50°.

The latitude dependence of $\left|Z_1^1\right|$ is shown in Fig. 3.14.4 for the dipole geomagnetic field (full and broken curves) and for the real field (dots). Below 50° latitude a real difference in $\left|Z_1^1\right|$ between these two approximations of the Earth's magnetic field is seen. The amplitude of the first harmonic of the diurnal variation is lowered most at high latitudes, but the run of $\left|Z_1^1\right|$ is not exactly proportional to cosΦ. At latitudes 50° – 70° the $\left|Z_1^1\right|$ are larger than at intermediate latitudes. This means that the largest observed amplitudes of the first harmonic of the solar-daily variation must be expected at latitudes

50°-70°. There should be a longitude difference of the amplitudes of 20% at intermediate latitudes and 30-40% at high latitudes. The values of $\left|Z_1^1\right|$ depend weakly on γ.

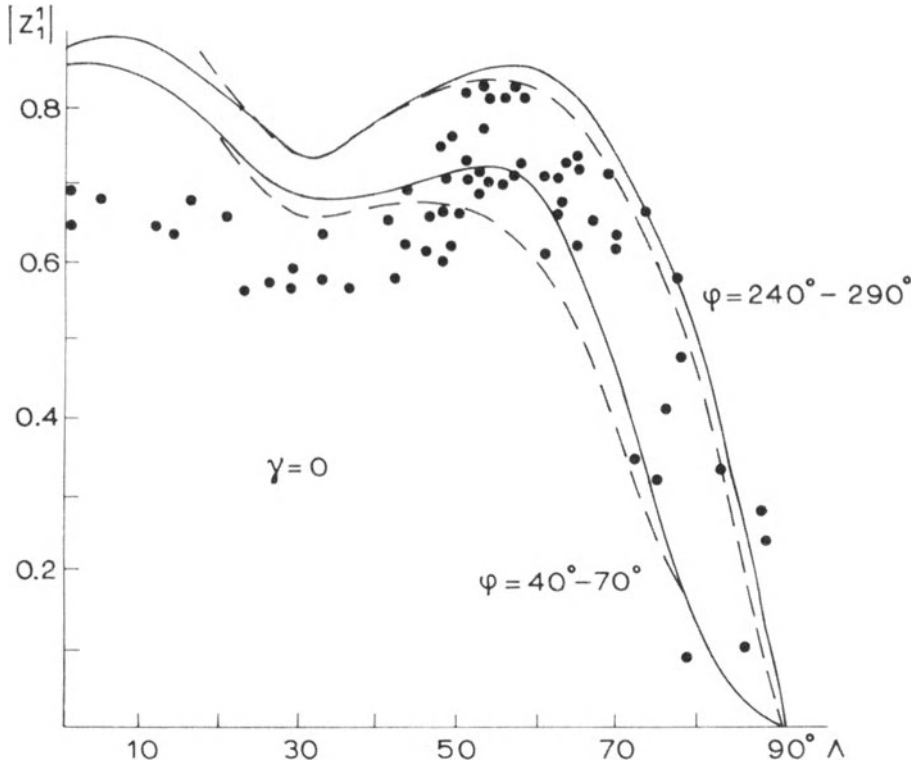

Fig. 3.14.4. Latitude dependence of $\left|Z_1^1\right|$ for the dipole representation of the geomagnetic field (full curves: solar minimum, dashed curves: solar maximum) and for the real field (dots).

The argument Ψ_1^1 (offset angle) is shown in Fig. 3.14.5 for different values of γ and b in the variation rigidity spectra and for the dipole and real representations of the geomagnetic field. The upper curves give Ψ_1^1 at longitudes 0° – 60°, where it is largest and the lower curves give Ψ_1^1 at longitudes 160° – 220°, where it is small. Differences (up to 15° and more) of the Ψ_1^1 computed for the real and dipole approximation are seen at nearly all latitudes.

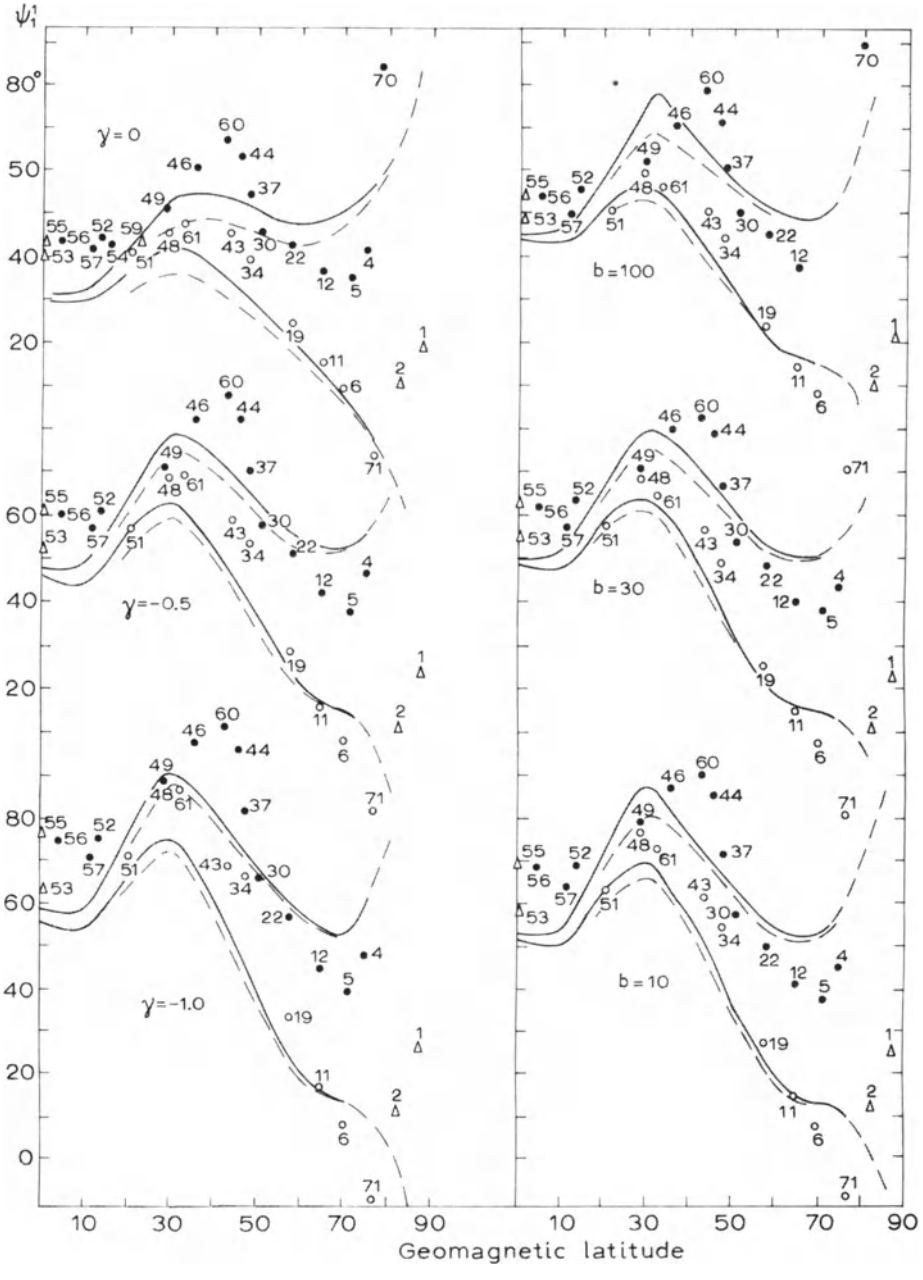

Fig. 3.14.5. Dependence of offset angle Ψ_1^1 on geomagnetic latitude. Curves refer to the dipole approximation (full curves: solar minimum; broken curves: solar maximum; upper set: longitudes 0°-60°; lower set: longitudes 160°-220°). Solid and open dots, marked with the station numbers of Table 3.14.1, refer to the real field in the two longitude regions. Left side for rigidity spectrum described by Eq. 3.14.24 at γ = 0, -0.5, and -1.0; right side – for spectrum described by Eq. 3.14.25 at b = 10, 30, and 100 GV.

As it can be seen from Fig. 3.14.5, the maximum Ψ_1^1 is reached not on the equator, but at latitudes 40°-50°. This is due to two competing factors: the geomagnetic field and the variation of CR rigidities with latitude. At the equator the geomagnetic field does not admit low-energy particles, but the high-energy particles are less subject to the influence of the geomagnetic field. At intermediate latitudes the contribution of lower-energy particles, for which the shift in the magnetic field is larger, will be significant. The largest scatter in Ψ_1^1, (and hence in the time of maximum of the first harmonic of the diurnal variation) is found at latitudes > 80°, where almost any value of Ψ_1^1 may be expected. With increasing exponent γ in the variation spectrum the Ψ_1^1 increase at intermediate and low latitudes but hardly vary at high latitudes. This is very important for determining the exponent γ in the spectrum of solar-daily variations.

The latitude dependence of the second spherical harmonics is shown in Fig. 3.14.6.

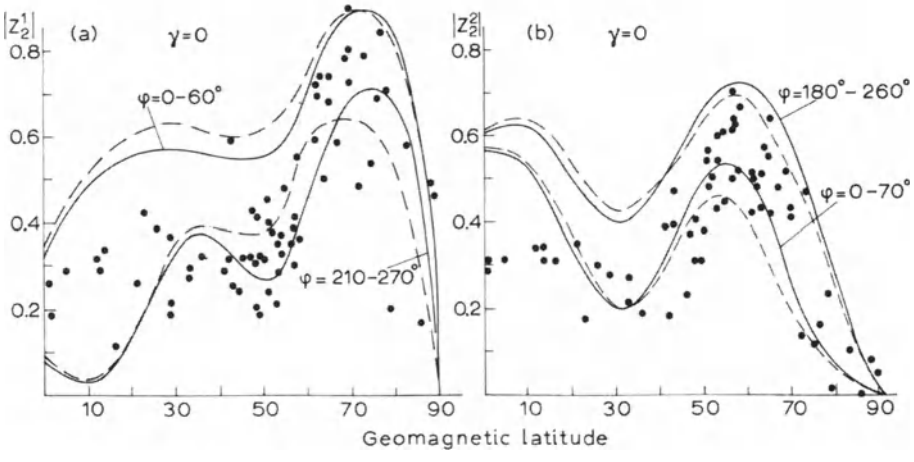

Fig. 3.14.6. Amplitudes $\left|Z_2^1\right|$ (left) and $\left|Z_2^2\right|$ (right). The same symbols as in Fig. 3.14.4 are used.

The left half of Fig. 3.14.6 shows $\left|Z_2^1\right|$, the modulus of the acceptance vector for contributing to the first harmonic of the diurnal variation. Its contribution is largest at latitudes 60°-80°, and drops strongly toward other latitudes. It has its maximum in Europe and its minimum in America. The right side of Fig. 3.14.6 shows the modulus $\left|Z_2^2\right|$ of the acceptance vector for the second harmonic of the diurnal variation. The largest difference in $\left|Z_2^2\right|$ between the real field and the dipole representation is observed at the equator. Since the observed amplitude of the second harmonic of the diurnal

variation must be proportional to $\left|Z_2^2\right|$, the largest amplitudes of the second harmonic are to be expected at latitudes 50° – 70°; at the equator it must be one third of this.

The arguments Ψ_2^1 and Ψ_2^2 are shown in Fig. 3.14.7, which is arranged as Fig. 3.14.5. At latitudes 0-70° the values of Ψ_2^1 vary by ± 2 hours for the actual magnetic field; for the dipole field the variation reaches, at the equator, 12 hours. The right-hand figure shows that the Earth's magnetic field shifts the time of maximum of the second harmonic of the solar-daily variation by 1 – 3 hours for American longitudes (φ = 170° - 250°) and 2-4 hours for European longitudes (φ = 40°-80°). The values of Ψ_2^2 computed for the real and the dipole representation of the geomagnetic field coincide.

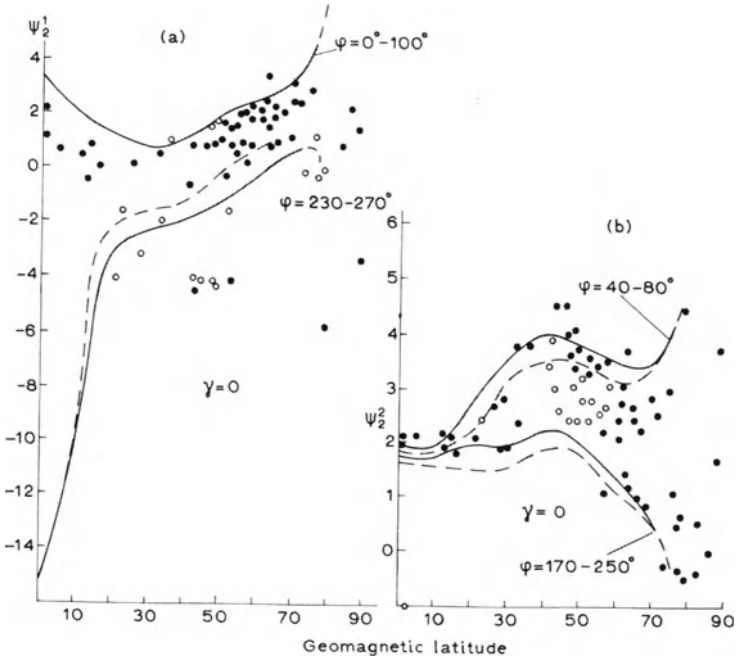

Fig. 3.14.7. The arguments Ψ_2^1 (left) and Ψ_2^2 (right) in dependence on geomagnetic latitude; the same arrangement as in Fig. 3.14.5.

3.14.5. Acceptance vectors for muon detectors

In computing acceptance vectors for muon detectors, differential coupling coefficients were used for zenith angles β = 0, 8, 16, 32, 48, 64° found in Krymsky et al. (1966b) for instruments placed at levels 0, 7, 20 and 60 m w.e. Directional diagrams for vertical muon detectors and inclined detectors (angles 30 and 60°) at various azimuths were calculated by Skripin (1965). Trajectory computations and threshold rigidities from Krymsky et al. (1966b) were used. The results for several muon detectors of the world-wide net are given in Table 3.14.2, those for the muon detectors of the Yakutsk complex (depths 0, 7, 20 and 60 m.w.e.) are in Table 3.14.3.

Table 3.14.2. Acceptance vectors for vertical muon telescopes.

No. of station	Station	Geographic coordinates	x_1^0						x_1^1					
			γ			b			γ			b		
			0	0.5	1.0	10	30	100	0	0.5	1.0	10	30	100
1	Apatity	67°33'N; 33°20'E	.77	.73	.70	.72	.74	.75	.43	.47	.51	.49	.47	.45
2	Ahmedabad	23°01'N; 72°36'E	.22	.17	.13	.14	.16	.19	.54	.42	.31	.35	.40	.46
3	Berkeley	37°52'N; 122°18'W	.0	−.16	−.25	−.21	−.16	−.09	.49	.36	.24	.33	.39	.44
4	Deep-River	46°06'N; 77°30'W	.52	.44	.36	.41	.44	.48	.67	.70	.72	.71	.70	.68
5	Climax	39°22'N; 106°11'W	.29	.16	.03	.11	.16	.22	.73	.72	.70	.72	.73	.73
6	Rio de Janeiro	22°54'S; 43°13'W	−.16	−.09	−.03	−.06	−.08	−.12	.63	.53	.41	.47	.52	.57
7	Trivandrum	8°29'N; 76°57'E	.13	.12	.11	.11	.12	.13	.56	.47	.38	.42	.45	.50
8	Wilkes	66°25'S; 110°27'E	−.73	−.75	−.77	−.76	−.75	−.74	.48	.49	.49	.49	.49	.48
9	Upsala	59°51'N; 17°55'E	−.14	−.12	−.09	−.10	−.11	−.12	.58	.45	.32	.38	.44	.50
10	Cape Schmidt	68°55'N; 179°29'W	.74	.69	.64	.67	.68	.71	.49	.56	.63	.59	.56	.53

No. of station	y_1^1						x_2^0						x_2^1					
	γ			b			γ			b			γ			b		
	0	0.5	1.0	10	30	100	0	0.5	1.0	10	30	100	0	0.5	1.0	10	30	100
1	.24	.29	.36	.33	.30	.27	.43	.35	.26	.31	.35	.38	.60	.64	.66	.65	.64	.62
2	.46	.53	.58	.57	.55	.52	−.32	−.36	−.38	−.37	−.36	−.35	.34	.29	.24	.26	.28	.30
3	.49	.58	.62	.61	.59	.55	−.17	−.20	−.22	−.21	−.20	−.19	−.11	−.04	−.11	−.08	−.04	.02
4	.28	.36	.43	.39	.36	.33	.0	−.10	−.20	−.14	−.10	−.05	.63	.56	.46	.52	.56	.60
5	.34	.42	.49	.45	.42	.39	−.16	−.22	−.26	−.25	−.23	−.20	.40	.24	.08	−.17	.24	.32
6	.43	.51	.58	.55	.52	.48	−.32	−.34	−.36	−.36	−.36	.34	−.31	−.25	−.21	−.22	−.24	−.27
7	.49	.54	.58	.57	.56	.53	−.40	−.41	−.42	−.42	−.41	−.41	.16	.14	.13	.13	.14	.15
8	−.05	−.06	−.06	−.06	−.06	−.06	.39	.42	.46	.44	.42	.40	−.67	−.70	−.73	−.72	−.71	−.69
9	.45	.53	.58	.56	.54	.51	−.36	−.38	−.40	−.39	−.38	−.37	−.25	−.23	−.21	−.22	−.22	−.24
10	.19	.23	.25	.24	.23	.21	.37	.27	.16	.22	.27	.32	.64	.68	.71	.70	.69	.67

No. of station	y_2^1						x_2^2						y_2^2					
	γ			b			γ			b			γ			b		
	0	0.5	1.0	10	30	100	0	0.5	1.0	10	30	100	0	0.5	1.0	10	30	100
1	.32	.39	.45	.42	.40	.37	.10	.11	.12	.11	.11	.11	.22	.31	.39	.34	.31	.27
2	.11	.10	.07	.08	.09	.11	.14	.02	−.07	−.46	.0	.05	.36	.34	.31	.33	.35	.36
3	−.21	−.35	−.43	−.39	−.34	−.28	.07	−.08	−.17	−.12	−.07	−.01	.39	.35	.26	.35	.39	.41
4	.20	.21	.20	.22	.22	.22	.30	.29	.28	.29	.29	.30	.38	.50	.62	.56	.50	.45
5	.07	.0	−.11	−.04	.0	.04	.35	.29	.21	.27	.30	.32	.48	.57	.64	.62	.59	.64
6	−.01	.03	.08	.06	.03	.01	.24	.11	.0	.04	.10	.15	.40	.40	.36	.39	.41	.41
7	.12	.12	.12	.12	.12	.12	.12	.01	−.09	−.06	−.02	.04	.33	.30	.26	.28	.30	.32
8	−.05	−.01	.03	.01	.0	−.03	.15	.18	.20	.19	.18	.16	−.10	−.09	−.09	−.09	−.09	−.09
9	−.20	−.10	−.09	−.10	−.10	−.10	.18	.04	−.08	−.04	−.01	.08	.37	.34	.28	.32	.34	.37
10	.25	.28	.29	.29	.28	.27	.21	.28	.35	.31	.28	.24	.22	.28	.34	.31	.28	.25

Table 3.14.3. Acceptance vectors for muon telescopes of Yakutsk complex (62°01' N, 129°43' E).

Depth m.w.e.	Direction	x_1^0						x_1^1					
		γ			b			γ			b		
		0	0.5	1.0	10	30	100	0	0.5	1.0	10	30	100
0	0°	.55	.47	.38	.43	.47	.51	.52	.56	.60	.59	.57	.55
	30°N	.61	.45	.31	.38	.44	.51	.29	.40	.49	.45	.41	.36
	30°W	.70	.61	.49	.56	.61	.66	.42	.48	.54	.51	.49	.46
	30°S	.45	.39	.32	.37	.39	.42	.76	.77	.77	.77	.77	.77
	30°E	.37	.25	.15	.20	.23	.28	.60	.66	.70	.68	.67	.64
7	0°	.63	.61	.57	.59	.60	.62	.48	.51	.54	.53	.52	.51
	30°N	.75	.67	.60	.62	.65	.69	.19	.25	.31	.29	.27	.24
	30°W	.80	.78	.76	.77	.78	.79	.37	.39	.42	.41	.40	.39
	30°S	.51	.49	.48	.48	.49	.50	.75	.76	.77	.76	.76	.76
	30°E	.48	.40	.33	.35	.38	.41	.55	.59	.63	.62	.60	.58
20	0°	.66	.67	.67	.67	.67	.67	.46	.47	.49	.48	.48	.47
	30°N	.84	.81	.78	.79	.79	.81	.12	.15	.18	.18	.17	.16
	30°W	.81	.82	.83	.83	.83	.82	.35	.36	.36	.36	.36	.37
	30°S	.53	.53	.52	.53	.53	.53	.75	.75	.75	.75	.75	.75
	30°E	.56	.52	.49	.50	.51	.52	.50	.52	.55	.54	.53	.52
60	0°	.74	.74	.75	.75	.75	.75	.41	.42	.42	.42	.42	.42
	30°N	.90	.90	.90	.81	.81	.80	.08	.09	.10	.35	.35	.35
	30°W	.79	.80	.81	.55	.55	.55	.35	.35	.35	.74	.74	.74
	30°S	.54	.55	.55	.65	.65	.65	.74	.74	.74	.47	.47	.47
	30°E	.65	.65	.65	.90	.90	.81	.46	.46	.47	.10	.10	.41

Depth m.w.e.	Direction	y_1^1						x_2^0					
		γ			b			γ			b		
		0	0.5	1.0	10	30	100	0	0.5	1.0	10	30	100
0	0°	.31	.41	.49	.45	.42	.38	.12	.01	−.10	−.04	.00	.05
	30°N	.48	.58	.64	.62	.60	.56	.25	.34	−.14	−.07	.00	−.10
	30°W	.09	.26	.40	.34	.28	.21	.36	.22	.06	.14	.21	.28
	30°S	.17	.27	.36	.31	.28	.23	−.10	−.16	−.23	−.19	.16	.14
	30°E	.55	.58	.60	.59	.58	.58	−.16	−.28	−.36	−.33	−.30	−.25
7	0°	.23	.30	.36	.34	.32	.29	.21	.16	.11	.13	.15	.18
	30°N	.40	.49	.56	.54	.52	.48	.44	.31	.18	.22	.26	.33
	30°W	−.05	.06	.15	.12	.09	.04	.50	.48	.42	.44	.46	.48
	30°S	.09	.14	.18	.17	.15	.13	−.05	−.06	−.08	−.07	−.06	−.06
	30°E	.53	.56	.58	.57	.57	.56	−.06	−.15	−.23	−.21	−.18	−.14
20	0°	.16	.20	.25	.24	.23	.21	.26	.26	.25	.25	.26	.26
	30°N	.31	.37	.43	.42	.40	.38	.60	.53	.47	.48	.50	.53
	30°W	−.17	−.11	−.05	−.06	−.07	−.10	.53	.55	.56	.56	.56	.56
	30°S	.04	.07	.09	.09	.08	.07	−.03	−.03	−.03	−.03	−.03	−.03
	30°E	.51	.53	.55	.55	.54	.53	.05	−.01	−.07	−.05	−.04	−.02
60	0°	.08	.10	.11	.11	.11	.10	.38	.39	.40	.40	.40	.39
	30°N	.17	.19	.20	−.26	−.26	−.27	.73	.72	.72	.52	.52	.51
	30°W	−.29	−.27	−.26	.01	.01	.00	.49	.51	.52	.00	.00	−.01
	30°S	−.01	.01	.01	.46	.46	.46	−.02	−.01	.00	.18	.18	.18
	30°E	.45	.46	.46	.20	.19	.13	.19	.18	.18	.72	.72	.51

Depth m.w.e.	Direction	x_2^1						y_2^1					
		γ			b			γ			b		
		0	0.5	1.0	10	30	100	0	0.5	1.0	10	30	100
0	0°	.46	.41	.34	.39	.41	.44	.23	.26	.25	.27	.27	.27
	30°N	.17	.17	.13	.15	.17	.18	.42	.38	.30	.35	.39	.43
	30°W	.49	.47	.42	.46	.48	.49	.01	.15	.21	.21	.19	.13
	30°S	.65	.57	.48	.53	.57	.61	.07	.10	.11	.12	.11	.09
	30°E	.33	.25	.16	.20	.24	.27	.37	.26	.16	.21	.25	.30
7	0°	.51	.52	.52	.52	.53	.53	.23	.29	.32	.33	.31	.28
	30°N	.20	.23	.24	.24	.24	.23	.48	.53	.54	.55	.55	.53
	30°W	.51	.54	.56	.55	.55	.54	−.09	.05	.17	.15	.11	.04
	30°S	.70	.70	.68	.71	.71	.71	.03	.07	.11	.09	.08	.07
	30°E	.42	.38	.39	.35	.37	.39	.48	.43	.37	.39	.41	.44
20	0°	.51	.55	.57	.56	.55	.54	.18	.23	.28	.29	.29	.26
	30°N	.17	.21	.24	.23	.22	.21	.43	.51	.57	.56	.55	.52
	30°W	.49	.51	.53	.53	.53	.51	−.25	−.15	−.06	−.07	−.10	−.15
	30°S	.74	.74	.74	.74	.74	.74	.00	.02	.04	.03	.03	.02
	30°E	.47	.46	.45	.45	.46	.48	.55	.54	.52	.53	.53	.54
60	0°	.52	.54	.56	.55	.55	.55	.09	.12	.13	.13	.13	.13
	30°N	.13	.15	.17	.50	.49	.49	.26	.29	.32	−.38	−.39	−.40
	30°W	.47	.48	.50	.77	.77	.77	−.43	−.41	−.38	−.02	−.02	−.03
	30°S	.76	.76	.77	.52	.52	.51	−.03	−.03	.03	.59	.59	.59
	30°E	.51	.51	.52	.17	.16	.17	.57	.58	.59	.32	.31	.31

Depth m.w.e.	Direction	x_2^2						y_2^2					
		γ			b			γ			b		
		0	0.5	1.0	10	30	100	0	0.5	1.0	10	30	100
0	0°	.12	.11	.09	.11	.12	.12	.34	.48	.61	.55	.50	.44
	30°N	−.17	−.16	−.15	−.16	−.17	.18	.37	.53	.67	.61	.55	.48
	30°W	.09	.08	.06	.07	.08	.08	.11	.29	.47	.39	.31	.23
	30°S	.46	.44	.39	.43	.45	.46	.28	.42	.55	.48	.43	.37
	30°E	.08	.11	.13	.13	.12	.10	.62	.72	.80	.77	.74	.69
7	0°	.11	.12	.13	.13	.12	.12	.22	.31	.38	.34	.33	.29
	30°N	−.19	−.22	−.23	−.23	−.23	−.22	.22	.31	.41	.38	.34	.29
	30°W	.09	.09	.09	.09	.10	.10	−.06	.03	.12	.09	.05	.01
	30°S	.49	.49	.50	.49	.49	.49	.16	.23	.30	.41	.25	.22
	30°E	.05	.06	.08	.07	.06	.05	.54	.61	.68	.66	.64	.60
20	0°	.11	.12	.12	.15	.15	.16	.13	.17	.22	.19	.18	.16
	30°N	−.15	−.18	−.20	−.20	−.19	−.18	.12	.16	.20	.29	.28	.16
	30°W	.10	.11	.12	.12	.12	.11	−.15	−.11	−.07	−.08	−.09	−.11
	30°S	.48	.49	.49	.49	.49	.49	.09	.12	.16	.15	.14	.13
	30°E	.03	.02	.02	.02	.02	.02	.46	.51	.55	.54	.53	.51
60	0°	.11	.11	.12	.12	.12	.12	.06	.08	.08	.08	.08	.08
	30°N	−.09	−.09	−.09	.09	.09	.09	.05	.05	.06	−.21	−.21	−.21
	30°W	.08	.09	.09	.46	.46	.46	−.23	−.22	−.21	.03	.03	.03
	30°S	.46	.46	.46	.05	.05	.05	.01	.02	.03	.38	.38	.38
	30°E	.05	.05	.05	−.09	−.09	−.07	.37	.38	.38	.06	.05	.10

3.14.6. Transformation matrices

The transformations of vectors **K** and **A** from one coordinate system to another are linear. In fact, any linear combination of distributions is maintained if the coordinate system is rotated and therefore the vector **A** is transformed linearly. Evidently the same holds for the vector **K**. Thus the transformations are expressed by matrices M_A and M_K. The scalar product **A•K** = I is invariant, and this requirement gives the relation between the matrices (Krymsky et al. 1966a,b):

$$M_A = \left(M_K^T\right)^{-1}, \tag{3.14.26}$$

where the upper index T denotes the transposed matrix. Since the Legendre functions in the expressions for the components of vector **K** can be normalized arbitrarily, one can choose the normalization such that $M_A = M_K$, i.e. both vectors are transformed by the same matrix. For n = 1, 2 the Legendre functions normalized in this way are

$$\begin{aligned} &P_1^0(\sin\theta) = \sin\theta, \quad P_1^1(\sin\theta) = \cos\theta, \quad P_2^0(\sin\theta) = \sqrt{3}\sin^2\theta - 1/3, \\ &P_2^1(\sin\theta) = \sin 2\theta, \quad P_2^2(\sin\theta) = \cos^2\theta. \end{aligned} \tag{3.14.27}$$

With this normalization the components of vector **A** have a simple meaning. If **A** is determined in the solar geographic coordinate system, $\left|r_1^1\right|$ is the amplitude of the diurnal variation owed to the first spherical harmonic recorded by an 'ideal' instrument at the equator, and the argument is its phase, r_2^1 gives amplitude and phase of the diurnal variation at latitude 45° N, and r_2^2 gives amplitude and phase of the semi-diurnal variation at the equator.

Transformation of Eq. 3.14.1 from one coordinate system to another cannot cause new spherical harmonics to appear or existing ones to disappear. In other words, when the coordinate system in Eq. 3.14.1 is rotated no values of the index n can appear or disappear. Hence the matrix M is quasi-diagonal and falls apart in a number of matrices corresponding to transformation of the first, second, etc., spherical harmonics. Thus to each value of n corresponds a transformation matrix M_n.

One may pass from one system of spherical coordinates to another by means of three successive rotations, given by the Euler angles ϕ, ξ, κ. The angles ϕ and κ correspond to rotations in longitude, and the angle ξ to a rotation in latitude. In order to find the matrix of any transformation it suffices to know two matrixes corresponding to rotation of coordinates in the equatorial and meridianal planes. Let us restrict ourselves to the first two harmonics. If the vector **K** is represented by the first harmonic only (n = l), i.e. **K** = $\{a_{10}, a_{11}, b_{11}\}$, it is an ordinary space vector, and therefore the transformation matrices for the first harmonic are given by the expressions:

$$M_1^{\text{long}}(\kappa)=\begin{pmatrix}1 & 0 & 0\\ 0 & \cos\kappa & \sin\kappa\\ 0 & -\sin\kappa & \cos\kappa\end{pmatrix},\quad M_1^{\text{lat}}(\xi)=\begin{pmatrix}\cos\xi & 0 & -\sin\xi\\ 0 & 1 & 0\\ \sin\xi & 0 & \cos\xi\end{pmatrix},\tag{3.14.27}$$

where the indices **long** and **lat** are the rotations of the plane of the equator in longitude and meridian (latitude) respectively.

In order to find the matrices for the second harmonic it is sufficient to note that the components of the vector **K** for $n = 2$ are expressed in the angles θ, ϕ so, that they are quadratic forms in the variables x_1^0, x_1^1, y_1^1

$$\begin{aligned}&x_2^0=\frac{2}{\sqrt{3}}\left(x_1^0\right)^2-\frac{1}{\sqrt{3}}\left(x_1^1\right)^2-\frac{1}{\sqrt{3}}\left(y_1^1\right)^2,\quad x_2^2=\left(x_1^1\right)^2+\left(y_1^1\right)^2,\\ &x_2^1=2x_1^0x_1^1,\quad y_2^1=2x_1^0y_1^1,\quad y_2^2=2x_1^1y_1^1.\end{aligned}\tag{3.14.28}$$

From this property and from the above matrices it follows that

$$M_2^{\text{long}}(\kappa)=\begin{pmatrix}1 & 0 & 0 & 0 & 0\\ 0 & \cos\kappa & \sin\kappa & 0 & 0\\ 0 & -\sin\kappa & \cos\kappa & 0 & 0\\ 0 & 0 & 0 & \cos 2\kappa & \sin 2\kappa\\ 0 & 0 & 0 & -\sin 2\kappa & \cos 2\kappa\end{pmatrix},\tag{3.14.29}$$

$$M_2^{\text{lat}}(\xi)=\begin{pmatrix}1-(3/2)\sin^2\xi & 0 & -\left(\sqrt{3}/2\right)\sin 2\xi & -\left(\sqrt{3}/2\right)\sin^2\xi & 0\\ 0 & \cos\xi & 0 & 0 & -\sin\xi\\ \left(\sqrt{3}/2\right)\sin 2\xi & 0 & \cos 2\xi & (1/2)\sin 2\xi & 0\\ -\left(\sqrt{3}/2\right)\sin^2\xi & 0 & -(1/2)\sin 2\xi & \left(1+\cos^2\xi\right)/2 & 0\\ 0 & \sin\xi & 0 & 0 & \cos\xi\end{pmatrix}.\tag{3.14.30}$$

One easily sees that these matrices have the property $M_A=\left(M_K^T\right)^{-1}$ described by Eq. 3.14.26. Also $M^{-1}(\xi)=M(-\xi)$. Therefore they can be used for the transformation of vector **K** and of vector **A** alike. The transformation given by the angles φ,ξ,κ is made using the matrix which is the product of the matrices for the respective rotations

$$M_n(\varphi,\xi,\kappa)=M_n^{\text{long}}(\kappa)M_n^{\text{lat}}(\xi)M_n^{\text{long}}(\varphi).\tag{3.14.31}$$

Suppose that a process connected with solar activity gives a CR distribution **A(r)** in the solar system, where **r** is the radius vector of the point in space where the observation is made. If the process is stationary, the mean of the distribution over the time of one revolution of the Sun **A(r)** at each point will be constant. If, moreover, the distribution in

each point of space is measured in the heliographic system of angular coordinates, the function **A(r)** will have axial symmetry with respect to the Sun's axis of rotation. Hence, neglecting the deviations of the Earth from the plane of the solar equator, we can assume that the distribution observed on the Earth will be constant in the **solar heliographic coordinate system.**

Assuming this distribution to be given we find the annual mean solar daily and sidereal daily variations. Vector **A** is split into two vectors:

$$\mathbf{A}_1 = \left\{r_1^0, r_1^1, 0\right\} \quad \text{and} \quad \mathbf{A}_2 = \left\{0, ..., r_2^0, r_2^1, r_2^2, 0, ...\right\} \tag{3.14.32}$$

corresponding to the first and second harmonics, respectively. For study of the solar-daily variations vector **A** must be represented in the solar geographic coordinate system. The transition to this system is made by three successive rotations: **solar heliographic; sidereal heliographic; sidereal geographic; solar geographic**, and is given by the angles $\varphi = t_1, \xi = \delta_o - \pi/2, \kappa = -t_2$, where $\delta_o = 64^o$ is the declination of the Sun's North pole, t_1 and t_2 are the longitudes of the point δ = 0, a = 1 hour in the solar heliographic and geographic coordinate systems respectively. The angles t_1 and t_2 differ by some degrees at most and one may put $t_1 \approx t_2 \approx t$, where in the course of the year t takes the values from 0 to 2π.

Thus, the annual mean vector $\mathbf{A}_{1,2}$ in the solar geographic system is obtained by multiplying the vector with the matrix

$$M_{1,2} = \overline{M_{1,2}^{\text{long}}(-t) M_{1,2}^{\text{lat}}(\delta_o - \pi/2) M_{1,2}^{\text{long}}(t)} \tag{3.14.33}$$

where the horizontal line indicates averaging over t. Performing this matrix multiplication and remembering that the orthogonally of the trigonometric functions makes $\cos^2 t, \cos^2 2t, \sin^2 t, \sin^2 2t$ equal to 1/2 and the other products to zero, we find that M_1 and M_2 are diagonal matrices with the following non-zero elements:

For M_1:

$$M_{11} = \sin\delta_o = 0.899, M_{22} = M_{33} = (1/2)(1 + \sin\delta_o) = 0.950\ ; \tag{3.14.34}$$

For M_2:

$$M_{11} = (3/2)\sin^2\delta_o - 1/2 = 0.712, M_{22} = M_{33} = (1/2)(\sin\delta_o - \cos 2\delta_o) = 0.758, \\ M_{44} = M_{55} = (1/4)(1 + \sin\delta_o)^2 = 0.902 \tag{3.14.35}$$

Thus the annual mean distribution vector differs little from the initial vector. Only the module of the complex components are changed, but their arguments remain. For finding the sidereal-daily variations one must pass to the equatorial coordinate system used in astronomy. This transition is done in the following order: solar heliographic; sidereal heliographic; sidereal geographic; equatorial. The corresponding Euler angles are:

$\varphi = t$, $\xi = \delta_o - \pi/2$, $\kappa = -1^{\mathrm{h}}04^{\mathrm{m}} = -16^o$. The matrices for finding the annual mean distribution in the equatorial system are

$$M_{1,2} = \overline{M_{1,2}^{\mathrm{long}}(\kappa) M_{1,2}^{\mathrm{lat}}(\delta_o - \pi/2) M_{1,2}^{\mathrm{long}}(t)} \,. \tag{3.14.36}$$

Evidently in matrices $M_{1,2}^{\mathrm{long}}(t)$ only one element is non-zero ($M_{11} = 1$), so multiplication according to Eq. 3.14.36 gives

$$M_1 = \begin{pmatrix} 0.899 \\ 0.121 \\ 0.420 \end{pmatrix}, \quad M_2 = \begin{pmatrix} 0.712 \\ 0.188 \\ -0.656 \\ -0.142 \\ -0.088 \end{pmatrix}. \tag{3.14.37}$$

This form of the matrices shows that the sidereal daily variations are due only to the components r_1^0 and r_1^2 of the vector represented in the solar heliographic system. Let us put $r_1^0 = 1$ and $r_1^2 = 1$. Then in the equatorial system

$$\begin{aligned} &r_1^0 = 0.899, \; r_1^1 = 0.437 \exp\left(i 286^o\right), \; r_2^0 = 0.712, \\ &r_2^1 = 0.683 \exp\left(i 286^o\right), \; r_2^2 = 0.167 \exp\left(i 212^o\right). \end{aligned} \tag{3.14.38}$$

The components r_1^1 and r_1^2 give the sidereal-daily variations which are symmetric and asymmetric relative to the geographic equator. The moment of maximum intensity in local sidereal time is the argument of these components expressed in hours: 286°/15 ≅ 19^{h}. In the southern hemisphere the second component gives the opposite time of maximum: 7^{h}. The component r_2^2 is responsible for the semi-diurnal variation with maximum at 212°/30 ≈ 7^{h} local sidereal time. The matrix method can also be employed to analyze concrete models of CR distribution. It is essential that the matrices can depend on time and on space coordinates, and that they can be averaged, subtracted, etc. This makes the method simple and flexible.

3.14.7. Method for determining the momentary anisotropy

Krymsky et al. (1966b) suggested a method for finding the anisotropy at any moment of time by using the acceptance vectors. The method is based on Eq. 3.14.3. Instruments with different **K** record at time t different CR intensities I. Let us assume that the series described by Eq. 3.14.1 contains no harmonics with n > l, then the vectors **A** and **K** contain $(l+1)^2$ real components. A complete description of the vector **A**, therefore, requires data from $(l+1)^2$ instruments with linearly independent **K**. Thus, for

finding the isotropic intensity (l = 0) one instrument is required; for finding the first spherical harmonic under the condition that the distribution contains no higher harmonics, four instruments and for the first two harmonics, nine instruments, properly distributed over the Earth. If the number of instruments is sufficient the vector $\mathbf{A}(t)$ at any moment can be found from a system of linear algebraic equations of the form as Eq. 3.14.3. The data of the worldwide net of neutron monitors can be treated by this method. However, their distribution over the globe is highly uneven. Therefore study of even the second spherical harmonic from these data is unreliable. A complication is the possible presence of zero line drifts. Since the measurements are made with respect to some mean level of the isotropic background, slow variations of instrumental or other local origin, different for different stations, are possible. To eliminate these one must provisionally correct all data by a linear 'filter' transmitting fluctuations with periods of the order of a day and not less. Such a filter can be used as follows:

$$I(t) = \int_{-\infty}^{\infty} F(t-\tau) I(\tau) d\tau \ . \qquad (3.14.39)$$

The nucleus $F(t-\tau)$ determines the pass band of the filter. In practice the integration limits are always finite. Since the CR data are discrete time series, the integral described by Eq. 3.14.39 becomes a sum. The simplest example of a filter is the operation of taking the difference between observed intensity and the sliding mean. The method described yields the anisotropy **A** at any moment (more properly, for each interval). However, at present its possibilities cannot be fully exploited, because many requirements are not met by the actual net of CR stations. First, on account of their uneven distribution over the Earth high spherical harmonics (already the second) cannot be properly studied. Moreover, owing to the influence of the geomagnetic field neutron monitors both at moderate latitudes and near the equator, collect radiation from regions close to the equator. Only few monitors, at geomagnetic latitudes above 60°–70°, are sensitive to high latitude radiation. This circumstance, and the necessity of correcting for instrumental variations, limits the possibilities of determining zonal harmonics.

Let us note that many applications of this method will be considered in the next book Dorman (M2005).

3.15. Experimental estimation of the ground detector's sensitivity to primary CR on the basis of data on observed CR variations

3.15.1. On the using of experimental data on CR variations for estimation of coupling functions and integral multiplicities for the detectors of secondary CR components

Above we considered in detail determination of integral multiplicities and coupling functions for detectors of secondary CR (nuclear or neutron component at different levels of observation in the atmosphere, muon component for different depths underground and at different levels of observation in the atmosphere, electron-photon component and others) on the basis of data on geomagnetic effects and by calculations of

meson-nuclear (hadronic) and electro-photon (electromagnetic) CR cascades in the atmosphere. In principle for this purpose can be used also data on observed CR variations with a big amplitudes of different secondary CR components: great FEP events observed by ground CR detectors (GLE – Ground Level Enhancement), long-term variations (11 and 22 year variations), big Forbush-effects, and so on.

In the first time, such possibility was used basing on the data of the greatest in the last 70 years FEP of February 23, 1956 (Dorman, M1957). As it was shown in Dorman (M1957) on the basis of data of many CR stations equipped by shielded 10 cm Pb ionization chambers, gas filled counters and scintillation telescopes of charged particles, and by neutron monitors of IGY type, in the first 30–40 min of event the planetary distribution of the CR intensity increase shows a big degree of solar CR flux anisotropy. However, in the next one-two hours, the distribution of solar CR out of the Earth's magnetosphere gradually transformed to practically isotropic (owed to solar energetic particle scattering in the interplanetary space). For isotropic distribution the amplitude of solar CR increase will be determine by primary solar CR flux near the Earth's orbit, by the integral multiplicity or coupling function of detector, and cutoff rigidity of the point of observations (see Section 3.1). For two points of observations with the same detectors but different cutoff rigidities we obtain (it is supposed that the corrections on meteorological effects and on geomagnetic variations are introduced):

$$\delta N_i(R_{c1},h_o,t)/N_i(R_{c1},h_o)=\int_{R_{c1}}^{\infty}\frac{\delta D(R,t)}{D_o(R)}W_i(R_{c1},R,h_o)dR, \tag{3.15.1}$$

$$\delta N_i(R_{c2},h_o,t)/N_i(R_{c2},h_o)=\int_{R_{c2}}^{\infty}\frac{\delta D(R,t)}{D_o(R)}W_i(R_{c2},R,h_o)dR, \tag{3.15.2}$$

where $W_i(R_{c1},R)$ and $W_i(R_{c2},R)$ are coupling functions for two points of observations. Let us rewrite Eq. 3.15.1 and 3.15.2 by using polar coupling functions $W_{io}(R,h_o)=W_i(0,R,h_o)$, described in Section 3.1, and relation

$$W_i(R_c,R,h_o)=(N_{io}(h_o)/N_i(R_c,h_o))W_{io}(R,h_o), \tag{3.15.3}$$

where $N_{io}(h_o)=N_i(0,h_o)$ is the CR intensity at $R_c=0$. So instead of Eq. 3.15.1 and 3.15.2 we obtain

$$\delta N_i(R_{c1},h_o,t)/N_i(R_{c1},h_o)=\frac{N_{io}(h_o)}{N_i(R_{c1},h_o)}\int_{R_{c1}}^{\infty}\frac{\delta D(R,t)}{D_o(R)}W_{io}(R,h_o)dR, \tag{3.15.4}$$

$$\delta N_i(R_{c2},h_o,t)/N_i(R_{c2},h_o)=\frac{N_{io}(h_o)}{N_i(R_{c2},h_o)}\int_{R_{c2}}^{\infty}\frac{\delta D(R,t)}{D_o(R)}W_{io}(R,h_o)dR, \tag{3.15.5}$$

If the difference between R_{c1} and R_{c2} is small, we obtain from Eq. 3.15.4 - 3.15.5 that

$$\frac{\delta N_i(R_{c1},h_o,t)}{N_i(R_{c1},h_o)}\frac{N_i(R_{c1},h_o)}{N_{io}(h_o)}-\frac{\delta N_i(R_{c2},h_o,t)}{N_i(R_{c2},h_o)}\frac{N_i(R_{c2},h_o)}{N_{io}(h_o)}=W_{io}(\overline{R})\int_{R_{c1}}^{R_{c2}}\frac{\delta D(R,t)}{D_o(R)}dR, \quad (3.15.6)$$

where $R_{c1}<\overline{R}<R_{c2}$ (it is assumed that $R_{c1}<R_{c2}$). The ratios $\frac{N_i(R_c,h_o)}{N_{io}(h_o)}$ in Eq. 3.15.3–3.15.6 characterized well known latitude effect. From Eq. 3.15.6 follows

$$W_{io}(\overline{R})=\left(\frac{\delta N_i(R_{c1},h_o,t)}{N_i(R_{c1},h_o)}\frac{N_i(R_{c1},h_o)}{N_{io}(h_o)}-\frac{\delta N_i(R_{c2},h_o,t)}{N_i(R_{c2},h_o)}\frac{N_i(R_{c2},h_o)}{N_{io}(h_o)}\right)$$
$$\times\left(\int_{R_{c1}}^{R_{c2}}\frac{\delta D(R,t)}{D_o(R)}dR\right)^{-1}. \quad (3.15.7)$$

Because R_{c1} and R_{c2} may cover the interval from zero to about 15 GV, on the basis of Eq. 3.15.7 can be found the polar coupling function for any CR secondary component if the spectrum of primary CR variation is known.

By the described method can be determined also integral multiplicities (yield functions). It can be made by two ways. In the first way we will use Eq. 3.1.4 of determination of coupling function, from which follows:

$$m_i(R,h_o)=\frac{W_{io}(R,h_o)N_{io}(h_o)}{D_o(R)}. \quad (3.15.8)$$

In the second way we will use Eq. 3.1.2, from which follows:

$$\delta N_i(R_{c1},h_o,t)-\delta N_i(R_{c2},h_o,t)=\int_{R_{c1}}^{R_{c2}}m_i(R,h_o)\delta D(R,t)dR, . \quad (3.15.9)$$

where $\delta D(R,t)$ is the spectrum of additional primary radiation which is assumed known from other measurements. From Eq. 3.15.9 we obtain

$$m_i(\overline{R},h_o)=(\delta N_i(R_{c1},h_o,t)-\delta N_i(R_{c2},h_o,t))\left(\int_{R_{c1}}^{R_{c2}}\delta D(R,t)dR\right)^{-1}, \quad (3.15.10)$$

where $R_{c1}<\overline{R}<R_{c2}$ (it is assumed again that $R_{c1}<R_{c2}$).

By using Eq. 3.15.7 the coupling functions for muon and charged CR components in the region of rigidities $R\le 7\ GV$ (where latitude effect of muon and charged CR components became very small and is much influenced by temperature effect according to Dorman, 1954) can be determined if the spectrum of primary solar CR is known. On the basis of the data of the FEP of 23 February 1956 this may be done rather reliably

since the flux of energetic particles in the low energy region was exceptionally large (owing to the great steepness of the spectrum) and effects may be detected even if the coupling functions in the region of such low energy is very small. In Dorman (M1957) the spectrum of primary CR variation $\delta D(R,t)/D_o(R)$ were determined on the basis of NM data (and controlled by data on balloons), and then for determining polar coupling functions for muon and charged CR components in small energy region according to Eq. 3.15.7 were used data at 5.00 UT 23 February (about 80 min after the start of FEP), when shielded by 10 cm Pb ionization chambers show following: at geomagnetic latitude 63° the amplitude of increase A = 45%, around geomagnetic latitude 50° it was observed A = 22%, 24%, 20%, 30%, and 26% (average 24%), and at geomagnetic latitude 36° A = 5%. We used also data obtained at 5.30 UT at 80° the amplitude of increase A = 33%, at 63° A = 30%, at 50° A = 12%, 13%, 16%, 12%, and 18% (average 14%), and at 36° A = 2.3%; at 6.00 UT at 80° A = 26%, at 63° A = 21%, at 50° A = 7.5%, 8%, 10%, 7%, and 10% (average 8.5%), and at 36° A = 1.4%; at 7.00 UT at 80° A = 16%, at 63° A = 12%, at 50° A = 4%, 4%, 6%, 4%, and 6% (average 4.8%), and at 36° A ≈ 0. We used also data at 8.00 UT and 10.00 UT, but the accuracy of these data is rather low. The final results are shown in Fig. 3.15.1 (here the coupling functions were determined in dependence of kinetic energy of primary particles).

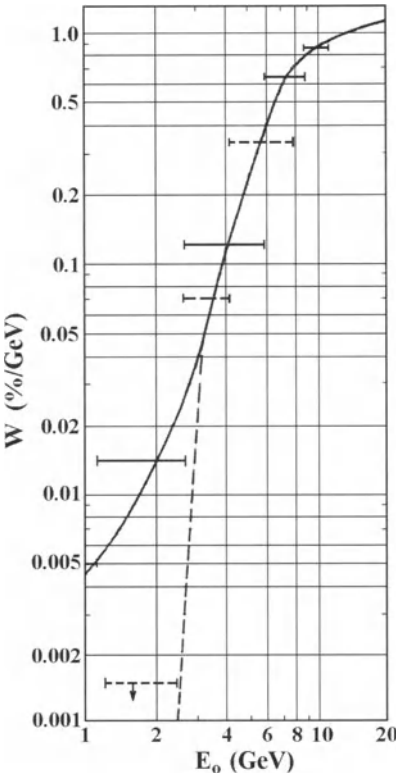

Fig. 3.15.1. Polar coupling functions for shielded by 10 cm Pb ionization chambers (solid curve; solid lines – experimental determinations), and for unshielded counter telescopes (total ionizing component – broken curve and broken lines), determined from data of GLE February 23, 1956. According to Dorman (M1957).

3.15.2. On the NM sensitivity to primary protons below 3 GeV derived from GLE data

As we mentioned in the previous Section 3.15.1, the biggest uncertainties in determining of integral multiplicities (yield functions) and coupling functions are in the region of small rigidities or small primary particle energies. But this region is especially important for investigations of solar CR characterized with a steepened energy spectrum. According to Belov and Struminsky (1997), ground level events on September 29, 1989 and June 15, 1991 provide a good opportunity to determine NM sensitivities to primary protons of energy below 2.5 GeV that are not currently as well known as for higher energy protons. During the late phase of these events the NM network has showed an isotropic enhancement with clear and large latitude effect. It is important that for these periods independent information on primary solar proton spectra was available from balloon and satellite measurements.

Besides mentioned above integral multiplicity and coupling function for describing the sensitivity of CR detectors to primary protons can be used also yield function $Y(R,h_o)$ or $Y(E,h_o)$ which characterized the dependence of counting rate per one primary proton from particle rigidity or energy:

$$Y_i(R,h_o)=\left(\frac{\partial(\delta N_i(R_c,h_o))}{\partial R_c}\right)_{R_c=R}(\delta D(R))^{-1}, \tag{3.15.11}$$

$$Y_i(E,h_o)=\left(\frac{\partial(\delta N_i(E_c,h_o))}{\partial E_c}\right)_{E_c=E}(\delta D(E))^{-1}, \tag{3.15.12}$$

where $\delta N_i(R_c,h_o)$ or $\delta N_i(E_c,h_o)$ is the enhancement of counting rate in dependence of primary protons cutoff rigidity or cutoff energy, and $\delta D(R)$ and $\delta D(E)$ is the enhancement of differential rigidity or energy primary CR spectrum. For the estimate of NM yield function Belov and Struminsky (1997) had choose the database of the late phase of GLE on September 29, 1989 and on June 15, 1991 (see Fig. 3.15.2).

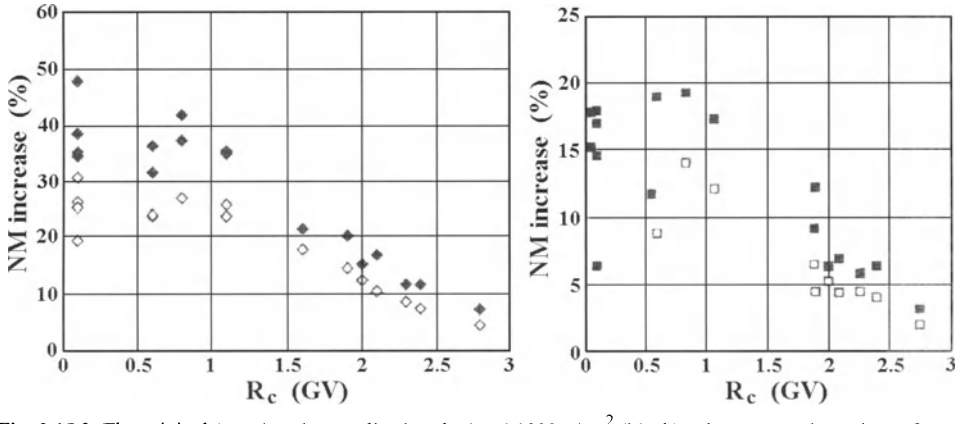

Fig. 3.15.2. The original (open) and normalized to the level 1033 g/cm^2 (black) enhancement dependence from cutoff rigidity at 20.00 UT on September 29, 1989 (left) and at 10.00 UT on June 15, 1991 (right). According to Belov and Struminsky (1997).

Fig. 3.15.2 shows the cutoff rigidity dependence of original NM data and of NM's percentage normalized to the atmospheric depth of 1033 g/cm^2 at 20.00 UT on September 29, 1989 and 10 UT on June 15, 1991. For normalization were used the atmospheric attenuation length for relativistic solar protons obtained by Ahluwalia and Xue (1993):

$$L_{SCR} = (2.8 \pm 0.4)R + (102.9 \pm 3.1)\ \mathrm{g/cm^2}, \tag{3.15.13}$$

where R in GV. The best fits of the normalized rigidity dependences from 1 to 2.8 GV are for data at 20.00 UT on September 29, 1989

$$N(R_c, h_o = 1033\,\mathrm{g/cm^2}) = (27.4 - 22.4 \ln R_c)\,\% \tag{3.15.14}$$

and for data at 10 UT on June 15, 1991

$$N(R_c, h_o = 1033\,\mathrm{g/cm^2}) = (12.3 - 9.83 \ln R_c)\,\% \tag{3.15.14}$$

The energy spectrums of the enhancements in the primary protons from the Sun for the events of September 29, 1989 and June 15, 1991 were obtained by different methods from independent data sets. The differential spectrum of solar protons at 20.00 UT on September 29, 1989 according to the balloon measurements of Akopyan et al. (1991) was:

$$\delta D(E) = 1.84 \times 10^9 E^{-4}\ \ \mathrm{cm^{-2} s^{-1} sr^{-1} MeV^{-1}}, \tag{3.15.15}$$

where E is the proton's kinetic energy in MeV. This result was obtained on the basis of regular balloon flights over Murmansk region $(R_c = 0.6\ \mathrm{GV})$ and over Moscow region $(R_c = 2.39\ \mathrm{GV})$, so these two points are most reliable on the spectrum. The differential spectrum of solar protons at 10 UT on June 15, 1991 was determined from satellite and NM's data for lower and higher energies respectively (see Fig. 3.15.3) by using the method of Belov and Eroshenko (1996).

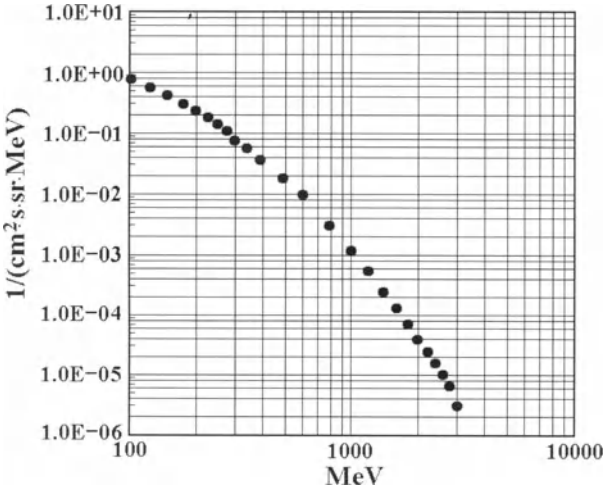

Fig. 3.15.3. The differential spectrum of solar protons at 10 UT on June 15, 1991. According to Belov and Struminsky (1997).

The final result of determining NM sensitivity to primary CR in small energy region calculated according to Eq. 3.15.12 taking into account described above data on primary energy

spectrum and rigidity dependence of NM enhancements is shown in Fig. 3.15.4 in comparison with expected according to formulae proposed by Nagashima et al. (1989).

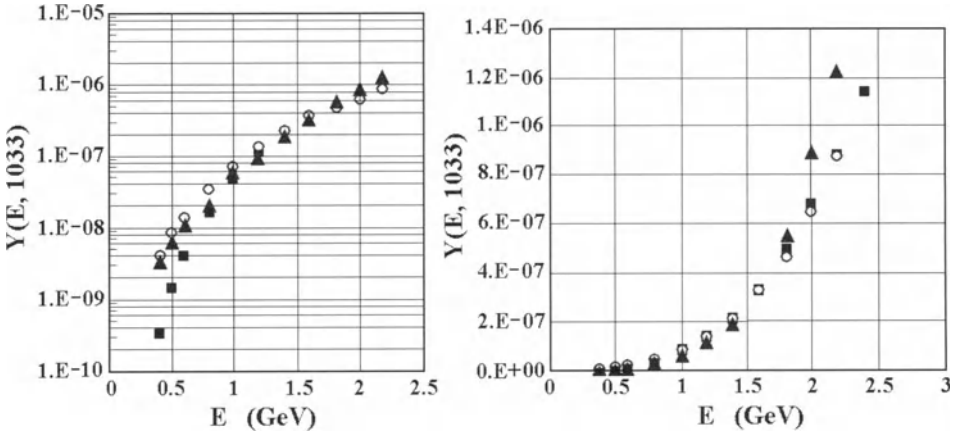

Fig. 3.15.4. Yield function for observations at sea level characterized the sensitivity of NM to primary CR protons in small energy region in logarithmic scale (left panel) and in linear scale (right panel). Open circles – obtained from data of GLE 29 September 1989; black triangles - from data of GLE 15 June 1991; black squares – calculations according to Nagashima et al. (1989). From Belov and Struminsky (1997).

From Fig. 3.15.4 follows that for both events obtained results for yield function in the most part of energy interval are coincided in the frame of statistical errors, and about coincide with expected from Nagashima et al. (1989). Only at kinetic energies smaller than 0.8 GeV the NM sensitivities obtained from both events coincide rather well with each other and show higher sensitivity than according to Nagashima et al. (1989) approximation (see the left panel of Fig. 3.15.4). The result obtained in Belov and Struminsky (1997) for the yield function in the low energy range (between the atmospheric cutoff about 400 MeV up to 3 GeV) can be approximated for the total neutron component by the power law:

$$Y_n\left(E, h_o = 1033 \text{ g/cm}^2\right) \approx 2.45 \times 10^{-17} E^{3.17} \text{ cm}^2.\text{s.sr}\,, \qquad (3.15.16)$$

where kinetic energy of primary protons E in MeV.

3.15.3. Using data on short and long term CR modulation; NM sensitivity changes vs. altitude and cutoff rigidity

In Pyle (1997) were used data on CR modulation effects (long term, 11 year solar cycle variations, and Forbush-decreases) obtained by NM for estimation of the NM sensitivity changes vs. altitude and cutoff rigidity. It is therefore often assumed that NM with the lowest vertical cutoff rigidity R_c should measure the greatest variation in counting rate. However, when the simultaneous development and attenuation of the cascade is taken into account, the altitude of the NM can be seen to play a very important role, especially at low to medium cutoff rigidity $\left(R_c \le 5-6 \text{ GV}\right)$. The latest is supported by Debrunner and Fluckiger's (1971a,b) calculations of response functions for the total

counting rate of NM (see Fig. 3.15.5). The altitude dependence of NM response function is reflected also in analytical presentation of integral multiplicities and coupling functions for NM (see Section 3.8).

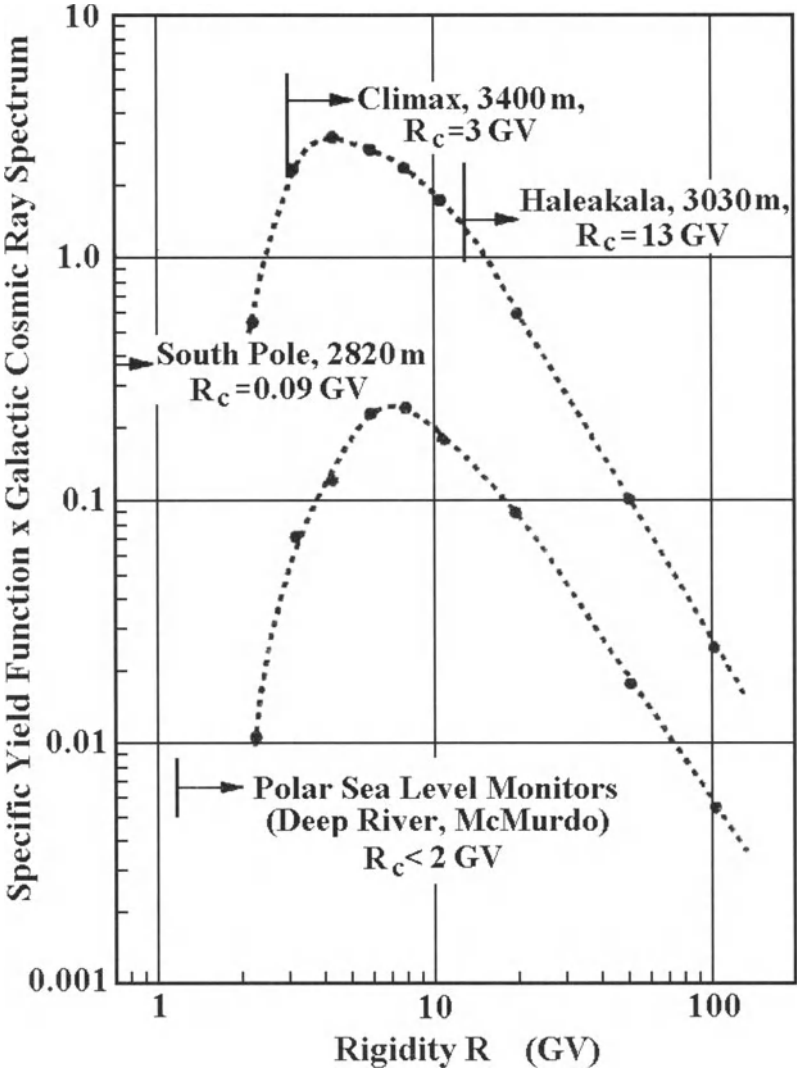

Fig. 3.15.5. Response function (equal to the product of yield function on the differential rigidity spectrum of primary galactic CR; the same as coupling function, but not normalized) for the total counting rate of NM at sea level and at mountains on the altitude about 3000 m. According to Debrunner and Flückiger (1971a,b)

For demonstration of the NM response function dependence from the altitude of observations, Pyle (1997) compare variations during Forbush-decrease of February 26, 1992 observed by Climax NM (altitude 3400 m, $R_c = 3.01$ GV) and Deep River NM (altitude 145 m, $R_c = 1.14$ GV). Results are shown in Fig. 3.15.6.

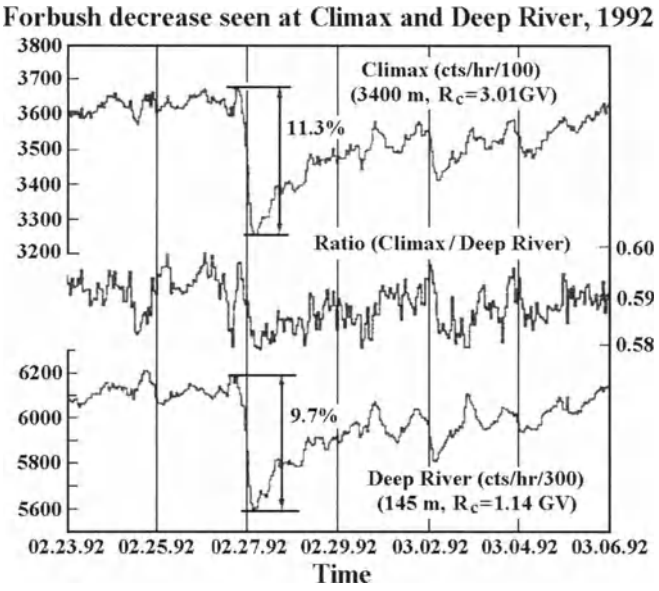

Fig. 3.15.6. A typical Forbush decrease at February 26, 1992 as seen at Climax NM and Deep River NM, and their ratio variation. According to Pyle (1997).

In Fig. 3.15.7 are shown results of comparison CR variations during the same Forbush-decrease but observed near two polar stations $(R_c \approx 0)$ with different elevations: South Pole (2820 m, $R_c = 0.09$ GV) and McMurdo (48 m, $R_c = 0.00$ GV).

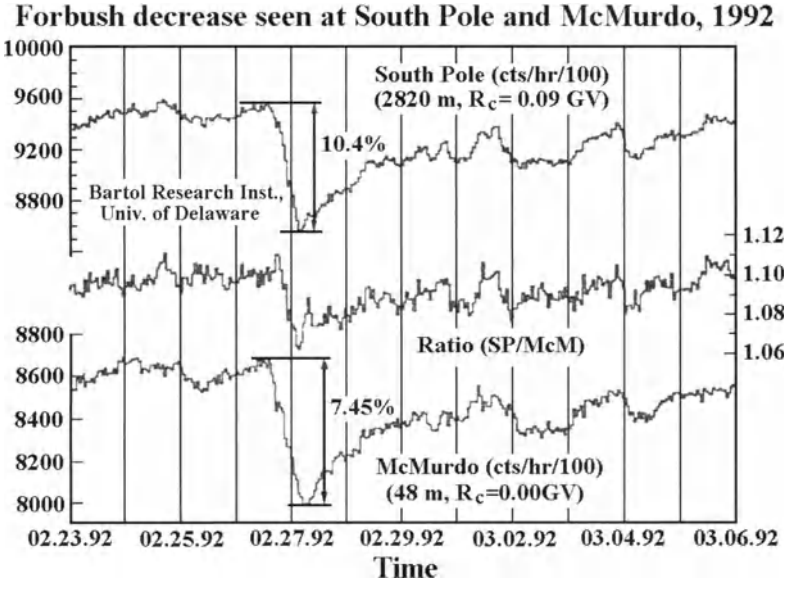

Fig. 3.15.7. Forbush decrease at February 26, 1992 as seen at South Pole NM and McMurdo NM, and their ratio variation. According to Pyle (1997).

From Fig. 3.15.6 can be seen that for this event the Climax NM sensitivity is about 16% greater than Deep River NM. From Fig. 3.15.7 follows that for near polar stations $(R_c \approx 0)$ the sensitivity of South Pole NM (2820 m) is about 40% greater than McMurdo NM (about sea level).

Results of comparison for long term modulation of Climax NM and Deep River NM are shown in Fig. 3.15.8 (monthly data normalized to the 1965 level, defined as 100%).

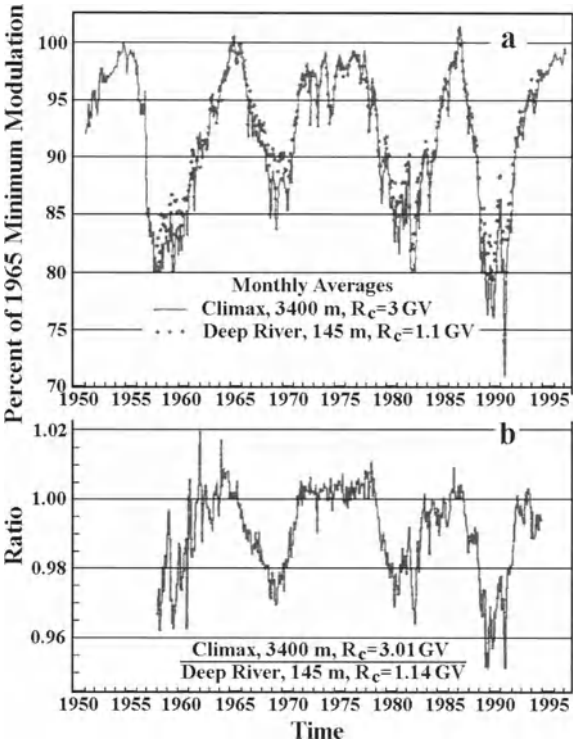

Fig. 3.15.8. (**a**) Monthly average counting rates of Climax NM and Deep River NM, normalized to 100% in 1965. (**b**) Climax NM/Deep River NM ratio (1958-1995). According to Pyle (1997).

From Fig. 3.15.8 can be seen that over the period 1958-1995 the ratio Climax NM/Deep River NM varies only about 4%, while the individual counting rates vary by more than 30%. In Figure 3.15.9 are plotted these two sets of monthly averages against each other and is shown the best-fit straight line. From Fig. 3.15.9 follows that the Climax NM at elevation 3400 m is again 16% more sensitive to long term CR solar modulation than Deep River NM near sea level (in accordance with obtained for the Forbush decrease, see Fig. 3.15.5). Let us note that this coincidence can be understand if we take into account that CR primary variation for both types of modulation (short and long term) is about the same: $\delta D(R)/D_o(R) \propto R^{-1}$. The other note is regarding to comparison of results of pairs Climax NM-Deep River NM and South Pole NM-McMurdo NM for Forbush decrease: 16% and 40%, respectively. This big difference can be understand if we take into account that in the case Climax NM-Deep River NM

cutoff rigidities are not equal: for Climax NM $R_c = 3.01$ GV and Deep River NM $R_c = 1.14$ GV. This gives sufficient decreasing of observed sensitivity effect (only 16%) in comparison with result about 40% for the pair South Pole NM-McMurdo NM with about the same cutoff rigidity $(R_c \approx 0)$.

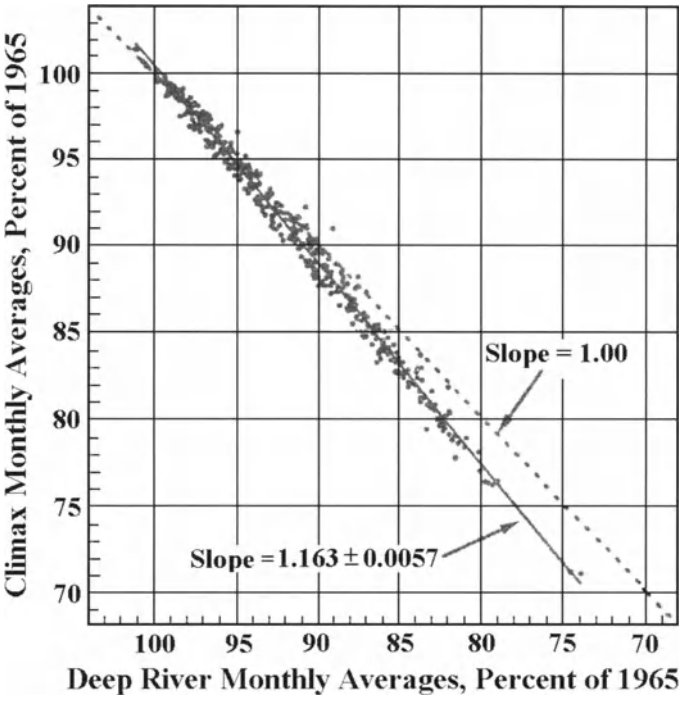

Fig. 3.15.9. Two sets of monthly averages of Climax NM and Deep River NM against each other; is shown also the best-fit straight line. According to Pyle (1997).

3.16. Effective rigidity and effective energy as characteristics of secondary CR detector sensitivity to primary CR

3.16.1. The effective rigidities and energies of CR detectors and their dependence from cutoff rigidity and primary CR spectrum of variation

In some rough estimations of dependence of CR variations from rigidity or energy of primary particles can be useful so called classical effective rigidities and effective energies of CR ground detectors of type *i* (Dorman, M1963b):

$$R_{\mathrm{ef},i}(R_c, h_o, \gamma) = \int_{R_c}^{\infty} R^{-\gamma+1} W_i(R_c, R, h_o) dR \times \left(\int_{R_c}^{\infty} R^{-\gamma} W_i(R_c, R, h_o) dR \right)^{-1}, \qquad (3.16.1)$$

where we assumed that the primary CR variation is described by expression

$$\delta D(R)/D_o(R) \propto R^{-\gamma} ; \tag{3.16.2}$$

and

$$E_{ef,i}(E_c,h_o,\gamma)=\int_{E_c}^{\infty} E^{-\gamma+1}W_i(E_c,E,h_o)dE \times \left(\int_{R_c}^{\infty} E^{-\gamma}W_i(E_c,E,h_o)dE\right)^{-1}, \tag{3.16.3}$$

where it is assumed that

$$\delta D(E)/D_o(E) \propto E^{-\gamma} . \tag{3.16.4}$$

Let us note that at $\gamma = 0$ Eq. 3.16.1 and 3.16.2 give effective rigidities and effective energies of CR ground detectors for nondisturbed intensity; at $\gamma \approx 1$ they determine effective rigidities and effective energies in the case of short term modulations (Forbush decreases) and long term variations (11 and 22 year solar cycle modulation); at $\gamma \approx 2$–5 they determine effective rigidities and effective energies in the case of solar CR events, so called GLE. From Eq. 3.16.1 and 3.16.3 follows that the effective rigidities and effective energies of CR ground detectors increase with increasing of cutoff rigidity and decrease with increasing γ: it means that effective rigidities and effective energies in case of modulation effects are smaller than for normal CR intensity, and in case of GLE they will be smaller than for modulation effects.

3.16.2. Using the analytical approximation for coupling functions

Let us use the analytical approximation for coupling functions (see Eq. 3.8.3 in Section 3.8). In this case instead of Eq. 3.16.2 we obtain for effective rigidity

$$R_{ef,i}(R_c,h_o,\gamma)=\int_{R_c}^{\infty} R^{-\gamma-k_i}\exp\left(-a_iR^{-k_i}\right)dR \times \left(\int_{R_c}^{\infty} R^{-\gamma-k_i-1}\exp\left(-a_iR^{-k_i}\right)dR\right)^{-1} . \tag{3.16.5}$$

To calculate the integrals in Eq. 3.16.5 we choose some R_1 for which $a_iR_1^{-k_i} << 1$ or $R_1 >> a_i^{1/k_i}$. In this case we obtain

$$\int_{R_c}^{\infty} R^{-\gamma-k_i}\exp\left(-a_iR^{-k_i}\right)dR = \int_{R_c}^{R_1} R^{-\gamma-k_i}\exp\left(-a_iR^{-k_i}\right)dR$$
$$+\int_{R_1}^{\infty} R^{-\gamma-k_i}\left[1-a_iR^{-k_i}+\left(a_i^2R^{-2k_i}/2!\right)-\left(a_i^3R^{-3k_i}/3!\right)+...\right]dR, \tag{3.16.6}$$

from which follows

$$\int_{R_c}^{\infty} R^{-\gamma-k_i}\exp\left(-a_iR^{-k_i}\right)dR = \int_{R_c}^{R_1} R^{-\gamma-k_i}\exp\left(-a_iR^{-k_i}\right)dR + \frac{R_1^{-\gamma-k_i+1}}{\gamma+k_i-1}$$
$$-\frac{a_iR_1^{-\gamma-2k_i+1}}{\gamma+2k_i-1}+\frac{a_i^2}{2!}\frac{R_1^{-\gamma-3k_i+1}}{\gamma+3k_i-1}-\frac{a_i^3}{3!}\frac{R_1^{-\gamma-4k_i+1}}{\gamma+4k_i-1}+..., \tag{3.16.7}$$

where the integral in the right hand must be calculated numerically.

3.16.3. Effective rigidities for muon detectors

For muon component at sea level (surveys data are compiled in Dorman, M1957, M1963b, M1974, M1975a) was found $\alpha_\mu = 19.4$, $k_\mu = 0.77$. As example we show in Fig. 3.16.1 calculated according to Eq. 3.16.5 and Eq. 3.16.7 R_{ef} for muon component at sea level.

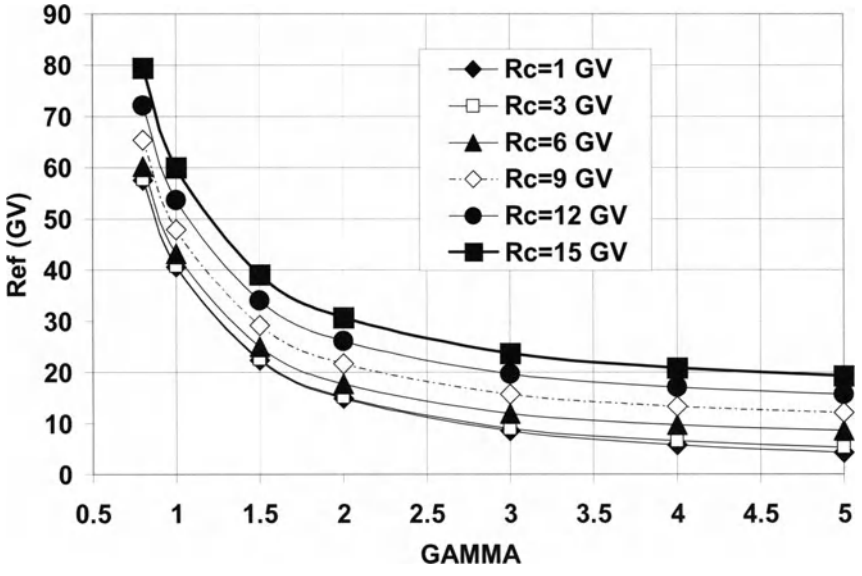

Fig. 3.16.1. Expected effective rigidity for muon CR component at sea level in dependence of cutoff rigidity and slope gamma in primary CR variation spectrum.

From Fig. 3.16.1 can be seen that effective rigidity of muon detector decreases with increasing of the slope in primary CR variation spectrum and increases with increasing of cutoff rigidity in the point of observation. The dependences of $R_{\text{ef},\mu}(R_c, h_o, \gamma)$ from γ at different R_c for observations at sea level can be approximated as following:

$$R_{\text{ef},\mu}(R_c = 1\ \text{GV}, h_o, \gamma) = 40.64 \times \gamma^{-1.414}\ \text{GeV} \tag{3.16.8}$$

with correlation coefficient of approximation 0.99975;

$$R_{\text{ef},\mu}(R_c = 3\ \text{GV}, h_o, \gamma) = 40.26 \times \gamma^{-1.315}\ \text{GeV} \tag{3.16.9}$$

with correlation coefficient of approximation 0.998;

$$R_{\text{ef},\mu}(R_c = 6\ \text{GV}, h_o, \gamma) = 42.12 \times \gamma^{-1.074}\ \text{GeV} \tag{3.16.10}$$

with correlation coefficient of approximation 0.991;

$$R_{ef,\mu}(R_c = 9\ \text{GV}, h_o, \gamma) = 46.80 \times \gamma^{-0.923}\ \text{GeV} \tag{3.16.11}$$

with correlation coefficient of approximation 0.973;

$$R_{ef,\mu}(R_c = 12\ \text{GV}, h_o, \gamma) = 52.64 \times \gamma^{-0.831}\ \text{GeV} \tag{3.16.12}$$

with correlation coefficient of approximation 0.984;

$$R_{ef,\mu}(R_c = 12\ \text{GV}, h_o, \gamma) = 59.01 \times \gamma^{-0.769}\ \text{GeV} \tag{3.16.12a}$$

with correlation coefficient of approximation 0.983. It is easy to see that Eq-s 3.16.8 – 3.16.12a can be combined with a good accuracy as

$$R_{ef,\mu}(R_c, h_o, \gamma) = F(R_c, h_o) \times \gamma^{-G(R_c, h_o)}\ \text{GeV}, \tag{3.16.13}$$

where functions $F(R_c, h_o)$ and $G(R_c, h_o)$ are presented in Fig. 3.16.2.

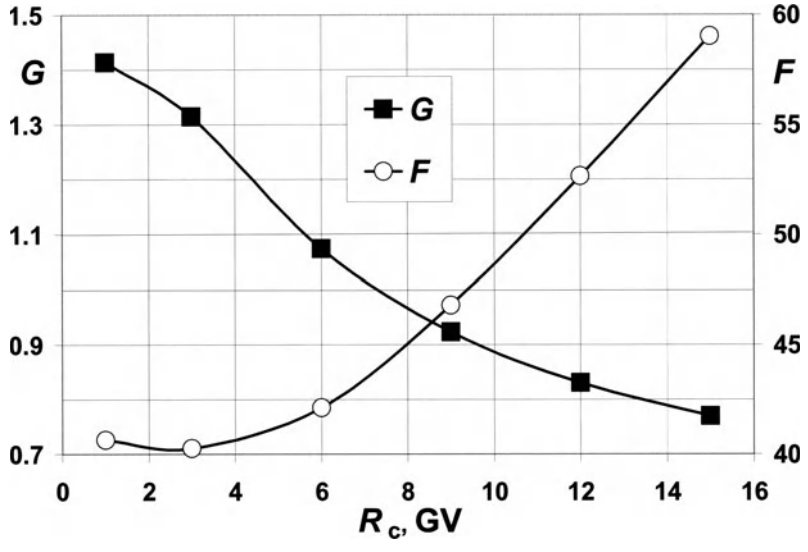

Fig. 3.16.2. Functions $F(R_c, h_o)$ and $G(R_c, h_o)$ in Eq. 3.16.13 for observations muon component at sea level.

From Fig. 3.16.2 follows that function $F(R_c, h_o)$ can be approximated as

$$F(R_c, h_o) = 41.59 - 1.164 R_c + 0.249 R_c^2 - 0.0063 R_c^3 \tag{3.16.14}$$

with correlation coefficient of approximation 0.99995. Function $G(R_c, h_o)$ can be approximated as

$$G(R_c, h_o) = 1.4309 + 0.00342R_c - 0.0204R_c^2 + 0.00206R_c^3 - 0.0000608R_c^4 \quad (3.16.15)$$

with correlation coefficient of approximation 0.9996.

3.16.4. Effective rigidities for total neutron component

For total neutron component at sea level near minimum of solar activity in surveys in 1976–1977 according to Aleksanyan et al. (1979a,b), and in survey in 1996–1997 according to Dorman et al. (1999, 2000) was obtained $\alpha_n = 9.92$, $k_n = 0.94$. By using these values we calculate R_{ef} for total neutron component at sea level according to Eq. 3.16.5 and Eq. 3.16.7. Results for $R_c = 1, 3, 6, 9, 12,$ and 15 GV are shown in Fig. 3.16.3.

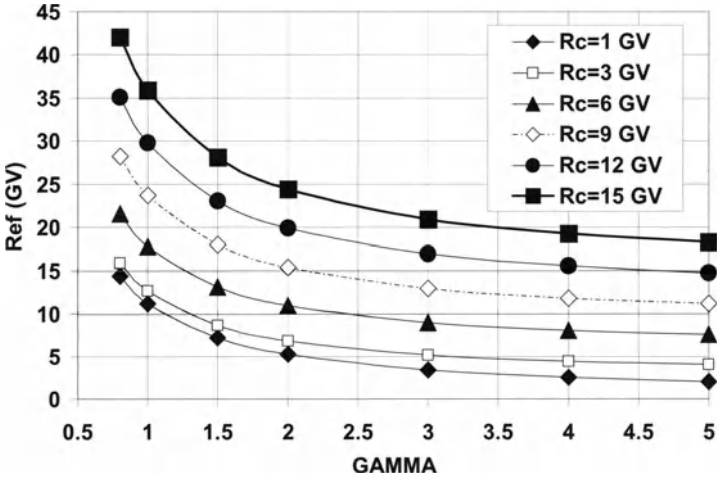

Fig. 3.16.3. Expected effective rigidity for total neutron component at sea level in dependence of cutoff rigidity and slope gamma in primary CR variation spectrum.

From Fig. 3.16.3 can be seen that effective rigidity of total neutron component detected at sea level by NM, decreases with increasing of the slope in primary CR variation spectrum and increases with increasing of cutoff rigidity in the point of observation. The dependences of $R_{\text{ef,n}}(R_c, h_o, \gamma)$ from γ at different R_c for observations at sea level can be approximated as following:

$$R_{\text{ef,n}}(R_c = 1 \text{ GV}, h_o, \gamma) = 11.188\,\gamma^{-1.072} \text{ GeV} \quad (3.16.16)$$

with correlation coefficient of approximation 0.9998;

$$R_{\text{ef,n}}(R_c = 3 \text{ GV}, h_o, \gamma) = 12.47\,\gamma^{-0.753} \text{ GeV} \quad (3.16.17)$$

with correlation coefficient of approximation 0.992;

$$R_{\mathrm{ef,n}}(R_c = 6\ \mathrm{GV}, h_o, \gamma) = 17.58\,\gamma^{-0.570}\ \ \mathrm{GeV} \tag{3.16.18}$$

with correlation coefficient of approximation 0.987;

$$R_{\mathrm{ef,n}}(R_c = 9\ \mathrm{GV}, h_o, \gamma) = 23.44\,\gamma^{-0.503}\ \ \mathrm{GeV} \tag{3.16.19}$$

with correlation coefficient of approximation 0.986;

$$R_{\mathrm{ef,n}}(R_c = 12\ \mathrm{GV}, h_o, \gamma) = 29.48\,\gamma^{-0.470}\ \ \mathrm{GeV} \tag{3.16.20}$$

with correlation coefficient of approximation 0.986;

$$R_{\mathrm{ef,n}}(R_c = 15\ \mathrm{GV}, h_o, \gamma) = 35.60\,\gamma^{-0.452}\ \ \mathrm{GeV} \tag{3.16.21}$$

with correlation coefficient of approximation 0.986. It is easy to see that Eq-s 3.16.16 – 3.16.21 can be combined with a good accuracy as

$$R_{\mathrm{ef,n}}(R_c, h_o, \gamma) = H(R_c, h_o)\,\gamma^{-J(R_c, h_o)}\ \mathrm{GeV}, \tag{3.16.22}$$

where functions $H(R_c, h_o)$ and $J(R_c, h_o)$ are presented in Fig. 3.16.4.

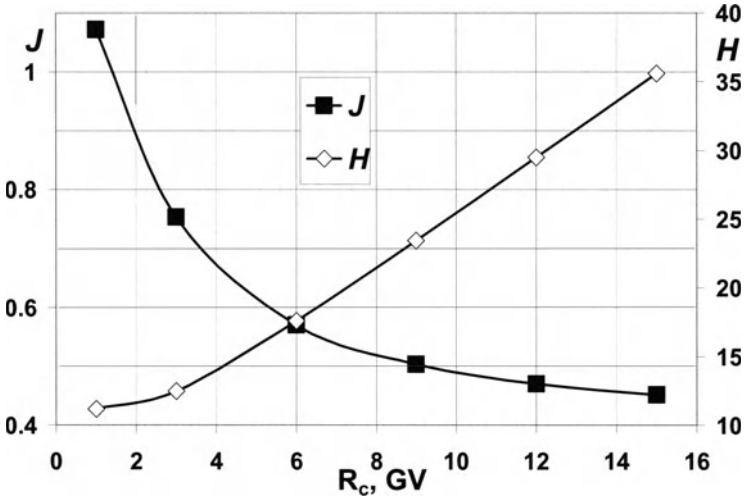

Fig. 3.16.4. Functions $H(R_c, h_o)$ and $J(R_c, h_o)$ in Eq. 3.16.22 for observations of total neutron component at sea level.

From Fig. 3.16.4 follows that function $H(R_c, h_o)$ can be approximated as

$$H(R_c, h_o) = 10.629 + 0.226R_c + 0.186R_c^2 - 0.00600R_c^3 \tag{3.16.23}$$

with correlation coefficient of approximation 0.9998. Function $J(R_c,h_o)$ can be approximated as

$$J(R_c,h_o)=1.3995-0.2865R_c+0.0402R_c^2-0.00261R_c^3+0.0000630R_c^4 \quad (3.16.24)$$

with correlation coefficient of approximation 0.9999.

From Fig. 3.16.1 and 3.16.3 can be seen that effective rigidities for muon component are sufficiently bigger than for total neutron component, and there are clear tendency of decreasing of effective rigidity for both components with increasing the slope gamma in primary CR variation spectrum and decreasing of cutoff rigidity. Let us note that numeral values of $a_i(h_o)$, $k_i(h_o)$ in dependence of h_o and level of solar activity for total neutron intensity and different multiplicities were determined by Eq. 3.8.6–3.8.9 in Section 3.8. By these values on the basis of Eq. 3.16.5 and 3.16.7 can be found $R_{\mathrm{ef},i}(R_c,h_o,\gamma)$ for many different cases in dependence of cutoff rigidity, primary spectrum of CR variation, from level of observation, and level of solar activity.

3.16.5. The integral effective energies of CR ground detectors for long-term CR modulation in dependence from cutoff rigidity

Alanko et al. (2003) presented a new concept of the effective energy of CR measured by neutron monitors. Using a 1D model of the heliospheric transport of CR and the specific yield function of a neutron monitor, it was shown that there is such an energy value, that the count rate of a given neutron monitor is directly proportional to the integral flux of primary CR with energy above this effective energy, irrespective of the phase of the solar cycle. To distinguish the effective energy introduced in Alanko et al. (2003) from classical effective energy (E_{ef} or R_{ef} considered above in Sections 3.16.1–3.16.4), let us call it as integral effective energy E_{inef}. In the basis of the Alanko et al. (2003) concept (developed specially for the long term CR modulation) is a spherically symmetric quasi-steady stochastic simulation model described in Usoskin et al. (2002), which reliably describes the long term galactic CR modulation during the last 50 years (see detail description of this and other models of CR long term modulation in the Heliosphere in Dorman, M2005). In this model the most important parameter of the long term modulation of galactic CR is the modulation strength Φ which according to Gleeson and Axford (1968) may be determined as

$$\Phi=u(r_H-r_E)/3\kappa_o\,, \quad (3.16.25)$$

where $r_H \approx 100$ AU is the radius of the Heliosphere, $r_E = 1$ AU is the radius of the Earth's orbit, $u = 400$ km/s is the constant solar wind velocity, and κ_o is the rigidity independent part of the CR diffusion coefficient in the interplanetary space changed with solar activity level (it sufficiently decreases with increasing of solar activity).

Alanko et al. (2003) calculate the galactic CR spectrum $D(E,\Phi)$ at 1 AU for different values of the modulation strength Φ, using the local interstellar spectrum of galactic CR as given by Burger et al. (2000). In order to calculate the NM count rate was

used the specific yield functions from Debrunner et al. (1982). Then was determined such an integral effective energy $E_{\text{inef}}(R_c,h_o)$ that the galactic CR flux above this energy is directly proportional to the NM count rate $N(R_c,h_o,\Phi)$ in the wide range of modulation strength Φ from 100 MV to 1000 MV:

$$\int_{E_{\text{inef}}(R_c,h_o)}^{\infty} D(E,\Phi)dE \propto N(R_c,h_o,\Phi). \tag{3.16.26}$$

In order to determine $E_{\text{inef}}(R_c,h_o)$, for each value of Φ was calculated ratio $R(E_{\text{inef}},R_c,h_o,\Phi)$ of the primary CR flux to the expected NM count rate:

$$R(E_{\text{inef}},R_c,h_o,\Phi)=B\times \int_{E_{\text{inef}}(R_c,h_o)}^{\infty} D(E,\Phi)dE \Big/ N(R_c,h_o,\Phi), \tag{3.16.27}$$

where coefficient B is determined by the normalization condition:

$$R(E_{\text{inef}},R_c,h_o,\Phi=600\,\text{MV})=1. \tag{3.16.28}$$

The obtained ratios were normalized to 1 at Φ = 600 MV. As example, in Fig. 3.16.5 are shown the dependences of normalized ratios from Φ for Oulu NM and Climax NM.

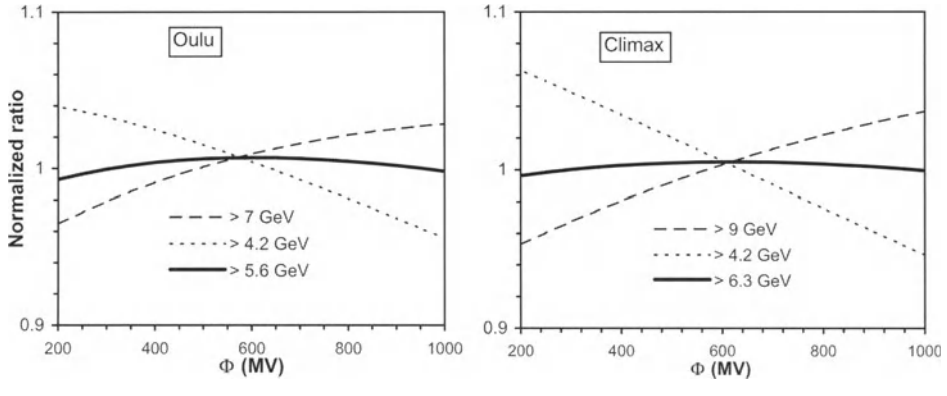

Fig. 3.16.5. Normalized ratios of the calculated galactic CR flux with energy above E_{inef} (as denoted in the legend) to the response of a neutron monitor, as a function of the modulation strength Φ for Oulu (R_c = 0.8 GV) and Climax ($R_c \approx 3$ GV). According to Alanko et al. (2003).

From Fig 3.16.5 can be seen that the normalized ratios in the range of Φ from 200 to 1000 MV are about constant for Oulu NM only at E_{inef} = 5.6 GeV and for Climax NM only at E_{inef} = 6.3 GeV. These values of E_{inef} where determined as minimized the standard deviation

$$Dst = \left(\frac{\sum_{\Phi} \left(R(E_{\text{inef}}, R_c, h_o, \Phi) - 1 \right)^2}{n-1} \right)^{1/2} = \min . \qquad (3.16.29)$$

In order to verify the described approach, Alanko et al (2003) calculated the galactic CR flux $\int_{E_{\text{inef}}(R_c,h_o)}^{\infty} D(E,\Phi)dE$ (scaled to the NM count rate) using the values of Φ obtained for the last 50 years by Usoskin et al. (2002), and compared with the actual annual NM count rates (see Fig. 3.16.6 for Oulu NM and Climax NM).

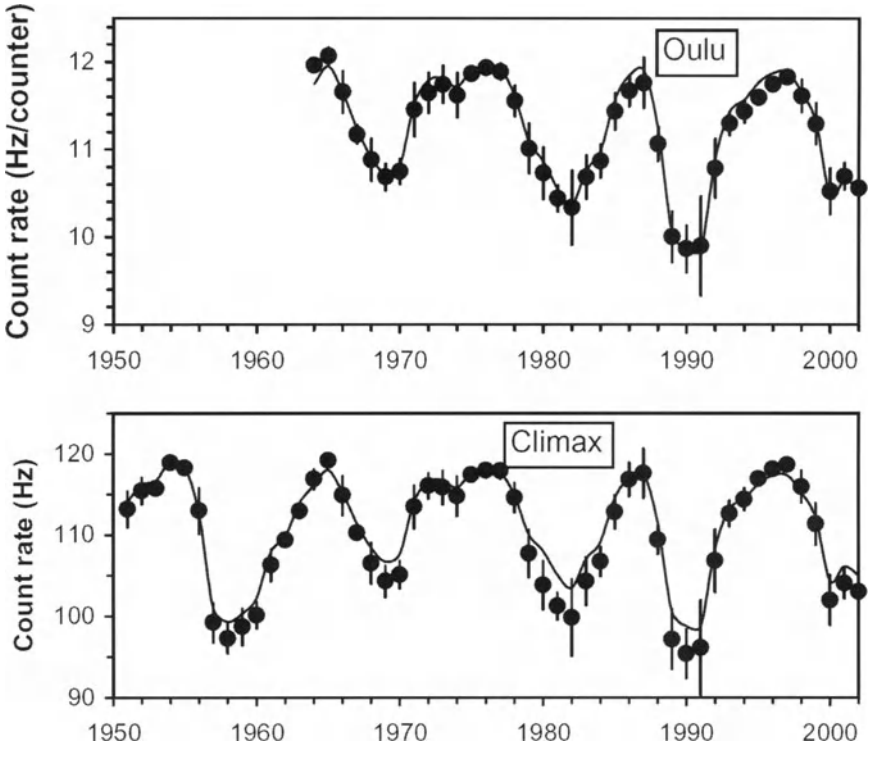

Fig. 3.16.6. Annual count rates of Oulu and Climax NMs. Dots denote the actual count rate with fluctuations of monthly values around the annual mean. Solid lines represent the calculated galactic CR flux (> E_{inef}) scaled to the NM count rate. According to Alanko et al. (2003).

From Fig. 3.16.6 can be seen that the correlation between the actual NM count rates and the calculated flux of galactic CR (with energy > E_{inef}) is very good (correlation coefficient bigger than 0.99 in all shown cases). The good agreement between modeled and observed values confirms the above calculation of E_{inef} and validates the used assumptions. Proper values of E_{inef} exist also for the other NMs (see Fig. 3.16.7).

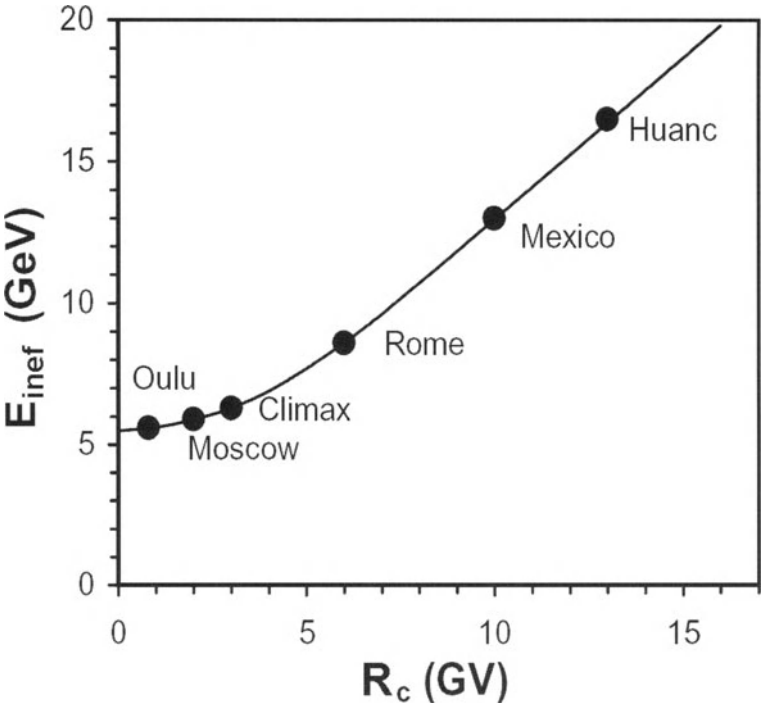

Fig. 3.16.7. The integral effective energy E_{inef} of a neutron monitor as a function of the geomagnetic cutoff rigidity R_C. Dots correspond to some neutron monitors from the world network. According to Alanko et al. (2003).

From Fig. 3.16.5 can be seen that the value of E_{inef} depends on the NM's geomagnetic cutoff rigidity, and it can be approximated by the following formula within 2% accuracy:

$$E_{\text{inef}} = 5.5 + R_c^{1.25} / \left(1 + 4\exp(-0.4R_c)\right), \qquad (3.16.30)$$

where E_{inef} and R_c are given in GeV and GV, respectively.

The described concept of Alanko et al. (2003) on the integral effective energy E_{inef} allows to regard the count rate of each neutron monitor as a direct measurement of the galactic CR flux with energy above E_{inef} specified for the station. The E_{inef} varies from about 5.5 GeV for polar NM up to about 20 GeV for equatorial NM (in comparison with E_{inef} for the cosmogenic polar ^{10}Be and global ^{14}C production rates which are about 1.3 GeV and 2.8 GeV, respectively; see Chapter 10, Section 10.5.7).

Chapter 4

Experimental Basis of Cosmic Ray Research

4.1. Worldwide network of CR Observatories and CR database

4.1.1. Worldwide network of CR detectors for geophysical, astrophysical, and space research applications

Using the theory of CR meteorological effects (see Part 2, Chapters 5–9), all CR data obtained by continuous registration in the atmosphere and underground on the worldwide network of CR Observatories can be corrected and then transformed to the boundary of atmosphere by applying coupling functions and spectrographic methods (as described above, in Chapter 3). The same methods can also be utilized to find the rigidity spectrum of primary CR variations and determine the time variation of cut off rigidities. Furthermore, use of the information on CR asymptotic directions allows the computation of the CR distribution function out of the atmosphere, and in the interplanetary space (using the global-spectrographic method, also based on coupling functions method, see Section 3.14). By this recalculation we mathematically transform the worldwide network of CR Observatories in the atmosphere and underground into a unique giant multidirectional detector in space, which moves and rotates with Earth for continuous determination of CR space-rigidity distribution function in the interval from about one GV up to about thousand GV. To prolong this spectrum into smaller and higher energy range are widely used measurements on balloons and satellites, deep underground and by EAS installations. These data give information not only on the CR spectrum but also on CR chemical and isotopic contents, on CR intensity space-time variations, they are widely used for geophysical, astrophysical, and space research applications.

4.1.2. Archives of CR data and formation of CR data database

CR intensity has been continuously measured by different detectors since 1933. The formation of CR data base for geophysical, astrophysical, and space research applications widely were discussed in papers of Belov and Yudakhin (1995), Shea and Smart (2000), Pyle (2000). Now these data are concentrated in Word Data Centers, mostly in Boulder (USA; available on CD and through Internet), Nagoya (Japan; available on CD and through Internet), and in Qazrin (Israel; only old data). The old CR data which are now in Israel were compiled on papers by Prof. A. E. Sandström in Sweden (WDC–2 for CR), and in 1994 the archive of CR data was transported from Sweden to Israel (the full catalog of these data is available through Internet in the website of Israel Cosmic Ray Center and Emilo Segre' Observatory). Let us note that now data from many CR Observatories are available also in real time scale.

Researches of different effects in CR require, as a rule, processing of significant number of data files. Belov and Yudakhin (1995) developed a special program formatted data database (see Fig. 4.1.1): it executes sorting in the desired order, linkage of the tables on key fields, search of a context, mark and deleting of strings, selection on set of formal conditions; the computing program receives the completed list of data, which it

should process. For example, it is possible to show on a screen of PC the plots of data and results of their processing by various methods simultaneously.

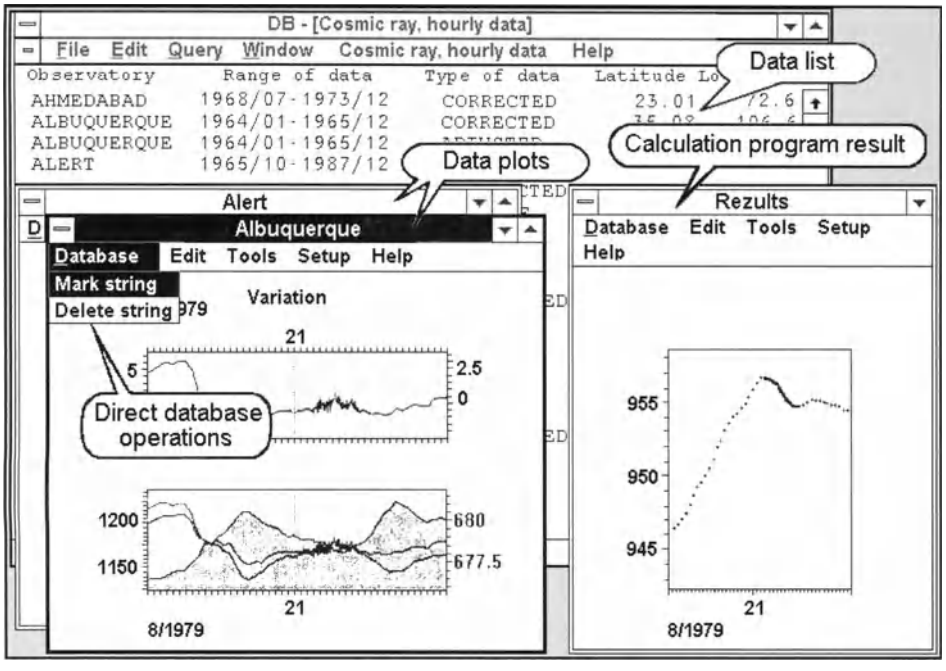

Fig. 4.1.1. Database screen example. According to Belov and Yudakhin (1995).

The program of CR data database formation of Belov and Yudakhin (1995) was successfully tested during Ground Level Enhancements research with including CR, IMF and other data in Belov et al. (1995).

Kozlov et al. (2003) founded the REal-time COsmic Ray Database (RECORD) with the aim to develop a unified database with data from different NM collected together, in unified format and to provide a user with several commonly used data access methods (currently the database includes Lomnitsky Stit, Moscow, Oulu; Tixie Bay, and Yakutsk CR observatories). The main database server is located in IKFIA (Yakutsk) but there will be several mirrors of the database; the database and all its mirrors are updated on the nearly real-time (1 hour) basis.

The formation of CR database on real time basis is very important for monitoring and forecasting of space weather. Munakata et al. (2000), Belov and Eroshenko (2002), Dorman (2002, 2003) show that the real time database (one hour data) from NM and TM worldwide networks is necessary for monitoring and forecasting of great geomagnetic storms accompanied with Forbush decreases and precursor effects. In Dorman et al. (2003, 2004) was proposed formation of CR database on the real time basis (1 min data) from combination of NM network and satellite CR observations with continue automatically processing for monitoring and forecasting of great solar proton events dangerous for spacecrafts electronics and people health in space and on regular air-lines at about 10 km altitude (see in more detail in Section 18.12 and in Dorman, M2005).

4.2. The network of ionization chambers

As mentioned in Section 1.2.7, the Nobel Laureate Prof. Arthur Compton founded the first worldwide network of several CR Observatories in 1934–1935. These pioneering CR Observatories were equipped with ionization chambers with a volume of 19.3 liters, shielded by 10.7 cm Pb, and with Compton's type compensation (Compton et al., 1934). During 1949–1951 this network of ionization chambers was significantly extended: these chambers in former USSR was developed and contained automatically operating chambers with a volume of 950 liters (ASC-1) and of 50 liters (ASC-2). Seven new CR Observatories in the former USSR (Moscow, Yakutsk, Sverdlovsk, Irkutsk, Cape Shmidt, Bay Tikhaya, Tbilisi) and one in China (Peking) were founded and equipped with ASC-1 and ASC-2. The detailed description of this type of ionization chambers was presented in Dorman (M1957). Ionization chambers measure mainly the flux of muons from all directions from the upper hemisphere. The sensitivity of ionization chamber *vs* the zenith angle of incident CR particles is shown in Fig. 4.2.1, compared with the zenith angle sensitivities of muon telescopes of different geometry (for more details see Section 4.3 below).

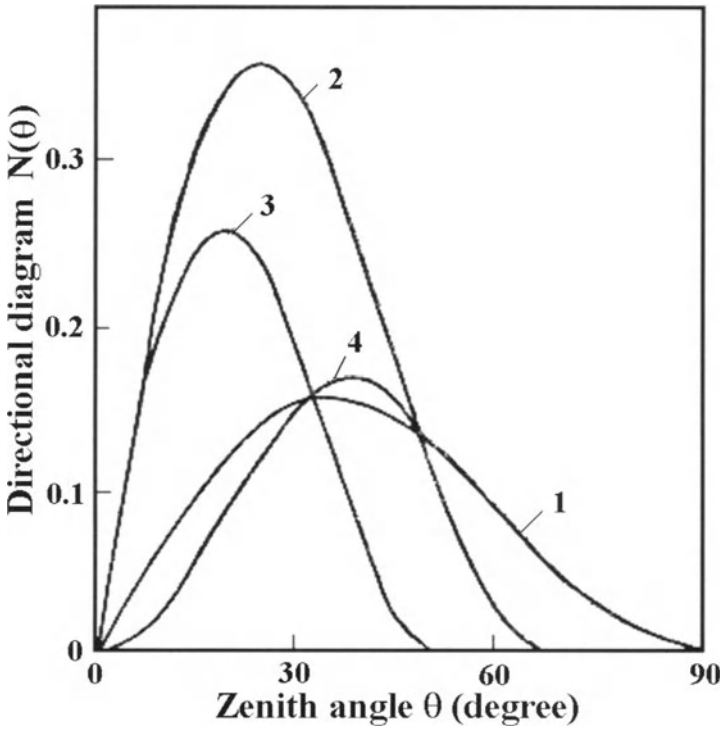

Fig. 4.2.1. Zenith angle sensitivity distribution for ionization chamber (curve 1), and for muon telescopes of different geometry: semi-cubical (curve 2), cubical (3), and inclined at 45° (4). From Dorman (M1975b).

Fig. 4.2.2 shows an ASC-1 (950 liters) type ionization chamber, developed in USSR during 1949–1951. An example of record detected by this chamber in Yakutsk in the period of great solar GLE at 19 November 1949 is shown in Fig. 4.2.3.

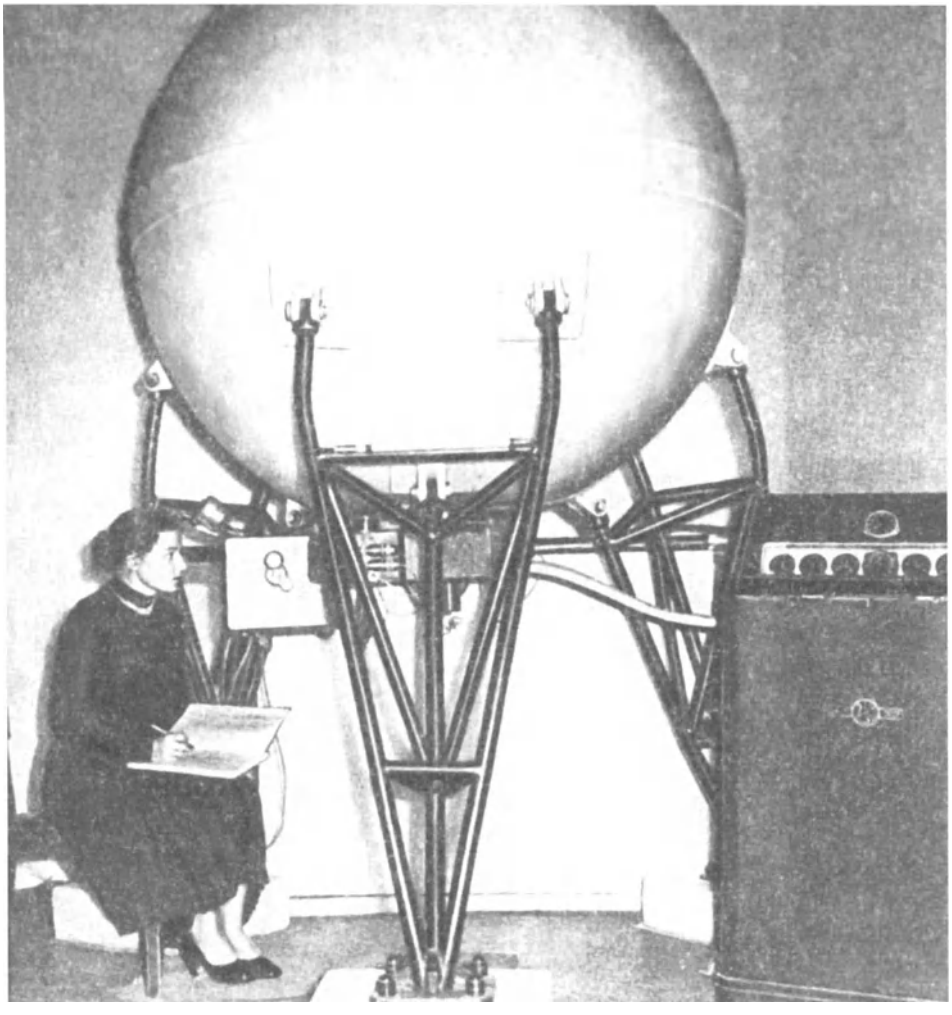

Fig. 4.2.2. A view of big ionization chamber ASC-1 (950 liters) near Moscow (IZMIRAN, Troitsk, Moscow region) in 1951. The young lady near the chamber is one of the designers of this type of chamber, Stalin Prize Winner Galina Shafer (Tyanutova), an enthusiast and propagandist of this detector. From Dorman (M1957).

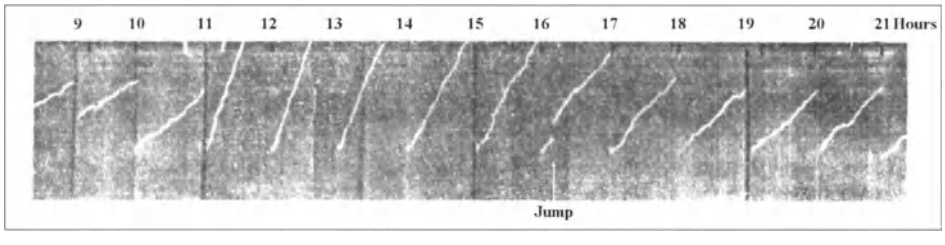

Fig. 4.2.3. An example of record detected by ASC-1 ionization chamber in Yakutsk in the period of great solar GLE at 19 November 1949.

The planetary distribution of ionization chambers shielded by 10.7 cm Pb and with compensation is shown in Fig. 4.2.4 (the situation at 1975 and earlier).

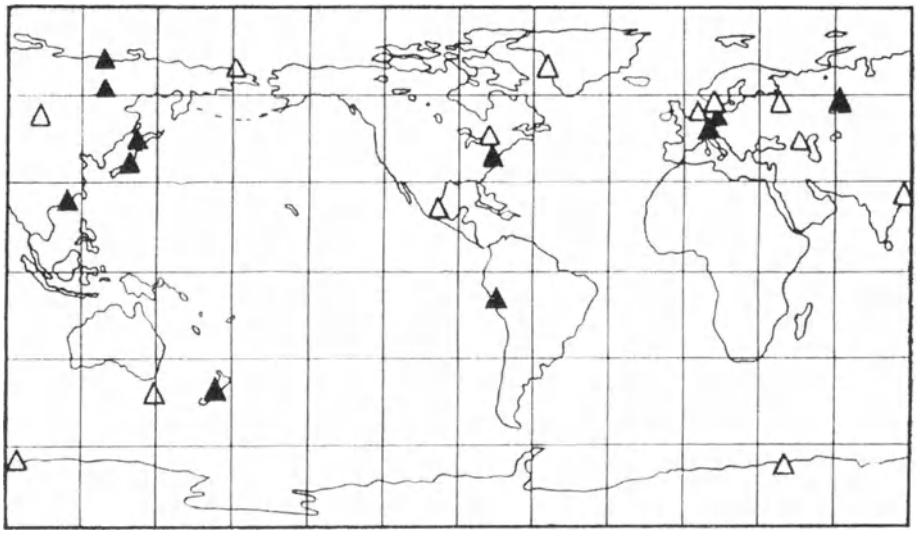

Fig. 4.2.4. Global distribution of ionization chambers shielded by 10.7 cm Pb with compensation. Black triangles: chambers operating in 1975, white triangles: chambers operating before 1972. From Dorman, M1975a.

Only a few ionization chambers still continue to work up to now. One of them is the 950 liters ASC-1 chamber in Yakutsk (since 1949).

4.3. The network of muon telescopes

Muon telescopes based on double or triple coincidences of Geiger–Muller, proportional, or scintillation counters were described in details in Dorman (M1957, M1963a, M1963b, M1974, M1975a) and Dorman et al. (M1979). Here we will describe briefly only the zenith directional diagrams of muon telescopes, properties of plastic scintillators (widely used for ground and underground detectors), and the distribution of telescopes in the world. The scientific results obtained by ground based and underground muon telescopes were reviewed in mention above books as well as in Duldig (2000) and will be one of main subjects of the next book Dorman (M2005).

4.3.1. Zenith directional diagrams

The chief characteristic of any telescope is its directional diagram $N(\theta)$, which shows the dependence of the intensity of the particles recorded by the telescope on the zenith angle θ. Knowledge of the directional diagram is very important, since CR variations of atmospheric as well as extra-atmospheric origin depend on the angle of incidence of the particles. If the dependence of CR intensity on azimuthally angle in the first approximation can be neglected, the number of particles recorded by a telescope per unit of time, incident under angles θ and φ in the intervals $d\theta$ and $d\varphi$ is equal to

$$N(\theta,\varphi)d\theta d\varphi = I(\theta)S_{\perp}(\theta,\varphi)d\omega\,, \tag{4.3.1}$$

where $S_{\perp}(\theta,\varphi)=S(\theta,\varphi)\cos\theta$ is the effective area perpendicular to the direction of incidence, $S(\theta,\varphi)$ is the area of the ground surface crossed by particles which enter under the angles θ and φ through the top surface; $d\omega=\sin\theta d\theta d\varphi$ is the element of solid angle; $I(\theta)=I_v\cos^2\theta$ is the number of particles passing per unit time per unit solid angle a unit area, perpendicular to the direction θ; and I_v is the intensity in the vertical direction.

If a is the side of the square base of the telescope and b its height, then

$$S(\theta,\varphi)=\left(a-b|\cos\varphi|tg\theta\right)\times\left(a-b|\sin\varphi|\mathrm{tg}\theta\right). \tag{4.3.2}$$

Substituting Eq. 4.3.2 in Eq. 4.3.1 and integrating over φ from 0 to 2π, we find for the cubical telescope:

$$N(\theta)=4a^2I_v\cos^3\theta\sin\theta\times\begin{cases}\left(\pi/2-\mathrm{tg}\theta+(1/8)\mathrm{tg}^2\theta\right) & \text{for } 0\le\theta\le 45^o\\ \left[\pi/2-2\alpha+2\mathrm{tg}\theta(\sin\alpha-\cos\alpha)+(1/2)\mathrm{tg}^2\theta\right.\\ \quad\left.\times\left(\cos^2\alpha-\sin^2\alpha\right)\right] & \text{for } 45^o\le\theta\le\mathrm{arctg}\sqrt{2}\\ 0 & \text{for } \theta\ge\mathrm{arctg}\sqrt{2}\end{cases} \tag{4.3.3}$$

and for the semi-cubical telescope:

$$N(\theta)=4a^2I_v\cos^3\theta\sin\theta\times\begin{cases}\left(\pi/2-\mathrm{tg}\theta+(1/8)\mathrm{tg}^2\theta\right) & \text{for } 0\le\theta\le\mathrm{arctg}2\\ \left[\pi/2-2\beta+\mathrm{tg}\theta(\sin\beta-\cos\beta)+(1/8)\mathrm{tg}^2\theta\right.\\ \left.\times\left(\cos^2\beta-\sin^2\beta\right)\right] & \text{for } \mathrm{arctg}2\le\theta\le\mathrm{arctg}2\sqrt{2}\\ 0 & \text{for } \theta\ge\mathrm{arctg}2\sqrt{2}\end{cases} \tag{4.3.4}$$

where

$$\alpha=\arccos\left(\frac{1}{\mathrm{tg}\theta}\right),\quad \beta=\arccos\left(\frac{2}{\mathrm{tg}\theta}\right). \tag{4.3.5}$$

The functions N(θ) were shown in Fig. 4.2.1. For comparison, the same figure also shows the directional diagram of the shielded spherical ionization chamber, the analytical form of which is

$$N(\theta)=2\pi^2r_o^2I_v\cos^2\theta\sin\theta\,, \tag{4.3.6}$$

where r_o is the radius of the chamber. Fig. 4.2.1 shows that the maximum number of particles in the cubical and semi-cubical telescopes arrives under zenith angles 19° and

24°, respectively. The 45° inclined telescope has its maximum at 35° and the shielded spherical ionization chamber at 38°.

The directional diagrams of telescopes from scintillators in the form of flat circles of radius r and at mutual distances b (Fig. 4.3.1) have been computed by Kaminer (1961).

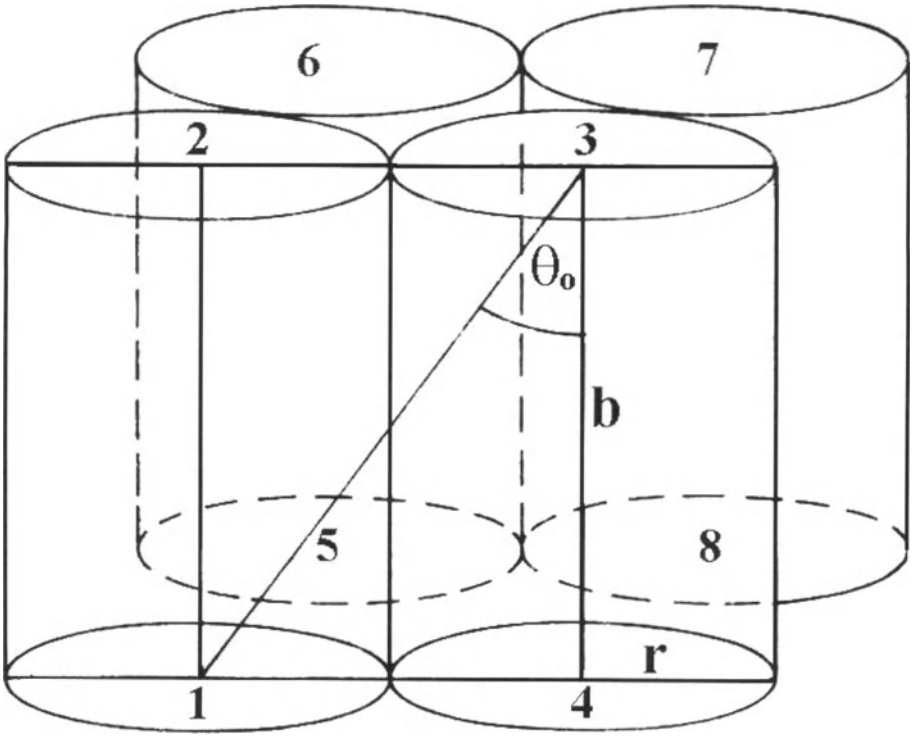

Fig. 4.3.1. Diagram for calculating zenith sensitivity of muon telescope from eight circular plastic scintillators (used double coincidences; r - radius of the scintillator; b - distance between the scintillators).

If it is assumed, as above, that the muon intensity depends on the zenith angle θ, as $I(\theta) = I_v \cos^2\theta$, and does not depend on the azimuth angle φ, then

$$N(\theta) = I_v \cos^3\theta \sin\theta \int_0^{2\pi} S(\theta,\varphi)\,d\varphi, \tag{4.3.7}$$

where $S(\theta,\varphi)$ is the effective recording area for particles incident under angles θ and φ. For a vertical telescope this gives

$$N(\theta) = I_v \pi b(2r - b\,\mathrm{tg}\,\theta)\cos^2\theta \sin^2\theta\,. \tag{4.3.8}$$

Directional diagrams for vertical and inclined telescopes are given in Fig. 4.3.2. Directional diagrams for telescopes of different geometry are calculated also by Lindgren (1966), and described in details in Dorman et al. (M1979).

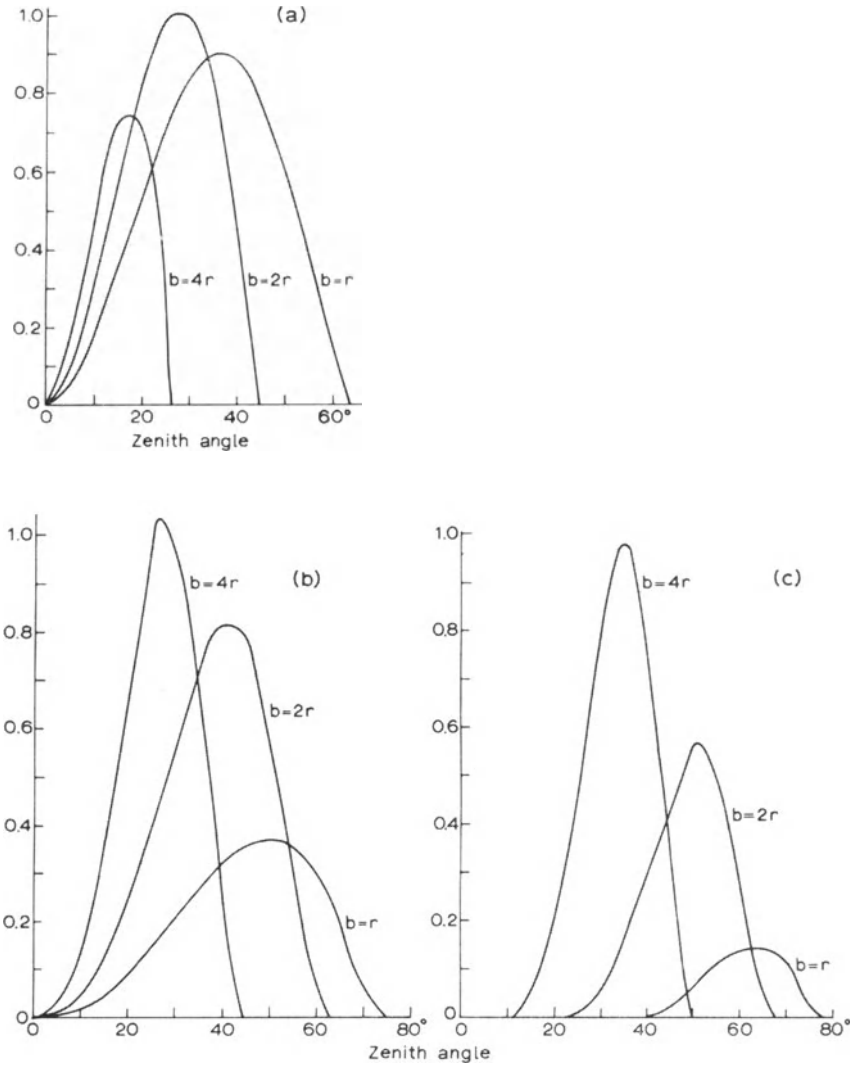

Fig. 4.3.2. Zenith diagrams of telescopes made of circular scintillators: a – for vertical telescope, b – for inclined telescopes of type 1–3 according to Fig. 4.3.1, c – for inclined telescopes of type 1–7. According to Kaminer (1961).

4.3.2. Using plastic scintillators for muon telescopes

The study of rapid intensity variations of the hard CR component and any variations of relatively small amplitude, requires an instrument with a small statistical error during short lime intervals, i.e., an instrument with a large effective area. For this purpose large plastic or liquid scintillators, instead of Geiger counters are used. Scintillators as detectors of charged particles have a number of advantages over Geiger counters. Among these is the short recovery time, about 10^{-8}–10^{-9} sec, which makes it possible to

measure large radiation intensities, collected on an area of several square meters. Not less important is the simplification of the electronics and the increased reliability of the recording equipment. The lifetime of the scintillators is practically unlimited, which cannot be said of the Geiger counters.

Common high quality organic plastic scintillators consist of a mixture of three aromatic hydrocarbons. As solvent a substance is used to collect a large part of the original excitation energy produced by the ionizing particles when passing through the scintillating material (on the mechanism of luminescence of plastic scintillators see in Rozman and Kilin, 1959). If no other components are present most of this energy is transformed into ultraviolet radiation, which is strongly absorbed and has a frequency beyond the sensitivity of the photomultiplier.

A second component, which may be called the transformer, is usually added in concentrations of the order of 1%. The excitation energy of the solvent is given to the transformer and afterwards radiated at lower frequencies than the fluorescent lighting of the pure solvent. For this light the solvent and the transformer are nearly transparent.

A third substance, the wavelength shifter, usually occurs in concentrations of the order of 0.05%. It absorbs the radiation of the transformer and emits part of the absorbed energy at longer wavelengths. This third component increases the efficiency of the mixture, displacing the wavelength of the radiation still farther away from the absorption bands of the solvent and the transformer, thus facilitating the egress of the fluorescent radiation. The wavelength shifter should be chosen to give radiation in a wavelength region close to the maximum sensitivity of the photomultiplier.

By a systematic study of a number of organic compounds plastic scintillators have been obtained with a very high efficiency. Among it these are the scintillators prepared by thermal polymerization of vinyltoluol with the addition of 2% PBD: 2-pheny-l-5-(4-biphenyl)-1,3,4-oxydiasol and 0.1% PPS: 4,4'-diphenylslilben.

Abrosimov (1963) has suggested an improved method for obtaining large plastic scintillators by high temperature polymerization of sterol without the aid of catalysts, which speeds up the process of preparing large scintillators for recording CR by about a factor of 10 over existing methods. Instead of plastic, also liquid scintillators (Ashton et al., 1965; Abrosimov et al., 1965) or paraffin scintillators (Barton and Crispin, 1965) can be used.

A high statistical accuracy requires scintillators of large dimensions. The important problem is how to collect the light pulses from the large surface of the scintillator with the aid of photomultipliers that have a relatively small collecting area of the photocathode. The pulse of the fluorescent light may be reflected many times by the walls of the scintillator, during which part of the light will gradually be absorbed by the material of the scintillator and in its walls; the remaining part of the light impulse will to a certain degree be scattered. As a result of these losses only a fraction η of the photons emitted by fluorescence reaches the photomultiplier. As an example a study made of plastic scintillators with a diameter of 100 cm (Clark et al., 1957) gave the following results: the thickness of the sheet was equivalent to 10 g/cm^2 CH; a relativistic singly charged particle loses on this way about 20 MeV, and since the production of photons in a scintillator is about 1 photon per 150 eV, so one relativistic particle produces about 1.3×10^5 photons. By the experiment was found that the emerging number of photoelectrons was about 50 for one relativistic particle, which shows that $\eta \approx 4\times10^{-4}$.

4.3.3. Design of muon telescopes with plastic scintillators

An example of standard cubic muon telescope on 8 plastic scintillators is shown in Fig. 4.3.3. This design of telescope was used widely in the world.

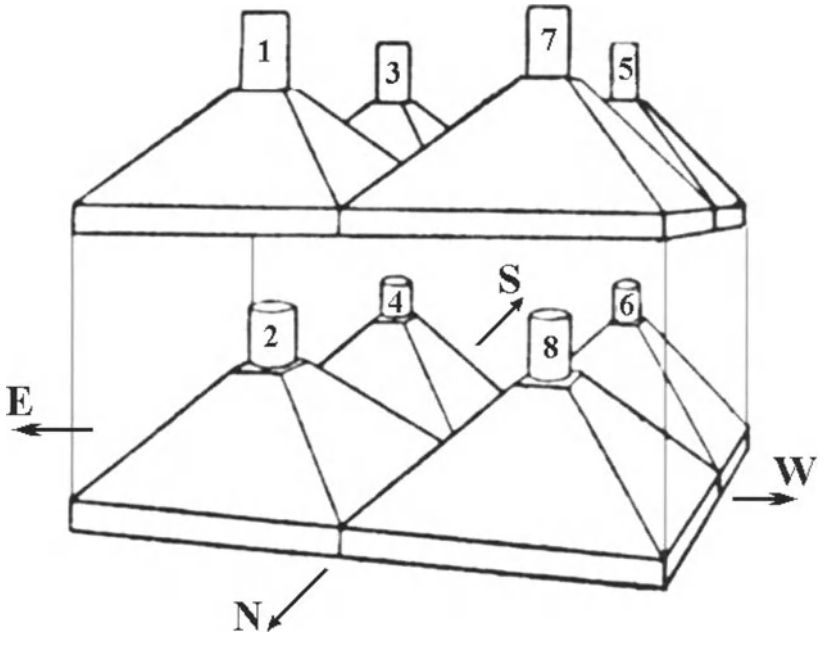

Fig. 4.3.3. Cubic muon telescope on plastic scintillators. According to Sandström et al. (1965).

A muon telescope of cubic geometry with 8 plastic scintillators of $120\times120\times5$ cm^3 with counting rates 1.1×10^6 and 1.6×10^5 per hour for vertical and inclined directions, respectively, was developed by Sandström et al. (1965) and erected in Uppsala in 1963. The geometry shown in Fig. 4.3.3 was extended in many CR Observatories: instead of 2×2 m^2, 6×6 m^2 was used (two underground telescopes in New Mexico, ground telescope in Nagoya, and other). As another design that uses plastic scintillators for the continuous recording of the muon intensity, we mention the telescope developed at the Massachusetts Institute of Technology (Palmeira and Williams, 1958). With the aid of this telescope, which has an effective area of about 10 m^2 and a counting rate at sea level of 1000 counts/sec (i.e. a statistical error of 0.4% for 1 min), such interesting phenomena were recorded as the rapid variations of CR intensity at the time of the magnetic storm of 11 February 1958, during the flare of 4 May 1960 (Palmeira and McCracken, 1960), etc. The apparatus consisted of three identical telescopes; each consisting of an upper and lower series of four circular disks of plastic scintillators with a diameter of 107 cm and a thickness of 9 cm. Coincidences between the upper and lower disks within 1.5×10^{-7} sec were recorded.

A many channel scintillation telescope for recording the vertical and directed CR components (North, South, East and West) is described by Chasson et al. (1965). It is located at Denver at 1,660 m above sea level. The telescope (see Fig. 4.3.4) consists of

eight circular scintillators (of thickness 7.62cm, diameter 107.7 cm) with shields of 10.2cm Pb. The heights $P_1P_7 = P_2P_8 = 5$ m; the side of the square basis is 4.5 m. The total weight is 11 tons.

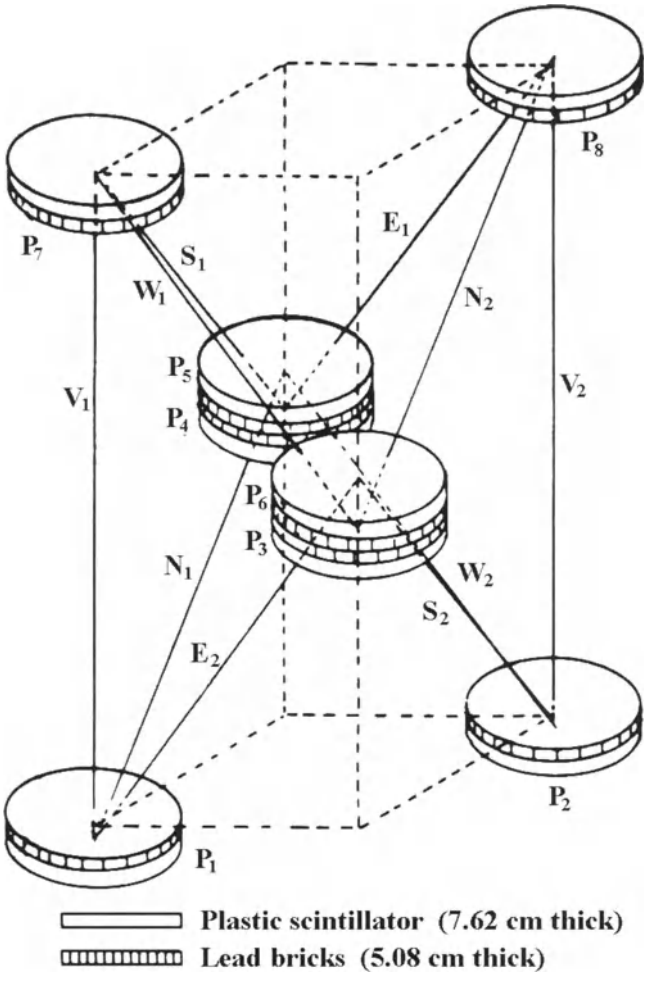

Fig. 4.3.4. Design of many channel scintillation telescope: N_1 – North directed telescope based on double coincidence of circle scintillators P_1 and P_5, N_2 – the same but on scintillators P_3 and P_8, etc. The main characteristics of this telescope are shown in Table 4.3.1. According to Chasson et al. (1965).

Table 4.3.1. The main characteristics of the scintillation telescope used in Denver.

Type of observation	Receiving angle	Solid angle, steradian	Shield, cm, Pb	Counts per minute
Wide angle, vertical	165°	5.46	10.2	15000
Narrow angle, vertical	30°	0.21	10.2	775
Inclined-1	38.5°	0.45	19.2	750
Inclined-2	55°	0.45	19.2	750

The construction of Bercovitch (1962) was recommended as a scintillators telescope for use during the 1QSY (see Fig. 4.3.5). In this design the telescope with 8 scintillators of 100x100x5 cm^3 (4 under and 4 above the lead; double coincidences are used) is combined with one 6-counter section of the super-monitor).

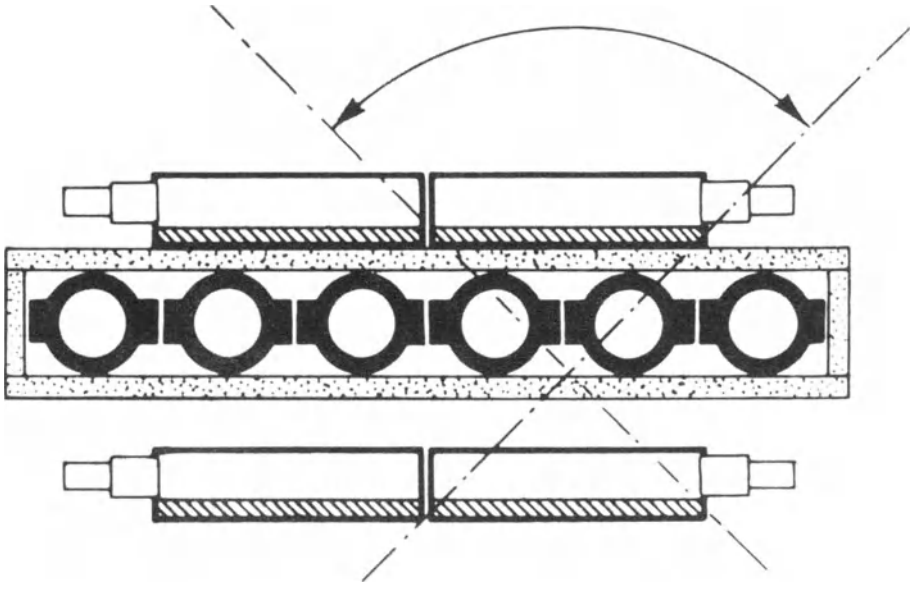

Fig. 4.3.5. Arrangement of muon scintillation telescope utilizing the lead of 6-counter section of NM-IQSY. According to Bercovitch (1962).

Muon telescopes with plastic scintillators have also been used for recording CR intensity from vertical and inclined directions under water, at depths of 20, 50, 90, 150, 220, 380, 715, 960 and 1380 meters (Higashi et al., 1965).

4.3.4. Narrow angle multi directional telescopes

Narrow angle multi-directional telescopes gave detail information on the angle distribution of arriving muons and its time variation. Especially it is important to search peculiarities in the CR angle distribution (decreases and increases of CR intensity in different directions) before great magnetic storms for using them as precursors of these phenomena for space weather forecasting (see Section 18.12 in the Chapter 12, and in more detail in Dorman, M2005). To observe such a beam-like precursory CR intensity decreases and increases effectively, a narrow angle multi-directional telescopes have been constructed in Moscow (Borog et al., 1995, 1997) and at Mt. Norikura (Ohashi et al., 1997). The telescope in Moscow consists of two pairs of layers with effective area 9 m^2 each (the distance between the payers of layers is about 1 m). Each of the layers includes 128 narrow strip scintillation counters with length 300 cm and cross section 2.5×1.0 cm^2. The telescope at Mt. Norikura consists of two layers of X- and Y-array each, made up of 44 cylindrical proportional counters of 4.4 m long with 10 cm diameter. In Fig. 4.3.6 is shown the schematic view and in Table 4.3.2 main characteristics of this telescope.

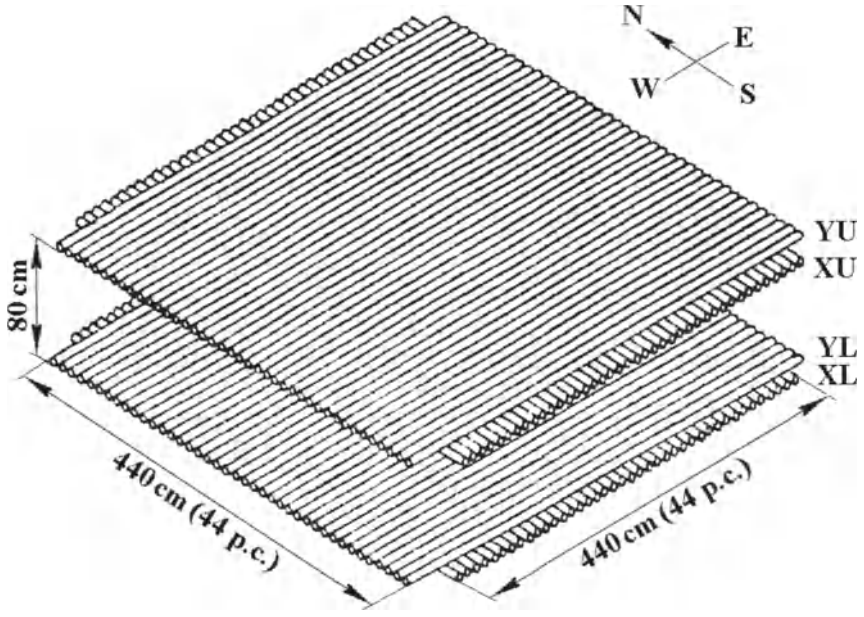

Fig. 4.3.6. The schematic view of narrow angle multi-directional telescope at Mt. Norikura. According to Ohashi et al. (1997).

Table 4.3.2. Main characteristics of narrow angle multi-directional telescope at Mt. Norikura. According to Ohashi et al. (1997).

Telescope	Center direction of viewing				SΩ (m^2sr)	Counting rate (10^3/h)
	Z(°)	Az.(°)	Lat.(°)	Long.(°E)		
T11-11	0	-	36N	137	0.3025	96
T11-16	32	90	30N	175	0.1385	28
T16-11	32	180	4N	137	0.1385	26
T11-06	32	270	30N	100	0.1385	29
T06-11	32	0	68N	137	0.1385	28
T16-16	41	135	4N	165	0.0748	10
T16-06	41	225	4N	110	0.0748	10
T06-06	41	315	55N	83	0.0748	10
T06-16	41	45	55N	192	0.0748	10

The block diagram of the electronic system of this telescope is shown in Fig. 4.3.7. After amplification, pulses from 44 proportional counters are mixed in each array of XL, YL, XU, and YU, and four-fold coincidence among them is taken as a gate pulse, and on-off information of the pulses of 44×4 proportional counters are recorded in the computer memory, through the parallel input-output circuit. Muon intensity data are transferred to HDD at every minute, along with data on atmospheric pressure and temperature. Contents of HDD can be monitored remotely through a satellite telephone line.

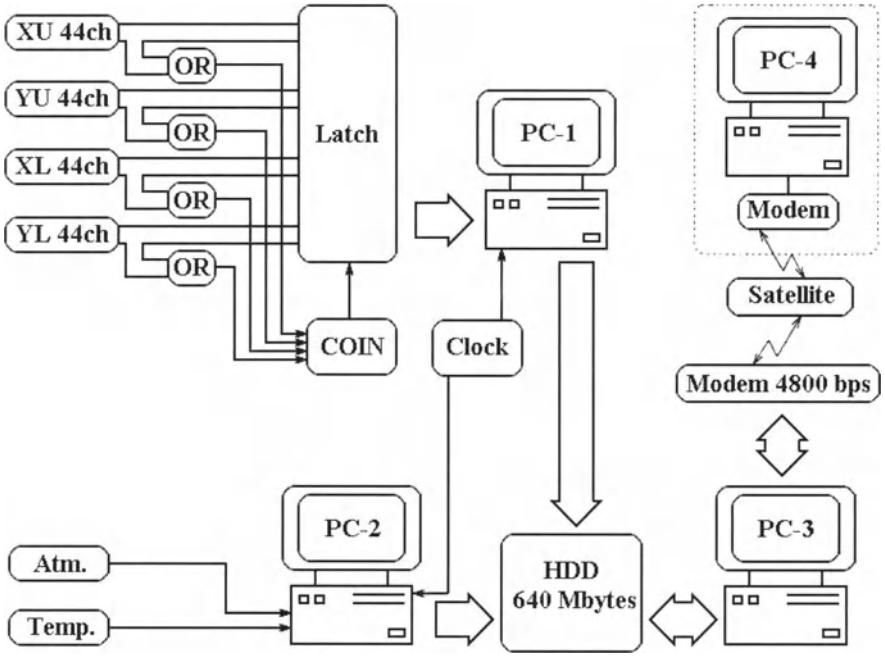

Fig. 4.3.7. The block diagram of electronic circuits of the narrow angle multi-directional telescope at Mt. Norikura. According to Ohashi et al. (1997).

4.3.5. World-wide distribution of ground and underground muon telescopes

Muon telescopes are widely used on the ground (see Fig. 4.3.8 for the situation at 1975) and at different depths underground (Fig. 4.3.9).

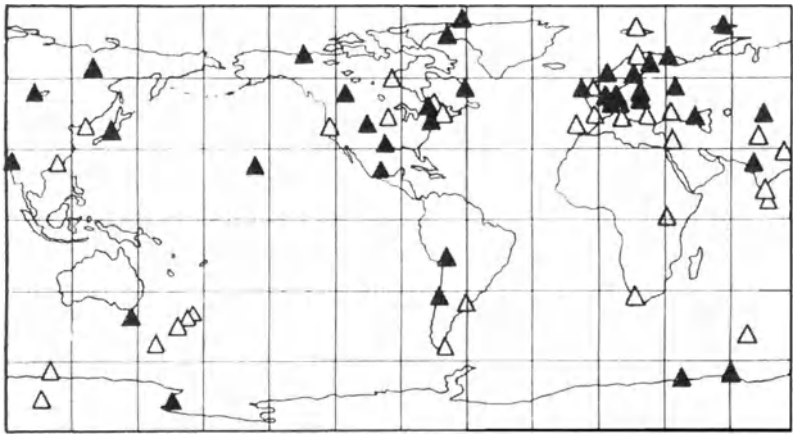

Fig. 4.3.8. Planetary distribution of ground based muon telescopes. Black triangles – operating in 1975, white triangles – operating before 1972. From Dorman, M1975a.

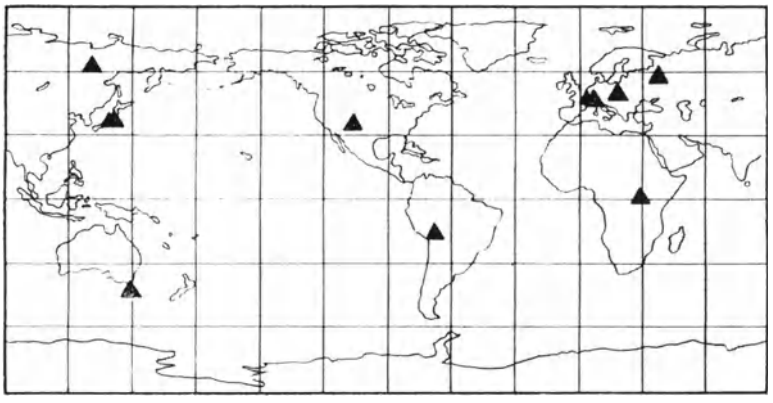

4.3.9. Planetary distribution of underground muon telescopes. Black triangles – operating in 1975. From Dorman, M1975a.

Some part of world-wide network of multi-directional muon telescopes is used by Munakata et al. (2000) for search of predictors in CR of large geomagnetic storms (see in details on this problem in the next book, Dorman, M2005). This network, together with asymptotic directions of arrived CR particles out of the Earth's magnetosphere, are shown in Fig. 4.3.10.

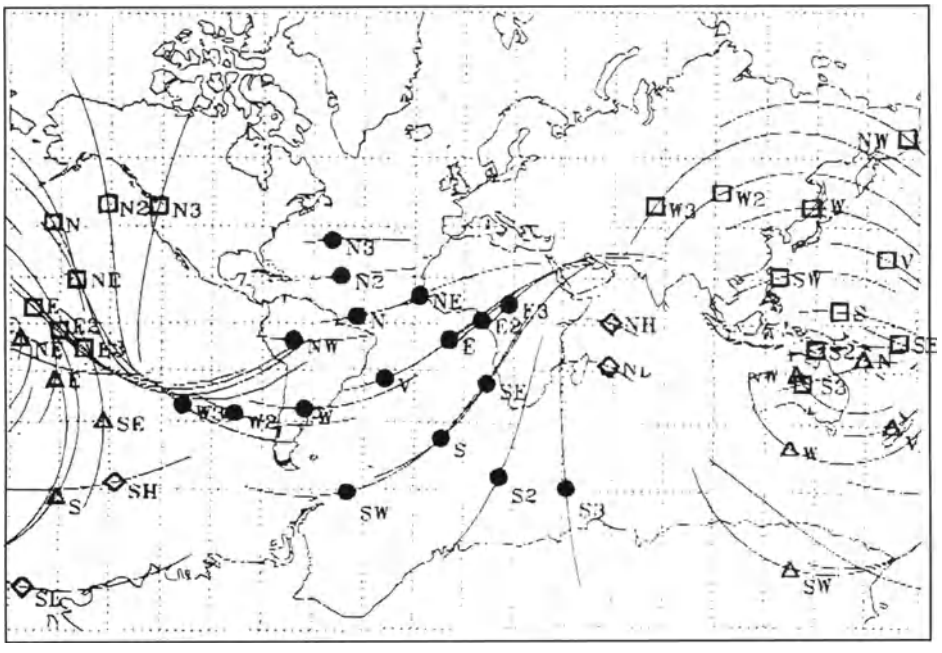

Fig. 4.3.10. Asymptotic viewing directions of muon telescopes at Nagoya (squares), Hobart (triangles), and Mawson (diamonds). The track through each symbol represents the spread of viewing directions corresponding to the central 80% of each telescope's energy response. By solid circles are shown the same for newly planned multi directional muon detector with 17 telescopes at Santa Maria, Brazil (29.44°S, 53.81°W). According to Munakata et al. (2000).

4.4. Network of neutron monitors of IGY type and neutron super-monitors of IQSY type

4.4.1. NM as main detector of worldwide network of ground based CR observatories; the tendency of combining NM and spacecraft data

In Section 1.2.9 we gave a very short description and history of neutron monitors of IGY type developed in USA in 1951–1952 by Simpson (M1955), and neutron super-monitors of IQSY type developed in 1961–1963 in Canada (see detailed description in Carmichael, M1964) and in USSR (where it was developed as energy spectrograph by using different times of neutrons collection, Blokh et al., 1971). These detectors became as main detectors of the worldwide network of CR Observatories. The detailed description of NM-IGY was given in Simpson (M1955), Dorman (M1957), and NM-IQSY – in Carmichael (M1964), Dorman (M1974, M1975a). Recent calculations of the coupling and response functions for NM IGY and NM IQSY were given in Clem and Dorman (2000), design of NM development – in Stoker et al. (2000), the design and operation of the NM world network – in Moraal et al. (2000), determination of coupling functions on the basis of latitude survey data – in Moraal et al. (1989), Dorman et al. (2000). Here we will give some brief information about NM-IGY and NM-IQSY world distribution at 1975 and at present time as well as about statistical errors for one hour registration for all existing NM (Section 4.4.2), about a possible new sensor for detecting neutrons (Section 4.4.3), about neutron monitors zenith diagrams (Section 4.4.4), about multiple neutrons phenomenon (Section 4.4.5), about sensitivity to CR secondary particles (Section 4.4.6) and about detection efficiency (Sections 4.4.7 and 4.4.8). In Sections 4.4.9 and 4.4.10 we will consider the concept of 'Spaceship Earth' and inter-calibration of the NM worldwide network.

During many years our main observational basis on dynamic electromagnetic processes in the interplanetary space were continue measurements of CR time variations by shielded 10 cm Pb ionization chambers and muon telescopes (from 1930s) and by neutron monitors (from 1950s). This information is regard to relatively high energy particles (with energy more than few GeV). Only from 1970s with the launch of satellites of IMP series and deep space missions Pioneer 10/11 and Voyager 1/2, and the journey of Ulysses and other spacecrafts became available practically continue information on low and medium CR energy as well as data on IMF and solar wind. As McDonald (2000) mentioned, many main results in the physics of Heliosphere and on dynamical processes inside and near boundary with the interstellar medium (on the distance about 100 AU from the Sun) were obtained on the basis of combination of NM and spacecrafts data. This combination gives important possibility to investigate CR variations in very wide energy interval from few MeV to many GeV. According to McDonald's (2000) opinion, in the future, with the new emphasis on carefully inter-calibrated of NM network (see Section 4.4.10) and the improved instrumentation for space studies (see Section 4.7.5), these symbiotic relations should prove to be even more productive in extending our understanding of the acceleration and transport of energetic particles (galactic and solar CR, anomaly CR, and energetic particles of interplanetary and planetary origin) in the Heliosphere. From other hand, solar observations from spacecrafts had great impact on interpreting results from NM (in particular the identification of coronal holes as the sources of high speed solar wind streams and the

recognition of the importance of coronal mass ejections in producing interplanetary disturbances and accelerating solar energetic particles (see in more details in Dorman, M2005).

4.4.2. Examples of CR Observatories equipped by NM

Figs. 4.4.1 and 4.4.2 show respectively a view of NM-IQSY, and of the Observatory on Mt. Jungfraujoch in Swiss Alps (equipped with NM-IQSY, NM-IGY, and with neutron telescope (for measurements of solar neutrons, see details in Section 4.9).

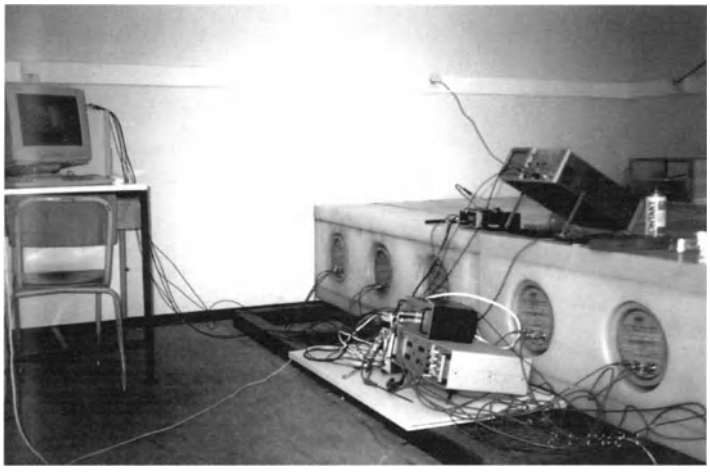

Fig. 4.4.1. A view of NM-IQSY in the process of mounting in Rome CR Observatory.

Fig. 4.4.2. The view on the Observatory on Mt. Jungfraujoch in Swiss Alps equipped with NM-IQSY and NM-IGY; on the nearest Mt. Cornergrat there is Neutron Solar Telescope (developed in Japan, see Section 4.9).

In Fig. 4.4.3 are shown the data acquisition system for LARC (Antarctic Laboratory for CR on King George Island, 62.2°S, 58.9°W; equipped by NM-IQSY) and scheme of database for the Chilean network of CR detectors according to Cordaro (1995).

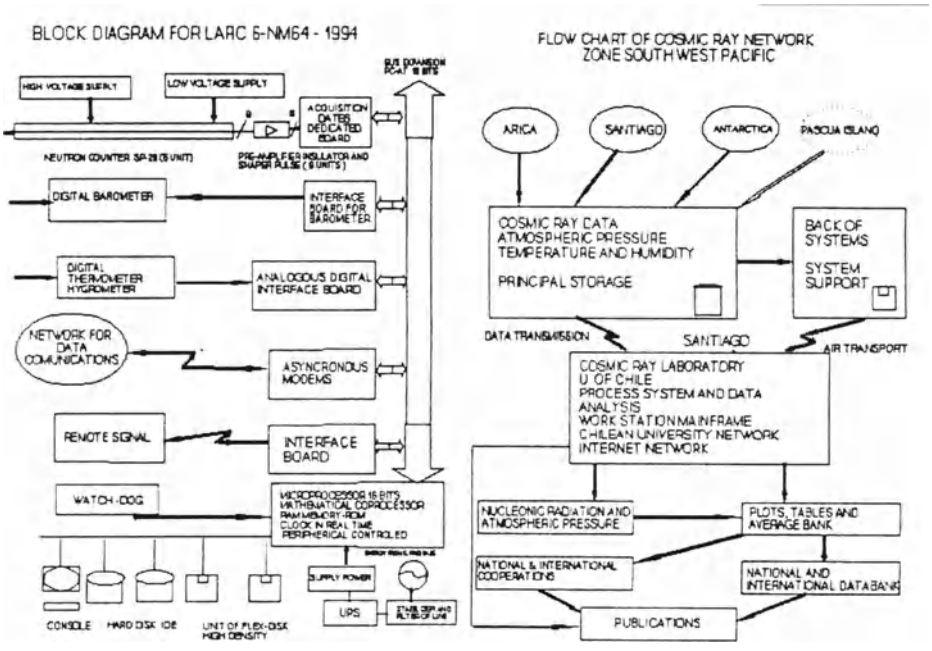

Fig. 4.4.3. Data acquisition system for LARC (left panel) and scheme of database for the Chilean network of CR detectors (right panel). According to Cordaro (1995).

4.4.3. Worldwide network of NM: planetary distribution

The global networks of NM-IGY and NM-IQSY are shown in Figs. 4.4.4 and 4.4.5 respectively (the situation at 1975).

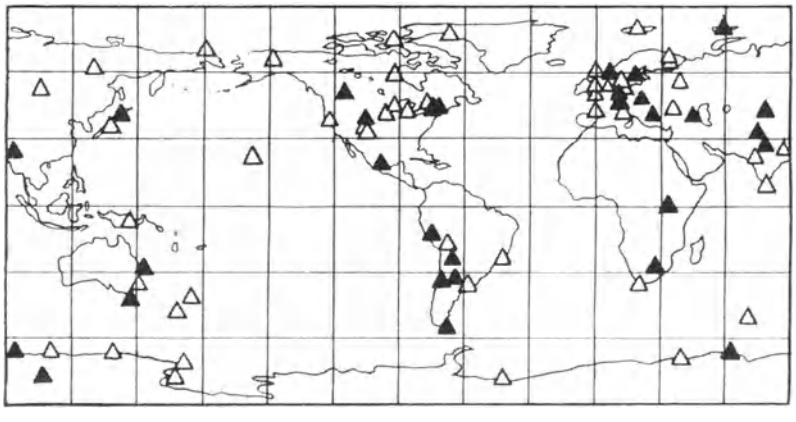

Fig. 4.4.4. The planetary distribution of NM-IGY. Black triangles – operating in 1975, white triangles – operating before 1972. From Dorman, M1975a.

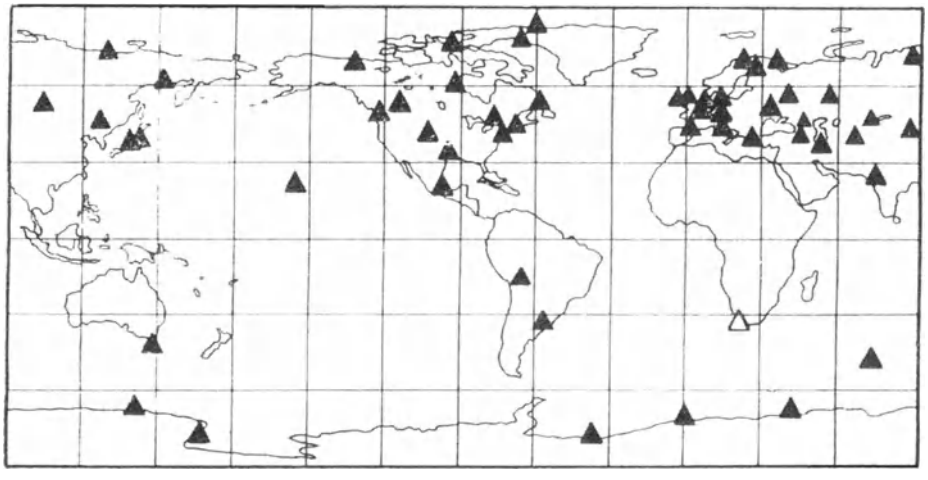

Fig. 4.4.5. The planetary distribution of NM-IQSY. Black triangles – operating in 1975, white triangles – operating before 1972. From Dorman, M1975a.

Fig. 4.4.6 shows the present (at 2002) world-wide network of neutron monitors of both types.

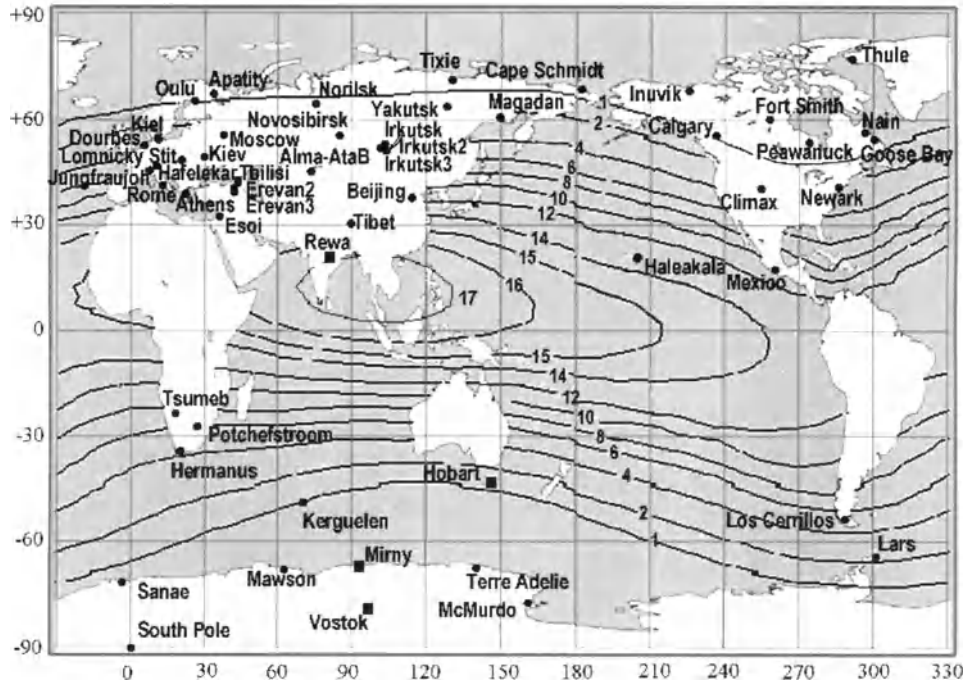

Fig. 4.4.6. The planetary distribution of neutron monitors of both types at 2002. Also shown are curves of cut off rigidities (numbers on curves in GV). Prepared by A.V. Belov and E.A. Eroshenko.

4.4.4. Worldwide network of NM: statistical errors

The statistical errors per one hour registration of NM-IGY and NM-IQSY of the worldwide network are presented in Fig. 4.4.7.

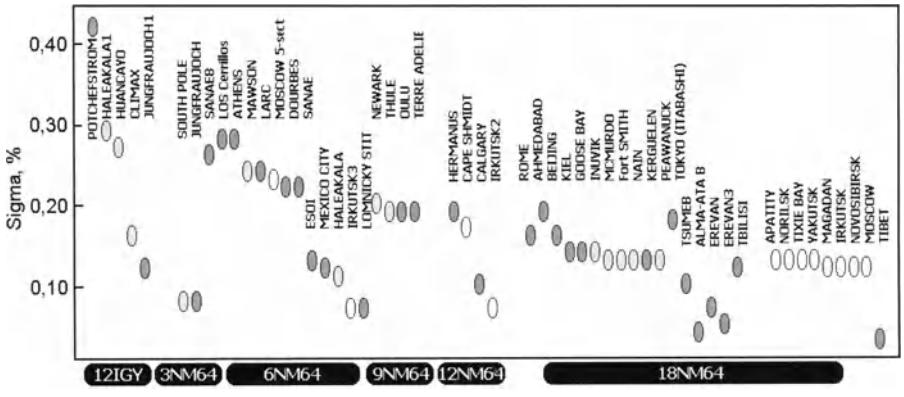

Fig. 4.4.7. Statistical errors per one hour registration (in %) for currently operating neutron monitors (situation at 2002). Prepared by A.V. Belov and E.A. Eroshenko.

In Table 4.4.1 are shown characteristics of 16 NM in the world with the highest counting rate (with the smallest statistical errors).

Table 4.4.1. Characteristics of 16 NM in the world with the highest counting rate (with the smallest statistical errors). On the basis of Moraal et al. (2000).

Station	Latitude (deg)	Altitude (m)	Pressure. (mb)	Cutoff (GV)	Counting rate (s^{-1})	Statist. error (%)	
						Per hour	Per minute
Tibet	30.1	4300	606	14.1	2970	0.031	0.24
Alma Ata B	43.1	3340	680	6.61	1205	0.047	0.36
Erevan	40.2	2000	815	7.58	1100	0.050	0.39
Haleakala	20.7	3030	700	12.9	970	0.054	0.42
Lomnicky Stit	49.2	2634	748	3.98	420	0.081	0.63
Jungfraujoch 2	46.5	3475	646	4.61	330	0.092	0.71
Tsumeb	-19.2	1240	880	9.21	310	0.095	0.73
Calgary	51.1	1128	883	1.08	270	0.101	0.79
South Pole	-90.0	2820	680	0.09	260	0.103	0.80
Irkutsk 3	52.3	3000	715	3.64	240	0.108	0.83
McMurdo	-77.9	48	1007	0	230	0.110	0.85
Irkutsk 2	52.3	2000	800	3.64	210	0.115	0.89
Moscow	55.5	200	1000	2.43	200	0.118	0.91
Kerguelen	-49.4	0	1000	1.14	190	0.121	0.94
ESO on Mt. Hermon	33.2	2025	800	10.8	171	0.127	0.99
Inuvik	68.3	21	1010	0.17	160	0.132	1.02
Novosibirsk	54.8	163	1000	2.87	160	0.132	1.02

4.4.5. Response of NM worldwide network to CR isotropic variation

The response of NM worldwide network to the primary CR isotropic variation of type $\delta D(R)/D_o(R) \propto R^{\gamma}$ for $\gamma = -1$ and -0.5 were calculated by Moraal et al. (2000) and

are shown in Fig. 4.4.8. It was assumed that at R = 10 GV the variation in primary intensity was 1%, and then for each station was calculated expected variation in NM counting rate (see Section 3.1 in Chapter 3).

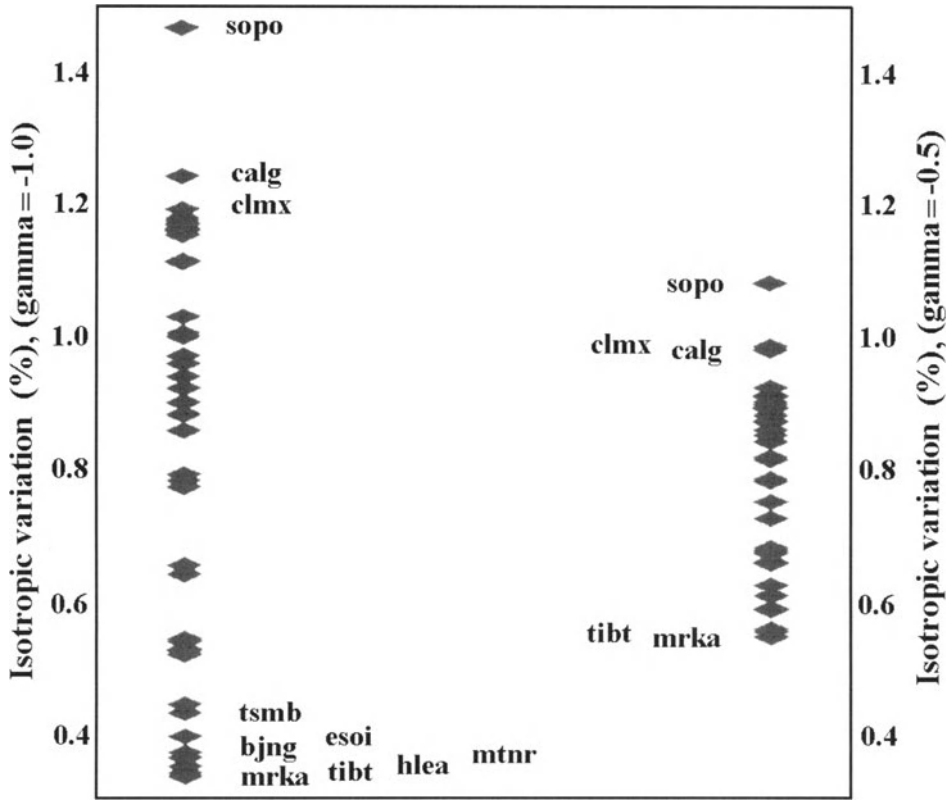

Fig. 4.4.8. Expected variations in NM counting rate caused by isotropic power variation in primary CR with amplitude 1% at R = 10 GV for slope in primary variation spectrum $\gamma = -1$ (left) and $\gamma = -0.5$ (right). **The list of station names for left ($\gamma = -1$) is** from top to bottom: South Pole (sopo), Calgary (calg), Climax (clmx), Cape Schmidt, Tixie Bay, Apatity, Oulu, Thule, Terre Adelie, McMurdo, Mt. Wellington, Goose Bay, Inuvik, Kerguelen, Mawson, Sanae, Yakutsk, Irkutsk (3000 m), Newark, Magadan, Moscow, Irkutsk (2000 m), Kiel, Lomnicky Stit, Jungfraujoch IGY, Jungfraujoch IQSY, Novosibirsk, Hafelekar, Kiev, Irkutsk, Hermanus, Alma Ata (3400 m), Potchefstroom, Alma Ata (800 m), Erevan, Rome, Tbilisi, Mexico City, Tsumeb (tsmb), Emilio Segre' Observatory on Mt. Hermon (esoi), Beijing (bjng), Mt. Norikura (mtnr), Haleakala (hlea), Tibet (tibt), Morioka (mrka). **The list for right ($\gamma = -0.5$) is** from top to bottom: South Pole, Climax, Calgary, Mt. Wellington, Irkutsk (3000 m), Sanae, Mawson, Apatity, Cape Schmidt, Tixie Bay, Oulu, Thule, Kerguelen, Terre Adelie, McMurdo, Goose Bay, Inuvik, Yakutsk, Irkutsk (2000 m), Lomnicky Stit, , Jungfraujoch IGY, Jungfraujoch IQSY, Magadan, Newark, Moscow, Kiel, Novosibirsk, Hafelekar, Irkutsk, Kiev, Alma Ata (3400 m), Hermanus, Potchefstroom, Erevan, Alma Ata (800 m), Tbilisi, Rome, Mexico City, Tsumeb, ESO on Mt. Hermon, Mt. Norikura, Haleakala, Beijing, Tibet, Morioka. According to Moraal et al. (2000).

From Fig. 4.4.8 can be seen that the most sensitive to primary CR isotropic variation with the slope $\gamma = -1$ are South Pole (R_c = 0.09 GV), Calgary (R_c = 1.08 GV), and Climax (R_c = 3.0 GV). Moraal et al. (2000) note that South Pole is more sensitive than other polar stations because of its high altitude of 2820 m. The stations with the lowest

response are Haleakala (R_c = 12.9 GV), Beijing (R_c = 10.1 GV), ESO on Mt Hermon (R_c = 10.8 GV), Tsumeb (R_c = 9.2 GV), and Mexico (R_c = 8.6 GV). Fig. 4.4.7 shows that the NM worldwide network is very high sensitive to the primary CR isotropic variation: the NM responses vary from about 1.5 to about 0.3 (factor 5) for the slope $\gamma = -1$, and from 1.1 to 0.5 (factor 2) for the slope $\gamma = -0.5$ in the primary CR spectrum variation.

4.4.6. Response of NM worldwide network to CR North-South asymmetry and solar-diurnal anisotropy

As we considered in Section 3.14 (Chapter 3), the observed by NM worldwide network the relative CR intensity variation can be presented as a sum of spherical harmonics:

$$\delta I = \delta I_{00} + (\delta I_{10} + \delta I_{11}) + (\delta I_{20} + \delta I_{21} + \delta I_{22}) + ..= C_{00}A_{00} + (C_{10}A_{10} + C_{11}A_{11}\cos(\Phi_{11} - \Psi_{11})) + \text{2nd and higher harmonics}, \quad (4.4.1)$$

where $A_{mn} = (\delta D(R)/D_o(R))_{mn}$ are the amplitudes of corresponding spherical harmonics of primary CR variation, and C_{mn} are corresponding coupling coefficients (McCracken et al., 1965; Krymsky et al., 1966; Nagashima, 1971; Yasue et al., 1982; see also Section 3.14 in Chapter 3). The term $\delta I_{00} = C_{00}A_{00}$ described the isotropic part of CR variation (in previous Section 4.4.5 was considered the sensitivity of the NM worldwide network to this part of CR variations). The terms of the first-order spherical harmonic $\delta I_{10} = C_{10}A_{10}$ and $\delta I_{11} = C_{11}A_{11}\cos(\Phi_{11} - \Psi_{11})$ described the North-South anisotropy and the solar diurnal variation (the angles Φ_{11} and Ψ_{11} are the effective asymptotic longitude of NM station and the phase of the diurnal variation). As we mentioned in Section 3.14, the 2nd harmonic $\delta I_{20} + \delta I_{21} + \delta I_{22}$ has three components: second zonal, asymmetric diurnal and semi-diurnal variations.

The response of NM worldwide network to CR North-South asymmetry and solar-diurnal CR anisotropy was calculated in Moraal et al. (2000), and results are shown in Fig. 4.4.9. It was assumed that these both anisotropies are caused by primary CR particles with rigidity up to 100 GV and their amplitude in primary CR is 1%. From Fig. 4.4.9 can be seen how NM worldwide network respond to the CR North-South asymmetry (left scale in Fig. 4.4.9): the polar and high latitude NM in North and South hemispheres have much bigger response to CR North-South asymmetry than middle and low latitude NM; the biggest response has a pair of NM Thule–McMurdo. The right scale in Fig. 4.4.9 shows the response of NM worldwide network to solar-diurnal CR anisotropy: it can be seen that more than 30 NM have coupling coefficients $C_{11} \geq 0.5$. It means that the solar-diurnal CR variation is well measured by the current NM worldwide network.

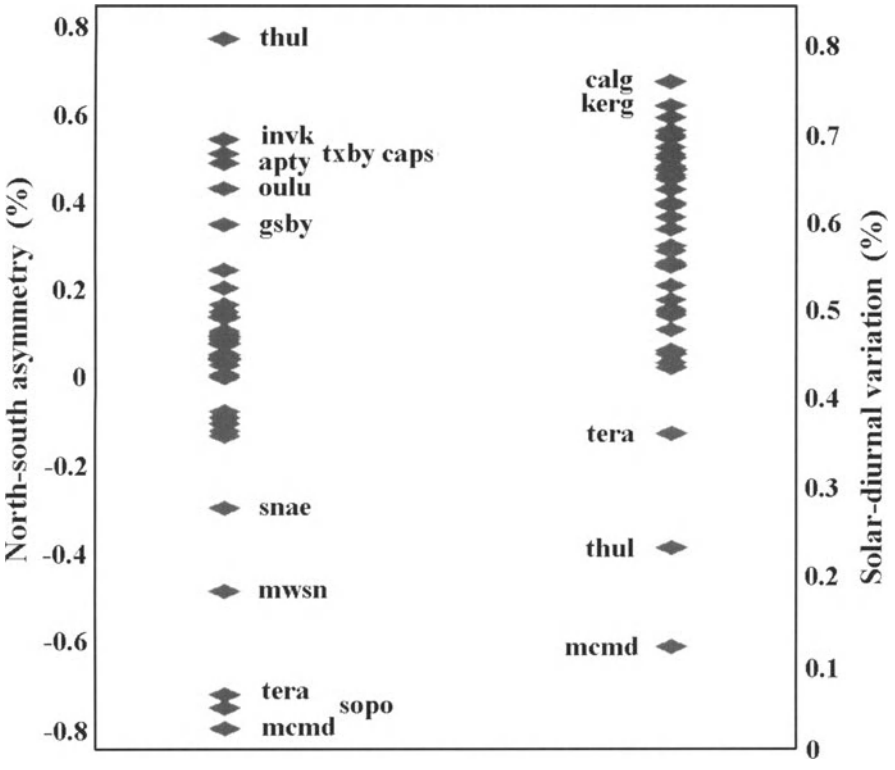

Fig. 4.4.9. Responses of NM to CR North-South asymmetry (left) and to solar-diurnal variation (right). **The list of station names for left (North-South asymmetry) is from top to bottom**: Thule, Inuvik, Tixie Bay, Cape Schmidt, Apatity, Oulu, Goose Bay, Yakutsk, Moscow, Kiel, Novosibirsk, Magadan, Kiev, Calgary, Lomnicky Stit, Rome, Hafelekar, Irkutsk, Tbilisi, Jungfraujoch IGY, Jungfraujoch IQSY, Hermanus, Potchefstroom, Beijing, Alma Ata (800 m), Erevan, Tsumeb, Newark, Alma Ata (3400 m), Morioka, Mt. Norikura, Mexico City, Haleakala, Kerguelen, Mt. Wellington, Climax, Sanae, Mawson, Terre Adelie, South Pole, McMurdo. **The list for right (solar-diurnal variation) is from top to bottom:** Calgary, Kerguelen, Mt. Wellington, Climax, Newark, Jungfraujoch IGY, Jungfraujoch IQSY, Lomnicky Stit, Sanae, Goose Bay, Yakutsk, Magadan, Moscow, Alma Ata (3400 m), Hafelekar, Kiel, Novosibirsk, Kiev, Irkutsk, Mawson, Alma Ata (800 m), Apatity, Cape Schmidt, Tixie Bay, Inuvik, Hermanus, Tbilisi, Erevan, Rome, Haleakala, Tibet, Mexico City, Potchefstroom, Morioka, Tsumeb, Beijing, South Pole, Terre Adelie, Thule, McMurdo. According to Moraal et al. (2000).

The asymptotic longitudes Φ_{11} of the 33 NM from the worldwide network characterized by coupling coefficients for solar diurnal variation C_{11} bigger than 0.5 are shown in Fig 4.4.10. It can be seen that NM of the worldwide network mostly sensitive to CR solar diurnal variation are not evenly distributed in asymptotic longitude, with a several large gaps of about 20–30°. Moraal et al. (2000) note that this uneven longitude spread is not very significant for investigations of steady-state CR anisotropies, but it is an important deficiency for measurements of transient CR anisotropies (e.g. in periods of Forbush decreases, in periods of solar CR increases). As it is considered in detail below in Section 4.4.14, polar and high latitude NM formed a sub-worldwide network which is very useful for investigations of transient CR anisotropies (the concept 'Space Earth', developed by Bieber and Evenson, 1995).

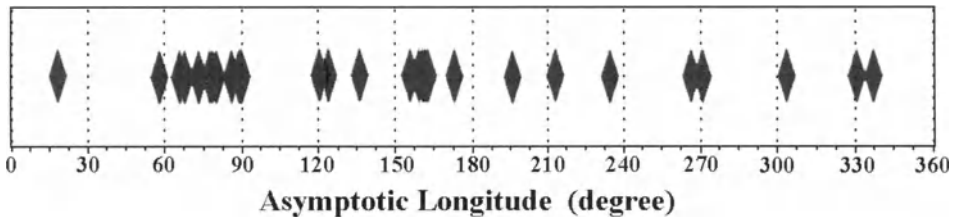

Fig. 4.4.10. Asymptotic longitudes of the 33 NM from the worldwide network with the biggest sensitivity to CR solar diurnal variations. The NM stations are from left to right: Sanae, Mawson, Kiel, Oulu, Apatity, Hermanus, Jungfraujoch IGY, Jungfraujoch IQSY, Hafelekar, Lomnicky Stit, Moscow, Kiev, Kerguelen, Rome, Tbilisi, Erevan, Novosibirsk, Alma Ata (800 m), Tixie Bay, Alma Ata (3400 m), Irkutsk (3000 m), Irkutsk (2000 m), Irkutsk, Yakutsk, Magadan, Mt. Wellington, Cape Schmidt, Inuvik, Haleakala, Calgary, Climax, Newark, Goose Bay. According to Moraal et al. (2000).

4.4.7. Sensitivity of NM worldwide network to solar neutron events

In the last 25 years only few solar neutron events were observed by NM: on 3 June 1982 at 11.45 Jungfraujoch NM detected an increase of ≈ 5% for about 10 minutes, on 24 May 1990 the Climax NM recorded an increase of ≈ 5% lasted about 25 minutes, on 22 March the Haleakala NM observed a neutron increase of 1.5%. Pyle (1993) calculated the probability that NM of the worldwide network will be able to observe these events (the criterion was the fraction of time that NM looks towards the Sun through less than 1000 g.cm^{-2}). Results are shown in Fig. 4.4.11.

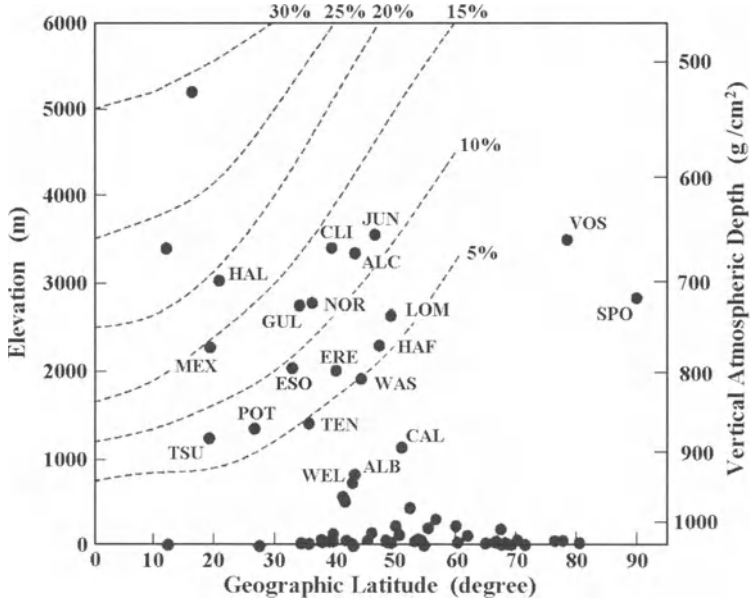

Fig. 4.4.11. The probability (fraction of time) that NM looks towards the Sun through less than 1000 g.cm^{-2}. NM stations with negligible probability have no name; NM station with sufficient probability have names: Haleakala, Climax, Mexico City, ESO on Mt. Hermon (added by L. Dorman), Gulmarg, Jungfraujoch, Alma Ata C (3400 m), Mt. Norikura, Tsumeb, Potchefstrum, Erevan, Lomnicky Stit, Hafelekar, Mt. Washington, Tehran, Wellington, Alma Ata B (800 m), Calgary, South Pole, Vostok. In the left top corner two points are closed now NM Chacaltaya and NM Huancayo. According to Pyle (1993).

From Fig. 4.4.11 follows that only small part of NM worldwide network has significant fraction of time that NM looks towards the Sun through less than 1000 g.cm^{-2}. In Table 4.4.2 is given a list of most favorable stations to observe solar neutron events.

Table 4.4.2. Most favorable stations to observe solar neutron events. On the basis of Pyle (1993).

Station name	Longitude range (°)	Cutoff (GV)
Jungfraujoch, Switzerland	-10 to 30	4.61
Hafelekar, Austria	0 to20	4.38
Tsumeb, Namibia	5 to 30	9.21
Lomnicky Stit, Slovakia	10 to 30	3.98
ESO on Mt. Hermon, Israel	10 to 60	10.8
Potchefstroom, South Africa	15 to 40	7.00
Erevan, Armenia	30 to 60	7.58
Gulmarg, India	50 to 100	11.58
Alma Ata (3400 m), Kazahstan	55 to 100	6.61
Mt. Norikura, Japan	115 to 160	11.48
Haleakala, U.S.A.	160 to 240	12.91
Climax, U.S.A.	230 to 280	3.08
Mexico City, Mexico	235 to 285	8.61

4.4.8. Possible new sensors for neutrons detecting

In the constructions of the NM-IGY and NM-IQSY proportional counters with the gas BF_3 enriched with the isotope ^{10}B were used as producers. The effective cross-section for thermal neutrons in the reaction $^{10}B(n,\alpha)^7Li$ is about 3770 barn. According to Voitovetskij and Tolmacheva (1959), Bollinger et al. (1962), the reaction $^6Li(n,\alpha)^3H$ may be used for neutron registration as well. Kopylov (1966) therefore suggests as sensor in a neutron monitor a lithium plate Li_2O with photomultiplier, keeping, as in an ordinary monitor, paraffin or polyethylene as the moderator and lead as the local neutron generator. The efficiency of the lithium plate is 74% for the natural isotopic composition and a plate thickness of 1 cm. Material enriched with ^6Li to 90.5% increases the efficiency rapidly, reaching 90% for a plate thickness of 0.2 cm and about 100% for 0.5 cm (Voitovetskij and Tolmacheva, 1959; Bollinger et al., 1962).

For recording the neutron CR component Granitskij and Sergeev (1966) suggested to use, besides counters filled with $^{10}BF_3$, also counters filled with ^3He. In these counters the reaction

$$^3He + n \rightarrow {}^3H + p + 7.65\ MeV \qquad (4.4.2)$$

is used; in the interval 0.001 – 0.03 eV the cross section is inversely proportional to neutron velocity, in the region 0.3 – 1.2 MeV it is approximately equal to 0.8 barn. The efficiency of ^3He counters is several times higher than that of counters with $^{10}BF_3$; the construction of the monitor is simplified considerably and besides integral measurements, spectrometric measurements become possible. The design of NM with ^3He counters is described in Stoker et al. (2000). In Clem (1999), Clem and Dorman (2000) it is shown that all the main characteristics of NM, such as sensitivity to various

secondary CR and to primary CR for NM equipped by $^{10}BF_3$ counters or by ^{3}He counters, are practically the same (see Section 4.4.13 for more details).

4.4.9. On neutron monitors zenith diagrams

Phillips and Parsons (1962) have computed the zenith diagram of the neutron monitors and checked it experimentally. According to the transformation of Gross:

$$I(Z)=I_v\left(1+\frac{h}{L\cos Z}\right)\exp\left(-\frac{h}{L\cos Z}\right), \tag{4.4.3}$$

where I_v is the neutron intensity in vertical direction, h is the depth of atmosphere in $g.cm^{-2}$, Z is the zenith angle and L is the absorption path of CR neutron component (also in $g.cm^{-2}$). According to Phillips and Parsons (1962), experiments with the aid of a mobile neutron monitor have shown that Eq. 4.4.2 gives too low a result for large zenith angles; the difference is attributed to substantial scattering of the neutrons in the terrestrial atmosphere (this effect is very important at observation of solar neutrons, see details in Dorman, M2005). If we assume that there is no dependence on azimuth angle φ, we obtain after integrating of Eq. 4.4.3 over φ for NM zenith sensitivity

$$N(Z)=2\pi I_v\left(1+\frac{h}{L\cos Z}\right)\exp\left(-\frac{h}{L\cos Z}\right)\sin Z\,. \tag{4.4.4}$$

In Fig. 4.4.12 we show the normalized zenith distributions (with the condition $\int_0^{\pi/2} N(Z)dZ=1$) for h = 1033, 850, 700 and 500 g.cm^{-2} at L = 145 g.cm^{-2}.

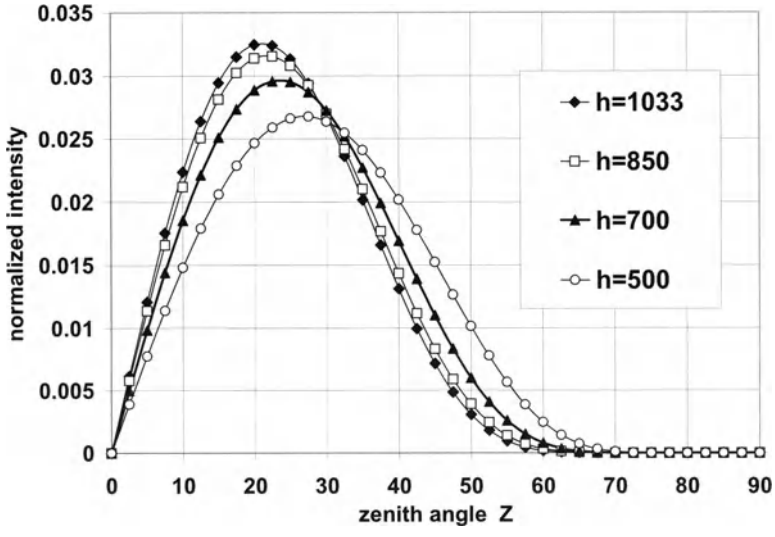

Fig. 4.4.12. Normalized zenith sensitivities of NM for h = 1033, 850, 700 and 500 g.cm^{-2} at L = 145 g.cm^{-2}.

From Fig. 4.4.12 can be seen that the maximum of zenith sensitivities is between 20° and 30°. If the opening angle of the sea level NM is limited to Z < 30° the counting rate must diminish by about a factor of 2 (Phillips and Parsons, 1962).

4.4.10. Recording of multiple neutrons by NM-IGY and NM-IQSY

Many years ago (Cocconi et al., 1950; Geiger, 1956) it was established that in each interaction of a CR nucleon with a heavy nucleus several neutrons are produced. Since the time spent by the different neutrons in the monitor is different, for a short dead time of the electronic circuits each incident nucleon gives several pulses, the so called 'multiple' neutrons. This phenomenon was first studied in detail by Meyer (1961), Hughes (1961), Fieldhouse et al. (1962), Bachelet et al. (1964), Meyer et al. (1964). Bachelet et al. (1964) after developing special circuits for separating multiple pulses found that the dependence of the counting rate in NM-IGY on the recovery time T_r is determined by multiple neutrons and the average life time T_{av} of the neutrons in the monitor. It was found that for $T_r < 100\,\mu\text{sec}$, neutrons with $T_{av} \approx 170\,\mu\text{sec}$ are the determining factor, but for $T_r > 100\,\mu\text{sec}$, neutrons with $T_{av} \approx 300\,\mu\text{sec}$ are the determining factor (according to Hatton and Carmichael (1964), for NM-IQSY this average time is $T_{av} \approx 326\,\mu\text{sec}$). The Bachelet et al. (1964) results on recording multiple neutrons in 1963 at various stations are given in Table 4.4.3.

Table 4.4.3. Number per hour of pulses of different multiplicities in a mobile NM-IGY. According to Bachelet et al. (1964).

Multiplicity	Rome R_c= 6.4 GV h_o = 1030 mb	Uppsala R_c=1.35GV h_o= 1029 mb	Monte Cavo R_c= 6.4 GV h_o= 926 mb	Haukeliseter R_c= 1.35 GV h_o= 922 mb
1	5213 ± 9	6573 ± 5	10336 ± 27	13380 ± 18
2	688 ± 3	861.9 ± 1.8	1478 ±10	1846 ± 7
3	140.3 ± 1.4	167.3 ± 0.8	310 ± 5	374 ± 3
4 and 5	57.4 ± 0.9	68.0 ± 0.5	140 ± 3	161 ± 2
6	9.9 ± 0.4	11.2 ± 0,2	23.6 ± 1.3	26.3 ± 0.8

Multiple neutrons were studied in detail by Nobles et al. (1965); for this purpose they developed a special monitor, with which any multiplicity can be recorded (see Fig. 4.4.13). It is a cube with a side of 1.2 m and weight 2700 kg. As neutron generator a thickness of 450 g/cm^2 of bismuth is used, which is about three times thicker than in ordinary NM-IGY and NM-IQSY where a layer of lead of 155 g/cm^2 is used. Measurements were made during 1965 with two instruments, located at sea level at Palo Alto (cut off rigidity 4.7 GV) and at 3800 m above sea level at White Mountain (cut off rigidity 4.5 GV). The distributions of the multiplicities for an observed spectrum of incident neutrons $N(E) = 1.5\times10^{-6}E^{-1.6}$ cm^{-2} sec^{-1} MeV^{-1} at 3,800 m, and $N(E) = 5\times10^{-8}E^{-2.2}$ cm^{-2} sec^{-1} MeV^{-1} at sea level, are shown in Fig. 4.4.14. Nobles et al. (1965) found that at mountain level the fractions of pulses due to capture of μ-mesons are 1.65%, 0.68% and only 0.3% for m = 1, 2 and 3, respectively, whereas at sea level these fractions are considerably higher: 8.94%, 6.7% and 2.6%. The relative fraction recorded with multiplicity m at mountain level was found for $10 < m < 400$ to fall with

increasing m as $m^{-3.3}$. Since multiple neutrons have a somewhat different sensitivity to the energies of the primary particles, recording them yields additional information about CR primary variations.

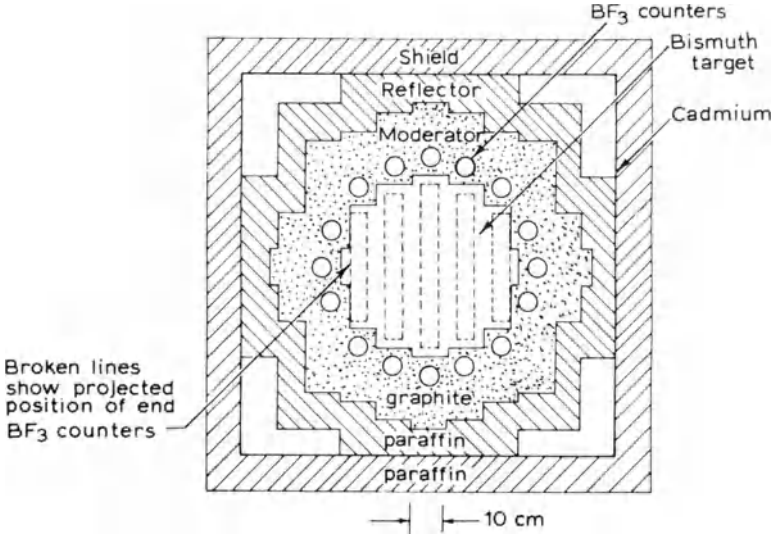

Fig. 4.4.13. Diagram of the multiplicity monitor in vertical cross section (Nobles et al., 1965).

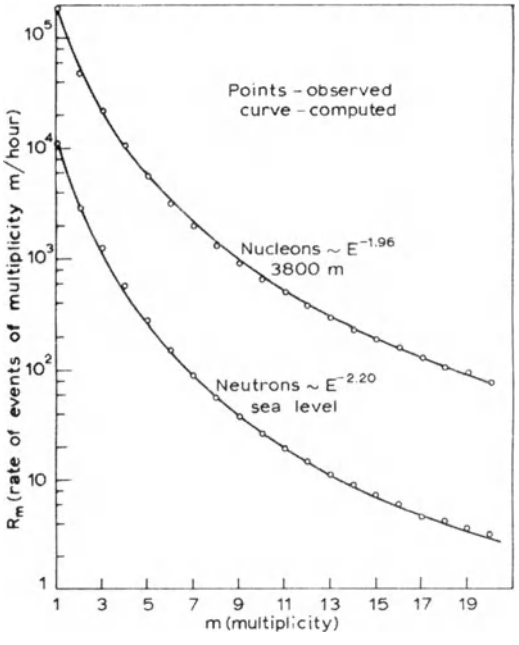

Fig. 4.4.14. Typical 3800 m and sea-level elevation multiplicity distributions. The data points are corrected for atmospheric pressure variations, for background (i.e. neutrons produced outside the bismuth target), for instrumental dead time, for muon capture neutron production, and for overlap of different multiplicity events in a single gate (Nobles et al., 1965).

In Chubenko et al. (2003) on the basis of measurements of multiple neutrons on Tien Shan NM-IQSY at the level 690 g.cm^{-2} and simulation was determined a relation between the observed multiplicity m of a neutron event and the average energy of the incident hadron E_h on the basis of agreement of the observed neutron multiplicity spectrum $P(m)$ with the energy spectrum $D(E_h)$ of cosmic ray hadrons. The latter spectrum has been measured earlier at mountain level by the Aragats magnetic spectrometer and Tien-Shan ionization calorimeter. According to Hatton and Carmichael (1964) the $P(m)$ and $D(E_h)$ spectra are connected by the equation

$$P(m) = S\Omega\eta \sum_{\nu=m}^{\infty} C_\nu^m \varepsilon^m (1-\varepsilon)^{\nu-m} \int_{E_{thresh}}^{\infty} D(E_h) W(\nu, E_h) dE_h , \qquad (4.4.5)$$

where $S\Omega$ is the neutron monitor's unit acceptance angle, η is the interaction probability of cosmic ray hadrons inside the monitor's lead absorber, ε = 0.05 is the registration efficiency of an evaporation neutron, ν is the multiplicity of evaporation neutrons and $W(\nu, E_h)$ is the probability distribution of the generation of ν neurons in interaction of a hadron having the energy E_h. The primary hadron spectrum at the level of 690 g/cm^2 was taken in the form:

$$F(E_h) = 32 \times E_h^{-2.55} \text{ m}^{-2}\text{ster}^{-1}\text{GeV}^{-1} \qquad (4.4.6)$$

which was obtained by the power-law fitting of the data of Aragats spectrometer in the energy range 2-10 GeV and the calorimeter data in the range above 300 GeV. Results of determining of the multiplicity spectrum $P(m)$ and the average number of neutrons evaporation *vs.* E_h are shown in Fig. 4.4.15.

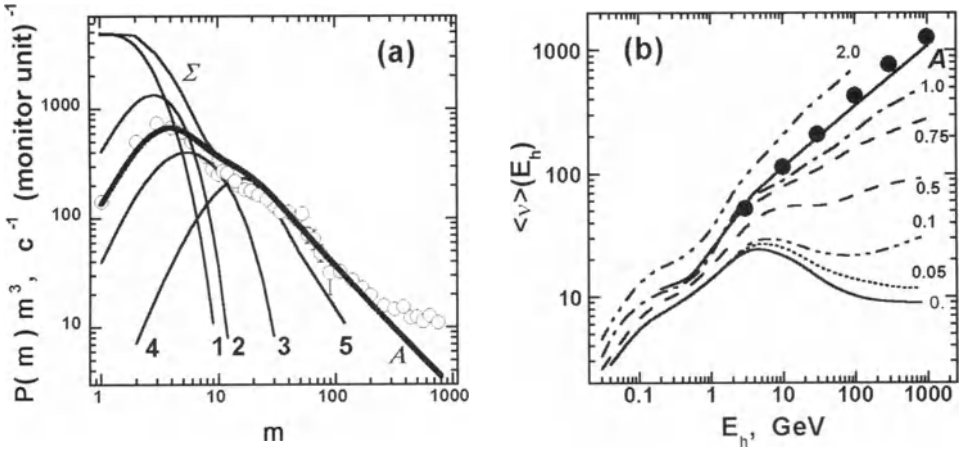

Fig. 4.4.15. Left panel **(a)**: neutron multiplicity spectra (points – experiment, curves – calculations). Right panel **(b)**: neutron production functions (curves with numbers – data from Hatton and Carmichael, 1964, curve *A* – results of the calculations, and circles – simulation by the SHIELD code according to Dementyev and Sobolevsky, 2003). From Chubenko et al. (2003).

4.4.11. Sensitivity of NM to various secondary CR particles

An important characteristic of a NM is the number of neutrons generated by protons and pions of various energies. Fig. 4.4.16 shows the results of experimental investigations by Hughes et al. (1962) with a standard NM-IGY of 12 counters, working together with a magnetic spectrograph.

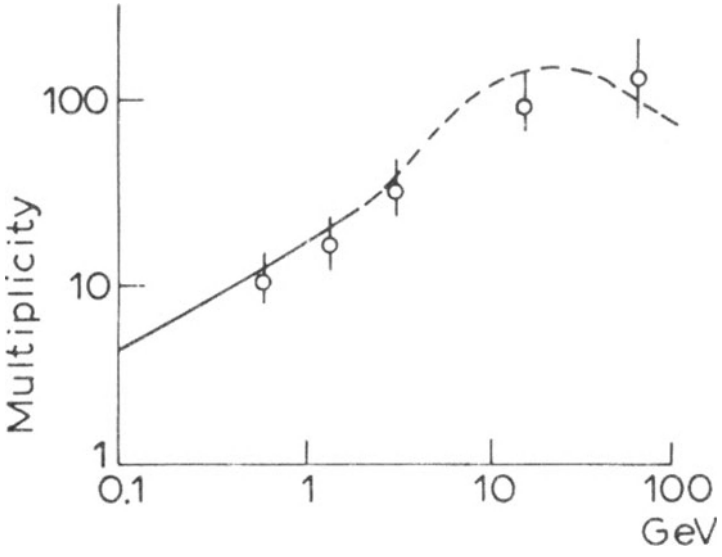

Fig. 4.4.16. Multiplicity of neutron generation, or yield function in the standard NM-IGY as a function of the kinetic energy of the incident protons. According to Hughes et al. (1962).

The multiplicity of neutron generation (Fig. 4.4.16) is seen to increase rapidly with increasing proton energy (about $\propto E_k$), reaching a maximum value of about 100 for a proton energy of some 10 GeV. The fraction of neutrons generated from pions formed in the monitor is about 0.05 in the energy region $E_k \approx 1 GeV$ and ~0.1 in the energy region 10 – 100 GeV. The distribution of multiplicities from 1 to 10 measured by Fieldhouse et al. (1962) gave an average effective multiplicity of 1.23. The same paper attributes 77% of the responses in the monitor to the incidence of neutrons, 14.8% to protons, and 6.8% to capture of muons. About 1% of the readings is caused by muons interacting in the air, nucleons in showers, and pions. Thus the neutrons give the chief contribution. The dependence on the energy of the incident nucleons was also, in first approximation, found by Fieldhouse et al. (1962).

Some important results about the sensitivity of the neutron monitor to various components of cosmic radiation found in Hughes et al. (1964), Meyer et al. (1964), and Hughes and Marsden (1966) are shown in Fig. 4.4.16, Table 4.4.4, and in Fig. 4.4.18. These investigations were made with the neutron monitor at Leeds (cut off rigidity 2.1 GV; recovery time 700 μsec). It is seen that 81.3 ± 2.4% of the impulses recorded are due to neutrons, 11.2 ± 1.1% to protons, 6–8 ± 1.2% to captured muons and less than 1% to fast muons, pions, and showers.

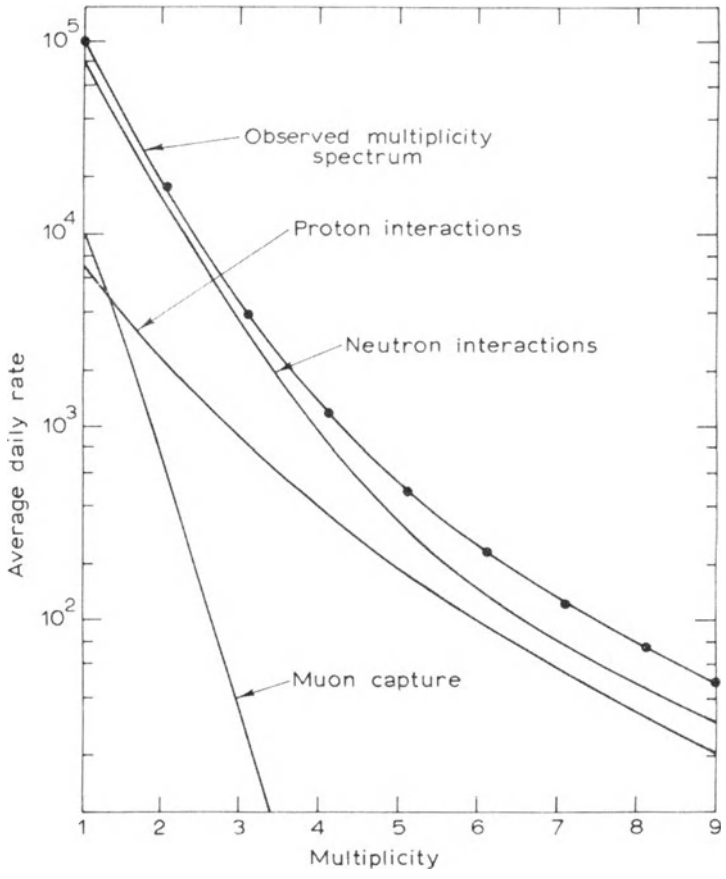

Fig. 4.4.17. The contributions to the multiplicity spectrum observed in the standard NM-IGY owed to neutron, proton, and muon interactions.

Table 4.4.4. Sensitivity of the Leeds NM-IGY to various secondary CR components

Component	Number of pulses per day	Fraction, %	For separate multiplicities								
			1	2	3	4	5	6	7	8	9
Total cosmic radiation	169064	100.0	104540	20064	4370	1305	520	245	133	78	49
Protons	18940	11.2 ± 1.1	7516	2410	905	381	190	97	55	33	20
Captured muons	11500	6.8 ± 1.2	10756	709	32	—	—	—	—	—	—
Passing muons	803	0.5	499	106	23	4	1	—	—	—	—
Pions	250	0.1	85	30	13	5	3	1	1	—	—
Showers	126	0.05	36	13	6	3	2	1	1	—	—
Neutrons	137445	81.3 ± 2.4	85648	16796	3391	912	324	145	76	44	29

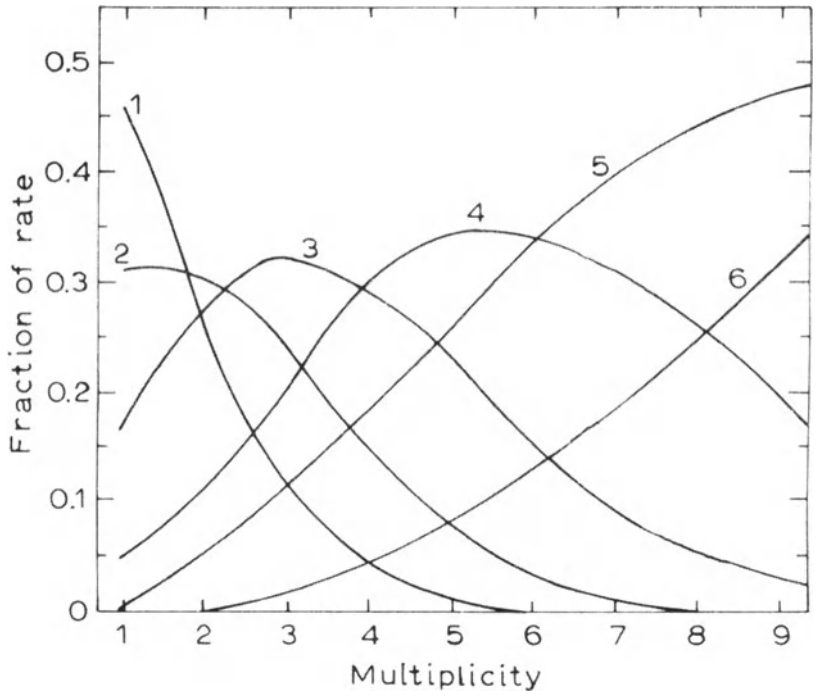

Fig. 4.4.18. Calculated curves showing the fraction of each multiplicity rate caused by the interactions of nucleons in six energy intervals: curve **1** – < 0.1 GeV; **2** – 0.1–0.3 GeV; **3** – 0.3–1.0 GeV; **4** – 1–3 GeV, **5** – 3–10 GeV; and **6** – > 10 GeV.

The more accurately measured neutron spectrum at sea level by Hughes and Marsden (1966) proved to be approximately exponential, with an exponent changing from about 2 in the energy region near 0.5 GeV to about 2.6 for energies around 10 GeV. The average nucleon energies at sea level corresponding to the generation of neutrons of multiplicities from 1 to 9 varies from 0.11 to 5.5 GeV. Hughes and Marsden (1966) showed that NM-IGY only record nucleons with energies above 50 MeV, but are practically insensitive to neutrons of lower energies, mainly owing to the presence of the lead generator of secondary neutrons. This is very important since according to Yamashita et al. (1966) near the Earth's surface the flux of neutrons in the region of the lowest energies (1 eV – 10^7 eV) suffers considerable fluctuations with variation of the properties of the soil (presence or absence of moisture) and other local factors which are hard to take into account.

4.4.12. Detection efficiency of NM-IGY and NM-IQSY

The detection efficiency of the neutron monitor was estimated by a simulation about 30 years ago (Hatton, 1971). Recently a new Monte Carlo calculation was performed by Clem (1999) and Clem and Dorman (2000). In order to determine the NM detection response of secondary particles at ground level, a simulation was carried out using a 3-dimensional particle transport package entitled FLUKA (Fassó el al., 1997) combined with specially prepared programs to simulate the proportional neutron counters and electronics response to energy deposition in the gas. The standard dimensions and

composition of materials of NM-IGY and NM-IQSY were used as input to the geometry according to Simpson (M1955) and Hatton (1971), correspondingly.

Fig. 4.4.19 displays the resulting detection efficiency of a NM-IQSY with $^{10}BF_3$ counters for 6 different particle species (neutrons, protons, positive and negative pions as well as positive and negative muons) for the vertical incident direction.

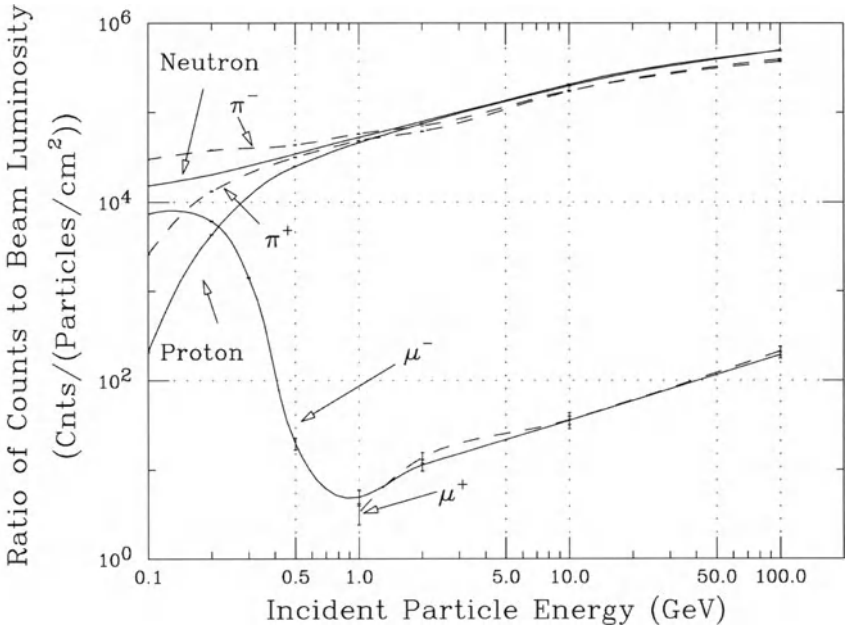

Fig. 4.4.19. Calculated detection efficiency of secondary particles arriving in the vertical direction for the NM-IQSY. According to Clem (1999), Clem and Dorman (2000).

From Fig. 4.4.19 can be seen that NM-IQSY response from muons above 1 GeV is roughly 3.5 orders of magnitude below the hadrons. In this energy region the primary mechanisms for muon induced counts are neutron production in photo-nuclear interactions and electromagnetic showers resulting in multiple ionization tracks in a counter. Below 1 GeV, stopping negative charge muons are captured by a lead nucleus into a meson orbit and absorbed by the nucleus. The de-excitation of the nucleus occurs with the emission of neutrons, which is reflected in the rise in detection efficiency with decreasing energy. As expected, there is practically no difference in the response between neutrons and protons in the high energy region, while at lower energies the ionization energy loss of protons become significant, greatly reducing the probability of an interaction, which is reflected in the decreasing detection efficiency. Positive and negative charged pions produce almost identical responses at high energies while at lower energies negative pions undergo nuclear capture like negative muons; however, the pion absorption time after capture is much less, compensating the pions shorter decay time as reflected in the rise in negative pion efficiency. Shown in Fig. 4.4.20 is the resulting detection efficiency for protons and neutrons in NM-IQSY and NM-IGY

compared with calculations of Hatton (1971) and for NM - IQSY with accelerator data (Shibata et al., 1997, 1999, 2001; see also below, Fig. 4.4.21).

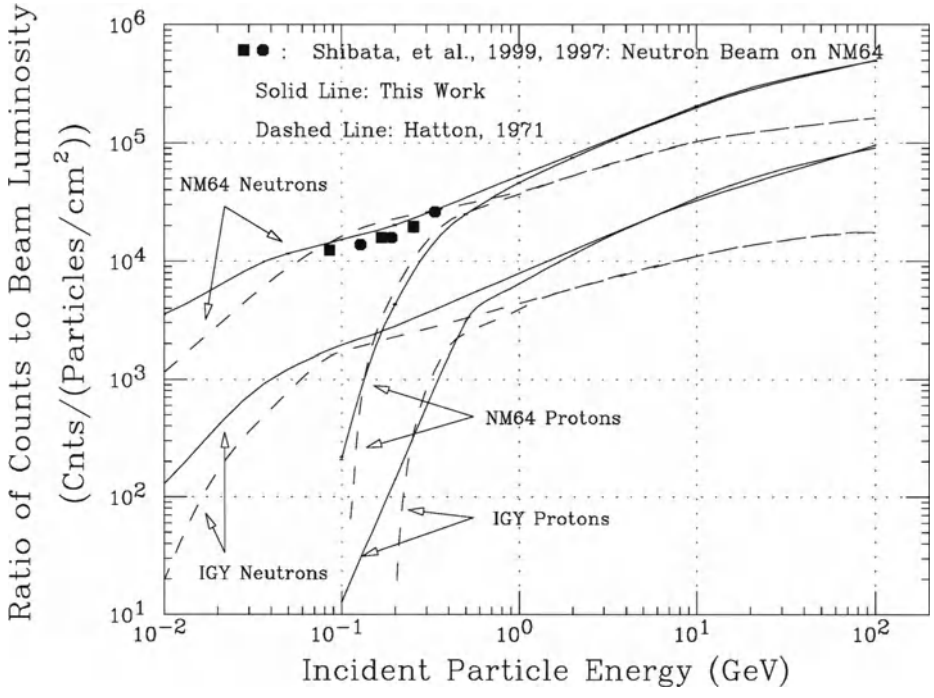

Fig. 4.4.20. Comparison of detection efficiency for neutrons and protons between NM-IQSY (or NM-64) and NM-IGY, expected according Clem (1999) – solid lines. Also shown is a comparison with calculations of Hatton (1971) – dashed lines. Full squares and full circles correspond respectively to detection efficiency for neutrons measured by neutron beam from accelerator for NM-64 by Shibata et al. (1999, 1997). From Clem (1999).

From Fig. 4.4.20 follows that: 1) both calculations of Clem (1999) and Hatton (1971) show that the detection efficiency for neutrons and protons for NM-IQSY (or NM-64) is much higher than for NM-IGY; 2) both calculations of Clem (1999) and Hatton (1971) show that the detection efficiency for neutrons and protons at $E_k \geq 1$ GeV is about the same, but for smaller energy detection efficiency for neutrons is much higher than for protons, 3) for neutrons the significant difference in the detection efficiency between Clem (1999) and Hatton (1971) lies in the energy regions $E_k \leq 60$ MeV (Clem's detection efficiency is higher than Hatton's, and this difference increases as neutron energy decreases, so at $E_k \approx 10$ MeV Clem's detection efficiency is higher than Hatton's by 2 times for NM-IQSY and 6 times for NM-IGY) and $E_k \geq 500$ MeV (Clem's detection efficiency again is higher than Hatton's, and this difference increases with neutron energy increases, so at $E_k \approx 100$ GeV Clem's detection efficiency is higher than Hatton's by 3 times for NM-IQSY and 5 times for NM-IGY), 4) only in region of neutrons $70\ \text{MeV} \leq E_k \leq 400\ \text{MeV}$ Clem's detection efficiency for NM-IQSY is

expected to be about the same as Hatton's, and ,namely, in this energy region was the experiment of Shibata et al. (1997, 1999) carried out. It can be seen in Fig. 4.4.14 that theoretical and experimental results are in good coincidence.

Let us note that the recent experimental checking of the neutron detection efficiency for NM-IQSY was made by the neutron beam from accelerator RCNP using the reaction Li(*p*,*n*)Be for neutron production (Shibata et el., 1997, 1999). Shown in Fig. 4.4.21 is the experimental scheme, and in Fig. 4.4.20 the comparison of experimental results with theoretical calculations of Clem (1999) and Hatton (1971).

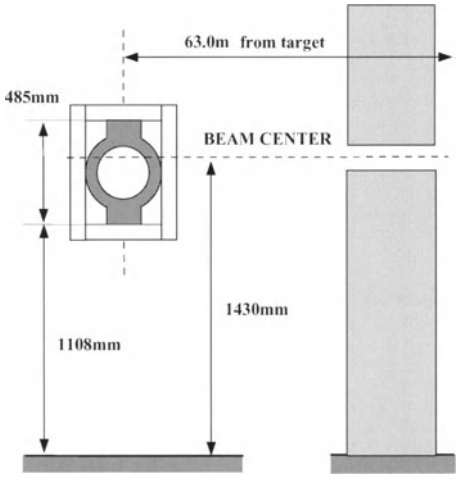

Fig. 4.4.21. The experimental scheme for NM-IQSY calibration. According to Shibata et al. (1999).

4.4.13. Comparison of detection efficiency of NM-IQSY with different neutron counters

In Section 4.4.8 we described the possibility of using in NM-IQSY neutron counters filled with ^{3}He. Table 4.4.5 summarizes the physical characteristics of the standard neutron counters BP-28 developed in Canada (or NM-15 developed in former USSR) filled by gas $^{10}BF_3$ and used widely in NM-IQSY (NM-64), of the new counters filled with ^{3}He, and of the neutron counters used in the NM-IGY. monitors.

Table 4.4.5. Physical characteristics of three types of neutron counters. According to Pyle et al. (1999).

	NM-64 Monitors		IGY Monitors
	BP-28	LND25373	NW G-15-34A
Diameter (cm)	14.8	4.8	3.8
Length (cm)	191	191	87
Gas Type	BF_3, 96% ^{10}B	97% ^3He + 3% CO_2	BF_3, 96% ^{10}B
Operating Voltage	2800V	1350V	1950V
Pressure (mm-Hg)	200	3040	450
Thermal Neutron Absorption Pathlength (cm)	41.0	1.9	18.2

Let us remember that in a NM, incident neutrons and neutrons generated in lead became thermal very soon (after few tens of collisions). From Table 4.4.5 it can be seen that for ^{3}He counters the absorption transport path of thermal neutrons is about 2.5 times smaller than the diameter of counter; for $^{10}BF_3$ counters the situation is reversed: the absorption transport path is bigger by about a factor of 3 (for NM-IQSY) or 5 (for NM-IGY) than the diameter of neutron counters. This is the main reason why the ^{3}He counters are so effective. Fig. 4.4.22 displays the comparison between the calculated detection efficiency of NM-IQSY based on standard neutron counters filled with $^{10}BF_3$ and based on neutron counters filled with ^{3}He for vertical incident neutron and proton beams (Clem,1999, Clem and Dorman, 2000) .

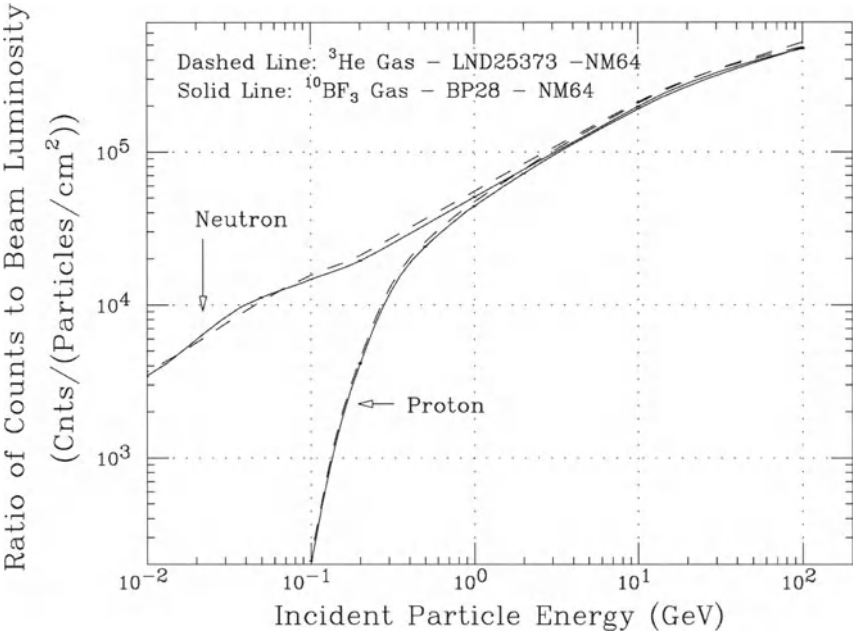

Fig. 4.4.22. Comparison between the detection efficiency for vertical incident neutron and proton beams of NM-IQSY (NM-64) based on standard neutron counters BP-28 filled with $^{10}BF_3$ (solid lines) and based on neutron counters LND25373 filled with ^{3}He (dashed lines), as calculated in Clem (1999), Clem and Dorman (2000) .

From Fig 4.4.22 it can be seen that the calculated ^{3}He NM-IQSY response is systemically slightly higher. Pyle et al. (1999) reported preliminary results from a recent latitude survey in which one of the monitor's three $^{10}BF_3$ neutron counters was replaced with a ^{3}He counter. This counter was operated during the voyage during the period November 1998 to April 1999 from Hawaii to McMurdo and then to Seattle (this is the first latitude survey using a ^{3}He counter in NM-IQSY instead of usually used $^{10}BF_3$ neutron counter). It was found that the dependence of intensity on cut off rigidity in the interval 0–17.4 GV is identical for both types of counters (in agreement with the results shown in Fig. 4.4.22), but the measured response of ^{3}He NM-IQSY is about 5% higher than predict theoretically (the cause of this small discrepancy is not clear; further details of the latitude survey data will be considered in Dorman, M2005).

4.4.14. The high latitude NM network as a basis of the 'Spaceship Earth' concept

Bieber and Evenson (1995) described the concept of 'Spaceship Earth' in which 11 high latitude NM are upgraded, redeployed, or newly constructed to establish a network with optimal directional sensitivity for the detection of transients such as GLE (Ground Level Enhancements of solar CR), Forbush decreases and precursory effects, as CR anisotropies. Nine of these NM have narrow cones of acceptance evenly spaced along the equatorial plane (important for continuous monitoring of CR daily and semi-daily anisotropy), while the Thule and McMurdo NM cover the North and South polar directions, respectively (important for continuous monitoring of North–South CR anisotropy). All these NM have the same (atmospherically determined) low cut off rigidity, which makes it particularly simple to reconstruct the free space density distribution function of any event. It is important that the NM responds to primary CR particles above a certain effective threshold rigidity: for mid latitude and low latitude stations this threshold is the geomagnetic cut off, but at high latitudes the geomagnetic cut off becomes very small, and the real threshold is governed instead by atmospheric absorption (see Fig. 4.4.23, which compares the relative response of Mawson, Antarctica, $R_c = 0.19$ GV with Newark, USA, $R_c = 2.08$ GV for a typical solar particle spectrum $D_S(R) \propto R^{-5}$).

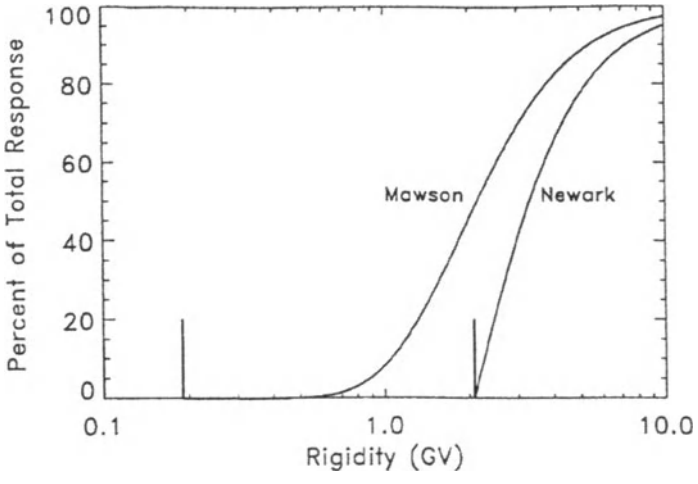

Fig. 4.4.23. Detector response as a function of rigidity for NM in Newark $(R_c = 2.08\ \text{GV})$ and Mawson $(R_c = 0.19\ \text{GV})$. Vertical lines indicate geomagnetic cut off rigidities. According to Bieber and Evenson (1995).

The relative response $F_i(R, R_c, D_S)$ of any CR component i to $D_S(R)$ can be determined as

$$F_i(R, R_c, h, D_S) = \int_{R_c}^{R} D_S(R) m_i(R,h) dR \left(\int_{R_c}^{\infty} D_S(R) m_i(R,h) dR \right)^{-1}, \qquad (4.4.7)$$

where $m_i(R,h)$ is integral multiplicity. Shifting the geomagnetic cut off within the range 0 to 0.6 GV has little effect on the NM response to solar particles. As a result all high latitude NM located near the sea level have nearly identical energy responses. It is also important to note that the atmosphere masks the near cut off region where CR asymptotic directions vary rapidly with energy. As a result high latitude monitors have much more confined viewing directions them mid or low latitude monitors.

To quantify this effect Bieber and Evenson (1995) define 'percentile rigidities' from the solar particle response. For example, the 10 percentile rigidity for Newark is 2.26 GV, the rigidity at which the 'Newark' curve in Fig. 4.4.23 rises above 10 percent. In Fig. 4.4.24 on a map of Earth's surface are plotted the viewing directions corresponding to the 10, 20, ..., and 90 percentile rigidities for CR vertically incident over 12 high latitude stations (geomagnetic cut offs below 1 GV), as well as two representative mid latitude stations (Newark in USA and Irkutsk in Russia).

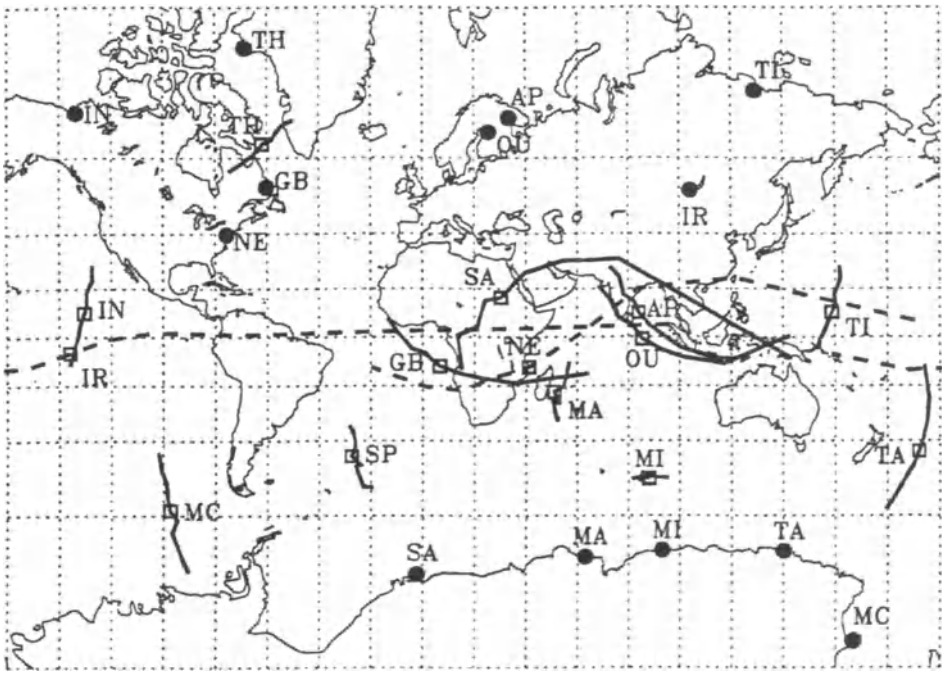

Fig. 4.4.24. Viewing directions of twelve high latitude neutron monitor stations (solid) and two mid latitude stations (dashed). The spread of viewing directions for each station encompasses the central 80% of the detector energy response to a typical solar particle spectrum. Squares denote asymptotic direction of median rigidity. According to Bieber and Evenson (1995).

Viewing directions plotted in Fig. 4.4.24 were computed for 1989 Day 272 at 13.30 UT using a trajectory code based on the Tsyganenko (1989) magnetosphere model according to Bieber et al. (1992). To characterize a stations angular resolution the angle between viewing directions of the 10 percentile and 90 percentile rigidities was computed. The advantages of high latitude sites for studying CR angular distributions are readily apparent in Fig. 4.4.24. Viewing directions for Newark (NE) spread over

more than half of Earth's circumference, and those for Irkutsk (IR) nearly circle the globe between the 10 and 90 percentile rigidities. In contrast, the high latitude stations have much more confined viewing directions. For the 8 stations with geomagnetic cut offs below 0.2 GV the angular resolution ranges from 9° to 48°, which compares favorably with the angular resolution typically achieved by modern particle detectors flown aboard spacecraft. Five of the stations with cut off below 0.2 GV are in Antarctica. As a result viewing directions towards southern mid latitudes are well covered by the existing neutron monitor network.

In contrast, coverage of the crucial equatorial region is seriously flawed. Large gaps pervade the western hemisphere, while stations viewing the eastern hemisphere have overlapping viewing directions, and, in many cases, comparatively poor angular resolution. Capabilities of the worldwide NM network could be greatly enhanced by rationalizing the distribution of monitor sites. One possible scenario is shown in Fig. 4.4.25, which depicts a 9 station network comprising Inuvik, Canada (IN), Tixie Bay, Russia (TI), and 7 new stations as follows: Uranium City, Canada (UC), Winisk, Canada (WI), Nutak, Canada (NU), Isafjördur, Iceland (IS), Elvebakken, Norway (EL), Napalkovo, Russia (NA), and Pevek, Russia (PE).

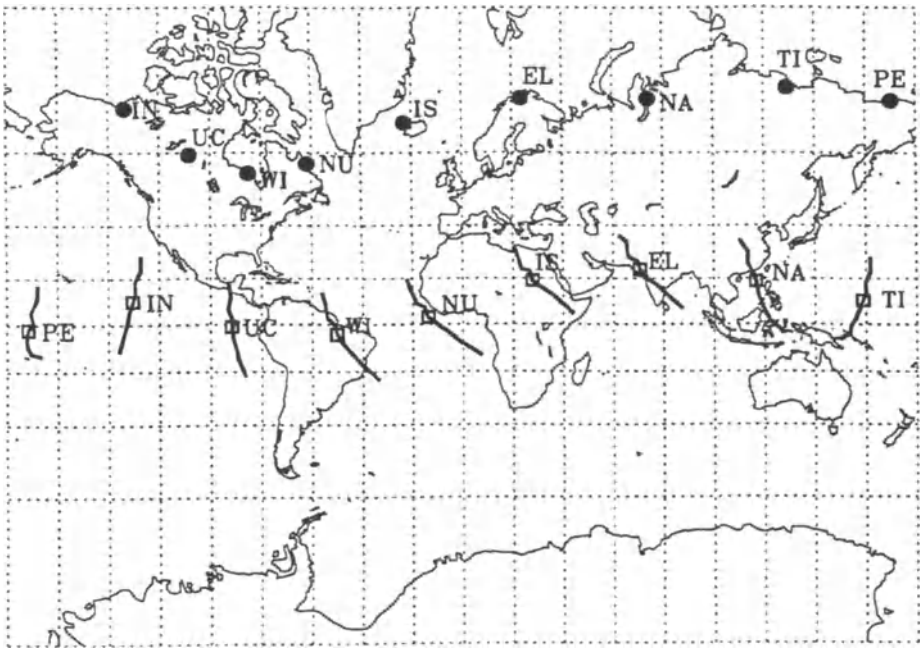

Fig. 4.4.25. Viewing directions for proposed network of Arctic/Subarctic high latitude NM. Angular resolution is better than 44° for all stations. According to Bieber and Evenson (1995).

According to Bieber and Evenson (1995), features of the proposed Arctic/Subarctic network include:

- excellent, nearly uniform, angular resolution ranging from 31° to 44°;

• viewing directions of median (50 percentile) rigidity spaced no more than 46° apart; and
• all stations view (median rigidity) within 24° of the equatorial plane.

The proposed network would thus provide a high resolution measurement of the equatorial angular distribution during CR events. Together with data returned by Thule and the Antarctic stations, we would then have highly sophisticated 'snapshot' observations of 3-dimensional CR fluxes with a degree of accuracy and completeness surpassing those provided by existing spacecraft detectors.

4.4.15. Inter-calibration of the NM worldwide network

As it was shown in Moraal et al. (2000, 2001), significant improvement can be realized if individual NM at different cut off rigidities can be calibrated against one another. The inter-calibration of stationary NM has been an implicit aim of many latitude surveys: when the latitudinal (or cut off rigidity) and altitude response of NM is known with sufficient accuracy, the counting rate of a stationary NM can be calibrated against that response function. The Italian group pursued this inter-calibration the furthest by actually transporting a NM to several European stations during 1963. From the results, described in Bachelet et al. (1972), it seems that the inherent accuracy of individual counting rates could be determined to about ±1%. The uncertainties in such an inter-calibration are mainly owed to: (a) different responses to primary intensity variations of NM of different design, (b) different atmospheric (pressure and temperature) responses of the NM, and (c) environmental differences. These systematic uncertainties are estimated to be about 0.2%. The statistical uncertainty of the calibration will be smaller than this if the calibrator counts at least 250,000 events per calibration. If this accuracy can be achieved, CR spectra can be determined from inter-calibrated NM counting rates down to 1.4 GV, which is equivalent to kinetic energy 740 MeV protons, and 230 MeV/nucleon fully stripped CR nuclei. This lower limit decreases to 600 MeV protons if the accuracy of inter-calibration is doubled to 0.1%. Typical space detectors, such as those on the Pioneer 10 and 11, Voyager 1 and 2, and IMP 8 spacecraft have proton channels up to 200 MeV and Helium channels up to 500 MeV/nucleon. This means that spectra deduced from NM would be entirely complementary to those measured in space. Good examples are: the crossovers in spectra, described by Reinecke et al. (1997), the analysis of Ground Level Enhancements by Lovell et al. (1998), determination of spectra variation (Bieber et al, 1995).

According to Krüger et al. (2003), two special calibration NM were completed in September 2002, with the following final design: the counter is a ^{3}He filled tube of the type LND25382, 51 mm in diameter and 652 mm long. It is surrounded by a polyethylene moderator with inner and outer diameters of 60.5 and 99.5 mm, a lead producer with diameters 101 and 193 mm, and finally an outer reflector with diameters 194 and 350 mm. All these cylinders are 653 mm long. The front and back of the counter are covered with 50 mm polyethylene ends with a diameter of 350 mm. The total active length of the monitor therefore is 653 + 100 = 753 mm. Its mass is 201 kg, of which 145 kg is lead. It rests on a cradle with storable wheels, and the total mass with cradle is 223 kg. The first calibrator was sent together with the US/Australian 3NM64 neutron monitor on a voyage by the US Coast Guard vessel Polar Sea between Seattle and McMurdo, Antarctica, from 4 November, 2002 until 19 April, 2003. The primary reason for this survey was to measure the latitude response of the calibrator against that of a

standard 3-counter NM64. Numerical simulations with the Fluka code, described in Clem and Dorman (2000), indicate that the counting ratio between the monitors may change as much as 3% from equator to pole, due to their different energy responses. The average hourly count rates of the two NM are shown as function of time in Fig.4.4.26 (panel A), starting on day 308 (4 November 2002), until day 473 (18 April 2003) for the calibrator, and day 482 (27 April 2003) for the 3NM64. The upper curve is for the 3NM64, and the bottom one for the calibrator. The ship departed from Seattle (cutoff rigidity $R_c \approx 2$ GV) on day 308, crossed the CR equator (maximum $R_c \approx 15.5$ GV) on day 332, and arrived at McMurdo, Antarctica at $R_c < 1$ GV on day 350. The return voyage started on day 427, crossed the CR equator again on day 461, and arrived back in Seattle on day 474.

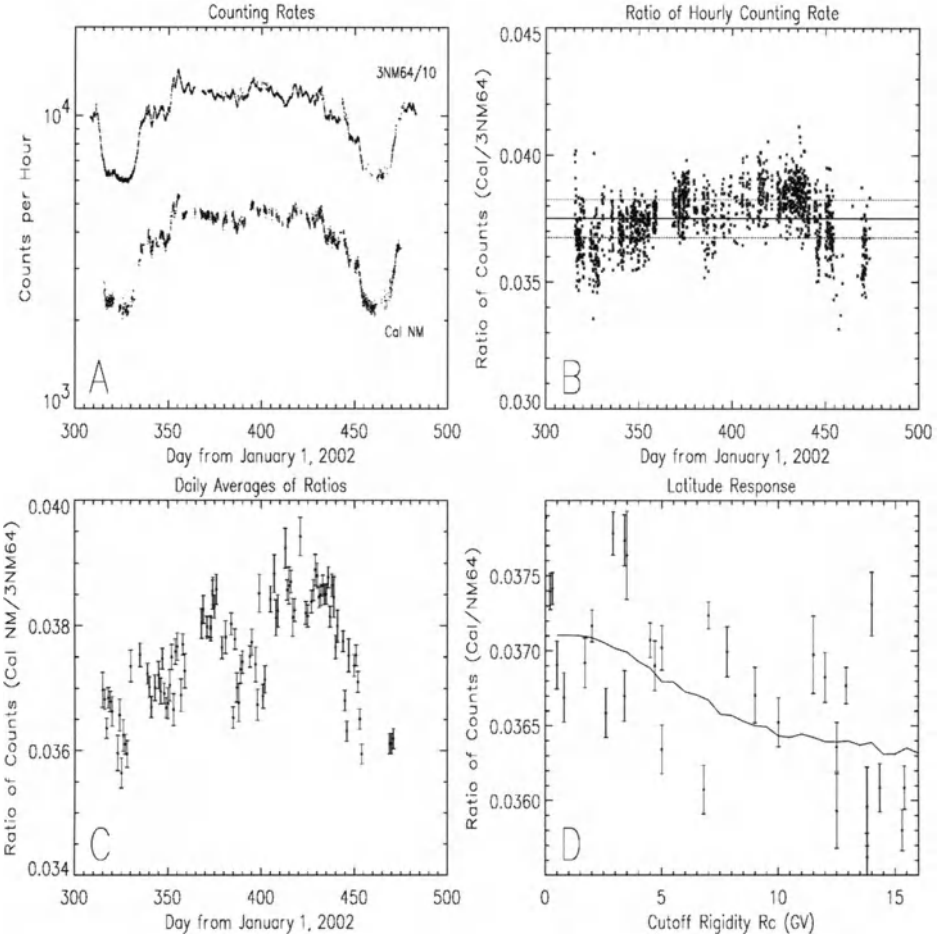

Fig. 4.4.26. Performance of the calibration NM on its voyage to Antarctica from 4 November 2002 (day 308), until 18 April 2003 (day 473). Panel A: Counting rates of 3NM64 (divided by 10), and calibrator. Panel B: Counting ratios on an hourly basis. Panel C: Daily averages of counting ratios. Panel D: Ratios as function of estimated (see text) cutoff rigidity. The line is the ratio calculated from the Fluka simulation of the calibrator. According to Krüger et al. (2003),

Panel B in Fig. 4.4.26 shows the ratio of these count rates. The overall average value is 0.0375± 0.0007, or an inverse 3NM64/Calibrator ratio of 26.7 ± 0.5. The Panel C in Fig. 4.4.26 shows the daily averages of these ratios, with the error bars calculated from the number of completed hours for that particular day. Finally, the ratios are binned into rigidity intervals in Panel D. The curve in Panel D of Fig. 4.4.26 shows the calculated ratio for these two monitors, with the Fluka code and Monte Carlo processing, described in Clem (1999).

Krüger et al. (2003) came to conclusion that the first voyage of the NM calibrator was successful: the average, overall ratio of calibrator counts/3NM64 counts is 0.0375 ± 0.0007, with an inverse ratio of 26.7 ±0.5; there is evidence that this ratio is latitude dependent as predicted. (this indicates that the physical processes of the calibrator are adequately understood; the experimental errors are still too big, so it needs additional more exact latitude surveys). The uncertainties on the observed ratios are too large for a firm final conclusion, however. This requires that the calibrator will have to make at least one more trip to Antarctica during 2003/2004.

According to Moraal et al. (2003), the second calibration NM from completed in September 2002 was used to calibrate in details the Sanae NM and preliminary the Hermanus NM. The Sanae NM is a 6 counter standard NM64 design, built inside the SANAE base of the South African National Antarctic Programme at Vesleskarvet, Antarctica. It is 1220 m above sea level, at geographic coordinates 71° S, 2° W, and at cutoff rigidity 0.79 GV. Nine calibrations of approximately 1 million counts each were done in three different positions (two inside the base and one – outside) between 19 December 2002 and 2 February 2003. Three calibrations were done in each of these three positions to test repeatability. As result, the Sanae NM was successfully calibrated, and its normalization is 50.845 ± 0.102 times the calibration standard. For eventual comparison with other NM of worldwide network, the calibrator's NM absolute count rate at that point must be increased with 1.91% to correct for the roof of the base. The calibrator was brought to the Hermanus NM for a calibration from 14 February until 6 May 2003. The preliminary result is that the 12NM64 monitor at Hermanus counts 106.84 times more than the calibrator. Moraal et al. (2003) supposed to calibrate in near future many NM of worldwide network.

4.5. Equipments for investigation of very high energy CR

4.5.1. Initial EAS equipments and research

Intensity variations of CR of super-high energy can be most efficiently studied from data on the frequency of extensive air showers (EAS), which cover areas exceeding many times the effective area of the detectors and thus give satisfactory statistics even for particles of very high energies. One such instrument was developed for the purpose of continuous recording by Krasil'nikov (1959a, 1960) in Yakutsk. The largest distance L between groups of counters with areas σ = 1/6, 1/2, and 1 m^2 is 80 m; by choosing various types of coincidences EAS can be recorded with numbers of particles from 1.5×10^4 (frequency about 330 per hour) to 2×10^6 (about 0.6 per hour). With the aid of this apparatus the barometric and temperature effects have been investigated in detail

(Krasil'nikov, 1958, 1959a) and also solar daily and sidereal daily variations (Krasil'nikov, 1959b).

Valuable data about time variations of the EAS frequency have also been obtained by means of other instruments, in particular, by a series of instruments of M.I.T. (Rossi, 1959): 'Kodaikanal' with linear dimensions L = 36 m and detector area σ =0.1 m^2, 'Agassiz' with L = 500 m and σ = 0.9 m^2, 'Alto' with L = 700 m and σ = 0.9 m^2, 'Vulcan R' with L = 2 km and σ = 3.5 m^2).

Large-area scintillation counters, described above in Section 4.3, are also extremely useful as detectors for recording EAS. In particular, valuable data about composition and spectrum of primary CR in very high-energy region were obtained with the complex apparatus in Moscow (Vernov et al., 1964) in which, besides detectors with Geiger counters, also 20 scintillation counters with area 0.5 m^2, 240 ionization chambers, etc. are used.

For continuously recording EAS the phenomenon of Cherenkov radiation of the showers upon their passing through the terrestrial atmosphere may also be used. Such an apparatus, containing ten light detectors of Cherenkov radiation and several hodoscopes with Geiger counters has been constructed by Chudakov et al. (1959). It permits recording of EAS with a number of particles from 2×10^4 to 1.3×10^7. An analogous instrument recording the Cherenkov radiation from EAS against the background of the light of the night sky was developed by Hill and Porter (1961). A detailed analysis of the problems of generation and recording of Cherenkov radiation of EAS was given by Jelley (1967).

A large apparatus was built near Sydney (Winn, 1966). It records EAS generated by primary particles with energies > 10^{18} eV. In the first stage the apparatus covers an area about 25 km^2 and consists of 25 separate stations. At each station 2 large plastic detectors are used as detectors. It is intended to increase the area afterwards to 260 km^2 (100 pairs of scintillators). Information about the EAS parameters will be recorded on a magnetic tape and be processed by a computer.

In the former Soviet Union near Yakutsk (Vernov et al., 1965) an apparatus with similar parameters has been established. In these instruments for measuring the total energy of the showers it is proposed to detect also the visual Cherenkov radiation. A very promising approach is also the detection of the polarized radio emission from showers formed in the atmosphere in the geomagnetic field. Pulses lasting < 0.15 μsec at wavelengths 6.8 and 2 m have been observed from showers with number of particles about 5×10^6 (Smith et al., 1965).

Analogues EAS complex installation at the Tyan-Shan Alpine station (3,340 m above sea level, near Alma Ata) is designed for the study of the interaction of the nuclear active particles and muons with the lead nucleons at energies above 10^{12} eV and of the interaction of nucleons with the nuclei of the atoms of air at energies of 10^{13}–10^{16} eV, for investigation of EAS properties and different type of CR variations (Erlykin et al., 1969). Fig. 4.5.1 shows the disposition of many types of detectors of this very effective EAS installation. The main part of EAS installation at the Tyan-Shan Alpine station is the large-size ionization calorimeter (surface 36 sq. m) which consists of 14 trains of ionization chambers (96 chambers per train) interlaid with 5 cm lead plates. Between the 1st and the 2nd trains, and between the 6th and the 7th trains, X-ray film magazines are

placed, covering the whole surface of the calorimeter. The calorimeter and the films are used for the investigation of the high energy nuclear active particles properties. The upper train of the calorimeter is shielded with 2.5 cm thick lead and it will allow the energy characteristics of the photon electronic component of the showers to be studied.

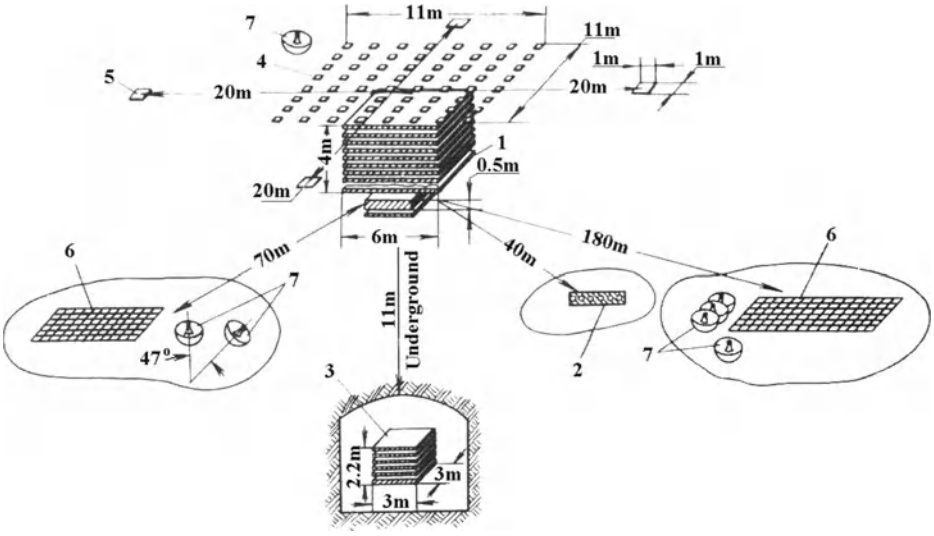

Fig. 4.5.1. The EAS installation at the Tyan-Shan Alpine station (see description in text).

The EAS installation shown in Fig. 4.5.1 includes beside described above the large-size ionization calorimeter (1), also:

(2) Standard NM-IQSY, placed at 40 m from the centre of the large calorimeter, serving as detector of the low-energy nuclear-active particles in the extensive air showers. It allows evaluating the total number of particles in a shower.

(3) Small size ionization calorimeter (surface 9 sq. m) that is installed underground at the depth of 11 m under the large calorimeter. It consists of 15 trains of ionization chambers (24 chambers on each train). The lead layers between the trains are 2.5 cm and 5 cm thick, depending on the experiment. This calorimeter is intended for the study of the muon component of the cosmic radiation.

(4) Central tray of scintillation counters, arranged above the calorimeter and covering the surface of 130 sq. m, consisting of 64 scintillation counters, 0.25 sq. m each. This tray is used to investigate the spatial distribution of the photon-electronic component near the core of the shower and to determine the point where the particles cross the axis and the complete number of the particles in low-power showers.

(5) Four scintillation counters, 1 sq. m each, placed at the corners of a square, 20 m from the centre of the calorimeter. These are used to measure the slope of the shower core.

(6) A block of peripheral scintillation counters, covering 16 sq. m, placed at the distance of 70 m from the centre. It serves to measure the total number N of particles at the observation level in showers with $N > 10^5$.

(7) Detectors of the Cherenkov radiation produced by shower particles in the atmosphere, placed at the distances of 10 m, 70 m and 180 m from the centre of the

calorimeter. Multiplier phototubes are used as light detectors; their sensitivity is enhanced with parabolic mirrors, 1.5 m in diameter. With the aid of the detectors data on the energy and the nature of showers evolving in the atmosphere will be collected.

4.5.2. Recent and planned EAS experiments for CR research in extremely high energy range

MILAGRO experiment

Milagro is the first detector designed to study air showers at energies near 1 TeV using Cherenkov techniques in water (McCullough et al., 1999). The detector is built in the Jemez Mountains near Los Alamos, New Mexico at an altitude of 2,650 m. The pond, which is 60m×80m×8m, is filled with clean water, covered with a light barrier and instrumented with 723 of 20 cm PMT's. The PMTs collect Cherenkov light produced by the shower particles which traverse the detector's water volume. Whenever a PMT pulse exceeds a preset discriminator threshold a multihit time–to–digital converter (TDC) is started. Each PMT has its own TDC which is capable of recording up to 16 discriminator level crossings per event with 0.5 ns resolution. These constitute the raw data from the PMT.

As it was shown in Gisler et al. (1995), Ahluwalia et al. (1996), Milagro can be effectively used also for research in solar and solar-terrestrial physics (high energy particles from solar flares and CR modulation effects in high energy region), for monitoring of space weather.

OWL–AIRWATCH experiment

According to Scarsi et al (1999), the OWL–AirWatch space mission, jointly supported by an Italian Consortium (Air Watch) and a US Consortium (OWL) with a possible extension to groups from Japan, is devoted to the imaging analysis of the UV atmospheric fluorescence induced by the Extreme Energy Cosmic Radiation ($E > 10^{19}$ eV). The objective is to obtain a detailed description of the CR energy spectrum at extremely high energies, together with a map of the arrival direction and to possibly open the channel of Cosmic Neutrino Astronomy in this energy range. The mission foresees a Midex class Free Flyer with a low ($H \sim 500$ km) circular near equatorial orbit and a target launch date around 2005.

LAAS Network Observation of Air Showers

According to Ochi et al. (1999) a network of air shower observations started in Japan. The network as a Large Area Air Shower (LAAS) group consists of eleven air shower arrays (stations), enclosing an area of 130,000 square kilometers (Fig. 4.5.2). Nine stations out of eleven are in operation, the remainders are under construction. Each station has 4–12 scintillation counters. Trigger conditions are different station-by-station; 2- to 8-fold coincidences are applied, yielding the trigger rates of (300–21000)/24h. Each station is equipped with the Global Positioning System as a common clock, so the arrival times of air showers can be recorded with an accuracy of one microsecond. By operating these stations simultaneously, the whole system can be regarded as a gigantic EAS detector, say, a cosmic ray interferometer. Ochi et al. (2003) note that the subjects which will be studying by this project include large-scale correlations in EAS, GRB-like

sporadic phenomena, extremely high energy CR around 10^{18} eV and large-scale atmospheric dynamics.

Fig. 4.5.2. The locations of eleven stations of the LAAS group. There are two stations in Kinki University.

Tibet-III Air Shower Array

The Tibet-III air shower array, which is still in the middle of construction, has been successfully operating at Yangbajing (4,300 m above sea level) since November of 1999 (Amenomori et al., 2001). In 2001, the Tibet-III array consisted of 533 scintillation detectors of each 0.5 m^2 (see Fig. 4.5.3 and Fig. 4.5.4). The threshold energy of observed air shower is estimated to be 1.5 TeV for protons, and the angular resolution is estimated to be $0.87 \pm 0.02°$ above 3 TeV using a Monte Carlo simulation. This angular resolution is well confirmed by observing the CR shadow produced by the Moon.

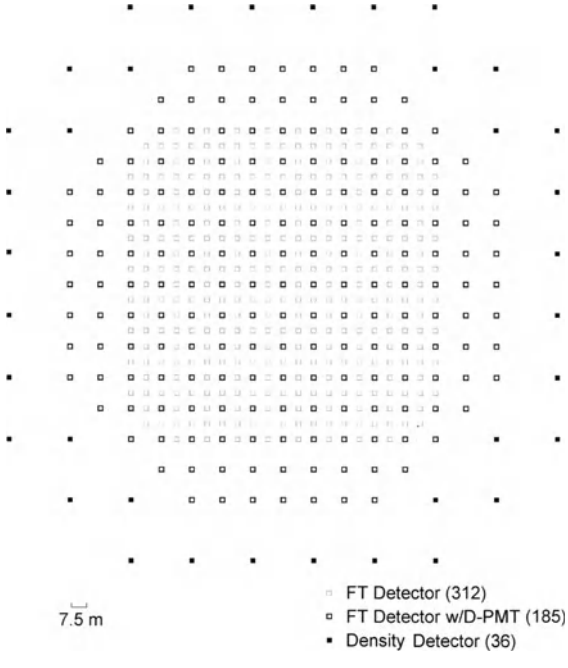

Fig. 4.5.3. The Tibet Air Shower Array in 2000. According to Amenomori et al. (2001).

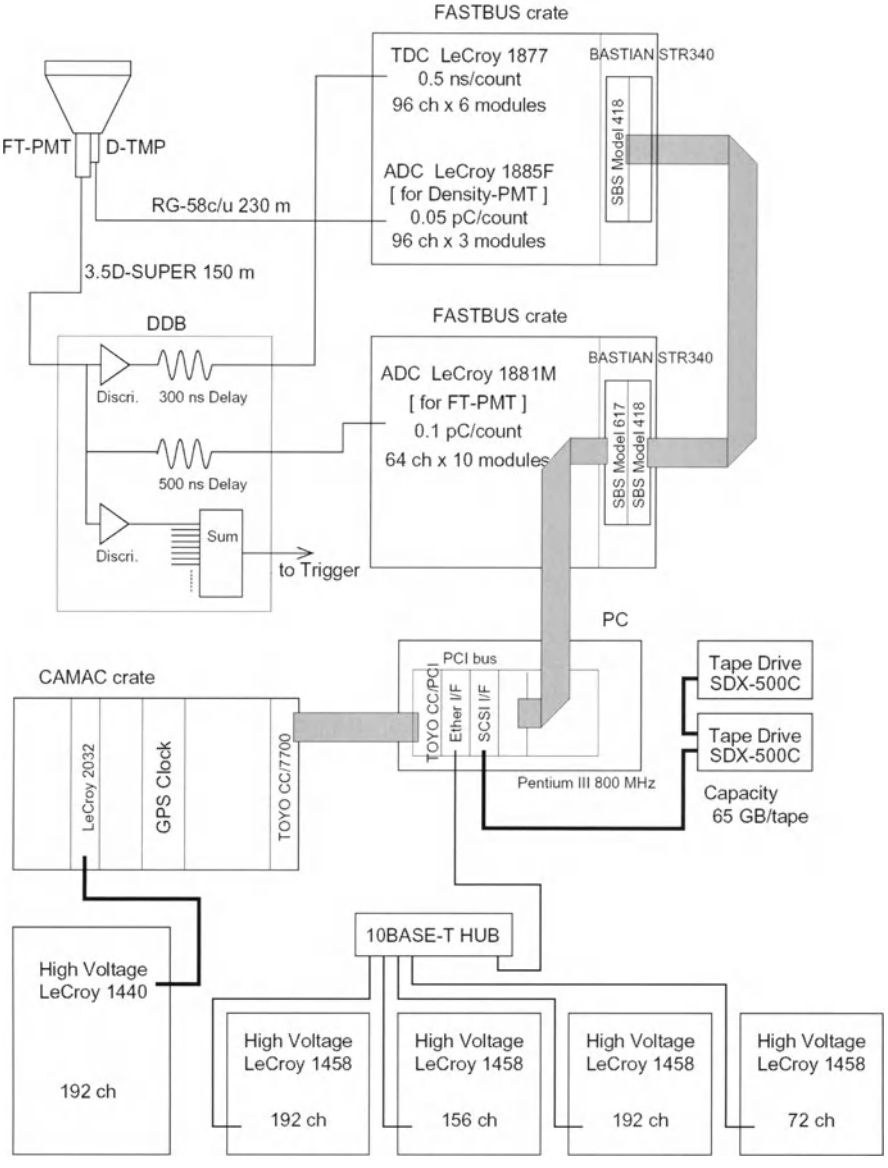

Fig. 4.5.4. Data acquisition system of the Tibet Air Shower Array. According to Amenomori et al. (2001).

TANGO Array I

The TANGO Array is an air shower experiment which has been recently constructed in Buenos Aires, Argentina (Bauleo et al., 2001). It became fully operational in September, 2000. The array consists of 4 water Cherenkov detector stations enclosing a geometrical area of about 30,000 m^2 and its design has been optimized for the observation of EAS produced by CR near the 'knee' energy region. Three of the

detectors have been constructed using 12,000 liter stainless steel tanks, and the fourth has been mounted in a smaller, 400 liter plastic container (see Fig. 4.5.5). The detectors are connected by cables to the data acquisition room, where a fully automatic system, which takes advantage of the features of a 4-channel digital oscilloscope, was set for data collection without the need of operator intervention. This automatic experiment control includes monitoring, data logging, and daily calibration of all stations.

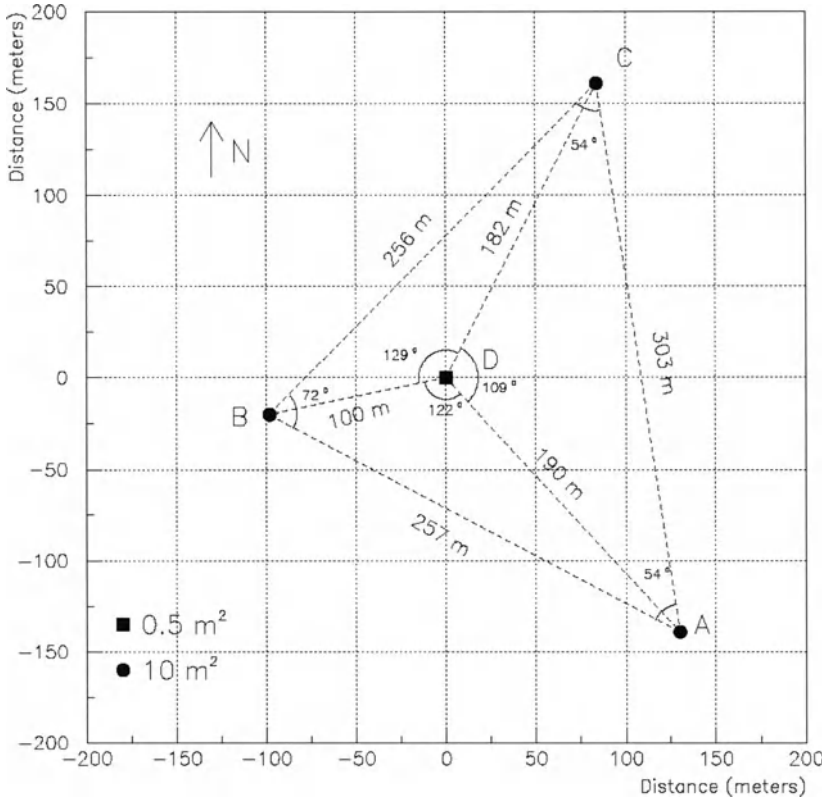

Fig. 4.5.5. TANGO Array Layout. Circles indicate the positions of the three 10 m^2 stations, whereas the square shows the position of the central, 0.5 m^2 detector. According to Bauleo et al. (2001).

Tunka EAS Cherenkov Array

Several years ago three groups began the construction of TUNKA Cherenkov EAS array (Budnev et al., 2001) in the Tunka Valley, 50 km to the west from the Lake Baikal (51.49° N, 103.04° E, at 680 m above sea level). Its purpose is the study of the energy spectrum, the chemical composition, and time variations of CR in the region of the 'knee' (3×10^{15} eV). The changes of the spectrum and composition in this region can play a key role in understanding of the galactic CR origin. The method of EAS Cherenkov light recording using the atmosphere of Earth as a huge calorimeter seems to be the most adequate one for studying the very high energy primary CR. TUNKA–13 array started data acquisition in 1996. It consisted of 13 phototubes (PMs) QUASAR–370 with 37 cm diameter photocathode, arranged within a square of 240 m side.

Auger Observatories for research of CR with E>10^{19} eV

According to Cronin (2001), the Pierre Auger Observatories will provide a comprehensive investigation of the nature and origin of CR with energies > 10^{19} eV. It is the greatest recent EAS Project. Sites in at Malargüe, Mendoza Provence, Argentina (southern hemisphere) and in Utah in the United States (northern hemisphere) have been chosen. The flux of CR is about 1/km^2/century/sr above 10^{20} eV so a large detection area of 3,000 km^2 has been chosen for each Observatory. As the first stage the Observatory in Argentina will be founded in near future (see Fig. 4.5.6).

Fig. 4.5.6. Layout of the Auger Observatory in Mendoza Province, Argentina. According to Cronin (2001).

The correct determination of the energy is of crucial importance so each observatory will detect the showers produced by the primary CR with both a surface array and by means of atmospheric fluorescence. There is a fine symbiosis between the two techniques. Coincidence timing between the surface detector (SD) and the fluorescence detector (FD) permits the precision of a single FD to be equivalent to a stereo view. Data from the FD permit the reconstruction of the core and direction of the shower with out appeal to density of particles observed in the SD. These are just a few examples of the advantages of a hybrid detector. The SD consists of a triangular grid of 1,600 water tanks spaced at a distance of 1.5 km. The tanks are 10 m^2 in area, 1.2 m deep and contain 12 metric tons of pure water. The tanks are lined with diffuse reflector and the Cherenkov light produced by the shower particles is detected by three 9″ photomultipliers placed on the upper surface of the tank looking downward. The large and steady flux of muons in the CR provides an easy calibration for each tank. The signals in each tank are expressed as Vertical Equivalent Muons (VEM) which is the light produced by a single muon passing vertically through the tank. The details of surface detectors are investigated by Mazur (2003), their triggering – by Szadkowski et al. (2003), calibration and monitoring – by Bertou (2003).

Table 4.5.1. Number of events per one year.

Energy eV	Surface $\geq$ 5 tanks	Hybrid $\geq$ 2 tanks + $\geq$ 1 FD
$\geq 6x10^{17}$	16000	45000
$\geq 10^{18}$	16000	30000
$\geq 3x10^{18}$	15000	4700
$\geq 10^{19}$	5200	520
$\geq 2x10^{19}$	1600	160
$\geq 5x10^{19}$	500	50
$\geq 10^{20}$	100	10
$\geq 2x10^{20}$	30	3
$\geq 5x10^{20}$	10	1

The surface array is fully efficient for CR with energy $\geq 10^{19}$ eV with zenith angles up to 60°. The FD consist of 30 units placed about the array so that all showers detected by the surface array will also be observed by at least one FD unit. Each FD unit covers from 1.7° to 30.3° in elevation and 30° in azimuth. Each pixel of the FD covers a hexagonal section of the sky of width 1.5°. The electronics in each tank of the SD is powered by solar panels. The relative timing of the arrival of the shower front is provided by GPS receivers and the data are sent to a central collection point by radio and microwave relay. The FD buildings are provided with power from the mains or by generators in remote areas. In Table 4.5.1 is shown expected number of events per one year operation in dependence of primary CR particle energy (according to Cronin, 2001).

The Telescope Array Project

The Telescope Array plans to deploy 10 large air fluorescence stations in the West desert of Utah covering the acceptance of 65,000 km^2sr with 10% duty factor (Aoki et al., 2001). It will be co-sited with the northern hemisphere Pierre Auger ground arrays of the similar exposure (see above the description of Pierre Auger Observatory in Argentina of the same type). The gamma ray primary will be identified with the modulation of the shower maximum; an elongation of the shower by the LPM effect and the north– south asymmetry by the geomagnetic cascade. A uniform detection of the air showers in the entire atmosphere will be most suited for the identification of the horizontal showers produced by the neutrinos. With a stereo reconstruction, an angular resolution of 0.6° is expected for the 10^{20}eV shower. The Telescope Array consists of 10 measurement stations, each separated by 30–40km, installed in the West Desert of USA, near Salt Lake City, Utah. At each station, 40 fixed telescopes covering a certain region of the sky are arranged in two concentric rings with a diameter of ~30m looking outward from the telescope housing as shown in Fig.4.5.7.

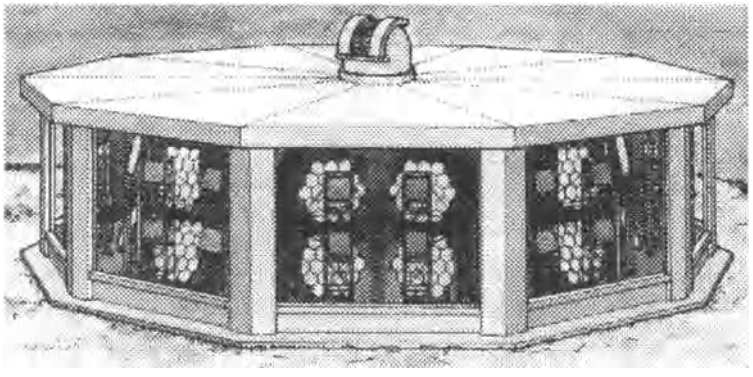

Fig. 4.5.7. Telescope Array station. According to Aoki et al. (2001).

Underground Multimuon Experiment

According to Enqvist et al. (2003) Underground Multimuon Experiment in Pyhäsalmi Mine (Finland) is preparing in order to observe simultaneous, multiple muon events originated from extensive air showers. The detection of the multimuon events is motivated by partly unknown composition and origin of the primary cosmic rays in the energy region of 10^{15} –10^{16} eV, i.e. the 'knee' region. The experiment will be carried out with two or three detector units of an area of about 100 m^2 each and with mutual separation of about 30 m (the existing free caverns in Pyhäsalmi Mine will be used. Detectors can be placed at different depths between 95 and 400 m (250–1000 m w.e.) for measuring different properties of the air shower. Detectors will consist of drift chambers formerly used in CERN as DELPHI barrel muon chambers (DELPHI-MUB); they have good enough spatial resolution (about 1 mm and 10 mm in horizontal directions) and can measure accurately the number and position of particles hitting the detectors. The DELPHI-MUB consisted of 1372 drift chambers arranged into 146 planks. About 100 planks are now available for the multimuon experiment. The active volume of each chamber is 20 cm wide, 1.6 cm high and 3.65 m long. The drift chambers operate in the proportional mode, with $Ar:CH_4:CO_2$ (90:5:5) nonflammable gas mixture. Each drift chamber can provide up to three signals, one anode signal and two delay line signals (near and far), which can be used to localize the points of particle passages through the chambers.

The ASHRA Detector

Aita et al. (2003) proposed a new air fluorescence and Cerenkov detector ASHRA (All-sky Survey High Resolution Air-shower telescope). The ASHRA observational station consists of 12 light collection telescopes covering entirely all sky with totally 80 mega pixels in the CMOS sensor arrays. The station site candidates are currently locations near the summits of the three mountains of Mauna Loa, Hualalai, and Mauna Kea on the Hawaii Big Island. In the first step, it is planning to install one full station including 12 telescopes at the site near the Mauna Loa summit and 4 telescopes in another station on the top of Hualalai which is distant from Mauna Loa by 35 km to start up all-sky survey for TeV gamma rays and precise measurement for arrival directions of extra high energy CR using stereo fluorescence technique (ASHRA-1). In the second step, enhancing the Hualalai site into one full station and installing one another station at the site on the higher side of Mauna Kea to complete the three full stations, will proceed to discovery and resolve higher energy phenomena in the Universe with lower flux (ASHRA-2). The telescope consists of four smaller sub-telescopes viewing the same field to ensure the high sensitivity and the cost-performance (Fig. 4.5.8).

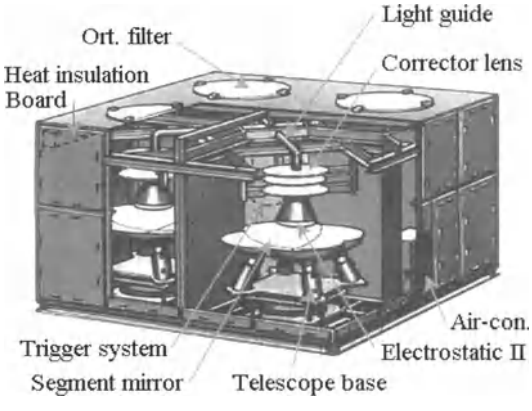

Fig. 4.5.8. The ASHRA telescope (it consists of four sub-telescopes viewing the same field). According to Aita et al. (2003).

KASCADE-Grande

According to Glasstetter et al. (2003) KASCADE-Grande extends the former KASCADE experiment by a large area scintillators array (0.5 km^2) for the detection of the charged component of extensive air showers. Its goal is to reconstruct the primary energy and composition of CR up to energies of 10^{18} eV thereby allowing a detailed investigation of the expected iron-knee. The former KASCADE has been extended by 37 new stations (Fig. 4.5.9). Each station contains a segmented 4 cm thick scintillator with a total detection area of 10 m^2. The stations are distributed over an area of 700×700 m^2 in a hexagonal grid with an average distance of 137 m.

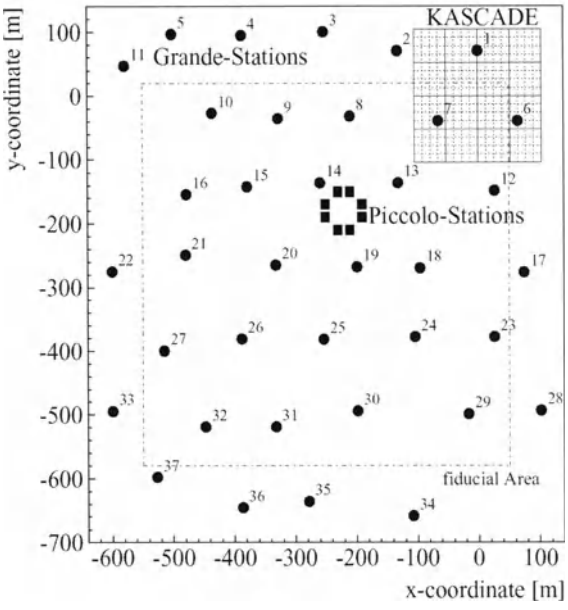

Fig. 4.5.9. Layout of the KASCADE-Grande experiment. According to Glasstetter et al. (2003)

Science-Education Experiment: Wide Area Small Air Showers Detection System Linked by Internet

Hamaguchi et al. (2003) developed an air shower detection system, consisting of widely distributed observational sites which are connected through the Internet. The obtained data at each site are exchanged in (quasi) real time. For science educational purposes, sites are set up at museums and schools. The system is intended to detect time-correlated air showers arriving over a wide area: possible existences of time correlated CR were first reported by Carrel and Martin (1994) and by Kitamura et al. (1997). According to Hamaguchi et al. (2003) each station consists of four scintillation counters, a data acquisition box (DA box) that has all the electronics for the station, a Windows PC, and a Global Positioning System (GPS) antenna, as shown in Fig. 4.5.10. Each counter is comprised of a pyramid-shaped vessel containing 70×70×4 cm^2 plastic scintillator at the bottom and a Hamamatsu H6410 2" Photo-Multiplier Tube (PMT) at the top. The counters are typically placed on the roof of the building at the square corners of an approximately 10×10 m^2. The DA box has four channels of ADCs and

TDCs, each having 12-bit resolution. Triggers are made of coincidences of hits in three out of four counters. The system can measure the trigger time with an accuracy of 1 μs. The electronic circuit is shown in Fig. 4.5.11.

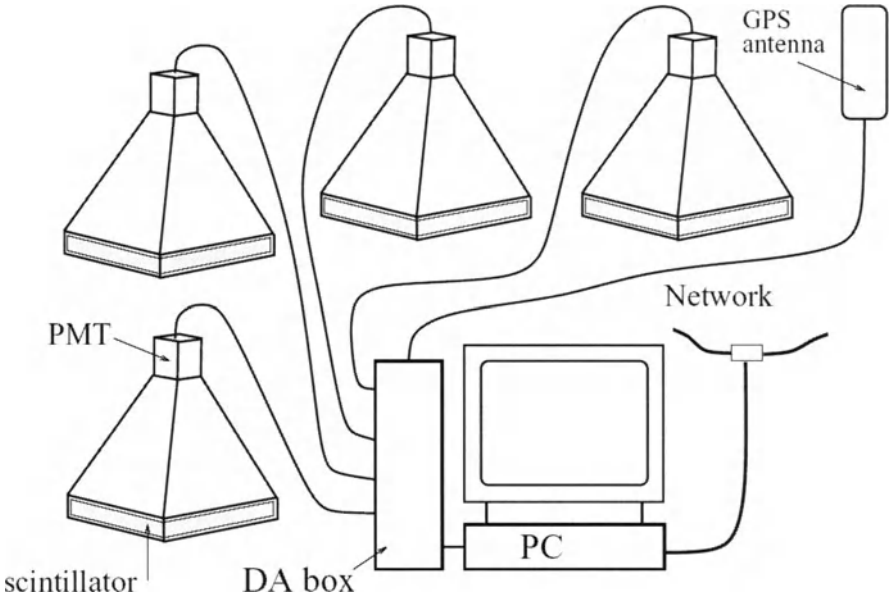

Fig.4.5.10. One standard station of the system. According to Hamaguchi et al. (2003).

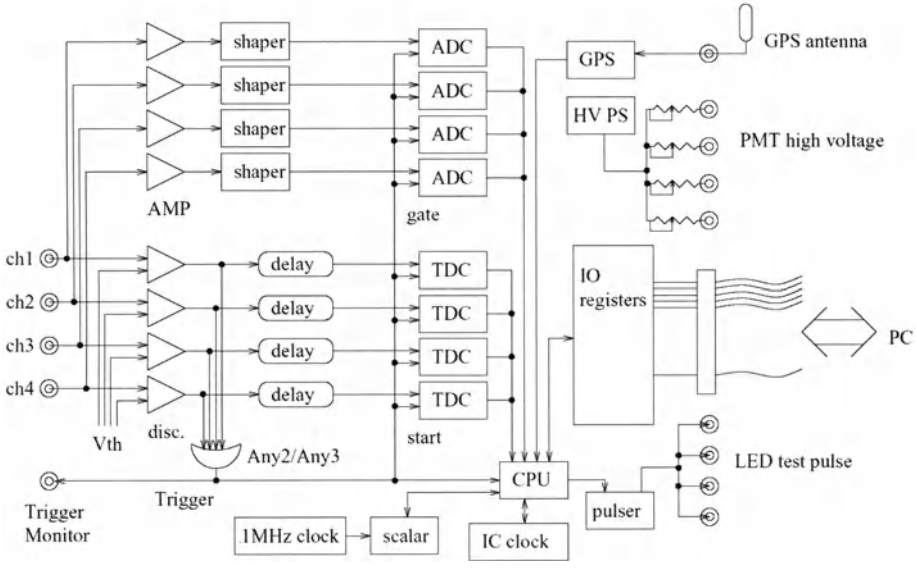

Fig. 4.5.11. Schematic of the electronics circuit. According to Hamaguchi et al. (2003).

4.6. CR experiments on aircrafts and balloons

4.6.1. The initial CR experiments on aircrafts

About 40–45 years ago the space distribution and time variations of CR were widely studied by measurements in aircraft at different altitudes by means of NM and telescopes for electron–photon and muon components with rather high accuracy. Thus, the instrument of Baradzei et al. (1961) at altitude 9 km had a statistical error for 5 minutes recording of 0.9%, 1.9% and 1.8%, respectively for the total ionizing, the muon and the neutron components (at 12 km these errors were 0.7%, 1.5% and 1.2%). By means of this instrument various CR modulation effects could be measured. Aircraft NM have been used by Sandström (1958) for determining the position of the CR equator, and by Coxell et al. (1966) for studying the planetary distribution of the geomagnetic cut off rigidities (for more details about these results see Dorman, M2005). The completely automatic three-sections aircraft NM have been developed by Bortnik and Granitskij (1967a,b), Bortnik et al. (1967). This aircraft NM, weighing about 300 kg, recorded also multiple neutrons. Granitskij and Bortnik (1968) developed combined aircraft detector containing NM and muon telescope, using as shield a lead neutron generator. A lot of such identical detectors were put in many airplanes and the rapid machine processing of the data of observation yield practically continuous information about the space distribution and the variations of CR intensity at various altitudes (Granitskij and Medvedev, 1968; Granitskij and Bortnik, 1968; Dorman et al., 1970).

4.6.2. Some example of recent aircraft CR experiments

According to Achenbach and Cobb (2001) the University of Oxford has started the design and development of the new experiment ADLER (Airborne Detector for Low Energy Rays). This apparatus will measure the CR muon flux at altitudes of 10–13 km. The detector should be flown by aircraft on transatlantic routes crossing the magnetic equator to investigate the flux at different geomagnetic latitudes. The method employed for distinguishing muons from other ionizing particles is the observation of delayed coincidences in an active absorber together with anti-coincidences in surrounding veto counters. The detector concept is similar to that developed by Conversi (1950), although scintillators are used in place of Geiger–Muller tubes. The dimensions of detector are $60\times85\times85$ cm^3 and the total weight including the inactive absorbers is about 350 kg. The detector will consist of three similar scintillator hodoscopes (see Fig. 4.6.1). Each hodoscope is composed of two planes of plastic scintillator bars. For the first one (S1) there are 16 strips of length 56 cm in each layer, while 8 strips of length 28 cm make up the second (S2) and third (S3). All strips are 3.5 cm wide by 2 cm thick. The maximum detectable zenith angle is defined by the hodoscopes S1 and S3 and amounts to 53.6°. The signals of the scintillators will be read out by the optical fibers to five small (3×3 cm^2) Hamamatsu multi-anode M16 (R5900) photomultiplier tubes operated at voltages of about 1,000 V. The total number of analogue channels is 96. The signal processing will be done by low powered electronics and a data acquisition system based on laptop PC. The trigger mode will be a coincidence of signals from the 3 hodoscopes together with an anti-coincidence of the veto counters. The time difference between trigger signal and delayed signal measures the decay time of the muon. The power consumption is about 30 Wt for the electronics and 20–30 Wt for the laptop.

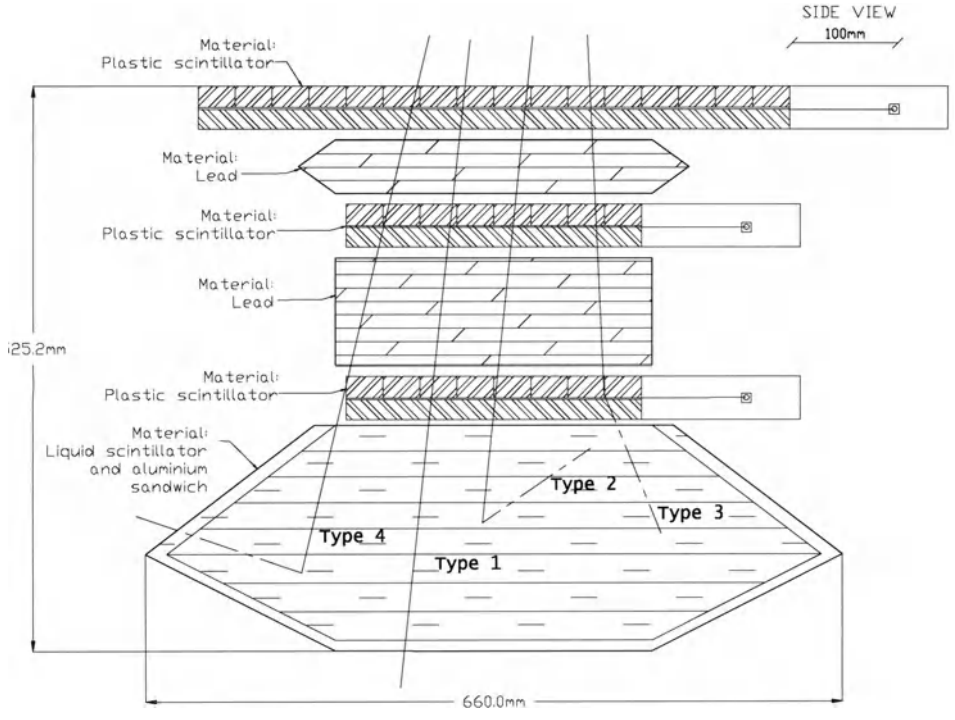

Fig. 4.6.1. Schematic drawing of the ADLER detector with a trapezoidal active absorber. Different types of particle tracks are distinguished by the timing of the detector response. Tracks of type originate from high energy muons, type 2 tracks originate from low energy muons which have stopped in the active absorber, type 3 tracks originate from muons which have stopped in the third trigger hodoscope and the decay electrons of type 4 tracks produce additional signals in one of the veto-counters and leave the active volume. According to Achenbach and Cobb (2001).

For measurements of the flux ratio of positive to negative muons, this provides important information on the interactions of the primary CR with nuclei in the atmosphere, capture of negative muons according to the reaction

$$\mu^- + p \rightarrow n + \nu_\mu \tag{4.6.1}$$

will be used in the ADLER experiment (Achenbach and Cobb, 2001). The positive excess is approximately 1.25 in the low energy range and most of the previous measurements have been carried out using magnetic deflection to determine the muon charge with simultaneous determination of the energy. Practically the entire energy liberated in this process is carried off by the neutrino and no signal will be produced in the detector. As a result the mean negative muon lifetime τ becomes

$$\tau^{-1} = \Lambda_c + \tau_\mu^{-1}, \tag{4.6.2}$$

where Λ_c is the capture probability and τ_μ the decay lifetime for a free muon. At Z = 11–12 the capture probability is almost equal to the decay probability, for iron (Z = 26) it is 90% of the total disappearance probability. For that reason the active absorber is designed flexible, making measurements with different absorbers (aluminum, steel, scintillator) possible. Thus the determination of the muon charge ratio will be achievable from a comparison of the total count rates.

4.6.3. The network of regular radio-balloon CR measurements

In the period of IGY in former USSR were organized regular (usually two times per day) CR observations on small meteorological balloons up to altitude about 35 km in Murmansk, near Moscow (in Dolgoprudnii), near Simferopol (in Crimea), and near Yakutsk. Later these regular observations were organized in Alma-Ata, Erevan, Apatity, Norilsk, and Tiksy. For these measurements two very simple detectors were developed: the first being RK-1 Geiger counter STS-6 for measurements of global intensity, and second RK-2, with weight 2.2 kg (together with the electrical battery) from two counter STS-6 (simultaneously measurements of global intensity from two separate counters and vertical intensity from double coincidences). These detectors were developed by Charakhchyan (1961). The detailed description is given also in Stozhkov (1980), Bazilevskaya and Svirzhevskaya (1998). These detectors were modernized for using near Yakutsk by Belomestnikh and Shafer (1958), and for using near Apatity by Lazutin and Franzus (1964). Asatrian et al. (1995) developed a detector for routine measurements on radio-balloons simultaneously charged CR component and neutron component (latter by small ^{3}He counter). Many regular measurements on balloons in the period of IGY were made by Winckler's group (Winckler, 1960) over Minneapolis (more than 60 flights in 1956–1958), near Guantanamo (Cuba), over Fairbanks (Alaska) and over Guam.

4.6.4. Special CR experiments on long duration balloons

Long duration balloon experiments can compete with satellite experiments in measuring the elemental energy spectra of high energy CR. They have many advantages including a much smaller cost per flight and the opportunity to repeat the flight a few times. The weight of an instrument can be relatively high (up to a few metric tons), size can be relatively large (~ 1×1 m^2) and there will be no obstructions in the geometry factor, which may be expected at the ISS (International Space Station) or other satellites and space probes. These advantages may compensate for the much smaller exposure time (2–4 weeks per single flight). Here we will consider shortly some examples of recent long duration balloon experiments (let us note that many long duration CR balloon experiments are used as prototypes for future satellite experiments).

SOFCAL

The **S**cintillating **O**ptical **F**iber **Cal**orimeter **(SOFCAL)** was designed by Christl et al. (1999) to measure the proton and helium spectra from 0.2 TeV to > 10 TeV, along with a limited number of heavier nuclei. SOFCAL is a hybrid instrument (see Fig. 4.6.2) that comprises a passive emulsion chamber with target and emulsion calorimeter and a thin ionization calorimeter utilizing scintillating fibers and lead plates (SciFiCal). The data for analysis was obtain from a 20-hour flight, from Ft. Sumner (New Mexiko) to Phoenix (Arizona) on May 20, 1997.

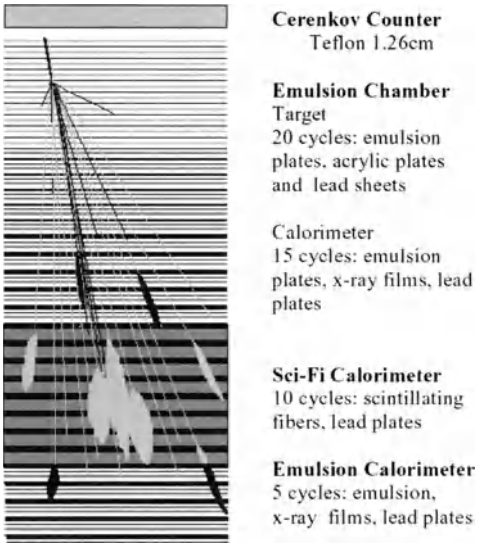

Fig. 4.6.2. SOFCAL configuration. According to Christl et al. (1999).

HEAT

The HEAT-pbar instrument (see Fig. 4.6.3) is designed by Bower et al. (1999) to detect the rare antiparticle species, antiprotons ($\bar{p}$) in the CR. The measurements of the $\bar{p}$ flux arriving near Earth serves as an important diagnostic tool for the understanding of the propagation of CR through the Galaxy.

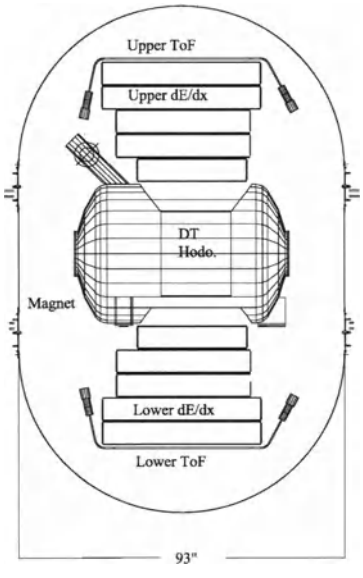

Fig. 4.6.3. Cross-section drawing of the HEAT magnet spectrometer showing the placement of the drift tube hodoscope. According to Bower et al. (1999).

CAPRICE

CAPRICE98 **(C**osmic **A**nti-**P**article **R**ing **I**maging **C**herenkov **E**xperiment, 1998**)** is the balloon borne detector built and flown by the WiZard collaboration (Ambriola et al., 1999). Its primary scientific objective is the study of antimatter in CR and the investigation of CR spectra and composition at different atmospheric depths. The CAPRICE98 apparatus is shown in Fig. 4.6.4. Inside a cylindrical aluminum vessel four detectors and a superconducting magnet were stacked, from the top to the bottom: the gas radiator RICH detector, a time of flight (ToF) system, a tracking system, a silicon-tungsten imaging calorimeter.

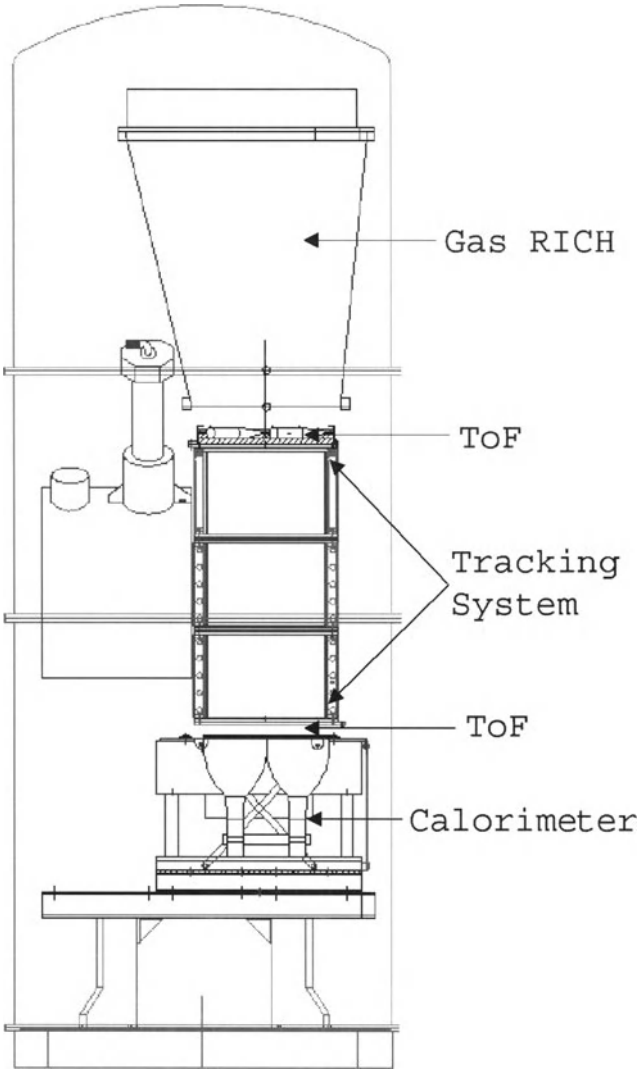

Fig. 4.6.4. The CAPRICE98 apparatus. According to Ambriola et al., 1999.

ATIC

According to Wefel (2001), the **A**dvanced **T**hin **I**onization **C**alorimeter (ATIC) balloon experiment had its maiden test flight from McMurdo, Antarctica from 28 December, 2000 to 13 January 2001, recording over 360 hours of data. The ATIC team is an international collaboration of researchers from the USA, Russia, South Korea, and Germany.

ATIC apparatus was designed to measure the composition and energy spectra of CR from ~ 10 GeV to near 100 TeV utilizing a Si matrix detector to determine charge in conjunction with a scintillator hodoscope which measures charge and trajectory (see Fig. 4.6.5). CR that interact in a carbon target have their energy determined from the shower that develops within a fully active calorimeter composed of a stack of scintillating BGO crystals. ATIC's geometry factor is about 0.25 m^2.ster . During line-of-sight operations much of the data stream was transmitted to the ground. For most of the flight, the data was recorded on board, yielding 45 GB of flight data for analysis.

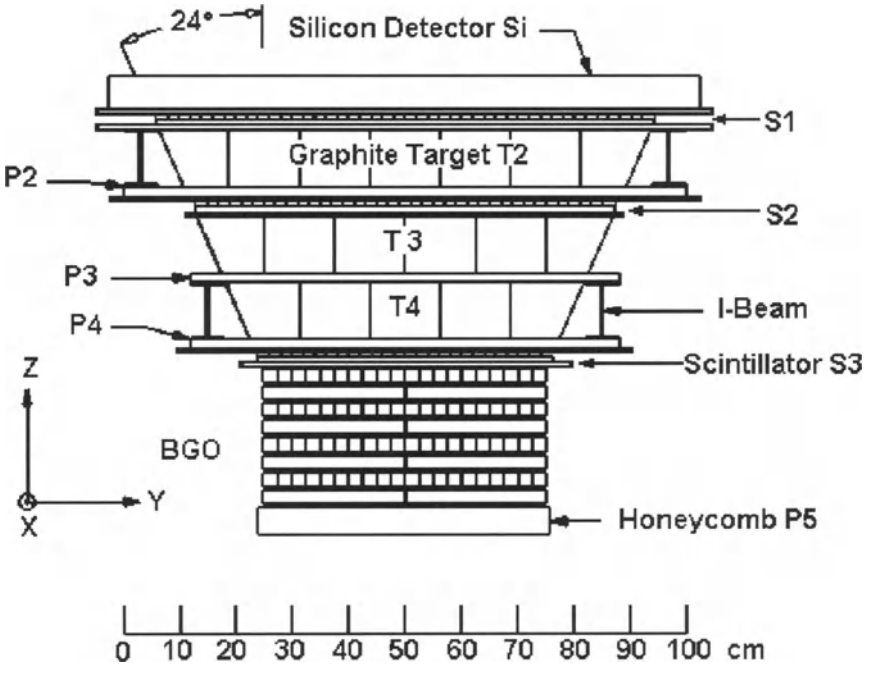

Fig. 4.6.5. ATIC instrument schematic diagram. According to Wefel (2001).

TIGER

The **T**rans **I**ron **G**alactic **E**lement **R**ecorder (TIGER), developed by Link et al. (2001), is a balloon borne CR instrument designed to measure the individual elemental abundances of galactic CR from $16 \leq Z \leq 40$ (see Fig. 4.6.6). It is expected to provide the first individual elemental abundance measurements of odd-Z of galactic CR nuclei with $30 < Z < 40$. TIGER was selected as the first scientific payload to fly onboard an Ultra Long Duration Balloon (ULDB) in December of 2001.

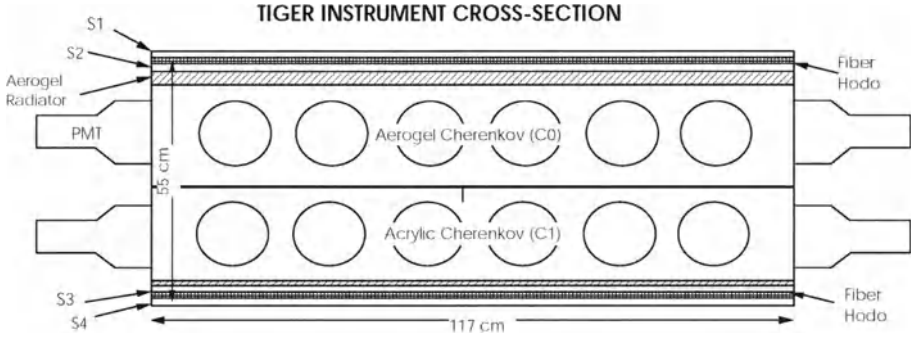

Fig. 4.6.6. A cross-section of the TIGER Detector: S1 and S2 are the top scintillator detectors, S3 and S4 are the bottom scintillation detectors (the TIGER instrument is about 117×117 cm^2 and 55 cm high). According to Link et al. (2001).

Polar BEAR

A new balloon experiment is proposed by Bashindzhagyan et al. (2001) for a long duration flight around the North Pole (Polar BEAR). The primary objective of the experiment is to measure the elemental energy spectra of high-energy CR in the region up to 10^{15} eV. The proposed instrument involves the combination of a large collecting area (1×1 m^2) KLEM (Kinematic Lightweight Energy Meter) device with an ionization calorimeter having a smaller collecting area (0.5×0.5 m^2) and integrated beneath the KLEM apparatus (see Fig. 4.6.7).

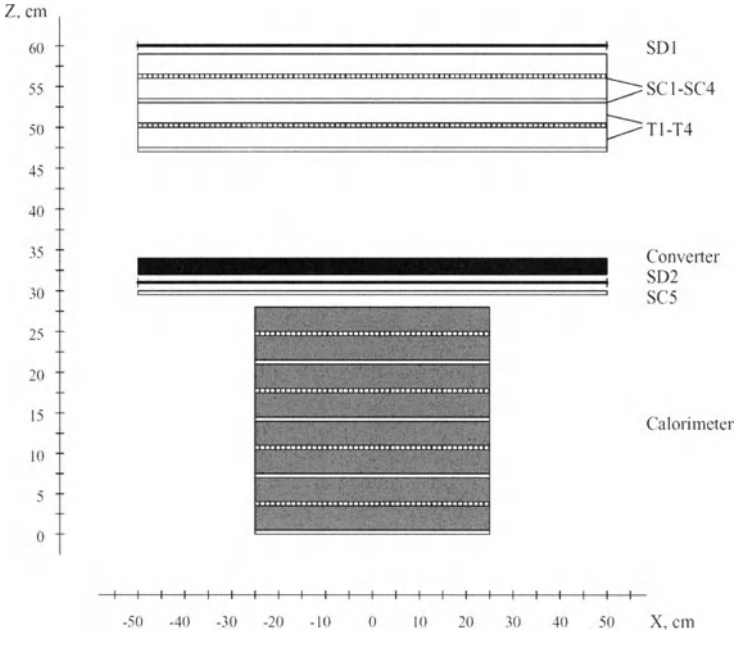

Fig. 4.6.7. The schematic layout of the Polar BEAR device. According to Bashindzhagyan et al. (2001).

BESS

According to Yamamoto et al. (2001), the **B**alloon borne **E**xperiment with a **S**uperconducting **S**pectrometer (BESS) were carried out with the aim of studying elementary particle phenomena in the early history of the Universe through precise measurements of low energy antiproton spectrum and search for antiparticle of cosmic origin. The low energy CR is anticipated with a similar objective. The search for anti-helium, progressed in BESS-1993 to BESS-2000 (Ormes et al., 1997; Saeki et al, 1998; Nozaki et al., 1999; Sasaki et al., 2001), is extended to study baryon asymmetry in the Universe. It is to reach the upper limit of anti-helium to helium ratio down to 10^{-7} in a flight period of 20 days. The spectrometer for the BESS-Polar experiment is designed to meet constraints/requirements of a science payload weight of 1,400 kg in maximum, a spectrometer wall material of < 5 g/cm^2 at the upper-half spectrometer, an electrical power balance of < 600 W, and a continuous operation time of over 20 days. Fig. 4.6.8 shows cross sectional views of the BESS-Polar spectrometer, and Table 4.6.1 gives general design parameters. The first BESS-Polar flight in Antarctica is expected in 2003/2004.

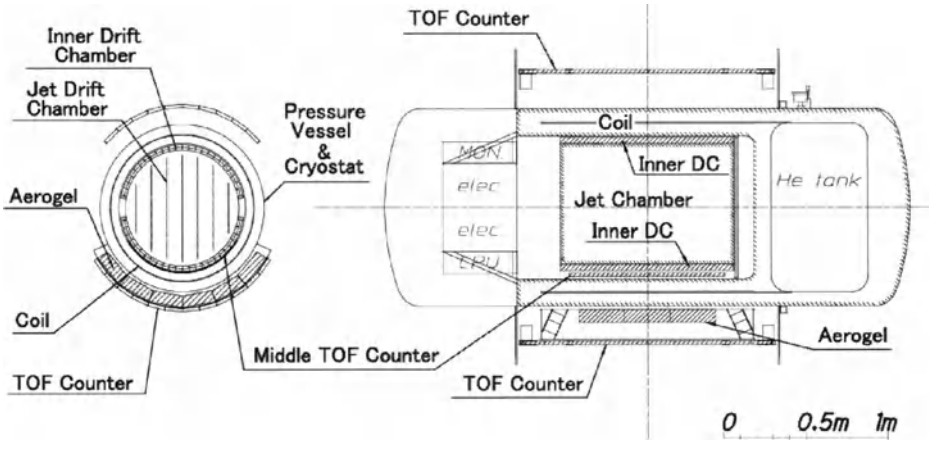

Fig. 4.6.8. Cross sections of the BESS-Polar spectrometer. The central tracker is placed inside the solenoid coil and others are placed outside the cryostat in vacuum. According to Yamamoto et al. (2001).

Table 4.6.1. BESS-Polar spectrometer design parameters. According to Yamamoto et al. (2001).

Geometrical acceptance	0.27 m^2•sr
Flight duration	10 ~ 20 days
Energy range for antiprotons (@ TOA)	0.1 ~ 4.2 GeV
Magnetic field	0.8 ~ 1 T
Distance between TOF counters	1.2 m
Diameter of Central tracker (JET/IDC)	0.75 m
Maximum detectable rigidity	150 ~ 200 GV
Power consumption	600 W
Material in upper-half detector wall	4.5 g/cm^2
Over-all payload size (x/y/z)	1.5m / 1.5m / 3m
Weight	1.4 ton

CREAM

According to Seo et al. (2003), the balloon-borne **C**osmic **R**ay **E**nergetics **A**nd **M**ass (CREAM) experiment is capable of extending direct measurements of CR to the supernova energy scale of 10^{15} eV in a series of Ultra Long Duration Balloon (ULDB) flights. The CREAM instrument consists of a variety of particle detectors as shown in Fig. 4.6.9. The Timing Charge Detector (TCD), Silicon Charge Detector (SCD), and S0/S1 provide particle charge measurements. The key design consideration for the charge detectors is to minimize the effects of backsplash particles from showers in the calorimeter. The TCD is a new technology being developed for CREAM (Beatty et al., 1999). It utilizes the fact that the incident particle enters the TCD before developing a shower in the calorimeter and the backscattered albedo particles arrive several nanoseconds later. S3 which is a single layer of scintillating fibers provides a reference time. A finely segmented silicon charge detector has been flown on the Advanced Thin Ionization Calorimeter, and a similar technique is employed for the CREAM SCD. Four layers of scintillating fibers, S0/S1, provide additional charge measurements as well as particle tracking information.

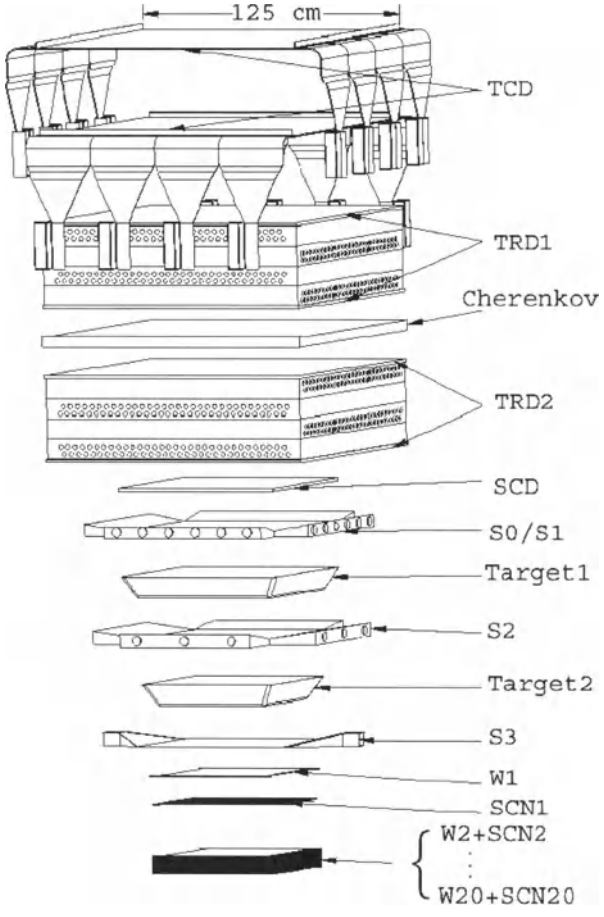

Fig. 4.6.9. Schematic view of the CREAM instrument. According to Seo et al. (2003).

Identification of Z = 1–26 particles in the CREAM experiment will be made with a timing-based charge detector and a pixilated silicon charge detector. Energy measurements will be made with a transition radiation detector and a tungsten/scintillating fiber calorimeter. The instrument has been tested with various particles in accelerated beams at the CERN SPS. The first flight is planned to be launched from Antarctica in December 2004.

4.7 CR research by geophysical rockets, on satellites and space-probes

4.7.1. The initial CR instruments on geophysical rockets

Although measurements of CR on geophysical (sounding) rockets are limited to short time intervals, the results are very interesting in studying the 11 year variations in the low-energy region, the nature of the high latitude cut off and the shift of the latitude 'knee' with changing of solar activity. New data about variations in the flux of protons, nuclei with different Z, and possibly also of electrons and gamma quanta during solar flares and geomagnetic storms may be obtained. The variations of the radiation zones can also be monitored by means of rocket flights. The instruments applied in the geophysical rockets are of many different types. The simplest instrument, developed by Shafer and Yarygin (1960) for standard measurements of variations of the primary flux of CR, consists of single halogen counters STS-6 (Vishnyakov, 1960) with an effective area of 14 cm^2, placed along the axis of the rocket and perpendicular to it, an ionization chamber with a volume of 7,020 cm^3 and the corresponding electronics. Comparison of the readings of the chamber and the counters gives the specific ionization caused by the particles and information about their nature. Brief technical and physical descriptions of the chief instruments used for measurements on rockets and satellites (in particular, of the ionization chambers for fast particles. Geiger Muller counters, proportional counters, scintillation counters, semi-conductor detectors) were given by Lindner (1964).

4.7.2. Early space instruments for total flux measurements of electrons, protons, alpha-particles and gamma rays

The first Soviet instruments designed for measuring CR on Earth satellites included gas discharge halogen counters (for determining the number of particles), ionization chambers (for determining the ionizing power of the radiation) and NaI scintillation counters for measuring energy production (Vernov et al., 1957, 1958a,b, 1961a,b; Shafer and Yarygin, 1960; Vernov and Chudakov, 1960; Savenko et al., 1961). Later developments were aimed at more detailed measurements.

Bartely et al. (1967) used on Pioneer 6 and 7 a detector capable of measuring the CR anisotropy with accuracy 10^{-4} in the energy interval 7.5–90 MeV/nucleon. It consists of a cylindrical plastic veto counter with closed bottom and open top through which the CR reach a CsI(Tl) crystal placed on the bottom; photomultipliers view both scintillators.

In order to separate fluxes of protons with energies 0.5–5 MeV and electrons with energies 30–300 keV, Maduev et al. (1965) used a magnetic analyzer allowing separation of the particles before they fall on the detector. Savenko et al. (1965) developed a four-channel to measure the proton spectrum in the energy range 3–100

MeV in the presence of intensive electron fluxes. A lead glass detector was used to select the particles with respect to dE/dx; the E–detector was a scintillation counter with CsI crystal, surrounded by a plastic anti-coincidence dome.

For observing solar gamma rays on the OSO-1 satellite Fazio and Hafner (1967) developed a telescope made of two scintillation counters between which a lead converter of 0.16 cm thickness has been placed. At a distance of 14 cm from them a Cherenkov counter is located. The gamma quanta are recorded from the electron-positron pairs formed by them in converter.

4.7.3. Early space instruments for measurements of nuclei flux time variations

Measurements of the variations in time and space of nuclei fluxes with different values of Z are important for the problem of the origin of CR as well as for studying the mechanism of generation of solar particles and the magnetic fields in interplanetary space. Most modulation effects and, generally, the character of the propagation of charged particles in space, are determined by two factors: the velocity of the particles and their rigidity. For equal rigidity the velocity of non-relativistic particles will depend on Z: for protons it is twice as large as for nuclei. Besides, data about the variations of the chemical composition in various energy intervals are exceedingly important. A series of investigations on the flux of nuclei aboard the third soviet satellite, the first, second and third rockets, and the second and third spaceships have been made by Kurnosova et al. (1958, 1960, 1961a,b), Ginzburg et al. (1961). In these investigations a detector of Dragun et al (1961) was used, in which the selection of nuclei with different Z was based on the strong dependence of the intensity of the burst of Cherenkov radiation on the charge Z of the nucleus:

$$I_c(Z,n,\beta,l) = KlZ^2\left(1-n^{-2}\beta^{-2}\right), \tag{4.7.1}$$

where K = 450 is a constant coefficient, n is the refraction index of the matter in the detector, β is the ratio of the velocity of the particle to the velocity of light, l is the free path of the particle in the detector. As detector a plexiglas cylinder was used, with a diameter of 26 mm and a height of 26 mm, which recorded all charged particles with $\beta >$ 0.66, which corresponds to a kinetic energy $E_k \geq 3\times10^2$ MeV/nucleon. The time variations of the intensity of the flux of nuclei were studied by a detector of integration type, which recorded all nuclei with atomic number larger than some given value, arriving from a rather large solid angle.

Jones et al. (1967) constructed three detector systems for detailed measurements on the satellite OGO-5 of the charge spectrum and differential energy spectra of galactic and solar CR, including protons and heavier nuclei (up to calcium) in the energy interval from about 4 MeV/nucleon to more than 1,000 MeV/nucleon. The detector for the particles with the highest energies contains 2 scintillation counters and one Cherenkov counter and serves for measuring charge and energy of particles in the energy intervals 50–220, 220–1000 and >1000 MeV/nucleon. The detector for particles of medium energies consists of a system of scintillation counters, measured charge and energy of particles in the energy range 20–300 MeV/nucleon. The detector for the low-energy

particles with energies 3.5–18.5 MeV/nucleon consists of a combination of semiconductor counters and a scintillation counter.

For studying modulation effects or solar CR, measurements of the variations in the flux of different nuclei in the low energy region are very important. The apparatus described by Savenko et al. (1965) is designed for this range; it contains silicon detectors of surface–barrier type for recording protons, α–particles and nuclei with $Z \geq 3$. Low energy protons are recorded in three energy intervals: 0.3–8.0, 7–11, and 11–14 MeV). Application of semiconductors for measuring the nuclear composition and the energy spectrum is also described in Engelmann et al. (1965).

Intensity variations of nuclei with different values of Z can also be studied excellently by the use of photo-emulsions aboard spacecraft which has the possibility of re-entry. The duration of the exposure must be restricted so that the number of particles recorded is not so large, that it becomes impossible to distinguish and identify the tracks of the individual nuclei. In order to be able to interrupt the exposure of the photo-emulsion at any given moment, Veprik et al. (1961) developed and applied in the second soviet satellite in-flight chemical processing. The apparatus performed automatically the cycle of operations comprised in exposing the photo-emulsion during a certain time, in developing and in fixation.

4.7.4. Early space instruments for high energy CR measurements

Grigorov et al. (1967) applied an efficient method for the study of the energy spectrum, time variations, and of various interaction parameters of primary CR up to energies of $10^{13} - 10^{14}$ eV on satellites of 'Proton' series. The space instruments developed includes an ionization calorimeter (described in detail in monograph of Veksler et al., M1959), used together with several detectors of other types, targets and electronics, and is made in the form of two identical parts, each of which can independently execute the whole program of measuring energy E, charge Z and interaction cross section σ. The effective surface of instrument is 60×41 cm^2. The first energy threshold of the apparatus is equal to 12.5 GeV. The interaction detector distinguishes between passage in the given solid angle of a single relativistic particle (1st threshold) and a shower of $n > 2$ relativistic particles formed in a target above the detector. It records the number of particles in the shower. The interaction detector is a plastic scintillator of 5x41x60 cm^3, covered with a Pb layer. The charge detector consists of two flat proportional counters, one above the other, divided in sections. Each counter contains 7 sections of 8×5×70 cm^3, filled with a mixture of argon + 10% methane at 280 mm Hg pressure. Singly charged relativistic particles are recorded with an efficiency of 80%. The probability of a proton being mistaken for an alpha–particle or conversely is about 10%. The detectors were calibrated with the aid of CR muons. The targets in the instrument were blocks of polyethylene (35 g/cm^2) and graphite (30.6 g/cm^2).

4.7.5. Recent space instruments for CR research

SilEye - Silicon Detector on the MIR Space Station

According to Furani et al. (1999), the SilEye Silicon Detector on the MIR Space Station experiment aims to study, using a silicon detector composed of six 380 micron thick strip planes, the nuclear radiation environment inside the MIR Space Station (see

Fig. 4.7.1). Particular interest has been devoted to the 'Light Flashes' phenomenon and to the study of its causes. Here we present preliminary results for nuclear discrimination of light nuclei from data collected inside the Space Station MIR. These measures show the abundance, inside the station, of secondary nuclei and may yield new results for dose absorbed by astronauts and electronics in space. The 'Light Flashes' phenomenon was studied in the past decades with dedicated observation programs on Apollo, Skylab and Apollo–Soyuz spacecraft, but new impulse has been given since 1995 with use, for the first time, of silicon detectors in SilEye-1 and SilEye-2 experiments.

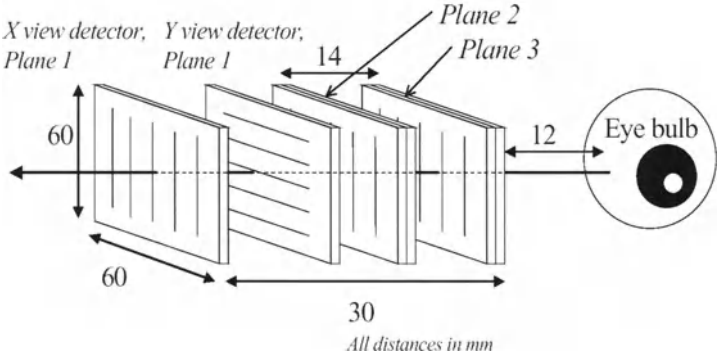

Fig. 4.7.1. Silicon detector setup scheme for SilEye-2. According to Furani et al. (1999).

NINA

The detector for CR nuclei study NINA on board the Russian satellite Resurs-01 n.4, is in orbit since July 10th, 1998 (Casolino et al., 1999). Its scientific scope is to study the low energy component of CR nuclei. The polar orbit of the satellite allows the telescope to detect particles of different nature during its revolution: galactic CR, solar energetic particles, trapped and untrapped anomalous CR. The space telescope NINA (see Fig. 4.7.2) is a silicon detector devoted to the study of CR of solar and galactic origin in the energy range 10-200 MeV/n at 1 AU.

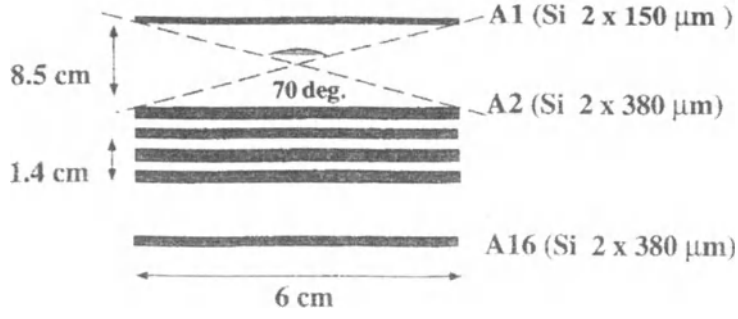

Fig. 4.7.2. Geometric configuration of NINA detector (A1-A16 are the silicon planes with orthogonal strips). According to Vacci (1997).

Detector NINA is capable of nuclear identification up to Iron and isotopic discrimination up to Nitrogen (Sparvoli, 1997), allowing the addressing of important

space physics issues such as the composition and energy spectra of galactic and solar particles (including Solar Energetic Particles). The importance of such measurements is underlined by the unprecedented number of probes which are studying the Heliosphere in different points of the Solar System to understand particle production and propagation mechanisms.

PAMELA

According to Piccardi et al. (1999), the PAMELA telescope will be installed on board of the Resurs–Arktika satellite (VNIIEM) and the launch is foreseen in 2002. The satellite will fly for at least 3 years in a polar orbit at about 700 km altitude. The main goals of the PAMELA experiment are the measurement of the antiproton and positron fluxes in CR, with large statistics in an energy range between 100 MeV and 150 GeV, and the search for anti-nuclei, up to 30 GeV/n, with a sensitivity better than 10^{-7} in the $\overline{\text{He}}/\text{He}$ ratio (Simon, 2003; Ambriola et al., 2003). PAMELA will also study phenomena connected with Solar and Earth physics (Casolino and Mikhailov, 2003). The PAMELA telescope consists of a magnetic spectrometer, a TRD detector, an imaging electromagnetic calorimeter and a TOF system including anticoincidence detectors (see Fig. 4.7.3).

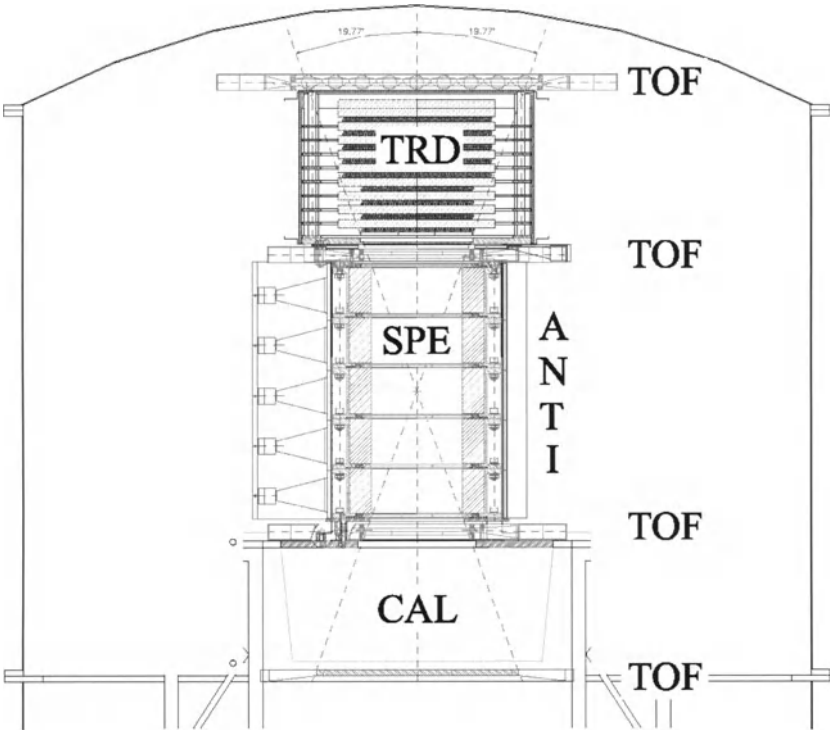

Fig. 4.7.3. The PAMELA telescope. The main detectors are: a transition radiation detector (TRD), a permanent magnet spectrometer equipped with silicon micro strip detector (SPE) and a silicon/tungsten calorimeter (CAL). There are also a time of flight detector (TOF) and an anti-coincidence system (ANTI) made by plastic scintillators. According to Piccardi et al. (1999).

ACCESS

The ACCESS (**A**dvanced **C**R **C**omposition **E**xperiment for International **S**pace **S**tation) is a new mission concept payload for the International Space Station (ISS) which has undergone a preliminary accommodation study. According to Wefel and Wilson (1999), ACCESS science goals include new measurements of the rare ultra-high energy and ultra-heavy components of the cosmic radiation above the Earth's atmosphere. The critical resource made available by the ISS is collecting power; up to 10,000 m^2.sr.days, for a four year stay in orbit, allows ACCESS to go beyond balloon-borne detectors. The instrument, consisting of a charge module, a transition radiation detector, and a imaging calorimeter, measures nuclei throughout the periodic table (see Fig. 4.7.4). The imaging calorimeter for ACCESS is described in more details by Rielage et al. (2001).

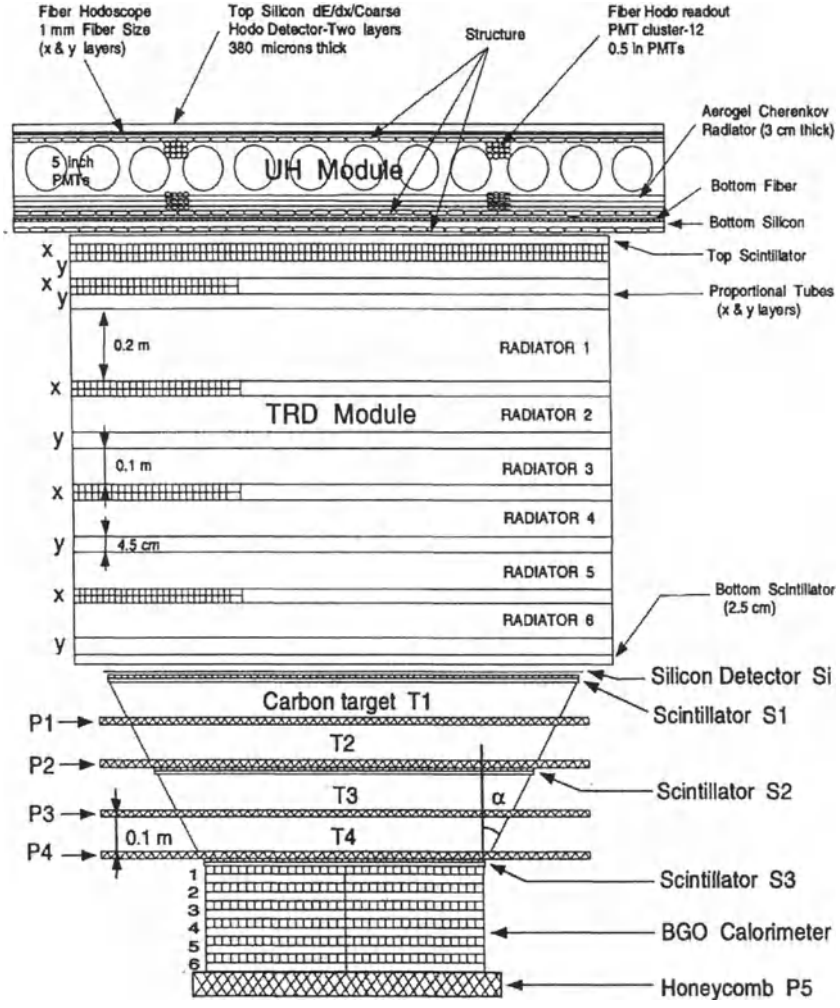

Fig. 4.7.4. The ACCESS Instrumentation. According to Wefel and Wilson (1999).

ECCO and ENTICE on HNX Mission

According to Binns et al (2001), the experimental goal of Heavy Nuclei eXplorer (HNX) mission is to measure the elemental abundances of all individual stable nuclei from neon through the actinides and possibly beyond. The HNX spacecraft will carry two high-precision instruments, the Extremely heavy Cosmic ray Composition Observer (ECCO), which measures elemental abundances of nuclei with $Z \geq 72$, and the ENergetic Trans-Iron Composition Experiment (ENTICE), which measures elemental abundances of nuclei with $10 \leq Z \leq 82$ (see Fig. 4.7.5). ECCO is a large array of glass track-etch detectors, which will measure individual elemental abundances for elements with $Z > 70$, with sufficient collecting power to collect > 100 actinides. ENTICE is an electronic instrument with a large dynamic range that will measure individual elemental abundances from Ne ($Z = 10$) through Bi ($Z = 83$) plus a handful of actinides. The two instruments will be configured such that a substantial number of Pt-Pb nuclei, as well as a few actinides, will traverse both instruments, thus inter-calibrating the two instruments. ECCO is designed to measure charges of ions with $E > 0.9$ GeV/nucleon. ENTICE will measure charges of nuclei with $E > 0.5$ GeV/nucleon and will measure energy spectra up to about 7 GeV/nucleon. Since ECCO must be recovered for data analysis, HNX will be launched and recovered by the Space Shuttle.

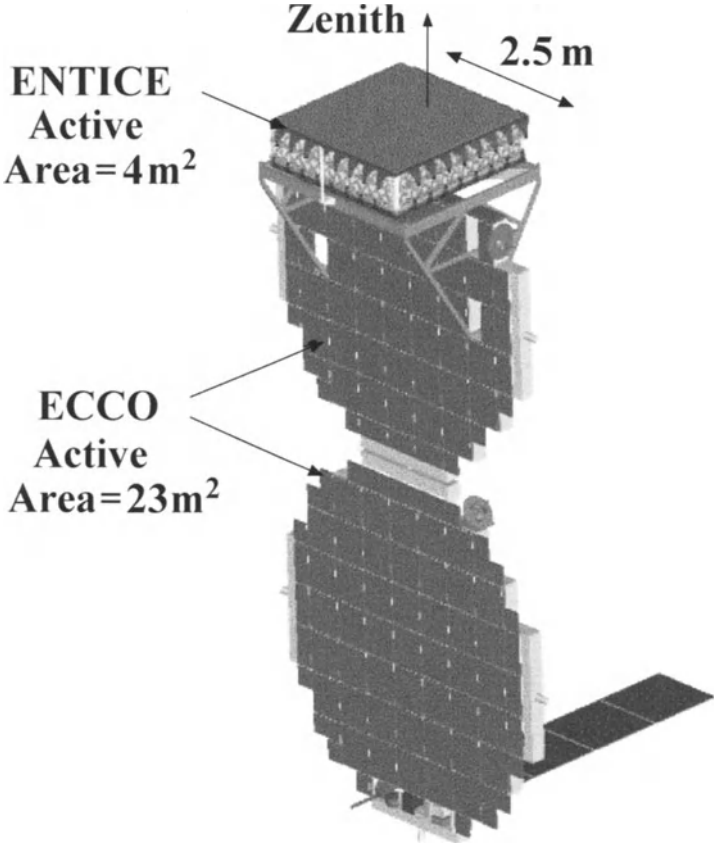

Fig. 4.7.5. HNX is shown in its deployed configuration. According to Binns et al (2001).

HIT on TSUBASA

According to Matsumoto et al. (2003), Japanese satellite TSUBASA has been operating well in the orbit of geostationary transfer orbit since February in 2002. HIT measures fluxes of heavy ions from helium to iron-nuclei in the energy range from 20 MeV/n for He to 179 MeV/n for Fe. The HIT instrument, based on the $\Delta E \times E$ particle identification method, consists of two position-sensitive-silicon-detectors and 16 PIN-typed Si-detectors with 420μm thickness. The geometric factor is 18–24 $cm^2 sr$ depending on energies of ions.

PS on SELENE

According to Takashima et al. (2003), the PS (**P**article **S**pectroscopy) sensor, that will be onboard the SELENE spacecraft for the first Japanese lunar mission to be launched in 2005, will measure the high energy CR particles to study their origin, acceleration and propagation in the solar system. The PS sensor consists of 4 detectors (HID, LPD-HE, LPD-p, LPD-e, these are Si stuck detectors using the $\Delta E \times E$ method) that are cover the energy range from 100 keV to 60 MeV for protons, from 30 keV to a few MeV for electrons, and from 3 MeV/n to 400 MeV/n for heavy ions, respectively.

AMS-02 on ISS

According to Gentile (2003), the **A**lpha **M**agnetic **S**pectrometer (AMS) is a particle physics experiment scheduled to be installed on the **I**nternational **S**pace **S**tation (ISS). The purpose of this experiment is to provide a high statistics measurement of CR charged particles and nuclei in rigidity range 0.5 GV to few TV, and to provide a sensitive search for cosmic antimatter (anti-helium) and dark matter, and to study the properties of CR. A preliminary version of the detector (so called AMS-01) operated successfully during a 10-day NASA Shuttle flight in June 1998. The AMS-02 detector construction (Fig. 4.7.6) is due to be completed by 2004 and installed in ISS in 2005. It contains the following main components (Gentile, 2003):

1. A 20 layer Transition Radiation Detector (TRD) to distinguish $p/\bar{p}$ from e^+/e^- with a rejection factor of $10^2 - 10^3$ in a range from 1.5 to 300 GeV (Burger and Gentile, 2003). This will be used in conjunction with an electromagnetic calorimeter to provide overall e^+/p rejection $< 10^{-6}$. Four layers of Time of Flight (TOF) hodoscopes provide precision time of flight measurements (≈ 120 ps), dE/dx measurements and the primary trigger (in more details see in Casadei, 2003).

2. The superconducting magnet which provides a bending power of $BL^2 \approx 0.8 \mathrm{Tm}^2$ (in more details see in Blau et al., 2003).

3. Eight layers (6.45 m2) of double-sided silicon tracker which provide a coordinate resolution of 10 μ in the bending plane and 30 μ in the non-bending plane.

4. Veto counters to ensure that only particles passing the magnet aperture will be accepted.

5. A Ring Imaging Cerenkov Counter (RICH) which measures the velocity (to 0.1 % accuracy) of particles or nuclei and their charge. This information, together with the momentum measurement in the magnet, will enable AMS to directly measure the mass of particles and nuclei (in more details see in Buénerd, 2003).

6. A 3-D sampling calorimeter (ECAL) to measure the energy of electrons, positrons and gamma rays and to distinguish electrons and positrons from hadrons in the range 1.5 GeV-1 TeV.

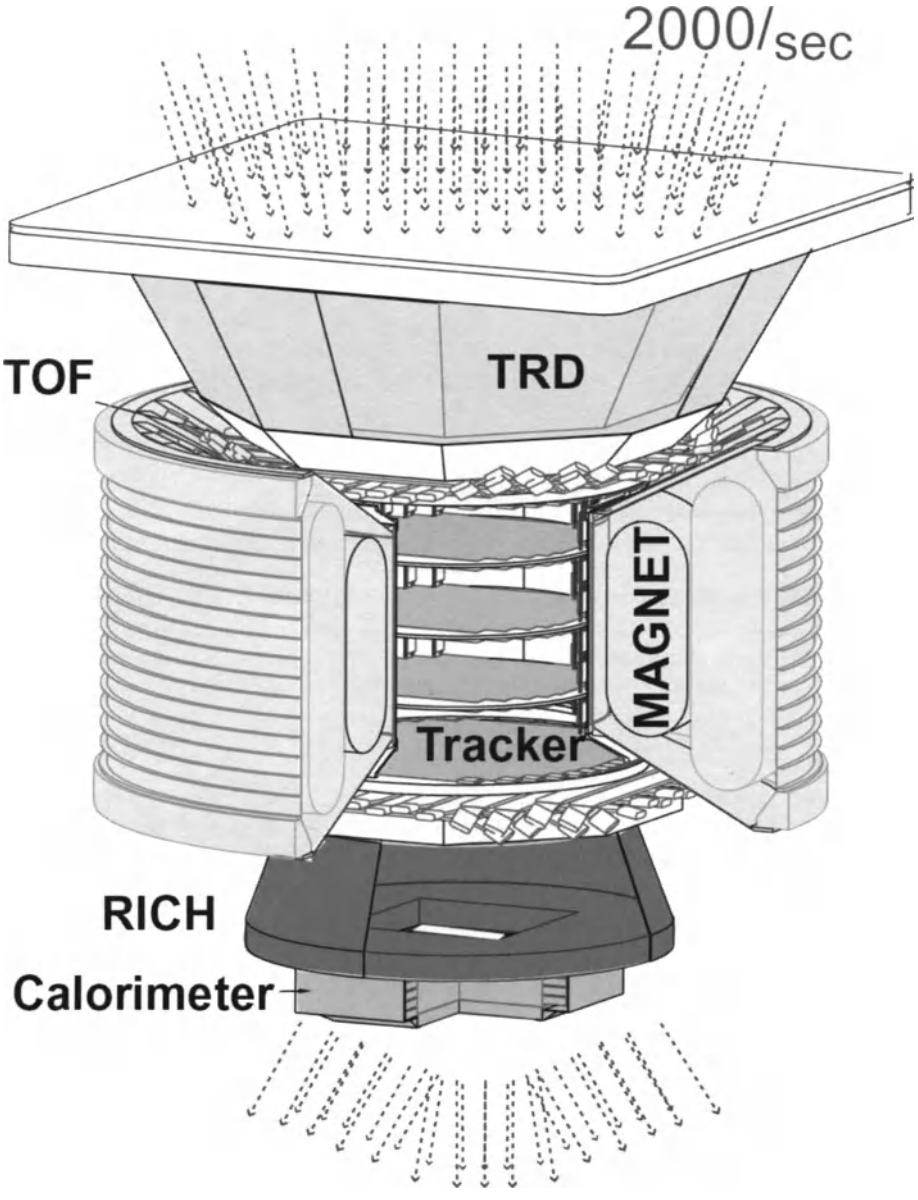

Fig. 4.7.6. The Alpha Magnetic Spectrometer (AMS-02). The detector components are: **T**ransition **R**adiation **D**etector (TRD), **T**ime-**o**f-**f**light Scintillators (TOF), Silicon Tracker (Tracker), **R**ing **I**maging **Ch**erenkov detector (RICH), lead/plastic fiber calorimeter (ECAL), the anticoincidence counters are located in inner side in the magnet. The arrows represent the acceptance of CR particles, ~ 2000 s^{-1}. According to Gentile (2003).

AMS-02 is a large acceptance, superconducting magnetic spectrometer which will measure, on board of ISS, charged CR spectra of individual elements below Z ~ 25 and up to TeV region (Casaus, 2003), high energy γ rays up to few hundreds GeV with good point-source localization; it will provide the most sensitive search in CR for the existence of antimatter nuclei and for the indirect studies of the origin of dark matter.

As example, in Fig. 4.7.7 are shown expected statistics in measurements ratios B/C and $^3He/^4He$ by AMS-02 in comparison with results obtained in other space experiments.

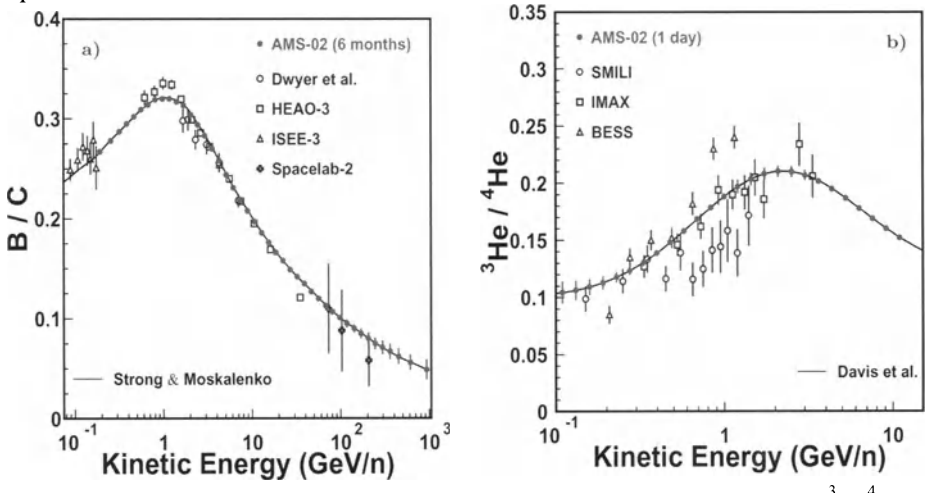

Fig. 4.7.7. AMS–02 expected performance on a) B/C ratio after 6 months of data taking and b) $^3He/^4He$ ratio after 1 day of data taking compared to other measurements. The ratios have been simulated following the models described in Strong and Moskalenko (1998, 2001) and Davis et al. (1995) respectively. According to Casaus (2003).

EUSU on ISS

According to Teshima et al (2003), Catalano et al. (2003) in near future will be realized very interesting and important experiment: the **E**xtreme **U**niverse **S**pace **O**bservatory (EUSO) on the ISS to measure with high sensitivity from space giant EAS caused by extremely high energy CR. The possibility to detect from space extreme high energy CR (charged particles, photons and neutrinos with energy $E \geq 10^{19}$ eV) was originally suggested about 25 years ago by Linsley (1979). In the middle of '90s, thanks to Takahashi (1995), conceptual studies such as the OWL and AIRWATCH Projects were carried out (see above Section 4.5.2). Based on the AIRWATCH concept and following a successful accommodation study on the ISS, the EUSO Project was eventually approved by ESA.

EUSO is a wide angle high resolution ((about 0.1°) telescope. It will be accommodated in the International Space Station, and look down the earth atmosphere from a ~ 400 km height ISS orbit. The full aperture for extreme high energy CR is estimated to be 500,000 km^2sr. Even conservatively assuming an observational duty cycle of 10%, one obtains an effective time averaged aperture of 50,000 km^2sr. This aperture is ~ 300 times larger than AGASA, and ~ 10 times larger than Auger detector which is now under construction in Malargue, Argentina (see above Section 4.5.2).

4.8. An example of automatically operating CR Observatory connected to the Internet

Here we will give, as example, a short description of the automatically operating Israel–Italian Emilio Segre' CR Observatory (in the framework of Israel CR Center), that provides real time one minute and one hour data on an internet site and monitors great radiation hazard in space, issuing alerts for the beginning of a great solar GLE (Ground Level Event).

4.8.1. Israel CR Center and Israeli–Italian Emilio Segre' Observatory

The Israel CR Center (ICRC) and Israeli–Italian Emilio Segre' Observatory (ESO) were established in 1998, with affiliation to Tel Aviv University, to the Technion (Israel Institute of Technology, Haifa) and to the Israel Space Agency (under the aegis of the Ministry of Science). The mobile CR Neutron Monitor was prepared by the collaboration of Israeli scientists of ICRC/ESO (headed by Prof. Lev Dorman) with Italian scientists of CR Group of Roma Tre University (headed by Prof. Nunzio Iucci) and of the Cosmic Radiation Sector IFSI/CNR (headed by Dr. Giorgio Villoresi), and transferred in June 1998 on Mt. Hermon (33°18' N, 35°47.2' E, 2,025 m above sea level, vertical cut off rigidity R_C = 10.8 GV). The results of measurements (data taken at one minute intervals of CR neutron total intensities at two separate 3NM–64 sections, as well as similar one minute data about the intensities relating to neutron multiplicities m = 1, 2, 3, 4, 5, 6, 7 and ≥ 8) are stored in the computer. Similar one minute data relating to the atmospheric electric field, wind speed, three components of geomagnetic field, air temperature outside, and humidity and temperature inside the CR Observatory are also recorded and archived. Each month one hour data of ESO are sent to the World Data Center in Boulder (USA, Colorado) and to many CR Observatories in the world. An automatic electric power supply using a UPS (Uninterruptible Power Supply) and a diesel generator guarantees continuous power for ESO. There is a direct radio connection in real time from ESO on Mt. Hermon to the central laboratory of ICRC in Qazrin, and to the Internet. Table 4.8.1 lists the characteristics of the different neutron monitor channels.

Table 4.8.1. Channels of the neutron monitor of ESO.

Channel title	Average counting rate per 1 hour	Statistical error for 1 hour, %	Statistical error for 1 min., %
Total	615930	0.13	0.98
***m* = 1**	282550	0.19	1.45
***m* = 2**	77850	0.36	2.8
***m* = 3**	26340	0.62	4.8
***m* = 4**	10215	0.99	7.6
***m* = 5**	4500	1.49	11.5
***m* = 6**	2195	2.13	16.4
***m* = 7**	1150	2.95	22.6
***m* ≥8**	1490	2.59	19.6

In Fig. 4.8.1 we show a block scheme of the main components of the Emilio Segre' Observatory (ESO) on Mt. Hermon and their connection with the central laboratory of Israel CR Center in Qazrin and with the internet.

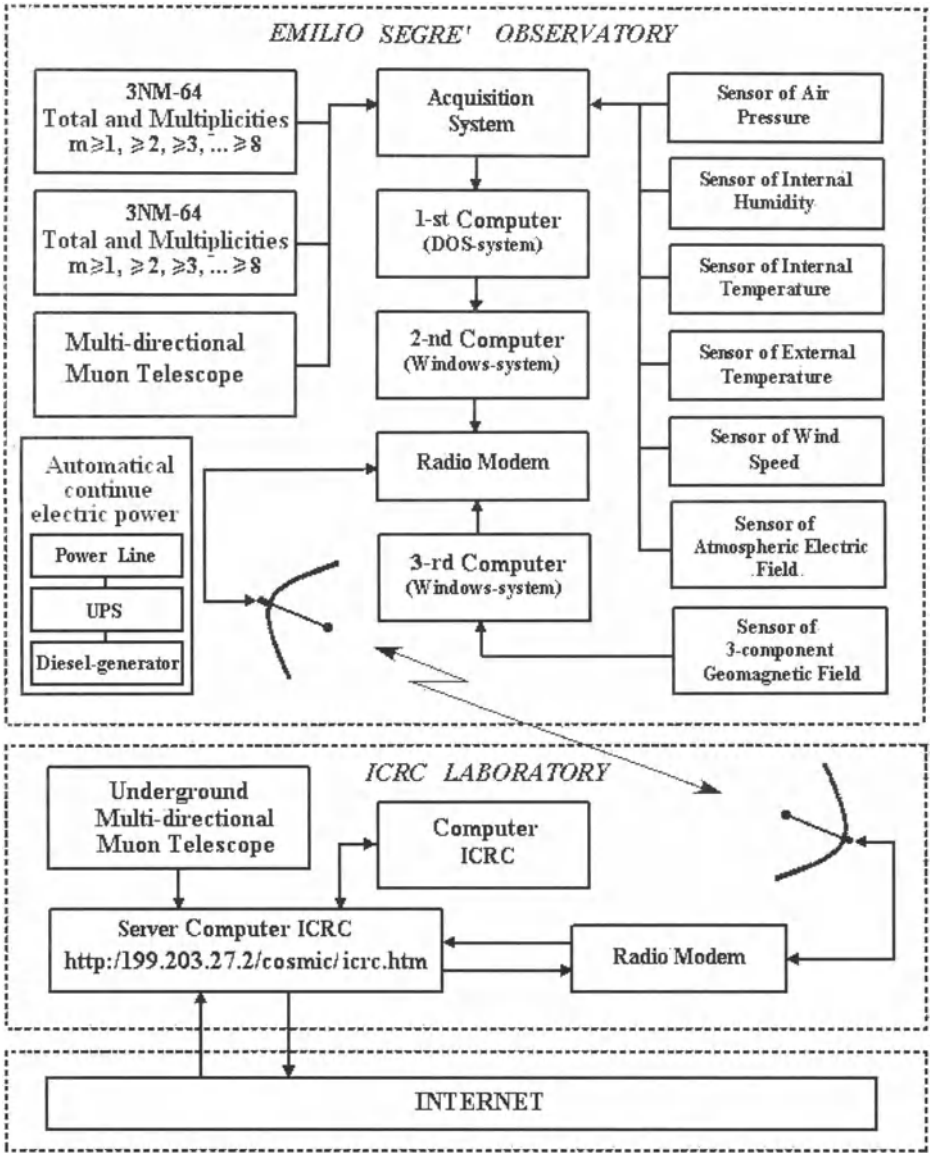

Fig. 4.8.1. Schematic description of the main components of the Israeli–Italian Emilio Segre' Observatory (ESO) and their connection with the central laboratory of Israel CR Center (ICRC) in Qazrin and with internet. Continuousl electric power is guaranteed by using in parallel a UPS connected to a UPS and a diesel-generator working automatically. Also shown are the multi-directional muon telescope planned for the near future (in combination with NM-IQSY, see Fig. 4.8.2). In the central laboratory of ICRC in Qazrin is shown the planned underground multi-directional muon telescope (see Fig. 4.8.3 and Fig. 4.8.4).

Fig. 4.8.2 depicts the cross-section of Emilio Segre' Observatory and disposition of both sections of NM-IQSY, as well as the multi-directional muon telescope planned to be installed in the near future in combination with NM-IQSY.

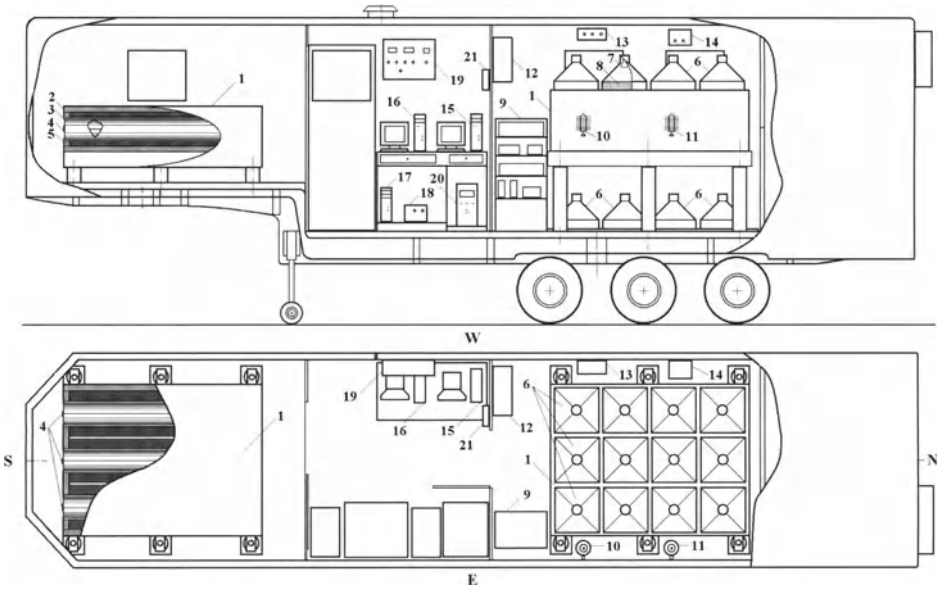

Fig. 4.8.2. Schematic view of the Israeli–Italian Emilio Segre' Observatory (ESO) on Mt. Hermon, showing both sections of NM-IQSY and the multi-directional muon telescope planned to be installed in the near future (the lead of NM will be used as a shield for the muon telescope): the top – vertical cross-section; the bottom – view from above. 1 – two 3-counters sections of NM-IQSY; 2 – polyethylene plates; 3 – polyethylene tubes; 4 – neutron counter $^{10}BF_3$; 5 – lead tubes; 6 – scintillation detector; 7 – photo-multiplayer; 8 – plastic scintillator 50 cm×50 cm×10 cm; 9 –acquisition system; 10 – sensor of humidity inside Observatory; 11 - sensor of air temperature inside Observatory; 12 – the system of continuous electric power supply; 13 – radio-modem; 14 – recording instrument of EFS-1000 (for measurements of atmospheric electric field); 15 – 1-st computer (DOS-system); 16 – 2-nd computer (Windows system); 17 – 3 rd computer for geomagnetic field (Windows system); 18 - recording instrument for registration of the 3 components of geomagnetic field; 19 – control panel of electric power; 20 – UPS.

4.8.2. Description of underground multi-directional muon telescope

An underground multi-directional muon telescope is presently under construction in collaboration with the CR Group of New Mexico University (headed by Prof. H. Ahluwalia). Fig. 4.8.3 shows the scintillation detector for this underground muon telescope.

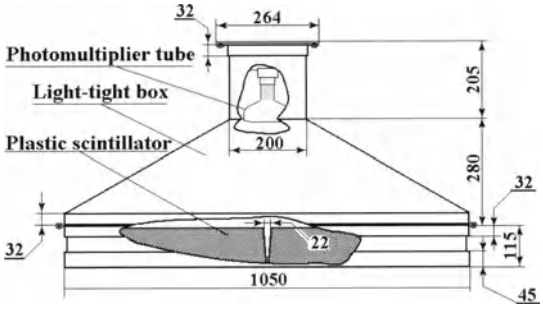

Fig. 4.8.3. Scintillation detector for the planned underground multi-directional muon telescope in ICRC. Dimensions are given in mm.

Figure 4.8.4 depicts the planned underground multidirectional muon telescope that will start to work in Qazrin in near future.

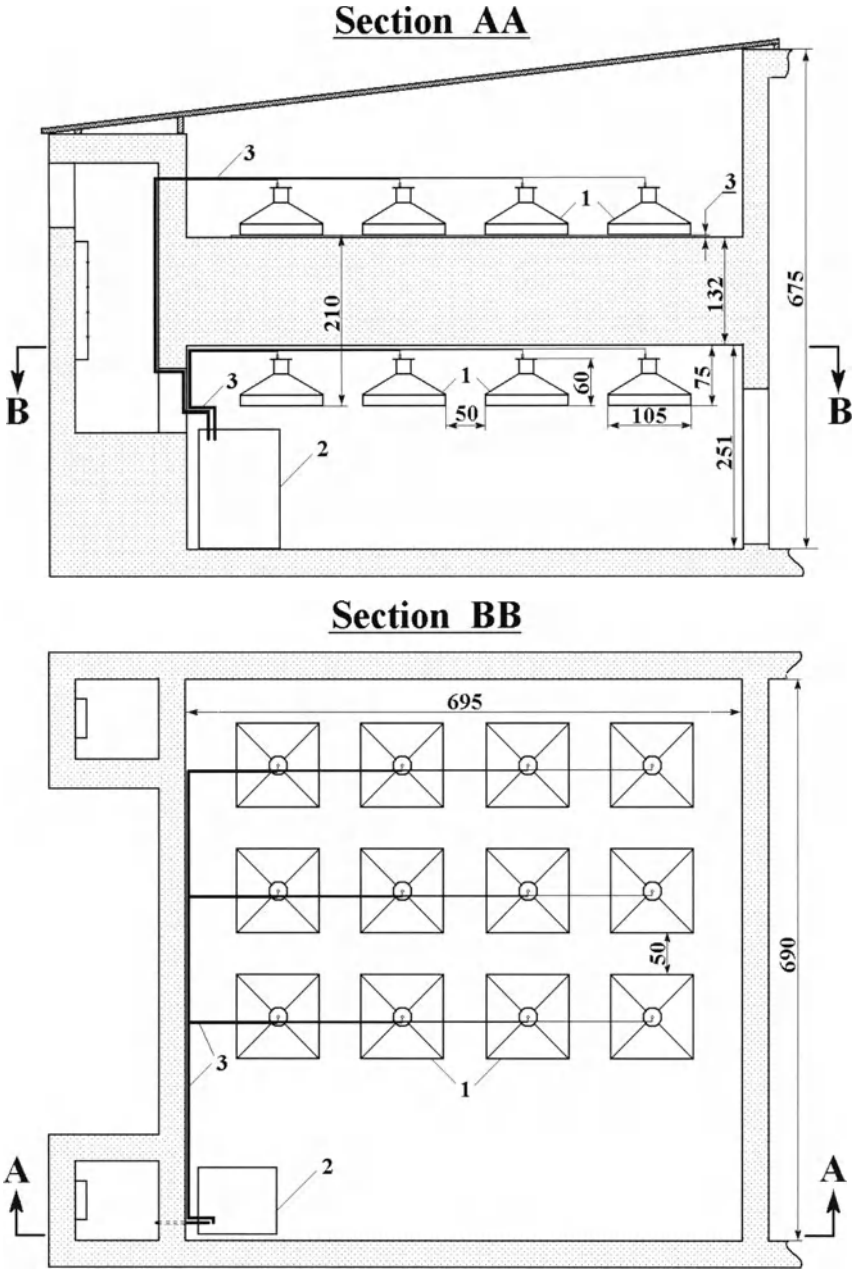

Fig. 4.8.4. The disposition of the planned underground multidirectional muon telescope in the Israel CR Center with characteristics listed in Table 4.8.2. 1- scintillation detectors; 2- acquisition system and computers; 3 – connection and power feeders. Dimensions are given in cm.

Table 4.8.2. Channels of planned underground multi-directional muon telescope in ICRC/ESO.

No	Channel title	Azimuth angle	Zenith angle	Number of telescopes	Expected counting rate	Statistical error for 1 hour, %
1	**VERTICAL**		**0°**	**12**	**5123000**	**0.044**
2	**N1**	0°	36.7°	8	1412000	0.084
3	**W1**	90°	36.7°	9	1588000	0.079
4	**S1**	180°	36.7°	8	1412000	0.084
5	**E1**	270°	36.7°	9	1588000	0.079
6	**GLOBAL (36.7°)**		**36.7°**	**34**	**6000000**	**0.041**
7	**NW1**	45°	46.5°	6	575000	0.13
8	**SW1**	135°	46.5°	6	575000	0.13
9	**SE1**	225°	46.5°	6	575000	0.13
10	**NE1**	315°	46.5°	6	575000	0.13
11	**GLOBAL (46.5°)**		**46.5°**	**24**	**2300000**	**0.066**
12	**N2**	0°	56.1°	4	164600	0.25
13	**W2**	90°	56.1°	6	246900	0.20
14	**S2**	180°	56.1°	4	164600	0.25
15	**E2**	270°	56.1°	6	246900	0.20
16	**GLOBAL (56.1°)**		**56.1°**	**20**	**833000**	**0.110**
17	**NNW**	26.6°	59.0°	3	89800	0.33
18	**SSW**	153.4°	59.0°	3	89800	0.33
19	**SSE**	206.6°	59.0°	3	89800	0.33
20	**NNE**	333.4°	59.0°	3	89800	0.33
21	**WNW**	63.4°	59.0°	4	119700	0.29
22	**WSW**	116.6°	59.0°	4	119700	0.29
23	**ESE**	243.4°	59.0°	4	119700	0.29
24	**ENE**	296.6°	59.0°	4	119700	0.29
25	**GLOBAL (59.0°)**		**59.0°**	**28**	**838000**	**0.109**
26	**NW2**	45°	64.6°	2	28825	0.59
27	**SW2**	135°	64.6°	2	28825	0.59
28	**SE2**	225°	64.6°	2	28825	0.59
29	**NE2**	315°	64.6°	2	28825	0.59
30	**GLOBAL (64.6°)**		**64.6°**	**8**	**115300**	**0.295**
31	**W3**	90°	65.9°	3	35600	0.53
32	**E3**	270°	65.9°	3	35600	0.53
33	**GLOBAL (65.9°)**		**65.9°**	**6**	**71200**	**0.375**
34	**WWWNW**	71.6°	67.0°	2	19880	0.71
35	**WWWSW**	108.4°	67.0°	2	19880	0.71
36	**EEESE**	251.6°	67.0°	2	19880	0.71
37	**EEENE**	288.4°	67.0°	2	19880	0.71
38	**GLOBAL (67.0°)**		**67.0°**	**8**	**79520**	**0.355**
39	**WWNW**	56.3°	69.6°	1	6320	1.26
40	**WWSW**	123.7°	69.6°	1	6320	1.26
41	**EESE**	236.3°	69.6°	1	6320	1.26
42	**EENE**	303.7°	69.6°	1	6320	1.26
43	**GLOBAL (69.6°)**		**69.6°**	**4**	**25280**	**0.63**
44	**TOTAL**			**144**	**15385300**	**0.0255**

From Table 4.8.2 it can be seen that besides 35 directional channels characterized by different azimuth and zenith angles, 8 additional channels will detect global intensities at different zenith angles, and 1 channel will measure the total intensity. By using

coincidences in different combinations of upper scintillators as well as telescopes in the same direction, it will be possible to detect small EAS (External Atmospheric Showers) that correspond to primary CR energies up to 10^{15}–10^{16} eV.

4.8.3. Automatic search of the start of great flare energetic particle events

Since the beginning of 2000, ICRC/ESO searches automatically for the start of solar radiation storms with NOAA magnitude scales of S5, S4 and S3, caused by Flare Energetic Particle (FEP) events. Such events are potentially dangerous for spacecraft electronics, astronauts in space station, and in some rarely cases even for technology and peoples on airplanes. The automatically detection of flux increase is made by comparing with intensity averaged from 120 to 61 minutes before the present Zth one minute data. For each Zth one minute data, the program 'FEP-Search-1 min' is applied. This program determines the values

$$D_{A1Z} = \left[\ln(I_{AZ}) - \sum_{k=Z-120}^{k=Z-60} \ln(I_{Ak})/60 \right] \Big/ \sigma_1 , \tag{4.8.1}$$

$$D_{B1Z} = \left[\ln(I_{BZ}) - \sum_{k=Z-120}^{k=Z-60} \ln(I_{Bk})/60 \right] \Big/ \sigma_1 , \tag{4.8.2}$$

where I_{Ak} and I_{Bk} are one minute total intensities in the sections of neutron super-monitor A and B, and σ_1 is the standard deviation of one minute data. If simultaneously

$$D_{A1Z} \geq 2.5, \quad D_{B1Z} \geq 2.5 , \tag{4.8.3}$$

the program 'FEP-Search-1 min' repeats the calculation for the next (Z+1)th minute and if Eq. 8.4.3 is satisfied again, the onset of great FEP is established and Alert is send to the Internet site of ICRC.

If Eq. 8.4.3 is not satisfied, the program 'FEP-Search-2 min' searches for the start of an increase by using two-min data characterized by $\sigma_2 = \sigma_1/\sqrt{2}$. In this case the program 'FEP-Search-2 min' will calculate values

$$D_{A2Z} = \left[\left(\ln(I_{AZ}) + \ln(I_{A,Z-1}) \right) \Big/ 2 - \sum_{k=Z-120}^{k=Z-60} \ln(I_{Ak}) \Big/ 60 \right] \Big/ \sigma_2 , \tag{4.8.4}$$

$$D_{B2Z} = \left[\left(\ln(I_{BZ}) + \ln(I_{B,Z-1}) \right) \Big/ 2 - \sum_{k=Z-120}^{k=Z-60} \ln(I_{Bk}) \Big/ 60 \right] \Big/ \sigma_2 . \tag{4.8.5}$$

If the result is negative (no simultaneous increases in both channels of total intensity $\geq 2.5\,\sigma_2$, i.e. the condition $D_{A2Z} \geq 2.5$, $D_{B2Z} \geq 2.5$ fails), then 'FEP-Search-3 min' uses the average of three minutes (Z-2)th, (Z-1)th, and Zth minutes with

$\sigma_3 = \sigma_1/\sqrt{3}$. If this program also gives a negative result, then the program 'FEP-Search-5 min' uses the average of five minutes Z-4, Z-3, Z-2, Z-1 and Z with $\sigma_5 = \sigma_1/\sqrt{5}$. If this program also gives negative result, i.e. all programs 'FEP-Search-K min' (where K = 1, 2, 3, 5) give negative result, the procedure is repeated for the next (Z+1)th minute, and so on. For each minute the final result of this automatic procedure is shown on the ICRC/ESO website (see Section 4.8.5). The block-scheme of programs 'FEP-Search' is shown in Fig. 4.8.5.

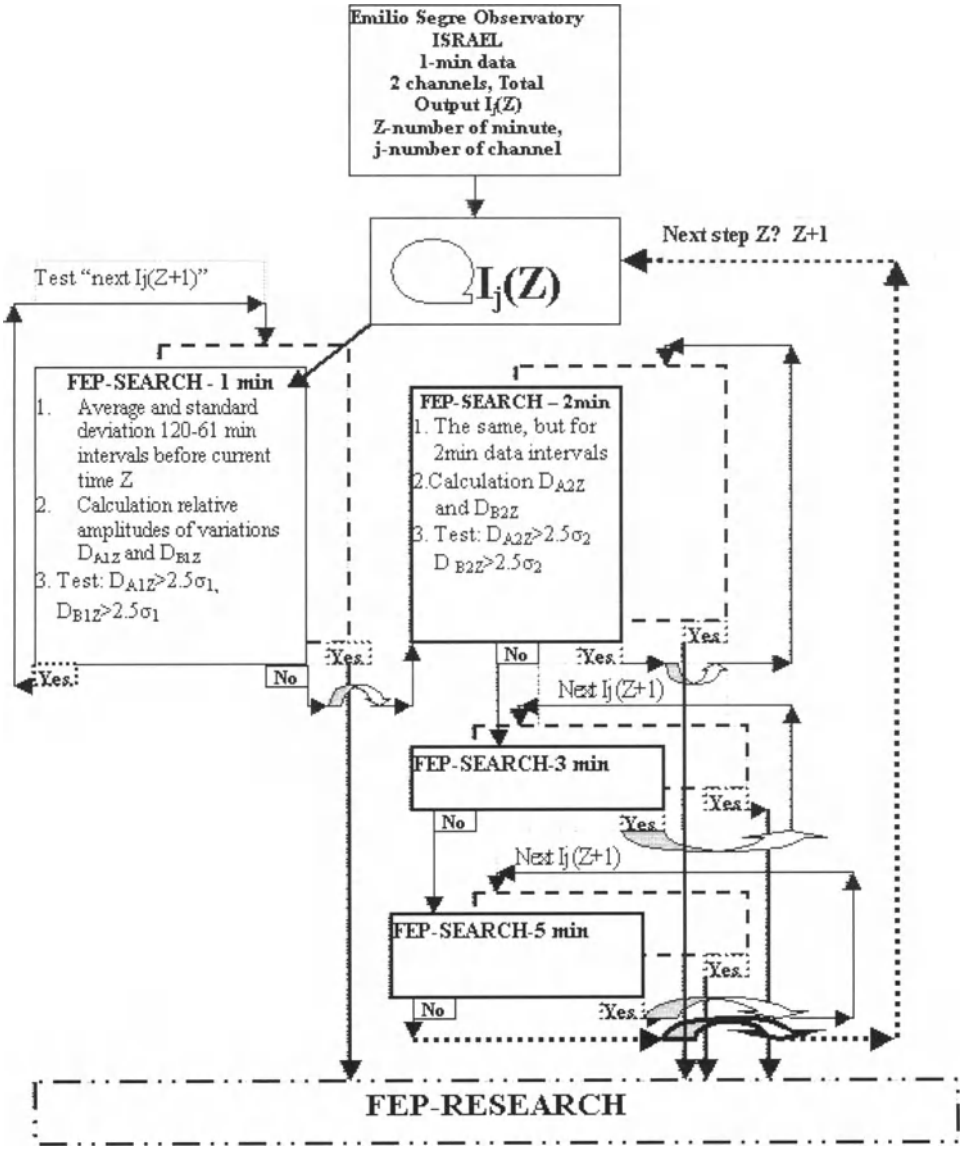

Fig. 4.8.5. Schematic description of the 'FEP-Search' programs.

4.8.4. The probability of false alarms

Because the probability function $\Phi(2.5)=0.9876$, **the probability of an accidental increase** with amplitude more than 2.5σ in **one channel** will be $(1-\Phi(2.5))/2=0.0062\,\mathrm{min}^{-1}$; that is, one in 161.3 minutes (in one day we expect 8.93 accidental increases in one channel). The probability of accidental increases simultaneously in **both channels** will be $((1-\Phi(2.5))/2)^2=3.845\times10^{-5}\,\mathrm{min}^{-1}$, corresponding to one in 26,007 minutes ≈ 18 days. The probability of an accidental increases of 2.5σ in **both channels in two successive minutes** is equal to $((1-\Phi(2.5))/2)^4=1.478\times10^{-9}\,\mathrm{min}^{-1}$; that is, one in 6.76×10^8 minutes ≈ 1,286 years. Issuing this false alarm (one in about 1,300 years) is not dangerous, because the first alarm is preliminary and can be cancelled if in the third successive minute there is no increase in both channels bigger than 2.5σ (it is not excluded that in the third minute there will be also an accidental increase, but the **probability of this false alarm** is negligible: $((1-\Phi(2.5))/2)^6=5.685\times10^{-14}\,\mathrm{min}^{-1}$ which means one in 3.34×10^7 years). Let us note that the false alarm can be sent in the case of solar neutron event, but this event usually is very short (only few minutes) and it will be automatically cancelled in the successive minute after the end of a solar neutron event.

4.8.5. The probability of missed triggers

The probability of missed triggers depends very strongly on the amplitude of the increase. Let us suppose for example that we have a real increase of 7σ in one channel (that for ESO corresponds to an increase of about 9.8 %). The trigger will be missed if in both channels and in two successive minutes the increase of intensity is less than 2.5σ as a result of statistical fluctuations. For this the statistical fluctuation must be negative with amplitude more than 4.5σ. The probability of this negative fluctuation in one channel in one minute is equal $(1-\Phi(4.5))/2=3.39\times10^{-6}\,\mathrm{min}^{-1}$, and the probability of a missed trigger for two successive minutes of observation simultaneously in two channels is 4 times larger: 1.36×10^{-5}. It means that a missed trigger is expected only one per about 70000 events. Table 4.8.3 lists the probabilities P_{mt} of missed triggers for ESO (where the standard deviation per one minute σ_1 = 1.4%) as a function of the amplitude of increase A.

Table 4.8.3. Probabilities P_{mt} of missed triggers as a function of the amplitude of increase A (in % and in σ)

A, %	5.6	6.3	7.0	7.7	8.4	9.1	9.8	10.5
A, σ	4.0	4.5	5.0	5.5	6.0	6.5	7.0	7.5
P_{mt}	0.27	0.091	0.025	0.0054	0.00093	0.00013	0.000014	0.0000011

The analysis described above shows that this automatic search for the onset of a great, dangerous FEP on the basis of one minute NM data practically does not give false alarms (the probability of false preliminary alarm is one in about 1,300 years, and for false final alarm one in 3.34×10^7 years). No dangerous solar neutron events can be separated automatically. We estimated also the probability of missed triggers; it was

shown that for events with amplitude of increase more than 10% the probability of a missed trigger for successive two minutes NM data is smaller than 1.36×10^{-5} (this probability decreases significantly with increasing amplitude A of the FEP flux, as shown in Table 4.8.3). Historical ground FEP events show very fast increase of amplitude in the start of event (Dorman, M1957; Dorman and Miroshnichenko, M1968; Duggal, 1979; Dorman and Venkatesan, 1993; Stoker, 1994). For example, in the biggest FEP event of February 23, 1956 amplitudes of increase in the Chicago NM were at 3.51 UT 1%, after one minute at 3.52 UT – 35%, at 3.53 UT – 180%, at 3.54 UT – 280 %. In this case the missed trigger can be only for the first minute at 3.51 UT. The described method can be used in many CR Observatories where one minute data are detected. Since the frequency of ground FEP events increases with decreasing cut off rigidity, it will be important to introduce the described method in high latitude CR observatories. For low latitude CR Observatories the FEP increase starts earlier and the increase is much faster; this is very important for forecasting of dangerous situation caused by great FEP events (this problem is considered in more detail in Dorman, M2005).

4.8.6. Website of ICRC/ESO in Internet and automatic alarms on the starting of big solar CR events

The first page of the ICRC/ESO website is shown in Fig. 4.8.6.

Israel Cosmic Ray Center & Emilio Segre' Israel-Italy Observatory

affiliated to Tel Aviv University, Technion, and Israel Space Agency

- INTRODUCTION
- EMILIO SEGRE' OBSERVATORY, ISRAEL (ESOI)
- WORLD DATA CENTER C1 (TRANSFERRED FROM SWEDEN) FOR COSMIC RAYS
- STAFF OF ICRC AND ESOI
- REAL-TIME ONE MINUTE DATA FOR THE LAST 28 HOURS (ASCII DATA)
- REAL-TIME ONE HOUR DATA FOR THE LAST 6 DAYS (ASCII DATA)
- REAL TIME DATA IMAGE (last 6 hours and last 6 days)
- ONE-DAY DATA FOR THE LAST 365 DAYS
- DATA ARCHIVE OF ESOI - 1998, 1999, 2000
- ANNUAL RESEARCH REPORT No 1, 1998
- ANNUAL RESEARCH REPORT No 2, 1999
- ANNUAL RESEARCH REPORT No 3, 2000
- IMPORTANT PUBLICATIONS BEFORE 1998
- PUBLICATIONS OF ICRC STAFF - 1998
- PUBLICATIONS OF ICRC STAFF - 1999
- PUBLICATIONS OF ICRC STAFF - 2000
- LECTURES "COSMIC RAY ASTROPHYSICS and GEOPHYSICS" - Prof. Lev Dorman, Tel Aviv University, March - June 2001 (content as html-page).
- Official Address
- Conditions for Use of Data

- USEFULL LINKS TO COSMIC RAY OBSERVATORIES
- USEFULL LINKS TO SPACE WEATHER

Fig. 4.8.6. The first page of the ICRC/ESO website on the Internet.

An example of the one minute and one hour data in real time scale (updated every minute) with information on the Alert for dangerous CR increases on the ground level is shown in Fig. 4.8.7.

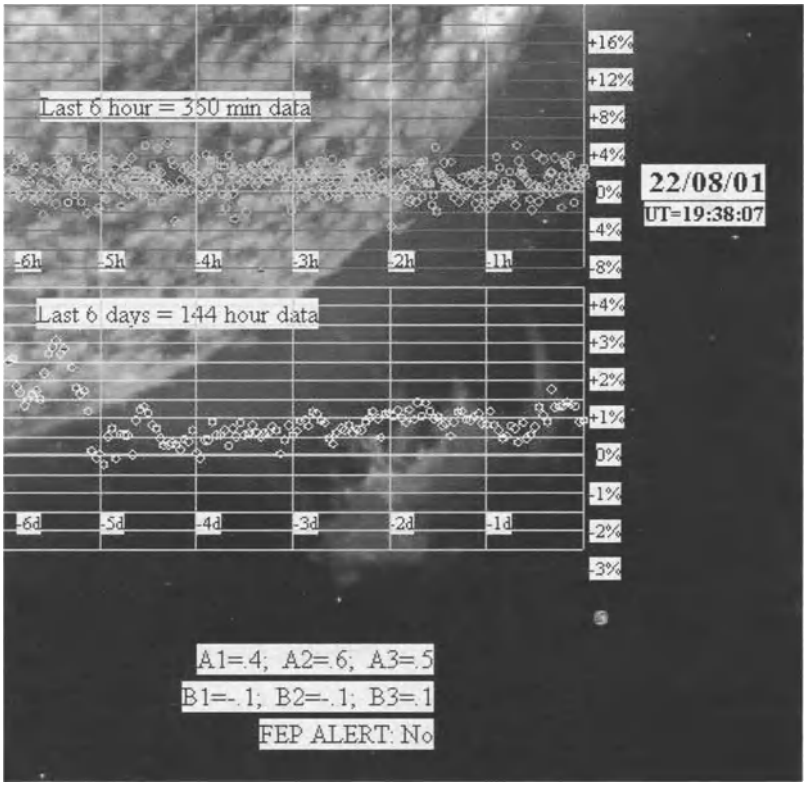

Fig. 4.8.7. Graphical presentation of ESO NM-IQSY real time data, updated each minute: upper circles – one-minute data of total neutron intensity from both sections for the last 360 minutes; lower circles – one-hour data for total neutron intensity for the last 144 hours; the numbers show at the bottom are the CR intensity variations in both sections for one-, two- and three-minutes data (in units σ), and the final conclusion for the Alert (for the moment shown on the figure, at 19.38 UT at 22 August 2001 Flare Energetic Particle Alert: No was obtained after 7 seconds).

4.9. Development of Solar Neutron Telescope (SNT) – a special detector for search and investigations of solar neutron events

4.9.1. The first SNT and formation of the SNT worldwide network

Here we will describe very shortly the development of a special detector for search and investigations of solar neutron events (SNE): the solar neutron telescope (SNT). The first SNT was developed for the CR Observatory on Mt. Norikura with an effective area of 1 m^2; it started to work in October 1990 (Muraki et al., 1992; in 1996 it was replaced by a new SNT with an effective area of 64 m^2). Let us note that the first great SNE in 1982 and 1990 were detected by the widely used NM described in Section 4.4 (see review in Usoskin et al., 1997). The NM, however, have no ability to measure the

energies of incident neutrons. For this reason, Japanese scientists developed new detectors called SNT and installed them on several high mountains (see Table 4.9.1).

Table 4.9.1. The first SNT worldwide network. According to Tsuchiya et al. (2001a,b).

Location (place)	Height (g/cm^2)	Longitude	Latitude	Area (m^2)	Start of observation
Switzerland (Gornergrat)	700	7.8° E	46.0° N	4	Jan. 1998
Armenia (Aragats)	700	40.5° E	44.2° N	4	Jun. 1997
Tibet (Yangbajing)	600	90.5° E	30.0° N	9	Sep. 1998
Japan (Mt. Norikura)	730	137.5° E	36.1° N	1	Oct. 1990
				64	Oct. 1996
USA (Mauna Kea)	610	203.7° E	19.8° N	8	Apr. 1997
Bolivia (Mt. Chacaltaya)	540	292° E	16.2° S	4	Sep. 1992

All SNT developed in Japan have a target layer, which consists of a thick scintillator or wood. Incoming neutrons are converted into protons by nuclear interactions in the target. Recoil protons which undergo a charge exchange process tend to be scattered in the direction of incident neutrons, almost conserving the energy of the incident neutrons. A schematic view of the SNT with effective area 4 m^2 is given in Fig. 4.9.1.

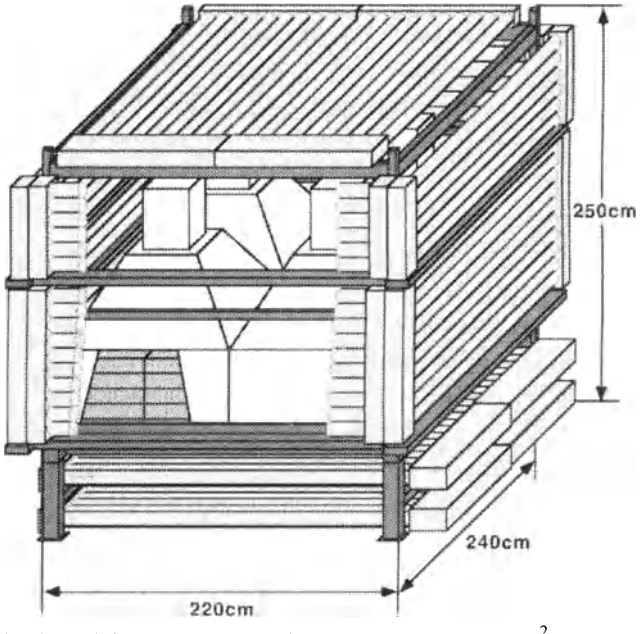

Fig. 4.9.1. Schematic view of the standard SNT with an effective area of 4 m^2. Scintillation counters are covered with proportional counters for excluding charged particles. Recoil protons converted in the scintillator are detected by a photomultiplier located above scintillators. The proportional counters under the scintillation counters are situated for measuring the arrival directions of neutrons. According to Matsubara et al. (1997).

In more details the SNT on Mt. Chacaltaya (Bolivia) is described in Matsubara et al. (1995), on Mt. Gornergrat (Switzerland) – in Bütikofer et al. (2003), on Mt. Aragats (Armenia) – in Chilingarian et al. (2003).

4.9.2. The largest SNT on Mt. Norikura (Japan)

Fig. 4.9.2 shows the schematic view of the world's largest Norikura SNT, developed in 1996. The scintillation counters cover an area of 64 m^2. Scintillators with a size of 100 cm×100 cm ×20 cm are placed inside each scintillation counter. Incoming neutrons are converted into protons in the scintillator. The measured energy deposits of recoil protons in the scintillator are > 20, > 40, > 60, and > 80 MeV. The scintillation counters are surrounded by proportional counters which reject charged particles.

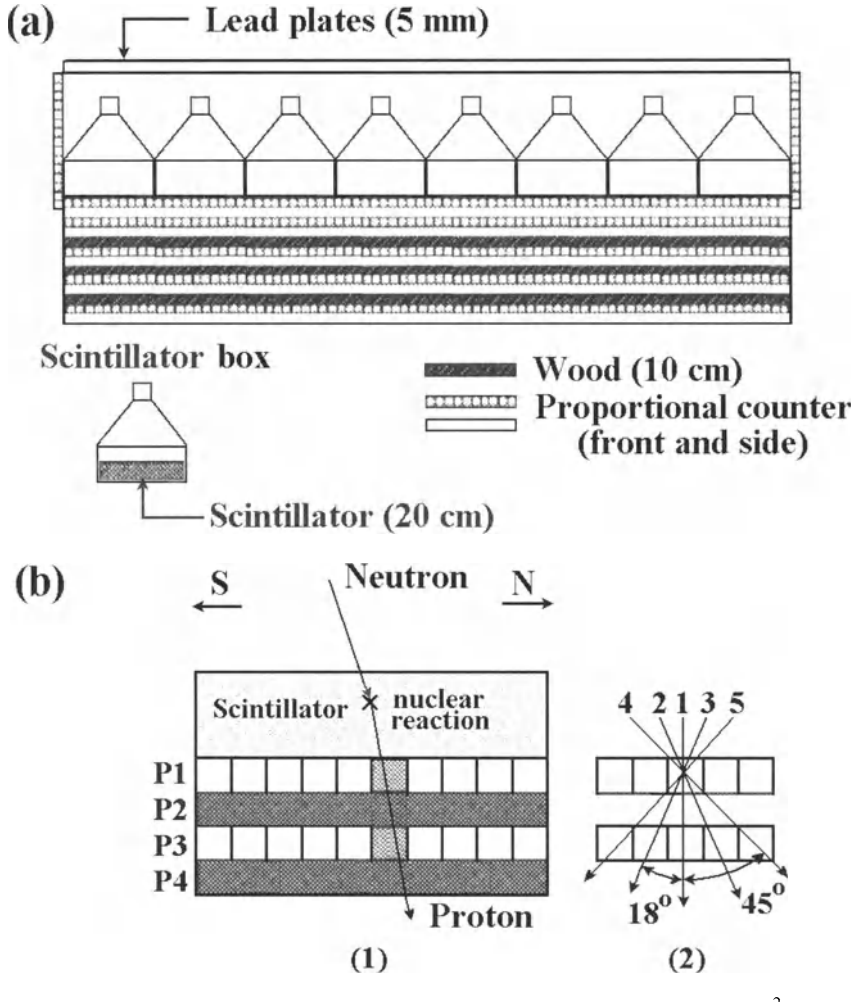

Fig. 4.9.2. (a) Schematic view of the largest SNT in the world, located on Mt. Norikura (64 m^2 detector), (b) Schematic diagram of the measurement of the direction of neutrons using the Norikura 64 m^2 detector. According to Muraki et al. (1997).

4.9.3. Calibrating of SNT

For the purpose of calibrating the detection efficiency of SNT, Tsuchiya et al. (2001) carried out between February 1996 and June 1999 accelerator experiments at the Research Center for Nuclear Physics of Osaka University, by using 100 m time-of-flight tunnel for accurate determination of neutron energy. Neutrons were produced using the reactions of ^{7}Li(p, n)^{7}Be. Protons were accelerated by the AVF cyclotron and the ring cyclotron. The thickness of Li target was 0.543 g/cm^{2}. The energies of bombarding protons for neutron production were 150, 230, 300 and 392 MeV in February and July 1996, and 100, 200, 300 and 392 MeV in December 1996 and June 1999. To obtain neutrons emitted in the incident direction of accelerated protons, neutrons were passed through a collimator which was placed at 5.93 m downstream from the Li target. All charged particles were bent by a magnet outside the target which prevented the entrance of protons into the neutron beam line. Each solar neutron detector was placed at a point 63–80 m away from the Li target; the neutron beam spread over ± (60–80) cm vertically and ± (50–70) cm horizontally. As example, in Fig. 4.9.3 are shown results of calibrating the detection efficiency of SNT on Mt. Chacaltaya in comparison with theoretical results of Monte Carlo simulation.

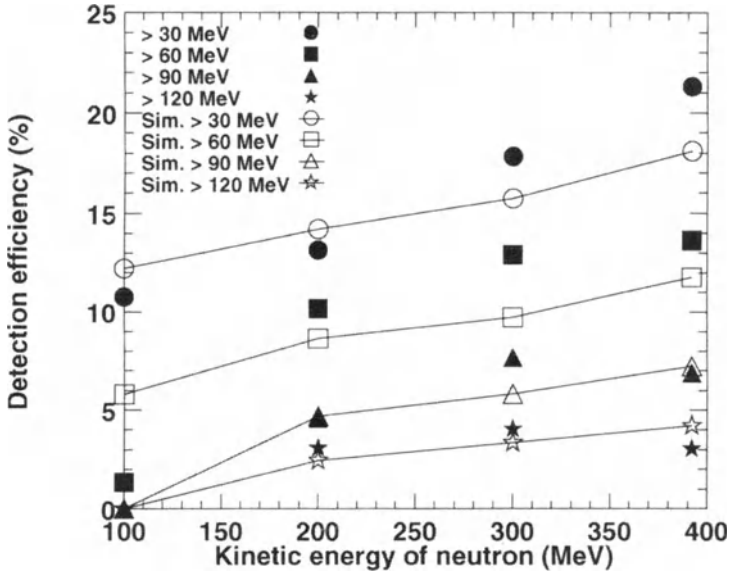

Fig. 4.9.3. Results of calibrating the detection efficiency of SNT on Mt. Chacaltaya (black points) in comparison with theoretical results of Monte Carlo simulations (white points, connected by lines) for channels >30, >60, >90, and >120 MeV. The ordinate gives the detection efficiency as a percentage and the abscissa gives the kinetic energy of neutrons in MeV. According to Tsuchiya et al. (2001a,b).

From Fig. 4.9.3 it can be seen that for the lowest channel (>30 MeV threshold), experimental results give the detection efficiencies as 11%, 13%, 18% and 21% for each incident energy of neutrons, while the prediction by the simulation gives them as 12%, 14%, 16% and 18%. The relative difference between the experimental results and simulations for this channel is therefore less than 15%.

4.9.4. Extending of SNT network: foundation of new SNT in Mexico

According to Valdes-Galicia et al. (2003), a new SNT has been constructed on Mt. Sierra Negra (4580m) in Mexico at 19.0° N, 97.3° W. It is the standard SNT shown in Fig. 4.9.1, but with increasing thickness of plastic scintillators from 20 cm to 30 cm. For data processing of Mexico SNT Sako et al. (2003a) applied Complex Programmable Logic Device (CPLD). It is supposed that CPLD in near future will be used for data processing also for other SNT of the worldwide network (see Table 4.9.1) as well as for new type of SNT, so called super SNT (see below, Section 4.9.5).

4.9.5. Developing of Super Solar Neutron Telescope (SSNT)

Sako et al. (2003b) proposed a new type of solar neutron detector, the Super Solar Neutron Telescope (SSNT), for the next solar cycle 24. It is assumed that the new detector should retain the function of the present SNT, i.e., the capability for energy measurement and determination of the arrival direction of solar neutrons with high detection efficiency. For this purpose SSNT should be composed of scintillators blocks with dimensions of 5cm×10cm×300cm. Those scintillators blocks will be aligned to compose a tracker and the proposed dimensions of the SSNT 300cm×300cm×150cm (total number of scintillators blocks 900). In Fig. 4.9.4 is shown the design of SSNT.

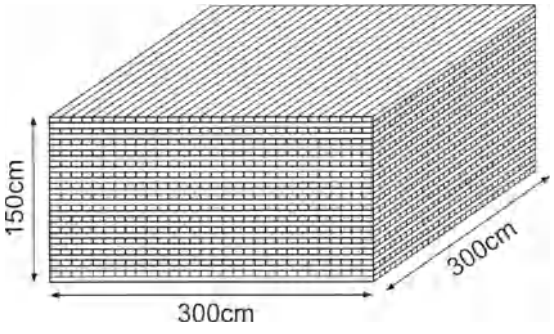

Fig. 4.9.4. Proposed design of the Super Solar Neutron Telescope (SSNT). According to Sako et al. (2003b).

The comparison of concept of the current observations of solar neutrons by SNT and concept of observations by SSNT is shown in Fig. 4.9.5.

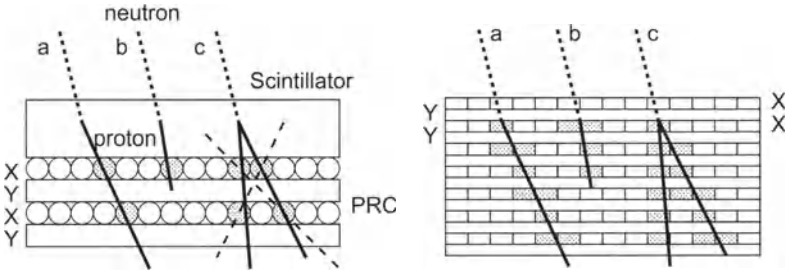

Fig. 4.9.5. Method of determining direction of neutrons arrival in SNT (left) and in SSNT (right). Incoming neutrons (dotted lines) are converted into protons (solid lines) in a plastic scintillators and the track of the recoiled particle is measured by the underlying proportional counters (PRCs) in SNT or much more exactly by scintillators blocks in SSNT. In SSNT will be possible avoid misidentification of the direction in case *c*. The data processing in SSNT supposed to be made automatically by Complex Programmable Logic Device (CPLD). According to Sako et al. (2003b).

Part 2

INFLUENCE OF THE CHANGING ATMOSPHERE ON COSMIC RAYS (METEOROLOGICAL EFFECTS)

Preface of Part 2

As we mentioned in Chapter 1, the barometric effect in CR was discovered in the middle of the 1920s, and the temperature effect about 10 years later. The barometric effect was interpreted as an absorber effect, and temperature effect as being caused by decay of muons. Only in the 1950s was a full theory of CR meteorological effects developed in the one-dimensional approximation (Dorman, 1951a,b, 1954a,b, M1957), and it was shown that, in fact, the barometric effect consists of three effects: absorption, decay and generation effects. The relative role of these effects depends very much on the altitude of observations and the value of the total detector shielding (for measurements on the ground and at different depths underground). It was also shown that the temperature effect is determined not only by the decay of muons, but also by the decay of pions and by the distribution function of pion generation in the atmosphere in nuclear reactions of protons, alpha–particles and heavier nuclei of primary CR with air atoms.

Part 2 contains five Chapters from 5 to 9. In **Chapter 5** is given the full theory of CR meteorological effects in the one-dimensional approximation (it is that pions, muons, and other secondary CR particles having the same direction as primary CR particles, generated these secondary CR). **Chapter 6** considers in detail experimental data for the snow effect, the Bernoulli effect (caused by winds in the atmosphere), and the barometric effect. **Chapter 7** is devoted to detailed analysis of temperature and humidity effects of different CR secondary components, and **Chapter 8** – to theoretical and experimental investigations of atmospheric electric field effects in muon, electron–photon, and neutron components (including different multiplicities).

In **Chapter 9** is given the development of the full theory of CR meteorological effects taking into account of muon angle and energy distribution at the decay of pions, Coulomb scattering of muons during propagation in the atmosphere, and possible generation of muons also through decay of kaons. In this Chapter we consider also the problem on the influence of magnetospheric and extra-terrestrial CR variations on the meteorological coefficients; for this purpose we introduce meteorological coefficients for integral multiplicity (partial meteorological coefficients). Especially important is the method of the partial barometric coefficient, and we determine this coefficient on the basis of observations of total barometric coefficient variations with cut off rigidity.

Chapter 5

Theory of Cosmic Ray Meteorological Effects for Measurements in the Atmosphere and Underground (One-Dimensional Approximation)

5.1. Meteorological effects of CR hard muon component

5.1.1. Expected pion intensity

Let us denote by $f_{\pi}(E_{\pi},h_1,Z)$ the $\pi^{\pm}$ – mesons (or, charged pions) generation function that depends on the air pressure level h_1, the total energy E_{π} and the zenith angle Z (this function will be defined quantitatively below, in Section 5.1.3, Eq. 5.1.22). Some part of the pions will be captured by air nuclei along with the generation of a lot of secondary particles, so that the energy of generated muons in this case will be too small to reach the ground level. The other part of the pions will decay with generation of muons. Let us suppose that l is the transport path of pions for nuclear interactions in the air. In this case, the fraction $dh/(l\cos Z)$ of the pions will be captured in the air layer dh. If m_{π} and τ_{π} are the mass and life time of charged pions at rest, the fraction of pions that decay in the air layer dh will be $d\tau/\tau$, where $d\tau = dh(c\rho(h)\cos Z)^{-1}$ is the time it takes to cross the layer dh, $\rho(h)$ is the density of air at the level h, and c is the velocity of light, which in the cases considered here will be about equal to the velocity of relativistic pions, and $\tau = \tau_{\pi}E_{\pi}/m_{\pi}c^2$ is the life time of pions in the system of coordinates fixed to the Earth. Therefore the probability $\varphi_{\pi}(E_{\pi},h_1,h,Z)$ that pions will be not be captured by nuclei and will not decay in the layer from h_1 to h will be determined by the equation

$$d\varphi_{\pi}(E_{\pi},h_1,h,Z) = \varphi_{\pi}(E_{\pi},h_1,h,Z)\left(-\frac{dh}{l\cos Z} - \frac{m_{\pi}c}{\tau_{\pi}E_{\pi}}\frac{dh}{\rho(h)\cos Z}\right). \qquad (5.1.1)$$

By integrating Eq. 5.1.1 from h_1 to h_2 with the boundary condition $\varphi_{\pi}(E_{\pi},h_1,h_1,Z)=1$, we obtain

$$\varphi_{\pi}(E_{\pi},h_1,h_2,Z) = \exp\left(-\frac{h_2-h_1}{l\cos Z}\right)\exp\left(-\frac{m_{\pi}c}{\tau_{\pi}E_{\pi}\cos Z}\int_{h_1}^{h_2}\frac{dh}{\rho(h)}\right). \qquad (5.1.2)$$

Since the pion generation starts at the boundary of atmosphere ($h_1 = 0$), the intensity of pions at level h_2 will be

$$N_\pi(E_\pi,h_2,Z)=\int_0^{h_2} f_\pi(E_\pi,h_1,Z)\varphi_\pi(E_\pi,h_1,h_2,Z)dh_1\ . \tag{5.1.3}$$

5.1.2. Expected hard muon intensity

Let us take into account that $\mu^\pm$ mesons (or, muons) are generated mostly through decay of charged pions:

$$\pi^+\to\mu^++\nu_\mu,\quad \pi^-\to\mu^-+\overline{\nu}_\mu \tag{5.1.4}$$

The direction of muon propagation will be about the same as that of pions (as for decay of ultra-relativistic pions). In this case the number of muons generated by pions with energy E in the layer between h_2 and h_2+dh_2 will be

$$f_\mu(E_\pi,h_2,Z)dh_2=\frac{d\tau}{\tau}N_\pi(E_\pi,h_2,Z)=\frac{m_\pi c}{\tau_\pi E_\pi}\frac{N_\pi(E_\pi,h_2,Z)dh_2}{\rho(h_2)\cos Z}, \tag{5.1.5}$$

where $N_\pi(E_\pi,h_2,Z)$ is determined by Eq. 5.1.3. Generated muons will be in the energy interval $\alpha^2E_\pi\le E_\mu\le E_\pi$ (where $\alpha=m_\mu/m_\pi$) distributed homogeneously, and can be described by the function

$$\omega(E_\mu)dE_\mu=\begin{cases}\left(E_\pi\left(1-\alpha^2\right)\right)^{-1}dE_\mu, & \text{if } \alpha^2E_\pi\le E_\mu\le E_\pi\\ 0, & \text{if } E_\mu<\alpha^2E_\pi,\ E_\mu>E_\pi.\end{cases} \tag{5.1.5a}$$

Therefore muons with energy E_μ will be generated by decay of pions with energy E_π from E_μ up to E_μ/α^2, and their generating function will be

$$\Omega_\mu(E_\mu,h_2,Z)=\int_{E_\mu}^{E_\mu/\alpha^2} f_\mu(E_\pi,h_2,Z)\left(E_\mu\left(\alpha^{-2}-1\right)\right)^{-1}dE_\pi\ , \tag{5.1.6}$$

As a first approximation we will use some average value of the interval of pion energy E_π from E_μ up to E_μ/α^2 as $\langle E_\pi\rangle\approx E_\mu/\alpha$. In this case instead of integral in Eq. 5.1.6, we obtain

$$\Omega_\mu(E_\mu,h_2,Z)\approx f_\mu(E_\pi=E_\mu/\alpha,h_2,Z). \tag{5.1.7}$$

Let us take into account that a muon generated on the level h_2 with energy $E_\mu=\alpha E_\pi$ from decay of a pion with energy E_π on the level h will have energy $\alpha E_\pi-a(h-h_2)/\cos Z$, where a is the energy lost by the muon passing 1 g/cm^2 of air

($a \approx 2\,\mathrm{MeV}/\left(\mathrm{g}/\mathrm{cm}^2\right)$ for relativistic singly charged particles). Since muons practically do not have nuclear interactions, the loss of muons will only be caused by their decay, with a life time corresponding to the rest muon life time τ_μ in reactions:

$$\mu^+ \to e^+ + \overline{\nu}_\mu + \nu_e, \quad \mu^- \to e^- + \nu_\mu + \overline{\nu}_e \,. \tag{5.1.8}$$

By repeating the calculations that lead to Eq. 5.1.2, but for muons, we finally obtain that the probability of muons to pass the layer from h_2 to the level of observation h_o without decaying will be

$$\varphi_\mu(E_\pi, h_2, h_o, Z) = \exp\left(-\frac{m_\mu c}{\tau_\mu} \int_{h_2}^{h_o} \frac{dh}{\rho(h)} \left(\alpha E_\pi \cos Z - a(h - h_2)\right)^{-1} \right). \tag{5.1.9}$$

Because muons are generated from the boundary of atmosphere ($h_2 = 0$) up to the level of observation h_o, we obtain for the intensity of muons

$$N_\mu(h_o, Z, E_{\mu\min}) = \int_{E_{\pi\min}}^{\infty} dE \int_0^{h_o} f_\mu(E_\pi, h_2, Z)\varphi_\mu(E_\pi, h_2, h_o, Z)dh_2 \,, \tag{5.1.10}$$

where $E_{\pi\min}$ is the minimal energy of pions that generated muon which have the energy $E_{\mu\min}$ at generation (detector's cut off energy for hard muons). The value of $E_{\pi\min}$ for observations underground or on the ground with a plate-parallel screen will be

$$E_{\pi\min} = \left(a(h_o - h_2) + E_{\mu\min}\right)/\alpha\cos Z \,, \tag{5.1.11}$$

and for spherically symmetric screen (10 cm Pb screen in ionization chambers of Compton type):

$$E_{\pi\min} = a(h_o - h_2)/\alpha\cos Z + E_{\mu\min}/\alpha \,. \tag{5.1.12}$$

By substituting Eq. 5.1.5 and Eq. 5.1.9 into Eq. 5.1.10 and taking into account Eq. 5.1.7, we obtain for the expected directed intensity of muons

$$N_\mu(h_o, Z, E_{\mu\min}) = \int_{E_{\pi\min}}^{\infty} dE_\pi \int_0^{h_o} dh_2 \int_0^{h_2} dh_1 F(E_\pi, h_1, h_2, h_o, Z), \tag{5.1.13}$$

where

$$F(E_\pi,h_1,h_2,h_o,Z)=\frac{m_\mu c f_\pi(E_\pi,h_1,Z)}{\tau_\pi E_\pi \rho(h_2)\cos Z}\exp\left(-\frac{m_\pi c}{\tau_\pi E_\pi \cos Z}\int_{h_1}^{h_2}\frac{dh}{\rho(h)}\right)$$
$$\times\exp\left(-\frac{h_2-h_1}{l\cos Z}\right)\exp\left(-\frac{m_\mu c}{\tau_\mu}\int_{h_2}^{h_o}\frac{dh}{\rho(h)}(\alpha E_\pi\cos Z-a(h-h_2))^{-1}\right). \quad (5.1.14)$$

5.1.3. Expected meteorological variations of muon intensity

In Eq. 5.1.13 we have the following variables that depend on meteorological conditions: $E_{\pi\min}$, h_o and $\rho(h)$. Let us vary Eq. 5.1.13 with respect to these variables:

$$\delta N_\mu(h_o,Z,E_{\mu\min})=-\delta E_{\pi\min}\int_0^{h_o}dh_2\int_0^{h_2}dh_1 F(E_{\pi\min},h_1,h_2,h_o,Z)$$
$$+\delta h_o\int_{E_{\pi\min}}^{\infty}dE_\pi\exp\left(-\frac{h_2-h_1}{l\cos Z}\right)\left\{\int_0^{h_o}dh_1 F(E_\pi,h_1,h_2,h_o,Z)\right.$$
$$\left.-\frac{m_\mu c}{\tau_\mu\rho(h_o)}\int_0^{h_o}dh_2\int_0^{h_2}dh_1\frac{F(E_\pi,h_1,h_2,h_o,Z)}{\alpha E_\pi\cos Z-a(h_o-h_2)}\right\}$$
$$-\int_{E_{\pi\min}}^{\infty}dE_\pi\int_0^{h_o}dh_2\frac{\delta\rho(h_2)}{\rho(h_2)}\int_0^{h_o}dh_1 F(E_\pi,h_1,h_2,h_o,Z) \quad (5.1.15)$$
$$+\int_{E_{\pi\min}}^{\infty}dE_\pi\int_0^{h_o}dh_2\int_0^{h_2}dh_1 F(E_\pi,h_1,h_2,h_o,Z)$$
$$\times\left\{\frac{m_\pi c}{\tau_\pi E_\pi\cos Z}\int_{h_1}^{h_2}\frac{dh\,\delta\rho(h)}{\rho^2(h)}+\frac{m_\mu c}{\tau_\mu}\int_{h_2}^{h_o}\frac{dh}{\rho^2(h)}\frac{\delta\rho(h)}{\alpha E_\pi\cos Z-a(h_o-h_2)}\right\}.$$

In Eq. 5.1.15 function $F(E_\pi,h_1,h_2,h_o,Z)$ was determined by Eq. 5.1.14. The first term in Eq. 5.1.15 reflects the absorption effect, caused by the change of $E_{\pi\min}$. Let us take into account that according to Eq. 5.1.11

$$\delta E_{\pi\min}=\left(a\delta h_o+\delta E_{\mu\min}\right)/\alpha\cos Z \quad (5.1.16)$$

for observations with plate-parallel screen, and according to Eq. 5.1.12

$$\delta E_{\pi\min}=a\delta h_o/\alpha\cos Z+\delta E_{\mu\min}/\alpha \quad (5.1.17)$$

for spherically symmetric screen. The first term in Eq. 5.1.16 and 5.1.17 corresponds to absorption barometric effect, and the second to the snow effect. The second term in Eq. 5.1.15 consists of two parts: the first, positive, reflects additional generation of pions with increasing h_o (this part dominates at high altitudes where total barometric effect becomes positive, but it is negligibly small near sea level). The second part, negative,

reflects the increase of muon decay with increasing h_o (caused by increasing height of the muon generation level with increasing h_o). The third and fourth terms in Eq. 5.1.15 reflect air density effects caused by the instability of pions and muons. Let us take into account that

$$\rho(h) = g\bar{h}/R(h)T(h), \tag{5.1.18}$$

where g is the gravity acceleration on the Earth, and, according to Uotila (1957),

$$g(\varphi,\lambda) = 978.0516\left[1 + 0.0052910\sin^2\varphi - 0.0000059\sin^2 2\varphi + 0.0000106\cos^2\varphi\cos 2\left(\lambda + 6^o\right)\right], \tag{5.1.19a}$$

where φ is the geographic latitude and λ is the geographic longitude of the measurement site. In Eq. 5.1.18 $\bar{h}$ is the air mass in the 1 cm^2 vertical column, $T(h)$ is the air temperature in °K and

$$R(h) = R_o\left(1 + 0.378e(h)/h\right) \tag{5.1.19b}$$

is the gas constant for air (here R_o is the gas constant of dry air, $e(h)$ is the pressure of water steam). From Eq. 5.1.18 follows

$$\frac{\delta\rho(h)}{\rho(h)} = \frac{\delta g}{g} - \frac{\delta R(h)}{R(h)} - \frac{\delta T(h)}{T(h)}; \quad \frac{\delta\rho(h)}{\rho^2(h)} = \frac{\delta g}{\rho(h)g} - \frac{R(h)}{h}\delta T(h) - \frac{T(h)}{h}\delta R(h); \tag{5.1.20}$$

and from Eq. 5.1.19b we have

$$\delta R(h) = 0.378R_o\delta e(h)/h. \tag{5.1.21}$$

For calculations of Eq. 5.1.15 we need to know the function $f_\pi(E,h_1,Z)$ of pion generation. According to a variety of experimental and theoretical data this function can be described approximately as

$$f_\pi(E_\pi,h_1,Z) = AE_\pi^{-(2+\gamma)}\exp(-h_1/L\cos Z), \tag{5.1.22}$$

where A is some constant, $0 \le \gamma \le 1$, and L is absorption path of meson-generating nucleon component of primary CR.

5.1.4. *Expected meteorological effects of different types*

Let us introduce the function

$$\Phi\left(E_\pi,h_1,h_2,h_o,Z,E_{\mu\min}\right) = F\left(E_\pi,h_1,h_2,h_o,Z\right)/N_\mu\left(h_o,Z,E_{\mu\min}\right), \tag{5.1.23}$$

where $N_\mu(h_o,Z,E_{\mu\min})$ is described by Eq. 5.1.13, and $F(E_\pi,h_1,h_2,h_o,Z)$ by Eq. 5.1.14. By substituting Eqs. 5.1.16–5.1.22 in Eq. 5.1.15, dividing by $N_\mu(h_o,Z,E_{\mu\min})$, and then by taking into account the definition Eq. 5.1.23, we obtain for meteorological effects of different types as following:

- For **snow effect** (of absorption origin) for spherically-symmetrical screen

$$\left.\frac{\delta N_\mu(h_o,Z,E_{\mu\min})}{N_\mu(h_o,Z,E_{\mu\min})}\right|_{\text{snow}} = -\delta E_{\mu\min}\alpha^{-1}\int_0^{h_o}dh_2\int_0^{h_2}dh_1\Phi(E_{\pi\min},h_1,h_2,h_o,Z,E_{\mu\min}) \quad (5.1.24)$$

(for the plate-parallel screen in this equation will be $(\alpha\cos Z)^{-1}$ instead of α^{-1}).

- For **barometric effect** (of absorption, decay and generation origin)

$$\left.\frac{\delta N_\mu(h_o,Z,E_{\mu\min})}{N_\mu(h_o,Z,E_{\mu\min})}\right|_{\text{bar}}$$

$$= \delta h_o\times\{-a\alpha^{-1}\int_0^{h_o}dh_2\int_0^{h_2}dh_1\Phi(E_{\pi\min},h_1,h_2,h_o,Z,E_{\mu\min})-$$

$$-\frac{m_\mu c}{\tau_\mu\rho(h_o)}\int_{E_{\pi\min}}^{\infty}dE_\pi\int_0^{h_o}dh_2\int_0^{h_2}dh_1\frac{\Phi(E_\pi,h_1,h_2,h_o,Z,E_{\mu\min})}{\alpha E_\pi\cos Z-a(h_o-h_2)}+$$

$$+\int_{E_{\pi\min}}^{\infty}dE_\pi\int_0^{h_2}dh_1\Phi(E_\pi,h_1,h_2,h_o,Z,E_{\mu\min})\}. \quad (5.1.25)$$

- For **temperature effect** (of pion decay and nuclear interactions, and muon ionization losses and decay origin)

$$\left.\frac{\delta N_\mu(h_o,Z,E_{\mu\min})}{N_\mu(h_o,Z,E_{\mu\min})}\right|_{\text{temp}} = \int_{E_{\pi\min}}^{\infty}dE_\pi\int_0^{h_o}dh_2\int_0^{h_2}dh_1\Phi(E_\pi,h_1,h_2,h_o,Z,E_{\mu\min})\times$$

$$\left\{\frac{\delta T(h_2)}{T(h_2)}-\frac{R_o m_\pi c}{E_\pi\tau_\pi\cos Z}\int_{h_1}^{h_2}\frac{dh\,\delta T(h)}{h}-\frac{R_o m_\mu c}{\tau_\mu}\int_{h_2}^{h_o}\frac{dh}{h}\frac{\delta T(h)}{\alpha E_\pi\cos Z-a(h-h_2)}\right\}. \quad (5.1.26)$$

- For **humidity effect** (of pion decay and nuclear interactions, and muon ionization losses and decay origin)

$$\left.\frac{\delta N_\mu(h_o,Z,E_{\mu\min})}{N_\mu(h_o,Z,E_{\mu\min})}\right|_{\text{humid}} = 0.378 \int_{E_{\pi\min}}^{\infty} dE_\pi \int_0^{h_o} dh_2 \int_0^{h_2} dh_1 \Phi(E_\pi,h_1,h_2,h_o,Z,E_{\mu\min})$$

$$\times\left\{\frac{\delta e(h_2)}{e(h_2)} - \frac{R_o m_\pi c}{E_\pi \tau_\pi \cos Z}\int_{h_1}^{h_2}\frac{dhT(h)\delta e(h)}{h^2} - \frac{R_o m_\mu c}{\tau_\mu}\int_{h_2}^{h_o}\frac{dh}{h^2}\frac{T(h)\delta e(h)}{\alpha E_\pi \cos Z - a(h-h_2)}\right\}. \quad (5.1.27)$$

- For **gravitational effect** (absorption and decay of pions and muons)

$$\left.\frac{\delta N_\mu(h_o,Z,E_{\mu\min})}{N_\mu(h_o,Z,E_{\mu\min})}\right|_{\text{gravit}} = \frac{\delta g}{g}\int_{E_{\pi\min}}^{\infty} dE_\pi \int_0^{h_o} dh_2 \int_0^{h_2} dh_1 \Phi(E_\pi,h_1,h_2,h_o,Z,E_{\mu\min})$$

$$\times\left\{-1 + \frac{m_\pi c}{E_\pi \tau_\pi \cos Z}\int_{h_1}^{h_2}\frac{dh}{\rho(h)} - \frac{m_\mu c}{\tau_\mu}\int_{h_2}^{h_o}\frac{dh}{\rho(h)}\frac{1}{\alpha E_\pi \cos Z - a(h-h_2)}\right\}. \quad (5.1.28)$$

5.1.5. Meteorological coefficients for hard muons

The parameter a in the previous equations characterizes energy losses of muons during crossing atmosphere. In Eq. 5.1.25–5.1.28 we assumed that a is constant, independent of muon energy. This is correct only for muon energies $\alpha E_\pi \le 10^{10}$ eV. For these energies $a \approx 2\times10^6$ eV/g.cm^{-2}. At higher energies, $\alpha E_\pi \ge 10^{11}$ eV, parameter a is not constant, but in this case $a(h-h_2) << \alpha E_\pi$, i.e. energy losses become negligible in comparison with total muon energy. Therefore in calculations of meteorological coefficients we can assume an approximately constant $a \approx 2\times10^6$ eV/g.cm^{-2}. Let us measure energy of pions and muons in units of 2 GeV and atmospheric pressure in units 1000 g.cm$^{-2} \approx$ atm ; in this case $a = 1$.

For calculations of meteorological coefficients it is necessary to choose the average profile of $T(h)$. Let us choose it in the form

$$T(h) = \begin{cases} 220, & \text{if } h \le 0.2 \text{ atm}, \\ 204 + 80h, & \text{if } h > 0.2 \text{ atm}. \end{cases} \quad (5.1.29)$$

The real $T(h)$ depends on the latitude and the climate in the region of observations and changes significantly during year. These changes will influence the values of meteorological coefficients and can be taken into account (see below, Section 5.1.6). Now we can calculate $N_\mu(h_o,Z,E_{\mu\min})$ and the meteorological coefficients. Results are as follows:

$$N_\mu(h_o,Z,E_{\mu\min})=A(\alpha\cos Z)^{1+\gamma}N_\gamma(h_o,Z,E_{\mu\min}), \tag{5.1.30}$$

$$\left.\frac{\delta N_\mu(h_o,Z,E_{\mu\min})}{N_\mu(h_o,Z,E_{\mu\min})}\right|_{\text{temp}}=\int_0^{h_o}W_T(h,h_o,E_{\mu\min},Z)\delta T(h)dh, \tag{5.1.31}$$

where

$$W_T(h,h_o,E_{\mu\min},Z)=W_T^{\pi}(h,h_o,E_{\mu\min},Z)+W_T^{\mu}(h,h_o,E_{\mu\min},Z) \tag{5.1.32}$$

and

$$N_\gamma(h_o,Z,E_{\mu\min})=\int_0^{h_o}\frac{\exp(-h_2/L\cos Z)\varphi_\gamma(s,v)dh_2}{(h_o-h_2+E_{\mu\min})^{1+\gamma}}, \tag{5.1.33}$$

$$W_T^{\pi}(h,h_o,E_{\mu\min},Z)=\frac{h\exp(-h/L\cos Z)\chi_\gamma(s,v)}{\alpha\lambda b_\pi(h)T(h)(h_o-h+E_{\mu\min})^{\gamma}N_\gamma\cos Z}, \tag{5.1.34}$$

$$W_T^{\mu}(h,h_o,E_{\mu\min},Z)=-\frac{m_\mu cR_o}{\tau_\mu hN_\gamma}\int_0^{h}\frac{\exp(-h_2/L\cos Z)f_\gamma(s,k,v)dh_2}{(h_o-h_2+E_{\mu\min})^{2+\gamma}}. \tag{5.1.35}$$

In Eq. 5.1.33–5.1.35 we used the following designations:

$$\varphi_\gamma(s,v)=\int_0^1 t^{1+\gamma}(t+s)^{-1}e^{vt}dt;\quad \chi_\gamma(s,v)=\int_0^1 t^{1+\gamma}(t+s)^{-2}e^{vt}dt; \tag{5.1.36}$$

$$f_\gamma(s,k,v)=\int_0^1 kt^{2+\gamma}(t+s)^{-1}(k-t)^{-1}e^{vt}dt, \tag{5.1.37}$$

where

$$s=\frac{h_2(h_o-h_2+E_{\mu\min})}{\alpha\lambda b_\pi(h_2)\cos Z},\quad k=\frac{h_o-h_2+E_{\mu\min}}{h-h_2},\quad \lambda=lL(L-l)^{-1}, \tag{5.1.38}$$

$$
v=\begin{cases}
\dfrac{\eta_{\mu 1}\ln\left[\dfrac{h_2}{h_o}\left(1-\dfrac{t(h_o-h_2)}{h_o-h_2+E_{\mu\min}}\right)\right]}{h_o-h_2(1-t)+E_{\mu\min}}, & \text{if } h_o\le 0.2 \text{ atm}\\[2ex]
\dfrac{\eta_{\mu 1}\ln\left[\dfrac{h_2}{h_o}\left(1-\dfrac{t(0.2-h_2)}{h_o-h_2+E_{\mu\min}}\right)\right]}{h_o-h_2(1-t)+E_{\mu\min}}+\dfrac{\eta_{\mu 3}}{t}\ln\left(\dfrac{1-\dfrac{t(h_o-h_2)}{h_o-h_2+E_{\mu\min}}}{1-\dfrac{t(0.2-h_2)}{h_o-h_2+E_{\mu\min}}}\right)\\[2ex]
\dfrac{\eta_{\mu 2}\ln\left[\dfrac{0.2}{h_o}\left(1-\dfrac{t(h_o-h_2)}{h_o-h_2+E_{\mu\min}}\right)\left(1-\dfrac{t(0.2-h_2)}{h_o-h_2+E_{\mu\min}}\right)^{-1}\right]}{h_o-h_2(1-t)+E_{\mu\min}}, & \text{if } h_o\ge 0.2 \text{ atm},\ h_2\le 0.2 \text{ atm}\\[2ex]
\dfrac{\eta_{\mu 2}\ln\left[\dfrac{h_2}{h_o}\left(1-\dfrac{t(h_o-h_2)}{h_o-h_2+E_{\mu\min}}\right)\right]}{h_o-h_2(1-t)+E_{\mu\min}}+\dfrac{\eta_{\mu 3}}{t}\ln\left(1-\dfrac{t(h_o-h_2)}{h_o-h_2+E_{\mu\min}}\right), & \text{if } h_2\ge 0.2 \text{ atm}.
\end{cases}
\tag{5.1.39}
$$

Here

$$
b_\pi(h)=\begin{cases}\eta_{\pi 1}, & \text{if } h\le 0.2 \text{ atm}\\ \eta_{\pi 2}+h\eta_{\pi 3}, & \text{if } h\ge 0.2 \text{ atm},\end{cases}\quad
b_\mu(h)=\begin{cases}\eta_{\mu 1}, & \text{if } h\le 0.2 \text{ atm}\\ \eta_{\mu 2}+h\eta_{\mu 3}, & \text{if } h\ge 0.2 \text{ atm},\end{cases}
\tag{5.1.40}
$$

where

$$
\begin{gathered}
\eta_{\pi 1}=220R_o m_\pi c\tau_\pi^{-1},\ \eta_{\pi 2}=204R_o m_\pi c\tau_\pi^{-1},\ \eta_{\pi 3}=80R_o m_\pi c\tau_\pi^{-1}\\
\eta_{\mu 1}=220R_o m_\mu c\tau_\mu^{-1},\ \eta_{\mu 2}=204R_o m_\mu c\tau_\mu^{-1},\ \eta_{\mu 3}=80R_o m_\mu c\tau_\mu^{-1}
\end{gathered}
\tag{5.1.41}
$$

Meteorological coefficients for humidity and gravity effects can be expressed through the temperature coefficient $W_T(h,h_o,E_{\mu\min},Z)$:

$$\left.\frac{\delta N_\mu(h_o,Z,E_{\mu\min})}{N_\mu(h_o,Z,E_{\mu\min})}\right|_{\text{hum}} = \int_0^{h_o} W_{\text{hum}}(h,h_o,E_{\mu\min},Z)\delta e(h)dh, \qquad (5.1.42)$$

where

$$W_{\text{hum}}(h,h_o,E_{\mu\min},Z) = 0.378(T(h)/h)W_T(h,h_o,E_{\mu\min},Z), \qquad (5.1.43)$$

and

$$\left.\frac{\delta N_\mu(h_o,Z,E_{\mu\min})}{N_\mu(h_o,Z,E_{\mu\min})}\right|_{\text{grav}} = \delta g\alpha_{\text{grav}}(h_o,E_{\mu\min},Z), \qquad (5.1.44)$$

where

$$\alpha_{\text{grav}}(h_o,E_{\mu\min},Z) = g^{-1}\int_0^{h_o} T(h)W_T(h,h_o,E_{\mu\min},Z)dh. \qquad (5.1.45)$$

The barometric effect, as we mentioned above (see Eq. 5.1.25), consists of absorption, decay, and generation contributions:

$$\delta N_\mu(h_o,E_{\mu\min},Z)/N_\mu(h_o,E_{\mu\min},Z)\big|_{\text{bar}} = \delta h_o(\beta_{\text{abs}}+\beta_{\text{dec}}+\beta_{\text{gen}}), \qquad (5.1.46)$$

where

$$\beta_{\text{abs}}(h_o,E_{\mu\min},Z) = -\frac{\cos Z}{N_\gamma(h_o,E_{\mu\min},Z)}\int_0^{h_o}\frac{\exp(-v_1-h_2/L\cos Z)dh_2}{(1+s)(h_o-h_2+E_{\mu\min})^{2+\gamma}}, \qquad (5.1.47)$$

$$\beta_{\text{dec}}(h_o,E_{\mu\min},Z) = -\frac{b_\mu(h_o)}{h_o}\int_0^{h_o}\frac{\exp(-h_2/L\cos Z)f_\gamma(s,k_o,v)dh_2}{(h_o-h_2+E_{\mu\min})^{2+\gamma}N_\gamma(h_o,E_{\mu\min},Z)}, \qquad (5.1.48)$$

$$\beta_{\text{gen}}(h_o,E_{\mu\min},Z) = \frac{\exp(-h_0/L\cos Z)\varphi_\gamma(s_o,v=0)}{N_\gamma(h_o,E_{\mu\min},Z)E_{\mu\min}^{1+\gamma}}. \qquad (5.1.49)$$

In Eq. 5.1.47 v_1 is determined by Eq. 5.1.39 at $t=1$; in Eq. 5.1.48 k_o is determined by Eq. 5.1.38 at $h=h_o$; in Eq. 5.1.49 s_o is determined by Eq. 5.1.38 at $h_2=h_o$. Let us note that all the formulas listed above for meteorological coefficients are obtained for the plane-parallel screen of muon detector. For spherically symmetrical screen, it is

necessary to use $E_{\mu\min}\cos Z$ instead of $E_{\mu\min}$ in all the formulas for meteorological coefficients. We used the following values of constants:

$$m_\mu = 215m_e,\ \tau_\mu = 2.15\times10^{-6}\,\text{sec},\ m_\pi = 276m_e,\ \tau_\pi = 2.5\times10^{-8}\,\text{sec}, \quad (5.1.50)$$

$$R_o = 2.87\times10^6\,\text{erg/g.grad},\ l = 60\,\text{g/cm}^2 = 0.06\ \text{atm},\ .L = 0.12\ \text{atm}. \quad (5.1.51)$$

Results of calculations of meteorological coefficients are shown in Fig. 5.1.1–5.1.9.

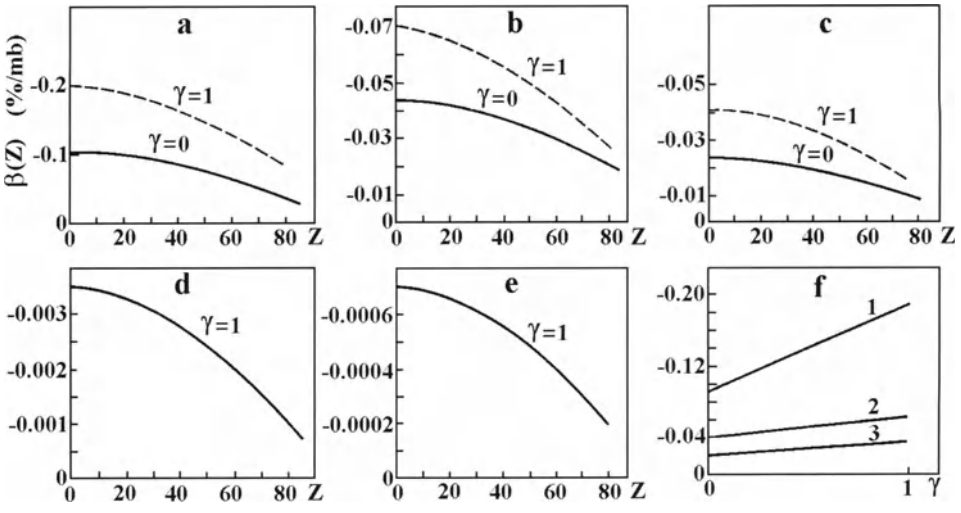

Fig. 5.1.1. Expected barometric coefficients for hard muon component (panels ***a*** – ***e***) at various values of γ detected under flat shield at sea level and underground with various $E_{\mu\min}$ as a function of the zenith angle Z: ***a*** – $E_{\mu\min} = 0.4$ GeV ; ***b*** – $E_{\mu\min} = 6.4$ GeV (corresponding to underground depth about 25 m w.e.); ***c*** – $E_{\mu\min} = 14.4$ GeV (about 55 m w.e.); ***d*** – $E_{\mu\min} = 100$ GeV (about 300 m w.e.); ***e*** – $E_{\mu\min} = 500$ GeV (about 1000 m w.e.). In panel **f** are shown barometric coefficients for various experimental conditions: ***1*** – cubical telescope at sea level with flat shield $E_{\mu\min} = 0.4$ GeV ; ***2*** – semi-cubical telescope underground about 25 m w.e., $E_{\mu\min} = 6.4$ GeV ; ***3*** - semi-cubical telescope underground about 55 m w.e., $E_{\mu\min} = 14.4$ GeV).

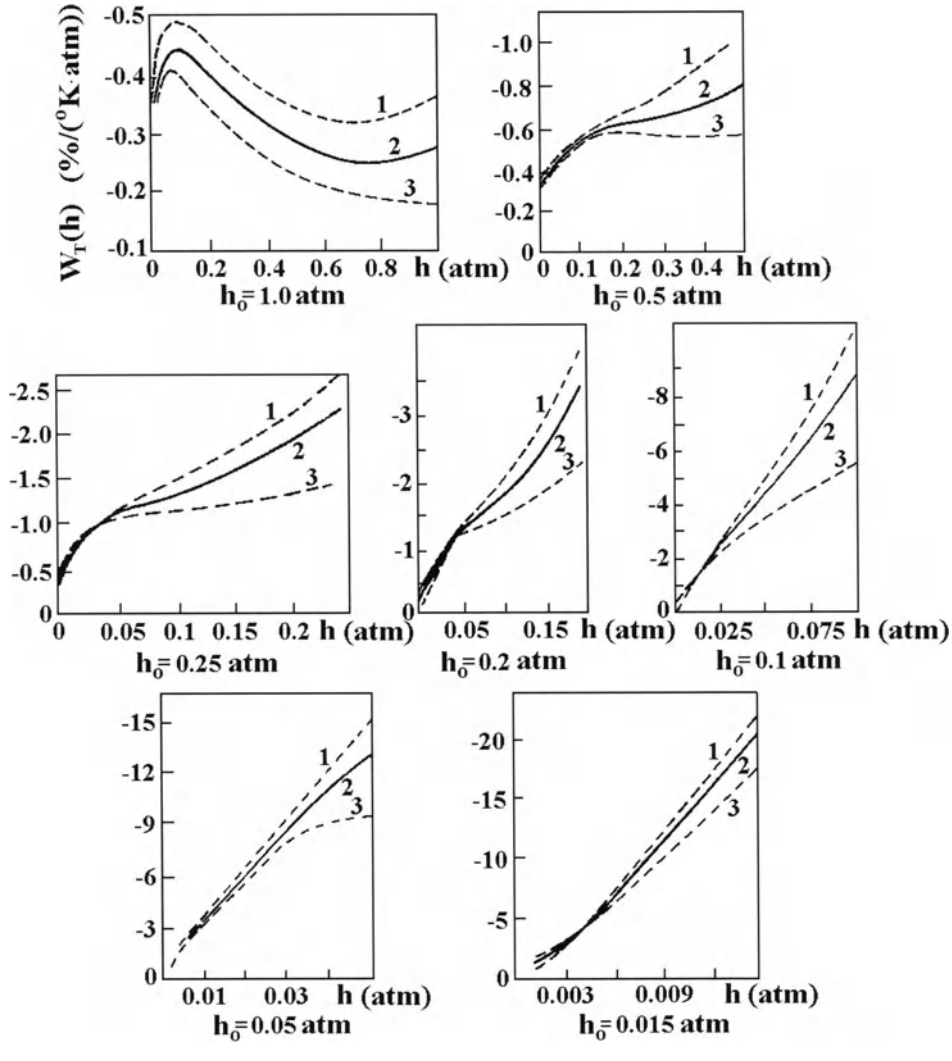

Fig. 5.1.2. Expected values of total temperature coefficients $W_T(h)$ for vertical arrival of hard muons ($E_{\mu\min} = 0.4$ GeV) as a function of h for different levels of observation h_o (from 1.0 atm up to 0.015 atm). Curves **1** – γ=1, **2** – γ=0.5, **3** - γ=0.

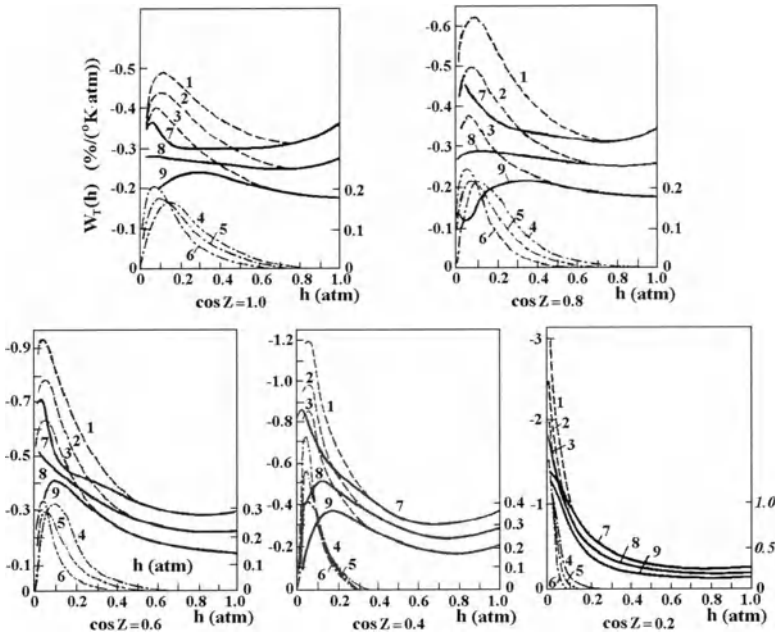

Fig. 5.1.3. Temperature coefficients $W_T(h)$ for hard muons at sea level at $E_{\mu\min} = 0.4$ GeV as a function of zenith angle *Z*. Muon effect (left scale): curve **1** – $\gamma = 1$, **2** – $\gamma = 0.5$, **3** – $\gamma = 0$. Pion effect (right scale): curve **4** – $\gamma = 1$, **5** – $\gamma = 0.5$, **6** – $\gamma = 0$. Total effect (left scale): curve **7** – $\gamma = 0$, **8** – $\gamma = 0.5$, **9** – $\gamma = 1$.

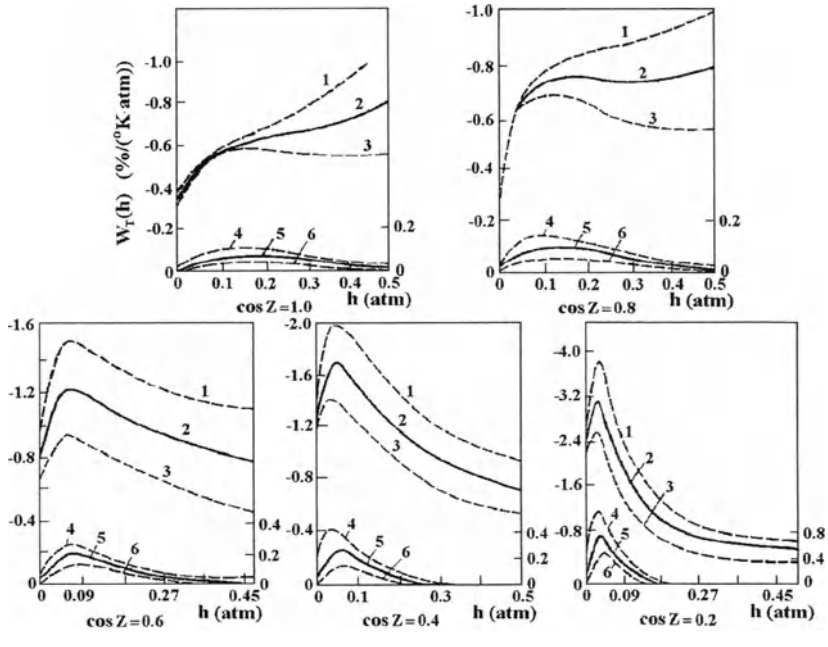

Fig. 5.1.4. The same as in Fig. 5.1.3, but for observations at the level $h_o = 0.5$ atm .

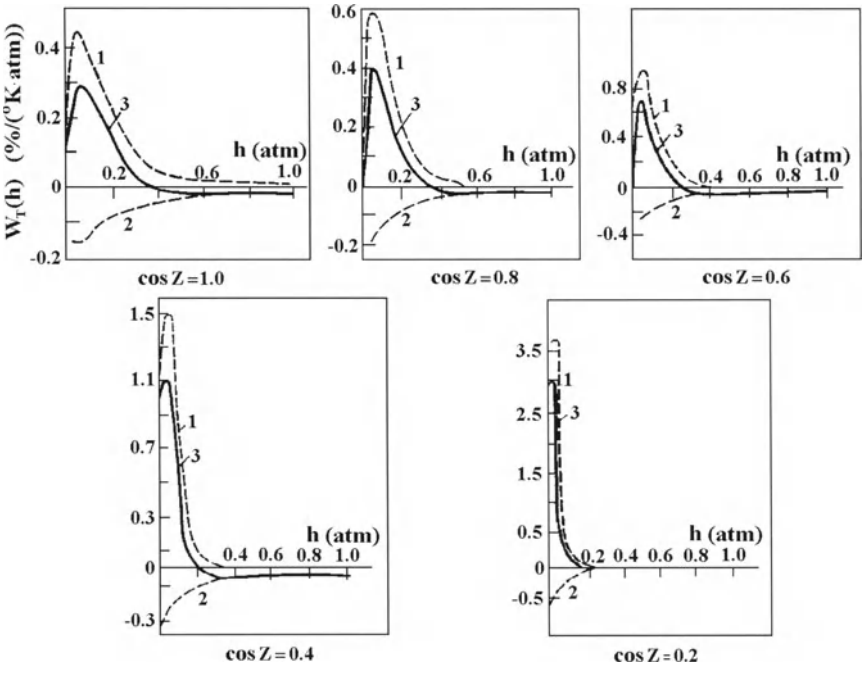

Fig. 5.1.5. Temperature coefficients $W_T(h)$ for hard muons at $\gamma = 0.5$ for observations underground on the depth 55 m w.e. ($E_{\mu\min} = 14.4$ GeV) for different zenith angles *Z*. Curves: ***1*** – pion effect, ***2*** – muon effect, **3** – total effect.

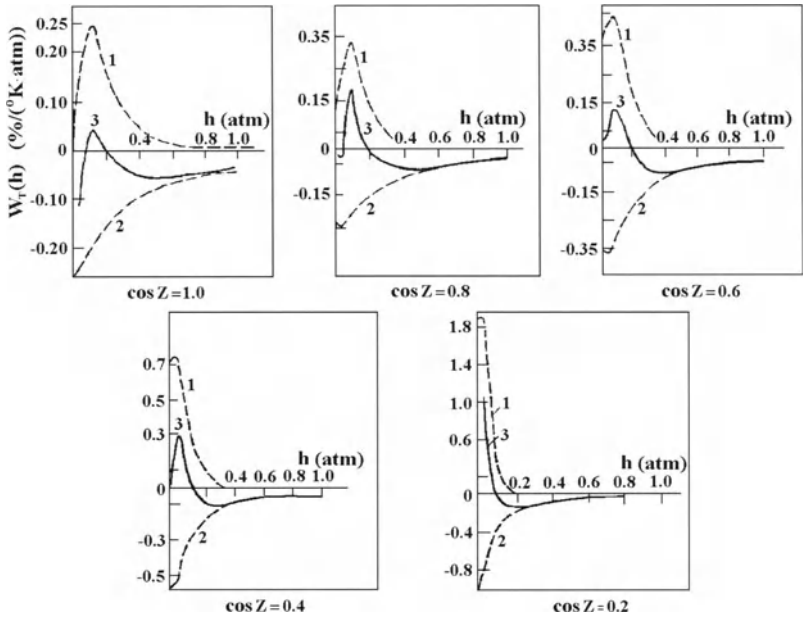

Fig. 5.1.6. The same as in Fig. 5.1.5, but for observations underground at the depth 25 m w.e. ($E_{\mu\,min} = 6.4\ GeV$).

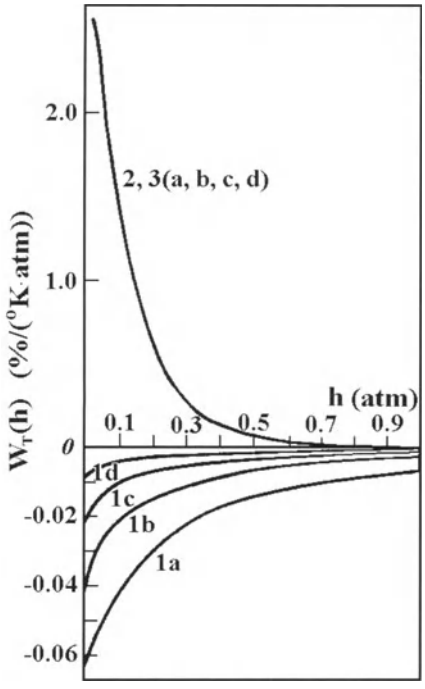

Fig. 5.1.7. Temperature coefficients $W_T(h)$ for hard muons at $\gamma = 1$ for observations in vertical direction deep underground on the depths:
a – 150 m w.e. ($E_{\mu\min} = 50$ GeV),
b – 300 m w.e. ($E_{\mu\min} = 100$ GeV),
c – 550 m w.e. ($E_{\mu\min} = 200$ GeV),
d – 1000 m w.e. ($E_{\mu\min} = 500$ GeV).
Curves: ***1*** – muon effect, ***2*** – pion effect, **3** – total effect.

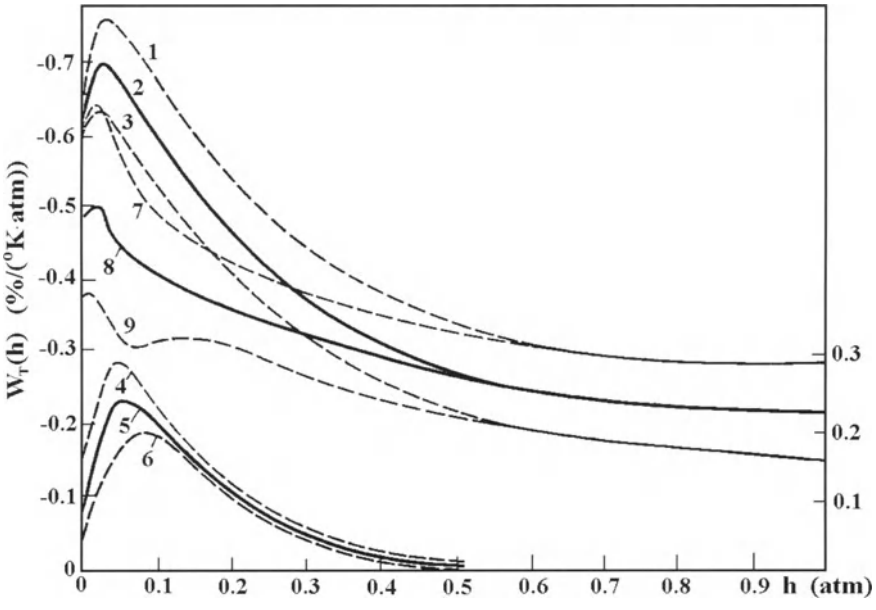

Fig. 5.1.8. Temperature coefficients $W_T(h)$ for global intensity of hard muons at sea level at $E_{\mu\min} = 0.4$ GeV . Muon effect (left scale): curve ***1*** – $\gamma = 1$, ***2*** – $\gamma = 0.5$, **3** – $\gamma = 0$. Pion effect (right scale): curve ***4*** – $\gamma = 0$, ***5*** – $\gamma = 0.5$, ***6*** – $\gamma = 1$. Total effect (left scale): curve ***7*** – $\gamma = 1$, ***8*** – $\gamma = 0.5$, ***9*** – $\gamma = 0$.

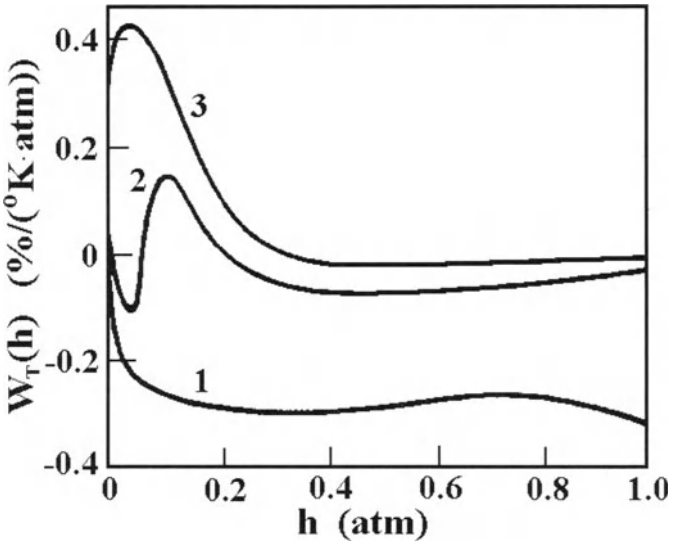

Fig. 5.1.9. The total temperature coefficients $W_T(h)$ for hard muons at sea level at $\gamma = 0.5$ for observations: *1* – by cubical telescope on the ground at $E_{\mu\min} = 0.4$ GeV, *2* – by semi-cubical telescope on the depth 25 m w.e. ($E_{\mu\min} = 6.4$ GeV), **3** – by semi-cubical telescope on the depth 55 m w.e. ($E_{\mu\min} = 14.4$ GeV),

5.1.6. Relative change of meteorological coefficients for hard muons with changing observation conditions

The relative change of meteorological coefficients with the changing observation conditions can be calculated according to formulas of meteorological coefficients given above. This was done by Kaminer (1960) and the results are shown in Tables 5.1.1–5.1.3. For normal conditions we take values for the depth of screen $X = 200\ \mathrm{g/cm^2}$ (corresponding $E_{\mu\min} = 0.4\ \mathrm{GeV}$), for $h_o = 1000\ \mathrm{g/cm^2}$, for temperature in stratosphere $T_{\mathrm{strat}} = 220^o\mathrm{K}$ (weight-average in layer higher than 200 $\mathrm{g/cm^2}$), and for temperature in troposphere according to Eq. 5.1.29.

Table 5.1.1. Dependence of the ratio β/β_n for hard muons from X, h_o, T_{strat}, T_{trop}.

X, $\mathrm{g/cm^2}$	β/β_n	h_o, atm	β/β_n	T_{strat}	β/β_n	T_{trop}	β/β_n
100	1.129	0.6	1.704	240	0.985	T^n_{trop}	1.000
200	1.000	0.8	1.242	220	1.000	T^a_{trop}	0.992
300	0.932	1.0	1.000	200	1.015	T^b_{trop}	0.985
400	0.886						

*For T^n_{trop} is used normal $T(h)$ described by Eq. 5.1.29, for T^a_{trop} is used $T(h) = 200 + 80h/h_o$ for $h \geq 0.2$, and for T^b_{trop} is used $T(h) = 180 + 80h/h_o$ for $h \geq 0.2$.

Table 5.1.2. Dependence of the ratio W_T^{π}/W_{Tn}^{π} for hard muons from X, h_o, T_{strat}.

X, g/cm^2	W_T^{π}/W_{Tn}^{π}	h_o, atm	W_T^{π}/W_{Tn}^{π}	T_{strat}	W_T^{π}/W_{Tn}^{π}
100	0.890	0.6	0.732	240	0.856
200	1.000	0.8	0.870	220	1.000
300	1.040	1.0	1.000	200	1.190
400	1.084				

Table 5.1.3. Dependence of the ratio W_T^{μ}/W_{Tn}^{μ} for hard muons from X, h_o, T_{trop}.

X, g/cm^2	W_T^{μ}/W_{Tn}^{μ}			h_o, atm	W_T^{μ}/W_{Tn}^{μ}		T_{trop}	W_T^{μ}/W_{Tn}^{μ}	
	h=0.8	0.5	0.4		0.5	0.4		0.8	0.4
100	1.174	1.090	1.083	0.6	1.871	1.823	T_{trop}^{n}	1.000	1.000
200	1.000	1.000	1.000	0.8	1.309	1.271	T_{trop}^{a}	1.019	1.011
300	0.875	0.900	0.920	1.0	1.000	1.000	T_{trop}^{b}	1.034	1.025
400	0.780	0.830	0.826						

From Table 5.1.1 it follows that the barometric coefficient sufficiently decreases with increasing of the screen depth X and with increasing pressure at the observation's level h_o, and practically does not depend on T_{strat} and T_{trop}. Tables 5.1.2 and 5.1.3 show that W_T^{π} increases significantly with increasing X and h_o, while W_T^{μ} decreases. From Table 5.1.2 it follows that W_T^{π} increases significantly with decreasing T_{strat} (let us note that W_T^{π} practically does not depend on T_{trop}). Table 5.1.3 shows that W_T^{μ} depends very weakly on T_{trop} (and does not depend on T_{strat}). Results listed in Tables 5.1.1–5.1.3 can be useful for correcting the calculated meteorological coefficients with local conditions for muon intensity observation taken into account.

5.2. Meteorological effects of CR soft muons

5.2.1. Expected intensity of soft muons

In Section 5.1 we considered meteorological effects for hard muons, i.e. muons that cross at least 10 *cm* Pb ($E_{\mu\min} \approx 0.4$ GeV, $E_{\mu\max} = \infty$). Special interest in connection with the problem of continuous CR registration by neutron monitors (NM) is the problem of meteorological effects for soft muons, i.e. muons absorbed by 10 *cm* Pb ($E_{\mu\min} \approx 0.1$ GeV, $E_{\mu\max} = 0.4$ GeV). Meteorological effects for soft muons in the one-dimensional approximation will be determined by the same formulas as in Section 5.1; however the integration over the energy of pions should be from $E_{\pi\min}^{\text{rest}}$ (for stopped muons) to $E_{\pi\min}$, instead of from $E_{\pi\min}$ to ∞. $E_{\pi\min}$ is determined by Eq. 5.1.11 for plate–parallel screen and by Eq. 5.1.12 for spherically–symmetrical screen. For the plate-parallel screen

$$E_{\pi\min}^{\text{rest}} = \left(a(h_o - h_2) + m_\mu c^2\right)/\alpha\cos Z \tag{5.2.1}$$

and for the spherically–symmetrical screen

$$E_{\pi\min}^{\text{rest}} = a(h_o - h_2)/\alpha\cos Z + m_\mu c^2/\alpha \ . \tag{5.2.2}$$

The expected intensity of soft muons will then be

$$N_\mu^s(h_o, Z, E_{\mu\min}) = \int_{E_{\pi\min}^{\text{rest}}}^{E_{\pi\min}} dE_\pi \int_0^{h_o} dh_2 \int_0^{h_2} dh_1 F(E_\pi, h_1, h_2, h_o, Z), \tag{5.2.3}$$

where function $F(E_\pi, h_1, h_2, h_o, Z)$ is determined by Eq. 5.1.14.

5.2.2. Expected meteorological variations of CR soft muons

Let us vary Eq. 5.2.3 over the independent variables characterized depth of screen and meteorological parameters:

$$\delta N_\mu^s(h_o, Z, E_{\mu\min}) = -\delta E_{\pi\min}^{\text{rest}} \int_0^{h_o} dh_2 \int_0^{h_2} dh_1 F\left(E_{\pi\min}^{\text{rest}}, h_1, h_2, h_o, Z\right)$$

$$+ \delta E_{\pi\min} \int_0^{h_o} dh_2 \int_0^{h_2} dh_1 F(E_{\pi\min}, h_1, h_2, h_o, Z) + \delta h_o \int_{E_{\pi\min}^{\text{rest}}}^{E_{\pi\min}} dE_\pi \exp\left(-\frac{h_2 - h_1}{l\cos Z}\right)$$

$$\times\left\{\int_0^{h_o} dh_1 F(E_\pi, h_1, h_2, h_o, Z) - -\frac{m_\mu c}{\tau_\mu \rho(h_o)} \int_0^{h_o} dh_2 \int_0^{h_2} dh_1 \frac{F(E_\pi, h_1, h_2, h_o, Z)}{\alpha E_\pi \cos Z - a(h_o - h_2)}\right\} - \int_{E_{\pi\min}^{\text{rest}}}^{E_{\pi\min}} dE_\pi \int_0^{h_o} dh_2$$

$$\times\frac{\delta\rho(h_2)}{\rho(h_2)} \int_0^{h_o} dh_1 F(E_\pi, h_1, h_2, h_o, Z) + \int_{E_{\pi\min}^{\text{rest}}}^{E_{\pi\min}} dE_\pi \int_0^{h_o} dh_2 \int_0^{h_2} dh_1 F(E_\pi, h_1, h_2, h_o, Z)$$

$$\times\left\{\frac{m_\pi c}{\tau_\pi E_\pi \cos Z} \int_{h_1}^{h_2} \frac{dh\,\delta\rho(h)}{\rho^2(h)} + \frac{m_\mu c}{\tau_\mu} \int_{h_2}^{h_o} \frac{dh}{\rho^2(h)} \frac{\delta\rho(h)}{\alpha E_\pi \cos Z - a(h_o - h_2)}\right\}, \tag{5.2.4}$$

where

$$\delta E_{\pi\min}^{\text{rest}} = \delta h_o a/\alpha\cos Z \tag{5.2.5}$$

for both cases of muon screen, and $\delta E_{\pi\min}$ is described by Eq. 5.1.16 for observations with plate-parallel screen and by Eq. 5.1.17 for spherically-symmetrical screen.

5.2.3. *Expected types of meteorological effects of soft muons*

It is convenient to introduce the function

$$\Phi_s\left(E_\pi,h_1,h_2,h_o,Z,E_{\mu\min}\right)=F\left(E_\pi,h_1,h_2,h_o,Z\right)\Big/N_\mu^s\left(h_o,Z,E_{\mu\min}\right), \qquad (5.2.6)$$

where $N_\mu^s\left(h_o,Z,E_{\mu\min}\right)$ is described by Eq. 5.2.3, and $F\left(E_\pi,h_1,h_2,h_o,Z\right)$ by Eq. 5.1.14. By substituting Eqs. 5.1.16 – 5.1.22 and Eq. 5.2.5 in Eq. 5.2.4, dividing by $N_\mu^s\left(h_o,Z,E_{\mu\min}\right)$, and then by taking into account the definition Eq. 5.2.6, we obtain for the different types of meteorological effects for soft muons the following:

- For soft muons, snow effect for the plate-parallel screen

$$\left.\frac{\delta N_\mu^s\left(h_o,Z,E_{\mu\min}\right)}{N_\mu^s\left(h_o,Z,E_{\mu\min}\right)}\right|_{\text{snow}}=\delta E_{\mu\min}\left(\alpha\cos Z\right)^{-1}$$
$$\times\int_0^{h_o}dh_2\int_0^{h_2}dh_1\Phi_s\left(E_{\pi\min},h_1,h_2,h_o,Z,E_{\mu\min}\right). \qquad (5.2.7)$$

For the spherically-symmetrical screen we obtain the same result, but with α^{-1} instead of $\left(\alpha\cos Z\right)^{-1}$ (let us note that the snow effect for soft muons became positive, in opposite to snow effect of hard muons what is negative, see Eq. 5.1.24);

- For soft muons, barometric effect (of absorption, decay and generation origin)

$$\left.\frac{\delta N_\mu^s\left(h_o,Z,E_{\mu\min}\right)}{N_\mu^s\left(h_o,Z,E_{\mu\min}\right)}\right|_{\text{bar}}=\delta h_o\left\{\alpha\alpha^{-1}\int_0^{h_o}dh_2\int_0^{h_2}dh_1\left[\Phi_s\left(E_{\pi\min},h_1,h_2,h_o,Z,E_{\mu\min}\right)\right.\right.$$
$$\left.-\Phi_s\left(E_{\pi\min}^{\text{rest}},h_1,h_2,h_o,Z,E_{\mu\min}\right)\right]-\frac{m_\mu c}{\tau_\mu\rho\left(h_o\right)}\int_{E_{\pi\min}^{\text{rest}}}^{E_{\pi\min}}dE_\pi\int_0^{h_o}dh_2\int_0^{h_2}dh_1$$
$$\left.\times\frac{\Phi_s\left(E_\pi,h_1,h_2,h_o,Z,E_{\mu\min}\right)}{\alpha E_\pi\cos Z-a\left(h_o-h_2\right)}+\int_{E_{\pi\min}^{\text{rest}}}^{E_{\pi\min}}dE_\pi\int_0^{h_2}dh_1\Phi_s\left(E_\pi,h_1,h_2,h_o,Z,E_{\mu\min}\right)\right\}. \qquad (5.2.8)$$

- For soft muons, temperature effect (of pion decay and nuclear interactions, and muon ionization losses and decay origin)

$$\left.\frac{\delta N_\mu^s(h_o,Z,E_{\mu\min})}{N_\mu^s(h_o,Z,E_{\mu\min})}\right|_{\text{temp}} = \int_{E_{\pi\min}^{\text{rest}}}^{E_{\pi\min}} dE_\pi \int_0^{h_o} dh_2 \int_0^{h_2} dh_1 \Phi_s(E_\pi,h_1,h_2,h_o,Z,E_{\mu\min})$$

$$\times\left\{\frac{\delta T(h_2)}{T(h_2)} - \frac{R_o m_\pi c}{E_\pi \tau_\pi \cos Z}\int_{h_1}^{h_2}\frac{dh\,\delta T(h)}{h} - \frac{R_o m_\mu c}{\tau_\mu}\int_{h_2}^{h_o}\frac{dh}{h}\frac{\delta T(h)}{\alpha E_\pi \cos Z - a(h-h_2)}\right\}. \quad (5.2.9)$$

- For soft muons, humidity effect (of pion decay and nuclear interactions, and muon ionization losses and decay origin)

$$\left.\frac{\delta N_\mu^s(h_o,Z,E_{\mu\min})}{N_\mu^s(h_o,Z,E_{\mu\min})}\right|_{\text{humid}} = 0.378\int_{E_{\pi\min}^{\text{rest}}}^{E_{\pi\min}} dE_\pi \int_0^{h_o} dh_2 \int_0^{h_2} dh_1 \Phi_s(E_\pi,h_1,h_2,h_o,Z,E_{\mu\min})$$

$$\times\left\{\frac{\delta e(h_2)}{e(h_2)} - \frac{R_o m_\pi c}{E_\pi \tau_\pi \cos Z}\int_{h_1}^{h_2}\frac{dh T(h)\delta e(h)}{h^2} - \frac{R_o m_\mu c}{\tau_\mu}\int_{h_2}^{h_o}\frac{dh}{h^2}\frac{T(h)\delta e(h)}{\alpha E_\pi \cos Z - a(h-h_2)}\right\}. \quad (5.2.10)$$

- For soft muons, gravitational effect (absorption and decay of pions and muons)

$$\left.\frac{\delta N_\mu^s(h_o,Z,E_{\mu\min})}{N_\mu^s(h_o,Z,E_{\mu\min})}\right|_{\text{gravit}} = \frac{\delta g}{g}\int_{E_{\pi\min}^{\text{rest}}}^{E_{\pi\min}} dE_\pi \int_0^{h_o} dh_2 \int_0^{h_2} dh_1 \Phi_s(E_\pi,h_1,h_2,h_o,Z,E_{\mu\min})$$

$$\times\left\{-1 + \frac{m_\pi c}{E_\pi \tau_\pi \cos Z}\int_{h_1}^{h_2}\frac{dh}{\rho(h)} - \frac{m_\mu c}{\tau_\mu}\int_{h_2}^{h_o}\frac{dh}{\rho(h)}\frac{1}{\alpha E_\pi \cos Z - a(h-h_2)}\right\}. \quad (5.2.11)$$

5.2.4. Meteorological coefficients for soft muons

Let us choose the average profile of $T(h)$ described by Eq. 5.1.29. In this case the results of calculations of $N_\mu^s(h_o,Z,E_{\mu\min})$ and meteorological coefficients are as following:

$$N_\mu^s(h_o,Z,E_{\mu\min}) = A(\alpha\cos Z)^{1+\gamma} N_{\gamma s}(h_o,Z,E_{\mu\min}), \quad (5.2.12)$$

$$\left.\frac{\delta N_\mu^s(h_o,Z,E_{\mu\min})}{N_\mu^s(h_o,Z,E_{\mu\min})}\right|_{\text{temp}} = \int_0^{h_o} W_{Ts}(h,h_o,E_{\mu\min},Z)\delta T(h)dh, \quad (5.2.13)$$

where

$$W_{Ts}(h,h_o,E_{\mu\min},Z) = W_{Ts}^{\pi}(h,h_o,E_{\mu\min},Z) + W_{Ts}^{\mu}(h,h_o,E_{\mu\min},Z) \quad (5.2.14)$$

and

$$N_{\gamma s}(h_o,Z,E_{\mu\min})=\int_0^{h_o}\frac{\exp(-h_2/L\cos Z)\varphi_{\gamma s}(s,v)dh_2}{(h_o-h_2+E_{\mu\min})^{1+\gamma}}, \tag{5.2.15}$$

$$W_{Ts}^{\pi}(h,h_o,E_{\mu\min},Z)=\frac{h\exp(-h/L\cos Z)\chi_{\gamma s}(s,v)}{\alpha\lambda b_{\pi}(h)T(h)(h_o-h+E_{\mu\min})^{\gamma}N_{\gamma s}\cos Z}, \tag{5.2.16}$$

$$W_{Ts}^{\mu}(h,h_o,E_{\mu\min},Z)=-\frac{m_{\mu}cR_o}{\tau_{\mu}hN_{\gamma s}}\int_0^h\frac{\exp(-h_2/L\cos Z)f_{\gamma s}(s,k,v)dh_2}{(h_o-h_2+E_{\mu\min})^{2+\gamma}}. \tag{5.2.17}$$

In Eq. 5.1.33–5.1.35 we used following designations:

$$\varphi_{\gamma s}(s,v)=\int_1^{E_{\pi\min}/E_{\pi\min}^{\text{rest}}}t^{1+\gamma}(t+s)^{-1}e^{vt}dt; \tag{5.2.18}$$

$$\chi_{\gamma s}(s,v)=\int_1^{E_{\pi\min}/E_{\pi\min}^{\text{rest}}}t^{1+\gamma}(t+s)^{-2}e^{vt}dt; \tag{5.2.19}$$

$$f_{\gamma s}(s,k,v)=\int_1^{E_{\pi\min}/E_{\pi\min}^{\text{rest}}}kt^{2+\gamma}(t+s)^{-1}(k-t)^{-1}e^{vt}dt, \tag{5.2.20}$$

where s,k,v were determined by Eq. 5.1.38–5.1.41.

Meteorological coefficients for humidity and gravity effects can be expressed through the temperature coefficient $W_{Ts}(h,h_o,E_{\mu\min},Z)$ determined by Eq. 5.2.14–5.2.17:

$$\left.\frac{\delta N_{\mu}^{s}(h_o,Z,E_{\mu\min})}{N_{\mu}^{s}(h_o,Z,E_{\mu\min})}\right|_{\text{hum}}=\int_0^{h_o}W_{\text{hum}}^{\text{soft}}(h,h_o,E_{\mu\min},Z)\delta e(h)dh, \tag{5.2.21}$$

where

$$W_{\text{hum}}^{\text{soft}}(h,h_o,E_{\mu\min},Z)=0.378(T(h)/h)W_{Ts}(h,h_o,E_{\mu\min},Z), \tag{5.2.22}$$

and

$$\left.\frac{\delta N_\mu^s(h_o,Z,E_{\mu\min})}{N_\mu^s(h_o,Z,E_{\mu\min})}\right|_{\text{grav}} = \delta g\,\alpha_{\text{grav}}^{\text{soft}}(h_o,E_{\mu\min},Z), \tag{5.2.23}$$

where

$$\alpha_{grav}^{soft}(h_o,E_{\mu\min},Z)=g^{-1}\int_0^{h_o}T(h)W_{Ts}(h,h_o,E_{\mu\min},Z)dh\,. \tag{5.2.24}$$

The barometric effect for soft muons consists also of absorption, decay and generation effects (as for hard muons):

$$\left.\frac{\delta N_\mu^s(h_o,Z,E_{\mu\min})}{N_\mu^s(h_o,Z,E_{\mu\min})}\right|_{\text{bar}} = \delta h_o\left[\beta_{\text{abs}}^{\text{soft}}(h_o,E_{\mu\min},Z)+\beta_{\text{dec}}^{\text{soft}}(h_o,E_{\mu\min},Z)+\beta_{\text{gen}}^{\text{soft}}(h_o,E_{\mu\min},Z)\right], \tag{5.2.25}$$

where

$$\beta_{\text{abs}}^{\text{soft}}(h_o,E_{\mu\min},Z)=-\frac{\cos Z}{N_{\gamma s}(h_o,E_{\mu\min},Z)}\int_0^{h_o}\frac{\exp(-\nu_1-h_2/L\cos Z)dh_2}{(1+s)(h_o-h_2+E_{\mu\min})^{2+\gamma}}\,, \tag{5.2.26}$$

$$\beta_{\text{dec}}^{\text{soft}}(h_o,E_{\mu\min},Z)=-\frac{b_\mu(h_o)}{h_o N_{\gamma s}(h_o,E_{\mu\min},Z)}\int_0^{h_o}\frac{\exp(-h_2/L\cos Z)f_{\gamma s}(s,k_o,\nu)dh_2}{(h_o-h_2+E_{\mu\min})^{2+\gamma}}\,, \tag{5.2.27}$$

$$\beta_{\text{gen}}^{\text{soft}}(h_o,E_{\mu\min},Z)=\frac{\exp(-h_0/L\cos Z)\varphi_{\gamma s}(s_o,\nu=0)}{N_{\gamma s}(h_o,E_{\mu\min},Z)E_{\mu\min}^{1+\gamma}}\,. \tag{5.2.28}$$

In Eq. 5.2.27 k_o is determined by Eq. 5.1.38 at $h=h_o$; in Eq. 5.2.28 s_o is determined by Eq. 5.1.38 at $h_2=h_o$. Let us note that all the formulas above for soft muon meteorological coefficients are obtained for the plane-parallel screen of detector. In the case of spherically symmetrical screen, it is necessary to use $E_{\mu\min}\cos Z$ instead of $E_{\mu\min}$. Results of calculations of soft muon meteorological coefficients are shown in Fig. 5.2.1–5.2.2.

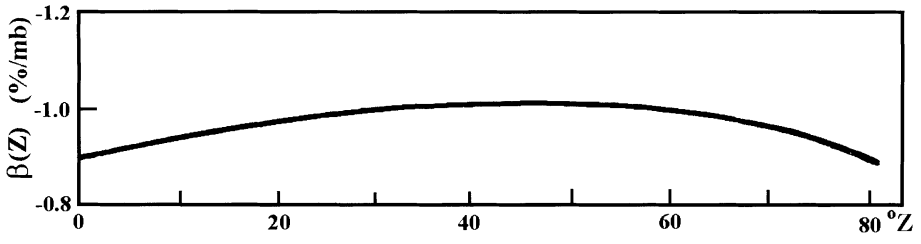

Fig. 5.2.1. Expected barometric coefficient $\beta(Z)$ for soft muons (absorbed by 10 cm Pb) in dependence from the zenith angle Z.

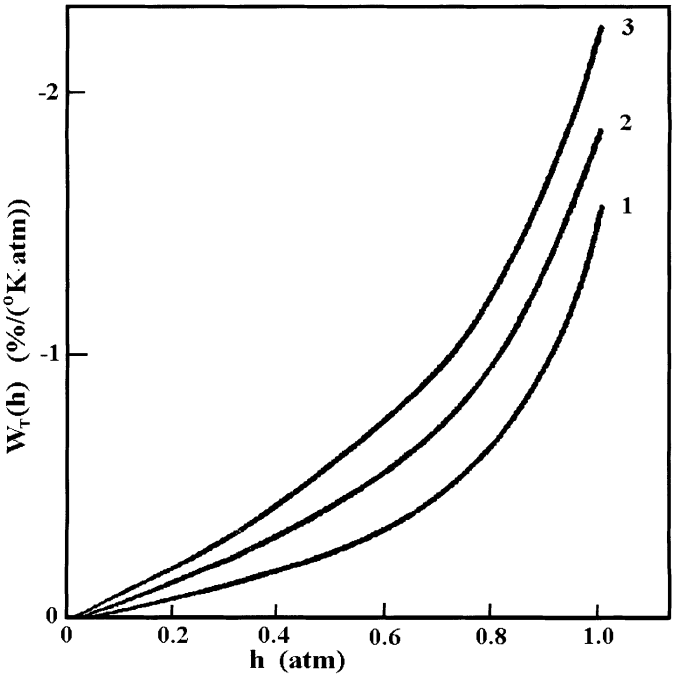

Fig. 5.2.2. The total temperature coefficients $W_T(h)$ for soft muons at sea level for different zenith angles Z of observations: curve *1* – $\cos Z = 1.0$, *2* – $\cos Z = 0.6$, and *3* – $\cos Z = 0.2$.

5.3. Meteorological effects of CR electron-photon, soft and general ionized components

5.3.1. CR general ionized, hard, soft and electron–photon components: main characteristics

The general ionized CR component, which can be measured by Geiger and proportional counters, ionization chambers, scintillators and other detectors, is traditionally separated to a hard component (that penetrates 10 cm Pb) and a soft component (absorbed by 10 cm Pb). The hard component consists mostly of hard muons;

meteorological effects of this component (in one-dimensional approximation) were considered in Section 5.1. It contains also nucleons penetrating 10 cm Pb.

The soft component of CR consists of equilibrium and non-equilibrium components. Soft equilibrium component is in equilibrium with the hard component of CR (with hard muons) and contains soft muons, electrons and positrons from charged muons decay and δ electrons knocked out by charged muons from atoms as result of direct interactions. Meteorological effects of soft muons (in one-dimensional approximation) were considered in Section 5.2. Soft non-equilibrium component is generated by decay of neutral pions on two gamma quanta and following cascade multiplying; it contains also nucleons absorbed by 10 cm Pb.

5.3.2. Expected intensity of electronic component from muon decay

Electrons and positrons generated in processes of high energy charged muon decay according to Eq. 5.1.8 have about 1/3 the energy of muon, enough for multiplying in accordance with cascade theory. Let us assume that E_{dec} is the energy transferred from muons to electrons as a result of muon decay on the way of 1 cascade unit t (let us remember that the cascade unit $t(h_o) = A/n(h_o)$, where $n(h_o)$ is number of atoms in 1 cm^3 of matter and A is determined by elements order number Z and atomic constants: for air $t = 34.2\ \text{g/cm}^2$, corresponding on the sea level at normal conditions to 260 m, for lead $t = 5.2\ \text{g/cm}^2$, corresponding to 0.46 cm) and that E_o is the energy lost in the same way by electron and all products of its cascade multiplying (so called critical energy: for air $E_o = 72$ MeV and for lead $E_o = 6.4$ MeV). The total number $n_e^{\text{dec}}(h_o)$ of decay electrons together with products of cascade multiplying can be determined from the condition of equilibrium:

$$n_e^{\text{dec}}(h_o)E_o = E_{\text{dec}}(h_o), \tag{5.3.1}$$

where $E_{\text{dec}}(h_o)$ is average energy of electrons from muon decay on the way of 1 cascade unit $t(h_o)$. The probability of muon decay on the path of 1 cm will be $m_\mu c \Big/ \left(\tau_\mu \sqrt{E_\mu^2 - m_\mu^2 c^4}\right)$; it means that the average energy transferred to electrons decay on 1 cm way will be $\frac{1}{3} E_\mu m_\mu c \Big/ \left(\tau_\mu \sqrt{E_\mu^2 - m_\mu^2 c^4}\right)$. From this it follows that

$$E_{\text{dec}}(h_o) = \frac{1}{3} t(h_o) E_\mu m_\mu c \Big/ \left(\tau_\mu \sqrt{E_\mu^2 - m_\mu^2 c^4}\right). \tag{5.3.2}$$

From comparison of Eq. 5.3.1 with Eq. 5.3.2 we can determine the number $n_e^{\text{dec}}(h_o)$ of decay electrons per one muon on the way of one cascade unit $t(h_o)$:

$$n_e^{\text{dec}}(h_o) = t(h_o) E_\mu m_\mu c \Big/ \left(3E_o \tau_\mu \sqrt{E_\mu^2 - m_\mu^2 c^4} \right). \tag{5.3.3}$$

Total number $N_e^{\text{dec}}(h_o)$ from all muons with differential energy spectrum $D(E_\mu, h_o)$ will be

$$N_e^{\text{dec}}(h_o) = \int_{m_\mu c^2}^{\infty} E_\mu m_\mu c\, t(h_o) D(E_\mu, h_o) dE_\mu \Big/ \left(3E_o \tau_\mu \sqrt{E_\mu^2 - m_\mu^2 c^4} \right). \tag{5.3.4}$$

5.3.3. Expected meteorological effects of electronic component from muon decay

Let us vary Eq. 5.3.4 with respect to $t(h_o)$ and $D(E_\mu, h_o)$ (that change with changing meteorological parameters):

$$\frac{\delta N_e^{\text{dec}}(h_o)}{N_e^{\text{dec}}(h_o)} = \frac{\delta t(h_o)}{t(h_o)} + \frac{\int_{m_\mu c^2}^{\infty} E_\mu \delta D(E_\mu, h_o) dE_\mu \Big/ \sqrt{E_\mu^2 - m_\mu^2 c^4}}{\int_{m_\mu c^2}^{\infty} E_\mu D(E_\mu, h_o) dE_\mu \Big/ \sqrt{E_\mu^2 - m_\mu^2 c^4}}. \tag{5.3.5}$$

Let us take into account that

$$t(h_o) \propto 1/n(h_o) \propto 1/\rho(h_o) = R(h_o) T(h_o) / g\, h_o, \tag{5.3.6}$$

from which it follows that

$$\frac{\delta t(h_o)}{t(h_o)} = \frac{0.378 \delta e(h_o)}{h_o (1 + 0.378 e(h_o)/h_o)} + \frac{\delta T(h_o)}{T(h_o)} - \frac{\delta g}{g} - \frac{\delta h_o}{h_o}, \tag{5.3.7}$$

where we take into account that $R(h_o) = R_o (1 + 0.378 e(h_o)/h_o)$.

Therefore on the basis of Eq. 5.3.5 and 5.3.7 we obtain

$$\frac{\delta N_e^{\text{dec}}(h_o)}{N_e^{\text{dec}}(h_o)} = \frac{0.378 \delta e(h_o)}{h_o (1 + 0.378 e(h_o)/h_o)} + \frac{\delta T(h_o)}{T(h_o)} - \frac{\delta g}{g} - \frac{\delta h_o}{h_o}$$

$$+ \frac{\int_{m_\mu c^2}^{\infty} E_\mu \delta D(E_\mu, h_o) dE_\mu \Big/ \sqrt{E_\mu^2 - m_\mu^2 c^4}}{\int_{m_\mu c^2}^{\infty} E_\mu D(E_\mu, h_o) dE_\mu \Big/ \sqrt{E_\mu^2 - m_\mu^2 c^4}}. \tag{5.3.8}$$

Eq. 5.3.8 shows that for muon decay electrons we have, in addition to the muon meteorological effects, also the following: positive local humidity effect, positive local temperature effect, negative gravitational effect and negative barometric effect.

5.3.4. Approximate solution for intensity and meteorological effects of electronic component from muon decay

Let us take into account that $D(E_\mu, h_o)$ decreases very quickly with decreasing E_μ so the relative fluxes at small energies are very small. A large fraction of muons have energy $E_\mu \geq (5 \div 6) m_\mu c^2$ but for these energies value $E_\mu / \sqrt{E_\mu^2 - m_\mu^2 c^4} \approx 1$ (see Table 5.3.1).

Table 5.3.1. Relative fluxes of muons in different energy intervals and values of $E_\mu / \sqrt{E_\mu^2 - m_\mu^2 c^4}$

$E_\mu / m_\mu c^2$	1.1–1.5	1.5–2.0	2.0–3.0	3.0–5.0	>5.0
Relative muon flux, %	0.3	0.6	2	5	92
$E_\mu / \sqrt{E_\mu^2 - m_\mu^2 c^4}$	2.2–1.34	1.34–1.15	1.15–1.06	1.06–1.02	1.02–1.00

Therefore with relative accuracy of a few percent, Eq. 5.3.4 can be transformed into

$$N_e^{\mathrm{dec}}(h_o) \approx \frac{t(h_o) m_\mu c}{3 E_o \tau_\mu} \int_{m_\mu c^2}^{\infty} D(E_\mu, h_o) dE_\mu = \frac{t(h_o) m_\mu c}{3 E_o \tau_\mu} N_\mu(h_o). \qquad (5.3.9)$$

The coefficient $t(h_o) m_\mu c / 3 E_o \tau_\mu$ determines the portion of electron decay flux relative to muon flux: at sea level ($h_o = 1030\,\mathrm{g/cm^2}$) this portion is about 0.20, and at mountain altitude ($h_o = 650\,\mathrm{g/cm^2}$) this portion is 0.32. By varying Eq. 5.3.9 on meteorological parameters we obtain

$$\left.\frac{\delta N_e^{\mathrm{dec}}(h_o)}{N_e^{\mathrm{dec}}(h_o)}\right|_{\mathrm{met}} \approx \frac{0.378 \delta e(h_o)}{h_o (1 + 0.378 e(h_o)/h_o)} + \frac{\delta T(h_o)}{T(h_o)} - \frac{\delta g}{g} - \frac{\delta h_o}{h_o} + \left(\frac{\delta N_\mu(h_o)}{N_\mu(h_o)}\right)_{\mathrm{met}}, \qquad (5.3.10)$$

where we take into account Eq. 5.3.7, and

$$\left(\frac{\delta N_\mu(h_o)}{N_\mu(h_o)}\right)_{\mathrm{met}} = -\delta h_o \beta_\mu(h_o) + \delta g \beta_g(h_o) + \int_0^{h_o} \delta T(h) W_T(h) dh + \int_0^{h_o} \delta e(h) W_e(h) dh, \qquad (5.3.11)$$

where meteorological coefficients for muons were determined in Sections 5.1 and 5.2.

5.3.5. *Expected intensity and meteorological effects of δ electrons*

In the case of equilibrium of muon component with δ electrons, each electron loses energy E_o on ionization on the way of one cascade unit *t*, and all $n_e^{\delta}(h_o)$ will lose total energy $E_o n_e^{\delta}(h_o)$. From other side, the total energy lost by a muon as a result of generation of δ electrons along one cascade unit *t* is

$$E_{\delta} = E_o \ln\left(E_{e\delta}^{\max}/E_{e\delta}^{\min}\right)\left\{\ln\left[\left(E_{\mu}-m_{\mu}c^2\right)^3/m_e c^2 J^2(Z)\right]\right\}^{-1}, \qquad (5.3.12)$$

where $E_{e\delta}^{\max}$ and $E_{e\delta}^{\min}$ are the maximal and minimal energies of δ electrons, $J(Z)$ is the effective ionization potential of air atoms. The dependence of $E_{e\delta}^{\max}$ on E_{μ} is shown in Table 5.3.1.

Table 5.3.1. The dependence of $E_{e\delta}^{max}$ on E_{μ}.

E_{μ}, *GeV*	1	2	5	20
$E_{e\delta}^{max}$, *GeV*	0.1	0.4	2	15

The dependence of $E_{e\delta}^{\max}$ (in GeV) on E_{μ} (also in GeV) can be approximated by

$$\ln\left(E_{e\delta}^{\max}\right) = -0.13765\left(\ln\left(E_{\mu}\right)\right)^2 + 2.08385\ln\left(E_{\mu}\right) - 2.30015 \qquad (5.3.13)$$

with correlation coefficient 0.999998. The minimal energy $E_{e\delta}^{\min}$ of δ electrons is determined by experiment and usually is about 0.3 MeV.

Because of the equilibrium condition $E_{\delta} = E_o n_e^{\delta}(h_o)$, the total number of δ electrons will be

$$N_e^{\delta}(h_o) = \int_{m_{\mu}c^2}^{\infty} n_e^{\delta}(h_o) D\left(E_{\mu}\right) dE_{\mu}$$

$$= \int_{m_{\mu}c^2}^{\infty} \ln\left(E_{e\delta}^{\max}/E_{e\delta}^{\min}\right)\left\{\ln\left[\left(E_{\mu}-m_{\mu}c^2\right)^3/m_e c^2 J^2(Z)\right]\right\}^{-1} D\left(E_{\mu}\right) dE_{\mu}. \qquad (5.3.14)$$

From Eq. 5.3.14, and taking into account Eq. 5.3.13, it follows that the relative role of δ electrons increases with increasing of muon energy E_{μ}. The dependence of ratio $N_e^{\delta}(h_o)/N_{\mu}(h_o)$ on E_{μ} is shown in Table 5.3.2.

Table 5.3.2. The dependence of ratio $N_e^{\delta}(h_o)/N_{\mu}(h_o)$ on E_{μ}.

E_{μ}, GeV	0.2	0.5	1	2	5	20	1000
$N_e^{\delta}(h_o)/N_{\mu}(h_o)$	0.06	0.13	0.15	0.17	0.19	0.22	0.23

By varying Eq. 5.3.14 over parameters that may change owing to meteorological conditions, we obtain

$$\frac{\delta N_e^{\delta}(h_o)}{N_e^{\delta}(h_o)} = \frac{\int_{m_{\mu}c^2}^{\infty} \ln\left(E_{e\delta}^{\max}/E_{e\delta}^{\min}\right)\left\{\ln\left[\left(E_{\mu}-m_{\mu}c^2\right)^3/m_e c^2 J^2(Z)\right]\right\}^{-1} \delta D(E_{\mu})dE_{\mu}}{\int_{m_{\mu}c^2}^{\infty} \ln\left(E_{e\delta}^{\max}/E_{e\delta}^{\min}\right)\left\{\ln\left[\left(E_{\mu}-m_{\mu}c^2\right)^3/m_e c^2 J^2(Z)\right]\right\}^{-1} D(E_{\mu})dE_{\mu}}. \quad (5.3.15)$$

Let us take into account that the factor in front of $D(E_{\mu})$ in Eq. 5.3.14 changes with E_{μ} logarithmically, very slowly, so that in the first approximation we obtain

$$N_e^{\delta}(h_o) \approx \left(\ln\left(E_{e\delta}^{\max}/E_{e\delta}^{\min}\right)\left\{\ln\left[\left(E_{\mu}-m_{\mu}c^2\right)^3/m_e c^2 J^2(Z)\right]\right\}^{-1} \right)_{\text{eff}} N_{\mu}(h_o). \quad (5.3.16)$$

In Eq. 5.3.16 the factor in front of $N_{\mu}(h_o)$ is about 0.15, which corresponds to $(E_{\mu})_{\text{eff}} \approx 1$ GeV, $E_{\delta}^{\max} \approx 0.1$ GeV, $E_{\delta}^{\min} \approx 0.3$ MeV. Therefore approximately

$$N_e^{\delta}(h_o) \approx 0.15 N_{\mu}(h_o); \quad \delta N_e^{\delta}(h_o)/N_e^{\delta}(h_o) \approx \delta N_{\mu}(h_o)/N_{\mu}(h_o), \quad (5.3.17)$$

i.e. meteorological effects of δ electrons are about the same as the muon component (for more exact research it is necessary to use Eq. 5.3.15 and Table 2, and take into account the very slowly increasing of δ electrons generation with increasing of muon energy E_{μ}).

5.3.6. Expected meteorological effects of non-equilibrium part of the electron–photon component

This part of the electron–photon component is generated by decay of neutral pions on two gamma quanta and is not in equilibrium with the muon component. The intensity of the non-equilibrium part of electron–photon component increases from zero on the

boundary of atmosphere ($h_o = 0$), reaches a maximum at the altitude 14–15 km (the depth about four *t*-units), and then decreases exponentially:

$$N_e^{\text{neq}}(h_o) \propto \exp(-h_o/L), \tag{5.3.18}$$

where $L \approx 120\,\text{g/cm}^2$. From Eq. 5.3.18 it follows that the non-equilibrium part of electron–photon component has only barometric effect:

$$\delta N_e^{\text{neq}}(h_o)/N_e^{\text{neq}}(h_o) = -\delta h_o/L \approx \beta_e^{\text{neq}} \delta h_o\,, \tag{5.3.19}$$

where the barometric coefficient

$$\beta_e^{\text{neq}} = -1/L = -0.84\,\%/(\text{g/cm}^2). \tag{5.3.20}$$

5.3.7. Expected intensity and meteorological effects of electron-photon component

Let us take into account Sections 5.3.2–5.3.6. The total intensity of electron-photon component can be presented as

$$N_e(h_o) = N_e^{\text{dec}}(h_o) + N_e^{\delta}(h_o) + N_e^{\text{neq}}(h_o), \tag{5.3.21}$$

where $N_e^{\text{dec}}(h_o)$ is determined by Eq. 5.3.4, $N_e^{\boldsymbol{\delta}}(h_o)$ by Eq. 5.3.14, and $N_e^{\text{nec}}(h_o)$ by Eq. 5.3.18. Let us suppose that

$$\begin{aligned} &N_e^{\text{dec}}(h_o) = F_{\text{dec}}(h_o) N_e(h_o),\ N_e^{\delta}(h_o) = F_{\delta}(h_o) N_e(h_o), \\ &N_e^{\text{neq}}(h_o) = F_{\text{neq}}(h_o) N_e(h_o);\ F_{\text{dec}}(h_o) + F_{\delta}(h_o) + F(h_o) = 1. \end{aligned} \tag{5.3.22}$$

In this case

$$\frac{\delta N_e(h_o)}{N_e(h_o)} = F_{\text{dec}}(h_o) \frac{\delta N_e^{\text{dec}}(h_o)}{N_e^{\text{dec}}(h_o)} + F_{\delta}(h_o) \frac{\delta N_e^{\delta}(h_o)}{N_e^{\delta}(h_o)} + F_{\text{neq}}(h_o) \frac{\delta N_e^{\text{neq}}(h_o)}{N_e^{\text{neq}}(h_o)}. \tag{5.3.23}$$

According to numerical experiments reviewed in Dobrotin (M1954), Rossi (M1966), Hayakawa (M1969), Murzin (M1988) the values of the factors *F* in Eq. 5.3.23 are as following:

- For sea level ($h_o = 1030\ \text{g/cm}^2$)

$$F_{\text{dec}}(h_o) = 0.5,\ F_{\delta}(h_o) = 0.4,\ F_{\text{neq}}(h_o) = 0.1; \tag{5.3.24}$$

- For mountain level (3900 m, $h_o = 650\ \mathrm{g/cm^2}$)

$$F_{\mathrm{dec}}(h_o) = 0.29,\ F_{\delta}(h_o) = 0.14,\ F_{\mathrm{neq}}(h_o) = 0.57; \tag{5.3.25}$$

- For height 10 km ($h_o = 300\ \mathrm{g/cm^2}$)

$$F_{\mathrm{dec}}(h_o) = 0.18,\ F_{\delta}(h_o) = 0.04,\ F_{\mathrm{neq}}(h_o) = 0.78. \tag{5.3.26}$$

Let us substitute Eqs. 5.3.10, 5.3.17 and 5.3.19 in Eq. 5.3.23 and take into account Eqs. 5.3.24–5.3.26. As result we obtain

- For sea level ($h_o = 1030\ \mathrm{g/cm^2}$, $T(h_o) \approx 280^{\circ}\mathrm{K}$)

$$\frac{\delta N_e(h_o)}{N_e(h_o)} = -0.13\{\%/\mathrm{mb}\}\delta h_o + 0.18\{\%/1^{\circ}\mathrm{K}\}\delta T(h_o) + 0.9\left(\delta N_{\mu}(h_o)/N_{\mu}(h_o)\right), \tag{5.3.27}$$

- For mountain's level (3900 m, $h_o = 650\ \mathrm{g/cm^2}$, $T(h_o) \approx 250^{\circ}\mathrm{K}$)

$$\frac{\delta N_e(h_o)}{N_e(h_o)} = -0.53\{\%/\mathrm{mb}\}\delta h_o + 0.12\{\%/1^{\circ}\mathrm{K}\}\delta T(h_o) + 0.43\left(\delta N_{\mu}(h_o)/N_{\mu}(h_o)\right), \tag{5.3.28}$$

- For height 10 km ($h_o = 300\ \mathrm{g/cm^2}$, $T(h_o) \approx 225^{\circ}\mathrm{K}$)

$$\frac{\delta N_e(h_o)}{N_e(h_o)} = -0.72\{\%/\mathrm{mb}\}\delta h_o + 0.08\{\%/1^{\circ}\mathrm{K}\}\delta T(h_o) + 0.22\left(\delta N_{\mu}(h_o)/N_{\mu}(h_o)\right). \tag{5.3.29}$$

Let us note that in Eq. 5.3.17–5.3.29 $\delta N_{\mu}(h_o)/N_{\mu}(h_o)$ denotes the meteorological effects of total muon intensity (including soft muons). For their determination it is necessary to use the results of both Sections 5.3.1 and 5.3.2.

5.3.8. Expected meteorological effects of CR general ionized component

The CR general ionized component consists of a soft component (electron–photon component + soft muons) and a hard component (mostly hard muons). Let us take into account that on sea level the soft component intensity is about 0.4 of that of the hard component; on mountain's level the ratio is about 1.1, and on the height 10 km it is about 3.8. Therefore by taking into account Eq. 5.3.27–5.3.29 we obtain

- For sea level ($h_o = 1030\ \mathrm{g/cm^2}$, $T(h_o) \approx 280^{\circ}\mathrm{K}$)

$$\frac{\delta N_g(h_o)}{N_g(h_o)} = -0.04\{\%/\mathrm{mb}\}\delta h_o + 0.05\{\%/1^{\circ}\mathrm{K}\}\delta T(h_o) + 0.97\left(\delta N_{\mu}(h_o)/N_{\mu}(h_o)\right), \tag{5.3.30}$$

- For mountain's level (3900 m, $h_o = 650\ \mathrm{g/cm^2}$, $T(h_o) \approx 250^{\circ}\mathrm{K}$)

$$\frac{\delta N_g(h_o)}{N_g(h_o)} = -0.38\{\%/\text{mb}\}\delta h_o + 0.06\{\%/1^\circ\text{K}\}\delta T(h_o) + 0.70\left(\delta N_\mu(h_o)/N_\mu(h_o)\right), \quad (5.3.31)$$

- For height 10 *km* ($h_o = 300$ g/cm^2, $T(h_o) \approx 225^\circ$K)

$$\frac{\delta N_g(h_o)}{N_g(h_o)} = -0.57\{\%/\text{mb}\}\delta h_o + 0.06\{\%/1^\circ\text{K}\}\delta T(h_o) + 0.38\left(\delta N_\mu(h_o)/N_\mu(h_o)\right). \quad (5.3.32)$$

Let us note again that in Eq. 5.3.30–5.3.32 $\delta N_\mu(h_o)/N_\mu(h_o)$ denotes the meteorological effects of total muon intensity (including soft muons).

5.4. Meteorological effects of CR total neutron component and different multiplicities

5.4.1. Formation of total neutron component and different multiplicities detected by neutron monitors

To determine the expected meteorological effects of CR total neutron component and different multiplicities is necessary to know the sensitivity of neutron monitor to different particles. Important results were obtained by Hughes et al. (1964), Meyer et al. (1964) and Hughes and Marsden (1966) by using standard neutron monitor at Leeds ($R_C = 2.1$ GV) together with magnetic spectrograph. Table 5.4.1 lists the counting rates for total and different multiplicities and relative role of neutrons, protons, captured muons (mostly soft muons, stopped in 10 cm Pb), passing muons (fast muons, crossing 10 cm Pb), pions and showers in formation of neutron monitor's (NM) counting rate.

Table 5.4.1. Counting rates for total and different multiplicities *m* (from 1 up to 9) and relative role of neutrons, protons, captured muons, passing muons, pions and showers in formation of counting rates in standard NM.

particles	Total intensity, %	multiplicities, in % from total			
		$m = 1$	$m = 2$	$m = 3$	$m = 4$
neutrons	81.30	50.660	9.935	2.006	0.539
protons	11.20	4.446	1.425	0.535	0.225
cap. muons	6.80	6.362	0.419	0.0189	
pas. muons	0.47	0.295	0.0627	0.0136	0.00236
pions	0.15	0.0503	0.0177	0.00769	0.00296
showers	0.08	0.0213	0.0136	0.00355	0.00177
total	100.00	61.8346	11.873	2.58474	0.77109

Table 5.4.1. (Continued)

particles	multiplicities, in % from total				
	$m = 5$	$m = 6$	$m = 7$	$m = 8$	$m = 9$
neutrons	0.1916	0.0858	0.0449	0.0260	0.01715
protons	0.1124	0.0574	0.0325	0.01952	0.01183
cap. muons					
pas. muons	0.00059				
pions	0.00177	0.00059	0.00059		
showers	0.00118	0.00059	0.00059		
total	0.30751	0.14438	0.07858	0.04552	0.02898

Therefore, the intensity observed by standard NM can be represented for m = tot, 1, 2, 3, ... as

$$N_m(h_o) = N_m^n(h_o) + N_m^p(h_o) + N_m^{c\mu}(h_o) + N_m^{p\mu}(h_o) + N_m^{\pi}(h_o) + N_m^{sh}(h_o), \quad (5.4.1)$$

where

$$\begin{aligned} &N_m^n(h_o) = a_m^n(h_o) N_m(h_o),\ N_m^p(h_o) = a_m^p(h_o) N_m(h_o), \\ &N_m^{c\mu}(h_o) = a_m^{c\mu}(h_o) N_m(h_o),\ N_m^{p\mu}(h_o) = a_m^{p\mu}(h_o) N_m(h_o), \\ &N_m^{\pi}(h_o) = a_m^{\pi}(h_o) N_m(h_o),\ N_m^{sh}(h_o) = a_m^{sh}(h_o) N_m(h_o). \end{aligned} \quad (5.4.2)$$

For any m in Eq. 5.4.2

$$a_m^n(h_o) + a_m^p(h_o) + a_m^{c\mu}(h_o) + a_m^{p\mu}(h_o) + a_m^{\pi}(h_o) + a_m^{sh}(h_o) = 1. \quad (5.4.3)$$

Values of these coefficients for m = tot, 1, 2, 3, 4, 5, 6, 7, 8 and 9 are listed in Table 5.4.2 (obtained on the basis of Table 5.4.1).

Table 5.4.2. Coefficients $a_m^n(h_o)$, $a_m^p(h_o)$, $a_m^{c\mu}(h_o)$, $a_m^{p\mu}(h_o)$, $a_m^{\pi}(h_o)$, $a_m^{sh}(h_o)$ for m = tot, 1, 2, ...9.

channel of NM	$a_m^n(h_o)$	$a_m^p(h_o)$	$a_m^{c\mu}(h_o)$	$a_m^{p\mu}(h_o)$	$a_m^{\pi}(h_o)$	$a_m^{sh}(h_o)$
total	0.8130	0.1120	0.0680	0.0047	0.0015	0.0008
$m = 1$	0.8193	0.0719	0.1029	0.00477	0.0008135	0.0003445
$m = 2$	0.8368	0.1200	0.03529	0.005281	0.001491	0.001145
$m = 3$	0.7761	0.2070	0.00731	0.005262	0.002975	0.001373
$m = 4$	0.6990	0.2918		0.003061	0.003839	0.002295
$m = 5$	0.6231	0.3655		0.001919	0.005756	0.003837
$m = 6$	0.5943	0.3976			0.004086	0.004086
$m = 7$	0.5714	0.4136			0.007508	0.007508
$m = 8$	0.5712	0.4288				
$m = 9$	0.5918	0.4082				

5.4.2. Expected meteorological effects in total neutron component and different multiplicities caused by different particles

By using information contained in Table 5.4.2, we can estimate the expected meteorological effects of total neutron component and different multiplicities caused by different particles. On the basis of Eq. 5.4.1–5.4.2 we obtain

$$\left(\frac{\delta N_m(h_o)}{N_m(h_o)}\right)_{\text{met}} = a_m^n(h_o)\left(\frac{\delta N_m^n(h_o)}{N_m^n(h_o)}\right)_{\text{met}} + a_m^p(h_o)\left(\frac{\delta N_m^p(h_o)}{N_m^p(h_o)}\right)_{\text{met}} + a_m^{c\mu}(h_o)\left(\frac{\delta N_m^{c\mu}(h_o)}{N_m^{c\mu}(h_o)}\right)_{\text{met}}$$
$$+ a_m^{p\mu}(h_o)\left(\frac{\delta N_m^{p\mu}(h_o)}{N_m^{p\mu}(h_o)}\right)_{\text{met}} + a_m^{\pi}(h_o)\left(\frac{\delta N_m^{\pi}(h_o)}{N_m^{\pi}(h_o)}\right)_{\text{met}} + a_m^{sh}(h_o)\left(\frac{\delta N_m^{sh}(h_o)}{N_m^{sh}(h_o)}\right)_{\text{met}} . \qquad (5.4.4)$$

Let us consider separately each term on the right hand side of Eq. 5.4.4.

5.4.3. Meteorological effects in total neutron component and different multiplicities caused by neutrons and protons: the first approximation.

In the first approximation the total number of neutrons and protons in the atmosphere decreases exponentially as

$$N_n(h_o) \propto \exp(-h_o/L_n),\ N_p(h_o) \propto \exp(-h_o/L_p), \qquad (5.4.5)$$

where L_n, L_p are the absorption paths for neutrons and protons, correspondingly (in the first approximation $L_n \approx L_p \approx 145\ \text{g/cm}^2$). It means that these parts of total neutron component and different multiplicities caused by neutrons and protons will give only barometric effect:

$$\delta N_n(h_o)/N_n(h_o) = \beta_n \delta h_o,\ \delta N_p(h_o)/N_p(h_o) = \beta_p \delta h_o, \qquad (5.4.6)$$

where barometric coefficients

$$\beta_n = -L_n^{-1} \approx -0.7\%/\text{mb},\ \beta_p = -L_p^{-1} \approx -0.7\%/\text{mb} . \qquad (5.4.7)$$

In reality L_n, L_p and correspondingly β_n, β_p change significantly during the 11-year solar cycle (caused by changes of primary CR spectrum) as well as from one station to another with changing of cut off rigidity (see below, Chapter 9).

Let us note that according to Table 5.4.2 neutrons and protons gave $a_m^n(h_o) + a_m^p(h_o) = 0.925$ in total counting rate of neutron monitor, 0.8912 in multiplicity m = 1, 0.9568 in m = 2, 0.9831 in m = 3, and more than 0.985 in multiplicities m = 4–9. It means that the main meteorological effect of total neutron component and different multiplicities detected by standard neutron monitors is a barometric effect.

5.4.4. Meteorological effects in the total neutron component and different multiplicities caused by neutrons and protons: the second approximation.

In the second approximation we need to take into account that in a nuclear–meson cascade of formation of neutron–proton CR component there take some part also non-stable particles: charged pions. With increasing air temperature the length for crossing the same depth of matter (in g/cm^2) will increase and the fraction of decayed pions will also increase, but the number of nuclear interacted pions will decrease. It leads to the well known positive temperature effect for the muon component (see above, Section 5.1) and to the negative temperature effect for the neutron-proton component. Let us estimate this effect very roughly. According to Grigorov and Murzin (1953) and Vernov et al. (1955) protons with energy $E_p \le 7$ GeV (the average energy about 3 GeV) in the nuclear interactions with air atoms transfer to neutrons and protons about 3/5 of their energy, and to charged pions only 1/4; from other side, protons with energy $E_p \ge 7$ GeV (the average energy about 20 GeV) in the nuclear interactions with air atoms transfer to charged pions much bigger part of energy about 1/2. Therefore we will suppose that about 1/3 (between ¼ and ½) of the observed neutron–proton component is formed through charged pions; this part will have air density effects caused by decay of pions. In Section 5.1 we were interested only in decay of pions because this decay generates muons. Here we will consider the other part of pions, which are absorbed by nuclei of air atoms and produce neutron and protons. We suppose that generated secondary neutrons and protons propagate down according to exponential law of absorption according to Eq. 5.4.5. Let us first determine the absorbed part of pions.

The transport path R_{dec} of pion with momentum p relative to decay will be $R_{\mathrm{dec}} = p\tau_\pi / m_\pi$, where τ_π and m_π are respectively the lifetime and the mass of charged pions in the rest system of coordinates. The transport path R_{abs} of pions relative to absorption by air atoms will be $R_{\mathrm{abs}} = l/\rho(h)$, where $l \approx 60\ g/cm^2$ and $\rho(h)$ is the air density. The relative part of pions, absorbed in a neutron monitor with generation of neutrons and protons will be

$$\varphi_{\mathrm{abs}}(p,h) = R_{\mathrm{dec}}/(R_{\mathrm{dec}} + R_{\mathrm{abs}}) = p\tau_\pi\rho(h)/(p\tau_\pi\rho(h) + lm_\pi). \qquad (5.4.8)$$

or for relativistic pions

$$\varphi_{\mathrm{abs}}(E_\pi,h) = E_\pi\tau_\pi\rho(h)/(E_\pi\tau_\pi\rho(h) + lm_\pi c). \qquad (5.4.9)$$

Eq. 5.4.9 shows that for pions with $E_\pi << lm_\pi c/\tau_\pi\rho(h)$ we obtain

$$\varphi_{\mathrm{abs}}(E_\pi,h) \approx \frac{E_\pi\tau_\pi\rho(h)}{lm_\pi c} << 1;\ \frac{\delta\varphi_{\mathrm{abs}}(E_\pi,h)}{\varphi_{\mathrm{abs}}(E_\pi,h)} \approx \frac{\delta\rho(h)}{\rho(h)}, \qquad (5.4.10)$$

and for high energy pions with $E_\pi >> lm_\pi c/\tau_\pi\rho(h)$ it will be

$$\varphi_{\text{abs}}(E_\pi,h)\approx 1-\frac{lm_\pi c}{E_\pi\tau_\pi\rho(h)}\approx 1;\ \frac{\delta\varphi_{\text{abs}}(E_\pi,h)}{\varphi_{\text{abs}}(E_\pi,h)}\approx\frac{lm_\pi c\delta\rho(h)}{E_\pi\tau_\pi\rho^2(h)}<<\frac{\delta\rho(h)}{\rho(h)},\quad (5.4.11)$$

where $\delta\rho(h)/\rho(h)$ and $\delta\rho(h)/\rho^2(h)$ were determined by Eq. 5.1.20 in Section 5.1. Results for $\varphi_{\text{abs}}(E_\pi,h)$ are shown in Table 5.4.3.

Table 5.4.3. The dependence of $\varphi_{\text{abs}}(E_\pi,h)$ from energy of pions E_π and air pressure h.

h, atm	E_π, GeV					
	1	3	10	30	100	300
0.05	0.0045	0.0134	0.0433	0.1195	0.3115	0.5758
0.1	0.0090	0.0264	0.0830	0.2135	0.4751	0.7308
0.2	0.0178	0.0515	0.1533	0.3519	0.6441	0.8445
0.3	0.0264	0.0753	0.2135	0.4489	0.7308	0.8907
0.4	0.0349	0.0980	0.2658	0.5206	0.7835	0.9157
0.5	0.0433	0.1195	0.3115	0.5758	0.8190	0.9314
0.6	0.0515	0.1401	0.3519	0.6196	0.8445	0.9422
0.7	0.0596	0.1597	0.3878	0.6552	0.8637	0.9500
0.8	0.0675	0.1784	0.4200	0.6847	0.8786	0.9560
0.9	0.0753	0.1964	0.4489	0.7096	0.8907	0.9607
1.0	0.0830	0.2135	0.4751	0.7308	0.9005	0.9645

The total number of neutrons and protons generated by pions will be

$$N_{np}^{\pi}(h_o)=B\times\int_{m_nc^2}^{\infty}dE_\pi\int_0^{h_o}\frac{dh_2}{l}\exp\left(-\frac{h_o-h_2}{L_{np}}\right)N_\pi(E_\pi,h_2),\quad (5.4.12)$$

where the constant B is determined from the condition that this part of neutron-proton component is equal to 1/3 of the observed, and $N_\pi(E_\pi,h_2)$ is the number of pions on the level h_2 propagated in vertical direction (compare Section 5.1, Eq. 5.1.3):

$$N_\pi(E_\pi,h_2)=\int_0^{h_2}f_\pi(E_\pi,h_1)\varphi_\pi(E_\pi,h_1,h_2)dh_1\ .\quad (5.4.13)$$

In Eq. 5.4.13 function of pion generation is given by

$$f_\pi(E_\pi,h_1)=AE_\pi^{-(2+\gamma)}\exp(-h_1/L),\quad (5.4.14)$$

where A is some parameter that changes with solar activity and depends on cut off rigidity. The probability that a pion generated on level h_1 will reach level h_2 is

$$\varphi_\pi(E_\pi,h_1,h_2)=\exp\left(-\frac{h_2-h_1}{l}\right)\exp\left(-\frac{m_\pi c}{\tau_\pi E_\pi}\int\limits_{h_1}^{h_2}\frac{dh}{\rho(h)}\right). \qquad (5.4.15)$$

By substituting Eq. 5.4.15 and 5.4.14 in Eq. 5.4.13, and then in Eq. 5.4.12, we obtain

$$N_{np}^{\pi}(h_o)=AB\int\limits_{m_nc^2}^{\infty}E_\pi^{-(2+\gamma)}dE_\pi\int\limits_0^{h_o}\frac{dh_2}{l}\exp\left(-\frac{h_o-h_2}{L_{np}}\right)$$
$$\times\int\limits_0^{h_2}\exp\left(-\frac{h_1}{L}-\frac{h_2-h_1}{l}\right)\exp\left(-\frac{m_\pi c}{\tau_\pi E_\pi}\int\limits_{h_1}^{h_2}\frac{dh}{\rho(h)}\right)dh. \qquad (5.4.16)$$

Let us take into account that $\rho(h)=gh/R(h)T(h)$ and that the interval (h_1, h_2) is very small and in this interval the changes of $R(h)$ and $T(h)$ are also small; in this case we obtain

$$\exp\left(-\frac{m_\pi c}{\tau_\pi E_\pi}\int\limits_{h_1}^{h_2}\frac{dh}{\rho(h)}\right)\approx\left(\frac{h_1}{h_2}\right)^{m_\pi cR(\bar{h})T(\bar{h})/g\tau_\pi E_\pi}, \qquad (5.4.17)$$

where $h_1\le\bar{h}\le h_2$. Then, the last integral in Eq. 5.4.16 can be approximated as

$$\int\limits_0^{h_2}\exp\left(-\frac{h_1}{L}-\frac{h_2-h_1}{l}\right)\exp\left(-\frac{m_\pi c}{\tau_\pi E_\pi}\int\limits_{h_1}^{h_2}\frac{dh}{\rho(h)}\right)dh_1$$
$$\approx\lambda_1\exp\left(-\frac{h_2}{l}\right)\left(\exp\left(\frac{h_2}{\lambda_1}\right)-1\right)k^{-m_\pi cR(\bar{h})T(\bar{h})/\tau_\pi E_\pi g}, \qquad (5.4.18)$$

where $\lambda_1^{-1}=l^{-1}-L^{-1}$ and $0\le k^{-1}\le 1$ (approximately $k\approx 2$). By substituting Eq. 5.4.18 in Eq. 5.4.16, we obtain

$$N_{np}^{\pi}(h_o)=AB\lambda_1 l^{-1}\exp\left(-\frac{h_o}{L_{np}}\right)\int\limits_0^{h_o}dh_2\exp\left(-\frac{h_2}{\lambda_2}\right)\left(\exp\left(\frac{h_2}{\lambda_1}\right)-1\right)$$
$$\times\int\limits_{m_nc^2}^{\infty}E_\pi^{-(2+\gamma)}k^{-m_\pi cR(\bar{h})T(\bar{h})/\tau_\pi E_\pi g}dE_\pi, \qquad (5.4.19)$$

where $\lambda_2^{-1}=l^{-1}-L_{np}^{-1}$. Finally, using $x(E_\pi)=m_\pi cR(\bar{h})T(\bar{h})\ln k/\tau_\pi E_\pi g$ the last integral in Eq. 5.4.19 can be transformed to

$$\int_{m_n c^2}^{\infty} E_\pi^{-(2+\gamma)} k^{-x(E_\pi)} dE_\pi = \left(\frac{\tau_\pi g}{m_\pi c R(\bar{h}) T(\bar{h}) \ln k} \right)^{1+\gamma} \int_0^{m_\pi c R(\bar{h}) T(\bar{h}) \ln k / \tau_\pi g m_n c^2} x^\gamma \exp(-x) dx$$

$$= \left(\frac{\tau_\pi g}{m_\pi c R(\bar{h}) T(\bar{h}) \ln k} \right)^{1+\gamma} \times \begin{cases} 1 - \exp\left(- \dfrac{m_\pi c R(\bar{h}) T(\bar{h}) \ln k}{\tau_\pi g m_n c^2} \right) & \text{for } \gamma = 0 \\ 1 - \left(1 + \dfrac{m_\pi c R(\bar{h}) T(\bar{h}) \ln k}{\tau_\pi g m_n c^2} \right) \exp\left(- \dfrac{m_\pi c R(\bar{h}) T(\bar{h}) \ln k}{\tau_\pi g m_n c^2} \right) & \text{for } \gamma = 1. \end{cases} \quad (5.4.20)$$

Let us take into account that interval (h_1, h_2) really is small (for small energies caused by fast decay of pions and for high energies caused by nuclear absorption), therefore we can approximately replace $\bar{h}$ by h_2. In this case we obtain from Eq. 5.4.19 (by taking into account Eq. 5.4.20)

$$N_{np}^{\pi}(h_o) = AB\lambda_1 l^{-1} \exp\left(- \frac{h_o}{L_{np}} \right) \int_0^{h_o} \Phi(h_2, \gamma, g, R(h_2), T(h_2)) dh_2 \,, \quad (5.4.21)$$

where

$$\Phi(h_2, \gamma, g, R(h_2), T(h_2)) = \exp\left(- \frac{h_2}{\lambda_2} \right) \left(\exp\left(\frac{h_2}{\lambda_1} \right) - 1 \right) \left(\frac{\tau_\pi g}{m_\pi c R(h_2) T(h_2) \ln k} \right)^{1+\gamma}$$

$$\times \int_0^{\frac{m_\pi c R(\bar{h}) T(\bar{h}) \ln k}{\tau_\pi g m_n c^2}} x^\gamma \exp(-x) dx = \exp\left(- \frac{h_2}{\lambda_2} \right) \left(\exp\left(\frac{h_2}{\lambda_1} \right) - 1 \right) \left(\frac{\tau_\pi g}{m_\pi c R(h_2) T(h_2) \ln k} \right)^{1+\gamma}$$

$$\times \begin{cases} 1 - \exp\left(- \dfrac{m_\pi c R(h_2) T(h_2) \ln k}{\tau_\pi g m_n c^2} \right) & \text{for } \gamma = 0 \\ 1 - \left(1 + \dfrac{m_\pi c R(h_2) T(h_2) \ln k}{\tau_\pi g m_n c^2} \right) \exp\left(- \dfrac{m_\pi c R(h_2) T(h_2) \ln k}{\tau_\pi g m_n c^2} \right) & \text{for } \gamma = 1. \end{cases} \quad (5.4.22)$$

Let us vary Eq. 5.4.21 with respect to the meteorological parameters h_o, g, $R(h_2)$, $T(h_2)$:

$$\left(\frac{\delta N^{\pi}_{np}(h_o)}{N^{\pi}_{np}(h_o)}\right)_{\text{met}} = \beta^{\pi}_{nph}(h_o)\delta h_o + \beta^{\pi}_{npg}(h_o)\delta g + \int_0^{h_o} W^{\pi}_{npe}(h_o,h_2,\gamma)\delta e(h_2)dh_2 + \int_0^{h_o} W^{\pi}_{npT}(h_o,h_2,\gamma)\delta T(h_2)dh_2, \quad (5.4.23)$$

where the barometric coefficient

$$\beta^{\pi}_{nph}(h_o) = -L^{-1}_{np} + \Phi(h_o,\gamma,g,R(h_o),T(h_o))\Big/\int_0^{h_o}\Phi(h_2,\gamma,g,R(h_2),T(h_2))dh_2, \quad (5.4.24)$$

the gravitational coefficient

$$\beta^{\pi}_{npg}(h_o) = \int_0^{h_o}\frac{\partial\Phi(h_2,\gamma,g,R(h_2),T(h_2))}{\partial g}dh_2 \Big/\int_0^{h_o}\Phi(h_2,\gamma,g,R(h_2),T(h_2))dh_2, \quad (5.4.25)$$

the humidity coefficient

$$W^{\pi}_{npe}(h_o,h_2,\gamma) = \frac{\delta\Phi(h_2,\gamma,g,R(h_2),T(h_2))}{\delta R(h_2)(0.378R_o/h_2)^{-1}}\Big/\int_0^{h_o}\Phi(h_2,\gamma,g,R(h_2),T(h_2))dh_2, \quad (5.4.26)$$

and the temperature coefficient

$$W^{\pi}_{npT}(h_o,h_2,\gamma) = \frac{\delta\Phi(h_2,\gamma,g,R(h_2),T(h_2))}{\delta T(h_2)}\Big/\int_0^{h_o}\Phi(h_2,\gamma,g,R(h_2),T(h_2))dh_2. \quad (5.4.27)$$

5.4.5. Expected meteorological effects in total neutron component and different multiplicities caused by captured muons

Soft negative muons that are stopped in 10 cm Pb are captured by lead nuclei with formation of mesoatoms according the reaction

$$\mu^- + {}^Z A \rightarrow {}^{Z-1}A^* + \nu_\mu. \quad (5.4.28)$$

Part of muon rest energy ($m_\mu c^2 \approx 100$ MeV) takes muon neutrino and other 10–20 MeV expends for the generation of one or a few neutrons. Experimental investigations of Babadzhanov (1969) show that average number of generated neutrons in lead $\langle M\rangle_{\text{Pb}} = 1.78 \pm 0.18$, in iron $\langle M\rangle_{\text{Fe}} = 1.11 \pm 0.17$, and in copper $\langle M\rangle_{\text{Cu}} = 1.20 \pm 0.07$. Results of numerical experimental data on generation of neutrons by soft muons in different materials characterized with atomic weight A can be approximated by the dependence

$$\langle M \rangle_A = bA^{1/3}, \quad b = 0.30 \pm 0.02 . \tag{5.4.29}$$

According to Table 5.4.2 captured muons give 6.8% in counting rate of total intensity, 10.29% in $m = 1$, 3.53% in $m = 2$, and 0.73% in $m = 3$. Therefore, meteorological effects in total neutron component and different multiplicities caused by captured muons will be

$$(\delta N_m(h_o)/N_m(h_o))_{\text{met}} = a_m^{c\mu}(h_o)\left(\delta N_m^{c\mu}(h_o)/N_m^{c\mu}(h_o)\right)_{\text{met}} , \tag{5.4.30}$$

where $\left(\delta N_m^{c\mu}(h_o)/N_m^{c\mu}(h_o)\right)_{\text{met}}$ are meteorological effects of soft muons, containing snow, barometric, temperature, humidity and gravitational effects, and were determined in Section 5.2; coefficients $a_m^{c\mu}(h_o)$ are listed in Table 5.4.2.

5.4.6. Expected meteorological effects in total neutron component and different multiplicities caused by fast muons

According to Cocconi et al. (1950), Cocconi and Cocconi-Tongiorgi (1951) fast muons (muons that cross 10 *cm* Pb) can, with very small probability, induce in lead and other materials nuclear disintegrations with generation of neutrons. From Table 5.4.1 it can be seen that the role of fast muons (passing the neutron monitor) in formation of total intensity is 0.47%, in the first multiplicity 0.48%, in $m = 2$ and $m = 3$ about 0.53%, in $m = 4$ and $m = 5$ correspondingly 0.31% and 0.19% (in multiplicities $m \geq 6$ this role becomes smaller than 0.1%). Therefore meteorological effects in total neutron component and different multiplicities caused by fast muons will be

$$(\delta N_m(h_o)/N_m(h_o))_{\text{met}} = a_m^{p\mu}(h_o)\left(\delta N_m^{p\mu}(h_o)/N_m^{p\mu}(h_o)\right)_{\text{met}} , \tag{5.4.31}$$

where $\left(\delta N_m^{p\mu}(h_o)/N_m^{p\mu}(h_o)\right)_{\text{met}}$ contains snow, barometric, temperature, humidity and gravitational effects, as determined in Section 5.1. The coefficients $a_m^{p\mu}(h_o)$ are listed in Table 5.4.2.

5.4.7. Expected meteorological effects in total neutron component and different multiplicities caused by charged pions inside NM

Near a neutron monitor the nuclear-active component of CR will generate charged pions. Some of these pions will decay into muons and neutrinos, and others will interact with matter while passing through the neutron monitor and give nuclear disintegrations, generating protons and neutrons that lead to additional counts in the NM. This contribution is determined by the coefficient $a_m^{\pi}(h_o)$ in Table 5.4.2. However, this coefficient is not constant. If the temperature of the ground layer of atmosphere of some depth increases, the decay of pions into muons and neutrino will also increase, the number of pions reaching neutron monitor will decrease, and correspondingly the relative number of the nuclear disintegrations decrease (through the decrease in the coefficient $a_m^{\pi}(h_o)$). Let us estimate this effect. The transport path R_{dec} of a pion with

momentum p relative to decay will be $R_{\rm dec} = p\tau_\pi / m_\pi$, where τ_π and m_π are respectively the life time and the mass of charged pions in the rest system of coordinates. The transport path $R_{\rm abs}$ of pions relative to absorption by air atoms will be $R_{\rm abs} = l/\rho(h_o)$, where $l \approx 60$ g/cm^2 and $\rho(h_o)$ is the air density. The relative part of decayed pions in the ground atmospheric layer will be

$$\varphi_{dec} = R_{abs}/(R_{dec} + R_{abs}) = lm_\pi/(p\tau_\pi \rho(h_o) + lm_\pi), \tag{5.4.32}$$

and relative part of pions, absorbed in neutron monitor with generation of neutrons and protons will be

$$\varphi_{\rm abs} = 1 - \varphi_{\rm dec} = R_{\rm dec}/(R_{\rm dec} + R_{\rm abs}) = p\tau_\pi \rho(h_o)/(p\tau_\pi \rho(h_o) + lm_\pi). \tag{5.4.33}$$

By varying Eq. 5.4.33 with respect to $\rho(h_o)$ we obtain

$$\frac{\delta\varphi_{\rm abs}}{\varphi_{\rm abs}} = \frac{\delta\rho(h_o)}{\rho(h_o)} - \frac{p\tau_\pi \delta\rho(h_o)}{p\tau_\pi \rho(h_o) + lm_\pi}. \tag{5.4.34}$$

By taking into account that $\rho(h_o) = gh_o/RT$, we obtain from Eq. 5.4.34

$$\left(\frac{\delta\varphi_{abs}}{\varphi_{abs}}\right)_{\rm met} = \frac{\delta g}{g} - \frac{\delta R(h_o)}{R(h_o)} - \frac{\delta T(h_o)}{T(h_o)} - \frac{p\tau_\pi h_o g \delta g / R(h_o)T(h_o)}{p\tau_\pi \rho(h_o) + lm_\pi}$$
$$- \frac{p\tau_\pi h_o g \delta R(h_o)/R^2(h_o)T(h_o)}{p\tau_\pi \rho(h_o) + lm_\pi} - \frac{p\tau_\pi h_o g \delta T(h_o)/R(h_o)T^2(h_o)}{p\tau_\pi \rho(h_o) + lm_\pi}, \tag{5.4.35}$$

where $T(h)$ is the air temperature in °K and $R(h_o) = R_o(1 + 0.378 e(h_o)/h_o)$ is the gas constant for air (here R_o is the gas constant of dry air, $e(h)$ is the pressure of water steam), and $\delta R(h) = 0.378 R_o \delta e(h_o)/h_o$. Eq. 5.4.35 describes the meteorological variations of coefficient $a_m^\pi(h_o)$.

5.4.8. Summary of temperature effects in total neutron component

As result of the considerations described above we can conclude that there are two temperature effects: one is local caused by pions captured in the neutron monitor (this effect is negative because with increasing temperature at the level of observation the probability of pion decay to muons and neutrinos increases and the relative number of absorbed pions with generation of neutrons inside neutron monitor will decrease), and the other is distributed over all the atmosphere caused by pions in the nuclear-meson cascade in atmosphere, by captured negative muons formatted mesoatoms inside monitor with following generation of neutrons inside the neutron monitor and by fast muons disintegrating lead atoms with generation neutrons:

$$\left(\frac{\delta N_n(h_o)}{N_n(h_o)}\right)_{\text{temp}} \approx \beta_T^n(h_o)\delta T(h_o) + \int_0^{h_o} W_T^n(h_o,h)\delta T(h)dh\,. \qquad (5.4.36)$$

As it was estimated above, on sea level ($\rho(h_o)\approx 10^{-3}$ g/cm^3, $T(h_o)\approx 270^\circ$K) $\beta_T^n(h_o)\approx -0.016$ %/1°K. In Fig. 5.4.1 we summarize all temperature coefficients for the second member in Eq. 5.4.36 for the total neutron component on sea level and mountain level at the latitude of 50° (cut off rigidity $R_c \approx 2.5\,GV$) and 0° ($R_c \approx 15$GV).

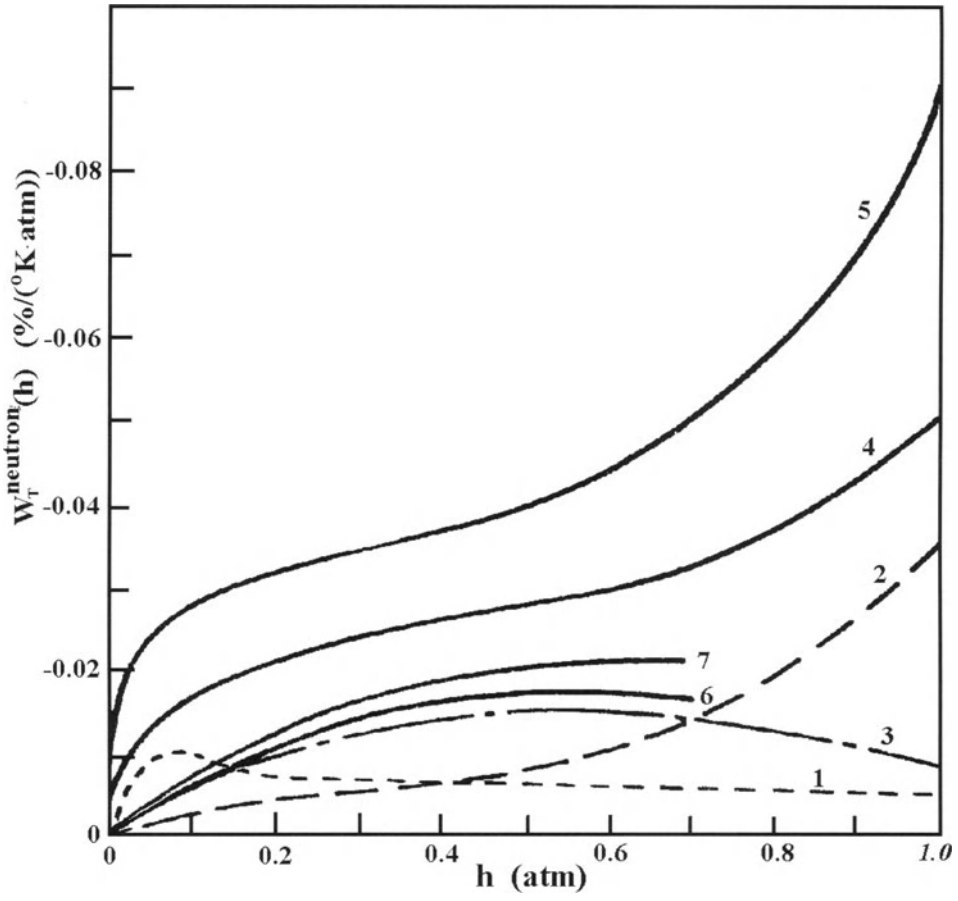

Fig. 5.4.1. Temperature coefficients $W_T^n(h)$ for neutron component at sea level and at mountain level for observations at latitude of about 50°, $R_c \approx 2.5$ GV and near equator, $R_c \approx 15$ GV. Curve **1** – caused by fast muons at sea level; **2** – caused by soft muons at sea level; **3** – caused by pions at sea level; **4** and **5** – total for observations at sea level (h_o = 1 atm) at $R_c \approx 2.5$ GV and at latitude near equator, $R_c \approx 15$ GV, respectively; **6** and **7** – total for observations at mountain level ($h_o = 0.7$ atm) at $R_c \approx 2.5$ GV and at $R_c \approx 15$ GV, respectively.

From Fig. 5.4.1 it can be seen that the total temperature coefficient for neutron component increases significantly with increasing cut off rigidity, and decreases with increasing measurement altitude: mostly this is caused by the relative change of neutron and muon fluxes with changing cut off rigidity and altitude of measurements (the change of the muon component intensity is much smaller than that of the neutron component).

Chapter 6

Experimental Investigations of CR Snow, Wind, and Barometric Effects

6.1. CR Snow effect

6.1.1. CR snow effect on mountains and high-latitude stations

When a neutron monitor station is covered with snow or water, two effects in counting rate arise: a negative absorption effect and positive effect of additional neutron generation in the absorber layer. Many CR stations on mountain heights have a problem with NM shielding with variable snow cover on the roof and near walls. Some CR stations near sea level at high latitudes also share this problem. It is a great pity because modern NM are characterized by a very high level of accuracy: the statistical error for one hour of observations is of order of 0.1%. Even regular cleaning of an Observatory from snow cannot prevent the disturbance of information in some short periods of time. The "snow' problem became especially acute in latter years when many mountain Observatories started to be operated automatically, as for example the Emilio Segre' Observatory on Mt. Hermon (Israel). One of the first investigations of the snow and water effect on neutron monitors was made by Blomster and Tanskanen (1970) on the basis of neutron monitor data in Oulu (Finland).

Dorman et al. (2001) developed a special method to determine quantitatively the snow effect in total NM counting rate as well as in different multiplicities without any measurements of the actual amount of snow on the roof and near walls of Observatory. The method can work in the near future automatically, allowing corrections of this effect by using on-line data of two or more NM. In the following we will describe this method. Dorman et al. (2001) also analyzed this effect during the periods from 15 December 1999 to 9 February 2000 (with maximal absorption effect about 16% in the first multiplicity) and from 1 January 2001 up to 5 March 2001 with maximal effect 13% in the total neutron intensity. The periods without snow are used for determining the regression coefficients between primary CR variations observed by NM of the Emilio Segre' Observatory, and by Rome NM. On the basis of the results obtained, it will be possible to correct for this effect automatically by using several NM hourly data. The method described below will be useful for on-line correction of NM data where the snow effect is important.

6.1.2. Regression relations in periods without snow

First we determine the regression relations between the ESO NM and the Rome NM for the total neutron intensity and for different multiplicities in periods without snow. One hour data of Rome NM (which is never covered by snow), corrected for the barometric effect, was used. Using one hour data of NM of the Emilio Segre' Observatory (also corrected on barometric effect) from 16 June 1998 up to 1 April 2001 in periods when there was no snow on Mt. Hermon, the regression relations between the two stations were determined:

$$\ln\left(I^{m}_{\mathrm{ESO}}\right)= B_m \times \ln\left(I^{\mathrm{tot}}_{\mathrm{Rome}}\right)+ C_m , \qquad (6.1.1)$$

where $m = \mathrm{tot}, 1, 2, 3, 4, 5, 6, 7, \geq 8$. Results for the regression coefficients B_m, C_m and the correlation coefficients R_m are shown in Table 6.1.1.

Table 6.1.1. Regression coefficients B_m, C_m and correlation coefficients R_m for total neutron intensity and different multiplicities, according to Eq. 6.1.1.

Channel	B_m	C_m	R_m
TOT	0.668 ± 0.001	4.63±0.02	0.966
$m = 1$	0.612 ± 0.002	4.58 ± 0.02	0.956
$m = 2$	0.766 ± 0.001	1.30 ± 0.02	0.977
$m = 3$	0.780 ± 0.002	2.54 ± 0.02	0.973
$m = 4$	0.739 ± 0.002	-3.90 ± 0.02	0.961
$m = 5$	0.660 ± 0.002	-1.81 ± 0.03	0.931
$m = 6$	0.569 ± 0.003	2.79 ± 0.04	0.860
$m = 7$	0.447 ± 0.004	1.22 ± 0.05	0.694
$m \geq 8$	0.142 ± 0.007	5.43 ± 0.09	0.169

6.1.3. Snow effect on Mt. Hermon for different multiplicities

Using Eq. 6.1.1 and the regression coefficients B_m, C_m listed in Table 6.1.1, one can determine the expected total neutron intensity and expected counting rates for different multiplicities on Mt. Hermon on the basis of Rome NM hourly data for neutron intensity and expected counting rates for different multiplicities on the basis of Rome NM hourly data for periods when the Emilio Segre' Observatory was covered by snow. To determine the snow effect we need to extract these expected intensities from those actually observed. The results are shown in Fig. 6.1.1 and Fig. 6.1.2 for winter of 1999/2000 for total intensity and different multiplicities. From Fig. 6.1.1 and Fig. 6.1.2 it can be seen that the biggest snow effect was observed on Mt. Hermon for multiplicity m=1; snow effect decreases with increasing neutron multiplicity m. The snow effects observed on Mt. Hermon in the winter of 2000/2001 in total intensity and in different neutron multiplicities are shown in Fig. 6.1.3.

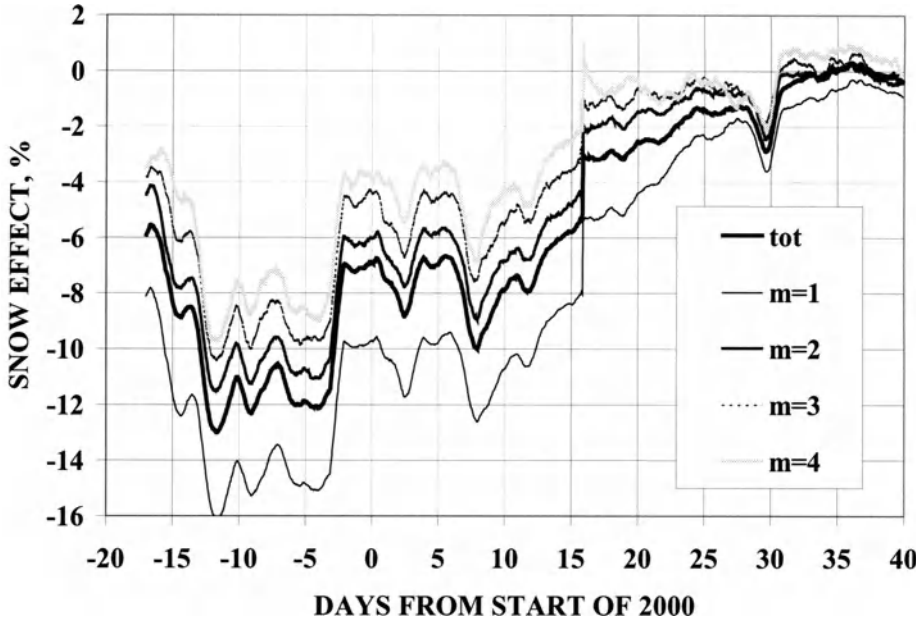

Figure 6.1.1. CR snow effect on Mt. Hermon in period of the winter 1999/2000 in the total neutron intensity and in the neutron multiplicities m = 1, 2, 3 and 4.

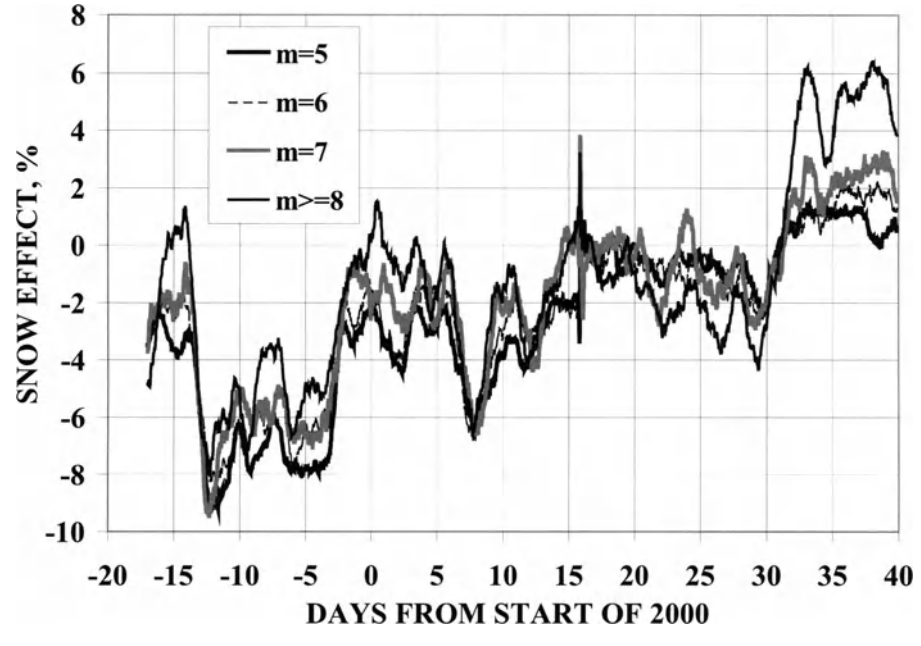

Figure 6.1.2. The same as in Fig. 6.1.1, but for multiplicities m = 5, 6, 7 and ≥ 8.

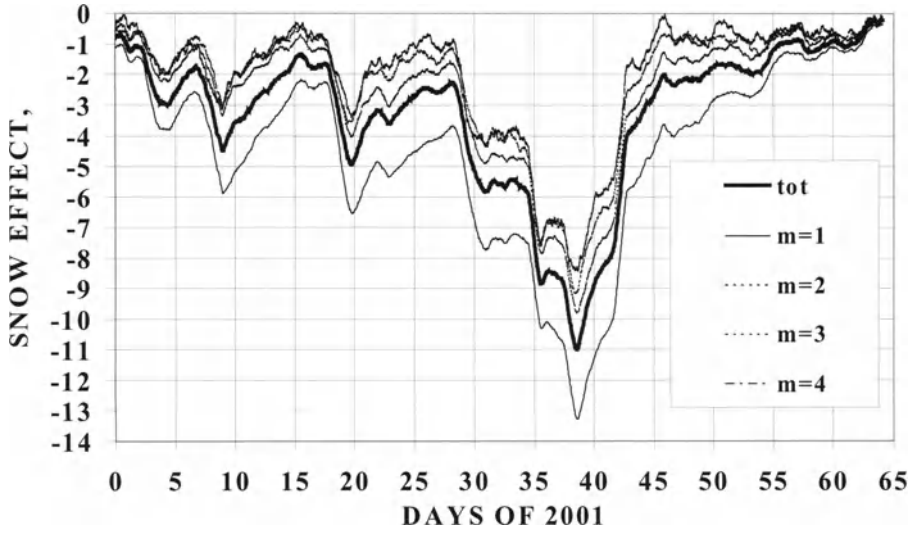

Figure 6.1.3. CR snow effects on Mt. Hermon in period of winter 2000/2001 in total neutron intensity and in neutron multiplicities m = 1, 2, 3 and 4

6.1.4. Regression relations between snow effects in total intensity and in different multiplicities

It can be seen from Fig. 6.1.1–6.1.3 that there are correlations of snow effects in total intensity and in different multiplicities. Fig. 6.1.4 and 6.1.5 show comparisons of snow effects observed in winter 1999/2000.

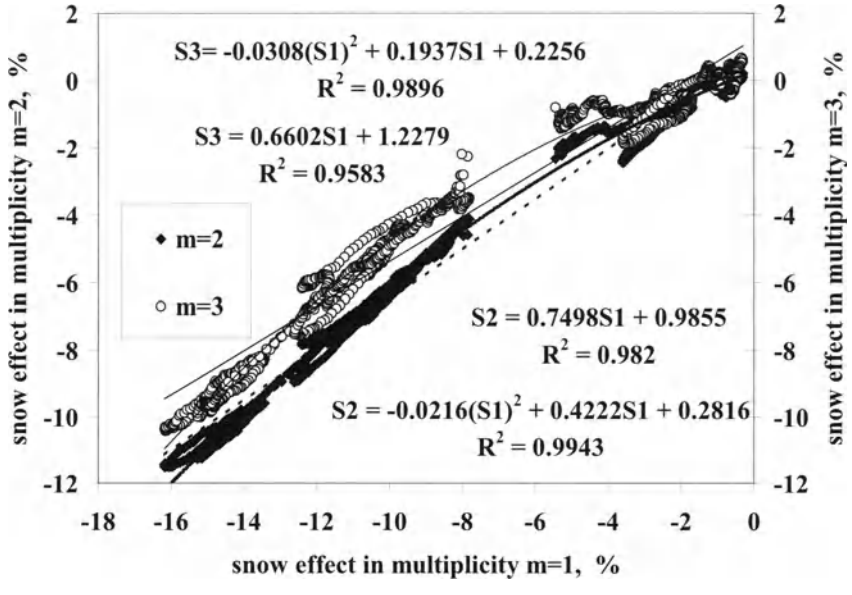

Figure 6.1.4. Comparison of snow effects in m = 2 and m = 3 with snow effect in m = 1. Linear and parabolic regression relations with correlation coefficients are also shown. Observations in winter 1999/2000.

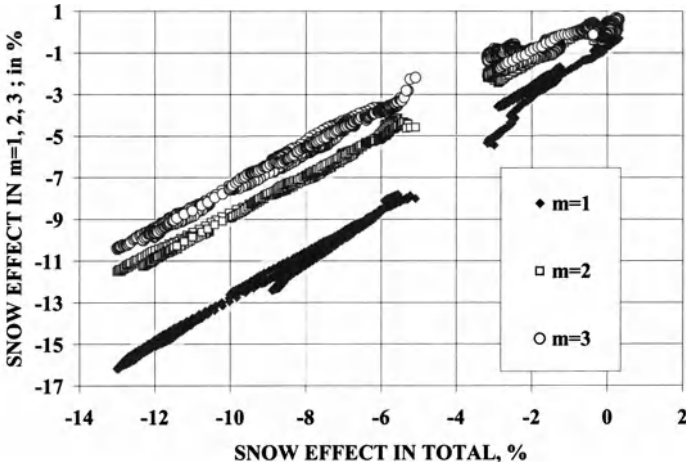

Figure 6.1.5. Comparison of snow effects in neutron multiplicities m = 1, 2 and 3 with snow effect in total neutron intensity. Observations in winter 1999/2000

The snow effect in different channels shown in Fig. 6.1.4 and 6.1.5 in the first approximation can be described by linear regression relations

$$S_m = D_{mt} S_t + E_{mt}; \quad S_m = D_{m1} S_1 + E_{m1} \tag{6.1.2}$$

between snow effects in different multiplicities S_m and in total neutron intensity S_t (see Table 6.1.2) or in the first multiplicity S_1 (see Fig. 6.1.4).

Table 6.1.2. Regression coefficients D_{mt}, E_{mt} and correlation coefficients R_{mt} for winters 1999/2000 and 2000/2001.

m	Winter 1999/2000			Winter 2000/2001		
	D_{mt}	E_{mt}	R_{mt}	D_{mt}	E_{mt}	R_{mt}
1	1.218	-0.008	0.996	1.201	-0.006	0.991
2	0.922	0.004	0.997	0.913	0.004	0.996
3	0.817	0.007	0.992	0.849	0.006	0.990
4	0.741	0.010	0.981	0.816	0.006	0.980
5	0.671	0.010	0.965	0.747	0.006	0.932
6	0.600	0.011	0.928	0.694	0.005	0.843
7	0.603	0.015	0.937	0.657	0.005	0.766
≥ 8	0.580	0.019	0.719	0.423	-0.001	0.370

Results show that snow effects in total neutron intensity and in different multiplicities on Mt. Hermon are comparable with great Forbush–decreases and with long–term CR variations connected with solar activity cycles. The method developed in Dorman et al. (2001) gives the possibility to determine snow effects with a good accuracy and then eliminate them from observed data. The found regression relations obtained between snow effects for total neutron intensity and for different multiplicities (see Table 6.1.2 and Fig. 6.1.4) can be explained by competition of two processes:

absorption by snow and by generation in snow of additional multiple neutrons. Application of the developed method will be useful for many mountain CR Observatories and for some Observatories near sea level with great snow effects.

6.2. Wind effect in CR

In applying corrections for barometric effect to measurements of the CR secondary components the possible difference between the air mass above the apparatus and the reading of the barograph should be noted. This difference, arising from the Bernoulli effect, is proportional to the square of the wind velocity w and is rather large for high velocities:

$$\Delta h_o \approx (1/2)\rho(h_o)w^2 \,. \tag{6.2.1}$$

The first investigations of the wind effect in CR was made by Falkoner (1947), Lockwood and Calawa (1957). The main result of Lockwood and Calawa (1957) is shown in Fig. 6.2.1.

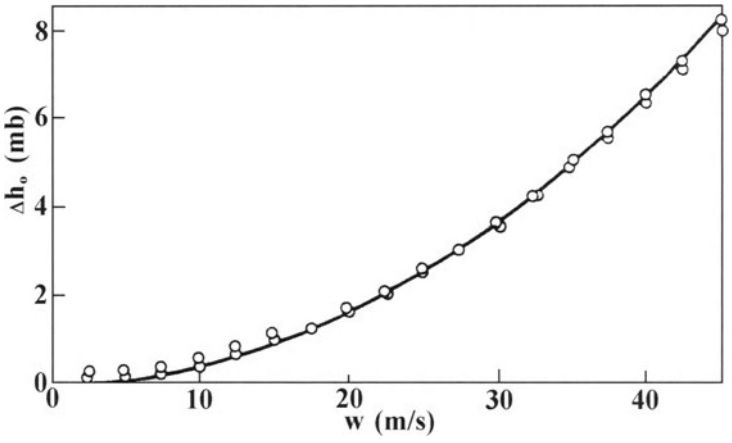

Fig. 6.2.1. The corrections Δh_o to the observed air pressure as a dependence upon wind velocity w. The curve is determined by Bernoulli effect $\Delta h_o = \rho(h_o)w^2/2$, and open circles are obtained from neutron monitor experimental data: $\Delta h_o = \Delta I_n/\beta_n$, where β_n is barometric coefficient of CR neutron component.

Fig. 6.2.1 shows that the influence of the wind on the measured air pressure becomes important for neutron monitor and muon telescope data corrections for periods when wind velocities $w \geq 10\ m/sec$ are observed. Lockwood and Calawa (1957) showed that after computing the barometric effect with this wind correction to the air pressure, the correlation coefficient of neutron intensity with wind velocity had dropped to 0.05, whilst it was 0.65 without correction on Bernoulli effect.

Dubinsky at al. (1960) studied this effect by NM data on Lomnitsky Stit. For a wind velocity ≈ 100 km/sec an effect of 2.6% was expected whereas the observations gave 5.5 ± 0.5%. Dubinsky at al. (1960) supposed that this great difference can be caused by the existence in the period of observations sufficient vertical component of wind velocity, which was not taken into account. The influence of wind on the barometric effect of neutron component was studied also by Kawasaki (1966) on the basis of neutron monitor

and wind velocity observations at Mt. Norikura. The latitude distribution of wind effect and its possible influence on CR latitude survey was studied by Dorman and Kaminer (1969). In this paper it was also shown that for more exact determination of wind effect it is necessary to take into account not only wind velocity in the level of observations but also the vertical component of wind velocity (especially important for CR observations on mountains), as well as vertical distribution of horizontal wind velocities.

The influence of strong turbulent winds in an alpine environment on neutron component pressure correction was investigated by Butikofer and Fluckiger (1999) on the basis of data obtained on Mt. Jungfraujoch (46.55°N, 7.98°E) during the period of solar CR event at 6 November 1997. There are two neutron monitors at Mt. Jungfraujoch: 18-NM-IGY at 3550 *m* above sea level (located at a saddle on the top of Sphinx rock and is therefore good exposed to winds), and 3-NM-64 (3-NM-IQSY) at 3475 *m* above sea level (situated on the south flank of the Mt. Jungfraujoch and is therefore less exposed to winds). Results of observations at 5–7 November 1997 (including solar CR event at 6 November) are shown in Fig. 6.2.2.

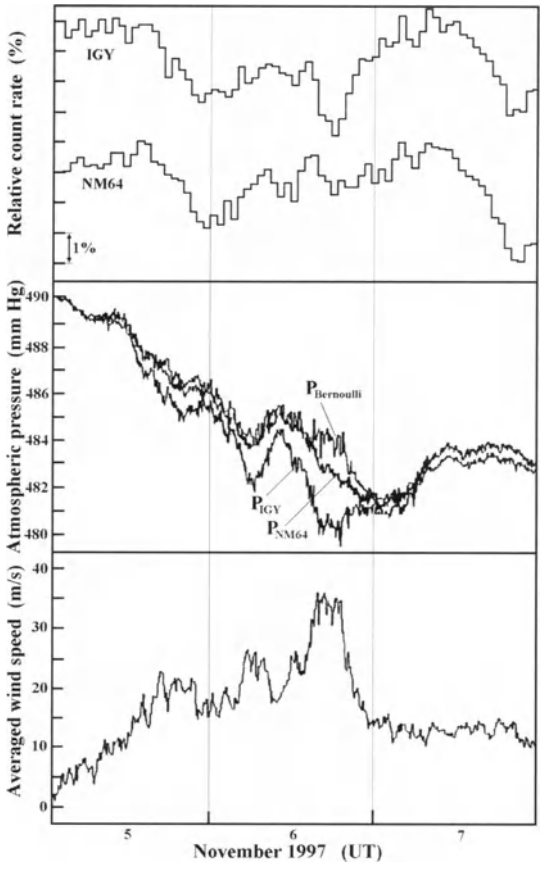

Fig. 6.2.2. Counting rates of IGY-type and NM-64 neutron monitors on Mt. Jungfraujoch in comparison with wind speed and expected Bernoulli effect during 5–7 November 1997. Details in text. According to Butikofer and Fluckiger (1999).

It was shown that the significant difference between counting rates of both neutron monitors is caused mostly by Bernoulli effect in location of 18-NM-IGY, determined from Eq. 6.2.1, with $\rho(h) \approx 0.83 \times 10^{-3}$ g.cm^{-3} for the height of the Mt. Jungfraujoch.

The role of the wind effect in CR latitude survey investigations will be considered in Chapter 16 (in the Section 16.2).

6.3. Barometric effect of EAS

6.3.1. Results for EAS caused by primary CR with energy from 100 TeV to 5000 TeV

Results of investigations of EAS (External Air Showers) barometric effect are shown in Table 6.3.1.

Table 6.3.1. Measurements of barometric coefficients for EAS.

Characteristics of EAS		Point of observations	Height above sea level, *m*	β, %/*mb*	References
Size of array	Primary energy				
$L \approx 5$ m	$\approx 10^{14}$ eV	Pic du Midi	2860	-0.75 ± 0.01	Daudin&Daudin (1953)
$L \approx 80$ m	$\approx 10^{14}$ eV	Pic du Midi	2860	-0.76 ± 0.02	Daudin&Daudin (1953)
$L \approx 51$ m	$\approx 10^{14}$ eV	Aucland (New Zealand)	Sea level	-0.73 ± 0.05	Farley&Storey (1957)
$L \approx 51$ m	$\approx 3 \times 10^{14}$ eV	Aucland (New Zealand)	Sea level	-0.77 ± 0.06	Farley&Storey (1957)
$L \approx 51$ m	$\approx 10^{15}$ eV	Aucland (New Zealand)	Sea level	-1.04 ± 0.13	Farley&Storey (1957)
$L \approx 51$ m	$\approx 3 \times 10^{15}$ eV	Aucland (New Zealand)	Sea level	-1.00 ± 0.27	Farley&Storey (1957)
$L \approx 20$ m	$\approx 5 \times 10^{14}$ eV	Mt. Chacaltaya	5220	-0.76 ± 0.17	Escobar et al. (1960)
$L \approx 20$ m	$\approx 5 \times 10^{15}$ eV	Mt. Chacaltaya	5220	-0.56 ± 0.16	Escobar et al. (1960)

6.3.2. Barometric effect for a single CR component of EAS

As it is mention in Boliev et al. (2003), recently interest to studying of CR variations with use a single component of Extensive Air Shower (EAS) arrays has risen. In particular, on Baksan EAS-arrays Andyrchy and Carpet (Alexeyev et al., 1991; Alexeenko et al., 1993; Karpov et al., 2003), on MILAGRITO (Ryan, 1999), and on GRAND (Poirier and D'Andrea, 2002) the significant variations caused by active processes on the Sun and in the interplanetary space were observed. For qualitative using of these data it is necessary to correct them on barometric and temperature effects. Corresponding coefficients can be calculated theoretically (see Chapters 5 and 8), and can be estimated experimentally. The latter was made by Boliev et al. (2003) on the basis of the 6 years (1996-2001) data of Andyrchy EAS array. This array consist of 37 detectors based on plastic scintillators with area 1×1 m^2 and with thickness 5 cm and the distance between detectors is about 40 m (total counting rate of the installation makes

11500 s^{-1}). The array located at a height of 2060 m above sea level in a point with geographical coordinates 43.28° N and 42.69° E with the geomagnetic cutoff rigidity 5.7 GV. For monthly intervals average value $\langle \beta_{\text{month}} \rangle = -0.36 \pm 0.14$ %/mb; for 3-day intervals it was found $\langle \beta_{3\text{days}} \rangle = -0.37 \pm 0.13$ %/mb. These values precisely coincide. However, errors are excessively great. To decrease the errors Boliev et al. (2003) excluded months or 3 days intervals for which the correlation coefficient between CR intensity and air pressure was smaller than 0.8 (it was made also for points with deviation from average more than 2σ; these points usually are poorly statistically provided, or distortion of β is caused by powerful variations not connected with meteorological effects). In this case the average values of barometric coefficients for 6 years data were found much more precisely:

$$\langle \beta_{\text{month}} \rangle = -0.382 \pm 0.0.053 \text{ %/mb}; \quad \langle \beta_{3\text{days}} \rangle = -0.376 \pm 0.059 \text{ %/mb}. \quad (6.3.1)$$

One can see that mean values of β for both monthly and 3-day points is practically equal to each other.

6.4. Barometric and temperature effects of ionization bursts

By the standard ionization chambers shielded with 10 cm Pb (of Compton type, see Section 1.2.7 and Section 4.2) it is possible to measure intensity of hard muons as well as ionization bursts (sudden great increasings of ionization inside the chamber). Ionization bursts in standard ionization chambers can be caused by several phenomena: 1) electron–nuclear showers generated in the chamber's shield; 2) EAS with a great density of charged particles; 3) radiation showers and δ showers generated by muons; and 4) strong ionized particles from nuclear disintegrations. According to Carmichael (1948), the relative role of these phenomena in generation of ionization bursts depends on the altitude and latitude of observations, and the volume of chamber. Cristy and Kusaka (1941) came to conclusion that on the sea level the main part of ionization bursts is caused by radiation from muons braking. But later George and Trent (1951) and Bridge and Rediker (1952) showed on the basis of experimental data and calculations of Cristy and Kusaka (1941) that at sea level only about half of observed ionization bursts are caused by radiation from muons braking. Moreover, Krasilnikov and Nikolsky (1955) on the basis of experimental data and theory developed by Belenky (M1948) reduced this part to about 0.1. Therefore, investigation of barometric effect of the frequency of ionization bursts is important for understanding of nature of ionization bursts.

According to Broxon (1951) the barometric coefficient at a height 1650 m above sea level for small ionization bursts (with total ionization equaling to ionization of few tenths of relativistic one charged particles) was found to be $\beta = -1.13$ %/mb. Stinchcomb (1951) for the height 3450 m above sea level for great ionization bursts (more than 200 relativistic particles) found $\beta = -1.54$ %/mb. Krasilnikov and Nikolsky (1955) for sea level for middle ionization bursts (150–250 relativistic particles) found $\beta = -2.5 \pm 0.5$ %/mb. Obtained values of barometric coefficients are in 10–20 times bigger than for hard muons, and about the same order as for electron–nuclear showers.

On the basis of ionization chamber ASC-1 data for 1954-1994 Krivoshapkin et al. (1997) investigated barometric and temperature effects of great ionization bursts *n1* (more than 1200 relativistic particles) and *n2* (more than 2400 relativistic particles). Barometric coefficients are found -1.54 ± 0.2 %/mb for *n1* and -3.45 ± 0.3 %/mb for *n2* ionization bursts. The temperature coefficients (relative to air temperature on the level of observation) were found -1.1 ± 0.1 %/^{o}C for *n1* and -2.2 ± 0.3 %/^{o}C for *n2* ionization bursts.

6.5. Barometric effect for underground observations of muon component

The results of measurements of barometric coefficients for muon component on different depths underground are listen in Table 6.5.1.

Table 6.5.1. Barometric coefficients for muon component on different depths underground.

Observations	Depth, m w.e.	β, %/mb	Apparatus	References
London (1950-1951)	60	-0.034 ± 0.002	Telescope on Geiger counters	MacAnuff (1951)
London (1960-1961)	60	-0.042 ± 0.004	Telescope on stintillators	Mathews (1963)
London (1961-1963)	60	-0.037 ± 0.002	Telescope on stintillators	Dutt and Tamby-aphillai (1965)
Hobart	40	-0.049 ± 0.002	Telescope on Geiger counters	Fenton et al. (1961)
Budapest	40	-0.062 ± 0.003	Telescope on Geiger counters	Sandor et al. (1962)

6.6. Barometric effect for hard muons

Zier and Knuts (1961) studied in detail the barometric effect of hard muons from observations at Kuhlungsborn in 1957-1960 with counter telescope and ionization chamber shielded by 10 cm Pb. Only quiet day (without geomagnetic storms and solar CR events) data are used. Using the correlation method, values of -0.176 %/mb and -0.132 %/mb were found for ionization chamber and counter telescope, respectively.

Barometric coefficients for counter telescopes (triple and double coincidences) shielded by 10 cm Pb were determined by Lapointe and Rose (1962) from observations at Ottawa, Churchill and Resolute made between July 1957 and December 1960 (see Fig. 6.6.1).

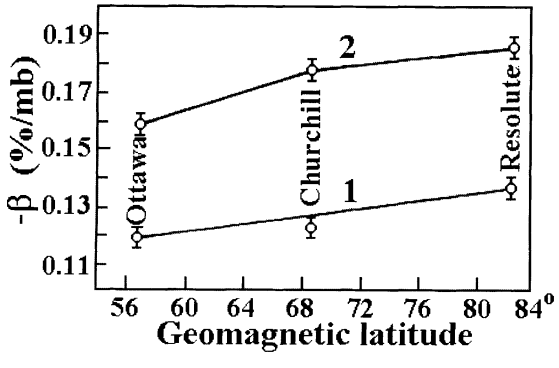

Fig. 6.6.1. Barometric coefficients for counter telescopes (curve **1** – triple coincidences, and **2** - double coincidences) shielded by 10 cm Pb at Ottawa, Churchill and Resolute (observations in period July 1957 - December 1960).

Lapointe and Rose (1962) conclude that:

- Within the error limits no seasonal variations of the barometric coefficient are observed, if strongly disturbed days are excluded from the analysis;
- During three and a half years the barometric coefficients practically did not vary;
- The barometric coefficient increases very slightly with increasing geomagnetic latitude (this can be explained by the decrease of mean energy of the secondary particles and the corresponding decrease of their free path for nuclear interactions).

Similar results for shielded muon telescopes ($\beta = -0.12 \pm 0.01$ %/mb and $\beta = -0.15 \pm 0.01$ %/mb) were obtained by Dawton and Elliot (1953) and Chasson (1954), respectively. Baker et al. (1993) obtained for barometric coefficients of the Mawson surface muon telescopes following results listed in Table 6.6.1.

Table 6.6.1. Barometric coefficients for the Mawson surface muon telescopes directed to North and to South.

year	1975		1976		1977		1984	
direction	North	South	North	South	North	South	North	South
β, %/mb	−0.13 ± 0.01	−0.12 ± 0.01	−0.12 ± 0.01	−0.13 ± 0.01	−0.07 ± 0.01	−0.08 ± 0.01	−0.13 ± 0.01	−0.13 ± 0.01

6.7. Barometric effect for general ionizing and soft CR components

Dawton and Elliot (1953) found from observations at Manchester in 1951–1952 for the general ionizing and soft CR components barometric coefficients $\beta = -0.18 \pm 0.01$ %/mb and $\beta = -0.34 \pm 0.02$ %/mb, respectively. Similar results was obtained by Chasson (1954): for the general ionizing and soft CR components $\beta = -0.211 \pm 0.015$ %/mb and $\beta = -0.343 \pm 0.048$ %/mb, respectively.

Barometric effect for a non-shielded ionization chamber (thickness of the wall 0.8 g/cm^2) at sea level was investigated by Shamos and Liboff (1966). Barometric coefficient was found to be $\beta = -0.29$ %/mb. Figure 6.7.1 shows the values of barometric coefficient for different values of total shielding: it can be seen that with increasing of shielding barometric coefficient decreases as

$$\beta = -(3.9 - 0.9 \lg d) \text{ %/cm}Hg = -(0.288 - 0.0664 \lg d) \text{ %/mb}, \qquad (6.7.1)$$

where d is the total shielding in g/cm^2.

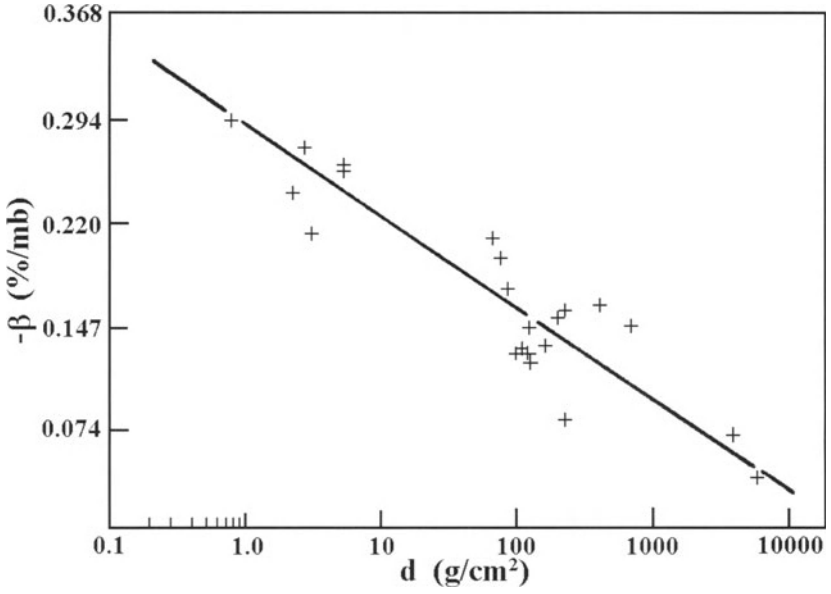

Fig. 6.7.1. Barometric coefficients for a non-shielded ionization chamber (thickness of the chamber's wall 0.8 g/cm^2) at sea level for different values of total shielding d (in g/cm^2).

6.8. Barometric effect for the total neutron component

6.8.1. Barometric coefficients for the first non-standard detectors of neutrons.

With the first instrument for recording the neutron component at Manchester (neutron counters surrounded by graphite) Adams and Braddick (1949) found for barometric coefficient $\beta = -0.70 \pm 0.02$ %/mb. With lead shields of 5, 10 and 15 *cm* thickness they found $\beta = -0.69 \pm 0.03, -0.65 \pm 0.02, -0.69 \pm 0.02$ %/mb, respectively. If the graphite is replaced by paraffin, the barometric coefficient increases somewhat to $\beta = -0.75 \pm 0.02$ %/mb. Tongiorgi (1949) found about the same value for neutron counters surrounded by paraffin: without lead $\beta = -0.78$ %/mb, and with a lead shield $\beta = -0.82 \pm 0.04$ %/mb.

6.8.2. Barometric coefficients for the standard IGY type neutron monitors.

For the standard neutron monitor of IGY (International Geophysical Year) type Simpson et al. (1953) found using the method of multiple correlation $\beta = -0.70 \pm 0.04$ %/mb.

McCracken and Johns (1959) used simultaneous observations N_1 and N_2 at two stations with nearly equal cut off rigidities for a more accurate determination of the barometric coefficient β for the neutron component:

$$\ln(N_1/N_2) = \beta(\Delta h_{o1} - \Delta h_{o2}) + \text{const}. \qquad (6.8.1)$$

They found for the IGY type neutron monitors in Murchison and Uppsala stations $\beta = -0.710 \pm 0.006$ %/mb; for Mawson and Mt. Wellington stations $\beta = -0.736 \pm 0.004$ %/mb; for neutron monitors on Resolute, Churchill and Ottawa stations $\beta = -0.725 \pm 0.005$ %/mb.

The same method was applied by Sergeev and Luzov (1961) to data obtained by IGY type neutron monitors at Irkutsk and Deep River in the periods: summer of 1958 (the found barometric coefficient $\beta = -0.74 \pm 0.02$ %/mb), autumn of 1958 ($\beta = -0.69 \pm 0.01$ %/mb), in winter 1958/1959 ($\beta = -0.65 \pm 0.005$ %/mb), and in spring 1959 ($\beta = -0.71 \pm 0.01$ %/mb). The mean value is

$$\beta = -0.69 \pm 0.01 \text{ %/mb}, \qquad (6.8.2)$$

in good agreement with results obtained by McCracken and Johns (1959) for neutron monitors on stations with about the same cut off rigidities.

6.8.3. Comparison of barometric coefficients for the standard IGY type (Simpson type) neutron monitor and for IQSY type (NM-64) super-monitor

Griffiths et al. (1965) found near the minimum of solar activity in January-May 1965 from simultaneously observations by standard IGY type (developed by Simpson, 1955) neutron monitor and by IQSY type (NM-64, developed by Carmichael, M1964) super-monitor at Leeds that within the error limits the barometric coefficients for these two types of neutron monitors are about equal:

$$\beta = -0.728 \pm 0.005 \text{ %/mb} \qquad (6.8.3)$$

for IGY type monitor and

$$\beta = -0.735 \pm 0.003 \text{ %/mb} \qquad (6.8.4)$$

for IQSY type monitor.

6.9. Variation of barometric coefficients for the total neutron component with altitude and geomagnetic cut off rigidity

6.9.1. The dependence of barometric coefficient at sea level on R_c

Carmichael et al. (1965) studied near the minimum of solar activity during April–June 1965 the barometric effect in neutron component. They carried out observations at 16 points near sea level and at 15 points at different heights above sea level by the mobile neutron monitor of IQSY type 3-NM-64 in the interval of cut off

rigidities R_c from 1 GV up to 10.5 GV (Canada, USA, Mexico). Fig. 6.9.1 shows the neutron component intensity dependence on R_c, while Fig. 6.9.2 shows the dependence of barometric coefficient for neutron component at sea level on R_c.

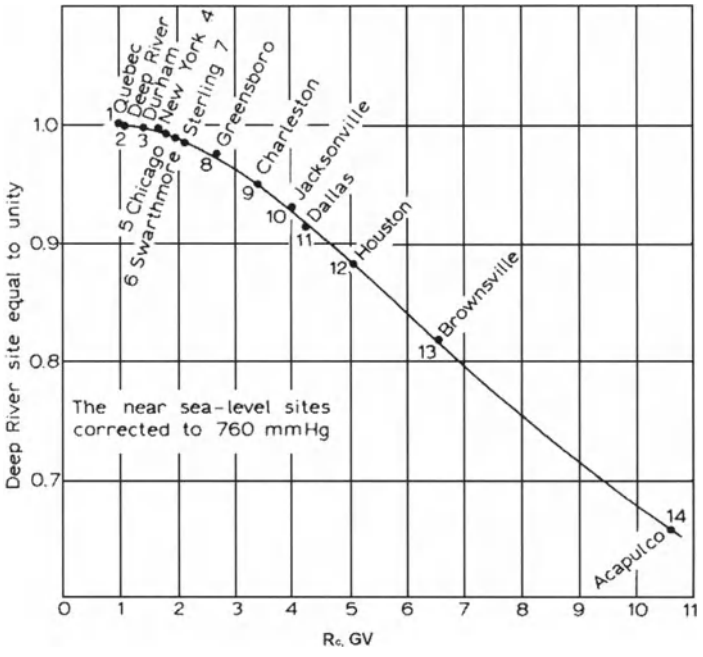

Fig. 6.9.1. The neutron component intensity dependence on R_c.

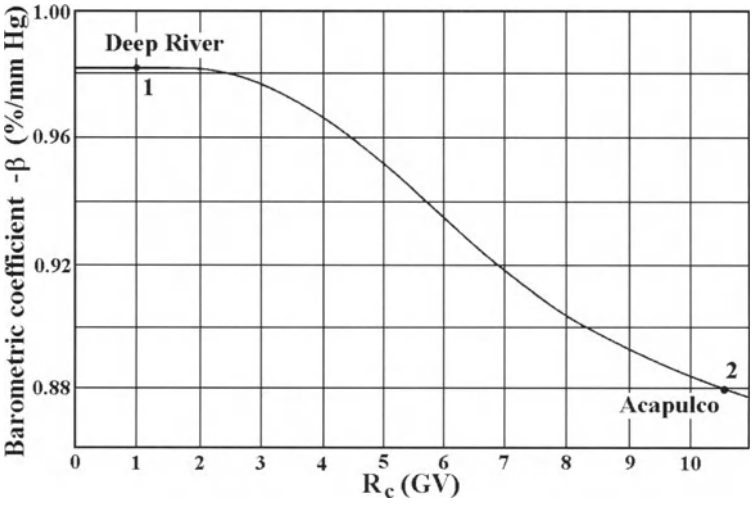

Fig. 6.9.2. Barometric coefficient for neutron component at sea level as a function of R_c.

The dependence of barometric coefficient for neutron component on R_c was found by Bachelet et al. (1965) from observations with many neutron monitors in 1962–1963 (see Fig. 6.9.3).

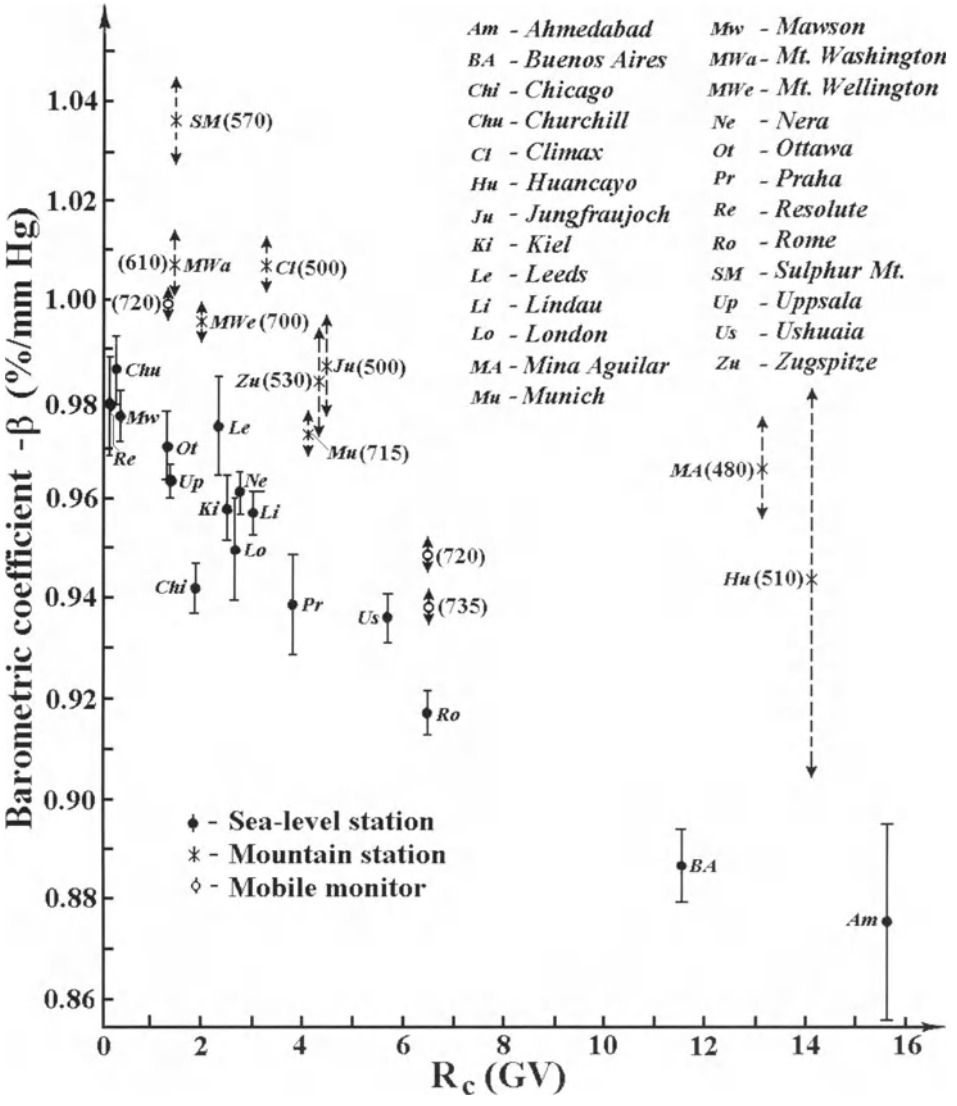

Fig. 6.9.3. The dependence of barometric coefficient for neutron component at sea level from R_c according to observations by mobile neutron monitor and by many stationary NM in 1962-1963 at sea level and at mountain levels (for mountain NM are shown pressure level in mm Hg).

Barometric coefficients for neutron component near minimum solar activity in 1964–1965 (see Fig. 6.9.4) were found by Dorman et al. (1968), and for various periods of solar activity (see Fig. 6.9.5) by Alania et al. (1968).

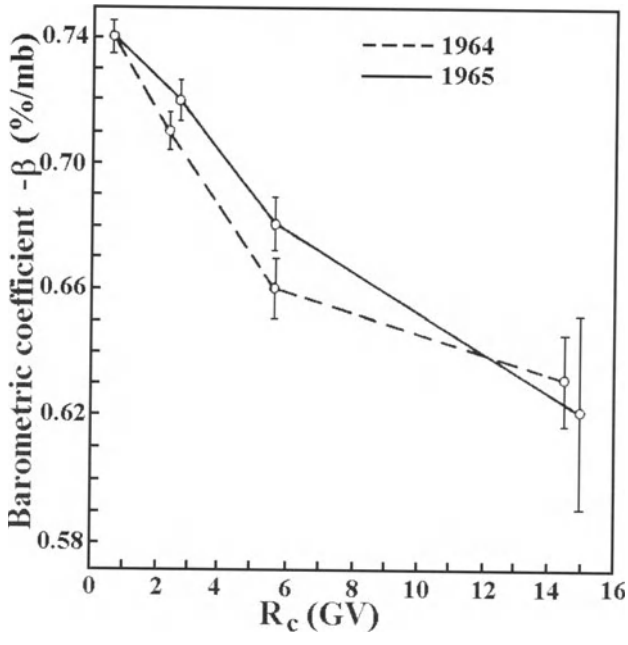

Fig. 6.9.4. Barometric coefficients for neutron component near minimum of solar activity in 1964–1965.

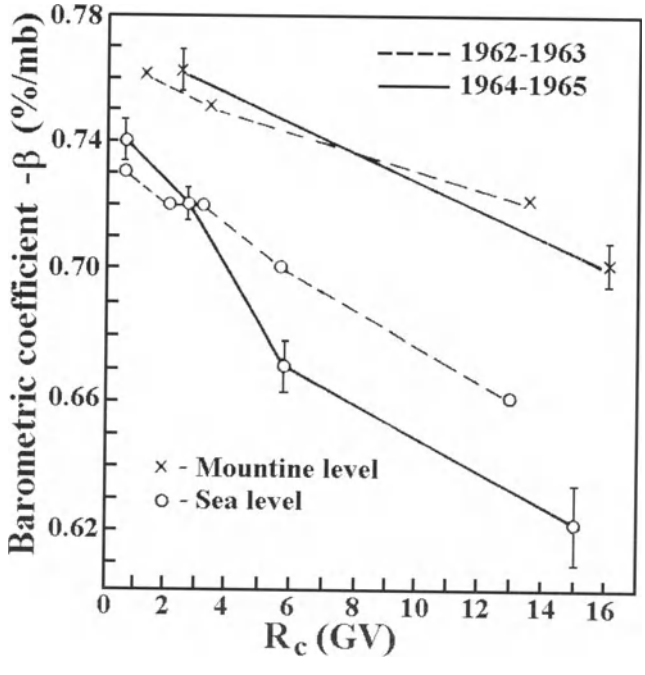

Fig. 6.9.5. The dependence of barometric coefficient for neutron component at sea level and at mountain level from R_c for various periods of solar activity.

6.9.2. The dependence of barometric coefficient on R_c and average air pressure on the level of observations

From latitude observations near the minimum of solar activity in 1965–1966 valuable results were obtained by Carmichael et al. (1968) about the dependence of barometric coefficient for total neutron component on cut off rigidity and also on pressure on the level of observation (see Fig. 6.9.6).

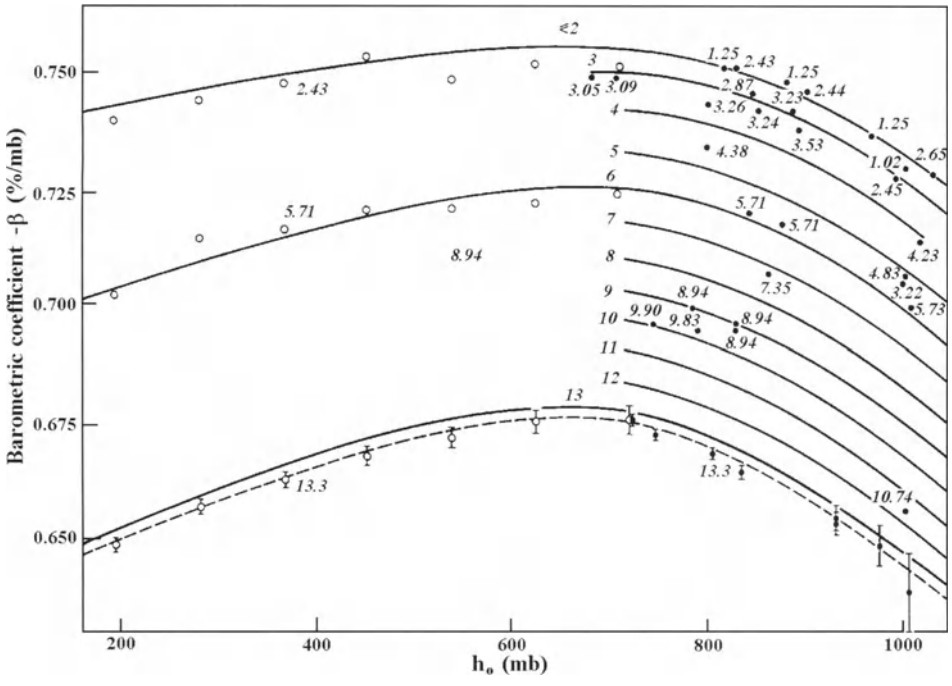

Fig. 6.9.6. The dependence of barometric coefficient $\beta(h_o, R_c)$ for total neutron component on cut off rigidity R_c and also on pressure on the level of observation h_o (obtained from latitude observations near minimum of solar activity in 1965–1966 as well as by stationary neutron monitors). Numbers near curves and points are values of R_c in GV.

6.10. Barometric coefficients for the total neutron component: airplane measurements

6.10.1. Results for the average air pressure about 680 mb *and 260–315* mb *in dependence of cut off rigidity near solar minimum*

The variation of the barometric coefficient with cut off rigidity at an average air pressure about 680 mb was studied by Coxell et al. (1966) with a neutron monitor aboard a plane. At $R_c = 2.5$ GV a mean free path for absorption $L = 136.1 \pm 0.3$ g/cm^2 what corresponds to a barometric coefficient $\beta = -0.735 \pm 0.002$ %/mb; with increasing R_c

the mean free path L also increases, what corresponds decreasing of barometric coefficient (see Fig. 6.10.1).

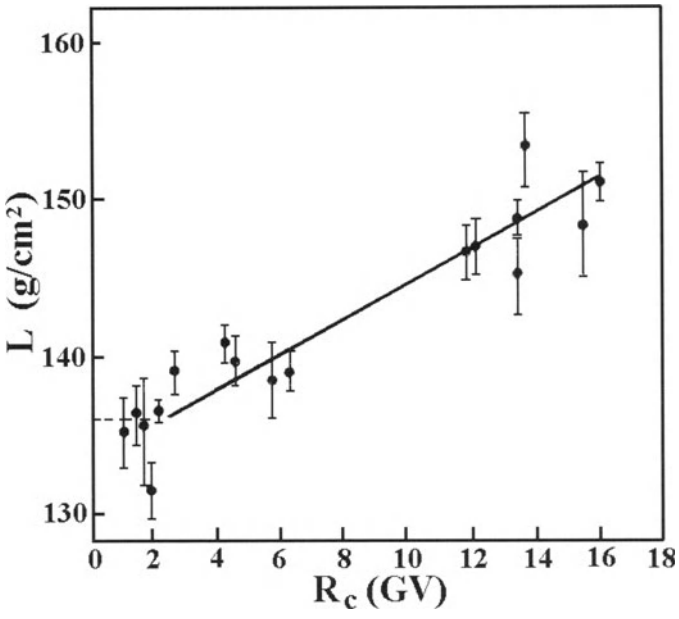

Fig. 6.10.1. The mean free path L in dependence from R_c at an average air pressure about 680 mb.

The relation between the barometric coefficient determined in the air pressure interval 260–315 mb and R_C was obtained by Granitsky et al. (1967) from measurements using a neutron monitor on an airplane near the solar minimum at January–February 1966 (see Fig. 6.10.2). It can be seen that the barometric coefficient is approximately constant for $R_C \leq 3\ GV$, and then gradually decreases with increasing R_C.

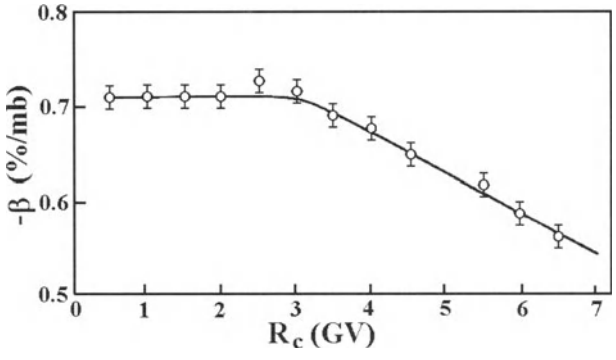

Fig. 6.10.2. The dependence of barometric coefficient $\beta(R_c)$ for total neutron component on cut off rigidity R_C (according to measurements by airplane neutron monitor near solar minimum at January-February 1966 at $h_0 = 260 \div 315$ mb).

6.10.2. Dependences $\beta(h)$ and $\beta_v(h)$ for air pressure interval 300–1030 mb *at cut off rigidities 4.94* GV *and 8.53* GV *near solar maximum*

The dependences of barometric coefficient for neutron component $\beta(h_o)$ and barometric coefficient for neutron component but for vertical direction $\beta_v(h_o)$ for air pressure interval 300–1030 *mb* at cut off rigidities 4.94 *GV* and 8.53 *GV* near solar maximum in August 1969 were obtained by air-plane neutron monitor by Raubenheimer and Stoker (1971). The recalculation of measured barometric coefficient $\beta(h_o)$ to barometric coefficient for vertical direction $\beta_v(h_o)$ was made according to Singh et al. (1970) by using of the Gross relation

$$\beta_v(h) = \left(h\beta^2(h) - h(\partial\beta(h)/\partial h)\right)/(1 + h\beta(h)). \qquad (6.10.1)$$

The observed data were corrected for the dead time of neutron monitors, for the radioactive background, and for the captured soft negative muons. Results for $\beta(h_o)$ are shown in Fig. 6.10.3 and for $\beta_v(h_o)$ in Fig. 6.10.4.

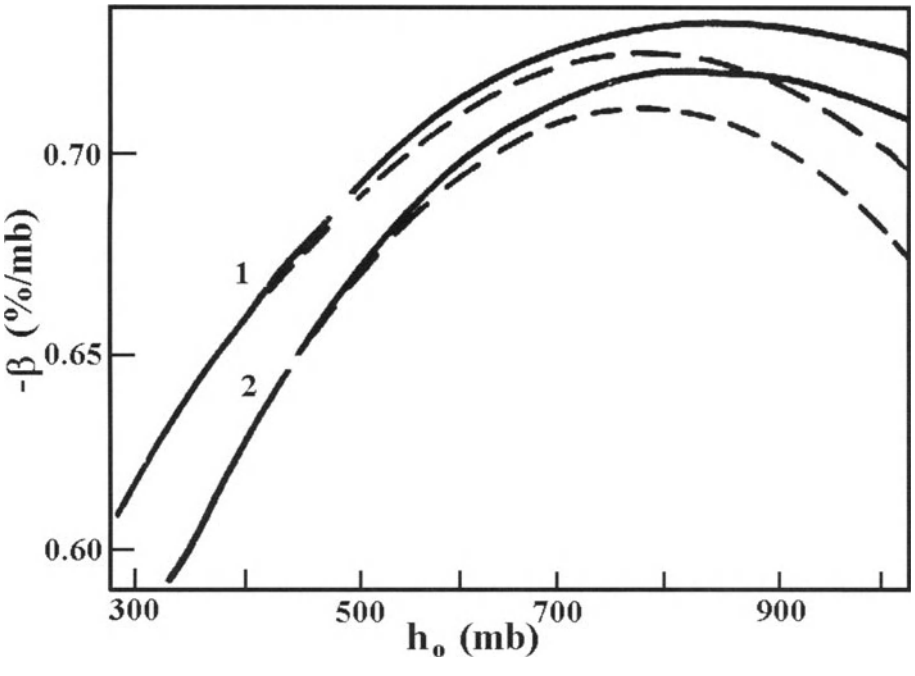

Fig. 6.10.3. The dependence of the barometric coefficient $\beta(h_o)$ for air-plane neutron monitor NM-64 with 15 cm paraffin reflector on air pressure in the interval 300 – 1030 mb at cut off rigidities 4.94 GV (curve 1) and 8.53 GV (curve 2) near the solar maximum in August 1969. Dashed lines – observation data with correction for the dead time of neutron monitor; solid lines - with corrections for the dead time of neutron monitor, for the radioactive background, and for the captured negative soft muons (generated meso-atoms).

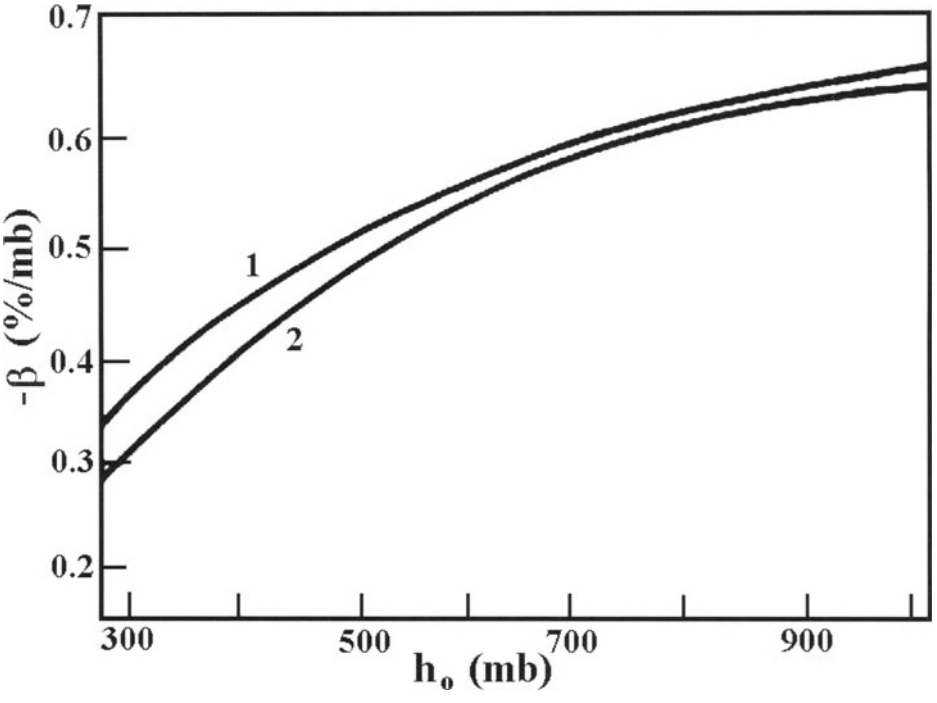

Fig. 6.10.4. The same as in Fig. 6.10.3, but for the barometric coefficient $\beta_v(h_o)$, recalculated for the vertical direction according to Eq. 6.10.1.

6.10.3. Dependences $\beta(h)$ and $\beta_v(h)$ vs. air pressure in the interval 200-1030 mb *at R_c of 1.6, 2.4; 5.7 and 13.3* GV *near solar minimum and solar maximum*

Carmichael et al. (1969), Carmichael and Peterson (1971), by using air-plane neutron monitors, investigated the dependences of barometric coefficient for neutron component $\beta(h_o)$ and barometric coefficient for vertical direction $\beta_v(h_o)$ for air pressure interval 200-1030 mb at cut off rigidities 1.6, 2.4; 5.7 and 13.3 *GV* in May-June 1966 near the solar minimum and in January 1970 near the solar maximum. Results are shown in Fig. 6.10.5a. Fig. 6.10.5b shows the results for data corrected for the dead time of the neutron monitors, the radioactive background, and the captured soft negative muons. The recalculation of $\beta(h_o)$ shown in Fig. 6.10.5b to barometric coefficient for vertical direction $\beta_v(h_o)$ was made according to Gross relation (Eq. 6.10.1) and the results are shown in Fig. 6.10.5c.

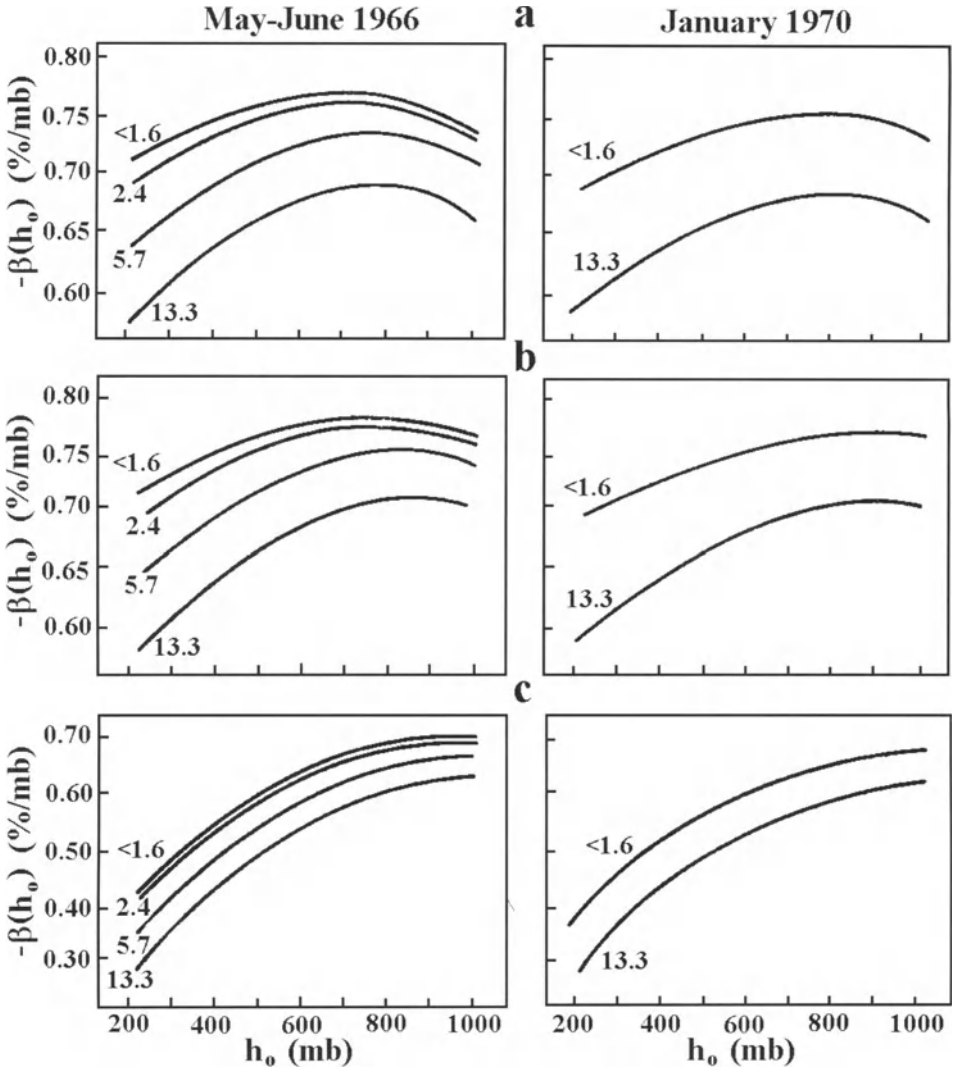

Fig. 6.10.5. The dependence of barometric coefficients for neutron component $\beta(h_o)$ and barometric coefficient for vertical direction $\beta_v(h_o)$ on the air pressure in the interval 200–1030 mb at cut off rigidities <1.6, 2.4; 5.7 and 13.3 GV (numbers near curves) in May–June 1966 near solar minimum (left) and in January 1970 near solar maximum (right). ***a*** - $\beta(h_o)$ without corrections, ***b*** - $\beta(h_o)$ with corrections on radioactive background and on capturing of negative soft muons (formatted meso-atoms), ***c*** – the same as in *b* but for $\beta_v(h_o)$.

Simpson and Slade (1971) by 2-NM-64 neutron monitor of IQSY type on balloons and airplanes made measurements of barometric coefficients in dependence of h at $R_c = 1.9, 3.1, 4.3, 7.2$ GV in 1968–1970. Obtained results are in good agreement with described above results of Carmichael et al. (1969) and Carmichael and Peterson (1971).

6.11. Dependence of barometric coefficient from *h* at different cut off rigidities and integral method of calculations of corrections on barometric effect

The results described above of the dependence of barometric coefficient on *h* show that the traditionally used method of calculations of barometric effect according to relation

$$N(h)=N(h_o)\exp(\beta(h-h_o)) \tag{6.11.1}$$

is correct only if the barometric coefficient β is constant Kisselbach and Chasson (1965) found that after correction of neutron monitor data in Climax and Dallas according to Eq. 6.11.1, the corrected data still correlated with air pressure; this correlation is especially high in periods of great changes of air pressure. From experimental data on barometric coefficient, it follows that $\beta \neq \text{const}$ and it is necessary to take into account the dependence of the barometric coefficient on *h*. Therefore, instead of Eq. 6.11.1 it is necessary to use the relation

$$N(h)=N(h_o)\exp\left(\int_{h_o}^{h}\beta(h)dh\right). \tag{6.11.2}$$

For observations at some level h_o for $|h-h_o|\leq 100\ mb$ the dependence of barometric coefficient on *h* with a good accuracy can be approximated by a parabolic function

$$\beta(h)=\beta(h_o)+\eta_1(h_o)(h-h_o)+\eta_2(h_o)(h-h_o)^2, \tag{6.11.3}$$

where coefficients η_1 and η_2 can be easily determined from observed data on $\beta(h)$ for different cut off rigidities and different levels of solar activity (see, for example, Fig. 6.9.6). By substituting Eq. 6.11.3 in Eq. 6.11.2 we obtain

$$N(h)=N(h_o)\exp\left(\beta(h_o)(h-h_o)+\eta_1(h_o)(h-h_o)^2/2+\eta_2(h_o)(h-h_o)^3/3\right). \tag{6.11.4}$$

Dorman and Kovalenko (1966), by using the data on $\beta(h)$ shown in Fig. 6.9.6 for different cut off rigidities, calculated the expected values $N(h)/N(h_o)$ for $h_o = 760$ mmHg according to Eq. 6.11.1 for $\beta(h)=\beta(h_o)=\text{const}$ and according to Eq. 6.11.2 or Eq. 6.11.3. Results are shown in Table 6.11.1.

Table 6.11.1. Expected values $N(h)/N(h_o)$ for $h_o = 760\ mmHg$ according to Eq. 6.11.1 for $\beta(h) = const$ and according to Eq. 6.11.4 for $\beta(h) \neq const$.

h- h_o , mm Hg	according to Eq. 6.11.4				Eq. 6.11.1
	$R_c = 3$ GV	$R_c = 4.5$ GV	$R_c = 6.4$ GV	$R_c = 9.5$ GV	$R_c = 3$ GV
-60	1.819	1.786	1.763	1.728	1.798
-50	1.644	1.619	1.601	1.574	1.630
-40	1.486	1.469	1.455	1.435	1.479
-30	1.345	1.333	1.323	1.310	1.341
-20	1.217	1.211	1.204	1.196	1.215
-10	1.104	1.100	1.097	1.093	1.103
0	1.000	1.000	1.000	1.000	1.000
10	0.907	0.910	0.913	0.921	0.907
20	0.823	0.829	0.834	0.839	0.822
30	0.748	0.755	0.763	0.770	0.746
40	0.680	0.689	0.698	0.707	0.676

From Table 6.11.1 it can be seen that Eq. 6.11.1 gives differences with the more exact Eq. 6.11.4: -0.021 at $h - h_o = -60$mb , -0.004 at $h - h_o = -30$ mb , and -0.004 at $h - h_o = 40$ mb (compare columns 2 and 6 for $R_c = 3$ GV).

6.12. Influence of primary CR variations on barometric coefficients for neutron monitors

6.12.1. Influence of solar CR on attenuation lengths and barometric coefficients

McCracken and Palmeira (1960) found that the amplitude of the neutron component intensity increase in the July 17, 1959 event for NM at Deep River (sea level) is smaller than the amplitude observed by NM at Mt. Sulfur (2280 *m* above sea level). McCracken and Palmeira (1960) supposed that this difference can be caused by the bigger absorption of neutron component generated by solar CR (characterized by attenuation length L_S) than those for neutron component generated by galactic CR (characterized by attenuation length L_G). For the July 17, 1959 event, they estimated $L_S = 89\ \mathrm{g/cm^2}$. This value is less than two-thirds of $L_G \approx 140\ \mathrm{g/cm^2}$ (according to Simpson and Fagot, 1953).

McCracken (1962) developed a two-attenuation-length method for applying a pressure correction to the counting rate of a NM data during solar CR events. Let L_G and L_S be the attenuation paths for absorption of the neutrons generated by galactic and solar CR, respectively; $N(h)$ and h are the counting rate of neutron monitor and air pressure on the level of observation before the solar CR event; $N(h+\Delta h)$ and $h+\Delta h$ are counting rate and air pressure during the solar CR event. Using the assumption that the intensity of galactic CR does not vary during short time of the solar event, the relative increase F of the neutron monitor counting rate reduced to the standard air pressure h_o according to McCracken (1962) will be

$$F = \left[\frac{N(h+\Delta h)}{N(h)}\exp\frac{\Delta h}{L_S} - \exp\frac{\Delta h}{L}\right]\exp\frac{h-h_o}{L}, \qquad (6.12.1)$$

where

$$L^{-1} = L_S^{-1} - L_G^{-1}, \quad L = L_S L_G/(L_G - L_S). \qquad (6.12.2)$$

Assuming $L_S = 100\ \mathrm{g/cm^2}$, $L_G = 138\ \mathrm{g/cm^2}$, we find from Eq. 6.12.2 $L = 363\ \mathrm{g/cm^2}$. Table 6.12.1 shows the neutron monitor intensity increases during the solar CR event at November 15, 1960 at seven stations with very near cut off rigidities and near sea level during isotropic phase of increase for three methods of determining of air pressure corrections: A – without barometric corrections; B – when the barometric corrections are computed by usual method (see above, Eq. 6.11.1); C – when the barometric corrections are computed according to Eq. 6.12.1.

Table 6.12.1. Comparison of different methods of applying barometric corrections for the period of increase at 5–6 UT, November 15, 1960; the amplitude of increase and the root mean square dispersion in % are given for methods *A*, *B* and *C* (McCracken, 1962).

VALUE	STATION	METHOD		
		A	*B*	*C*
INCREASE, %	Churchill	61.5	61.1	64.1
INCREASE, %	College	69.4	67.9	66.4
INCREASE, %	Mawson	65.0	65.5	65.0
INCREASE, %	McMurdo	67.1	66.6	66.6
INCREASE, %	Ottawa	69.1	66.9	66.9
INCREASE, %	Resolute	57.3	58.2	63.8
INCREASE, %	Thule	66.8	67.5	64.4
DISPERSION, %		4.3	3.6	1.2

For the average value of L_S determined on the basis of data on many solar CR events during 1960–1977 for particle rigidity $R < 7$ GV was obtained $\langle L_S \rangle = 100 \pm 5\ \mathrm{g/cm^2}$ (Duggal, 1979). Let us note that Eq. 6.12.1 can still father be improved because according to McCracken (1962), the quantity F in Eq. 6.12.1 is expressed relative to the intensity level at the given station before the event, but for determining energy spectrum of solar CR and anisotropy of flux it would be necessary to determine F relative to the intensity at some world standard pressure h_{ow}, the same for stations with near level of observations. In this case according to Kaminer (1967) instead of Eq. 6.12.1 will be

$$F = \frac{N(h+\Delta h)}{N(h_{ow})}\exp\frac{h-h_{ow}+\Delta h}{L_s} - \exp\frac{h-h_{ow}+\Delta h}{L}, \qquad (6.12.3)$$

where L is determined by Eq. 6.12.2. Attenuation path for absorption of the neutrons generated by solar CR L_S can be determined on the basis of Eq. 6.12.3 by using data of two stations on different pressure levels but with about equal cut off rigidities:

$$L_S = (h_2 - h_1 + \Delta h_2 - \Delta h_1) \left[\ln \left(\frac{\frac{N_1(h_1+\Delta h_1)}{N_1(h_{ow})} - \exp\left(\frac{-h_1 - h_{ow} + \Delta h_1}{L_G}\right)}{\frac{N_2(h_2+\Delta h_2)}{N_2(h_{ow})} - \exp\left(\frac{-h_2 - h_{ow} + \Delta h_2}{L_G}\right)} \right) \right]^{-1} . \quad (6.12.4)$$

Let us note also that the quantity L_S may vary from one event to other because of the varying solar CR spectrum, and also from one station to other with varying cut off rigidity. It was shown by Ahluwalia and Xue (1993) on the basis of observation data of solar CR event of 29 September 1989: by using neutron monitor 5 – min data of 3 pairs stations Mt. Norikura – Tokyo (average $\langle R_c \rangle = 11.5$ GV), Mt. Tyan-Shan (near Alma Ata) – Tbilisi ($\langle R_c \rangle = 6.68$ GV) and Mt. Washington – Durham ($\langle R_c \rangle = 1.33$ GV). Results are shown in Fig. 6.12.1.

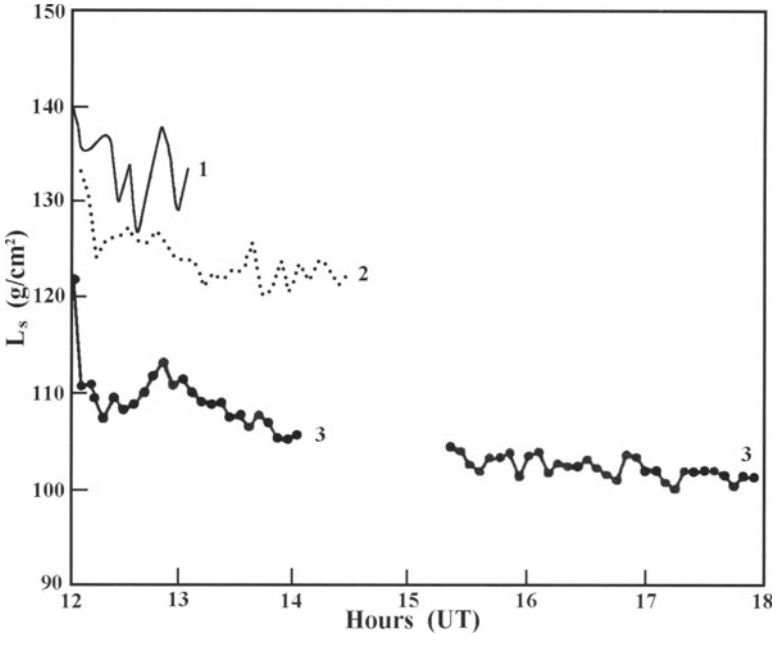

Fig. 6.12.1. The variation of L_S with time during solar CR event of 29 September 1989 according to following pairs stations: curve *1* - Mt. Norikura – Tokyo (average $\langle R_c \rangle = 11.5$ GV), *2* - Mt. Tyan-Shan – Tbilisi ($\langle R_c \rangle = 6.68$ GV), and *3* – Mt. Washington – Durham ($\langle R_c \rangle = 1.33$ GV).

From Fig. 6.12.1 can be seen: 1) there are tendencies of decreasing of L_S with time (it caused by softening of solar CR spectrum with time owed to propagation in the interplanetary space), and 2) there are also tendency of decreasing of $\langle L_S \rangle$ with decreasing of $\langle R_c \rangle$ (see Table 6.12.2).

Table 6.12.2. Mean values of $\langle L_S \rangle$ for 3 station pairs, event 29 September 1989 (according to Ahluwalia and Xue, 1993).

Station pairs	$\langle R_c \rangle$, GV	Number of points	$\langle L_S \rangle$, g/cm^2
Mt. Norikura - Tokyo	11.50	13	134.3±4.0
Mt. Tyan-Shan - Tbilisi	6.68	29	124.2±2.9
Mt. Washington - Durham	1.33	57	105.6±4.1

Table 6.12.2 shows that there are clear tendency of decreasing of $\langle L_S \rangle$ with decreasing of $\langle R_c \rangle$. According to Ahluwalia and Xue (1993) this dependence can be approximated by the following equation

$$\langle L_S \rangle = (2.8 \pm 0.4)\langle R_c \rangle + (102.9 \pm 3.1) \text{ g/cm}^2 , \qquad (6.12.5)$$

where $\langle R_c \rangle$ is measured in GV.

6.12.2. Influence of the 11–year solar activity cycle on CR barometric coefficients

It is well known that the decrease of solar activity in the 11–year cycle is accompanied by an increase of CR intensity and by softening of spectrum of observed galactic CR. Hence the value of the barometric coefficient $|\beta(h)|$ is expected to increase with decreasing solar activity. This was verified by Kamphouse (1963) from observations of the neutron component at College (Alaska) in 1956–1962. It was found that $|\beta(h)|$ had a minimum in 1957–1958 (solar activity maximum), when the energy spectrum of galactic CR on the Earth was hardest. The variation of $|\beta(h)|$ have about one year's time lag relative to sunspot number, in good agreement with the observed hysteresis effect in connection of CR intensity with solar activity cycle (caused by great dimension of the Heliosphere, see in Dorman, M2005).

Forman (1967, 1968) on the basis of Climax and Chicago neutron monitor data in 1953–1965 found a relative change of barometric coefficient with solar cycle of about 5%. The increase of $|\beta(h)|$ by 3.2% for the Canadian stations Ottawa, Churchill and Resolute from -0.697 ± 0.003%/mb in 1958–1960 to -0.720 ± 0.004%/mb in 1962–1963 was found by Bachelet et al. (1965). The total change of about 6% from maximum to minimum solar activity (from 1959 to 1965) was confirmed for the Upsala neutron monitor by Dyring et al. (1966).

Fig. 6.12.2 shows the variation of the barometric coefficients for Leeds, College and Chicago neutron monitors during solar cycle 1954–1964 according to Griffiths et al. (1966). It can be seen that the barometric coefficient for Leeds NM increases by 6% from maximum to minimum solar activity; data for College and Chicago do not contradict this dependence of $|\beta(h)|$ on solar activity.

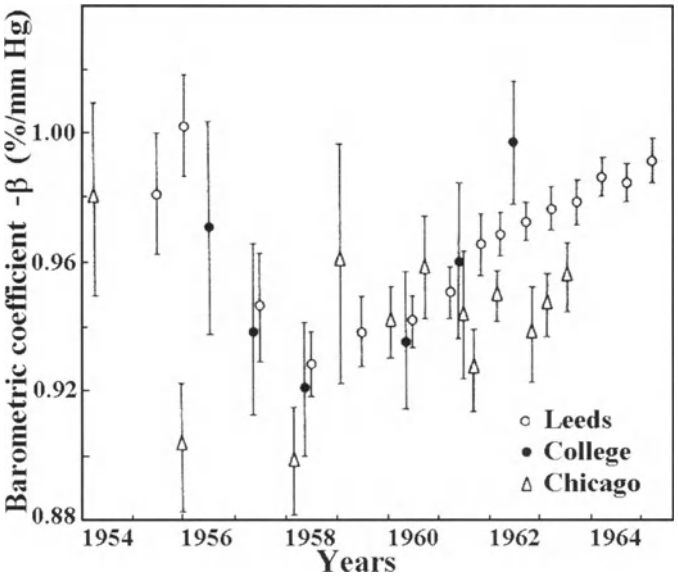

Fig. 6.12.2. Variations of barometric coefficients for Leeds, College and Chicago neutron monitors during solar cycle 1954-1964.

Bachelet et al. (1967) determined the dependence of $\Delta\beta = \left(|\beta| - \langle|\beta|\rangle\right)/\langle|\beta|\rangle$ on solar activity from observations with many neutron monitors in the period 1957–1965 (see Fig. 6.12.3).

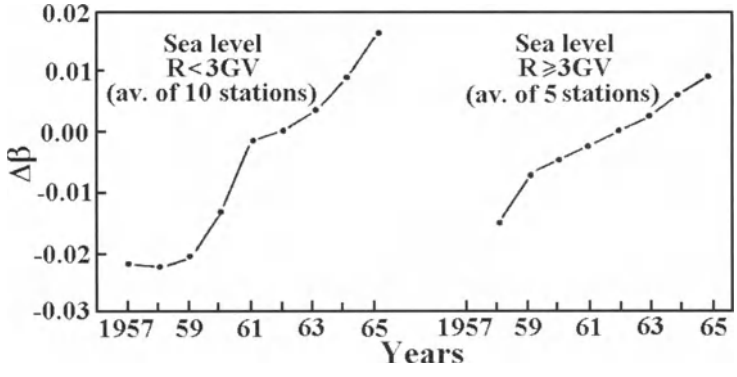

Fig. 6.12.3. The dependence of $\Delta\beta = \left(|\beta| - \langle|\beta|\rangle\right)/\langle|\beta|\rangle$ on solar activity from observations with many neutron monitors in the period 1957-1965 (from maximum to minimum of solar activity) for two groups of stations at sea level with $R_c < 3$ GV and with $R_c \geq 3$ GV .

From Fig. 6.12.3 can be seen that for neutron monitors with $R_c < 3$ GV , $|\beta(h)|$ increases by about 4% from 1957 (maximum of solar activity) to 1965 (minimum of solar activity); for neutron monitors with $R_c > 3$ GV this increase is about two times smaller.

The pronounced dependence of barometric coefficient on solar activity was confirmed with high accuracy by Kent and Pomerantz (1966), Bercovitch (1967), Forman (1967, 1968), Bachelet et al. (1967), Carmichael et al. (1968), Rogava and Shatashvili (1991), Nagashima et al. (1994), Shatashvili and Rogava (1995).

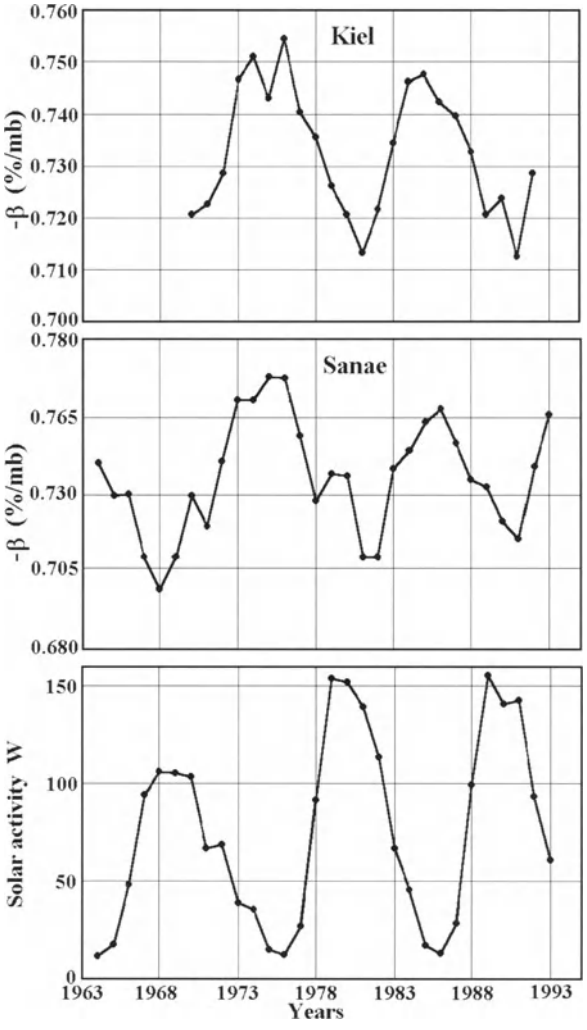

Fig. 6.12.4. The cyclic variations of the neutron component barometric coefficient $\beta(h)$ according to sea level data of Sanae NM ($R_c = 1.06$ GV) for 1964–1993 and data of Kiel NM ($R_c = 2.32$ GV) for 1970–1992.

Fig. 6.12.4 shows the cyclic variations of the neutron component barometric coefficient $\beta(h)$ according to sea level data of Sanae NM ($R_c = 1.06$ GV) for 1964–1993 and data of Kiel NM ($R_c = 2.32$ GV) for 1970–1992 (Shatashvili and Rogava, 1995). It can be seen from this figure that the relative cyclic change of $\beta(h)$ is

about 9.3% for Sanae NM and 5.5% for Kiel NM. From comparison of cyclic variations of $\beta(h)$ with cyclic variations of solar activity (sunspot numbers W on the bottom of Fig. 6.12.4) is can be clear seen that $\beta(h)$ has a time lag about 1–2 years relative to variations of W, in good agreement with the same time lag for neutron CR intensity.

The analyze of solar cycle variation of $\beta(h)$ for neutron component on the basis of Deep River, Moscow, Novosibirsk, and Irkutsk NM for 1987-1993 was made also by Yanchukovsky (1995).

6.12.3. On the connection of barometric coefficient variations with primary time modulations of CR intensity

CR intensity modulations of different type (caused by 11-year solar activity cycle and 22-year solar magnetic cycle, by interplanetary shock waves, 27-day and annual variations, and so on have about the same spectrum of primary variations $\Delta D(R)/D_o(R) \propto R^{-1}$; therefore it can be expected that the barometric coefficient change for modulation effects will be connected with variations of CR intensity. According to Griffiths et al., $df(h)/dh$ the connection of barometric coefficient primary time variations with variations of CR intensity (caused by the 11–year solar activity cycle, 22–year magnetic cycle, interplanetary shock waves leads to Forbush-decreases, and so on) can be understood as follows. Let $\beta_o(h) = dN_o(h)/N_o(h)dh$, $f(h) = N(h)/N_o(h)$. Then

$$\frac{dN(h)}{dh} = f(h)\frac{dN_o(h)}{dh} + N_o(h)\frac{df(h)}{dh} = N(h)\left(-\beta_o(h) + \frac{df(h)}{f(h)dh}\right), \qquad (6.12.5)$$

which gives

$$\beta(h) = -\frac{dN(h)}{N(h)dh} = \beta_o(h) - \frac{df(h)}{dh} \times \frac{1}{f(h)}. \qquad (6.12.6)$$

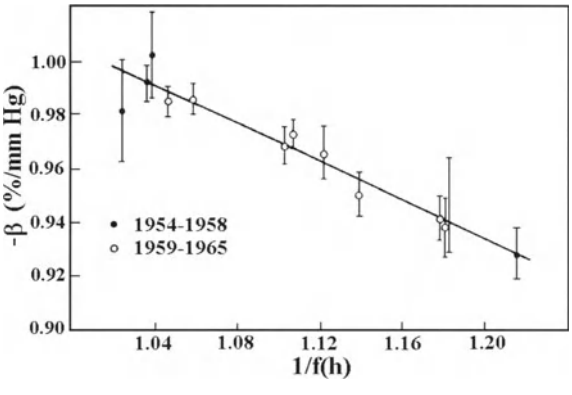

Fig. 6.12.5. The variation of barometric coefficient $\beta(h)$ with $1/f(h) = N_o(h)/N(h)$ for Leeds neutron monitor observations during two periods: 1954–1958 (increasing of solar activity) and in 1959–1965 (decreasing of solar activity).

Fig. 6.12.5 shows how $\beta(h)$ varied with $1/f(h) = N_o(h)/N(h)$ for Leeds NM observations during two periods: 1954–1958 (increasing of solar activity) and in 1959–1965 (decreasing of solar activity). Here $\beta_o(h)$ and $N_o(h)$ are the barometric coefficient and the counting rate of Leeds NM in October 1954. For both periods result of determination of regression coefficient $df(h)/dh$ in Eq. 6.12.6 is about the same:

$$df(h)/dh \approx (1.92 \pm 0.11) \times 10^{-3}\ \text{mb}^{-1}. \qquad (6.12.7)$$

According to Griffiths et al. (1965), the regression coefficient $df(h)/dh$ in Eq. 6.12.6 for neutron monitor at Mt. Washington for observations in 1954-1957 was found $df(h)/dh \approx (1.69 \pm 0.67) \times 10^{-3}\ \text{mb}^{-1}$, which agrees within the error limits with the values for Leeds NM (Eq. 6.12.7). Therefore in the first approximation, the regression coefficient $df(h)/dh$ is about the same for mountain and sea level neutron monitors.

6.13. Various influences on barometric coefficients for neutron monitors

6.13.1. Influence of radioactive contaminations on barometric coefficients for neutron monitors

It is well known that some small part (few percents) of counting rate in neutron monitors of both types (IGY and IQSY) is caused by radioactive contaminations in neutron counters. This part of counting rate is about constant in time and does not depend on the air pressure (barometric coefficient is zero). With increasing CR intensity, the relative role of radioactive contaminations decreases, and barometric coefficient slightly increases. Alania et al. (1970) estimated the expected changes of barometric coefficient caused by radioactive contaminations (see Fig. 6.13.1).

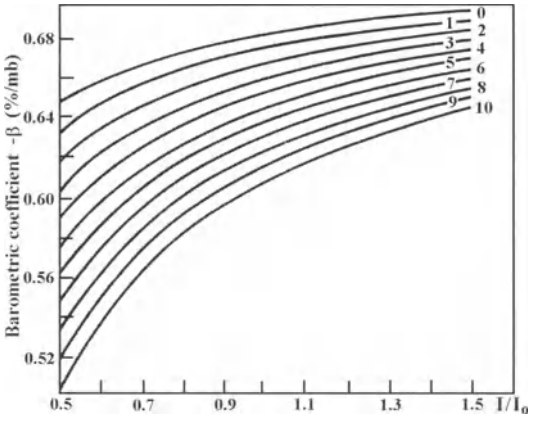

Fig. 6.13.1. The expected changes of barometric coefficient caused by radioactive contaminations in dependence of CR intensity changes I/I_0. Numbers near curves – values of relative counting rates caused by radioactive contaminations (in percents).

6.13.2. Influence of accidental coincidences and generation of mesoatoms by captured soft negative muons on barometric coefficients for neutron monitors

Kapustin et al. (1970) showed that accidental coincidences of pulses and generation of mesoatoms by captured soft negative muons influence on barometric coefficients for neutron monitors. This influence is different for different multiplicities. The accidental coincidences of pulses leads to an apparent decrease of the barometric coefficient for multiplicity $m = 1$ and to an apparent increase for $m = 2$. The results of correction of barometric coefficients for the accidental coincidences for multiplicities $m = 1, 2, 3$, and 4 are shown in Table 6.13.1.

Another phenomenon that influences the barometric coefficients is the generation of mesoatoms by captured soft negative muons (Nobles et al., 1966). This influence is maximal for $m = 1$, much smaller for $m = 2$ and 3 and negligible for $m \geq 4$. The results of correction of barometric coefficients for both effects: accident coincidences according to Kapustin et al. (1970) and generation of mesoatoms by captured soft negative muons according to Nobles et al. (1966) are shown in the last row of Table 6.13.1.

Table 6.13.1. Observed and corrected barometric coefficients for neutron component.

BAROMETER COEFFICIENTS	multiplicities			
	$m = 1$	$m = 2$	$m = 3$	$m = 4$
observed	-0.57	-0.69	-0.72	-0.74
corrected on accident coincidences	-0.66	-0.72	-0.73	-0.74
corrected both on accident coincidences and on generation of mesoatoms	-0.71	-0.75	-0.75	-0.74

6.14. Barometric coefficients for counting rates of various neutron multiplicities

6.14.1. Connection between barometric coefficients for total neutron counting rate and for multiplicities

The total counting rate of neutron monitor

$$N_t(h) = \sum_{m=1}^{\infty} m N_m(h), \tag{6.14.1}$$

where $N_m(h)$ is the counting rate of multiplicity m. The barometric coefficient for the total counting rate of neutron monitor on the basis of Eq. 6.14.1 can be expressed through barometric coefficients of various multiplicities:

$$\beta_t(h) = \frac{\partial N_t(h)}{N_t(h)\partial h} = \sum_{m=1}^{\infty} m \frac{\partial N_m(h)}{N_t(h)\partial h} = \sum_{m=1}^{\infty} \frac{m N_m(h)}{N_t(h)} \beta_m(h), \tag{6.14.2}$$

where

$$\beta_m(h) = \partial N_m(h) / (N_m(h)\partial h) \tag{6.14.3}$$

is the barometric coefficient for counting rate of multiplicity m.

Neutron monitors can also detect counting rate of pulses

$$N_p(h) = \sum_{m=1}^{\infty} N_m(h). \tag{6.14.4}$$

Barometric coefficient for counting rate of pulses will be

$$\beta_p(h) = \frac{\partial N_p(h)}{N_p(h)\partial h} = \sum_{m=1}^{\infty} \frac{\partial N_m(h)}{N_p(h)\partial h} = \sum_{m=1}^{\infty} \frac{N_m(h)}{N_p(h)} \beta_m(h). \tag{6.14.5}$$

6.14.2. Results for neutron monitors of IGY type

Barometric coefficients for various multiplicities were determined from measurements with neutron monitors of IGY type by Dyring and Sporre (1965, 1966), Bachelet et al. (1965a,b). Results are shown in Table 6.14.1.

Table 6.14.1. Barometric coefficients $\beta_m(h)$ (in %/mb) for various multiplicities m for IGY-type neutron monitors at Uppsala ($R_c = 1.4$ GV) in 1964–1965 and at Rome ($R_c = 6.4$ GV) in 1964.

m	Uppsala, 1964-1965	m	Rome, 1964
1	−0.712 ± 0.004	1	−0.66 ± 0.01
2	−0.777 ± 0.008	2	−0.76 ± 0.01
3	−0.817 ± 0.017	≥3	−0.83 ± 0.02
≥4	−0.832 ± 0.037		

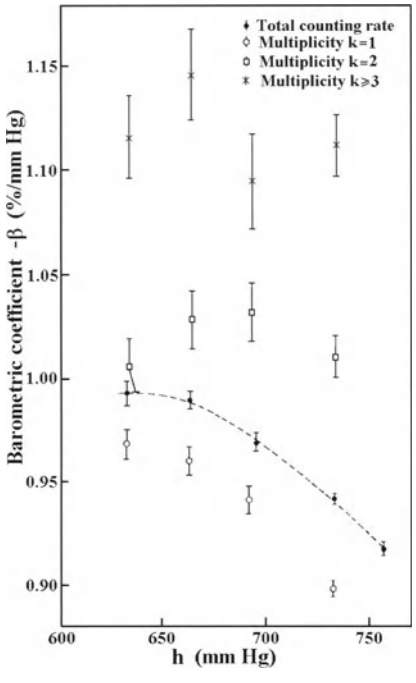

With the expedition neutron monitor of IGY type, Bachelet et al. (1965c) measured $\beta_m(h)$ in the autumn of 1964 as function of altitude in interval 630–760 mm Hg not far from Rome ($R_c \approx 6.4$ GV). Results for $\beta_t(h)$ and $\beta_m(h)$ for $m = 1, 2, \geq 3$ are shown in Fig. 6.14.1.

Fig. 6.14.1 Barometric coefficients for total counting rate and different multiplicities according to measurements by expedition neutron monitor of IGY type in the autumn of 1964 as function of altitude in interval 630–760 mm Hg not far from Rome ($R_c \approx 6.4$ GV).

6.14.3. Comparison of results for NM of IGY type and stationary and shipboard NM of IQSY type

Kodama and Ishida (1967), on the basis of measurements during the period September – November 1966, determined the barometric coefficients for various multiplicities $\beta_m(h)$ according to Eq. 6.14.3, as well as for total counting rate $\beta_t(h)$ according to Eq. 6.14.2 and for all pulses $\beta_p(h)$ according to Eq. 6.14.5. Results are shown in Table 6.14.2.

Table 6.14.2. Barometric coefficients $\beta_m(h)$, $\beta_p(h)$ and $\beta_t(h)$ (in %/*mb*) according to measurements during the period September - November 1966 by neutron monitors of IGY type and stationary and ship-board neutron monitors of IQSY type.

BAROMETRIC COEFFICIENTS	neutron monitor of IGY type	neutron monitors of IQSY type	
		stationary	shipboard
$\beta_1(h)$	−0.62 ± 0.05	−0.55 ± 0.01	−0.56 ± 0.01
$\beta_2(h)$	−0.60 ± 0.10	−0.67 ± 0.02	−0.71 ± 0.01
$\beta_3(h)$	−0.64 ± 0.24	−0.73 ± 0.02	−0.74 ± 0.03
$\beta_4(h)$	−0.81 ± 0.39	−0.73 ± 0.05	−0.86 ± 0.05
$\beta_5(h)$		−0.72 ± 0.07	−0.95 ± 0.08
$\beta_{\geq 6}(h)$		−0.79 ± 0.06	−0.96 ± 0.08
$\beta_p(h)$	−0.62 ± 0.04	−0.59 ± 0.01	−0.60 ± 0.01
$\beta_t(h)$	−0.65 ± 0.02	−0.62 ± 0.01	−0.66 ± 0.01

Kodama and Ohuchi (1968) found barometric coefficients for points with three different cut off rigidities using NM of IQSY type on board a ship (see Table 6.14.3).

Table 6.14.3. Barometric coefficients $\beta_m(h)$, $\beta_p(h)$ and $\beta_t(h)$ (in %/mb) for three points with different cut off rigidities according to measurements during the period September-November 1966 by ship-board neutron monitor of IQSY type.

BAROMETRIC COEFFICIENTS	Syowa (R_c = 0.4 GV)	Freemantle (R_c = 4.3 GV)	Tokyo (R_c = 11.5 GV)
$\beta_1(h)$	−0.78	−0.71	−0.57
$\beta_2(h)$	−0.86	−0.81	−0.71
$\beta_3(h)$	−0.89		−0.74
$\beta_4(h)$	−0.96		−0.83
$\beta_5(h)$	−1.00		−0.90
$\beta_{\geq 6}(h)$	−1.06		−0.96
$\beta_p(h)$	−0.81	−0.74	−0.61
$\beta_t(h)$	−0.83	−0.75	−0.66

Agrawal et al. (1970), on the basis of measurements with stationary 18-NM-64 (of IQSY type) in 1968–1969 at Ahmedabad ($R_c \approx 16$ GV), determined the barometric coefficients for various multiplicities.

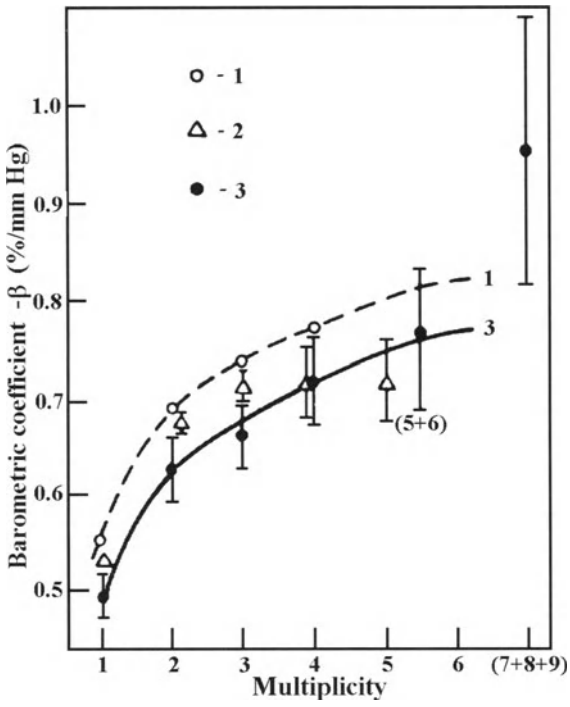

It was shown (see Fig. 6.14.2) that the results obtained are in good agreement with those obtained in Japan also by 18-NM-64 at Itabashi and in expeditionary measurements by Kodama and Ohuchi (1968).

Fig. 6.14.2 Barometric coefficients for various multiplicities obtained on the basis of latitude measurements on the ship (*1*), by measurements with stationary 18-NM-64 (of IQSY type) in 1968-1969 at Itabashi (*2*) and at Ahmedabad (*3*).

6.14.4. Dependence of β (%/mb) for various multiplicities on R_c

Kodama and Ohuchi (1968) by ship-board NM of IQSY type during period December 1966-April 1967 along the route Japan – Australia – Antarctic – South Africa – Ceylon – Japan found dependences of barometric coefficients for various multiplicities on the cut off rigidity (results are shown in Fig. 6.14.3).

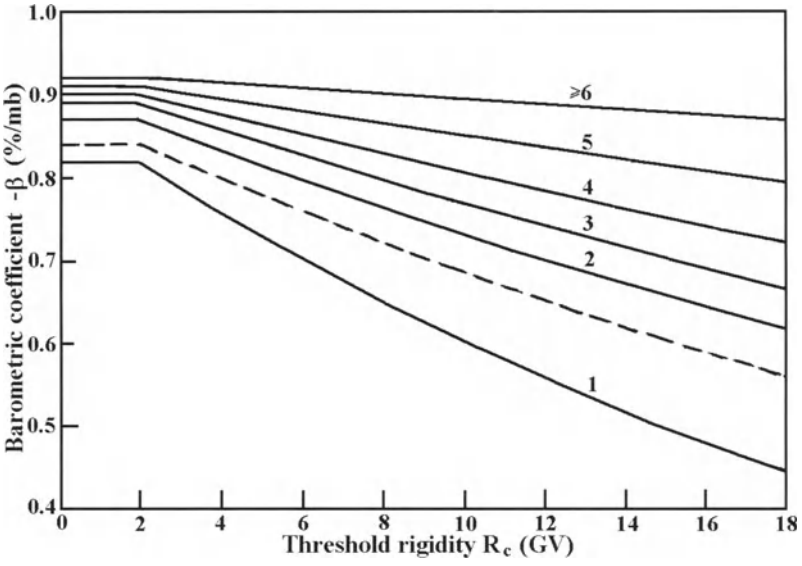

Fig. 6.14.3. The dependences of barometric coefficients from cut off rigidity for various multiplicities (numbers near full curves) and for total intensity (dashed curve) according to expedition measurements by shipboard neutron monitor of IQSY type during period December 1966-April 1967 along the route Japan – Australia – Antarctic – South Africa – Ceylon – Japan.

By the same detector Kodama and Inoue (1970) continued this research on the basis of expeditionary measurements in 1967-1968 in the interval of cut off rigidities 0.4–17.6 GV (see Fig. 6.14.4).

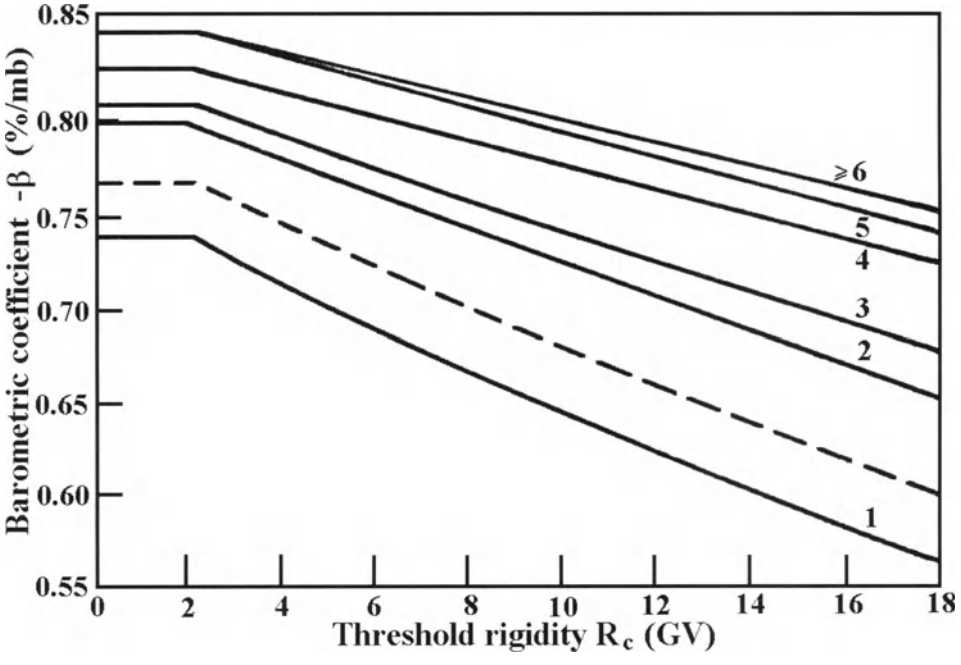

Fig. 6.14.4. The same as in Fig. 6.14.3, but according to expedition measurements during 1967–1968.

6.14.5. Mean multiplicities for neutron monitor of IGY type and stationary and shipboard neutron monitors of IQSY type

The mean multiplicity $m_{av}(h)$ for neutron monitor can be determined as

$$m_{av}(h) = \sum_{m=1}^{\infty} mN_m(h) \Big/ \sum_{m=1}^{\infty} N_m(h) = N_t(h)/N_p(h), \tag{6.14.6}$$

where $N_t(h)$ is total counting rate (determined by Eq. 6.14.1) and $N_p(h)$ is counting rate of pulses (determined by Eq. 6.14.4). The dependence of $m_{av}(h)$ on R_c was obtained by Kodama and Ohuchi (1968) on the basis of measurements by ship borne neutron monitor 3-NM-64 of IQSY type in December 1966 – April 1967 (Fig. 6.14.5). It can be seen that relative increases of $m_{av}(h)$ with increasing R_c from 0 to 17 GV is 1.89%, what corresponds of average increase 0.111 %/GV.

The dependencies of $m_{av}(h)$ on the air pressure for different types of neutron monitors, obtained by Kodama and Ishida (1967), are shown in Fig. 6.14.6.

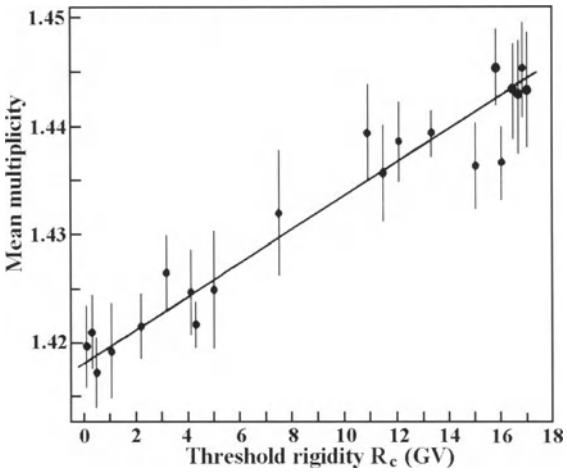

Fig. 6.14.5. The dependence of $m_{av}(h)$ from R_c obtained on the basis of measurements by ship borne neutron monitor 3-NM-64 of IQSY type in December 1966 – April 1967.

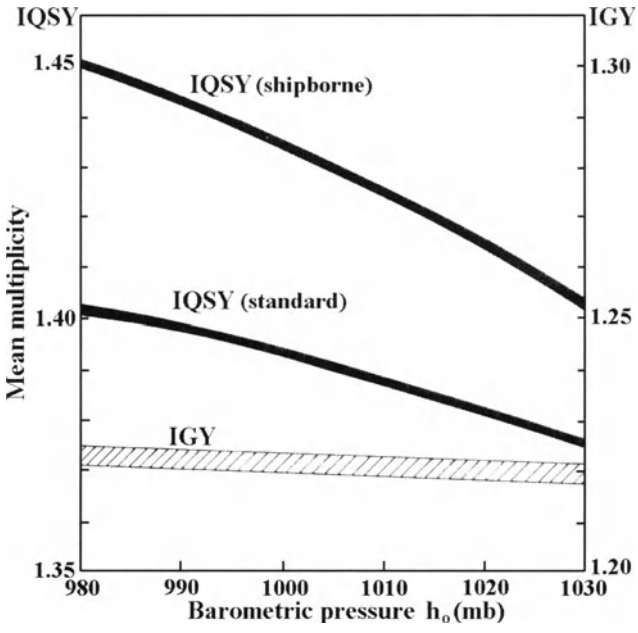

Fig. 6.14.6. The dependencies of $m_{av}(h)$ from air pressure for different types of neutron monitors.

From Fig. 6.14.6 one can determine the barometric coefficients for $m_{av}(h)$:

$$\beta_{m_{av}}(h) = d\ln(m_{av}(h))/dh\,. \tag{6.14.7}$$

Results are as follows:

$$\beta_{m_{av}}(h) = -0.070, -0.035, -0.0066\ \%/\text{mb} \qquad (6.14.8)$$

correspondingly for the shipboard neutron monitor of IQSY type, for the stationary neutron monitor of IQSY type, and for neutron monitor of IGY type. These results are in good agreement with obtained by Niemi (1968) on the basis of measurements by stationary neutron monitor 9-NM-64 of IQSY type at Oulu (Finland) during the period November 5 1965 to April 30 1967:

$$\beta_{m_{av}}(h) = -(0.027 \pm 0.005)\ \%/\text{mb}\ . \qquad (6.14.9)$$

Niemi (1968) found also that during the solar CR event of 28 January 1967, when the total counting rate at Oulu increased by 14%, $m_{av}(h)$ decreased from 1.408 to 1.385, i.e. by 15.9%; this decrease of $m_{av}(h)$ is caused by significant softening of primary CR energy spectrum in the period of solar CR increasing (in this period $\Delta D(R)/D_o(R) \propto R^{-\gamma_S}$). According to Niemi (1968), in the period of Forbush–decrease on 22 March 1966 when the total counting rate at Oulu NM decreased by 6.5%, $m_{av}(h)$ increased from 1.405 to 1.410, i.e. by 0.36%; this increase of $m_{av}(h)$ is caused by hardening of primary CR energy spectrum in the period of Forbush–decrease (in this period $\Delta D(R)/D_o(R) \propto -R^{-\gamma_F}$). From these results it follows that $m_{av}(h)$ is very sensitive to the change of primary CR energy spectrum.

6.14.6. Analytical approximation for dependence of barometric coefficient for total neutron intensity and different neutron multiplicities from the level of observation

According to Yanchukovsky and Philimonov (1997), the all available experimental data on the barometric coefficient for the total count of NM-IQSY at low solar activity (used data for 1974-1977, 1986-1987, and 1994-1995) in the cutoff rigidity range 2.9-3.6 GV in the interval of observation pressure h from 200 mbar to 1045 mbar can be approximated by expression:

$$\beta(h) = \beta(h_o) + \beta_1[\exp(\alpha_1(h-h_o)) - \exp(\alpha_2(h-h_o))]\ \%/\text{mbar}, \qquad (6.14.10)$$

where $h_o = 1013.25$ mbar, and parameters $\beta(h_o)$, β_1 as well as α_1, α_2 were determined by fitting to available experimental data on barometric coefficients (see Fig. 6.14.7):

$$\beta(h_o) = 0.694\ \%/\text{mbar},\ \beta_1 = 0.1842\ \%/\text{mbar}, \qquad (6.14.11)$$

and

$$\alpha_1 = 1.852\times10^{-3}\ \text{mbar}^{-1},\ \alpha_2 = 4.628\times10^{-3}\ \text{mbar}^{-1}. \qquad (6.14.12)$$

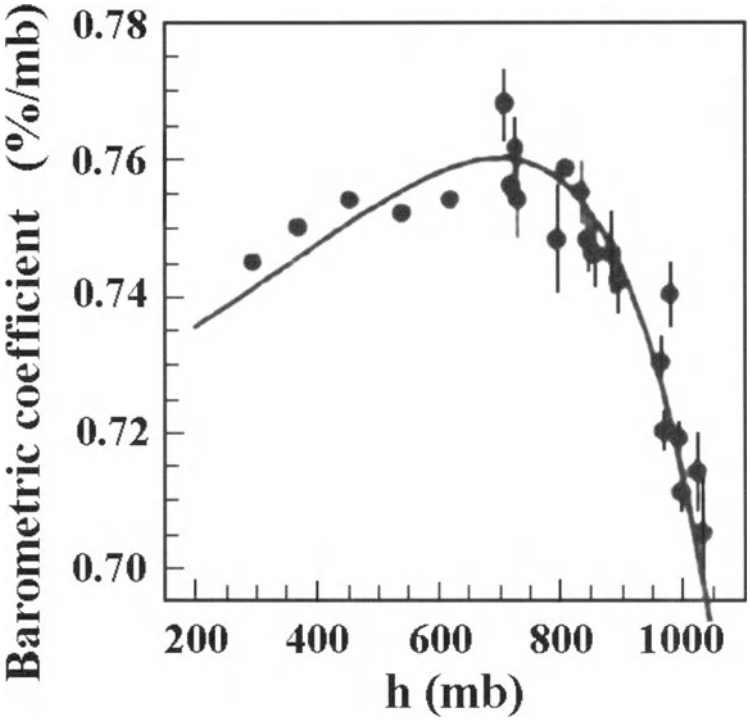

Fig. 6.14.7. The dependence of NM barometric coefficient from thr pressure on the level of observations: black circles – experimental data, curve – fitting according Eq. 6.14.7. From Yanchukovsky and Philimonov (1997).

The same procedure were applied by Yanchukovsky and Philimonov (1997) to data on barometric coefficients $\beta(h,m)$ for neutron multiplicities m from 1 to 8; it was found that:

$$\beta(h,m)=\frac{\beta(h)[F(m)-C]}{F_1(h)F(m)-F_2(h)}, \tag{6.14.13}$$

where $\beta(h)$ is determined by Eq. 6.14.10, $F(m)$ is the relative sensitivity of NM to detect multiplicity m, $C = 0.0594$, and

$$F_1(h)=b_1-b_2[\exp(\alpha_1(h-h_o))-\exp(\alpha_2(h-h_o))], \tag{6.14.14}$$

$$F_2(h)=b_3+b_2[\exp(\alpha_1(h-h_o))-\exp(\alpha_2(h-h_o))]. \tag{6.14.15}$$

In Eq. 6.14.14 and 6.14.15 parameter α_1 is determined by Eq. 6.14.11, parameter α_2 by Eq. 6.4.12, and

$$b_1=0.1183,\ b_2=0.3233,\ b_3=0.7955. \tag{6.14.16}$$

6.15. Determination of barometric coefficients by the method of consecutive approximations

6.15.1. The method of consecutive approximations for determination of barometric coefficients

Determination of the CR barometric effect is very important for exact correction of observed data for the barometric effect, taking into account its variation with the cut off rigidity and with the solar activity cycle (see review in Dorman, M1957, M1963a,b, M1972, M1974). Investigations of the dependence of the barometric effects on the cut off rigidity gave the possibility to determine the barometric coefficients of integral multiplicities (differential barometric coefficients, introduced in Dorman, M1972). This research is also important for exact the correction of CR latitude survey data (Iucci et al., 2000; see also Chapter 16). Dorman et al. (1999a) determined the attenuation coefficients for Emilio Segre' Observatory for total neutron intensity and for different multiplicities approximately on the basis of measurements of air pressure, total neutron monitor counting rate and intensities of neutron multiplicities ≥1, ≥2, ≥3, ≥4, ≥5, ≥6, ≥7 and ≥8 in three points on different altitudes: port Haifa (sea level), at low station of sky lift (626 mm Hg), and on the final position of Emilio Segre' Observatory on Mt. Hermon (33°18.3′N, 35°47.2′E, 598 mm Hg, 2025 m above sea level, $R_c = 10.8$ GV). The barometric coefficients determined by this method were used in Dorman et al. (1999b) as the basis for iteration processes for more exact determination of barometric coefficients by using hourly data between June – December 1998. By these data CR barometric coefficients for total neutron monitor counting rate, as well as separately for multiplicities 1, 2, 3, 4, 5, 6, 7, was determined approximately by taking into account also information on primary CR variations on the basis of Rome NM data. In Dorman et al. (2001b) the method of determining of barometric coefficients for total neutron intensity and different multiplicities step by step in three approximations was developed. As the first approximation there were used barometric coefficients determined by widely used correlation of CR data for all period of observations with variations of air pressure. Then obtained corrected on barometric effect in the first approximation data were correlated with Rome data, also corrected on the barometric effect. By obtained regression coefficients original data of ESO NM were corrected on CR primary variations. Corrected data were again correlated with air barometric pressure and determined barometric coefficients in the second approximation. Then with obtained barometric coefficients original data of ESO NM were corrected on barometric effect with much better accuracy and new data of intensity again correlated with corrected Rome data. By obtained new regression coefficients CR data of Emilio Segre' Observatory were more exactly corrected on primary variations. Then barometric coefficients for total neutron intensity and different multiplicities were determined in the third approximation by data corrected on primary variations in the second approximation.

6.15.2. Barometric coefficients for Rome 17-NM-64 of IQSY type

First we determined by regression method the barometric coefficients for the total intensity and the different multiplicities for Rome NM. Results for 1998–2001 are shown in Table 6.15.1.

Table 6.15.1. Barometric coefficients (in %/mm Hg) for total intensity and different multiplicities for Rome NM in 1998–2001.

2001	2000	1999	1998	YEARS
759.57	761.41	760.63	761.97	$\langle h_o \rangle$, mm Hg
−0.926 ± 0.007	−0.847 ± 0.004	−0.942 ± 0.003	− 0.884 ± 0.003	total
−0.820 ± 0.007	−0.740 ± 0.004	−0.836 ± 0.003	− 0.771 ± 0.003	$m = 1$
−0.993 ± 0.008	−0.908 ± 0.004	−1.009 ± 0.004	− 0.952 ± 0.003	$m = 2$
−1.051 ± 0.008	−0.971 ± 0.004	−1.068 ± 0.004	−1.015 ± 0.003	$m = 3$
−1.086 ± 0.008	−1.015 ± 0.005	−1.103 ± 0.004	−1.055 ± 0.004	$m = 4$
−1.108 ± 0.009	−1.037 ± 0.005	−1.116 ± 0.005	−1.078 ± 0.005	$m = 5$
−1.108 ± 0.007	−1.063 ± 0.004	−1.120 ± 0.003	−1.096 ± 0.003	$m = 6$
−1.126 ± 0.014	−1.054 ± 0.009	−1.143 ± 0.009	−1.094 ± 0.009	$m = 7$
−1.124 ± 0.011	−1.065 ± 0.006	−1.115 ± 0.007	−1.091 ± 0.007	$m \geq 8$

6.15.3. Barometric coefficients for ESO NM-64 (Mt. Hermon): first approximation

As a first approximation for barometric coefficients for ESO NM for total intensity and different multiplicities, we used as usual the regression coefficients in the relation between change of atmospheric pressure $h - h_o$ and natural logarithms of NM counting rates of observed total neutron intensity and of different multiplicities $\ln(I_m(h))_{\text{obs}}^{\text{ESO}}$:

$$\ln(I_m(h))_{\text{obs}}^{\text{ESO}} = B_{m1} \times (h - h_o) + C_{m1} \ , \qquad (6.15.1)$$

where $m =$ total, 1, 2, 3, 4, 5, 6, 7, ≥ 8. We used hourly data from June 1998 up to April 2001. For each m we determined also the correlation coefficients R_{m1}. Results are listed in Table 6.15.2. From Table 6.15.2 it can be seen that in case when data are not corrected for primary variations, the correlation between the change of atmospheric pressure and CR intensity in different channels is very low, especially for a high multiplicities.

Table 6.15.2. Barometric coefficients B_{m1} in the first approximation (in %/mm Hg) for total intensity and for different multiplicities for ESO NM. Also are shown corresponding correlation coefficients R_{m1}.

channel	B_{m1}	R_{m1}
total	− 0.855 ± 0.008	0.644
$m = 1$	− 0.676 ± 0.008	0.583
$m = 2$	− 0.905 ± 0.009	0.614
$m = 3$	−1.015 ± 0.010	0.642
$m = 4$	−1.093 ± 0.010	0.663
$m = 5$	−1.154 ± 0.011	0.666
$m = 6$	−1.201 ± 0.012	0.632
$m = 7$	−1.243 ± 0.015	0.569
$m \geq 8$	−1.301 ± 0.015	0.580

6.15.4. Barometric coefficients for ESO NM (Mt. Hermon): second approximation

Using the barometric coefficients thus found, we corrected the observed data according to the relation

$$\ln(I_m)_{\text{cor1}}^{\text{ESO}} = \ln(I_m(h))_{\text{obs}}^{\text{ESO}} - B_{m1}(h-h_o) - C_{m1}. \qquad (6.15.2)$$

The corrected data was correlated with the Rome NM data, also corrected for the barometric effect using the barometric coefficients listed in Table 6.15.1. The results can be described by relations

$$\ln(I_m)_{\text{cor1}}^{\text{ESO}} = \ln(I_t)_{\text{cor1}}^{\text{Rome}} \times D_{m1} + E_{m1}, \qquad (6.15.3)$$

where the regression coefficients are listed in Table 6.15.3 (together with the corresponding correlation coefficients).

Table 6.15.3. Regression coefficients D_{m1}, E_{m1} and correlation coefficients Ω_{m1} for connection of ESO NM data with Rome NM data according to Eq. 6.15.3.

channel	D_{m1}	E_{m1}	Ω_{m1}
total	0.669 ± 0.002	4.635 ± 0.024	0.946
$m = 1$	0.613 ± 0.002	4.577 ± 0.025	0.935
$m = 2$	0.740 ± 0.006	1.758 ± 0.076	0.717
$m = 3$	0.750 ± 0.007	0.548 ± 0.086	0.677
$m = 4$	0.708 ± 0.007	0.130 ± 0.097	0.611
$m = 5$	0.627 ± 0.008	0.378 ± 0.110	0.515
$m = 6$	0.533 ± 0.010	0.859 ± 0.129	0.400
$m = 7$	0.409 ± 0.012	1.831 ± 0.155	0.267
$m \geq 8$	0.099 ± 0.013	6.095 ± 0.165	0.063

We then determined the CR variations on Mt. Hermon corrected on primary variations according to:

$$\ln(I_m)_{\text{cor1/pr}}^{\text{ESO}} = \ln(I_m)_{\text{obs}}^{\text{ESO}} - \ln(I_t)_{\text{cor1}}^{\text{Rome}} \times D_{m1} - E_{m1}, \qquad (6.15.4)$$

using the regression coefficients D_{m1} and E_{m1}. Now we can determine the 2-nd approximation of barometric coefficients according to regression relations:

$$\ln(I_m(h))_{\text{cor1/pr}}^{\text{ESO}} = B_{m2} \times (h-h_o) + C_{m2}. \qquad (6.15.5)$$

Barometric coefficients B_{m2} and corresponding correlation coefficients R_{m2} are listen in Table 6.15.4.

Table 6.15.4. Barometric coefficients B_{m2} (in %/*mm* Hg) and correlation coefficients R_{m2} for the second approximation for total intensity and for different multiplicities for ESO NM.

channel	B_{m2}	R_{m2}
total	-0.904 ± 0.003	0.941
$m = 1$	-0.721 ± 0.003	0.909
$m = 2$	-0.958 ± 0.003	0.934
$m = 3$	-1.069 ± 0.004	0.918
$m = 4$	-1.145 ± 0.005	0.876
$m = 5$	-1.200 ± 0.007	0.805
$m = 6$	-1.240 ± 0.010	0.711
$m = 7$	-1.273 ± 0.014	0.604
$m \geq 8$	-1.308 ± 0.015	0.584

6.15.5. Barometric coefficients for ESO NM (Mt. Hermon): third approximation

Using the barometric coefficients for ESO NM listed in Table 6.15.4, we correct the observed data according to relation

$$\ln(I_m)_{\text{cor2}}^{\text{ESO}} = \ln(I_m(h))_{\text{obs}}^{\text{ESO}} - B_{m2}(h - h_o) - C_{m2}\,. \tag{6.15.6}$$

The corrected data is correlated with Rome NM data also corrected on barometric effect. The results can be described by relations

$$\ln(I_m)_{\text{cor2}}^{\text{ESO}} = \ln(I_t)_{\text{cor1}}^{\text{Rome}} \times D_{m2} + E_{m2}\,, \tag{6.15.7}$$

where regression coefficients are listed in Table 6.15.5 (together with the corresponding correlation coefficients).

Table 6.15.5. Regression coefficients D_{m2}, E_{m2} and correlation coefficients Ω_{m2} for connection of ESO NM data with Rome NM data according to Eq. (6.15.7).

channel	D_{m2}	E_{m2}	Ω_{m2}
total	0.670 ± 0.002	4.612 ± 0.024	0.947
$m = 1$	0.615 ± 0.002	4.556 ± 0.024	0.936
$m = 2$	0.768 ± 0.002	1.276 ± 0.027	0.950
$m = 3$	0.782 ± 0.003	0.010 ± 0.034	0.925
$m = 4$	0.740 ± 0.004	-0.399 ± 0.046	0.861
$m = 5$	0.660 ± 0.005	-0.176 ± 0.065	0.733
$m = 6$	0.569 ± 0.007	0.288 ± 0.090	0.556
$m = 7$	0.446 ± 0.009	1.245 ± 0.123	0.357
$m \geq 8$	0.140 ± 0.010	5.473 ± 0.133	0.110

Let us now determine the CR variations on Mt. Hermon corrected for the primary variations according to:

$$\ln(I_m)^{\mathrm{ESO}}_{\mathrm{cor2/pr}} = \ln(I_m)^{\mathrm{ESO}}_{\mathrm{obs}} - \ln(I_t)^{\mathrm{Rome}}_{\mathrm{cor1}} \times D_{m2} - E_{m2} \quad . \tag{6.15.8}$$

We can then determine the 3rd approximation of barometric coefficients according to regression relations:

$$\ln(I_m(h))^{\mathrm{ESO}}_{\mathrm{cor2/pr}} = B_{m3} \times (h - h_o) + C_{m3} \quad . \tag{6.15.9}$$

The barometric coefficients B_{m3} and the corresponding correlation coefficients R_{m3} are listed in Table 6.15.6.

Table 6.15.6. Barometric coefficients B_{m3} (in %/mm Hg) in the second approximation for total intensity and for different multiplicities for ESO NM. Also are shown corresponding correlation coefficients R_{m3}.

channel	B_{m3}	R_{m3}
total	–0.904 ± 0.003	0.941
$m = 1$	–0.721 ± 0.003	0.909
$m = 2$	–0.960 ± 0.003	0.935
$m = 3$	–1.072 ± 0.004	0.919
$m = 4$	–1.147 ± 0.005	0.877
$m = 5$	–1.202 ± 0.007	0.806
$m = 6$	–1.243 ± 0.010	0.712
$m = 7$	–1.275 ± 0.014	0.605
$m \geq 8$	–1.311 ± 0.015	0.585

6.15.6. Comparison of the three approximations for barometric coefficients

Let us compare the three approximations of found barometric coefficients and corresponding correlation coefficients for ESO NM for total neutron intensity and different multiplicities (see Table 6.15.7).

Table 6.15.7. Comparison of three approximations for ESO NM.

channel	B_{m1}	B_{m2}	B_{m3}	R_{m1}	R_{m2}	R_{m3}
total	–0.855 ± 0.008	–0.904 ± 0.003	–0.904 ± 0.003	0.644	0.941	0.941
$m = 1$	–0.676 ± 0.008	–0.721 ± 0.003	–0.721 ± 0.003	0.583	0.909	0.909
$m = 2$	–0.905 ± 0.009	–0.958 ± 0.003	–0.960 ± 0.003	0.614	0.934	0.935
$m = 3$	–1.015 ± 0.010	–1.069 ± 0.004	–1.072 ± 0.004	0.642	0.918	0.919
$m = 4$	–1.093 ± 0.010	–1.145 ± 0.005	–1.147 ± 0.005	0.663	0.876	0.877
$m = 5$	–1.154 ± 0.011	–1.200 ± 0.007	–1.202 ± 0.007	0.666	0.805	0.806
$m = 6$	–1.201 ± 0.012	–1.240 ± 0.010	–1.243 ± 0.010	0.632	0.711	0.712
$m = 7$	–1.243 ± 0.015	–1.273 ± 0.014	–1.275 ± 0.014	0.569	0.604	0.605
$m \geq 8$	–1.301 ± 0.015	–1.308 ± 0.015	–1.311 ± 0.015	0.580	0.584	0.585

From Table 6.15.7 it can be seen that: 1) for total neutron intensity and for small multiplicities (up to $m = 4$) the second approximation has much better accuracy than the first approximation, statistical errors decrease by a factor of 2–3 from the first to the second approximation and the correlation coefficients increase significantly (it means that for these NM channels correction on primary variations is very important); 2) for higher multiplicities ($m \geq 5$) the second approximation has about the same accuracy as the first approximation and the correlation coefficients increase very little (for these multiplicities the accuracy is determined mostly by poor statistics, correction on primary variations is not so important); 3) the difference between the second and the third approximations is negligible, correlation coefficients and statistical errors are about the same and very small differences of barometric coefficients for total neutron intensity and for different multiplicities are in frame of statistical errors (it means that two approximations for determining barometric coefficients is enough; the third approximation we made for control of obtained results).

Chapter 7

Experimental Investigations of Cosmic Ray Temperature and Humidity Effects

7.1. Experimental investigations of temperature effect and the encountered difficulties

The atmospheric conditions in the empirical method for determining of temperature effect are characterized by one or two of the following parameters: the air temperature on the ground, the height and air temperature of the level where main muon generation is assumed to take place (usually levels of 100 or 200 mb), the average mass temperature of the atmosphere, and so on. Very useful work in developing and checking the empirical method has been performed by Duperier (1949, 1951). Adopting the explanation by Blackett (1938) of the hard muons temperature effect, he used two parameters: the height $H(h_g)$ and air temperature $T(h_g)$ at the level h_g where the main part of muons is generated (about 100-200 mb). Therefore the total regression equation (with taking into account also barometric effect) has the form:

$$(\Delta M/M_o)_{\text{met}} = \beta \Delta h_o + C_H \Delta H(h_g) + C_T \Delta T(h_g), \qquad (7.1.1)$$

where $(\Delta M/M_o)_{\text{met}}$ is the relative variation of hard muon intensity of meteorological origin. This method has been checked also by Bachelet and Conforto (1956), Trefall (1957), Mathews (1959), French and Chasson (1959), Ehmert (1960), Wada (1961), Tanskanen (1965), Wang and Lee (1967). Thus, Tanskanen (1965) found by triple correlation described by Eq. 7.1.1, from hard muon observations with the cubical telescope at Oula (Finland) in 1964 the following regression coefficients (here was supposed that $h_g = 100\,\text{mb}$):

$$\beta = -0.12 \pm 0.02\,\%/\text{mb}, \quad C_H = -4.66 \pm 0.58\ \%/\text{km}, \quad C_T = +0.06 \pm 0.01\%/^{\circ}\text{C}. \quad (7.1.2)$$

Wang and Lee (1967) found for observations at Hong Kong ($R_c = 16.3$ GV) by two muon cubical telescopes:

$$\beta = -0.085 \pm 0.003\%/\text{mb}, \quad C_H = -3.1 \pm 0.8\ \%/\text{km}, \quad C_T = +0.15 \pm 0.03\%/^{\circ}\text{C}. \quad (7.1.3)$$

Many investigations show that the regression coefficients in Eq. 7.1.1 vary significantly from one station to another, with season, from one period to other. Although empirical method was rather widely used in the 1950s and 1960s (since it is simple and free from possible errors in the computation of theoretical coefficients), it has important defects. The difficulties encountered are ultimately due to the circumstance that for the temperature CR effect the distribution of air mass in the atmosphere is

essential. This mass distribution is completely and uniquely determined by the temperature profile from the level of observation to the boundary of the atmosphere. Moreover, the temperature corrections computed by regression coefficients of empirical method (Eq. 7.1.1) will have only statistical significance. We can never feel convinced that an individual temperature correction obtained by Eq. 7.1.1 for a concrete moment really will be close to the true one. As it was shown in Dorman (1954b), only integral method by using balloons weather probing or other data of temperature profile can solve this problem exactly .

7.2. Integral method for determining of temperature effect for hard muon component

An approximate check of the theoretical temperature coefficients described in Chapter 5 was made by Wada (1961) from observations in Japan. He found the regression coefficient for the correlation of the hard muon intensity, corrected for barometric effect, with the average temperature of the atmosphere (the average being taken with weights according to masses of atmospheric layers). The coefficient was found to be $-0.255 \pm 0.009\ \%/^{\circ}\mathrm{C}$. If this coefficient is computed with the temperature coefficient $W_T(h)$ found by Dorman (1954a), then it is $-0.276\ \%/^{\circ}\mathrm{C}$; and with the coefficients of Maeda and Wada (1954) it is $-0.250\ \%/^{\circ}\mathrm{C}$. Thus the experimental value lies between these two theoretical ones. Wada (1961) supposes that one of the causes of the small difference between the two theoretical results may be the difference in the assumed mean atmosphere temperature distribution (see Fig. 7.2.1).

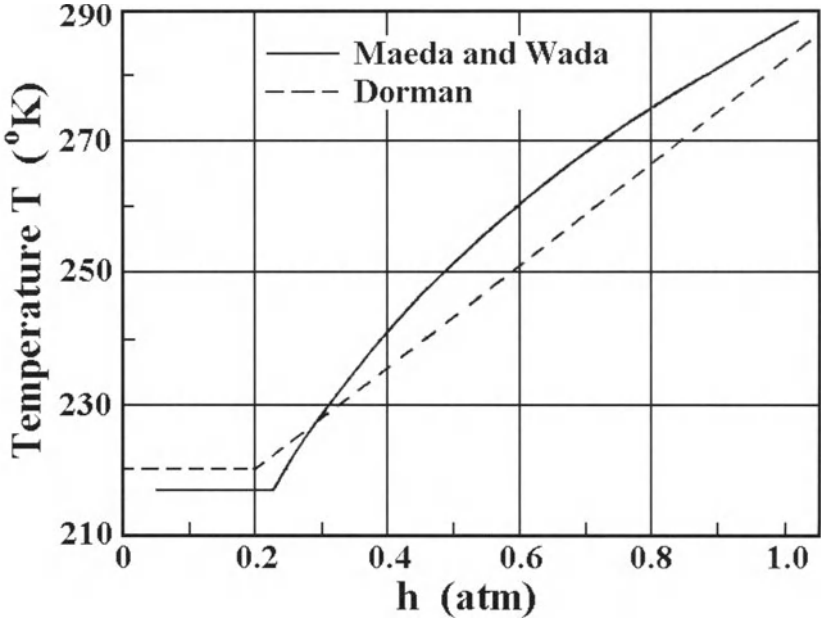

Fig. 7.2.1. The mean assumed atmosphere temperature distribution in two models.

Fig. 7.2.2 shows a comparison of the experimental values of determining of temperature coefficients by Ehmert (1960), by Wada and Kudo (1954), and by Wada (1961) with the theoretical temperature coefficients according to Dorman (1954a) and Maeda and Wada (1954).

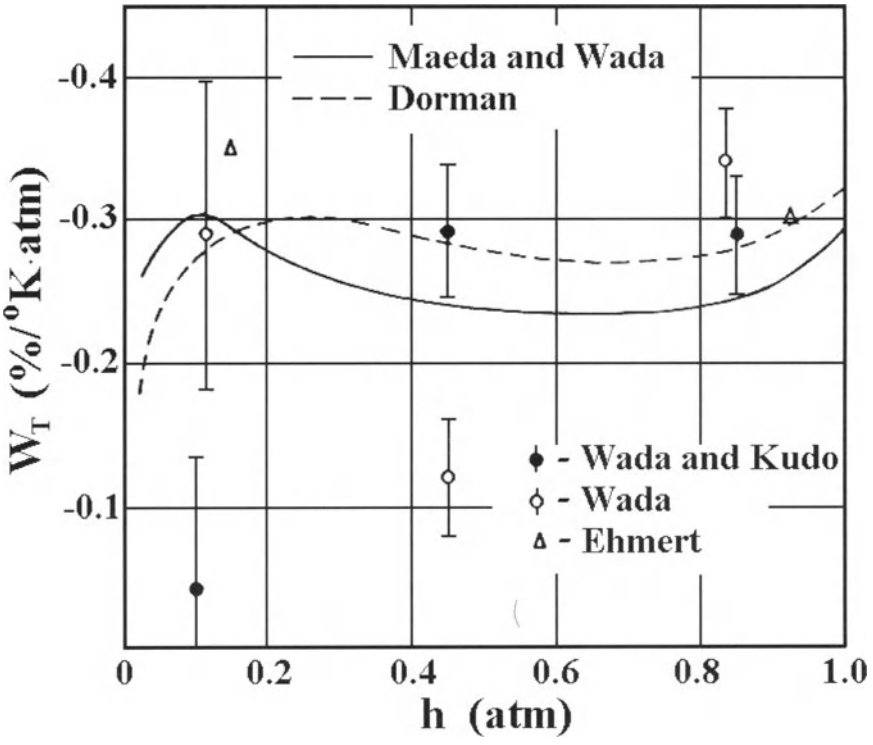

Fig. 7.2.2. Comparison of experimental values of determining of temperature coefficients by Ehmert (1960), by Wada and Kudo (1954), and by Wada (1961) with theoretical values according to Dorman (1954a) and Maeda and Wada (1954).

Evidently, no definite conclusions can be drawn from Fig. 7.2.2 until the experimental errors are significantly reduced.

Much more exact results were obtain by Carmichael et al. (1963, 1965a). They investigated meteorological effects of hard muons on the basis of observations during May 1962 – April 1963 by muon super-telescope and neutron monitor of IQSY type at Deep River, using radiosonde air temperature data at 7 and 19 LT each day from the aerological station Maniawaku (about 120 km west of Deep River). Three methods for finding the temperature corrections with the aid of regression equations were tested:

$$\delta M = C_N \delta N + \beta \Delta h_o + \begin{cases} C_H \Delta H & \text{according to Duperier,} \\ C_M \Delta T_M & \text{according to Maeda,} \\ C_D \Delta T_D & \text{according to Dorman,} \end{cases} \qquad (7.2.1)$$

where $\delta M = \Delta M / M_o$ and $\delta N = \Delta N / N_o$ are the relative intensity variations of the hard muon and neutron components (for neutron component are used data corrected on barometric effect), $\beta \Delta h_o$ takes into account barometric effect, H is the elevation of the 200 mb level (according to Duperier, 1949, 1951), ΔT_M and ΔT_D are the temperature corrections computed from radiosonde data with the aid of the temperature coefficients according to Maeda and Wada (1954) and Dorman (1954a), respectively. Monthly total regression coefficients for the hard muon component, corrected according to Eq. 7.2.1 are given in Fig. 7.2.3.

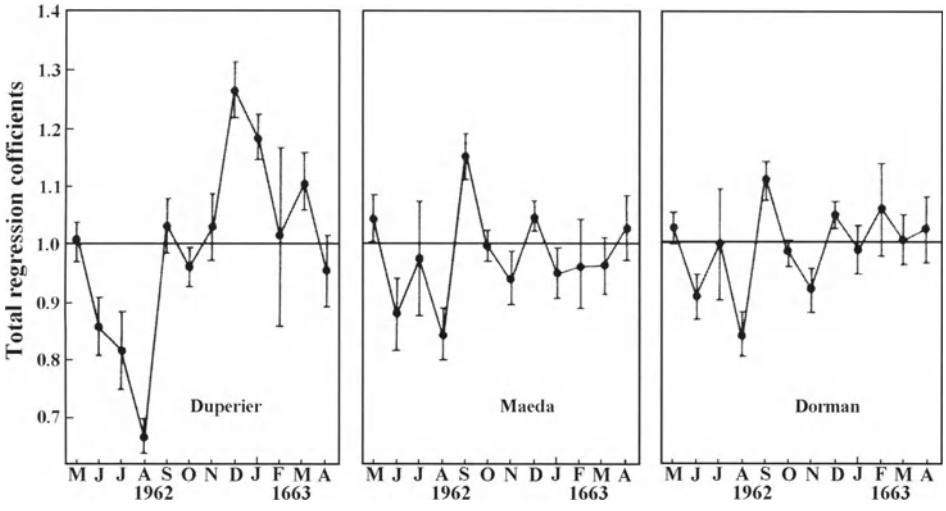

Fig. 7.2.3. Monthly averages of total regression coefficients for correlation between observed hard muon component intensities with expected according to models of Duperier, Maeda and Dorman (Eq. 7.2.1) during May 1962–April 1963.

It can be seen that the integral methods (Maeda's and Dorman's) give much smaller dispersion than Duperier's empirical method. The regression coefficients in the three formulae of Eq. 7.2.1 for the period May 1962 - April 1963 are:

$$C_N = 0.401\%/\%, \beta = -0.120\%/mb, C_H = -4.150\%/km \text{ (Duperier's method)}, \quad (7.2.2)$$

$$C_N = 0.371\%/\%, \beta = -0.159\%/mb, C_M = 1.078 \text{ (Maeda's method)}, \quad (7.2.3)$$

$$C_N = 0.382\%/\%, \beta = -0.156\%/mb, C_D = 1.018 \text{ (Dorman's method)}. \quad (7.2.4)$$

From Eq. 7.2.2 – 7.2.4 it can be seen that the regression coefficient for connection of computed temperature corrections with the observed one is the nearest to unity for Dorman's method $(C_D = 1.018)$. Carmichael et al. (1963, 1965a) came to the following conclusion: the fact that the regression coefficient C_D is found to be very close to 1 indicates that the temperature coefficient found in Dorman (1954a) is correct.

This investigations were continued by Carmichael et al. (1965b) using observations from May 1, 1963 to April 30, 1964 at Deep River by a wide-angle scintillation telescope with a counting rate of 1.3×10^6 pulses/hr. The expected theoretical temperature effects were computed by using balloons weather probing data, and corrections for extra-terrestrial variations were made by using neutron super-monitor data at the same station (counting rate 0.6×10^6 pulses/hr). The regression coefficients for the counting rate of the meson telescope M are defined by the equation

$$\delta M = \beta\Delta h_o + C_N\delta N + C_T\Delta T_{\text{int}} + \overline{C}_N\delta\overline{N} + \overline{C}_T\overline{\Delta T}_{\text{int}}, \tag{7.2.5}$$

where $\delta M = \Delta M/M_o$ and $\delta N = \Delta N/N_o$ are the relative intensity variations of the hard muon and neutron components (for neutron component, data are corrected for the barometric effect), $\beta\Delta h_o$ takes into account barometric effect of hard muons, $C_N\delta N$ and $\overline{C}_N\delta\overline{N}$ are corrections on primary variations based on hour data and on data smoothed with a period of 31 days, respectively; ΔT_{int} and $\overline{\Delta T}_{\text{int}}$ are computed by integral method on the basis of weather balloon data temperature corrections for hourly data and data smoothed with a period of 31 days, respectively. Results for the regression coefficients in Eq. 7.2.5 and correlation coefficient are shown in Table 7.2.1.

Table 7.2.1. Regression coefficients in Eq. 7.2.5 and correlation coefficients for different integral methods.

regression and correlation coefficients	integral method		
	Dorman	Maeda	Wada
β, %/*mb*	−0.159 ± 0.001	−0.160 ± 0.001	−0.160 ± 0.001
C_N	0.34 ± 0.02	0.34 ± 0.02	0.34 ± 0.02
C_T	0.98 ± 0.02	1.03 ± 0.02	0.98 ± 0.02
$\overline{C}_N$	−0.07 ± 0.02	−0.07 ± 0.02	−0.08 ± 0.02
$\overline{C}_T$	0.26 ± 0.02	0.24 ± 0.02	0.32 ± 0.02
correlation coefficient	0.99755	0.99751	0.99755

From Table 7.2.1 it can be seen that all three integral methods for determining the temperature effect give, within the error limits, about the same results for the regression coefficients $\beta, C_N, C_T, \overline{C}_N$ and for the correlation coefficients. This is due to the fact that the temperature coefficients used in the three methods differ only very little.

Carmichael et al. (1965b) extended the method described above by using observations with wide-angle muon telescopes simultaneously at two stations Deep River (station 1) and Inuvik (station 2), with nearly the same altitude and equal cut-off rigidities. By means of the regression equation

$$(\delta M_1 - \delta M_2) - \beta(\Delta h_{o1} - \Delta h_{o2}) = C_T(\Delta T_{\text{int}1} - \Delta T_{\text{int}2}), \tag{7.2.6}$$

it was found that $C_T = 1.13$ with Maeda's temperature coefficient and $C_T = 1.08$ with Dorman's temperature coefficient.

Experimental checks of the integral method have been made in many papers for hard muon component observations at sea level (Dorman et al., 1954; Bachelet and Conforto, 1956; Mathews, 1959; Glokova, 1960a). With the aid of the integral method described in Chapter 2, the following contributions to the temperature effect were determined: annual variations (Dorman et al., 1954; Glokova, 1956, 1960a,b; Berdichevskaya et al., 1957), the 27-day variations (Glokova et al., 1955), the solar-daily variations (Dorman et al., 1954; Kuzmin, 1954, 1955; Krasil'nikov, 1955; Berdichevskaya et al., 1957; Glokova et al., 1958), the siderial-daily variations (Glokova et al., 1958, 1960c, 1961), variations during great geomagnetic storms (Kuzmin and Skripin, 1960) and in periods of solar CR enhancements (Dorman et al., 1954; Kaminer, 1960).

7.3. Experimental investigations of temperature effect of the hard muon component intensity underground

The integral method described above was checked also by investigations of the temperature effect of the hard muon component intensity underground (Blokh et al., 1959; Kuzmin and Danilov, 1960; Blokh et al., 1961; Messerschmidt, 1961; Kuzmin and Skripin, 1962; Sandor et al., 1962; Kuzmin et al., 1963). From continuous recording of the CR muon component at Yakutsk in 1957-1959 with Geiger counter telescope on the ground surface and underground at depth of 7, 20 and 60 m w. e. Kuzmin and Skripin (1962) derived the temperature coefficient for various observation levels. The values found agree with those expected from Dorman's theory (see Chapter 5), if only it is assumed that the effective exponent of the muon energy spectrum varies smoothly from 1.3 at the ground level, to about 2.0 at the depth 60 *m* w. e. (corresponding to a change of γ in Chapter 5 from $\gamma = 0.3$ at the ground level to $\gamma = 1.0$ at the depth 60 *m* w. e., in good agreement with direct measurements of muon energy spectrum in high energy region).

7.4. Experimental investigations of the temperature and humidity effects in the neutron component

7.4.1. Estimation of possible temperature effect in neutron component by using of empirical method of Duperier

Bachelet et al. (1965) estimated the temperature effect in the neutron component as follows. Since muons through formation of meso-atoms contribute about 8-9% in the total counting rate of the IGY neutron monitor at Rome ($R_C \approx 6.4\ GV$), and the decay regression coefficient according to Duperier's (1949, 1951) method (see Section 7.1) is about 5 %/*km*, there must also be a temperature effect for the neutron monitor characterized by the decay coefficient of about 0.4 %/*km*. This must give an annual wave of meteorological origin with amplitude ≈0.3 %. These values are too small to observe because they are within the error margin of Duperier's method. Let us note that this estimate, based on measurements of the temperature effect for hard muons, is not exact since: 1) meso-atoms in the neutron monitor are produced mainly by slow negative muons with a relatively larger temperature effect than for hard muons, and 2) it necessary to use integral method instead of empirical method (see the theory in the Section 2.4 and discussion on empirical and integral methods in the Section 7.1).

7.4.2. The checking of the integral method of estimation of temperature effect in neutron component

The expected temperature effect in the counting rate of neutron monitor was calculated in Section 21.3 in Dorman (M1957) by taking into account the relative role of non-stable particles in the meson-nuclear cascade in the atmosphere, as well as role of negative soft muons in formation of lead mesoatoms (in more details see above in Section 2.4). Early attempts to check this theory (e.g. Manzano et al., 1959) had no success since the large neutron intensity variations of extra-atmospheric origin were much larger than the expected small temperature effect. The first important result on the checking of the integral method of estimation of temperature effect in neutron component by observation data was obtained by Kaminer et al. (1964a,b,c, 1965): they removed the large neutron intensity variations of extra-atmospheric origin by subtracting the data of one station from those of another station with about the same geomagnetic cut-off rigidity and lying in the opposite hemisphere. Thus the seasonal temperature effect is nearby doubled. On the basis of monthly averages of neutron intensity observed in 1960–1962 by IGY neutron monitors at Hobart (Australia) and Chicago (USA), the seasonal neutron intensity variations were found: the phase was in good agreement with the one expected from the integral method (using weather balloon data), but the amplitude found (1.2–1.6%) was bigger than expected by the factor about 2. For the higher solar activity period in 1957-1960 this factor for the same stations was found to be 1.7.

Harman and Hatton (1968) determined the temperature effect of IGY neutron monitors and IQSY neutron super-monitors by the multiple correlation method on the basis of observations in 1962–1965. The effect found for IGY neutron monitors exceeded Dorman's (1957) theoretical results by a factor 1.57 ± 0.10. For the IQSY neutron super-monitors this factor was found to be somewhat closer to unity: 1.20 ± 0.13. Harman and Hatton (1968) are inclined to ascribe the obtained difference between two factors to a possible difference of the contribution of captured negative soft muons (with formation of meso-atoms) to the counting rate of IGY and IQSY neutron monitors.

7.4.3. The measurements of temperature and humidity effects in neutron component

As was shown in Chapter 5 (see Section 5.4), the temperature and humidity effects of neutron component are very closely connected; therefore it is necessary to investigate them simultaneously. The first attempt of this type of analysis was made by Bercovitch and Robertson (1965) on the basis of neutron intensity observations at Inuvik, Churchill, Goose Bay and Deep River during the period June 15, 1964 – January 30, 1965 and corresponding weather balloon data on temperature and humidity twice daily. They determined the regression coefficients between the observed differences of intensities at a pair of the above mentioned stations (in order to eliminate most of the variations of extra-atmospheric origin), as well as the difference of the temperature corrections computed according to Dorman (M1957) for the same pair of stations (regression coefficient C_T), the difference of humidity (water in the atmosphere, regression coefficient C_W), and the difference of air pressure (barometric coefficient β). The barometric coefficients were found to be

$$\beta = 0.726 \pm 0.002,\ 0.728 \pm 0.002,\ 0.734 \pm 0.003 \text{ and } 0.736 \pm 0.003\ \%/\text{mb} \quad (7.4.1)$$

for stations Inuvik, Churchill, Deep River and Goose Bay, respectively. The values for regression coefficients C_T and C_W obtained are listed in the Table 7.4.1.

Table 7.4.1. Regression coefficients C_T and C_W for the neutron component temperature and humidity effects.

PAIR OF STATIONS	C_T	C_W, $\%/\left(\text{g/cm}^2\right)$
Inuvik – Churchill	1.10 ± 0.13	-0.075 ± 0.036
Churchill – Deep River	1.60 ± 0.12	-0.15 ± 0.034
Deep River – Inuvik	1.13 ± 0.12	-0.06 ± 0.026
AVERAGE	1.28 ± 0.10	-0.09 ± 0.03

Bercovitch and Robertson (1965) came to conclusion that the absorption effect of the neutron component in water is

$$\beta_W = \beta + C_W = -0.82 \pm 0.03\ \%/\left(\text{g.cm}^{-2}\right), \quad (7.4.2)$$

which gives for the ratio

$$\beta_W / \beta = 1.12 \pm 0.04\,. \quad (7.4.3)$$

This means that the absorption effect of the neutron component in water is on 12±4 % higher than in air.

Chasson et al. (1966) studied the influence of the atmospheric water vapor content on the barometric coefficient of the neutron component. With this aim an aluminum container filled with water was placed above the neutron monitor and the decrease of neutron intensity was measured. The mean of four series of measurements gave for this weakening coefficient

$$\overline{\beta_W} = -0.43 \pm 0.02\ \%/\left(\text{g.cm}^{-2}\right). \quad (7.4.4)$$

Comparison with the value shown in Eq. 7.4.2 found by Bercovitch and Robertson (1965) shows that the concentration of the water from the atmosphere in a thin layer above the monitor reduces the effect by about a factor of two.

Kaminer and Khadakhanova (1966) showed that the correction of their earlier results (Kaminer et al., 1964a,b,c, 1965; see previous Section 7.4.2) for the humidity effect according to Bercovitch and Robertson (1965) considerably decreases the difference between observations and Dorman's theory: from 2.1 to 1.45, close to the ratio 1.28±0.10 obtained by Bercovitch and Robertson (1965), see Table 7.4.1.

7.5. Temporal and latitudinal dependencies of the temperature effect for CR neutron component

7.5.1. The problem of separation of temperature effect and North–South anisotropy in the CR neutron component

In papers reviewed in the previous section, it was supposed that the annual CR variation of extra-atmospheric origin is about the same on all stations. In this case the difference between the data from a pair of CR stations gives a clean temperature effect. In the last ten years it was shown that this suggestion is not correct: simultaneously with the symmetrical annual CR annual wave of extra-atmospheric origin, there exists also a non-symmetrical North–South CR anisotropy. The problem is how to separate CR temperature effect and North-South CR anisotropy. To solve this problem and to investigate the temporal and latitudinal dependencies of the temperature effect of CR neutron component, Belov et al. (1995, 1997) used data of the atmospheric temperature balloons weather probing during 1957–1968 at Resolute, Mawson, Hermanus, Chicago and Churchill (data from 'Monthly Climatic Data', Asheville, WDC-A, Meteorology, 1957-1968), and during 1979–1980 at Deep River, Kerguelen, Hermanus, Kiel, Moscow, Mawson, Sanae, Inuvik, Rome, Hobart and Potchefstroom (data from CEDEX CR-ROM, NASA Climate Data System, Goddard Space Flight Center, Greenbelt, 1992). Expected temperature effects were computed by the Dorman's integral method for each station and pairs of stations on the basis of these temperature balloons weather probing data and following theoretical temperature coefficients:

$$W_{Tn}^{\mathrm{IGY}}(h) = 0.03 \times W_{T\pi}(h) + 0.02 \times W_{T\mu f}(h) + 0.03 \times W_{T\mu c}(h) \qquad (7.5.1)$$

for IGY neutron monitors, and

$$W_{Tn}^{\mathrm{IQSY}}(h) = 0.02 \times W_{T\pi}(h) + 0.03 \times W_{T\mu f}(h) + 0.068 \times W_{T\mu c}(h) \qquad (7.5.2)$$

for IQSY neutron super-monitors. In Eq. 7.5.1 and Eq. 7.5.2 the temperature coefficient $W_{T\pi}(h)$ is for pions, $W_{T\mu f}(h)$ is for fast muons, and $W_{T\mu c}(h)$ is for captured (soft) muons. These coefficients were taken for three variants: according to Dorman, M1957 (see in detail Section 5.4 in Chapter 5), Dorman and Yanke (1971a,b) and Dorman et al., 1990 (see Chapter 9, Section 9.6).

To separate seasonal temperature effect and seasonal North-South anisotropy the system of regression equations (for each pair *i, k* of mentioned above stations) was considered

$$(\Delta N/N)_{ik}^{\mathrm{obs}} = C_T\left((\Delta N/N)_i^T - (\Delta N/N)_k^T\right) + A_{NS}\left(C_{10}^i - C_{10}^k\right), \qquad (7.5.3)$$

where the first member in the right hand is the difference of seasonal temperature effects for the station pair *i, k,* and the second member reflects the difference of seasonal North-

South anisotropy (here C_{10}^{i} and C_{10}^{k} are coupling coefficients for the first harmonic of CR anisotropy for the spectrum variations index $\gamma = 0$ and upper limit of rigidity $R_u = 100\ GV$, according to Yasue et al., M1982). In Eq. 7.5.3 C_T is a factor determined from comparison of observed and theoretical results of determination temperature effect in neutron component, and A_{NS} is the amplitude of c CR anisotropy (let us note that the wave caused by North-South anisotropy is particularly essential for the high latitude stations with $R_c \leq 2$ GV).

7.5.2. The seasonal temperature effect and North¬South anisotropy in the CR neutron component; determination of factor C_T .

In Fig. 7.5.1 are shown examples for 5 pairs of neutron monitor stations of observed seasonal waves and computed according to temperature coefficients obtained in Dorman (M1957), Dorman and Yanke (1971a,b), and in Dorman et al. (1990) at $C_T = 1$.

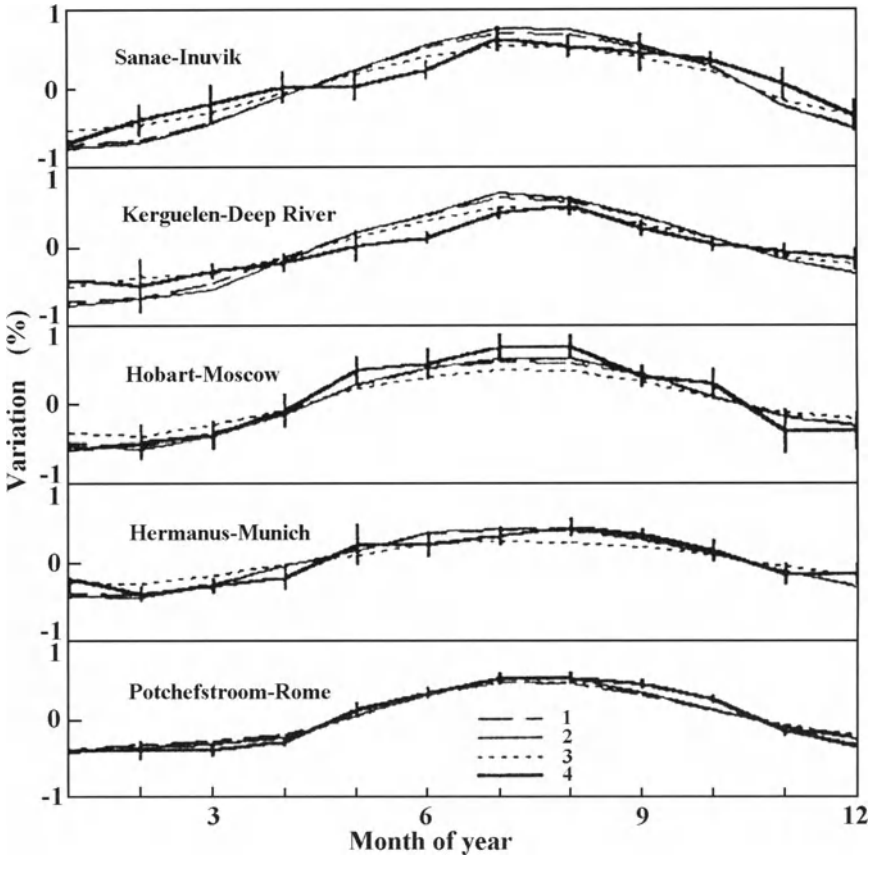

Fig. 7.5.1. Observed seasonal waves for 5 pairs of neutron monitor stations (curves *1*) and those computed according to the temperature coefficients obtained in Dorman, M1957 (curves *2*), Dorman and Yanke, 1971a,b (curves *3*), and in Dorman et al., 1990 (curves *4*) at $C_T = 1$.

The observed seasonal waves shown in Fig. 7.5.1 contain the temperature effect and North–South anisotropy. By solving the system of Eq. 7.5.3 the factor C_T was determined in Belov et al. (1995, 1997) for the three temperature coefficients mentioned above. It was shown that within statistical errors, for all three temperature coefficients, factor C_T is about the same:

$$C_T = 1.0 \pm 0.1 . \tag{7.5.4}$$

The system of Eq. 7.5.3 was solved again by the fixed value of C_T according to Eq. 7.5.4 and for each pair of stations temperature seasonal waves and North–South anisotropies were determined. As an example, Fig. 7.5.2 shows results for the pair of high latitude stations Sanae–Inuvik (where the North–South anisotropy is significant) and pair of low latitude stations Potchefstroom–Rome (where the North–South anisotropy is negligible).

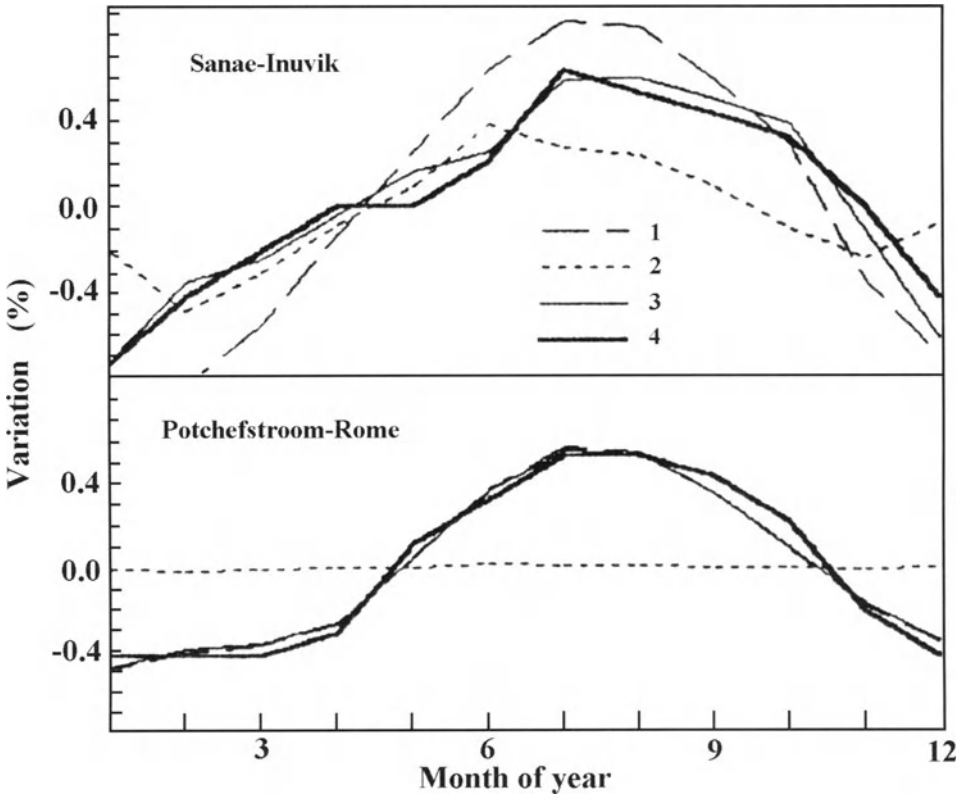

Fig. 7.5.2. Seasonal waves for the pair of high latitude stations Sanae–Inuvik (where the North–South anisotropy is significant) and pair of low latitude stations Potchefstroom–Rome (where the North–South anisotropy is negligible). Curves *1 – 4* – the same as in Fig. 7.5.1.

Belov et al. (1995, 1997) came to the following conclusions:

1) Consideration of the North–South anisotropy and seasonal temperature effect simultaneously for many pairs of neutron monitor stations gave the possibility to determine these two effects separately;
2) All three temperature coefficients of Dorman (M1957), Dorman and Yanke (1971a,b), and of Dorman et al. (1990) gave within experimental errors about the same result and the connection between observations and theory is characterized according to Eq. 7.5.4 by the a factor of about unity.

Chapter 8

Atmospheric Electric Field Effects in Cosmic Rays

8.1. Discovery and detail investigations of atmospheric electric field effects in CR on the Baksan EAS array

Discussions on the possible acceleration of charged particles by atmospheric electric fields in periods of thunderstorms started to appear in the scientific literature many years ago. Wilson (1925) assumed that electrons in thunderstorms clouds can be accelerated up to very high energies, as in CR. There were many attempts to observe effects of charged particle acceleration by atmospheric electric fields before or during thunderstorms (e.g., Shonland, 1930; Shonland and Vilfoen, 1933; Clay et al., 1952), but the results were contradictory and not clear. The first real CR fluctuations connected with precipitations out of cumulous-nimbus and nimbostratus clouds were observed by Attolini et al. (1971), but they suggested that the most probable cause of the observed phenomenon are the air temperature variations in the atmosphere.

Alexeenko et al. (1985, 1987) were the first to examine in detail the relationship of temporal CR variations to atmospheric electric field (at about 20 kV/m and up to 30 kV/m field intensities) using 4 min counts of the Baksan EAS array at 90 MeV threshold energy $E_{k\min} \approx 90$ MeV (height 1700 m, cut off rigidity 6.5 GV, the effective area of scintillators was 200 m^2, the average counting rate $I_{90} = 1.2 \times 10^7$ per 4 min) and at $E_{k\min} \approx 20$ MeV (the effective area was 6.9 m^2 and $I_{20} = 3.6 \times 10^6$ per 4 min). The observations were carried out since 1975. The main characteristics of the phenomenon, accompanied by heavy rains and thunderstorms with atmospheric electric field $E \geq 20 kV/m$, were found to be the following. There were short term CR intensity fluctuations (the time between maximum and minimum intensity about 8–16 min, the duration of fluctuations not more than 15–20 min, and total duration of phenomenon was up to 5 hours, about the same as duration of thunderstorm); the increase in I_{90} does not exceed 0.5–0.7% (usually 0.2–0.3%) and the respective decrease is smaller than 2–3% (usually 0.8–1.5%), the variations in I_{20} are, as a rule, larger than in I_{90} (by a factor of 1.2 on average). Fig. 8.1.1 shows the event on July 13, 1984 correlated with rain and great atmospheric electric field fluctuations. It can be seen that during 14.00–17.00 LT there were large variations of $E(h_o)$ and CR intensities I_{90} and I_{20}, but not of ground pressure h_o and ground temperature $T(h_o)$. Alexeenko et al. (1985) came to conclusion that the main cause of the observed CR fluctuations can only be the acceleration and deceleration of charged particles by atmospheric electric field. Alexeenko et al. (1985) mentioned that possible changing in the air temperature at high altitudes cannot be considered to be the main cause of the observed variations, since in this case according to Dorman's theory (M1957, M1972), the effect for I_{90} is expected to be bigger than for

I_{20}, in total contradiction with the observations. This investigation was continued in Alexeenko et al. (1987, 2001).

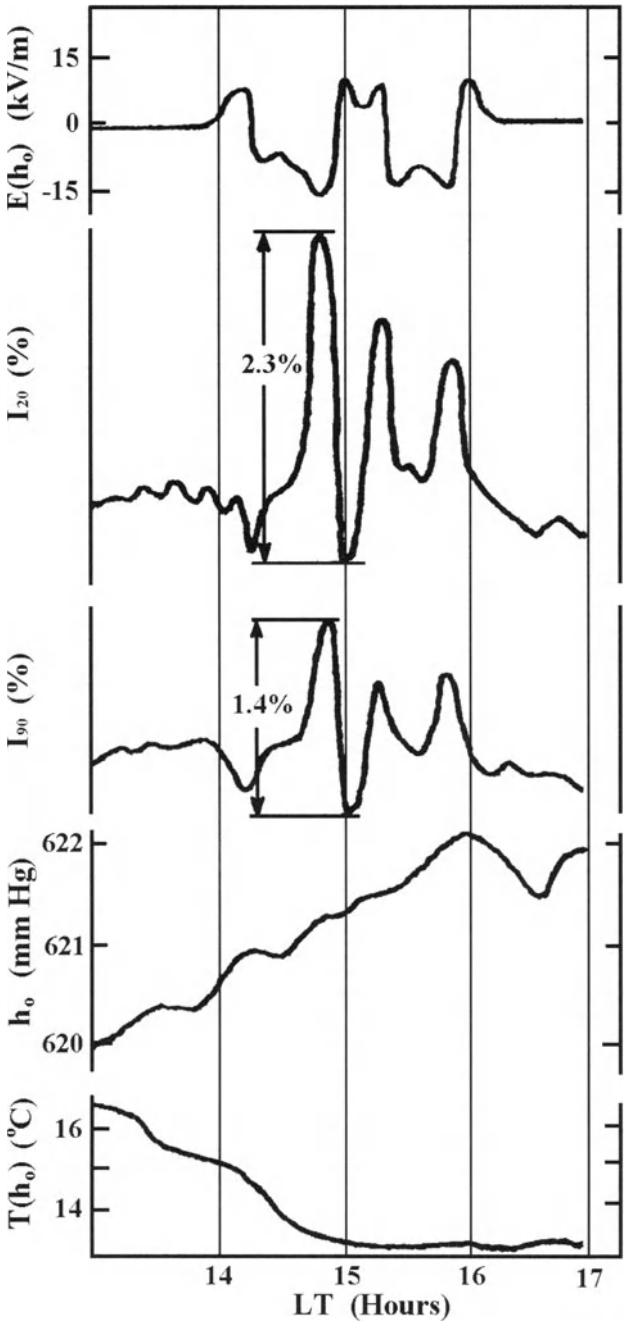

Fig. 8.1.1. The event of July 13, 1984. Explanations are in the text. According to Alexeenko et al. (1985).

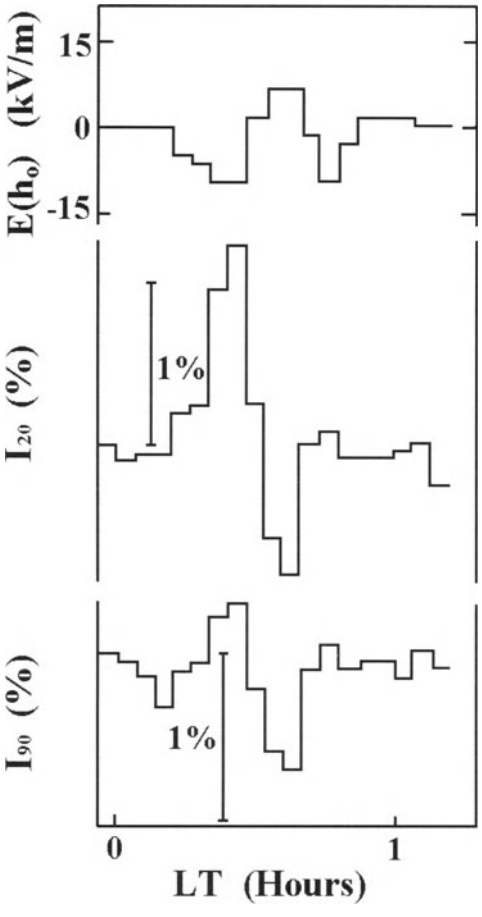

In Fig. 8.1.2 is shown what is typically observed in I_{20} and in I_{90} in connection with strong variations of atmospheric electric field $E(h_o)$ on the level of CR measurements. In Fig. 8.1.3 is shown an example of negative correlation of I_{20} with $E(h_o)$ in the period of the thunderstorm on September 7, 2000, and in Fig. 8.1.4 the correlation of I_{90} with $E(h_o)$ in the period of the thunderstorm on September 24, 2000. On September 7, 2000 strong enhancements in I_{20} with amplitude up to 20% were observed without sufficient variations in I_{90} (see Fig. 8.1.5). The statistical results of the connection of amplitudes of variations of I_{20} and I_{90} with $E(h_o)$ are shown in Fig. 8.1.6 and 8.1.7.

Fig. 8.1.2. Variations typically observed in I_{20} and in I_{90} in connection with strong variations of atmospheric electric field $E(h_o)$ on the level of CR measurements. According to Alexeenko et al. (1985, 1987).

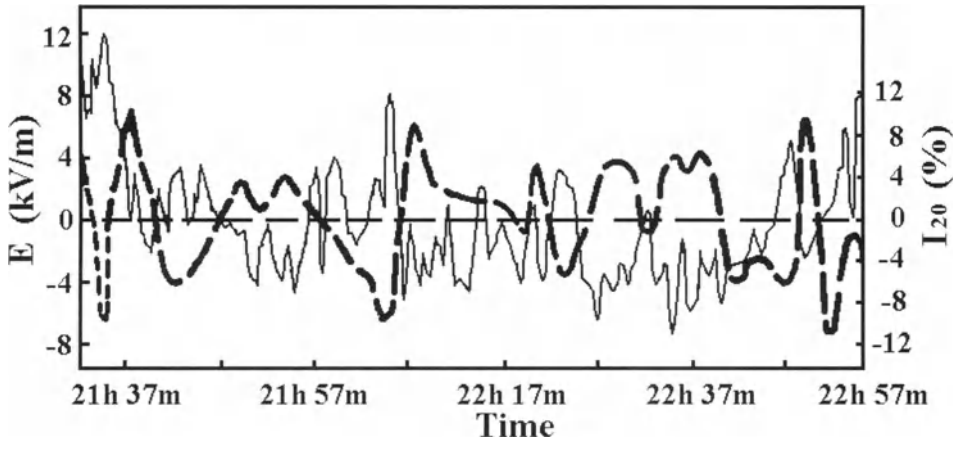

Fig. 8.1.3. An example of negative correlation of I_{20} (thick curve) with $E(h_o)$ (thin curve) in the period of thunderstorm on September 7, 2000. According to Alexeenko et al. (2001).

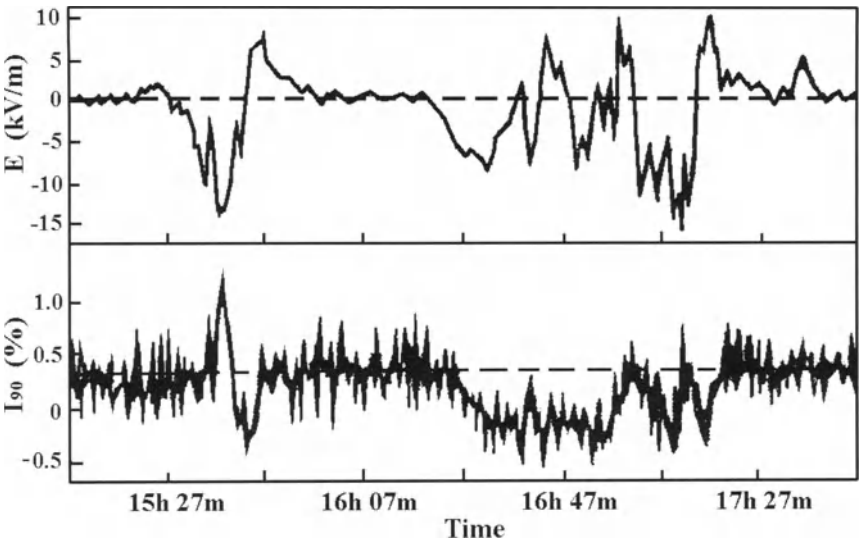

Fig. 8.1.4. An example of correlation of I_{90} with $E(h_o)$ in the period of thunderstorm on September 24, 2000. According to Alexeenko et al. (2001).

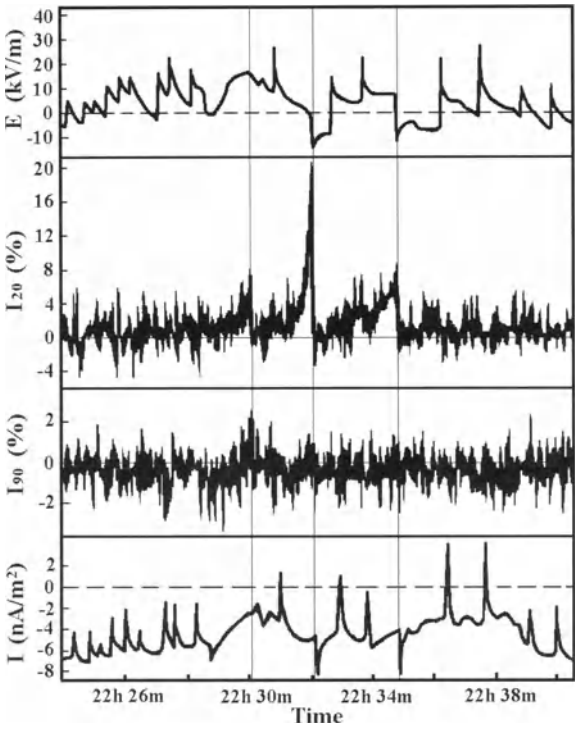

Fig. 8.1.5. A strong enhancements in I_{20} with amplitude up to 20% (without sufficient variations in I_{90}) on September 7, 2000. According to Alexeenko et al. (2001).

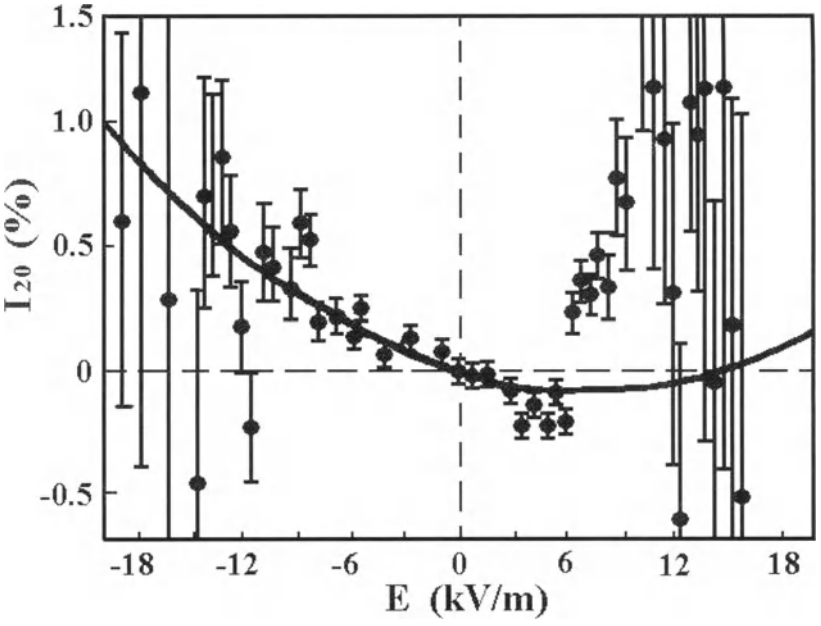

Fig. 8.1.6. The statistical results of connection of amplitudes of variations of I_{20} with $E(h_o)$. According to Alexeenko et al. (2001).

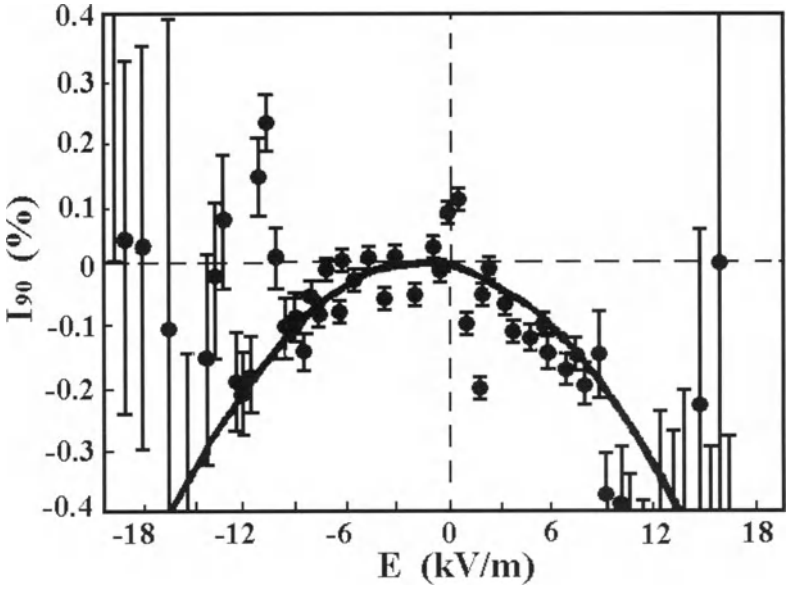

Fig. 8.1.7. The same as in Fig. 8.1.6, but for I_{90}. According to Alexeenko et al. (2001).

The detail investigations of atmospheric electric field effects in CR on the Baksan EAS array were continued in Alexeenko et al. (2002), Khaerdinov et al. (2003a-d). For

measurements of distance to lightning discharges Khaerdinov et al. (2003a) developed a special detector (see Fig. 8.1.8).

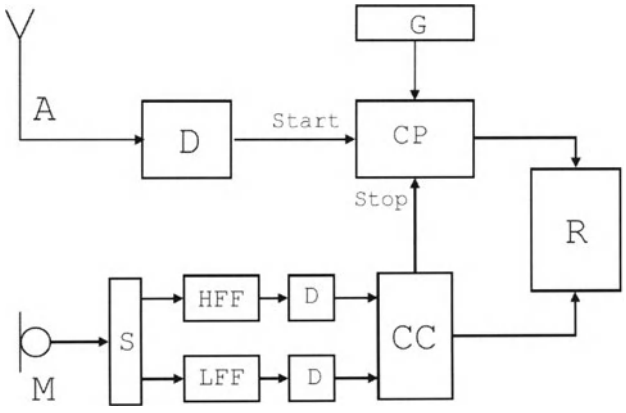

Fig. 8.1.8. A block diagram of measuring the distance to lightning. A and M are, respectively, an antenna and a microphone. D means discriminator, S is splitter, HFF and LFF represent HF and LF filters, CC is the coincidence circuit, G is generator, CP is the counter of pulses, and R is the recording system. According to Khaerdinov et al. (2003a).

For example, for Δt = 540 s (far from lightning instants) the average effect in the soft component I_{20} is found to equal to –0.0382 ± 0.0015 % per kV/m (Khaerdinov et al., 2003d).

8.2. Possible explanations of the observed atmospheric electric field effects in CR

Alexeenko et al. (2001) assumed that the observed electric field effects in I_{90} (mostly the muon component) can be understood in the framework of Alexeenko et al. (1987) model by taking into account the influence of atmospheric electric field with some profile $E(h)$ on energy of muons, and through this on absorption and decay of muons, resulting in the influence of atmospheric electric field on muon intensity.

Alexeenko et al. (2001) suggested that for electric field effects in I_{20} (mostly the electron–photon component) two mechanisms can be important: one is caused by the influence of atmospheric electric field on propagation of CR secondary electrons of equilibrium (generated by decay of muons) and non-equilibrium (electromagnetic cascades generated by decay of neutral pions on two gamma-quanta) electron-photon components. The second mechanism can be caused by direct acceleration of electrons in EAS and knock-out electrons by atmospheric electric fields in periods before or during thunderstorms, as suggested many years ago by Wilson (1925) and recently developed by Gurevich at al. (1992, 1999). The inverse influence of CR on atmospheric electric field phenomena, and, in particular, on lightning processes is also very important (see review in Gurevich and Zybin, 2001; we will consider this problem in Chapter 11).

Dorman (1987) showed that the atmospheric electric field effect in hard muon CR component mainly can be understood in the framework of general theory of CR

meteorological effects (Dorman, 1954a,b; M1957; M1972), if the following are taken into account:

1) the existence of a small positive excess in the secondary components of CR near the sea level and on mountain heights (because primary CR are mostly protons, α–particles and heavier nucleus).
2) acceleration and deceleration of secondary CR particles by atmospheric electric field are relatively small in comparison with energy looses on ionization and can be described as effective change of energy losses (decreasing at acceleration and increasing at deceleration).

Dorman (1987) came to the conclusion that the atmospheric electric field effects in any CR secondary components can be described in the frame of general theory of CR meteorological effects by calculating of the small changes in the integral multiplicities due to acceleration and deceleration of secondary charged CR particles by atmospheric electric fields. This theory was developed in Dorman and Dorman (1995a,b), Dorman et al. (1995), Dorman and Dorman (1999, 2000), and is described below in Sections 8.5–8.7. In these papers it was also shown that atmospheric electric field effects must be not only in charged secondary components, but are expected in neutron monitor counting rates for total intensity and for different multiplicities as well (Section 8.8). More recently atmospheric electric field effects in neutron component were experimentally discovered by observations on Mt. Hermon (Dorman et al., 2001, 2002). These experimental results will be described in Section 8.9.

The atmospheric electric field influences not only on the energy of positive and negative muons, but also accelerates and decelerates electrons and positrons of secondary electron-photon component as well as electrons and positrons in EAS (External Atmospheric Showers), accompanied by increasing of bremsstrahlung X-ray and gamma-ray radiation and by short time variations in intensity of electron-photon component and in EAS counting rate. Evidence of these effects was obtained in many experimental investigations: Shaw (1967), Parks et al. (1981), McCarthy and Parks (1985), Eack et al. (1996), Eack and Beasley (1996), Suszynsky and Roussel-Dupre (1996), Cecchini et al. (1997), Aglietta et al. (1999), Brunetti et al. (2000), Takami et al. (2001), Vernetto et al. (2001), Khaerdinov et al. (2003a-d), Muraki et al. (2003), Cattani et al. (2003). Important results were obtained by CR observations on the top of Gran Sasso (see Section 8.3) and on Mt. Norikura (Section 8.4). For example, according to Aglietta et al. (1999), Brunetti et al. (2000), Vernetto et al. (2001), on the top of Gran Sasso in periods of strong thunderstorms the counting rate of EAS (generated by primary particles with energy > 80 TeV) during periods 10–20 minutes increases by 10–15% accompanied by similar effects in the single ionizing particle rate in scintillators (threshold energy of electrons 3.0 ± 0.5 MeV). The observed effects can be explained by mechanism developed in Gurevich et al. (1992, 1999): EAS electrons with energy $E > E_c \approx 1$ MeV moving inside an atmospheric electric field of magnitude larger than $100 - 200$ kV/m are accelerated and initiate an electron avalanche (owing to collisions with air molecules they can generate knocked–out electrons with $E > E_c$ that in turn are accelerated and produce new knocked–out electrons and so on, the number of electrons increases exponentially and initiated 'runaway' electron process). This mechanism can play important role also for generation of discharges lightning between electrically charged cloud and ground, and between two clouds (see in detail below, Ch. 11).

8.3. Observations on the top of Gran Sasso

Aglietta et al. (1999) investigate the temporal variations of the environmental radiation (secondary CR and airborne radionuclides) correlated with rainfalls and thunderstorms. The data are provided by a NaI(Tl) detector (sensitive to gamma rays of energyE > 0.1 MeV) and by the EASTOP (air shower array, sensitive to particles of energy E > 2.5 MeV and E > 25 MeV and detecting EAS generated by primary CR of energy above 100 TeV).

8.3.1. Observations with NaI(Tl)

The NaI(Tl) detector consists of a cylindrical NaI(Tl) monocrystal with hight 10 cm and diameter 20 cm with sides and bottom shielded by 1.0 cm Pb, 0.2 mm Cu and 0.3 mm Al. During four months of operation (from July 5 to November 4 1996) the following data sets have been obtained: a) Counting rate per minute in the energy range 0.4–20 MeV (including both radioactivity and secondary CR); b) Counting rate per hour in the energy range 0.1–2.8 MeV (radioactivity+ secondary CR); c) Counting rate per hour in the energy range 3–10 MeV (secondary CR); these data are corrected for the atmospheric pressure effect, the barometric coefficient being $\beta = -(0.50 \pm 0{:}04)\%/\text{mbar}$. In a few occasions of perturbed weather significant increases in the counting rates have been observed in all data sets. In Fig. 8.3.1 an event with particular interesting features, occurred on July 11, 1996 is shown.

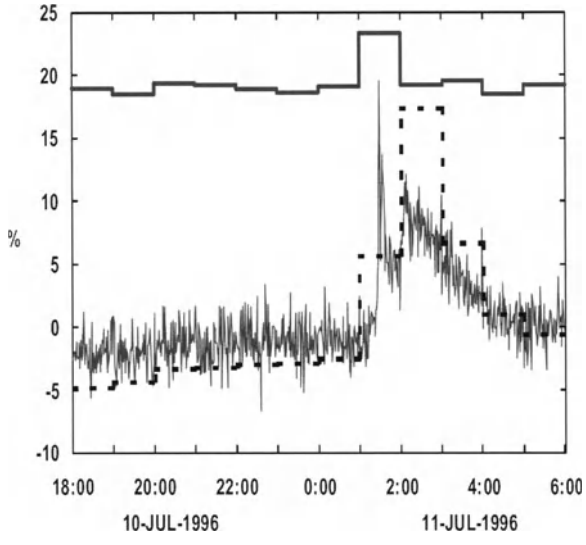

Fig. 8.3.1. Data of NaI(Tl) measurements during the event of July 11, 1996. Thin line: percent increase of the counts per minute at energy range 0.4-20 MeV (radioactivity + secondary CR); thick dashed line: hourly counting rates in the energy range 0.1-2.8 MeV (radioactivity + secondary CR); thick continuous line: hourly counting rate in the energy range 3-10 MeV (only secondary CR). According to Aglietta et al. (1999).

From Fig. 8.3.1 can be seen that the counting rate in the energy range 0.4–20 MeV (radioactivity+ secondary CR) shows a fast increase, lastings about 10 minutes, of magnitude exceeding 20%, superimposed to a slower and smoother one, lasting few

hours. It is interesting to note the different behaviors of the hourly counting rates in the two different energy ranges: intensity in 0.1–2.8 MeV range (radioactivity+ secondary CR) follows the curve of 0.4–20 MeV, while in the 3–10 MeV range (only secondary CR) it shows an increase only at the time of the first peak, demonstrating that the long duration increase is a lower energy effect. These data suggest that the short duration increase and the longer one, even if both produced in conditions of perturbed weather, could have a different origin.

8.3.2. Observations with EASTOP

The EASTOP electromagnetic detector is made of 35 plastic scintillators (each of area 10 m^2 and thickness 4 cm) spread over an area of about 10^5 m^2. Results for the event of July 11, 1996 are shown in Fig. 8.3.2.

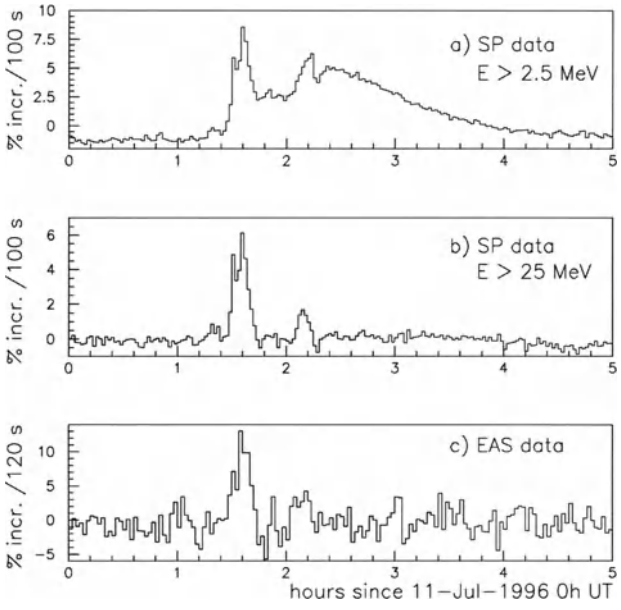

Fig. 8.3.2. EASTOP data during the July 11 event: *a*) percent increase of the single particle counting rate for detector energy E > 2.5 MeV; *b*) single particle counting rate at E > 25MeV; *c*) Extensive Air Shower rate. According to Aglietta et al. (1999).

Results shown in Fig. 8.3.2 are based on two data sets which are used in analysis of Aglietta et al. (1999):

SP (single particle) data: the single particle counting rate of any individual scintillators recorded every 100 seconds at an energy threshold E_{th} = 3:0 ± 0:5 MeV. Ten out of the 35 detectors have an additional wooden cover that increases the energy threshold of charged particles to E_{th} = 25MeV. The average SP counting rate is ~ 500 and 400 m^{-2} s^{-1} respectively for "external" and "covered" detectors. The SP counting rate is mostly due to secondary particles (muons and electrons) generated in the atmosphere by low energy primary CR and is modulated by the atmospheric pressure, the 24 hours anisotropy and

the solar activity. Besides these modulations, significant increases in the SP counting rate are observed in coincidence with rainfalls and thunderstorms. The increase usually starts with the beginning of the rain and reaches a magnitude of the order of ~ 5–15% in a time of ~ 0.5–1 hour; when the rain stops the counting rate returns to its normal value with a slow decay, lasting few hours.

EAS data: Extensive Air Showers generated by primary CR of energy E > 100 TeV (with the trigger condition requires at least 5 contiguous detectors hit in a time coincidence of 300 ns, the trigger rate is about 28 s^{-1}.

In Fig. 8.3.2 (panels *a* and *b*), the SP counting rate of EASTOP detectors are shown during the increase occurred on July 11 1996. The panel *a*, corresponding to "external" detectors, shows the same temporal behavior as the NaI(Tl) in the energy range 0.4-20 MeV (compare with Fig. 8.3.1), while panel *b* corresponding to "covered" detectors shows only two short duration peaks. These observations agree with the NaI(Tl) detector data and confirm the observed difference in the energy range between long duration and short duration increases.

Concerning EAS data, a significant excess in the air shower counting rate is observed in coincidence with the short duration peaks (see panel *c* in Fig. 8.3.2). During the first peak the increase reaches a magnitude of more than 10% and lasts ~ 10 minutes (an interesting feature is the arrival directions of the excess showers, about perpendicular to the ground at the EASTOP site, i.e. an irregular mountain slope of about 15° oriented to South).

Aglietta et al. (1999) mentioned that in a few other occasions similar events have been also observed. All of them have a similar behavior: a short duration (10–15 minutes) increase of the air showers counting rate, superimposed to a slower increase of the single particle one (the shower increase always occurs when the single particle counting rate is still raising). In one occasion an operator could report the local weather conditions during an air showers increase and he verified that a thunderstorm was in progress, with lightnings and hail fall. These events are quite rare, while the long duration increases in the single particle counting rate appear to be strongly correlated with rainfalls.

8.3.3. On the different nature of long and short duration events: relative role of radioactive aerosols and AEF

Aglietta et al. (1999) came to conclusion that two different types of counting rate increases have been observed in described above measurements:

Long duration event: an increase directly related to rainfalls, observed in the energy range E < 3 MeV; it lasts a few hours and has a slow decrease.

Short duration event: a ~10 minutes increase, observed also at energies E > 3 MeV, usually superimposed to a slow increase of type A; this type of event is accompanied by a significant excess of the air shower counting rate.

According to Aglietta et al. (1999) a possible explanation of **long duration events** could be related to the gamma ray emission from radioactive aerosols transported to the ground by the rain, as Radon daughters (that, as it is well known, constitute condensation nuclei for raindrops). This 'washout' effect interpretation is supported by the results obtained from the difference between the spectrum measured during the increase and the spectrum in normal conditions. In Fig. 8.3.3, showing such difference spectrum with the

identification of the photoelectric peaks, the contribution of gamma decays from Radon daughters is visible: similar events according to Cecchini et al. (1997) were observed during a measurements on board of the ship 'Italica' along the Ravenna – Terra Nova Bay – Ravenna course of the XI Italian expedition to Antarctica, when with the aid of a meteorological station, it was possible to pinpoint the coincidence of precipitations with increments in the detector counting rate and ascribe them to gamma emission from Radon daughters.

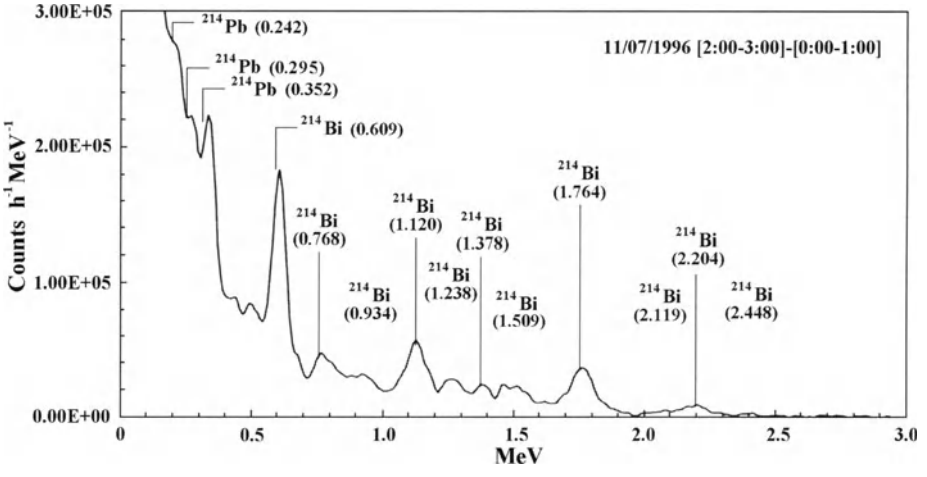

Fig. 8.3.3. Difference between the spectrum obtained during the counting rate increase occurred on July 11, 1996 and the spectrum obtained in normal conditions. The gamma ray photoelectric peaks of the Radon daughters are well identified. According to Aglietta et al. (1999).

Concerning the origin of **short duration events**, atmospheric pressure effects can be excluded since the data are corrected for pressure variations. An increase of the primary CR flux is excluded as well by contemporary measurements by the neutron monitors at Rome and Jungfraujoch. According to Aglietta et al. (1999) a possible origin of short duration events can be due to the effect of strong atmospheric electric fields on the propagation of the secondary CR particles. As it was considered in Section 8.1, variations of the single particle counting rate (of energy E > 20 MeV and E > 90MeV) have been observed by the BAKSAN air shower array in correlation with electric field variations during thunderstorms: it was observed the same time duration as the events on Gran Sasso, while the amplitudes are smaller (less than 3%) and with both signs (i.e. increases and decreases are observed, while only increases are observed in the Gran Sasso experiment). Aglietta et al. (1999) assumed that can be effective direct secondary CR particle acceleration by AEF (Dorman and Dorman, 1995a,b) as well as the mechanism developed in Gurevich et al. (1992, 1999): the EAS electrons can be accelerated by electric fields of magnitude more than some critical field $E_c \approx 1–2$ KV cm^{-1} and initiate an 'avalanche' process producing more and more fast electrons by collisions with air molecules (see in detail in Chapter 11). The process would be more effective on larger and more energetic air showers. Such effect would increase the size of air showers (total number of secondary CR particles in shower) and consequently increase the rate of the events observed over a given detection threshold.

8.4. Atmospheric electric field effects in charged CR components and in NM counting rate on Mt. Norikura

8.4.1. Particle acceleration in thunderstorms over Mt. Norikura during 4–8 August 2000

Takami et al. (2001) present evidence for particle acceleration in several events of thunderstorms using the large area (64 m^2) proportional counters and scintillators array located at Mt. Norikura CR Observatory at an altitude of 2770m. More detail results were obtained for the period 4–8 August 2000. Atmospheric conditions at Mt. Norikura in the Japanese Alps during the 4–8 August 2000, were very unstable: thunderstorms developed, followed by rainfall lasting several hours. In Fig. 8.4.1 are shown results of observations at 8 August 2000.

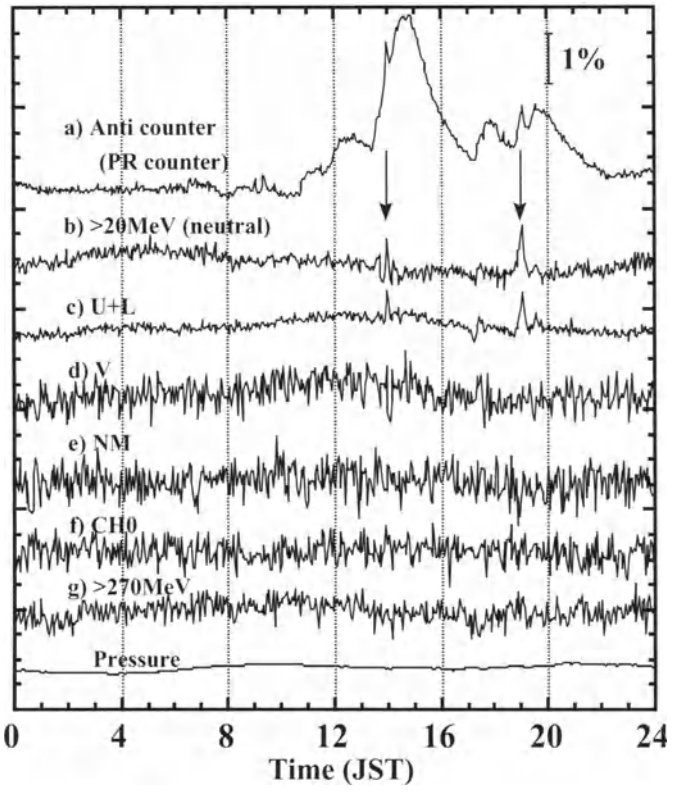

Fig. 8.4.1. The time profile of the counting rate on August 8th 2000 at Mt. Norikura: (a) 64 m^2 proportional counters, (b) 64 m^2 scintillation counters with anti-counters, (c) 36m^2 scintillation counter without anti-counters, (d) the same detector but for the coincidence channel, (e) the neutron monitor 10NM-64, (f) 1 m^2 ×50 cm plastic scintillation detector, (g) the > 270 MeV channel of the 64 m^2 detector. As shown by the arrow, at 14 JST and 19 JST, two spikes can be seen, as an evidence for electrons produced by the thunderstorm run down mechanism. The excess could not be seen at higher channel of which deposit energy is higher than 270 MeV. The data show 3 minutes value. The scale is indicated by the barred line indicating 1%. According to Takami et al. (2001).

According to Takami et al. (2001), during the period of rainfall the large area (64 m^2) proportional counters showed an **long duration increase** which must be caused by low energy gamma rays (presumably from the radon family, e.g. Bi-214, 609 keV). As the rainfall decreased the count rate decreased gradually. This observation of long duration event is in accordance with results obtained on Gran Sasso (see Section 8.3.3). On Mt. Norikura were observed also **short-lived events**. As can be seen from panels **b** and **c** of Fig. 8.4.1 there were sharp and short lived (~ 10 min) enhancements at about 14.00 JST and about 1900 JST corresponding to the start and end of the rainfall respectively (the data shown in panel **b** was taken from the 64 $m^2 \times 20$ cm thick plastic scintillators and that shown in panel **c** – from a 36 $m^2 \times 5$ cm thick plastic detector having a double layer structure). Coincidences between signals in the double layer structure are shown in panel **d** and the neutron monitor data are shown in panel **e**. It is evident from these results that **short-lived events** were not produced by protons (the anti-coincidence circuit worked), nor by muons (which would easily penetrate two layers of the 36 $m^2 \times 5$ cm detector), nor by neutrons/hadrons (there is no increase in the 10NM-64 neutron monitor). Takami et al. (2001) conclude that the signal must be caused by gamma rays with energies exceeding 40 MeV, since the scintillators threshold for charged particles (electron-positron pairs) was set at over 20 MeV. The energy of electrons that produced the gamma rays must have been > 100 MeV.

8.4.2. On the monthly and daily distributions of AEF effects in CR

The investigations of thunderstorm effects in CR on Mt. Norikura were continued by Muraki et al. (2003). AEF events in CR were selected using the criterion that the variation of CR intensity should exceed 1% in the U+L channel of the 36 $m^2 \times 5$ cm thick plastic detector having a double layer structure. In Fig. 8.4.2. is shown the monthly distribution of the thunderstorm events obtained on the basis of 11 years observations on Mt. Norikura from 1991 up to 2001. From Fig. 8.4.2 it is evident that the thunderstorm effects in CR are most frequent during the summer but also occur in the winter.

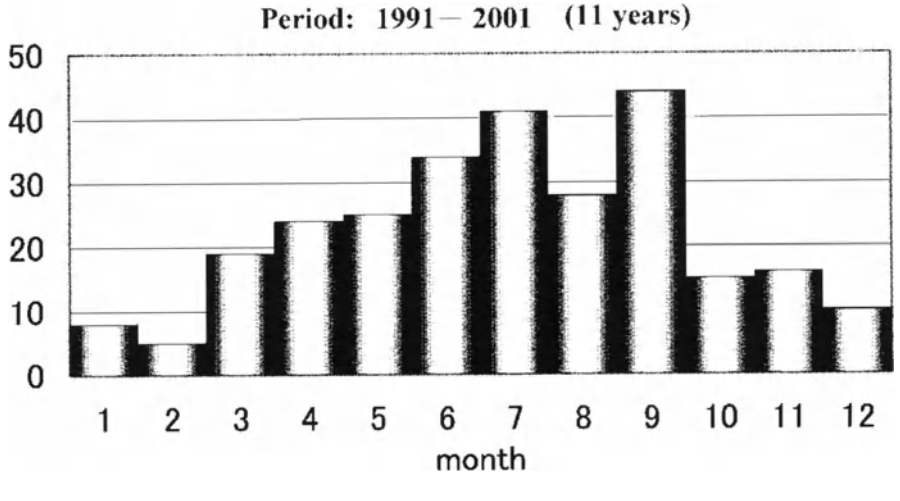

Fig. 8.4.2. Monthly distribution of the thunderstorm effects in CR. According to Muraki et al. (2003).

A periodicity analysis using the maximum entropy method (Fig. 8.4.3) indicates that there is a periodicity of about 26 days. Muraki et al. (2003) suggest that this might be associated with the solar activity since this period lies between the synodic and sidereal periods of the Sun.

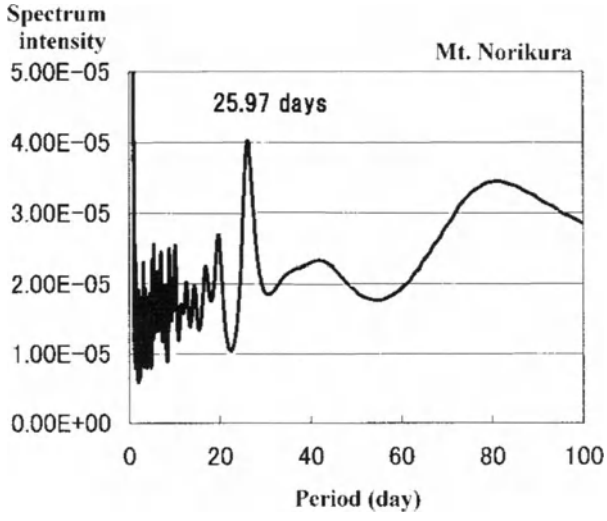

Fig. 8.4.3. Periodicity of days with thunderstorms effects in CR on Mt. Norikura. According to Muraki et al. (2003).

8.4.3. AEF influence on CR at 17 July 2002: NM and charged component data

According to Muraki et al. (2003) very interesting event of AEF influence on CR was observed on Mt. Norikura at 17 July 2002 (see Fig. 8.4.4, where are shown CR data from different detectors together with data from the AEF mill). The electric field was measured to be +17 kV/m between 09.40 and 10.30 local time while between 10.30 and 11.30 it was measured as −12 kV/m. The neutron monitor showed two 3σ enhancements between 09.50 and 10.55. According to Muraki et al. (2003), several interesting events were observed during the summers of 2001–2002. In particular, it was found an event in which the soft component was increased by a positive electric field, whereas on the Baksan it was observed such increases only during periods of negative electric field (see Section 8.1). Thus, in the event of 17 July, 2002, increases of the soft component were seen with both positive and negative AEF (see Fig. 8.4.4) and moreover, the neutron monitor recorded short enhancements in the middle of each increase. By the opinion of Muraki et al. (2003), these NM enhancements can be the result of proton acceleration by a positive electric field. Hence there must have been a region of positive field continuously above Mt. Norikura between 09.40 and 11.30 even though the field at ground level measured by the AEF mill was sometimes negative. Let us note that as it was shown by Dorman and Dorman (1995a,b), the cause of NM enhancements more probably are negative muons acceleration and their capture by lead nucleuses inside NM with formation mesoatoms and then generation of additional neutrons (see in more details in Dorman et al., 2001, 2003, and below in Sections 8.8 and 8.9).

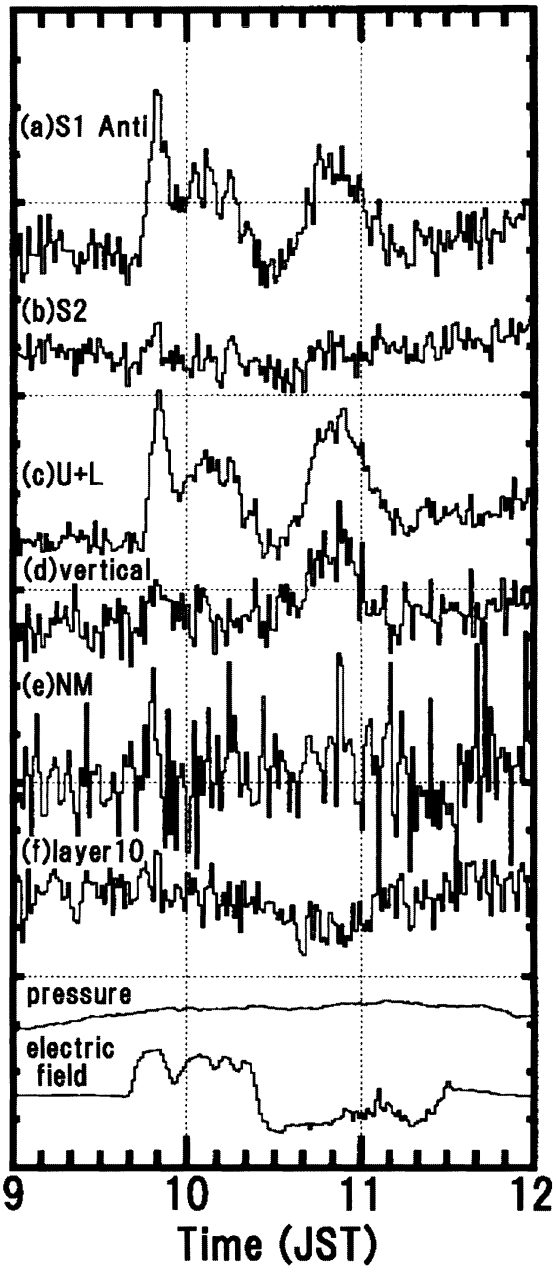

Fig. 8.4.4. Time profile of July 17th, 2002 event. (a) 64 m^2 scintillation counters with anti- coincidence (photons E > 20 MeV), (b) 64 m^2 scintillation counters without anti-coincidence (E > 40 MeV), (c) 36 m^2 scintillation counters without anti-coincidence, (d) the same detector but for coincidence channel, (e) the neutron monitor 10NM-64 and (f) 64 m^2, the bottom proportional counters (E > 110 MeV). The scale divisions correspond to 0.5% variation for (a), (b), (c) and 1% for (d), (e), (f). For electric field, the division correspond to 10 kV/m. According to Muraki et al. (2003).

8.4.4. Possible causes of the difference of AEF effects in CR in Baksan valley and on Mt. Norikura

According to opinion of Muraki et al. (2003), the difference between the observations made in the Baksan valley (Section 8.1) and on Mt. Norikura is perhaps the result of differing local topographies. As indicated in Fig. 8.4.5, observations at Baksan are made in a valley where the negatively-charged region is ~ 2 km above the ground, whereas at Mt. Norikura, the CR Observatory is on the top of the mountain, usually in the clouds, and may penetrate the negatively-charged region as well as being often in the positively-charged region.

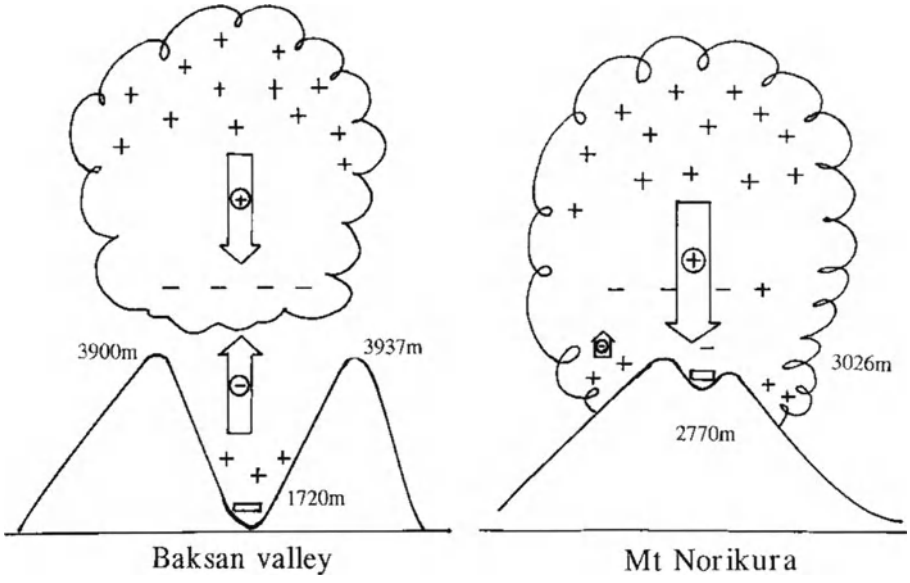

Fig. 8.4.5. A hypothetical picture of the charge distribution in clouds, for Baksan valley and Mt. Norikura. Symbols ⊕ and ⊖ represent positive and negative AEF directions respectively. According to Muraki et al. (2003).

8.4.5. Monte Carlo simulations of expected AEF effects in CR data on Mt. Norikura

A Monte Carlo simulation of the behavior of muons below 10 km altitude has been made in Muraki et al. (2003) using the GEANT 4 program, modified to allow for the presence of a vertical electric field in the atmosphere. It was assumed the spectrum of muons observed at 10 km altitude and the observed ratio $\mu^+/\mu^- \approx 1.5$ according to Grieder (M2002) as inputs (see also above in Section 2.5, Chapter 2). Preliminary results on the Monte Carlo simulation are shown in Fig. 8.4.6. As can be seen in panel **(a)** of Fig. 8.4.6, electrons and positrons with energies > 40 MeV shows a net increase with the electric field which approaches 100 kV/m. The reason for the increase is that in a positive electric field, positive muons are preferentially accelerated and these decay into positrons which in turn produce bremsstrahlung photons that can be detected in the 'S1

Anti' channel of the system on Mt. Hermon. The Monte Carlo calculation suggests that an increase at small negative electric fields (about −5 kV/m) is produced by the acceleration of knock-on electrons (Takami et al., 2001; see also Section 8.4.1)). The variation of the expected variations of > 1 GeV muon flux with electric field strength is shown in the panel **(b)** of Fig. 8.4.6.

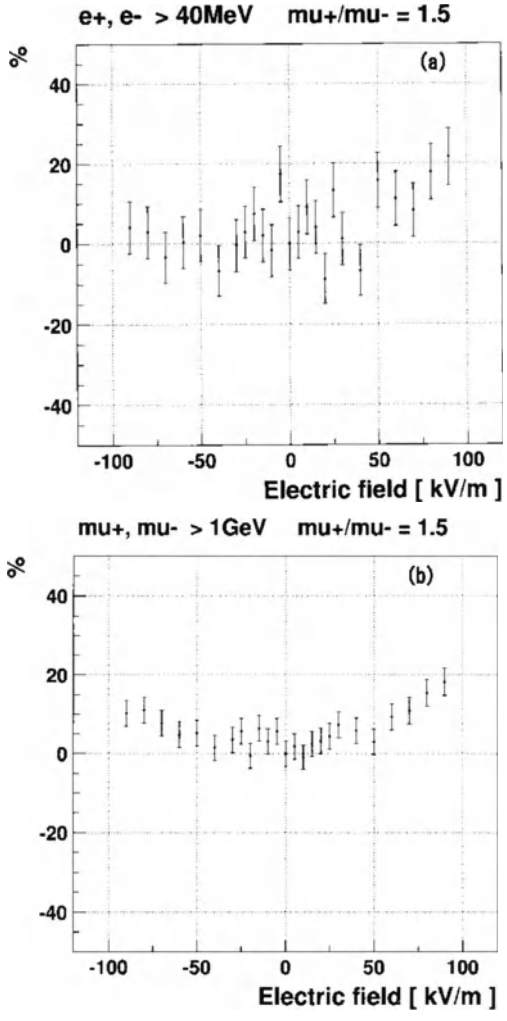

Fig. 8.4.6. Results of a Monte Carlo calculations for **(a)** electrons and positrons induced by muons (E > 40 MeV) and **(b)** the variation (in %) of muon flux with E > 1 GeV. According to Muraki et al. (2003).

According to Takami et al. (2001), Muraki et al. (2003) by observations on Mt. Norikura were obtained evidence that, in association with thunderstorms, charged particles (probably electrons) were accelerated to energies higher than 40 MeV (perhaps higher than 100 MeV) in the atmosphere somewhere above the detector; it is proposed that the observed effect in CR is the result of the acceleration of high energy knock-on electrons or decay electrons of muons.

8.5. The general theory of atmospheric electric field effects in the CR secondary components

Any secondary CR component $I_i(h_o,R_c,g,T(h),e(h),\mathbf{E}(h))$ of type i observed at the level of air pressure h_o at the point with cut off rigidity R_c, gravitational acceleration g, and with vertical distributions of air temperature $T(h)$, of humidity $e(h)$ and of atmospheric electric field vector $\mathbf{E}(h)$ can be described by the relation

$$I_i(h_o,R_c,g,T(h),e(h),\mathbf{E}(h))=\int_{R_c}^{\infty}D(R)m_i(h_o,R,g,T(h),e(h),\mathbf{E}(h))dR\,, \tag{8.5.1}$$

where $m_i(h_o,R,g,T(h),e(h),\mathbf{E}(h))$ is the integral multiplicity and $D(R)$ is the primary CR spectrum out of the atmosphere. Let us suppose that at some time we have change only of the atmospheric electric field on

$$\Delta\mathbf{E}(h)=\mathbf{E}(h)-\mathbf{E}_o(h)\,. \tag{8.5.2}$$

Then from Eq. 8.5.1 for the atmospheric electric field effects we obtain

$$\left(\frac{\Delta I_i(h_o,R_c,g_o,T_o(h),e_o(h),\mathbf{E}(h))}{I_i(h_o,R_c,g_o,T_o(h),e_o(h),\mathbf{E}_o(h))}\right)_E=\int_0^{h_o}W_{iE}(h,h_o,R_c)\Delta\mathbf{E}(h)dh\,, \tag{8.5.3}$$

where the atmospheric electric field coefficient

$$W_{iE}(h,h_o,R_c)=\int_{R_c}^{\infty}\frac{\delta m_i(h_o,R,g_o,T_o(h),e_o(h),\mathbf{E}(h))}{m_i(h_o,R,g_o,T_o(h),e_o(h),\mathbf{E}_o(h))\delta\mathbf{E}(h)}W_{iR_c}(h_o,R,g_o,T_o(h),e_o(h),\mathbf{E}_o(h))dR. \tag{8.5.4}$$

In Eq. 8.5.4 the coupling function

$$W_{iR_c}(h_o,R,g_o,T_o(h),e_o(h),\mathbf{E}_o(h))=\frac{D_o(R)m_i(h_o,R,g_o,T_o(h),e_o(h),\mathbf{E}_o(h))}{I_i(h_o,R_c,g_o,T_o(h),e_o(h),\mathbf{E}_o(h))}\,. \tag{8.5.5}$$

8.6. The theory of atmospheric electric field effects in the hard muon component.

8.6.1. Expected intensity of hard positive and negative muons

Because the atmospheric electric field effects are opposite for different charged muons, let us determine the expected intensity of positive and negative muons separately. According to the theory Dorman's (1954, M1957) of atmospheric variations

of CR muon component without taking into account atmospheric electric field $(E(h)=0)$, the observed intensity of hard muons will be determined by the expression

$$I_{\mu h}(h_o, E_{\mu\min}, Z) = I^{+}_{\mu h}(h_o, E_{\mu\min}, Z) + I^{-}_{\mu h}(h_o, E_{\mu\min}, Z), \qquad (8.6.1)$$

where h_o is the atmospheric pressure on the level of observation, Z is the zenith angle, $E_{\mu\min}$ is the apparatus muon energy threshold, and indexes + and – regard to positive and negative muons. Here

$$I^{\pm}_{\mu h}(h_o, E_{\mu\min}, Z) = \int_0^{h_o} dh_2 \int_{E^{\pm}_{\pi\min}}^{\infty} dE_\pi \int_0^{h_2} dh_1 F^{\pm}(E_\pi, h_1, h_2, h_o, Z), \qquad (8.6.2)$$

where E_π is the energy of pions, h_1 is the level of pion generation, h_2 is the level of muon generation,

$$E^{\pm}_{\pi\min} = \left(E^{\pm}_{\mu\min} + \int_{h_1}^{h_o} a^{\pm}(h)dh \right)(\beta\cos Z)^{-1} \qquad (8.6.3)$$

is the lowest pion energy for producing positive and negative muons what can be detected by apparatus with threshold energy $E_{\mu\min}$ (in the case of a plane-parallel screen). In Eq. 8.6.2 function

$$F^{\pm}(E_\pi, h_1, h_2, h_o, Z) = \frac{m_\pi c}{\tau_\pi} \frac{f^{\pm}_\pi(E_\pi, h_1, Z)}{E_\pi \rho(h_2)\cos Z} \exp\left(-\frac{h_2 - h_1}{l\cos Z}\right)$$

$$\times \exp\left(-\frac{m_\pi c}{\tau_\pi E_\pi \cos Z}\int_{h_1}^{h_2}\frac{dh}{\rho(h)}\right)\exp\left(-\frac{m_\mu c}{\tau_\mu}\int_{h_2}^{h_o}\frac{dh}{\rho(h)}\left(\beta E_\pi \cos Z - \int_{h_2}^{h} a^{\pm}(h')dh'\right)^{-1}\right). \qquad (8.6.4)$$

Here $m_\pi, m_\mu, \tau_\pi, \tau_\mu$ are the appropriate rest masses and life times of charged pions and muons, $\beta = m_\mu/m_\pi$, $\rho(h)$ is air density, $a^{\pm}(h)$ is muon energy loss per 1 g/cm^2 (at $E(h)=0$, $a^{+}(h)=a^{-}(h)\approx 2$ MeV/(g/cm^2)), $f^{\pm}_\pi(E_\pi, h_1, Z)$ is the pion

generation function for positive and negative pions[1]. If $E(h)\neq 0$ then owing to acceleration or deceleration of charged muons their loses of energy will be change for positive and negative muons in opposite directions (decrease or increase correspondingly for accelerated or decelerated electric field), and in this case $a^{+}(h)\neq a^{-}(h)$.

8.6.2. Expected influence of atmospheric electric field on intensity of hard positive and negative muons

As mentioned in the previous section 8.6.1, if we take into account the atmospheric electric field, $a^{+}(h)$ and $a^{-}(h)$ for positive and negative muons become significantly different. For example, if $E(h)=+30\,\mathrm{kV/m}=+3\times10^{5}\,V/\left(\mathrm{g/cm^{2}}\right)$ near sea level ($\rho\,(h)\approx10^{-3}\,\mathrm{g/cm^{3}}$), then for vertically arriving positive muons $a^{+}(h)=1.7\,\mathrm{MeV/}\left(\mathrm{g/cm^{2}}\right)$ and for negative muons $a^{-}(h)=2.3\,\mathrm{MeV/}\left(\mathrm{g/cm^{2}}\right)$ (in this case $\Delta a^{\pm}(h)=\mp 0.3\,\mathrm{MeV/}\left(\mathrm{g/cm^{2}}\right)$ correspondingly for positive and negative muons). For the general case of muons arriving at zenith angle Z on the depth h with air density $\rho(h)$ one obtains

$$\Delta a^{\pm}(h)=\mp eE(h)\cos Z/\rho(h). \tag{8.6.5}$$

Using Eq. 8.6.2–8.6.5, we obtain for atmospheric electric field effect in positive and negative muon intensity the following changes (caused by changes in muon energy looses according to Eq. 8.6.5):

$$\Delta I^{\pm}_{\mu h}(h_o,E_{\mu\min},Z)=$$
$$-\frac{1}{\beta\cos Z}\int_0^{h_o}dh_2\int_0^{h_2}dh_1F^{\pm}\left(E^{\pm}_{\pi\min},h_1,h_2,h_o,Z\right)\int_{h_2}^{h_o}\Delta a^{\pm}(h)dh-\int_0^{h_o}dh_2$$
$$\times\int_{E^{\pm}_{\pi\min}}^{\infty}dE_{\pi}\left(\frac{m_{\mu}c}{\tau_{\mu}}\int_{h_2}^{h_o}\frac{dh\int_{h_2}^{h}\Delta a^{\pm}(h')dh'}{\rho(h)\left(\beta E_{\pi}\cos Z-\int_{h_2}^{h}\Delta a^{\pm}(h')dh'\right)^{2}}\right)\int_0^{h_2}dh_1F^{\pm}(E_{\pi},h_1,h_2,h_o,Z). \tag{8.6.6}$$

---

[1] Because primary CR out of the atmosphere are mostly positive particles (protons, α – particles and heavies nucleus), there is a positive excess in the pion generation function: $f^{+}_{\pi}(E_{\pi},h_1,Z)>f^{-}_{\pi}(E_{\pi},h_1,Z)$ (see Chapter 3).

8.6.3. Expected influence of atmospheric electric field on the total intensity of hard muons

For the relative variation of the total intensity of hard muons caused by atmospheric electric field effect we obtain from Eq. 8.6.6 with taking into account Eq. 8.6.5:

$$\left(\frac{\Delta I_{\mu h}}{I_{\mu h}}\right)_E = \frac{\left(\Delta I^{+}_{\mu h} + \Delta I^{-}_{\mu h}\right)_E}{I_{\mu h}} = I^{-1}_{\mu h} \int_0^{h_o} dh_2 E_1(h_2, h_o) \Phi(h_2, h_o, E_{\pi \min}, Z)$$

$$+ I^{-1}_{\mu h} \int_0^{h_o} dh_2 \int_{E_{\pi \min}}^{\infty} dE_\pi E_2(h_2, h_o, E_\pi, Z) \Phi(h_2, h_o, E_\pi, Z), \qquad (8.6.7)$$

where

$$E_1(h_2, h_o) = \int_{h_2}^{h_o} \frac{eE(h)dh}{\beta p(h)}; \quad E_2(h_2, h_o, E_\pi, Z) = \frac{m_\mu c}{\tau_\mu} \int_{h_2}^{h_o} \frac{dh \int_{h_2}^{h_o} dh' \left(eE(h')/\rho(h')\right)}{\rho(h)\left(\beta E_\pi \cos Z - a(h - h_2)\right)^2} \qquad (8.6.8)$$

$$\Phi(h_2, h_o, E_\pi, Z) = \int_0^{h_2} dh_1 \left(F^{+}(E_\pi, h_1, h_2, h_o, Z) - F^{-}(E_\pi, h_1, h_2, h_o, Z)\right). \qquad (8.6.9)$$

8.6.4. Absorption contribution to the atmospheric electric field effects in total hard muon intensity

The first integral in the right part of Eq. 8.6.6 and Eq. 8.6.7 describes the atmospheric electric field muon effect owed to changes of muon absorption. On the basis of calculations of integrals in Eq. 8.6.6 and Eq. 8.6.7 as made in Dorman (M1957, M1972; see also here, Section 5.1), taking into account the difference between functions of positive and negative pion production in the Earth's atmosphere $f^{+}_{\pi}(E_\pi, h_1, Z)$ and $f^{-}_{\pi}(E_\pi, h_1, Z)$ we can roughly estimate the role of the absorption contribution in the muon atmospheric electric field effect. Let us assume that $E(h) \neq 0$ only in the region between h_o and some level h_3, and have one sign. For $E(h) = 10$ kV/m and 30 kV/m, $h_o = 1000\ \mathrm{g/cm^2}$, $h_3 = 700\ \mathrm{g/cm^2}$ and $Z = 0^\circ$ (vertical direction) we obtain the expected value of the effect at sea level 0.2% and 0.6% for hard muons (10 cm Pb absorber). For Baksan station ($h_o \approx 800\ \mathrm{g/cm^2}$) at the same $h_3 \approx 700\ \mathrm{g/cm^2}$ we expect 0.22–0.36% and 0.10–0.30% for threshold kinetic energies of muons 20 MeV and 90 MeV, in a good agreement with observations of Alexeenko et al. (1985, 1987).

8.6.5. Decay contribution to the atmospheric electric field effects in total hard muon intensity

The second integral in the right hand side of Eq. 8.6.6 and Eq. 8.6.7 describes the atmospheric electric field muon effect owed to changes of muon decay. For the same

conditions that were considered in the previous Section 8.6.4 let us estimate the expected the decay contribution in the atmospheric electric field effects in the total intensity of hard muons on the sea level. The result of rough calculations is: 0.12% and 0.36% correspondingly for $E(h)=10$ kV/m and 30 kV/m. For Baksan station we estimate 0.23% and 0.69% for 20 MeV threshold energy and 0.19% and 0.57% for 90 MeV threshold energy, correspondingly for $E(h)=10$ kV/m and 30 kV/m. These values do not contradict those observed by Alexeenko et al. (1985, 1987).

8.7. The theory of atmospheric electric field effects in soft muon intensity

Atmospheric electric field effects of soft muons (muons with small energy, absorbed by 10 cm Pb) are especially interesting because they contribute in some part of the neutron monitor's and super-monitor's counting rates. We see above that this leads to the temperature effect in the neutron component (see above, Section 5.4). As will be shown in the Section 8.5, this will lead also to the appearance of atmospheric electric field effects in the neutron monitor's and super-monitor's counting rates.

8.7.1. General expression for expected intensity of positive and negative soft muons in an atmospheric electric field

The intensities of positive and negative soft muons according to Section 2.2 will be determined by the expression

$$I^{\pm}_{\mu s}(h_o,R_c,Z)=\int_0^{h_o}dh_2\int_{E^{\pm}_{\pi 1}}^{E^{\pm}_{\pi\min}}dE_{\pi}\int_0^{h_2}dh_1F^{\pm}(E_{\pi},h_1,h_2,h_o,Z), \tag{8.7.1}$$

where $F^{\pm}(E_{\pi},h_1,h_2,h_o,Z)$ was determined by Eq. 8.6.4 (see previous Section 8.6), and

$$E^{\pm}_{\pi 1}=\left(m_{\mu}c^2+\int_{h_1}^{h_o}a^{\pm}(h)dh\right)\Big/\beta\cos Z;\quad E^{\pm}_{\pi\min}=\left(E_{\mu\min}+\int_{h_1}^{h_o}a^{\pm}(h)dh\right)\Big/\beta\cos Z. \tag{8.7.2}$$

In Eq. 8.7.2 the energy losses at the existing of atmospheric electric field $E(h)$ will be

$$a^{\pm}(h)=a+\Delta a^{\pm}(h)=a\pm eE(h)/\rho(h). \tag{8.7.3}$$

8.7.2. Expected variations of positive and negative soft muon intensity in an atmospheric electric field

On the basis of Eq. 8.7.1 and Eq. 8.7.2 we obtain for the variations of positive and negative soft muons intensity in an atmospheric electric field:

$$\left(\Delta I^{\pm}_{\mu s}\right)_E = \frac{1}{\beta \cos Z}\int_0^{h_o} dh_2 \int_0^{h_2} dh_1$$

$$\times\left(F^{\pm}\left(E^{\pm}_{\pi 1}, h_1, h_2, h_o, Z\right) - F^{\pm}\left(E^{\pm}_{\pi \min}, h_1, h_2, h_o, Z\right)\right)\int_{h_2}^{h_o} \Delta a^{\pm}(h)dh - \frac{m_\mu c}{\tau_\mu}\int_0^{h_o} dh_2$$

$$\times \int_{E^{\pm}_{\pi 1}}^{E^{\pm}_{\pi \min}} dE_\pi \int_{h_2}^{h_o} \frac{dh \int_{h_2}^{h} \Delta a^{\pm}(h')dh'}{\rho(h)\left(\beta E_\pi \cos Z - \int_{h_2}^{h} a^{\pm}(h')dh'\right)^2} \int_0^{h_2} dh_1 F^{\pm}(E_\pi, h_1, h_2, h_0, Z). \qquad (8.7.4)$$

By taking into account Eq. 8.6.5 or Eq. 8.7.3 (where e is the charge of muons, and $E(h)$ is the vertical component of atmospheric electric field, positive in direction to the ground), we obtain from Eq. 8.7.4 for the relative change of positive and negative soft muon intensity caused only by atmospheric electric field effect the following expressions:

$$\left(\Delta I^{\pm}_{\mu s}/I^{\pm}_{\mu s}\right)_E = \left(I^{\pm}_{\mu s}\right)^{-1}\int_0^{h_o} dh_2 E_1(h_2, h_o)\left(\Phi^{\pm}(h_2, h_o, E_{\pi \min}, Z) - \Phi^{\pm}(h_2, h_o, E_{\pi 1}, Z)\right)$$

$$+\left(I^{\pm}_{\mu s}\right)^{-1}\int_0^{h_o} dh_2 \int_{E_{\pi 1}}^{E_{\pi \min}} dE_\pi E_2(h_2, h_o, E_\pi, Z)\Phi^{\pm}(h_2, h_o, E_\pi, Z), \qquad (8.7.5)$$

where

$$E_1(h_2, h_o) = \int_{h_2}^{h_o} \frac{eE(h)dh}{\beta \rho(h)}; \quad E_2(h_2, h_o, E_\pi, Z) = \frac{m_\mu c}{\tau_\mu}\int_{h_2}^{h_o} \frac{dh \int_{h_2}^{h} dh'\left(eE(h')/\rho(h')\right)}{\rho(h)\left(\beta E_\pi \cos Z - a(h - h_2)\right)^2}; \qquad (8.7.6)$$

$$\Phi^{\pm}(h_2, h_o, E_\pi, Z) = \int_0^{h_2} dh_1 F^{\pm}(E_\pi, h_1, h_2, h_o, Z). \qquad (8.7.7)$$

8.7.3. Absorption part of atmospheric electric field influence on soft positive and negative muon intensity

The first term in Eq. 8.7.5 describes the atmospheric electric field effect caused by absorption. According to Eq. 8.7.6 and Eq. 8.7.7 we obtain approximately:

$$\left(\Delta I^{\pm}_{\mu s}/I^{\pm}_{\mu s}\right)_{E,abs} \approx \pm E_1(h_3,h_o)\left(1-b^{\gamma+1}\right)\left(\left(m_\mu c^2 + a(h_o-L)\right)\left(1-b^{\gamma}\right)\right)^{-1}, \qquad (8.7.8)$$

where $L \approx 120\ \mathrm{g/cm^2}$ is the attenuation path of primary CR in the atmosphere, $b = E_{\pi 1}/E_{\pi\,\min}$ and γ is the power integral pion spectrum index for high energy region ($\geq 2\,\mathrm{GeV}$). Let us suppose that $E(h)$ = 10 kV/m and 30 kV/m between $h_3 = 700\ \mathrm{g/cm^2}$ and $h_o = 1000\ \mathrm{g/cm^2}$. In this case we expect for soft positive and negative muons an effect of about 2.8 % and 8.4 %, respectively.

8.7.4. Decay part of atmospheric electric field influence on soft positive and negative muon intensity

The second term in Eq. 8.7.5 describes the atmospheric electric field effect caused by the influence of acceleration and deceleration processes of muons on their decay. For this part we obtain approximately

$$\left(\Delta I^{\pm}_{\mu s}/I^{\pm}_{\mu s}\right)_{E,\mathrm{dccay}} \approx \pm\frac{Kcm_\mu \cos Z}{\rho(h_4)\tau_\mu}(h_o-h_3)\left(a(h_o-h_4)\right)^{-2}E_1(h_3,h_4), \qquad (8.7.9)$$

where $h_3 \leq h_4 \leq h_o$, the function $E_1(h_3,h_4)$ was determined by Eq. 8.7.6, and

$$K = \left(1-\frac{(\gamma+1)\left(E_{\mu\min}+m_\mu c^2\right)}{a(h_o-L)}\right)\Bigg/\left(\left(1+\frac{m_\mu c^2}{a(h_o-h_4)}\right)\left(1+\frac{E_{\mu\min}}{a(h_o-h_4)}\right)\right). \qquad (8.7.10)$$

Using the same assumptions as in Section 8.7.3, we obtain for the expected amplitude of decay part of atmospheric electric field effect 1.1% and 3.3% for $E(h)$=10 and 30 kV/m between $h_3 = 700\ \mathrm{g/cm^2}$ and $h_o = 1000\ \mathrm{g/cm^2}$.

8.8. Expected atmospheric electric field effects in neutron monitor total counting rate and in different multiplicities

8.8.1. Possible atmospheric electric field effects in neutron monitor

In Dorman & Dorman (1995), Dorman et al. (1995), the model of atmospheric electric field influence on CR was extended on the case of neutron monitor and super-monitor for total intensity, and in Dorman & Dorman (1999) also for different multiplicities. It was taken into account that some part of the neutron monitor counting rate caused by negative soft muons captured by lead nucleons and formed mesoatoms with generation of neutrons of several MeV energy from lead. In this case, the neutron monitor or neutron super-monitor works as analyzer, which detect muons of only one, negative sign. It is very important because the atmospheric electric field effect has

opposite signs for positive and negative muons that the main part of this effect in the muon telescope or in ionization chamber is compensated.

The counting rate $I_m(h_o, R_c)$ of neutron monitor total intensity ($m = t$), or different multiplicities ($m = 1, 2, 3, ...$) at the pressure level h_o and at the point with cut off rigidity R_c, is determined by

$$I_m(h_o, R_c) = I_{mN}(h_o, R_c) + I^-_{m\mu s}(h_o, R_c), \tag{8.8.1}$$

where the first term on the right hand of Eq. 8.8.1 $I_{mN}(h_o, R_c)$ reflects the main, nucleonic part of the neutron monitor counting rate (e.g. for the total neutron intensity $I_{tN}(h_o, R_c)/I_t(h_o, R_c) \approx 0.93$). This part describes the generation of neutrons in the high atmosphere and their transport down to the observation level by scattering and absorption processes (the transport path for absorption is ≈ 145 g/cm^2 ; the atmospheric electric field has practically no influence on this part). The second term on the right hand of Eq. 8.8.1 $I^-_{m\mu s}(h_o, R_c)$ reflects a very small part of the neutron monitor counting rate (e.g. for the total neutron intensity $I^-_{t\mu s}(h_o, R_c)/I_t(h_o, R_c) \approx 0.07$), caused by soft negative muons, producing lead mesoatoms with generation of neutrons in the detector (the atmospheric electric field influences only this part).

Let us denote

$$I^-_{m\mu s}(h_o, R_c)/I_m(h_o, R_c) = b_m(h_o, R_c). \tag{8.8.2}$$

Then the relative variation in neutron monitor counting rate due to the atmospheric electric field effect will be

$$\left(\frac{\Delta I_m(h_o, R_c)}{I_m(h_o, R_c)}\right)_E = \left(\frac{\Delta I^-_{m\mu s}(h_o, R_c)}{I_m(h_o, R_c)}\right)_E = b_m(h_o, R_c)\left(\frac{\Delta I^-_{m\mu s}(h_o, R_c)}{I^-_{m\mu s}(h_o, R_c)}\right)_E . \tag{8.8.3}$$

8.8.2. Formation of lead mesoatoms in neutron monitor by soft negative muons

The atmospheric electric field effect is determined mostly by soft negative muons generating lead mesoatoms with ejection of neutrons. Let us consider data on the frequency of lead mesoatoms formation in neutron monitors as a function of multiplicity and altitude. According to Nobles et al. (1967), special measurements were made in the region of middle cut off rigidity ($R_c \approx 4 - 5$ GV) and in the period of low solar activity (near 1965). It was found that the relative part of counting rate caused by formation of lead mesoatoms on the sea level is

$$b_m(h_o, R_c \le 5\ \text{GV})\Big|^{\text{s.l.}}_{\text{low SA}} = 8.94\% \text{ for } m=1;\ 6.7\% \text{ for } m=2;\ 2.6\% \text{ for } m=3\,. \quad (8.8.4)$$

For the mountain level (about 3 km) the relative part of counting rate caused by formation of lead mesoatoms is several times smaller:

$$b_m(h_o, R_c \le 5\ \text{GV})\Big|^{\text{m.l.}}_{\text{low SA}} = 1.65\% \text{ for } m=1;\ 0.68\% \text{ for } m=2;\ 0.3\% \text{ for } m=3\,. \quad (8.8.5)$$

According to these data the largest atmospheric electric field effect at low solar activity is expected at sea level for multiplicities $m = 1$ and $m = 2$. At the mountain level the atmospheric electric field effect is expected to be about 5 times smaller (it is caused by much faster increase with increasing of altitude of the secondary neutron intensity in comparison with the secondary muon intensity).

8.8.3. Dependence of lead mesoatoms formation in neutron monitor on cut off rigidity and solar activity

The relative part of neutron monitor counting rate caused by formation of lead mesoatoms is directly proportional to muon component intensity and inversely proportional to nucleonic component intensity. The muon component intensity decreases from $R_c \le 2$ GV to $R_c \approx 15$ GV only by about 10%, but intensity of neutron component decreases by about 50%. This means that the relative part of neutron monitor counting rate caused by the formation of lead mesoatoms is expected to increase by about 40% from $R_c \le 2$ GV to $R_c \approx 15$ GV, and that on sea level this part will be increase and as result we expect:

$$b_m(h_o, R_c \approx 15\ \text{GV})\Big|^{\text{s.l.}}_{\text{low SA}} = 12.5\% \text{ for } m=1;\ \ 9.4\% \text{ for } m=2;\ \ 3.6\% \text{ for } m=3\,. \quad (8.8.6)$$

From the minimum to the maximum of solar activity at $R_c \le 5$ GV intensity of muon component decreases by about 6% and neutron component by about 20%; it means that the relative part of neutron monitor counting rate caused by formation of lead mesoatoms expected to be increase by about 14% from minimum to maximum of solar activity, and as result we expect:

$$b_m(h_o, R_c \le 5\ \text{GV})\Big|^{\text{s.l.}}_{\text{high SA}} = 10.2\% \text{ for } m=1;\ 7.6\% \text{ for } m=2;\ 3.0\% \text{ for } m=3\,. \quad (8.8.7)$$

Near equator ($R_c \approx 15$ GV) from the minimum to the maximum of solar activity intensity of muon component decreases by about 4% and intensity of neutron component by about 12%; it means that the relative part of neutron monitor counting rate caused by formation of lead mesoatoms expected to be increase by about 8% from minimum to maximum of solar activity, and as result we expect:

$$b_m(h_o, R_c \approx 15\ \text{GV})\Big|^{\text{s.l.}}_{\text{high SA}} = 13.5\% \text{ for } m=1;\ 10.2\% \text{ for } m=2;\ 3.9\% \text{ for } m=3\,. \quad (8.8.8)$$

8.8.4. Atmospheric electric field coefficients for total neutron monitor counting rate and for different multiplicities

Here we will use results by Dorman and Dorman (1995) of calculations of expected atmospheric electric field effect for soft muons (see also Sections 8.7.3 and 8.7.4). According to Dorman and Dorman (1995), the total atmospheric electric field coefficients for soft negative muons in the lower atmosphere can be approximated by

$$W_{\mu sE}(h,h_o,R_c)\approx 1.3\times10^{-3}\ \%(\mathrm{kV/m})^{-1}\left(\mathrm{g/cm^2}\right)^{-1}. \qquad (8.8.9)$$

By taking into account the results of Sections 8.8.2 and 8.8.3, we obtain for observations on sea level in the period of low solar activity on high and middle latitudes that

$$W_{nE}(h,h_o,R_c\le 5\ \mathrm{GV},m=1,2,3)\Big|^{\mathrm{s.l.}}_{\mathrm{low\ SA}}$$
$$\approx(11.6;\ 8.7;\ 3.4)\times10^{-5}\ \%(\mathrm{kV/m})^{-1}\left(\mathrm{g/cm^2}\right)^{-1} \qquad (8.8.10)$$

respectively for multiplicities m = 1, 2 and 3. For $E(h)\approx 30$ kV/m between $h_o=1000$ g/cm^2 and $h_3=700$ g/cm^2 this gives changes of about 1.05%, 0.75%, and 0.3% in neutron monitor counting rates for multiplicities m = 1, 2, and 3 respectively.

With increasing solar activity the total atmospheric electric field coefficients will increase slightly according to the results of Section 8.8.3, so that at the maximum of solar activity we obtain instead of Eq. 8.8.10

$$W_{nE}(h,h_o,R_c\le 5GV,m=1,2,3)\Big|^{\mathrm{s.l.}}_{\mathrm{high\ SA}}$$
$$\approx(12.5;\ 9.4;\ 3.6)\times10^{-5}\ \%(\mathrm{kV/m})^{-1}\left(\mathrm{g/cm^2}\right)^{-1}. \qquad (8.8.11)$$

The total atmospheric electric field coefficients will increase with increasing cut off rigidity. For example, for the period of low solar activity near the equator the atmospheric electric field coefficients will be (according to results of Section 8.8.3):

$$W_{nE}(h,h_o,R_c\approx 15\ \mathrm{GV},m=1,2,3)\Big|^{\mathrm{s.l.}}_{\mathrm{low\ SA}}$$
$$\approx(16.2;\ 12.2;\ 4.7)\times10^{-5}\ \%(\mathrm{kV/m})^{-1}\left(\mathrm{g/cm^2}\right)^{-1}. \qquad (8.8.12)$$

Similarly, according to the results of Section 8.8.3, for the period of high solar activity near the equator the atmospheric electric field coefficients will be:

$$W_{nE}(h,h_o,R_c\approx 15\ \mathrm{GV},\ m=1,2,3)\Big|^{\mathrm{s.l.}}_{\mathrm{high\ SA}}$$
$$\approx(17.5;\ 13.2;\ 5.1)\times10^{-5}\ \%(\mathrm{kV/m})^{-1}\left(\mathrm{g/cm^2}\right)^{-1}. \qquad (8.8.13)$$

With increasing of altitude of observations, the atmospheric electric field coefficients decrease significantly. For example, for observations on mountains (about 3 km) in the period of low solar activity on high and middle latitudes

$$W_{nE}(h,h_o,R_c \le 5\ \text{GV},\ m=1,2,3)\Big|_{\text{low SA}}^{\text{m.l.}}$$

$$\approx (2.1;\ 0.9;\ 0.4)\times 10^{-5}\ \%(\text{kV/m})^{-1}\left(\text{g/cm}^2\right)^{-1}. \qquad (8.8.14)$$

For total neutron intensity $I_t(h_o,R_c)$ atmospheric electric field coefficients can be obtained very easily by using Eq. 8.8.10–8.8.14, if we take into account that

$$I_t(h_o,R_c)=\sum_{m=1}^{\infty} mI_m(h_o,R_c). \qquad (8.8.15)$$

On the basis of Eq. 8.8.15 we obtain

$$W_{nE}(h,h_o,R_c,tot)=\sum_{m=1}^{\infty}\frac{mI_m(h_o,R_c)}{I_t(h_o,R_c)}W_{nE}(h,h_o,R_c,m). \qquad (8.8.16)$$

In Eq. 8.8.16 the summation is actually up to m = 3, because $W_{nE}(h,h_o,R_c,m\ge 4)\approx 0$ (see example of calculations of $W_{nE}(h,h_o,R_c,tot)$ for Mt. Hermon in the next Section 8.8.5).

Our conclusions are as following:

- Atmospheric electric field coefficient for observations at sea level decreases from $11.6\times10^{-5}\ \%(\text{kV/m})^{-1}\left(\text{g/cm}^2\right)^{-1}$ to $8.7\times10^{-5}\ \%(\text{kV/m})^{-1}\left(\text{g/cm}^2\right)^{-1}$ and then to $3.4\times10^{-5}\ \%(\text{kV/m})^{-1}\left(\text{g/cm}^2\right)^{-1}$ with increasing neutron multiplicity from m = 1 to m = 2 and then to m = 3.
- Atmospheric electric field coefficient increases with increasing cut off rigidity and solar activity.
- Atmospheric electric field coefficient decreases significantly with increasing altitude of measurements.
- The typical atmospheric electric field effect at sea level (for $E(h)\approx 30\,\text{kV/m}$ between $h_o = 1000\,\text{g/cm}^2$ and $h_3 = 700\,\text{g/cm}^2$) is expected to be about 1.05%, 0.75%, and 0.3% respectively for multiplicities m = 1, 2, and 3.
- Simultaneous measurements of atmospheric electric field effect in different neutron multiplicities on different latitudes and altitudes in periods of different levels of solar activity give important possibility to investigate this phenomenon in details.

8.8.5. AEF coefficients for NM on Mt. Hermon

On the basis of Eq. 8.8.10–8.8.16 we can determine atmospheric electric field coefficients for observations by neutron monitor of the Emilio Segre' Observatory on Mt. Hermon (height 2025 m above sea level, R_c = 10.8 GV). To calculate atmospheric electric field coefficients for total neutron intensity we need to determine coefficients $mI_m(h_o,R_c)/I_t(h_o,R_c)$ in Eq. 8.8.16. It can be done by data listed in Table 8.8.1, based on continuous registration of total intensity and different multiplicities on Mt. Hermon for 3 years in June 1998–May 2001.

Table 8.8.1. Counting rates per one minute of total neutron intensity and different multiplicities on Mt. Hermon, averaged for 3 years (June 1998–May 2001) and the coefficients $mI_m(h_o,R_c)/I_t(h_o,R_c)$.

parameter	total	$m=1$	$m=2$	$m=3$	$m=4$	$m=5$	$m=6$	$m=7$	$m\geq 8$
count. rate	10256.82	4683.69	1302.55	441.37	170.94	75.20	36.57	19.10	23.30
$mI_m(h_o,R_c)$		4683.69	2605.10	1324.12	683.78	376.01	219.43	133.73	230.97
$mI_m(h_o,R_c)/I_t(h_o,R_c)$		0.4672	0.2598	0.1321	0.0682	0.0375	0.0219	0.0133	0.0230

Results for the atmospheric electric field coefficients for total neutron intensity on the basis of Table 8.8.1 and Eq. 8.8.16 as well as for different multiplicities are as follows: for the period of low solar activity

$$W_{nE}(h,h_o,R_c=10.8\ \text{GV}, m=tot;1;2;3)\Big|_{\text{low SA}}^{\text{Mt. Hermon}} \approx (4.37;\ 6.48;\ 4.32;1.71)\times 10^{-5}\ \%(\text{kV/m})^{-1}\left(\text{g/cm}^2\right)^{-1}, \qquad (8.8.17)$$

and for the period of high solar activity

$$W_{nE}(h,h_o,R_c=10.8\ \text{GV}, m=tot;1;2;3)\Big|_{\text{high SA}}^{\text{Mt. Hermon}} \approx (4.72;\ 6.99;\ 4.66;1.83)\times 10^{-5}\ \%(\text{kV/m})^{-1}\left(\text{g/cm}^2\right)^{-1}. \qquad (8.8.18)$$

8.9. First observations of atmospheric electric field effects in total neutron intensity and in different multiplicities

8.9.1. Simultaneous measurements of AEF effects in total neutron intensity and different multiplicities in the Emilio Segre' Observatory on Mt. Hermon

Dorman et al. (2001, 2003), on the basis of CR and AEF one minute data obtained by neutron monitor and electric field sensor EFS-1000 in the Emilio Segre' Observatory on Mt. Hermon in Israel (33°18.3′N, 35°47.2′E, height 2025 m above sea level, cut off rigidity for vertical direction 10.8 GV), were the first to investigate the AEF effect in CR for total neutron intensity and for different multiplicities (for the description of the Observatory, see Section 4.8). For comparison purposes and for exclusion of primary CR variations, we also used data obtained in the Rome neutron super-monitor (about sea level, cut off rigidity 6.7 GV). According to the theoretical calculations described in Section 8.8 the electric field effect in the neutron monitor counting rate caused mainly following the capture of slow negative muons by lead nucleus with escape of few neutrons. As was shown in Sections 8.8.4 and 8.8.5, the biggest electric field effect is expected in the multiplicity m = 1, smaller in m = 2, much smaller in m = 3 and negligible effect is expected in higher multiplicities. This conclusion was controlled on the basis of Mt. Hermon experimental data. The results obtain give the possibility to estimate the total acceleration and deceleration of CR particles by the atmospheric electric field.

8.9.2. Measurements of AEF on Mt. Hermon; characteristics of thunderstorm periods

The AEF sensor EFS-1000 started to work in the Emilio Segre' Observatory on Mt. Hermon in February 2000. It made measurements on top of the Observatory each minute for negative field up to –160 kV/m and for positive field up to +16 kV/m (if the electric field has intensity near the ground $E > +16$ kV/m, EFS-1000 shows only the upper limit +16 kV/m). In Fig. 8.9.1 and 8.9.2 are shown examples of these measurements.

In Table 8.9.1 are shown periods of thunderstorms on Mt. Hermon, their times of start and finish, total duration and maximum of AEF $E_{\max}$ (in kV/m) observed with the EFS-1000 in each period.

From Table 8.9.1 it can be seen that very high atmospheric electric fields characterized by $E_{\max} = 80 - 110$ kV/m were observed on several occasions. Fields of this intensity are very dangerous for the neutron monitor, the electronics, and the computers in the Emilio Segre' Observatory. To save the Observatory from this dangerous electric field, we use a ground connected Faraday net protector which covers the Observatory.

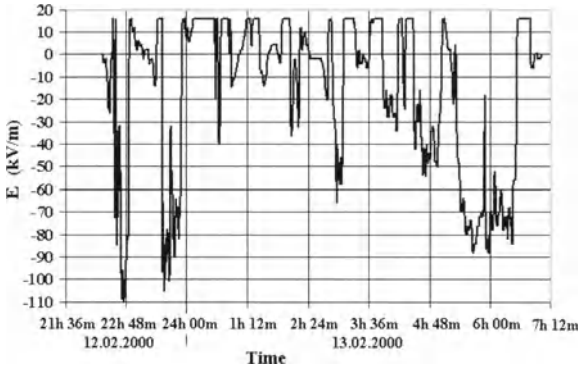

Fig. 8.9.1. One-minute data of AEF on Mt. Hermon during a thunderstorm period in February 2000.

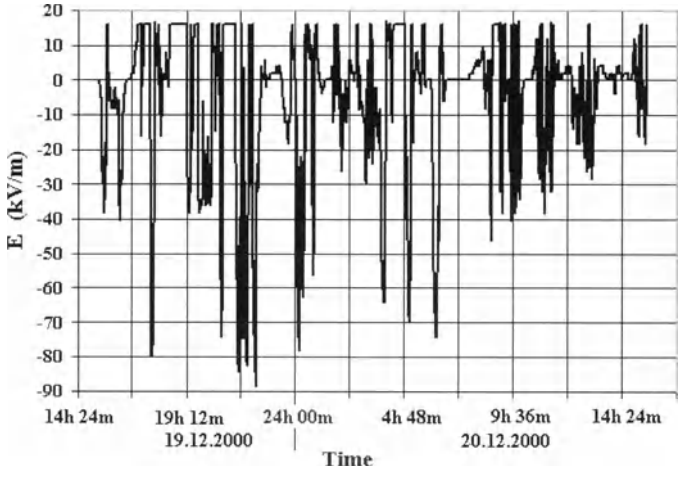

Fig. 8.9.2. The same as in Fig. 8.9.1, but for a thunderstorm period in December 2000.

Table 8.9.1. List of 49 thunderstorm periods on Mt. Hermon, observed by the sensor EFS-1000 of Emilio Segre' Observatory on Mt. Hermon in February–May, October–December 2000, and in January–May 2001.

No.	Start, UT	Finish, UT	Duration, min	E_{max}, kV/m
1	05.02.00, 15:10	06.02.00, 03:25	735	34
2	12.02.00, 17:36	13.02.00, 08:44	908	110
3	13.02.00, 17:32	14.02.00, 00:20	408	54
4	15.02.00, 18.39	16.02.00, 12:42	1083	80
5	19.02.00, 11:55	19.02.00, 19.16	441	36
6	22.02.00, 14:43	23.02.00, 03:56	793	48
7	27.02.00, 11:31	27.02.00, 12.31	60	14
8	01.03.00, 01:05	01.03.00, 18:22	1037	112
9	04.03.00, 09:04	04.03.00, 14:45	341	64
10	06.03.00, 20:25	07.03.00, 02:16	351	16
11	08.04.00, 17:35	08.04.00, 20:10	155	26
12	08.04.00, 22:59	09.04.00, 06:07	428	70
13	09.04.00, 10:51	09.04.00, 18:38	467	56
14	19.04.00, 01:49	19.04.00, 02:46	57	26
15	20.04.00, 01:42	20.04.00, 04:48	186	56
16	03.05.00, 21:19	04.05.00, 00:11	172	10
17	08.05.00, 06:08	08.05.00, 07:38	90	8
18	22.10.00, 21:51	23.10.00, 04:18	387	12
19	23.10.00, 10:18	23.10.00, 12:23	125	22
20	23.10.00, 14:58	24.10.00, 15:23	1465	70
21	25.10.00, 01:34	25.10.00, 07:07	333	10
22	25.10.00, 11:59	25.10.00, 14:55	176	14
23	29.11.00, 05:31	29.11.00, 06:20	49	10
24	29.11.00, 18:23	30.11.00, 05:11	648	20
25	30.11.00, 14:09	01.12.00, 03:10	781	50
26	12.12.00, 08:27	13.12.00, 07:15	1368	80
27	19.12.00, 01:20	20.12.00, 22:09	2689	88
28	24.12.00, 09:00	24.12.00, 13:39	279	30
29	02.01.01, 15:03	03.01.01, 04:10	787	26
30	17.01.01, 10:41	17.01.01, 13:12	151	76
31	18.01.01, 14:49	19.01.01, 01:14	625	70
32	19.01.01, 06:45	19.01.01, 15:26	521	50
33	19.01.01, 23:56	20.01.01, 01:11	75	14
34	23.01.01, 18:58	25.01.01, 05:58	2100	62
35	03.02.01, 06:47	04.02.01, 18:21	2134	88
36	13.02.01, 20:52	15.02.01, 01:12	1700	60
37	15.02.01, 12:45	15.02.01, 15:44	179	24
38	20.02.01, 00:09	20.02.01, 23:21	1392	48
39	23.02.01, 12:24	23.02.01, 13:36	72	40
40	14.03.01, 01:19	14.03.01, 01:52	33	12
41	23.03.01, 22:54	24.03.01, 01:58	184	72
42	02.04.01, 13:43	02.04.01, 16:07	144	40
43	07.04.01, 13:45	07.04.01, 15:02	77	52
44	01.05.01, 20:16	02.05.01, 01:32	316	16
45	02.05.01, 08:57	02.05.01, 09:49	52	40
46	09.05.01, 04:44	09.05.01, 05:11	27	28
47	09.05.01, 07:58	09.05.01, 10:10	132	20
48	13.05.01, 03:30	13.05.01, 03:58	28	20
49	13.05.01, 04:45	13.05.01, 07:33	168	40

Fig. 8.9.3 shows values of E_{max} as a function of the thunderstorms duration T.

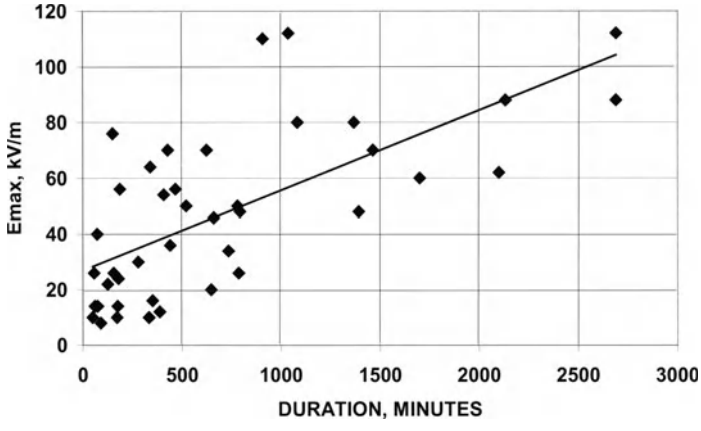

Fig. 8.9.3. $E_{\max}$ *vs* thunderstorm's period of duration T.

From Fig. 8.9.3 it can be seen that there is a clear positive correlation of $E_{\max}$ with thunderstorms duration T (in minutes):

$$E_{\max}[\mathrm{kV/m}] = 0.029[\mathrm{kV/(m.min)}] \times T[\mathrm{min}] + 27\,\mathrm{kV/m} \tag{8.9.1}$$

with a correlation coefficient of 0.68.

Our EFS-1000 for all E > +16 kV/m gives the same value as at E=+16 kV/m. Therefore we excluded from our analysis all terminal data at E=+16 kV/m. In Fig. 8.9.4 is shown the distribution function of the AEF according to our observations on Mt. Hermon in February 2000.

From Fig. 8.9.4 it can be seen that the distribution function has a sharp maximum at $E = 0$, a very flat decrease at high negative values of E (this explains the $E_{\max} \propto T$ dependence according to Fig. 8.9.3), and for $|E| \le 15\,\mathrm{kV/m}$ is almost symmetrical relative to $E = 0$.

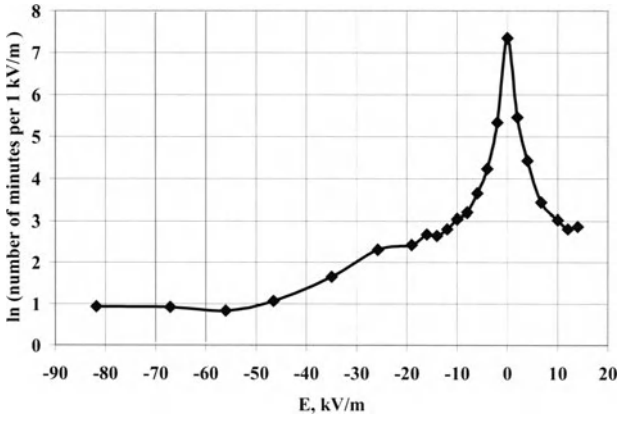

Fig. 8.9.4. The distribution function of the AEF according to observations of seven thunderstorms on Mt. Hermon in February 2000.

8.9.3. Data on electric field and CR observations

Because the expected AEF effect for measurements by NM on mountain heights is very small (see above, Sections 8.8.4 and 8.8.5), it is necessary to decrease fluctuations in CR intensity caused by other causes than AEF effects. Therefore we corrected data of the total and different multiplicities on barometric effect (see in Dorman et al., 2001a; also in Section 6.15), on snow effect (Dorman et al., 2001b; also in Section 6.1), and on primary variations (by using Rome NM data for comparison). Our one minute data are characterized with statistical errors of 0.98%, 1.45%, 2.76% and 4.74% for total intensity, m = 1, 2, and 3, respectively. Therefore we used averaged data. In Table 8.9.2 are shown the averaged results of observations of the AEF and neutron monitor counting rate in total intensity and in different multiplicities.

Table 8.9.2. Averaged results of observations on Mt. Hermon in February 2000 of the AEF and neutron monitor counting rates in total intensity and in multiplicities m = 1, 2, and 3.

E, kV/m	Interval of E	minutes	*tot*, %	m = 1, %	m = 2, %	m = 3, %
–81.8	–110 to –72	71	–0.08 ± 0.16	–0.43 ± 0.17	0.14 ± 0.29	–0.03 ± 0.54
–67.1	–70 to –62	25	–0.76 ± 0.29	–0.69 ± 0.31	–0.54 ± 0.46	0.54 ± 0.85
–56.1	–60 to –52	23	0.00 ± 0.33	–0.27 ± 0.32	–1.18 ± 0.43	–0.61 ± 0.77
–46.6	–50 to –42	29	–0.22 ± 0.27	–0.60 ± 0.30	0.26 ± 0.67	–0.62 ± 0.83
–35.0	–40 to –32	52	–0.73 ± 0.24	–0.77 ± 0.18	–0.41 ± 0.38	–0.60 ± 0.63
–25.8	–30 to –24	100	–0.38 ± 0.15	–0.54 ± 0.15	–0.48 ± 0.30	0.45 ± 0.37
–19.1	–22 to –18	45	–0.45 ± 0.20	–0.27 ± 0.22	–0.85 ± 0.47	–0.25 ± 0.70
–16.0	–17 to –15	29	–0.23 ± 0.25	0.01 ± 0.27	–0.57 ± 0.48	0.73 ± 0.88
–14.0	–15 to –13	28	–0.09 ± 0.36	0.15 ± 0.32	–0.41 ± 0.49	1.64 ± 0.94
–12.0	–13 to –11	33	–0.12 ± 0.26	0.05 ± 0.28	–0.43 ± 0.55	0.60 ± 0.75
–10.0	–11 to –9	42	–0.04 ± 0.21	–0.20 ± 0.24	0.04 ± 0.40	–0.05 ± 0.81
–8.0	–9 to –7	49	0.07 ± 0.20	0.23 ± 0.27	–0.23 ± 0.45	0.28 ± 0.71
–6.0	–7 to –5	77	0.13 ± 0.18	0.26 ± 0.16	–0.03 ± 0.32	–0.20 ± 0.50
–4.0	–5 to –3	138	0.04 ± 0.14	–0.03 ± 0.13	-0.30 ± 0.20	0.05 ± 0.37
–2.0	–3 to –1	415	0.02 ± 0.08	–0.03 ± 0.07	0.18 ± 0.12	0.16 ± 0.22
0.0	–1 to +1	3111	0.00 ± 0.03	0.05 ± 0.03	0.00 ± 0.05	–0.03 ± 0.09
+2.0	1 to 3	470	0.10 ± 0.08	0.02 ± 0.08	0.05 ± 0.13	0.32 ± 0.21
+4.0	3 to 5	167	0.07 ± 0.13	0.18 ± 0.13	–0.11 ± 0.22	–0.18 ± 0.37
+6.7	5 to 8	124	0.32 ± 0.15	0.09 ± 0.13	0.62 ± 0.27	–0.38 ± 0.44
+10.0	8 to 11	41	0.26 ± 0.24	0.12 ± 0.23	0.40 ± 0.49	0.03 ± 0.82
+12.0	11 to 13	33	–0.05 ± 0.31	0.02 ± 0.30	0.17 ± 0.53	–1.06 ± 0.77
+14.0	13 to 16	35	–0.06 ± 0.31	0.14 ± 0.28	0.42 ± 0.40	–0.73 ± 0.80

8.9.4. Regression relations between AEF and counting rates of total neutron intensity and different multiplicities

Unfortunately we cannot use directly the theoretical Eq. 8.8.3 for regression analysis, since information on the space–time distribution of AEF $E(h,t)$ is not available.

In the Emilio Segre' Observatory on Mt. Hermon we have one minute data of continuous measurements only of $E(h_o,t)$ in the place occupied by our Observatory. We suppose that $E(h_o,t)$ is in good correlation with distribution function $E(h,t)$. In this case instead of Eq. 8.8.3 we obtain approximately

$$(\Delta I_m(t)/I_{mo})_E = \int_{h_3}^{h_o} W_{mE}(h)E(h,t)dh \approx \overline{W}_{mE}\times(h_o - h_3)\times E(h_o,t), \tag{8.9.2}$$

where h_3 is the air pressure on altitude of charged clouds caused thunderstorms., We also assume that

$$\overline{W}_{mE} \approx \int_{h_3}^{h_o} W_{mE}(h)dh \Big/ (h_o - h_3)\ . \tag{8.9.3}$$

The expected values of $\overline{W}_{mE}$ were discussed above, in Section 8.8. On the other hand, on the basis of the experimental data on $E(h_o,t)$ and on $(\Delta I_m(t)/I_{mo})_E$ described above we can determine by Eq. 8.9.2 the regression coefficient $\overline{W}_{mE}\times(h_o - h_3)$.

As an example we present the results of regression analysis for seven thunderstorms periods in February 2000 (total duration of thunderstorms periods more than 5000 minutes). Our EFS-1000 for all $E \geq +16$ kV/m gives the value $E = +16$ kV/m. Therefore we need to exclude from regression analyses all points with $E = +16$ kV/m. In Fig. 8.9.5 are shown the total neutron intensity variations as a function of the AEF E.

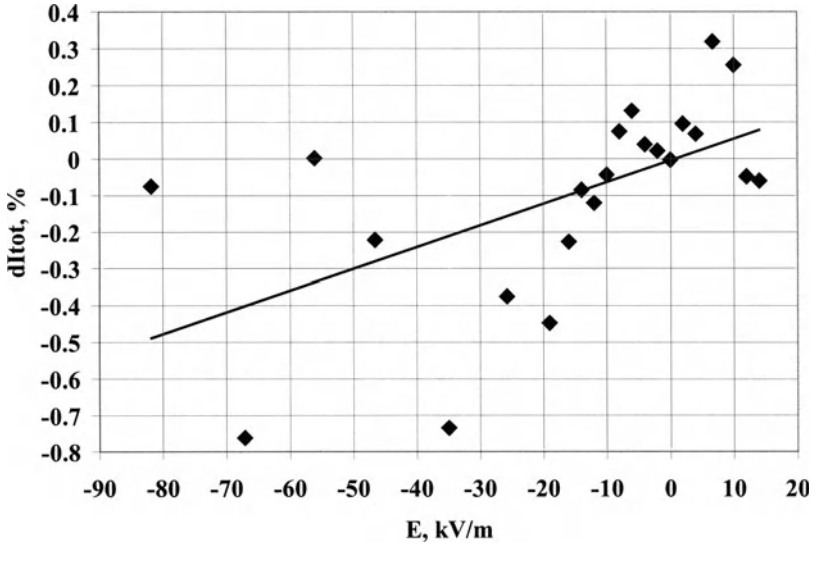

Fig. 8.9.5. CR intensity variations *vs* AEF E for total neutron intensity according to measurements on Mt. Hermon in February 2000. The straight line reflects the linear correlation between CR intensity and AEF E according to Eq. 8.9.4.

According to the data in Fig. 8.9.5, the statistical relation between variations of total neutron intensity and E is as following:

$$(\Delta I_t(t)/I_{to})_E \propto \overline{W}_{tE} \times (h_o - h_3) \times E(h_o, t) \tag{8.9.4}$$

with correlation and regression coefficients

$$R_t = 0.56 \pm 0.09;\ \overline{W}_{tE} \times (h_o - h_3) = (0.0059 \pm 0.0018)\,\%(\mathrm{kV/m})^{-1}. \tag{8.9.5}$$

In Fig. 8.9.6-8.9.8 are shown the intensity variations of the multiplicities m = 1, 2, and 3 *vs* AEF E.

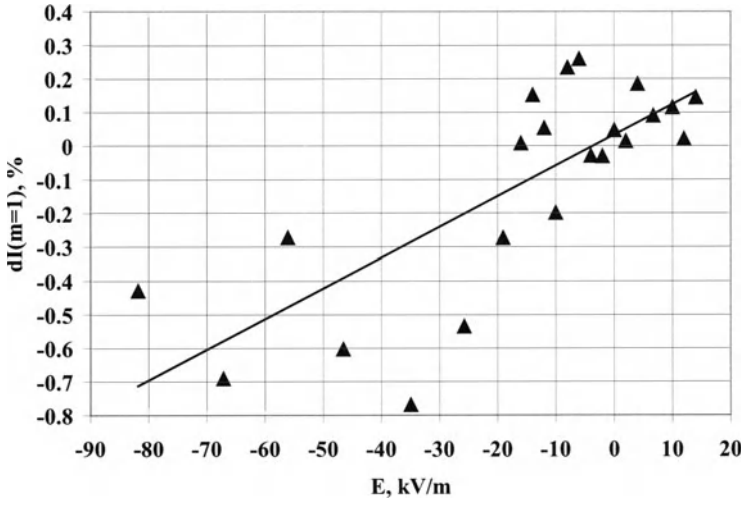

Fig. 8.9.6. The same as in Fig. 8.9.5 but for multiplicity m = 1. The straight line reflects the linear correlation according to Eq. 8.9.6 with regression coefficient Eq. 8.9.8.

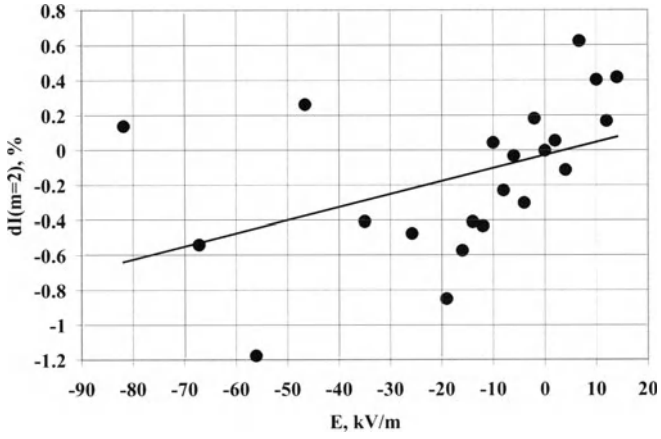

Fig. 8.9.7. The same as in Fig. 8.9.5 but for multiplicity m = 2. The straight line reflects the linear correlation according to Eq. 8.9.6 with regression coefficient Eq. 8.9.9.

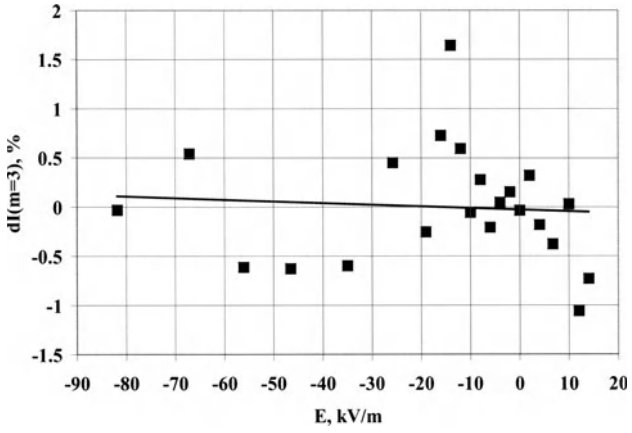

Fig. 8.9.8. The same as in Fig. 8.9.5 but for multiplicity m = 3. The straight line reflects the linear correlation according to Eq. 8.9.6 with regression coefficient Eq. 8.9.10.

According to data in Fig. 8.9.6–8.9.8, the statistical relations between variations of multiplicities m = 1, 2, 3 and E are as following:

$$(\Delta I_m(t)/I_{mo})_E \propto \overline{W}_{mE} \times (h_o - h_3) \times E(h_o, t) \tag{8.9.6}$$

with correlation coefficients

$$R_1 = 0.77 \pm 0.06, \quad R_2 = 0.45 \pm 0.11, \quad R_3 = -0.07 \pm 0.14, \tag{8.9.7}$$

and regression coefficients

$$\overline{W}_{1E} \times (h_o - h_3) = (0.0091 \pm 0.0016)\,\%(\mathrm{kV/m})^{-1}, \ . \tag{8.9.8}$$

$$\overline{W}_{2E} \times (h_o - h_3) = (0.0075 \pm 0.0032)\,\%(\mathrm{kV/m})^{-1}, \tag{8.9.9}$$

$$\overline{W}_{3E} \times (h_o - h_3) = -(0.0016 \pm 0.0048)\,\%(\mathrm{kV/m})^{-1}, \tag{8.9.10}$$

8.9.5. Comparison of experimental results and theoretical predictions of AEF effects in NM total intensity and different multiplicities

The comparison of experimental results reflected in Fig. 8.9.5–8.9.8 and Eq. 8.9.4–8.9.10 shows that the best correlation with the highest regression coefficient was observed for the multiplicity m = 1. Lower correlation and smaller regression coefficients were observed for the total neutron intensity and for multiplicity m = 2. Practically null correlation and negligible regression coefficient were observed for the multiplicity m = 3. These results are in good qualitative agreement with those predicted by the theory of Dorman and Dorman (1995), Dorman et al. (1995), Dorman and Dorman (1999) that was described above in Section 8.8.

Quantitative comparison of experimental results with theory is much more difficult. On the one hand, the influence of AEF on charged energetic particles of CR has an integral character in vertical direction from the level of observations to the level of charged clouds and from great horizontal surface (neutron monitor detects particles arrived mostly from zenith angles smaller than about 30° which means from the surface about 10 km^2 on the height of charged clouds of few km). On the other hand, the sensor of AEF EFS-1000 gives information only on the local AEF on the top of our Observatory on Mt. Hermon. Nevertheless we can try to do this comparison. Since the observations were carried out during a period of high solar activity (February 2000), we will use for comparison the theoretical prediction for Mt. Hermon, described by Eq. 8.8.18 (see Section 8.8.5). Let us first compare the theoretical result for the multiplicity $m = 1$ in Eq. 8.8.18 with the experimental result described by Eq. 8.9.8, that has the smallest relative error. From this comparison it follows that

$$(h_o - h_3)_{m=1} \approx \frac{(0.0091 \pm 0.0016)\%(\mathrm{kV/m})^{-1}}{6.99\times10^{-5}\ \%(\mathrm{kV/m})^{-1}\left(\mathrm{g/cm^2}\right)^{-1}} = (130 \pm 23)\mathrm{g/cm^2} \qquad (8.9.11)$$

From comparison of the theoretical Eq. 8.8.18 for total intensity and multiplicity $m = 2$ with experimental results described by Eq. 8.9.5 and 8.9.9, we obtain

$$(h_o - h_3)_{tot} \approx \frac{(0.0059 \pm 0.0018)\%(\mathrm{kV/m})^{-1}}{4.72\times10^{-5}\ \%(\mathrm{kV/m})^{-1}\left(\mathrm{g/cm^2}\right)^{-1}} = (125 \pm 38)\mathrm{g/cm^2} \qquad (8.9.12)$$

$$(h_o - h_3)_{m=2} \approx \frac{(0.0075 \pm 0.0032)\%(\mathrm{kV/m})^{-1}}{4.66\times10^{-5}\ \%(\mathrm{kV/m})^{-1}\left(\mathrm{g/cm^2}\right)^{-1}} = (160 \pm 68)\mathrm{g/cm^2} \qquad (8.9.13)$$

For multiplicity $m = 3$ the expected effect is very small (see Eq. 8.8.18) in agreement with experimental result described by Eq. 8.9.10. The relative errors of determining $h_o - h_3$ by measurements of total intensity and multiplicities $m = 1$ and $m = 2$ are

$$\sigma_{tot} = \pm 38/125 = \pm 0.304;\ \ \sigma_1 = \pm 23/130 = \pm 0.177;\ \ \sigma_2 = \pm 68/160 = \pm 0.425; \qquad (8.9.14)$$

so the average value of $h_o - h_3$ with taking into account the relative weights of results Eq. 8.9.11–8.9.13 will be

$$(h_o - h_3)_{av} = \left\{\sigma_{tot}^{-2}(h_o - h_3)_{tot} + \sigma_1^{-2}(h_o - h_3)_{m=1} + \sigma_2^{-2}(h_o - h_3)_{m=2}\right\}$$

$$\times\left(\sigma_{tot}^{-2} + \sigma_1^{-2} + \sigma_2^{-2}\right)^{-1} = 132\ \mathrm{g/cm^2} \qquad (8.9.15)$$

with relative statistical error

$$\sigma_{av}^{-2} = \sigma_{tot}^{-2} + \sigma_1^{-2} + \sigma_2^{-2}; \quad \sigma_{av} = \pm 0.144\,, \tag{8.9.16}$$

so the final average result will be

$$(h_o - h_3)_{av} = (132 \pm 19)\,\mathrm{g/cm^2} \tag{8.9.17}$$

The results show that the theory of AEF effects in total neutron intensity and different multiplicities (Section 8.8) is in good agreement with experimental data obtained on Mt. Hermon. Determination of $(h_o - h_3)_{av}$ (see Eq. 8.9.17) shows that the average vertical distance from the Emilio Segre' Observatory on Mt. Hermon to thunderstorm clouds that generate the AEF is about 1.5–2.0 km (altitude above sea level 3.5–4.0 km), in good agreement with the meteorological observations.

Chapter 9

Development of the Theory and Methods of Determination of Cosmic Ray Variations of Atmospheric Origin

9.1. Determination of CR temperature effect by heights of isobaric levels

Some aero-meteorological stations give regular data on the heights of isobaric levels. These data also can be used for the determination of CR temperature effect by integral method, as was shown in Dorman (1960). Let us take into account that the height $H(h_o,h)$ of isobaric level h and its variation $\delta H(h_o,h)$ are (here we use $\rho(h)=h/R_oT$, where R_o is the gas constant for air at normal conditions)

$$H(h_o,h)=\int_h^{h_o} dh'/\rho(h'); \quad \delta H(h_o,h)=\delta h_o/\rho(h_o)+\int_h^{h_o}(R_o/h')\delta T(h')dh'. \tag{9.1.1}$$

By differentiation of Eq. 9.1.1 over h we obtain

$$d\delta H(h_o,h)/dh=-(R_o/h)\delta T(h); \quad \delta T(h)=-(h/R_o)(d\delta H(h_o,h)/dh). \tag{9.1.2}$$

From Eq. 9.1.2 follows

$$\left(\frac{\delta I(h_o)}{I_o}\right)_T=-\int_0^{h_o}\frac{h}{R_o}W_T(h)\frac{d\delta H}{dh}dh=R_o^{-1}\int_0^{h_o}\left(W_T(h)+h\left(\frac{dW_T(h)}{dh}\right)\right)\delta H dh$$

$$\approx\sum_{i=0}^{n}\kappa_i\delta H_i, \text{ where } \kappa_i=R_o^{-1}(h_iW_T(h_i)-h_{i+1}W_T(h_{i+1})). \tag{9.1.3}$$

The air pressure h is measured in atm, and $W_T(h)$ in $\%/\left({}^{o}\mathrm{C}\times\mathrm{atm}\right)$; in this case the gas constant $R_o=0.029$ km$/{}^{o}$C, and the coefficients κ_i will be in %/km.

9.2. The first, second, and higher approximations in the integral method

9.2.1. The general formula for the n-th approximation for the integral method

Let us assume that the observed CR data are corrected on variations of magnetospheric and extraterrestrial origin, so that we have only variations of atmospheric origin. The atmospheric variations described in the previous Chapters 5–8 were considered in the first approximation, which is enough when the observed

variations are very small (the relative amplitude << 1). Here we will consider the more general case when it is necessary to use the higher approximations; we will also estimate the errors in determining of CR atmospheric variations as a function of the level of approximation used.

Let us consider the intensity of any secondary CR component $I_i(h_o(t),T(h,t))$ of type i determined only by the air mass in vertical column over observation level $h_o(t)$ and by vertical distribution of air temperature $T(h,t)$. Here we consider the generalized temperature which includes the distribution of humidity:

$$T(h,t)=T_{tr}(h,t)(1+0.378e(h,t)/h(t)), \tag{9.2.1}$$

where $T_{tr}(h,t)$ is the vertical distribution of the true air temperature, and $e(h,t)$ is the pressure water vapors. In the general case

$$I_i(h_o(t),T(h,t))=\int_0^{h_o(t)}F_i(h_o(t),T(h,t),h)dh,\quad I_{io}=I_i(h_o,T_o(h))=\int_0^{h_o}F_i(h_o,T_o(h),h)dh, \tag{9.2.2}$$

where the function $F_i(h_o(t),T(h,t),h)$ accounted the processes of generation and propagation of the i-th CR secondary component. The total change of CR intensity caused by finite variations of meteorological conditions

$$\Delta T(h,t)=T(h,t)-T_o(h),\quad \Delta h_o(t)=h_o(t)-h_o \tag{9.2.3}$$

will be

$$\Delta I_i(h_o(t),T(h,t))=I_i(h_o(t),T(h,t))-I_i(h_o,T_o(h))$$

$$=\sum_{k=1}^{n}\frac{1}{k!}\left[\frac{\delta}{\delta T_o(h)}\Delta T(h,t)+\frac{\partial}{\partial h_o}\Delta h_o(t)\right]^k I_i(h_o,T_o(h))+R_n, \tag{9.2.4}$$

where $\dfrac{\delta}{\delta T_o(h)}$ is the functional deviation, and the rest term

$$R_n=\frac{1}{(n+1)!}\left[\frac{\delta}{\delta T_o(h)}\Delta T(h,t)+\frac{\partial}{\partial h_o}\Delta h_o(t)\right]^{n+1} I_i(h_o+\theta_h\Delta h_o(t),T_o(h)+\theta_T\Delta T(h,t)) \tag{9.2.5}$$

where θ_h and θ_T are between 0 and 1.

9.2.2. Commonly used first approximation for the integral method

At the lowest level of approximation ($n=1$ in Eq. 9.2.4) for the relative atmospheric variation we obtain:

$$\left(\frac{\Delta I_i(h_o(t),T(h,t))}{I_i(h_o,T_o(h))}\right)_{n=1}=\frac{\delta I_i(h_o,T_o(h))}{I_i(h_o,T_o(h))\delta T_o(h)}\Delta T(h,t)+\frac{\partial I_i(h_o,T_o(h))}{I_i(h_o,T_o(h))\partial h_o}\Delta h_o(t)$$

$$=\int_0^{h_o}W_{Ti}(h_o,T_o(h),h)\Delta T(h,t)dh+W_{hi}(h_o,T_o(h))\Delta h_o(t). \quad (9.2.6)$$

In Eq. 9.2.6 we accounted that

$$\frac{\delta I_i(h_o,T_o(h))}{I_i(h_o,T_o(h))\delta T_o(h)}\Delta T(h,t)=\frac{1}{I_i(h_o,T_o(h))}\int_0^{h_o}\frac{\partial F_i(h_o,T_o(h),h)}{\partial T_o(h)}\Delta T(h,t)dh$$

$$=\int_0^{h_o}W_{Ti}(h_o,T_o(h),h)\Delta T(h,t)dh, \quad (9.2.7)$$

and

$$\frac{\partial I_i(h_o,T_o(h))}{I_i(h_o,T_o(h))\partial h_o}\Delta h_o(t)=W_{hi}(h_o,T_o(h))\Delta h_o(t), \quad (9.2.8)$$

where $W_{Ti}(h_o,T_o(h),h)$ and $W_{hi}(h_o,T_o(h))$ are the commonly used temperature and barometric coefficients for the first approximation (see Chapters 5–8). If $\Delta T(h,t)$ and $\Delta h_o(t)$ are such that the amplitudes of CR meteorological effects are relatively very small, the first approximation for the integral method is enough.

9.2.3. The second approximation for the integral method

In some cases, when the expected amplitudes of CR meteorological effects are relatively big, the first approximation for the integral method is not enough. In these cases it is necessary to use at least the second approximation for the integral method, that can be obtained from Eq. 9.2.4 at $n=2$:

$$\left(\frac{\Delta I_i(h_o(t),T(h,t))}{I_i(h_o,T_o(h))}\right)_{n=2}=\left(\frac{\Delta I_i(h_o(t),T(h,t))}{I_i(h_o,T_o(h))}\right)_{n=1}+\frac{\partial^2 I_i(h_o,T_o(h))}{2I_i(h_o,T_o(h))\partial h_o^2}(\Delta h_o(t))^2$$

$$+\frac{\Delta h_o(t)}{2I_i(h_o,T_o(h))}\int_0^{h_o}\left\{\frac{\delta}{\delta T_o(h)}\left(\frac{\partial I_i(h_o,T_o(h))}{\partial h_o}\right)+\frac{\partial}{\partial h_o}\left(\frac{\delta I_i(h_o,T_o(h))}{\delta T_o(h)}\right)\right\}\Delta T(h,t)dh$$

$$+\frac{1}{2I_i(h_o,T_o(h))}\int_0^{h_o}\left[\frac{\delta}{\delta T_o(h)}\left(\frac{\delta I_i(h_o,T_o(h))}{\delta T_o(h)}\right)\right](\Delta T(h,t))^2dh. \quad (9.2.9)$$

Usually used temperature and barometric coefficients $W_{Ti}(h_o,T_o(h))$ and $W_{hi}(h_o,T_o(h))$ are meteorological coefficients of the first order. Let us introduce now the meteorological coefficients of second order in accordance with Eq. 9.2.9:

$$W_{hhi}(h_o,T_o(h))=\frac{\partial^2 I_i(h_o,T_o(h))}{2I_i(h_o,T_o(h))\partial h_o^2}=\frac{1}{2}\left[\frac{\partial W_{hi}(h_o,T_o(h))}{\partial h_o}+(W_{hi}(h_o,T_o(h)))^2\right], \quad (9.2.10)$$

$$W_{hTi}(h_o,T_o(h),h)=\frac{1}{2I_i(h_o,T_o(h))}\frac{\delta}{\delta T_o(h)}\left(\frac{\partial I_i(h_o,T_o(h))}{\partial h_o}\right)$$
$$=\frac{1}{2}\left[\frac{\delta W_{hi}(h_o,T_o(h))}{\delta T_o(h)}+W_{hi}(h_o,T_o(h))W_{Ti}(h_o,T_o(h),h)\right], \quad (9.2.11)$$

$$W_{Thi}(h_o,T_o(h),h)=\frac{1}{2I_i(h_o,T_o(h))}\frac{\partial}{\partial h_o}\left(\frac{\delta I_i(h_o,T_o(h))}{\delta T_o(h)}\right)=$$
$$=\frac{1}{2}\left[\frac{\partial W_{Ti}(h_o,T_o(h),h)}{\partial h_o}+W_{hi}(h_o,T_o(h))W_{Ti}(h_o,T_o(h),h)\right], \quad (9.2.12)$$

$$W_{TTi}(h_o,T_o(h),h)=\frac{1}{2I_i(h_o,T_o(h))}\frac{\delta}{\delta T_o(h)}\left(\frac{\delta I_i(h_o,T_o(h))}{\delta T_o(h)}\right)$$
$$=\frac{1}{2}\left[\frac{\delta W_{Ti}(h_o,T_o(h),h)}{\delta T_o(h)}+(W_{Ti}(h_o,T_o(h),h))^2\right]. \quad (9.2.13)$$

Using the notation described by Eq. 9.2.10–9.2.13, the second approximation for the integral method, Eq. 9.2.9, can be rewritten as

$$\left(\frac{\Delta I_i(h_o(t),T(h,t))}{I_i(h_o,T_o(h))}\right)_{n=2}=[W_{hi}(h_o,T_o(h))+W_{hhi}(h_o,T_o(h))\Delta h_o(t)]\Delta h_o(t)$$
$$+\int_0^{h_o}[W_{Ti}(h_o,T_o(h),h)+W_{TTi}(h_o,T_o(h),h)\Delta T(h,t)]\Delta T(h,t)dh$$
$$+\Delta h_o(t)\int_0^{h_o}[W_{hTi}(h_o,T_o(h),h)+W_{Thi}(h_o,T_o(h),h)]\Delta T(h,t)dh. \quad (9.2.14)$$

In Eq. 9.2.14 meteorological coefficients of the second order can be determined through well known meteorological coefficients of the first order by the help of Eq. 9.2.10–9.2.13 and the deviations $\partial W_{hi}/\partial h_o$, $\delta W_{hi}/\delta T_o(h)$, and so on. The estimation of these deviations was made in Chapter 5. For the hard muon component near sea level some necessary results are listen below:

$$\frac{\partial W_h}{W_h\partial h_o}=-0.99\times10^{-3}\ \text{mb}^{-1}, \quad \frac{\partial W_h}{W_h\partial T(h)}=-3.8\times10^{-4}\ \text{deg}^{-1},$$
$$\frac{\partial W_{T\pi}}{W_{T\pi}\partial h_o}=6.5\times10^{-4}\ \text{mb}^{-1}, \quad \frac{\partial W_{T\pi}}{W_{T\pi}\partial T_{str}}=-7.4\times10^{-4}\ \text{deg}^{-1}, \quad (9.2.15)$$
$$\frac{\partial W_{T\mu}}{W_{T\mu}\partial h_o}=-1.45\times10^{-3}\ \text{mb}^{-1}, \quad \frac{\partial W_{T\mu}}{W_{T\mu}\partial T_{trop}}=-8.4\times10^{-4}\ \text{deg}^{-1}.$$

9.2.4. The partial case of stable component or when $\Delta T(h,t)=0$

In the partial case of stable secondary component or when $\Delta T(h,t)=0$ we obtain from Eq. 9.2.4 at $n=\infty$:

$$\left(\frac{\Delta I_i(h_o(t),T(h,t))}{I_i(h_o,T_o(h))}\right)_{n=\infty}=\sum_{k=1}^{\infty}\frac{1}{k!}\frac{\partial^k I_i(h_o,T_o(h))}{I_i(h_o,T_o(h))\partial h_o^k}(\Delta h_o(t))^k. \qquad (9.2.16)$$

If the absorption of $I_i(h_o,T_o(h))$ with depth in the vicinity of h_o is exponential with the some effective length for absorption L as $I_i(h_o,T_o(h))\propto\exp(-h_o/L)$, it will be

$$\frac{\partial I_i(h_o,T_o(h))}{I_i(h_o,T_o(h))\partial h_o}=-\frac{1}{L}=W_h(h_o,T_o(h)),....\frac{\partial^k I_i(h_o,T_o(h))}{I_i(h_o,T_o(h))\partial h_o^k}=(W_h(h_o,T_o(h)))^k. \qquad (9.2.17)$$

By introducing Eq. 9.2.17 in Eq. 9.2.16, we obtain the natural result

$$\left(\frac{\Delta I_i(h_o(t),T(h,t))}{I_i(h_o,T_o(h))}\right)_{n=\infty}=\left(\frac{\Delta I_i(h_o(t),T(h,t))}{I_i(h_o,T_o(h))}\right)_h=\exp(-\Delta h_o(t)/L)-1. \qquad (9.2.17)$$

9.3. Calculations of barometric coefficients for different neutron multiplicities and total neutron intensity

Theoretical calculations of expected barometric coefficients $\beta_m(R_c,h_o)$ for different neutron multiplicities m and total neutron intensity were carried out by Hatton and Griffiths (1968). The calculations were made in the framework of Cranshow and Hillas (1960) model of the secondary nucleonic component generation and propagation in the atmosphere. In this model it is supposed that:

1. Primary particles on the top of atmosphere are only protons with the energetic spectrum

$$D(E_p)dE_p=aE_p^{-\gamma}dE_p \qquad (9.3.1)$$

2. The coefficient of inelasticity in the elementary act $f=\text{const}$.
3. In each interaction only one nucleon is generated.
4. The energy losses on ionization can be neglected.

According to the Cranshow and Hillas (1960) model, the primary proton with energy E_p after k interactions will generate secondary nucleons with energy

$$E_n(k)=f^k E_p. \qquad (9.3.2)$$

Let l_n be the transport path for nucleon interaction in air. In this case, the probability that on the path h will be k interactions, is determined by the Poisson distribution:

$$P(k,h/l_n)=\frac{(h/l_n)^k}{k!}\exp(-h/l_n). \tag{9.3.3}$$

Therefore the number of secondary nucleons in the interval of energies E_n, E_n+dE_n generated as result of k interactions from primary protons in the energy interval E_p, E_p+dE_p will be

$$N_k(E_n,h)dE_n=\left(\frac{(h/l_n)^k}{k!}\exp(-h/l_n)\right)\frac{a}{f^k}\left(\frac{E_n}{f^k}\right)^{-\gamma}dE_n. \tag{9.3.4}$$

The total number of secondary nucleons $N(E_n,h)dE_n$ will be found by summing Eq. 9.3.4 over all possible k:

$$N(E_n,h)dE_n=aE_n^{-\gamma}\sum_{k=k_{\min}}^{\infty}f^{k(\gamma-1)}\left(\frac{(h/l_n)^k}{k!}\exp(-h/l_n)\right)dE_n, \tag{9.3.5}$$

where $k_{\min}$ is determined by the geomagnetic cut off energy for primary protons E_{pc} according to the relation

$$E_{pc}=E_nf^{-k_{\min}}. \tag{9.3.6}$$

The average multiplicity $\langle m\rangle$ of neutrons generated in the neutron monitor as function of energy E_n of arriving nucleons was found experimentally by Hughes and Marsden (1966) and calculated theoretically by Wainio (1967). The probability to detect multiplicity m at average multiplicity $\langle m\rangle$ will be determined by the relation

$$P(m,\langle m\rangle(E_n),\xi)=C_m^{\langle m\rangle}\xi^m(1-\xi)^{\langle m\rangle-m}, \tag{9.3.7}$$

where ξ is the efficiency of detecting neutrons generated inside the neutron monitor. The counting rate of neutron multiplicity m will be

$$I_m(E_{pc},h)=\int_{E_{n\min}}^{\infty}N(E_n,h)P(m,\langle m\rangle(E_n),\xi)dE_n, \tag{9.3.8}$$

where $E_{n\min}$ is the minimal energy of nucleons detected by neutron monitor: according to Harman (1967) $E_{n\min}\approx 20$ MeV for neutron supermonitors NM-64 and $E_{n\min}\approx 50$ MeV for neutron monitors of IGY type. In Eq. 9.3.8 $N(E_n,h)$ is determined by Eq. 9.3.5, and $P(m,\langle m\rangle(E_n),\xi)$ by Eq. 9.3.6. From Eq. 9.3.8 follows

$$I_m(E_{pc},h_1)/I_m(E_{pc},h_2)=\exp\left(\frac{h_2-h_1}{L_n(m)}\right), \tag{9.3.8}$$

where $L_n(m)$ is the absorption path for neurons of multiplicity m. Barometric coefficients $\beta_m(E_{pc},h)$ for the depth $h=(h_1+h_2)/2$ can be found very easy from $L_n(m)$ by the Gross formula. The barometric coefficient $\beta_{tot}(E_{pc},h)$ for the total neutron intensity can be found according to relation:

$$\beta_{tot}(E_{pc},h)=\sum_{m=1}^{\infty} mI_m(E_{pc},h)\beta_m(E_{pc},h)\Big/\sum_{m=1}^{\infty} mI_m(E_{pc},h). \tag{9.3.9}$$

By this way in Hatton and Griffiths (1968) were found $\beta_m(E_{pc},h)$ for $m=1,\ 2,$ and ≥ 4 at $E_{pc}=2,\ 4,\ 8,$ and 16 GeV for observations by neutron super-monitors NM-64 and neutron monitors of IGY type near sea level (the average depth $h=1020\ \mathrm{g/cm^2}$). Results are shown in Fig. 9.3.1.

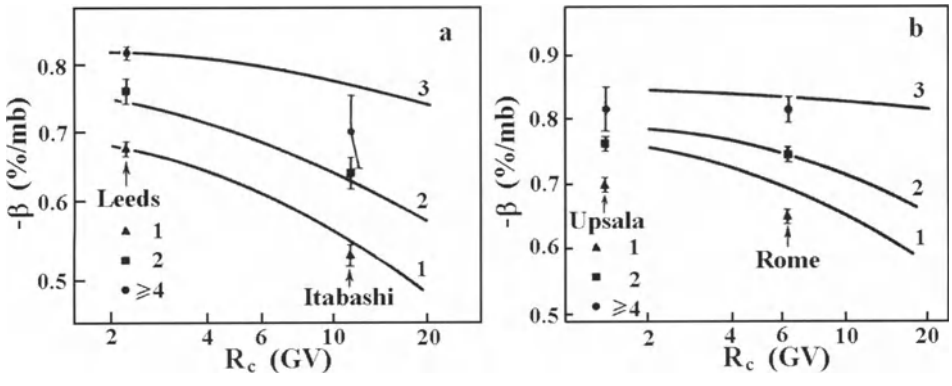

Fig. 9.3.1. Barometric coefficients $\beta_m(E_{pc},h)$ for $m=1,\ 2,$ and ≥ 4 at $E_{pc}=2,\ 4,\ 8,$ and 16 GeV for observations by neutron super-monitors NM-64 of IQSY type (*a* – left) and by neutron monitors of IGY type (*b* – right) near sea level (the average depth $h=1020\ \mathrm{g/cm^2}$). Curves *1* (for $m=1$), *2* (for $m=2$), and *3* (for $m\geq 4$) – expected from theoretical calculations described in text.

In addition, Hatton and Griffiths (1968) calculated $\beta_m(E_{pc},h)$ for neutron monitors of IGY type at $E_{pc}=2$ GeV for $h=420$ and $840\ \mathrm{g/cm^2}$. For these calculations the following values of parameters were assumed: $\xi=0.02$ and 0.05 for neutron monitors of NM-64 and IGY types, accordingly (correspondingly to Harman, 1967); $\gamma=2.35$; $l_n=80\ \mathrm{g/cm^2}$ and $f=0.5$ in accordance with Brooke et al., 1964). For high

multiplicities m equilibrium between primary and secondary energy spectrums must be established. In this case the relation

$$l_n/L_n = 1 - f^{\gamma-1} \tag{9.3.10}$$

must be valid. From Eq. 9.3.10 follows $L_n = 132\ \mathrm{g/cm^2}$ (i.e., $\beta_{m>>1} \approx -0.846\ \%/\mathrm{mb}$).

9.4. Calculations of barometric coefficients for frequency of external atmospheric showers

Murthy et al. (1968) calculated the expected barometric coefficients for the frequency of external atmospheric showers (EAS) for different models of elementary act using the Monte Carlo method (see Table 9.4.1).

Table 9.4.1. The models of elementary act used in Murthy et al. (1968) for calculating of expected barometric coefficients of the frequency of EAS by the Monte Carlo method

Values	Model I		Model II		Model III		Model IV		
	Nucl eons	Pio ns	Nucle- ons	Pio ns	Nucle -ons	Pions	Nucleons		Pions
							Fire- balls	Iso- bars	
Multiplicity	$2.7\times E_o^{1/4}$		$5.6\times \lg\left(1+\frac{E_o}{18}\right)$		$0.96\times E_o^{1/2}$		$0.25\times E_o^{1/2}$	3	$0.96\times E_o^{1/2}$
inelasticity coefficient	0.5	1.0	0.5	1.0	0.5	1.0	0.2	≈0.3	1.0
Transport path, $\mathrm{g/cm^2}$	80	120	80	120	80	120	80	80	120

In all models it was supposed that the part of generation nucleon–antinuclear pairs is

$$P_{n-a}(E_o) = [7\times(1+500/E_o)]^{-1} \tag{9.4.1}$$

(where E_o is in GeV), and energy spectrum of generated particles is described by an exponential function. The distribution of transverse momentum was assumed to be

$$\varphi(p_\perp)dp_\perp = (p_\perp/p_o)^2 \exp(-p_\perp/p_o)dp_\perp, \tag{9.4.2}$$

where the average value of transverse momentum

$$\langle p_\perp \rangle = 2p_o = 0.36\ \mathrm{GeV/c}. \tag{9.4.3}$$

The results of calculation of barometric coefficients for different models and different size of showers at the sea level (in the interval $10^4 - 10^8$, corresponding to primary particle energies of $10^{14} - 10^{18}$ eV), compared with experimental data are shown in Fig. 9.4.1.

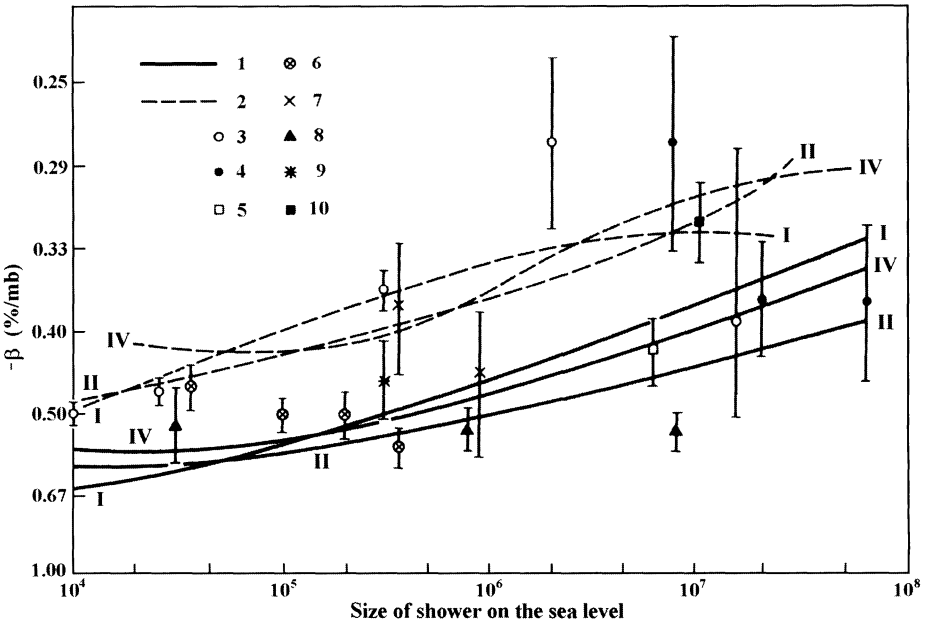

Fig. 9.4.1. Comparison of theoretical calculations of Murthy et al. (1968) of barometric coefficients for frequency of EAS as a function of the size of shower at sea level with experimental data. Full curves (*1*) – with the assumption that nucleon–antinuclear pairs are not generated, dashed curves (*2*) – with the assumption that nucleon–antinuclear pairs are generated. Roman numbers near curves – theoretical models according to Table 9.4.1. Points *3* – *10* with error bars reflects experimental results of different authors.

From Fig. 9.4.1 it can be seen that experimental errors in determining barometric coefficients are too big, so it is not possible to choose the correct model of elementary act from these data.

9.5. Theory of hard muon meteorological effects accounting the muon generation spectrum at pions decay

9.5.1. Muon generation spectrum at charged pions decay

In Chapter 5 we considered the theory of hard muon meteorological effects with the assumption that muons generated at pion decay have energy spectrum described by δ – function:

$$\omega(E_\mu) = \delta(E_\mu - \alpha E_\pi), \tag{9.5.1}$$

where E_μ and E_π are total energies of muons and charged pions, m_μ and m_π are masses of muons and pions, and $\alpha = m_\mu / m_\pi$. Dorman and Yanke (1971a) took into account the real energy spectrum of muons generated by decay of charged pions (see in Baldin et al., M1968):

$$\omega(E_\mu)=\begin{cases}\dfrac{1}{2\gamma_\pi\beta_\pi p^*_\mu} & \text{if} \quad \gamma_\pi\left(E^*_\mu-\beta_\pi p^*_\mu\right)\le E_\mu\le\gamma_\pi\left(E^*_\mu+\beta_\pi p^*_\mu\right),\\ 0, & \text{if} \quad E_\mu<\gamma_\pi\left(E^*_\mu-\beta_\pi p^*_\mu\right) \text{ or } E_\mu>\gamma_\pi\left(E^*_\mu+\beta_\pi p^*_\mu\right),\end{cases} \tag{9.5.2}$$

where

$$p^*_\mu=c\left(m^2_\pi-m^2_\mu\right)/2m_\pi,\ E^*_\mu=c^2\left(m^2_\pi+m^2_\mu\right)/2m_\pi,\ \gamma_\pi=E_\pi/m_\pi c^2,\ \beta_\pi=v_\pi/c\,. \tag{9.5.3}$$

Only pions in the energy interval $E^+_\pi\le E_\pi\le E^-_\pi$ can give a contribution to the flux of muons with energy E_μ, with probability $P(E_\mu)=dE_\pi/\left(E^-_\pi-E^+_\pi\right)$. Here E^+_π and E^-_π can be determined using Eq. 9.5.2 as:

$$E^\pm_\pi=\left(E^2_\mu+p^{*2}_\mu c^2\right)\left[E^2_\mu\left(1+\alpha^2\right)/2-\alpha^2\left(E^2_\mu+p^{*2}_\mu c^2\right)\pm E_\mu p_\mu c\left(1-\alpha^4\right)/2\right]^{-1/2}. \tag{9.5.4}$$

At very high energies, when $\beta_\pi\approx1$, Eq. 9.5.4 can be transformed to a much simpler form:

$$E^+_\pi\approx E_\mu,\quad E^-_\pi\approx E_\mu/\alpha^2\ . \tag{9.5.5}$$

Moreover, at these energies the Coulomb scattering of muons can be neglected, i.e. muons generated in pion decay conserve the direction of pions: in the laboratory system of coordinates more than 90% of muons are moving inside the cones with angle $\Omega\approx3/\gamma_\pi$.

9.5.2. Expected muon intensity at the level of observation

In Dorman and Yanke (1971a) it was assumed that muons are generated only through decay of charged pions. Let us describe the charged pion generation with energy E_π moving at zenith angle Z by the function $f_\pi(E_\pi,h_1,Z)$. As in Section 2.1.1, let us suppose that l is the transport path of pions for nuclear interactions in the air. In this case the fraction $dh/l\cos Z$ will be captured in the air layer dh. If m_π and τ_π are the mass and life time of rest charged pions, that the part of pions decayed in the air layer dh will be $d\tau/\tau$, where $d\tau=dh(c\rho(h)\cos Z)^{-1}$ is the time crossing of the layer dh ($\rho(h)$ is the density of air on the level h and c is the velocity of relativistic pions), and $\tau=\tau_\pi E_\pi/m_\pi c^2$ is the life time of pions in the system of coordinates connected with the Earth. Therefore, the probability $\varphi_\pi(E_\pi,h_1,h_2,Z)$ that pions will be not nuclear captured and not decayed in the layer from h_1 to h_2 will be determined by

$$\varphi_\pi(E_\pi,h_1,h_2,Z)=\exp\left(-\frac{h_2-h_1}{l\cos Z}\right)\exp\left(-\frac{m_\pi c}{\tau_\pi E_\pi\cos Z}\int_{h_1}^{h_2}\frac{dh}{\rho(h)}\right). \tag{9.5.6}$$

The total flux of pions through the level h_2 will be

$$N_\pi(E_\pi,h_2,Z)=\int_0^{h_2} f_\pi(E_\pi,h_1,Z)\varphi_\pi(E_\pi,h_1,h_2,Z)dh_1 . \qquad (9.5.7)$$

The number of pions which will decay in the layer h_2, h_2+dh_2 will be

$$\chi_\pi(E_\pi,h_2,Z)=\frac{d\tau}{\tau}N_\pi(E_\pi,h_2,Z)=\frac{m_\pi c^2}{\tau_\pi E_\pi}\frac{dh_2}{c\rho(h_2)\cos Z}N_\pi(E_\pi,h_2,Z). \qquad (9.5.8)$$

On the basis of Eq. 9.5.2–9.5.8 we can determine the muon generation function

$$f_\mu(E_\mu,h_2,Z)=\int_{E_\pi^+}^{E_\pi^-}\frac{m_\pi c}{\tau_\pi E_\pi}\frac{N_\pi(E_\pi,h_2,Z)dE_\pi}{\rho(h_2)\cos Z(E_\pi^- - E_\pi^+)}. \qquad (9.5.9)$$

Now we can determine the expected muon intensity at the level of observation

$$N_\mu(h_o,Z,E_{\mu\,\mathrm{det}})=\int_{E_{\mu\min}}^{\infty}dE_\mu\int_0^{h_o}f_\mu(E_\mu,h_2,Z)\varphi_\mu(E_\mu,h_2,h_o,Z)dh_2 , \qquad (9.5.10)$$

where $E_{\mu\min}$ is the minimal energy of generated muons which have energy on the level of observation $E_{\mu\,\mathrm{det}}$ (detector's cut off energy for hard muons). The value of $E_{\mu\min}$ for observations underground or on the ground with plate-parallel screen will be

$$E_{\mu\min}=\left(a(h_o-h_2)+E_{\mu\,\mathrm{det}}\right)/\cos Z , \qquad (9.5.11)$$

and for spherically symmetric screen (as for screened by 10 cm Pb ionization chambers of Compton type):

$$E_{\mu\min}=E_{\mu\,\mathrm{det}}+a(h_o-h_2)/\cos Z . \qquad (9.5.12)$$

In Eq. 9.5.10 $\varphi_\mu(E_\mu,h_2,h_o,Z)$ is the probability for muon to arrive from the level h_2 to observation level h_o:

$$\varphi_\mu(E_\mu,h_2,h_o,Z)=\exp\left(-\frac{m_\mu c}{\tau_\mu}\int_{h_2}^{h_o}\frac{dh}{\rho(h)}\left(E_\mu\cos Z-a(h-h_2)\right)^{-1}\right), \qquad (9.5.13)$$

where a is the energy loses by muon at passing of one $\mathrm{g/cm^2}$ of air ($a\approx 2\,\mathrm{MeV}/\left(\mathrm{g/cm^2}\right)$ for relativistic one-charge particles).

Eq. 9.5.10 by accounting Eq-s. 9.5.6, 9.5.7, 9.5.9 and 9.5.13 can be rewritten as

$$N_\mu(h_o,Z,E_{\mu\min})=\int_0^{h_o}dh_2\int_0^{h_2}dh_1\int_{E_{\mu\min}}^{\infty}dE_\mu\int_{E_\pi^+}^{E_\pi^-}dE_\pi F(E_\pi,E_\mu,h_1,h_2,h_o,Z), \quad (9.5.14)$$

where

$$F(E_\pi,E_\mu,h_1,h_2,h_o,Z)=\frac{m_\pi c f_\pi(E_\pi,h_1,Z)}{\tau_\pi E_\pi \rho(h_2)(E_\pi^- - E_\pi^+)\cos Z}\exp\left(-\frac{h_2-h_1}{l\cos Z}\right)$$

$$\times\exp\left(-\frac{m_\pi c}{\tau_\pi E_\pi}\int_{h_1}^{h_2}\frac{dh}{\rho(h)}\right)\exp\left(-\frac{m_\mu c}{\tau_\mu}\int_{h_2}^{h_o}\frac{dh}{\rho(h)}\left(E_\mu\cos Z-a(h-h_2)\right)^{-1}\right). \quad (9.5.15)$$

For the function of pion generation we choose the same as in Section 5.1:

$$f_\pi(E_\pi,h_1,Z)=AE_\pi^{-\gamma}\exp(-h_1/L\cos Z), \quad (9.5.16)$$

where A is some constant, and L is absorption path of meson-generating nucleon component of primary CR. The connection between air density in Eq. 9.5.15 and air temperature is determined by the classical relation

$$\rho(h)=gh/R_oT, \quad (9.5.17)$$

where g is the gravitational acceleration, $T(h)$ is the air temperature in °K, and R_o is the gas constant for dry air. Calculations in Dorman and Yanke (1971a) were carried for three vertical distributions of air temperature, shown in Fig. 9.5.1.

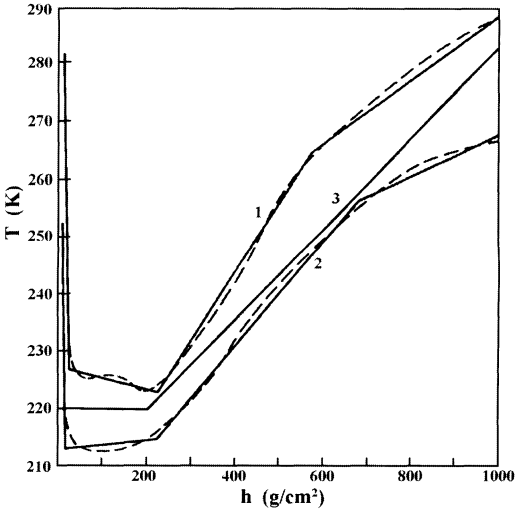

Fig. 9.5.1. Air temperature distribution in the atmosphere. Dashed curves: averaged for many years observed temperature distribution over Moscow (*1* – for June, *2* – for January). Full curves: *1* and *2* – approximations in Dorman and Yanke (1971a) as averages for summer and winter, *3* - approximation in Dorman (1954a, M1957) as annual average.

9.5.3. Comparison of theory with observations for muon energy spectrum, zenith angle distribution, and altitude dependence of intensity

The comparison of theory with observations for muon energy spectrum, zenith angle distribution and altitude dependence of intensity is important for controlling a lot of parameters γ, l, L, and others, determined meteorological coefficients. In Section 5.1 we chose $\gamma = 2.5$, $l = 60\ \mathrm{g/cm^2}$, $L = 120\ \mathrm{g/cm^2}$. According to experimental investigations of pion energy spectrum in the interval 0.7–150 GeV of Brooke et al. (1964), $L = 127 \pm 4\ \mathrm{g/cm^2}$. So we will assume here $L = 120\ \mathrm{g/cm^2}$, but for comparison we will carry out calculations also for $L = 90$ and $150\ \mathrm{g/cm^2}$.

Usually it is supposed that the transport path for pion absorption (attenuation length) is $l \approx 60\ \mathrm{g/cm^2}$. It is about the same as the transport path for pion interaction (corresponding to the geometrical cross-section of air atoms). But for very high energy pions they can interact more than once before absorption, therefore some increase of l with increasing pion energy is expected. For example, in Cini-Castagnoli and Dodero (1967) it was shown on the basis of investigation of temperature effect at the depth 70 m w. e. that $l = 142 \pm 10\ \mathrm{g/cm^2}$ for pions in energy interval 30–60 GeV. So in Dorman and Yanke (1971a) calculations are carried out at different values of l from 60 to 150 $\mathrm{g/cm^2}$. Another very important parameter is the slope γ of pion generation spectrum. In Table 9.5.1 are presented the experimental data of Hayman and Wolfendale (1962) and values calculated by Dorman and Yanke (1971a) at $\gamma = 2.65$.

Table 9.5.1. The comparison of experimental data (in $\mathrm{cm^{-2}.sec^{-1}.ster^{-1}.(GeV/c)^{-1}}$)of Hayman and Wolfendale (1962) with calculated by Eq. 9.5.14 according to Dorman and Yanke (1971a) at $\gamma = 2.65$.

Momentum, p_μ, GeV/c	Observed differential intensity,	Relative error, %	Theoretical differential intensity,	$\frac{I_{\mu\ obs} - I_{\mu\ theor}}{I_{\mu\ obs}}$, %
5.45	3.21×10^{-4}	± 4.2	3.42×10^{-4}	−6.5
6.45	1.95×10^{-4}	± 2.8	1.92×10^{-4}	+1.5
10.8	8.51×10^{-5}	± 3.0	8.71×10^{-5}	−2.3
14.6	4.35×10^{-5}	± 2.6	4.32×10^{-5}	+0.7
22.6	1.39×10^{-5}	± 2.6	1.42×10^{-5}	−2.2
34.3	5.85×10^{-6}	± 2.6	5.85×10^{-6}	0
56.1	1.22×10^{-6}	± 4.5	1.08×10^{-6}	+12.5
75.5	5.75×10^{-7}	± 8	4.91×10^{-7}	+14.6
112	1.36×10^{-7}	± 10	1.23×10^{-7}	+9.6
153	5.18×10^{-8}	± 18	4.43×10^{-8}	+14
244	1.14×10^{-8}	± 20	0.93×10^{-8}	+18
413	1.98×10^{-9}	+60/−37	1.48×10^{-9}	+25
894	1.84×10^{-10}	+70/−42	0.95×10^{-10}	+48

It can be seen from Table 9.5.1 that the differences between the theoretical and the experimental results are within experimental errors. Only for momentum higher than 50 GeV/c there is a tendency of some systematic deficit in the theoretical differential intensity in comparison with observations. It can be caused by the increasing of l with increasing of pions energy according to Cini-Castagnoli and Dodero (1967), as discussed above.

In Fig. 9.5.2 we show the comparison of the differential muon energy spectrum observed by Hayman and Wolfendale (1962), with theoretical values according to Dorman and Yanke (1971a) at $\gamma = 2.5$ and at $\gamma = 2.1$.

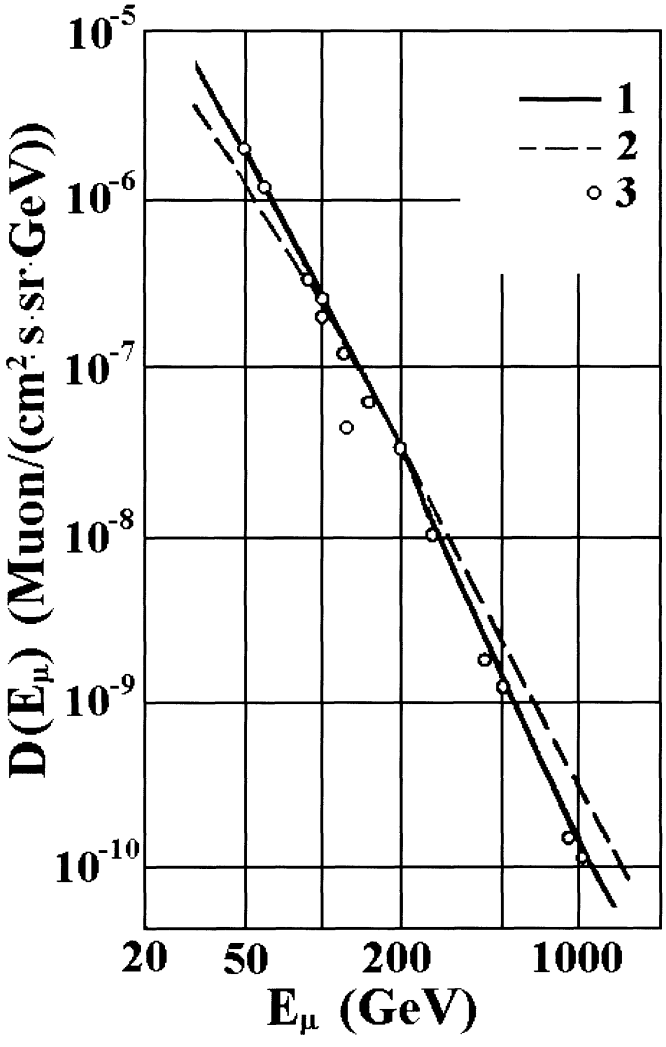

Fig. 9.5.2. Comparison of observed by Hayman and Wolfendale (1962) differential muon energy spectrum (open circles *3*) with theoretical according to Dorman and Yanke (1971a) at $\gamma = 2.5$ (full curve *1*) and at $\gamma = 2.1$ (dashed curve *2*).

It can be seen that theoretical the results at $\gamma = 2.1$ contradict the observed data, and for $\gamma = 2.5$ there is good agreement. Fig. 9.5.3 shows the expected zenith angle distribution.

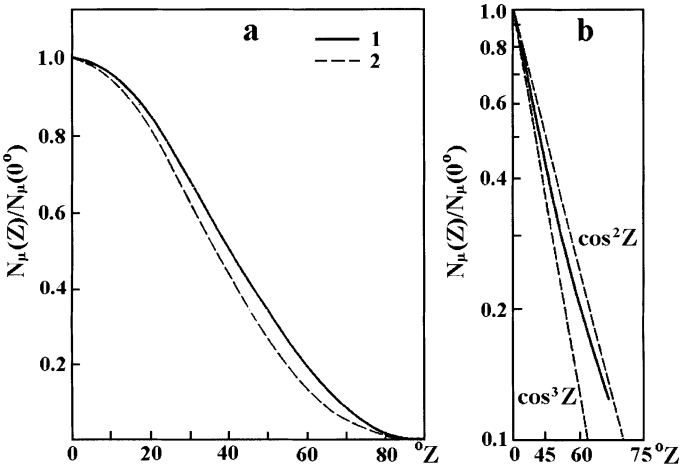

Fig. 9.5.3. Expected zenith angle distribution at sea level for $E_{\mu\,\min} = 0.4$ GeV : *a* – for $\gamma = 2.5$ (full curve *1*) and for $\gamma = 2.1$ (dashed curve *2*); *b* – for $\gamma = 2.5$ (full curve) in double logarithmic scale (for comparison by dashed curves are shown dependences $\cos^2 Z$ and $\cos^3 Z$).

Fig. 9.5.4 gives a comparison between the observed and the predicted altitude dependence of muon intensity at $\gamma = 2.6$, $L = 140$ g/cm^2, and $E_{\mu\,\min} = 0.4$ GeV .

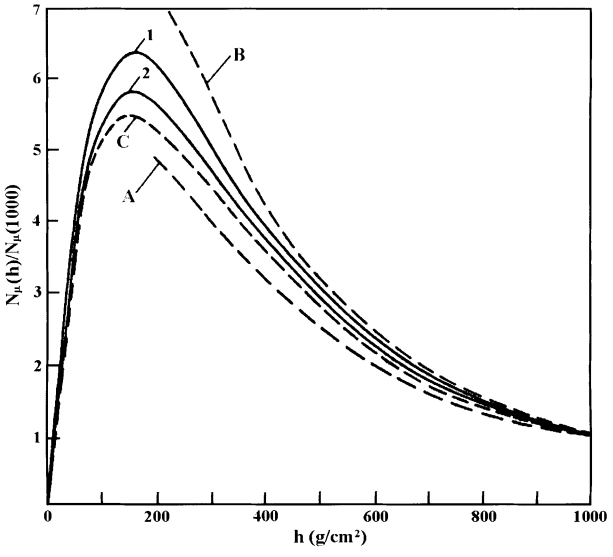

Fig. 9.5.4. Comparison of observed altitude dependence of muon intensity (dashed curves: *A* and *B* – according to Rossi, 1949 at equator and at high latitudes, correspondingly; *C* – according to Pullar and Dymond, 1953 at latitude 56°S) with the expected for $l = 150$ and 60 g/cm^2 (full curves *1* and *2*).

To estimate the sensitivity of muon intensity altitude dependence from γ, L and l, we show in Fig. 9.5.5 the expected ratio

$$R_\mu(150/1000)=\frac{N_\mu\left(h_o=150\ \mathrm{g/cm^2}\right)}{N_\mu\left(h_o=1000\ \mathrm{g/cm^2}\right)} \tag{9.5.18}$$

at different γ as a function of L and l.

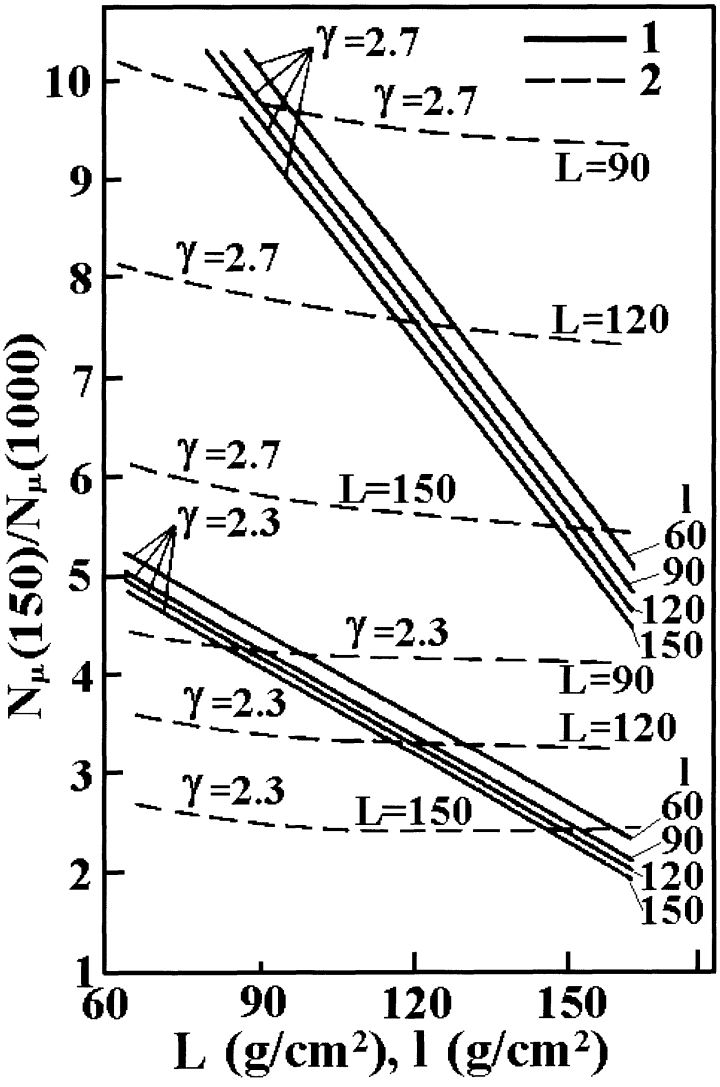

Fig. 9.5.5. Expected ratio $R_\mu(150/1000)$ at different γ in dependence from L at constant l (full curves *1*), and in dependence from l at constant L (dashed curves *2*).

It can be seen from Fig. 9.5.5 that the ratio $R_\mu(150/1000)$ is very sensitive to the value of γ: the change of γ from 2.7 to 2.3 leads to a decrease of $R_\mu(150/1000)$ by about a factor of 2. Increasing of L from 90 to 150 g/cm^2 led to decreasing of $R_\mu(150/1000)$ also about two times. The sensitivity of $R_\mu(150/1000)$ to l is very weak: increasing of l from 60 to 150 g/cm^2 led to decreasing of $R_\mu(150/1000)$ only on 10÷20%. Results of theoretical calculations of $R_\mu(150/1000)$ in Fig. 9.5.5 for different values of γ, L and l in comparison with experimental data can be used for estimation of effective values of these parameters important for calculations of meteorological coefficients.

9.5.4. Calculations of barometric coefficients for ground and underground observations of hard muons

To obtain expressions for barometric coefficients, it is necessary to vary Eq. 9.5.14 over h_o taking into account Eq. 9.5.11:

$$\left(\frac{\Delta N_\mu(h_o,Z,E_{\mu\min})}{N_\mu(h_o,Z,E_{\mu\min})}\right)_h = -\frac{a\Delta h_o}{\cos Z}\int_0^{h_o} dh_2 \int_0^{h_2} dh_1 \int_{E_\pi^+}^{E_\pi^-} dE_\pi \frac{F(E_\pi,E_{\mu\min},h_1,h_2,h_o,Z)}{N_\mu(h_o,Z,E_{\mu\min})}$$

$$-\frac{m_\mu c\Delta h_o}{\tau_\mu \rho(h_o) N_\mu(h_o,Z,E_{\mu\min})}\int_0^{h_o} dh_2 \int_0^{h_2} dh_1 \int_{E_{\mu\min}}^{\infty} dE_\mu \int_{E_\pi^+}^{E_\pi^-} dE_\pi \frac{F(E_\pi,E_\mu,h_1,h_2,h_o,Z)}{E_\mu \cos Z - a(h_o-h_2)}$$

$$+\frac{\Delta h_o}{N_\mu(h_o,Z,E_{\mu\min})}\int_0^{h_o} dh_1 \int_{E_{\mu\min}}^{\infty} dE_\mu \int_{E_\pi^+}^{E_\pi^-} dE_\pi F(E_\pi,E_\mu,h_1,h_o,h_o,Z). \qquad (9.5.19)$$

The first term on the right hand side of Eq. 9.5.19 reflects the negative absorption effect $\beta_a(h_o,E_{\mu\min},Z)$, the second term reflects negative muon decay effect $\beta_d(h_o,E_{\mu\min},Z)$ – increasing of muon decay with increasing of h_o (caused by increasing of the height of the level of muon generation with increasing of h_o). The third term reflects the positive generation effect $\beta_g(h_o,E_{\mu\min},Z)$ – increasing of pion and muon fluxes with increasing of h_o; this part dominates at high altitudes where total barometric effect became positive, but it is negligibly small near sea level).

Results of calculations of $\beta_a(h_o,E_{\mu\min},Z)$, $\beta_d(h_o,E_{\mu\min},Z)$, $\beta_g(h_o,E_{\mu\min},Z)$, and total barometric coefficient $\beta(h_o,E_{\mu\min},Z)$ are shown in Fig. 9.5.6 *vs* the zenith angle Z for different values of $E_{\mu\min}$ from 0.4 up to 500 GeV.

In Fig. 9.5.7 are shown the altitude dependences of β_a,β_d,β_g, and $\beta=\beta_a+\beta_d+\beta_g$ at $\gamma=2.5$, and $E_{\mu\min}=0.4$ GeV.

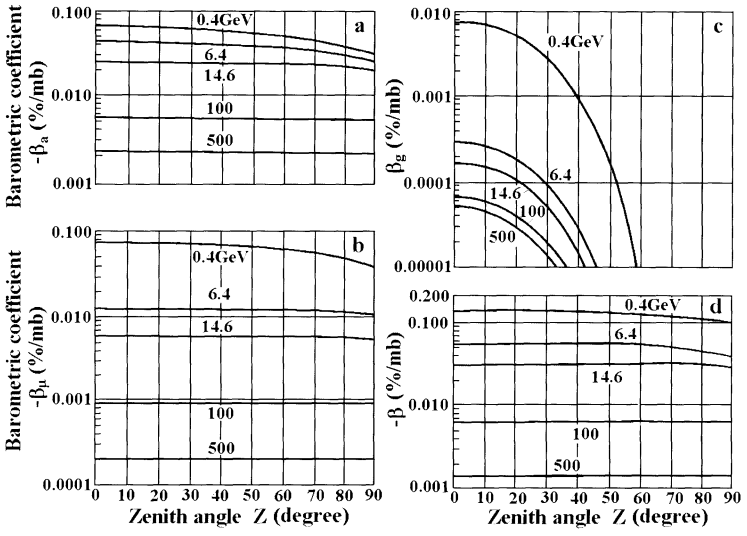

Fig. 9.5.6. Results of calculations: *a* – absorption part of barometric coefficient $\beta_a(h_o, E_{\mu\min}, Z)$; *b* – decay part of barometric coefficient $\beta_d(h_o, E_{\mu\min}, Z)$; *c* – generation part of barometric coefficient $\beta_g(h_o, E_{\mu\min}, Z)$; and *d* – total barometric coefficient $\beta(h_o, E_{\mu\min}, Z)$ in dependence of zenith angle *Z* for different values of $E_{\mu\min}$ from 0.4 GeV up to 500 GeV (numbers near curves).

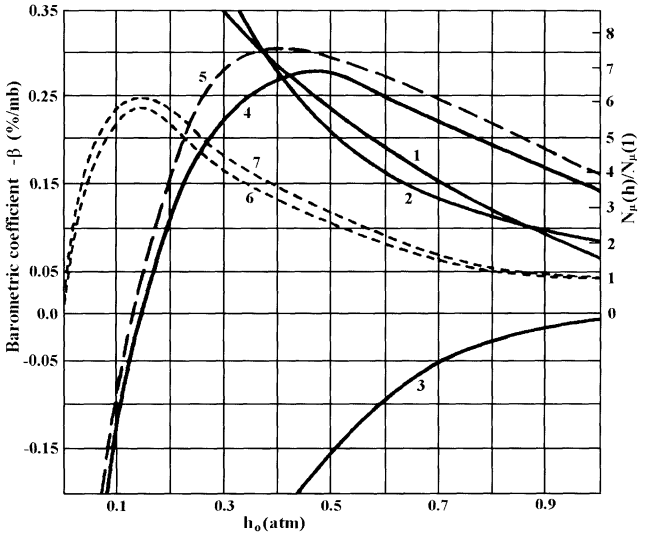

Fig. 9.5.7. Altitude dependences of $\beta_a, \beta_d, \beta_g$, and $\beta = \beta_a + \beta_d + \beta_g$ at $\gamma = 2.5$, and $E_{\mu\min} = 0.4$ GeV. *1* – absorption part of barometric coefficient β_a; *2* – decay part of barometric coefficient β_d; *3* – generation part of barometric coefficient β_g; *4* – total barometric coefficient β for air temperature distribution *3* in Fig. 9.5.1; *5* - total barometric coefficient β for air temperature distribution *2* in Fig. 9.5.1; curves *6* and *7* – altitude dependences of muon intensity (right scale) for air temperature distributions *3* and *2* in Fig. 9.5.1.

The dependence of β on $E_{\mu\min}$ at $\gamma = 2.5$ and $Z = 0^\circ$ is shown in Fig. 9.5.8.

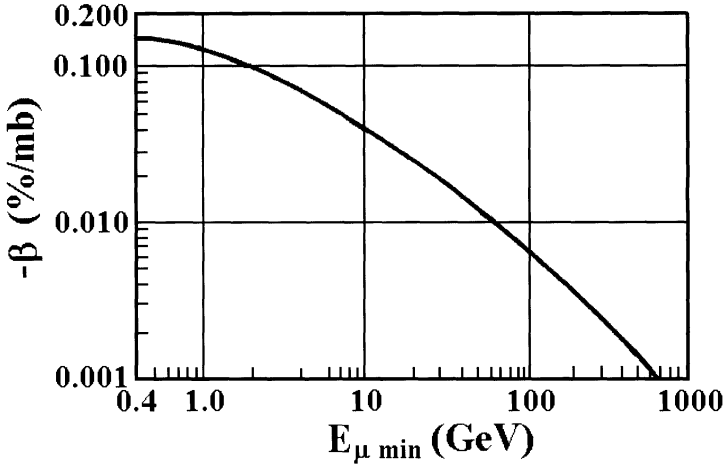

Fig. 9.5.8. The dependence of barometric coefficient β at sea level from $E_{\mu\min}$ at $\gamma = 2.5$ and $Z = 0^\circ$.

In Fig. 9.5.9 are shown the dependences of barometric coefficients at sea level on the value of γ in the interval from 2.0 to 3.0.

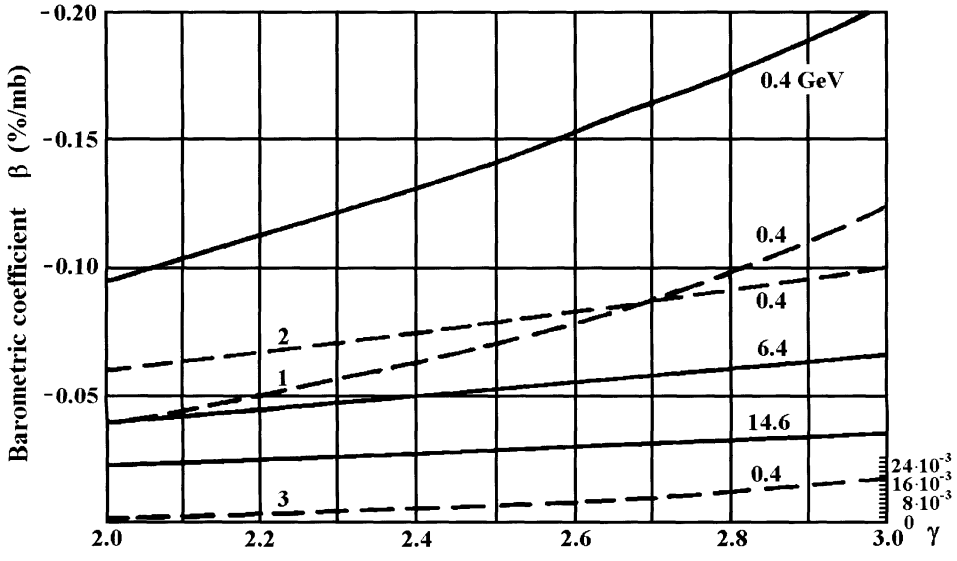

Fig. 9.5.9. The dependences of barometric coefficients at sea level from value of γ in the interval from 2.0 to 3.0. Dashed curves for $E_{\mu\min} = 0.4$ GeV : *1* – absorption part of barometric coefficient; *2* – decay part of barometric coefficient; *3* – generation part of barometric coefficient (right scale). Full curves: total barometric coefficients for different values of $E_{\mu\min}$ (numbers near curves in GeV).

The dependences of $\beta_a, \beta_d, \beta_g$, and β at $\gamma = 2.5$ on the zenith angle Z are shown in Fig. 9.5.10.

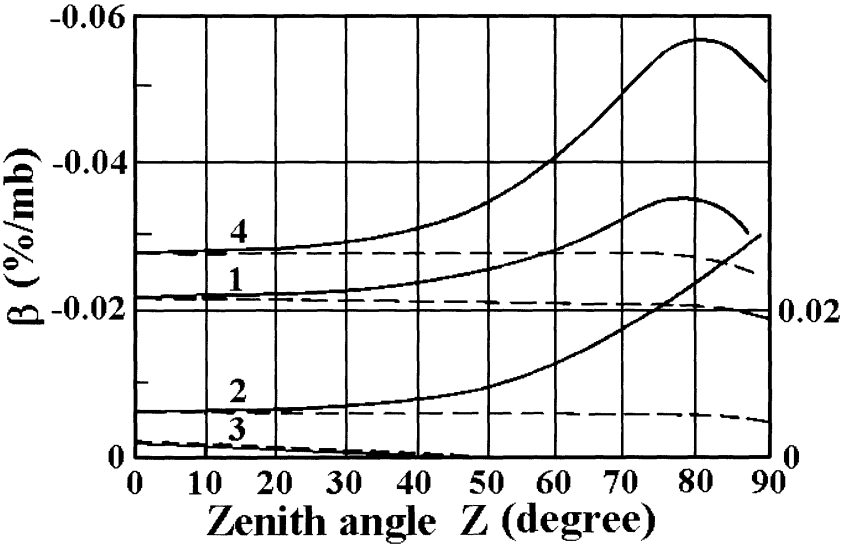

Fig. 9.5.10. The dependences of $\beta_a, \beta_d, \beta_g$, and β at $\gamma = 2.5$, $E_{\mu\min} = 14.6$ GeV from zenith angle Z at sea level for plane-horizontal shield (dashed curves) and for spherical-symmetrical shield (full curves). *1* – absorption part of barometric coefficient; *2* – decay part of barometric coefficient; *3* – generation part of barometric coefficient (right scale); *4* - total barometric coefficient.

9.5.5. Calculations of temperature coefficients for ground and underground observations of hard muons

Temperature effect of hard muons for ground and underground observations is caused by the change of air density $\rho(h)$, influenced on decay of pions and muons. The expression for this effect can be obtained from Eq. 9.5.14 for muon intensity by varying over $\rho(h)$:

$$\left(\frac{\Delta N_\mu(h_o,Z,E_{\mu\min})}{N_\mu(h_o,Z,E_{\mu\min})}\right)_T = -\int_{E_{\mu\min}}^{\infty} dE_\mu \int_0^{h_o} dh_2 \frac{\Delta\rho(h_2)}{\rho(h_2)} \int_0^{h_2} dh_1 \int_{E_\pi^+}^{E_\pi^-} dE_\pi \frac{F(E_\pi,E_\mu,h_1,h_2,h_o,Z)}{N_\mu(h_o,Z,E_{\mu\min})}$$

$$+ \int_{E_{\mu\min}}^{\infty} dE_\mu \int_0^{h_o} dh_2 \int_0^{h_2} dh_1 \int_{E_\pi^+}^{E_\pi^-} dE_\pi \frac{F(E_\pi,E_\mu,h_1,h_2,h_o,Z)}{N_\mu(h_o,Z,E_{\mu\min})} \frac{m_\pi c}{\tau_\pi E_\pi \cos Z} \int_{h_1}^{h_2} \frac{dh\Delta\rho(h)}{\rho^2(h)}$$

$$+ \int_0^{h_o} dh_1 \int_{E_{\mu\min}}^{\infty} dE_\mu \int_{E_\pi^+}^{E_\pi^-} dE_\pi \frac{F(E_\pi,E_\mu,h_1,h_2,h_o,Z)}{N_\mu(h_o,Z,E_{\mu\min})} \frac{m_\mu c}{\tau_\mu} \int_{h_2}^{h_o} \frac{dh\Delta\rho(h)/\rho(h)}{E_\mu \cos Z - a(h-h_2)}. \qquad (6.5.20)$$

Taking into account Eq. 9.5.17 for variation of air density caused only by change of air temperature, we obtain

$$\frac{\Delta\rho(h)}{\rho(h)} = -\frac{\Delta T(h)}{T(h)};\ \frac{\Delta\rho(h)}{\rho^2(h)} = -\frac{R_o}{gh}\Delta T(h)\,. \tag{9.5.21}$$

After introducing Eq. 9.5.21 in Eq. 9.5.20, we obtain

$$\left(\frac{\Delta N_\mu(h_o,Z,E_{\mu\min})}{N_\mu(h_o,Z,E_{\mu\min})}\right)_T = \int_{E_{\mu\min}}^{\infty} dE_\mu \int_0^{h_o} dh_2 \int_0^{h_2} dh_1 \int_{E_\pi^+}^{E_\pi^-} dE_\pi \frac{F(E_\pi,E_{\mu\min},h_1,h_2,h_o,Z)}{N_\mu(h_o,Z,E_{\mu\min})}$$

$$\times\left\{\frac{\Delta T(h_2)}{T(h_2)} - \frac{m_\pi c}{\tau_\pi E_\pi}\int_{h_1}^{h_2}\frac{\Delta T(h)dh}{h\cos Z} - \frac{m_\mu cR_o}{\tau_\mu g}\int_{h_2}^{h_o}\frac{\Delta T(h)dh}{h\left(E_\mu\cos Z - a(h-h_2)\right)}\right\}. \tag{9.5.22}$$

Eq. 9.5.22 can be rewritten as

$$\left(\frac{\Delta N_\mu(h_o,Z,E_{\mu\min})}{N_\mu(h_o,Z,E_{\mu\min})}\right)_T = \int_0^{h_o} W_T(h,h_o,Z,E_{\mu\min})\Delta T(h)dh\,, \tag{9.5.23}$$

where

$$W_T(h,h_o,Z,E_{\mu\min}) = W_{T\mu}(h,h_o,Z,E_{\mu\min}) + W_{T\pi}(h,h_o,Z,E_{\mu\min}) \tag{9.5.24}$$

and

$$W_{T\mu}(h,h_o,Z,E_{\mu\min}) = -\frac{(m_\mu cR_o/\tau_\mu g)}{N_\mu(h_o,Z,E_{\mu\min})}$$

$$\times \int_{E_{\mu\min}}^{\infty} dE_\mu \int_0^{h} dh_2 \int_0^{h_2} dh_1 \int_{E_\pi^+}^{E_\pi^-} dE_\pi \frac{F(E_\pi,E_\mu,h_1,h_2,h_o,Z)}{h\left(E_\mu\cos Z - a(h-h_2)\right)}, \tag{9.5.25}$$

$$W_{T\pi}(h,h_o,Z,E_{\mu\min}) = \frac{1}{N_\mu(h_o,Z,E_{\mu\min})}$$

$$\times \int_{E_{\mu\min}}^{\infty} dE_\mu \int_0^{h} dh_1 \int_{E_\pi^+}^{E_\pi^-} dE_\pi \left\{\frac{1}{T(h)} - \frac{m_\pi c}{\tau_\pi E_\pi\cos Z}\int_{h_1}^{h_2}\frac{dh}{T(h)}\right\} F(E_\pi,E_\mu,h_1,h_2,h_o,Z). \tag{9.5.26}$$

Results of calculations of negative $W_{T\mu}$, positive $W_{T\pi}$ and total W_T for zenith angles 0, 45, 60 and 75° in dependence of the depth of atmosphere for different $E_{\mu\min}$ are shown in Fig. 9.5.11–9.5.14. In all cases it is assumed that the observations are at sea

level ($h_o = 1$ atm); $E_{\mu\,\min} = 0.4$ GeV corresponding to a standard shield of 10 cm Pb, and with bigger $E_{\mu\,\min}$ – observations underground on different depths.

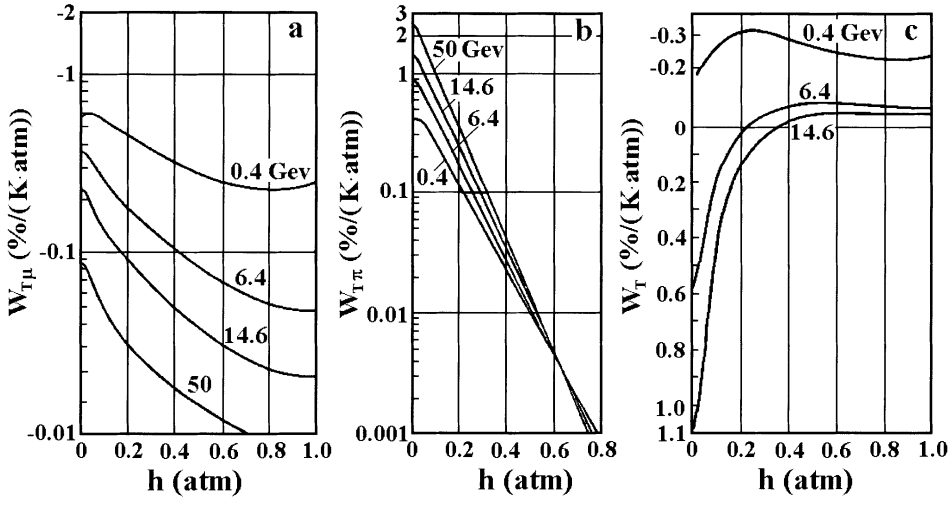

Fig. 9.5.11. Negative part of muon temperature coefficient $W_{T\mu}$ (*a*), positive part $W_{T\pi}$ (*b*), and total temperature coefficient W_T (*c*) for zenith angle $Z = 0°$ and observations at sea level ($h_o = 1$ atm) in dependence of the depth of atmosphere h for different values of $E_{\mu\,\min}$ (numbers near curves in GeV). Value $E_{\mu\,\min} = 0.4$ GeV corresponds observations with the standard shield 10 cm Pb, and with bigger $E_{\mu\,\min}$ – observations underground on different depths.

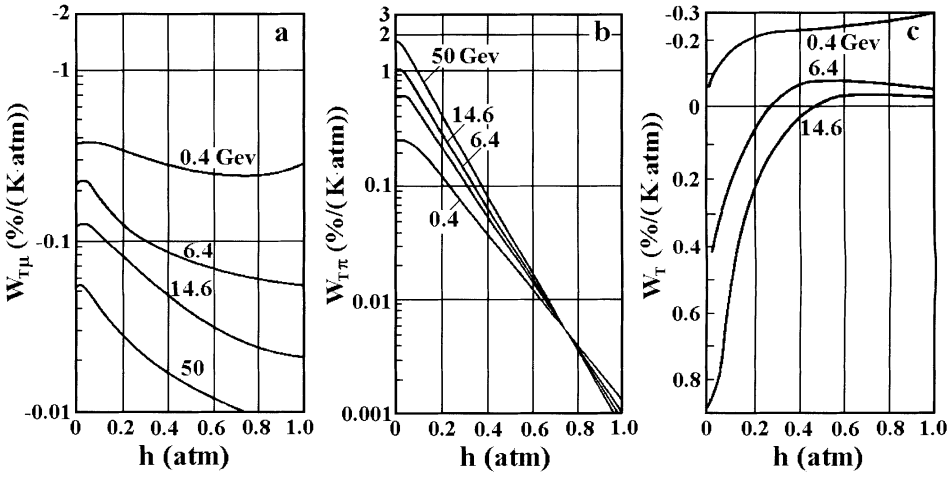

Fig. 9.5.12. The same as in Fig. 9.5.11, but for zenith angle $Z = 45°$.

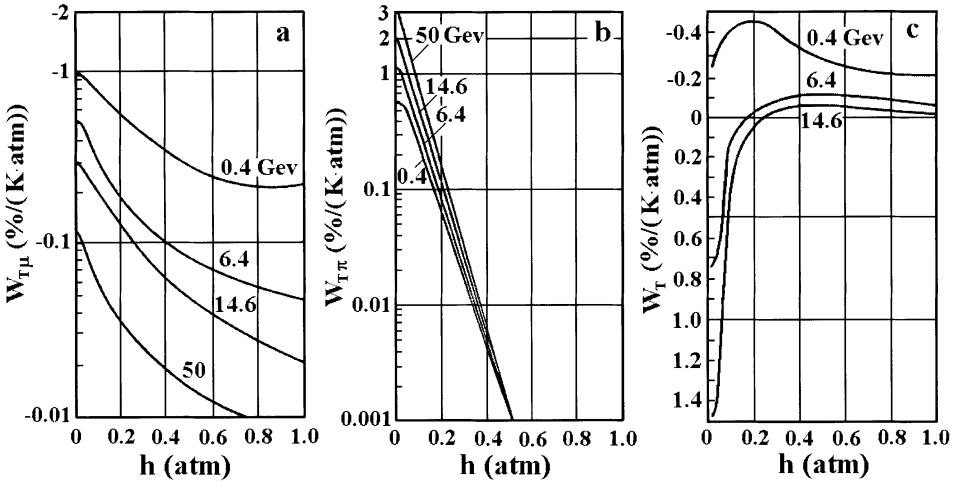

Fig. 9.5.13. The same as in Fig. 9.5.11, but for zenith angle $Z = 60°$.

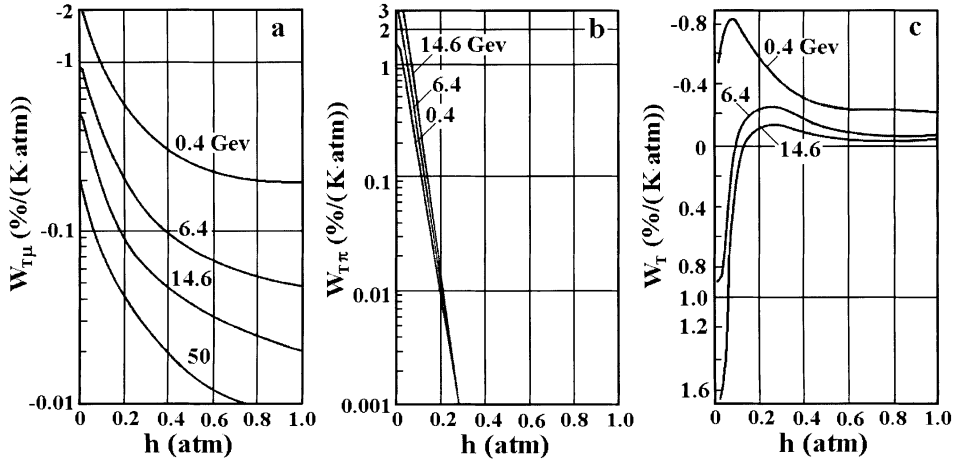

Fig. 9.5.14. The same as in Fig. 9.5.11, but for zenith angle $Z = 75°$.

It can be seen that for vertically arriving primary particles (Z = 0°), $W_{T\mu}$ has a maximum near 100 g/cm^2, near the region of muon generation. This position of maximum moves to smaller h with increasing zenith angle Z and with increasing $E_{\mu\min}$.

The dependence of $W_{T\mu}$, $W_{T\pi}$ and W_T for observations at sea level ($h_o = 1$ atm) on the zenith angle Z is shown in Fig. 9.5.15–9.5.18.

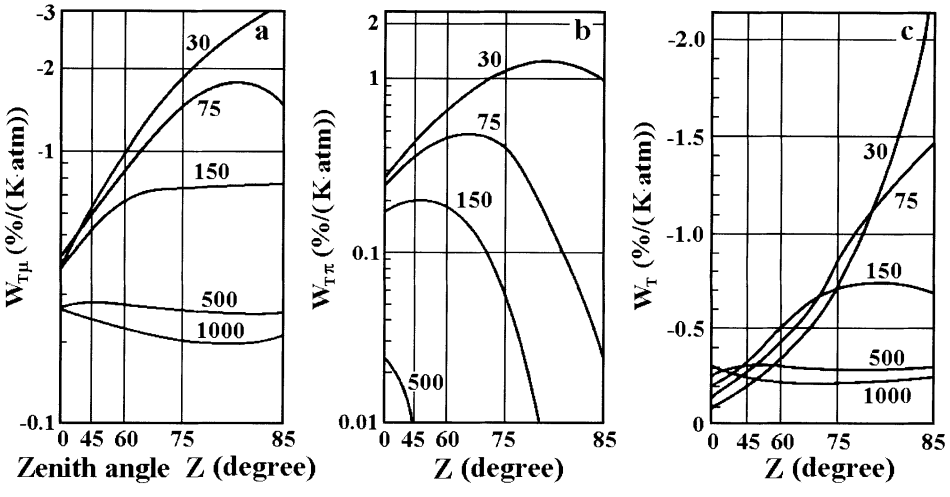

Fig. 9.5.15. The dependences of $W_{T\mu}$, $W_{T\pi}$ and W_T on the zenith angle Z at $\gamma = 2.5$ and $E_{\mu\min} = 0.4$ GeV for different levels of atmosphere (numbers near curves in g/cm^2).

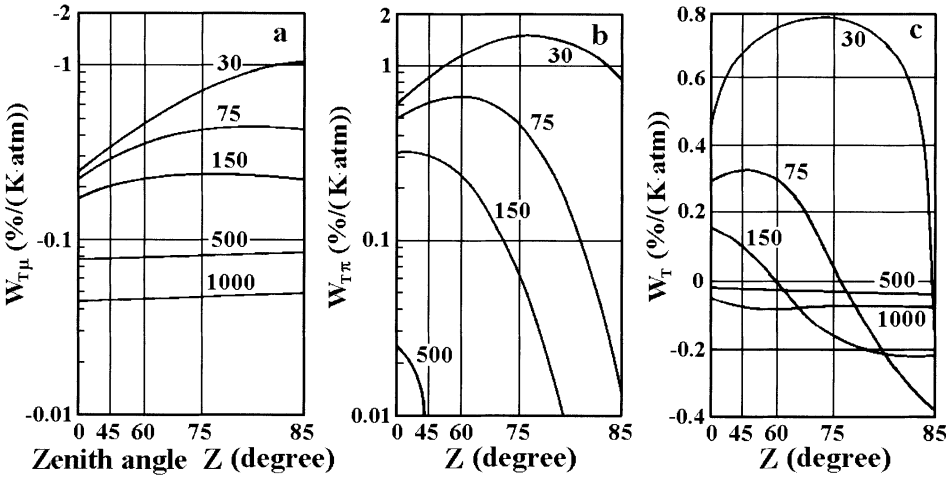

Fig. 9.5.16. The same as in Fig. 9.5.15, but for $E_{\mu\min} = 6.4$ GeV.

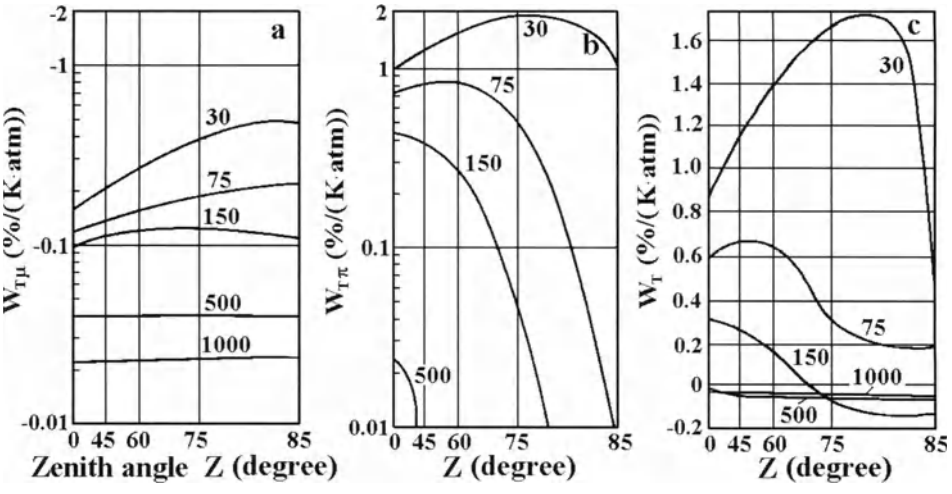

Fig. 9.5.17. The same as in Fig. 9.5.15, but for $E_{\mu\min} = 14.6$ GeV.

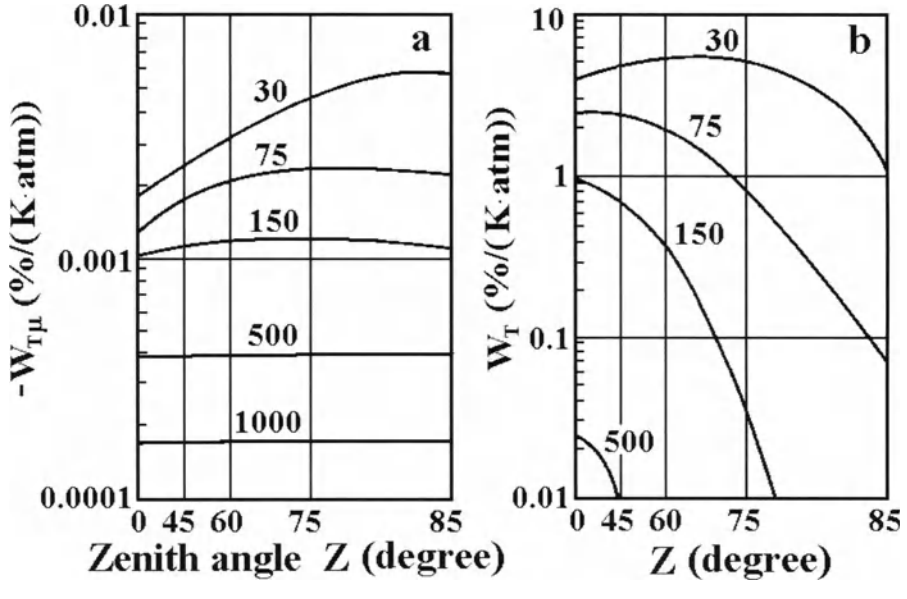

Fig. 9.5.18. The dependences of $W_{T\mu}$, and W_T from zenith angle Z at $\gamma = 2.5$ for observations deep underground $(E_{\mu\min} = 2000$ GeV$)$ for different levels of atmosphere (numbers near curves in g/cm^2).

The sensitivity of the temperature coefficients to the average vertical distribution of temperature can be seen from Fig. 9.5.19, which shows the temperature coefficients for Moscow in June and in January (the vertical distributions of temperature were shown in Fig. 9.5.1). It can be seen from Fig. 9.5.19 that this sensitivity is very weak.

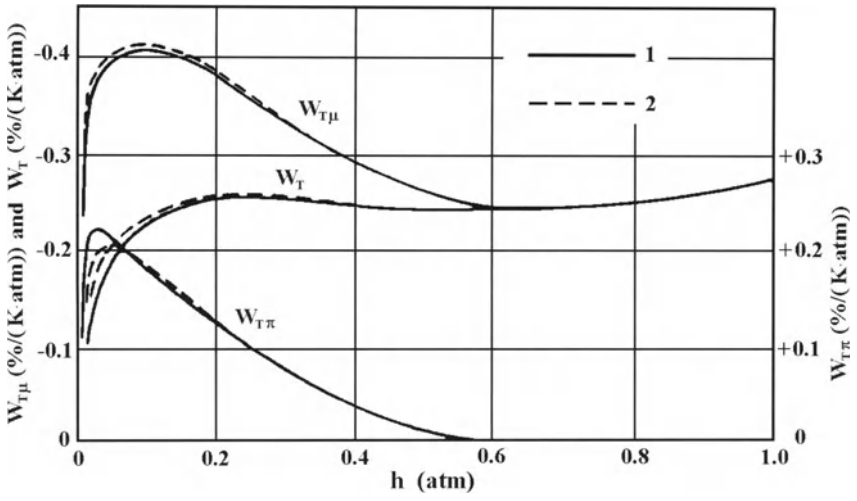

Fig. 9.5.19. Temperature coefficients negative $W_{T\mu}$, positive $W_{T\pi}$ (left scale), and total W_T for Moscow in June (full curves *1*) and in January (dashed curves *2*) for $\gamma = 2.5$ and $E_{\mu\,\min} = 0.4$ GeV. Corresponding average vertical distributions of air temperature were shown in Fig. 9.5.1.

The sensitivity of temperature coefficients to the chouse of values of attenuation length l for pions can be seen from Fig. 9.5.20, which shows the results for $W_{T\mu}$ and $W_{T\pi}$ at $L = 120$ g/cm^2 for $l = 60, 120$ and 240 g/cm^2.

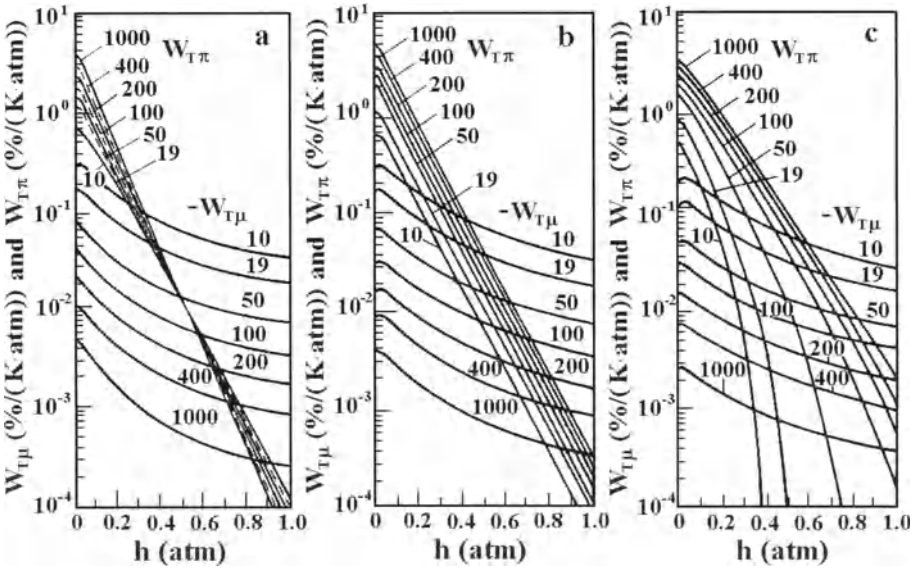

Fig. 9.5.20. Temperature coefficients negative $W_{T\mu}$ and positive $W_{T\pi}$ in dependence of attenuation length l for pions at $L = 120$ g/cm^2 : *a*, *b* and *c* - for $l = 60$, 120 and 240 g/cm^2.

To obtain temperature coefficients for real detectors (ionization chambers, cubical, semi-cubical, and multi-directional muon telescopes) it is necessary to take into account the zenith–azimuth sensitivity diagram $\Psi(Z,Y)$, where Y is the azimuth angle. We suppose that zenith-azimuth sensitivity diagrams are normalized:

$$\int_0^{\pi/2} \sin Z dZ \int_0^{2\pi} \Psi(Z,Y) dY = 1. \tag{9.5.27}$$

In this case the detector's temperature coefficients will be

$$W_T(h,h_o,\Psi,E_{\mu\min}) = \int_0^{\pi/2} \sin Z dZ \int_0^{2\pi} W_T(h,h_o,Z,E_{\mu\min})\Psi(Z,Y)dY, \tag{9.5.28}$$

$$W_{T\mu}(h,h_o,\Psi,E_{\mu\min}) = \int_0^{\pi/2} \sin Z dZ \int_0^{2\pi} W_{T\mu}(h,h_o,Z,E_{\mu\min})\Psi(Z,Y)dY, \tag{9.5.29}$$

$$W_{T\pi}(h,h_o,\Psi,E_{\mu\min}) = \int_0^{\pi/2} \sin Z dZ \int_0^{2\pi} W_{T\pi}(h,h_o,Z,E_{\mu\min})\Psi(Z,Y)dY. \tag{9.5.30}$$

According to Kawasaki et al. (1957) the function $\Psi(Z,Y)$ for vertical directed detectors with angular aperture Λ can be approximately described as

$$\Psi(Z,Y) \propto 4(\Lambda - 2Z)/\Lambda^2. \tag{9.5.31}$$

In Fig. 9.5.21 are shown detector's temperature coefficients for angle apertures $\Lambda = 0, 90, 120, 170^o$.

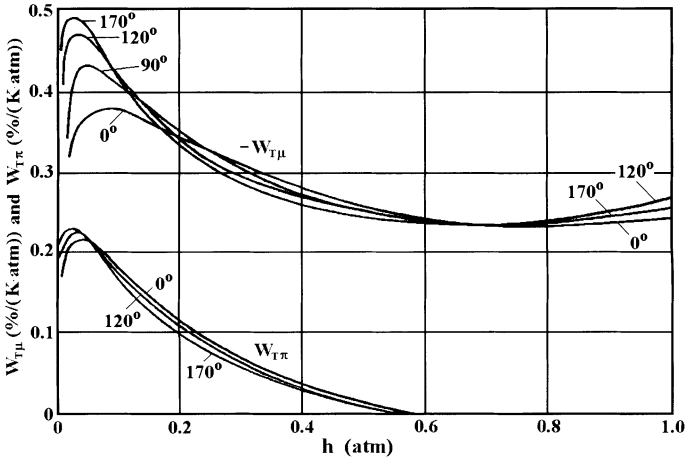

Fig. 9.5.21. Temperature coefficients negative $W_{T\mu}$ and positive $W_{T\pi}$ for vertical muon telescope for $E_{\mu\min} = 0.4$ GeV with angle aperture $\Lambda = 0, 90, 120, 170^o$ (numbers near curves).

9.6. Development of the theory of soft muon meteorological effects

Dorman and Yanke (1971b) developed the theory of soft muon meteorological effects accounting the spectrum of muon generation and angle distribution at pions decay, and coulomb scattering. As we showed in Section.9.5, for hard muons the angle scattering is very small and can be neglecting. The other situation is for soft muons: to obtain more exact results it is necessary to take into account these processes as well as the spectrum of muon generation at pions decay.

9.6.1. Expected intensity and energy spectrum of soft muons

Soft muons are generated by decay of pions mostly on the height $150-250\ \mathrm{g/cm^2}$. Therefore, muons at this height must be generated with average energy about 1 GeV to become soft muons near sea level. According to Baldin et al. (M1968), Coulomb scattering for these muons will give change of moving direction not more than $5\div 8^{o}$ from the primary direction of muon. For calculation of expected intensity and energy spectrum of soft muons, we can use Eq. 9.5.14 for the intensity and energy spectrum of hard muons

$$N_{\mu}\left(h_o,Z,E_{\mu\,\mathrm{det}}\right)=\int_0^{h_o}dh_2\int_0^{h_2}dh_1\int_{E_{\mu\,\min}}^{E_{\mu\,\max}}dE_{\mu}\int_{E_{\pi}^{+}}^{E_{\pi}^{-}}dE_{\pi}F\left(E_{\pi},E_{\mu},h_1,h_2,h_o,Z\right), \quad (9.6.1)$$

where E_{π}^{+} and E_{π}^{-} were determined by Eq. 9.5.4, and $E_{\mu\,\mathrm{det}}\approx 0.4$ GeV is the minimal energy of muons which can cross 10 *cm* Pb. In Eq. 9.6.1 for the plate-parallel screen

$$E_{\mu\,\min}=m_{\mu}c^2+a\left(h_o-h_2\right)/\cos Z,\quad E_{\mu\,\max}=E_{\mu\,\mathrm{det}}+a\left(h_o-h_2\right)/\cos Z, \quad (9.6.2)$$

and

$$F\left(E_{\pi},E_{\mu},h_1,h_2,h_o,Z\right)=\frac{m_{\pi}cf_{\pi}\left(E_{\pi},h_1,Z\right)}{\tau_{\pi}E_{\pi}\rho\left(h_2\right)\left(E_{\pi}^{-}-E_{\pi}^{+}\right)\cos Z}\exp\left(-\frac{h_2-h_1}{l\cos Z}\right)$$

$$\times\exp\left(-\frac{m_{\pi}c}{\tau_{\pi}E_{\pi}}\int_{h_1}^{h_2}\frac{dh}{\rho\left(h\right)}\right)\exp\left(-\frac{m_{\mu}c}{\tau_{\mu}}\int_{h_2}^{h_o}\frac{dh}{\rho\left(h\right)}\left(E_{\mu}\cos Z-a\left(h-h_2\right)\right)^{-1}\right). \quad (9.6.3)$$

For the function of pion generation we choose the same as in Section 9.5:

$$f_{\pi}\left(E_{\pi},h_1,Z\right)=AE_{\pi}^{-\gamma}\exp\left(-h_1/L\cos Z\right), \quad (9.6.4)$$

where A is some constant, and L is absorption path for meson-generating nucleon component of primary CR.

In Fig. 9.6.1 are shown the expected differential energy spectra of soft muons for different values of $\gamma=2.3$, 2.5, and 2.7 in the region of energy from $m_{\mu}c^2\approx 0.1$ GeV up to 0.4 GeV.

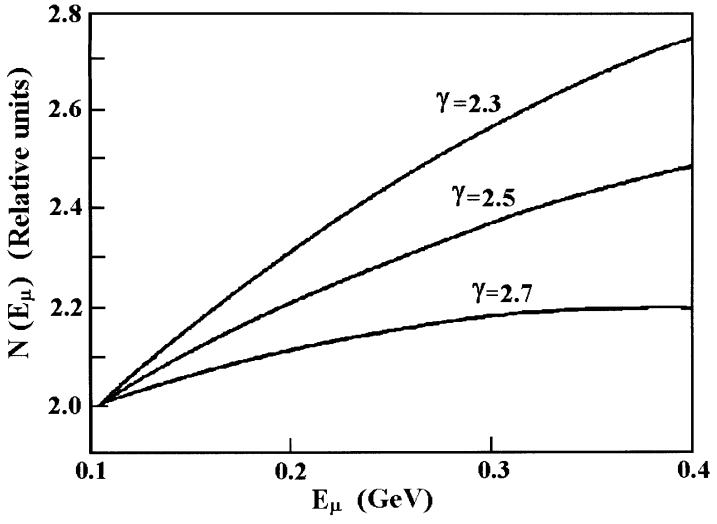

Fig. 9.6.1. Expected differential energy spectrums of soft muons at sea level for different values of $\gamma = 2.3$, 2.5, and 2.7 in the region of energy from $m_\mu c^2 \approx 0.1$ GeV up to $E_{\mu\,\mathrm{det}} = 0.4$ GeV.

It can be seen that the expected spectra are characterized by increasing of flux with increasing of energy (in opposite for higher energy region for hard muons, see Section 9.6.2). To our regret, experimental data in the energy interval from $m_\mu c^2 \approx 0.1$ GeV up to 0.4 GeV have a big errors, but all they show the tendency of increasing of flux with increasing of energy, in agreement with results presented in Fig. 9.6.1.

Fig. 9.6.2 shows the altitude dependence of soft muon intensity at $\gamma = 2.5$; it can be seen that the maximum of intensity is expected at $h \approx 0.1$ atm.

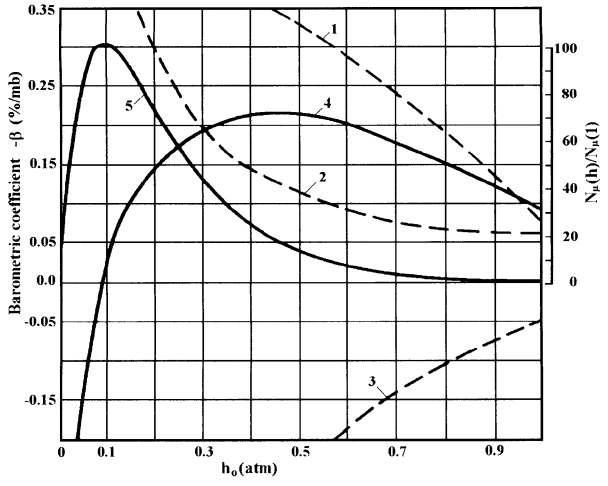

Fig. 9.6.2. The altitude dependence of soft muon intensity (full curve *5*, right scale) and barometric coefficients for soft muons at $\gamma = 2.5$ and $E_{\mu\,\mathrm{det}} = 0.4$ GeV: dashed curves *1*, *2*, and *3* – absorption, decay and generation parts of barometric coefficient; full curve *5* – total barometric coefficient.

9.6.2. Calculations of barometric coefficients for soft muons

Varying Eq. 9.6.1 over h_o we obtain

$$\left(\frac{\Delta N_\mu(h_o,Z,E_{\mu\,\mathrm{det}})}{N_\mu(h_o,Z,E_{\mu\,\mathrm{det}})}\right)_h = -\Delta E_{\mu\,\min}\int_0^{h_o} dh_2 \int_0^{h_2} dh_1 \int_{E_\pi^+}^{E_\pi^-} dE_\pi \frac{F(E_\pi,E_{\mu\,\min},h_1,h_2,h_o,Z)}{N_\mu(h_o,Z,E_{\mu\,\mathrm{det}})}$$

$$+\Delta E_{\mu\,\max}\int_0^{h_o} dh_2 \int_0^{h_2} dh_1 \int_{E_\pi^+}^{E_\pi^-} dE_\pi \frac{F(E_\pi,E_{\mu\,\max},h_1,h_2,h_o,Z)}{N_\mu(h_o,Z,E_{\mu\,\mathrm{det}})}$$

$$-\frac{m_\mu c\Delta h_o}{\tau_\mu \rho(h_o) N_\mu(h_o,Z,E_{\mu\,\mathrm{det}})}\int_0^{h_o} dh_2 \int_0^{h_2} dh_1 \int_{E_{\mu\,\min}}^{E_{\mu\,\max}} dE_\mu \int_{E_\pi^+}^{E_\pi^-} dE_\pi \frac{F(E_\pi,E_\mu,h_1,h_2,h_o,Z)}{E_\mu\cos Z - a(h_o-h_2)}$$

$$+\frac{\Delta h_o}{N_\mu(h_o,Z,E_{\mu\,\mathrm{det}})}\int_0^{h_o} dh_1 \int_{E_{\mu\,\min}}^{E_{\mu\,\max}} dE_\mu \int_{E_\pi^+}^{E_\pi^-} dE_\pi F(E_\pi,E_\mu,h_1,h_o,h_o,Z), \qquad (9.6.5)$$

where according to Eq. 9.6.2:

$$\Delta E_{\mu\,\min} = \Delta E_{\mu\,\max} = a\Delta h_o/\cos Z\,. \qquad (9.6.6)$$

The first two terms in Eq. 9.6.5 describe the absorption barometric effect, so the absorption barometric coefficient will be

$$\beta_a(h_o,Z,E_{\mu\,\mathrm{det}}) = -\frac{a}{N_\mu(h_o,Z,E_{\mu\,\mathrm{det}})\cos Z}$$

$$\times\int_0^{h_o} dh_2 \int_0^{h_2} dh_1 \int_{E_\pi^+}^{E_\pi^-} dE_\pi \left[F(E_\pi,E_{\mu\,\min},h_1,h_2,h_o,Z) - F(E_\pi,E_{\mu\,\max},h_1,h_2,h_o,Z)\right]. \qquad (9.6.7)$$

The third term in Eq. 9.6.5 describes the negative part of the barometric effect, caused by the decay of muons (increasing of the height of generation level with increasing of h_o) so the decay barometric coefficient will be

$$\beta_d(h_o,Z,E_{\mu\,\mathrm{det}}) = -\frac{m_\mu c}{\tau_\mu \rho(h_o) N_\mu(h_o,Z,E_{\mu\,\mathrm{det}})}$$

$$\times\int_0^{h_o} dh_2 \int_0^{h_2} dh_1 \int_{E_{\mu\,\min}}^{E_{\mu\,\max}} dE_\mu \int_{E_\pi^+}^{E_\pi^-} dE_\pi \frac{F(E_\pi,E_\mu,h_1,h_2,h_o,Z)}{E_\mu\cos Z - a(h_o-h_2)}. \qquad (9.6.8)$$

The last term in Eq. 9.6.5 describes the positive part of the barometric effect, caused by the generation of muons near the level of observation (with increasing of h_o will be increased number of generated pions and muons), so the positive generation barometric coefficient will be

$$\beta_g(h_o,Z,E_{\mu\,\mathrm{det}})=+\int_0^{h_o} dh_1 \int_{E_{\mu\,\min}}^{E_{\mu\,\max}} dE_\mu \int_{E_\pi^+}^{E_\pi^-} dE_\pi \frac{F(E_\pi,E_\mu,h_1,h_o,h_o,Z)}{N_\mu(h_o,Z,E_{\mu\,\mathrm{det}})}. \qquad (9.6.9)$$

Results of calculations of barometric coefficients for soft muons are shown in Fig. 9.6.2-9.6.4.

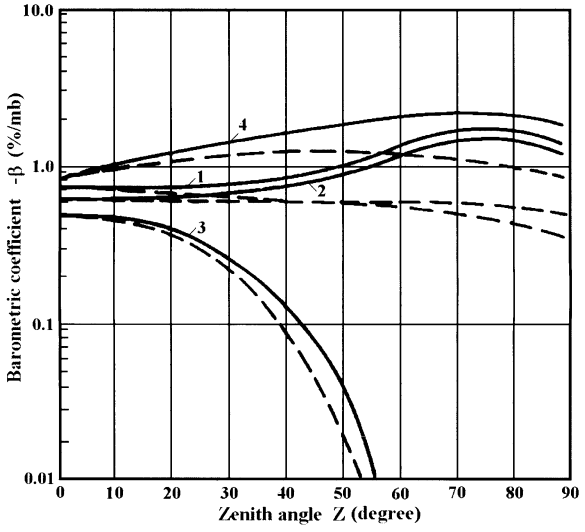

Fig. 9.6.3. The dependence of barometric coefficients for soft muons at $\gamma=2.5$ and with energy in the interval from $m_\mu c^2$ to $E_{\mu\,\mathrm{det}}=0.4$ GeV from zenith angle Z: dashed curves for plane-horizontal shield, and full curves for spherical symmetric shield. Curves *1, 2, 3* – absorption, decay and generation parts of barometric coefficient; curves *4* – total barometric coefficient.

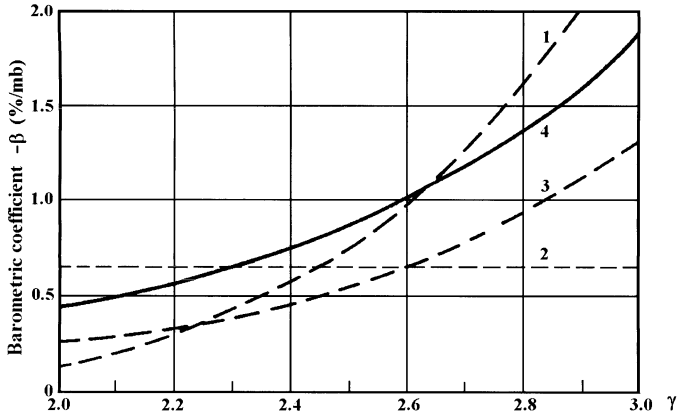

Fig. 9.6.4. The dependence of barometric coefficients for soft muons at $\gamma=2.5$ and with energy in the interval energy from $m_\mu c^2$ to $E_{\mu\,\mathrm{det}}=0.4$ GeV from γ. Dashed curves 1, 2, 3 – absorption, decay and generation parts of barometric coefficient; full curve 4 –total barometric coefficient. Left scale – for absorption, decay and total barometric coefficients; right scale – for generation barometric coefficient.

It can be seen that the barometric coefficients for soft muons ($E_\mu < 0.4$ GeV) are $5-6$ times bigger than for hard muons ($E_\mu > 0.4$ GeV, see Section 9.4). The dependences of barometric coefficients for soft muons on altitude, zenith angle, and γ in the spectrum of pion generation (Eq. 9.6.4) have about the same tendency as for hard muons.

9.6.3. Calculations of temperature coefficients for soft muons

By varying of Eq. 9.6.1 over air density, we obtain

$$\left(\frac{\Delta N_\mu(h_o,Z,E_{\mu\,\mathrm{det}})}{N_\mu(h_o,Z,E_{\mu\,\mathrm{det}})}\right)_T = -\int_{E_{\mu\min}}^{E_{\mu\max}} dE_\mu \int_0^{h_o} dh_2 \frac{\Delta\rho(h_2)}{\rho(h_2)} \int_0^{h_2} dh_1 \int_{E_\pi^+}^{E_\pi^-} dE_\pi \frac{F(E_\pi,E_\mu,h_1,h_2,h_o,Z)}{N_\mu(h_o,Z,E_{\mu\,\mathrm{det}})}$$

$$+ \int_{E_{\mu\min}}^{E_{\mu\max}} dE_\mu \int_0^{h_o} dh_2 \int_0^{h_2} dh_1 \int_{E_\pi^+}^{E_\pi^-} dE_\pi \frac{F(E_\pi,E_\mu,h_1,h_2,h_o,Z)}{N_\mu(h_o,Z,E_{\mu\,\mathrm{det}})} \frac{m_\pi c}{\tau_\pi E_\pi \cos Z} \int_{h_1}^{h_2} \frac{dh\Delta\rho(h)}{\rho^2(h)}$$

$$+ \int_0^{h_o} dh_1 \int_{E_{\mu\min}}^{E_{\mu\max}} dE_\mu \int_{E_\pi^+}^{E_\pi^-} dE_\pi \frac{F(E_\pi,E_\mu,h_1,h_2,h_o,Z)}{N_\mu(h_o,Z,E_{\mu\,\mathrm{det}})} \frac{m_\mu c}{\tau_\mu} \int_{h_2}^{h_o} \frac{dh\,\Delta\rho(h)/\rho(h)}{E_\mu \cos Z - a(h-h_2)}. \qquad (9.6.10)$$

Eq. 9.6.10 by taking into account Eq. 9.6.21, can be rewritten as

$$\left(\frac{\Delta N_\mu(h_o,Z,E_{\mu\,\mathrm{det}})}{N_\mu(h_o,Z,E_{\mu\,\mathrm{det}})}\right)_T = \int_0^{h_o} W_T(h,h_o,Z,E_{\mu\,\mathrm{det}})\Delta T(h)dh, \qquad (9.6.11)$$

where

$$W_T(h,h_o,Z,E_{\mu\,\mathrm{det}}) = W_{T\mu}(h,h_o,Z,E_{\mu\,\mathrm{det}}) + W_{T\pi}(h,h_o,Z,E_{\mu\,\mathrm{det}}), \qquad (9.6.12)$$

$$W_{T\mu}(h,h_o,Z,E_{\mu\,\mathrm{det}}) = -\frac{(m_\mu c R_o/\tau_\mu g)}{N_\mu(h_o,Z,E_{\mu\,\mathrm{det}})} \times \int_{E_{\mu\min}}^{E_{\mu\max}} dE_\mu \int_0^{h} dh_2 \int_0^{h_2} dh_1 \int_{E_\pi^+}^{E_\pi^-} dE_\pi \frac{F(E_\pi,E_\mu,h_1,h_2,h_o,Z)}{h(E_\mu \cos Z - a(h-h_2))}, \qquad (9.6.13)$$

$$W_{T\pi}(h,h_o,Z,E_{\mu\,\mathrm{det}}) = \frac{1}{N_\mu(h_o,Z,E_{\mu\,\mathrm{det}})} \times \int_{E_{\mu\min}}^{E_{\mu\max}} dE_\mu \int_0^{h} dh_1 \int_{E_\pi^+}^{E_\pi^-} dE_\pi \left\{\frac{1}{T(h)} - \frac{m_\pi c}{\tau_\pi E_\pi \cos Z} \int_{h_1}^{h_2} \frac{dh}{T(h)}\right\} F(E_\pi,E_\mu,h_1,h_2,h_o,Z). \qquad (9.6.14)$$

Results of calculations of total temperature coefficient W_T for soft muons are presented in Fig. 9.6.5–9.6.6.

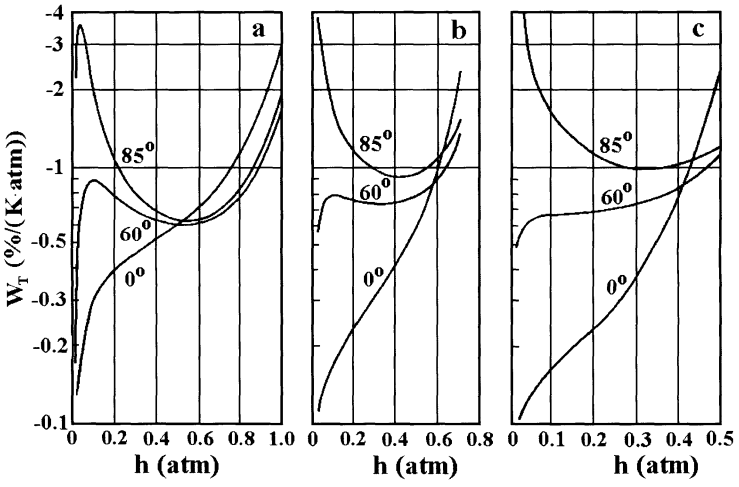

Fig. 9.6.5. Total temperature coefficients for soft muons in the interval energy from $m_\mu c^2$ to $E_{\mu\,\mathrm{det}} = 0.4$ GeV for different zenith angles (numbers near curves) for observations on the levels: *a* – $h_o = 1$ atm ; *b* – $h_o = 0.7$ atm ; *c* – $h_o = 0.5$ atm .

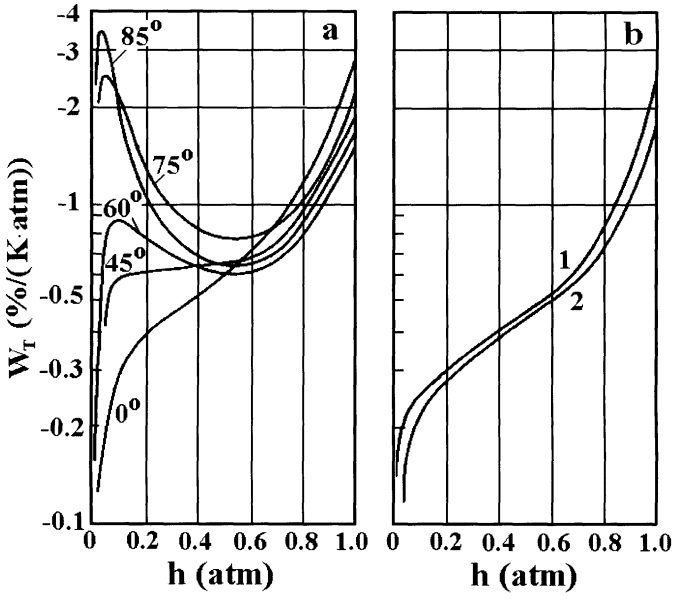

Fig. 9.6.6. Total temperature coefficients for soft muons for observations on the sea level: *a* – at different zenith angles (numbers near curves) for the energy interval $m_\mu c^2 - 0.4$ GeV ; *b* – at zenith angle $Z = 0^\circ$ in the energy interval $0.19 - 0.405$ GeV (curve *1*) and energy interval $0.14 - 0.365$ GeV (curve *2*).

9.6.4. Temperature coefficients for soft muons with accounting the angle distribution at pions decay, and Coulomb scattering

Consider a pion moving at zenith angle Z_π decay and the generated muon moving at zenith angle Z_μ. Let us denote the angle between trajectories of pion and muon as α. Because the spin of pion is zero, the distribution of the pion's products of decay (neutrino and muons) will be isotropic in the pion's system of coordinates. In the C-system the momentum and energy of muon $p^*_{o\mu}$ and $E^*_{o\mu}$ are constant and can be determined from the kinematics of decay:

$$p^*_{o\mu} = c\left(m_\pi^2 - m_\mu^2\right)/2m_\pi; \quad E^*_{o\mu} = c^2\left(m_\pi^2 + m_\mu^2\right)/2m_\pi \quad . \tag{9.6.15}$$

Therefore, the angle and energy muon distribution in C-system will be

$$\frac{d^2 A^*_\pi}{A^*_\pi dE^*_\mu d\Omega^*} = \frac{1}{4\pi}\delta\left(E^*_\mu - E^*_{o\mu}\right) . \tag{9.6.16}$$

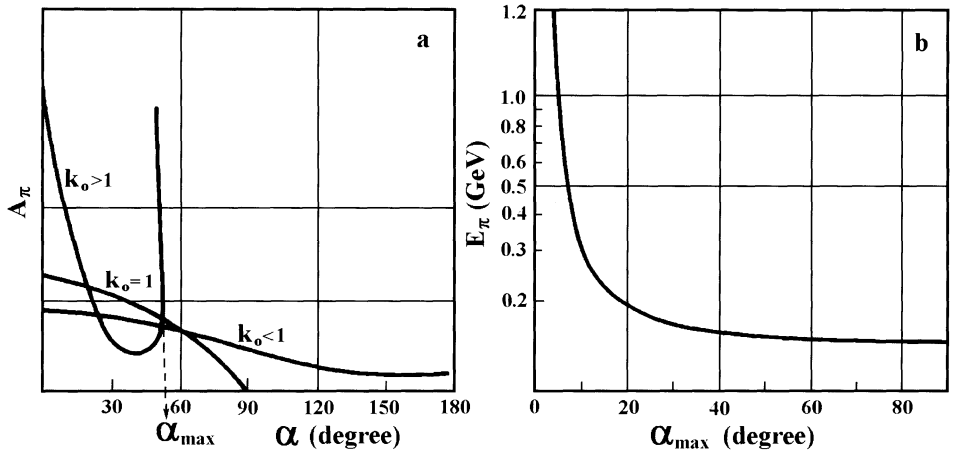

Fig. 9.6.7. The angle distribution of muons at pion decay in the laboratory system of coordinates (*a*), and the dependence of α_{max} from the pion energy (*b*).

By the transformation of the distribution in the C-system described by Eq. 9.6.16 to the laboratory system of coordinates (see Fig. 9.6.7a), we obtain according to Baldin et al. (M1968):

$$A_\pi(E_\pi,\alpha)=\begin{cases}\dfrac{1}{2\pi}\dfrac{\gamma_\pi^2\left[E_{o\mu}^{*2}\left(1+\beta_\pi^2\cos^2\alpha\right)-m_\mu^2b^2c^4\right]}{cb^4p_{o\mu}^*\sqrt{E_{o\mu}^{*2}-m_\mu^2b^2c^4}}, & \text{if } \kappa_o>1;\ 0\le\alpha\le\alpha_{\max}\\ \dfrac{1}{\pi}\dfrac{\cos\alpha}{\gamma_\pi^2\left(1-\beta_\pi^2\cos^2\alpha\right)^2}, & \text{if } \kappa_o=1;\ 0\le\alpha\le\pi/2\\ \dfrac{1}{4\pi}\dfrac{\gamma_\pi^2\left[\beta_\pi E_{o\mu}^*|\cos\alpha|+\dfrac{\cos\alpha}{|\cos\alpha|}\sqrt{E_{o\mu}^{*2}-m_\mu^2b^2c^4}\right]^2}{cb^4p_{o\mu}^*\sqrt{E_{o\mu}^{*2}-m_\mu^2b^2c^4}}, & \text{if } \kappa_o<1;\ 0\le\alpha\le\pi\end{cases} \tag{9.6.17}$$

where

$$\kappa_o=\beta_\pi E_{o\mu}^*/cp_{o\mu}^*,\quad b=\gamma_\pi\sqrt{1-\beta_\pi^2\cos^2\alpha} \tag{9.6.18}$$

and $\alpha_{\max}$ is determined by equation

$$\lg(\alpha_{\max})=\left(\gamma_\pi\sqrt{\kappa_o^2-1}\right)^{-1}. \tag{9.6.19}$$

In Fig. 9.6.7b we show the dependence of $\alpha_{\max}$ on E_π. The expected $\alpha_{\max}\approx 10^\circ$ for $E_\pi=0.3\ GeV$. For pions with energy of several GeV the expected $\alpha_{\max}$ is negligible; so the angle expansion at pion decay is significant only for soft muons.

Let us introduce azimuthal angle ω as it is shown in Fig. 9.6.8. The angles $Z_\pi,Z_\mu,\alpha,\omega$ are connected by the relation

$$\cos\boldsymbol{\alpha}=\cos Z_{\boldsymbol{\pi}}\cos Z_{\boldsymbol{\mu}}+\sin Z_{\boldsymbol{\pi}}\sin Z_{\boldsymbol{\mu}}\cos\boldsymbol{\omega}\ . \tag{9.6.20}$$

Therefore, the angle distribution $A_\pi(E_\pi,\alpha)\Rightarrow A_\pi\left(E_\pi,Z_\pi,Z_\mu,\omega\right)$, and for muon generation function we obtain

$$f_\mu\left(E_\mu,h_2,Z_\mu\right)=\int_{E_\pi^+}^{E_\pi^-}dE_\pi\int_{(\cos\omega)_{\min}}^{(\cos\omega)_{\max}}d(\cos\omega)\int_{(\cos Z_\pi)_{\min}}^{(\cos Z_\pi)_{\max}}d(\cos Z_\pi)$$
$$\times\frac{m_\pi c}{\tau_\pi E_\pi}\frac{f_\pi(E_\pi,h_2,Z_\pi)A_\pi\left(E_\pi,Z_\pi,Z_\mu,\omega\right)}{\left(E_\pi^--E_\pi^+\right)\rho(h_2)\cos Z_\pi}. \tag{9.6.21}$$

Then by the same transformations as used in Section 9.4 for hard muons, we obtain for the intensity of soft muons:

$$N_\mu\left(h_o, Z_\mu, E_{\mu\,\mathrm{det}}\right) = \int_0^{h_o} dh_2 \int_0^{h_2} dh_1 \int_{E_{\mu\min}}^{E_{\mu\max}} dE_\mu \int_{E_\pi^+}^{E_\pi^-} dE_\pi \int_{(\cos\omega)_{\min}}^{(\cos\omega)_{\max}} d(\cos\omega)$$

$$\times \int_{(\cos Z_\pi)_{\min}}^{(\cos Z_\pi)_{\max}} d(\cos Z_\pi) F\left(E_\pi, E_\mu, h_1, h_2, h_o, Z_\pi, Z_\mu\right) A_\pi\left(E_\pi, Z_\pi, Z_\mu, \omega\right). \qquad (9.6.22)$$

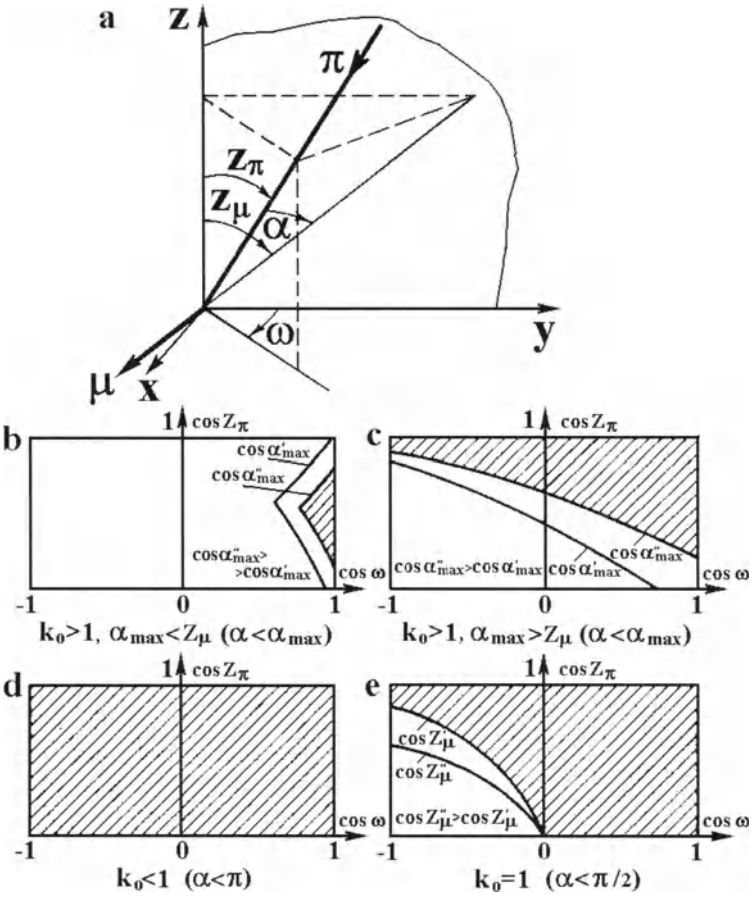

Fig. 9.6.8. The used system of coordinates (*a*), and regions of integrating over zenith and azimuthal angles: *b* – for $\kappa_o > 1$, $\alpha_{\max} < Z_\mu$, *c* – for $\kappa_o > 1$, $\alpha_{\max} > Z_\mu$, *d* – for $\kappa_o < 1$, $\alpha < \pi$, *e* – for $\kappa_o = 1$, $\alpha < \pi/2$.

In Eq. 9.6.22

$$\left(\cos Z_\pi\right)_{\min} = \frac{\cos\alpha_{\max}\cos Z_\mu - \sin Z_\mu \cos\omega\sqrt{\cos^2 Z_\mu - \cos^2\alpha_{\max} + \sin^2 Z_\mu \cos^2\omega}}{\cos^2 Z_\mu + \sin^2 Z_\mu \cos^2\omega}, \qquad (9.6.23)$$

$$(\cos Z_\pi)_{\max} = \frac{\cos\alpha_{\max}\cos Z_\mu + \sin Z_\mu \cos\omega\sqrt{\cos^2 Z_\mu - \cos^2\alpha_{\max} + \sin^2 Z_\mu \cos^2\omega}}{\cos^2 Z_\mu + \sin^2 Z_\mu \cos^2\omega}, \quad (9.6.24)$$

$$(\cos\omega)_{\min} = \begin{cases} \sqrt{\cos^2\alpha_{\max} - \cos^2 Z_\mu}\,/\sin^2 Z_\mu, & \text{if } \cos\alpha_{\max} > \cos Z_\mu; \\ -1, & \text{if } \cos\alpha_{\max} < \cos Z_\mu \end{cases}$$

$$(\cos\omega)_{\max} = 1. \quad (9.6.25)$$

Let us consider now the relative role of Coulomb multi-scattering of muons. Assume that a muon with the starting energy $\gamma_{\mu 1}$ (in units of muon rest energy) crosses the layer Δh and its energy becomes $\gamma_{\mu 2}$. In this case according to Rossi and Greisen (M1948) the average scattering angle will be determined by

$$\left\langle \alpha_c^2 \right\rangle = \frac{E_s^2 \Delta h}{m_\mu^2 c^4 t_o} \frac{\ln\left|\left(1+\gamma_{\mu 1}\right)/\left(1+\gamma_{\mu 2}\right)\right|\sqrt{\left(\gamma_{\mu 1}^2-1\right)\left(\gamma_{\mu 2}^2-1\right)}}{\gamma_{\mu 1} + \left(\gamma_{\mu 1}\right)^{-1} - \gamma_{\mu 2} - \left(\gamma_{\mu 2}\right)^{-1}}, \quad (9.6.26)$$

where t_o is the radiation length for air, and $E_s = 137 m_e c^2/4\pi = 0.022$ GeV. The angle distribution after crossing the layer Δh will be described by Gauss function:

$$A_c(\alpha, E_\mu, \Delta h) = \left(2\pi\left\langle \alpha_c^2 \right\rangle\right)^{-1/2} \exp\left(-\alpha^2/2\left\langle \alpha_c^2 \right\rangle\right). \quad (9.6.27)$$

The starting and final muon energies are connected by the relation

$$E_{\mu 1} = E_{\mu 2} + a\Delta h/\cos Z_\mu, \quad (9.6.28)$$

In Fig. 9.6.9a is shown the dependence of $\left\langle \alpha_c^2 \right\rangle^{1/2}$ on the final muon energy and level of muon generation. Fig. 9.6.9b shows the dependence of $\left\langle \alpha_c^2 \right\rangle^{1/2}$ on the starting and final muon kinetic energies $E_{\mu 1} - m_\mu c^2$, $E_{\mu 2} - m_\mu c^2$. Taking into account Coulomb multi-scattering of muons, the function of muon generation will be

$$f_\mu(E_\mu, h_2, Z_\mu) = \int_{E_\pi^+}^{E_\pi^-} dE_\pi \int_{(\cos\omega)_{\min}}^{(\cos\omega)_{\max}} d(\cos\omega) \int_{(\cos Z_\pi)_{\min}}^{(\cos Z_\pi)_{\max}} d(\cos Z_\pi) \times$$
$$\times \frac{m_\pi c}{\tau_\pi E_\pi} \frac{f_\pi(E_\pi, h_2, Z_\pi) A_c(E_\pi, Z_\pi, Z_\mu, \omega)}{\left(E_\pi^- - E_\pi^+\right)\rho(h_2)\cos Z_\pi}, \quad (9.6.29)$$

where $A_c\left(E_\pi, Z_\pi, Z_\mu, \omega\right)$ is determined by Eq. 9.6.27 and Eq. 9.6.20. Then for intensity of soft muons we obtain

$$N_\mu\left(h_o, Z_\mu, E_{\mu\,\mathrm{det}}\right) = \int_0^{h_o} dh_2 \int_0^{h_2} dh_1 \int_{E_{\mu\min}}^{E_{\mu\max}} dE_\mu \int_{E_\pi^+}^{E_\pi^-} dE_\pi \int_{(\cos\omega)_{\min}}^{(\cos\omega)_{\max}} d(\cos\omega)$$

$$\times \int_{(\cos Z_\pi)_{\min}}^{(\cos Z_\pi)_{\max}} d(\cos Z_\pi) F\left(E_\pi, E_\mu, h_1, h_2, h_o, Z_\pi, Z_\mu\right) A_c\left(E_\pi, Z_\pi, Z_\mu, \omega\right). \qquad (9.6.30)$$

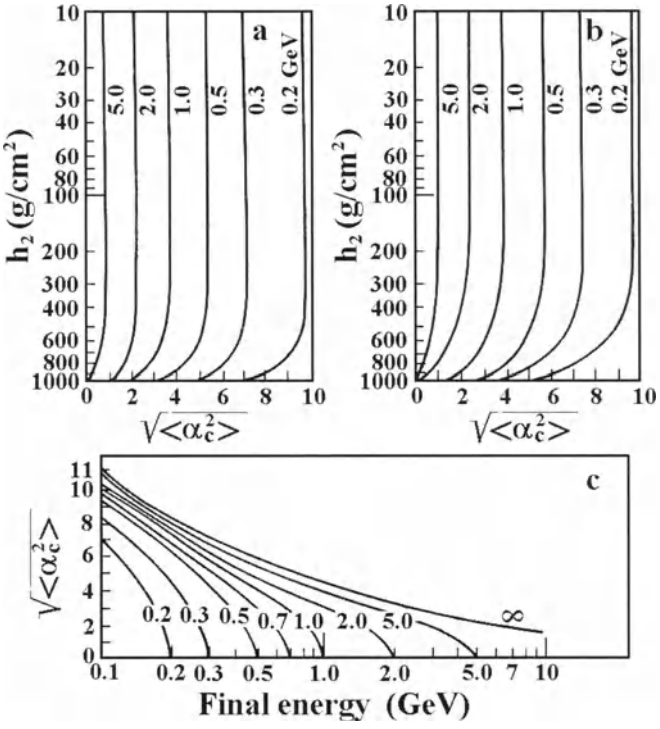

Fig. 9.6.9. The dependence of $\sqrt{\left\langle \alpha_c^2 \right\rangle}$ on final muon energy (numbers near curves in GeV) and on the level of muon generation h_2 (in $\mathrm{g/cm^2}$) for zenith angles $Z_\mu = 0^\circ$ (*a*) and $Z_\mu = 60^\circ$ (*b*), as well as on starting $E_{\mu 1} - m_\mu c^2$ (numbers near curves in GeV) and final $E_{\mu 2} - m_\mu c^2$ muon kinetic energy (*c*).

The expressions for temperature coefficients can be obtained from Eq. 9.6.30 in the same way as in the Section 9.6.3; only instead of $A_\pi\left(E_\pi, Z_\pi, Z_\mu, \omega\right)$ we use $A_c\left(E_\pi, Z_\pi, Z_\mu, \omega\right)$. Results of numerical calculations of temperature coefficients for soft muons with accounting of coulomb multi-scattering of muons are shown in Fig. 9.6.10–9.6.12.

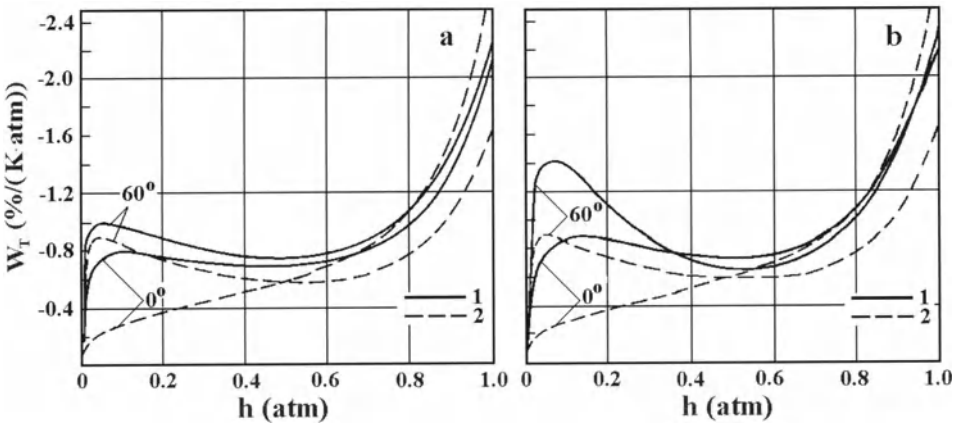

Fig. 9.6.10. Temperature coefficients for soft muons at sea level for zenith angles $Z_\mu = 0^\circ$ and $Z_\mu = 60^\circ$ (numbers near curves) with accounting (full curves *1*) and without accounting (dashed curves *2*) of coulomb multi-scattering of muons (*a*) and of angle distribution of muons at pion decay (*b*).

From Fig. 9.6.10 one can see the relative role of angle extended at pion decay and coulomb multi-scattering of muons in formation of temperature coefficients for soft muons.

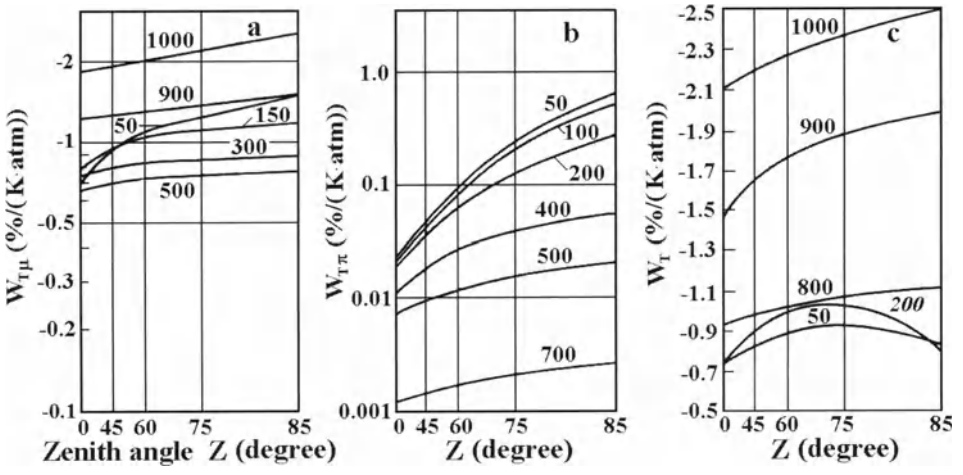

Fig. 9.6.11. The dependence of temperature coefficients for soft muons at sea level from zenith angle on different h (numbers near curves in g/cm^2) with accounting of coulomb multi-scattering of muons: *a* – muon part $W_{T\mu}$; *b* – pion part $W_{T\pi}$; *c* – total temperature coefficient W_T.

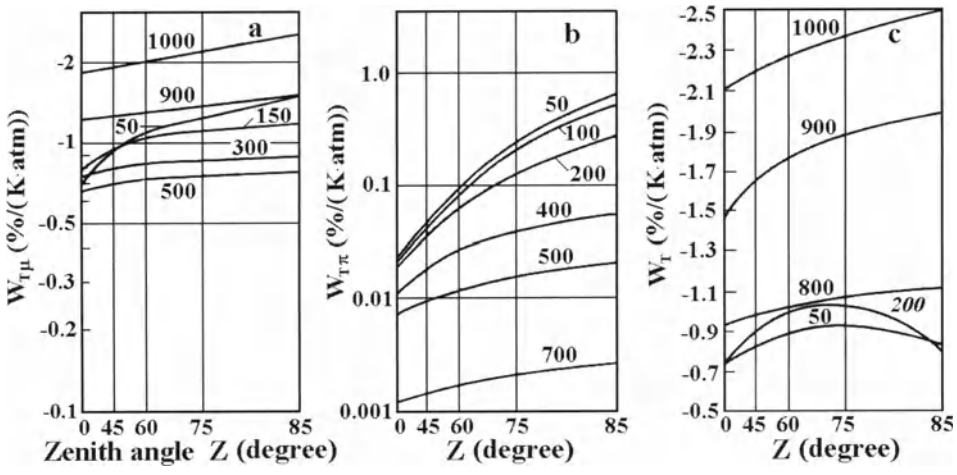

Fig. 9.6.12. Temperature coefficients for soft muons at sea level for different zenith angles of soft muons arriving (numbers near curves) at $\gamma = 2.5$ with accounting of coulomb multi-scattering of muons: *a* – muon part $W_{T\mu}$; *b* – pion part $W_{T\pi}$; *c* – total temperature coefficient W_T .

9.7. Theory of super-high energy muons temperature effects

At present there are several giant deep underground muon detectors in the world which measure fluxes of super-high energy muons. For these experiments the approximations considered above are not enough: for super-high energy region one must consider formation of muons not only through decay of pions, but also through decay of kaons. Furthermore, it is important to take into account not only ionization losses but also Cherenkov radiation, formation of pair and other processes (increasing of energy loses with increasing of particle energy) and generation of mesons also by mesons. An attempt to account for these factors was made by Volkova (1970).

9.7.1. Expected muon spectrum in the super-high energy region

In Volkova (1970) the functions of direct generation of mesons of any type i ($i = 1,2,3$ corresponds to pions, kaons and muons) are the same as was used in Dorman (M1957) and described in Chapter 5:

$$f_i(h,E,Z) = A_i E^{-\gamma} \exp(-h/L\cos Z), \tag{9.7.1}$$

where A_i are constants, and L is the attenuation length for the meson generating component of primary CR. It is supposed that the direction of mesons moving is the same as of particle generated mesons. After the introduction of the non-dimensional variable $y_i = h/(l_i \cos Z)$ and denoting $x_i = l_i/L$ we obtain the kinetic equation describing the transport of mesons in the atmosphere:

$$\frac{\partial N_i(y_i,E,Z)}{\partial y_i} = -\left(1+\frac{m_i c^2 l_i}{c\tau_i \rho(v_i l_i \cos Z)}\right) N_i(y_i,E,Z) + A_i E^{-\gamma}\exp(-x_i y_i). \qquad (9.7.2)$$

The solution of Eq. 9.7.2 can be written as

$$N_i(y_i,E,Z) = \int_0^{y_i} A_i E^{-\gamma}\exp\left\{-\int_0^{t_i}\frac{m_i c^2 l_i dt_i'}{c\tau_i\rho(v_i l_i\cos Z)E} - x_i t_i + t_i - y_i\right\} dt_i. \qquad (9.7.3)$$

At super-high energies it is necessary to take into account the dependence of losses of energy from the energy (important are not only losses on ionization, but also on Cherenkov radiation, formation of pairs and others). It can be made by following expression:

$$dE/dy_i = -(a(E)+b(E)E)l_i, \qquad (9.7.4)$$

where coefficients $a(E)$, $b(E)$ are listen in Table 9.7.1.

Table 9.7.1. Coefficients $a(E)$, $b(E)$ in Eq. 9.7.4 for E in GeV.

E, GeV	a, $\mathrm{GeV}\left(\mathrm{g/cm^2}\right)^{-1}$	b, $\left(\mathrm{g/cm^2}\right)^{-1}$
10^2	3.0×10^{-3}	2.28×10^{-6}
10^3	3.1×10^{-3}	3.20×10^{-6}
10^4	3.2×10^{-3}	3.18×10^{-6}

Taking into account Eq. 9.7.4, we obtain kinetic equation for transport in the atmosphere muons generated by mesons of type i:

$$\frac{\partial N_{i\mu}(y_i,E,Z)}{\partial y_i} = -\frac{m_\mu c^2 l_i N_{i\mu}(y_i,E,Z)}{c\tau_\mu\rho(y_i l_i\cos Z)E} + \frac{\partial}{\partial E}\left[a(E)N_{i\mu}(y_i,E,Z)\right] + f_{i\mu}(y_i,E,Z), \qquad (9.7.5)$$

where $f_{i\mu}(y_i,E,Z)$ is the function of generation muons by mesons of type i, and

$$f_{\mu\mu}(y_\mu,E,Z) = A_\mu E^{-\gamma}\exp(-x_\mu y_\mu), \qquad (9.7.6)$$

in the case in which muons are generated directly in nuclear interactions. If muons are generated through decay of pions (i = 1) or kaons (i = 2), the muon generation function will be

$$f_{i\mu}(y_i,E,Z)=\int_{E}^{E(m_i/m_\mu)^2} dE' \int_0^{y_i} A_i(E')^{-(\gamma+2)}$$

$$\times\exp\left\{-\int_t^{y_i}\frac{m_ic^2l_idt'}{c\tau_i\rho(t'l_i\cos Z)E'}-x_it+t-y_i\right\}\frac{m_ic^2l_idt}{c\tau_i\rho(y_il_i\cos Z)\left(1-(m_\mu/m_i)^2\right)}. \quad (9.7.7)$$

Expected differential energy spectrum of muons will be found by solution of equation:

$$N_{i\mu}(y_i,E,Z)=\int_0^{y_i} f_{i\mu}[t,E_i(E,y_i-t),Z]$$

$$\times\exp\left\{-\int_t^{y_i}\frac{m_\mu c^2l_idt'}{c\tau_\mu\rho(t'l_i\cos Z)E_i(E,y_i-t')}+bl_i(y_i-t)\right\}dt, \quad (9.7.8)$$

where

$$E_i(E,y_i-t)=E\exp(bl_i(y_i-t))+\frac{a}{b}(\exp(bl_i(y_i-t))-1). \quad (9.7.9)$$

By introducing Eq. 9.7.9 and Eq. 9.7.6 in Eq. 9.7.8 we found the differential energy spectrum of muons generated directly in nuclear reactions:

$$N_{\mu\mu}(y_\mu,E,Z)=\int_0^{y_\mu} A_\mu[E_\mu(E,y_\mu-t)]^{-\gamma}$$

$$\times\exp\left\{-x_\mu t-\frac{m_\mu c^2L}{c\tau_\mu}\int_t^{y_\mu}\frac{dt'}{\rho(t'l_\mu\cos Z)E_\mu(E,y_\mu-t')}+bL(y_\mu-t)\right\}dt. \quad (9.7.10)$$

By introducing Eq. 9.7.9 and Eq. 9.7.7 in Eq. 9.7.8 we found the differential energy spectrum of muons generated by decay of pions ($i = 1$) and kaons ($i = 2$):

$$N_{i\mu}(y_i,E,Z)=\int_0^{y_i}dt\int_{E_i(E,y_i-t)}^{(m_i/m_\mu)^2E_i(E,y_i-t)} dE'\,A_i(E')^{-(\gamma+2)}\int_0^t dt'$$

$$\times\exp\left\{-\int_{t'}^{t}\frac{m_ic^2l_idt''}{c\tau_i\rho(t''l_i\cos Z)E'}-x_it'+t'-t\right\}\frac{m_ic^2l_i}{c\tau_i\rho(tl_i\cos Z)\left(1-(m_\mu/m_i)^2\right)}$$

$$\times\exp\left\{-\frac{m_\mu c^2l_i}{c\tau_\mu}\int_t^{y_i}\frac{dt''}{\rho(t''l_i\cos Z)E_i(E,y_i-t)}-bl_i(y_i-t)\right\}. \quad (9.7.11)$$

9.7.2. Expressions for temperature effect of super-high energy muons

By varying Eq. 9.7.10 and Eq. 9.7.11 over air density $\rho(h)$ we obtain muon intensity variations caused by change of temperature. For $i=3$ (muons generated directly in nuclear interactions, Eq. 9.7.10) we obtain:

$$\left(\frac{\Delta N_{\mu\mu}(y_\mu,E,Z)}{N_{\mu\mu}(y_\mu,E,Z)}\right)_T = \frac{1}{N_{\mu\mu}(y_\mu,E,Z)}\int_0^{y_\mu} A_\mu\left[E_\mu(E,y_\mu-t)\right]^{-\gamma}$$

$$\times\left[\int_t^{y_\mu}\frac{m_\mu c^2 L\Delta\rho(t' l_\mu\cos Z)dt'}{c\tau_\mu\rho^2(t' l_\mu\cos Z)E_\mu(E,y_\mu-t')}\right]\times$$

$$\times\exp\left\{-x_\mu t-\frac{m_\mu c^2 L}{c\tau_\mu}\int_t^{y_\mu}\frac{dt'}{\rho(t' l_\mu\cos Z)E_\mu(E,y_\mu-t')}+bL(y_\mu-t)\right\}dt. \quad (9.7.12)$$

For $i=1,2$ (for muons generated correspondingly through decay of pions and kaons, see Eq. 9.7.11) we obtain:

$$\left(\frac{\Delta N_{i\mu}(y_i,E,Z)}{N_{i\mu}(y_i,E,Z)}\right)_T = \int_0^{y_i} dt\int_{E_i(E,y_i-t)}^{(m_i/m_\mu)^2 E_i(E,y_i-t)} dE'\int_0^t dt'\frac{A_i(E')^{-(\gamma+2)}}{N_{i\mu}(y_i,E,Z)}$$

$$\times\frac{m_i c^2 l_i}{c\tau_i\rho(tl_i\cos Z)\left(1-(m_\mu/m_i)^2\right)}\exp\left\{-\int_{t'}^{t}\frac{m_i c^2 l_i dt''}{c\tau_i\rho(t'' l_i\cos Z)E'}-x_i t'-t'-t\right\}$$

$$\times\exp\left\{-\frac{m_\mu c^2 l_i}{c\tau_\mu}\int_t^{y_i}\frac{dt''}{\rho(t'' l_i\cos Z)E_i(E,y_i-t)}-bl_i(y_i-t)\right\}$$

$$\times\left[\int_{t'}^{t}\frac{m_i c^2 l_i\Delta\rho(t'' l_i\cos Z)dt''}{c\tau_i\rho^2(t'' l_i\cos Z)E'}+\frac{m_\mu c^2 l_i}{c\tau_\mu}\int_t^{y_i}\frac{dt''}{\rho(t'' l_i\cos Z)E_i(E,y_i-t)}-\frac{\Delta\rho(t'' l_i\cos Z)}{\rho(t'' l_i\cos Z)}\right]. \quad (9.7.13)$$

Let us take into account that $\Delta\rho/\rho=-\Delta T/T$. Then the terms of type [ ] contained $\Delta\rho/\rho$ in Eq. 9.7.12 and Eq. 9.7.13 will be, consequently:

$$[\,]_{\text{Eq.9.7.12}}=\left[-\int_t^{y_\mu}\frac{\Delta T(t')}{T(t')}\frac{m_\mu c^2 L dt'}{c\tau_\mu\rho(t' l_\mu\cos Z)E_\mu(E,y_\mu-t')}\right], \quad (9.7.14)$$

$$[\ ]_{\text{Eq. 9.7.13}} = \left[-\int_{t'}^{t} \frac{\Delta T(t'')}{T(t'')} \frac{m_i c^2 l_i dt''}{c\tau_i \rho(t'' l_i \cos Z) E'} \right.$$

$$\left. - \frac{m_\mu c^2 l_i}{c\tau_\mu} \int_{t}^{y_i} \frac{\Delta T(t')}{T(t')} \frac{dt'}{\rho(t' l_i \cos Z) E_i(E, y_i - t')} + \frac{\Delta T(t)}{T(t)} \right]. \qquad (9.7.15)$$

9.7.3. Calculations of temperature coefficients for observations of super-high energy muons

Using Eqs. 9.7.14–9.7.15, one can rewrite Eq. 9.7.12 and Eq. 9.7.13 for differential energy spectrum as

$$\left(\frac{\Delta N_{i\mu}(y_i, E, Z)}{N_{i\mu}(y_i, E, Z)} \right)_T = \int_0^{y_i} W_{i\mu}(y_i, t, E, Z) \Delta T(t) dt, \qquad (9.7.16)$$

and for the integral energy spectrum as

$$\left(\frac{\Delta N_{i\mu}(y_i, > E, Z)}{N_{i\mu}(y_i, > E, Z)} \right)_T = \int_0^{y_i} W_{i\mu}(y_i, t, > E, Z) \Delta T(t) dt, \qquad (9.7.17)$$

where

$$W_{i\mu}(y_i, t, E, Z) = W_{i\mu 1}(y_i, t, E, Z) + W_{i\mu 2}(y_i, t, E, Z) + W_{i\mu 3}(y_i, t, E, Z), \qquad (9.7.18)$$

$$W_{i\mu}(y_i, t, > E, Z) = W_{i\mu 1}(y_i, t, > E, Z) + W_{i\mu 2}(y_i, t, > E, Z) + W_{i\mu 3}(y_i, t, > E, Z). \qquad (9.7.19)$$

Numerical calculations of temperature coefficients were carried out by Volkova (1970) for $\gamma = 2.65$, $l_\pi = l_k = L = 120\ \text{g/cm}^2$. In accordance with Eq. 9.7.12 and Eq. 9.7.14, for muons generated in direct nuclear interactions there is only one temperature effect, a negative effect, caused by decay of muons during their transport from level of generation to the level of observation (denoted as $W_{\mu\mu 3}$). In accordance with Eq. 9.7.13 and Eq. 9.7.15, for muons generated through decay of pions and kaons, there are three temperature effects: index 1 in Eq. 9.7.18 and Eq. 9.7.19 corresponds to the positive temperature effect caused by relative increasing of pion and kaon decay in the layer of muon generation (the relative role of this effect increased very much with increasing of muons energy); index 2 corresponds to the negative temperature effect caused by increasing of pion and kaon decay in the layer above the level of muon generation (for small energy of muons, considered in Section 2, this effect is negligible in comparison with positive effect 1); index 3 corresponds to the negative temperature effect caused by decay of muons during their transport from level of generation to the level of observation (the same nature as $W_{\mu\mu 3}$, the relative role of this effect decreased very much with

increasing of muons energy). Results of numerical calculations of temperature coefficients according to Volkova (1970) are shown in Fig. 9.7.1–9.7.5.

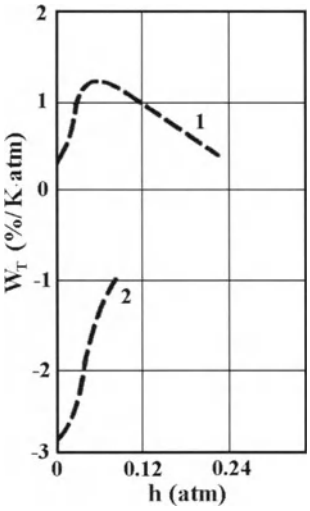

Fig. 9.7.1. Temperature coefficients at sea level and $Z = 0^o$ for differential energy spectrum of muons generated through pion decay (energy $E_\mu = 10^2$ GeV): curve *1* – $W_{\pi\mu 1}$; curve *2* – $W_{\pi\mu 2}$.

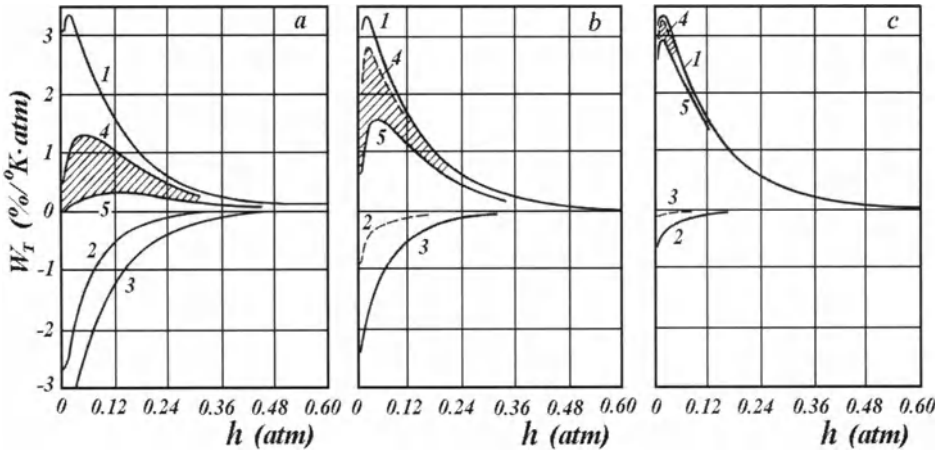

Fig. 9.7.2. Temperature coefficients at sea level for integral flux of muons with energy $E_\mu \geq E_{\mu\min}$ for $E_{\mu\min} = 10^2$ GeV (*a*); $E_{\mu\min} = 10^3$ GeV (*b*); $E_{\mu\min} = 10^4$ GeV (*c*); Curves *1* – $W_{T1\pi}\left(h, E_\mu \geq E_{\mu\min}, Z = 0^\circ\right)$ and $W_{T1k}\left(h, E_\mu \geq E_{\mu\min}, Z = 0^\circ\right)$; *2* – $W_{T2\pi}\left(h, E_\mu \geq E_{\mu\min}, Z = 0^\circ\right)$; *3* – $W_{T2k}\left(h, E_\mu \geq E_{\mu\min}, Z = 0^\circ\right)$; *4* and *5* – total temperature coefficients $W_{T\pi}\left(h, E_\mu \geq E_{\mu\min}, Z = 0^\circ\right)$ and $W_{Tk}\left(h, E_\mu \geq E_{\mu\min}, Z = 0^\circ\right)$.

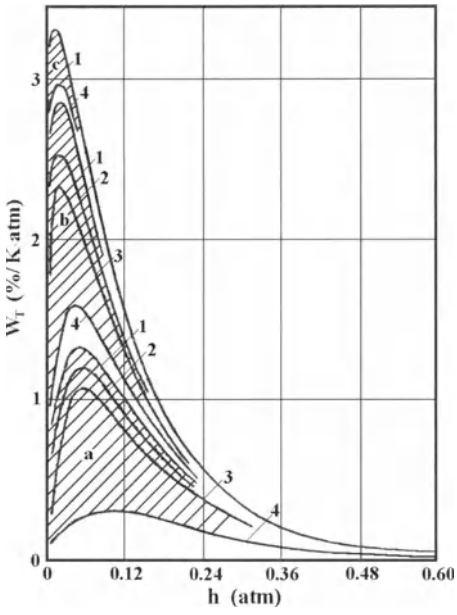

Fig. 9.7.3. Total temperature coefficients at sea level for integral flux of muons with energy $E_\mu \geq 10^2$ GeV (dashed region *a*), $E_\mu \geq 10^3$ GeV (dashed region *b*), $E_\mu \geq 10^4$ *GeV* (dashed region *c*) at different suppositions: curves *1* – all muons are generated only by decay of pions; curves *2* – 80% of muons are generated by decay of pions and 20% by decay of kaons; curves *3* – 60% of muons are generated by decay of pions and 40% by decay of kaons; curves *4* – all muons are generated only by decay of kaons.

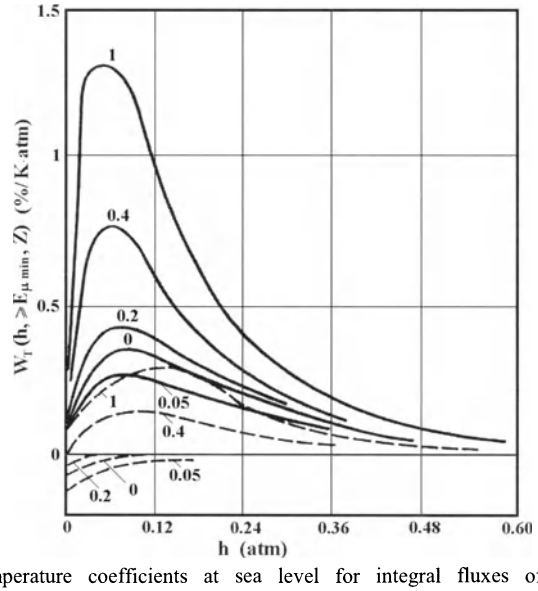

Fig. 9.7.4. Total temperature coefficients at sea level for integral fluxes of muons with energy $E_\mu \geq 10^2$ GeV arrived at different zenith angles (numbers near curves – values of $\cos Z$) for two suppositions: full curves – all muons are generated only by decay of pions; dashed curves – all muons are generated only by decay of kaons.

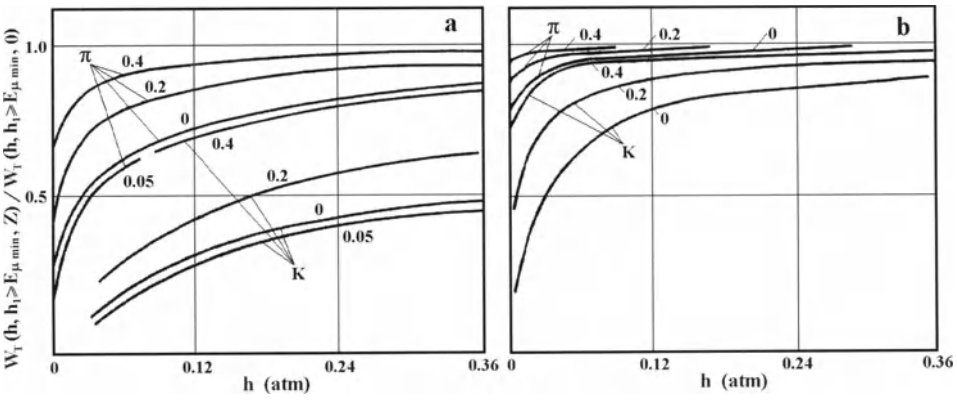

Fig. 9.7.5. Ratios of total temperature coefficients at zenith angle Z (numbers near curves are values of $\cos Z$) to temperature coefficients at zenith angle 0° for observations at sea level of integral fluxes of muons with $E_{\mu\min} = 10^3$ GeV (*a*) and $E_{\mu\min} = 10^4$ GeV (*b*) for two suppositions: curves π – all muons are generated only by decay of pions; curves K – all muons are generated only by decay of kaons.

9.8. Meteorological effects of integral multiplicities, partial coefficients, and interference of variations of different origin

9.8.1. General theory of meteorological effects and classification of time variations

Let us consider the CR intensity

$$I_i(h_o, R_c, D(R), T(h), \mathbf{E}(h)) = \int_{R_c}^{\infty} D(R) m_i(R, h_o, T(h), \mathbf{E}(h)) dR \qquad (9.8.1)$$

measured by detector of type i (it can denote muon or electron–photon intensity, total counting rate of neutron monitor, multiplicities 1, 2, 3 and others) in some point with cut off rigidity R_c, by the mass h_o of air in the vertical column with unity cross-section under the detector, by the energy spectrum of primary CR $D(R)$, by the vertical distribution under detector of generalized temperature $T(h) = T_r(h)(1 + 0.378e(h)/h)$ (here $T_r(h)$ is the real absolute temperature and $e(h)$ is the air humidity vertical distribution) and of atmospheric electric field $\mathbf{E}(h)$. In the right hand side of Eq. 9.8.1 m_i denote the integral multiplicity (the number of secondary particles of type i generated by one primary particle with rigidity R).

Variation of Eq. 9.8.1 on R_c will describe the CR intensity changing due to the change of the geomagnetic field (geomagnetic variations)

$$(\Delta I_i / I_{io})_{gm} = -\Delta R_c W_i(R_c, \overline{h_o}, \overline{T(h)}, \overline{\mathbf{E}(h)}). \qquad (9.8.2)$$

Variation on $D(R)$ will describe the CR intensity changing due to the change of primary CR spectrum (primary variations)

$$\left(\frac{\Delta I_i}{I_{io}}\right)_{pr} = \int_{R_c}^{\infty} \frac{\Delta D(R)}{D_o(R)} W_i\left(R, \overline{h_o}, \overline{T(h)}, \overline{\mathbf{E}(h)}\right) dR \,, \tag{9.8.3}$$

and variation on m_i will describe the CR intensity changing owed to the change of meteorological conditions in the Earth's atmosphere (meteorological variations)

$$\left(\frac{\Delta I_i}{I_{io}}\right)_{mt} = \int_{R_c}^{\infty} \frac{\Delta m_i\left(R, h_o, T(h), \mathbf{E}(h)\right)}{m_{io}\left(R, \overline{h_o}, \overline{T(h)}, \overline{\mathbf{E}(h)}\right)} W_i\left(R, \overline{h_o}, \overline{T(h)}, \overline{\mathbf{E}(h)}\right) dR \,. \tag{9.8.4}$$

In Eq. 9.8.2–9.8.4

$$W_i\left(R, \overline{h_o}, \overline{T(h)}, \overline{\mathbf{E}(h)}\right) = D_o(R) m_{io}\left(R, \overline{h_o}, \overline{T(h)}, \overline{\mathbf{E}(h)}\right) / I_{io} \tag{9.8.5}$$

is the coupling function, and $\overline{h_o}, \overline{T(h)}, \overline{\mathbf{E}(h)}$ are values and distributions averaged for long time period and characterized the average meteorological situation in the point of observations. In Eq. 9.8.2–9.8.5 I_{io} is determined by Eq. 9.8.1 at $R_c = \overline{R_c}$, $h_o = \overline{h_o}$, $T(h) = \overline{T(h)}$, $\mathbf{E}(h) = \overline{\mathbf{E}(h)}$. From our opinion, Eq. 9.8.4 described all known in the present time meteorological effects with taking into account the dependence of the meteorological coefficients from cut off rigidity and CR primary spectrum (through changing of coupling function according to Eq. 9.8.5).

9.8.2. Partial meteorological coefficients

Let us consider in more details Eq. 9.8.4 which can be rewritten in the form:

$$\left(\frac{\Delta I_i}{I_{io}}\right)_{mt} = \left(\frac{\Delta I_i}{I_{io}}\right)_{h} + \left(\frac{\Delta I_i}{I_{io}}\right)_{T} + \left(\frac{\Delta I_i}{I_{io}}\right)_{\mathbf{E}} , \tag{9.8.6}$$

where effect of atmospheric mass changing (barometric effect) owed by changing of h_o is

$$\left(\frac{\Delta I_i}{I_{io}}\right)_{h} = \Delta h_o \times \int_{R_c}^{\infty} \Omega_{hi}\left(R, h_o, \overline{T(h)}, \overline{\mathbf{E}(h)}\right) W_i\left(R, \overline{h_o}, \overline{T(h)}, \overline{\mathbf{E}(h)}\right) dR, \tag{9.8.7}$$

and where

$$\Omega_{hi}\left(R, h_o, \overline{T(h)}, \overline{\mathbf{E}(h)}\right) = \frac{\partial m_i\left(R, h_o, \overline{T(h)}, \overline{\mathbf{E}(h)}\right)}{\partial h_o \times m_{io}\left(R, \overline{h_o}, \overline{T(h)}, \overline{\mathbf{E}(h)}\right)} \tag{9.8.9}$$

is the partial mass coefficient (or partial barometric coefficient). The temperature effect due to changing of $T(h)$ will be determined by

$$\left(\frac{\Delta I_i}{I_{io}}\right)_T = \int_0^{h_o} \Delta T(h)dh \int_{R_c}^{\infty} \Omega_{Ti}\left(h,R,\overline{h_o},T(h),\overline{\mathbf{E}(h)}\right) W_i\left(R,\overline{h_o},\overline{T(h)},\overline{\mathbf{E}(h)}\right)dR, \quad (9.8.9)$$

where

$$\Omega_{Ti}\left(h,R,\overline{h_o},T(h),\overline{\mathbf{E}(h)}\right) = \frac{\delta m_i\left(R,\overline{h_o},T(h),\overline{\mathbf{E}(h)}\right)}{\delta T(h) \times m_{io}\left(R,\overline{h_o},\overline{T(h)},\overline{\mathbf{E}(h)}\right)} \quad (9.8.10)$$

is the partial temperature coefficient and δ in Eq. 9.8.10 denote the functional derivative; the atmospheric electric field effect owed to the changing of $\mathbf{E}(h)$ will be determined by

$$\left(\frac{\Delta I_i}{I_{io}}\right)_{\mathbf{E}} = \int_0^{h_o} \Delta E(h)dh \int_{R_c}^{\infty} \Omega_{\mathbf{E}}\left(h,R,\overline{h_o},\overline{T(h)},\mathbf{E}(h)\right) W_k^i\left(R,\overline{h_o},\overline{T(h)},\overline{\mathbf{E}(h)}\right)dR, \quad (9.8.11)$$

where

$$\Omega_{\mathbf{E}}\left(h,R,\overline{h_o},\overline{T(h)},\mathbf{E}(h)\right) = \frac{\delta m_i\left(R,\overline{h_o},\overline{T(h)},\mathbf{E}(h)\right)}{\delta \mathbf{E}(h) \times m_{io}\left(R,\overline{h_o},\overline{T(h)},\overline{\mathbf{E}(h)}\right)} \quad (9.8.12)$$

is the partial atmospheric electric field coefficient.

9.8.3. On the connection between partial and total meteorological coefficients

The commonly used total meteorological coefficients $W_{hi}, W_{Ti}, W_{\mathbf{E}i}$ can be determined from Eq. 9.8.7–9.8.12, taking into account their dependence on R_c and $D(R)$ and on averaged meteorological conditions:

$$W_{hi}\left(R_c,D(R),h_o,\overline{T(h)},\overline{\mathbf{E}(h)}\right) = \int_{R_c}^{\infty} \Omega_{hi}\left(R,h_o,\overline{T(h)},\overline{\mathbf{E}(h)}\right) W_i\left(R,\overline{h_o},\overline{T(h)},\overline{\mathbf{E}(h)}\right)dR, \quad (9.8.13)$$

$$W_{Ti}\left(h,R_c,D(R),\overline{h_o},T(h),\overline{\mathbf{E}(h)}\right) = \int_{R_c}^{\infty} \Omega_{Ti}\left(h,R,\overline{h_o},T(h),\overline{\mathbf{E}(h)}\right) W_i\left(R,\overline{h_o},\overline{T(h)},\overline{\mathbf{E}(h)}\right)dR, \quad (9.8.14)$$

$$W_{\mathbf{E}i}\left(h,R_c,D(R),\overline{h_o},\overline{T(h)},\mathbf{E}(h)\right) = \int_{R_c}^{\infty} \Omega_{\mathbf{E}i}\left(h,R,\overline{h_o},\overline{T(h)},\mathbf{E}(h)\right) W_i\left(R,\overline{h_o},\overline{T(h)},\overline{\mathbf{E}(h)}\right)dR. \quad (9.8.15)$$

Let us note that the dependence of total meteorological coefficients $W_{hi}, W_{Ti}, W_{\mathbf{E}i}$ on $D(R)$ is included in the coupling function according to Eq. 9.8.5.

9.8.4. Theory of meteorological effects accounting the interference of variations of different origin

In Sections 9.8.1–9.8.3 it was assumed that CR variations are relatively very small:

$$(\Delta I_i/I_{io})_{\text{magn}} << 1, \quad (\Delta I_i/I_{io})_{\text{prim}} << 1, \quad (\Delta I_i/I_{io})_{\text{met}} << 1. \tag{9.8.16}$$

But in many cases this assumption is not justified for primary variations (in periods of big ground level increases of solar CR, in periods of Forbush-decreases, during 11 solar cycle variations), for geomagnetic variations (during main phase of big geomagnetic storms and in connection with long-term variations of main geomagnetic field), and for meteorological variations (seasonal and daily temperature variations in places with strong continental climate, big atmosphere pressure variations during crossing of meteorological fronts, etc). In these cases we will have interference of CR effects of different origin with influence of primary variation on geomagnetic variation, and with influence of primary and geomagnetic variations on meteorological CR variations.

Let us start again from Eq. 9.8.1, but now we suppose that

$$\Delta m_i(R,h_o,T(h),\mathbf{E}(h)) = m_i(R,h_o,T(h),\mathbf{E}(h)) - m_{io}\left(R,\overline{h_o},\overline{T(h)},\overline{\mathbf{E}(h)}\right),$$
$$\text{or } \Delta m_i = m_i - m_{io};\ \Delta R_c = R_c - R_{co};\ \Delta D(R) = D(R) - D_o(R);\ \Delta I_i = I_i - I_{io}, \tag{9.8.17}$$

are not small relative to m_{io}, R_{co}, $D_o(R)$, and I_{io}. From Eq. 9.8.1, by using Eq. 9.8.17, we obtain

$$\frac{\Delta I_i\left(R_c,h_o,T(h),\mathbf{E}(h)\right)}{I_{io}\left(R_{co},\overline{h_o},\overline{T(h)},\overline{\mathbf{E}(h)}\right)} = \int_{R_{co}}^{\infty} \frac{\Delta m_i\left(R,h_o,T(h),\mathbf{E}(h)\right)}{m_{io}\left(R,\overline{h_o},\overline{T(h)},\overline{\mathbf{E}(h)}\right)} W_i\left(R_{co},R,\overline{h_o},\overline{T(h)},\overline{\mathbf{E}(h)}\right)$$

$$\times\left\{1+\delta\left(R-\overline{R_c}\right)\Delta R_c\left[1+\frac{\Delta D(R)}{D_o(R)}\right]+\frac{\Delta D(R)}{D_o(R)}\right\}dR - \Delta R_c W_i\left(R_{co},R_{co},\overline{h_o},\overline{T(h)},\overline{\mathbf{E}(h)}\right)$$

$$\times\left[1+\frac{\Delta D\left(\overline{R_c}\right)}{D_o(R_{co})}\right]+\int_{R_{co}}^{\infty}\frac{\Delta D(R)}{D_o(R)}W_i\left(R_{co},R,\overline{h_o},\overline{T(h)},\overline{\mathbf{E}(h)}\right)dR, \tag{9.8.18}$$

where $\overline{R_c}$ is in the interval $R_{co}, R_{co}+\Delta R_c$. In Eq. 9.8.18 the first term describes meteorological effects accounting the influence of geomagnetic and extra-terrestrial CR variations on meteorological coefficients; the second term describes geomagnetic effects with accounting the influence of extra-terrestrial CR variations, and the third term described only extra-terrestrial CR variations.

Let us consider in more details the first term that describes meteorological effects. In this case, the partial meteorological coefficients will be the same as determined by Eq. 9.8.9, 9.8.10 and 9.8.12, but for total meteorological coefficients we obtain:

$$W_{hi}\left(R_{co},\Delta R_c,D_o(R),\Delta D(R),h_o,\overline{T(h)},\overline{\mathbf{E}(h)}\right)=\int_{R_{co}}^{\infty}\Omega_{hi}\left(R,h_o,\overline{T(h)},\overline{\mathbf{E}(h)}\right)$$
$$\times W_i\left(R,\overline{h_o},\overline{T(h)},\overline{\mathbf{E}(h)}\right)\left[1+\delta\left(R-\overline{R_c}\right)\Delta R_c\left(1+\Delta D(R)/D_o(R)\right)+\Delta D(R)/D_o(R)\right]dR, \quad (9.8.19)$$

$$W_{Ti}\left(R_{co},\Delta R_c,D_o(R),\Delta D(R),\overline{h_o},T(h),\overline{\mathbf{E}(h)}\right)=\int_{R_{co}}^{\infty}\Omega_{Ti}\left(R,\overline{h_o},T(h),\overline{\mathbf{E}(h)}\right)$$
$$\times W_i\left(R,\overline{h_o},\overline{T(h)},\overline{\mathbf{E}(h)}\right)\left[1+\delta\left(R-\overline{R_c}\right)\Delta R_c\left(1+\Delta D(R)/D_o(R)\right)+\Delta D(R)/D_o(R)\right]dR, \quad (9.8.20)$$

$$W_{\mathbf{E}i}\left(R_{co},\Delta R_c,D_o(R),\Delta D(R),\overline{h_o},\overline{T(h)},\mathbf{E}(h)\right)=\int_{R_{co}}^{\infty}\Omega_{\mathbf{E}i}\left(R,\overline{h_o},\overline{T(h)},\mathbf{E}(h)\right)$$
$$\times W_i\left(R,\overline{h_o},\overline{T(h)},\overline{\mathbf{E}(h)}\right)\left[1+\delta\left(R-\overline{R_c}\right)\Delta R_c\left(1+\Delta D(R)/D_o(R)\right)+\Delta D(R)/D_o(R)\right]dR, \quad (9.8.21)$$

From Eq. 9.8.19–9.8.21 it follows that total meteorological coefficients can be presented as a constant (usually used) part and two variables parts caused by the influence of geomagnetic and extra-terrestrial CR variations on meteorological coefficients:

$$W_{ki}=W_{ki,c}+W_{ki,gm}+W_{ki,e-t}, \quad (9.8.22)$$

where $k=h,T$, or $\mathbf{E}$, and $W_{ki,c}$ is constant parts of total meteorological coefficients determined by Eq. 9.8.13-9.8.15. The second term on the right hand side of Eq. 9.8.22 describes variable parts of total meteorological coefficients caused by influence of geomagnetic CR variations on meteorological coefficients:

$$W_{ki,gm}=\Delta R_c\left(1+\Delta D\left(\overline{R_c}\right)/D_o\left(\overline{R_c}\right)\right)\Omega_{ki}\left(\overline{R_c},\overline{h_o},\overline{T(h)},\overline{\mathbf{E}(h)}\right)W_i\left(\overline{R_c},\overline{h_o},\overline{T(h)},\overline{\mathbf{E}(h)}\right). \quad (9.8.23)$$

The third term describes the influence of extra-terrestrial CR variations on meteorological coefficients:

$$W_{ki,e-t}=\int_{R_{co}}^{\infty}\frac{\Delta D(R)}{D_o(R)}\Omega_{ki}\left(R,\overline{h_o},\overline{T(h)},\overline{\mathbf{E}(h)}\right)W_i\left(R,\overline{h_o},\overline{T(h)},\overline{\mathbf{E}(h)}\right)dR. \quad (9.8.24)$$

9.9. CR meteorological coefficients for hard muons on the basis of 3-D model of meson–nuclear cascades in the atmosphere

Viskov and Dorman (1965) derived general formulas for computing integral multiplicity for hard muons on the basis of 3-D model of meson-nuclear cascades in the atmosphere, and in Viskov et al. (1967) were obtained general formulas for computing partial temperature coefficient for hard muons on the basis of this model.

9.9.1. Determination of integral multiplicity for hard muons

According to Viskov et al. (1967) the integral multiplicity for hard muons will be determined by expression

$$M_\mu(E_o,h_o,T(h))=\frac{(m_\pi R_o/\tau_\pi)m_\pi^3c^3}{2\pi\left(m_\pi^2-m_\mu^2\right)}\sum_{i=1}^{i_{\max}}\frac{A_N^i}{(i-1)!}\int_0^1\frac{d\cos Z}{(l\cos Z)^i}\int_0^{h_o}\frac{T(h)}{h}dh$$

$$\times\int_{E_{\mu\min}}^{E_{\mu\max}(i)}\frac{dE_\mu}{E_\mu}\int_{\alpha_1}^{\alpha_2}\frac{d\cos\theta}{\cos\theta}\int_{\overline{E_\mu}}^{E_\mu}\frac{E_\pi^{-\gamma}\left(-q\overline{T}(h,h')-\dfrac{h}{l\cos\theta}\right)}{\Phi\left(E_\pi^2-m_\pi^2c^4\right)}$$

$$\times\int_0^h\exp\left(-\frac{h'}{l}\frac{\cos Z-\cos\theta}{\cos Z\cos\theta}\right)(h')^{i-1}dh'\exp\left(-\frac{m_\mu R_o}{\tau_\mu}\overline{\overline{T}}(h,E_\mu,\cos\theta)\right), \tag{9.9.1}$$

where $\overline{E_\mu}$ is determined by equation

$$\frac{m_\pi^2}{m_\mu^2}\left[\overline{E_\mu}+\frac{a(h_o-h)}{\cos\theta}\right]\le E_{\pi\max}(i) \tag{9.9.2}$$

and

$$q=\frac{m_\pi R_o c}{g\tau_\pi\cos\theta\sqrt{E_\pi^2-m_\pi^2c^4}};\ \overline{T}(h',h)=\int_{h'}^{h}\frac{T(h'')}{h''}dh'';\ \overline{\overline{T}}(h,E_\mu,\cos\theta)=\int_h^{h_o}\frac{T(h')dh'}{h'\left(E_\mu-\dfrac{a(h-h')}{\cos\theta}\right)};$$

$$\alpha_{1,2}=\sqrt{\frac{E_\pi^2-m_\pi^2c^4-p_\perp^2c^2}{E_\pi^2-m_\pi^2c^4}}\cos Z\mp\frac{p_\perp c}{\sqrt{E_\pi^2-m_\pi^2c^4}}\sin Z;\ \Phi=\left[1-\frac{E_\pi^2-m_\pi^2c^4-p_\perp^2c^2}{E_\pi^2-m_\pi^2c^4}\right.$$

$$\left.-\cos^2\theta-\cos^2 Z+2\cos Z\cos\theta\sqrt{\frac{E_\pi^2-m_\pi^2c^4-p_\perp^2c^2}{E_\pi^2-m_\pi^2c^4}}\right]^{1/2}. \tag{9.9.3}$$

In Eq. 9.9.1–9.9.3 h_o is the level of observation, h is the level of pion generation, Z – the zenith angle of primary particle arriving, θ is the angle between trajectory of generated in elementary act pion and trajectory of primary particle, L and l are the transport paths for nuclear interactions of primary particles and pions, all other are the same what we used above. For further calculations, it was assumed that $L = l$ and new variables were introduced:

$$y=h/h_o;\ \ E_1=\overline{E_\mu}-E_{\mu\min};\ \ z=\left(E_\mu-E_{\mu\min}\right)/E_1;\ \ Q=m_\mu R_o c/\tau_\mu g;$$
$$F=E_1 z+ah_o(1-y)/\cos Z. \tag{9.9.4}$$

After introducing Eq. 9.9.4 in Eq. 9.9.1 and simplification of the equation on the basis of estimation of relative role of different terms in different regions of pressure and primary particle energy, we obtain

$$M_\mu(E_o,h_o,T(h))=\frac{m_\pi^4 R_o c^3}{2\pi\tau_\pi g\left(m_\pi^2-m_\mu^2\right)}\sum_{i=1}^{i_1}\frac{A_{Ni}E_1 h_o^i}{(i-1)!}\int_0^1\frac{d\cos Z}{(l\cos Z)^i}\int_0^1\frac{T(y)}{y}dy$$

$$\times\int_0^1\frac{dz}{E_1 z+E_{\mu\min}}\int_F^{\frac{m_\pi^2}{m_\mu^2}F\le E_{\pi\max}(i)}\frac{E_\pi^{-\gamma}dE_\pi}{\left(E_\pi^2-m_\pi^2c^4\right)}\int_{\alpha_1}^{\alpha_2}\frac{d\cos Z}{\Phi\cos^2 Z}\exp\left[-\overline{\overline{QT}}(y,h_o)\right]$$

$$\times\int_0^y(h')^{i-1}\exp\left(-g\overline{T}(y,h')-\frac{yh_o}{l\cos Z}\right)\exp\left(-\frac{h_o h'}{l}\frac{\cos Z-\cos\theta}{\cos Z\cos\theta}\right)dh', \qquad (9.9.5)$$

where $\gamma\approx 2.5\div 2.7$ is the slope in the pion generation differential spectrum.

9.9.2. *Calculation of temperature effect of muon integral multiplicity*

By varying of integral multiplicity described by Eq. 9.9.5 on $T(h)$, we obtain

$$\frac{\Delta M_\mu(E_o,h_o,T(h))}{M_\mu(E_o,h_o,T(h))}=\frac{m_\pi^4 R_o c^3}{2\pi\tau_\pi g\left(m_\pi^2-m_\mu^2\right)m_\mu(E_o,h_o,T(h))}\sum_{i=1}^{i_1}\frac{A_{Ni}E_1 h_o^i}{(i-1)!}(A+B+C), \qquad (9.9.6)$$

where

$$A=\int_0^1\frac{\Delta T(y)}{y}dy\int_0^1\frac{d\cos Z}{(l\cos Z)^i}\int_0^1\frac{dz}{E_1 z+E_{\mu\min}}\int_0^y(h')^{i-1}dh'\int_{\alpha_1}^{\alpha_2}\frac{d\cos Z}{\cos^2 Z}\exp\left(-\frac{h_o h'}{l}\frac{\cos Z-\cos\theta}{\cos Z\cos\theta}\right)$$

$$\times\int_F^{\frac{m_\pi^2}{m_\mu^2}F\le E_{\pi\max}(i)}\frac{E_\pi^{-\gamma}dE_\pi}{\Phi\left(E_\pi^2-m_\pi^2c^4\right)}\exp\left(-g\overline{T}(y,h')-\frac{yh_o}{l\cos Z}\right)\exp\left[-\overline{\overline{QT}}(y,h_o)\right]; \qquad (9.9.7)$$

$$B=-\int_0^1\frac{\Delta T(h'')}{h''}dh''\int_{h''}^1\frac{T(y)}{y}dy\int_0^1\frac{d\cos Z}{(l\cos Z)^i}\int_0^1\frac{dz}{E_1 z+E_{\mu\min}}\int_0^y(h')^{i-1}dh'\int_{\alpha_1}^{\alpha_2}\frac{d\cos Z}{\cos^2 Z}$$

$$\times\exp\left(-\frac{h_o-h_1}{l}\frac{\cos Z-\cos\theta}{\cos Z\cos\theta}\right)\times\int_F^{\frac{m_\pi^2}{m_\mu^2}F\le E_{\pi\max}(i)}\frac{qE_\pi^{-\gamma}dE_\pi}{\Phi\left(E_\pi^2-m_\pi^2c^4\right)}$$

$$\times\exp\left(-g\overline{T}(y,h')-\frac{yh_o}{l\cos Z}\right)\exp\left[-\overline{\overline{QT}}(y,h_o)\right]; \qquad (9.9.8)$$

$$C=\int_0^1\frac{\Delta T(h'')}{h''}dh''\int_0^h\frac{T(y)}{y}dy\int_0^1\frac{d\cos Z}{(l\cos Z)^i}\int_0^1\frac{dz}{E_1 z+E_{\mu\min}}\int_F^y(h')^{i-1}dh'\int_{\alpha_1}^{\alpha_2}\frac{d\cos Z}{\cos^2 Z}$$

$$\times\exp\left(-\frac{h_o-h'}{l}\frac{\cos Z-\cos\theta}{\cos Z\cos\theta}\right)\times\int_F^{\frac{m_\pi^2}{m_\mu^2}F\le E_{\pi\max}(i)}\frac{E_\pi^{-\gamma}dE_\pi}{\Phi\left(E_\pi^2-m_\pi^2c^4\right)}\exp\left(-\overline{\overline{QT}}(y,h_o)\right)$$

$$\times\left(-\frac{Q}{(E_1 z+E_{\mu\min})\cos Z}\right)\exp\left(-g\overline{T}(y,h')-\frac{yh_o}{l\cos Z}\right). \qquad (9.9.9)$$

9.10. The method of partial barometric coefficient

Nowadays the main ground CR detectors in the World are neutron monitors and super-monitors. These detectors have a very small temperature effect, but a big barometric effect. It means that for obtaining accurate data it is necessary to make very accurate corrections for the barometric effect. This is not so easy to do because, as was shown above, barometric coefficients change significantly with changing of the primary CR spectrum (caused by modulation effects in the Heliosphere of galactic CR and by generation of solar CR in the flare–coronal acceleration processes), as well as with changes of averaged air pressure and cut off rigidity. To solve this problem Dorman (1966) introduced the method of partial barometric coefficient (in addition to the generally used total barometric coefficient).

9.10.1. Total and partial barometric coefficients

Let us start from expression for CR intensity of type i in some point with cut off rigidity R_C and air pressure h:

$$I_i(R_C,h)=\int_{R_C}^{\infty}D(R)m_i(R,h)dR\,, \qquad (9.10.1)$$

where $m_i(R,h)$ is the integral multiplicity. The total barometric coefficient is determined as

$$\beta_i(R_C,h)=\partial\ln(I_i(R_C,h))/\partial h=I_i^{-1}(R_C,h)\int_{R_C}^{\infty}(\partial m_i(R,h)/\partial h)D(R)dR. \qquad (9.10.2)$$

According to Dorman (1966), the partial barometric coefficient has a sense as barometric coefficient of integral multiplicity:

$$B_i(R,h)=\partial\ln(m_i(R,h))/\partial h\,. \qquad (9.10.3)$$

The connection between total and partial barometric coefficients is described by relation (on the basis of Eq. 9.10.2 and 9.10.3):

$$\beta_i(R_c,h)=\int_{R_c}^{\infty}B_i(R,h)W_i(R_c,R,h)dR\,, \tag{9.10.4}$$

where $W_i(R_c,R,h)$ is the local coupling function what depends from the primary CR spectrum $D(R)$, integral multiplicity $m_i(R,h)$ and cut off rigidity R_c:

$$W_i(R_c,R,h)=D(R)m_i(R,h)/I_i(R_c,h). \tag{9.10.5}$$

9.10.2. Determination of partial barometric coefficient by using data of total barometric coefficient at different cut off rigidities

By differentiating of Eq. 9.10.4 on R_c we obtain:

$$\frac{\partial\beta_i(R_c,h)}{\partial R_c}=-B_i(R_c,h)W_i(R_c,R_c,h)-\int_{R_c}^{\infty}B_i(R,h)\frac{D(R)m_i(R,h)}{I_i^2(R_c,h)}\frac{\partial I_i(R_c,h)}{\partial R_c}dR. \tag{9.10.6}$$

From Eq. 9.10.6 by using Eq. 9.10.5 and Eq. 9.10.1 these follows

$$\frac{\partial\beta_i(R_c,h)}{\partial R_c}=(\beta_i(R_c,h)-B_i(R_c,h))W_i(R_c,R_c,h)\,, \tag{9.10.7}$$

from which we finally obtain

$$B_i(R_c,h)=\beta_i(R_c,h)-W_i^{-1}(R_c,R_c,h)(\partial\beta_i(R_c,h)/\partial R_c)\,. \tag{9.10.8}$$

Eq. 9.10.8 can be used for determining the partial barometric coefficient $B_i(R,h)$ on the basis of observation data of the planetary distribution of the total barometric coefficient $\beta_i(R_c,h)$. This was done in Dorman and Sergeev (1969), where it was shown that all available data on the total barometric coefficient in intervals $0\le R_c\le 15$ GV and $600\text{ mb}\le h\le 1050$ mb can be described (with relative error ± 0.015) as

$$\beta_i(R_c,h)=((b_1+b_2h)+(b_3+b_4h)R_c)^{-1}\%/\text{mb}\,, \tag{9.10.9}$$

where

$$b_1=1.277,\ b_2=8.58\times10^{-5},\ b_3=-1.298\times10^{-2},\ b_4=2.56\times10^{-5}. \tag{9.10.10}$$

To determine $W_i^{-1}(R_c,R_c,h)$ in Eq. 9.10.8 let us use an analytical approximation for the coupling function (see in Chapter 3, Section 3.8); in this case

$$W_i^{-1}(R_c,R_c,h)=\frac{R_c^{k_i+1}}{a_i k_i}\left(\exp\left(a_i R_c^{-k_i}\right)-1\right). \qquad (9.10.11)$$

By introducing Eq. 9.10.9 and Eq. 9.10.11 in Eq. 9.10.8, we finally obtain

$$B_i(R,h)=-(b_3+b_4R)^{-1}\left(1+(a_i k_i(b_3+b_4R))^{-1}b_4R^{k_i+1}\left(\exp\left(a_i R^{-k_i}\right)-1\right)\right), \qquad (9.10.12)$$

where values of coefficients b_1,b_2,b_3 and b_4 were given by Eq. 9.10.10.

9.10.3. Calculation of partial barometric coefficient for total neutron component

In Section 3.5.2 we calculated the integral multiplicity $M_n\,(E_o,\theta_o,h)$ for the total neutron component within the framework of the theory of meson-nuclear cascade development in the atmosphere according to Dorman and Yanke (1981). In Fig. 3.5.3 were shown the dependences of $M_n\,(E_o,\theta_o,h)$ from h for vertical primary CR arriving ($\theta_o=0^o$). From these data one can evaluate the partial barometric coefficient:

$$B(E_o,\,\theta_o,\,h)=\partial \ln M_n\,(E_o,\theta_o,h)/\partial h. \qquad (9.10.13)$$

Results are shown in Fig. 9.10.1 for h = 1030, 760, 490 and 40 g.cm^{-2} as a dependence on the energy of primary particles E_o. Using the results of Fig. 9.10.1 on the partial barometric coefficient and Eq. 9.10.4 described the relation between total and partial barometric coefficients, we can determine the total barometric coefficient:

$$\beta(h,R_c)=\int_{R_{\min}}^{\infty} dR \int_0^{\pi/2} S(\theta_o)G(R,\theta_o)B(R,\theta_o,h)\frac{M_n(R,\theta_o,h)D(R)}{I(h,R_c)}\sin\theta_o d\theta_o\,, \qquad (9.10.14))$$

where $S(\theta_o)$ is the effective surface of NM in direction θ_o, $G(R,\theta_o)$ is the penumbra function (see above Section 3.3). For differential energy spectrum of primary CR it is supposed that at high rigidities $D(R)\propto R^{-2.7}$. Results of calculation of $\beta(h,R_c)$ in comparison with experimental data are shown in Fig. 9.10.2.

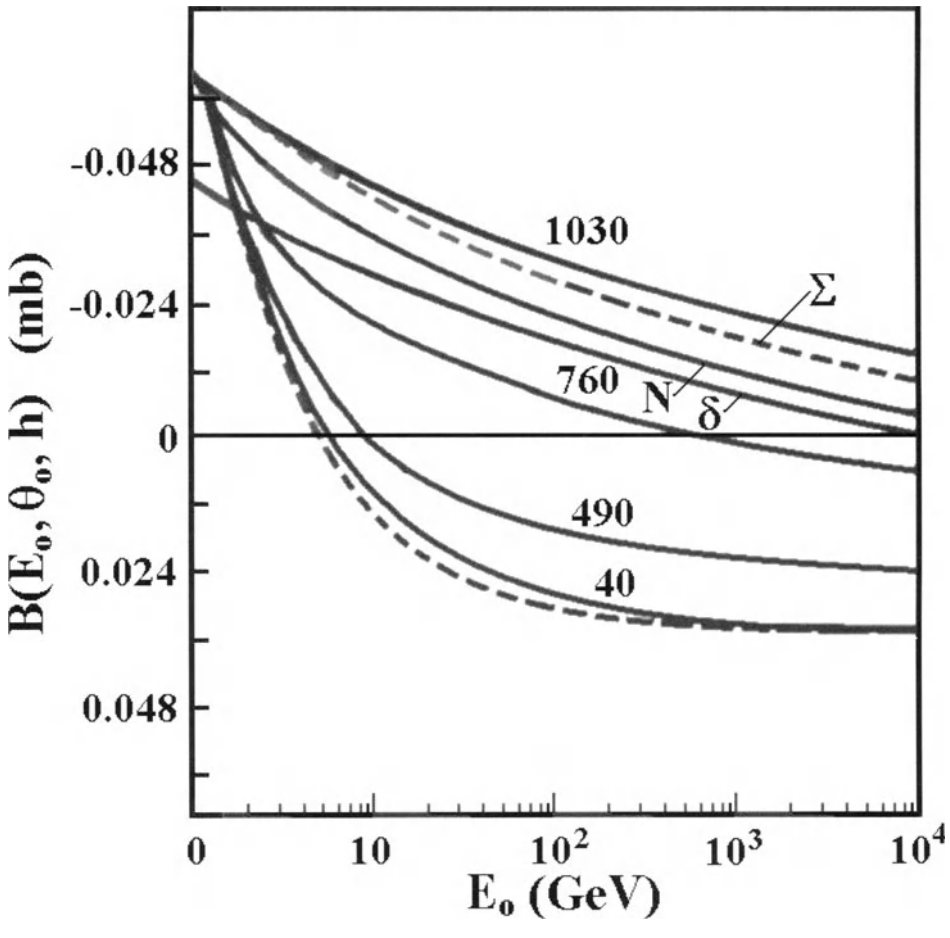

Fig. 9.10.1. The partial barometric coefficient $B(E_O, \theta_O, h)$ in units mb^{-1} for h = 1030, 760, 490 and 40 $g.cm^{-2}$ as a dependence on the energy of primary particles E_0 for vertical primary CR arriving for inelastic coefficient 0.5 (by dashed curve for h = 1030 $g.cm^{-2}$ and dotted curve for h = 40 $g.cm^{-2}$ are shown the expected partial barometric coefficients for inelastic coefficient 0.45). For h = 1030 $g.cm^{-2}$ are also shown the parts from energetic nucleons (N) and from δ-nucleons (δ). According to Dorman and Yanke (1981).

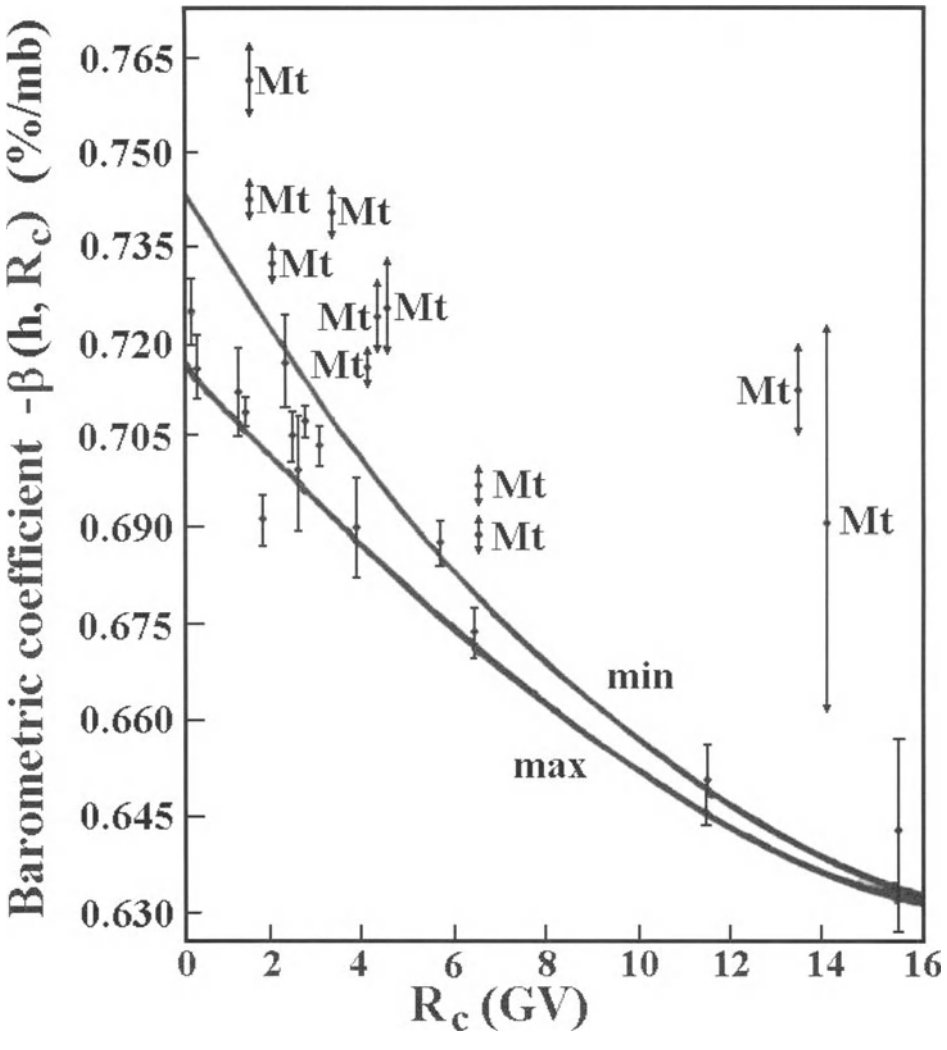

Fig. 9.10.2. Calculated total barometric coefficient for neutron component at sea level for minimum and maximum of solar activity in comparison with experimental data (full vertical lines for NM near sea level, and vertical lines with Mt near bars for NM at mountain levels). According to Dorman and Yanke (1981).

Part 3

COSMIC RAY INFLUENCE ON THE ATMOSPHERE AND ATMOSPHERIC PROCESSES

Preface of Part 3

In Part 2 we considered the direct problem: how the changed atmosphere influences the cosmic radiation; here we consider the inverse problem: how cosmic radiation influences the atmosphere. Namely, in Part 3 (Chapters 10–14) we consider the problem of galactic and solar CR influence on the Earth's atmosphere and atmospheric processes through nuclear reactions of primary and secondary CR with air and aerosols matter accompanied with the formation of a lot of unstable and stable cosmogenic nuclides; through generation in the atmosphere of secondary relativistic electrons and positrons, played a key role in atmospheric electric field phenomena; through air ionization influences on the low ionosphere and radio wave propagation; through induced chemical reactions influences on the chemistry of the atmosphere and ozone layer, as well as on long-term global climate change (through CR influence on planetary cloud covering).

In **Chapter 10** we consider in details the production of many cosmogenic nuclides in nuclear reactions of CR with ground, water, and air atoms, the vertical and global mixing in the atmosphere, and exchange between different planetary reservoirs, data on producing by CR of cosmogenic isotopes ^{3}H, ^{3}He, ^{7}Be, ^{10}Be. On the basis of ^{10}Be data in Antarctic and Greenland ice very important information on long term CR variations in the past caused by solar activity cycles and big change of geomagnetic field was obtained.

In **Chapter 11** we consider the problem of CR influence on the atmospheric electric field and thunderstorms, on the global Earth's charge and global electric current; we consider the key role of CR in discharges inside charged clouds, between clouds, and between the ground and clouds, the possible role of EAS (External Atmospheric Showers) generated by high energy CR particles; on the CR role in the equilibrium between charged and discharged global atmospheric electric currents, and in supporting the stability of the Earth's charge.

The problem of CR influence on the ionosphere and radio wave propagation we consider in **Chapter 12**: we start from the famous GLE of 23 February 1956, when were observed enormous disturbances in the ionosphere and interruptions in radio wave communications; then we present calculations of the expected ionization rate and radio-wave absorption for different solar energetic particles (SEP) energy spectrums, analyze the riometer measurements of polar absorptions as method of small energy solar CR monitoring, and consider recent calculations of expected ionization rates during GLE in October 1989, July 2000, and April 2001 with observations comparison, we develop also the ionosphere CR coupling function method.

In **Chapter 13** we consider the problem of CR influence on the chemical processes in the atmosphere, especially on the formation of nitrates in the mesosphere and very important experimental data on their abundances in Antarctic and Greenland ice columns (which are used for wide research of many interesting phenomena in the past), of CR influence on stratospheric chemistry and ozone layer.

In **Chapter 14** we consider the problem on CR influence on planetary cloud covering and long term climate change; on the possible influence of long term CR variation on long term changing of the planetary surface temperature (especially, CR influence on weather during a Maunder minimum); CR influence on precipitation in periods of big magnetic storms (Forbush–decreases) and big solar CR events. We will consider shortly also the Project CLOUD as important step in understanding the link CR–cloud formation–climate change.

Chapter 10

Nuclear Reactions of Cosmic Rays with Ground, Water, and Air Atoms; Production of Cosmogenic Nuclides

10.1. Production of stable and unstable cosmogenic nuclides in space, in bodies, and in atmospheres

In any astrophysical object containing CR (of local and/or external origin) and matter a lot of stable and unstable cosmogenic isotopes will be continuously produced. This production is caused by nuclear reactions with matter of primary protons and nuclei as well as of secondary CR nuclear active particles. It takes place **in space** where secondary energetic particles generated in interactions of primary CR particles with space matter become a part of CR with changing elemental and isotopic contents. On the other hand the space matter also is changed by these nuclear interactions with generation of cosmogenic stable and unstable nuclides. The abundance and composition of cosmogenic nuclides will be determined by the variations of CR intensity (which lead to the time variation of cosmogenic generation rate) by the amount and composition of matter, by the decay time of unstable cosmogenic nuclides, and by exchange processes in the space (this problem will be considered in details in Dorman, M2005).

Production of cosmogenic nuclides takes place also **in bodies** in interplanetary space: asteroids; meteorites; comets; planets and satellites of planets without or with very thin atmospheres (much smaller than one mean nuclear transport path, as for example on Mars). In this case CR of galactic origin (modulated by solar activity) and CR of local origin (solar, planetary and interplanetary CR) will produce a lot of cosmogenic nuclides inside these bodies in the depth from the surface to about several mean nuclear transport paths (several hundred $g.cm^{-2}$). The number of secondary nuclear active particles from CR interactions with matter as a result of nuclear meson cascades will increase very much with increasing primary CR particle energy. The total number of generated cosmogenic nuclides can be even greater than the total number of incident CR particles. Moreover in bodies with solid state structure CR will produce a lot of structural disturbances in the form of tracks (especially by CR particles with a great charge *Ze*) which also contain important information on CR for many millions of years (see in more details in Dorman, M2005).

We have a much more complicated situation **in the atmospheres** of the Sun and the planets: besides the production of cosmogenic nuclides in the atmospheres by galactic and local CR and the nuclear active secondary particles generated in the atmospheres in the processes of nuclear meson cascades, it is necessary to take into account modulation effects produced by solar wind and the influence of own magnetic fields on CR trajectories (and consequently cut off rigidities), as well as the mixing of elements in the atmospheres and exchange of elements between different planetary reservoirs or between different layers of atmosphere with different production rate of cosmogenic nuclides. Let us note that for Earth some very small production rates of cosmogenic

nuclides is expected also **in rocks in the ground** and **in the waters of the sea and oceans.**

In this Chapter we will consider vertical mixing of cosmogenic nuclides in the atmosphere and introduce local coupling functions (Section 10.2), planetary mixing and planetary coupling functions (Section 10.3). cosmogenic nuclides exchange between different reservoirs (Section 10.4), and some results on direct measurements of cosmogenic nuclides production rate (Section 10.5). Main results obtained by measurements of cosmogenic nuclides ^{7}Be and ^{10}Be will be considered in Sections 10.6 and 10.7, respectively.

10.2. Cosmogenic nuclides and vertical mixing of elements in the Earth's atmosphere; local cosmogenic coupling functions

10.2.1. The production rate of cosmogenic nuclides in the atmosphere, ground, and water

The production rate of cosmogenic nuclides will be determined by the depth h in the atmosphere, in the ground or in the water (calculated from the upper boundary of the atmosphere in units g.cm^{-2}) and by the cut off rigidity R_c. Let us suppose that $M_l(R,Z_l,E_l,h)$ is the total differential multiplicity on the depth h in the atmosphere of nuclear active particles of type l with kinetic energy per nucleon E_l and charge $Z_l e$ (l denotes protons, neutrons, charged pions, nuclei and nuclei fragments, etc.), i.e. includes all nuclear active nuclear active particles at the depth h generated by one primary particle with charge Ze and rigidity R. In this case we obtain for the production rate of cosmogenic nuclides:

$$q_i(R_c,h,t)=\sum_Z \int_{R_c}^{\infty} D_Z(R,t)dR \sum_l \sum_k \int_0^{E(R)} M_l(R,Z_l,E_l,h)\sigma_{ilk}(E_l)N_k(h)dE_l, \quad (10.2.1)$$

where $D_Z(R,t)$ is the rigidity differential spectrum of primary CR out of the atmosphere with rigidity R and charge Ze,

$$E(R)=Ze\left(R^2+\left(Am_nc^2/Ze\right)^2\right)^{1/2}-Am_nc^2 \quad (10.2.2)$$

is the kinetic energy of primary particle of atomic number A, rigidity R and charge Ze, $\sigma_{ilk}(E_l)$ is the effective cross-section of generation of a cosmogenic isotope of type i in the interaction of l type nuclear active particle with background nuclei in the atmosphere, in ground or in water of type k (H, He, C, N, O, Si, Ca, Fe, etc.) with concentration $N_k(h,t)$.

Let us note that in the first approximation all $D_Z(R,t)$ for galactic CR have about the same shape (see above, Section 1.4) and therefore we can suppose that

$$D_Z(R,t) \approx B_Z D(R,t), \tag{10.2.3}$$

where B_Z determines the relative abundance of particles with charge Ze in primary CR and $\sum_Z B_Z = 1$. By putting Eq. 10.2.3 in Eq. 10.2.1 we obtain

$$q_i(R_c,h,t) = \int_{R_c}^{\infty} D(R,t) M_i(R,h,t) dR, \tag{10.2.4}$$

where

$$M_i(R,h,t) = \sum_Z \sum_l \sum_k \int_0^{E(R)} M_l(R,Z_l,E_l,h) \sigma_{ilk}(E_l) B_Z N_k(h,t) dE_l \tag{10.2.5}$$

is the integral multiplicity of the cosmogenic nuclides of type *i* produced by one average primary particle with rigidity *R*.

10.2.2. Calculations of cosmogenic nuclides production rate as a function of altitude and geomagnetic latitude

Many authors made calculations of expected cosmogenic nuclide production rates by consideration of CR cascade in atmosphere and nuclear interactions with air atoms: Hess et al. (1961), Newkirk (1963), Lingenfelter (1963), Lal and Peters (1967), Oeschger et al. (1969), Light et al. (1973), O'Brien (1979), Blinov (1988), Masarik and Reedy (1995), Masarik and Beer (1997, 1999). An important result found in these calculations is the dependence of expected cosmogenic production rates on the altitude and the geomagnetic latitude. Extensive results were obtained recently by Masarik and Beer (1999). We described in Chapter 2 (Section 2.8) results on secondary protons and neutrons obtained in this paper. Here we will describe the results of Masarik and Beer (1999) on the production rates of different cosmogenic nuclides. In Fig. 10.2.1 is shown the depth dependence of latitudinal production rates of ^{36}Cl ($T_{1/2} = 3\times10^5$ years) and ^{10}Be ($T_{1/2} = 1.5\times10^6$ years).

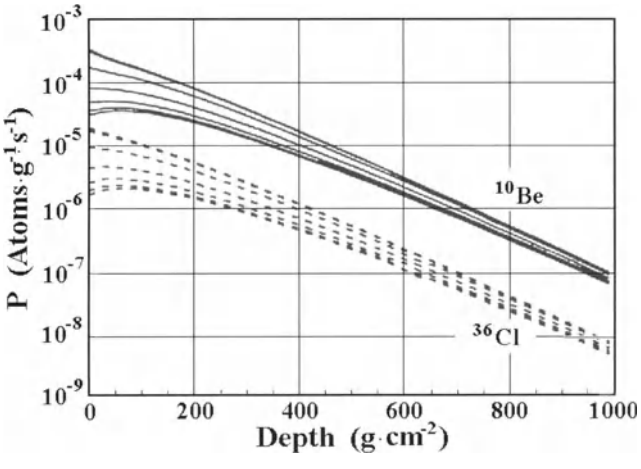

Fig. 10.2.1. The depth dependence of latitudinal production rates of ^{36}Cl and ^{10}Be in the Earth's atmosphere. Each line represents a latitude interval of 10° (for both nuclides the production rates decrease with geomagnetic latitude decreasing; the top curves are for 80–90°; and bottom – for 0–10°). According to Masarik and Beer (1999).

The relative contribution of the stratosphere in the total production rate of cosmogenic nuclides ^{10}Be ($T_{1/2} = 1.5\times10^6$ years), ^{36}Cl ($T_{1/2} = 3\times10^5$ years), and ^{14}C ($T_{1/2} = 5730$ years) is shown in Fig. 10.2.2 (it can be seen that at low latitudes this contribution is about 30%, and increases to more than 80% at high latitudes).

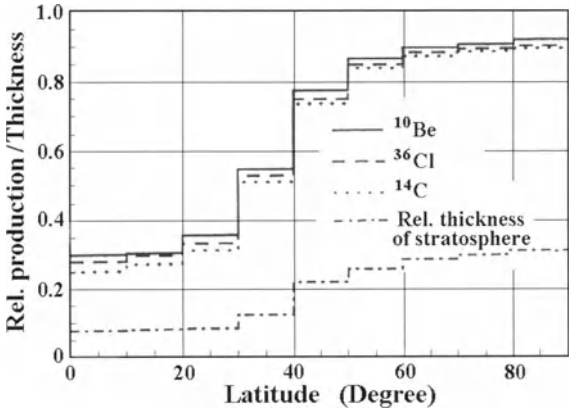

Fig. 10.2.2. Relative contribution of the stratosphere in the total production rate of cosmogenic nuclides ^{10}Be, ^{36}Cl and ^{14}C. According to Masarik and Beer (1999).

10.2.3. The vertical mixing of elements and integral cosmogenic multiplicity

Let us take into account the vertical mixing of elements in the atmosphere with characteristic time T_{iv} and determine the total production rate of cosmogenic nuclides $Q_i(R_c,h_o,t)$ in the vertical column per cm^2 from the atmosphere's top $h=0$ to the bottom $h=h_o$:

$$Q_i(R_c,h_o,t) = T_{iv}^{-1}\sum_Z \int_{R_c}^{\infty} dR \int_{t-T_{iv}}^{t} D_Z(R,t) M_{Zi}(R,h_o,t)dt\,, \tag{10.2.6}$$

where

$$M_{Zi}(R,h_o,t) = \int_0^{h_o} dh \sum_l \sum_k \int_0^{E(R)} M_{Zl}(R,Z_l,E_l,h)\sigma_{ilk}(E_l)N_k(h,t)dE_l \tag{10.2.7}$$

is the integral cosmogenic multiplicity in the vertical column per cm^2 from $h=0$ to $h=h_o$ of cosmogenic nuclides of type i per one primary particle Ze with rigidity R.

In the frame of approximation described by Eq. 10.2.3 we obtain

$$Q_i(R_c,h_o,t) = T_{iv}^{-1}\int_{R_c}^{\infty} dR \int_{t-T_{iv}}^{t} D(R,t) M_i(R,h_o,t)dt\,, \tag{10.2.8}$$

where $M_i(R,h_o,t)$ is determined by Eq. 10.2.5.

Let us note that for cosmogenic nuclides in the water of the oceans and seas the vertical mixing is also important, but in this case the characteristic time T_{iv} is much bigger then that for the atmosphere; for cosmogenic nuclides in rocks and ground it can be supposed that $T_{iv} \to \infty$.

Table 10.2.1 lists the expected production rates of different cosmogenic nuclides integrated over vertical column in different latitudinal zones, as calculated by Masarik and Beer (1999) (details of calculations were described in the previous Section 10.2.1).

Table 10.2.1. Expected production rates (in atoms.cm^{-2}.sec^{-1}) of different cosmogenic nuclides integrated over vertical column in different latitudinal zones, and global average production rates for average value of modulation parameter $\Phi = 550$ MeV. According to Masarik and Beer (1999).

NUCLIDE	LATITUDINAL ZONES						
	0–10°	10–20°	20–30°	30–40°	40–50°	50–60°	60–90°
^{3}H	0.118	0.129	0.159	0.224	0.380	0.565	0.602
^{7}Be×10	0.148	0.161	0.197	0.285	0.478	0.710	0.740
^{10}Be×100	0.775	0.841	1.04	1.47	2.48	3.68	3.86
^{14}C	0.83	0.90	1.10	1.56	2.63	3.92	4.55
^{36}Cl×1000	0.791	0.860	1.05	1.51	2.52	3.75	3.96

10.2.4. Time-variations and local coupling functions for production rate of cosmogenic nuclides in the vertical column of the atmosphere

The relative time variation of production rate of cosmogenic nuclides in the vertical column of the atmosphere can be determined from Eq. (10.2.6):

$$\frac{\delta Q_i(R_c,h_o,t)}{Q_{io}(R_{co},h_o)} = \sum_Z \int_{R_{co}}^{\infty} dR \int_{t-T_v}^{t} \frac{\delta D_Z(R,t)}{D_{Zo}(R)} W_{iZR_{co}}(R,h_o)dR$$

$$+\sum_Z \int_{R_{co}}^{\infty} dR \int_{t-T_v}^{t} \frac{\delta M_{iZ}(R,h_o,t)}{M_{iZo}(R,h_o)} W_{iZR_{co}}(R,h_o)dR - \delta R_c(t)\sum_Z W_{iZR_{co}}(R_{co},h_o), \qquad (10.2.9)$$

where

$$W_{iZR_{co}}(R,h_o) = D_{Zo}(R)M_{iZo}(R,h_o)/Q_{io}(R_{co},h_o) \qquad (10.2.10)$$

is the local coupling function between production rate of cosmogenic nuclides in the vertical column of the atmosphere and differential rigidity spectrum of primary CR with charge *Ze* (the method of coupling functions for cosmogenic nuclides production rate and its time variations was introduced for radiocarbon investigations by Dorman, 1977a–g, 1978). In Eq. 10.2.9 and 10.2.10 we denote:

$$Q_{io}(R_{co},h_o)=Q_i(R_{co},h_o,0),\ \delta Q_i(R_c,h_o,t)=Q_i(R_c,h_o,t)-Q_{io}(R_{co},h_o),\ R_{co}=R_c(0),$$

$$\delta R_c(t)=R_c(t)-R_{co},\ D_{Zo}(R)=D_Z(R,0),\ \delta D_Z(R,t)=D_Z(R,t)-D_{Zo}(R), \qquad (10.2.11)$$

$$M_{iZo}(R,h_o)=M_{iZ}(R,h_o,0),\ \delta M_{iZ}(R,h_o,t)=M_{iZ}(R,h_o,t)-M_{iZo}(R,h_o).$$

The first term in Eq. 10.2.9 describes the relative change in production rate caused by the variation of differential rigidity spectrum (primary variation). The second term (atmospheric variation) reflects the change in the production rate caused by the change of integral multiplicity; that is, the change in conditions for developing of meson nuclear cascade in the atmosphere. According to Eq. 10.2.7 it can be caused by change in h_o (barometric effect) and by possible change of the vertical distribution $N_k(h,t)$ of element contents in the atmosphere (elements distribution effect):

$$\delta M_{iZ}(R,h_o)=\delta h_o\sum_l\sum_k\int_0^{E(R)}M_{iZl}(R,Z_l,E_l,h_o)\sigma_{ilk}(E_l)N_k(h_o,t)dE_l$$

$$+\int_0^{h_o}dh\sum_l\sum_k\int_0^{E(R)}M_{iZl}(R,Z_l,E_l,h)\sigma_{ilk}(E_l)\delta N_k(h,t)dE_l. \qquad (10.2.12)$$

The third term in Eq.10.2.9 reflects the change in cosmogenic nuclide production rate caused by variation of cut off rigidity R_c (geomagnetic variation).

Using the approximation described in Eq. 10.2.3 we obtain from Eq. 10.2.8:

$$\frac{\delta Q_i(R_c,h_o,t)}{Q_{io}(R_{co},h_o)}=\int_{R_{co}}^{\infty}dR\int_{t-T_{iv}}^{t}\frac{\delta D(R,t)}{D_o(R)}W_{iR_{co}}(R,h_o)dR$$

$$+\int_{R_{co}}^{\infty}dR\int_{t-T_{iv}}^{t}\frac{\delta M_i(R,h_o,t)}{M_{io}(R,h_o)}W_{iR_{co}}(R,h_o)dR-\delta R_c(t)W_{iR_{co}}(R_{co},h_o), \qquad (10.2.13)$$

where

$$W_{iR_{co}}(R,h_o)=D_o(R)M_{io}(R,h_o)/Q_{io}(R_{co},h_o) \qquad (10.2.14)$$

is the local coupling function between production rate of cosmogenic nuclides in the vertical column of the atmosphere and differential rigidity spectrum of primary CR with rigidity R in approximation described by Eq. 10.2.3 (in this case $M_i(R,h_o,t)$ is determined by Eq. 10.2.5).

10.2.5. Expected changes of cosmogenic nuclides integral production rates in different latitudinal zones with variation of modulation parameter

The solar cycle variations of galactic CR energy spectrum in the first approximation can be described by the variations of the modulation parameter Φ according to Eq.2.8.2 of Section 2.8 (Chapter 2). The change of Φ with solar activity was shown in Fig. 2.8.5 (also in Section 2.8). Therefore in order to determine the expected long term variations of production rates for different nuclides, it is necessary to calculate the expected integral production rates (in the total vertical column) for modulation parameter Φ varying from 0 up to 1000 MeV. This was done by Masarik and Beer (1999) according to the procedure described in Section 2.8. Results for cosmogenic nuclides ^{7}Be, ^{10}Be, ^{14}C, and ^{36}Cl are shown in Fig. 10.2.3 for $\Phi = 0, 200, 400, 600, 800, 1000$ MeV as a function of the geomagnetic latitude.

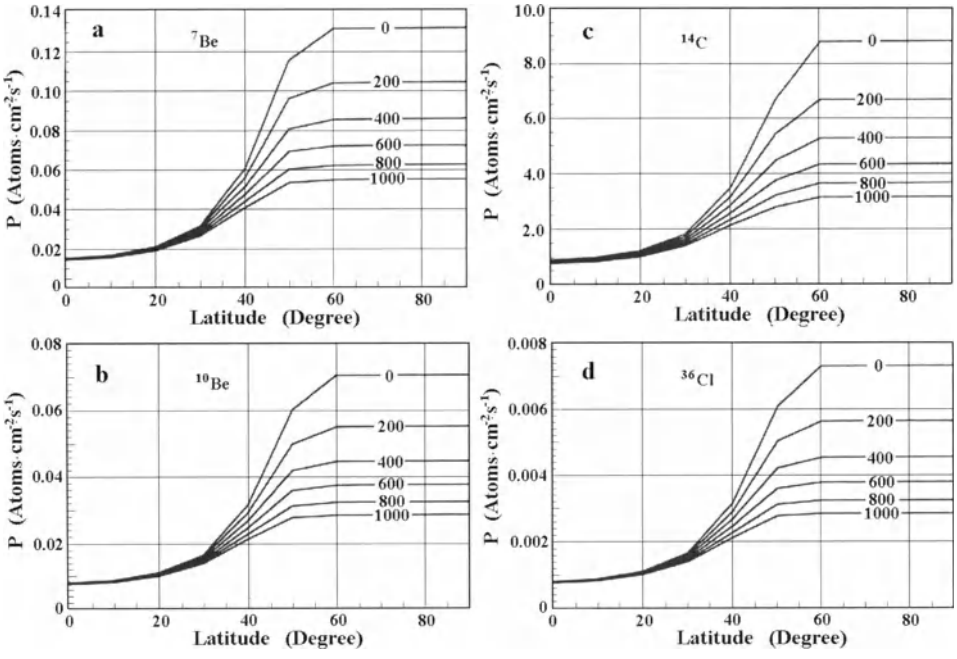

Fig. 10.2.3. Depth integrated latitudinal production rates of cosmogenic nuclides ^{7}Be (*a*), ^{10}Be (*b*), ^{14}C (c) and ^{36}Cl (*d*) in the Earth's atmosphere for modulation parameter Φ = 0, 200, 400, 600, 800, and 1000 MeV (numbers near curves). According to Masarik and Beer (1999).

In Fig. 10.2.4 are shown results on expected production rates of the same cosmogenic nuclides for different latitudinal zones *vs* the solar modulation parameter Φ.

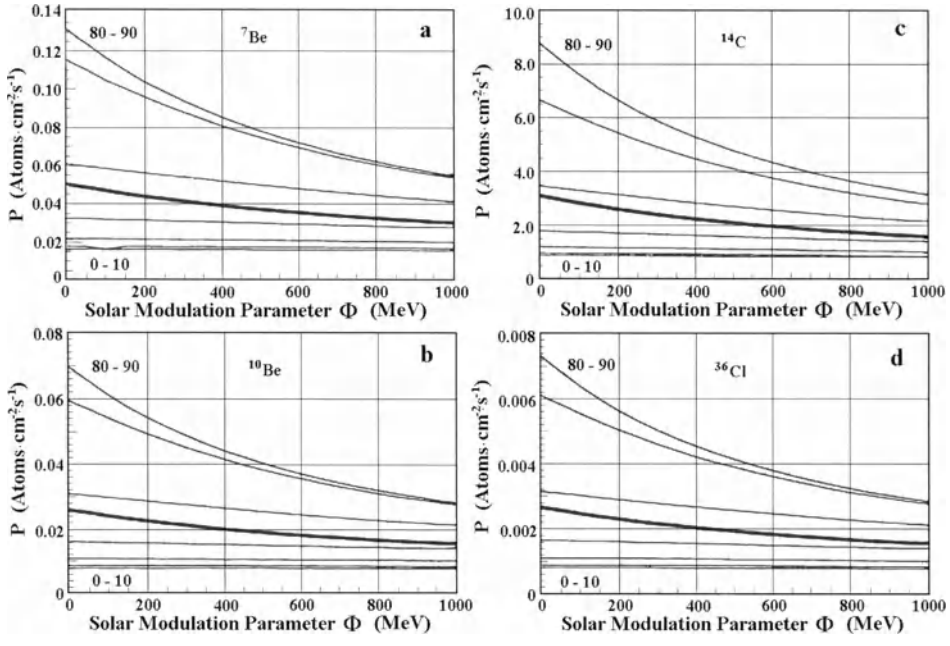

Fig. 10.2.4. Dependences of global average production rates (thick lines) and latitudinal production rates (thin lines) of cosmogenic nuclides ^{7}Be (a), ^{10}Be (b), ^{14}C (c) and ^{36}Cl (d) in the Earth's atmosphere from the solar modulation parameter Φ. According to Masarik and Beer (1999).

10.2.6. Expected changes of cosmogenic nuclides integral production rates in different latitudinal zones with possible variation of the Earth's magnetic field

Masarik and Beer (1999) also calculated the expected influence of geomagnetic field intensity change on cosmogenic nuclides production rates (for details of calculations see in Section 2.8 of the Chapter 2).

Results are shown in Fig. 10.2.5 for ^{10}Be, ^{14}C, and ^{36}Cl for the geomagnetic field intensities relative to present: 0, 0.25, 0.5, 0.75, 1.0 (present level), 1.25, 1.5, 1.75 and 2.0 as a function of geomagnetic latitude.

It can be seen that at latitudes higher 60° the production rate is the same as at 0 geomagnetic field, but with decreasing of latitude the influence of geomagnetic field intensity on cosmogenic nuclides production rate becomes important (near equator the increasing of geomagnetic field from 0 to 0.25 from present value decreases production rate about two times).

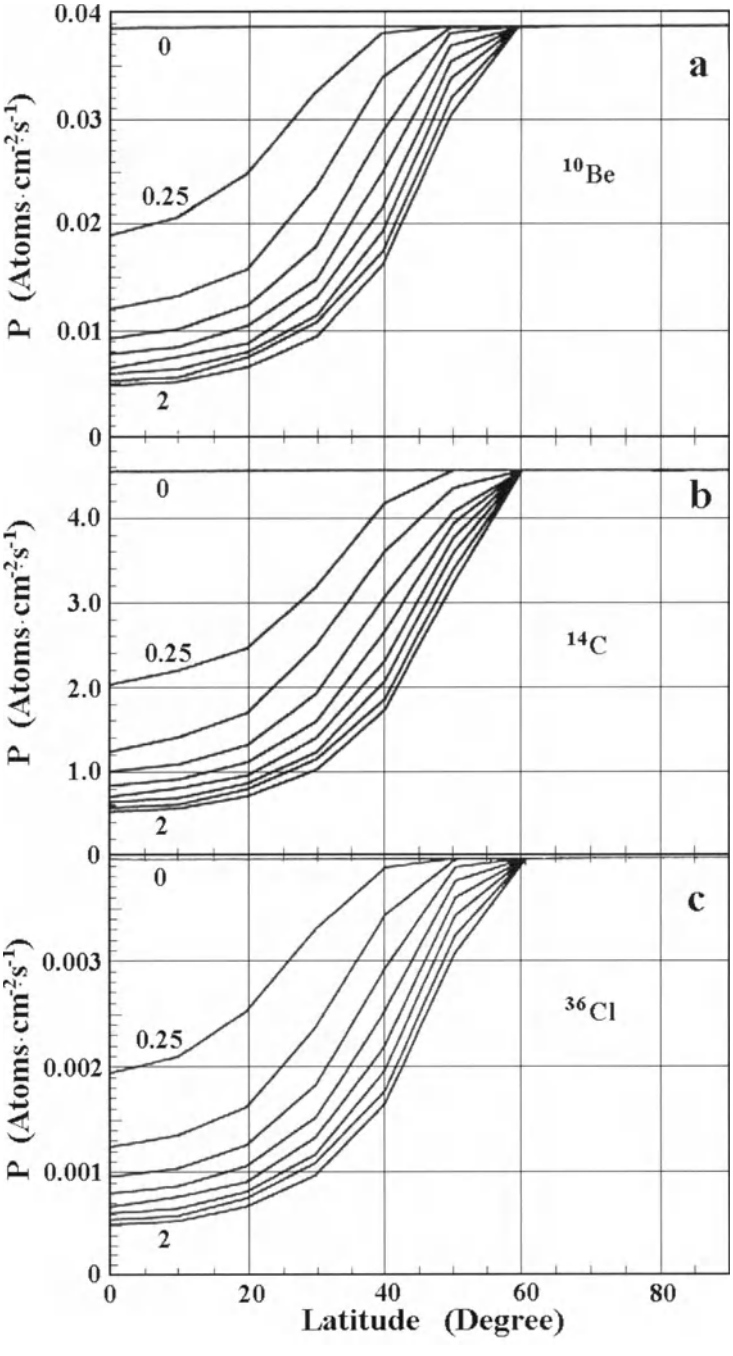

Fig. 10.2.5. Expected influence of the geomagnetic field intensity changes on cosmogenic nuclides production rates of ^{10}Be (*a*), ^{14}C (*b*), and ^{36}Cl (c). Each curve describes the production rate as a function of latitude for geomagnetic field intensities relative to present: 0, 0.25, 0.5, 0.75, 1.0 (present level), 1.25, 1.5, 1.75 and 2.0. According to Masarik and Beer (1999).

10.2.7. Expected cosmogenic nuclide contents in the vertical column of the atmosphere and its time variations.

If we take into account only vertical mixing of elements in the atmosphere then the expected contents in the vertical column of the atmosphere of cosmogenic nuclide of type i with time decay constant λ_i will be determined by the equation

$$dN_i(R_c,h_o,t)/dt = Q_i(R_c,h_o,t) - \lambda_i N_i(R_c,h_o,t), \tag{10.2.15}$$

whose solution is

$$N_i(R_c,h_o,t) = \exp(-\lambda_i t)\left(\int_0^t Q_i(R_c,h_o,\tau)\exp(\lambda_i\tau)d\tau + N_{io}(R_c,h_o)\right), \tag{10.2.16}$$

with the initial condition

$$N_i(R_c,h_o,t=0) = N_{io}(R_c,h_o). \tag{10.2.17}$$

In Eq. 10.2.15 $Q_i(R_c,h_o,t)$ changes with time according to Eq. 10.2.9 or Eq. 10.2.13. From Eq. 10.2.15 it can be seen that if $Q_i(R_c,h_o,t) \approx \text{const} = Q_{io}(R_c,h_o)$ then

$$N_i(R_c,h_o,t) = (Q_{io}(R_c,h_o)/\lambda_i)(1-\exp(-\lambda_i t)) + N_{io}(R_c,h_o)\exp(-\lambda_i t), \tag{10.2.18}$$

which $\rightarrow Q_{io}(R_c,h_o)/\lambda_i$ at $t >> \lambda_i^{-1}$, coinciding with the steady state solution of Eq.10.2.10 at $dN_i(R_c,h_o,t)/dt = 0$.

Let us suppose that on the background of the steady state solution at $t = t_o$ there is a local supernova explosion or an extremely great solar flare which gives a very short (relative to $t - t_o$) increase in production rate with relative amplitude A_{SN} that can be described by expression

$$Q_i(R_c,h_o,t) = Q_{io}(R_c,h_o)(1 + A_{SN}\delta(t-t_o)). \tag{10.2.19}$$

In this case according to Eq.10.2.16 we obtain

$$N_i(R_c,h_o,t) = (Q_{io}(R_c,h_o)/\lambda_i)(1 + A_{SN}\lambda_i \exp(-\lambda_i(t-t_o))). \tag{10.2.20}$$

Let us suppose now that the steady state solution $Q_{io}(R_c,h_o)/\lambda_i$ is modulated by a cyclic process of cosmogenic nuclides production of the form

$$Q_i(R_c,h_o,t) = Q_{io}(R_c,h_o)(1 + A_m\cos(\omega(t-t_m))), \tag{10.2.21}$$

where A_m is the amplitude of modulation, ω is the cycle frequency of modulation and t_m is the time of maximum of production rate of cosmogenic nuclides. Then the solution of Eq.10.2.16 will be

$$N_i(R_c,h_o,t)=(Q_{io}(R_c,h_o)/\lambda_i)$$

$$\times\left(1+A_m\lambda_i\left(\lambda_i^2+\omega^2\right)^{-1/2}\cos\left(\omega\left(t-t_m-\omega^{-1}\arctan\left(\omega\lambda_i^{-1}\right)\right)\right)\right). \quad (10.2.22)$$

Eq.10.2.22 shows that in cosmogenic nuclides' contents we expect also cyclic modulation with the same frequency ω as for the production rate, but the amplitude of modulation will be smaller by the factor $\lambda_i\left(\lambda_i^2+\omega^2\right)^{-1/2}$ and there will be some delay in time of the maximum on the value $\omega^{-1}\arctan\left(\omega\lambda_i^{-1}\right)$. Only if $\lambda_i >> \omega$, will the amplitude of contents modulation be about the same as for the production rate, and the time delay of phase be about λ_i^{-1}. If $\lambda_i << \omega$ then the amplitude of contents modulation will be much smaller than for the production rate by the factor about $\lambda_i\omega^{-1}$ and delay time of phase will be about $\omega^{-1}(\pi/2)=T_m/4$, where T_m is the period of modulation.

10.3. The planetary mixing in the atmosphere, variations in planetary cosmogenic nuclides production rate and planetary coupling functions

10.3.1. Cosmogenic nuclides global production rate at the planetary mixing in the atmosphere

The planetary mixing of some elements in the atmosphere can be so strong that the characteristic time of mixing T_{ip} can be significantly smaller than λ_i^{-1} for some cosmogenic nuclides. In these cases it is convenient to consider the planetary production rate of cosmogenic nuclides averaged over the planetary mixing time T_{ip} over the full surface of the Earth. Let us use Eq. 10.2.6 to determine the total production rate of cosmogenic nuclides $Q_i(R_c,h_o,t)$ in the vertical column per cm^2 from the atmosphere's top $h=0$ to the bottom $h=h_o$, taking into account the vertical mixing of elements in the atmosphere with characteristic time T_{iv} (or on the basis of Eq. 10.2.8 in the frame of approximation described by Eq. 10.2.3). Let us take into account also that R_c and h_o are functions from latitude θ and longitude φ. We then obtain for the planetary cosmogenic production rate (in number of cosmogenic atoms of type *i* per sec per cm^2):

$$Q_{ip}(R_{cp},h_{op},t)=(4\pi T_{ip})^{-1}\int_{t-T_{ip}}^{t}d\tau\int_{-\pi/2}^{\pi/2}\sin\theta d\theta\int_{0}^{2\pi}d\varphi Q_i(R_c(\theta,\varphi,\tau),h_o(\theta,\varphi,\tau),\tau) \quad (10.3.1)$$

where R_{cp} and h_{op} are some effective values of R_c and h_o averaged over the planetary surface. For approximate calculations, one can use the dipole presentation of the Earth's magnetic field. In this case θ and φ are geomagnetic coordinates, and R_c will depend only on geomagnetic latitude θ as

$$R_c(\theta,t)=R_c(0,t)\cos^4\theta=e\mathrm{M}_p(t)(4cr_p^2)^{-1}\cos^4\theta \quad (10.3.2)$$

where e is the proton charge, $M_p(t)$ is the planetary magnetic moment, c is the velocity of the light, and r_p is the planetary radius. From Eq. 10.3.2 follows:

$$R_c(\theta,t)=R_c(\theta,0)M_p(t)/M_p(0). \quad (10.3.3)$$

Masarik and Beer's (1999) results of calculations (see details above, in Section 10.2.2) of global average production rates in the Earth's atmosphere for long term mean solar activity (modulation parameter $\Phi=550$ MeV) are shown in Table 10.3.1 for five cosmogenic nuclides.

Table 10.3.1. The global average production rates (in atoms.cm^{-2}.sec^{-1}) of different cosmogenic nuclides in the Earth's atmosphere for long term mean solar activity (modulation parameter $\Phi=550$ MeV). According to Masarik and Beer (1999).

NUCLIDE	GLOBAL AVERAGE
^{3}H	0.281
^{7}Be×10	0.354
^{10}Be×100	1.84
^{14}C	2.02
^{36}Cl×1000	1.88

10.3.2. Time variation of planetary cosmogenic nuclides production rate

The expected time variation of $Q_{ip}(R_{cp},h_{op},t)$ will be determined by variation of Eq. 10.3.1, taking into account Eq. 10.2.6 and Eq. 10.2.8:

$$\frac{\delta Q_{ip}(R_{cp},h_{op},t)}{Q_{ipo}}=\int_{R_{cpo}}^{\infty}\frac{\delta D(R,t)}{D_o(R)}W_{ip}(R,h_{opo})dR+\beta_{iph}\delta h_{op}(t)+\beta_{ipm}\delta R_{cp}(t), \quad (10.3.4)$$

where

$$Q_{ipo} = Q_{ip}(R_{cp}, h_{op}, 0), \quad \delta Q_{ip}(R_{cp}, h_{op}, t) = Q_{ip}(R_{cp}, h_{op}, t) - Q_{ipo},$$
$$D_o(R) = D(R,0), \quad \delta D(R,t) = D(R,t) - D_o(R), \quad h_{opo} = h_{op}(0), \tag{10.3.5}$$
$$\delta h_{op}(t) = h_{op}(t) - h_{opo}, \quad R_{cpo} = R_{cp}(0), \quad \delta R_{cp}(t) = R_{cp}(t) - R_{cpo}.$$

In Eq. 10.3.4

$$W_{ip}(R, h_{opo}) = D_o(R) M_{ip}(R, h_{opo}) / Q_{ipo} \tag{10.3.6}$$

is the planetary cosmogenic coupling function and $M_{ip}(R, h_{opo})$ is the planetary cosmogenic integral multiplicity obtained from Eq. 10.2.9 taking into account Eq. 10.2.3 and averaging over the planetary surface according to Eq. 10.3.1. In Eq. 10.3.4 the parameter

$$\beta_{iph} = \int_{R_{cpo}}^{\infty} \frac{\partial \ln M_{ip}(R, h_{opo})}{\partial h_{opo}} W_{ip}(R, h_{opo}) dR \tag{10.3.7}$$

is the planetary cosmogenic barometric coefficient, and parameter

$$\beta_{ipm} = W_{ip}(R_{cpo}, h_{opo}) \tag{10.3.8}$$

is the planetary cosmogenic magnetic coefficient.

The expected variations of the planetary production rates of cosmogenic nuclides ^{7}Be, ^{10}Be, ^{14}C and ^{36}Cl in the Earth's atmosphere caused by the change of solar modulation parameter Φ were found by Masarik and Beer (1999). Results were shown by thick lines in Fig. 10.2.4 (see Section 10.2.5).

10.4. Two-reservoir model of elements exchange: the planetary contents of cosmogenic nuclides in the atmosphere and their time-variations

10.4.1. General solution

As a first approximation let us suppose that the planetary elements exchange can be described in the frame of a two-reservoir model: the first reservoir is the atmosphere with the planetary production rate of cosmogenic nuclides. Its time variations were analyzed in Section 10.3. The second reservoir is where we can neglect the production rate of cosmogenic nuclides (this reservoir includes everything that is at the bottom and below the bottom of the atmosphere where the expected intensity of nuclear active particles to be negligible). If λ_{12} is the probability of exchange of elements per unit time from reservoir 1 to reservoir 2 and λ_{21} is the probability for inverse exchange of elements, then the planetary contents (in atoms per cm^2) of cosmogenic nuclides

$N_{ip1}(t)$ and $N_{ip2}(t)$ in the first and second reservoirs and their time-variations will be described by the system of equations:

$$d N_{ip1}(t)/dt = Q_{ip}(R_{cp}(t),h_{op}(t),t)-(\lambda_i+\lambda_{12})N_{ip1}(t)+\lambda_{21}N_{ip2}(t),$$
$$d N_{ip2}(t)/dt = -(\lambda_i+\lambda_{21})N_{ip2}(t)+\lambda_{12}N_{ip1}(t). \tag{10.4.1}$$

The solution of this system with initial conditions

$$N_{ip1}(t=0)=N_{ip1o},\quad N_{ip2}(t=0)=N_{ip2o} \tag{10.4.2}$$

is

$$N_{ip1}(t)=\exp(-\lambda_i t)\left[\frac{\lambda_{21}}{\lambda_{12}+\lambda_{21}}\int_0^t \exp(\lambda_i\tau)Q_{ip}(R_{cp}(\tau),h_{op}(\tau),\tau)d\tau\right.$$
$$\left.+\frac{\lambda_{21}(N_{ip1o}+N_{ip2o})}{\lambda_{12}+\lambda_{21}}\right]+\exp(-(\lambda_i+\lambda_{12}+\lambda_{21})t)\left[\frac{\lambda_{12}}{\lambda_{12}+\lambda_{21}}\right.$$
$$\left.\times\int_0^t \exp((\lambda_i+\lambda_{12}+\lambda_{21})_i\tau)Q_{ip}(R_{cp}(\tau),h_{op}(\tau),\tau)d\tau+\frac{\lambda_{12}N_{ip1o}-\lambda_{21}N_{ip2o}}{\lambda_{12}+\lambda_{21}}\right], \tag{10.4.3}$$

$$N_{ip2}(t)=\exp(-\lambda_i t)\left[\frac{\lambda_{12}}{\lambda_{12}+\lambda_{21}}\int_0^t \exp(\lambda_i\tau)Q_{ip}(R_{cp}(\tau),h_{op}(\tau),\tau)d\tau\right.$$
$$\left.+\frac{\lambda_{12}(N_{ip1o}+N_{ip2o})}{\lambda_{12}+\lambda_{21}}\right]-\exp(-(\lambda_i+\lambda_{12}+\lambda_{21})t)\left[\frac{\lambda_{12}}{\lambda_{12}+\lambda_{21}}\right.$$
$$\left.\times\int_0^t \exp((\lambda_i+\lambda_{12}+\lambda_{21})_i\tau)Q_{ip}(R_{cp}(\tau),h_{op}(\tau),\tau)d\tau+\frac{\lambda_{12}N_{ip1o}-\lambda_{21}N_{ip2o}}{\lambda_{12}+\lambda_{21}}\right]. \tag{10.4.4}$$

10.4.2. Steady state solution

It follows from Eq. 10.4.3 and Eq. 10.4.4 that at $(\lambda_i+\lambda_{12}+\lambda_{21})t >> 1$ the solution for $N_{ip1}(t)$ and $N_{ip2}(t)$ does not depend on the initial conditions. If $Q_{ip}(R_{cp}(t),h_{op}(t),t)\approx \text{const} = Q_{ipo}$ we obtain steady-state solution

$$N_{ip1st}=Q_{ipo}\frac{\lambda_i+\lambda_{21}}{\lambda_i(\lambda_i+\lambda_{12}+\lambda_{21})},\quad N_{ip2st}=Q_{ipo}\frac{\lambda_{12}}{\lambda_i(\lambda_i+\lambda_{12}+\lambda_{21})}. \tag{10.4.5}$$

If $\lambda_{12} << \lambda_{21}$ it follows from Eq. 10.4.5 that in this case

$$N_{ip1st} \approx \frac{Q_{ipo}}{\lambda_i}, \quad N_{ip2st} \approx \frac{Q_{ipo}}{\lambda_i}\frac{\lambda_{12}}{\lambda_i + \lambda_{21}} << N_{ip1st}. \tag{10.4.6}$$

In the opposite case, when $\lambda_{12} >> \lambda_{21}$, we obtain from Eq. 10.4.5

$$N_{ip1st} \approx \frac{Q_{ipo}}{\lambda_i + \lambda_{12}}, \quad N_{ip2st} \approx \frac{Q_{ipo}}{\lambda_i}\frac{\lambda_{12}}{\lambda_i + \lambda_{12}}. \tag{10.4.7}$$

For cosmogenic nuclides with $\lambda_i << \lambda_{12}$ (as, for example, for cosmogenic radiocarbon, see Chapter 17), we have from Eq. 10.4.7:

$$N_{ip1st} \approx \frac{Q_{ipo}}{\lambda_{12}}, \quad N_{ip2st} \approx \frac{Q_{ipo}}{\lambda_i} >> N_{ip1st}, \tag{10.4.8}$$

i.e. in this case the content of cosmogenic nuclides in the second planetary reservoir will be much bigger than in the atmosphere (even though cosmogenic nuclides are generated mainly in the atmosphere).

10.4.3. Expected time variations of planetary cosmogenic nuclides contents from local supernova explosion

Let us suppose the variation in the production rate of cosmogenic nuclides in the form of Eq. 10.2.19 describes an increase of production rate of cosmogenic nuclides at $t = t_o$ with very short duration in comparison with $t - t_o$ (local supernova explosion, extremely great solar CR event, etc.). Then from Eq. 10.4.3–10.4.5 we obtain

$$N_{ip1}(t) = N_{ip1st}[1 + A_{sn}(B_1 \exp(-\lambda_i(t - t_o)) + B_2 \exp(-(\lambda_i + \lambda_{12} + \lambda_{21})(t - t_o)))], \tag{10.4.9}$$

where

$$B_1 = \frac{\lambda_i\lambda_{21}(\lambda_i + \lambda_{12} + \lambda_{21})}{(\lambda_{12} + \lambda_{21})(\lambda_i + \lambda_{21})}, \quad B_2 = \frac{\lambda_i\lambda_{12}(\lambda_i + \lambda_{12} + \lambda_{21})}{(\lambda_{12} + \lambda_{21})(\lambda_i + \lambda_{21})}, \tag{10.4.10}$$

and

$$N_{ip2}(t) = N_{ip2st}[1 + A_{sn}B_3(\exp(-\lambda_i(t - t_o)) - \exp(-(\lambda_i + \lambda_{12} + \lambda_{21})(t - t_o)))], \tag{10.4.11}$$

where

$$B_3 = \frac{\lambda_i(\lambda_i + \lambda_{12} + \lambda_{21})}{\lambda_{12} + \lambda_{21}}. \tag{10.4.12}$$

10.4.4. The inverse problem: estimation of local supernova explosion parameters from data on planetary cosmogenic nuclides contents

It is important that on the basis of Eq. 10.4.9–10.4.12 it is possible to obtain the solution of the inverse problem: to determine the time t_o of supernova explosion and the amplitude A_{sn} of the integral effect of this explosion on the production rate of cosmogenic nuclides (relative to steady state production rate). Below we will show that the exact results for the inverse problem can be obtained by measurements of one type cosmogenic nuclide contents in the atmosphere, but at two different times (for example, by using dated samples):

$$\frac{N_{ip1}(t_1)}{N_{ip1st}} - 1 = A_{sn}[B_1 \exp(-\lambda_i x) + B_2 \exp(-(\lambda_i + \lambda_{12} + \lambda_{21})x)], \tag{10.4.13}$$

$$\frac{N_{ip1}(t_2)}{N_{ip1st}} - 1 = A_{sn}[B_1 \exp(-\lambda_i (x + \Delta t)) + B_2 \exp(-(\lambda_i + \lambda_{12} + \lambda_{21})(x + \Delta t))], \tag{10.4.14}$$

where $x = t_1 - t_o$, $\Delta t = t_2 - t_1$, and the parameters B_1, B_2 are determined by Eq. 10.4.10. Dividing Eq. 10.4.13 by Eq. 10.4.14 we obtain an equation for determining x (and then it is easy to determine $t_o = t_1 - x$):

$$\frac{\delta N_{ip1}(t_1)}{\delta N_{ip1}(t_2)} = \frac{B_1 \exp(-\lambda_i x) + B_2 \exp(-(\lambda_i + \lambda_{12} + \lambda_{21})x)}{B_1 \exp(-\lambda_i (x + \Delta t)) + B_2 \exp(-(\lambda_i + \lambda_{12} + \lambda_{21})(x + \Delta t))}, \tag{10.4.15}$$

where

$$\delta N_{ip1}(t_1) = \frac{N_{ip1}(t_1) - N_{ip1st}}{N_{ip1st}}, \quad \delta N_{ip1}(t_2) = \frac{N_{ip1}(t_2) - N_{ip1st}}{N_{ip1st}} \tag{10.4.16}$$

are relative variations of cosmogenic nuclides contents in times t_1 and t_2. From Eq. 10.4.15 follows

$$\frac{\delta N_{ip1}(t_1)}{\delta N_{ip1}(t_2)} = \frac{B_1 + B_2 \exp(-(\lambda_{12} + \lambda_{21})x)}{B_1 \exp(-\lambda_i \Delta t) + B_2 \exp(-(\lambda_i + \lambda_{12} + \lambda_{21})(x + \Delta t))}, \tag{10.4.17}$$

and the solution of this equation can be obtained very easily:

$$x = (\lambda_{12} + \lambda_{21})^{-1} \ln\left(\frac{B_2\left(\left(\delta N_{ip1}(t_1)/\delta N_{ip1}(t_2)\right)\exp(-(\lambda_i + \lambda_{12} + \lambda_{21})\Delta t) - 1\right)}{B_1\left(1 - \left(\delta N_{ip1}(t_1)/\delta N_{ip1}(t_2)\right)\exp(-\lambda_i \Delta t)\right)} \right). \tag{10.4.18}$$

After obtaining the solution determined by Eq. 10.4.18, it is easy to determine A_{sn} from Eq. 10.4.13 or Eq. 10.4.14:

$$A_{sn} = \delta N_{ip1}(t_1)\left[B_1 \exp(-\lambda_i x) + B_2 \exp(-(\lambda_i + \lambda_{12} + \lambda_{21})x)\right]^{-1}$$

$$= \delta N_{ip1}(t_2)\left[B_1 \exp(-\lambda_i (x + \Delta t)) + B_2 \exp(-(\lambda_i + \lambda_{12} + \lambda_{21})(x + \Delta t))\right]^{-1}. \quad (10.4.19)$$

In order to verify the solution of the inverse problem it will be very important to have measurements for some third time t_3 also.

For the inverse problem one can also use data on two different cosmogenic nuclides i and k, obtained for the same time t_1 :

$$\delta N_{ip1}(t_1) = A_{sn}\left[B_{1i} \exp(-\lambda_i x) + B_{2i} \exp(-(\lambda_i + \lambda_{12} + \lambda_{21})x)\right], \quad (10.4.20)$$

$$\delta N_{kp1}(t_1) = A_{sn}\left[B_{1k} \exp(-\lambda_k x) + B_{2k} \exp(-(\lambda_k + \lambda_{12} + \lambda_{21})x)\right], \quad (10.4.21)$$

where $\delta N_{ip1}(t_1)$ and $\delta N_{kp1}(t_1)$ are determined by Eq. 10.4.16, the parameters B_{1i}, B_{2i}, B_{1k}, B_{2k} are determined by Eq. 10.4.10, and $x = t_1 - t_o$. Dividing of Eq. 10.4.20 by Eq. 10.4.21 we obtain

$$\frac{\delta N_{ip1}(t_1)}{\delta N_{kp1}(t_1)} = \exp(-(\lambda_i - \lambda_k)x) \times \frac{B_{1i} + B_{2i} \exp(-(\lambda_{12} + \lambda_{21})x)}{B_{1k} + B_{2k} \exp(-(\lambda_{12} + \lambda_{21})x)}, \quad (10.4.22)$$

from which it follows that

$$x = (\lambda_i - \lambda_k)^{-1} \ln\left(\frac{\delta N_{kp1}(t_1)\left[B_{1i} + B_{2i} \exp(-(\lambda_{12} + \lambda_{21})x)\right]}{\delta N_{ip1}(t_1)\left[B_{1k} + B_{2k} \exp(-(\lambda_{12} + \lambda_{21})x)\right]}\right). \quad (10.4.23)$$

and $x = t_1 - t_o$ can be determined by the iteration method. It is then easy to determine A_{sn} from Eq. 10.4.20 or Eq. 10.4.21:

$$A_{sn} = \delta N_{ip1}(t_1)\left[B_{1i} \exp(-\lambda_i x) + B_{2i} \exp(-(\lambda_i + \lambda_{12} + \lambda_{21})x)\right]^{-1}$$
$$= \delta N_{kp1}(t_1)\left[B_{1k} \exp(-\lambda_k x) + B_{2k} \exp(-(\lambda_k + \lambda_{12} + \lambda_{21})x)\right]^{-1}. \quad (10.4.24)$$

10.4.5. Expected time variations of planetary cosmogenic nuclides contents from cyclic variations of production rate

Let us consider now the cyclic modulation of production rate of cosmogenic nuclides in the form described by Eq. 10.2.21. In this case on the basis of Eq. 10.4.3 and Eq. 10.4.4 we obtain:

$$N_{ip1}(t) = N_{ip1st}\left[1 + A_m C_{1i} \cos(\omega(t - t_m - C_{2i}))\right], \quad (10.4.25)$$

$$N_{ip2}(t) = N_{ip2st}\left[1 + A_m C_{3i}\cos(\omega(t - t_m - C_{4i}))\right], \tag{10.4.26}$$

where

$$C_{1i} = \frac{\lambda_i(\lambda_i + \lambda_{12} + \lambda_{21})\left(D_{11i}^2 + D_{12i}^2\right)^{1/2}}{(\lambda_{12} + \lambda_{21})\left(\lambda_i^2 + \omega^2\right)(\lambda_i + \lambda_{21})\left(\omega^2 + (\lambda_i + \lambda_{21} + \lambda_{12})^2\right)}, \tag{10.4.27}$$

$$C_{2i} = \omega^{-1}\arctan(D_{12i}/D_{11i}), \tag{10.4.28}$$

$$C_{3i} = \frac{\lambda_i(\lambda_i + \lambda_{12} + \lambda_{21})\left(D_{31i}^2 + D_{32i}^2\right)^{1/2}}{(\lambda_{12} + \lambda_{21})\left(\lambda_i^2 + \omega^2\right)\left(\omega^2 + (\lambda_i + \lambda_{21} + \lambda_{12})^2\right)}, \tag{10.4.29}$$

$$C_{4i} = \omega^{-1}\arctan(D_{32i}/D_{31i}). \tag{10.4.30}$$

In Eq. 10.4.27–10.4.30 the following notations are used:

$$D_{11i} = \omega\left[\lambda_{21}\left(\omega^2 + (\lambda_i + \lambda_{21} + \lambda_{12})^2\right) + \left(\lambda_i^2 + \omega^2\right)(\lambda_i + \lambda_{21})\right], \tag{10.4.31}$$

$$D_{12i} = \lambda_i\lambda_{21}\left(\omega^2 + (\lambda_i + \lambda_{21} + \lambda_{12})^2\right) + (\lambda_i + \lambda_{12} + \lambda_{21})\left(\lambda_i^2 + \omega^2\right)(\lambda_i + \lambda_{21}), \tag{10.4.32}$$

$$D_{31i} = \lambda_i\left(\omega^2 + (\lambda_i + \lambda_{21} + \lambda_{12})^2\right) - (\lambda_i + \lambda_{12} + \lambda_{21})\left(\lambda_i^2 + \omega^2\right), \tag{10.4.33}$$

$$D_{32i} = \omega\left((\lambda_i + \lambda_{12} + \lambda_{21})^2 - \lambda_i^2\right). \tag{10.4.34}$$

Eq. 10.4.25–10.4.34 show that the contents of cosmogenic nuclides in reservoirs 1 and 2 will undergo cyclic modulations with the same frequency ω as the production rate, but the amplitudes $A_m C_{1i}$ and $A_m C_{3i}$ as well as the time delay in the phase of modulation C_{2i} and C_{4i} will depend on ω, λ_i, λ_{12}, λ_{21}.

10.5. Direct measurements of production rates of cosmogenic isotopes ^{10}Be, ^{3}He, and ^{3}H

Direct measurements of cosmogenic production rates of ^{10}Be, ^{3}He, and ^{3}H were made by Brown et al. (2000) during about 15 months from February 1993 to May 1994 (468–487 days) at three sites near Mt. Blanc in the French Alps ($R_c \approx 4.7$ GV) at elevations 4745 m ($h_o = 570$ g/cm^2), 3810 m ($h_o = 644$ g/cm^2), 620 m ($h_o = 960$ g/cm^2), and underground at 1780 m w.e. (for controlling measurements). Results are shown in Table 10.5.1. In Table 10.5.1 are shown for comparison also

results obtained at high latitudes ($R_c \leq 2$ GV) near sea level by Lal (1991), Pomerantz and Agrawal (1962), and Dunai (2000).

Table 10.5.1. Measured production rates of ^{10}Be, ^{3}He, and ^{3}H (in atoms/g.year)

R_c, GV	h_o, g/cm^2	production rates, atoms/g.year			Reference
		^{10}Be	^{3}He	^{3}H+^{3}He	
4.7	570	114 ± 10	1838 ± 30	2407 ± 161	Brown et al, 2000
4.7	644	70 ± 5	1022 ± 17	1337 ± 84	Brown et al, 2000
4.7	960	5.9 ± 0.7	135 ± 12	177 ± 77	Brown et al, 2000
≤ 2	≈1000	4.4 ± 0.9		99 ± 12	Lal, 1991
≤ 2	≈1000	3.8 ± 0.2		88 ± 19	Pomerantz and Agrawal, 1962
≤ 2	≈1000	3.9 ± 0.2		92 ± 20	Dunai, 2000

Brown et al. (2000) found also ratios of production rates 0.32±0.08 for ^{3}H: ^{3}He, and 20.2 ± 1.5 for (^{3}H + ^{3}He): ^{10}Be. These ratios are consistent with theoretical and meteorite estimates (e.g., Craig and Lal, 1961; Kruger and Heymann, 1968). Production rates of ^{10}Be obtained by Brown et al (2000) are consistent with measurements at high latitudes near sea level (see Table 10.5.1), but are lower than those obtained by Nishiizumi et al. (1996).

10.6. Peculiarities and main results regarding to ^{7}Be

10.6.1. Importance of cosmogenic isotope ^{7}Be investigations for space and atmospheric physics

Galactic CR and solar energetic particles (SEP) interact with the Earth's atmospheric nuclei and produce many different isotopes. In particular, ^{7}Be is a short-lived radioisotope (half-life is 53.3 days) which result from nuclear reactions of energetic protons with atmospheric N and O nuclei. According to Lal and Peters (1967) galactic CR produce about two thirds of ^{7}Be in the stratosphere and one third in the upper troposphere. The ^{7}Be emits a gamma-ray line at 478 keV from the electron-capture process. **For space physics** is important that the ^{7}Be production rate is expected to exhibit the 11 year and other time variations in accordance with galactic CR modulation in the Heliosphere. For space physics is important also that highly intense solar proton fluxes arrived at the Earth in association with a large solar proton events, will produce additional amount of ^{7}Be.

On the other hand, the study of ^{7}Be in the atmosphere provides important information on **atmospheric transport processes**. The source distribution of galactic CR produced ^{7}Be peaks around 20 km in altitude (Lal and Peters, 1967). Produced ^{7}Be nuclei rapidly attach to aerosol particle in the upper atmosphere and fall to the Earth's surface. The ground-level measurement of ^{7}Be radioactivity gives a clue on the air mass mixing between the stratosphere and troposphere. Yoshimori et al. (2003b) note that galactic CR produce most of ^{7}Be in the stratosphere and the mean residence time is

thought to be 14 months (from the long-term temporal variations in ^{90}Sr radioactivity according to Rehfeld and Heimann, 1995; ^{90}Sr is an artificial radioisotope due to nuclear weapon test in high altitudes). This means that the residence time in stratosphere is much longer than the half life of ^{7}Be.

The mean residence time of ^{7}Be produced in the troposphere by galactic CR is only 22-35 days (according to Martell and Moore, 1974; Bleichrodt, 1978). The tropospheric ^{7}Be contribute to the ^{7}Be radioactivity at the ground level. If the ground level ^{7}Be radioactivity significantly enhances, it is expected that the stratospheric ^{7}Be suddenly fall to the troposphere by the atmospheric processes. As a possible mechanism, Reiter (1975) suggested stratospheric/tropospheric air mass exchange process and Shapiro (1980) proposed that turbulent mixing within tropopause folds as a mechanism for the exchange of chemical constituents between the stratosphere and troposphere. Implications on stratosphere/troposphere air exchange were discussed from the distribution of ^{7}Be in the troposphere (Viezee and Singh, 1980). Dibb (1989) and Feely et al. (1989) indicated that the stratospheric/tropospheric air mass mixing takes place in spring. The seasonal variation in the ^{7}Be radioactivity at the ground level (see below in Section 10.6.4) is likely due to air mass mixing in spring and fall seasons between the stratosphere and troposphere.

10.6.2. Peculiarities of ^{7}Be *production in atmosphere*

For production of ^{7}Be by galactic and solar CR are important information on the cross sections of reactions p + N and p + O with formation ^{7}Be. In Fig. 10.6.1 are shown these cross sections in dependence of energy of protons determined on accelerators by Bodemann et al. (1993).

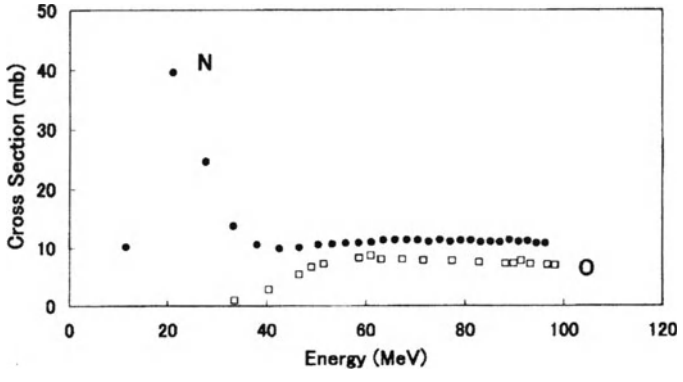

Fig. 10.6.1. Cross sections for production of ^{7}Be in reactions p + N and p + O. According to Bodemann et al. (1993).

These data were used by Yoshimori et al. (2003a) for determining of ^{7}Be production rate by galactic CR in dependence of atmospheric depth at different geomagnetic latitudes 60, 47, 30, and 0° (see Fig. 10.6.2). In these calculations was supposed that the cutoff rigidity for vertical arriving of primary CR at geomagnetic latitude λ is

determined approximately by $R_c(\lambda) \approx 15 \times \cos^4 \lambda$ GV. The used primary differential spectrum of galactic CR is shown in Fig. 6.10.3, where is shown also spectrum of solar energetic particles (SEP) during event of July 14, 2000.

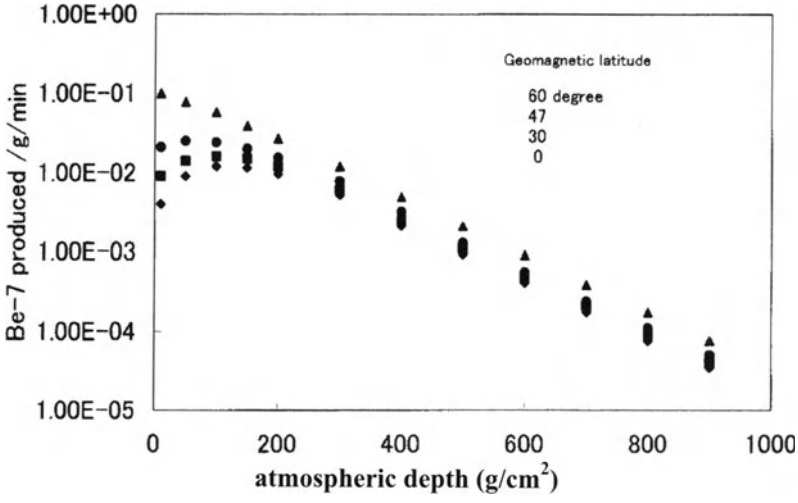

Fig. 10.6.2. The number of ^{7}Be cosmogenic nuclei at geomagnetic latitudes 60, 47, 30 and 0° produced by galactic CR per minute per gram of air. According to Yoshimori et al. (2003a).

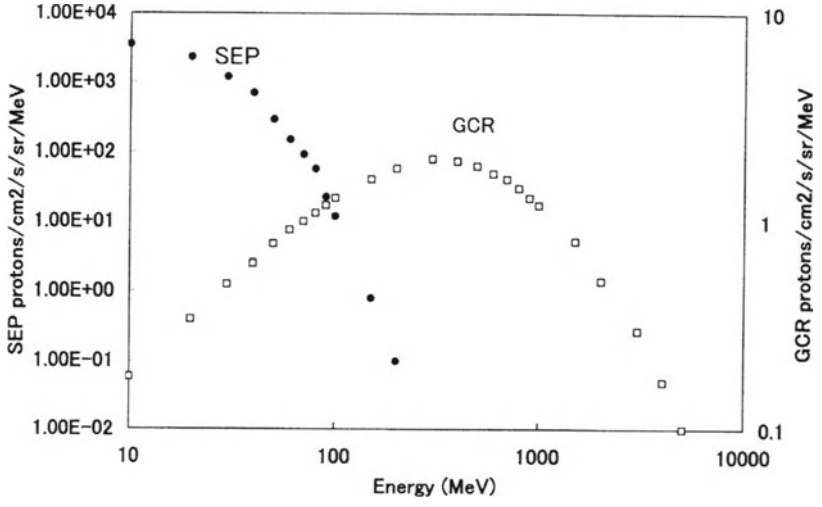

Fig. 10.6.3. Galactic CR (GCR) and solar energetic particles (SEP) proton energy spectra, used in calculations of ^{7}Be production rate. According to Yoshimori et al. (2003a).

According to Yoshimori et al. (2003a) the global average production rate by galactic CR is estimated to be about 0.1 (0.07 in the stratosphere and 0.03 in the troposphere) ^{7}Be cm^{-2} s^{-1}. The calculations for SEP event at July 14, 2000 according to

the spectrum shown in Fig. 10.6.3 give for the global average production rate during this event 2.4 ^{7}Be cm^{-2} s^{-1}, more than 20 times bigger than by galactic CR. The total contribution of such events in monthly or yearly values of ^{7}Be production is negligible (in comparison with caused by galactic CR) because SEP events are very shortly (lasting not longer than few days) and are very rarely (even in the maximum of solar activity).

10.6.3. Long-term variation of the concentration of ^{7}Be *in the atmosphere (on the basis of yearly data)*

According to Lal and Peters (1967) cosmogenic ^{7}Be in the Earth's atmosphere is a product owed to nuclear interactions of galactic and solar CR with air atoms in the stratosphere and troposphere. Concentration of ^{7}Be in air at ground level shows various time variations on the basis of daily, monthly and yearly data. The yearly data values of ^{7}Be concentration are anti-correlated to the number of sunspots with 11 years solar cycle (Raisbeck and Yiou, 1979; Matsunami and Megumi, 1994; Sakurai et al., 1997). According to Sakurai et al. (1997), ^{7}Be concentration in air is continuously monitored (by detection of the peak 477.6 keV from ^{7}Be decay in the gamma ray spectrum from samples on a fiber glass filter with the cross section 20.3 cm×25.4 cm) from November 1992 (and daily data are obtained from August 1993) at the campus of Yamagata University (38°15.2'N, 140°20.9'E, 152.5 m above sea level). The error for daily measurements was about 5%, and the values obtained are distributed in the range from about 0.4 mBq/m^3 (low limit of measurements) up to about 7 mBq/m^3.

In Fig. 10.6.4 are shown yearly data of ^{7}Be concentration in air and yearly data of sunspot numbers for 1993–1996.

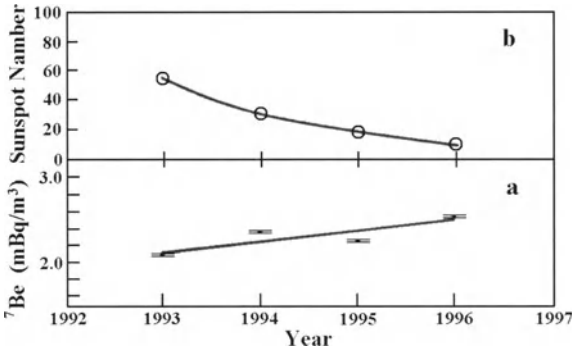

Fig. 10.6.4. Yearly data of ^{7}Be concentration in air (*a*); and yearly data of sunspot numbers (*b*) for 1993–1996. According to Sakurai at al. (1997).

It can be seen from Fig. 10.6.4 that the concentration of ^{7}Be is anti-correlated to the number of sunspots. It was found that the concentration of ^{7}Be in 1996 (near minimum of solar activity) was approximately 20% higher than that in 1993.

10.6.4. Seasonal variations of ^{7}Be *contents in atmosphere*

The seasonal variations in Sakurai et al. (1997) are also clearly observed (see Fig. 10.6.5): the average concentration of ^{7}Be during spring and fall is approximately 3 times higher than that during summer.

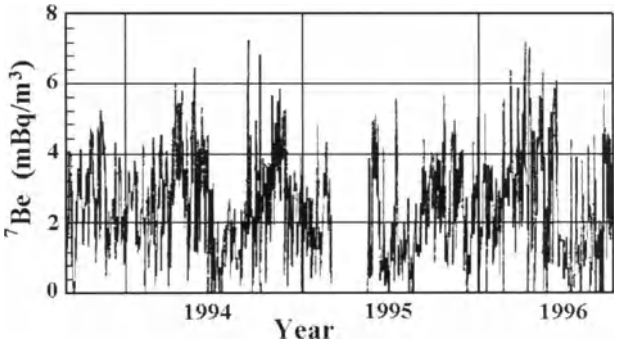

Fig. 10.6.5. Seasonal variation of ^{7}Be concentration in air (based on daily data observations). According to Sakurai et al. (1997).

The investigation of seasonal variations of ^{7}Be contents in atmosphere was continued in Yoshimori et al. (2003). Results are shown in Fig. 10.6.6.

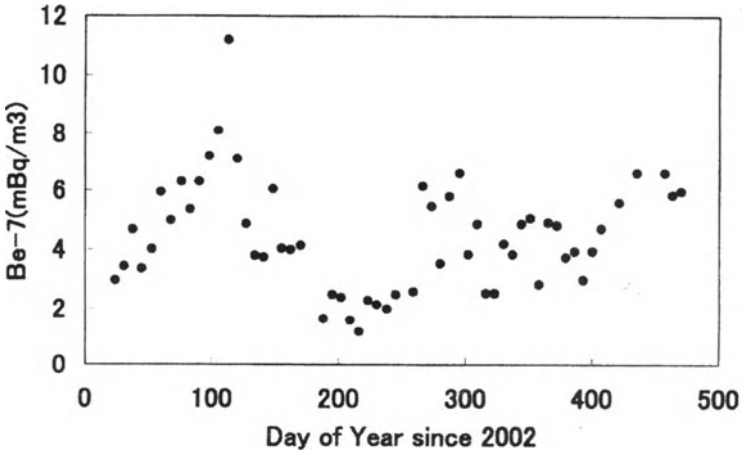

Fig. 10.6.6. Variations in ^{7}Be contents in January 2002 – May 2003. According to Yoshimori et al. (2003).

According to opinion of Sakurai et al. (1997), Yoshimori et al. (2003) the seasonal variations ^{7}Be contents near ground level are caused mostly by atmospheric exchange processes between stratosphere and troposphere (see Section 10.6.1 for more details). This conclusion is supported by the simultaneously measurements of about the same seasonal variations in the ^{210}Pb radioactivity with gamma-ray line at 46.5 keV (a part of

^{210}Pb is emanated out of the Earth's crust into the higher atmosphere). According to Yoshimori et al. (2003), the ^{210}Pb data support the suggesting on seasonal air mass mixing between the stratosphere and troposphere, mainly in spring and in fall, followed from observations of ^{7}Be seasonal variations.

10.6.5. Variation of ^{7}Be contents with rotation period of the Sun

Sakurai et al. (2001) on the basis of daily data for 2000 found periodicities of 18 and 28 days in daily data of ^{7}Be concentration (in daily data of sunspot numbers for the same year periodicities of 21 and 26 days were found). More detail investigation was made by Sakurai et al. (2003) on the basis of daily data for three years, 2000–2002. According to Sakurai et al. (2003), the daily ^{7}Be concentration in the air is continuously observed at the top of a building 15 m in height, at Yamagata University (Japan). The location is at 38°15.2' N, 140°20.9' E and its altitide is 152.2 m from sea level. A high-volume air sampler (HV-1000F) was employed for the collection of the air mass. The volume rate of the air mass intake is regulated to 1380 m^3 per 23 hours, with the accuracy of 0.02%. The dust in the air mass including ^{7}Be is trapped in a glass-fiber filter with the cross section of 203 mm × 254 mm (ADVANTEC GB-100R). The specific activity of the ^{7}Be in the filter was measured with a high-purity germanium gamma-ray detector GEM-25185, surrounded by shielding materials. The specific activity of the ^{7}Be was measured with 477.6 keV gamma rays.

To investigate the periodicity of the ^{7}Be contents in comparison with the periodicity in sunspot number (SSN), the Power Spectral Densities (PSD) were calculated for the three years data (2000–2002). Fig. 10.6.7 shows the PSD for ^{7}Be contents, the SSN, and the Beijing NM data as a function of period in unit of day.

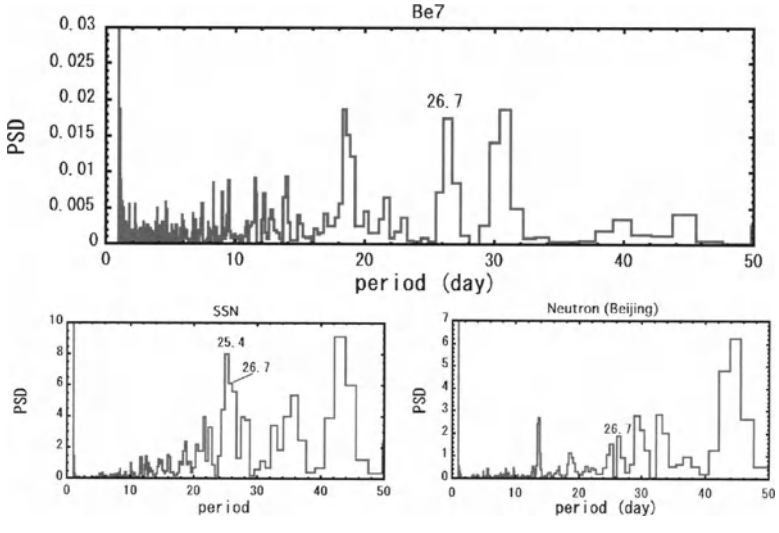

Fig. 10.6.7. Power Spectral Densities (PSD) for each time series of the ^{7}Be contents, the sunspot numbers (SSN), and the CR neutron intensity according to Beijing NM. All of spectra show a peak at 26.7 days that corresponds to the rotation period of the Sun. According to Sakurai et al. (2003).

In Sakurai et al. (2003) the three years daily data of the ^{7}Be contents, SSN, and the NM data from 2000 to 2002 were folded with a same folding period of 26 days and normalized to the value per day, respectively. The NM data were used for four observation sites of Beijing, Calgary, Kiel and Moscow. In Fig. 10.6.8 the moving averages of 5 points for all of the folding data are shown with the relative variations to their averages, respectively.

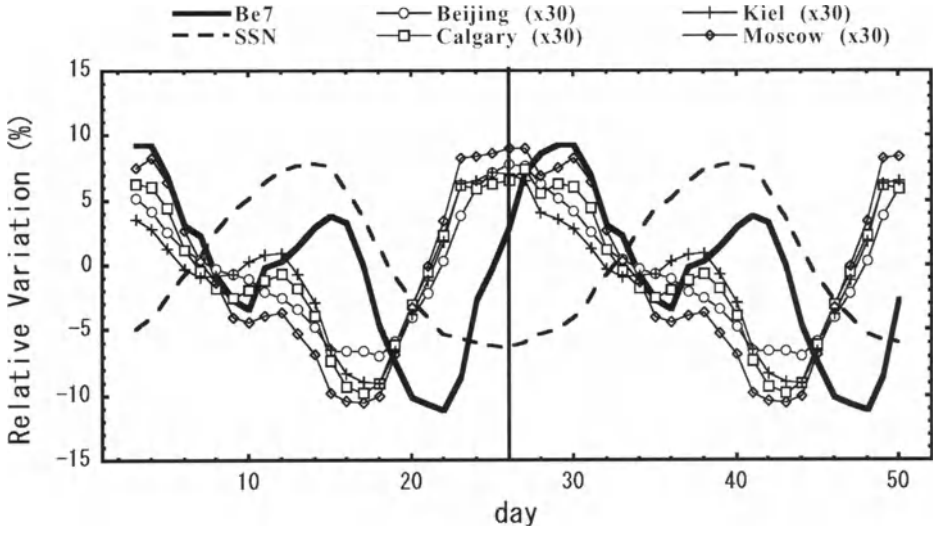

Fig. 10.6.8. Contents of ^{7}Be, sunspot numbers SSN, and neutron intensity data from four NM folded with the folding period of 26 days for the each time series. Note the neutrons are shown the net values multiplied by 30. According to Sakurai et al. (2003).

As it can be seen from Fig. 10.6.8, the relative variations of the ^{7}Be contents, the SSN and the neutron intensity were approximately 20%, 13% and 0.7% for the peak to peak, respectively. The phase for the minimum portions of the ^{7}Be contents and the neutron intensity are delayed approximately 8 days and 3 days, respectively, compared with that for the maximum portion of the SSN. The delay time of 3 days for the neutron intensity is inferred a propagation time from the Sun to the Earth for disturbances corresponding to the SSN, considering the travel time of solar wind plasma from the Sun to the Earth. Also, the phase delay of 5 days from the neutron intensity to the ^{7}Be contents indicates an average residence time of the ^{7}Be in the troposphere. These indicate that the time variation with 26 days of the ^{7}Be contents is caused by the solar modulation of galactic CR. However, it is a problem that the relative variation of the ^{7}Be contents are quite larger than that of the neutron intensity, although the variation pattern of the ^{7}Be contents is similar to that of the neutron intensity. The difference can not clarify from simple comparison of both quantities, because the production rate of ^{7}Be is high in an altitude of the polar region with low cutoff rigidities and the ^{7}Be is transported from the high latitude to the middle one by air mass motion (Masarik and Beer, 1999).

10.6.6. Effect of SEP events in ^{7}Be *contents*

Sakurai et al. (1997) investigated the correlation between the daily concentration of ^{7}Be and 61 solar H_α flare events by Cree method (as zero days were choused the days of H_α flare events) using data in 1994 (see Fig. 10.6.9).

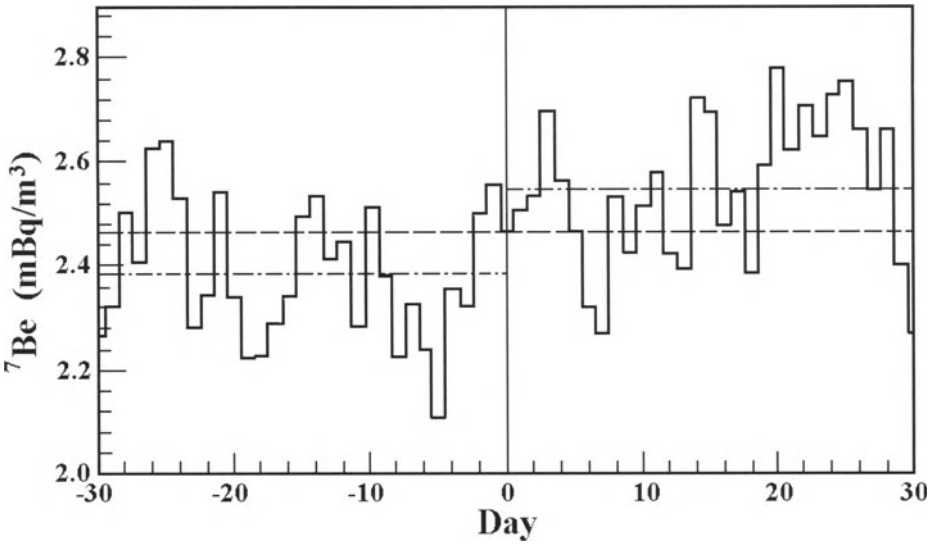

Fig. 10.6.9. Average concentration of ^{7}Be in the air before and after H_α – flare events. Each dash dotted lines shows the averages of ^{7}Be for 30 days before and 30 days after H_α – flare event.

It was found that the average concentration of ^{7}Be over 30 days after the flare events is 7% higher than that before the flare events.

10.7. Peculiarities and main results regarding to ^{10}Be

10.7.1. Mean global ^{10}Be *production rate in dependence of the solar activity level and of geomagnetic field intensity*

In Section 10.2 we considered results of Masarik and Beer (1999) on the latitudinal distribution of ^{10}Be production rate (see Fig. 10.2.1). On the basis of these results Masarik and Beer (1999) calculated expected mean global ^{10}Be production rate in dependence of the solar activity level (characterized by the value of modulation parameter Φ from 0 to 1000 MV) and of geomagnetic field intensity (from 0 to 2 relative to the present intensity taken as 1). Results are shown in Fig. 10.7.1. It can be seen from Fig. 10.7.1 that the dynamic range between high solar activity (Φ ~ 1000 MV)/large magnetic field (two times bigger than present) and quiet Sun (Φ ~ 0)/no magnetic field is about an order of magnitude.

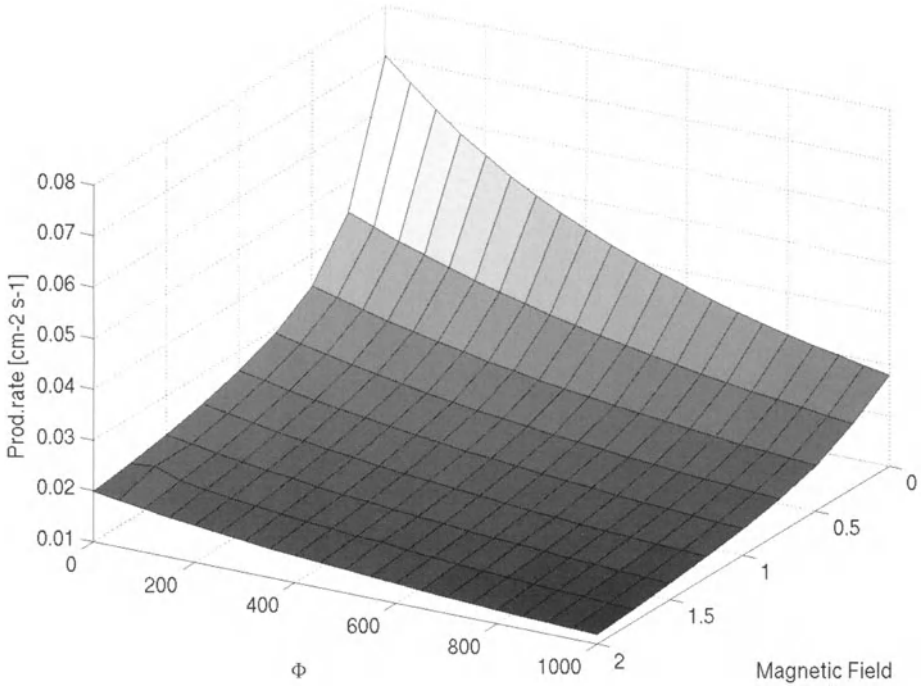

Fig. 10.7.1. Dependence of the mean global ^{10}Be production rate on the solar activity Φ and the geomagnetic field intensity (rel. units; 1: present field). According to Masarik and Beer (1999).

10.7.2. On the sensitivity of ^{10}Be data to primary CR modulation, to the change of geomagnetic field, and to atmosphere mixing models

In McCracken (2003) a mathematical model has been developed that computes the ^{10}Be flux precipitated to the polar caps based upon:

- the time varying geomagnetic field (scalar magnitude and location of pole) derived from archeomagnetic observations (McElhinny and McFadden, M2000);
- a number of models of the inter-latitudinal mixing in the atmosphere;
- the averaging effects of the circumpolar motion of the atmosphere;
- values of the modulation parameter in the range $0 < \Phi < 1000$ MV.

The developed model computes the ^{10}Be production rate on a 1080 point grid at a spacing of 5° in latitude and 30° in longitude, using the dipole approximation to the geomagnetic field. The response function used in the calculation of the ^{10}Be production rate was computed using the results of Masarik and Beer (1999) and is given in Fig. 10.7.2 (Panel A). The response function in Panel A of Fig. 10.7.2 shows that the ^{10}Be measurements sample a lower portion of the galactic CR spectrum than does the ground level NM (according to Nagashima et al., 1989; see also Chapters 3 and 4).

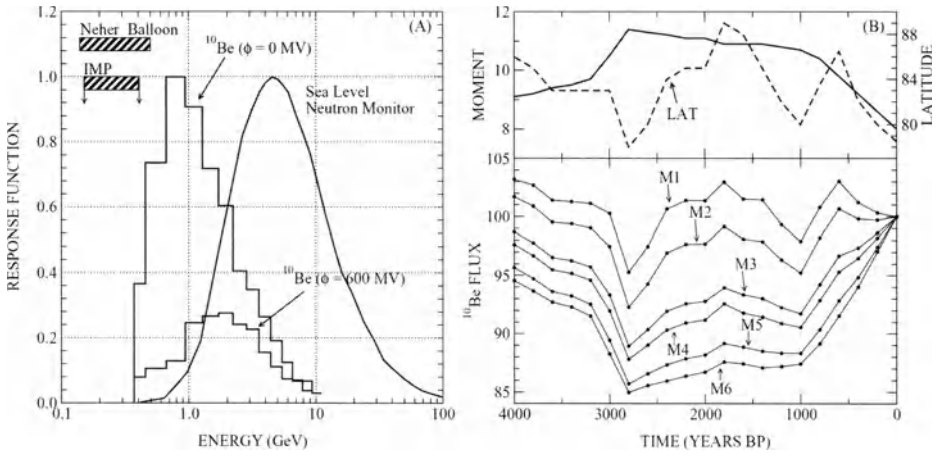

Fig. 10.7.2. Panel **A:** Comparison of the response functions of the ^{10}Be measurements at $\Phi = 0$ and $\Phi = 600$ MV with a high latitude NM, and with balloon and satellite measurements. Panel **B:** on the top – the causal changes in the geomagnetic field during the last 4000 years; on the bottom – the computed variation of the ^{10}Be planetary contents due to geomagnetic effects for different models M1-M6 (see explanation in text) of planetary elements mixing. According to McCracken (2003).

From the Panel A of Fig. 10.7.2 can be seen that the peak response of ^{10}Be is at 1.8 GeV/nucleon for contemporary times (Φ = 600MV), shifting to the vicinity of 0.8 GeV/nucleon for $\Phi = 0$. Panel B of Fig. 10.7.2 displays the variability introduced into the ^{10}Be measurements by the known variations of the geomagnetic field over the past 4000 years according to McElhinny and McFadden (M2000). These calculations are for six different models for inter-latitudinal mixing in the atmosphere prior to the precipitation of the ^{10}Be in the polar caps. Model M1 is the case where all the ^{10}Be is from latitudes above 60°; M6 is where the flux represents the global average production; and M2, M3, and M4 represent contributions that extend to 40°, 20°, and the equator, respectively. Note that polar wander is the primary contributor to the variability in the case of the ^{10}Be produced in or near the polar cap (Models M1 and M2); while scalar changes in the geomagnetic dipole moment dominate the global average, M6.

In Fig. 10.7.3 are shown the relative role of mixing models M1-M6 in formation of flux (planetary production rate) and concentration of ^{10}Be. The Panel A of Fig. 10.7.3 displays the computed dependence of the ^{10}Be flux upon mixing model (for $\Phi = 0$). It can be seen that changes in inter-latitudinal mixing will result in large changes in the ^{10}Be measurements that might be interpreted as changes in the galactic CR. The ^{10}Be record exhibits a large decrease since the Maunder and Dalton minima (1700 and 1810), which were coincident with the 'little ice ages', and it has been proposed that this was largely due to changes in latitudinal mixing (Lal, 1987). For example, the Panel A of Fig. 10.7.3 shows that if the inter-latitudinal mixing changed from model M1 to model M2, the ^{10}Be flux to the polar caps would decrease by 10%.

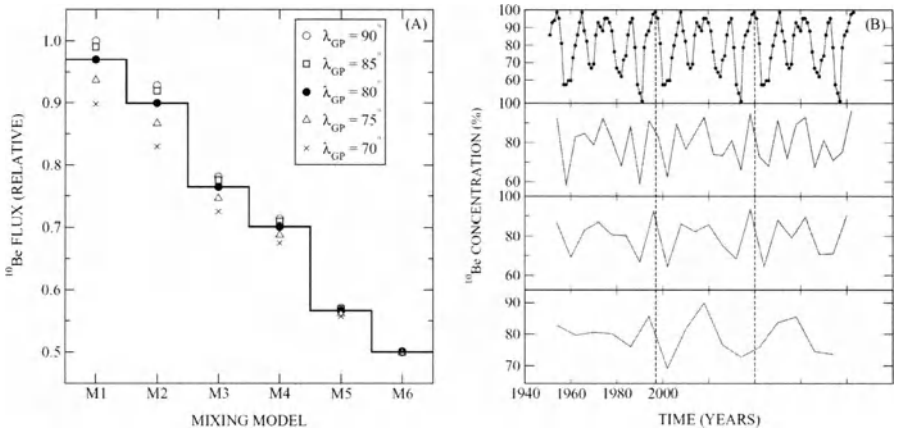

Fig. 10.7.3. Panel A: The computed dependence of the ^{10}Be flux to the polar regions as a function of 6 different mixing models (M1–M6; see text), and the location of the geomagnetic pole. Panel B: On the top - the input 11 year variation of the ^{10}Be (the Climax NM data for the period 1954–1997 were used as an input of time series, converted to the equivalent ^{10}Be production rate time series using the regression relation), and down are shown the results obtained when 4, 6, and 8 year samples of the ice are used to measure the ^{10}Be. According to McCracken (2003).

In the panel B of Fig. 10.7.3 can be seen the 11 year input (on the top) and the resulting output series. McCracken (2003) note that (1) the character of the 11 year variation has been lost; (2) the output series resembles random noise ; (3) the range is a large percentage of the amplitude of the 11 year variation used as the input. Beer et al. (1990) have estimated that annual ^{10}Be data contains 4-10% of measurement and sampling noise, and therefore panel B of Fig. 10.7.3 shows that the unresolved 11 year variation can be the largest source of noise in the ^{10}Be data (signal processing techniques allow this pseudo-noise to be eliminated).

McCracken (2003) concluded that

- the response function of ^{10}Be data has its maximum in the range 0.8-1.8 GeV/nucleon in dependence of the level of solar activity;
- known changes in the geomagnetic field have introduced up to 15% variations into the ^{10}Be data over the past 4000 years;
- less than 4% variability is introduced into the ^{10}Be data by climate controlled changes in atmospheric circulation;
- under some circumstances, the dominant 'random noise' in the ^{10}Be data is due to the 11 year variation of galactic CR.

10.7.3. 11-year variation of ^{10}Be *concentration in ice and the problem of* ^{10}Be *planetary mixing*

Beer et al. (1990, 2003) reported on the annual concentrations of ^{10}Be in ice columns obtained in Dye 3 in Southern Greenland (65°N) for the period 1783–1985 in which individual 11-year cycles are clearly evident with amplitudes of 20–30%.

Important results on 11-year variations of ^{10}Be concentration in ice for solar cycles 4–20 (1784–1976) and on the problem of ^{10}Be planetary mixing were obtained recently by McCracken (2001) based on the data of Beer et al. (1990). To reduce high frequency noise prior to analysis, all ^{10}Be data have been passed through a time series filter with weights of 1, 2, 1. Results are shown in Fig. 10.7.4. According to these results, the 11-year variation of ^{10}Be concentration in ice averaged over solar cycles 19 and 20 (see Fig. 10.7.4b) has an amplitude of 34.8%.

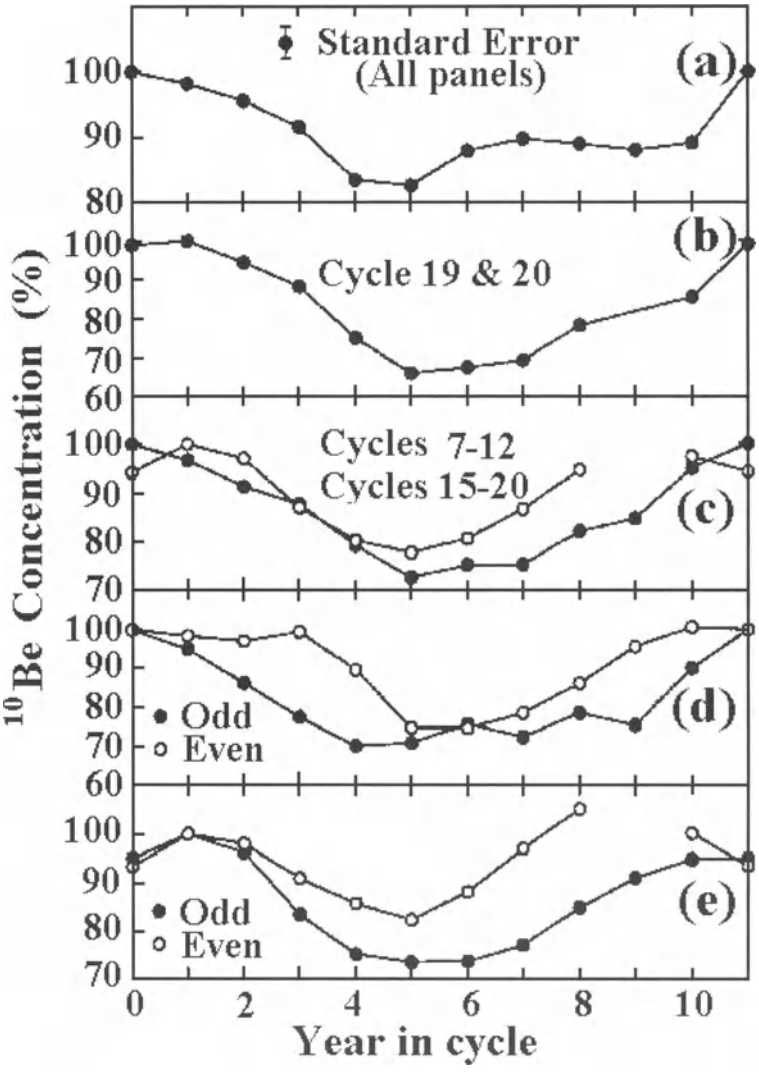

Fig. 10.7.4. Superposed epoch analysis of the 11-year variations in the ^{7}Be concentration in ice for 4–20 solar cycles (1784–1976): (***a***) –average of solar cycles 5, 6, 12, 14; (***b***) –average of solar cycles 19 and 20; (***c***) –averages of solar cycles 7–12 and 15–20; (***d***) –averages of odd and even cycles from solar cycles 7–12; (***e***) –averages of odd and even cycles from solar cycles 15–20 (McCracken, 2001).

On the other hand, according to calculations by Masarik and Beer (1999), the production rate of ^{10}Be at high latitudes is as high as 2.7 times the planetary average. The expected amplitude of the 11-year variations of ^{10}Be concentration in ice averaged over solar cycles 19 and 20 is 34.4% at high latitudes ($R_c \leq 1.0$ GV) if there is no planetary mixing of ^{10}Be, but for planetary averaged production rate of ^{10}Be (global planetary mixing) the expected amplitude of the 11-year variations is much smaller: only 21.6%. So McCracken (2001) on the basis of calculations Masarik and Beer (1999), came to the conclusion that good agreement of observed and predicted amplitudes (34.8% and 34.4%) shows that the conditions in the Earth's atmosphere do not allow sufficient planetary mixing of ^{10}Be. This important conclusion is in accordance with the results of Steig et al. (1996) and Bard et al. (1997). Steig et al. (1996) and Bard et al. (1997) have concluded that ≥ 70% of the ^{10}Be precipitated at Taylor Dome (78°S) and at the South Pole has been produced at high latitudes ($R_c \leq 1.0$ GV).

10.7.4. Reflection of 22-year helio-magnetic cycles in ^{10}Be concentrations in ice

From NM data it is well known (Dorman, 2001; Dorman et al., 2001a,b; see details in Dorman, M2005) that in the odd 11-year solar cycles (e.g., 17, 19) there are relatively broad CR variations, while the even cycles (e.g., 18, 20) have had a shorter lived decrease and return to the CR sunspot minimum value several years prior to sunspot minimum. This difference in behavior of CR variation is caused by energetic particle drifts which reverse their direction of motion at about the solar activity maximum during the 22-year helio-magnetic cycle. McCracken (2001) showed that the data on ^{10}Be concentrations in ice exhibit a similar difference between the odd (7, 9, 11) and even (8, 10, 12) solar cycles (see Fig. 10.7.4d). Similar differences are also found between the odd cycles 15, 17, 19 and the even cycles 16, 18, 20 (Fig. 10.7.4e).

10.7.5. Geomagnetic field changes during 1000AD–2000AD, circumpolar atmosphere motions, reflection in ^{10}Be concentrations in ice

According to McElhinny and McFadden (M2000), the geomagnetic field changed considerably during the last thousand years: the geomagnetic pole has moved some 21° (see Fig. 10.7.5) and the Earth's magnetic dipole strength has changed by about 25%. It leads to big changes in CR cut off rigidities: e.g., at the location 48°N, 285°E (North America) in 2000 cut off rigidity for primary CR was $R_c \approx 1$ GV for vertical direction, but at 1000 AD it was $R_c \approx 7$ GV .

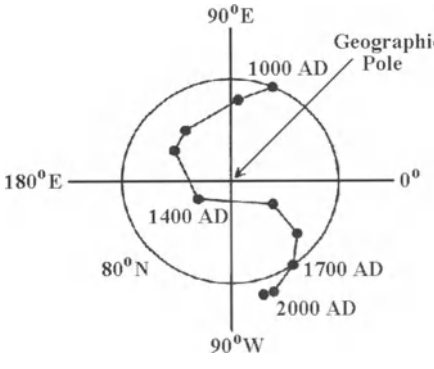

Fig. 10.7.5. The motion of the North geomagnetic pole during 1000–2000. From McCracken (2001).

According to McCracken (2001) the zonal (circumpolar) motions of the atmosphere is needs to be included for determining the expected ^{10}Be concentrations in polar ice. In Fig. 10.7.6 are shown McCracken's (2001) results of expected changes in ^{10}Be precipitated to three polar locations owing the long term changes of the geomagnetic dipole during 1000–2000. It can be seen that at the South Pole, where $R_C \approx 0$ no variations are expected, but at two other polar locations about 2% and 4% long term variations are expected in ^{10}Be concentrations in polar ice.

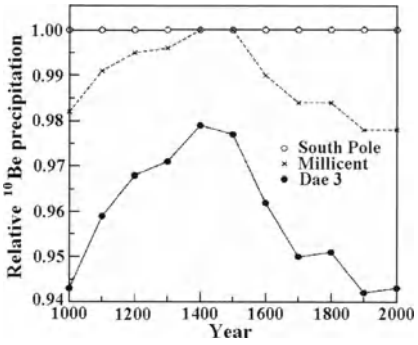

Fig. 10.7.6. The calculated changes in ^{10}Be precipitated to three polar locations owed the long term changes of the geomagnetic dipole. According to McCracken (2001).

10.7.6. Reflection in ^{10}Be data long term Heliospheric modulation in periods of low and high solar activity

On the basis of ^{10}Be data in polar ice Beer et al. (1998) came to conclusion that the galactic CR exhibited substantial modulation even during the Maunder minimum. To study this further, the upper graphs in Fig. 10.7.7 display the ^{10}Be data from Dye 3, applying a weighted average to the annual data with weights 1, 2, and 1.

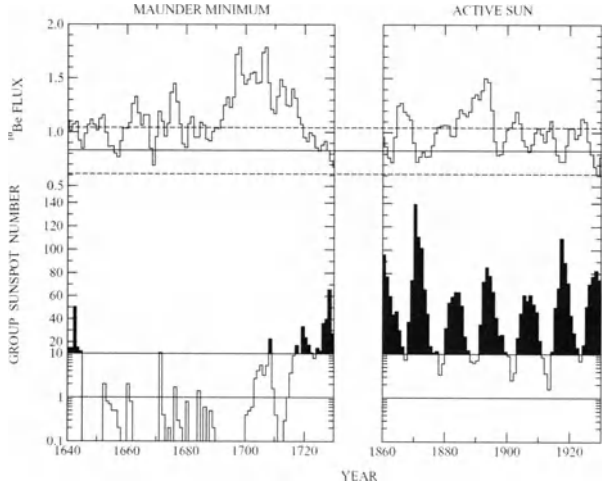

Fig. 10.7.7. Comparison of the ^{10}Be data, and the sunspot numbers (a) during the Maunder minimum, and (b) during a period of high solar activity. According to McCracken et al. (2003).

From Fig. 10.7.7 can be seen that there are large, rapid changes in both intervals, the ^{10}Be data varying by ±30% between 0.7 and 1.3x10^4 atoms/g in each case. The modulation of the galactic CR requires the presence of magnetic fields, and Fig. 10.7.7 indicates that the strength and properties of the heliomagnetic field were similar during both periods. The lower panels in Fig. 10.7.7 show the group sunspot numbers NG (according to Hoyt and Schatten, 1996; note that for NG<10 are used the logarithmic scale). Comparing the panels, note that while the amplitudes of the variations in ^{10}Be were similar during the two periods, NG differed by a factor of about 50. Since 1950, the galactic CR intensity has shown an approximately linear regression with NG, however Fig. 10.7.7 shows that this regression relationship did not pertain during the Maunder minimum.

10.7.7. Long term CR variations on the basis of ^{10}Be *data*

In Fig. 10.7.8 is shown long term CR variation on the basis of the 11 and 22 year average ^{10}Be data from Dye 3 and South Pole for the period 800–2000.

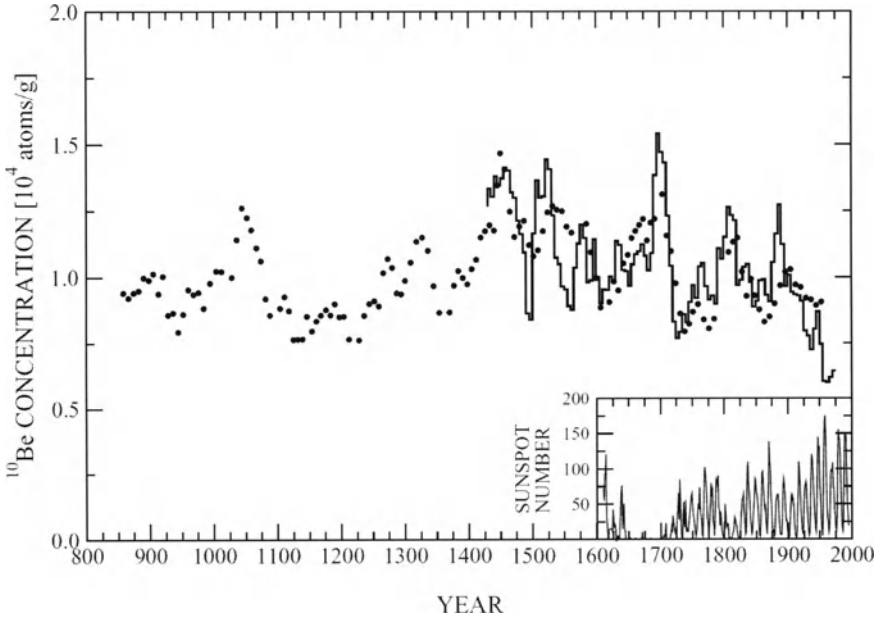

Fig. 10.7.8. The 11 year average ^{10}Be data from Dye 3, Greenland (histogram) and 21–24 year averages (dots) from South Pole for the period 800-2000; are shown also sunspot numbers for 1600-2000. According to McCracken et al. (2003).

According to Beer et al. (2003) the ^{10}Be flux record from Greenland during a non-glacial period (e.g., the last 12,000 years) can be interpreted as a record of the heliospheric and geomagnetic modulation of the galactic CR. To illustrate the extraction of the heliospheric modulation it was choused the ^{10}Be flux from the GISP2 ice core (Masarik and Beer, 1999) covering the period 8000 to almost 3000 years before present (present being 1950). Results are shown in Fig. 10.7.9.

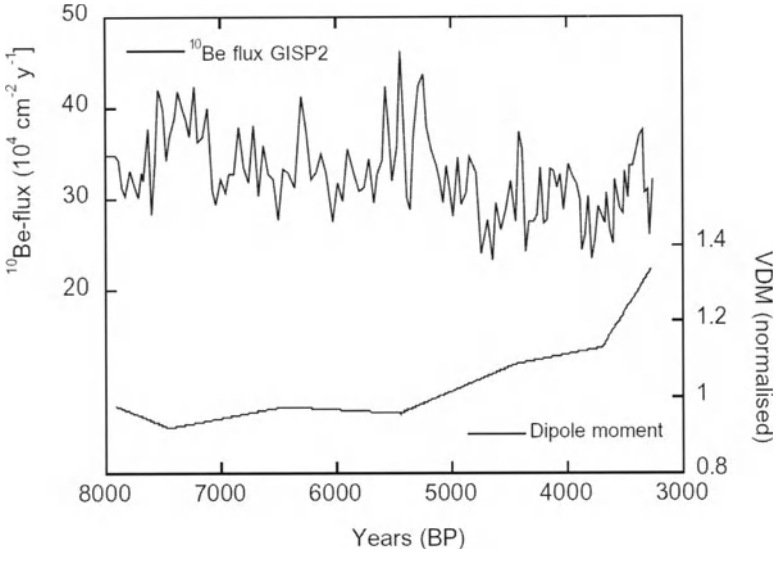

Fig. 10.7.9. Data of ^{10}Be flux from the GISP2 ice core and the geomagnetic dipole moment (units relative to today). According to Beer et al. (2003).

In order to reconstruct the heliospheric modulation, Beer et al. (2003) first remove the effects of the changing geomagnetic dipole, using a time dependence based on a large number of archeomagnetic measurements (Fig. 10.7.9, lower panel). The modulation parameter Φ was then derived using the relationship between ^{10}Be production rate, geomagnetic dipole moment (M) and solar modulation (Φ) shown above in Fig. 10.7.1. Fig. 10.7.10 displays the results after applying low pass filters with cut-off periodicities of 50 and 500 years.

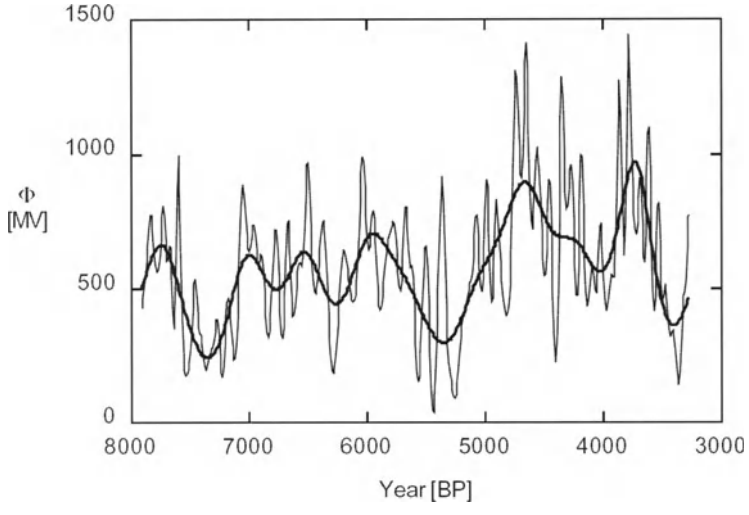

Fig. 10.7.10. Heliospheric modulation parameter Φ as derived from the ^{10}Be record (Fig. 10.7.9) filtered with 50 years (thin curve) and 500 years (thick curve) low pass filters. According to Beer et al. (2003).

As can be seen from Fig. 10.7.10, modulation parameter Φ extended over the range 0–1500 MV, compared to an average Φ since 1950 of ~ 800 MV, and that there were distinct periods with higher and lower CR modulation than the present. Spectral analysis made in Beer et al. (2003) reveals the 88 years (Gleissberg) and 208 years (Suess or DeVries) periodicities, and others. This example shows that cosmogenic radionuclides have the potential to reconstruct the solar modulation parameter Φ over the past 10 millennia. The changes in Φ were much larger in earlier times than experienced during the instrumental period. Careful comparison of ^{10}Be and ^{36}Cl records from different ice cores with the ^{14}C tree ring record will eventually improve the temporal resolution to 1-2 years, reduce the noise, and provide a means to estimate the uncertainties.

On the basis of long term CR variations by ^{10}Be data McCracken et al. (2003) came to following conclusions:
(1) the 11 and 22 year average galactic CR intensity near 2 GeV/nucleon has varied by a factor of ~ 2.5 over the past 1150 years, and that it has been at its lowest value since ~ 1965;
(2) there was strong modulation of the galactic CR during the Maunder minimum, implying substantial interplanetary magnetic fields;
(3) at a time of only mild solar activity (1700–1725), there was a precipitous ~ 50% decrease in the galactic CR intensity that indicates that the modulation process developed to a strength that was not achieved again until 225 years later.

10.7.8. On the expected changes of ^{10}Be contents in polar ice caused by very great solar particle events

McCracken et al. (2001) estimated that the ^{10}Be total production for the big solar particle event (SPE) of 23 February 1956 (the fluence of protons with energy > 30 MeV was about $10^9\,\mathrm{cm}^{-2}$ according to Shea and Smart, 1990) was probably $3.1\times10^2\,\mathrm{atoms/g}$. This value is very small in comparison with $\approx10^4\,\mathrm{atoms/g}$ produced by galactic CR per year. But, according to nitrate data in polar ice (see below, Section 13.1), in September 1859 there was a SPE about 20 times greater than SPE of 23 February 1956; so in this case ^{10}Be about $6\times10^3\,\mathrm{atoms/g}$ was produced, which is comparable with what is produced by galactic CR per year. McCracken et al. (2001) came to the conclusion that very great SPEs in the past (bigger than SPE of 23 February 1956) can be measured not only by nitrates, but also by ^{10}Be data in polar ice.

10.7.9. On the integral effective energy of primary CR to which are sensitive ^{10}Be and other cosmogenic nuclides

Masarik and Beer (1999) calculated the expected fluxes of secondary neutrons generated by CR, and then – the expected production rate of several cosmogenic nuclides, including ^{10}Be. On the basis of these calculations McCracken (2001, 2003) estimated the dependence of polar ^{10}Be production rate response from CR primary energy at different values of modulation parameter Φ in comparison with NM, balloon and satellite measurements (see panel A of Fig. 10.7.2).

In Alanko et al. (2003) was introduced a concept on integral effective energy E_{inef} for long term CR modulation (it means that the integral flux of primary CR above E_{inef} is proportional to the some ground detector count rate or to some cosmogenic isotope production rate; see in detail Chapter 3, section 3.15.5). Calculations of Alanko et al. (2003) for polar production rate of ^{10}Be gave E_{inef} = 1.3 GeV and for global production rate of ^{14}C gave E_{inef} = 2.8 GeV, much smaller than for polar NM (E_{inef} = 5.5 GeV).

Chapter 11

Cosmic Ray Influence on Atmospheric Electric Field and Thunderstorms, Earth's Global Charge and Global Electric Current

11.1. On two mechanisms of CR connection with thunderstorm discharges

In Chapter 8 we considered the problem of the influence of atmospheric electric field on cosmic rays. But there is also another very important and interesting inverse problem: is there or is there not some influence of cosmic rays on thunderstorms and the atmospheric electric field? We mentioned this problem very briefly in Section 8.1. The first to suggest that secondary cosmic ray electrons can be influenced by the strong cloud electric fields was Wilson (1916, 1925a,b). In the last decade this problem was developed very intensively by A.V. Gurevich and colleagues (see Gurevich et al., 1992, 1999, 2001; Gurevich and Milikh, 1999; Gurevich and Zybin, 2001). They showed that the secondary CR relativistic electrons in the atmospheric electric field create runaway electron avalanches, which can be main cause of thunderstorm discharges (see Sections 11.2 and 11.3). On the other hand, Ermakov (1992), Ermakov and Stozhkov (2002, 2003) also connected thunderstorms discharges with CR, but they assumed that the main cause is EAS (External Atmospheric Showers) generated by primary CR with energy $\geq 10^{14}$ eV (see Section 11. 4).

11.2. Necessary conditions for atmospheric electric field discharges in the atmosphere

It is well known that to obtain big current electrical discharges (usually used in technology, see Mesjaz and Korolev, M1991; Babich et al., 1990) it is necessary to have a very strong electrical field E in the atmosphere, determined by the classical relation

$$E \geq E_{\mathrm{sf}} = \frac{4\pi e^3 Z N_m}{2.72\overline{E}}, \qquad (11.2.1)$$

where Z is the effective charge of atoms and N_m number of molecules in the atmosphere in cm^3, $\overline{E} \approx J_z \approx ZE_i$ (E_i is the ionization potential). In this case all electrons are transferred very quickly in the regime of acceleration, leading to a great current electrical discharge. The problem is that the condition determined by Eq. 11.2.1 is never realized in the natural processes connected with atmospheric electric field phenomena and thunderstorms: the observed values of E are about 200 times smaller than E_{sf}.

Let us note that the observed values of E are also much smaller (about 10 times) than the critical field E_{th} for the usual discharges in the atmosphere (at the sea level

$E_{th} \approx 23$ kV/cm). The usual discharges are caused by runaway electrons from background atmosphere in the high energy tail of Maxwell distribution.

Nevertheless, the atmospheric electric field discharges in the atmosphere as lightnings in periods of thunderstorms are realized and were observed very often at much smaller electric fields. What is the main cause of this phenomenon? Let us consider this problem in more details, following the treatment of Gurevich et al. (1992).

The behavior of electrons in the atmosphere is determined by the electric field E and ionization loose of energy F:

$$m\frac{dv}{dt} = eE\cos\theta - F(E_k); \quad \frac{dE_k}{dt} = e\sqrt{\frac{2E_k}{m}}\left(E\cos\theta - \frac{F(E_k)}{e}\right), \tag{11.2.2}$$

where m, e, v and E_k are the rest mass, charge, velocity and kinetic energy of electrons, θ is the angle between electric field E and direction of electron moving (we will put θ = 0), and $F(E_k)$ is ionization loose of energy. In the non-relativistic region ($E_k << mc^2$)

$$F(E_k) = \frac{4\pi N_m Z e^4}{mv^2}\ln\left(\frac{mv^2}{zE_i}\right), \tag{11.2.3}$$

where $Z = 2z \approx 14.5$ (here z is the mean nuclear charge of the nitrogen and oxygen atoms of air), and $E_i \approx 15$ eV is the characteristic ionization energy. In the relativistic region ($E_k >> mc^2$)

$$F(E_k) = \frac{4\pi N_m Z e^4}{mc^2}\ln\left(\frac{mc^2\gamma}{E_i}\right), \tag{11.2.4}$$

where $\gamma = E_k/mc^2 = \left(1 - v^2/c^2\right)^{-1/2}$ and $E_i \approx 270$ eV . When $E_k << mc^2$ the ionization force in Eq. 11.2.2 decreases with an increase of the electron energy as $F(E_k) \propto E_k^{-1}\ln(E_k)$. But in the relativistic region it begins to increase as $F(E_k) \propto \ln(\gamma)$. Therefore there is a minimum of F

$$F_{\min}(\gamma) = \frac{4\pi N_m Z e^4}{mc^2}a, \text{ where } a \approx 10, \tag{11.2.5}$$

The minimum (Eq. 11.2.5) is attained at $\gamma_{\min} \approx 3 \div 4$ (corresponding to $E_{k\min} \approx 1.4$ MeV). The dependence of $F/F_{\min}$ on E_k is shown in Fig. 11.2.1. Let us introduce the dimensionless parameter

$$\delta_o = \frac{Emc^2}{4\pi N_m Z e^3 a} = 0.5 \times \frac{E}{1\text{kV/cm}}\frac{N_{mo}}{N_m}\frac{10}{a}, \tag{11.2.6}$$

where $N_{mo} = 2.7 \times 10^{19}$ cm^{-3} is the number of air atoms at normal conditions (h_o =1 atm).

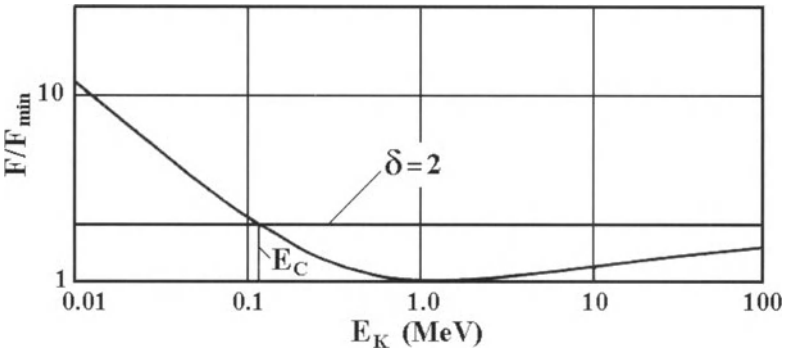

Fig. 11.2.1. The dependence of brake force F on the energy of electron E_k (the braking force is normalized to the minimal braking force $F_{\min}$ at $E_k \approx 1.4$ MeV). It is shown the critical electric field E_c at $\delta = 2$. According to Gurevich and Zybin (2001).

Let us consider the case $\delta_o > 1$ (which corresponds to $E>F/e$) when electrons can be accelerated (the right hand side of Eq. 11.2.2 is positive). The critical value of E will be determined from the balance equation $eE - F(v) = 0$, which has two roots. One root is in the non-relativistic region

$$v_1^2 = c^2/\delta_o, \; E_{k1} = mc^2/2\delta_o, \tag{11.2.7}$$

which is unstable: for electrons with velocity $v < v_1$ we have $E<F/e$ and the electrons slow down, while for electrons with $v > v_1$ (the high energy tail of the Maxwell distribution of background electrons) have $E > F/e$, and the electrons accelerate, they become runaways (Gurevich, 1960). The first root corresponds to a critical electric field in the atmosphere at normal conditions $E_{\text{th}} \approx 23$ kV/cm. This solution can not be realized in periods of thunderstorms because of the very high value of E_{th}. The second root is in the relativistic region $\gamma_2 \approx \exp(a(\delta_o - 1))$ and is stable: when $\gamma < \gamma_2$ electron accelerates and γ increases, but when $\gamma > \gamma_2$ it slows down and γ decreases. The critical electric field corresponding to this root

$$E_c = \frac{F_{\min}}{e} = \frac{4\pi N_m Z e^3}{mc^2} a \tag{11.2.8}$$

is more than 10 times smaller than E_{th} (here $a \approx 10$). The energy of electrons in the high energy tail of Maxwell distribution of background electrons for realization of the second solution is not enough: energies several thousand times bigger are needed. Only cosmic ray secondary relativistic electrons with energy

$$E_k > E_{kc} \approx E_c mc^2 / 2E \tag{11.2.9}$$

will be continuously accelerated (see Fig. 11.2.1) and become runaway. It is important that these electrons, by ionization, will generate new electrons which will also be accelerated and become runaway. The number of these electrons along a unit length with energy more than E_{k1} is determined by Eq. 11.2.7 (see also Fig. 11.2.1) and generated by fast electron with energy $E_k >> E_{k1}$ will be determined according to Landau and Lifshitz (M1960) by

$$\frac{dN(E_{k1})}{ds} = \frac{\pi N_m Z e^4}{mc^2 E_{k1}}. \tag{11.2.10}$$

If $E_{k1} > E_{kc}$ all generated electrons will be runaway. Then from Eq. 11.2.9 and 11.2.10 one can determine the characteristic path l_a for generation of runaway electrons:

$$l_a = \left(\frac{dN}{ds}\right)^{-1} = \frac{\left(mc^2\right)^2}{2\pi N_m Z e^4}\frac{E_c}{E}, \tag{11.2.11}$$

and total increasing of runaway electrons will be determined by

$$N = N_o \exp(s/l_a), \tag{11.2.12}$$

where according to Eq. 11.2.11

$$l_a \approx 50m \times \frac{E_c}{E}\frac{N_{mo}}{N_m}, \tag{11.2.13}$$

where $N_{mo} = 2.7 \times 10^{19}\,\mathrm{cm}^{-3}$ is the number of air atoms at normal conditions ($h_o = 1$ atm). Together with runaway electrons the number of thermal electrons also increases exponentially, leading to a very dramatic increase of conductivity and to electrical discharge.

11.3. Measurements of atmospheric electric field, critical electric field, lightnings, and sprites

In Fig. 11.3.1 are shown the results of atmospheric electric field measurements on different heights by balloons (Marshall et al., 1996a,b; general information see in Uman, M1984, M1987; Volland, M1984; MacGorman and Rust, M1988). Also shown are the critical electric field E_c according to Eq. 11.2.8 and moments of lightning. It can be seen that always the observed atmospheric electric field is smaller or about the same as the

field E_c, and in many cases when $E \approx E_c$ lightnings are formed. These results support the model described above in Section 11.2.

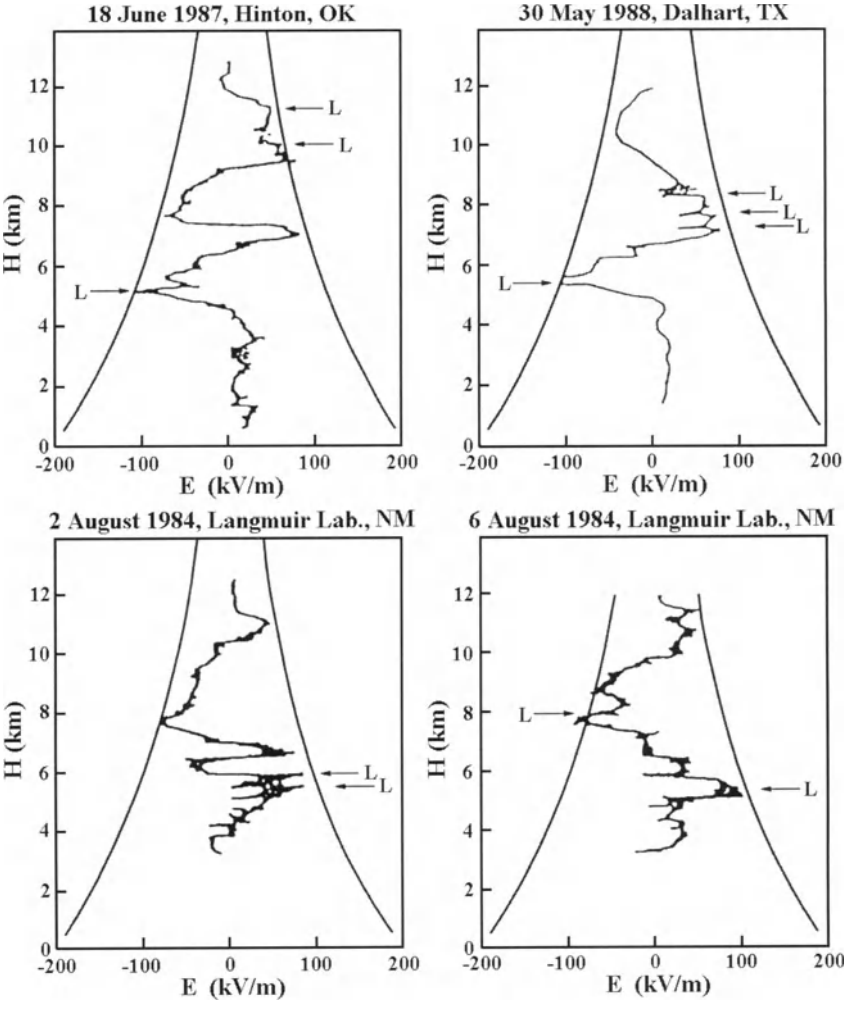

Fig. 11.3.1. The balloon measurements of atmospheric electric field in periods of thunderstorms in different States of USA in 1984–1988 (Marshall et al., 1996a,b). Are shown the critical electric field E_c according to Eq. 11.2.8 *vs* the altitude H, and by L are shown moments of lightnings. According to Gurevich and Zybin (2001).

According to the theory of Gurevich at al. (1992, 1999, 2001) described above, the necessary conditions for lightning are the following:

1. The atmospheric electric field must be

$$E \geq E_c = 2.16h \text{ kV/cm} = 216\exp(-H/H_o) \text{ kV/m}, \qquad (11.3.1)$$

where E_c is determined from Eq. 11.2.8. Here h is the atmospheric pressure in atmospheres, H is the height above sea level in km and $H_o \approx 8$ km . As follows from Eq. 11.3.1, E_c decreases exponentially with altitude: at $H \approx 6.3$ km, $E_c \approx 100$ kV/m , and at $H \approx 11$ km, $E_c \approx 50$ kV/m .

2. Magnitude of the dimension *L* over which the condition described by Eq. 11.3.1 is satisfied, must be much bigger than the length of exponential increase of avalanche exponential multiplication l_a:

$$L >> l_a \approx \frac{E_c}{E}\exp(-H/H_o)\times 50 \text{ m} \tag{11.3.2}$$

where l_a was determined by Eq. 11.2.11 and 11.2.13. Really this condition is satisfied in thunderstorm clouds, between them, and between clouds and ground, where dimensions are measured in km.

3. There must be seed relativistic electrons with energy

$$E_k \geq E_{kc} = \frac{mc^2 E_c}{2E} . \tag{11.3.3}$$

Seed relativistic electrons are formed continuously in the atmosphere at any place and at any time by galactic cosmic rays: according to Daniel and Stephens (1974), Fulks and Meyer (1974), Bazilevskaya and Svirzhevskaya (1988) the average flux of these electrons on altitudes 4–8 km is about 10^3 electron.m^{-2}.sec^{-1} (see in more detail above, Section 2.11 in Chapter 2). Because secondary cosmic ray electrons move in all directions, the discharge can develop in any direction, dependening on the direction of atmospheric electric field: lightnings between clouds, from clouds to ground and from ground to clouds, and giant sprits between clouds and ionosphere (up to about 100 km).

The existing of great electric field E in the atmosphere depends on the relation between processes of generation and relaxation of E. There are two mechanisms of generation E:

1. Usual gradual increase of E inside and near boundaries of clouds caused by action of atmospheric winds, gravitation forces and capturing charged particles by water drops, ice particles and aerosols (the characteristic time of this process is 1-10 min);

2. Sudden change of electric charge in clouds caused by powerful discharge from cloud to the ground (the characteristic time of this process is milliseconds).

The relaxation of E is determined by the conductivity of air:

$$T_r = (4\pi\sigma)^{-1}, \tag{11.3.4}$$

where T_r is the time of relaxation and σ is the air conductivity, determined mainly by cosmic ray ionization (and terrestrial radioactive sources very near the ground). The air conductivity is mainly caused by ions because thermal electrons stick to molecules after a

time $\approx 10^{-7}$ sec. Near the ground at sea level $T_r \approx 400$ sec, on the altitude 10 km $T_r \approx 100$ sec, and on 30–50 km $T_r \approx 1-10$ sec (see Fig. 11.3.2).

The comparison of two characteristic times leads to conclusion that for the first mechanism of electric field generation realized in the lower layers of thunderstorm atmosphere (usually lower than about 8 km), value of E can be only little more than E_c, but the time of existence of this field can be as long as a few minutes (these fields have usually caused lightnings between clouds and between clouds and ground).

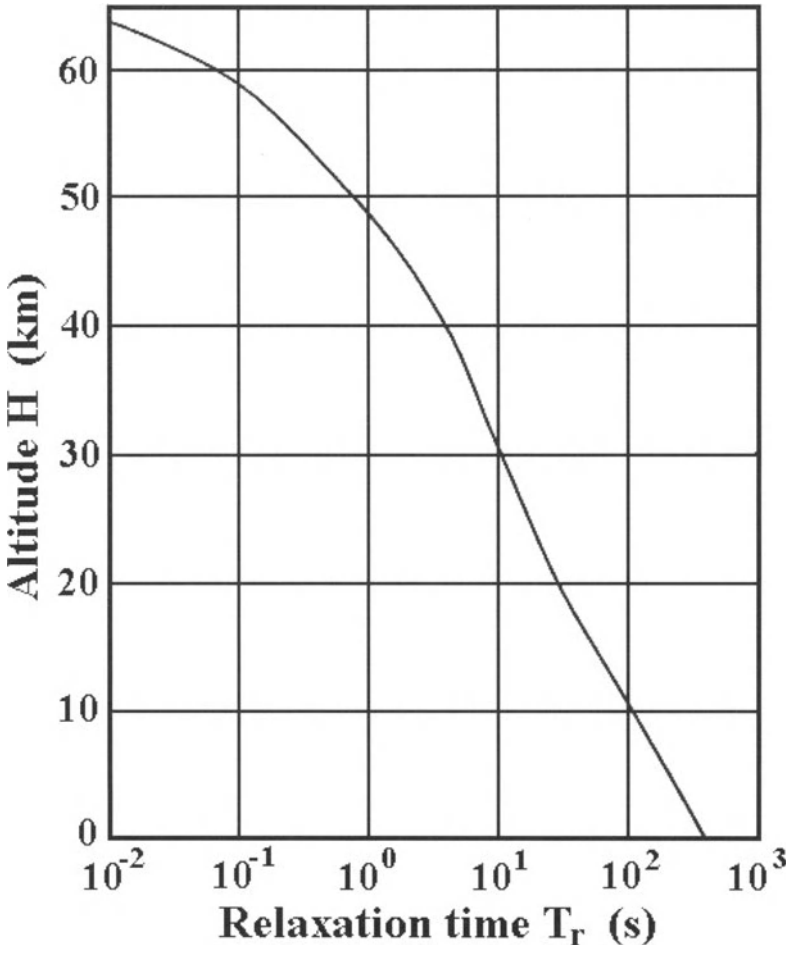

Fig. 11.3.2. The time of relaxation T_r *vs* the altitude *H*. According to Gurevich and Zybin (2001).

For the second mechanism realized in the highest layers of thunderstorm atmosphere (usually from about 20 km to 100 km), value of E can be much more than E_c, but for a very short time, not longer than about 10 sec (these fields caused so called sprites, see Fig. 11.3.3 and Fig. 11.3.4).

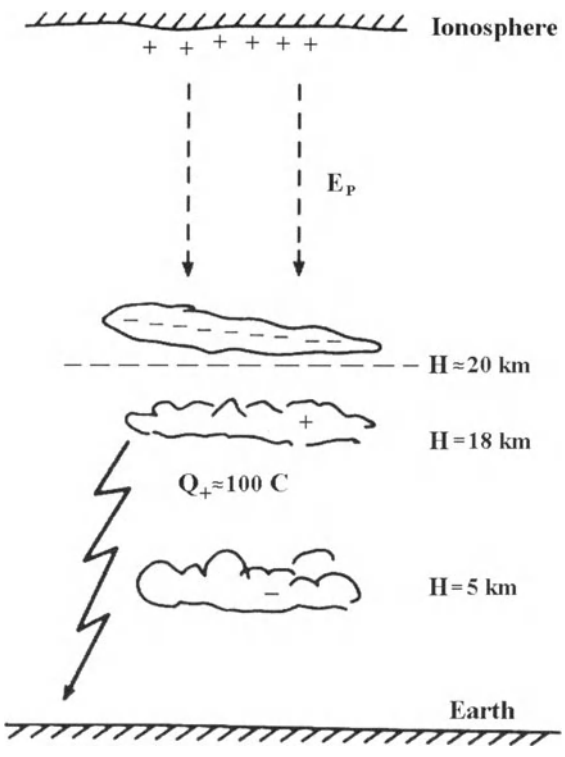

Fig. 11.3.3. The model describing the evolution of the conditions for sprite discharge. According to Gurevich and Zybin (2001).

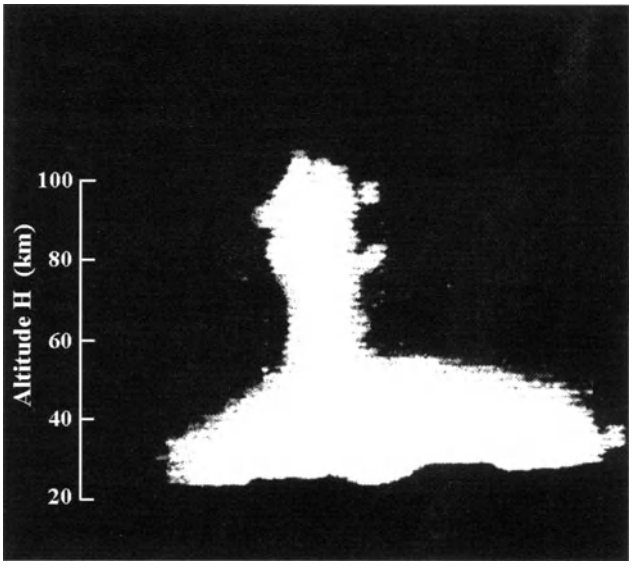

Fig. 11.3.4. An example of sprite discharge. According to Gurevich and Zybin (2001).

According to direct measurements on planes and sounding balloons (see McCarthy and Parks, 1985; Eack, 1996; Eack et al., 1996a,b, 2000; Beasley et al., 2000), thunderstorms and sprites are accompanied by X-ray and gamma ray radiation (see example of X-ray radiation in the period of thunderstorm in Fig. 11.3.5).

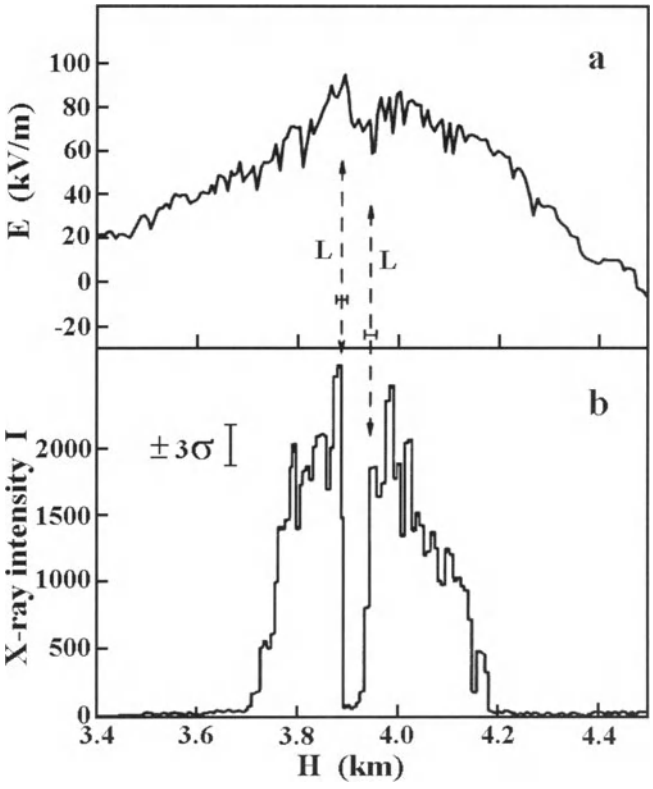

Fig. 11.3.5. An example of simultaneous observations of atmospheric electric field E (*a*) and X-ray radiation I (*b*) in the period of lightning at altitudes $3.7 \text{ km} \le H \le 4.2 \text{ km}$ (at this time on altitudes $H < 3.7$ km and $H > 4.2$ km was observed the standard background X-ray intensity). According to Gurevich and Zybin (2001).

These results are in good agreement with theoretical calculations of Gurevich et al. (2001) in accordance with the model described above, in Section 11.2. This agreement also shows that in formation of thunderstorms and sprites the secondary relativistic cosmic ray electrons play a key role.

11.4. External Atmospheric Showers (EAS) generated by high energy CR particles and thunderstorm discharges

11.4.1. EAS and inter-cloud discharges

Ermakov (1992), Ermakov and Stozhkov (1999, 2002, 2003), Stozhkov (2002) suggested that main cause of thunderstorm discharges are EAS (External Atmospheric

Showers) which are generated by primary CR particles with energy more than 10^{14} eV. In Fig. 11.4.1 is shown the schematic view of EAS produced by high energy CR particle in thundercloud.

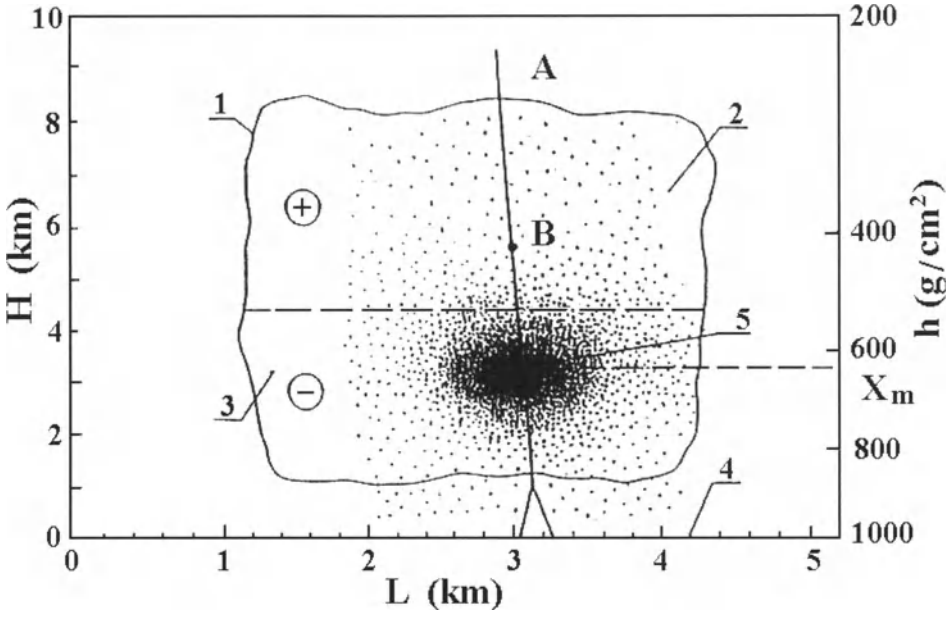

Fig.11.4.1. Schematic view of extensive air shower (EAS) produced by a high energy cosmic ray particle in thundercloud: ***H*** -altitude in the atmosphere in km; ***h*** - atmospheric pressure in g/cm^2; ***L*** - horizontal size of thundercloud in km; ***1*** – thundercloud boundary; ***2, 3*** - regions of positive and negative electric charges (dashed line separates these regions); ***4*** - the Earth's surface; ***5*** - region of maximum number of EAS particles which are shown by dots. This region is at the atmospheric pressure level $\mathbf{X_m}$; straight line ***A*** - track of primary cosmic ray particle with $E_0 > 10^{15}$ eV; ***B*** - site of high energy cosmic ray particle interaction with air nuclear; straight line below ***B*** shows the EAS core; most of EAS secondary particles is connected by ionized channels with the track of primary particle ***A***. According to Ermakov and Stozhkov (2002, 2003).

The position of maximum concentration of EAS particles according to Murzin (M1988) is defined as

$$X_m = 500 + 75 \times \lg\left(E_o / 10^{15}\,\text{eV}\right)\ \text{g/cm}^2\,, \tag{11.4.1}$$

where E_o is the energy of primary CR particle. The lengthwise size of EAS can get more than 10 km, and the lateral dimension of EAS is about several hundreds meters. As soon as atmospheric electric field E_{atm} within the thundercloud reaches the critical value about 200–300 kV/m, the discharges within the cloud arise. They run along secondary particle tracks of EAS and transfer electric charge Q, as shown in Fig. 11.4.2a.

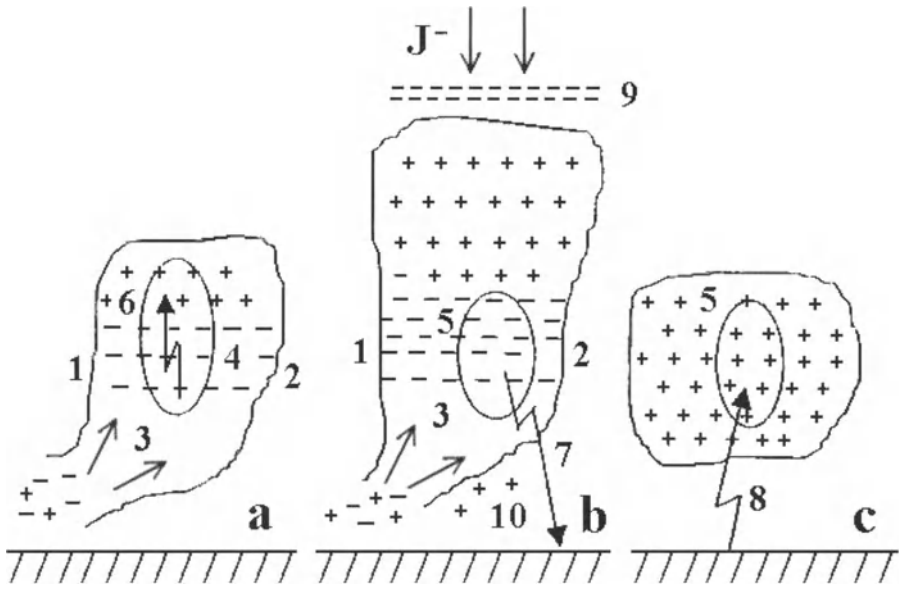

Fig.11.4.2. The phases of thundercloud existence: ***a***-generation, ***b***-maturity; ***c***-degradation. Notations: ***1*** - region of a warm front; ***2*** - region of a cold front; ***3*** - ascending fluxes of wet ionized air; ***4*** and ***5*** - extensive air showers produced by primaries with the energies $E_0 \geq 10^{14}$ eV and $E_0 \geq 10^{15}$ eV ; ***6*** – intra-cloud electric discharges; ***7, 8*** - descending and ascending discharges; ***9*** - negative screen layer, ***10*** - positive charge in the cloud base; J^- – current of negative ions running from the ionosphere to the top of cloud. According to Ermakov and Stozhkov (2002, 2003).

In EAS primary CR particles with energy $E_o \geq 10^{14}$ eV will generate simultaneously more than 10^4–10^5 relativistic electrons, and about 10^{10} free electrons in the numerous ionized tracks of EAS in the atmosphere. The linear density of these electrons is $n_e \approx 10^2\,\mathrm{cm}^{-1}$. By the action of atmospheric electric field E_{atm} within the thundercloud these electrons give electron avalanches increasing ionization inside the tracks of EAS particles. At the moment of a discharge the radius of an electron avalanche is $r_a \approx 1$ mm, the gain coefficient of avalanche $k_a \approx 7\times10^8$, and electron concentration n within the track is according to Raiser (M1987), Ermakov and Stozhkov (2002, 2003):

$$n = (n_a k_a)/(\pi r_a) \approx 2\times10^{12}\ \mathrm{cm}^{-3}. \qquad (11.4.2)$$

Each discharge in the volume of EAS decreases E_{atm} by hundred times: from about 200 kV/m to about 1–2 kV/m (Raiser, M1987). The frequency of intra-cloud discharges is defined by the rate of E_{atm} strength gain, and this frequency does not depend on the intensity of EAS inside the cloud: according to Amatuni et al. (1987) inside the cloud with

the base $S_{cl} \approx 13\ \text{km}^2$ the frequency of EAS from CR primary particles with $E_o \geq 10^{14}$ eV falling on this cloud equals to $F_{\text{EAS}} \approx 1300\ \text{sec}^{-1}$.

From the moment of intra-cloud discharge emergence the cloud begins itself to generate electric charges. The number of electron–ion pairs produced by electron avalanches in extensive air shower tracks is more than 7×10^{20} pairs and the value of charge (positive or negative signs) is no less than Q ~ 110 C. Most of these ion pairs disappear as a result of recombination in the various processes. The rest attach to the neutral aerosols gives the new charged nuclei of condensation. These nuclei together with ones coming up from the lower atmosphere take part in the process of unlike charge separation described above. The process of charge generation via intra-cloud discharges increases mainly the frequency of these discharges and gives the essential growth of unlike charges within the cloud. Owing to the discharges within the cloud the concentrations of charged nuclei condensation increases and, accordingly, the concentrations of water drops growing on these nuclei increase. The growth of cloud is enhanced because there is a strong electric field that is favorable to vapor condensation not only on the charged droplets but on the neutral ones also (Rusanov and Kuzmin, 1977). The release of latent heat in the condensation process amplifies air upstream and, accordingly, amplifies electrical activity and water content in the incipient cloud.

11.4.2. EAS discharge mechanism and descending lightning (from cloud to ground)

Ermakov and Stozhkov (2002, 2003) considered the application of EAS discharge mechanism to the possible explanation of descending lightning (from cloud to ground). The thundercloud electric dipole formed with the negative volume charge at the bottom and positive one at the top of the thundercloud becomes asymmetric for the following reason. Under the action of electric charges of the dipole an electric current of light negative ions flows from the atmosphere to the top of the cloud and positive ion current flows from the ground to the bottom of the cloud (see Fig. 11.4.2b). Besides, the positive charges on which water vapor was not condensed go up to the atmosphere from the cloud. The negative ion current (flowing to the top of the cloud) is higher than the positive ion current (flowing to the base of the cloud) ~ 10 times. It is because the mobility and concentration of ions above the cloud are higher than these values under the cloud. The measurements made with balloons and aircrafts showed that the average value of a total current above the top of the cloud is J ~ 1 A and a negative ion current J^- flowing from the ionosphere to the thundercloud top equals to a half of this value (Gish and Wait, 1950; Stergis et al., 1957). This current of negative ions compensates partially the volume positive charge of the thundercloud. In this case the negative charged layer is formed near the top of the cloud (see Fig. 11.4.2b). As a result of the compensation of volume positive charge, the electric dipole of the cloud becomes asymmetric with the prevalence of the negative charge in the low part of the cloud. It gives the increase of the electric field between the cloud and the Earth's surface and the appearance of descending lightning transferring the negative charge from the cloud to the Earth's surface.

From the moment of the 'cloud to ground' lightning emergence the cloud is in the phase of maturity that extends about 20 min. In this phase, owing to a large number of

'cloud to ground' lightning, the water vapor condensation rate peaks maximum values and owing to a release of maximum values of latent heat upstream rate, electric activity and water content of thundercloud also increase up to maximum levels. The descending lightnings run along the ionized tracks of the EAS particles that reach the Earth's surface. Such EAS are produced by the high energy primary particles with $E_o \geq 10^{15}$ eV. The frequency of 'cloud to ground' lightning is defined as the rate of the electric field strength growth within the cloud or the value of negative ion current J^- flowing to the cloud top. This frequency does not depend practically on the intensity of extensive air showers with $E_o \geq 10^{15}$ eV. The number of such showers falling on the cloud with the base of about 13 km^2 is rather high and equals to ≈ 30 sec^{-1} (Amatuni et al., 1987). As a rule a descending lightning consists of several discharges. The first discharge is running along the tracks of secondary particles of the EAS produced by the high energy primary particle with energy $E_o \geq 10^{15}$ eV. The other discharges are running along the non-cooled channel of the first discharge and along other nearby channels of the smaller extensive air showers produced by primary particles with lower energies $E_o \geq 10^{14}$ eV within the cloud. Usually the intra-cloud discharges are propagated along tracks of these EAS. Since the geometrical size of a high energy EAS is larger than the size of a low energy EAS, the charge value transferred to the Earth's surface during the first discharge is larger than the charges transferred in the successive strikes. If the average radii of EAS produced by primaries with $E_o \geq 10^{14}$ eV and $E_o \geq 10^{15}$ eV equal to $R_{14} \approx 200$ m and $R_{15} \approx 300$ m then most of 'cloud to ground' lightning has to consist of not more than

$$N \approx 2\pi \times (R_{14} + R_{15}) / R_{14} \approx 8 \tag{11.4.3}$$

discharges. Each descending lightning takes the excess charge from the cloud volume enclosed EAS with $E_o \geq 10^{15}$ eV. For the most part of events the time interval between discharges has to be no less than

$$T = \left\{\pi \Phi_{14} \left[(R_{15} + 2R_{14})^2 - R_{15}^2\right]\right\}^{-1} \approx 10^{-2} \text{ sec}, \tag{11.4.4}$$

where $\Phi_{14} \approx 100$ km^{-2} sec^{-1} is the EAS intensity with $E_o \geq 10^{14}$ eV (Amatuni et al., 1987). From the observations it is known that each descending lightning transfers to the Earth's surface the negative charge Q ~ (10–20) C. If the average current of negative ions J^- flowing to the cloud top equals to $J^- \approx 0.5$ A then the descending lightning has to arise in

$$t \approx Q / J^- \approx (20 - 40) \text{ sec}, \tag{11.4.5}$$

which is observed in the atmosphere (Raiser, M1987). Each descending lightning takes the excess charge from the cloud volume

$$V \approx \pi \Delta H (R_{14} + R_{15})^2 \approx 3.14 \times 3 \times (0.3 + 0.4)^2 \approx 5 \text{ km}^3 . \quad (11.4.6)$$

Thus, the density of excess charge in the cloud is

$$\rho = Q/\text{eV} \approx (10 - 20) C / \left(1.6 \times 10^{-19} C \times 5 \times 10^{15} \text{ cm}^3\right) \approx (1 - 2) \times 10^4 \text{ cm}^{-3} , \quad (11.4.7)$$

which is corroborated by the observations (Chalmers, M1967).

11.4.3. EAS discharge mechanism and ascending ('ground to cloud') lightnings

Ermakov and Stozhkov (2002) considered also the application of EAS discharge mechanism to the possible explanation of ascending ('ground to cloud') lightnings. With time within the thundercloud the growth of unfrozen and frozen water drops takes place as a result of processes of water vapor condensation and droplet coagulation. In so doing the drops become heavier and begin to go down by gravity. This causes precipitation and scattering cloud. Together with the precipitation from the lower part of the cloud the negative charge goes away and the positive charge being on hydrometeors in the upper part of the cloud comes into this place (see Fig. 11.4.2c). As a consequence the direction of the electric field between the cloud and the Earth's surface is reversed (Baker and Dash, 1994). It opens up opportunities for the 'ground to cloud' lightning production that transfer a negative charge from the Earth's surface to the cloud. The ascending lightning as well as the descending ones are running along the ionized tracks of EAS particles produced by primaries with $E_o \geq 10^{15}$ eV. At the precipitation the ascending fluxes of air decrease strongly and with it the processes of new electric charge generation and its separation decrease also. For this reason the ascending lightning eliminates a part of positive volume charge that was in the upper part of the cloud earlier. The rest of the charge falls down to the Earth's surface together with the precipitation or it is scattered in the atmosphere. Since the positive charge value in the upper part of the cloud is less than negative charge, the number of 'ground to cloud' lightnings in a thundercloud is much less than number of 'cloud to ground' lightnings. As it is known from the observations the number of 'ground to cloud' lightnings is less than ~10 % of the total number of discharges between the Earths surface and clouds (Uman, 1988).

11.4.4. Application of EAS discharge mechanism to explanations of red sprites and blue jets

According to Ermakov and Stozhkov (2002, 2003), the EAS discharge mechanism can be used to explain red sprites and blue jets. When lightning discharges run along the ionized tracks of EAS secondary charged particles these tracks begin to fluoresce. In the case of intra-cloud and descending discharges this fluorescence in the most part is invisible because the cloud shields this light from the observer. However, when the cloud goes down and 'ground to cloud' lightning arise, an observer above the cloud top can see the fluorescence of the numerous tracks of secondary particles of EAS. Many such cases were observed from airplanes and satellites (Vaughan and Vonnegut, 1989; Rodger, 1999). Such fluorescence is observed when the cloud top is at the altitude of $H \sim$ (5–10) km.

In the third phase of thundercloud life (see Fig. 11.4.2c) the electric dipole is formed by the cloud positive charge and its 'image' under the conductive surface of the Earth at a depth that equals the cloud altitude. When ascending lightning occurs some part of a cloud positive charge flows down to the upper conducting layer of the Earths surface. The charges of a cloud and its 'image' decrease by the same value. The relaxation time of the charge which flowed on the upper layer surface is a definite value. It depends on the capacity of the Earth (~700 μF), the surface upper layer conductivity under a cloud (this value can change within wide limits), and the charge leakage through a thundercloud to the ionosphere. It follows from the measurements of the electric field below thunderclouds this time falls in the range from several ms to 100 ms, its averaged value equals ~20 ms (Beasley et al., 1982).

From the moment that ascending lightning appears the electric field over the thundercloud is the sum of fields produced by the symmetric dipole and the positive surface charge arising from the discharge. At high altitudes H over the thundercloud (in the ionosphere) there is a field from the positive surface charge mainly because the dipole part of the field decreases as H^{-3}, whereas the electric field from the surface charge decreases as H^{-2}.

It is known from measurements that the ascending lightning can transfer to the Earth's surface a positive charge of Q ≅ 50 C. At the altitudes of 22.5, 45 and 90 km (these altitudes were chosen for the convenience of calculations) this charge gives the electric field strengths of $E_{\text{atm}} \approx 9,\ 2.2,\ 0.55$ V/cm and the electric potentials of φ ~ 20, 10 and 5 MV. The values of φ and E_{atm} were calculated from the expressions

$$\varphi = Q/(4\pi\chi H), \quad E_{\text{atm}} = Q/\left(4\pi\chi H^2\right), \tag{11.4.8}$$

where H is the altitude and $\chi = 8.85\times10^{-12}$ C/(V.m).

In response to electric field free electrons move from the ionosphere to the cloud top. Over the interval between collisions with air molecules electrons increase their energy and then lose it in the processes of atom excitation and ionization. The calculations show that in the ionosphere the electrons between the collisions can get enough energy to excite vibratory levels of nitrogen molecules. At the de-excitation of these excited molecules photons of red color are mainly emitted. This radiation observed in the lower ionosphere during thunderstorms was given the name of red sprites (Sentman and Wescott, 1982).

Some part of EAS secondary electrons moving from the ionosphere to the cloud top can have minimum collisions with ambient air molecules and then can travel large distances. In this case such electrons can get the cloud top gaining a large energy. At the collisions with air atoms and molecules these electrons with energy up to several MeV produce photons in visible and ultraviolet regions and give short-wave radiation. So, the scattered light observed in jets between the ionosphere and cloud top is enriched with short-wave photons (according to Rayleigh's law scattered light intensity is inversely related to the fourth power of wavelength); it explains the blue color of luminous jets observed above thunderclouds (Sentman and Wescott, 1982).

11.4.5. EAS discharge mechanism and thundercloud activity over oceans

Ermakov and Stozhkov (2002, 2003) tried to explain the peculiarities of the thundercloud activity over oceans in the frame of the EAS discharge mechanism. It is known from the observations that the thunderstorm activity over oceans is lower than over continents (Fullekrug, 1999; Christian et al., 1999). In the framework of mechanisms given above this experimental fact can be explained in the following way. As was shown above, to apply this mechanism the fulfillment of several conditions is required. It is necessary to have (1) rather powerful upstream of wet and ionized air from the low boundary layer of the atmosphere to form thundercloud, (2) a sufficient number of aerosols performing role of condensation nuclei, and (3) the EAS availability. Over oceans the dynamic and thermal convections that are responsible for the strong upstream occurrence are weakly developed. Air over the oceans is mainly ionized by cosmic rays and the role of radioactivity in this process is negligible. So in the boundary layer of oceans the level of air ionization is lower than over continents. Also the aerosol concentration over the oceans is lower by several times in comparison with the continents. The number of EAS arising in the atmosphere over oceans does not depend on geographic latitude and time. Most of the electric activity of thunderclouds is observed when 'cloud to ground' discharges arise and each discharge transfers a large amount of electric charge (up to several tens coulomb) on the Earth's surface. Such transfer is possible merely in the case if the relaxation time of electric charge transferred from the cloud to the Earth's surface is rather short. Seawater has rather high electro-conductivity. However, its conductivity is ionic and not electronic conductivity. Because of that the electric charge transferred from the thundercloud to water cannot go away quickly from the lightning strike site and its electric field hinders the lightning discharge development. As a result the restriction of current in the lightning channel and, correspondingly, the restriction of charge value transferred to water surface. This is the main reason for the attenuation of lightning channel luminosity and because of it sailors do not see descending and ascending lightning over sea surface. It should be remembered that the EAS intensity arriving at the ocean surface is a little smaller than the EAS intensity getting the continent surface because the continents are spaced above sea level in average at 875 m.

11.5. On the connection between CR intensity and discharged atmospheric electric current

It is well known that the Earth has about constant negative charge $Q \cong -6 \cdot 10^5$ C. As result, in the quiet conditions there are electric fields directed to the Earth's surface of about – 130 V/m. Between the Earth's surface and neutral layer in ionosphere at the altitudes 55–80 km there flows an electric current with average density $J \approx 10^{-12}\ \mathrm{A/m^2}$. The total discharged current in all atmosphere is about 1800 A, and this current may discharge the negative charge of the Earth in 5– 6 minutes (Chalmers, M1961), but this discharge really is compensated by many thousands thunderstorms and precipitations charged the Earth negatively. The work of global electric circuit in the low atmosphere provides by CR which through the air atoms ionization assure air conductivity. As will be

shown in Section 11.7, CR may play an important, key role in keeping the Earth's global negative charge about constant.

According to Stozhkov et al. (2001) in the interval of altitudes 3 km ≤ H ≤ 35 km the connection between CR intensity and atmospheric electric current is linear. Indeed, the ion production rate $q(h)$ is connected with CR intensity $I(h)$ and cross-section for ionization $\sigma(h)$ by the following relation

$$q(h) = I(h)\sigma(h)\rho(h)/M\,, \tag{11.5.1}$$

where $\rho(h)$ is the air density, and M the average mass of air atoms. On the other hand, the density of electric current J in the quiet atmosphere is

$$J = \lambda(h)\Phi(h) = en(h)k(h)\Phi(h), \tag{11.5.2}$$

where $\lambda(h)$ is the air conductivity, $\Phi(h)$ the electric field tension in the atmosphere, e the electron's charge, $n(h)$ the ion density, $k(h)$ the mobility of light ions. Let us take into account that according to Ermakov et al. (1997)

$$q(h) = \beta(h,T(h))n(h)\,, \tag{11.5.3}$$

where $\beta(h,T)$ is the coefficient of linear recombination, and $T(h)$ is the air temperature. From Eq. 11.5.1–11.5.3 follows that

$$J = eI(h)\sigma(h)\rho(h)k(h)\Phi(h)/M\,\beta(h,T(h))\,. \tag{11.5.4}$$

All the parameters on the right hand side of Eq. 11.5.4, excluding the CR intensity $I(h)$, practically do not change with the time (or their dependence on time are very weak); it means that the electric current in the quiet atmosphere J and CR intensity $I(h)$ are expected to change with time in phase, about linearly.

Fig. 11.5.1 shows the time variations for 17 years observations of discharged electric current J according to Roble (1985) and of CR intensity $I(h)$ according to balloon CR measurements at polar latitudes on the altitude H = 8 km, h ~ 350 mb (Stozhkov et al., 2001).

From Fig. 11.5.1 one can see a good about linear connection between J and $I(h)$. The correlation coefficient between J and $I(h)$ is relatively high: 0.77 ± 0.10 (the correlation of J with sunspot numbers W is much lower, with coefficient – 0.32 ± 0.22).

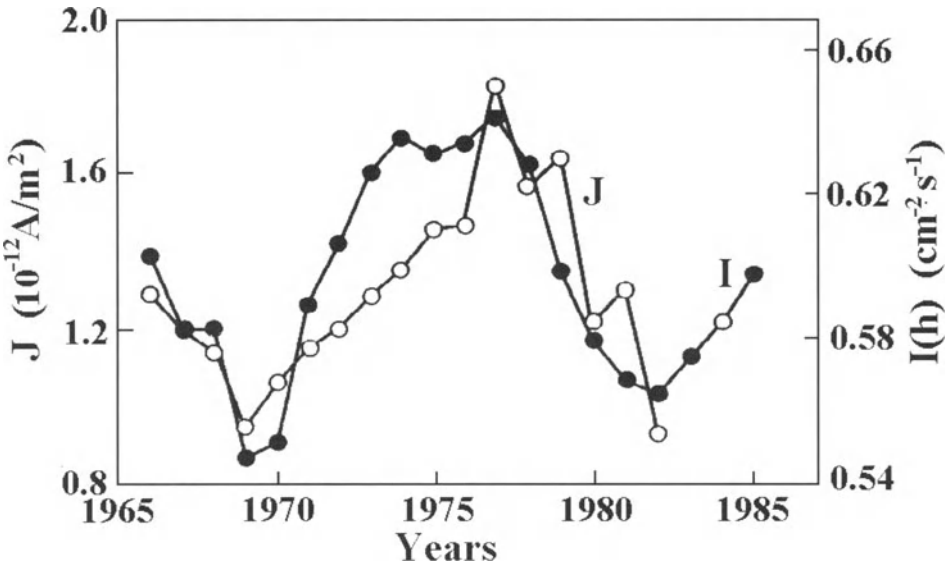

Fig. 11.5.1. Time variations for 17 years observations of discharged electric current ***J*** (light circles) according to Roble (1985) and of CR intensity ***I(h)*** (black circles). According to Stozhkov et al. (2001).

11.6. On the connection between CR intensity and frequency of thunderstorm discharges; charged electric current

In Sections 11.2 and 11.3 we considered the mechanism of thunderstorm discharges based on the formation of accelerated electrons avalanche grown from secondary CR relativistic electrons (Gurevich et al., 1992, 1999, 2001; Gurevich and Milikh, 1999; Gurevich and Zybin, 2001). In this case the annual number of thunderstorm discharges integrated over a great territory will be in the first approximation connected with CR intensity time variation: with increasing of intensity of secondary CR relativistic electrons there are expected about the same increasing of the number of thunderstorm discharges per year (in the 11-year solar activity cycle it is expected time variation of the yearly number of thunderstorm discharges with amplitude more than 10–20%).

On the other hand, Ermakov (1992), Ermakov and Stozhkov (1999, 2002, 2003), Stozhkov (2002) suggested that the main cause of thunderstorm discharges are EAS (External Atmospheric Showers) which are generated by primary CR with energy more than 10^{14} eV (in these EAS more than 10^4–10^5 relativistic electrons will be generated about simultaneously; see Section 11.4). The time variations of EAS frequency are investigated very well (see review in Dorman, M1957, M1963a,b), and it was found that the amplitude of primary variations (after correction data on barometric effect) is very small, not more than 1%. Therefore in this case the 11-year time variation of the year number of thunderstorm discharges is expected with amplitude smaller than 1%.

In Fig. 11.6.1 are shown the time profiles of the frequency of thunderstorm discharges over USA in 1989–1998 according to Orville and Huffines (1999, 2001) and time variation of ion production rate q in the column of atmosphere between 2 and 10 km (these values were calculated on the basis of regular balloon measurements of CR

intensity on the middle latitude with vertical cut-off rigidity 2.4 GV in the same period 1989–1998 in Stozhkov et al., 2001).

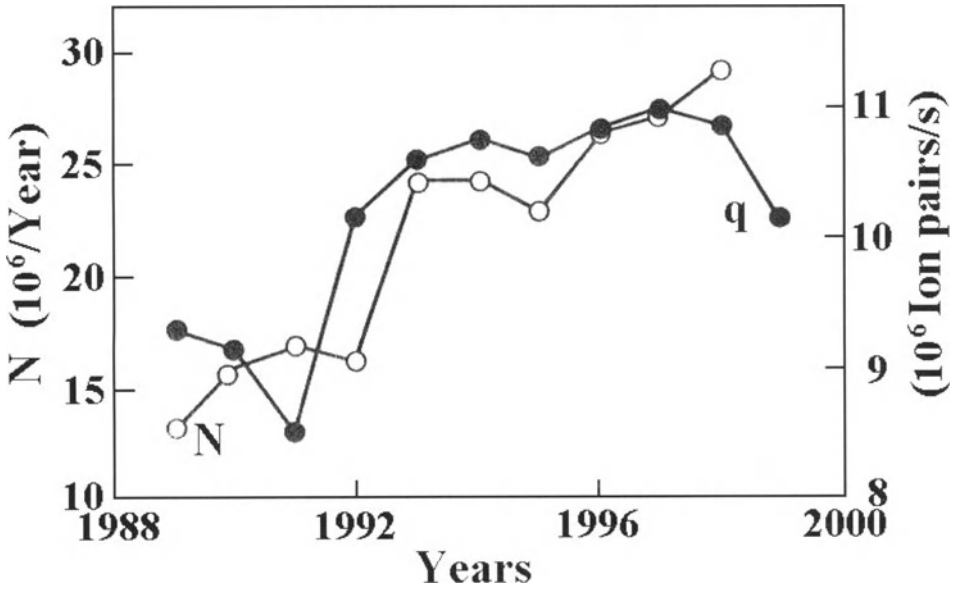

Fig. 11.6.1. The annual number of thunderstorm discharges ***N*** (open circles) over the territory of the USA in 1989–1998 according to Orville and Huffines (1999) and time variation of yearly average ion production rate ***q*** (black circles) in the column of atmosphere between 2 and 10 km (calculated on the basis of balloon CR measurements). According to Stozhkov et al. (2001).

Fig. 11.6.1 shows a clear positive correlation between the annual number of thunderstorm discharges N and time variation of annual average ion production rate q (with correlation coefficient $+0.85 \pm 0.09$). The amplitude of time variation is several tens percent, supporting, from the first view, the model of thunderstorm discharges considered in Sections 11.2 and 11.3, and contradicts to EAS model discharges of Ermakov (1992), Ermakov and Stozhkov (1999, 2002, 2003), Stozhkov (2002). But, in fact, according to Stozhkov et al. (2001), the obtained strong positive correlation can be understand if we take into account that with increasing of CR intensity increases the ion production rate in the atmosphere, and increases the concentration of ions. But, as we will see in Chapter 14, the increasing of ion concentration in atmosphere leads to increasing of clouds coverage, and correspondingly, to increasing of thunderstorm discharge rate, to increasing of global atmospheric charged currents. In this case the result shown in Fig. 11.6.1 does not contradict either of the considered mechanisms of CR influence on thunderstorm discharges. Let us note that the intensity increase of secondary CR seed relativistic electrons (which give the start of formation of accelerated electrons avalanches) will have a tendency also to increase the number of thunderstorm discharges.

11.7. On the CR role in the equilibrium between charged and discharged global atmospheric electric currents, and in the supporting the stability of the Earth's Charge

Stozhkov et al. (2001) assumed that CR play an important role in supporting the equilibrium between charged and discharged global electric currents, providing the stable value of the total negative charge of the Earth. Let us consider again Fig. 11.6.1, but from another point of view: it can be seen that with increasing ion production rate q (caused by increasing of CR intensity) the number of thunderstorm discharges N increases, i.e. the power of charged generator (charged electric current) increases, leading to an increase of Earth's total negative charge. Let us note that increasing the primary CR flux, which consists mostly of positive protons and different nuclei, leads to increasing the discharged electric current, but the total value of this current

$$J_{CR} = eI_{CR} \approx 1.6\times10^{-19}\,\mathrm{C}\times10^{4}\,\mathrm{m}^{-2}\,\mathrm{sec}^{-1} \approx 2\times10^{-15}\,\mathrm{A/m}^{2} \qquad (11.7.1)$$

is negligible in comparison with currents caused by the global thunderstorm activity $J \approx 10^{-12}\,\mathrm{A/m}^{2}$, and usually the variation of this CR current J_{CR} is not taken into account.

From other hand, Fig. 11.5.1 shows that the increase of CR intensity I (increase of ion production rate q) leads to an increase of discharged global electric currents. This will mostly compensate the increasing charged electric currents caused according to Fig. 11.6.1 by increasing thunderstorms discharges frequency (caused by the same increasing of CR intensity).

Chapter 12

Air Ionization by CR, Influence on the Ionosphere and Radio Wave Propagation

12.1. Observed disturbances in the ionosphere and interruptions in radio wave communications during great GLE of February 23, 1956

The first observations of CR influence on the ionosphere and radio wave propagation were made during event of February 23, 1956 – the biggest Ground Level Event (GLE), observed in the last approximately 80 years. Let us consider some important results obtained in connection with this GLE.

Ellison and Reid (1958) found that the intensity of atmospherics caused by lightnings in different places in the world, and observed at Edinburgh at 24 kHz suddenly decreased during 10 minutes, starting at 3.45 UT on 23 February 1956: no such effect had been observed before during 6 years of continuous recording. Strong absorption of the radio emission from the discrete source Virgo A at 22.2 MHz was observed in this period at Washington by Forbush and Burke (1956).

A detailed analysis of the anomalous ionization on 23 February 1956 in the altitude interval 30–110 km was made by Bailey (1959). He distinguished an 'early' type of cosmic radio radiation absorption observed on the dark hemisphere of the Earth and immediately related to the rapid increase of solar CR flux (which was observed by Belrose et al., 1956; Pierce, 1956; Bailey, 1957), and the 'late' type related to isotropic phase of solar CR flux (Bailey, 1957; Little and Leinbach, 1958; Shapley and Knecht, 1957; Minnes et al., 1957; Lied, 1957). According to Bailey (1959) the process of ionization of the Earth's atmosphere by CR particles is described by the following set of equations:

$$dN_e/dt = q - \alpha_d N_e N^+ - \eta n_1 N_e + k n_2 N^- + \rho s N^-, \tag{12.1.1}$$

$$dN^-/dt = -\alpha_i N^- N^+ + \eta n_1 N_e - k n_2 N^- - \rho s N^-, \tag{12.1.2}$$

$$dN^+/dt = q - \alpha_d N^- N^+ - \alpha_i N^- N^+, \tag{12.1.3}$$

where N_e, N^-, N^+ are respectively the densities of electrons, negative and positive ions, n_1 is the density of the neutral particles, to which electrons can be attached (in particular O_2), n_2 is the density of the neutral particles which can tear electrons away when colliding with negative ions ($n_2 \approx 5n_1$), q is the rate of electron production by solar CR particles, η is the attachment coefficient of electrons to O_2, k is the detachment coefficient of electrons from O_2^- during collisions, ρs is the rate of photo-

detachment of electrons from O_2^- (s is the intensity of solar photons what is equal to zero at night), α_d is the effective value of the recombination coefficient for collisions between electrons and positive ions, and α_i is the coefficient of neutralization between negative and positive ions.

Bailey (1959) adopted the following values:

$$\alpha_d = 3\times10^{-8}\,\mathrm{cm^3 s^{-1}}, \quad \alpha_i = 3\times10^{-9}\,\mathrm{cm^3 s^{-1}}, \quad \rho s = 0.44\,\mathrm{s^{-1}},$$
$$k = 2.4\times10^{-17}\,\mathrm{cm^3 s^{-1}} \text{ for } n_2 \approx 5n_1. \tag{12.1.4}$$

In the most interesting altitude range from 30 to 110 km, the characteristic times of the various processes in the ionosphere are very small compared to the times of variation of q. Therefore only the stationary case is interesting, where all derivatives with respect to time in Eq. 12.1.1–12.1.3 may be put equal to zero. Eq. 12.1.3 may then be written in the form

$$q = (1+\lambda)\alpha N_e^2, \tag{12.1.5}$$

where

$$\lambda = N^-/N_e, \quad \alpha = \alpha_d + \alpha_i, \tag{12.1.6}$$

and from Eq. 12.1.2 we can determine

$$\lambda \approx \eta n_1/(kn_2 + \rho s). \tag{12.1.7}$$

In Fig. 12.1.1 and 12.1.2 are shown the expected distributions of the electron density N_e and absorption of cosmic radio waves of 32 MHz with height at different geomagnetic latitudes at noon and at midnight for the event February 23, 1956.

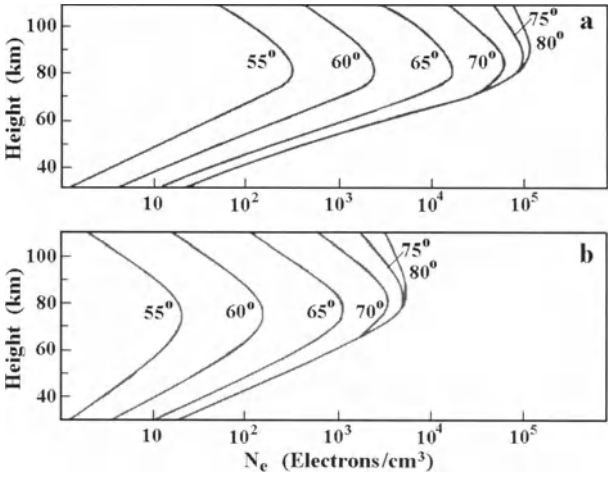

Fig. 12.1.1. The expected distribution of the electron density N_e with height at different geomagnetic latitudes at noon (***a***) and at midnight (***b***) for the event February 23, 1956. According to Bailey (1959).

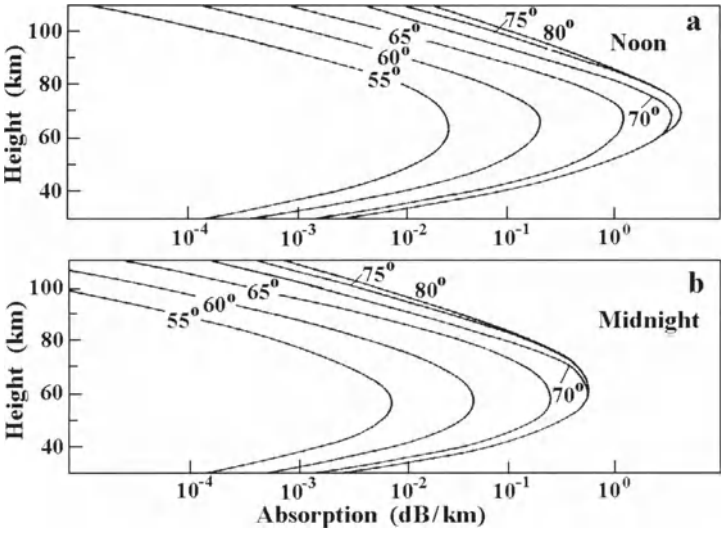

Fig. 12.1.2. The expected distributions of the absorption of cosmic radio waves of 32 MHz with height at different geomagnetic latitudes at noon and at midnight for the event February 23, 1956. According to Bailey (1959).

12.2. Expected ionization rate and radio-wave absorption for different SEP energy spectrums

Reid (1961) found the expected rate of electron formation as a function of height (Fig. 12.2.1) and electron density distribution in day and night (Fig. 12.2.2) assuming a differential spectrum of solar energetic particles (SEP) (mostly, protons) in the form

$$D(E_k) = 2.24 \times 10^{10} E_k^{-5} \text{ proton.MeV}^{-1}.\text{cm}^{-2}.\text{sec}^{-1} \qquad (12.2.1)$$

with low energy cut off $E_{k\,\min} = 20$ and 40 MeV.

Adams and Masley (1965) computed the expected $q(H)$ at altitudes H from 30 to 100 km for great GLE of 18 and 20 July 1959 (Fig. 12.2.3).

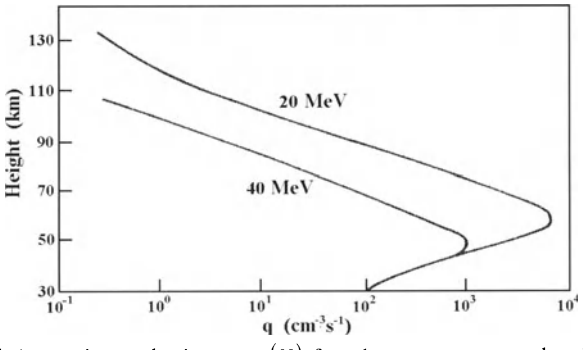

Fig. 12.2.1. Expected electron-ion production rate $q(H)$ for solar proton spectrum described by Eq. 12.2.1 for two values of the low-energy cutoff, 20 and 40 MeV. According to Reid (1961).

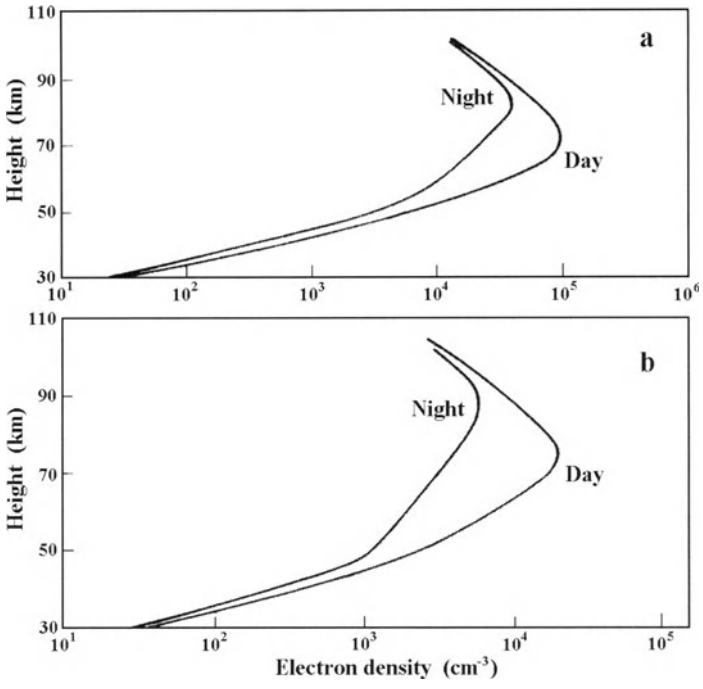

Fig. 12.2.2. Expected height distribution of the electron (or ion) density for day and night corresponding to production rate $q(H)$ in Fig. 12.2.1: (a) – for a low energy cut off 20 MeV; (b) – for a low energy cut off 40 MeV. According to Reid (1961).

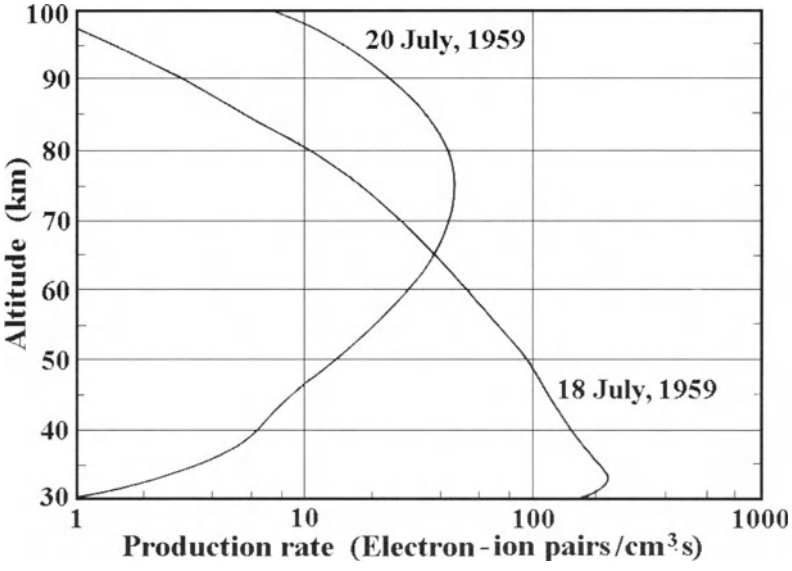

Fig. 12.2.3. Expected electron-ion production rate $q(H)$ for solar proton events 18 and 20 July, 1959. According to Adams and Masley (1965).

12.3. Riometer measurements of polar absorptions as method of low energy solar CR monitoring

Little and Leinbach (1959) supposed to use measurements of polar absorptions for a low energy solar CR monitoring. They developed a spectral apparatus for continuous recording of the intensity of cosmic radio emission at 27.6 MHz (so called riometers) in Thule (Greenland), at Barrow and College (Alaska), at Farewell and Kiruna (Sweden). On the basis of the well known formula of Appleton–Hartree, the amplitude of the polar absorption A (in dB) at frequency 27.6 MHz is connected with electron density $N_e(H)$ as

$$A = 0.46 \times \int_0^\infty \frac{N_e(H)\nu(H)dH}{3.34\times10^{16} + \nu^2(H)}, \tag{12.3.1}$$

where $\nu(H)$ is the frequency of electron encounters. On the other hand, according to Eq. 12.1.5 for a stationary process

$$N_e(H) = (q(H)/\alpha_{\text{eff}}(H))^{1/2}, \tag{12.3.2}$$

where $q(H)$ is the rate of electron formation, and $\alpha_{\text{eff}}(H)$ is the effective recombination coefficient. Because $q(H)$ is about proportional to the intensity $I(\geq E_{k\,\min})$ of solar CR, we obtain

$$A \propto \sqrt{I(\geq E_{k\,\min})}, \text{ or } I(\geq E_{k\,\min}) \propto A^2. \tag{12.3.3}$$

This means that measurements of the polar absorption can be used as a sensitive method of recording solar CR flux in the small energy region (from about 1–5 Mev to 30-50 MeV) penetrating into the atmosphere to heights from 90 to 50 km.

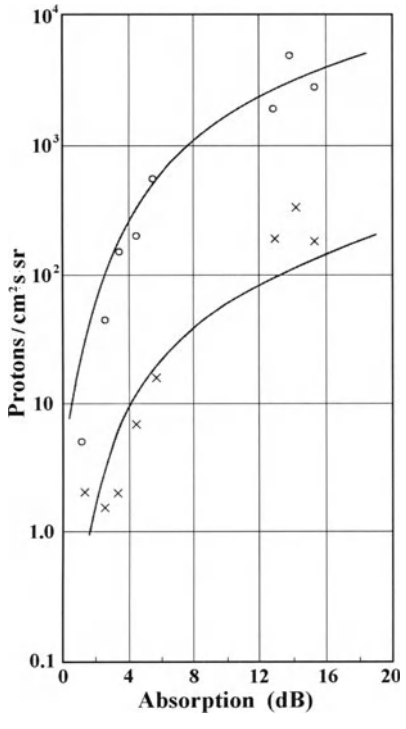

Fig. 12.3.1. Relation between the intensity of solar particles with energy ≥ 10 MeV (circles) and ≥ 100 MeV (crosses) and the absorption of cosmic radio noise at 27.6 MHz; both curves represent the square root of the relation. According to Davis and Ogilvie (1962).

Fig. 12.3.1, which is based on the rocket observations Davis and Ogilvie (1962) above Churchill during great SEP events in November 1960 shows that in the first approximation the absorption of cosmic radio noise is proportional to the square root of the intensity of solar protons, in agreement with Eq. 12.3.3. If A is expressed in dB, $I(\geq E_{k\,\min})$ in protons/$\left(\text{cm}^2.\text{sec.sterad}\right)$, we obtain

$$I(\geq E_{k\,\min}) = A^2 \times \begin{cases} 16.5 & \text{for } E_{k\,\min} = 10 \text{ MeV}, \\ 0.8 & \text{for } E_{k\,\min} = 100 \text{ MeV}. \end{cases} \tag{12.3.4}$$

12.4. Galactic and solar CR influence on the low ionosphere: analytical approach

12.4.1. Comparison of different ionizing agents

Ivanov-Kholodny and Nikolsky (M1969) computed the ionization at heights lower than 100 km for periods with different levels of solar activity, owed to different ionizing agents: L_α – radiation, ultraviolet and X-ray radiation, and galactic CR. It was shown that galactic CR give larger ionization than all other agents together at heights below 75 km and 65 km at solar minimum and maximum, respectively. As it was shown in Sections 12.1–12.3, in periods of great SEP events ionization by CR became important also for much higher atmospheric levels (in comparison with other ionizing agents). In Dorman and Dorman (1973a,b), Dorman (1977a) analytical formulas were obtained that described the formation of ionization by protons and nuclei of different Z of solar and galactic CR by taking into account electron capturing and energy change of incident particles down to thermal energies kT.

12.4.2. Analytical approach for protons

Let us first consider protons with kinetic energy $E_k \leq 200$ MeV . In this range, up to the energy $E_k = 2.5\times10^{-2}$ MeV (corresponding to protons with the velocity equal to velocity of orbital electron in hydrogen atom), the energy loss for ionization will be approximately presented as

$$dE_k / dh = -245 \times E_k^{-0.785} \text{ MeV}/\left(\text{g.cm}^{-2}\right), \tag{12.4.1}$$

where E_k is measured in MeV, and h is the air thickness in g.cm^{-2}. At $E_k < 2.5\times10^{-2}$ MeV the character of energy loss changes (energy loss decreases with decreasing of proton energy):

$$dE_k / dh = -2.804\times10^4 \times E_k^{1/2} \text{ MeV}/\left(\text{g.cm}^{-2}\right), \tag{12.4.2}$$

where the numerical factor 2.804×10^4 has been determined from the condition of jointing of Eq. 12.4.1 and Eq. 12.4.2 at $E_k = 2.5\times10^{-2}$ MeV .

For higher energies, up to 100 GeV, the ionization energy losses can be approximated as (in units $\text{MeV}/\left(\text{g.cm}^{-2}\right)$):

$$\frac{dE_k}{dh}=\begin{cases}-41.6\times E_k^{-0.54} & \text{if } 200 \text{ MeV} \le E_k \le 900 \text{ MeV},\\ -1.9 & \text{if } 900 \text{ MeV} \le E_k \le 5\times10^3 \text{ MeV},\\ 0.723\times E_k^{0.123} & \text{if } 5\times10^3 \text{ MeV} \le E_k \le 10^5 \text{ MeV}.\end{cases} \tag{12.4.3}$$

In the ionosphere the most important role is played by small energy particles, so let us first consider the case where the initial proton energy at the boundary of atmosphere $E_{ko} \le 200$ MeV. On the basis of Eq. 12.4.1 and Eq. 12.4.2 we obtain for the proton energy dependence on h:

$$E_k(E_{ko},h)=\begin{cases}\left(E_{ko}^{1.785}-245\times1.785h\right)^{1/1.785} & \text{if } h \le h_4,\\ \left[\left(2.5\times10^{-2}\right)^{1/2}-1.402\times10^4(h-h_4)\right]^2 & \text{if } h_4 \le h \le h_5,\\ kT & \text{if } h \ge h_5,\end{cases} \tag{12.4.4}$$

where

$$h_4(E_{ko})=\frac{E_{ko}^{1.785}-\left(2.5\times10^{-2}\right)^{1.785}}{245\times1.785} \text{ g.cm}^{-2}, \tag{12.4.5}$$

is the atmospheric depth at which the energy of proton equals $E_k = 2.5\times10^{-2}$ MeV (and velocity equals the orbital electron velocity in hydrogen atom);

$$h_5(E_{ko})=7.133\times10^{-5}\left[\left(2.5\times10^{-2}\right)^{1/2}-(kT)^{1/2}\right]+h_4(E_{ko}) \text{ g.cm}^{-2}, \tag{12.4.6}$$

is the atmospheric depth, where the energy of a proton $E_k = kT$.

Analogous expressions for $E_k(E_{ko},h)$ can be obtained for higher energies by using Eq. 12.4.3. Let us suppose that 5×10^3 MeV $< E_{ko} < 10^5$ MeV. In this case we obtain

$$E_k(E_{ko},h)=\begin{cases}\left(E_{ko}^{0.885}-0.885\times0.723h\right)^{1/0.885} & \text{if } h \le h_1,\\ 5\times10^3-1.9(h-h_1) & \text{if } h_1 \le h \le h_2,\\ \left[900^{1.54}-41.6\times1.54(h-h_2)\right]^{1/1.54} & \text{if } h_2 \le h \le h_3,\\ \left(200^{1.785}-245\times1.785(h-h_3)\right)^{1/1.785} & \text{if } h_3 \le h \le h_4,\\ \left[\left(2.5\times10^{-2}\right)^{1/2}-1.402\times10^4(h-h_4)\right]^2 & \text{if } h_4 \le h \le h_5,\\ kT & \text{if } h \ge h_5,\end{cases} \tag{12.4.7}$$

where

$$h_1(E_{ko}) = \frac{E_{ko}^{0.885} - \left(5\times10^3\right)^{0.885}}{0.885\times0.723} \text{ g.cm}^{-2}, \tag{12.4.8}$$

is the atmospheric depth at which the energy of proton $E_k = 5\times10^3$ MeV;

$$h_2(E_{ko}) = \left(5\times10^3 - 900\right)/1.9 + h_1(E_{ko}) \text{ g.cm}^{-2}, \tag{12.4.9}$$

is the atmospheric depth at which the energy of proton $E_k = 900$ MeV;

$$h_3(E_{ko}) = \left(900^{1.54} - 200^{1.54}\right)/(41.6\times1.54) + h_2(E_{ko}) \text{ g.cm}^{-2}, \tag{12.4.10}$$

is the atmospheric depth at which the energy of proton $E_k = 200$ MeV;

$$h_4(E_{ko}) = \frac{200^{1.785} - \left(2.5\times10^{-2}\right)^{1.785}}{245\times1.785} + h_3(E_{ko}) \text{ g.cm}^{-2}, \tag{12.4.11}$$

is the atmospheric depth at which the energy of proton $E_k = 2.5\times10^{-2}$ MeV. The depth $h_5(E_{ko})$ at which the energy of proton $E_k = kT$ will be determined by Eq. 12.4.6, but $h_4(E_{ko})$ in this expression is determined by Eq. 12.4.11. Let us note that here are only ionization energy looses of protons are taken into account. Nuclear interactions are not considered.

The electron-ion production rate $q_1(h)$ for the primary proton (Z = 1) spectrum $D_1(E_{ko})$ will be

$$q_1(h) = \frac{\rho(h)}{Q}\int_{E_{k\min}}^{\infty} D_1(E_{ko})\left(-dE_k(E_{ko},h)/dh\right)dE_{ko}, \tag{12.4.12}$$

where $\rho(h)$ is the density of the atmosphere at the depth h, Q is the energy loss in production of one electron-ion pair (for air $Q \approx 35$ eV $= 3.5\times10^{-5}$ MeV), and $E_{k\min}$ is the minimal energy in proton spectrum determined by geomagnetic cut off or by some other cause. Let us for simplicity consider $D_1(E_{ko})$ for $E_{ko} < 200$ MeV (important for the upper atmosphere). Let us consider three possible cases.

Case 1. When $E_{k\min} \geq E_{k1}(h)$, where

$$E_{k1}(h) = \left[245\times1.785h + \left(2.5\times10^{-2}\right)^{1.785}\right]^{1/1.785}; \tag{12.4.13}$$

in this case we obtain

$$q_1(h)=\frac{\rho(h)}{Q}\int_{E_{k\min}}^{\infty}D_1(E_{ko})245\times\left[E_{ko}^{1.785}-245\times1.785h\right]^{-0.785/1.785}dE_{ko}\,. \qquad (12.4.14)$$

Case 2. When $E_{k1}(h)\geq E_{k\min}\geq E_{k2}(h)$, where

$$E_{k2}(h)=\left[1.381\times10^{-3}+437.3\left(h-7.133\times10^{-5}\left(0.158-(kT)^{0.5}\right)\right)\right]^{1/1.785}, \qquad (12.4.15)$$

we obtain

$$\begin{aligned}q_1(h)=2.804\times10^4\times\frac{\rho(h)}{Q}&\int_{E_{k\min}}^{E_{k1}(h)}D_1(E_{ko})\\&\times\left[0.158+1.402\times10^4\left(\frac{E_{ko}^{1.785}-1.381\times10^{-3}}{245\times1.785}-h\right)\right]^{-0.785/1.785}dE_{ko}\\&+\frac{\rho(h)}{Q}\int_{E_{k1}(h)}^{\infty}D_1(E_{ko})245\times\left[E_{ko}^{1.785}-245\times1.785h\right]^{-0.785/1.785}dE_{ko}\,. \qquad (12.4.16)\end{aligned}$$

Case 3. When $E_{k\min}\leq E_{k2}(h)$. In this case the expression for $q_1(h)$ coincides with Eq. 12.4.16, but the lower limit $E_{k\min}$ in the first integral should be replaced by $E_{k2}(h)$.

12.4.3. Analytical approach for nuclei with charge Z

For nuclei with charge Z we get instead of Eq. 12.4.1 the following relation

$$dE_k/dh=-245\times\left(Z^2/A\right)E_k^{-0.785}\ (\text{MeV/nucleon}).\text{g.cm}^{-2}\,, \qquad (12.4.17)$$

where E_k is measured in MeV/nucleon, and A is the atomic number of nuclei of charge Z. Eq. 12.4.17 is valid up to

$$E_{ka}=2.5\times10^{-2}Z^2\ \text{MeV/nucleon}; \qquad (12.4.18)$$

at lower energies an electron is captured by nuclei first in the K shell, then in the L shell and so on, and the effective charge of the nuclei becomes $Z^*(E_k)<Z$. Such process will take place until the particle is singly charged with energy

$$E_{kb}=2.5\times10^{-2}\ \text{MeV/nucleon}\,. \qquad (12.4.19)$$

Though the effective value of charge $Z^*(E_k)$ varies discretely in the energy range from E_{ka} to E_{kb}, it may be assumed approximately that

$$Z^*(E_k) \approx \left(E_k / \left(2.5\times10^{-2}\right)\right)^{1/2} \text{ for } E_{kb} \le E_k \le E_{ka}. \tag{12.4.20}$$

Substituting $Z^*(E_k)$ determined by Eq. 12.4.20 in Eq. 12.4.17 instead of Z for the energy range $E_{kb} \le E_k \le E_{ka}$, we obtain

$$dE_k / dh = -9.8\times10^3 A^{-1} E_k^{0.215} \text{ (MeV/nucleon).g.cm}^{-2}. \tag{12.4.21}$$

As a result, for the energy of nuclei Z with initial energy at the boundary of atmosphere $E_{ko} \le 200$ MeV/nucleon we obtain

$$E_k(E_{ko},h) = \begin{cases} \left(E_{ko}^{1.785} - 245\times1.785\left(Z^2/A\right)h\right)^{1/1.785} & \text{if } h \le h_4 \\ \left[\left(0.025Z^2\right)^{0.785} - 7.693\times10^3(h-h_4)\right]^{1/0.785} & \text{if } h_5 \ge h \ge h_4 \\ \left[\left(2.5\times10^{-2}\right)^{1/2} - 1.402\times10^4(h-h_5)\right]^2 & \text{if } h_6 \ge h \ge h_5 \\ kT & \text{if } h \ge h_6, \end{cases} \tag{12.4.22}$$

where

$$h_4(E_{ko},Z) = \frac{E_{ko}^{1.785} - \left(0.025\times Z^2/A\right)^{1.785}}{1.785\times245\times\left(Z^2/A\right)} \text{ g.cm}^{-2}, \tag{12.4.23}$$

$$h_5(E_{ko},Z) = h_4(E_{ko},Z) + \frac{\left(0.025Z^2/A\right)^{0.785} - (0.025)^{0.785}}{0.785\times9.8\times10^3} \text{ g.cm}^{-2}, \tag{12.4.24}$$

$$h_6(E_{ko},Z) = h_5(E_{ko},Z) + 7.133\times10^{-5}\left[(0.025)^{1/2} - (kT)^{1/2}\right] \text{ g.cm}^{-2}. \tag{12.4.25}$$

Substituting Eq. 12.4.17, 12.4.21 and 12.4.2 in the expression of the form Eq. 12.4.12 but written for nuclei with charge Z, we shall obtain the following expressions, including Eq. 12.4.22–12.4.25, depending on the geomagnetic threshold $E_{k\,\min}$ (expressed in MeV/nucleon) for the nuclei with charge Z:

The 1-st case: $E_{k\,\min} > E_{k1}(h,Z)$, where

$$E_{k1}(h,Z) = \left[245\times1.785\times hZ^2 + 0.025\times1.785\times Z^2\right]^{1/1.785}. \tag{12.4.26}$$

In this case we obtain

$$q_Z(h)=\frac{\rho(h)}{Q}\int_{E_{k\min}}^{\infty}D_Z(E_{ko})245Z^2\left[E_{ko}^{1.785}-245\times1.785\times hZ^2\right]^{-\frac{0.785}{1.785}}dE_{ko} \quad (12.4.27)$$

The 2-nd case: $E_{k1}(h,Z)\geq E_{k\min}\geq E_{k2}(h,Z)$, where

$$E_{k2}(h,Z)=\left[0.00138Z^{3.57}+437.3Z^2\left(h-\frac{0.0553\left(Z^{1.57}-1\right)}{0.785\times9.8\times10^3}\right)\right]^{0.5602}. \quad (12.4.28)$$

In this case we will have

$$q_Z(h)=\frac{\rho(h)}{Q}\int_{E_{k\min}}^{E_{k1}(h,Z)}D_Z(E_{ko})\times9800$$
$$\times\left[\left(0.025Z^2\right)^{0.785}-7693\times\left(h-\frac{E_{ko}^{1.785}-\left(0.025Z^2\right)^{1.785}}{245\times1.785Z^2}\right)\right]^{-\frac{0.215}{0.785}}dE_{ko}$$
$$+\frac{\rho(h)}{Q}\int_{E_{k1}(h,Z)}^{\infty}D_Z(E_{ko})\times245Z^2\left(E_{ko}^{1.785}-245\times1.785Z^2h\right)^{-\frac{0.785}{1.785}}. \quad (12.4.29)$$

The 3-rd case: $E_{k2}(h,Z)\geq E_{k\min}\geq E_{k3}(h,Z)$, where

$$E_{k3}(h,Z)=\left\{\left(0.025Z^2\right)^{1.785}+245\times1.785\times Z^2\times\left[h-\frac{\left(0.025Z^2\right)^{0.785}-(0.025)^{0.785}}{0.785\times9.8\times10^3}\right.\right.$$
$$\left.\left.-7.13\times10^{-5}\left((0.025)^{0.5}-(kT)^{0.5}\right)\right]\right\}. \quad (12.4.30)$$

In this case we obtain

$$q_Z(h)=\frac{\rho(h)}{Q}\int_{E_{k\min}}^{E_{k2}(h,Z)} D_Z(E_{ko})\times 2.804\times 10^4\left\{(0.025)^{0.5}-1.402\times\left[h\right.\right.$$
$$\left.\left.-\frac{E_{ko}^{1.785}-\left(0.025Z^2\right)^{1.785}}{245\times 1.785Z^2}-\frac{\left(0.025Z^2\right)^{0.785}-(0.025)^{0.785}}{0.785\times 9.8\times 10^3}\right]\right\}dE_{ko}$$
$$+\frac{\rho(h)}{Q}\int_{E_{k2}(h,Z)}^{E_{k1}(h,Z)} D_Z(E_{ko})\times 9.8\times 10^3\left\{\left(0.025Z^2\right)^{0.785}-0.785\times 9.8\times 10^3\right.$$
$$\left.\times\left[h-\frac{E_{ko}^{1.785}-\left(0.025Z^2\right)^{1.785}}{245\times 1.785Z^2}\right]\right\}^{\frac{0.215}{0.785}} dE_{ko}$$
$$+\frac{\rho(h)}{Q}\int_{E_{k1}(h,Z)}^{\infty} D_Z(E_{ko})\times 245Z^2\left(E_{ko}^{1.785}-245\times 1.785Z^2h\right)^{\frac{0.785}{1.785}} dE_{ko}. \qquad (12.4.31)$$

The 4-th case: $E_{k\min}\le E_{k3}(h,Z)$, where $E_{k3}(h,Z)$ is determined by Eq. 12.4.30. In this case the resultant expression for $q_Z(h)$ will be the same as Eq. 12.4.31, but the lower limit of integration $E_{k\min}$ in the first integral will be replaced by $E_{k3}(h,Z)$.

The above consideration of the four possible cases completely solves the formulated problem of finding the rate of ionization by the nuclei with charge Z including the electron capture and the deviation from the Bethe–Bloch formula in low energy range.

12.5. Expected ionization rates during GLE in October 1989, July 2000, and April 2001

12.5.1. Differential proton fluxes in the range 15-850 MeV during three GLE

In Fig. 12.5.1 are shown the proton fluxes during the GLE in October 1989 (in the energy intervals 15–44, 39–82, 84–200, 110–500 MeV); in July 2000 and April 2001 (in energy intervals 15–44, 39–82, 84–200, 110–500, 640–850 MeV). GLE in October 1989 and in July 2000 with especially great fluencies (total integral fluxes of flare energetic particles during all event) are called as rogue GLE (Kallenrode and Cliver, 2001a,b).

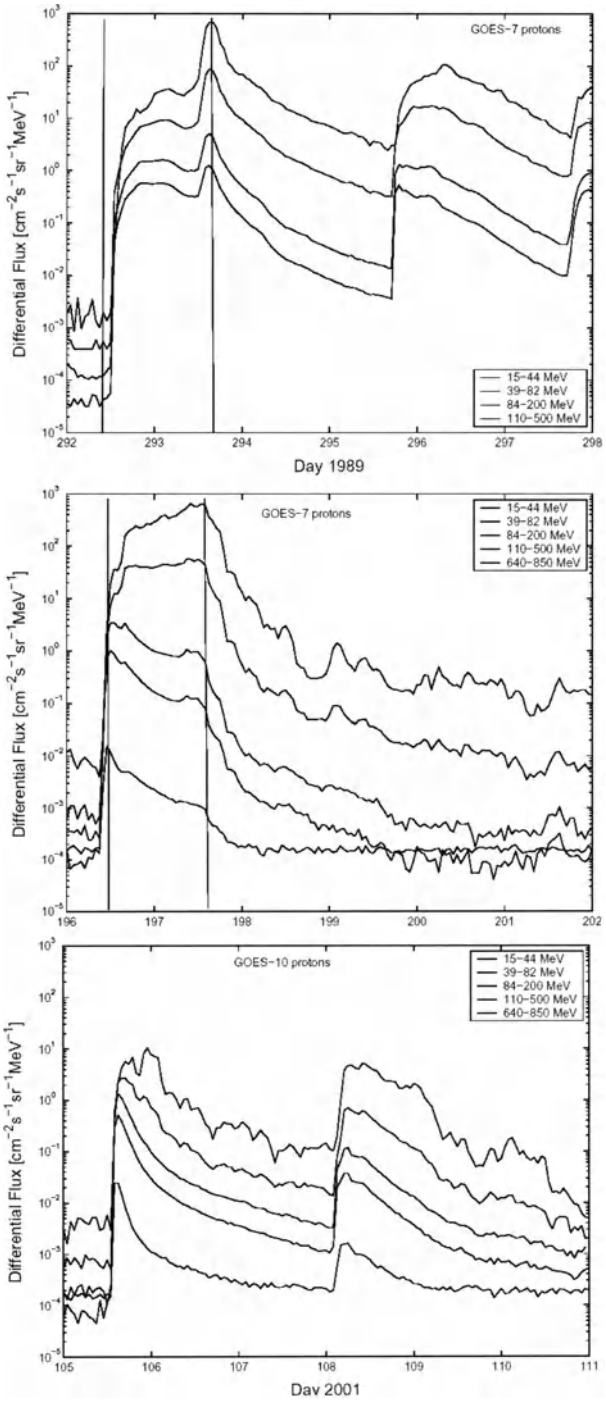

Fig. 12.5.1. Time profiles of proton fluxes in different energy ranges for GLE in October 1989, July 2000, and April 2001 (measurements on satellites GOES-7 and GOES-10). According to Quack et al. (2001).

12.5.2 Expected ionization rates during three GLE

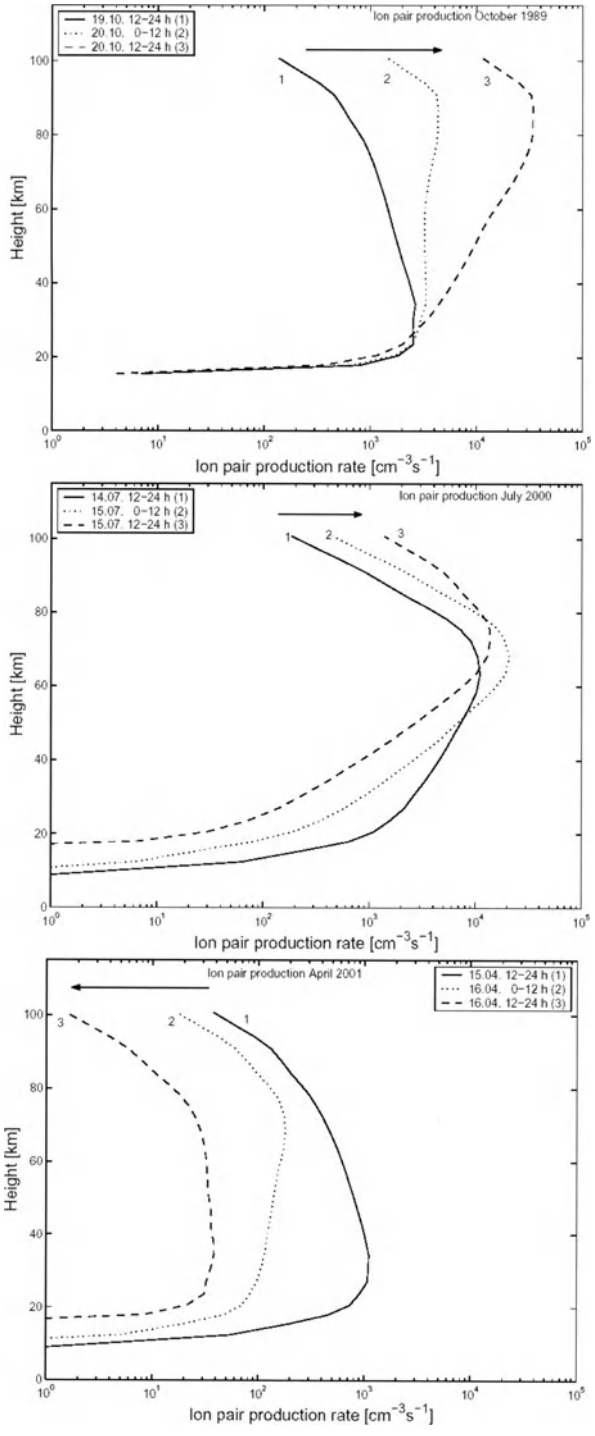

Time profiles of proton fluxes in different energy ranges, which were used in Quack et al. (2001) for calculations of ionization rates for GLE in October 1989, July 2000, and April 2001, are shown in Fig. 12.5.1.

For each moment of time proton fluxes were approximated by the power low of the type $I(E_k) = I_o(E_k/E_{ko})^{-\gamma}$, which was extrapolated up to $E_{k\,\min} = 4$ MeV. These fluxes in each energy range were averaged for a period of 12 hours, and for these averaged energy spectra the Bethe–Bloch equation was solved numerically for atmospheric composition of 78% N_2, 21% O_2, and 1% Ar. Energy loss rates from the Bethe-Bloch equation are then converted to ionization rates assuming the typical average ionization energy for air of $Q \approx 35$ eV. Results of Quack et al. (2001) of ionization rate profiles calculations are shown in Fig. 12.5.2 for the same three GLE in October 1989, July 2000, and April 2001.

Fig. 12.5.2. Expected ionization rate profiles for GLE in October 1989, July 2000, and April 2001. According to Quack et al. (2001).

In Quack et al. (2001) calculations of ionization rates for these GLE, energy spectra of FEP were considered only up to 800 MeV; higher energies start to decrease very early and their contribution becomes negligible at later times.

From Fig. 12.5.2 (the top panel) it can be seen that the October 1989 SEP event initially led to a strong ionization in the lower stratosphere while the ionization in the mesosphere was about an order of magnitude smaller. As time increased, the ionization in the lower stratosphere did not change (since high energy particle intensities were roughly constant), while the mesospheric ionization increased significantly as intensities in the low energies continued to rise. The temporal development of ionization rates in the July 2000 event (Fig. 12.5.2, middle panel) was more complex: initial ionization in the lower stratosphere was comparable to that in October 1989 while ionization in the middle mesosphere was larger and in the upper mesosphere lower. Since particle intensities in the higher energies started to decrease rather early, ionization rates in the stratosphere decreased, too, as the event evolved. Only upper mesospheric ionization rates increased with time. In the GLE of April 2001 (Fig. 12.5.2, bottom panel), initial ionization profiles were comparable to those of the October 1989 event in shape although numbers were smaller by about a factor of 2 to 3. However, ionization decreased with increasing time at all heights.

Consequently, the total ionization as shown in Fig. 12.5.3 was significantly larger in the two rogue events in October 1989 and in July 2000 compared to the GLE in April 2001.

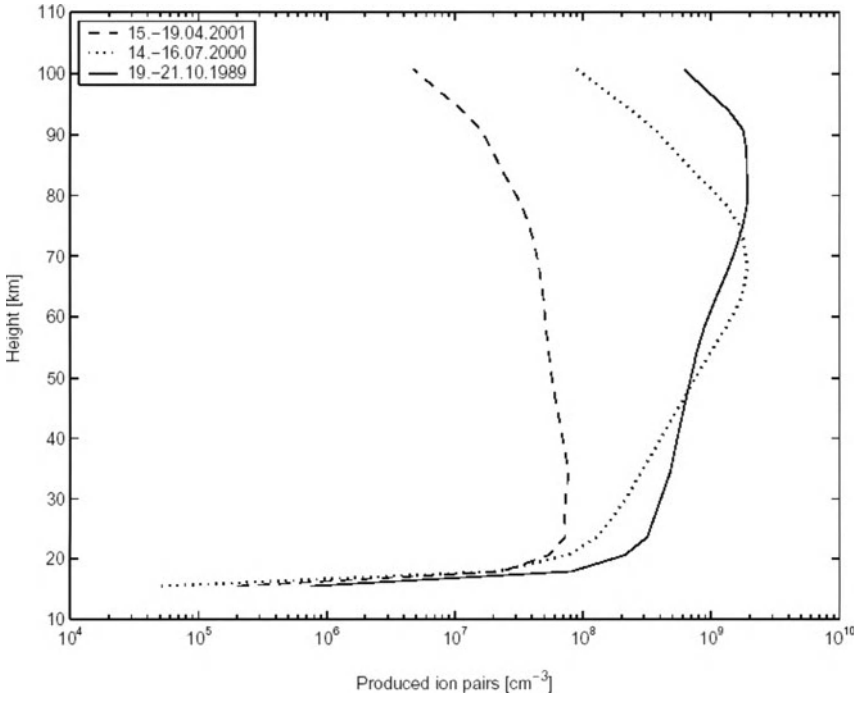

Fig. 12.5.3. Total ionization during GLE in October 1989, July 2000, and April 2001. According to Quack et al. (2001).

12.6. The inverse problem: possible use of ionospheric measurements for estimation of galactic and solar CR variations

12.6.1. How to use ionospheric data for galactic and solar CR research?

The ionospheric method for studying the CR variations (Dorman, 1977b), which is based on the examination and application of the effects of the galactic and solar CR on the state of the ionosphere to derive information on the variations of the geomagnetic cut off rigidity and the extraterrestrial variations of the CR energy spectrum, is very promising (Velinov et al., M1974). With this purpose, use may be made of the riometric measurements on various frequencies and other methods of obtaining practically continuous information on the state of the ionosphere (mainly the lower ionosphere, the so called CR layer region which appears owing to the ionization produced by CR), namely the vertical and inclined sounding, the propagation of long and super long radio-waves (Dorman and Krupitskaya, 1972, 1975; Dorman et al., 1972; Dorman and Kozin, 1977, M1983). It will be shown below that any measurement method of the ionospheric ionization rate due to CR at various altitudes makes it possible to obtain, using the method of ionospheric integral multiplicities and coupling functions developed in Dorman (1977b), and described below, important information on CR variations, especially in low energy range (up to several MeV) during SEP events.

12.6.2. General expression for ionization rate profiles owed to CR of galactic and solar origin; ion production multiplicity

Let the CR flux be characterized by a set of differential rigidity spectra $\sum_Z D_Z(R,\theta,\varphi)$, where R is the particle rigidity; Ze is the particle charge; summation is over all Z = 1, 2, 3...; particles are incident onto the atmospheric boundary at zenith angle θ and azimuthally angle φ. Nuclear interactions will produce secondary particles of type j (protons, $\pi^{\pm}$ – mesons, $\mu^{\pm}$ – mesons, electrons and positrons, photons, etc). The total number of the primary particles and the secondary particles of type j (including the unstable $\pi^{\pm}$ – and $\mu^{\pm}$ – mesons and the electro-magnetic cascade generated by these particles, namely electrons, positrons, and photons) at the level with pressure h at kinetic energy E_{kj} from a single primary particle with charge Z and rigidity R is determined by the integral generation multiplicity $m_j(Z,R,\theta,h,E_{kj})$. The energy loss for ionization of a particle of type j with energy E_{kj} is determined by the value $\varepsilon_j(E_{kj})$. Considering that energy Q = 35 eV is lost for production of an ion pair in air (taking into account that about 2/3 of the total energy loss is spent for excitation and heating of the medium whilst the rest is lost for ionization proper), the ion production rate will be (in units of ion.cm^{-3}.sec^{-1}):

$$q(R_c,h)=\frac{\rho(h)}{Q}\sum_Z\int_0^{2\pi}d\varphi\int_0^{\pi/2}d\theta \times\int_{R_c(\theta,\varphi)}^{\infty}dR\left[D_Z(R,\theta,\varphi)\sum_j\int_0^{\infty}m_j(Z,R,\theta,h,E_{kj})\varepsilon_j(E_{kj})dE_{kj}\right], \quad (12.6.1)$$

where $\rho(h)$ is the density of the air at the level with pressure h, $R_c(\theta,\varphi)$ is the effective geomagnetic cut off rigidity. If the spectrum of the incident particles is isotropic we shall find after integrating over θ and φ in Eq. 12.6.1, that

$$q(R_c,h)=\sum_Z\int_{R_c}^{\infty}D_Z(R)M_Z(R,h,\rho(h))dR\,, \quad (12.6.2)$$

where

$$M_Z(R,h,\rho(h))=\frac{\rho(h)}{Q}\sum_j\int_0^{\infty}m_j(Z,R,\theta,h,E_{kj})\varepsilon_j(E_{kj})dE_{kj} \quad (12.6.3)$$

is the number of the ion pairs produced in 1 cm of the atmosphere (in the vertical direction) at level h by a single primary particle with charge Z and rigidity R at the atmospheric boundary and by the secondary radiation produced by such primary particle. For the sake of brevity, we shall call this value the ion production multiplicity.

12.6.3. Temporal variations of the ionization rate $q(R_c,h)$ and determination of the ionospheric coupling coefficients for the nuclei Z

The following values in Eq. 12.6.2 may vary with time: the geomagnetic cut off rigidity R_c (the geomagnetic variations.), the density of air $\rho(h)$, the temperature, the chemical composition and rigidity spectra $D_Z(R)$ (the extraterrestrial variations of CR). Varying Eq. 12.6.2 in these parameters, we obtain

$$\delta q(R_c,h)=-\delta R_c\sum_Z D_Z(R_c)M_Z(R_c,h,\rho(h))+\sum_Z\int_{R_c}^{\infty}\delta D_Z(R)M_Z(R,h,\rho(h))dR +\sum_Z\int_{R_c}^{\infty}D_Z(R)\frac{\delta M_Z(R,h,\rho(h))}{\delta\rho(h)}\delta\rho(h)dR. \quad (12.6.4)$$

Dividing Eq. 12.6.4 by $q(R_c,h)$ and inserting the denomination of ionospheric coupling function for primary particles with charge Z

$$U_Z(R_c,R,h,\rho(h))=\frac{D_Z(R)M_Z(R,h,\rho(h))}{q(R_c,h)}\,, \quad (12.6.5)$$

we shall obtain

$$\frac{\delta q(R_c,h)}{q(R_c,h)} = -\delta R_c \sum_Z U_Z(R_c,R_c,h,\rho(h)) + \sum_Z \int_{R_c}^{\infty} \frac{\delta D_Z(R)}{D_Z(R)} U_Z(R_c,R,h,\rho(h))dR - \frac{\delta T(h)}{T(h)} \sum_Z \int_{R_c}^{\infty} U_Z(R_c,R,h,\rho(h))dR. \quad (12.6.6)$$

It was taken into account when calculating the last term in Eq. 12.6.6 that, according to Eq. 12.6.3

$$\frac{\partial M_Z(R,h,\rho(h))}{M_Z(R,h,\rho(h))\partial\rho(h)} \delta\rho(h) = \frac{\delta\rho(h)}{\rho(h)} = -\frac{\delta T(h)}{T(h)}, \quad (12.6.7)$$

where $T(h)$ is the temperature of the layer with pressure h in °K (it has been taken into account here that $\rho(h) \propto 1/T(h)$. It follows from Eq. 12.6.5 and Eq. 12.6.2 that

$$\sum_Z \int_{R_c}^{\infty} U_Z(R_c,R,h,\rho(h))dR = 1, \quad (12.6.8)$$

so that the discussed term in Eq. 12.6.6 is merely $\propto \delta T(h)/T(h)$, and reflects the temperature variation of the ion production rate (the atmospheric variation). The first and second terms describe the geomagnetic and extraterrestrial variations respectively. The Eq. 12.6.5 determines the ionospheric local coupling coefficient for the flux of nuclei with charge Z.

12.6.4. The total local and polar ionospheric coupling coefficients

Summation of Eq. 12.6.5 over Z gives the total local ionospheric coupling coefficient for a point with geomagnetic cut off rigidity R_c:

$$U(R_c,R,h,\rho(h)) = \sum_Z U_Z(R_c,R,h,\rho(h)) = q^{-1}(R_c,h) \sum_Z D_Z(R) M_Z(R,h,\rho(h)). \quad (12.6.9)$$

It follows from Eq. 12.6.8 that the total coupling coefficient has been normalized to 1. Let us insert the total polar ionospheric coupling coefficient at $R_c = 0$:

$$U_o(R,h,\rho(h)) = \sum_Z U_{oZ}(R,h,\rho(h)) = q_o^{-1}(h) \sum_Z D_Z(R) M_Z(R,h,\rho(h)). \quad (12.6.10)$$

It can be easily seen that in this case the total local coupling coefficient will be

$$U(R_c,R,h,\rho(h)) = \begin{cases} 0 & \text{if } R < R_c, \\ U_o(R,h,\rho(h)) \left[\int_{R_c}^{\infty} U_o(R,h,\rho(h))dR \right]^{-1} & \text{if } R \geq R_c, \end{cases} \quad (12.6.11)$$

that is the total local coupling coefficient for any point on the Earth can be easily determined through the total polar ionospheric coefficient.

12.6.5. The case of a constant chemical composition of CR

If the chemical composition is constant in time (for example, for the modulation effects in the galactic CR) and the energy spectra of various nuclei are similar, then in this case

$$D_Z(R) = A_Z D(R), \tag{12.6.12}$$

where $A_Z = \text{const}$ and $D(R)$ is the total CR spectrum (let us note that $\sum_Z A_Z = 1$). Then

$$U(R_c, R, h, \rho(h)) = \frac{D(R) M(R, h, \rho(h))}{q(R_c, h)}, \tag{12.6.13}$$

where

$$M(R, h, \rho(h)) = \sum_Z A_Z M_Z(R, h, \rho(h)). \tag{12.6.14}$$

Considering the above, the variation equation (12.6.6) may be rewritten in the form

$$\frac{\delta q(R_c, h)}{q(R_c, h)} = -\frac{\delta T(h)}{T(h)} - \delta R_c \sum_Z U(R_c, R_c, h, \rho(h)) + \int_{R_c}^{\infty} \frac{\delta D(R)}{D(R)} U(R_c, R, h, \rho(h)) dR. \tag{12.6.15}$$

12.6.6. The set of ionospheric spectrographic equations for continuous observations at several levels above a single point

The various methods have been developed for continuously sounding the electron concentration and determining the ionization rate at various atmospheric levels (see in Velinov et al. (M1974) and the monographs on the atmospheric physics and radio wave propagation). Besides that, the observation conditions should be so selected that one may be sure that the CR are the single source of ionization at given altitudes and in given period. Consider the case in which the correction for the temperature variations have been taken into account. It will be assumed that the values

$$b_i = \delta q(R_c, h_i)/q(R_c, h_i) + \delta T(h_i)/T(h_i) \tag{12.6.16}$$

are known at some three levels h_i (i = 1, 2, 3). The following set of three ionospheric equations may then be written on the basis of Eq. 12.6.15:

$$b_i = \delta R_c U_i + a f_i(\gamma), \tag{12.6.17}$$

where the power form of the extraterrestrial variation

$$\delta D(R)/D_o(R) = aR^{-\gamma} \tag{12.6.18}$$

is suggested and the designations

$$U_i \equiv U(R_c, R_c, h_i, \rho(h_i)); \quad f_i(\gamma) \equiv \int_{R_c}^{\infty} R^{-\gamma} U(R_c, R, h_i, \rho(h_i)) dR \tag{12.6.19}$$

has been inserted for the sake of brevity. We shall solve the set of Eq. 12.6.17 using the procedure described above in Chapter 3 (Section 3.11). It can be found from the first two equations of the set 12.6.17 at $i = 1$ and $i = 2$ that

$$a = (b_1 U_2 - b_2 U_1)[f_1(\gamma) U_2 - f_2(\gamma) U_1]^{-1}. \tag{12.6.20}$$

It can be obtained from the set of Eq. 12.6.17 at $i = 1$ and $i = 3$ that

$$a = (b_1 U_3 - b_3 U_1)[f_1(\gamma) U_3 - f_3(\gamma) U_1]^{-1}. \tag{12.6.21}$$

The equation for determining γ will be obtained from Eq. 12.6.19 and Eq. 12.6.20:

$$\frac{b_1 U_2 - b_2 U_1}{b_1 U_3 - b_3 U_1} = \Psi(\gamma). \tag{12.6.22}$$

where the function

$$\Psi(\gamma) = \frac{f_1(\gamma) U_2 - f_2(\gamma) U_1}{f_1(\gamma) U_3 - f_3(\gamma) U_1} \tag{12.6.23}$$

may be tabulated beforehand using the known functions $f_i(\gamma)$ and the known values of U_i for given levels h_1, h_2, h_3 over the point with geomagnetic cut off rigidity R_c. The left part of Eq. 12.6.22 contains the experimental data on b_i and the known values of U_i. Thus the value γ can be easily obtained using Eq. 12.6.22. Substituting the found γ in Eq. 12.6.19 or Eq. 12.6.20, we find a and then Eq. 12.6.16 will be used to find δR_c:

$$\delta R_c = [a f_i(\gamma) - b_i]/U_i, \tag{12.6.24}$$

where i may take on any value (i = 1, 2, 3). If it is possible to take synchronous measurements of $q(h)$ at more than four observation levels, the spectrum of the extraterrestrial variation may be set in a more complex form including the possible deviations of the spectrum from the power form. Thus it has been shown that the continuous ionospheric and riometric measurements (on several frequencies) bearing on the variations in $q(h)$ make it possible to obtain practically continuous information on

the variations δR_c and the extraterrestrial variations of the primary CR spectrum using Eq. 12.6.20-12.6.24 on the basis of the appropriate computer-processing of the observation data.

12.6.7. The set of spectrographic equations for continuous observations of ionization rates above two points at two levels

In this case the set of spectrographic equations is of the form

$$b_{ik} = \delta R_{ck} U_{ik} + a f_{ik}(\gamma), \tag{12.6.25}$$

where U_{ik} and $f_{ik}(\gamma)$ are determined by the formulas similar to Eq. 12.6.19; the index k = 1, 2 indicates the number of the observation point, i = 1, 2 is the number of the observation level. Following Eq. 12.6.6, we shall calculate first the function

$$\varphi(\gamma) = \frac{f_{12}(\gamma)U_{11} - f_{11}(\gamma)U_{12}}{f_{22}(\gamma)U_{21} - f_{21}(\gamma)U_{22}}. \tag{12.6.26}$$

which then shall be used to find γ on the basis of the experimental data on b_{ik} from the equation

$$\frac{b_{12}U_{11} - b_{11}U_{12}}{b_{22}U_{21} - b_{21}U_{22}} = \varphi(\gamma). \tag{12.6.27}$$

After that, the rest of the unknown parameters can be easily found:

$$a = (b_{12}U_{11} - b_{11}U_{12})[f_{12}(\gamma)U_{11} - f_{11}(\gamma)U_{12}]^{-1}, \tag{12.6.28}$$

$$\delta R_{c1} = (b_{12}f_{11}(\gamma) - b_{11}f_{12}(\gamma))[f_{12}(\gamma)U_{11} - f_{11}(\gamma)U_{12}]^{-1}, \tag{12.6.29}$$

$$\delta R_{c2} = (b_{22}f_{21}(\gamma) - b_{21}f_{22}(\gamma))[f_{22}(\gamma)U_{21} - f_{21}(\gamma)U_{22}]^{-1}. \tag{12.6.30}$$

The solutions described by Eq. 12.6.27–12.6.30 completely solve the problem of determination of the cut off rigidity variations at two points and the extraterrestrial CR variation on the basis of the ionospheric data.

12.7. Altitude distribution of ionization in the troposphere and stratosphere owed by galactic CR and ion balance equation

The altitude distribution of ionization in the troposphere and stratosphere were measured on radio balloons by Ermakov and Komotskov (1992), Ermakov et al. (1992, 1997a,b). The ion concentration n was measured with ion-aspiration chambers lifted by balloons. The airflow through a chamber was maintained by balloon rising. The instrument collects almost all negative ions on the altitudes $H \geq 7$ km. The ion

observations were conducted at quiet conditions (no SEP events and no Forbush decreases) at different sites: Thumba (8° N, 77° E; cutoff rigidity for vertical CR arriving $R_c = 17.3$ GV), Balkhash (46° N, 73° E; $R_c = 5.3$ GV), Rylsk (52° N, 35° E; $R_c = 3.3$ GV), Molodezhnaya (67° S, 46° E; $R_c = 0.4$ GV). Results are shown in Fig. 12.7.1 (five points running averages).

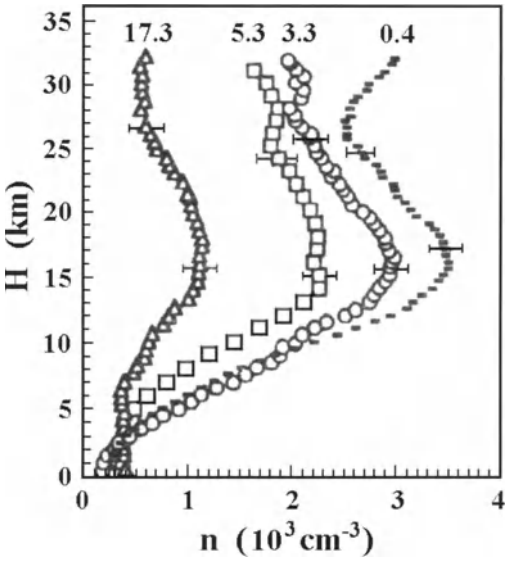

Fig. 12.7.1. The altitude ion concentration profiles at the sites with different geomagnetic cutoff rigidities (the values in GV are denoted at the top). The horizontal bars give the typical values of standard deviations. According to Ermakov et al. (1997a,b).

Then the ion concentration data were compared with values of ionization production rate q. The long-term measurements of ionization rate q in the atmosphere with ionization chambers at different R_c were made by Neher (1961, 1967, 1971). These observations partly overlap with regular balloon observations of CR intensity made in former USSR, and Ermakov et al. (1997a,b) analyzed, the is some relation between these two sets of data or not. It was found that the relationship between the CR flux I and the ionization rate q has the form:

$$q_c(H) \approx 81 \times I(H), \tag{12.7.1}$$

where $q_c(H)$ is in ion pairs/(sm^{3}s.atm) and $I(H)$ is in counts/(cm^{2}s). The ionization rate in the atmosphere $q(H)$ is connected with the ionization rate $q_c(H)$ in the ionization chamber by the relation:

$$q(H) = q_c(H)\rho(H)/\rho_c\,, \tag{12.7.2}$$

where $\rho(H)$ is the air pressure in the atmosphere, and ρ_c is the constant pressure of air in the Neher's ionization chamber. From Eq. 12.7.1 and Eq. 12.7.2 follows

$$q(H) = 81 \times I(H)\rho(H)/\rho_c \,. \tag{12.7.3}$$

By using Eq. 12.7.3 and experimental data of the long-term observations of CR intensity by balloons Ermakov et al. (1997) found ion production rate in the atmosphere vs. altitude for different cutoff rigidities and different levels of solar activity. In Fig. 12.7.2 are shown the absorption curves of CR in the atmosphere at different cutoff rigidities 17.3, 5.2, 3.4, and 0.03 GV.

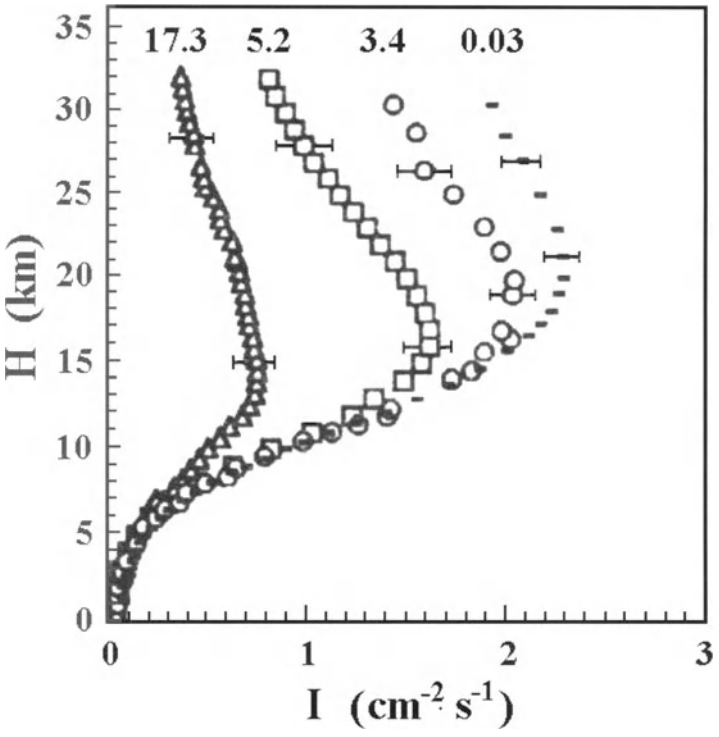

Fig. 12.7.2. The absorption curves of CR in the atmosphere at different cutoff rigidities (numbers on the top in GV). By horizontal bars are shown standard deviations. According to Ermakov et al. (1997).

For quasi-state conditions the common relationship between q and n is

$$q(H) = \alpha(H)n^2(H), \tag{12.7.4}$$

where $\alpha(H)$ is the Thompson's coefficient of ion recombination. Let us consider ratios of I, n, and n^2 at two different cutoff rigidities R_{c1} and R_{c2} vs. altitude: $I_1(H)/I_2(H)$, $n_1(H)/n_2(H)$, and $n_1^2(H)/n_2^2(H)$. From Eq. 12.7.4 and Eq. 12.7.3 follows that

$$n_1^2(H)/n_2^2(H) = q_1(H)/q_2(H) = I_1(H)/I_2(H). \tag{12.7.5}$$

So, if Eq. 12.7.4 is correct, it will be expect that ratios $n_1^2(H)/n_2^2(H)$ and $I_1(H)/I_2(H)$ will show the same dependence vs. H for any R_{c1} and R_{c2}. The different ratios for polar and equatorial latitudes in the interval of altitudes 7–30 km are shown in Fig. 12.7.3.

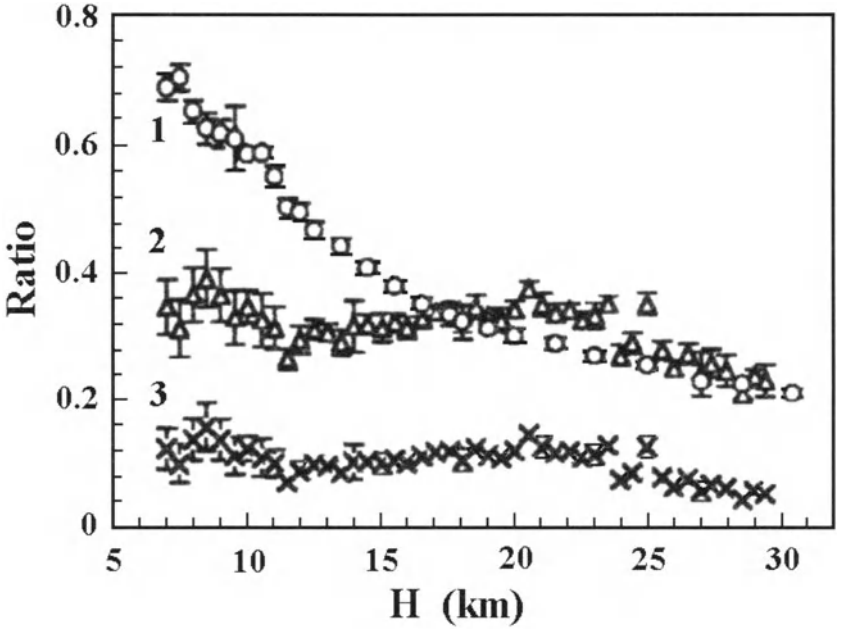

Fig. 12.7.3. The ratios of CR fluxes (1), ion concentrations (2), and ion concentrations squared (3) vs. altitude for the stations Thumba (R_C = 17.3 GV) and Molodezhnaya (R_C = 0.4 GV). The standard deviations are depicted by vertical bars. According to Ermakov et al. (1997).

From Fig. 12.7.3 can be seen a big difference between ratios $I_1(H)/I_2(H)$ and $n_1^2(H)/n_2^2(H)$ what means that Eq. 12.7.4 is not valid in any part of the interval of altitudes 7–30 km. From other hand, a good coincidence is observed in the interval of altitudes 15–30 km for the ratios $I_1(H)/I_2(H)$ and $n_1(H)/n_2(H)$; it means that in this interval of altitudes is realized linear dependence of n from q and I

$$q(H) = \beta(H) n(H), \tag{12.7.6}$$

and in this case instead of Eq. 12.7.5 will be

$$n_1(H)/n_2(H) = q_1(H)/q_2(H) = I_1(H)/I_2(H). \tag{12.7.7}$$

From Fig. 12.7.3 can be seen also that at altitudes lower than 15 km both relations between ion production rate q (which is proportional to CR intensity I) and ion concentration n (squared and linear, described by Eq. 12.7.4 and Eq. 12.7.6., respectively), – are not valid.

12.8. Spatial and temporal changes of the ionization in the low atmosphere induced by galactic CR

12.8.1. Importance of investigations induced by galactic CR ionization in the low atmosphere

Usoskin et al. (2004) in the extended paper investigate in details the expected spatial and temporal changes of the ionization in the low atmosphere induced by galactic CR. Obtained results are very important for many applications which will be considered below: CR influence through ionization on chemical composition in the atmosphere and ozone layer (Chapter 13), CR role through ionization in formation of low clouds and possible influence on global climate change in the past and in present time, for example, according to Yu (2002), Marsh and Svensmark (2003), one of the most probable candidates for mechanism of solar activity influence on cloudiness and climate is ionization of the lower atmosphere by CR which in turn may affect the clouds formation (Chapter 14). It is well known that CR are the main source of the ionization of lower atmosphere. Primary CR initiate a nucleonic-electromagnetic cascade in the atmosphere, with the main energy losses at altitudes below 30 km resulting in ionization, dissociation and excitation of molecules (see, e.g., Bazilevskaya and Svirzhevskaya, 1998; Bazilevskaya et al., 2000). Therefore, one needs long data set on spatial distribution and time profiles of the CR induced ionization to build quantitative models relating CR to cloud formation. Typical ionization detectors measure not the ambient ion concentration but rather the ion production rate inside themselves. Also, since used as an index of CR, such measurements are performed onboard high-altitude balloon flights at few g/cm^2 of the residual atmosphere (e.g., a review by Bazilevskaya and Svirzhevskaya, 1998).

Since there are no routine worldwide measurements of the ion concentrations in the low atmosphere, Usoskin et al. (2004) employed model calculations in this study. In contrast to earlier phenomenological approaches using either parameterization or regression methods (e.g., Heaps, 1978; Hensen and Van Der Hage, 1994; Bazilevskaya et al., 2000), Usoskin et al. (2004) build a complete physical model which can calculate CR induce air ionization starting from the solar modulation of galactic CR, without employing any phenomenological regression or parameterization.

12.8.2. The scheme of the step by step calculations of air ionization in the low atmosphere induced by galactic CR

Fife main processes determined the air ionization in the low atmosphere induced by galactic CR: 1) modulation of galactic CR in the Heliosphere (convection-diffusion and drift modulation, which leads to different effects in odd and even solar cycles, see in Dorman, 2001; Dorman et al., 2001a,b; in more details see in Dorman, M2005), this process determined the intensity and energy spectrum of galactic CR near the boundary of the Earth's magnetosphere; 2) the geomagnetic shielding which is determined by the planetary distribution of cutoff rigidities, also changed in time (see Section 3.3; in more details see in Dorman, M2005), this process determined the intensity and energy spectrum of galactic CR near the boundary of the Earth's atmosphere; 3) nuclear-electromagnetic cascade of CR inside the atmosphere and generation of secondary CR (see Chapter 2), this process determined fluxes of different charged particles in the atmosphere and their energy spectra; 4) energy losses by primary and secondary CR on

ionization, dissociation and excitation of molecules (see Sections 12.4 – 12.6), this process determined the pair ions production rate; 5) recombination (see Sections 12.1 and 12.7), this process determined finally the steady-state ionization (ion concentration).

In Usoskin et al. (2004) to take into account all these processes the according five following approaches were made. **For the process 1** (modulation in the Heliosphere) Usoskin et al. (2002a) have recently reconstructed the time-variable flux and energy spectrum of cosmic rays for the NM era since 1951, using the data of the entire world network of NM from equatorial to polar stations. **For the process 2** (geomagnetic shielding) the virtual dipole moment M of the Earth was calculated. Then the local magnetic latitude λ_m of the site can be determined, and finally the local vertical geomagnetic cutoff (in GV) can be estimated using the Størmer's formula (Elsasser, Nay and Winckler, 1956):

$$R_c \approx 1.9 \times M \cos^4 \lambda_m (r_e/r)^2 \text{ GV}, \tag{12.8.1}$$

where r_e = 6371 km is the mean Earth's radius, r is the distance to the actual dipole center, and M is the virtual geomagnetic dipole moment in 10^{25} gauss cm^3 (M = 7.8 for the 2000 epoch). For calculation of M were used the Gauss coefficients as tabulated in the DGRF/IGRF model (http://nssdc.gsfc.nasa.gov/space/model/magnetos/igrf.html) with 5-year time epochs (between the epochs was applied a simple linear interpolation of the geomagnetic parameters). **For the Process 3** (development in the atmosphere CR nuclear-electromagnetic cascade) was employed the CORSIKA Monte Carlo package (Heck et al., 1998) which is specially designed for this purpose and includes recent and reliable description of various physical processes and cross sections. Primary CR are assumed to consist of protons (94%) and α–particles (6%). The package CORSIKA can calculate energy losses deposited by the developing cascade for ionization of the ambient air at every step. First was calculated such ionization energy $\Delta E_{ion}(E,h)$ spent by secondaries of the atmospheric cascade initiated by a CR particle with initial energy E, in a thin layer around the residual atmospheric thickness h (in g/cm^2). The value of $\Delta E_{ion}(E,h)$ rises with the increasing energy of primary CR particles. The atmospheric layer is assumed to be not too thick (it was consider Δh = 25 g/cm^2), i.e., its thickness is small in comparison with the characteristic size of a nucleonic cascade, and atmospheric parameters can be considered roughly constant within the layer. The real width of the layer can be defined as $\Delta H = \Delta h/\rho(h)$, where $\rho(h)$ is the corresponding mean density of the air in this layer. The real altitude H corresponding to the atmospheric thickness h can be calculated as follows

$$H = a_1 + a_2 \exp(-h/a_3), \tag{12.8.2}$$

where coefficients $a_1, a_2,$ and a_3 are defined from the corresponding atmospheric model. Usoskin et al. (2004) used the standard chemical composition of the atmosphere with the volume fractions of N_2, O_2 and Ar as 78.1%, 21% and 0.9%, respectively. As the physical model of the atmosphere was used the well tabulated US standard atmosphere, 1976. **For the Process 4** (ion pairs production) it was assumed that on the

average it takes about 35 eV to produce one ion pair in the air (Porter et al., 1976). One can calculate the number of ion pairs produced in one cm layer by the CR induced cascade as follows

$$q(E,H)=\frac{1}{35\,\mathrm{eV}}\frac{\Delta E_{ion}(E,H)}{\Delta H}. \qquad (12.8.3)$$

Assuming isotropic flux of primary CR particles and locally flat atmosphere, it was define the 'yield function' (or integral multiplicity) of CR induced ionization, similar to, e.g., yield function of a neutron monitor (e.g., Clem and Dorman, 2000; see also Chapter 3). The concept of the yield function $Y(E,H)$ defines the ion-pair production rate corresponding to the mono-energetic unit flux of cosmic rays beyond the Earth's magnetosphere (see Fig. 12.8.1).

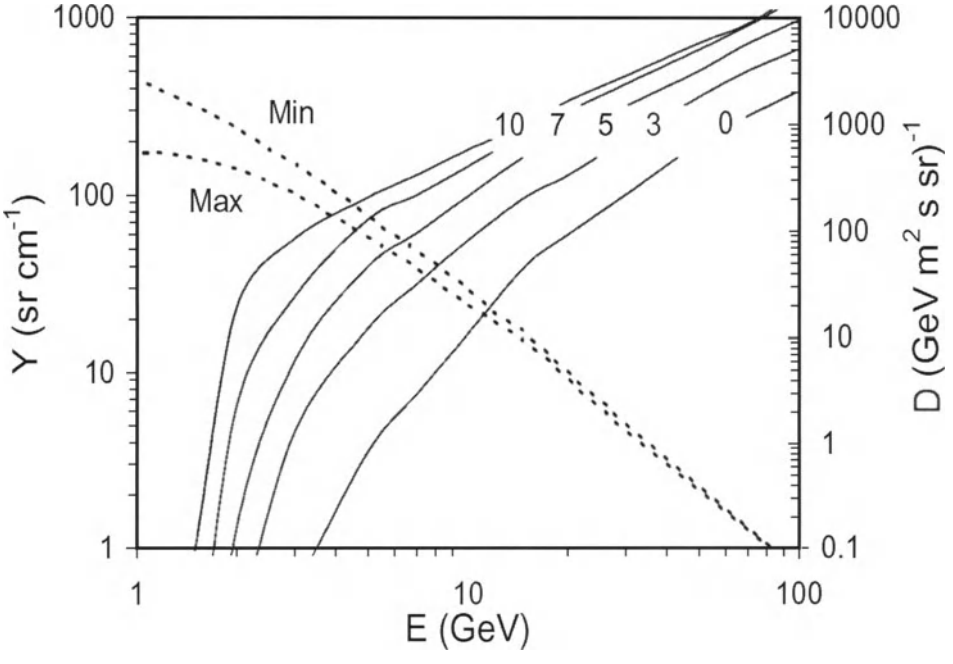

Fig. 12.8.1. The ionization yield function Y in polar regions (solid curves, left axis) is shown vs. the energy of primary galactic CR for different altitudes (in km) as denoted near the curves. The differential energy spectrum $D(E)$ of galactic CR (dotted curves, right axis) is shown for the solar minimum and maximum conditions as denoted next to the curves. According to Usoskin et al. (2004).

By using the ionization yield function the total ionization rate at a given location can be calculated as the integral of a product of the galactic CR differential spectrum $D(E)$ and the yield function $Y(E,H)$ (both are shown in Fig. 12.8.1):

$$Q(R_c,H)=\int_{E_{cp}(R_c)}^{\infty}Y_p(E,H)D_p(E)dE+\int_{E_{c\alpha}(R_c)}^{\infty}Y_\alpha(E,H)D_\alpha(E)dE, \qquad (12.8.4)$$

where $E_{cp}(R_c)$ is the cutoff energy of protons corresponded to the local geomagnetic rigidity cutoff R_c; $E_{c\alpha}(R_c)$ is the same for α–particles; the $Y_p(E,H)$ and $Y_\alpha(E,H)$ are ionization yield functions for primary protons and α–particles of energy E per nucleon at altitude H; $D_p(E)$ and $D_\alpha(E)$ are the differential energy spectra of primary protons and α–particles of galactic CR at 1 AU. The integrand of Eq. 12.8.4, i.e. the differential ion production function $F = Y \times D$, is the product of the sharply decreasing galactic CR energy spectrum and the increasing yield function, and therefore has a peak-like shape (see Fig. 12.8.2).

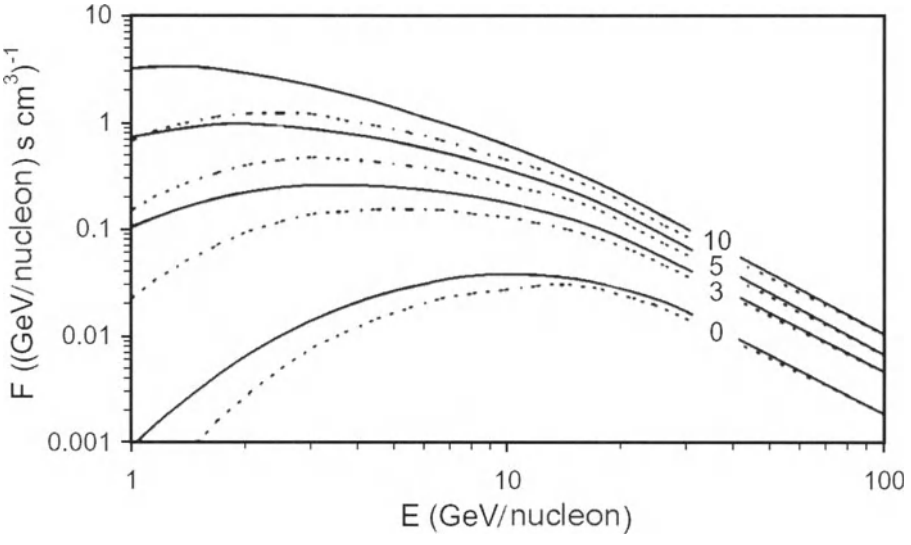

Fig. 12.8.2. The differential ion production function $F = Y \times D$ in polar regions vs. the energy of primary galactic CR corresponding to the solar minimum (solid curves) and solar maximum (dotted curves) conditions for different altitudes as denoted (in km) next to curves. According to Usoskin et al. (2004).

As can be seen in Fig. 12.8.2, the peak of F-function is broad, with the maximum varying from 1 to 10 GeV/nucleon depending on the altitudes and phase of the solar cycle. With increasing solar activity this peak moves slightly to higher energies due to the hardening of galactic CR spectrum, while it moves towards lower energies with increasing altitude. Usoskin at al. (2004) mentioned that in the NM terminology it is common to use the effective energy, so that the time profile of galactic CR flux at this energy is directly proportional to the NM count rate (Alanko et al., 2003; see in detail Section 3.16 in the Chapter 3), or median energy which halves the integral in Eq. 12.8.4 (Ahluwalia and Dorman, 1997) . The similarly defined effective/median energy of the cosmic ray induced ionization at a few km altitude takes the wide range of values from about 10 GeV/nucleon for polar up to about 50 GeV/nucleon for equatorial sites, which is quite close to the neutron monitors. Usoskin at al. (2004) have compared described calculations with the measured ion-pair production rate (Fig. 12.8.3). The agreement between calculations and the actual measurements is quite good, especially taking into

account that the calculations present some average value while measurements have been performed within a short period of flight.

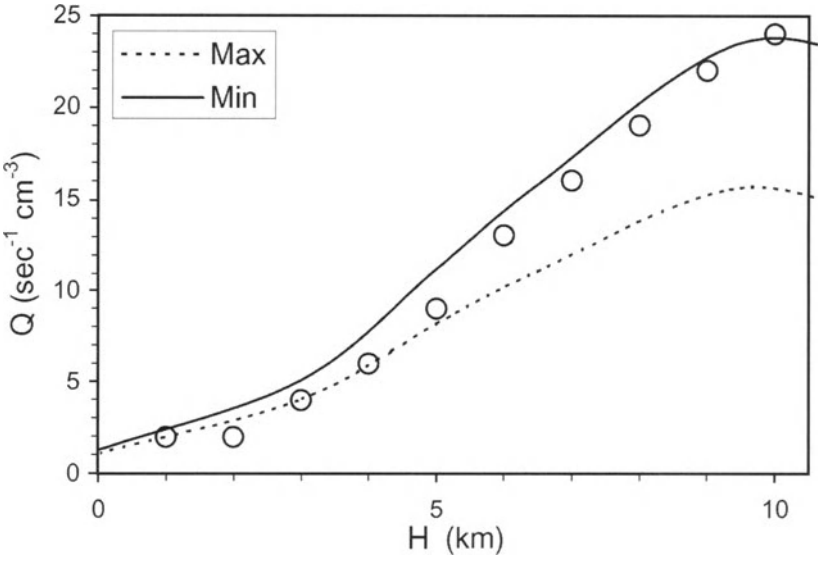

Fig. 12.8.3. The altitude profile of the ion production rate in polar regions calculated for the solar minimum (solid line) and maximum (dotted line) conditions. Open dots represent the measured values of Q by Neher (1967, 1971) for the solar minimum conditions. According to Usoskin et al. (2004).

For the process 5 (formation of ion pairs concentration) Usoskin et al. (2004) have calculated the equilibrium ion concentration due to CR ionization, taking into account the recombination processes in the atmosphere. The equilibrium condition between the ionization rate Q and the ion concentration n is usually considered as described by Eq. 12.7.4 (see above, Section 12.7).

$$Q(R_c,H)=\alpha(H,T)n^2(R_c,H); \quad n(R_c,H)\approx\left(Q(R_c,H)/\alpha(H,T)\right), \tag{12.8.5}$$

where $\alpha(H,T)$ is the recombination coefficient which depends on the local pressure and temperature (e.g., Bates, 1982; Rosen et al., 1982; Smith and Adams, 1982). On the other hand, a possible role of aerosols and 'large ions' in the recombination has been discussed (e.g., Ermakov et al., 1997a,b; Bazilevskaya et al., 2000; see also above, Section 12.7) that may lead to essential deviation from Eq. 12.8.5. Usoskin et al. (2004) have adopted the values of the effective recombination coefficient $\alpha(H,T)$ according to Rosen and Hofmann (1981) and Bates (1982) which agree with the observations. In Fig. 12.5.4 the calculated altitude profile of the ion concentration in polar regions have compared with the actually measured values of n obtained by the same instrument during several balloon flights in 1989–1990 (solar maximum). The calculated profile is in a good agreement with the observations for the altitude ≥ 7 km and systematically higher for lower altitudes. However, as mentioned by Ermakov et al. (1997b), this instrument

might have missed a fraction of the ions at altitudes below 7 km, resulting in underestimate of the ion concentration.

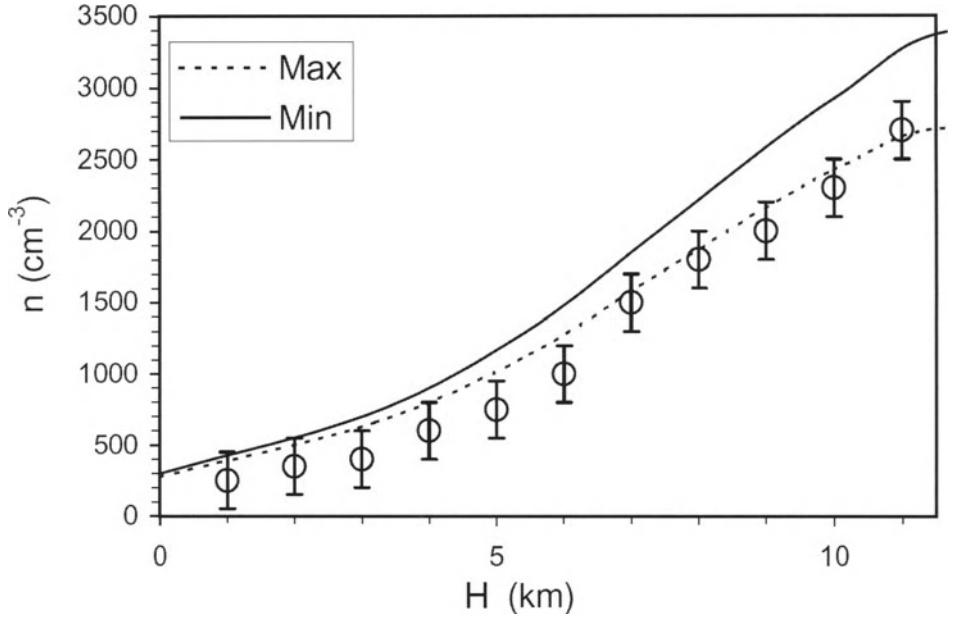

Fig. 12.8.4. The altitude profile of the ion concentration in polar regions calculated for the solar minimum (solid line) and maximum (dotted line) conditions. Open dots with error bars represent the measured values of *n* by Ermakov et al. (1992, 1997a,b) for the solar maximum conditions. According to Usoskin et al. (2004).

12.8.3. The expected 3-D distribution air ionization in the low atmosphere and long term variations induced by galactic CR

Thus, using the galactic CR time-variable flux (Usoskin et al., 2002), geomagnetic rigidity cutoff (Eq. 12.8.1), and the pre-calculated yield function (Fig. 12.8.2), it became possible to calculate the ion-pair production rate Q and finally, using Eq. 12.8.5, the CR induced ionization for a given location and time. Actually we calculate the 3D (longitude, latitude and altitude) time-variable distribution of the cosmic ray induced ionization. As a snapshot, a surface distribution of the cosmic ray induced ionization at 3 km altitude is shown in Fig. 12.8.5 for the year 2000. As expected, the ionization increases with the latitude, changing by 20–25% between the equatorial and polar regions. The ionization is nearly constant beyond the last grid line of 710 cm^{-3} implying the 'knee' in this latitudinal dependence, in agreement with observations (Neher, 1961; Heaps, 1978). This knee at 50–60° geomagnetic latitude corresponds to the geomagnetic cutoff rigidity of 2–2.5 GV. Primary CR particles with lower rigidity/energy do not really contribute to the ion production rate (see Fig. 12.8.2), and thus the decreasing effective rigidity cutoff does not result in further increase of the ion concentration. Also, the South Atlantic Anomaly is clearly seen in Fig. 12.8.5 as the region of enhanced ion concentration due to the shift of the geomagnetic dipole center with respect to the Earth's center.

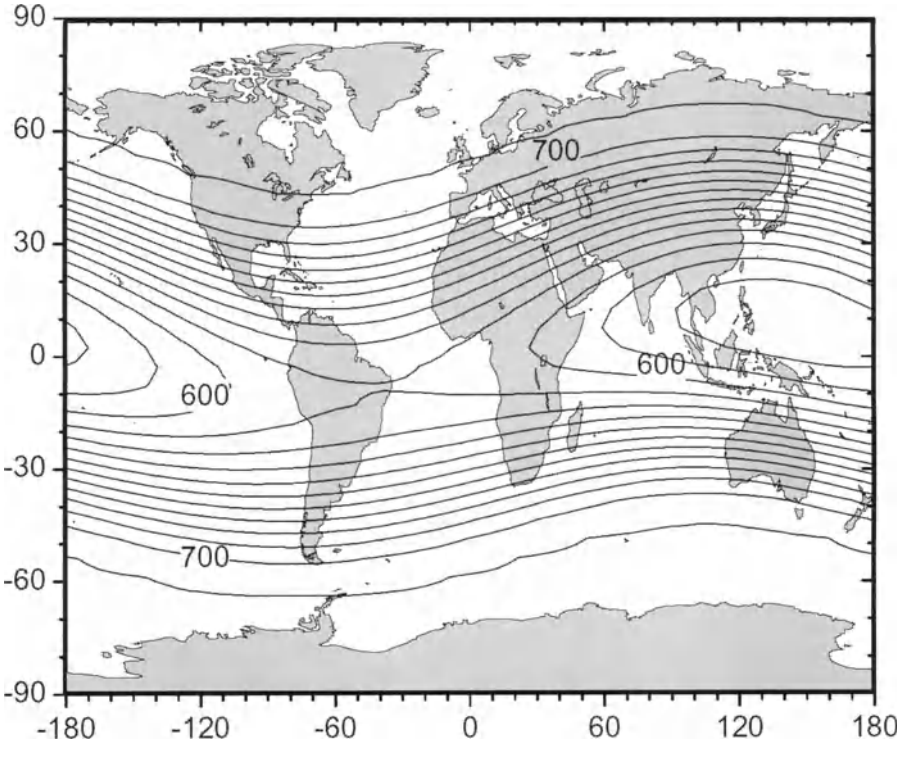

Fig. 12.8.5. Calculated equilibrium cosmic ray induced ionization at the altitude of 3 km (h = 725 g/cm^2) for the year 2000. Contour lines are given as the number of ion pairs per cm^3 with the step of 10 cm^{-3}. According to Usoskin et al. (2004).

So, in Usoskin et al. (2004) are present, for the first time, detailed calculations of the time-variable spatial distribution of CR induced ionization of the lower atmosphere. For this purpose, a physical model has been applied including the CR differential spectrum long term modulation, Monte-Carlo simulation of the CR initiated atmospheric cascade, ion-pair production by the cascade as well as the balance between ionization and recombination. A comparison of the calculation results with the actual measurements validates the calculation method since no fitting or parameterization has been used in the model. The calculated CR induced ionization reproduces the observed altitudinal and latitudinal profiles of the ion concentration in the low atmosphere.

The other example of Usoskin et al. (2004) results is Fig. 12.8.6 which shows time profiles of CR induced ionization calculated for the 3 km altitude (h = 725 g/cm^2) for three different regions: polar (R_c < 1 GV), mid-latitudes ($R_c \approx$ 6 GV) and equatorial ($R_c \approx$ 15 GV).

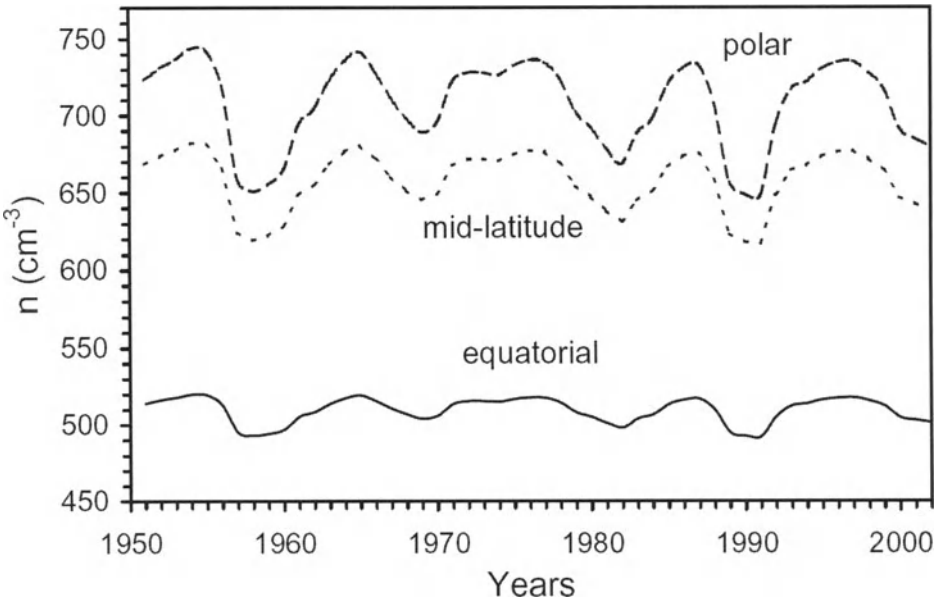

Fig. 12.8.6. Calculated time profiles of the annual CR induced ionization at the altitude of 3 km (h = 725 g/cm^2) for three regions: polar (R_c < 1 GV), mid-latitudes ($R_c \approx$ 6 GV) and equatorial ($R_c \approx$ 15 GV) regions. According to Usoskin et al. (2004).

From Fig. 12.8.6 can be seen that the amplitude of 11-year cycle variations of the CR induced ionization in the atmosphere on the altitude 3 km changes greatly between the polar region (about 80 cm^{-3} or 11% of the solar minimum ionization level) and equatorial regions (about 20 cm^{-3} or less than 5%). The 11-year cycle variation amplitude in the globally average CR induced ionization is about 8% of the solar minimum ionization level.

The described calculations have been carried out for the period since 1951 using the CR differential flux as computed from the worldwide NM network data (Usoskin et al., 2002a). However, this calculated CR induced ionization series can be extended backwards in time for about four centuries, using the CR flux reconstruction since 1610 (Usoskin et al., 2002b). Moreover, by using cosmogenic isotopes data (e.g., ^{10}Be and ^{14}C, see correspondingly Chapters 10 and 17), the information on CR intensity variation can be prolonged into the past for more than 10,000 years. In this case, the described results provide a basis for a quantitative study of the solar-terrestrial relationships through CR induced ionization in the low atmosphere on very long time scales. From other hand the CR induced ionization in the low atmosphere influenced on air conductivity and atmospheric electric processes (see Chapter 11), on chemical composition in the atmosphere and formation ozone layer (Chapter 13), on cloudiness formation and climate change (Chapter 14).

Chapter 13

Cosmic Ray Influence on the Chemical Processes in the Atmosphere and Formation of Ozone Layer

13.1. CR influence on the chemistry in the mesosphere

Zeller et al. (1986) revealed a strong correlation between nitrate fallouts and great solar proton events by measuring abundances of nitrates in Antarctic snow. It was observed that the nitrate concentration peak for solar GLE (Ground Level Events) in August 1972 was 2–3 times as much as the mean level. Jackman et al. (1990) performed the calculations of expected increase of the concentration for

$$NO_y = N + NO + NO_2 + NO_3 + HNO_3 + HNO_4 + 2N_2O_5 + ClNO_3 \qquad (13.1.1)$$

from ground level up to 30 km altitude caused by solar protons in August 1972. But after summation of all expected fallouts for 1 month in August 1972 the value of maximum expected excess abundance of nitrates was obtained

$$A(NO_y) \approx 0.45 \text{ mg.m}^{-2}.\text{month}^{-1}, \qquad (13.1.2)$$

whereas the observed nitrate peak in Antarctic snow according to Zeller et al. (1986) was about 3 times higher. On the other hand, according to calculations of Crutzen et al. (1975), the number of *NO* molecules produced by solar protons above 30 *km* is almost one order higher than that for ground level layer (see Fig. 13.1.1).

On the other hand, according to Vitt et al. (2000), a two-dimensional photochemical transport model which has inputs that characterize the odd nitrogen production associated with galactic CR, solar particle events (SPEs), and lower thermospheric contributions (auroral electrons and solar EUV and soft X-rays) is used to compute odd nitrogen concentrations in the polar middle atmosphere during 1970–1994. It was found that the SPE contributions to annual average odd nitrogen concentrations in the polar stratosphere (latitudes > 50°) are computed to be significant (>10%) only for the larger events of August 1972 and October 1989. So the influence of CR on formation of nitrates is much more effective than on formation of odd nitrogen.

Gladysheva and Kocharov (1995) suggested that the transfer of a fraction of nitrates from mesosphere to ground layers could explain the observed by Zeller et al. (1986) the nitrate peak in Antarctic snow. The principal source of nitric oxide molecule production in the upper atmosphere is the reaction

$$N(^2D) + O_2 \rightarrow N_2^+ + 2e^- . \qquad (13.1.3)$$

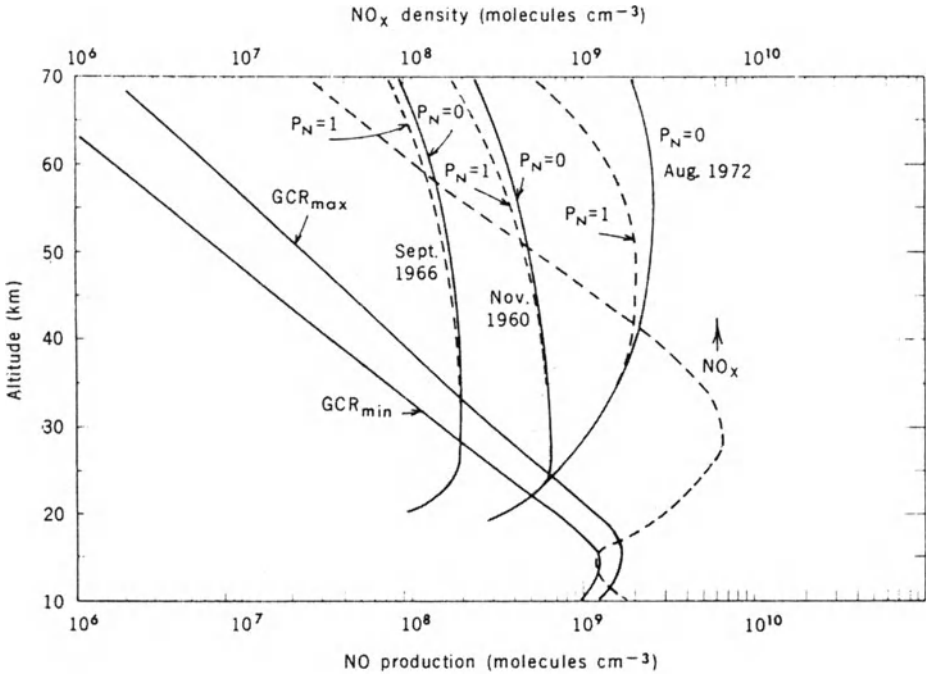

Fig. 13.1.1. Total production of NO during the FEP events of November 1960, September 1966, and August 1972 (lower scale) for hights 10–70 km. The curves labeled $P_N = 0$ give the production obtained by assuming that all nitrogen atoms are in excited states, and $P_N = 1$ – in the ground state. Curves GCR_{max} and GCR_{min} show annual production of NO by galactic CR in minimum and maximum of solar activity, respectively. The background distribution of NO_x ($NO + NO_2$) is also given (upper scale). According to Crutzen et al. (1975).

Solar protons generate in the upper atmosphere an intensive flux of secondary electrons with energy of tens and hundreds of eV, which make a substantial contribution to generation of excited $N(^2D)$ atoms with following reactions:

$$N_2 + e^- \rightarrow N_2^+ + 2e^-;\ N_2 + e^- \rightarrow N^+ + N + 2e^-;\ N_2 + e^- \rightarrow 2N + e^-. \quad (13.1.4)$$

The decay of NO molecules takes place mainly because of reaction with atoms of nitrogen at ground state:

$$N(^4S) + NO \rightarrow N_2 + O. \quad (13.1.5)$$

As shown by Atkin (1994), the concentration of nitric acid in the mesosphere increases markedly during the injection of high energy particles: an ionization rate $q_e \approx 1.2\times10^{-3}\,\mathrm{cm}^{-3}.\mathrm{sec}^{-1}$ at the altitude 50 km leads to an increase for one day of the abundance of HNO_3 from $3\times10^5\,\mathrm{cm}^{-3}$ to $6\times10^7\,\mathrm{cm}^{-3}$. Then HNO_3 molecules transform in few days to nitric oxide molecules, and then into aerosol particles or small crystals like those observed in silver 'mustard' clouds at the altitudes 40–90 km. The nitrate peak revealed in Antarctic snow has a maximum height at the end of 1972 and the

beginning of 1973, about 5 months after the great GLE in August 1972; so Gladysheva and Kocharov (1995) came to conclusion that the sedimentation velocity of particles from altitude about 85 km to the ground is about $u_s \approx 0.6$ km/day (in good agreement with observations of the polarization shift of the sky before sunset, from which follows particle sedimentation velocity of ≈ 0.62 km/day).

13.2. Nitrate abundances in Antarctic and Greenland snow and ice columns: information on FEP events in the past

Over the past 10–15 years there have been a number of publications (for example Dreschhoff and Zeller, 1990; Zeller and Dreschhoff, 1995) that have advanced the hypothesis that short term (approximately two months or less) increases in the nitrate component of polar ice are the consequence of flare energetic particle (FEP) events. Gladysheva et al. (1995) supposed that by measurements of nitrate abundance in the dated Antarctic and Greenland ice columns for the last 10,000 years on the basis of established quantitative correlation between the abundance of the nitrate NO_3 and total energy of protons emitted, it is possible to determine the upper limit of total energy induced by solar flare energetic protons.

In McCracken et al. (2001a-d) the geophysical significance of the thin nitrate-rich layers found in both Arctic and Antarctic ice cores is examined in details. The ice cores are sampled to yield about 20 contiguous samples per year, and NO_3 concentrations (in nanograms of nitrate/gram of water) and electrical conductivities (in micro-Siemens/cm) are measured for each sample. In Fig. 13.2.1 are shown examples of the impulsive nitrate events associated with the great white light flare of 1 September, 1859 (observed by Carrington, 1860), several events in 1890-1898, and associated with GLE of 25 July 1946.

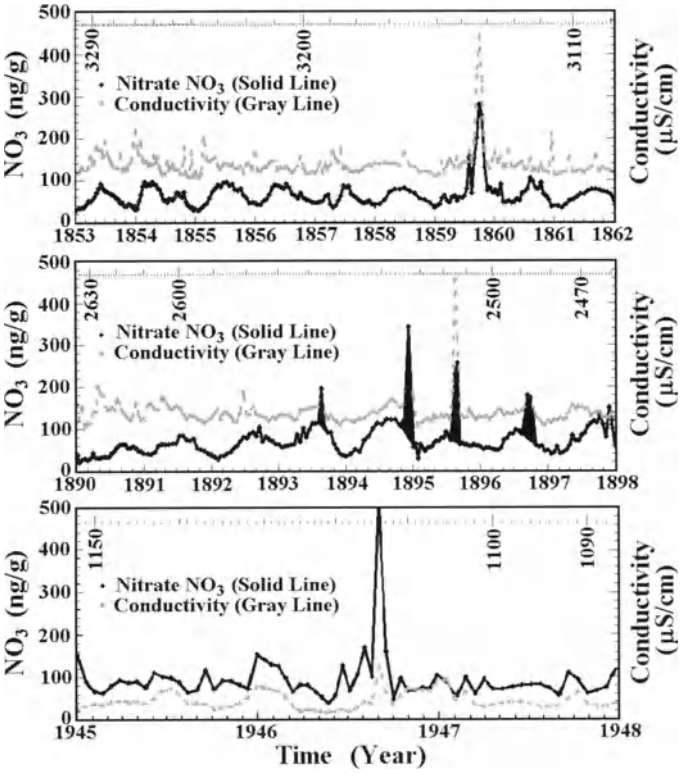

Fig. 13.2.1. Examples of the impulsive nitrate events associated with great events on the Sun and in CR: ***a*** – associated with the great white light flare of 1 September 1859; ***b*** – events in 1890–1898; ***c*** - associated with GLE of 25 July 1946. According to McCracken et al. (2001b).

Fig. 13.2.2 shows the times of occurrence of >30 Mev FEP events for the 125 impulsive nitrate events with fluence exceeding 1.0×10^{9} cm^{-2} for the period 1561–2000 in comparison with annual sunspot numbers.

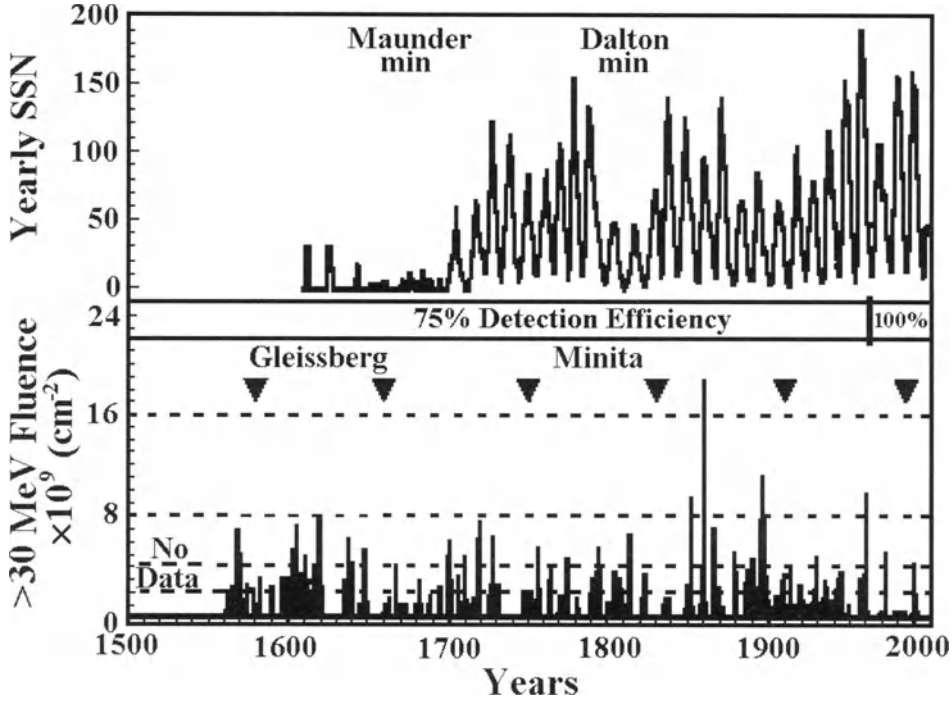

Fig. 13.2.2. The times of occurrence and fluencies of >30 Mev FEP events for 125 impulsive nitrate events for the period 1561–2000 with fluencies exceeding 1.0×10^{9} cm^{-2} in comparison with annual sunspot numbers. According to McCracken et al. (2001a).

13.3. Cumulative probabilities of the FEP events vs. their fluencies for > 30 MeV solar protons on the basis of nitrate abundances in Antarctic and Greenland ice columns, satellite data and cosmogenic isotopes in moon rocks

The data shown in Fig. 13.2.1 and 13.2.2 for 1500–2000 were used By McCracken et al. (2001a-d) for determining the cumulative probabilities of the FEP events with fluencies for >30 MeV solar protons up to 2.0×10^{10} cm^{-2} (about 20 times bigger than for the FEP event of 23 February 1956). To prolong the interval of fluencies in the region of much smaller values were used also satellite data, and for prolonging in the region much bigger fluencies – data on cosmogenic isotopes in moon rocks. Results are shown in Fig. 13.3.1.

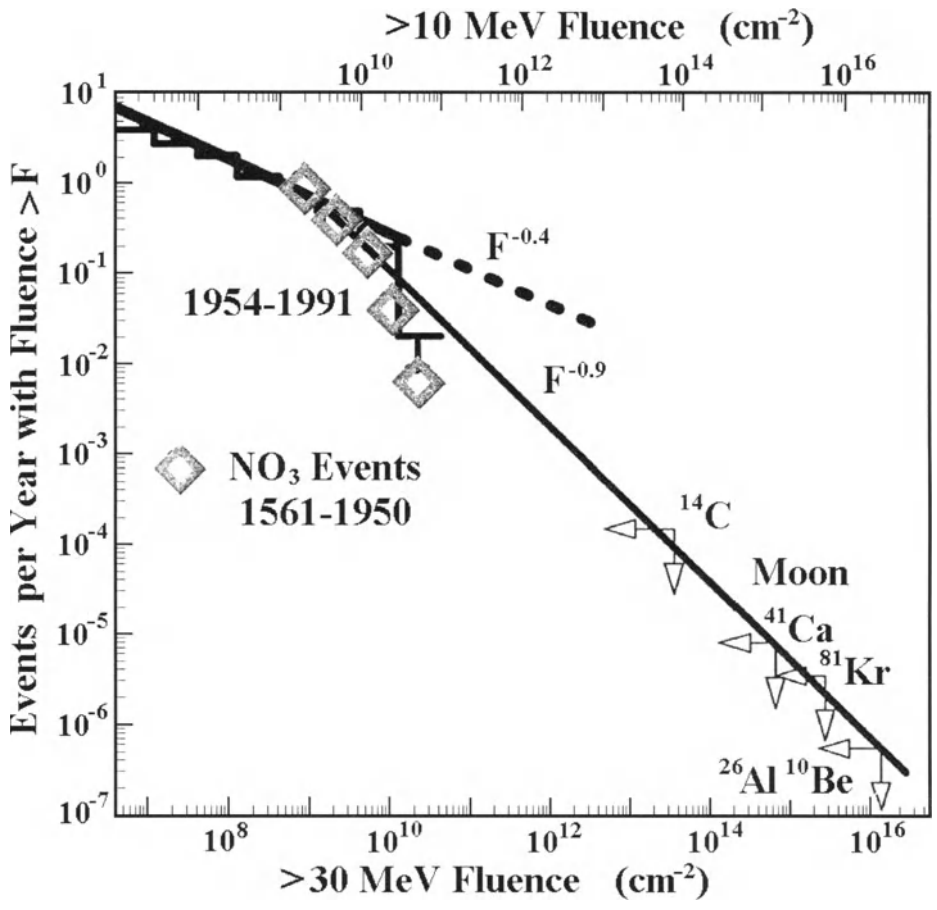

Fig. 13.3.1. Cumulative probabilities of the FEP events vs. the fluence observed by satellites, and derived from the nitrate data; the diamond shaped symbols refer to the nitrate data, the histogram and lines – to the satellite data, and fluence limits derived from cosmogenic isotopes in moon rocks. According to McCracken et al. (2001b).

The results shown in Fig. 13.3.1 in the range of fluencies $< 10^9$ cm^{-2} for particles with energy > 30 MeV are in good agreement with obtained by Dorman et al. (1993), Dorman and Pustil'nik (1995, 1999) on the basis of satellite and NM data for about five solar cycles.

13.4. On the seasonal dependency of great FEP occurrence according to nitrate data in arctic polar ice

Using solar proton event measurements from 1950 to 1990, McCracken et al. (2001c) derived a relationship between the excess nitrates and the > 30 MeV omni-directional solar proton fluence, and applied this relationship to the excess nitrate measurements from an Arctic ice core that was dated from 1561 to 1992. In Shea et al. (2003) the concentrates on a sub-set of that data — the 62 nitrate events with a > 30

MeV omni-direction fluence above 5×10^8 cm^{-2} from 1840–1950. These dates are consistent with a semi-homogeneous list of major geomagnetic storms for the same period. The intent of this study was to ascertain if there was a seasonal dependency in the nitrate enhancements and to see if there was any relationship between major geomagnetic disturbances and subsequent (i.e. within a few months) impulsive nitrate enhancements. The 62 impulsive nitrate enhancements during 1840–1950 were divided into two groups: 46 events with a derived > 30 MeV omni-directional solar proton fluence > 10^9 cm^{-2} and 16 events with a derived omni-directional solar proton fluence between 5×10^8 cm^{-2} and 1×10^9 cm^{-2}. Fig. 13.4.1 shows the distribution of these events as a function of decimal year.

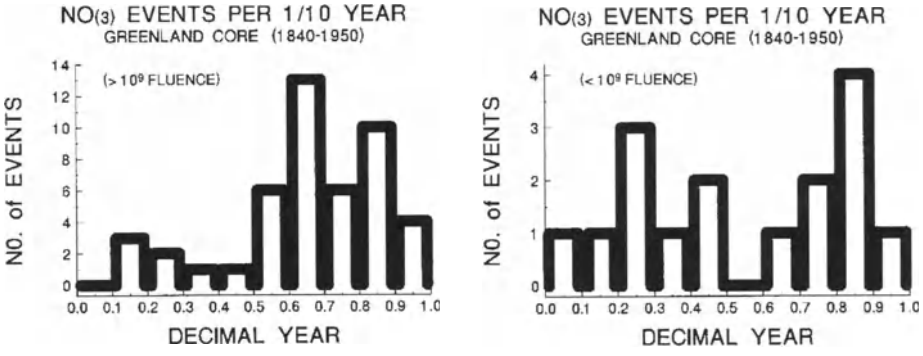

Fig. 13.4.1. Impulsive nitrate events (1850–1950) as a function of decimal year. According to Shea et al. (2003).

The distribution of the largest events, shown on the left side of Fig. 13.4.1, has a pronounced increase in the number of events during July-October. This distribution is independent of the size of the event above the 10^9 cm^{-2} fluence threshold. At this point Shea et al. (2003) do not have a physical explanation for the excessive nitrate enhancements occurring in the Northern Hemisphere late summer and early autumn time period. Nevertheless it is broadly consistent with the estimate in McCracken et al. (2001d) that the probability that a solar proton event would be detected in the NO(Y) record is 75%. The impulsive nitrate enhancements with a total derived > 30 MeV omni-directional fluence between 5×10^8 cm^{-2} and 1.0×10^9 cm^{-2} exhibited a different pattern with the maximum number of events around the periods of solar equinoxes as illustrated in the right side of Fig. 13.4.1. This pattern is similar to the annual distribution of geomagnetic disturbances noted by Russell and McPherro (1973).

13.5. On the possible connection of nitrate enhancements with geomagnetic storms and auroras

McCracken et al. (2001c) assumed that the nitrate deposition in polar ice begins approximately within 6–8 weeks after the occurrence of the proton event and may continue for another 6–8 weeks. Thus it seemed reasonable to assume that many of the impulsive nitrate events in the period 1840–1950 would be associated with geomagnetic

activity a few weeks preceding the nitrate enhancement event (GLE) in recorded history (Smart and Shea, 1991) at which time protons with energies > 20 GeV were recorded (Swinson and Shea, 1990). To ascertain if a geomagnetic disturbance occurred prior to the identified impulsive nitrate enhancements, Shea et al. (2003) inspected geomagnetic records from Royal Greenwich Observatory (Nevanlinna et al., 1993; Nevanlinna and Kataja, 1973) for significant activity for the three-month period prior to the nitrate enhancement. Additional information such as major sunspot groups near central meridian or sequences of geomagnetic activity over a short period of time was also identified if these records were available in the above publications or references therein. Of the 62 impulsive nitrate enhancements with a derived > 30 MeV omni-directional solar proton fluence above 5×10^8 cm^{-2} between 1840–1950, 52 of them (84%) appear to have some association with significant geomagnetic disturbances. When separating these events into the same categories as mentioned previously, the 46 larger fluence events have an 80% association while the 16 smaller fluence events have a 94% association. This 94% association is in agreement with the seasonal distribution of both the nitrate events shown in the right side of Fig. 13.4.1 and the known seasonal distribution of geomagnetic disturbances. The statistical significance of these results are being evaluated.

Auroras records also can be used for this purpose. Mid-latitude aurorae are often sighted during major geomagnetic storms. Using the data from Krivsky and Pejml (1988) Fig. 13.5.1 illustrates the commonality between the impulsive nitrate events and mid-latitude auroras from 1840–1900.

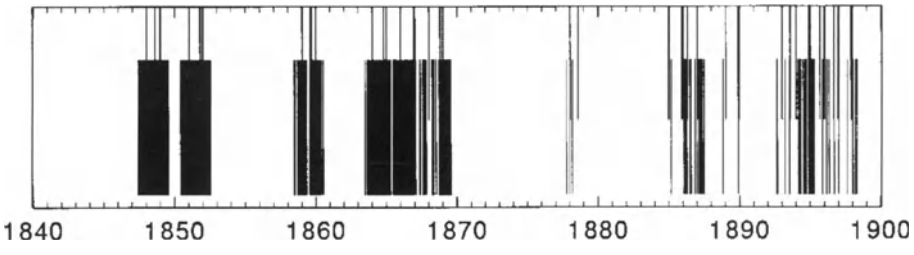

Fig. 13.5.1. Impulsive nitrate events (top) and mid-latitude auroras (bottom). According to Shea et al. (2003).

Fig. 14.4.2 reflects that the nitrate events are frequently associated with mid-latitude auroras sightings reflecting a common source.

13.6. Nitrate signals on the long term CR variations in the 415 year ice core record

According to Dreschhoff and Zeller (1995), a 120 meter ice core was retrieved from the summit area of the Central Greenland Ice Sheet in 1992. The entire core was sampled at 1.5 cm intervals, resulting in a total of almost 8000 data points representing 415 years of snow and ice accumulation at the site 72° N, 38° W. All nitrate measurements were performed by UV absorption using the super clean methods employed in handling the samples and cores. The nitrate anomalies superimposed on a seasonal background signal were primary concern. The high resolution examination made it possible to resolve these

anomalies, which represent short-term pulse-like inputs into the winter stratosphere within the polar region. The anomalies (with the background removed) are plotted in the top panel of Fig. 13.6.1. For comparison in the bottom panel of Fig. 13.6.1 the sunspot data are represented by monthly values available from 1749, and further back in time by yearly values. All data are plotted at the position of the equivalent sample number along the core. Both data series, nitrates and sunspot numbers are also plotted as a 150 point moving average.

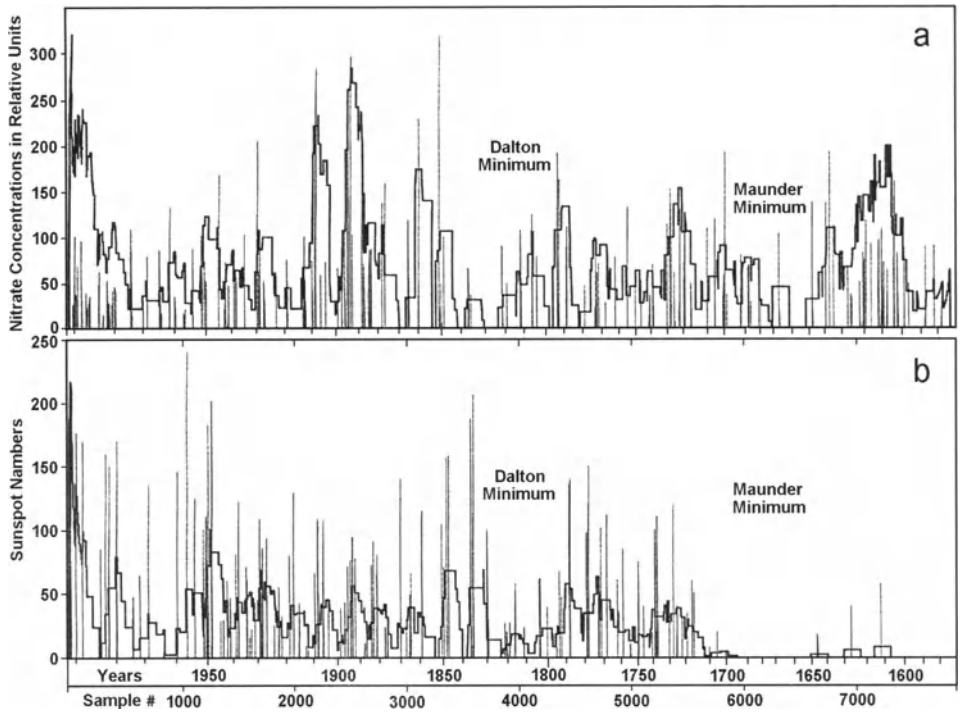

Fig. 13.6.1. Nitrate anomalies (top panel **a**) and 'winter' sunspots (bottom panel **b**) plotted along Greenland ice core. According to Dreschhoff and Zeller (1995).

From Fig. 13.6.1 can be seen the agreement between the nitrate anomalies and adjusted sunspots remarkable. Most important is the fact that the broad periods of maxima and minima do correspond and both, the well known Maunder and Dalton Minima are indicated in the Fig. 13.6.1. Dreschhoff and Zeller (1995) note that the extending of the record further into the past would be a tremendous help as can be considered from studies by Attolini et al. (1990): their investigations led to the conclusion that the Sun's behavior can be described as a non-linear system forced by an oscillator having the Hale frequency: 1 cycle/22 years. This conclusion is supported by Dreschhoff and Zeller (1994) showed on the basis of nitrate and cosmogenic isotopes data that ~ 22 year nitrate and CR periodicity having been maintained even during the Maunder Minimum (see also in Chapters 10 and 17).

13.7. CR influence on stratospheric chemistry

For investigation of CR influence on stratospheric chemistry, Quack et al (2001) used a two-dimensional chemical and transport model extended from 90°S to 90°N, and from 0 to 100 km altitude. It consists of the dynamical module 'THIN AIR' of Kinnersley (1996) and chemistry module 'TOMCAT' of Chipperfield (M1996). The dynamical module calculates temperature, pressure, horizontal and vertical transport, and includes also planetary waves and a gravity wave scheme. The chemistry module uses 57 species, considering 181 chemical reactions and 37 photolysis reactions, are considered also gas-phase and heterogeneous reactions, formation of stratospheric particles; families NO_x, HO_x and O_x are calculated in photochemical equilibrium according to Porter et al. (1976) and Solomon et al. (1981).

Quack et al (2001) considered three GLE: in October 1989 and July 2000 (data on proton fluxes from 4 MeV to 850 MeV from GOES-7), and April 2001 (data from GOES-10). In Fig. 13.7.1 are shown as example results of modeled variations of NO_x ($N+NO+NO_2$) and measured variations of NO_x for the event in July 2000.

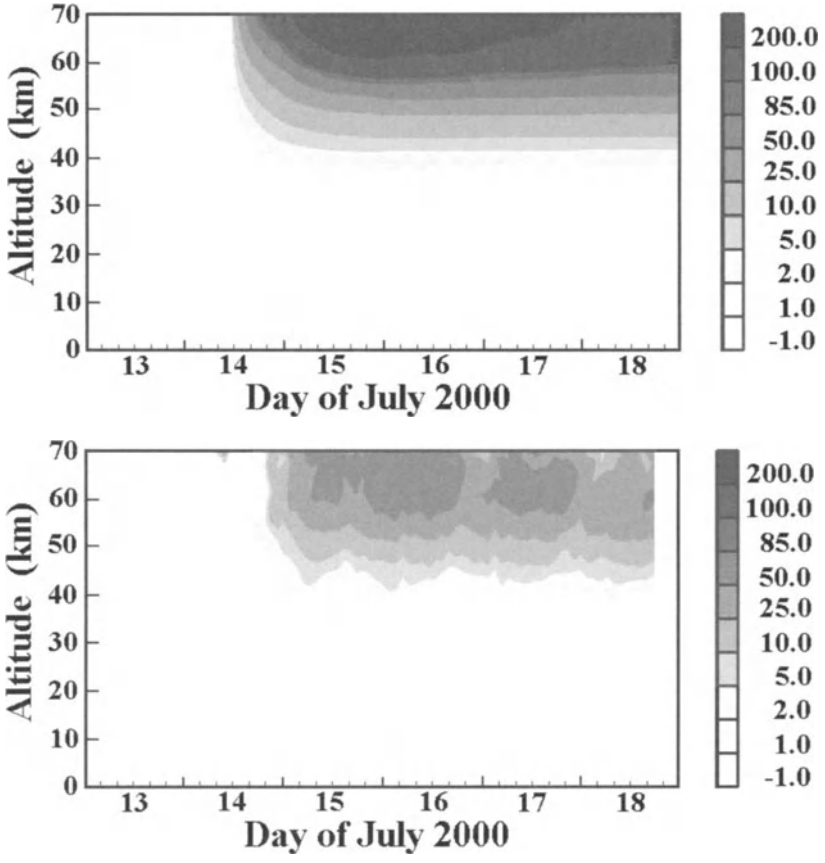

Fig. 13.7.1. Variations compared to background level in NO_x in ppb (top panel modeled, and bottom – observed by HALOE). According to Quack et al (2001).

From Fig. 13.7.1 it can be seen that both measurements and model show a similar temporal and vertical distribution: significant changes in NO_X start on 14 July 2000 at altitudes above 40 km and as NO_X is very long lived in the upper stratosphere, the enhanced values of NO_X last in the stratosphere for weeks or months (in accordance with results of Jackman et al., 2000).

In Fig. 13.7.2 are shown results of modeled variations of NO_X ($N+NO+NO_2$) for the event in April 2001.

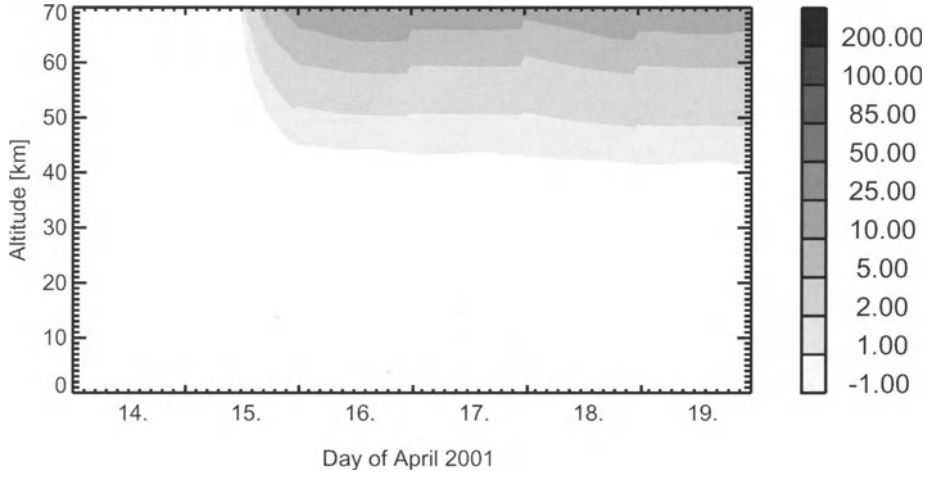

Fig. 13.7.2. Modeled of NO_X during the ground level event on April 14, 2001. According to Quack et al (2001).

13.8. Long-term galactic CR influence on the ozone layer

Martin et al. (1997) used four sets of stratospheric ozone measurements from ground by Dobson spectrophotometer and Russian one type M-124 in 1960–1995 covering polar, mid-latitude and equatorial regions: in Campinas (Brazilia) at 23°S, 45°W; Tbilisi (Georgia) at 42°N, 43°E; Belsk (Poland) at 51°N, 21°E; and in Tromso (Norway) at 69°N, 19°E (see Fig. 13.8.1).

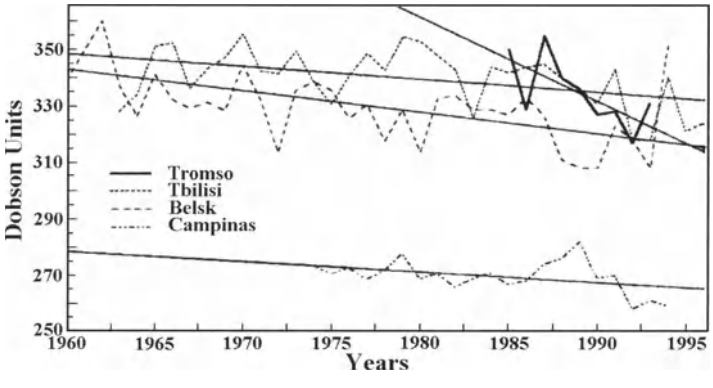

Fig. 13.8.1. Stratospheric ozone variability over Tromso, Belsk, Tbilisi and Campinas. According to Martin et al. (1997)

From Fig. 13.8.1 can be seen that only in high latitude was a great decrease of total ozone abundance observed; in other regions the decrease was only about 10%. It was found also (see Fig. 13.8.2) that there is a correlation between total ozone abundance with CR intensity in stratosphere according to balloon measurements near Moscow, as well as with solar activity (better correlation, about 0.7 correlation coefficient with CR, was observed for high and mid-latitude regions, and only about 0.3 correlation coefficient for equatorial region).

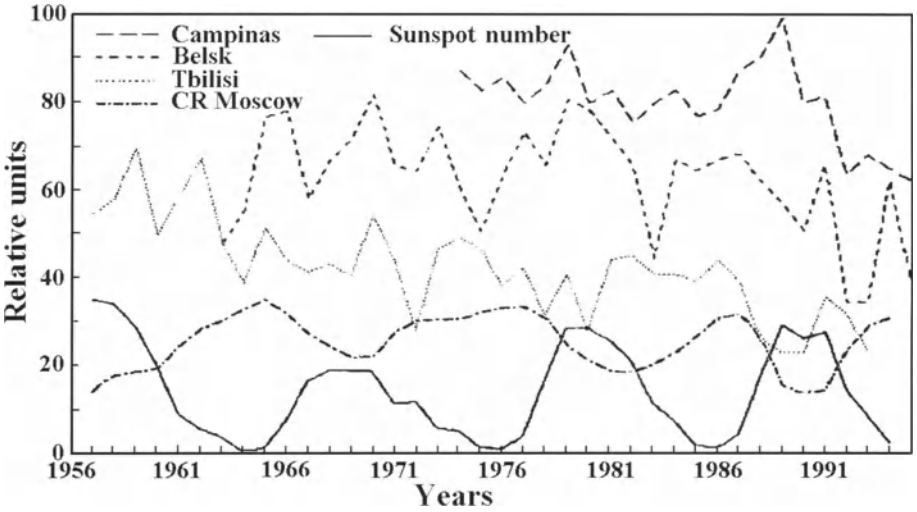

Fig. 13.8.2. Comparison of long-term variations of ozone abundance with variations of galactic CR intensity and solar activity. According to Martin et al. (1997).

13.9. On the possible relationship of atmospheric ozone dynamics with global auroral activity, CR Forbush effects, and IMF clouds

It is well known that the global auroral activity, CR Forbush effects, and IMF clouds are connected with geomagnetic storms and influenced on CR leaded, as rule, to the decrease of their intensity and air ionization. From other hand, particles and radiation of aurora can lead to increasing of air ionization. It is expected that the change in air ionization will lead to some change of the atmosphere chemistry and ozone contents (see Sections 13.7 and 13.10 which described results of simulation).

The possible relationship between atmospheric ozone dynamics (characterized by daily index A) and global auroral activity (daily values of the auroral activity index AE) were investigate by Marcucci et al. (1995) by using data on the daily total ozone content from the TOMS instrument on board NIMBUS-7 for the southern high latitudes (> 60° S) during springtime periods of 1980-1985 epoch. The index $A(N_o)$ characterized the area of ozone layer enclosed by a contour of a chosen O_3 level N_o From the different possible $A(N_o)$ Marcucci et al. (1995) selected the one in which the $A(N_o)$ border roughly coincided with the lower boundary of the auroral oval. The A-time evolution was found to be characterized by increasing values in the early September

(contemporary to the formation of the Antarctic ozone hole). To check better a possible relationship between aurora activity and ozone depletion Marcucci et al. (1995) look for daily data associated with a stable polar vortex (its border approximately coincide with the one of the auroral oval. In Fig. 13.9.1 are shown correlation coefficients between daily indexes A for ozone and AE for auroras in dependence of time lag. For all periods a statistical significant lag is found at the 99% confidence level, except for 1983 (98% level).

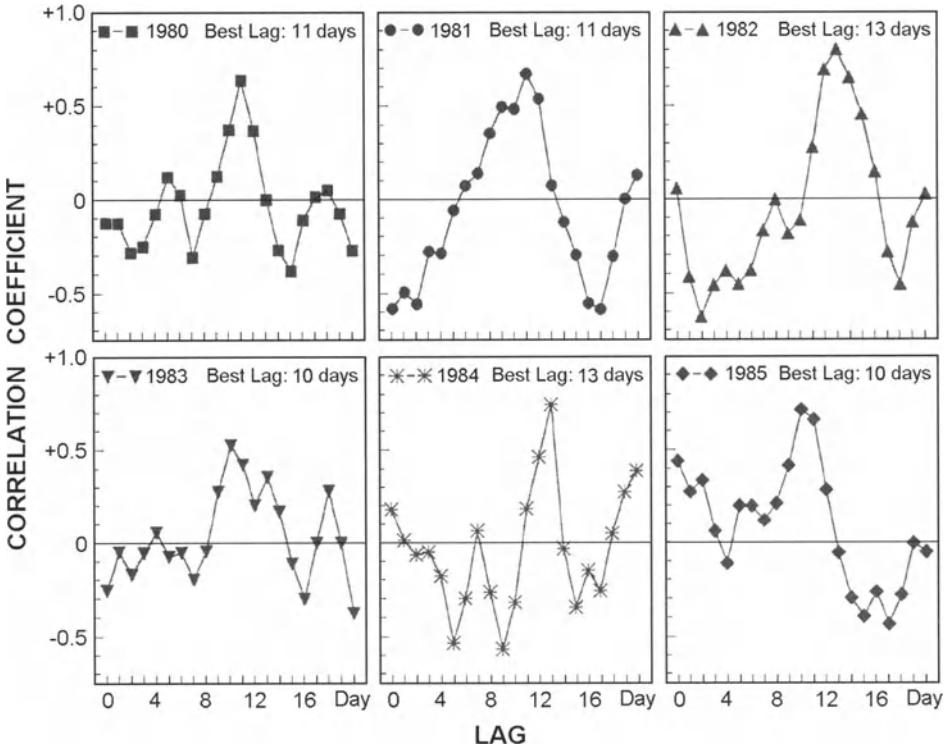

Fig. 13.9.1. Correlation coefficients between daily indexes A for ozone and AE for auroras in dependence of time lag separately for each year 1980-1985. According to Marcucci et al. (1995).

From Fig. 13.9.1 can be seen that the time lag between ozone characteristics and auroral activity is about 10–13 days according to data for 6 years from 1980 to 1985.

The possible influence of CR Forbush-decreases and IMF clouds on ozone contents was investigate by Nachkebia et al. (2003) on the basis of 231 ozone-sounds flown at Boulder (USA) in 1997–2002 (ozone data, http://www.cmdl.noaa.gov/info/ftpdata.html). It was considered 45 cases of galactic CR Forbush decreases which are observed by the Tbilisi NM and other NM of world network (data of events of Forbush CR intensity decreases, http://helios.izmiran.rssi.ru/cosray/events00.htm). Were used also data on 51 events of the IMF clouds were used as sign of the IMF disturbances (WIND/MFI Magnetic Cloud Data, http://lepmfi.gsfc.nasa.gov/mfi/mag_cloud_pub1.html). The data set used for the investigation enables to reveal only 23 events of the IMF disturbances accompanied with ozone-sound flights. It was found that the IMF cloud may be one of reasons of the ozone depletions (see Fig. 13.9.2).

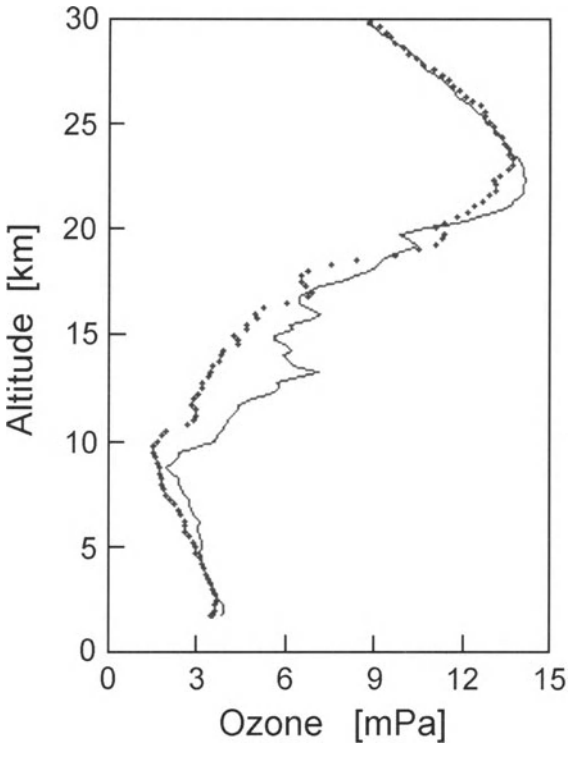

Fig. 13.9.2. Averaged ozone vertical profiles before (lines) and after IMF magnetic clouds (points). According to Nachkebia et al. (2003).

From Fig 13.9.2 can be seen that the maximum depletion is observed at the altitude about 13 km, which is about 20 % of main ozone peak value. There were observed a narrow layer of ozone increase. Averaged total ozone decreases from 326 to 303 DU. It was also determined the temperature effect in the ozone depletion. It is neglected due to small differences between the temperatures before and after magnetic clouds. The estimation of the magnetic cloud effect in CR is shown in Fig. 13.9.3 which represents the superposed epoch analyses for Oulu NM daily data during discussed period 1997–2002. In this case 51 zero days are selected as days of arrival at Earths orbit of the IMF clouds. From the Fig. 13.9.3 can be seen that the IMF cloud affect on galactic CR intensity is small (about 1 %). The same analyses on the basis of Tbilisi NM data reveal even smaller effect (in accordance with expected because geomagnetic cutoff rigidity for Tbilisi is much bigger than for Oulu). The determined average IMF cloud effect in galactic CR intensity is sufficiently smaller than the average amplitude of CR Forbush decrease. Nachkebia et al. (2003) came to conclusion that the IMF cloud affect to ozone depletion goes not only via the galactic CR intensity variation, which amplitude is rather small. From other hand, for air ionization and formation of ozone layer in the upper troposphere and in stratosphere much more important must be galactic CR with sufficiently smaller energy; the Forbush decrease and effect of IMF clouds in this energy range expected much bigger than observed by NM, may be about the same order as it is observed in ozone data.

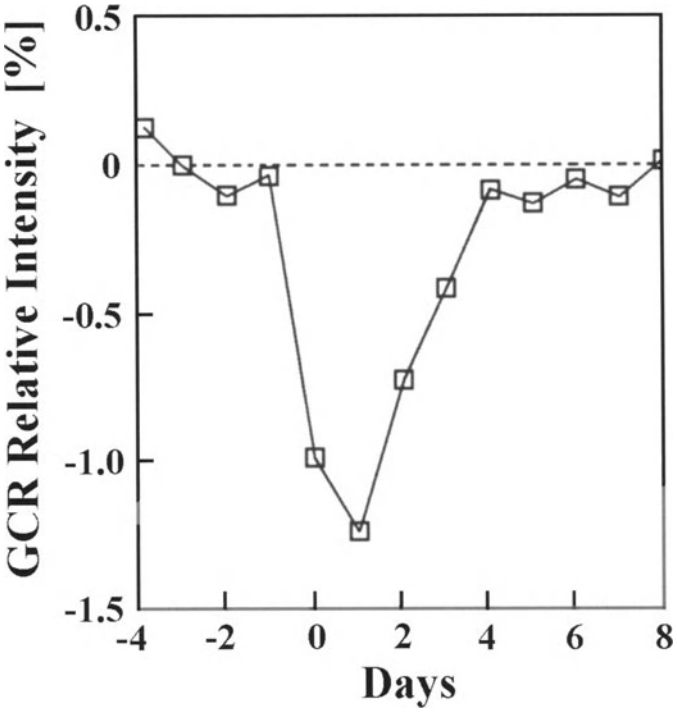

Fig. 13.9.3. Magnetic cloud affect in Oulu NM daily relative intensity (51 zero days are selected as the start days of the IMF clouds during 1997–2002). According to Nachkebia et al. (2003).

13.10. Short-term solar CR influence on the ozone layer

13.10.1. Discovery and modeling of GLE influence on the ozone layer

The influence of precipitating solar energetic particles (SEP) on high latitude ozone first has been observed in the large August 1972 flare (e.g. Heath et al., 1977) and has led to the discovery of the influence of NO_x on stratospheric and in particular on ozone chemistry (Crutzen et al., 1975). The strongest modifications so far have been observed during the August 1972 and October 1989 events (Heath et al., 1977; Vitt et al., 2000; Jackman et al., 2000), an event comparable in size and consequences was in July 2000 (Jackman et al., 2001). For three GLE in October 1989, July 2000, and April 2001, Quack et al (2001) extended their calculations of CR influence on chemical processes in the stratosphere (see Section 13.7) to determine the expected influence also on ozone layer.

13.10.2. GLE in August 1972

For the GLE in August 1972 results are shown in Fig. 13.10.1 and Fig. 13.10.2. From Fig. 13.10.1 can be seen that in the total O_3 contents above 4 mb level in the equatorial zone (5° S to 5° N) with a big cut off rigidity (about 15 GV) there is no any significant effect owed by GLE; in latitude zone 55° N to 65° N there is significant, but

short effect on ozone contents (decrease about 10% during two days after GLE); but in high latitude zone 75° N to 80° N there is big effect in ozone contents (decrease about 20% during more than 20 days after GLE). More detail information on the dynamic of ozone layer in high latitude zone 75° N to 80° N owed by August 1972 GLE can be seen from Fig. 13.10.2. Heath et al. (1977) came to conclusion that the long duration effect of solar CR influence on ozone layer is mostly due to the catalytic effect of solar energetic protons produced NO.

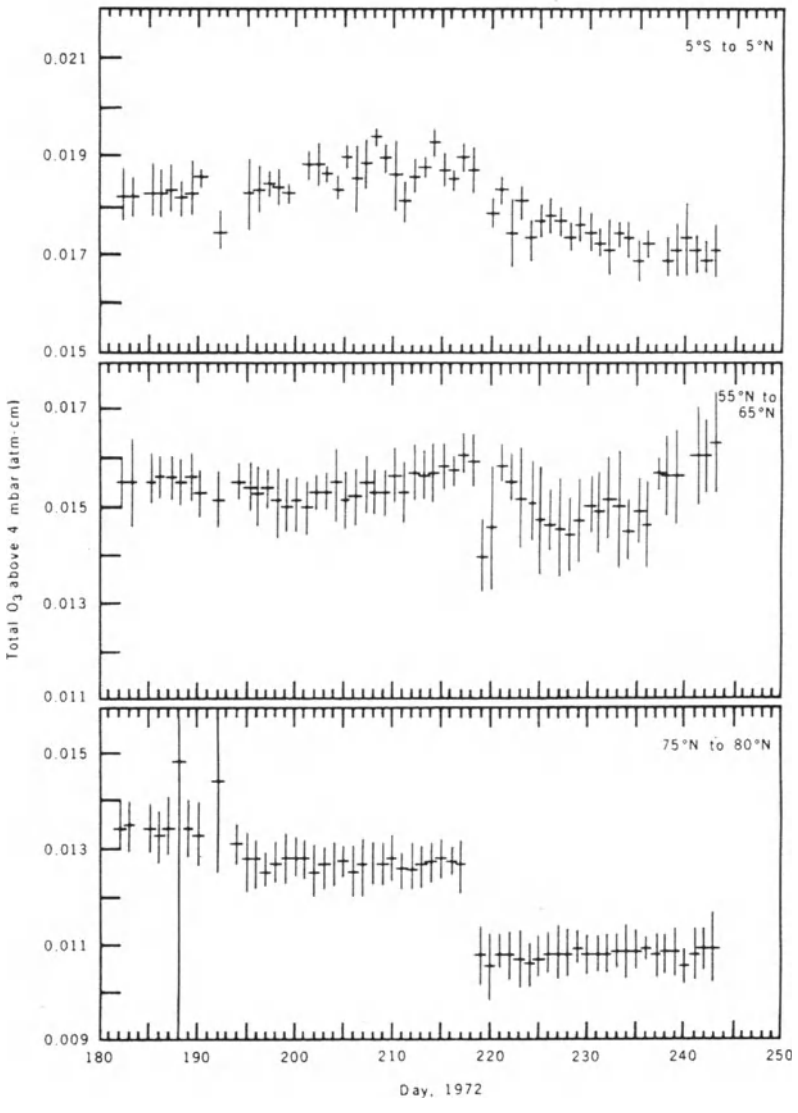

Fig. 13.10.1 Zonally averaged total O_3 above the 4 mb pressure surface for equatorial (top panel), middle latitudes (middle), and high latitudes (bottom) during July–August 1972. The GLE occurred on 4 August 1972 (day 217). According to Heath et al. (1977).

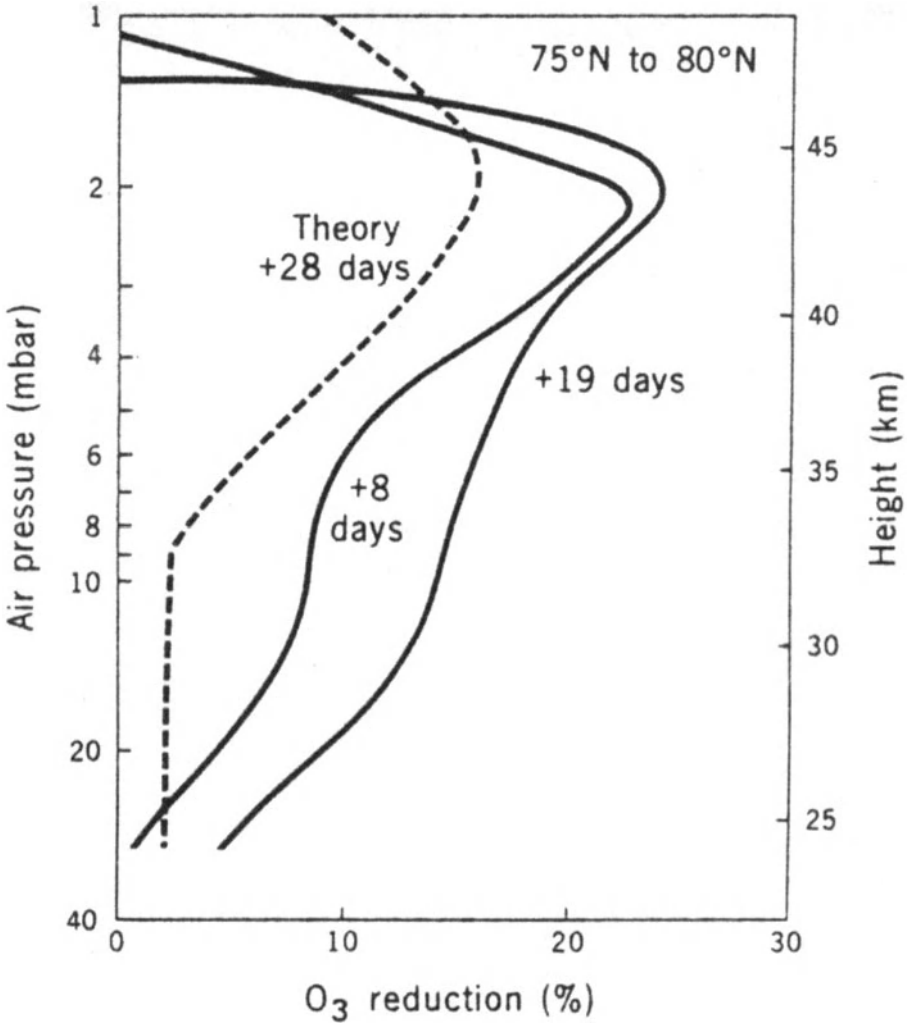

Fig. 13.10.2. Percentage decrease of the O_3 partial pressure versus air pressure derived from the average of the 7 days before 4 August 1972 and 7 day periods centered on 8 and 19 days after the GLE (solid lines). The dashed line is a calculation of the O_3 reduction for 1 September 1972 (28 days after GLE) owed to the catalytic effect solar energetic protons produced NO. According to Heath et al. (1977).

13.10.3. GLE in July 2000

Results for the event July 2000 are shown in Fig. 13.10.3 in comparison with observations: it can be seen that model calculations based on experimental data of GOES-7 on solar energetic proton fluxes in interval 4–850 MeV are in good agreement with observed sufficient decreases of ozone abundance.

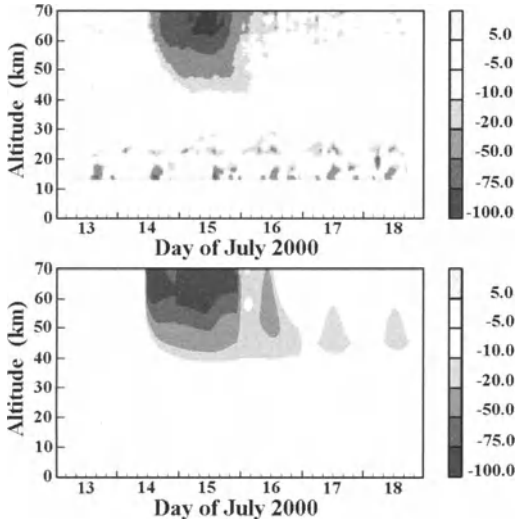

Fig. 13.10.3. Variations compared to background level in O_3 in % (down panel modeled and upper panel observed) during the event in July 2000. According to Quack et al (2001).

In Fig. 13.10.4 are shown results of observations and modeling for July 2000 event by Jackman et al. (2001).

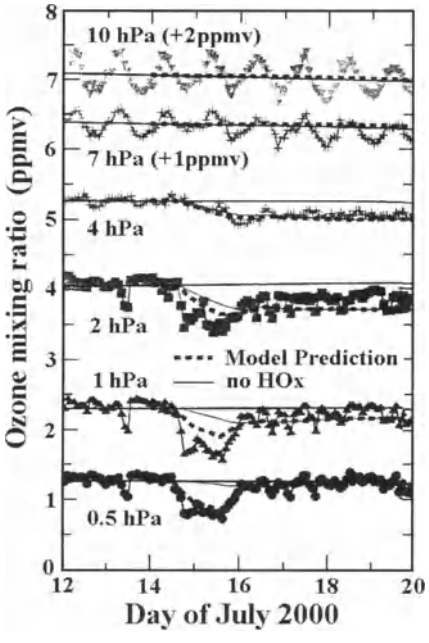

Fig. 13.10.4. Polar Northern Hemisphere ozone observations from NOAA 14 SBUV/2 measurements and model computations for the 10, 7, 4, 2, 1, and 0.5 hPa levels during the July 12-19, 2000. The dashed lines indicate the 2-D model prediction with both SPE-driven HO_X increases. According to Jackman et al. (2001).

13.10.4. GLE in April 2001

For event of April 2001 results are shown in Fig. 13.10.5.

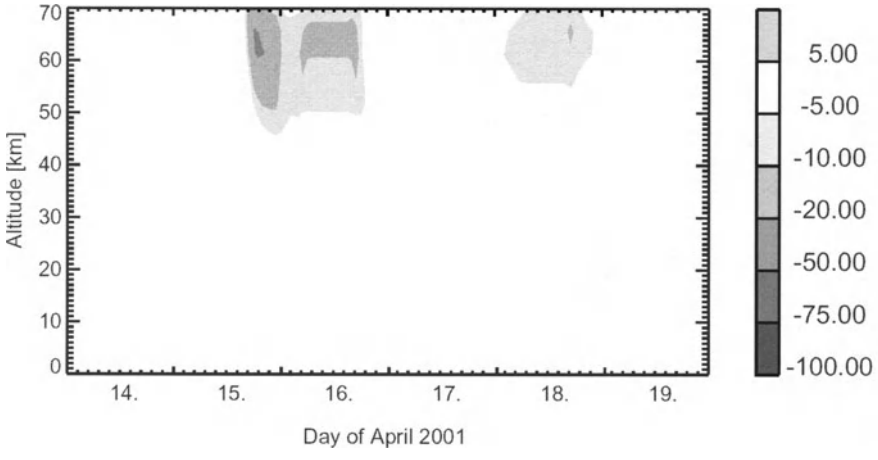

Fig. 13.10.5. The expected changing in O_3 contents during GLE of April 14, 2001 (Quack et al., 2001).

13.11. Peculiarities of GLE influence on chemistry and ozone layer in the upper stratosphere and lower mesosphere

According to Quack et al. (2001), measurements of HO_X in high altitude region are extremely sparse, but as ozone destruction in this altitude is mainly caused by HO_X, comparison of ozone measurements to modeled O_3 can be used as an indicator of the validity of HO_X production during the event. As HO_X is extremely short lived in the upper stratosphere and lower mesosphere, HO_X will decrease to background level as soon as the energetic particle fluxes decrease. Equally, ozone depletion owed to HO_X will last only as long as the event lasts. Again, measurement and model show similar temporal and vertical behavior, but the amount of ozone loss is overestimated in the model. The model produces almost the same results if the particle spectrum extends up to 500 MeV or 800 MeV: although ionization curves are markedly different because higher energies can penetrate down into the lower stratosphere or even the troposphere, modifications caused by them vanish since atmospheric density is too large. Thus changes of atmospheric chemistry due to solar energetic particles seem to be limited to altitudes of above about 35–40 km; even in the October 1989 event despite much larger particle fluencies variations in NO_X and O_3 cannot be found below 30–35 km (Quack et al, 2001).

Chapter 14

Cosmic Ray Influence on Planetary Cloud Covering and Long Term Climate Change

14.1. Short historical review

Several possible causes of global climate change have been discussed in the scientific literature (see in Swensmark, 2000): 1) orbital changes in the Earth's motion around the Sun; 2) internal variability in the climate system, e.g., changes in atmospheric and ocean circulation; 3) large volcanic eruptions, which are known to cause a sudden cooling lasting several years; 4) changes in concentration of greenhouse gases (increase of atmospheric CO_2 concentration during the last 100 years by about 30% has led to an increase approximately 0.7 °C in the global surface temperature); 5) changes in solar activity and in CR intensity. This last possible cause will be the main subject of this Chapter.

About two hundred years ago the famous astronomer William Herschel (1801) suggested in London that the price of wheat is directly controlled by the number of sunspots, based on his observation that less rain fell when there was a small number of sunspots (this research has been continued recently, see below in Section 14.5). The solar activity level is known from direct observations over about 450 years, and from data of cosmogenic nuclides for more than 10,000 years (Eddy, 1976; see also Chapters 10 and 17). For this long time there has been a striking qualitative correlation between cold and warm climate periods and low and high solar activity, correspondingly.

As an example, Fig. 14.1.1 shows the change in the concentration of radiocarbon during the last millennium (a higher concentration of ^{14}C corresponds to a higher intensity of CR and to lower solar activity, see Chapter 17).

It can be seen that during 1000–1300 AD the CR intensity was very low and solar activity very high, which coincided with the warm medieval period (during this period Vikings settled in Greenland). After 1300 AD solar activity decreased considerably and CR intensity increased, and a long cold period followed (the so called Little Ice Age, which included the Maunder minimum 1645–1715 AD and lasted until the middle of 19th century).

Friis-Christiansen and Lassen (1991) and Lassen and Friis-Christiansen (1995) found on the basis of 400 years' data that the filtered solar activity cycle length is closely connected with the variations of average surface temperature in the northern hemisphere. Labitzke and Van Loon (1993) showed on the basis of data of solar cycles 18–21 that the height of the pressure surfaces in the lower stratosphere varies in phase with solar activity (which means that the air temperature increases with increasing of the level of solar activity). Swensmark (2000) also discussed the problem of the possible influence of solar activity on the Earth's climate through the changes in solar irradiance. But the direct satellite measurements of the solar irradiance during the last two solar cycles show that the variations during a solar cycle is only about 0.1%, corresponding to about 0.3 $W.m^{-2}$. This value is too small to explain the observed changes in the global

temperature (Lean et al., 1995). Much bigger change during a solar cycle occur in UV radiation (about 10%, which is important in the formation of the ozone layer). High (1996), and Shindell et al. (1999) suggested that the heating of the stratosphere by UV radiation can be dynamically transported into the troposphere.

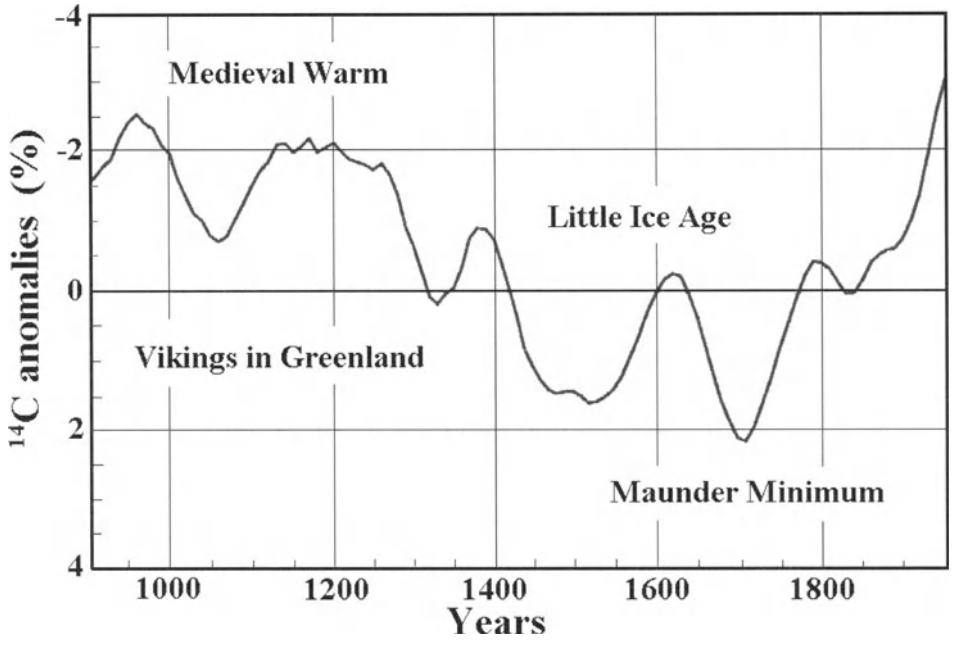

Fig. 14.1.1. The change of CR intensity reflected in radiocarbon concentration during the last millennium. The Maunder minimum refers to the period 1645–1715. According to Swensmark (2000).

Many authors considered galactic and solar CR as an important link between solar activity and changing of the climate. As was shown in Chapter 12, CR is the main source of air ionization below 40–35 km (only near the ground level, lower than 1 km, are radioactive gases from the soil also important in air ionization). The first to suggest a possible influence of air ionization by CR on the climate was Ney (1959). Swensmark (2000) noted that the variation in air ionization caused by CR could potentially influence the optical transparency of the atmosphere, by either a change in aerosol formation or an influence on the transition between the different phases of water. Many authors considered these possibilities: Ney (1959), Dickinson (1975), Pudovkin and Raspopov (1992), Pudovkin and Veretenenko (1992, 1996), Tinsley (1996), Swensmark and Friis-Christiansen(1997), Swensmark (1998), Marsh and Swensmark (2000a,b). The possible statistical connections between the solar activity cycle and the corresponding long term CR intensity variations with characteristics of climate change were considered in Dorman et al. (1987, 1988a,b). This problem for the middle ages in England was considered in Dorman, Pustil'nik and Yom Din (2003a,b) through available data on wheat market dynamics (see below, Section 14.5). Dorman (2003) reconstructed CR intensity variations for the last 400 years on the basis of solar activity data, taking into account parameters of convection-diffusion and drift mechanisms obtained from investigation of CR-SA hysteresis phenomenon; results obtained are compared with

radiocarbon and climate change data (more details on the CR-SA hysteresis phenomenon can be found in Dorman, M2005).

As it was shown in Ch. 11, CR play a key role in the formation of thunderstorms and lightnings. Many authors considered atmospheric electric field phenomenon as a possible link for the solar activity influence on the Earth's climate: Markson (1978), Price (2000), Tinsley (2000), Schlegel et al. (2001), Dorman and Dorman (2003), Dorman et al. (2003).

Let us note that in the general for a possible CR link it is necessary to take into account also the influence of long term changes of the geomagnetic field on CR intensity through the change of cut off rigidity (Shea and Smart, 2003). So the general hierarchical relationship determining the part of long-term climate change caused by CR will be: (solar activity cycles + long-term changes in the geomagnetic field) → (CR long term modulation in the Heliosphere + long term variation of cut off rigidity) → long term variation of clouds covering → climate change. The subject of the first link in this hierarchical connection is beyond the scope of the present monograph, and will be considered in detail in our next book Dorman (M2005).

14.2. On the connection of CR solar cycle variation with variation of planetary cloud coverage

A very important result for an understanding of the mechanism of the influence of solar activity cycle on the Earth's climate has recently been obtained: it was found that the Earth's cloud coverage (observed by satellites) is strongly correlated with CR intensity (Swensmark and Friis-Christensen, 1997; Swensmark, 1998, 2000; Marsh and Swensmark, 2000a,b). Clouds influence irradiative properties of the atmosphere by both cooling through reflection of incoming short wave solar radiation, and heating through trapping of outgoing long wave radiation. The total result depends mostly on the height of the clouds. According to Hartmann (1993), high optically thin clouds tend to heat while low optically thick clouds tend to cool (see Table 14.2.1).

Table 14.2.1. Global annual mean forcing owed to various types of clouds, from the Earth Radiation Budget Experiment (ERBE), according to Hartmann (1993). The positive forcing increases the net radiation budget of the Earth and leads to a warming; negative forcing decreases the net radiation and causes a cooling.

Parameter		High clouds		Middle clouds		Low clouds	Total
		Thin	Thick	Thin	Thick	All	
Global fraction	(%)	10.1	8.6	10.7	7.3	26.6	63.3
Forcing (relative to clear sky):							
Albedo (SW radiation)	(Wm^{-2})	-4.1	-15.6	-3.7	-9.9	-20.2	-53.5
Outgoing LW radiation	(Wm^{-2})	6.5	8.6	4.8	2.4	3.5	25.8
Net forcing	(Wm^{-2})	2.4	-7.0	1.1	-7.5	-16.7	-27.7

From Table 14.2.1 it can be seen that low clouds give a cooling of about 17 $W.m^{-2}$, so they play an important role in the Earth's radiation budget (Ohring and Clapp, 1980; Ramanathan et al., 1989; Ardanuy et al., 1991). So even small changes in the lower

cloud coverage can give important changes in the radiation budget and considerably influence the Earth's climate (let us remember that the solar irradiance changes during solar cycle by only about $0.3\ W.m^{-2}$). Fig. 14.2.1 shows the composite of satellite observations of the Earth's total cloud coverage in comparison with CR intensity (according to Climax NM) and solar activity data (intensity of 10.7 cm solar radio flux).

From Fig. 14.2.1 it can be seen that the correlation of global cloud coverage with CR intensity is much better than with solar activity. Marsh and Swensmark (2000a) came to conclusion that CR intensity connects very well with low global cloud coverage, but not with high and middle clouds (see Fig. 14.2.2).

It is important to note that low clouds lead, as rule, to the cooling of the atmosphere. It means that with increasing CR intensity and cloud coverage (see Fig. 14.2.1), the surface temperature is expected to decrease. It is in good agreement with the situation shown in Fig. 14.1.1 for the last 1000 years, and with direct measurements of the surface temperature for the last four solar cycles (sees below, Section 14.3).

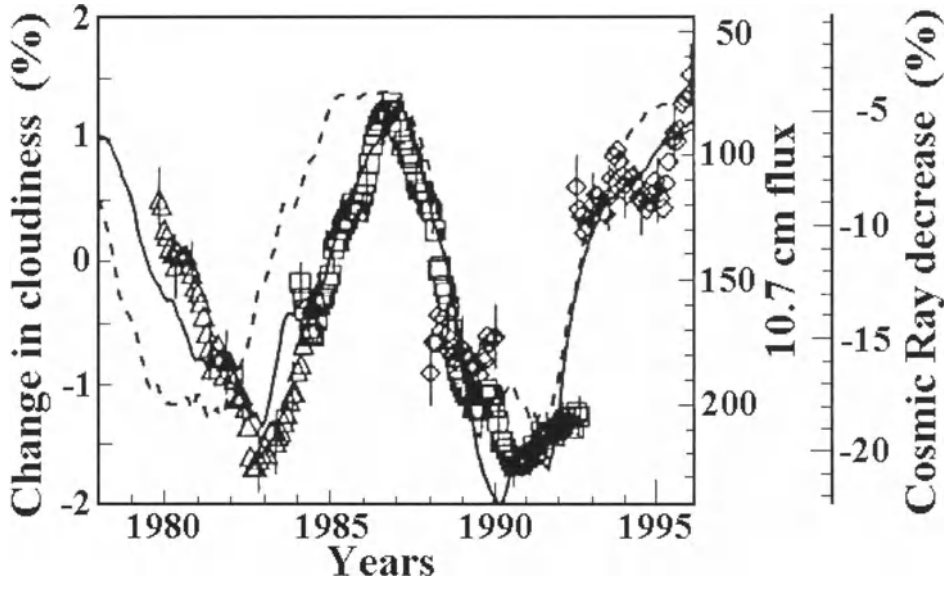

Fig. 14.2.1. Changes in the Earth's cloud coverage: triangles - from satellite Nimbus 7, CMATRIX project, (Stowe et al., 1988); squares - from the International Satellite Cloud Climatology Project, ISCCP, (Rossow and Shiffer, 1991); diamonds – from the Defense Meteorological Satellite Program, DMSP (Weng and Grody, 1994, Ferraro et al., 1996). Solid curve – CR intensity variation according to Climax NM, normalized to May 1965. Broken curve – solar radio flux at 10.7 cm (in units $10^{-22}\ W.m^{-2}.Hz^{-1}$). All data are smoothed using 12 months running mean. According to Swensmark (2000).

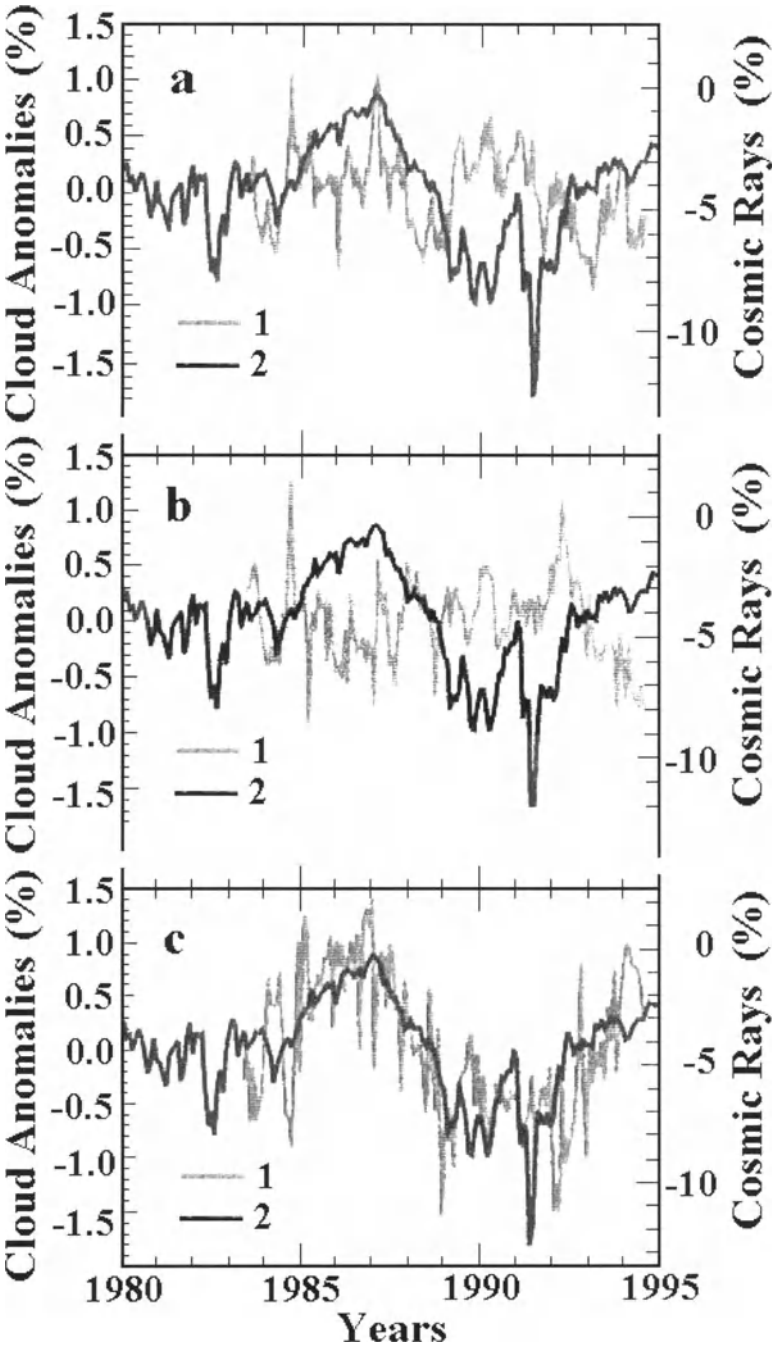

Fig. 14.2.2. CR intensity according to Huancayo/Haleakala NM (cut off rigidity 12.9 GV, normalized to October 1965, curve *2*) in comparison with global average of monthly cloud coverage anomalies (curves *1*) for: ***a*** – high clouds, H > 6.5 km, ***b*** – middle clouds, 6.5 km >H > 3.2 km, and ***c*** – low clouds, H < 3.2 km. According to Marsh and Swensmark (2000a).

14.3. On the possible influence of long-term CR variation on long term changing of planetary surface temperature

In Fig. 14.3.1 are shown 11 year moving average of Northern Hemisphere marine and land air temperature anomalies for 1935–1995 in comparison with CR intensity according to ion chamber data (constructed from Cheltenham/Fredericksburg for 1937–1975 and Yakutsk for 1953–1994, according to Ahluwalia, 1997) and Climax NM data, as well as with other parameters (unfiltered solar cycle length, sunspot numbers, and reconstructed solar irradiance).

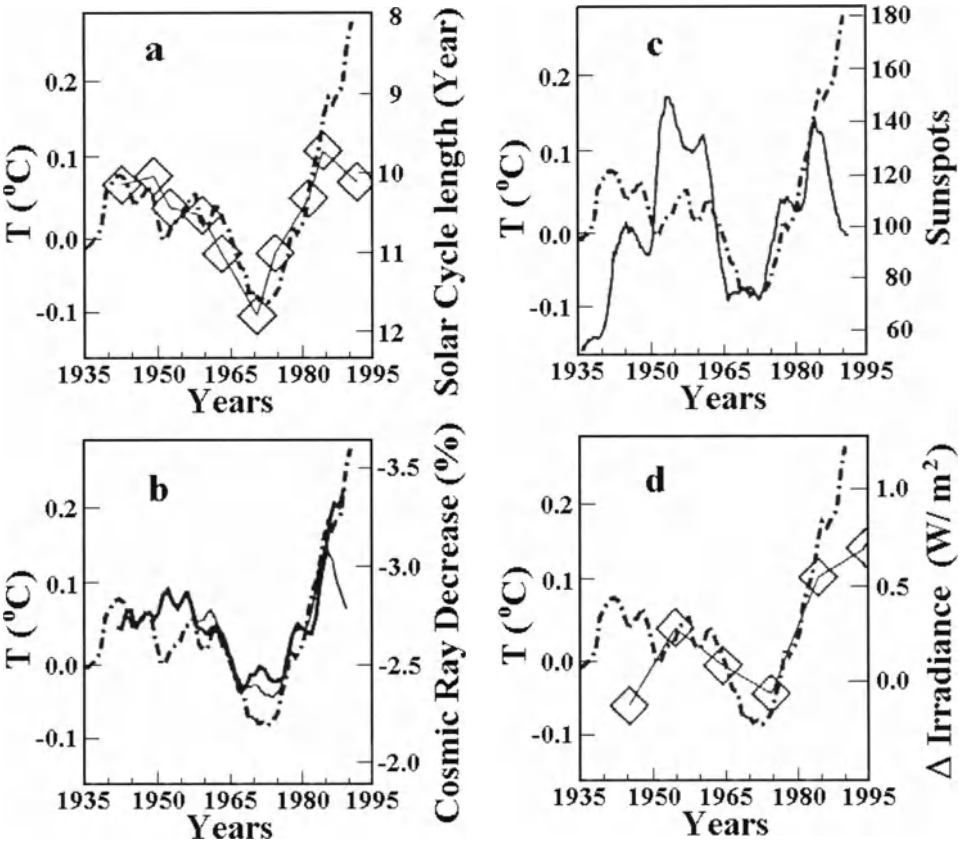

Fig. 14.3.1. 11 year moving average of Northern hemisphere marine and land air temperature anomalies (broken curve) compared with: (***a***) unfiltered solar cycle length; (***b***) 11 year moving average of CR intensity (thick solid curve – from ion chambers 1937–1994, normalized to 1965, and thin solid curve – from Climax NM, normalized to ion chambers); (*c*) 11 year moving average of sunspot numbers; and (***d***) decade variation in reconstructed solar irradiance from Lean et al., 1995 (zero level corresponds to 1367 $W.m^{-2}$). According to Swensmark (2000).

From Fig. 14.3.1 one can see that the best correlation of air global temperature is with CR intensity, in accordance with the results described in Section 14.2. According to Swensmark (2000), the comparison of Fig. 14.3.1 with Fig. 14.2.1 shows that the increase of air temperature by 0.3 °C corresponds to a decrease of CR intensity measured

by ionization chambers on 3.5% and a decrease of global cloudiness on 3%; this is equivalent to an increase of solar irradiance on the Earth's surface by about 1.5 $W.m^{-2}$ (according to Rossow and Cairns, 1995) which is about 5 times bigger than the actual solar cycle change of solar irradiance (only 0.3 $W.m^{-2}$, see Section 14.1).

14.4. CR influence on weather during Maunder minimum.

Fig. 14.4.1 shows the situation in the Maunder minimum according to data of reconstructed solar irradiance (Lean et al., 1992, 1995), data on concentration of the cosmogenic isotope ^{10}Be (Beer et al., 1991), proportional to CR intensity variation (see Ch. 10), and recently reconstructed air surface temperature for the northern hemisphere (Jones et al., 1998).

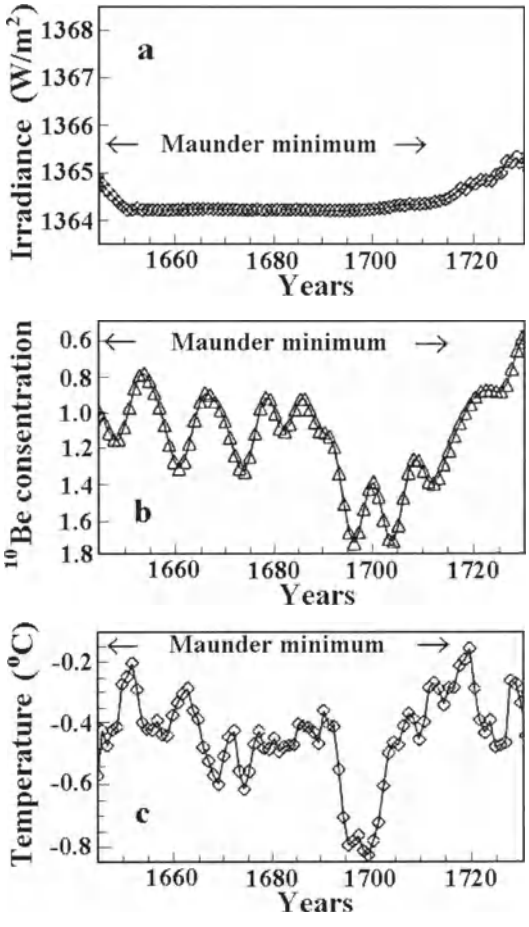

Fig. 14.4.1. Situation in the Maunder minimum: ***a***) variation in reconstructed solar irradiance from Lean et al. (1995); ***b***) variation in ^{10}Be concentration from Beer et al. (1991); ***c***) reconstructed air surface temperature for the northern hemisphere from Jones et al. (1998). According to Swensmark (2000).

The solar irradiance is almost constant during the Maunder minimum and about 0.24% (or about 0.82 $W.m^{-2}$) lower than the present value (see Fig. 14.4.1a), but CR intensity and air surface temperature have very similar variations in the same manner as was described in previous sections: with increasing CR intensity there is a decrease in air surface temperature (see Fig. 14.4.1b and 14.4.1c). The highest level of CR intensity was in 1690–1700, which corresponds to the minimum of air surface temperature at about the same time (Mann et al., 1998, also show that the coldest decade was 1690–1700).

14.5. Possible influence of solar activity/cosmic ray intensity long term variations on wheat prices (through weather changes) in medieval England

As we mentioned in Section 14.1, Herschel (1801) was the first who paid attention to an evident correlation between the observed number of sunspots and the state of the wheat market, based on a series of wheat prices published by Smith (M1776). Herschel showed that five prolonged periods of few sunspots correlated with costly wheat. The next scientist in this field was the well known English economist and logician William Stanley Jevons (1875), one of the creators of Neoclassical Economic Theory. He directed his attention to the first part of the data, published later in the first volume of a series of monographs by Rogers (M1887). In this volume were presented wheat prices over 140 years, from 1259 up to 1400. Jevons (1875) discovered that the time intervals between high prices were close to 10–11 years. The coincidence of these intervals with the period of the recently discovered 11 year cycle of solar activity led him to suggest the solar activity cycle as a 'synchronization' factor for fluctuations in wheat prices (Jevons, 1878). As a next step he extrapolated his theory to stock markets of the 19^{th} Century in England and was impressed by a close coincidence of five stock exchange panics with five minima in solar spot numbers that preceded these panics. He suggested that both solar and economic activities are subjected to a harmonic process with the same constant period equal to 10.86 year. However, the subsequent discovery of the non-harmonic behavior of solar cycles, with periods varying from 8 to 15 years, and the later observation of lack of coincidence between panics predicted by Jevons and the actual ones, destroyed his arguments. A notable statement by one of his critics, Prof. Proctor (1880), remarks that, under conditions of variable periods of solar activity, it would be more effective not to use the ephemeral 'harmonic period', but to confront a chosen phase of solar activity with the state of the market, and to search for any correlation between them.

The Rogers (M1887) database included wheat prices in England in the Middle Ages (1249–1703) was used by Dorman, Pustil'nik and Yom Din (2003a,b), Pustil'nik et al. (2003) to search for possible manifestations of solar activity and CR intensity variations' influence on wheat prices (through weather changes). The graph of the time series of wheat prices (Fig. 14.5.1) contains two specific features:

1. A transition from 'low price' state to 'high price' state during 1530–1630, possibly owed to access to sources of cheap silver in the recently discovered New World. We use a logistic curve for fitting our data, aiming at long term extrapolation of this transition.
2. The existence of two populations in the price sample: noise-like variations with low amplitude bursts and several bursts of large amplitude.

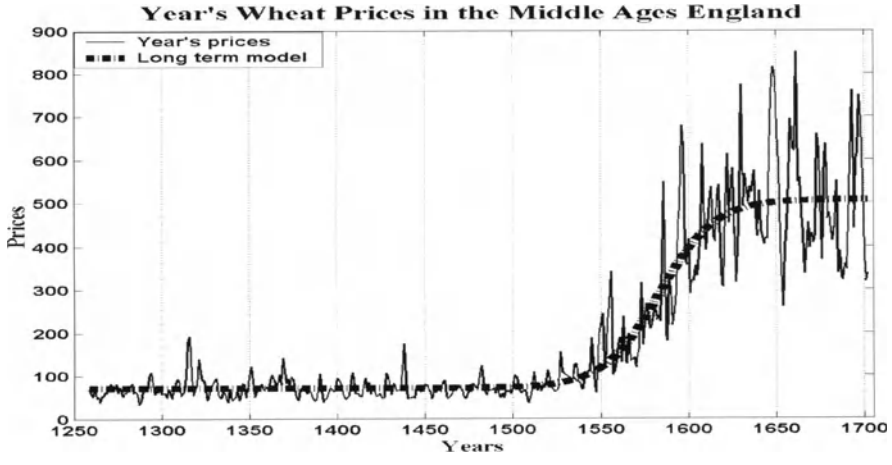

Fig. 14.5.1. Wheat prices in England 1259–1702 with price transition 1530–1630.

Our first step was to estimate parameters of the logistic curve as a long term model $\hat{P}(t_i)$ for the transition of the prices $P(t_i)$ from 'low' to 'high'. Deviations in annual prices, from year to year, were calculated as $\Delta P(t_i) = P(t_{i+1}) - P(t_i)$, normalized with respect to the value $\hat{P}(t_i)$ of the long-term model: $\delta P(t_i) = \Delta P(t_i) / \hat{P}(t_i)$, reflecting price bursts. We used absolute values of the normalized deviations (AD) of prices: $ADP(t_i) = \mathrm{Abs}(\delta P(t_i))$, which are sensitive not only to sharp increases, but also to sharp falls. The second step of our analysis was to choose a discrimination level, filtering out low amplitude bursts, generated by the noise component of the variation. This enabled us to select only anomalous price bursts, potentially connected with the space weather and solar cycles (evidently, as a result of the filtering we can lose a part of the real low amplitude bursts). For our data a discrimination level $\delta P(t) \approx 0.52$ was chosen. We compared the distribution of intervals of price bursts with the distribution of the intervals between extremes (minimum phases) of solar cycles (see Fig. 14.5.2).

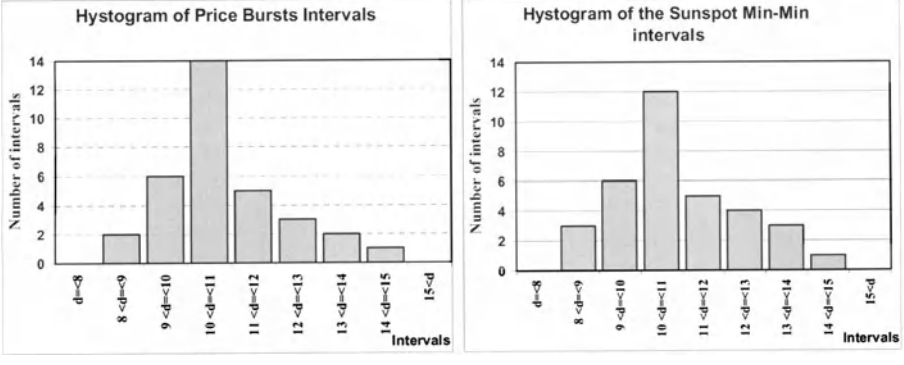

Fig. 14.5.2. Histograms of the interval distribution for price bursts for the period over 450 years (1249–1702), and of minimum–minimum intervals of sunspots during the last 300 years (1700–2000).

Conclusions from the interval analysis are following:

i) For sunspot minimum–minimum interval distribution the estimated parameters are: median – 10.7 years; mean – 11.02 years; standard deviation – 1.53 years.
ii) For price burst interval distribution the estimated parameters are: median – 11.0 years; mean – 11.14 years; and standard deviation – 1.44 years.
iii) The null hypothesis that the frequency distributions are the same for both of the samples (intervals between price bursts and intervals between minima of sunspots) was not rejected with the χ^2-test (significance level > 95%).

The main problem for a comparison between price levels and solar activity is the absence of the time interval common to sunspot observation data (the years 1700–2001) and wheat price data (the years 1259–1702). However, the discovery of the strong correlation between concentration of ^{10}Be isotopes in Greenland ice with CR intensity according to data of direct CR intensity measurements in the last about 60 years (see for details Chapter 10) opens a new possibility for searching for an answer to our question. In Fig. 14.5.3 prices for 1600–1702 are shown in comparison with ^{10}Be data according to Beer et al. (1998). White marks show prices, averaged for 3-year intervals centered on moments of minimums CR intensity, which are marked by yellow lines. Black marks correspond to average prices in 3-year intervals for maximum CR intensity.

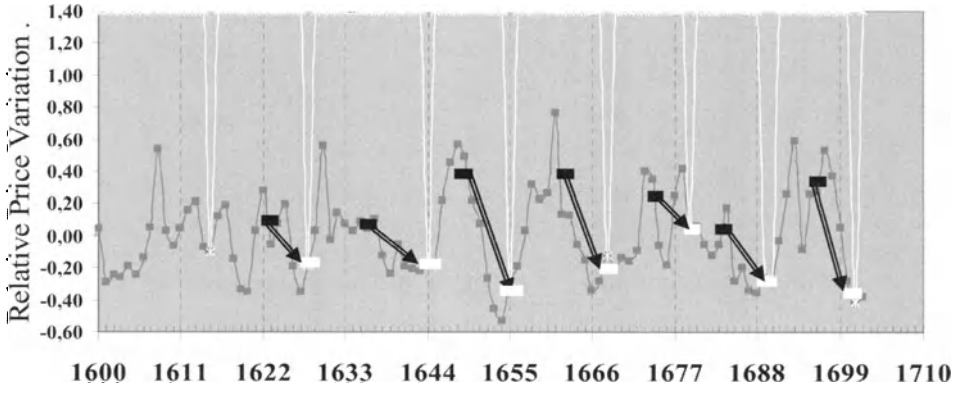

Fig. 14.5.3. Systematic differences in prices at moments of minimum and maximum CR intensity determined according ^{10}Be data (Beer et al., 1998). White rectangles show prices averaged for 3-year intervals centered on moments of minimum CR intensity, black rectangles show prices averaged for 3-year intervals centered on moments of maximum CR intensity

As can be seen from Fig. 14.5.3, all prices in the neighborhoods of the seven maxima of CR intensity (correspond approximately to minima of solar activity) are systematically higher than those in the neighborhoods of the seven minima of CR intensity (maxima of solar activity) in the long term variation of CR intensity according to ^{10}Be data of Beer et al. (1998). The probability of a random occurrence of this systematic difference may be estimated with the help of the criterion of the sign correlation as $(1/2)^7 < 1\%$.

14.6. On the connection between integral rate of ion generation in the atmosphere by CR and total surface of clouds

The time variation of the integral rate of ion generation q in the middle latitude atmosphere in the altitude interval 2–5 km was found in Stozhkov et al. (2001) for the period January 1984–August 1990 on the basis of regular CR balloon measurements. As was mentioned in Section 11.5 (see Eq. 11.5.1), in the troposphere on some level h the values $q(h)$ and CR intensity $I(h)$ are connected by the relation $q(h) = AI(h)$, where A = const. On the other hand, according to Eq. 11.5.3 the rate of ion generation $q(h)$ is connected with ion concentration $n(h)$ as $q(h) \propto n(h)$, so we obtain, in the first approximation

$$\Delta q(h)/q(h) \approx \Delta I(h)/I(h) \approx \Delta n(h)/n(h) . \qquad (14.6.1)$$

The relative change of integral rate of ion generation q in the altitude interval 2–5 km was found in Stozhkov et al. (2001) by integration of Eq. 14.6.1. Results are shown in Fig. 14.6.1 in comparison with relative changes of the total surface of clouds over Atlantic Ocean.

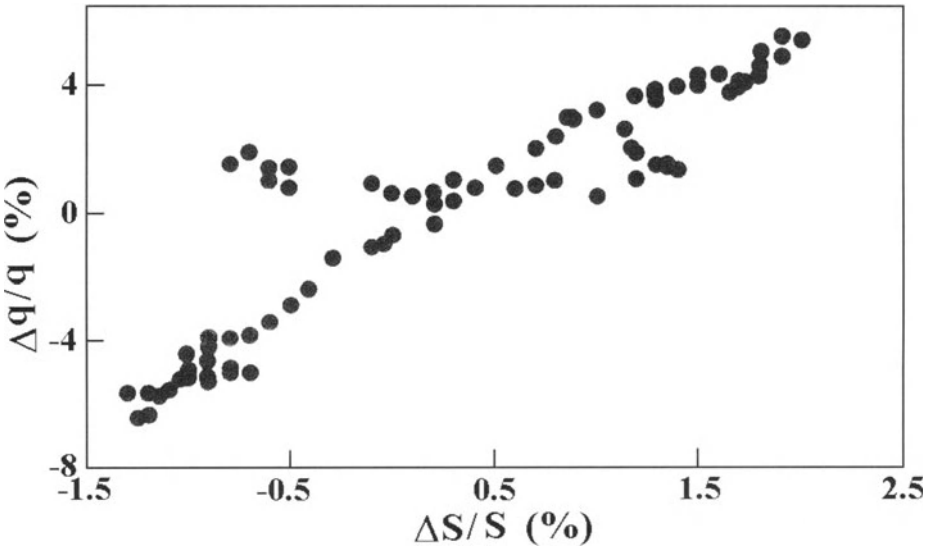

Fig. 14.6.1. The connection of relative changes of total clouds covering surface over Atlantic Ocean $\Delta S/S$ in the period January 1984–August 1990 (according to Swensmark and Friis-Christensen, 1997) with the relative changes of integral rate of ion generation $\Delta q/q$ (or relative changes of ion concentration $\Delta n/n$ according to Eq. 14.6.1) in the middle latitude atmosphere in the altitude interval 2–5 km. According to Stozhkov et al. (2001).

From Fig. 14.6.1 it can be seen that the is a close connection between $\Delta S/S$ and $\Delta q/q$ (or $\Delta n/n$): the correlation coefficient is 0.91 ± 0.04. This result is in good agreement with results described above in Sections 14.1–14.5.

14.7. CR influence on precipitation in periods of big magnetic storms (Forbush decreases) and solar CR events

The decreasing of atmosphere ionization leads to a decreasing of the concentration of charge condensation centers; in these periods decreasing of total cloudiness and atmosphere turbulence, and increasing of isobaric levels are observed (Veretenenko and Pudovkin, 1994). As a result of cloudiness decrease, decrease of total precipitation is also expected. Stozhkov et al. (1995a,b; 1996), Stozhkov (2002) analyzed 70 events of Forbush decreases (caused by big geomagnetic storms) observed in 1956–1993 and compared with the situation in the total precipitation over former USSR. Results obtained by the method of superposed epochs are shown in Fig. 14.7.1.

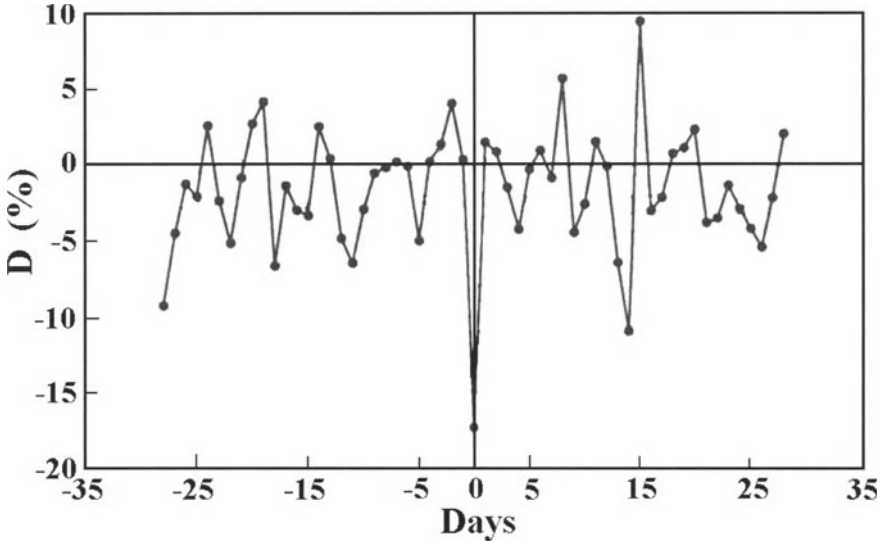

Fig. 14.7.1. The changes of the daily precipitation level, D (in %), relative to mean value evaluated from the precipitation data during one month before (-30 to -1 days) and **one** month after (1 **to** 30 days) Forbush decrease event. The day '0' corresponds to the Forbush decrease main phase. According to Stozhkov (2002).

It was found that during the main phase of the Forbush decrease (minimum of CR intensity) the daily precipitation level decreases by

$$D_{FD}(0) = -(17.4 \pm 2.7)\%. \qquad (14.7.1)$$

The probability of the occasional appearance of this result is less than 10^{-4}. The result described by Eq. 14.7.1 is in agreement with described above results: with decreasing of CR intensity the cloudiness decreases what leads to decreasing of the precipitation level.

During big solar CR events when the CR intensity and ionization in the atmosphere significantly increase, an inverse situation is expected: increasing cloudiness that leads to an increase in the precipitation level. Stozhkov et al. (1995a,b; 1996), Stozhkov (2002) analyzed more than 53 events of solar CR enhancements in 1942-1993. The amplitude of positive increase was found (see Fig. 14.7.2):

$$D_S(0) = +(13.3 \pm 5.3)\% . \qquad (14.7.2)$$

The probability of this effect appearing by chance is less than 0.01.

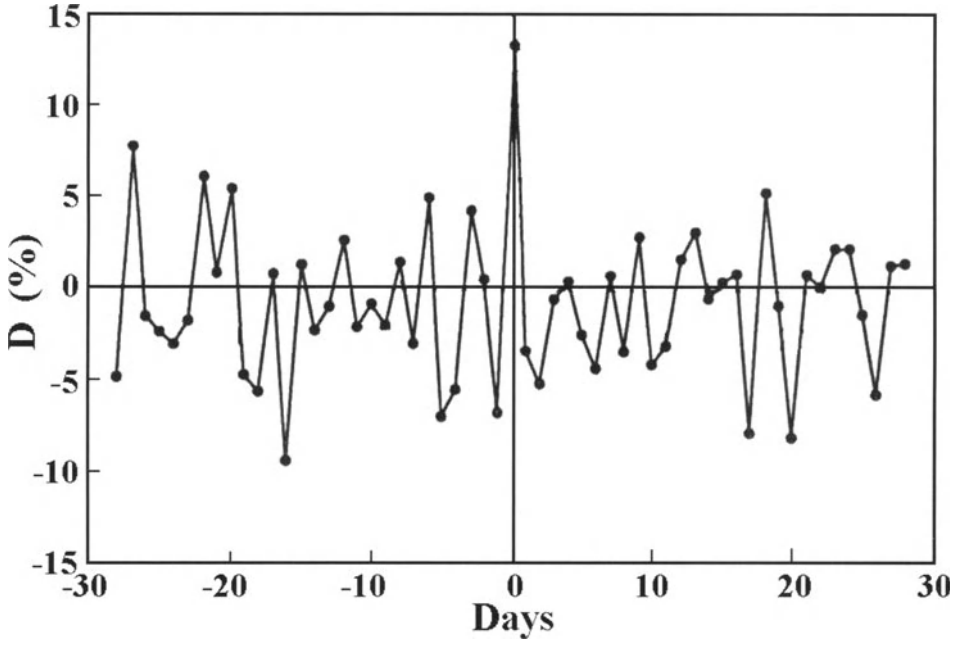

Fig. 14.7.2. The changes of the daily precipitation level D (in %), relative to the mean value evaluated from the precipitation data during one month before and one month after solar proton events recorded by ground based neutron monitors (chosen as the day 0). According to Stozhkov (2002).

14.8. On the possible influence of geomagnetic disturbances and solar activity on the rainfall level through energetic particle precipitation from the inner radiation belt

14.8.1. On the possible influence on climate parameters particle precipitation from inner radiation belt

The phenomena of correlation of the solar and geomagnetic activity with climate parameters (cloudiness, temperature, rainfalls and others) were considered above. The possible physical mechanisms partly also were considered above, but mostly are in process. The clearly pronounced connection observed at high and middle latitudes is explained by the decrease of the MeV-GeV galactic CR with increasing of solar and geomagnetic activity, and by appearance of FEP fluxes ionizing the atmosphere (Tinsley and Deen, 1991). This mechanism can work efficiently at high latitudes, because CR particles with energy up to 1 GeV penetrate more easily to this region due to its very low cut off rigidity. Near equator in the Brazilian Magnetic Anomaly (BMA) region the main part of galactic and solar CR is shielded by geomagnetic field; only at the altitude above

200–300 km exist the large fluxes of energetic protons and electrons trapped in the inner radiation belt. The significant magnetic disturbances can produce precipitation of these particles and subsequent ionization of the atmosphere. According to Pugacheva et al. (1995), these phenomena can influence on climate parameters even in low latitude region of BMA. For example, Campinas (23° S, 47° W) is located at the south foot of the magnetic line $L = 1.16$ populated by electrons of ~ 1 $cm^{-2}s^{-1}sr^{-1}$ at energy > 100 MeV and protons of ~ 300 $cm^{-2}s^{-1}sr^{-1}$ at energy > 400 MeV. Precipitating the particles can reach the meteorologically sensitive layers of the atmosphere: < 20 km for electrons, and < 10 km for protons. The energy contained in these components is 0.1 GeV $cm^{-2}s^{-1}sr^{-1}$ (electrons) and 100 GeV $cm^{-2}s^{-1}sr^{-1}$ (protons), the last one is by a factor 1000 higher than in the galactic CR and FEP fluxes at BMA region. The influence of solar-terrestrial connections on climate in the BMA region was studied by Pugacheva et al. (1995). Two types of correlations were observed: 1) a significant short and long time scale correlation between the index of geomagnetic activity Kp and rainfalls in Sao Paulo State; 2) the correlation-anticorrelation of rainfalls with the 11 and 22 year cycles of solar activity for 1860-1990 in Fortaleza.

14.8.2. Comparison of Kp-index with rainfall level on the daily data basis

Fig. 14.8.1 shows the time dependences of Kp-index and level of rain in Campinas (23° S, 47° W) and in Ubajara (3° S, 41° W) during 1986.

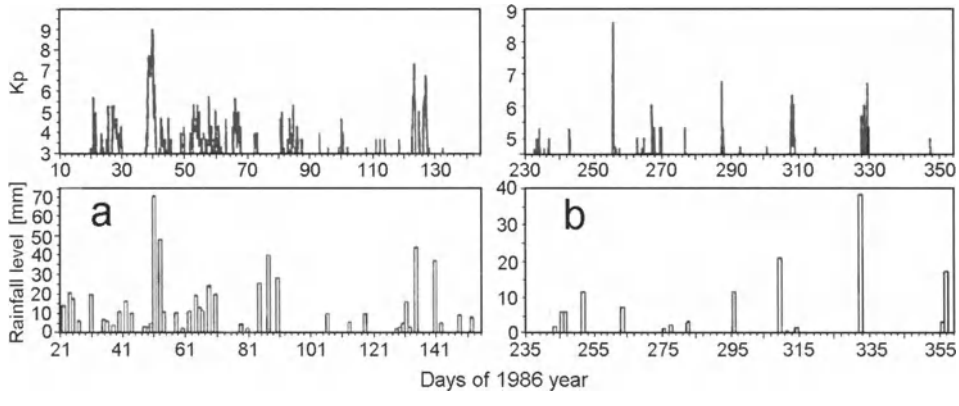

Fig. 14.8.1. The Kp-index of geomagnetic activity (top panels) and rainfall level (bottom panels) in Campinas (left panels ***a***) and in Ubajara (right panels ***b***) in 1986. According to Pugacheva et al. (1995).

From Fig. 14.8.1 can be seen that with a delay of 5–11 days, almost every significant (> 3.0) increase of Kp-index is accompanied by an increase in the rainfall level. The effect is especially seen at the time of the great geomagnetic storm of February 8 1986, when the electron fluxes of inner radiation belt were thrown down into the atmosphere during several days of February 18-21 (Martin et al., 1995) and greatest rainfall of the 1986 year was observed in February 19. After the series of solar flares of March 19–22, 1991 the great magnetic disturbances associated with the flares were

registered and energetic solar flare particles were injected into magnetosphere. A Sao Paolo station on the March 22 showed the greatest rainfall of the year.

14.8.3. On the connection of the long term variations of annual rainfalls with variations of solar and geomagnetic activity

The long term variations of annual rainfalls in Campinas, the Kp-index and sunspot numbers are shown in Fig. 14.8.2 and Fig. 14.8.3.

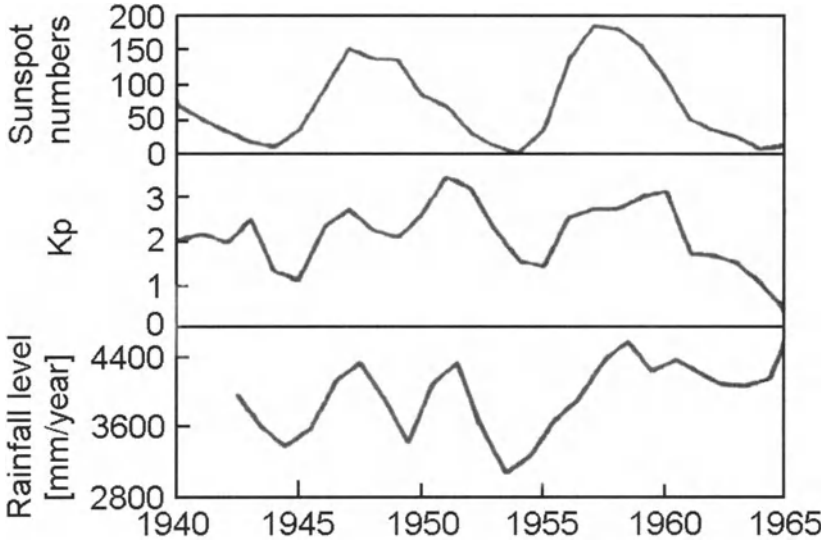

Fig. 14.8.2. Long-term variations of rainfalls (Campinas, the bottom panel) in comparison with variations of solar and geomagnetic activity (the top and middle panels, respectively) for 1940–1965. According to Pugacheva et al., 1995).

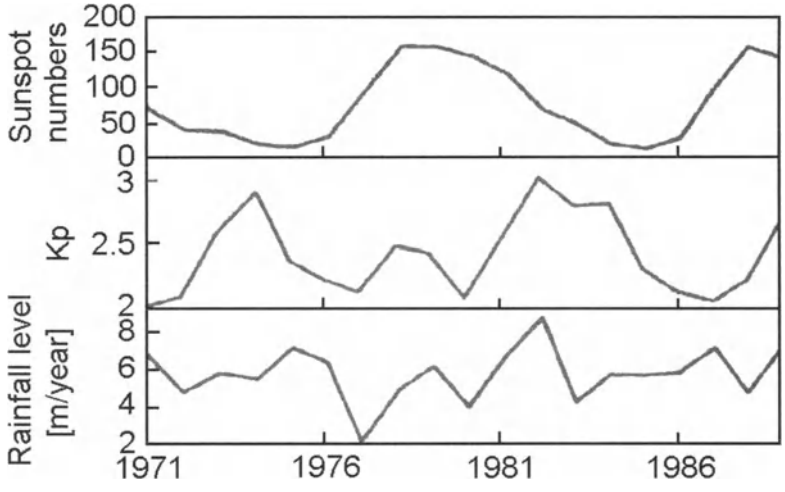

Fig. 14.8.3. The same as in Fig. 14.8.2, but for 1971-1990. According to Pugacheva et al., 1995).

From Fig. 14.8.2 and Fig. 14.8.3 can be seen the clear double peak structure of rainfall variation similar to the Kp-index. Only during the 20 solar cycle (1964–1975), weakest of the last 6 cycles, a correlation of rainfalls and Kp-index is absent and anticorrelation between rainfalls and sunspot numbers is observed in most of Brazil. The Kp – rainfall correlation is more pronounced in the regions connected with magnetic lines occupied by trapped particles.

In Fortaleza (4° S, 39° W), located in an empty magnetic tube (L = 1.054), it is the other kind of correlation (see Fig. 14.8.4).

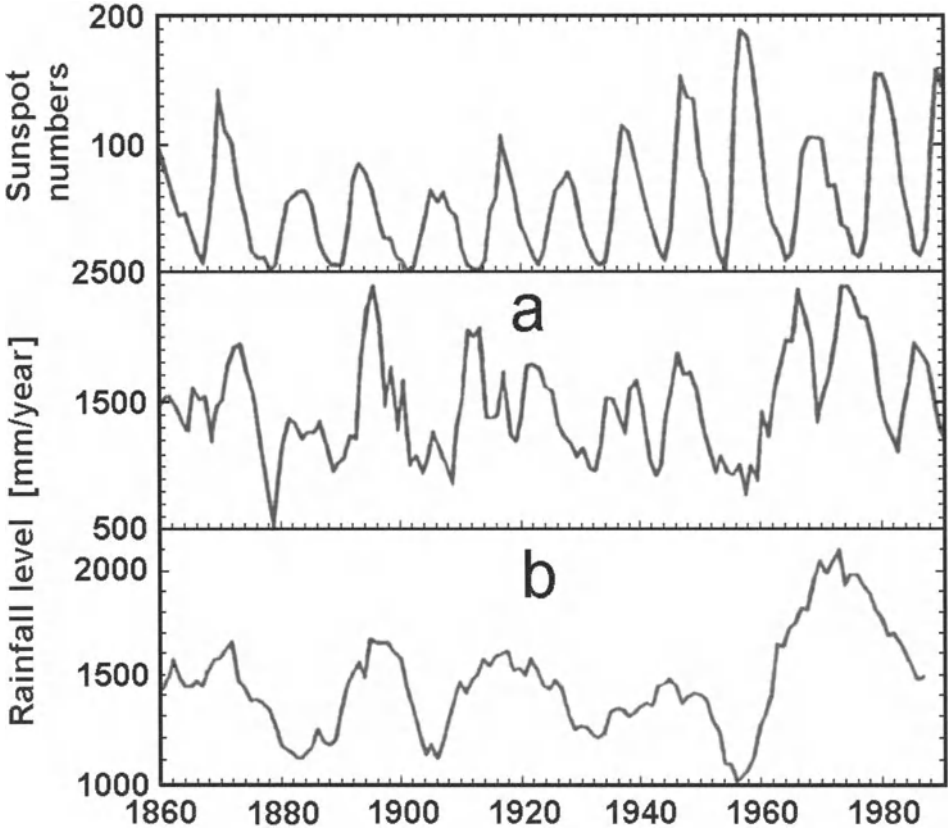

Fig. 14.8.4. The comparison of yearly sunspot numbers long-term variation (the top panel) with 3 years and 11 years running averaged rainfalls (panels ***a*** and ***b***, respectively) in Fortaleza (4° S, 39° W) during 1860-1990. According to Pugacheva et al., 1995).

From Fig. 14.8.4 can be seen that the correlation exist between sunspot numbers and rainfalls during the 1860–1900 years (3 solar cycles: 11, 12 and 13 cycles) and 1933–1954 years (2 cycles: 17 and 18 cycles). The anticorrelation was observed during 1900–1933 years (3 cycles: 14, 15 and 16) and 1954–1990 years (3 cycles: 19, 20 and 21 cycles). As far as sunspot numbers mainly anticorrelate with the CR flux, an anticorrelation of sunspot numbers with rainfalls could be interpreted as a correlation of rainfalls with the CR. The positive and negative phases of the correlation interchange

several times during the long time interval 1860–1990, that was observed earlier in North America (King, 1975). Some climate events have a 22-year periodicity similar to the 22-year solar magnetic cycle. The panel *b* in Fig. 14.8.4 demonstrate 22-year periodicity of 11-year running averaged rainfalls in Fortaleza. The phenomenon is clearly observed during 5 periods from 1860 to 1990. During the 11–16 solar cycles (from 1860 until 1930), the maxima of rainfalls correspond to the maxima of sunspot numbers of odd solar cycles 11, 13, 15 and minima of rainfalls correspond to maxima of even solar cycles 12, 14, 16. During the 17th solar cycle the phase of the 22-year periodicity is changed to the opposite and the sunspot number maxima of odd cycles 19 and 21 correspond to the minima of rainfall. The effect is not pronounced (excluding years 1957–1977) in Sao Paolo.

14.8.4. On the difference of galactic and solar CR influence on climate parameters at middle and low latitudes

In Section 14.7 were demonstrate effects of galactic CR Forbush decreases and solar FEP events on climate parameters at high and middle latitudes (regions of former USSR). From other hand, the influence of Forbush decreases of CR intensity and the increases of solar flare particles on climate parameters in region with much higher rigidity in the Brazilian Magnetic Anomaly (BMA) region was studied in Pugacheva et al. (1995). The 17 greatest Forbush decreases during wet seasons (October - March) of 1956–1985 in the Sao Paulo state were selected. The corresponding data of Washington NM (R_c = 6.7 GV) and Huancayo NM (R_c = 13 GV) were used. The method of superposed epochs for rainfalls of about 100 station of Sao Paulo state (plotting the 20 days before and 20 days after key days of CR intensity decreases) was used. No statistically proved correlation appeared. The solar events with high energy proton fluxes for wet seasons (from 1966 up to 1994) were found using the data of the Sanae NM in the South hemisphere detected the solar CR ground level events (GLE) owned by high rigidity particles. Only GLE with the amplitudes more than 10% were selected. The same method of superposed epochs for rainfalls of about 100 station of Sao Paulo state did not reveal any effect that overcomes the error limits.

The difference in results obtained by Stozhkov (2002) and by Pugacheva et al. (1995) can be easy understand if we take into account the big value of cutoff rigidity in the BMA region; this is a cause why the variations in galactic and solar CR intensity in the BMA region practically do not reflected in the air ionization and not influenced on the climate parameters. From other hand, in the BMA region will be important the other mechanism of solar and magnetic activity influence on climate parameters: energetic particle precipitation from the inner radiation belt (see Sections 14.8.1–14.8.3).

14.9. On the possible influence of galactic CR on formation of cirrus hole and global warming

According to Ely (1977), Ely and Huang (1987) there are expected variations of upper tropospheric ionization caused by long-term variations of galactic CR intensity. These variations of upper tropospheric ionization will lead to formation of the associated cirrus hole (a strong latitude dependent modulation of cirrus). The upper tropospheric ionization is caused mainly by particles with energy smaller than 1 GeV but bigger than about 500 MeV. In Fig. 14.9.1 is shown the long term modulation of the difference Mt.

Washington NM (R_c = 1.24 GV) and Durham NM (R_c = 1.41 GV), what corresponds protons with kinetic energy between ~ 650 MeV and ~ 850 MeV.

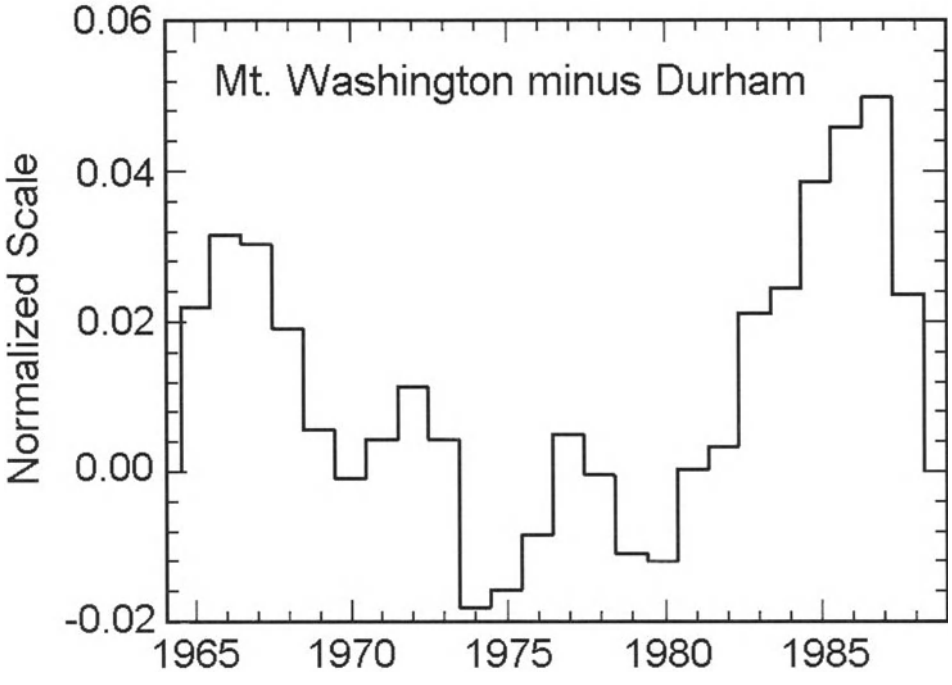

Fig. 14.9.1. The observed 22-year modulation of galactic CR between 1.24 GV and 1.41 GV rigidity (i.e., protons with kinetic energy between ~ 650 MeV and ~ 850 MeV, ionizing heavily in the 200–300 g/cm^2 range). According to Ely et al. (1995).

The Fig. 14.9.1 clearly shows the 22-year modulation of galactic CR intensity in the range 650–850 MeV with amplitude more than 3%. The 2% amplitude in the NM 22-year difference plot is estimated to produce a variations of upper tropospheric ionization much over 30% at 10 km altitude (Lockwood et al., 1974). Variations of upper tropospheric ionization influences on the cirrus covering. The "cirrus hole" is expected corresponding to decreasing phase of CR intensity variation shown in Fig. 14.9.1. According to Ely et al. (1995), the "cirrus hole" really was observed in different latitude zones of the whole world between 1962 and 1971, centered in 1966 (see Fig. 14.9.2). The Fig. 14.9.2 shows that data for the whole world give about 7% amplitude of depression in the cirrus covering, for the equatorial zone (30° S–30° N) about 4%, and for the northern zone (30° N–90° N) about 17% depression in the cirrus covering. With decreasing of cirrus covering leads to increasing heat loss to outer space (note that only ~ 4 % change in total cloud cover is equivalent to a factor of 2 changes in carbon dioxide). Especially big influence of cirrus hole is expected in the northern latitude zone (30° N – 90° N) where the cirrus covering is reduced by 17 %, greatly increasing heat loss to outer space what influences on climate parameters in northern winter (the effect of the cirrus hole is reduced in summer by the increase in lower clouds resulting from the enhanced insulation) The low temperatures produced from mid to high latitude

significantly increase the pressure of the polar air mass and cause frequent "polar break troughs" at various longitudes in which, for example, cold air from Canada may go all the way even to Florida and freeze the grapefruits (Ely et al., 1995). However, when the cirrus hole is not present, the heat loss from mid to high latitudes is much less, and the switching of the circulation patterns (represented by the well known Rossby waves) is much less frequent.

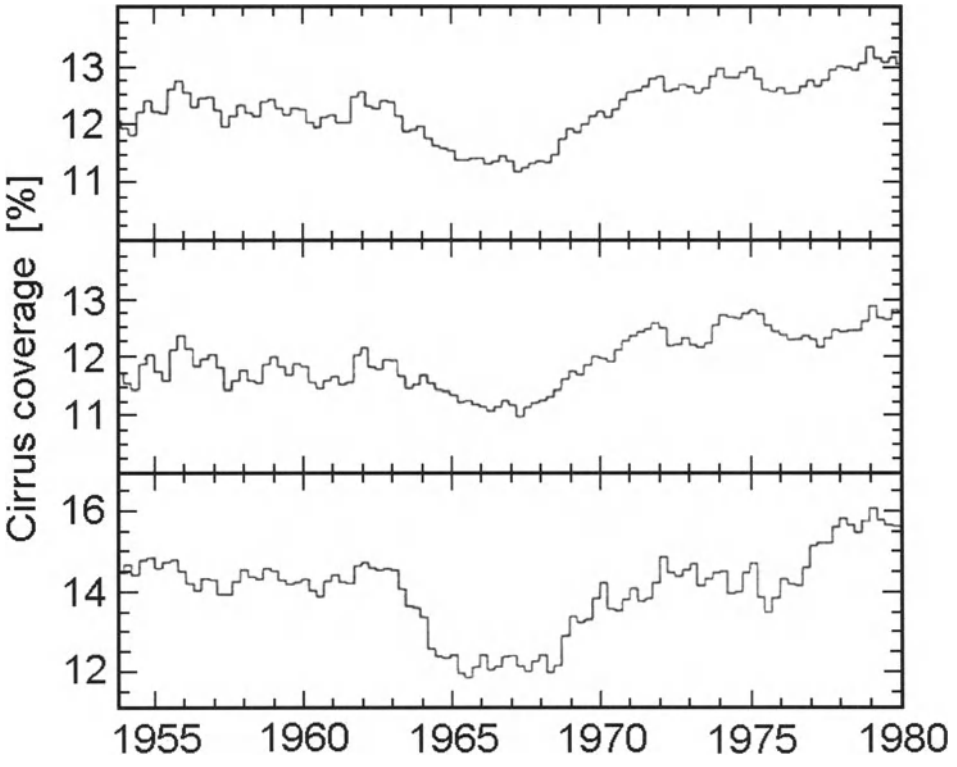

Fig. 14.9.2. The "cirrus hole" of the 1960's. The 3 plots, from top to bottom, show depression in % cirrus coverage (between 1962 and 1971, centered in 1966) for the whole world (the top panel), the equatorial zone (30° S-30° N; middle panel), and the northern zone (30° N-90° N; bottom panel). The fractional decreases in cirrus coverage are 7%, 4%, and 17%, respectively for the whole world, equatorial, and northern zone. According to Ely et al. (1995).

14.10. On the possible influence of long-term variation of main geomagnetic field on global climate change through CR cutoff rigidity variation

14.10.1. Expected CR intensity variation owed to cutoff rigidity change

If the cutoff rigidity change is relatively small, the expected CR intensity variation owed only to the cutoff rigidity change will be determined by the second member of right hand of Eq. 3.1.2 (see Section 3.1 in Chapter 3). In this case we obtain

$$\delta N_i(R_c(t),h_o,t)/N_{io} = -\delta R_c(t) W_i(R_{co},R_{co},h_o), \tag{14.10.1}$$

where $\delta R_c(t) = R_c(t) - R_{co}$, R_{co} and N_{io} are the cutoff rigidity and CR intensity at present time, respectively, and

$$W_i(R_{co},R,h_o) = D_o(R) m_i(R,h_o)/N_{io} \tag{14.10.2}$$

is the coupling function between secondary CR of type *i* and primary CR. In Eq. 14.10.2 $D_o(R)$ is the primary CR spectrum and $m_i(R,h_o)$ is the integral multiplicity. From papers Fluckiger et al. (2003), Smart and Shea (2003), and Shea and Smart (2003) follows that long-term variations of cutoff rigidities are not small, are comparable with values of R_c. In this case Eq. 14.10.1 does not valid, and it is necessary to determine the expected CR intensity variation by the relation

$$\Delta N_i(R_c(t),h_o,t)/N_{io} = \left[\int_{R_c(t)}^{\infty} D_o(R) m_i(R,h_o) dR - \int_{R_{co}}^{\infty} D_o(R) m_i(R,h_o) dR\right] \Big/ N_{io}$$
$$= \int_{R_c(t)}^{R_{co}} W_i(R_{co},R,h_o) dR. \tag{14.10.3}$$

14.10.2. Long-term variation of cut-off rigidity planetary distribution during 1600-2000

Shea and Smart (1977, 1990, 1997) have shown that in the present era the geomagnetic cutoff rigidities are rapidly changing in several areas of the world with increases of the order of 1% per year in the North Atlantic Ocean area and decreases > 0.5% per year in the South Atlantic Ocean area. They show that these changes are non-linear in time and for precise CR intensity measurements the geomagnetic cutoff rigidities must be calculated using a field model appropriate for the time of the measurements. The dipole and non-dipole components of the magnetic field are rapidly changing. The non-dipole terms contribute about 18 percent of the total magnetic field. At our current point in geological time the earth's magnetic field is rapidly decreasing. The magnitude of the dipole term alone has changed by 39% over 400 years (from 1600 to 2000). This change is so rapid and non-uniform that the magnetic field Working Group 8 of IAGA Division V provides updates to the International Geomagnetic Reference Field every five years (Sabaka et al., 1997). These changes affect the geomagnetic cutoff rigidities and hence the magnitude of the cosmic radiation incident on the atmosphere at a specific location is a function of time what is very important for the problem of air ionization and atmosphere chemistry owed by CR. There has been considerable interest in constructing models of the Earth's magnetic field in the past (Merrill et al., M1997). Through various international research efforts, models of the Earth's magnetic field extending back centuries (Barraclough, 1974, 1978) and even millennia in time (Constable et al., 2000) have been derived, although with decreasing confidence in the model accuracy.

Smart and Shea (2003) have calculated a world grid of CR geomagnetic cutoff rigidities in the vertical direction every 50 years to establish the long-term changes in the geomagnetic cutoff rigidities during 1600–2000. They have utilized the International Geomagnetic Reference Field Models for these calculations for epochs between 2000 and 1900 and the British Geological Survey models (restricted to degree and order 5) for epochs between 1850 and 1600. The CR trajectory-tracing method was used to determine the geomagnetic cutoff rigidity parameters for a set of world grids every 5 degrees in latitude and 15 degrees in longitude. As example, in Fig. 14.10.1 – 14.10.5 are shown these results for 1600, 1700, 1800, 1900, and 2000.

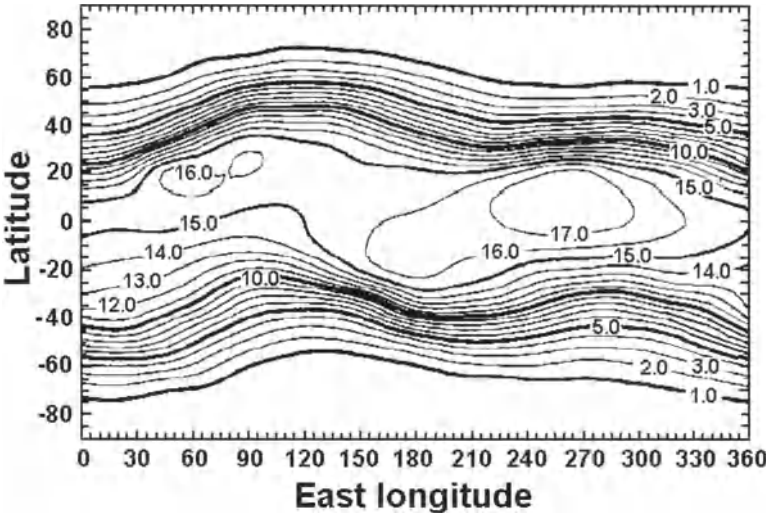

Fig. 14.10.1. Geomagnetic CR cutoff rigidity contours for 1600. According to Smart and Shea (2003).

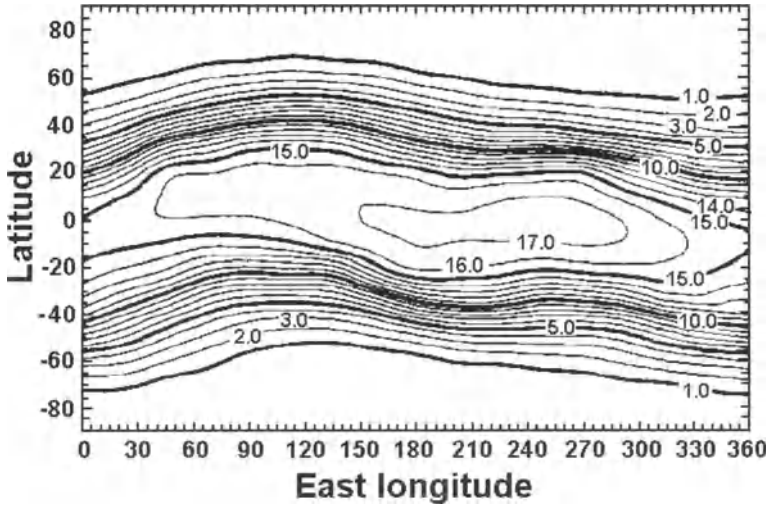

Fig. 14.10.2. Geomagnetic CR cutoff rigidity contours for 1700. According to Smart and Shea (2003).

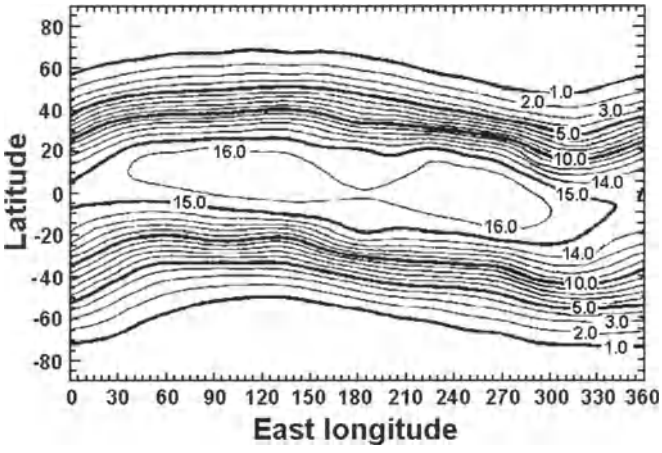

Fig. 14.10.3. Geomagnetic CR cutoff rigidity contours for 1800. According to Smart and Shea (2003).

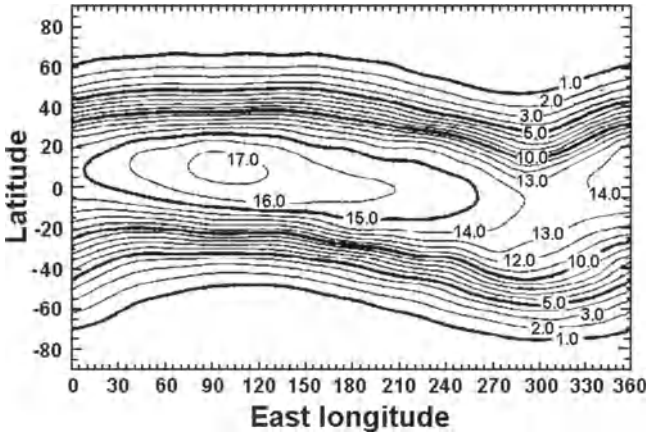

Fig. 14.10.4. Geomagnetic CR cutoff rigidity contours for 1900. According to Smart and Shea (2003).

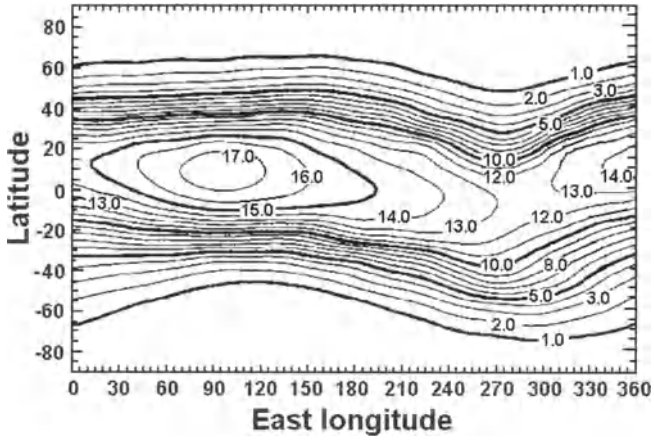

Fig. 14.10.5. Geomagnetic CR cutoff rigidity contours for 2000. According to Smart and Shea (2003).

From Fig. 14.10.1-14.10.5 can be seen a big change in cutoff rigidity planetary distribution. For example, in 1600 the highest vertical cutoff rigidity values were over South America whereas in 2000 the highest vertical cutoff rigidity values were close to India. This is consistent with the migration of the North geomagnetic polar axis from over Northern Europe to over North America: the position of the eccentric dipole from the center of the Earth changed at the rate 0.8 km per year from 1650 to 1800 increasing to a rate of 0.9 km per year from 1800 to the present (the north dipole axis position had a steady movement of 0.11 degree per year westward and 0.03 degree southward per year from 1650 to 1850; after 1850 the southward drift became very small).

14.10.3. On the long-term change of cutoff rigidities and expected change of CR intensity owed to geomagnetic field variation

The amount of cosmic radiation reaching the top of the atmosphere is a function of the Earth's geomagnetic field. Since there is a long-term evolution of the Earth's magnetic field, any variation in this field may also have climatic effects (Anderson, 1992). While the total field is decreasing, the changes are non-uniform over the Earth. Shea and Smart (2003a) show that the amount of cosmic radiation impinging at the top of the atmosphere has a considerable variation from place to place over the past 400 years; these variations should be considered in long-term climatic studies.

On the basis of results discussed in previous Section 14.10.2, Shea and Smart (2003a) calculated the expected long-term change of cutoff rigidities during 1600-1900. Results are shown in Fig. 14.10.6.

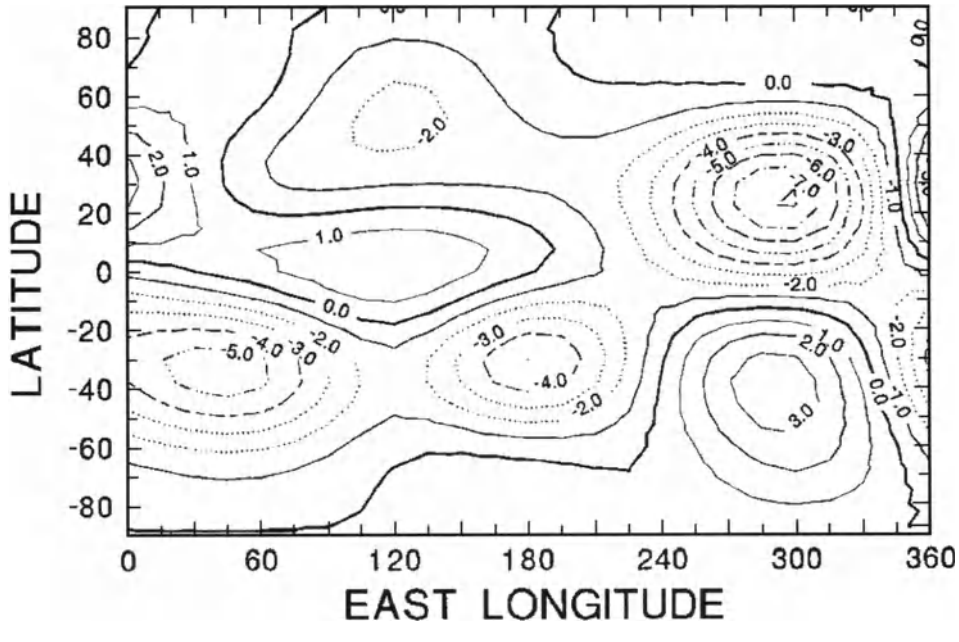

Fig. 14.10.6. Contours of the change in vertical cutoff rigidity values (in GV) between 1600 and 1900. Full lines reflect positive trend (increasing of cutoff rigidity from 1600 to 1900); dotted lines reflect negative trend. According to Shea and Smart (2003a).

From Fig. 14.10.6 can be seen that on the Earth there are several regions with big negative and positive changes of CR cutoff rigidities (up to 7 GV).

The vertical cutoff rigidity values and changes in the galactic cosmic radiation calculated by Smart and Shea (2003a), are shown in Table 14.10.1 which reflect major changes at individual locations over a 300-year period. These changes are not uniform. There are also locations (e.g. 55N, 30E; 20N, 300E; 35S, 300E) where the 300-year trend reverses between 1900 and 2000.

Table 14.10.1. Vertical cutoff rigidities (in GV) for various epochs 1600–2000, and galactic CR intensity variation during 1600–1900 owed to changes of geomagnetic field. According to Shea and Smart (2003a).

Lat.	Long. (E)	Epoch 2000	Epoch 1900	Epoch 1800	Epoch 1700	Epoch 1600	Change in GCR flux (1600–1900)	
55	30	2.30	2.84	2.31	1.49	1.31	−48%	Europe
50	0	3.36	2.94	2.01	1.33	1.81	−37%	Europe
50	15	3.52	3.83	2.85	1.69	1.76	−55%	Europe
40	15	7.22	7.62	5.86	3.98	3.97	−58%	Europe
45	285	1.45	1.20	1.52	2.36	4.14	+214%	N. Amer.
40	255	2.55	3.18	4.08	4.88	5.89	+118%	N. Amer.
20	255	8.67	12.02	14.11	15.05	16.85	+68%	N. Amer.
20	300	10.01	7.36	9.24	12.31	15.41	+195%	N. Amer.
50	105	4.25	4.65	5.08	5.79	8.60	+132%	Asia
40	120	9.25	9.48	10.24	11.28	13.88	+76%	Asia
35	135	11.79	11.68	12.40	13.13	14.39	+37%	Japan
−25	150	8.56	9.75	10.41	11.54	11.35	+25%	Australia
−35	15	4.40	5.93	8.41	11.29	12.19	+178%	S. Africa
−35	300	8.94	12.07	13.09	10.84	8.10	−63%	S. Amer.

According to the opinion of Shea and Smart (2003a), the derivation of a physical relationship between galactic cosmic radiation and cloud cover (and hence climate) is complex. There are two sources of climatology records: long-term measurements for individual locations and approximations derived from these measurements to estimate global trends. While reliable cloud cover data exist for some individual locations, full global coverage data are available only since 1983. Kristjánsson et al. (2003) suggest that correlation coefficients between solar-terrestrial parameters such as cosmic radiation and/or solar irradiance and climatic parameters computed at different geographical locations would be more meaningful than global correlations. Shea and Smart (2003a) suggest that investigations of a possible relation between galactic cosmic radiation and climate for specific areas of the world where reliable climatic data are available should include the changes in the cosmic radiation flux at that particular location over the time period under investigation. This does not have to be done on a point by point basis, but can be done over a regional basis such as northern Europe. In using the more recent global cloud cover data, it is now possible, using world grids of vertical cutoff rigidity values calculated for 1980 and 2000, to estimate the changes in cosmic radiation over the entire globe during that period or over a specific region of the globe. There are some regions of the world where the vertical cutoff rigidity is changing by as much as 1% per year (Shea and Smart, 1990) and the changes in galactic cosmic radiation over these regions over the 20-year period may be sufficient to provide meaningful insight to the cosmic radiation/cloud cover hypothesis.

The total strength of the Earth's magnetic dipole has decreased significantly between 1600 and the present time. Smart and Shea (2003b) have estimated a globally averaged increase in the CR flux of ~18% over this 400-year period.

14.10.4. The global cutoff rigidities and their change during the last 2000 years

In Sections 14.10.1-14.10.3 were used vertical cutoff rigidities R_c. Flückiger et al. (2003) investigate the evaluation of global CR cutoff rigidities for the past 2000 years. The state-of-the-art technique for the determination of cutoff rigidities is the calculation of particle trajectories in a magnetic field model representing the Earth's magnetic field at a specific time. For a specified location (geographic latitude λ and longitude φ), and a specified arrival direction (zenith angle θ, azimuth angle ϕ), allowed and forbidden trajectories are determined by numerically integrating the equation of motion of charged particles as a function of particle rigidity. The effective cutoff rigidity $R_{c,eff}(\lambda,\varphi,\theta,\phi)$ takes into account geomagnetic filtering effects in the penumbra region (see Section 3.3). For air ionization and influence on climate are important not only vertical arrived particles but also arrived at different zenith angles. At a specific location, the global cutoff rigidity

$$R_{c,gl}(\theta_{\max},\lambda,\varphi)=\frac{\int_0^{2\pi} d\phi \int_0^{\theta_{\max}} R_{c,eff}(\theta,\phi)\sin\theta d\theta}{2\pi \int_0^{\theta_{\max}} R_{c,eff}(\theta,\phi)\sin\theta d\theta}. \qquad (14.10.3)$$

is a valuable parameter describing the lower rigidity limit of CR particles arriving at this location. During the past 2000 years the magnetic dipole moment of the Earth decreased by ~ 30% to today's value of ~ 7.8×10^{25} Gs.cm^3, and the location of the North geomagnetic pole has changed within a limited latitudinal range near the geographic pole (Merrill and McElhinny, M1983). Examples of contour lines of 2π-averaged global cutoff rigidities at $\theta_{\max}=85^o$ are plotted in Fig. 14.10.7 for dipole moment 11.7×10^{25} Gs.cm^3 (corresponds to about 2000 years ago) and in Fig. 14.10.8 for dipole moment 7.8×10^{25} Gs.cm^3 (corresponds to the present time). For the corresponding calculations the information about the position and direction of the magnetic dipole inside the Earth was deduced from the International Geomagnetic Reference Field (IGRF). In Fig. 14.10.9 are shown the contour lines $R_{c,gl}(\theta_{\max},\lambda,\varphi)$ = 2 GV for $\theta_{\max}=85^o$ in the Northern and Southern hemispheres for geocentric and eccentric dipole field models (geomagnetic dipole moment 7.8×10^{15} Vsm, present time). The total area enclosed by the solid contours (geocentric dipole) in the North and South corresponds to ~ 15% of the Earth's surface. With the eccentric dipole instead of the geocentric dipole the surface inside the 2 GV contour line is reduced in the North by ~ 7% and enlarged in the South by ~ 6%. In particular, as illustrated in Fig. 14.10.9, the use of a geocentric instead of the

eccentric dipole field model may lead to considerable differences between the Northern and Southern hemispheres (Flückiger et al., 2003).

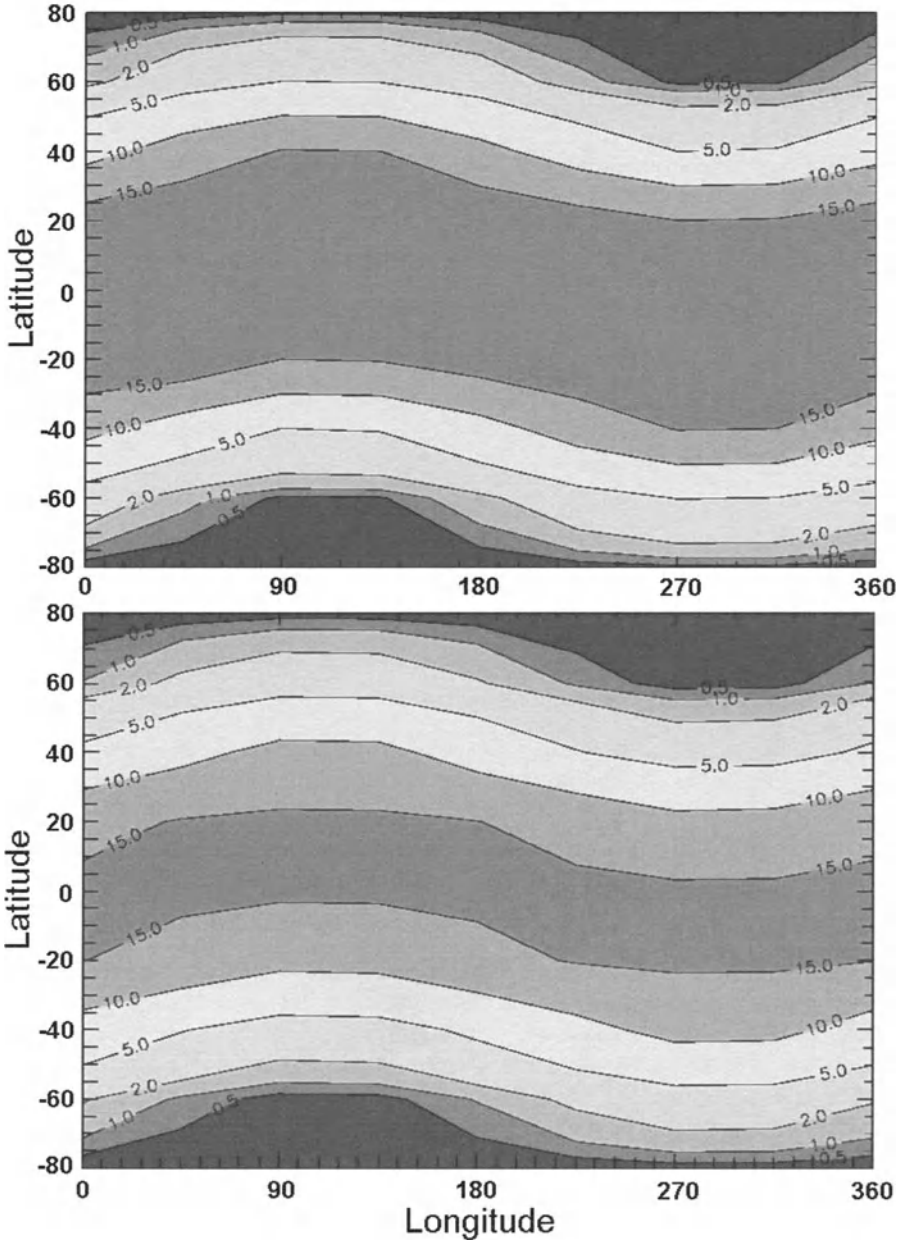

Fig. 14.10.7. Planetary contours of trajectory-derived averaged global magnetic cutoff rigidities determined by Eq. 14.10.3 for the geocentric dipole field model with dipole moment 11.7×10^{25} Gs.cm^3 (top panel, 2000 years ago) and 7.8×10^{25} Gs.cm^3 (bottom panel, present time) at $\theta_{\max}=85^{o}$. According to Flückiger et al. (2003).

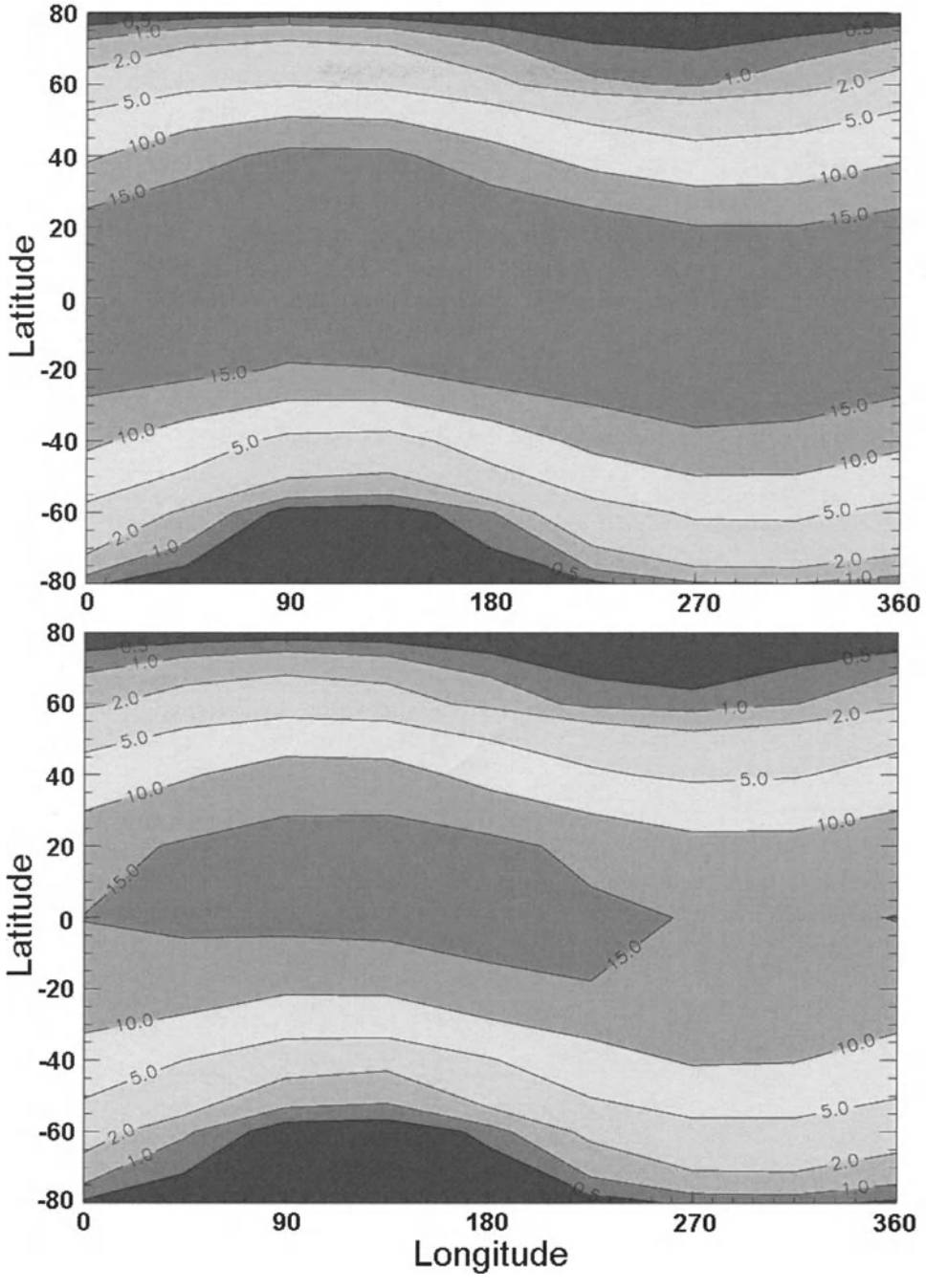

Fig. 14.10.8. The same as in Fig. 14.10.7., but for the eccentric dipole field model with dipole moment 11.7×10^{25} Gs.cm^3 (top panel, 2000 years ago) and 7.8×10^{25} Gs.cm^3 (bottom panel, present time) at $\theta_{\max} = 85^o$. According to Flückiger et al. (2003).

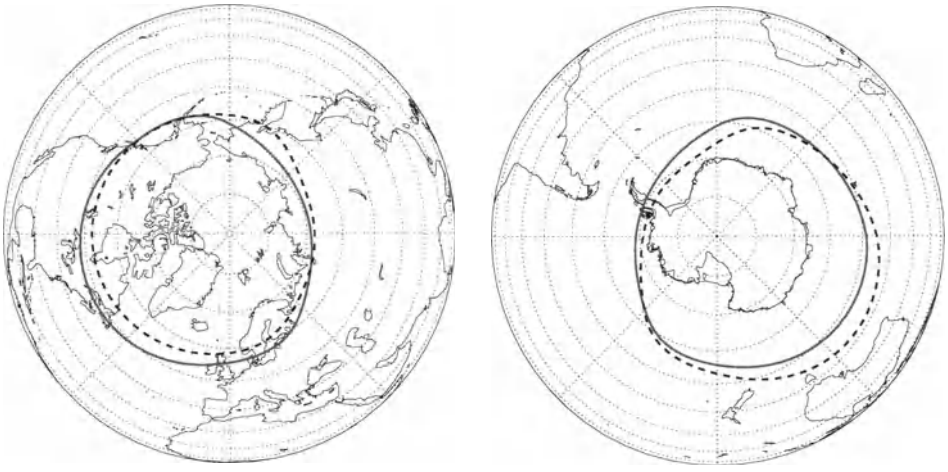

Fig. 14.10.9. Contour lines for global cutoff rigidity 2 GV in the Northern (left) and Southern (right) hemispheres for geomagnetic dipole moment 7.8×10^{25} Gs.cm^3 . The solid lines refer to a geocentric magnetic dipole, whereas the dashed lines refer to an eccentric dipole. According to Flückiger et al. (2003).

14.11. Cosmic rays and the current trend of the global warming

It is now commonly thought of that the current trend of the global warming is causally related to the accelerating consumption of fossil fuels in the industrial nations. However, it has been suggested that this warming might have been produced as the result of the gradual increase of the solar and magnetic activity for more than a century since the year 1870 (see Fig. 14.11.1 and Fig. 14.11.2).

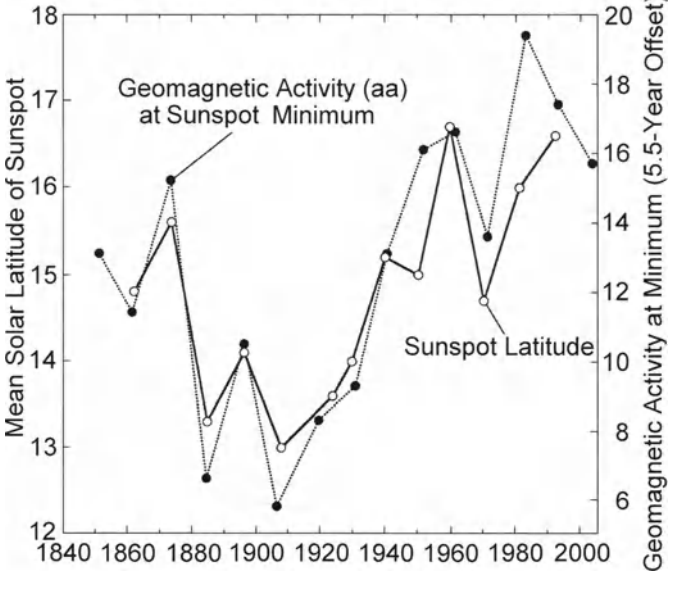

Fig. 14.11.1. The time variation of geomagnetic activity (index *aa*) at minimums of solar activity in comparison with the time variation of the mean sunspots latitude. According to Pulkkinen et al. (2000).

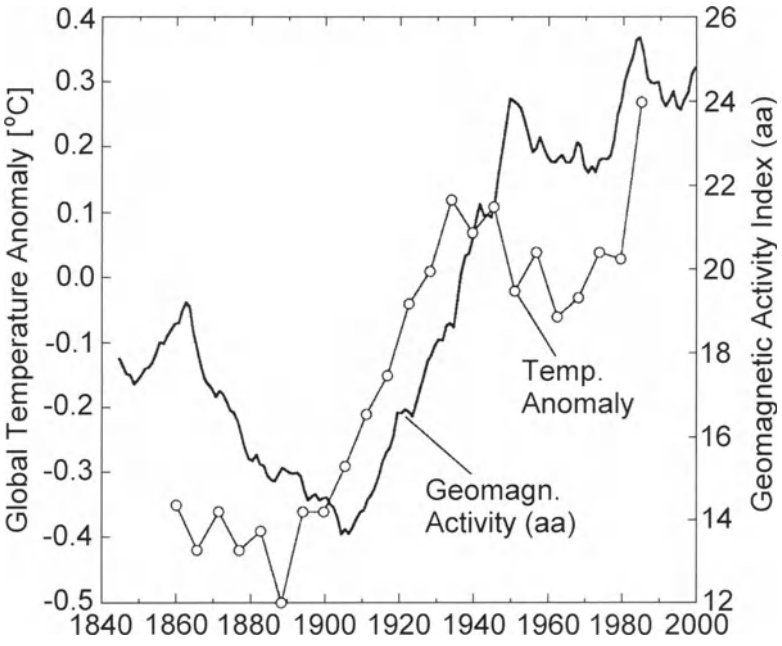

Fig. 14.11.2. The time variation of geomagnetic activity (index *aa*) at minimums of solar activity in comparison with the time variation of the solar cycle mean of the global temperature anomaly. According to Pulkkinen et al. (2000).

According to Pulkkinen et al. (2000), as shown in Fig. 14.11.1 and Fig. 14.11.2, the solar and magnetic activity has been increasing since the year 1900, though there exists a gap indicating that this activity slightly decreased in the last half of the 19th century. It is clear from Fig. 14.11.1 and Fig. 14.11.2 that the *aa* index of geomagnetic activity, as a measure of the variability of the IMF, is varying almost in parallel with the sunspot activity and with global temperature anomaly.

In fact, it has been well established that the brightness of the Sun varies in proportion with the solar activity, though the variability of this brightness is very small and cannot explain the total global warming. From other hand, the gradual increase of the solar activity for such a long period as more than a hundred years seems to have been accompanied by the gradual decrease of the CR intensity in the interplanetary space (Lockwood et al., 1999). As have been analyzed by Lockwood et al. (1999), the CR intensity as being observed at the Earth has a tendency to steadily decrease for more than hundred years in the recent past with the enhancement of the IMF being originated in the solar photosphere. This enhancement of the magnetic fields in the interplanetary space is shown by the long term variation of the a-a indices of the geomagnetic activity, which is causally connected with the behavior of these magnetic fields being transported from the Sun by the solar wind.

The discovery of the important links between CR and cloudiness (Sections 14.1–14.6, 14.9), between CR and precipitation rainfall level (Sections 14.7–14.8), between CR and thunderstorm discharges (Chapter 11) described above gave a basis for assuming that CR may be considered as one of the possible causes of the global climate change observed in the last hundred years (Stozhkov et al., 2001). The direct

measurements of CR intensity on the ground by the global network of NM as well as regular CR intensity measurements on balloons in the troposphere and stratosphere for a period of more than 40 years show that there is a small negative trend of galactic CR intensity $I(t)$ (Stozhkov et al., 2000). In Fig. 14.11.3 are shown the yearly averaged CR fluxes measured in four successive solar activity minimum periods in the Northern polar atmosphere (near Murmansk) at the level 180–200 mb (the negative trend is shown by the straight line and its value is $d\ln(I(t))/dt \approx -(0.09 \pm 0.02)\,\%/\text{year}$). As a result of four solar cycles of balloon measurements in Moscow, the trend was found to be $d\ln(I(t))/dt \approx -(0.08 \pm 0.01)\,\%/\text{year}$. Similar results were obtained on the basis of NM data. For example, NM at the stations Thule, Apatity, Moscow, Jungfraujoch show the same trend as measurements on balloons: $d\ln(I(t))/dt \approx -(0.08 \pm 0.01)\,\%/\text{year}$.

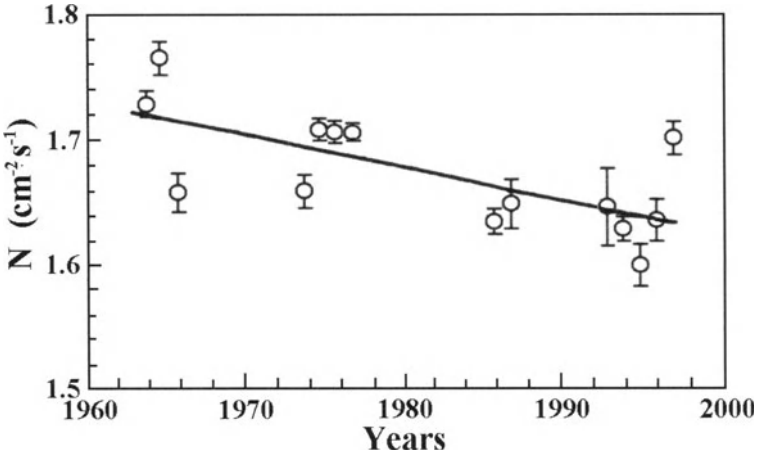

Fig. 14.11.3. Yearly averaged CR fluxes measured in four successive solar activity minimum periods in the Northern polar atmosphere (near Murmansk) at level 180–200 mb (the negative trend is shown by the straight line). According to Stozhkov et al. (2000).

The average over many measurements of CR intensity by NM and on balloons for four solar cycles gives

$$d\ln(I(t))/dt \approx -0.08\ \%/\text{year}. \qquad (14.11.1)$$

If the trend (Eq. 14.11.1) determined on the basis of direct CR measurements during the last 40 years is stable, for 100 years it gives a CR intensity decrease of 8%. From Fig. 14.6.1 it can be seen that the decreasing of CR intensity by 8% will lead to a decrease of cloud coverage of about 2%. According to Dickinson (1975), decreasing cloud coverage by 2% corresponds to increasing the solar radiation power falling on the Earth's ground by about 0.5%. Stozhkov et al. (2001) come to conclusion that the observed global climate change (increasing of average planetary ground temperature by 0.4–0.8°C during the last 100 years) may be caused by the negative trend of CR intensity.

To the same conclusion came Sakurai (2003) on the basis of analyzing data on solar activity and results on the observed connection of solar activity with CR intensity.

14.12. The Project CLOUD as an important step in understanding of the links CR–cloud formation–climate change

According to Fastrup et al (2000), in the last two years a special Collaboration was organized in the framework of European Organization for Nuclear Research, which included 17 Institutes and Universities, for preparing measurements under controlled laboratory conditions in a beam at the CERN Proton Synchrotron (PS), which provides an adjustable source of 'cosmic rays'. The experiment, which is named **CLOUD**, is based on a cloud chamber (which is designed to duplicate the conditions prevailing in the atmosphere) and 'cosmic rays' from CERN Proton Synchrotron (see Fig. 14.12.1). It may be hoped that Project CLOUD will make the next very important step in understanding the link CR–clouds formation.

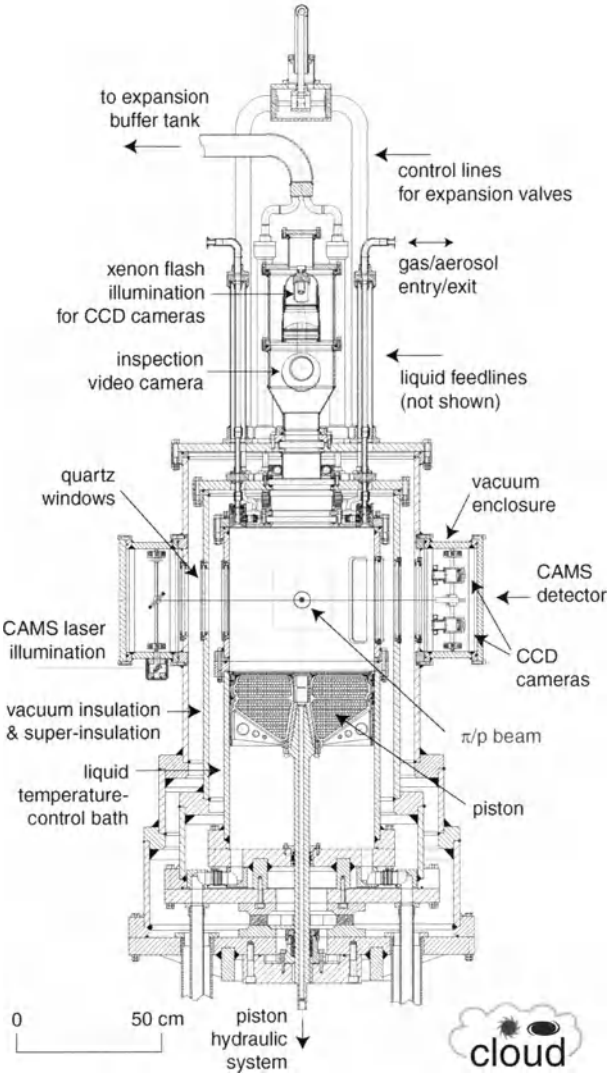

Fig. 14.12.1. Vertical section through the **CLOUD** detector. According to Fastrup et al (2000).

14.13. Possible CR paths in atmosphere forming intermediate links between variable Sun and the Earth's climate change

These paths are shown in Fig. 14.13.1. They may form an intermediate link: the variable Sun through solar wind and general solar magnetic field leaded to CR modulation in the Heliosphere and then to the Earth's climate change (according to Fastrup et al., 2000).

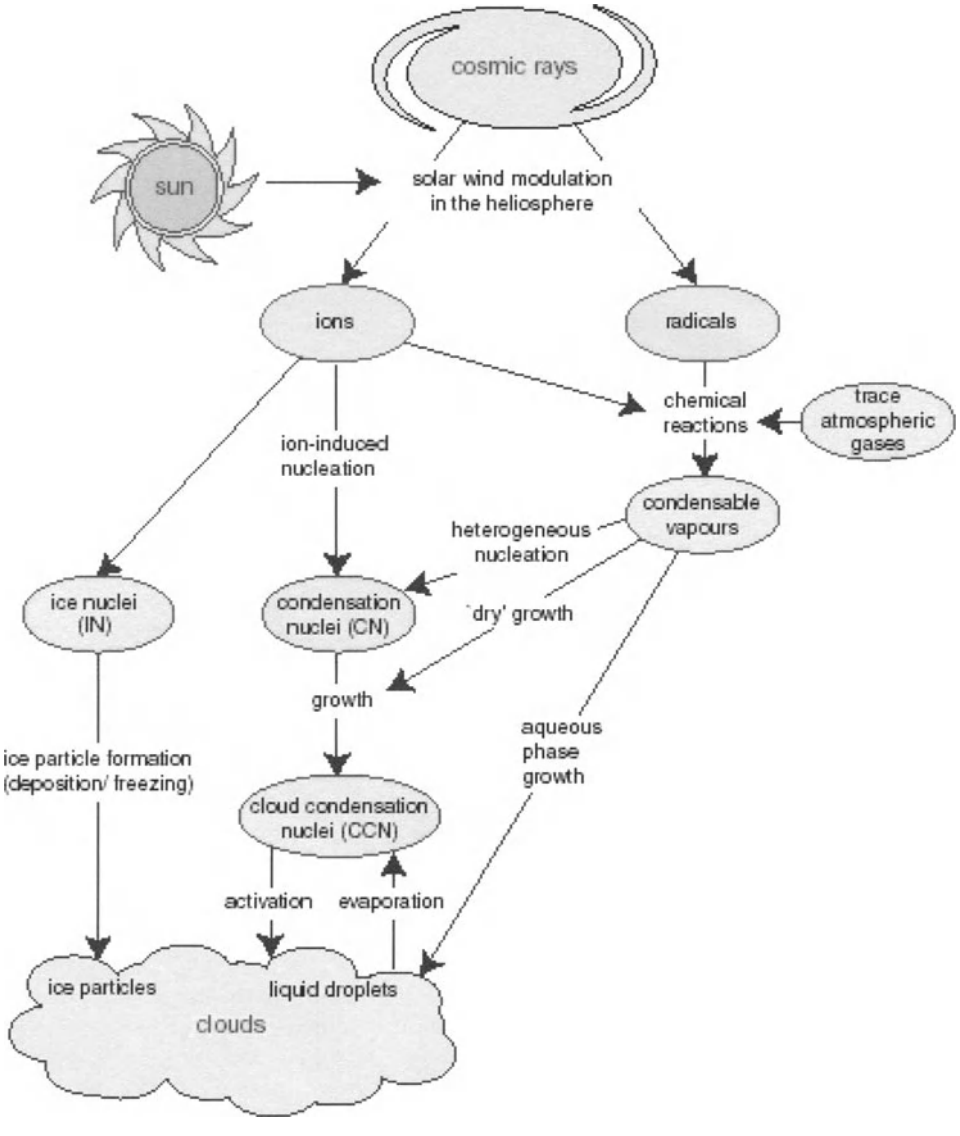

Fig. 14.13.1. Scheme of solar modulation influence on CR intensity and possible influence of CR on different processes in atmosphere leaded to formation of clouds and through clouds on influence on the long term climate change. According to Fastrup et al (2000).

Increasing air ionization with increasing CR intensity can give some increase also in global rain fall (it will be very interesting to check this statement not only on the basis of the data of one country, as in Section 14.7, but on the planetary scale). The main causes of long term change of CR intensity will be considered in detail in Dorman (M2005). Further development of the mechanisms of the paths shown in Fig. 14.13.1 will stimulate deep research of the problem of CR influence on cloud formation, on precipitation, and both in Nature (Sections 14.1–14.11) and in laboratory conditions (Section 14.12); this will lead to some significant progress in the understanding of this very interesting scientific problem, which also has important practical applications.

14.14. On the possible role of CR in long-term climate and landscape change (e.g., Netherlands)

According to Van der Plicht et al. (1998), CR can play an important role in long-term climate and landscape change. How could a relatively small reduction in solar irradiation during low solar activity induce the relatively large change in global climate inferred for 2650 BP? Answering this question involves a considerable degree of speculation, since the effect of solar variability on the Holocene climate is controversial. Two theories are available that explain how a relatively small reduction of solar irradiation and an accompanying increase in CR flux may effect the lower stratosphere.

The first theory is based on the notion that a reduction of ultraviolet radiation may also lead to a decline in ozone production in the lower stratosphere. This could trigger the inferred climate changes (see above, Sections 14.1 and 14.13).

The second theory is based on the idea that an increase of the CR flux may directly lead to an increase in global cloud cover. This relation may be explained by ionization in the atmosphere by CR, thus positively affecting aerosol formation and cloud nucleation. Swensmark H. and E. Friis-Christiansen (1997) found an excellent correlation between the variation in CR flux and the observed global cloud cover for the most recent solar cycle (see Section 14.2). An increase in the global cloud cover is believed to cause a cooling of the earth, especially when low altitude clouds are involved, because more incoming radiation is reflected. Indeed the correlation between CR flux and cloud cover increases going from the equator towards the poles.

A direct increase in cloudiness and accompanying cooling would be in agreement with the reconstructed wetter and cooler conditions at middle latitudes around 2650 BP. The inferred drier conditions in the tropics are less easily explained by this second theory. One may speculate, however, that the proposed changes in cloud cover and temperature may invoke changes in the atmospheric circulation, possibly involving an increase in the number of El Niño events and drier conditions at several places in the tropics. A weakening of the thermohaline circulation in the Atlantic Ocean, as a result of the displacement of the mid-latitudinal storm tracks, could have played an additional role. Such a weakening could have caused a relatively strong cooling of Europe through the reduced release of heat by the Gulf stream and through the positive ice-albedo feedback. This evidence supports the idea that solar/CR forcing is an important factor in the present climate and may also dominate climatic changes in the near future. The above mechanism can be connected to the following observations from prehistory and palaeoecology: more CR mean more clouds and precipitation (the simplified illustration of landscape changes see in Fig. 14.14.1).

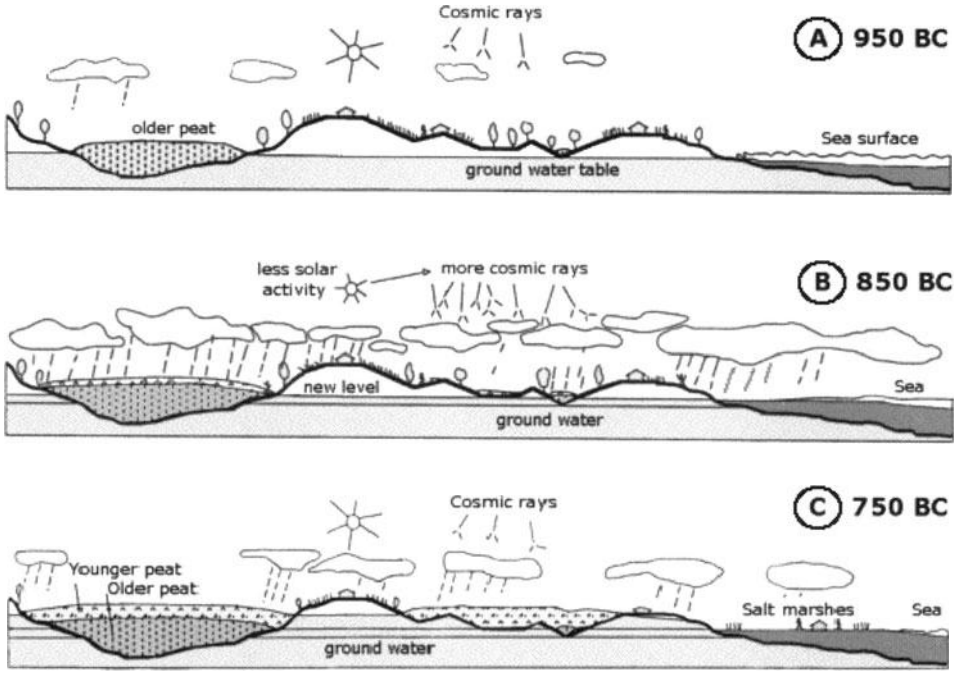

Fig. 14.14.1. Diagram showing the development of the landscape in the northern Netherlands during the older parts of the first millennium BC. Between phases A and B a decline of solar activity caused an increase in cosmic rays, which resulted in an sharp increase of the atmospheric ^{14}C content and also in more clouds, more precipitation and lower temperatures (change of atmospheric patterns). As a consequence there was a sharp increase of the ground water level and enhanced bog growth. Farmers in hydrological marginal regions had to move to drier sites. Salt marshes emerged, probably as a consequence of thermal contraction of ocean water, and these areas were colonized. When the solar activity changed again to less extreme values, the atmospheric circulation patterns did not move to their earlier positions and, as a consequence, the relatively coll and wet climate persisted. According to Van der Plicht et al. (1998),

Van der Plicht et al. (1998) came to following conclusions:

1. In European raised bog deposits, the changing spectrum of peat forming mosses and a sharp decline in decomposition of the peat indicate a sudden change from relatively dry and warm to cool, moist climatic conditions.
2. As a consequence of climate change there was a fast and considerable rise of the ground water table so that peat growth started in areas which were already marginal from a hydrological point of view.
3. The rise of the ground-water table in low-lying areas of the Netherlands resulted in the abandonment of settlement sites.
4. The contemporaneous earliest human colonization of newly emerged salt marshes in the northern Netherlands (after loss of cultivated land) may have been related to thermal contraction of ocean water, causing a temporary stagnation in the relative sea-level rise.

Part 4

APPLICATIONS OF COSMIC RAY RESEARCH

Preface of Part 4

In Part 4 we consider realized and potential applications of CR research in the atmosphere and underground for many different branches of science and technology. This Part contains Chapters 15–18. In Chapters 15–17 these realized applications wich have a considerable prospects in future development are considered in detail, and in Chapter 18 most potential applications for different branches of Science and Technology are considered shortly (some of them will be considered in detail in Dorman, M2005).

Chapter 15 is the theoretical basis for CR application in meteorology – the use of CR for continues determination of the vertical distribution of air temperature (by simultaneous measurements of CR intensity of different secondary components and data processing by the general spectrographic method).

Chapter 16 is an example of CR meteorological effects as a research application to CR latitude survey data processing with an accurate correction of observation data on the barometric effect (with the barometric coefficient changed with latitude), on Bernoulli and effects of state of the sea (sea-state effect), on temperature effect changed with time and latitude. This type of applications widely used in investigations of many CR time variations of magnetospheric and extra-terrestrial origin, which are significantly disturbed by meteorological effects (the magnetospheric and extra-terrestrial CR variations will be considered in details in Dorman, M2005).

Above, in Chapter 10 we introduced the special method of radionuclide coupling functions (for investigations of cosmogenic radionuclide planetary production by CR, mixing and exchange). This method we applied widely in **Chapter 17**, in which the radiocarbon coupling functions method developed for investigations of planetary mixing and exchange processes, influence of H-bombs explosion on the environment, radiocarbon data using for CR variations in the past caused by the change of geomagnetic field, solar activity cycles, supernova explosions.

Chapter 18 contains the short descriptions of a lot of realized and potential applications in Meteorology and in the service of great airports, in Hydrology and Agriculture, in the research of atmospheric electric field phenomena, in Geology and geophysical prospecting, in Environmental science (chemical elements planetary mixing and exchange), in Archeology, potential CR applications for Police and Criminalities, and for Navigation, important applications for the Physics of the Earth's magnetosphere, and for the Physics of the Heliosphere (see details in Dorman, M2005), in the research on global climate change, important applications for space weather monitoring and forecasting (the development of this problem will be in Dorman, M2005), for environmental monitoring of radioactive clouds from nuclear explosions or nuclear plant failures, applications to the problem of forecasting dangerous earthquakes, applications to CR interactions with the atmospheres of the Sun and other planets and their satellites, with the Moon, asteroids and meteorites in the interplanetary space (details in Dorman, M2005), CR applications to some medical and car road accidents problems connected with the influence of space phenomena on people's health and people's speed of reaction in dangerous situations.

Chapter 15

The Possible Application of the Inverse Problem: Determination of Atmospheric Conditions by Cosmic Ray Data

15.1. Determination of air temperature variations in the upper atmosphere by data on underground muon component variations

Investigation of the CR variations of meteorological origin helps, in its turn, in the study of the temperature fluctuations in the Earth's atmosphere on pressure levels smaller than 100–200 mb. From this point of view measurements made underground are of particular interest because, as was found in the previous Chapters 5 and 9, the large value of the temperature coefficient $W_T(h)$ at small h and the very small value of $W_T(h)$ at large h imply that the intensity of muons underground is very sensitive to variations of the temperature in the upper layers of the atmosphere and practically insensitive to temperature changes in the lower layers. A favorable circumstance is that the variations in the extra-atmospheric origin of the muon intensity underground are considerably smaller than at the surface.

About 50 years ago aerologists had serious problems caused by errors connected with the Sun's irradiative heating in meteorological sounding balloons: they came to a wrong conclusion about the existence in $h \leq 200$ mb of daily air temperature variation with enormous amplitude of about 20–25 °C. But, as it was shown by Dorman at the beginning of 1950s on the Seminar in the Central Aerological Observatory (Dolgoprudny, Moscow region), this result strongly contradicts the muon underground measurements at a depth of 60 m w.e. according to MacAnuff (1951) and other authors; corresponding to muon underground data the amplitude of diurnal wave of air temperature at $h \leq 200$ mb does not exceed 1 °C (see review of this problem in Dorman, M1957, Section 20.3). This result formed the basis for the irradiative corrections to be applied to the meteorological sounding balloon temperature data according to the *Methodical Instructions for Meteorological Sounding Balloon Measurements* (1955).

According to Chapters 5 and 9 the temperature coefficient $W_T(h)$ at the depth of 60 m w.e. at the zenith angle 60° has a sharp maximum above the pressure level 20–30 mb. This was used by Kuzmin et al. (1965) for the rough estimation of possible temperature variations in the layer above 20–30 mb. It was found that over Yakutsk the amplitude of the seasonal variations of the effective temperature of the layer above 20–30 mb is 35-50 °C and of the 27-days variations about 15–20 °C.

15.2. Determination of vertical distribution of air temperature by simultaneous measurements of several CR secondary components

More general formulation of the inverse problem–determination of atmospheric conditions by measurements of several secondary CR components with sufficiently different temperature coefficients $W_{Ti}(h)$ was formulated by Miyazaki and Wada (1970). They relied on $W_{Ti}(h)$ which was described above in Chapter 5 for hard and soft muons at sea level, and hard muons underground at the depth of 60 m w.e. (see Fig. 15.2.1).

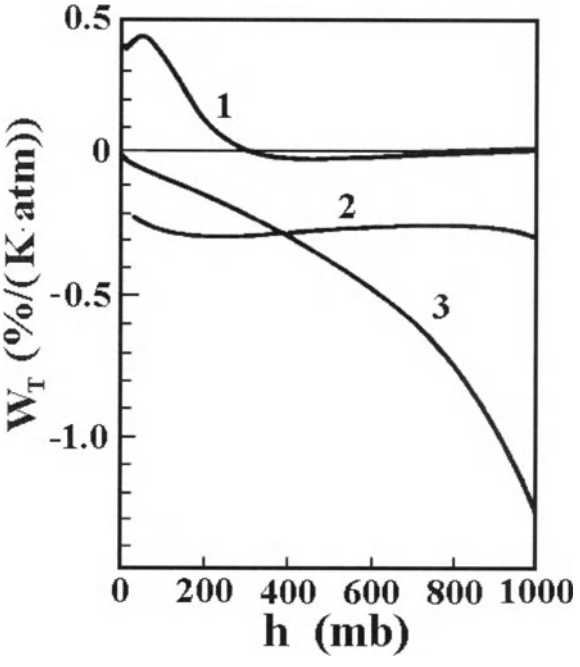

Fig. 15.2.1. The comparison of temperature coefficients: *1* for observations underground at the depth 60 m w.e.; *2* for hard muons at the sea level; *3* for soft muons at sea level. According to Miyazaki and Wada (1970).

For any moment of time t

$$\delta I_i(t) = (\Delta I_i(t)/I_{oi})_T = \int_o^{h_o} W_{Ti}(h)\Delta T(h,t)dh \approx \sum_{k=1}^{k=3} W_{ik}\Delta T_k(t), \qquad (15.2.1)$$

where $i = 1, 2, 3$ is the type of CR component, and the atmosphere is divided on three layers $k = 1, 2, 3$ with average pressure 100, 500 and 700 mb. In this case

$$W_{ik} \approx \int_{h_k}^{h_{k+1}} W_{Ti}(h)dh, \quad \Delta T_k(t) \approx \int_{h_k}^{h_{k+1}} \Delta T(h,t)dh, \qquad (15.2.2)$$

where

$$h_1 = 0, \quad h_2 = 100\,\text{mb}, \quad h_3 = 500\,\text{mb}, \quad h_4 = 700\,\text{mb}, \quad h_5 = h_o. \tag{15.2.3}$$

The solution of the system Eq. 15.2.1 will be

$$\Delta T_1(t) = \begin{vmatrix} \delta I_1(t) & W_{12} & W_{13} \\ \delta I_2(t) & W_{22} & W_{23} \\ \delta I_3(t) & W_{32} & W_{33} \end{vmatrix} \Bigg/ \begin{vmatrix} W_{11} & W_{12} & W_{13} \\ W_{21} & W_{22} & W_{23} \\ W_{31} & W_{32} & W_{33} \end{vmatrix}, \quad \Delta T_2(t) = \begin{vmatrix} W_{11} & \delta I_1(t) & W_{13} \\ W_{21} & \delta I_2(t) & W_{23} \\ W_{31} & \delta I_3(t) & W_{33} \end{vmatrix} \Bigg/ \begin{vmatrix} W_{11} & W_{12} & W_{13} \\ W_{21} & W_{22} & W_{23} \\ W_{31} & W_{32} & W_{33} \end{vmatrix},$$

$$\Delta T_3(t) = \begin{vmatrix} W_{11} & W_{12} & \delta I_1(t) \\ W_{21} & W_{22} & \delta I_2(t) \\ W_{31} & W_{32} & \delta I_3(t) \end{vmatrix} \Bigg/ \begin{vmatrix} W_{11} & W_{12} & W_{13} \\ W_{21} & W_{22} & W_{23} \\ W_{31} & W_{32} & W_{33} \end{vmatrix}. \tag{15.2.4}$$

In Fig. 15.2.2 are shown the variations of daily averaged temperature on layers $h_4 = 700$ mb, $h_3 = 500$ mb, $h_2 = 100$ mb observed in December 1965, in comparison with those calculated from CR observations according to Eq. 15.2.4.

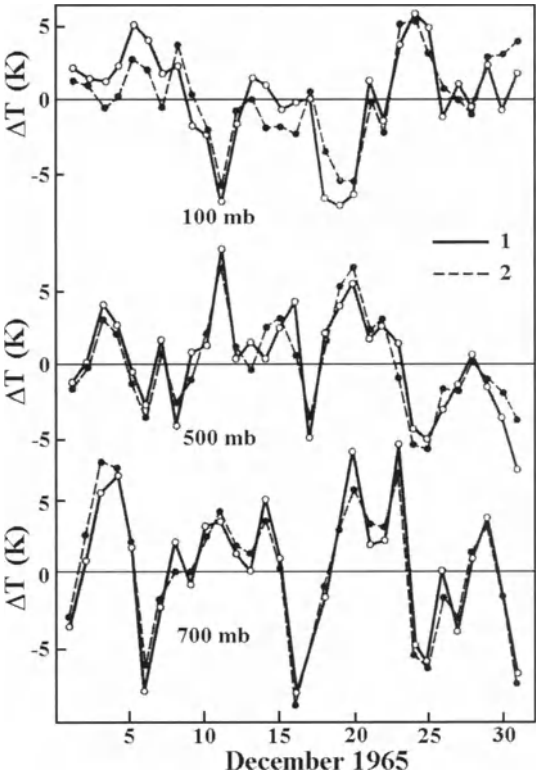

Fig. 15.2.2. The comparison of observed daily averaged temperatures on levels 100, 500 and 700 mb (full curves *1*) with obtained from CR data (dashed curves *2*). According to Miyazaki and Wada (1970).

It can be seen that in principle continuous measurements of vertical temperature distribution in the atmosphere can be carried out using CR. Much better results can be obtained by CR detectors with bigger effective area on the basis of spectrographic method.

15.3. The use of spectrographic method to exclude geomagnetic and extraterrestrial variations

To obtain real exact information on the meteorological conditions by means of CR it is necessary first of all to exclude from observational data variations of geomagnetic and extraterrestrial origin. In principle this can be made with good accuracy by using the spectrographic method described in Sections 3.11 and 3.12. This was demonstrated in Dorman and Krestyannikov (1977) by using observation data of the Sayan spectrographic array in 1969–1975. This array consists of three neutron monitors on levels 435, 2000 and 3000 m above sea level and hard muon detector on level 435 m. The set of equations that describe the observed variations of geomagnetic, extraterrestrial, and temperature origin (all data are preliminary corrected on barometric effect) will be

$$b_{n1}(t)=\Delta I_n(R_c,h_1,t)/I_{no}(R_c,h_1)=-\Delta R_c(t)W_{n1}+af_{n1}(\gamma(t)), \tag{15.3.1}$$

$$b_{n2}(t)=\Delta I_n(R_c,h_2,t)/I_{no}(R_c,h_2)=-\Delta R_c(t)W_{n2}+af_{n2}(\gamma(t)), \tag{15.3.2}$$

$$b_{n3}(t)=\Delta I_n(R_c,h_3,t)/I_{no}(R_c,h_3)=-\Delta R_c(t)W_{n3}+af_{n3}(\gamma(t)), \tag{15.3.3}$$

$$b_{\mu1}(t)=\Delta I_\mu(R_c,h_1,t)/I_{\mu o}(R_c,h_1)=-\Delta R_c(t)W_{\mu1}+af_{\mu1}(\gamma(t))+C_{\mu T}(h_1,t), \tag{15.3.4}$$

where

$$W_{ni}=W_n(R_c,R_c,h_i),\quad f_{ni}(\gamma)=\int_{R_c}^{\infty}R^{-\gamma}W_n(R,R_c,h_i)dR,\quad W_{\mu1}=W_\mu(R_c,R_c,h_1),$$
$$f_{\mu1}(\gamma)=\int_{R_c}^{\infty}R^{-\gamma}W_\mu(R,R_c,h_1)dR,\quad C_{\mu T}(h_1,t)=\int_0^{h_1}W_{\mu T}(h,h_1)\Delta T(h,t)dh. \tag{15.3.5}$$

The solution of the first three Eq. 15.3.1–15.3.3 is as following:

1. The slope $\gamma(t)$ in the relation $\Delta D(R,t)/D_o(R)=a(t)R^{-\gamma(t)}$ will be determined from equation

$$\Psi_{\text{Sayan}}(\gamma)=[W_{n1}b_{n2}(t)-W_{n2}b_{n1}(t)]/[W_{n2}b_{n3}(t)-W_{n3}b_{n2}(t)], \tag{15.3.6}$$

where for the Sayan spectrograph

$$\Psi_{\text{Sayan}}(\gamma)=[W_{n1}f_{n2}(\gamma)-W_{n2}f_{n1}(\gamma)]/[W_{n2}f_{n3}(\gamma)-W_{n3}f_{n2}(\gamma)]. \tag{15.3.7}$$

2. After determining $\gamma(t)$ from Eq. 15.3.6 it is very easy to determine

$$a(t)=[b_{n2}(t)W_{n1}-b_{n1}(t)W_{n2}]/[W_{n1}f_{n2}(\gamma(t))-W_{n2}f_{n1}(\gamma(t))]. \quad (15.3.8)$$

$$\Delta R_c(t)=[b_{n2}(t)f_{n1}(\gamma(t))-b_{n1}(t)f_{n2}(\gamma(t))]/[W_{n1}f_{n2}(\gamma(t))-W_{n2}f_{n1}(\gamma(t))], \quad (15.3.9)$$

Then from Eq. 15.3.4 by using solutions for $\gamma(t)$, $a(t)$, and $\Delta R_c(t)$ we determine

$$C_{\mu T}(h_1,t)=b_{\mu 1}(t)+[W_{n1}f_{n2}(\gamma(t))-W_{n2}f_{n1}(\gamma(t))]^{-1}$$

$$\times\{W_{\mu 1}[b_{n2}(t)f_{n1}(\gamma(t))-b_{n1}(t)f_{n2}(\gamma(t))]-f_{\mu 1}(\gamma(t))[b_{n2}(t)W_{n1}-b_{n1}(t)W_{n2}]\}. \quad (15.3.10)$$

On the other hand, we can determine $C_{\mu T}(h_1,t)$ according to the last equation in Eq. 15.3.5 on the basis of meteorological balloon data. The comparison of $C_{\mu T}(h_1,t)_{sp}$ found by the spectrographic method without using any information on the vertical air temperature distribution (according to Eq. 15.3.10) and $C_{\mu T}(h_1,t)_{int}$ found by the integral method described in Chapter 5 on the basis of meteorological balloon data on the time variations of the vertical air temperature distribution are shown in Fig. 15.3.1.

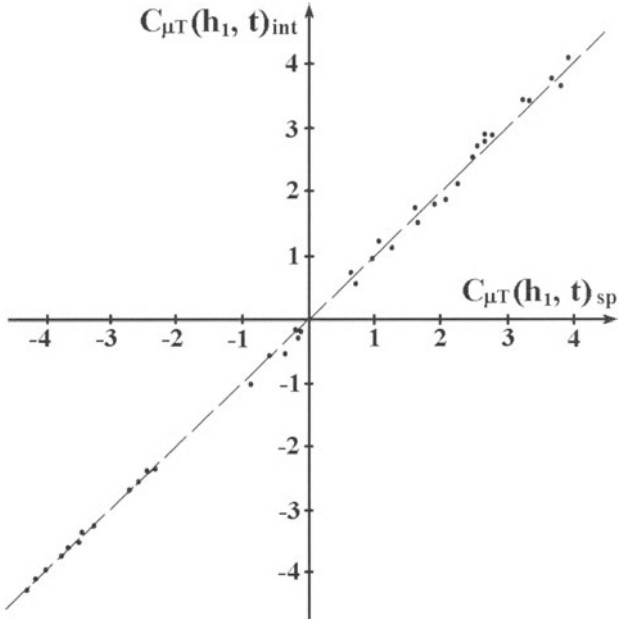

Fig. 15.3.1. The comparison of $C_{\mu T}(h_1,t)_{sp}$ found by spectrographic method (without using any information on the vertical air temperature distribution according to Eq. 15.3.10) and $C_{\mu T}(h_1,t)_{int}$ found by integral method on the basis of aero-sound data on the time variations of the vertical air temperature distribution.

From this figure it can be seen that the relative difference between the two values of $C_{\mu T}(h_1,t)$ is not more than 0.2–0.3%; regression and correlation coefficients are very near to 1. It means that by spectrographic method we can determine the CR temperature variations with very high accuracy. These results can then be used for determining the vertical air temperature distribution.

15.4. Determination of altitudinal air temperature profile using CR data and ground temperature

Belov et al. (1986, 1987, 1990) developed a method for determining the altitudinal air temperature profile by using CR data and ground temperature measurements. It is suggested that CR measurements were made continuously by the ground muon telescope $I_g(t)$ (energy of detected muons more than 350 MeV) and by the underground muon telescope $I_u(t)$ (energy of detected muons more than 20 GeV). It is also assumed that are continuous measurements of ground temperature $T_g(t)$. Observational data of CR intensity are corrected for CR variations of extra-terrestrial and geomagnetic origin (by using on-line data of neutron monitor at the same point or from other CR stations). In this case according to Belov et al. (1986, 1987, 1990) the connection between the temperature $T_i(t)$ at some isobaric level i will be determined by the following linear regression equation:

$$\delta T_i(t) = a_i \delta I_g(t) + b_i \delta I_u(t) + c_i \delta T_g(t), \qquad (15.4.1)$$

where the regression coefficients a_i, b_i, c_i are determined in the following manner. Because these coefficients vary negligibly with time they can be determined for some long period of simultaneous measurements of CR intensity by ground and underground muon telescopes and ground temperature on the one hand, and temperature data obtained by meteorological balloons over the point of CR measurements on the other. In this case regression coefficients a_i, b_i, c_i will be determined for each atmospheric layer i by the least squares method:

$$\sum_k \left[\delta T_i(t_k) - \left(a_i \delta I_g(t_k) + b_i \delta I_u(t_k) + c_i \delta T_g(t_k)\right)\right]^2 = \min, \qquad (15.4.2)$$

where $\delta T_i(t_k)$ are results of temperature balloon sounding of atmospheric layer i at the moment t_k. Let us note the following:

1) the accuracy of this method will increase with decreasing statistical errors of CR measurements;
2) by using averaged data the method will work better than for one-hour data;
3) the number of control layers can be determined experimentally: it depends on the number of CR secondary components and character of interconnection between temperatures of different atmospheric layers;
4) regression coefficients a_i, b_i, c_i may be different for different points of observations;

5) it is not excluded that there are seasonal variations of the regression coefficients a_i, b_i, c_i.

In any case it is necessary to make a special investigation on the basis of a few years of CR data as well as ground air temperature and balloon sounding temperature data on the stability and possible time variations of the regression coefficients a_i, b_i, c_i. And even after this it is not excluded that at some particular times (passing of cyclones, warm and cold fronts, etc) the method considered will not work well. The physical method, which will be considered below, will work well in any weather situation.

15.5. The general spectrographic method and inverse problem

The methods described above in Sections 15.1 and 15.2, applied in Kuzmin et al. (1965) and Miyazaki and Wada (1970) are not quite correct since the variations of extraterrestrial origin were not completely excluded (disregarding the temporal variations of the geomagnetic cut off rigidity and the exponent of the extraterrestrial variation spectrum). In Dorman (1977a,b) it was proposed to use the generalized spectrographic method to isolate and separately study the CR variations of the extraterrestrial, geomagnetic and atmospheric origin.

15.5.1. The case of detection of three stable and one or several unstable CR components at a single point.

Let us consider first the simplest case in which a spectrographic array is able to detect the variations of the stable CR components with (at least) three instruments with essentially different coupling coefficients, and several unstable components with essentially different temperature coefficients (for example, electron-photon component, hard and soft muon components, the components arriving from the vertical and various zenith angles, etc.). The set of stable CR components could provide the possibility of finding the parameters ΔR_c, a, and γ, which determine respectively the variations of magnetospheric origin (characterized by values of ΔR_c), and extraterrestrial origin (characterized by values of $\Delta D(R,t)/D_o(R) = aR^{-\gamma}$). This can be made by solving the set of three spectrographic equations examined for any moment of time t according to Section 3.11 in Chapter 3. The set of equations for three stable components (for example, for three different neutron multiplicities m) will be presented in the form

$$b_m(t) = -\Delta R_c(t) W_m + a(t) f_m(\gamma(t)), \tag{15.5.1}$$

where the notations

$$b_m(t) = \Delta I_m(R_c,t)/I_{mo}(R_c), \quad W_m = W_m(R_c,R_c), \quad f_m(\gamma) = \int_{R_c}^{\infty} R^{-\gamma} W_m(R,R_c)\,dR, \tag{15.5.2}$$

are used. The equations for n unstable components $i = 4, 5, 6, \ldots, n+3$ will be presented in the form

$$b_i(t) = -\Delta R_c(t) W_i + a(t) f_i(\gamma(t)) + C_{Ti}(t), \tag{15.5.3}$$

where $C_{Ti}(t)$ is the temperature effect of the i-th unstable component (which is determined by the vertical distribution of the atmospheric temperature above the observation level), and

$$b_i(t) = \Delta I_i(R_c,t)/I_{io}(R_c), \quad W_i = W_i(R_c,R_c), \quad f_i(\gamma) = \int_{R_c}^{\infty} R^{-\gamma} W_i(R,R_c)\,dR. \tag{15.5.4}$$

We assume that in Eq. 15.5.1 and Eq. 15.5.3 all observed CR variations $b_m(t)$ and $b_i(t)$ are corrected for the barometric effect (here m = 1, 2, and 3; i = 4, 5, … , n+3. Therefore we have total system of n+3 equations described by Eq. 15.5.1 and 15.5.3 with the unknown variables $\Delta R_c(t)$, $a(t)$, $\gamma(t)$ and $C_{Ti}(t)$. The following procedure will be used to solve the set of Eq. 15.5.1 and 15.5.3. First of all, the function

$$\Psi(\gamma) = [W_1 f_2(\gamma) - W_2 f_1(\gamma)]/[W_2 f_3(\gamma) - W_3 f_2(\gamma)] \tag{15.5.5}$$

will be tabulated in accordance with the procedure described in Section 3.11 and then $\gamma(t)$ can be easily found from the equation

$$\Psi(\gamma) = [W_1 b_2(t) - W_2 b_1(t)]/[W_2 b_3(t) - W_3 b_2(t)]. \tag{15.5.6}$$

Substituting the found $\gamma(t)$ in the set Eq. 15.5.1 we obtain

$$\Delta R_c(t) = [b_2(t) f_1(\gamma(t)) - b_1(t) f_2(\gamma(t))]/[W_1 f_2(\gamma(t)) - W_2 f_1(\gamma(t))], \tag{15.5.7}$$

$$a(t) = [b_2(t) W_1 - b_1(t) W_2]/[W_1 f_2(\gamma(t)) - W_2 f_1(\gamma(t))]. \tag{15.5.8}$$

By substituting the found $\gamma(t)$, $\Delta R_c(t)$ and $a(t)$ in Eq. 15.5.3, we obtain

$$C_{Ti}(t) = b_i(t) + [W_1 f_2(\gamma(t)) - W_2 f_1(\gamma(t))]^{-1}$$

$$\times \{W_i [b_2(t) f_1(\gamma(t)) - b_1(t) f_2(\gamma(t))] - f_i(\gamma(t))[b_2(t) W_1 - b_1(t) W_2]\}. \tag{15.5.9}$$

On the other hand, according to Chapters 5 and 9

$$C_{Ti}(t) = \int_0^{h_o} W_{Ti}(h_o,h) \Delta T(h,t)\,dh = \sum_{j=1}^{n} W_{Tij} \Delta T_j(t), \tag{15.5.10}$$

where $W_{Ti}(h_o,h)$ is the temperature coefficient for the i-th unstable component and $\Delta T(h,t)$ characterizes the variation of the vertical distribution of air temperature (strictly speaking, according to Chapter 5, $T(h,t)$ is the generalized temperature determined by the relation

$$T(h,t)=T_{tr}(h,t)+0.378e(h,t)/h \tag{15.5.11}$$

where the $T_{tr}(h,t)$ is the true temperature and $e(h,t)$ is the pressure of water vapor; in this case both temperature and humidity effects for the unstable components are taken into account). In Eq. 15.5.10 $\Delta T_j(t)$ is the change of the effective temperature of the corresponding layer, and

$$W_{Tij}=\int_{h_j}^{h_{j+1}} W_{Ti}(h,h_o)dh, \tag{15.5.12}$$

where j = 1, 2, 3, ..., n, and $h_1=0,.....,h_{n+1}=h_o$. By comparison of Eq. 15.5.9 with Eq. 15.5.10 we obtain a set of n linear equations relevant to $\Delta T_j(t)$. The solution for such set of equations is determined by the formulas

$$\Delta T_j(t)=\left(\det\left|W_{Tij}\right|\right)^{-1}\times\sum_{i=4}^{n+3}\overline{W_{Tij}}\{b_i(t)+[W_1f_2(\gamma(t))-W_2f_1(\gamma(t))]^{-1}$$

$$\times[W_i(b_2(t)f_1(\gamma(t))-b_1(t)f_2(\gamma(t)))-f_i(\gamma(t))(b_2(t)W_1-b_1(t)W_2)]\}, \tag{15.5.13}$$

where $\overline{W_{Tij}}$ is the algebraic addition to the element W_{Tij} in $\det\left|W_{Tij}\right|$. Eq. 15.5.13, together with the definitions of $\gamma(t)$, $a(t)$, $\Delta R_c(t)$ according to Eq. 15.5.6–15.5.8, show that the three stable and n unstable components may be used to realize the continuous location of the temporal variations of the vertical temperature distribution in the atmosphere by means of CR. Let us note that in this case the errors associated with the specific conditions of atmosphere sounding by meteorological balloons, i.e. the irradiative heating, inertness, etc, can be naturally eliminated.

15.5.2. The case when all components are unstable; passive location of the variations in the vertical distribution of the atmospheric temperature

Let us consider now the more general case when the neutron components are considered also as unstable (because they have some small temperature effect, see Sections 5.4 and 7.4). In this case, we will have the set of n equations:

$$b_i(t)=-\Delta R_c(t)W_i+a(t)f_i(\gamma(t))+C_{Ti}(t), \tag{15.5.14}$$

where $i=1,2,3,...,n$ $(n\geq 4)$, designations of $b_i(t)$, W_i, $f_i(\gamma(t))$ were given in Eq. 15.5.4, and $C_{Ti}(t)$ is the temperature variation of the i-th unstable component determined by the vertical distribution of the air temperature above the observation level and by the i-th temperature coefficient according to Chapters 5 and 9:

$$C_{Ti}(t)=\int_0^{h_o} W_{Ti}(h_o,h)\Delta T(h,t)dh\,, \tag{15.5.15}$$

The problem is that in the set of n equations described by Eq. 15.5.14 we have $n+3$ unknown variables: $\gamma(t)$, $a(t)$, $\Delta R_c(t)$, and $C_{Ti}(t)$ ($i=1,2,3,...,n$). To solve this problem let the atmosphere from the level of observation $h=h_o$ to the boundary of the atmosphere $h=0$ be broken into $n-3$ layers. In this case the Eq. 15.5.15 may be rewritten in the form

$$C_{Ti}(t)=\sum_{j=1}^{n-3} W_{Tij}\Delta T_j(t)\,, \tag{15.5.16}$$

where $\Delta T_j(t)$ is the mean value of temperature in the h_j-h_{j+1} layer, and

$$W_{Tij}=\int_{h_j}^{h_{j+1}} W_{Ti}(h,h_o)dh. \tag{15.5.17}$$

If, further, not $C_{Ti}(t)$ but $\Delta T_j(t)$ is considered as new $n-3$ unknown variables, we will have a set from n equations with total n unknown variables:

$$b_i(t)=-\Delta R_c(t)W_i+a(t)f_i(\gamma(t))+\sum_{j=1}^{n-3} W_{Tij}\Delta T_j(t). \tag{15.5.18}$$

Examine the first $n-3$ equations of the set Eq. 15.5.18. Let the first two terms in them be transposed to the left hand side; then $\Delta T_j(t)$ will be found:

$$\Delta T_j(t)=\left\{\sum_{i=1}^{n-3}\overline{W_{Tij}}\left[b_i(t)+\Delta R_c(t)W_i-a(t)f_i(\gamma(t))\right]\right\}\Big/\det\left|W_{Tij}\right|\,. \tag{15.5.19}$$

where $\overline{W_{Tij}}$ is the algebraic addition to the element W_{Tij} in the $\det\left|W_{Tij}\right|$. Substituting Eq. 15.5.19 in the last three equations of the set Eq. 15.5.18 we obtain

$$b_i(t)-\left(\det\left|W_{Tij}\right|\right)^{-1}\sum_{j=1}^{n-3}W_{Tij}\sum_{l=1}^{n-3}\overline{W_{Tlj}}b_l(t)=-\Delta R_c(t)\left[W_i-\left(\det\left|W_{Tij}\right|\right)^{-1}\sum_{j=1}^{n-3}W_{Tij}\sum_{l=1}^{n-3}\overline{W_{Tlj}}W_l\right]$$

$$+a(t)\left[f_i(\gamma(t))-\left(\det\left|W_{Tij}\right|\right)^{-1}\sum_{j=1}^{n-3}W_{Tij}\sum_{l=1}^{n-3}\overline{W_{Tlj}}f_l(\gamma(t))\right], \qquad (15.5.20)$$

where $i=n-2, n-1$, and n. The left hand side of Eq. 15.5.20 contains the known values, while the right hand side contains three unknowns $\Delta R_c(t)$, $a(t)$, and $\gamma(t)$ which determine the magnetospheric and extraterrestrial variations of CR. The solution of the set of three equations Eq. 15.5.20 will be found as follows. First of all, it is necessary to tabulate the following special function for a given set of instruments and the given separation of atmosphere on $n-3$ layers:

$$\Omega(\gamma)=[\omega_{n-2}\varphi_{n-1}(\gamma)-\omega_{n-1}\varphi_{n-2}(\gamma)]/[\omega_{n-1}\varphi_n(\gamma)-\omega_n\varphi_{n-1}(\gamma)], \qquad (15.5.21)$$

where

$$\omega_i=W_i-\left(\det\left|W_{Tij}\right|\right)^{-1}\sum_{j=1}^{n-3}W_{Tij}\sum_{l=1}^{n-3}\overline{W_{Tlj}}W_l, \qquad (15.5.22)$$

$$\varphi_i(\gamma(t))=f_i(\gamma(t))-\left(\det\left|W_{Tij}\right|\right)^{-1}\sum_{j=1}^{n-3}W_{Tij}\sum_{l=1}^{n-3}\overline{W_{Tlj}}f_l(\gamma(t)) \qquad (15.5.23)$$

can be easily obtained through the known coupling and temperature coefficients. The slope $\gamma(t)$ is determined by solving the equation

$$\Omega(\gamma)=[\omega_{n-2}\beta_{n-1}(t)-\omega_{n-1}\beta_{n-2}(t)]/[\omega_{n-1}\beta_n(t)-\omega_n\beta_{n-1}(t)], \qquad (15.5.24)$$

where

$$\beta_i(t)=b_i(t)-\left(\det\left|W_{Tij}\right|\right)^{-1}\sum_{j=1}^{n-3}W_{Tij}\sum_{l=1}^{n-3}\overline{W_{Tlj}}b_l(t). \qquad (15.5.25)$$

After $\gamma(t)$ has been determined, the parameters $a(t)$ and $\Delta R_c(t)$ can be easily determined:

$$a(t)=[\omega_{n-2}\beta_{n-1}(t)-\omega_{n-1}\beta_{n-2}(t)]/[\omega_{n-2}\varphi_{n-1}(\gamma(t))-\omega_{n-1}\varphi_{n-2}(\gamma(t))], \qquad (15.5.26)$$

$$\Delta R_c(t)=\frac{\varphi_{n-2}(\gamma(t))\beta_{n-1}(t)-\varphi_{n-1}(\gamma(t))\beta_{n-2}(t)}{\omega_{n-2}\varphi_{n-1}(\gamma(t))-\omega_{n-1}\varphi_{n-2}(\gamma(t))}. \qquad (15.5.27)$$

The temperature variations for each of the components will be, in its turn, determined from Eq. 15.5.14 taking into account the solutions obtained for $\gamma(t)$, $a(t)$, and $\Delta R_c(t)$:

$$C_{Ti}(t) = b_i(t) + \{W_i[\varphi_{n-2}(\gamma(t))\beta_{n-1}(t) - \varphi_{n-1}(\gamma(t))\beta_{n-2}(t)] - f_i(\gamma(t))$$

$$\times[\omega_{n-2}\beta_{n-1}(t) - \omega_{n-1}\beta_{n-2}(t)]\}[\omega_{n-2}\varphi_{n-1}(\gamma(t)) - \omega_{n-1}\varphi_{n-2}(\gamma(t))], \qquad (15.5.28)$$

where $i = 1, 2, 3, ..., n$. By substituting the found by Eq. 15.5.24, 15.5.26 and 15.5.27 values of $\gamma(t)$, $a(t)$, and $\Delta R_c(t)$ in Eq. 15.5.19 we shall find the time variation of the unknown vertical air temperature profile:

$$\Delta T_j(t) = \left(\det|W_{Tij}|\right)^{-1} \sum_{i=1}^{n-3} \overline{W_{Tij}} \{b_i(t) + [W_i(\varphi_{n-2}(\gamma(t))\beta_{n-1}(t) - \varphi_{n-1}(\gamma(t))\beta_{n-2}(t))$$

$$- f_i(\gamma(t))][\omega_{n-2}\beta_{n-1}(t) - \omega_{n-1}\beta_{n-2}(t))][\omega_{n-2}\varphi_{n-1}(\gamma(t)) - \omega_{n-1}\varphi_{n-2}(\gamma(t))]^{-1}\}, \qquad (15.5.29)$$

where $j = 1, 2, 3, ..., n-3$.

15.6. The continuous passive sounding of the variations in the vertical distribution of the atmospheric temperature and the air column mass over the observation level by means of CR

It was assumed in the previous Section 15.5 that the corrections for the barometric effect are inserted into all the observational data prior to spectrographic analysis. Under some conditions, however, the insertion of the barometric corrections on the basis of the data of measurements of the air pressure at the observation level seems to be extremely difficult or even impossible (for example, during strong wind motions the Bernoulli effect significantly distorts the results of the measurements of the air column's mass over the observation point, see Section 6.2). To study the effect of the various distorting factors on the measurements of the barometric effect, it is of interest to develop the method for determining the air column mass over the instruments on the basis of the data of CR observations. Such a method developed in Dorman (1977a,b,c; 1979) would make it possible to independently and objectively obtain continuous information not only about the temperature profile of the atmosphere but also about the variations of the air column mass over the observation level, and then, by comparison with direct measurements of dynamic air pressure to obtain some continue information on the wind velocity distribution in the atmosphere.

So consider the case of detection of n different unstable components at level h_o. The appropriate set of spectrographic equations will be written, taking account of the division of the atmosphere into $n-4$ layers, in the form

$$b_i(t) = -\Delta R_c(t)W_i + a(t)f_i(\gamma(t)) + B_i\Delta h_o(t) + \sum_{j=1}^{n-4} W_{Tij}\Delta T_j(t), \qquad (15.6.1)$$

where $i = 1, 2, 3, ..., n$; B_i are the barometric coefficients, and $\Delta h_o(t)$ is the unknown variation of the air column mass over the observation level, and the rest of the designations are given by

$$b_i(t) = \Delta I_i(R_c, t)/I_{io}(R_c), \quad W_i = W_i(R_c, R_c), \quad f_i(\gamma) = \int_{R_c}^{\infty} R^{-\gamma} W_i(R, R_c) dR, . \quad (15.6.2)$$

$$W_{Tij} = \int_{h_j}^{h_{j+1}} W_{Ti}(h, h_o) dh, \quad (15.6.3)$$

and $W_i(R, R_c)$ are the coupling functions and $W_{Ti}(h, h_o)$ are the temperature coefficients. In the set of n equations Eq. 15.6.1 we have n unknowns: $\gamma(t)$, $a(t)$, $\Delta R_c(t)$, $\Delta h_o(t)$, and $\Delta T_j(t)$, where $j = 1, 2, 3, ..., n-4$. Any three equations from the set Eq. 15.6.1 will be used for determining the parameters $\gamma(t)$, $a(t)$, and $\Delta R_c(t)$. Let us denote these equations as $i = n-2$, $n-1$ and n. The rest $n-3$ equations can be rewritten as

$$b_i(t) + \Delta R_c(t) W_i - a(t) f_i(\gamma(t)) = B_i \Delta h_o(t) + \sum_{j=1}^{n-4} W_{Tij} \Delta T_j(t), \quad (15.6.4)$$

where $i = 1, 2, 3, ..., n-3$. Let us denote

$$x_j(t) = \begin{cases} \Delta T_j(t) \text{ if } 1 \le j \le n-4, \\ \Delta h_o(t) \text{ if } j = n-3, \end{cases} \quad (15.6.5)$$

$$V_{ij} = \begin{cases} W_{ij} \text{ if } 1 \le j \le n-4, \\ B_i \text{ if } j = n-3. \end{cases} . \quad (15.6.6)$$

In this case instead of Eq. 15.6.4 we obtain

$$b_i(t) + \Delta R_c(t) W_i - a(t) f_i(\gamma(t)) = \sum_{j=1}^{n-3} V_{ij} x_j(t), \quad (15.6.7)$$

The solution of set Eq. 15.6.7 will be of the form

$$x_j(t) = \left(\det \left| V_{kj} \right|\right)^{-1} \sum_{k=1}^{n-3} \overline{V_{kj}} \left[b_k(t) + \Delta R_c(t) W_k - a(t) f_k(\gamma(t)) \right], \quad (15.6.8)$$

where $\overline{V_{kj}}$ is the algebraic addition to the element V_{kj} in $\det\left|V_{kj}\right|$. Substituting the solution Eq. 15.6.8 in Eq. 15.6.7 at $i = n-2, n-1$, and n, we obtain the set from three equations for determining $\gamma(t)$, $a(t)$, and $\Delta R_c(t)$:

$$b_i(t) - \left(\det\left|V_{kj}\right|\right)^{-1} \sum_{j=1}^{n-3} W_{Tij} \sum_{l=1}^{n-3} \overline{V_{lj}} b_l(t) = -\Delta R_c(t) \left[W_i - \left(\det\left|V_{kj}\right|\right)^{-1} \sum_{j=1}^{n-3} V_{ij} \sum_{l=1}^{n-3} \overline{V_{lj}} W_l \right]$$

$$+ a(t) \left[f_i(\gamma(t)) - \left(\det\left|V_{kj}\right|\right)^{-1} \sum_{j=1}^{n-3} V_{ij} \sum_{l=1}^{n-3} \overline{V_{lj}} f_l(\gamma(t)) \right], \tag{15.6.9}$$

where $i = n-2, n-1$, and n. The solution of the set of three equations Eq. 15.6.9 will be found as follows. First of all, it is necessary to tabulate the following special function for given set of instruments and the given broken of atmosphere on $n-3$ layers:

$$\overline{\Omega}(\gamma) = \frac{\overline{\omega}_{n-2}\overline{\varphi}_{n-1}(\gamma) - \overline{\omega}_{n-1}\overline{\varphi}_{n-2}(\gamma)}{\overline{\omega}_{n-1}\varphi_n(\gamma) - \overline{\omega}_n\overline{\varphi}_{n-1}(\gamma)}, \tag{15.6.10}$$

where

$$\overline{\omega}_i = W_i - \left(\det\left|V_{ij}\right|\right)^{-1} \sum_{j=1}^{n-3} V_{ij} \sum_{l=1}^{n-3} \overline{V_{lj}} W_l , \tag{15.6.11}$$

$$\overline{\varphi}_i(\gamma(t)) = f_i(\gamma(t)) - \left(\det\left|V_{ij}\right|\right)^{-1} \sum_{j=1}^{n-3} V_{ij} \sum_{l=1}^{n-3} \overline{V_{lj}} f_l(\gamma(t)) \tag{15.6.12}$$

can be easily obtained through the known coupling and temperature coefficients.

The slope $\gamma(t)$ is determined by solving the equation

$$\overline{\Omega}(\gamma) = \frac{\overline{\omega}_{n-2}\overline{\beta}_{n-1}(t) - \overline{\omega}_{n-1}\overline{\beta}_{n-2}(t)}{\overline{\omega}_{n-1}\overline{\beta}_n(t) - \overline{\omega}_n\overline{\beta}_{n-1}(t)}, \tag{15.6.13}$$

where

$$\overline{\beta}_i(t) = b_i(t) - \left(\det\left|V_{ij}\right|\right)^{-1} \sum_{j=1}^{n-3} V_{ij} \sum_{l=1}^{n-3} \overline{V_{lj}} b_l(t). \tag{15.6.14}$$

After $\gamma(t)$ has been determined, the parameters $a(t)$ and $\Delta R_c(t)$ can be easily calculated:

$$a(t)=\frac{\overline{\omega}_{n-2}\overline{\beta}_{n-1}(t)-\overline{\omega}_{n-1}\overline{\beta}_{n-2}(t)}{\overline{\omega}_{n-2}\overline{\varphi}_{n-1}(\gamma(t))-\overline{\omega}_{n-1}\overline{\varphi}_{n-2}(\gamma(t))}, \tag{15.6.15}$$

$$\Delta R_c(t)=\frac{\overline{\varphi}_{n-2}(\gamma(t))\overline{\beta}_{n-1}(t)-\overline{\varphi}_{n-1}(\gamma(t))\overline{\beta}_{n-2}(t)}{\overline{\omega}_{n-2}\overline{\varphi}_{n-1}(\gamma(t))-\overline{\omega}_{n-1}\overline{\varphi}_{n-2}(\gamma(t))}. \tag{15.6.16}$$

By substituting the calculated $\gamma(t)$, $a(t)$, and $\Delta R_c(t)$ in Eq. 15.6.8, we obtain the final solution in the form

$$x_j(t)=\left(\det\left|V_{ij}\right|\right)^{-1}\sum_{i=1}^{n-3}\overline{V_{ij}}\{b_i(t)+\left[W_i\left(\overline{\varphi}_{n-2}(\gamma(t))\overline{\beta}_{n-1}(t)-\overline{\varphi}_{n-1}(\gamma(t))\overline{\beta}_{n-2}(t)\right)\right.$$

$$\left.-f_i(\gamma(t))\left(\overline{\omega}_{n-2}\overline{\beta}_{n-1}(t)-\overline{\omega}_{n-1}\overline{\beta}_{n-2}(t)\right)\right]\left[\overline{\omega}_{n-2}\overline{\varphi}_{n-1}(\gamma(t))-\overline{\omega}_{n-1}\overline{\varphi}_{n-2}(\gamma(t))\right]^{-1}\}. \tag{15.6.17}$$

Then, taking into account Eq. 15.6.16, we shall find the time variation of the vertical air temperature profile ($j=1, 2, 3, ..., n-4$):

$$\Delta T_j(t)=\left(\det\left|V_{ij}\right|\right)^{-1}\sum_{i=1}^{n-3}\overline{V_{ij}}\{b_i(t)+\left[W_i\left(\overline{\varphi}_{n-2}(\gamma(t))\overline{\beta}_{n-1}(t)-\overline{\varphi}_{n-1}(\gamma(t))\overline{\beta}_{n-2}(t)\right)\right.$$

$$\left.-f_i(\gamma(t))\left(\overline{\omega}_{n-2}\overline{\beta}_{n-1}(t)-\overline{\omega}_{n-1}\overline{\beta}_{n-2}(t)\right)\right]\left[\overline{\omega}_{n-2}\overline{\varphi}_{n-1}(\gamma(t))-\overline{\omega}_{n-1}\overline{\varphi}_{n-2}(\gamma(t))\right]^{-1}\}, \tag{15.6.18}$$

and variation of air mass in the vertical column over observation level $(j=n-3)$:

$$\Delta h_o(t)=\left(\det\left|V_{ij}\right|\right)^{-1}\sum_{i=1}^{n-3}\overline{V_{i,n-4}}\{b_i(t)+\left[W_i\left(\overline{\varphi}_{n-2}(\gamma(t))\overline{\beta}_{n-1}(t)-\overline{\varphi}_{n-1}(\gamma(t))\overline{\beta}_{n-2}(t)\right)\right.$$

$$\left.-f_i(\gamma(t))\left(\overline{\omega}_{n-2}\overline{\beta}_{n-1}(t)-\overline{\omega}_{n-1}\overline{\beta}_{n-2}(t)\right)\right]\left[\overline{\omega}_{n-2}\overline{\varphi}_{n-1}(\gamma(t))-\overline{\omega}_{n-1}\overline{\varphi}_{n-2}(\gamma(t))\right]^{-1}\}. \tag{15.6.19}$$

Let us note that in the described procedure the most complicated part is determining of the slope $\gamma(t)$ of the extra-terrestrial CR variation by solving Eq. 15.6.13. Many types of extra-terrestrial CR variations (long term, 22-year and 11-year, 27-day, Forbush decreases and other) have a slope $\gamma(t)$ near 1. In the small interval near 1 the function described by Eq. 15.6.10 can be approximated by linear dependence:

$$\overline{\Omega}(\gamma)=\frac{\overline{\omega}_{n-2}\overline{\varphi}_{n-1}(\gamma)-\overline{\omega}_{n-1}\overline{\varphi}_{n-2}(\gamma)}{\overline{\omega}_{n-1}\overline{\varphi}_{n}(\gamma)-\overline{\omega}_{n}\overline{\varphi}_{n-1}(\gamma)}\approx A_1+A_2\gamma\,, \tag{15.6.20}$$

where the parameters A_1 and A_2 are determined by the set of used CR detectors of type n, $n-1$, $n-2$ and depend from R_C. In this case we obtain from Eq. 15.6.13

$$\gamma(t)\approx A_2^{-1}\left[\frac{\overline{\omega}_{n-2}\overline{\beta}_{n-1}(t)-\overline{\omega}_{n-1}\overline{\beta}_{n-2}(t)}{\overline{\omega}_{n-1}\overline{\beta}_{n}(t)-\overline{\omega}_{n}\overline{\beta}_{n-1}(t)}-A_1\right], \tag{15.6.21}$$

and then it is very easy to determine $a(t)$ and $\Delta R_C(t)$ according to Eq. 15.6.15 and Eq. 15.6.16. One can then easily determine all $\Delta T_j(t)$ and $\Delta h_o(t)$ according to Eq. 15.6.18 and Eq. 15.6.19.

Only in periods of ground solar CR events does the slope $\gamma(t)$ vary very much during the event and from one event to another (from about 0.5 to 6). In this case it is necessary to approximate $\Omega(\gamma)$ more exactly and solve the Eq. 15.6.13 more precisely to determine $\gamma(t)$.

Chapter 16

Meteorological Effects Application to Cosmic Ray Latitude Survey Data Processing

16.1. CR latitude surveys and meteorological effects

Together with direct measurements of primary CR, either with space probes outside the geomagnetic field, or with balloons in the upper atmospheric layers, the technique of continuous measurements of the secondary components by ground based detectors gives unique information on the time variations of the CR distribution function outside the magnetosphere, as well as of the cut off rigidity planetary distribution. On the other hand, the time variations of the CR distribution function out of the magnetosphere are produced by two main causes: 1) the continuous modulation of the galactic CR flux by Heliosphere dynamic processes over various time scales (from hours to the solar cycle time span); and 2) the sporadic emission from the Sun of energetic particles accelerated in solar flare regions and reaching the Earth after propagation through the solar corona and interplanetary space. Therefore these variations contain important information on dynamic processes in the Heliosphere and acceleration phenomena in solar atmosphere; their study is an essential tool for determining the models appropriate to the different modulation processes.

The 'great instrument' consisting of all CR detectors located on the Earth's surface provides a continuous monitoring of primary variations in a wide rigidity interval and for every direction of the incoming particles out of the magnetosphere. The global spectrographic method (Dorman, M1974; Belov et al., 1983) based on the knowledge of coupling functions (Dorman, M1957) furnishes an efficient mathematical tool for this purpose. The core of the 'great instrument' is the worldwide network of CR neutron monitors at sea level and at mountain heights, which are sensitive to time variations of primaries with rigidities up to 30–40 GV, and of muon telescopes on the ground and underground, which are sensitive to primaries with rigidities over 1000 GV. The technique of latitude surveys of CR nucleonic and muonic components is the most reliable method to calibrate the 'CR geomagnetic spectrometer' and to determine the coupling functions necessary for studying time variations of the primary CR spectrum by the data of the neutron monitors and muon telescope stations network (see review in Dorman, M1974, M1975a and investigations of individual CR latitude surveys in Bachelet et al., 1965, 1972, 1973; Dorman et al., 1966, 1967a,b,c; Lockwood and Webber, 1967; Kodama, 1968; Keith et al., 1968; Carmichael and Bercovitch, 1969; Allkofer et al., 1969; Aleksanyan et al., 1979a,b, 1985; Potgieter et al., 1980a,b; Moraal et al., 1989; Nagashima et al., 1989; Stoker, 1993; Stoker and Moraal, 1995; Bieber et al., 1997; Villoresi et al., 1997). Moreover, it is also possible by latitude surveys to verify the evaluation of geomagnetic cut off rigidities and detect geomagnetic anomalies for cut off rigidities R_C (see Stoker, 1995; Stoker et al., 1997; Clem et al., 1997). However, to obtain reliable latitude effects of CR nucleonic and muonic components it is necessary to apply refined analysis techniques on the original data registered along the survey.

It is well known that with increasing latitude in both directions (from the equator to the North and South poles), the average temperature, as well as the cut off rigidity R_C decrease. With decreasing R_C CR intensity will increase according to the relation

$$N_i(R_C, h_O, T(h)) = \int_{R_C}^{\infty} D(R) m_i(R, h_O, T(h)) dR, \tag{16.1.1}$$

where h_O is the air pressure on the level of CR latitude measurements, $T(h)$ is the vertical distribution of air temperature, $D(R)$ is the spectrum of primary CR, and $m_i(R, h_O, T(h))$ is the integral multiplicity. By using Eq. 16.1.1 from CR latitude survey data it is possible to determine the coupling function

$$W_i(R_C, R, h_O, T(h)) = \frac{D(R) m_i(R, h_O, T(h))}{N_i(R_C, h_O, T(h))} = -\frac{(\partial N_i(R_C, h_O, T(h))/\partial R_C)_{R_C \to R}}{N_i(R_C, h_O, T(h))} \tag{16.1.2}$$

and integral multiplicity

$$m_i(R, h_O, T(h)) = -\frac{(\partial N_i(R_C, h_O, T(h))/\partial R_C)_{R_C \to R}}{D(R)}. \tag{16.1.3}$$

The problem is that with increasing latitude h_O and $T(h)$ also change, producing an important part of latitude change in CR intensity caused by meteorological effects. As was shown in Dorman (1954c), this influence of meteorological effects on latitude CR intensity dependence is very important for the hard muon component: the correction for the temperature effect leads to a significant change of latitude curve (at latitudes higher than about 40° it becomes about plate, meaning that primary particles with rigidity lower than 6–7 GV mainly cannot produce muons that can be detected on sea level). A lot of CR latitude survey investigations with accounting of meteorological effects was made for soviet CR expeditions inside USSR and in the world (see for example, Dorman et al., 1967a,b, 1970; Blokh et al., 1974; and in review papers Dorman, 1969, M1975b, 1987). Let us note that for the neutron component the temperature effect for CR latitude survey data processing is not so important as for the muon component, but much more important is the barometric effect (the change of barometric coefficients with latitude and with solar activity), the wind effect (caused by Bernoulli phenomenon), and others. As an example of the precise accounting of this and some other influences, we note a recent CR latitude survey to Antarctica in 1996–1997 that is described in Villoresi at al. (1997, 1999, 2000), Iucci et al. (1999, 2000) and in Dorman et al. (1999, 2000, 2001), Danilova et al. (2001).

Studies by ground based detectors of CR spectral changes over different time scales rely on the accurate knowledge of the energy response of detectors to primary CR (coupling function). During the 1996–1997 austral summer a 3NM-64 neutron monitor was operated on board the ship 'Italica' to record CR neutron intensities at sea from Italy to Antarctica and back. Moreover, the flux of thermalized neutrons was measured by two

bare BF_3 counters. The main purpose of this research was the determination of an accurate latitude curve of CR nucleonic intensity during solar minimum to be utilized for obtaining the coupling function appropriate for this phase of solar cycle. This was achieved through reliable instrumentation and accurate management of the experiment and by determining and applying for the first time all necessary corrections on latitude survey neutron monitor data: (i) changes in vertical atmospheric mass column, by taking into account the wind effect; (ii) oscillations of the ship produced by sea roughness; (iii) atmospheric temperature changes; (iv) interplanetary CR North-South asymmetry; (vi) primary CR time variations; (vii) time changes of CR East West effect, caused by the asymmetric shielding effect on the ship.

16.2. The Bernoulli effect on measurements of atmospheric mass for latitude surveys

In Lockwood and Calawa (1957), Dubinsky et al. (1960), Gushchina et al. (1969), Dorman and Kaminer (1969), Kawasaki (1972), the influence of the Bernoulli effect caused by wind flows in the atmosphere on atmospheric pressure measurements was investigated (see review in Dorman, M1963a,b, M1972, M1974, and in this book, Section 6.2). This influence leads to smaller estimates of the vertical mass of air M, as determined by barometric measurements of the dynamic air pressure P. The relation between M and the measured P is:

$$M(\varphi,\lambda)=1033.2\times Pg_o[P_o g(\varphi,\lambda)]^{-1}\ \text{g.cm}^{-2}, \tag{16.2.1}$$

where φ is the geographic latitude and λ the geographic longitude of the place of measurements; $P_o=1013$ hP corresponds to the normal air pressure 760 mm Hg, $g_o=980.6\ \text{cm/sec}^2$ is the normal Earth's gravitational acceleration and, according to Uotila (1957),

$$g(\varphi,\lambda)=978.0516\Big[1+0.0052910\sin^2\varphi$$

$$-0.0000059\sin^2 2\varphi+0.0000106\cos^2\varphi\cos 2\left(\lambda+6^o\right)\Big]. \tag{16.2.2}$$

The effect on M of the ship's speed relative to the atmosphere (wind speed) can be evaluated by using Bernoulli's theorem on the basis of direct and indirect measurements of wind speed. We used 5-min data of wind speed W with respect to the ship and determined for each 3-hourly interval the average values of

$$\left\langle W^2\right\rangle=(1/36)\sum_{j=1}^{36}W_j^2\,. \tag{16.2.3}$$

The correction for Bernoulli effect can be written as

$$\Delta M_b=f\cdot M_b=(1/2)f\rho\left\langle W^2\right\rangle g^{-1}(\varphi,\lambda), \tag{16.2.4}$$

where $\rho = \rho_o PT_o / P_o T$, ρ_o is the density of air near sea level at normal conditions $P_o = 760$ mmHg, $T_o = 290$ °K, and P, T are the average pressure and temperature for each 3-hourly interval. In Eq. 16.2.4 the coefficient $f < 1$ accounts for the fact that in low atmosphere the wind action is mainly limited to some fraction (up to 3–4 km) of total atmospheric layer. For stratospheric strong wind (with speed about 20–30 m.sec^{-1}) at the altitude of about 10–12 km, Bernoulli effect can be neglected because it is about one order of magnitude smaller than that determined by Eq. 16.2.4 and it is about constant with time. An evaluation of parameter f will be given in Section 16.4 by using the data of our latitude survey.

The wind effect, as far as we know, has never been considered before in the analysis of survey data; sometimes it was taken into account for CR stations at mountain altitude (see *e.g.* Kawasaki, 1972). Data of $\langle W^2 \rangle$ are available until February 13, 1997 when the wind speed sensor was damaged during a big storm. After 13 February 1997 $\langle W^2 \rangle$ has been evaluated by means of the good correlation between sea state index F_S and $\langle W^2 \rangle$ (in m^2.sec^{-2}) determined in the previous period of survey (December 20, 1996 – February 13, 1997):

$$\langle W^2 \rangle = 12.2 F_S^2 - 41.2 F_S + 73.2 \qquad (16.2.5)$$

with correlation coefficient $+0.852 \pm 0.016$ (see Fig. 16.2.1).

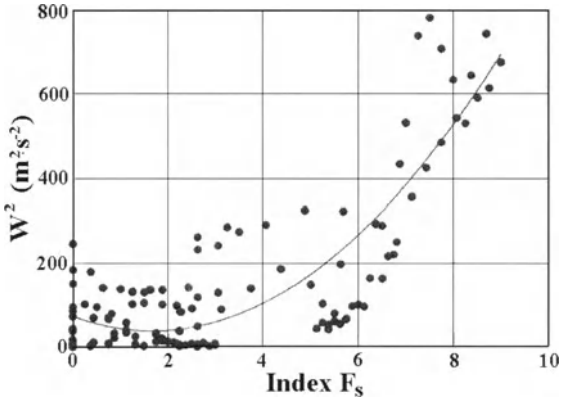

Fig. 16.2.1. 3-hourly averages of the square of wind speed (relative to the ship) W^2 as a function of sea state index F_S (December 20, 1996 to February 13, 1997). Best fit curve is represented by Eq. 16.2.5.

We note that the constant term in Eq. 16.2.5 is very close to the square of the average velocity of the ship, as expected. By Eq. 16.2.5 we computed $\langle W^2 \rangle$ from the measured F_S and by Eq. 16.2.4 we evaluated M_b.

16.3. Nature and evaluation of sea state effect on the NM counting rate

The sea state effect, which was experimentally investigated by Bieber et al. (1995), was analyzed in Iucci et al. (2000) with regards to its physical nature. Let us call $F(\theta)d\theta$ the flux of nuclear active particles (mainly neutrons) approaching sea level with zenith angle between θ and $\theta + d\theta$ and integrated over azimuth angle. The flux of these particles on a horizontal NM with effective surface S will be $SF(\theta)d\theta$ and the total counting rate, for integrated flux over all zenith angles, will be

$$I_o = S\int_0^{\pi/2} F(\theta)\cos\theta\cdot\varphi(\theta)d\theta = S\int_0^{\pi/2} F(\theta)\Psi(\theta)d\theta, \qquad (16.3.1)$$

where $\varphi(\theta)$ is the average probability to detect a neutron approaching at zenith angle θ. $F(\theta)$, $\varphi(\theta)$, $\Psi(\theta) = \cos\theta\times\varphi(\theta)$ are even functions, and $F(\theta)$ goes rapidly to zero for $\theta = \pi/2$. If the NM is inclined by the angle θ_o, the counting rate will be:

$$I(\theta_o)/S = (1/2)\int_0^{\pi/2} F(\theta)\Psi(\theta-\theta_o)d\theta + (1/2)\int_0^{\pi/2-\theta_o} F(\theta)\Psi(\theta+\theta_o)d\theta$$

$$= (1/2)\int_0^{\pi/2} F(\theta)[\Psi(\theta-\theta_o)+\Psi(\theta+\theta_o)]d\theta - (1/2)\int_{\pi/2-\theta_o}^{\pi/2} F(\theta)\Psi(\theta+\theta_o)d\theta; \qquad (16.3.2)$$

under the hypothesis that the almost horizontal CR are fully absorbed by the inclined ship before reaching the neutron monitor (that is why the second integral is computed up to $\theta = \pi/2 - \theta_o$). For sufficiently small θ_o, namely for

$$\Psi(\theta\pm\theta_o) = \Psi(\theta)\pm\Psi'(\theta)\theta_o + \Psi''(\theta)\theta_o^2/2 \pm \Psi'''(\theta)\theta_o^3/6, \qquad (16.3.3)$$

the corresponding change in counting rate can be written, being $\Psi(\theta) = \varphi(\theta)\cos\theta$ an even function, as:

$$I(\theta_o) - I_o \approx \frac{1}{2}S\int_0^{\pi/2} F(\theta)[\Psi(\theta+\theta_o)+\Psi(\theta-\theta_o)-2\Psi(\theta)]d\theta - \frac{1}{2}S\int_{\pi/2-\theta_o}^{\pi/2} F(\theta)\Psi(\theta+\theta_o)d\theta$$

$$\approx \frac{1}{2}\theta_o^2 S\int_0^{\pi/2} F(\theta)\Psi''(\theta)d\theta - \frac{1}{2}S\int_{\pi/2-\theta_o}^{\pi/2} F(\theta)\Psi(\theta+\theta_o)d\theta = \Delta I_1 + \Delta I_2. \qquad (16.3.4)$$

The first integral ΔI_1 in Eq. 16.3.4 gives the decrease in counting rate produced by the geometrical effect of rotation of the NM-64 by the angle θ_o; this decrease can simply be estimated for the most likely condition of $\varphi(\theta)$ slowly changing with θ, *i.e.*

for $\varphi'(\theta) \approx 0$. In this case, there holding $\Psi''(\theta) \approx -\Psi(\theta)$, we obtain:

$$(\Delta I_1/I) = (I(\theta_o) - I_o)_1 / I_o \approx -\theta_o^2/2 . \qquad (16.3.5)$$

In the case of harmonic rolling motion of the ship, $\theta_o = \theta_m \cos\omega t$, $\left\langle \theta_o^2 \right\rangle = \theta_m^2/2$ and the average effect will be:

$$\left\langle \Delta I_1/I \right\rangle \cong -\theta_m^2/4 . \qquad (16.3.6)$$

The second integral ΔI_2 in Eq. 16.3.4, representing the decrease in counting rate produced by half CR flux approaching the monitor with zenith angle $\theta > \pi/2 - \theta_o$ (absorption effect through the inclined ship), is negligible. In fact, for $\theta_o \le 0.2$, *i.e.* for $\alpha = \pi/2 - \theta \le \theta_o \le 0.2$ we can approximate $F(\theta)$ and $\Psi(\theta)$ as: $F(\theta) \propto \cos^k\theta = \sin^k\alpha \cong \alpha^k$, with $k \ge 2$, $\Psi(\theta) \propto \cos(\theta + \theta_o) = \sin(\alpha - \theta_o) \approx \alpha - \theta_o$, and, as a consequence,

$$\left\langle \Delta I_2/I \right\rangle \cong -\frac{\gamma}{2}\int_0^{\theta_o} \alpha^{k+1} d\alpha = -\frac{\gamma}{k+2}\cdot\frac{\theta_o^{k+2}}{2} < -\frac{\gamma}{4}\cdot\frac{\theta_o^4}{2} \approx -\frac{\gamma}{16}\cdot\theta_m^4 , \qquad (16.3.7)$$

γ being a constant of the order of some units. A similar negligible contribution of particles with $\theta > 75^o$ has been obtained when computing the weights of different zenith zones (Dorman et al., 2000). By taking into account the Eq. 16.3.4, 16.3.6 and 16.3.7 we obtain for $\theta_m \le 0.2$

$$\left\langle \frac{\Delta I}{I} \right\rangle = \left\langle \frac{\Delta I_1}{I} \right\rangle + \left\langle \frac{\Delta I_2}{I} \right\rangle \approx -\theta_m^2/4 , \qquad (16.3.8)$$

which gives for $\theta_m = 0.2$ a decrease of 1.0% in the NM counting rate. Therefore according to Eq. 16.3.8 the determination of sea state effect on NM counting rate depends on the knowledge of the maximum inclination angle θ_m. Unfortunately we could not achieve continuous measurements of θ_m on the ship 'Italica' in digital form, but it was possible to do a number of determinations of the angle $\theta_m \approx 0.20 - 0.21$ for sea state strength $F_S \approx 8$ and to derive the empirical relationship:

$$F_S \approx 750 \times \theta_m^2/4. \qquad (16.3.9)$$

From Eq. 16.3.8 and Eq. 16.3.9 it ensues that

$$\left(\left\langle I(F_S) \right\rangle - I_o \right) / I_o = K_{NM} F_S \approx -1.3 \times 10^{-3} F_S . \qquad (16.3.10)$$

We can compare Eq. 16.3.10 with the only other numerical evaluation of the variations of neutron monitor counting rate in dependence on sea state strength, done by Bieber et al. (1995) on board an icebreaker during the period December 1994–April 1995. They found a decrease in counting rate of about 1.1% from $F_S = 0$ to $F_S = 8$, leading to the relationship:

$$\left(\langle I(F_S)\rangle - I_o\right)/I_o \approx -1.5\times10^{-3} F_S, \qquad (16.3.11)$$

which is very close to our determination. We remark that it is difficult to interpret the result of comparison between Eq. 16.3.10 and Eq. 16.3.11, the real variations of NM counting rate on a rolling ship in dependence of sea state index F_S being mainly determined by the relation between θ_m and F_S. This relation should depend on the particular type of ship and stabilizing systems for wave motion. The comparison between Eq. 16.3.10 and Eq. 16.3.11 is also rather uncertain because from the distribution of experimental points given by Bieber et al. (1995) there could be inferred a very low correlation and as a consequence a large error bar on the regression coefficient for Eq. 16.3.11. Moreover, it is not known whether or not the Bernoulli effect has been taken into account by Bieber et al. (1995); the correlation is expected to be largely affected by the presence of Bernoulli effect which is statistically connected to sea state effect, according to Eq. 16.2.5 and Eq. 16.2.4.

16.4. Determination of atmospheric absorption, Bernoulli and sea state effects in the Antarctic region

16.4.1. Conditions for multi-correlation analysis

An accurate correction of NM and BC (bare counters) intensity for the small CR primary variations has already been applied by using the data of the NM station network (Villoresi at al., 2000). Proper atmospheric absorption coefficients β for correcting NM data have been determined by Carmichael and Bercovitch (1969) and Bachelet et al. (1972) for different cut off rigidities and solar activity levels. Since β is also dependent on individual detectors (geometry, shielding, electronics parameters, radioactive background), a direct computation of β by survey data is worthwhile for NM and necessary for BC. Moreover, sea state and wind effects should also be determined by analysis of the survey data. From January 27 to February 18, 1997 the survey detectors operated in the Antarctic and near-Antarctic region (rigidity threshold $R_{cp} \leq 1$ GV). Atmospheric pressure, sea state strength, and wind speed being extremely variable in this period, it is possible in principle to obtain an accurate evaluation of the effects by regression analysis:

$$\ln I(M, F_S, M_b) = \beta M + KF_S + (f\beta)M_b, \qquad (16.4.1)$$

where $f M_b$ was defined by Eq. 16.2.4.

16.4.2. Multi-correlation analysis for NM data

The analysis can be done only in the period in which wind speed has been measured (132 of 3-hourly data from 18^h January 27 to 06^h February 13). We consider a multi-correlation analysis between $\Delta\ln I = \ln I - \langle \ln I \rangle = Y_0$ with $\Delta M = M - \langle M \rangle = Y_1$, $\Delta F_S = F_S - \langle F_S \rangle = Y_2$ and $\Delta M_b = M_b - \langle M_b \rangle = Y_3$, where $\langle x \rangle$ is the average of 132 x values. By writing the regression as

$$Y_0 = A_1 Y_1 + A_2 Y_2 + A_3 Y_3 , \tag{16.4.2}$$

the regression coefficients A_k (k = 1, 2 and 3) are determined, according to the least square method, as:

$$A_1 = \beta = \begin{vmatrix} a_{10} & a_{12} & a_{13} \\ a_{20} & a_{22} & a_{23} \\ a_{30} & a_{32} & a_{33} \end{vmatrix} \cdot D^{-1}; \qquad A_2 = K = \begin{vmatrix} a_{11} & a_{10} & a_{13} \\ a_{21} & a_{20} & a_{23} \\ a_{31} & a_{30} & a_{33} \end{vmatrix} \cdot D^{-1}; \tag{16.4.3}$$

$$A_3 = (f \cdot \beta) = \begin{vmatrix} a_{11} & a_{12} & a_{10} \\ a_{21} & a_{22} & a_{20} \\ a_{31} & a_{32} & a_{30} \end{vmatrix} \cdot D^{-1}, \text{ with } D = \begin{vmatrix} a_{11} & a_{12} & a_{13} \\ a_{21} & a_{22} & a_{23} \\ a_{31} & a_{32} & a_{33} \end{vmatrix}, \tag{16.4.4}$$

with $a_{ij} = \sum Y_i \cdot Y_j$ extended over the 132 values. The total correlation coefficient R, *i.e.* the correlation between $(\Delta\ln I)_o$ observed and $(\Delta\ln I)_c$ computed according to Eq. 16.4.1, can be evaluated as $R = \left(1 - (\mathrm{StD}/\sigma)^2\right)^{1/2}$, where StD is the standard deviation of $(\Delta\ln I)_o - (\Delta\ln I)_c$, and σ the standard deviation of $(\Delta\ln I)_o$. As a result of the analysis, partial correlation coefficients between variables M, M_b, F_S are:

$$R_{M,F_S} = -0.285 \pm 0.054,\ R_{M,M_b} = -0.422 \pm 0.048,\ R_{M_b,F_S} = 0.752 \pm 0.025; \tag{16.4.5}$$

partial correlation coefficients between $\ln I$ and variables M, M_b, F_S are:

$$R_{M,I} = -0.9599 \pm 0.0046,\ R_{F_S,I} = -0.248 \pm 0.055,\ R_{M_b,I} = 0.392 \pm 0.049; \tag{16.4.6}$$

parameters of multi-correlation are:

$$R = 0.9956 \pm 0.0005,\ \beta = (-0.754 \pm 0.011)\frac{\%}{\mathrm{g/cm^2}},\ K = (-0.073 \pm 0.006)\%/F_S , \tag{16.4.7}$$

$$\beta \times f = (-0.055 \pm 0.004)\%/\left(\mathrm{g/cm^2}\right), \text{ and } f = (\beta \times f)/\beta = 0.072 \pm 0.007. \tag{16.4.8}$$

We notice that the very high value of the total correlation coefficient R shows that the experimental data can be well represented by Eq. 16.4.1, but in the presence of high

values of partial correlation coefficients between variables M, M_b, F_S (strong/weak sea state is often associated with strong/weak wind and frequently with low/high pressure). These high partial coefficients make the determination of individual regression coefficients doubtful: correlation coefficient R is consistent, within the statistical uncertainty, with its maximum value, in a wide region of the 3-D space (β, K, f). This can be seen in Table 16.4.1 in which we present some examples of double-correlation analysis for three fixed values of f.

Table 16.4.1. Results of double-correlation analysis $\ln I(M, F_S) = \beta M + K F_S$ for three fixed values of f

f	$\beta, \%(g\,cm^{-2})^{-1}$	$K, \%/F_S$	R
0	–0.753	–0.086	0.99553±0.00052
1/3	–0.759	–0.022	0.99537±0.00054
1	–0.770	+0.112	0.99553±0.00052

Therefore it is necessary to follow a different approach: (i) evaluate the global (Bernoulli and sea state) effect for constant pressure conditions; (ii) separate Bernoulli from sea state effects by utilizing Eq. 16.3.10; (iii) compute by regression analysis the atmospheric absorption coefficients, by using the neutron intensity data corrected for sea state effect and atmospheric mass M corrected for Bernoulli effect.

16.4.3. Sea state, Bernoulli and atmospheric absorption effects for NM detector

The correlation of the 3-hourly data of $\ln(I_{NM})$, corrected for primary variations, with M is shown in Fig. 16.4.1.

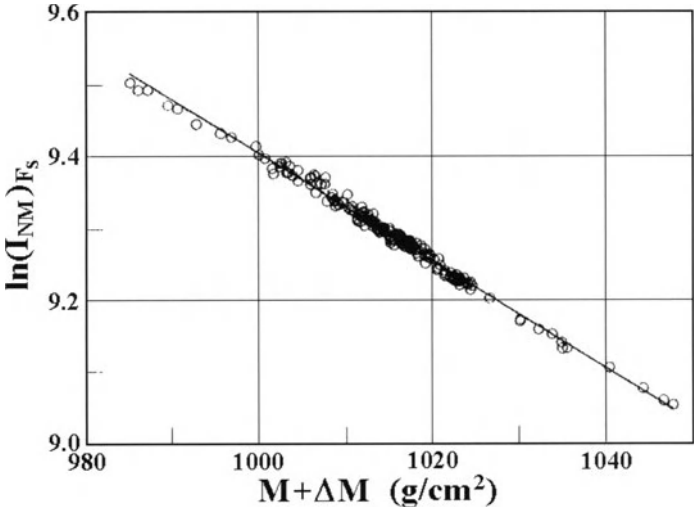

Fig. 16.4.1. The logarithm of NM intensity (corrected for CR primary variations and sea state effect) as a function of atmospheric mass $M + \Delta M_b$ (3-hourly averages), for $R_{cp} \leq 1$ GV (January 27–February 18, 1997). Best fit line is represented by Eq. 16.4.15.

It was found that

$$\ln(I_{NM}) = -0.0072235 \times M + 16.61489 \qquad (16.4.9)$$

with correlation coefficient $R = -0.992 \pm 0.006$ (atmospheric absorption coefficient $\beta_{NM} = -(0.722 \pm 0.007)\%/(\text{g.cm}^{-2})$). After correction for this "apparent" absorption effect the standard deviation of the 3-hourly I_{NM} data in Antarctic region ($R_{cp} \leq 1$ GV) decreases from StD = 7.34% to StD = 0.93% (to be compared with StD = 0.24% obtained for a pure Poisoning distribution of 3-hourly NM intensity data).

Let us now divide the I_{NM} data into three subgroups according to different ranges of sea state strength F_S, namely: F_{S1} for $F_S \leq 3.5$, F_{S2} for $3.5 < F_S \leq 6.5$, and F_{S3} for $F_S > 6.5$. In Table 16.4.2 we report the average values of M, W^2 and F_S for the three subgroups.

Table 16.4.2. Average values of M, W^2, and F_S for three different ranges of F_S in the Antarctic region ($R_{cp} \leq 1$ GV, January 27 to February 18, 1997)

F_S	$\langle M \rangle$, g cm^{-2}	$\langle W^2 \rangle$, m^{2}s^{-2}	$\langle F_S \rangle$
F_{S1} ($F_S \leq 3.5$)	1017	65	1.2
F_{S2} ($3.5 < F_S \leq 6.5$)	1016	150	5.9
F_{S3} ($F_S > 6.5$)	1011	565	8.3

For $F_S > 6.5$, the missing $\langle W^2 \rangle$ data after February 13, 1998 (see Section 16.2) have been derived from the measured F_S by means of Eq. 16.2.5. The result for periods with low sea state strength F_{S1}, characterized by relatively small pressure fluctuations, is

$$\ln(I_{NM}) = -0.0078672 \times M + 17.27468, \qquad (16.4.10)$$

with correlation coefficient $R = -0.9917$. The result for periods of the intermediate sea state F_{S2}:

$$\ln(I_{NM}) = -0.0075185 \times M + 16.91186 \qquad (16.4.11)$$

with correlation coefficient $R = -0.9975$. The result for periods of high sea state F_{S3}:

$$\ln(I_{NM}) = -0.0075592 \times M + 16.93852 \qquad (16.4.12)$$

with correlation coefficient $R = -0.9915$.

The differences between the Eq. 16.4.10–16.4.12 allow giving an overall estimate of the change in counting rate due to the combined contribution of Bernoulli and sea state effects as a function of M. This rough estimation done for the difference between the extreme cases F_{S1} and F_{S3} gives, for $\langle M \rangle = 1014$ g.cm^{-2}:

$$\langle \Delta I/I \rangle = \langle \Delta I/I \rangle_{F_S} + \langle \Delta I/I \rangle_{Ber} = K_{NM} \Delta F_S + \beta \times f \left[\frac{\rho}{2g} \Delta \langle W^2 \rangle \right] \cong -1.6\%, \quad (16.4.13)$$

where β is the atmospheric absorption coefficient in $\%/\left(\mathrm{g/cm^2}\right)$ and $\Delta F_S \cong 7.1$, $\Delta \langle W^2 \rangle \approx 500\ \mathrm{m^2 s^{-2}}$. By means of Eq. 16.3.10 it is possible to compute the sea state effect for $F_S = 7.1$: $\langle \Delta I/I \rangle_{F_S} = K_{NM} \Delta F_S = -0.9\%$ and from Eq. 16.4.13 $\langle \Delta I/I \rangle_{\mathrm{Ber}} = -0.7\%$. From this evaluation of Bernoulli effect for $\Delta W^2 \approx 500\,\mathrm{m^2 s^{-2}}$ we can determine the value of parameter f in Eq. 16.2.4:

$$\Delta M_b \times \beta = \frac{f \times 500 \times 10^4 \times 1.3 \times 10^{-3} \times \beta}{2 \times 983.21} = -0.7\%. \quad (16.4.14)$$

If the value of atmospheric absorption coefficient is $\beta = -0.75\%/\left(\mathrm{g/cm^2}\right)$, then from Eq. 16.4.14 we obtain $f \cong 0.3$. This value of f is in agreement with the evaluation of Kawasaki (1972) and indicates that atmospheric winds, causing significant effects on the determination of atmospheric absorbing mass, are mainly confined to 1/3 of the total atmospheric layer.

With these results we can correct the I_{NM} Antarctic data for sea state effect and the M data for Bernoulli effect and determine the correlation between $(I_{NM})_{F_S}$ and $M + \Delta M_b$ for $R_{cp} \leq 1$ GV. The result can be represented by the following regression line

$$\ln(I_{NM})_{F_S} = -0.0075077 \times (M + \Delta M_b) + 16.91178 \quad (16.4.15)$$

with very high correlation coefficient $R = -0.9955 \pm 0.0005$ (atmospheric absorption coefficient $\beta_{NM} = -(0.751 \pm 0.005)\%/\mathrm{g.cm^{-2}}$). After correction for this 'real' atmospheric absorption effect the standard deviation of the 3-hourly I_{NM} data is StD = 0.70%, instead of StD = 0.93% as computed on the data corrected for the 'apparent' atmospheric absorption effect (see Eq. 16.4.9).

The correlation between the intensity corrected for primary variations and atmospheric absorption effect (to the level of atmospheric mass $M_o = 1034\ \mathrm{g.cm^{-2}}$), and sea state index F_S, based on all data collected in near-Antarctic region ($R_{cp} \leq 1$ GV), is:

$$\ln(I_{NM}) = -0.00109 F_S + 0.00432 \quad (16.4.16)$$

with correlation coefficient $R = -0.441 \pm 0.045$ and regression coefficient $K_{NM} = -(0.109 \pm 0.017)\%/(\Delta F_S = 1)$ which is very close to the empirical determination of the see state effect given by Eq. 16.3.10.

16.4.4. Sea state, Bernoulli, and atmospheric absorption effects for BC detector

The correlation of the 3-hourly data of $\ln(I_{BC})$, corrected for primary variations, with M is found that

$$\ln(I_{BC}) = -0.0071271 \times M + 14.13259 \tag{16.4.17}$$

with correlation coefficient $R = -0.964 \pm 0.013$ (atmospheric absorption coefficient $\beta_{BC} = -(0.713 \pm 0.015)\%/(\text{g.cm}^{-2})$). After correction for this 'apparent' atmospheric absorption effect the standard deviation of 3-hourly I_{BC} data decreases from StD = 7.58% to StD = 1.28% (to be compared with StD = 0.6% obtained for a pure Poisoning distribution of 3-hourly BC intensity data).

A detailed comparison between I_{NM} and I_{BC} data revealed that the I_{BC} data were affected by additional small (some percent) increases owing to 'near-port' effect when the ship was close to the Italian Antarctic Base (the majority of such increases have been already removed from I_{BC} data). The whole period 3-12 February, 1998 is not sufficiently reliable to be used for the determination of the sea state and atmospheric absorption effects. So we obtain a new regression (as in Eq. 16.4.17, but computed without the period 3–12 February, 1998):

$$\ln(I_{BC}) = -0.0072589 \times M + 14.25262 \tag{16.4.18}$$

with correlation coefficient $R = -0.985 \pm 0.012$ (the atmospheric absorption coefficient $\beta_{BC} = -(0.726 \pm 0.013)\%/\text{g.cm}^{-2}$). We can notice the remarkable increase of R with respect to Eq. 16.4.17.

For BC detector we can use the evaluation of Bernoulli effect (f = 0.3) obtained in the analysis of NM data; therefore it is necessary to determine only the sea state and the 'real' atmospheric absorption effects. The regression between the 3-hourly data of $\ln(I_{BC})$ and $M + \Delta M_b$ is found that

$$\ln(I_{BC}) = -0.0074035 \times (M + \Delta M_b) + 14.40438 \tag{16.4.19}$$

with correlation coefficient $R = -0.987 \pm 0.011$ (the atmospheric absorption coefficient $\beta_{BC} = -(0.740 \pm 0.012)\%/\text{g.cm}^{-2}$).

As it was done for I_{NM}, the I_{BC} data have been divided into three groups according to different ranges of sea state strength F_S (see Table 16.4.2). Without the period 3-12 February, the group F_{S1} vanishes almost completely, so that the analysis is restricted to groups F_{S2} and F_{S3}. It is found that for periods characterized by sea state strength F_{S2}:

$$\ln(I_{BC}) = -0.0079482 \times (M + \Delta M_b) + 14.95871 \tag{16.4.20}$$

with correlation coefficient $R = -0.9928$. For periods with sea state F_{S3}:

$$\ln(I_{BC}) = -0.0077941 \times (M + \Delta M_b) + 14.79685 \qquad (16.4.21)$$

with correlation coefficient $R = -0.9839$.

The difference between the relationships of Eq. 16.4.20 and Eq. 16.4.21 allows to estimate the change in counting rate owed to sea state effect as a function of *M*. For $\langle M \rangle = 1013.5\ g \cdot cm^{-2}$:

$$\langle \Delta I / I \rangle = \langle \Delta I / I \rangle_{\Delta F_S = 2.4} \approx -0.6\% . \qquad (16.4.22)$$

The sea state effect for BC counters can then be written as:

$$\langle (I(F_S) - I_o)/I_o \rangle = K_{BC} F_S \cong -2.5 \times 10^{-3} F_S . \qquad (16.4.23)$$

We can correct the I_{BC} Antarctic data for the sea state effect and determine the correlation between $(I_{BC})_{F_S}$ and $M + \Delta M_b$ for $R_{cp} \leq 1$ GV.

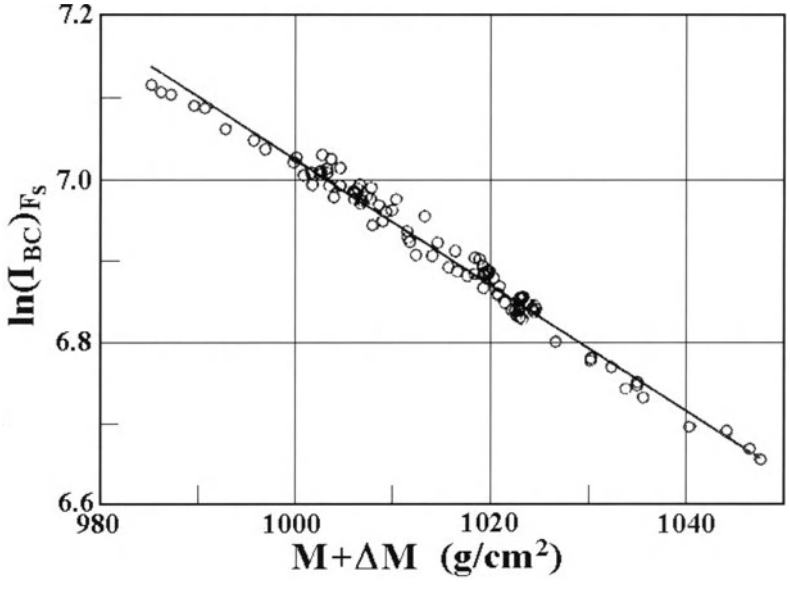

Fig. 16.4.2. The logarithm of BC intensity (corrected for CR primary variations and sea state effect) as a function of atmospheric mass $M + \Delta M_b$ (3-hourly averages), for $R_{cp} \leq 1$ GV (January 27–February 2; February 13–18, 1997). Best fit line is represented by Eq. 16.4.24.

The result given in Fig. 16.4.2 is represented by the following regression line:

$$\ln(I_{BC})_{F_S} = -0.0076556 \times (M + \Delta M_b) + 14.67805 \qquad (16.4.24)$$

with correlation coefficient $R=-0.991\pm0.009$ (the atmospheric absorption coefficient $\beta_{BC}=-(0.766\pm0.011)\%/\mathrm{g.cm}^{-2}$). After correction for this 'real' atmospheric absorption effect the standard deviation of the 3-hourly I_{BC} decreases from StD = 10.0% to StD = 1.36%.

As for NM data, we can compute the correlation of the BC intensity corrected for primary variations and atmospheric absorption effect (to the level of atmospheric mass $M_o=1034\,\mathrm{g.cm}^{-2}$) with the index of sea state F_S, based on data collected in near Antarctic region ($R_{cp}\le1\mathrm{GV}$), disregarding the aforementioned period influenced by 'near port' effect:

$$\ln(I_{BC})=-0.00283F_S+0.0168 \tag{16.4.25}$$

with correlation coefficient $R=-0.514\pm0.059$ and regression coefficient $K_{BC}=-(0.283\pm0.049)\%/(\Delta F_S=1)$. K_{BC} is very close to the result given in Eq. 16.4.23, as expected, the two computations being based on almost the same data.

16.4.5. Summary of the results on the determination of Bernoulli, sea state, and atmospheric absorption effects for NM and BC detectors

In Table 16.4.3 we summarize the results on the determination of Bernoulli, sea state and atmospheric absorption effects for NM and BC detectors.

Table 16.4.3. Summary of determinations of Bernoulli, sea state, and barometric effects for NM-64 and BC detectors in Antarctic region ($R_{cp}\le1$ GV, January 27 to February 18, 1997)

aEffects	NM-64		BC	
Bernoulli effect	$f=0.3$		$f=0.3$	
Sea state (F_S) effect	$\Delta I/I=K_{NM}F_S=-1.3\times10^{-3}F_S$		$\Delta I/I=K_{BC}F_S=-2.5\times10^{-3}F_S$	
Barometric effect, β, $\%(\mathrm{g.cm}^{-2})^{-1}$	β	R	β	R
Original data	−0.722 ± 0.007	−0.9919 ± 0.0006	−0.726 ± 0.013	−0.9850 ± 0.0012
Data corrected for Bernoulli	−0.737 ± 0.006	−0.9945 ± 0.0005	−0.740 ± 0.012	−0.9873 ± 0.0010
Data corrected for Bernoulli and F_S	−0.751 ± 0.005	−0.9955 ± 0.0005	−0.766 ± 0.011	−0.9908 ± 0.0009

It is worthwhile noting that the disregarding of the Bernoulli and sea state effects leads to very low values of atmospheric absorption coefficients and to lower correlation coefficients between M and I. Moreover, the difference between sea state effects of NM and BC detectors is remarkable. The bigger effect for BC could be owed to the comparatively larger view angle of this detector (sensitive to thermal neutrons) and consequently to a larger fraction of particle absorption through the ship and sea waves.

16.5. The atmospheric absorption effect as a function of cut off rigidity

16.5.1. Remarks on the atmospheric absorption effect of NM and BC

In Section 16.4 we determined the atmospheric absorption coefficients of NM and BC in Antarctic region (where $R_{cp} \leq 1$ GV), $\beta_{NM} = -(0.751 \pm 0.005)\%/\text{g.cm}^{-2}$ and $\beta_{BC} = -(0.766 \pm 0.011)\%/\text{g.cm}^{-2}$, together with the Bernoulli and sea state effects for both detectors. To correct the data for atmospheric absorption effect in the region $R_{cp} \geq 1$ GV we should take into account the dependence of atmospheric absorption coefficient upon cut off rigidity. Villoresi et al. (2000) evaluated the atmospheric absorption coefficients at $R_{cp} = 6.2$ GV in Colli (13.52 °E, 41.67 °N, 230 m above sea level, ~80 km South-East of Rome) before (*B*) and after (*A*) the latitude survey:

$$(\beta_{NM})_B = -(0.665 \pm 0.010)\frac{\%}{\text{g.cm}^{-2}}, \qquad (\beta_{NM})_A = -(0.694 \pm 0.019)\frac{\%}{\text{g.cm}^{-2}}, \quad (16.5.1)$$

$$(\beta_{BC})_B = -(0.613 \pm 0.021)\frac{\%}{\text{g.cm}^{-2}}, \qquad (\beta_{BC})_A = -(0.610 \pm 0.040)\frac{\%}{\text{g.cm}^{-2}}. \quad (16.5.2)$$

In Colli atmospheric absorption coefficients for NM and BC detectors look systematically different, whilst in the Antarctic region they are almost equal (the slightly higher value for BC could be indicative of a higher response of this detector to low energy particles). In Colli the radioactive background on soil, which is usually higher than on the seas could cause a decrease in β_{BC}, as compared with β_{BC} on the seas at the same cut off rigidities. This problem can be neglected for NM. To determine whether there is any difference between the cut off dependence of β_{NM} and β_{BC} we compared NM and BC data, corrected for sea state effect, as a function of cut off rigidity and atmospheric mass. The regression between $\ln(I_{NM})$ and $\ln(I_{BC})$ recorded during the whole survey (only port and near port periods have been removed) is described by:

$$\ln(I_{BC}) = 1.1230 \times \ln(I_{NM}) - 3.5220, \quad (16.5.3)$$

with correlation coefficient $R = 0.9990$. In Fig. 16.5.1 we show the dependence of I_{BC}/I_{NM} *vs.* R_{cp}. The linear best fit for $R_{cp} > 1$ GV (for $R_{cp} \leq 1$ GV a constant ratio is assumed) is:

$$I_{BC}/I_{NM} = -0.0005636 \times R_{cp} + 0.09232, \quad (16.5.4)$$

with correlation coefficient $R = -0.9335$. The pole–equator effect is owed to the $\cong 10\%$ difference in the latitude effects of I_{NM} and I_{BC} (see in Villoresi et al., 2000). The standard deviation StD of points about the best fit line is a factor 1.5 bigger than

$(\mathrm{StD})_{\mathrm{stat}}$ owing to pure statistics in the interval $0\ \mathrm{GV} \le R_{cp} < 9\ \mathrm{GV}$; $\mathrm{StD} \cong 2.0 \times (\mathrm{StD})_{\mathrm{stat}}$ for $9\ \mathrm{GV} \le R_{cp} < 13\ \mathrm{GV}$ and $\mathrm{StD} \cong 1.3 \times (\mathrm{StD})_{\mathrm{stat}}$ for $R_c \ge 13\ \mathrm{GV}$.

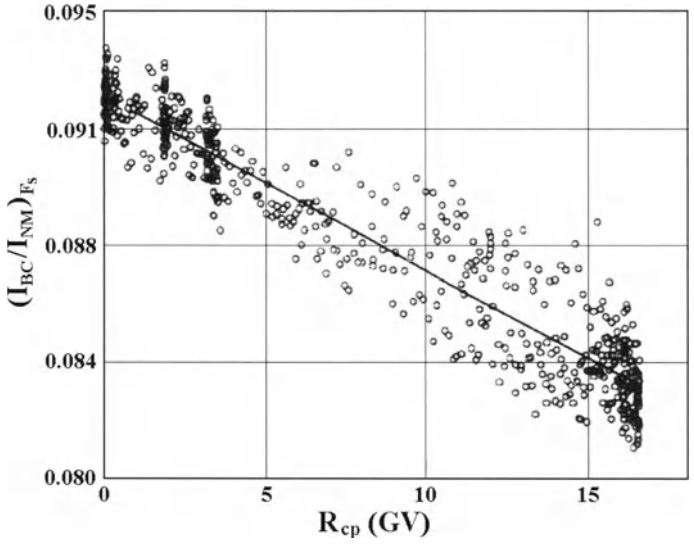

Fig. 16.5.1. The ratio I_{BC}/I_{NM} corrected for sea state effect, as a function of cut off rigidity R_{cp}. Best fit line (for $R_{cp} > 1$ GV) is represented by Eq. 16.5.4.

In Fig. 16.5.2 are shown the fluctuations of the ratio I_{BC}/I_{NM} about the best fit line described by Eq. 16.5.4 as a function of atmospheric mass M. No appreciable dependence of these fluctuations on M is found (correlation coefficient $R = 0.02$).

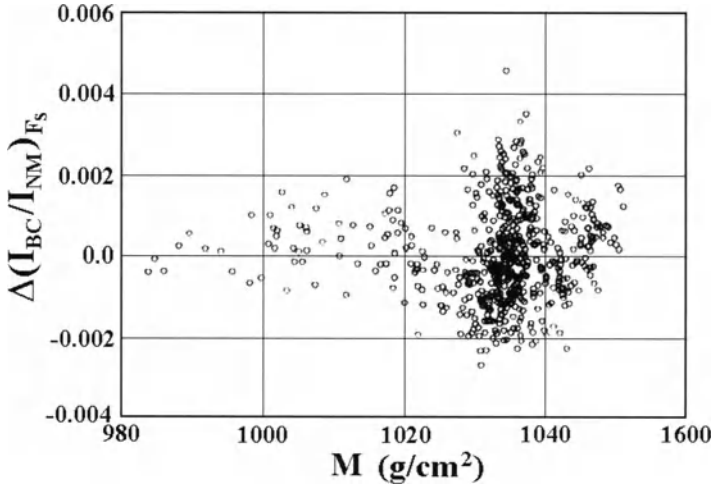

Fig. 16.5.2. The fluctuations about the best fit line of Fig. 16.5.1, as a function of atmospheric mass M. Correlation coefficient $R = 0.02$.

These results indicate that within the statistical sensitivity of the data it is not possible to observe any appreciable difference between β_{NM} and β_{BC} as a function of geomagnetic cut off rigidity. Apparently this result is in contradiction with what is expected from the different contribution of stopping muons in I_{NM} (about 7%) and I_{BC} (about zero). This effect would lead to about 5–6% increase of β_{BC} with respect to β_{NM}, owing to the much smaller (by a factor 6-7 at the pole) atmospheric absorption coefficient of stopping muons. The reason why we do not observe this increase could be owing to the contribution of local radioactivity in I_{BC}. Local radioactivity, having $\beta = 0\ \%/\left(\text{g/cm}^2\right)$, will decrease the value of β_{BC}. In our experiment on board of ship 'Italica' and on the seas, a 6% of local radioactivity at the pole could be enough to decrease β_{BC} to the level of β_{NM} all along the latitude survey.

16.5.2. Analytical approximation of atmospheric absorption coefficient vs. cut off rigidity

We utilize the dependence of atmospheric absorption coefficient on cut off rigidity obtained for the period of minimum solar activity by Carmichael and Bercovitch (1969) and Bachelet et al. (1972), by taking into account our determination in Antarctic region. The dependence of the NM-64 atmospheric absorption coefficient β_{NM} upon the vertical cut off rigidity R_{cp} can be approximated by the same function introduced by Dorman (1969) to describe CR latitude dependencies and coupling functions:

$$\beta_{NM} = \beta_o\left(1 - \exp\left(-\alpha R_{cp}^{-k}\right)\right), \tag{16.5.5}$$

where $\beta_o = -0.751\%/\left(\text{g/cm}^2\right)$ is the atmospheric absorption coefficient determined in Antarctic region ($R_{cp} \le 1$ GV).

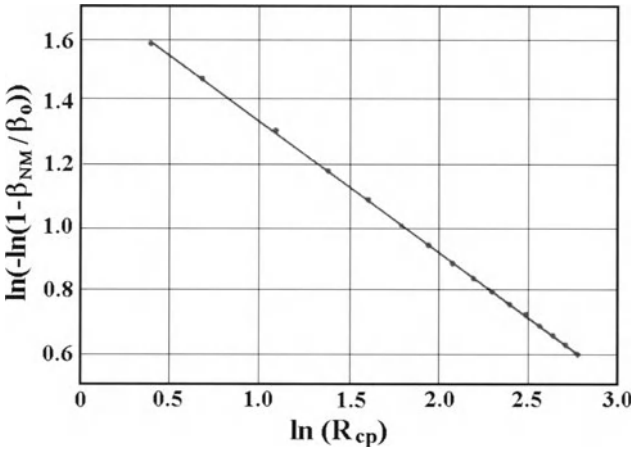

Fig. 16.5.3. Correlation between $\ln\left(-\ln\left(1-\beta_{NM}/\beta_o\right)\right)$ and $\ln\left(R_{cp}\right)$. Best fit line is plotted.

Parameters α and k are obtained by the correlation between $\ln(-\ln(1-\beta_{NM}/\beta_o))$ and $\ln(R_{cp})$ (see Fig. 16.5.3):

$$\ln(-\ln(1-\beta_{NM}/\beta_o)) = -0.4113\times\ln(R_{cp}) + 1.74395\,, \qquad (16.5.6)$$

with correlation coefficient $R = -0.9997$. Therefore for the survey detectors during minimum solar activity the dependence of the atmospheric absorption coefficient on R_{cp} at sea level can be described by Eq. 16.5.5, with

$$\beta_o = -0.751\%/(\text{g/cm}^2),\ \alpha = \exp(1.74395) = 5.69\pm0.03,\ k = 0.411\pm0.002, \qquad (16.5.7)$$

in which α and k are determined by comparing Eq. 16.5.5 and Eq. 16.5.6 and the errors are determined by taking into account the value of correlation coefficient.

16.6. Corrections for temperature effect *vs.* time and cut off rigidity

16.6.1. Temperature coefficient for neutron monitor vs. cut off rigidity

The temperature effect in neutron monitor intensity is caused by the contribution of unstable particles in secondary CR: pions, hard and soft muons. An especially important role is played by low energy negative muons (usually called soft muons) captured inside the NM-64 by lead nuclei, with further release of a few neutrons from the excited nuclei. Temperature effect of neutron monitor intensity was considered theoretically and was checked experimentally by many authors (see above, Sections 5.4, 7.4. and 7.5). According to Dorman (M1957, M1972), Dorman et al. (1990), the temperature effect in neutron monitor counting rate can be written as:

$$(\Delta I_{NM}(t)/I_{NM})_{T,R_{cp}} = \int_0^{h_o} W_{TNM}(h,R_{cp})\Delta T(h,R_{cp},t)dh\,, \qquad (16.6.1)$$

where h_o is the atmospheric pressure at the observation level, $\Delta T(h,R_{cp},t)$ is the change in temperature and

$$W_{TNM}(h,R_{cp}) = f_\pi(R_{cp})W_{T\pi}(h) + f_{\mu h}(R_{cp})W_{T\mu h}(h) + f_{\mu s}(R_{cp})W_{T\mu s}(h) \qquad (16.6.2)$$

is the temperature coefficient. In Eq. 16.6.2 $W_{T\pi}(h)$, $W_{T\mu h}(h)$, and $W_{T\mu s}(h)$ are the temperature coefficients for pions, hard and soft muons, correspondingly. These functions were calculated on the basis of theory and experimental data on CR nuclear meson and electromagnetic cascades in atmosphere by Dorman (M1957, M1972), Dorman et al. (1990). Coefficients $f_\pi(R_{cp})$, $f_{\mu h}(R_{cp})$, $f_{\mu s}(R_{cp})$ are the relative contributions to the neutron monitor counting rate owed to pions, hard and soft muons,

respectively; they depend on the type of neutron monitor. They were determined mainly experimentally by accelerators (see review in Dorman, M1957, M1963a,b, M1972, M1974, M1975a). For a NM-64 located at middle–high geomagnetic latitudes $\geq 50^o$ $\left(R_{cp} \leq 2.5 \text{ GV}\right)$

$$f_\pi\left(R_{cp} \leq 2.5 \text{ GV}\right) \approx 0.02,\ f_{\mu h}\left(R_{cp} \leq 2.5 \text{ GV}\right) \approx 0.03,\ f_{\mu s}\left(R_{cp} \leq 2.5 \text{ GV}\right) \approx 0.068. \quad (16.6.3)$$

The dependence of these coefficients on R_{cp} is determined by the dependencies of muon $I_\mu\left(R_{cp}\right)$ and neutron $I_n\left(R_{cp}\right)$ components on R_{cp}:

$$f_i\left(R_{cp}\right) \approx f_i\left(R_{cp} \leq 2.5\ GV\right)\left[I_\mu\left(R_{cp}\right)/I_n\left(R_{cp}\right)\right]/\left[I_\mu\left(R_{cp} \leq 2.5\ GV\right)/I_n\left(R_{cp}\right)\right] \quad , \quad (16.6.4)$$

where index i can be $\pi, \mu h, \mu s$ respectively.

The analytical approximation of $I_\mu\left(R_{cp}\right)$ and $I_n\left(R_{cp}\right)$ can be written as (see Dorman, 1969, and above, Section 3.8):

$$I_\mu\left(R_{cp}\right) = I_\mu(0)\left(1 - \exp\left(-\alpha_\mu R_{cp}^{-k_\mu}\right)\right), \quad I_n\left(R_{cp}\right) = I_n(0)\left(1 - \exp\left(-\alpha_n R_{cp}^{-k_n}\right)\right), \quad (16.6.5)$$

where the coefficients a_μ, k_μ, a_n, k_n have been determined on the basis of latitude surveys in periods near the minimum solar activity. For muon component (surveys data are compiled in Dorman (M1957, M1963b, M1974, M1975a))

$$\alpha_\mu = 19.4, \quad k_\mu = 0.77\ ; \quad (16.6.6)$$

and for neutron component (1976–1977 survey, according to Aleksanyan et al., 1979a,b):

$$\alpha_n = 8.10 \pm 0.05, \quad k_n = 0.88 \pm 0.02\ . \quad (16.6.7)$$

In this case $I_\mu\left(R_{cp} \leq 2.5 \text{ GV}\right) \approx I_\mu(0)$ and $I_n\left(R_{cp} \leq 2.5 \text{ GV}\right) \approx I_n(0)$ with accuracy of about 0.1%. Therefore, we obtain

$$f_i\left(R_{cp}\right)/f_i\left(R_{cp} \leq 2.5 \text{ GV}\right) \approx \left(1 - \exp\left(-\alpha_\mu R_{cp}^{-k_\mu}\right)\right)\Big/\left(1 - \exp\left(-\alpha_n R_{cp}^{-k_n}\right)\right) = F_{\mu n}\left(R_{cp}\right). \quad (16.6.8)$$

The function $F_{\mu n}\left(R_{cp}\right)$, plotted in Fig. 16.6.1, shows that from polar to equatorial regions the temperature coefficient increases by about 1.8 times.

A recent comparison between the described theory of temperature effect on neutron monitor intensity and experimental data of many neutron monitors in the northern and

southern hemispheres showed that the regression coefficient between theoretical and experimental data is 1.1 ± 0.1 (Belov et al., 1995). Therefore, we can use the theoretically calculated $W_{TNM}(h,R_{cp})$, by taking into account Eq. 16.6.3 and Eq. 16.6.8 (see Fig. 16.6.1), with relative accuracy of about ±10%.

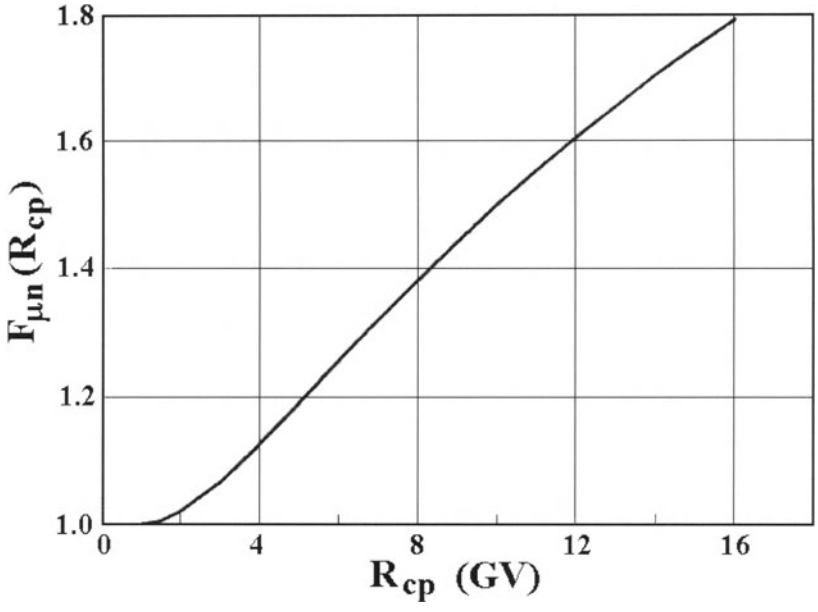

Fig. 16.6.1. The atmospheric temperature function $F_{\mu n}(R_{cp})$ *vs.* cut off rigidity R_{cp} .

16.6.2. Sea level and vertical air temperature distributions vs. cut off rigidity

To calculate the temperature corrections of the NM-64 counting rate according to Eq. 16.6.1 we should know $\Delta T(h,R_{cp},t)$, i.e. the dependence of sea level and vertical air temperature distributions upon cut off rigidity in the period of survey. The 3-hourly data of sea level air temperature have been obtained by averaging the 5-min temperature data measured on the ship during the survey. To determine the vertical air temperature distribution, we used data measured by satellites NOOA-9 and NOOA-10 in the period 1985-1988 (averaged for layers sea level–500 mb, 500 mb–300 mb, 300 mb–100 mb, and 100 mb–30 mb), for different geographic latitudinal zones: –90° to –70°, –70° to –50°, –50° to –30°, –30° to –10°, –10° to +10°, +10° to +30°, +30° to +50°, +50° to +70°, and +70° to +90°. Seasonal changes in temperature at different altitudes in different geographic latitudinal zones have been estimated by using the data taken in the same period of the year of our survey. Since the change from year to year temperature for layers higher than 500 mb is relatively small, we used for each day of the survey the average temperature distribution at different geographic latitudinal zones, obtained by averaging the data over time (1985–1988) and over atmospheric layers (500 mb–300 mb, 300 mb–100 mb, and 100 mb–30 mb). For layer sea-level–500 mb we used the

same four-year average, but for all 3-hourly values of survey period we applied corrections by taking into account the 3-hourly sea level air temperature data measured on the ship.

To illustrate the air temperature dependence upon cut off rigidity, we show in Fig. 16.6.2 the average (over the survey period) distribution of air temperature in layers sea level–500 mb, 500 mb–300 mb, 300 mb–100 mb and 100 mb–30 mb *vs.* latitude from Antarctic to Arctic zones.

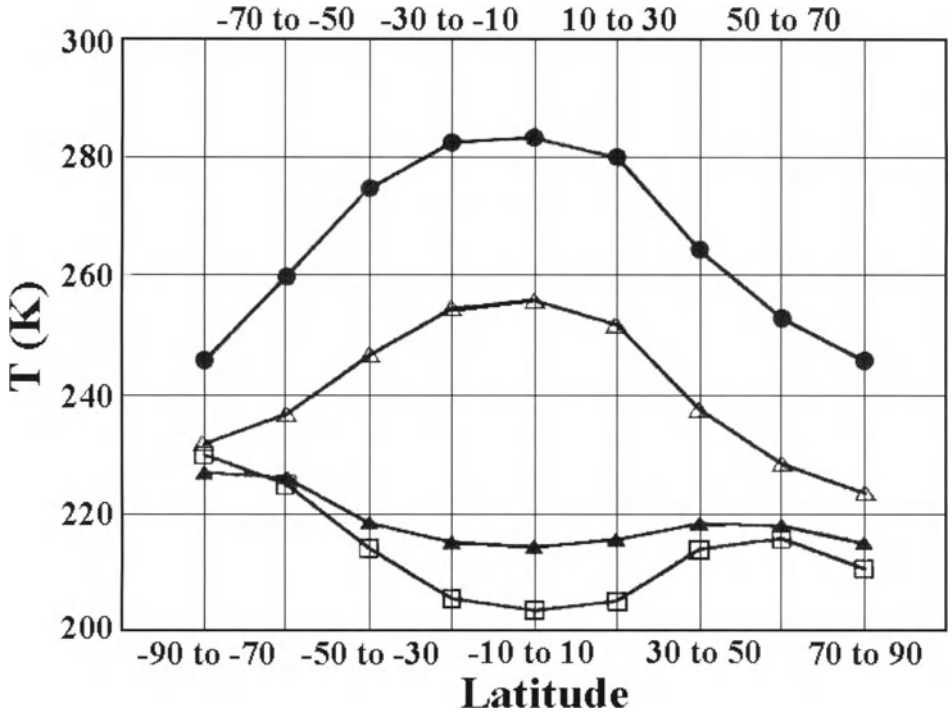

Fig. 16.6.2. Average (over the survey period) temperature distribution, as a function of geographic latitude, for different atmospheric layers (from top to bottom: sea level–500 mb, (500–300) mb, (300–100) mb and (100–30) mb).

From Fig. 16.6.2 it can be seen that the biggest increase in air temperature of about 40° is observed between Antarctica and equatorial zone in the layer sea level–500 *mb*, and of about 25° increase in the layer 500 mb–300 mb. The temperature effect in the neutron monitor counting rate caused by these two layers (producing a decrease in intensity in the equatorial zone relative to Antarctic and Arctic zones) will be partly compensated by the opposite tendency in the higher layers 300 mb–100 mb and 100 mb–30 mb (air temperature decreases by about 15° and 25° from Antarctic to equatorial zone, respectively).

To illustrate the air temperature variability in the survey period, we show in Fig. 16.6.3 the standard deviation of air temperature in each layer *vs.* latitude from Antarctic to Arctic zones.

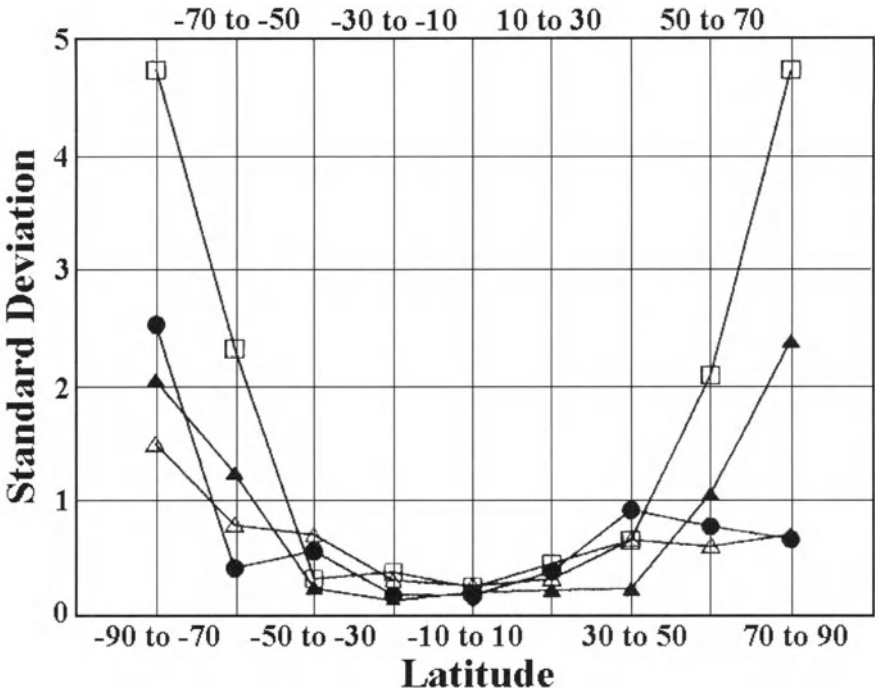

Fig. 16.6.3. Average (over the survey period) standard deviation of atmospheric temperature, as a function of latitude, for the same different atmospheric layers as in Fig. 16.6.2.

We can see from Fig. 16.6.3 that the standard deviations of air temperature at middle and equatorial zones in all layers are very small (for geographic latitudes –50° to +50° they are smaller than 1 °C), but they increase in Antarctic zone up to 2.5 °C in layer sea-level–500 mb, 1.5 °C in layer 500 mb–300 mb, 2.1 °C in layer 300 mb–100 mb, and 4.7 °C in layer 100 mb–30 mb.

16.6.3. Temperature corrections of NM-64 counting rate vs. cut off rigidity

On the basis of the 3-hourly data of $\Delta T(h, R_{cp}, t)$ averaged in layers sea level–500 mb, 500 mb–300 mb, 300 mb–100 mb and 100 mb–30 mb we computed the temperature corrections for the NM-64 counting rate in dependence of cut off rigidity according to

$$(\Delta I_{NM}(t)/I_{NM})_{T,R_{cp}} = \sum_{j=1}^{4} W_{Tj}(R_{cp})\Delta T_j(R_{cp}, t), \qquad (16.6.9)$$

which follows from Eq. 16.6.1. Index $j = 1, 2, 3, 4$ corresponds to the different layers sea level–500 mb, 500 mb–300 mb, 300 mb–100 mb and 100 mb–30 mb, correspondingly, and $W_{Tj}(R_{cp})$ are the integrals of $W_{TNM}(h, R_{cp})$ in the same layers:

$$W_{T1}(R_{cp}) = -0.0366\,F_{\mu n}(R_{cp})\%/^{\circ}\mathrm{C}, \quad W_{T2}(R_{cp}) = -0.0104\,F_{\mu n}(R_{cp})\%/^{\circ}\mathrm{C},$$
$$W_{T3}(R_{cp}) = -0.0085\,F_{\mu n}(R_{cp})\%/^{\circ}\mathrm{C}, \quad W_{T4}(R_{cp}) = -0.0020\,F_{\mu n}(R_{cp})\%/^{\circ}\mathrm{C}, \tag{16.6.10}$$

where the function $F_{\mu n}(R_{cp})$, determined by Eq. 16.6.8, is shown in Fig. 16.6.1. Values $\Delta T_j(h, R_{cp}, t)$ in Eq. 16.6.9 have been computed relatively to the average vertical distribution of air temperature in the equatorial zone (where this distribution is very stable; the standard deviation over the whole survey period is smaller than 0.5 °C in all layers, see Fig. 16.6.3).

In Fig. 16.6.4 we show the computed temperature corrections relative to the equatorial zone for the NM for each day of survey and for each layer, as well as the total temperature corrections. It can be seen that the total temperature correction changes from about –(0.10–0.15)% in the low latitude region up to about +(1.0–1.1)% in Antarctica and in northern Italy. The lowest layer, sea-level–500 mb, plays the most important role for temperature correction (more than 85% of total); the temperature corrections for layers 300 mb–100 mb and 100 mb–30 mb in the sum are smaller than 0.15%. We used daily data of temperature corrections relative to each layer to obtain the 3-hourly data of these corrections, by taking into account the 3-hourly data of sea-level air temperature measured on the ship and utilized by extrapolation for higher layers. We think that this procedure is sufficiently accurate because of the dominant role of lowest layer for which the temperature corrections have been computed more precisely.

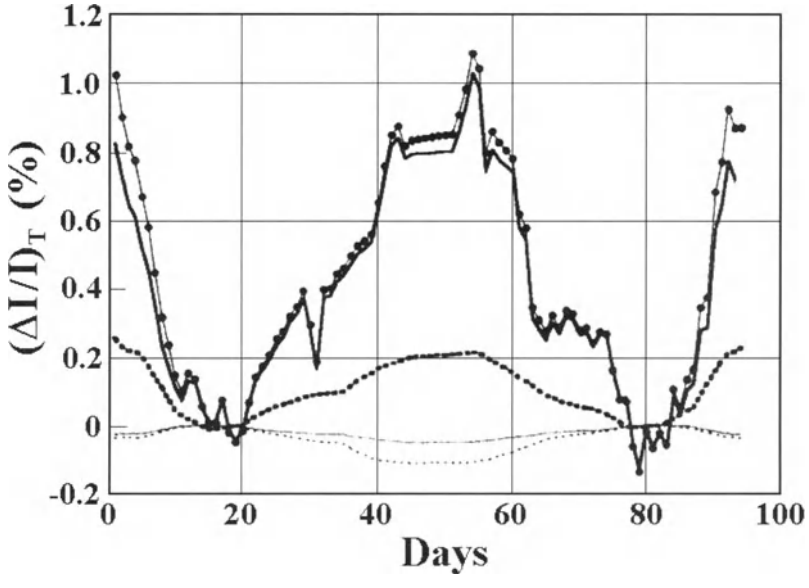

Fig. 16.6.4. Temperature corrections (in percent) relative to equatorial zone for NM-64 for each day of survey; solid circles denote total correction; thick solid line denotes correction for layer sea level–500 mb, thick dashed line denotes corrections for layer 500–300 mb, thin line denotes corrections for layer 300–100 mb and thin dashed line denotes corrections for layer 100–30 mb.

16.6.4. On the temperature effect in the counting rate of bare neutron counters

Bare neutron counters, not surrounded by lead and polyethylene, will detect thermal neutrons from the CR cascade in the atmosphere, locally produced thermal neutrons from CR interactions in nearby matter and thermal neutrons from local radioactivity. Therefore we expect that the relative role of soft muons in the counting rate of BC is negligible, as compared with NM in which soft muons have a greater probability of producing mesoatoms in lead with subsequent release of additional neutrons. Also for hard muons and pions, their contribution to the counting rate of BC is also negligible in comparison with NM. For this reason we will not consider the temperature effect for BC.

16.7. Correction of survey data for primary variations and all meteorological effects

16.7.1. Correction of survey data for primary variations

In Villoresi et al. (2000) we corrected the survey data for time variation in primary CR intensity on the basis of Rome NM and many NM of world network stations. The contribution of this correction is shown in Fig. 16.7.1 as $(\Delta I)_{\text{prim}}(\%)$ for each 3-hour from the beginning of survey. It can be seen that the contribution of this variation is about 3%. In Fig. 16.7.1 we show also the change of cut off rigidity R_{cp} in GV and the Earth's gravitational acceleration g in cm.sec^{-2} along the survey.

16.7.2. Determination of vertical atmospheric mass corrected for wind effect

As was done in the Antarctic area, the atmospheric pressure data P have been transformed to the mass M of vertical air column by taking into account the distribution of gravity acceleration value on the Earth's surface, by considering the rotation, the ellipsoidal shape and great anomalies of the Earth, according to Eq. 16.2.1 and Eq. 16.2.2. Then, we computed $f \times M_b$, owed to wind effect (Bernoulli effect), according to Eq. 16.2.4 with f = 0.3, as determined in Section 16.4.2. The vertical atmospheric mass $M + f \times M_b$ has been computed on 3-hourly basis for the whole survey. We remind that after February 13, 1997 $\langle W^2 \rangle$ has been derived by the index of the sea state F_S, according to Eq. 16.2.5. In Fig. 16.7.1 we plotted for comparison g, M and $f \times M_b$ for the whole survey period.

16.7.3. Correction for sea state effect

The correction for the sea state effect was applied to the survey data by using Eq. 16.4.16 for NM and Eq. 16.4.23 for BC, assuming that the sea state effect, evaluated in Sections 16.3 and 16.4 on the base of data in Antarctic region ($R_{cp} \leq 1$ GV), is the same at different latitudes. In Fig. 16.7.1 we show the computed NM intensity changes for the

sea state effect. We can see that the expected decrease in intensity is not bigger than 2% and that the sea state effect takes place on most days; for BC the expected sea state effect is about 2 times bigger than for NM. To obtain the 3-hourly corrections for the sea state effect we interpolated the daily values under the assumption that the F_S index changed gradually from day to day.

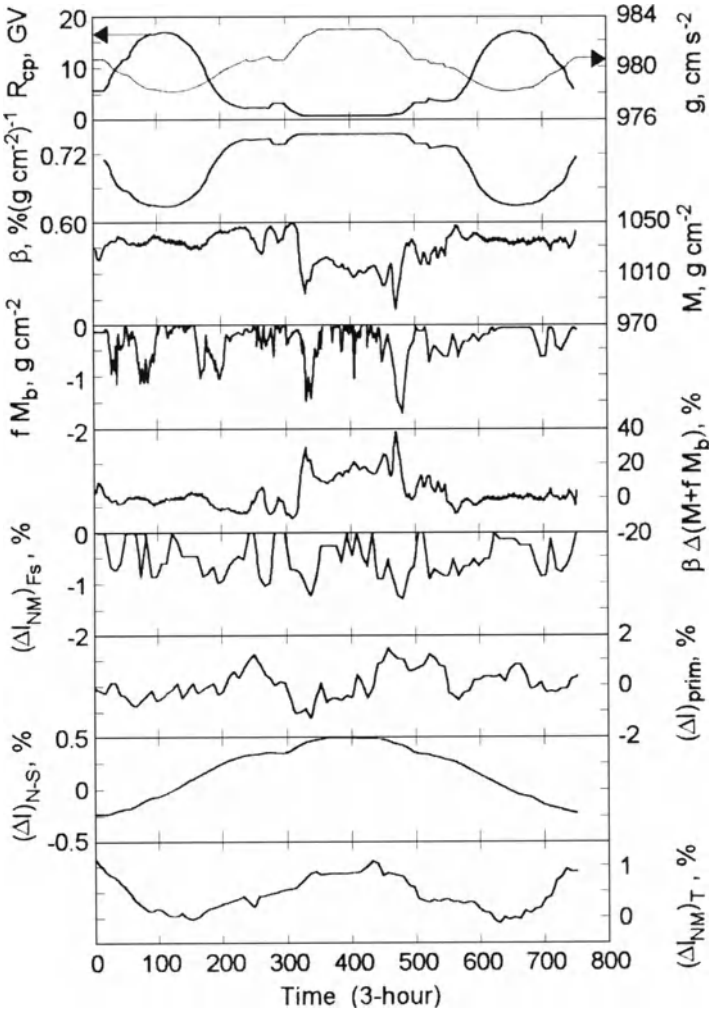

Fig. 16.7.1. Summary of meteorological effects on NM intensity and atmospheric mass, together with the effect of CR primary variations and the changes in gravity acceleration g and vertical cut off rigidity R_{cp} along the survey time span. From top to bottom: cut off rigidity R_{cp} and g (in the same panel); atmospheric absorption coefficient β; atmospheric mass M; wind effect on atmospheric mass $f \times M_b$; the effect of atmospheric mass ($M + f \times M_b$) changes on counting rate; the sea state effect on NM counting rate (for BC the effect is 2 times bigger); the effect of CR primary variations; the effect of atmospheric temperature changes on the NM counting rate.

16.7.4. Correction for atmospheric absorption effect

In Antarctic region for the period January–February 1997 (near solar activity minimum) we obtained in Section 16.4 $\beta_{NM} = -(0.751 \pm 0.05)\%/\left(\mathrm{g/cm^2}\right)$ and $\beta_{BC} = -(0.766 \pm 0.011)\%/\left(\mathrm{g/cm^2}\right)$. Since $\beta_{NM} \cong \beta_{BC}$ within the statistical errors, we have used Dorman's analytical approximation described by Eq. 16.5.5 with parameters given in Eq. 16.5.7 for computing the atmospheric absorption coefficients *vs.* R_{cp} for both NM and BC. In Fig. 16.7.1 we show the β behavior, together with the atmospheric absorption effect on neutron intensity (equal for NM and BC),

$$\Delta \ln I = \beta(R_{cp}) \cdot \Delta(M + f \times M_b). \tag{16.7.1}$$

We did not apply any time change in atmospheric absorption coefficients because the CR survey Italy-Antarctica was carried during very quiet period in the minimum of solar activity cycle. This possible variation is expected to be negligible along the survey time span.

16.7.5. Corrections for temperature effect

In Fig. 16.7.1 we also show the effect on NM counting rate owed to atmospheric temperature variations, according to the evaluations presented in Section 16.6.

16.8. Application of CR meteorological effects to latitude survey research: summary and conclusions

In Sections 16.1–16.7 we tried, for the first time in the case of CR latitude surveys on the seas, to perform a 'complete' determination of meteorological effects having some influence on the recorded data. For this purpose we measured the necessary data (P, W, F_S, T), and developed and/or utilized theoretical and/or numerical methods for an adequate evaluation of these effects. For a statistical determination of the main phenomena, we utilized the period of measurements in Antarctic area ($R_{cp} \le 1$ GV) where the sea level extra-terrestrial CR intensity (corrected for primary variations) is constant with time in the case of invariable meteorological conditions. In particular, for the determination of the absorption effect on the detected CR intensity, owing to the actual atmospheric mass M over the detector ($\Delta \ln I = -\beta \times \Delta M$) it is necessary: (i) to correct the evaluation of atmospheric mass for Bernoulli effect ($\Delta M_b = (1/2) f \times (\rho/g) \times \langle W^2 \rangle$); and (ii) to correct CR intensity for the inclination of the detector, owed to the sea state effect ($\langle \Delta I/I \rangle_{SF} = K F_S$). In Antarctic region ($R_{cp} \le 1$ GV) the high variability of M, W^2 and F_S made it possible to obtain reliable estimates of β, f, and K for the NM-64, in spite of W^2 and F_S (responsible for rather small, but not negligible, effects on M and $\ln I$) being well correlated and usually more effective during a low M regime. Indeed, the β values, determined by regression analysis between the raw M and $\ln I$ data, are particularly low, in

disagreement with independent evaluations performed on data from mobile laboratories or fixed CR stations at sea level and in the same phase of solar cycle (see *e.g.* Carmichael and Bercovitch, 1969; Bachelet et al., 1972) (for such detectors there is no sea state effect and the Bernoulli effect is usually much smaller). On the other hand, by a multiple correlation analysis of our data for $\ln I$, M, F_S and $(1/2)\times\rho\times W^2$ we found a wide region in the coordinate system (β, f, K) in which the correlation coefficients are very high and not statistically different. For this reason it was necessary to determine the total contribution of the small Bernoulli and sea state effects, by comparing data characterized by similar conditions in $\langle M \rangle$ and great variations in W^2 and F_S. The assessment of the two separate effects has been done: (i) by determining K through the evaluation of $\Delta I/I$ by a number of measurements of the ship's oscillations at $F_S = 8$, on the basis of a sea state effect model; and (ii) by computing f (by a simple difference procedure) and comparing this value with independent determinations performed at high altitude stations, where sea state effect is absent.

Due to the high correlation between W^2 and F_S (see Fig. 16.2.1) the computed correction coefficients for Bernoulli and sea state effects make us confident that the global correction for the two effects has been properly applied on all the survey data. For the first time, as far as we know, it was possible to do such simultaneous evaluation of the effects and compare the results with the expectations of simple models.

For bare counters (BC) it was not possible to develop any model able to connect the counting rate to the ship's inclination angle and, as a consequence, to F_S by the measured angles. For BC the contribution to the counting rate of incoming particles at large zenith angles, near $\pi/2$, is not known. Moreover, it is not possible to consider bare counters as plane detectors. On the other hand, after the determination of the Bernoulli coefficient f by the analysis of NM data in Antarctic area, it was possible to evaluate the sea state effect also for BC through the estimate of the global (sea state plus wind) effect, and compute the value of β by correlation between the corrected M and $\ln I_{BC}$ data, obtaining: $K_{BC} \cong 2 \cdot K_{NM}$ and $\beta_{BC} \cong \beta_{NM}$ within the statistical errors. The higher value of K_{BC} is probably owed to the non-negligible contribution of quasi-horizontally approaching particles to the counting rate of BC; in case of high F_S the inclined ship and waves might constitute an efficient shield for such particles.

The comparison between β_{BC} and β_{NM} has been extended to the whole survey (up to $R_{cp} \approx 16$ GV) by studying the dependence of I_{BC}/I_{NM} on M on the data corrected for the sea state effect. The lack of any correlation (R = 0.02) shows that $\beta_{BC}(R_{cp}) = \beta_{NM}(R_{cp})$ within the statistical errors. In contrast, computations on contemporary data recorded before and after survey (near Rome at $R_{cp} \approx 6.2$ GV) showed that for ground based detectors β_{BC} was significantly lower than β_{NM}. This result is in agreement with the increases in BC counting rate as large as 20%, observed when the ship was inside ports; when the detector was located near ground the contribution of ambient radioactivity, much bigger than at sea, increased the counting rate and consequently decreased β_{BC}, as compared with β_{NM} (the higher sensitivity

of BC to low energy primary CR is demonstrated by the $\cong 10\%$ increase in the equator to pole variation of I_{BC}/I_{NM}).

The values of β_{NM} and β_{BC} computed in the Antarctic area, together with the results of Carmichael et al. (1969) and Bachelet et al. (1972), allowed to determine the $\beta_{NM}(R_{cp}) \cong \beta_{BC}(R_{cp})$ function and correct all survey data for atmospheric absorption effect. Finally, the NM data have been corrected also for temperature variations in different atmospheric layers by using the Dorman (M1957, M1972), Dorman et al. (1990) model. Temperature data measured by the satellites NOOA-9 and NOOA-10 in the period 1985-1988 have been used, together with temperature data recorded on the ship. In this way it was possible to have continuous information about the time variations of the atmospheric temperature distribution and to take into account the influence of meteorological perturbations in the lower atmospheric layers. The expected pole-to-equator temperature effect of NM was found to be rather small ($\Delta I/I \approx 1\%$). Naturally, this correction is not necessary for BC, since the expected contribution of soft muons to the counting rate is negligible.

Chapter 17

Applications of the Radiocarbon Coupling Function Method to Investigations of Planetary Mixing and Exchange Processes; Influence of H-Bomb Explosions on the Environment; Cosmic Ray Variations in the Past

17.1. Cosmogenic nuclides and radiocarbon method for CR variations, for geophysical and astrophysical research

In Chapter 10 we considered the general equations and its solutions determining the space-time variations of cosmogenic nuclides production by CR and its contents in the space, inside astrophysical bodies, in atmospheres of stars and planets by the coupling function method which were developed before for CR variations research. Here we introduce and calculate the local and polar radiocarbon coupling functions for the Earth's atmosphere, taking into account vertical mixing of elements. We then introduce and calculate the planetary coupling function, taking into account the planetary element mixing and influence of geomagnetic field on CR planetary distribution. For the contents of radiocarbon in the atmosphere and in dated samples there are very important exchange processes between several reservoirs on the Earth. As a first approximation we consider two-reservoir model and then the model of five-reservoir element exchange. By comparison with experimental data on radiocarbon contents we estimate the exchange constants. On the basis of methods developed and solutions of equations obtained we determine the time evolution of the radiocarbon production rate and contents in the Earth's atmosphere. We consider data of H-bomb explosions in the atmosphere, on CR time variations in the past, caused by changes of geomagnetic field, by solar activity cycles, and by possible local supernova explosions.

The radiocarbon method has wide applications in archaeology for dating of historical samples and phenomena (assuming that the history over time of radiocarbon contents in the atmosphere is known). On the other hand, the application of the radiocarbon method to samples with an exactly known date of radiocarbon formation (so called dated samples: annual tree rings, old wines, stalactites, and others) gives important information on the time history of the radiocarbon contents in the atmosphere for long periods of time in the past (up to about 40,000 years). This information can then be directly used in archaeology and forensic issues for more exact application of radiocarbon method. The problem is how to obtain useful data on the time history of the radiocarbon contents in the atmosphere also for CR research, how to extract from these data information on CR intensity variations in the past and on related phenomena: on the change in time of the CR cut off rigidities and on the Earth's magnetic field variations, on the CR intensity cycle variations and solar activity and magnetic cycles, on the periods of gradual CR intensity increases connected with periods of very low solar activity levels (like the well known Maunder minimum), on the possible specific CR intensity increases connected with local supernova explosions, etc.. Here we try to develop the radiocarbon method for

different applications and CR research by 4 steps. In the first step we introduce the polar and local radiocarbon coupling functions connecting the primary CR spectrum variations in the interplanetary space with the local radiocarbon production rate in the total vertical column of the atmosphere, taking into account the vertical mixing processes in the Earth's atmosphere. On the basis of Lingenfelter's (1963) detailed calculations of the neutron and radiocarbon production rate by galactic CR as a function of altitude and geomagnetic latitude we determine the radiocarbon coupling functions and find its analytical approximation to high accuracy: correlation coefficient greater than 0.99 (Section 17.2). In the second step we introduce the planetary radiocarbon coupling functions connected the primary CR spectrum variations in the interplanetary space with the planetary radiocarbon production rate in the total Earth's atmosphere, taking into account the planetary elements mixing as well as planetary distribution of CR cut off rigidities (Section 17.3). In the third step we formulate the system of two differential equations, determined the connection of the planetary radiocarbon production rate with the radiocarbon contents in dated samples by also taking into account the planetary exchange processes of elements on the Earth in the framework of the 2-reservoir model (Section 17.4). On the basis of experimental data of radiocarbon contents change in dated samples connected with the great H-bomb explosions carried out by USSR and USA in 1962 we determine the probabilities of elements exchange between two planetary reservoirs (one – the atmosphere, and the other – world ocean + biosphere + humus) (Section 17.5). We investigate the reflection of different types of CR variations in radiocarbon contents considering inverse problems: on the basis of data on radiocarbon contents in dated samples, determining CR variations caused by change of geomagnetic field, by solar activity cycles and by possible local supernova explosions in the past (Sections 17.6 and 17.7). We then go to the fourth step and consider the more complicated 5-reservoir model (atmosphere, biosphere and humus, highest and deep parts of the World Ocean). We determine the probabilities of elements exchange between these 5 planetary reservoirs, formulate the system of 5 differential equations and determine the connection between the time variation of planetary radiocarbon production rate in the atmosphere (connected with CR intensity variation by the planetary coupling function) with the radiocarbon contents in each of 5 planetary reservoirs (Section 17.8). In Section 17.9 we present a short review on the research by the radiocarbon method of CR variations and related phenomena in the past: variation of geomagnetic field, solar activity cycles, and local supernova explosions.

17.2. Radiocarbon production rate *vs* latitude, altitude, and level of solar activity; vertical mixing in the atmosphere and local coupling functions for radiocarbon

17.2.1. Production rate of radiocarbon in the Earth's atmosphere as a function of atmospheric depth and geomagnetic latitude

The production rate $Q(R_C,h,t)$ of radiocarbon ^{14}C in the Earth's atmosphere at the point with cut off rigidity R_C at the depth h (in units g.cm^{-2}) and at time t as for any other cosmogenic nuclides will be determined according to Section 10.2 by the nuclear meson cascade of CR in the atmosphere with generation of secondary nuclear active

particles, by rigidity spectrum and contents of primary CR, by cross-sections of formation of radiocarbon atoms in nuclear interactions of energetic particles with atoms of background matter, and by cut off rigidity:

$$Q(R_c,h,t)=\sum_Z \int_{R_c}^{\infty} D_Z(R,t)dR \sum_l \sum_k \int_0^{E(R)} M_l(R,E_l,h)\sigma_{lk}(E_l)N_k(h)dE_l\,. \quad (17.2.1)$$

Here $D_Z(R,t)$ is the differential rigidity spectrum of primary particles with charge *Ze*, $M_l(R,E_l,h)$ is the total differential multiplicity at the depth *h* in the atmosphere of nuclear active particles of type *l* with kinetic energy per nucleon E_l (*l* indicates protons, neutrons, pions, nuclei and nuclei fragments, etc.), i.e. including all nuclear active particles at the depth *h* generated by one primary particle with charge *Ze* and rigidity *R*; $\sigma_{lk}(E_l)$ is the effective cross-section of generation of radiocarbon atoms in the interaction of *l* type nuclear active particle with background nuclei of *k*-type with concentration $N_k(h)$. In Eq. 17.2.1 $E(R)$ is the kinetic energy of primary particle corresponding to the atomic number *A*, rigidity *R* and charge *Ze*:

$$E(R)=Ze\left(R^2+\left(Am_nc^2/Ze\right)^2\right)^{1/2}-Am_nc^2, \quad (17.2.2)$$

where m_n is the rest mass of a nucleon. As in section 10.2, let us assume that in the first approximation for all *Ze* in the primary galactic CR the rigidity spectra $D_Z(R,t)$ have about the same shape, that

$$D_Z(R,t)\approx B_Z D(R,t), \quad \sum_Z B_Z=1. \quad (17.2.3)$$

After introducing Eq. 17.2.3 into Eq. 17.2.1 we obtain

$$Q(R_c,h,t)=\int_{R_c}^{\infty} D(R,t)M(R,h)dR, \quad (17.2.4)$$

where

$$M(R,h)=\sum_Z \sum_l \sum_k \int_0^{E(R)} M_l(R,E_l,h)\sigma_{lk}(E_l)B_Z N_k(h)dE_l \quad (17.2.5)$$

is the integral multiplicity of radiocarbon production by one average primary particle with rigidity *R* at depth *h*. The detailed calculations of radiocarbon production rate were made in Lingenfelter (1963), taking into account the data on nuclear active particles in the atmosphere. It was considered that several types of reactions produce ^{14}C. The main reaction is $^{14}\mathrm{N}(n,p)^{14}\mathrm{C}$. If the production rate of radiocarbon by this reaction is taken as 1, then other reaction rates are: $<3\times10^{-3}$ for $^{16}\mathrm{O}(n,{}^3\mathrm{He})^{14}\mathrm{C}$, 2.3×10^{-6} for $^{17}\mathrm{O}(n,\alpha)^{14}\mathrm{C}$, $<4\times10^{-5}$ for $^{15}\mathrm{N}(n,d)^{14}\mathrm{C}$, 1.1×10^{-9} for $^{13}\mathrm{C}(n,\gamma)^{14}\mathrm{C}$, and

$<1.2\times10^{-7}$ for reactions of spallation of ^{20}Ne, ^{21}Ne and ^{22}Ne with formation of ^{14}C. The reaction ^{14}N$(n,p)^{14}$C gives more than 99% of the total ^{14}C production rate and all other reactions give less than 1% of the total production rate of radiocarbon in the Earth's atmosphere (let us note that the importance of this reaction for generation of radiocarbon by CR neutrons was suggested more than 60 years ago by Montgomery and Montgomery, 1939). It means that in Eq. 17.2.5 the summation over l will have only one member (for neutrons) and the summation over k will have also only one member (for ^{14}N). Results of Lingenfelter's (1963) calculations of radiocarbon production rate in 1 g of air in solar minimum (as in 1953–1954) as a function of geomagnetic latitude and atmospheric depth are shown in Fig. 17.2.1. Let us note that recently Aoki et al. (2003) start to made new calculations of radiocarbon production rate in dependenceof altitude and latitude for minimum and maximum of solar activity on the basis of Geant-4 program, and we hope that final results will published in near future.

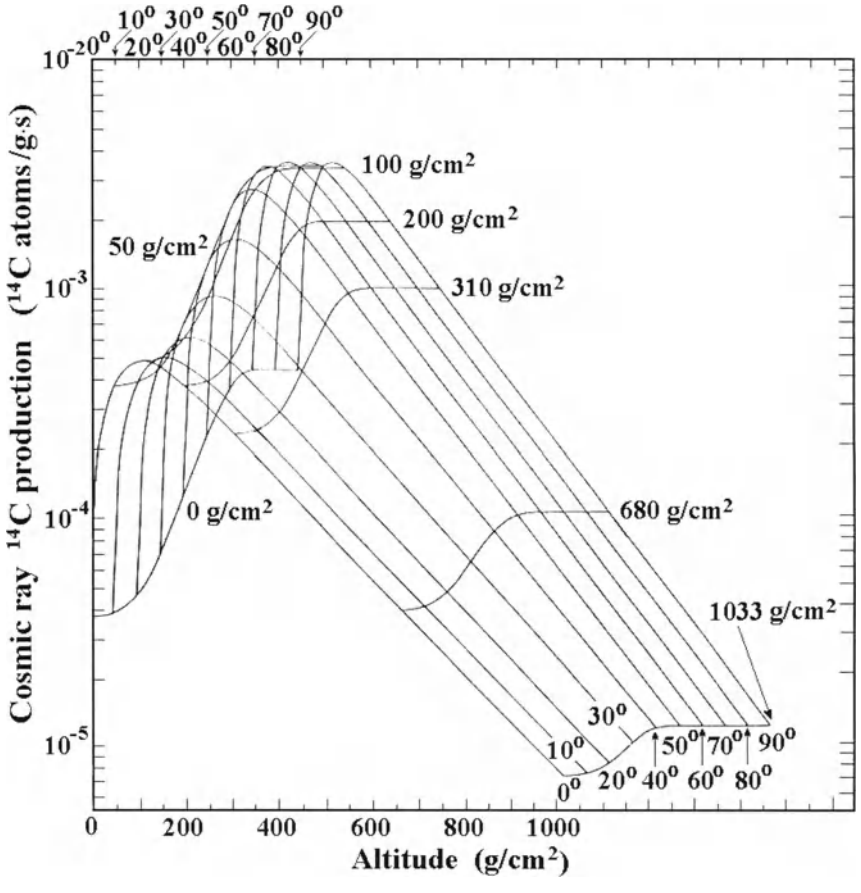

Fig. 17.2.1. The solar minimum radiocarbon production rate from galactic CR neutrons (in radiocarbon atoms per gram per second) as a function of mass level (in grams per square centimeter), and geomagnetic latitude. Results of calculations are normalized to a total neutron production rate of 1 neutron per square centimeter column of air per second at the geomagnetic pole during the solar minimum. According to Lingenfelter (1963).

From Fig. 17.2.1 it can be seen that radiocarbon is mostly formed at small depths from about 50 g.cm^{-2} up to about 300 g.cm^{-2} and decreases with increasing h as

$$Q(R_c, h, t) \propto \exp(-h/L(R_c)), \tag{17.2.6}$$

where $L(R_c)$ decreases with increasing geomagnetic latitude (decreasing of R_c) from 214 g.cm^{-2} at 0° ($R_c \approx 15$ GV) to 164 g.cm^{-2} at high latitudes ≥ 60° ($R_c \leq 1$ GV) in accordance with behavior of neutron flux. The maximum of radiocarbon production rate is expected to be about 2.1×10^{-2} atom ^{14}C per 1 g per 1 sec at the depth of about 90 g.cm^{-2} at high geomagnetic latitudes and about one order lower at geomagnetic equator (at a depth of about 130 g.cm^{-2}). For solar maximum (1957–1958) the expected radiocarbon production rate (see Fig. 17.2.2) is lower by about 20% than the maximum rate at high latitudes ≥ 60° ($R_c \leq 1$ GV) and lower only by 5% than the maximum rate near equator for solar activity minimum.

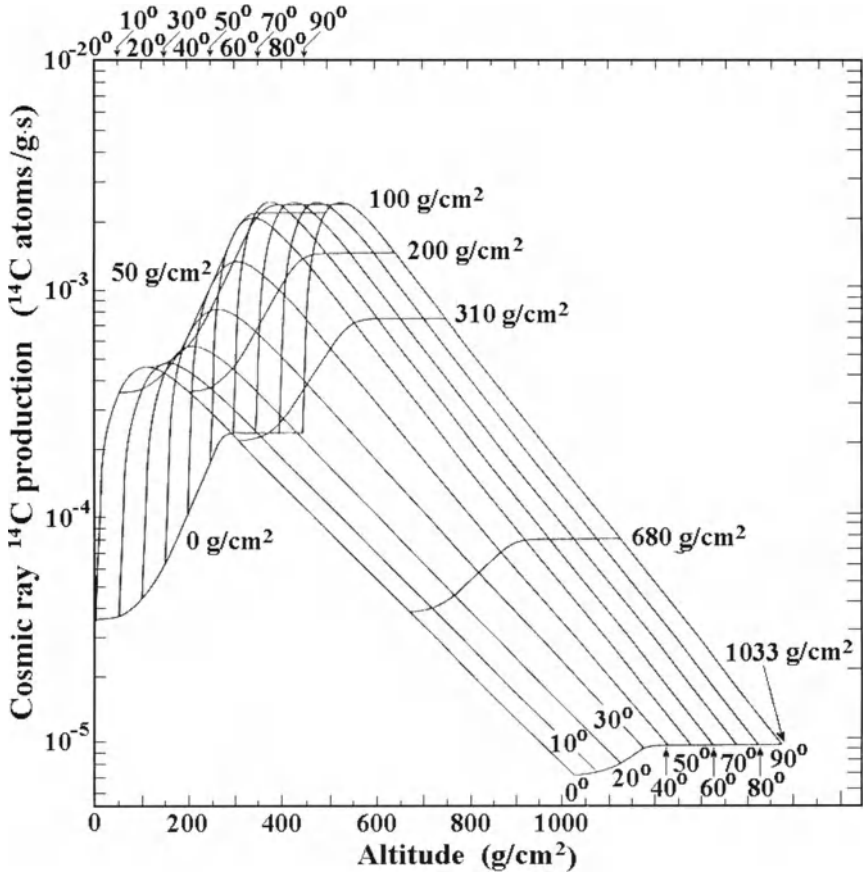

Fig. 17.2.2. The same as in Fig. 17.2.1, but for solar maximum. According to Lingenfelter (1963).

17.2.2. Vertical mixing of elements in the Earth's atmosphere, radiocarbon production rate in the total vertical column

Let us take into account the vertical mixing of elements in the Earth's atmosphere with some characteristic time T_v and determine the total production rate of radiocarbon $Q_v(R_c,h_o,t)$ in the vertical column per cm^2 in the atmosphere from top $(h=0)$ to the bottom $(h=h_o)$. Then from Eq. 17.2.4 we obtain:

$$Q_v(R_c,h,t)=\int_{R_c}^{\infty} D_v(R,t)M_v(R,h_o(t))dR, \tag{17.2.7}$$

where

$$D_v(R,t)=T_v^{-1}\int_{t-T_v}^{t} D(R,\tau)d\tau,\ M_v(R,h_o(t))=\int_{0}^{h_o(t)} M(R,h)dh. \tag{17.2.8}$$

Here $D_v(R,t)$ is the primary CR rigidity spectrum averaged over the time T_v of vertical mixing and $M_v(R,h_o(t))$ is the integral multiplicity of radiocarbon in the vertical column per cm^2 from $h=0$ to $h_o(t)$ per one averaged primary particle with rigidity R. In Lingenfelter (1963) on the basis of results described above in Section 17.2.1 the expected values of $Q_v(R_c,h_o,t)$ were calculated for sea level $h_{oo}=1033$ g.cm^{-2} as a function of geomagnetic latitude θ for solar activity minimum (1953-1954) and maximum (1957–1958). These data are listed in Table 17.2.1, where we give also the values of R_c for the Earth's magnetic field in dipole approximation according to

$$R_c = R_o(\cos\theta)^4, \tag{17.2.9}$$

where $R_o \approx 14.9$ GV is the cut off rigidity for vertical direction at geomagnetic equator at the present time ($t = 0$).

Table 17.2.1. Values of $Q_v(R_c,h_o,t)$ in units of atoms ^{14}C per cm^2 per sec at solar activity minimum $(Q_{v\min})$ and maximum $(Q_{v\max})$. According to Lingenfelter (1963).

θ	0°	10°	20°	30°	40°	50°	60°	70°	80°	90°
R_c, GV	14.9	14.0	11.6	8.38	5.13	2.54	0.93	0.20	0.01	0
$Q_{v\min}$	0.98	1.01	1.22	1.83	3.02	4.52	5.26	5.38	5.38	5.38
$Q_{v\max}$	0.93	0.96	1.15	1.63	2.45	3.44	3.79	3.79	3.79	3.79

Table 17.2.1 shows that $Q_v(R_c,h_o,t)$ increases with increasing of geomagnetic latitude from 0° to 70° (i.e. with decreasing R_c from 14.9 GV to 0.20 GV) by 5.5 times at solar minimum and by 4.1 times at solar maximum. The change of $Q_v(R_c,h_o,t)$ with solar activity depends on R_c: about 5% at R_c=14.9 GV up to 42% at $R_c \le$ 0.20 GV. It is

important to note that at solar minimum 1953–1954 the radiocarbon production rate by primary particles with rigidity $R_c \leq 0.20$ GV was negligible, and for solar maximum the same is true for primary particles with $R_c \leq 0.93$ *GV*. The share in the radiocarbon production rate by primary particles with rigidity $R \geq 14.9$ GV at solar minimum is about 18% and at solar maximum 25%. About half of the radiocarbon production rate is caused by primary particles in the rigidity interval 2.5–8.4 GV.

An important quantity is the global average radiocarbon production rate $\langle Q_g \rangle$. The first rough estimation of this rate was made by Libby (1946) on the basis of CR neutron measurements: $\langle Q_g \rangle \approx 0.8$ ^{14}C.cm^{-2}.sec^{-1}. Utilizing the improvements in the accuracy of CR neutron measurements, Anderson and Libby (1951) and Anderson (1953) revised the initial estimate mentioned above, increasing it by about three times: $\langle Q_g \rangle \approx 2.8$ ^{14}C.cm^{-2}.sec^{-1}. Similar estimates were made also by Pfotzer (1952): $\langle Q_g \rangle \approx 2.2 \pm 0.3$ ^{14}C.cm^{-2}.sec^{-1}; by Landenburg (1952) and Kouts and Yuan (1952): $\langle Q_g \rangle \approx 2.4$ ^{14}C.cm^{-2}.sec^{-1}. According to Lingenfelter (1963): $\langle Q_g \rangle \approx 2.5 \pm 0.5$ ^{14}C.cm^{-2}.sec^{-1}. The change of $\langle Q_g \rangle$ with cycle of solar activity is considered below, in Section 17.3.1.

17.2.3. Radiocarbon production rate in vertical column of the atmosphere and its time variations

From Eq. 17.2.7 we can determine the expected relative variations of $Q_v(R_c, h_o, t)$ caused by changes in the primary CR spectrum (local supernova explosions, modulation processes in the Heliosphere, generation of energetic particles in solar flares), by change of integral multiplicity in vertical column of atmosphere (variation of atmospheric depth h_o), and by change of geomagnetic field (leading to change in R_c):

$$\frac{\delta Q_v(R_c,h_o,t)}{Q_{vo}(R_{co},h_o)} = \int_{R_c}^{\infty} \frac{\delta D_v(R,t)}{D_{vo}(R)} W_v(R_c,R,h_o(t))dR$$

$$+ \int_{R_c}^{\infty} \frac{\partial \ln M_v(R,h_o(t))}{\partial h_o(t)} W_v(R_c,R,h_{oo})dR - \delta R_c(t) W_v(R_c,R_c,h_{oo}), \quad (17.2.10)$$

where

$$W_v(R_{co},R,h_{oo}) = D_{vo}(R) M_{vo}(R,h_{oo}) / Q_{vo}(R_{co},h_{oo}). \quad (17.2.11)$$

is the local coupling function between radiocarbon production rate in the vertical column of the atmosphere and differential rigidity spectrum of primary CR particles (Dorman, 1976, 1977a-g). Here we denote:

$$R_{co}=R_c(0),\ \ \delta R_c(t)=R_c(t)-R_{co};\ \ h_{oo}=h_o(0),\ \ \delta h_o(t)=h_o(t)-h_{oo};$$
$$Q_{vo}(R_{co},h_{oo})=Q_v(R_c,h_{oo},0),\ \ \delta Q_v(R_c,h_o,t)=Q_v(R_c,h_o,t)-Q_{vo}(R_{co},h_{oo});\quad (17.2.12)$$
$$D_{vo}(R)=D_v(R,0),\ \ \delta D_v(R,t)=D_v(R,t)-D_{vo}(R).$$

17.2.4. Calculations of local and polar radiocarbon coupling functions; analytical approximation for coupling functions

The local coupling function $W_v(R_{co},R,h_{oo})$ determined by Eq.17.2.11, can be found from Eq. 17.2.7, if we know the dependence of $Q_v(R_c,h_o,t)$ on R_c (or on geomagnetic latitude). By differentiating Eq. 17.2.7 for $Q_{vo}(R_{co},h_o)$ over R_{co} we obtain

$$\partial Q_{vo}(R_{co},h_{oo})/\partial R_{co}=-D_{vo}(R_{co})M_{vo}(R_{co},h_{oo}),\quad (17.2.13)$$

and then

$$W_v(R_{co},R_{co},h_{oo})=-(\partial Q_{vo}(R_{co},h_{oo})/\partial R_{co})/Q_{vo}(R_{co},h_{oo}),\quad (17.2.14)$$

On the basis of Lingenfelter (1963) results listed in Table 17.2.1 and using Eq. 17.2.14, we can determine $W_v(R_{co},R,h_{oo})$ up to about 15 GV. We can extrapolate to higher rigidities by taking into account that in Eq. 17.2.11 $D_{vo}(R)$ and $M_{vo}(R,h_{oo})$ are power functions for $R \geq 15$ GV and that $W_v(R_{co},R,h_{oo})$ are normalized functions:

$$\int_{R_{co}}^{\infty} W_v(R_{co},R,h_{oo})dR=1\quad (17.2.15)$$

which follows from definition Eq. 17.2.11 and Eq. 17.2.7 for $Q_{vo}(R_{co},h_{oo})$. We can try to use also the approximation function for CR coupling functions introduced in Dorman (1969, M1972, M1974). In this case the data on the radiocarbon production rate as a function of R_{co} is approximated by the function

$$Q_{vo}(R_{co},h_{oo})\Big/Q_{vo}(0,h_{oo})=1-\exp\left(-a(h_{oo})R_{co}^{-k(h_{oo})}\right).\quad (17.2.16)$$

By the least square regression fitting to the data listed in Table 1 for $h_{oo}=1033$ g.cm^{-2} we determined for solar minimum parameters $a_{\text{min s.a.}}$, $k_{\text{min s.a.}}$ and correlation coefficient $\text{C}_{\text{min s.a.}}$ between Eq. 17.2.16 and data in Table 17.2.1:

$$a_{\text{min s.a.}}=4.246\pm0.006,\ \ k_{\text{min s.a.}}=1.1105\pm0.0016,\ \ \text{C}_{\text{min s.a.}}=0.9965\,.\quad (17.2.17)$$

For the solar maximum we obtained

$$a_{\text{max s.a.}}=7.5729\pm0.0006,\ \ k_{\text{max s.a.}}=1.22805\pm0.00005,\ \ \text{C}_{\text{max s.a.}}=0.9999.\quad (17.2.18)$$

According to Dorman (1969, M1972, M1974) the polar coupling function (for R_{CO} =0) will be

$$W_{vo}(0,R,h_{oo}) = akR^{-(k+1)}\exp\left(-aR^{-k}\right) \tag{17.2.19}$$

with maximum

$$W_{vo\max} = (k+1)\left(\frac{k+1}{ak}\right)^{1/k}\exp\left(-\frac{k+1}{k}\right) \quad \text{at} \quad R_{\max} = \left(\frac{ak}{k+1}\right)^{1/k} \tag{17.2.20}$$

By using Eq. 17.2.17 and Eq. 17.2.18 we obtain for solar minimum

$$(W_{vo\max})_{\min\text{ s.a.}} = 15.3\ \%/\text{GV},\ (R_{\max})_{\min\text{ s.a.}} = 2.06\ \text{GV} \tag{17.2.21}$$

and for solar maximum

$$(W_{vo\max})_{\max\text{ s.a.}} = 11.3\ \%/\text{GV},\ (R_{\max})_{\max\text{ s.a.}} = 3.20\ \text{GV} \tag{17.2.22}$$

In Fig. 17.2.3 (in the interval 0–20 GV) and Fig. 17.2.4 (interval 0.1–1000 GV) we show the polar radiocarbon coupling functions for minimum and maximum of solar activity.

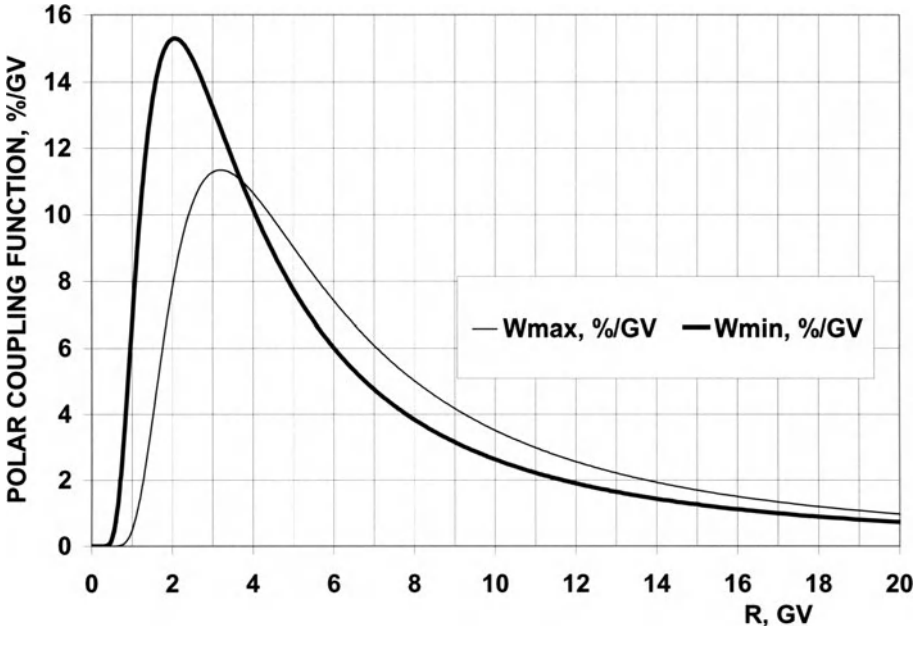

Fig. 17.2.3. Polar radiocarbon coupling functions for minimum (thick line) and maximum (thin line) of solar activity in double-linear scale.

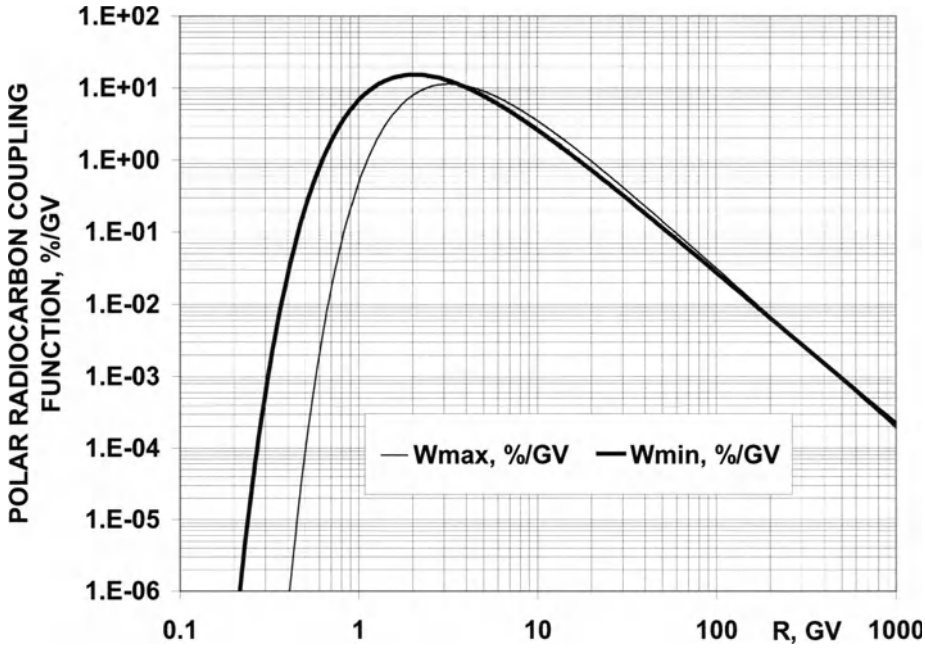

Fig. 17.2.4. Polar radiocarbon coupling functions for minimum (thick line) and maximum (thin line) of solar activity in double-logarithmic scale.

The local coupling functions for any R_{co} according to Dorman (M1963a,b) can be found through polar coupling function:

$$W_v(R_{co},R,h_{oo})=\begin{cases}0 & \text{at } R<R_{co}\\ W_{vo}(0,R,h_{oo})\left(\int\limits_{R_{co}}^{\infty}W_{vo}(0,R,h_{oo})dR\right)^{-1} & \text{at } R\geq R_{co}\end{cases} \qquad (17.2.23)$$

By taking into account Eq. 17.2.19 we obtain for $R \geq R_{co}$:

$$W_v(R_{co},R,h_{oo})=akR^{-(k+1)}\exp\left(-aR^{-k}\right)\left[1-\exp\left(-aR_{co}^{-k}\right)\right]^{-1}. \qquad (17.2.24)$$

17.2.5. Expected variation of radiocarbon coupling functions during solar activity cycle

Let us take into account the change of parameters a and k with solar activity. The annual average of Wolf sunspot numbers W for the solar minimum years 1953–1954 was 9.1 and for solar maximum years 1957–1958 was 187.5 (let us mention that namely for these periods were found in Eq. 17.2.21 and 17.2.22 values of parameters a and k).

Let us assume that in the first approximation the dependence of a and k on W is linear. In this case

$$a(\mathrm{W}) = 4.0763 + 1.865\times10^{-2}\,\mathrm{W}, \quad k(\mathrm{W}) = 1.104 + 6.614\times10^{-4}\,\mathrm{W}. \qquad (17.2.25)$$

For solving many problems of CR variations long time ago usually are used radiocarbon data averaged for 10 and more years. For this the important quantity is the coupling function averaged over many solar cycles (see Fig. 17.2.5).

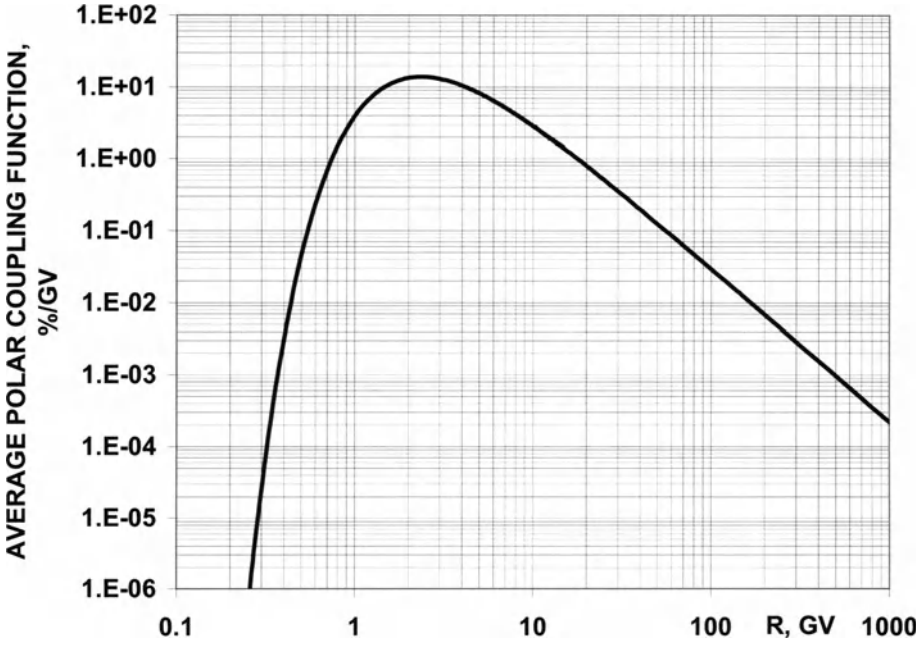

Fig. 17.2.5. Polar radiocarbon coupling function averaged for many solar cycles.

To determine this average coupling function we used the average value of W for about 10 solar cycles from 1844 through 1954 and found $W_{av} = 47.7$. The expected values of parameters a and k averaged over many years will be according to Eq. 17.2.25:

$$a_{av} = 4.966, \quad k_{av} = 1.136. \qquad (17.2.26)$$

The polar radiocarbon coupling function averaged over many solar cycles and shown in Fig. 17.2.5, was determined according to Eq. 17.2.19 and Eq. 17.2.26.

Eq. 17.2.21–17.2.26 determine the polar and local radiocarbon coupling functions for any cut off rigidity and any level of solar activity, as well as those averaged over many years radiocarbon coupling functions.

17.3. Planetary mixing in the atmosphere and the planetary coupling function for radiocarbon; analytical approximation and change with solar activity

17.3.1. Planetary mixing of elements in the Earth's atmosphere and planetary radiocarbon production rate

Besides the vertical mixing in the Earth's atmosphere there is the very important planetary mixing of elements with effective time $T_p \approx 1-2$ years. If we consider data for times greater than T_p it is necessary to take into account the planetary mixing of elements in the Earth's atmosphere. That is, we must average the radiocarbon production rate determined by Eq. 17.2.7 in the vertical column of the atmosphere over time T_p and over all surface of the Earth:

$$Q_p(t) = (4\pi T_p)^{-1} \int_{t-T_p}^{t} d\tau \int_{-\pi/2}^{\pi/2} \cos\theta d\theta \int_{0}^{2\pi} Q_V(R_c(\theta,\varphi,\tau), h_o(\theta,\varphi,\tau), \tau) d\varphi, \quad (17.3.1)$$

where θ is the latitude (counted from equator, in the North, positive, in the South, negative), φ is the longitude and $Q_V(R_c(\theta,\varphi,t), h_o(\theta,\varphi,t), t)$ was determined from Eq. 17.2.7. Here we take into account that R_c as well as h_o depend on θ, φ, and t. The planetary production rate of radiocarbon was calculated by Lingenfelter (1963) using the results of radiocarbon production rate distribution in the atmosphere (see above, Section 17.2) for solar minimum 1953-1954. It was found that

$$(Q_p)_{\min s.a.} = 2.61 \text{ atom}^{14}\text{C.cm}^{-2}.\text{sec}^{-1}. \quad (17.3.2)$$

For solar maximum 1957-1958 according to Lingenfelter (1963)

$$(Q_p)_{\max s.a.} = 2.08 \text{ atom}^{14}\text{C.cm}^{-2}.\text{sec}^{-1}. \quad (17.3.3)$$

Let us take into account the observations that during solar minimum 1953–1954 the average value of sunspot number W = 9.1 and during solar maximum 1957–1958 W = 187.5. For linear dependence of Q_p on W, as was assumed by Lingenfelter (1963),

$$Q_p(W) = 2.637 - 2.971\times10^{-3}\times W \text{ atom}^{14}\text{C.cm}^{-2}.\text{sec}^{-1}. \quad (17.3.4)$$

This gives

$$Q_{pav} \approx 2.5 \text{ atom}^{14}\text{C.cm}^{-2}.\text{sec}^{-1} \quad (17.3.5)$$

for the average of about 10 solar cycles from 1844 to 1954 ($W_{av} = 47.7$).

If we approximate the magnetic field of the Earth by a dipole field and θ, φ are geomagnetic coordinates, then R_c will depend only on θ as

$$R_c(\theta,t) = R_o(\mu(t)/\mu_o)(\cos\theta)^4 \text{ GV}, \tag{17.3.6}$$

where R_o is the equatorial value of the vertical cut off rigidity at present time ($R_o \approx 14.9$ GV), $\mu(t)$ is the magnetic moment of the Earth at time t, μ_o is the present value of the Earth's magnetic moment. Let us introduce Eq. 17.2.7 into Eq. 17.3.1, taking into account Eq. 17.3.5:

$$Q_p(R_{cp},h_{op},t) = T_p^{-1}\int_{t-T_p}^{t} d\tau \int_0^{\infty} dR \int_{\Phi(R,\tau)}^{\pi/2} D_v(R,\tau)M_v(R,h_o(\theta,\tau))\cos\theta d\theta, \tag{17.3.7}$$

where

$$\Phi(R,\tau) = \begin{cases} \arccos(R/R_o\tau)^{1/4} & \text{if } 0 \le R \le R_o\tau, \\ 0 & \text{if } R > R_o\tau, \end{cases} \tag{17.3.8}$$

and

$$R_o\tau = R_o\mu(\tau)/\mu_o, \quad \mu_o = \mu(0), \quad R_o \approx 14.9\ GV. \tag{17.3.9}$$

After integrating Eq. 17.3.7 over θ taking into account Eq. 17.3.8 and 17.3.9, and that

$$\int_{\arccos x}^{\pi/2} \cos\theta d\theta = 1 - \left(1-x^2\right)^{1/2}, \tag{17.3.10}$$

we obtain

$$Q_p(\mu(t),h_{op}(t),t) = T_p^{-1}\int_{t-T_p}^{t} d\tau \int_0^{\infty} D_v(R,\tau)M_v(R,h_{op}(\tau))dR$$

$$- T_p^{-1}\int_{t-T_p}^{t} d\tau \int_0^{R_o\tau} D_v(R,\tau)M_v(R,h_{op}(\tau))\left(1-(R/R_o\tau)^{1/2}\right)^{1/2} dR. \tag{17.3.11}$$

Let us take into account that $\mu(\tau)$ and $M_v(R,h_{op}(\tau))$ are very slowly varying functions during the time period of planetary mixing $T_p \approx 1-2$ years. Therefore, we can factor these functions out of the integral over time and use them at some moment of time between $t-T_p$ and t; with a good accuracy, we can use also the average of these functions over time between $t-T_p$ and t. So, we will use the following functions:

$$D_p(R,t) = T_p^{-1}\int_{t-T_p}^{t} D_v(R,\tau)d\tau, \quad \mu_p(t) = T_p^{-1}\int_{t-T_p}^{t} \mu(\tau)d\tau,$$
$$M_p(R,h_{op}(t)) = T_p^{-1}\int_{t-T_p}^{t} M_v(R,h_{op}(\tau))d\tau. \tag{17.3.12}$$

On the basis of Eq. 17.3.12 we obtain instead of Eq. 17.3.5:

$$Q_p(\mu_p(t),h_{op}(t),t)=\int_0^\infty D_p(R,t)M_p(R,h_{op}t)\Psi(R,\mu_p(t))dR\,, \qquad (17.3.13)$$

where

$$\Psi(R,\mu_p(t))=\begin{cases}1-\left(1-(R\mu_o/R_o\mu_p(t))^{1/2}\right)^{1/2} & \text{if } R\le R_o\mu_p(t)/\mu_o\,,\\ 1 & \text{if } R>R_o\mu_p(t)/\mu_o\,.\end{cases} \qquad (17.3.14)$$

17.3.2. Time variations of planetary production rate and planetary radiocarbon coupling functions

Let us take into account that in Eq. 17.3.13 $D_p(R,t)$, $\mu_p(t)$, and $h_{op}(t)$ can change with time. Then by variation of Eq. 17.3.13 over these parameters we obtain

$$\frac{\delta Q_p(\mu_p(t),h_{op}(t),t)}{Q_{po}}=\int_0^\infty\frac{\delta D_p(R,t)}{D_{po}(R)}W_p(R,h_{op})dR+\beta_{pm}\frac{\delta\mu_p(t)}{\mu_o}+\beta_{ph}\delta h_{op}(t)\,. \qquad (17.3.15)$$

Here

$$\begin{aligned}&Q_{po}=Q_p(\mu_p(0),h_{op}(0),0),\ \ \delta Q_p(\mu_p(t),h_{op}(t),t)=Q_p(\mu_p(t),h_{op}(t),t)-Q_{po},\\ &D_{po}(R)=D_p(R,0),\ \ \delta D_p(R,t)=D_p(R,t)-D_{po}(R);\ \ \mu_{po}=\mu_p(0),\\ &\delta\mu_p(t)=\mu_p(t)-\mu_{po},\ \ h_{opo}=h_{op}(0),\ \ \delta h_{op}(t)=h_{op}(t)-h_{opo}.\end{aligned} \qquad (17.3.16)$$

In Eq. 17.3.15 we introduced the planetary coupling function for radiocarbon production rate in the Earth atmosphere:

$$W_p(R,h_{opo})=D_{po}(R)M_p(R,h_{opo})\Psi_o(R)/Q_{po}\,, \qquad (17.3.17)$$

and

$$\Psi_o(R)=\begin{cases}1-\left(1-(R/R_o)^{1/2}\right)^{1/2} & \text{if } 0\le R\le R_o\,,\\ 1 & \text{if } R>R_o\,.\end{cases} \qquad (17.3.18)$$

The part of planetary coupling function $D_{po}(R)W_p(R,h_{opo})/Q_{po}$ can be approximated by a function proportional to Eq. 17.2.19, and by taking into account Eq. 17.3.18 we obtain the analytical approximation of $W_p(R,h_{opo})$:

$$W_p(R,h_{opo})=\begin{cases}abkR^{-(k+1)}\exp\left(-aR^{-k}\right)\left[1-\left(1-(R/R_o)^{1/2}\right)^{1/2}\right] & \text{if } R\le R_o\,,\\ abkR^{-(k+1)}\exp\left(-aR^{-k}\right) & \text{if } R>R_o\,.\end{cases} \qquad (17.3.19)$$

The coefficient of proportionality b will be determined from the normalization condition

$$\int_0^\infty W_p(R, h_{opo})dR = 1, \tag{17.3.20}$$

giving

$$b = \left(1 - ak\int_0^{R_o} R^{-(k+1)} \exp\left(-aR^{-k}\right)\left(1-(R/R_o)^{1/2}\right)^{1/2} dR\right)^{-1}, \tag{17.3.21}$$

where parameters a and k were determined by Eq. 17.2.17 for solar minimum and by Eq. 17.2.18 for solar maximum. These parameters for average value of W for about 10 solar cycles from 1844 through 1954 were determined by Eq. 17.2.26.

According to Eq. 17.3.21 parameter b will be:

$$b_{\min \text{ s.a.}} = 2.1092, \quad b_{\max \text{ s.a.}} = 1.8257, \quad b_{av} = 2.0131. \tag{17.3.22}$$

Taking into account the relatively small change of parameter b, let us assume a linear dependence of b on solar activity. In this case we obtain:

$$b(\mathrm{W}) = 2.1237 - 1.589\times10^{-3}\,\mathrm{W}. \tag{17.3.23}$$

17.3.3. Planetary radiocarbon magnetic and barometric coefficients

The planetary magnetic coefficient β_{pm} will be determined through the planetary coupling function (Eq. 17.3.19):

$$\beta_{pm} = -(abk/4)\int_0^{R_o} R^{-(k+1)} \exp\left(-aR^{-k}\right)(R/R_o)^{1/2}\left(1-(R/R_o)^{1/2}\right)^{1/2} dR. \tag{17.3.24}$$

Inserting in Eq. 17.3.24 the equatorial value of the cut off rigidity $R_o = 14.9$ GV, and taking into account Eq. 17.3.21, Eq. 17.2.17 and Eq. 17.2.18, we find for solar minimum $\beta_{pm} = -1.81$ and for solar maximum $\beta_{pm} = -1.61$. It means that relative increase of the Earth's magnetic moment, for example, by 10%, will be reflected in the planetary radiocarbon production rate by a decrease of about 18% and 16% during the periods of solar activity minimum and maximum.

The planetary barometric coefficient β_{ph} can be also determined through planetary coupling function

$$\beta_{ph} = \int_0^\infty \left(\partial \ln M_p(R, h_{op})/\partial h_{op}\right) W_p(R, h_{opo})dR. \tag{17.3.25}$$

This coefficient is positive (with increasing of air pressure the number of generated radiocarbon atoms increases). This is different from the barometric coefficient for the neutron component generated by galactic CR, which is negative. On the basis of Eq.

17.3.25, taking into account Eq. 17.3.21, and the results of Lingenfelter (1963) on the expected distribution of radiocarbon production rate in the Earth's atmosphere by galactic CR in solar minimum 1953-1954 and in solar maximum 1957-1958 we determined that $\beta_{ph} \approx 1.7\times10^{-5}$ %/mb during the solar minimum and $\beta_{ph} \approx 2.2\times10^{-5}$ %/mb during the solar maximum. If we take into account that when averaged over 1–2 years (the time of planetary mixing of elements) and over all Earth's surface, the planetary pressure at the bottom of atmosphere $h_{op}(t)$ changes very little, we come to conclusion that barometric effect in radiocarbon production rate time variations is negligible. Only extraterrestrial variations caused by processes in Galaxy (local supernova explosions), in the Heliosphere (modulation of galactic CR intensity), on the Sun (generation of solar CR) and described by the first member in the left side of Eq. 17.3.15 and variations caused by the planetary change of geomagnetic field described by the second member in Eq. 17.3.15, are important.

17.3.4. On the influence of the planetary mixing of elements on the time variation of radiocarbon production rate

Let us consider the function in Eq. 17.3.11

$$F(\tau) = \int_0^\infty D_v(R,\tau) M_v\left(R, h_{op}(\tau)\right) dR - \int_0^{R_{o\tau}} D_v(R,\tau) M_v\left(R, h_{op}(\tau)\right)\left(1-(R/R_{o\tau})^{1/2}\right)^{1/2} dR, \qquad (17.3.26)$$

which determines the time variation of production rate before averaging over planetary mixing time T_p. This function can be represented by

$$F(\tau) = Q_{po}\left(1+\sum_n A_n \cos\left(\omega_n(\tau-\tau_n)\right)\right), \qquad (17.3.27)$$

where A_n is the relative amplitude of the harmonic with frequency ω_n and time of maximum τ_n. After introducing Eq. 17.3.27 into Eq. 17.3.11 we obtain

$$Q_p(t) = T_p^{-1}\int_{t-T_p}^{t} F(\tau)d\tau = Q_{po}\left(1+\sum_n \alpha_n \cos\left(\omega_n(t-\beta_n)\right)\right), \qquad (17.3.28)$$

where

$$\alpha_n = 2A_n\left(\omega_n T_p\right)^{-1}\sin\left(\omega_n T_p/2\right), \quad \beta_n = \tau_n + T_p/2., \qquad (17.3.29)$$

Thus we come to the conclusion that harmonics after planetary mixing do not change their frequency ω_n, the time maximum for all harmonics occurred later on time $T_p/2$

and amplitudes are reduced by the factor $2(\omega_n T_p)^{-1}\sin(\omega_n T_p/2)$, which is about 1 only for $\omega_n^{-1} >> T_p/2$; if $\omega_n^{-1} << T_p/2$ then the amplitude is reduced significantly ($\alpha_n/A_n << 1$). The time profile of radiocarbon production rate variation will not be changed after planetary mixing if this profile contains only low frequency harmonics with $\omega_n << (T_p/2)^{-1}$, but if it contains high frequency harmonics with $\omega_n >> (T_p/2)^{-1}$ which will be reduced very much, the time profile of radiocarbon production rate after planetary mixing will be changed considerably.

17.3.5. Situation in the case of giant solar flare event or local supernova explosion

Let us consider the case of CR burst (giant solar flare event or local supernova explosion) described by the following function $F(\tau)$ in Eq. 17.3.11:

$$F_b(\tau) = Q_{po}\left\{1 + A_b(2\pi\kappa(\tau-\tau_b))^{-3/2}\exp\left(-r_b^2/(4\kappa(\tau-\tau_b))\right)\right\}, \qquad (17.3.30)$$

where A_b is the relative amplitude of the production rate burst before planetary mixing of elements in the Earth's atmosphere, $\kappa = V\Lambda/3$ is the diffusion coefficient of CR particles with velocity V and transport path Λ in the interplanetary space (for a giant solar flare event) or in local part of Galaxy (for the local supernova explosion), τ_b is the time of burst and r_b is the distance from the Earth to the source of CR burst. After planetary elements mixing we obtain:

$$Q_p(t) = Q_{po}\begin{cases} 1 & \text{if } t \le t_b, \\ 1 + A_b\alpha_b(1 - \mathrm{erf}(x_1)) & \text{if } t_b < t < t_b + T_p, \\ 1 + A_b\alpha_b(\mathrm{erf}(x_2) - \mathrm{erf}(x_1)) & \text{if } t \ge t_b + T_p, \end{cases} \qquad (17.3.31)$$

where

$$\alpha_b = \left(2\sqrt{\pi}\kappa r_b T_p\right)^{-1}, \quad x_1 = r_b(4\kappa(t-t_b))^{-1/2}, \quad x_2 = r_b\left(4\kappa(t-t_b-T_p)\right)^{-1/2}, \qquad (17.3.32)$$

and erf(x) is the probability integral. The maximum CR burst on the Earth will be according to Eq. 17.3.30 at the moment $t_{\max} = t_b + r_b^2/4\kappa$. If $r_b^2/4\kappa << T_p$ (a giant solar flare event) then Eq. 17.3.31 turns out to be

$$Q_p(t) = Q_{po}\begin{cases} 1 & \text{if } t \le t_b, \\ 1 + A_b\left(r_b^2/4\kappa T_p\right)\left(er_b^3\right)^{-1} & \text{if } t_b < t < t_b + T_p, \\ 1 & \text{if } t \ge t_b + T_p, \end{cases} \qquad (17.3.33)$$

with very small amplitude increase of production rate (reduced by the factor $r_b^2/4\kappa T_p << 1$ after planetary mixing of elements). In the opposite case, when $T_p << r_b^2/4\kappa$ (a local supernova explosion) instead of Eq. 17.3.31 we obtain

$$Q_p(t) = Q_{po}\begin{cases}1 & \text{if } t \le t_b, \\ 1 + A_b(2\pi\kappa(t-t_b))^{-3/2}\exp\left(-x_1^2\right) & \text{if } t > t_b,\end{cases} \tag{17.3.34}$$

where x_1 was determined in Eq. 17.3.32. Eq. 17.3.34 shows that in the case of local supernova explosion the planetary mixing of elements does not influence the time profile of production rate variation (in accordance with above conclusion on planetary mixing influence on very low frequency harmonics).

17.4. Radiocarbon contents and planetary elements exchange in the frame of 2-reservoir model

17.4.1. Radiocarbon contents in dated samples

Because radiocarbon atoms ^{14}C for bio-chemical reactions are absolutely the same as carbon atoms ^{12}C, these atoms will be accumulated at time t by biological objects in the same proportionality which was in this time in the Earth's atmosphere. It is very important that there are several biological objects which can be used as dated samples for radiocarbon contents: years rings of trees, old exact dated wines, etc.. The radiocarbon contents in some dated sample $N_s(t_o)$ measured at time t_o in these samples, but dated (exposed) at time t, will be reflect the radiocarbon contents $N_A(t)$ in the atmosphere at time t according to relation

$$N_A(t) = N_s(t_o)\exp(\lambda(t-t_o)), \tag{17.4.1}$$

where λ is the decay constant of radiocarbon, and corresponds to $T_{1/2} = 5730$ years. The dated annual rings in trees are obtained by comparison of widths of rings in living trees with rings in relative to not so old trees found underground; then dated underground trees are used for dating more old trees, etc.. Now there are trees samples with annual rings dated up to about 40,000 years ago.

17.4.2. Non-stationary solution for radiocarbon contents in the framework of the 2-reservoir model of elements exchange on the Earth at any initial condition

The radiocarbon contents in the planetary mixing atmosphere will be determined by the planetary production rate of radiocarbon and exchange processes between the atmosphere and other reservoirs, which we combine into one. Let us take into account that radiocarbon is produced only in the atmosphere – in reservoir A. In the other reservoir, let us call it F (which includes oceans, biosphere and humus), the flux of CR

nuclear active particles is at least $10^3 - 10^4$ times smaller than in the atmosphere. Therefore we can neglect the radiocarbon production in the reservoir F in comparison with production in the Earth's atmosphere. For the 2-reservoir model of elements exchange on the Earth we will have the system of equations:

$$dN_A(t)/dt = Q_p(t.) - \lambda N_A(t) - \lambda_{AF} N_A(t) + \lambda_{FA} N_F(t), \tag{17.4.2}$$

$$dN_F(t)/dt = -\lambda N_F(t) - \lambda_{FA} N_F(t) + \lambda_{AF} N_A(t), \tag{17.4.3}$$

where $\lambda = \ln 2 / T_{1/2} = 1.21 \times 10^{-4}$ year^{-1} is the radioactive decay constant for ^{14}C, λ_{AF} is the probability per one year for radiocarbon atoms to pass from reservoir A to reservoir F and λ_{FA} is the probability to pass in the opposite direction.

The solution of this system with initial conditions

$$N_A(t=0) = N_{Ao}, \quad N_F(t=0) = N_{Fo} \tag{17.4.4}$$

is

$$N_A(t) = \exp(-\lambda t)\left[\frac{\lambda_{FA}}{\lambda_{AF} + \lambda_{FA}} \int_0^t \exp(\lambda\tau) Q_p(\tau) d\tau + \frac{\lambda_{FA}(N_{Ao} + N_{Fo})}{\lambda_{AF} + \lambda_{FA}}\right]$$

$$+ \exp(-(\lambda + \lambda_{AF} + \lambda_{FA})t)$$

$$\times\left[\frac{\lambda_{AF}}{\lambda_{AF} + \lambda_{FA}} \times \int_0^t \exp((\lambda + \lambda_{AF} + \lambda_{FA})\tau) Q_p(\tau) d\tau + \frac{\lambda_{AF} N_{Ao} - \lambda_{FA} N_{Fo}}{\lambda_{AF} + \lambda_{FA}}\right], \tag{17.4.5}$$

$$N_F(t) = \exp(-\lambda t)\left[\frac{\lambda_{AF}}{\lambda_{AF} + \lambda_{FA}} \int_0^t \exp(\lambda\tau) Q_p(\tau) d\tau + \frac{\lambda_{AF}(N_{Ao} + N_{Fo})}{\lambda_{AF} + \lambda_{FA}}\right]$$

$$- \exp(-(\lambda + \lambda_{AF} + \lambda_{FA})t)$$

$$\times\left[\frac{\lambda_{AF}}{\lambda_{AF} + \lambda_{FA}} \times \int_0^t \exp((\lambda + \lambda_{AF} + \lambda_{FA})\tau) Q_p(\tau) d\tau + \frac{\lambda_{AF} N_{Ao} - \lambda_{FA} N_{Fo}}{\lambda_{AF} + \lambda_{FA}}\right]. \tag{17.4.6}$$

17.4.3. Solution for the total contents of radiocarbon on the Earth

Let us consider the total contents of radiocarbon on the Earth:

$$N(t) = N_A(t) + N_B(t). \tag{17.4.7}$$

The equation for $N(t)$ follows from Eq. 17.4.2 and Eq. 17.4.3:

$$dN(t)/dt = Q_p(t) - \lambda N(t) \tag{17.4.8}$$

with the solution at initial condition $N(t=0) = N_o$:

$$N(t) = \exp(-\lambda t)\left[\int_0^t \exp(\lambda\tau) Q_p(\tau) d\tau + N_o\right]. \tag{17.4.9}$$

Let us assume that after $t = 0$, $Q_p(t) = \text{const} = Q_{po}$, then from Eq. 17.4.9 we obtain

$$N(t) = Q_{po}/\lambda + (N_o - Q_{po}/\lambda)\exp(-\lambda t), \tag{17.4.10}$$

which gives for $t >> \lambda^{-1}$ the stationary value

$$N_{\text{st}} = Q_{po}/\lambda . \tag{17.4.11}$$

If we use the value of $Q_{av} = 2.495$ atom ^{14}C.cm^{-2}.sec^{-1} obtained in Section 10.3.1 by averaging over about 10 solar cycles as stationary value of Q_{po}, we obtain from Eq. 17.4.11:

$$N_{\text{st}} = 6.186 \times 10^{11} \text{ atom } ^{14}\text{C.cm}^{-2} . \tag{17.4.12}$$

17.4.4. Steady state solution for radiocarbon contents in both reservoirs on the Earth; relation between probabilities of elements exchange

The system of steady state equations for radiocarbon contents follows from Eq. 17.4.2 and Eq. 17.4.3 at $d/dt = 0$:

$$Q_{av} - \lambda N_A - \lambda_{AF} N_A + \lambda_{FA} N_F = 0; \qquad -\lambda N_F - \lambda_{FA} N_F + \lambda_{AF} N_A = 0 . \tag{17.4.13}$$

The solution of this system will be

$$N_{A\text{st}} = Q_{av}(\lambda + \lambda_{FA})(\lambda(\lambda + \lambda_{AF} + \lambda_{FA}))^{-1}, \tag{17.4.15}$$

$$N_{F\text{st}} = Q_{av}\lambda_{AF}(\lambda(\lambda + \lambda_{AF} + \lambda_{FA}))^{-1} . \tag{17.4.16}$$

According to data reviewed in Kocharov et al. (1972),

$$N_{A\text{st}} = 7.5 \times 10^{9} \text{ atom } ^{14}\text{C.cm}^{-2} . \tag{17.4.17}$$

Then, taking into account Eq. 17.4.12 we obtain

$$N_{Fst} = 6.11 \times 10^{11} \text{ atom } {}^{14}\text{C.cm}^{-2}. \qquad (17.4.18)$$

The relation between λ_{AF} and λ_{FA} can be obtained by comparison of Eq. 17.4.15 and Eq. 17.4.16:

$$\lambda_{AF} = (N_{Fst}/N_{Ast})(\lambda + \lambda_{FA}) = 9.86 \times 10^{-3} + 81.5 \times \lambda_{FA}. \qquad (17.4.19)$$

17.4.5. Non-stationary solution at initial condition of stationary contents

In many cases time variations of radiocarbon contents are realized with the initial condition of stationary contents in both reservoirs. Let us use the stationary solutions described by Eq. 17.4.15 and Eq. 17.4.16 as initial conditions for the system Eq. 17.4.5 and Eq. 17.4.6. In this case the solution of this system of equations will be

$$N_A(t) = \frac{\lambda_{FA}}{\lambda_{AF} + \lambda_{FA}} \exp(-\lambda t)\left[\int_0^t \exp(\lambda\tau) Q_p(\tau) d\tau + Q_{av}/\lambda\right] + \frac{\lambda_{AF}}{\lambda_{AF} + \lambda_{FA}} \exp(-\lambda_1 t)\left[\int_0^t \exp(\lambda_1\tau) Q_p(\tau) d\tau + Q_{av}/\lambda_1\right], \qquad (17.4.20)$$

$$N_F(t) = \frac{\lambda_{AF}}{\lambda_{AF} + \lambda_{FA}} \exp(-\lambda t)\left[\int_0^t \exp(\lambda\tau) Q_p(\tau) d\tau + Q_{av}/\lambda\right] + \frac{\lambda_{AF}}{\lambda_{AF} + \lambda_{FA}} \exp(-\lambda_1 t)\left[\int_0^t \exp(\lambda_1\tau) Q_p(\tau) d\tau + Q_{av}/\lambda_1\right], \qquad (17.4.21)$$

where we designate $\lambda_1 = \lambda + \lambda_{AF} + \lambda_{FA}$.

17.5. H-bomb explosions, generation of radiocarbon, and estimation of parameters of the elements exchange model; influence on global environment

17.5.1. The reflection in radiocarbon production rate of H-bomb explosions taking into account vertical and planetary mixing

Let us suppose that at $t < t_o$ and at $t > t_o + \Delta t$ we had stationary values of radiocarbon production rate, but in the period between these time moments there was a sudden increase described by the function described by Eq. 17.3.26 in the form:

$$F(t) = \begin{cases} Q_{av} & \text{if } t < t_o, \\ Q_{av}(1 + A) & \text{if } t_o \le t < t_o + \Delta t, \\ Q_{av} & \text{if } t > t_o + \Delta t. \end{cases} \qquad (17.5.1)$$

First we must take into account the planetary mixing of elements with characteristic time T_p and because $T_p \geq T_v$ it will include also the vertical mixing.

Let us consider two cases.

In the **first case** $\Delta t \leq T_p$ and by introducing Eq. 17.5.1 into Eq. 17.3.11 we obtain

$$Q_p(t)=\begin{cases} Q_{av} & \text{if } t<t_o, \\ Q_{av}\left(1+A(t-t_o)/T_p\right) & \text{if } t_o \leq t<t_o+\Delta t, \\ Q_{av}\left(1+A\Delta t/T_p\right) & \text{if } t_o+T_p \leq t<t_o+\Delta t+T_p, \\ Q_{av} & \text{if } t>t_o+\Delta t+T_p. \end{cases} \tag{17.5.2}$$

In the **second case** $\Delta t \geq T_p$ and by introducing Eq. 17.5.1 into Eq. 17.3.11 we obtain:

$$Q_p(t)=\begin{cases} Q_{av} & \text{if } t<t_o, \\ Q_{av}\left(1+A(t-t_o)/T_p\right) & \text{if } t_o \leq t<t_o+T_p, \\ Q_{av}(1+A) & \text{if } t_o+T_p \leq t<t_o+\Delta t, \\ Q_{av}\left(1+A\left(t_o+\Delta t+T_p-t\right)/T_p\right) & \text{if } t_o+\Delta t \leq t<t_o+\Delta t+T_p, \\ Q_{av} & \text{if } t>t_o+\Delta t+T_p. \end{cases} \tag{17.5.3}$$

17.5.2. The H-bomb explosions effect in radiocarbon contents taking into account elements exchange between planetary reservoirs

Let us take into account the exchange of elements on the Earth according to Eq. 17.4.20 and Eq. 17.4.21. These equations include exponents with characteristic times λ^{-1} and $\lambda_1^{-1}=(\lambda+\lambda_{AF}+\lambda_{FA})^{-1}$. Because the time of production rate burst Δt and characteristic time of planetary mixing T_p are very small in comparison with λ^{-1} and $\lambda_1^{-1}=(\lambda+\lambda_{AF}+\lambda_{FA})^{-1}$, in the first approximation we can replace functions described by Eq. 17.5.3 and 17.5.4 by δ function:

$$Q_p(t)=Q_{av}(1+A\Delta t\delta(t-t_o)). \tag{17.5.4}$$

By substituting Eq. 17.5.4 in Eq. 17.4.20 and Eq. 17.4.21, we obtain

$$N_A(t)=N_{Ast}\left[1+\frac{\lambda\lambda_1 A\Delta t\exp(-\lambda(t-t_o))}{\lambda_2(\lambda+\lambda_{FA})}\left(\lambda_{AF}\exp(-\lambda_2(t-t_o))+\lambda_{FA}\right)\right], \tag{17.5.5}$$

$$N_F(t)=N_{Fst}\left[1+\frac{\lambda_1 A\Delta t\exp(-\lambda(t-t_o))}{\lambda_2}\left(1-\exp(-\lambda_1(t-t_o))\right)\right], \tag{17.5.6}$$

where $\lambda_1 = \lambda + \lambda_{AF} + \lambda_{FA}$ and $\lambda_2 = \lambda_{AF} + \lambda_{FA}$.

The maximum of radiocarbon content in the atmosphere according to Eq. 17.5.5 will be at $t = t_o$ and we determine it by taking into account value for $N_{A\mathrm{st}}$ (Eq. 17.4.12) and the value of $N_{A\mathrm{st}}$ (Eq. 17.4.17):

$$N_{A\max} = N_{A\mathrm{st}}\left(1 + \lambda A \Delta t\left(N_{\mathrm{st}}/N_{A\mathrm{st}}\right)\right) = N_{A\mathrm{st}}\left(1 + 9.98\times10^{-3} A\Delta t\right). \qquad (17.5.7)$$

17.5.3. Application to USSR and USA H-bomb explosions in 1962; estimation of total radiocarbon production

In Fig. 17.5.1 are shown recent results of Muraki et al. (1998), and Kato et al. (2001) from the tree that was cut down in 1994 on the effect in radiocarbon of H- bomb explosions in 1962.

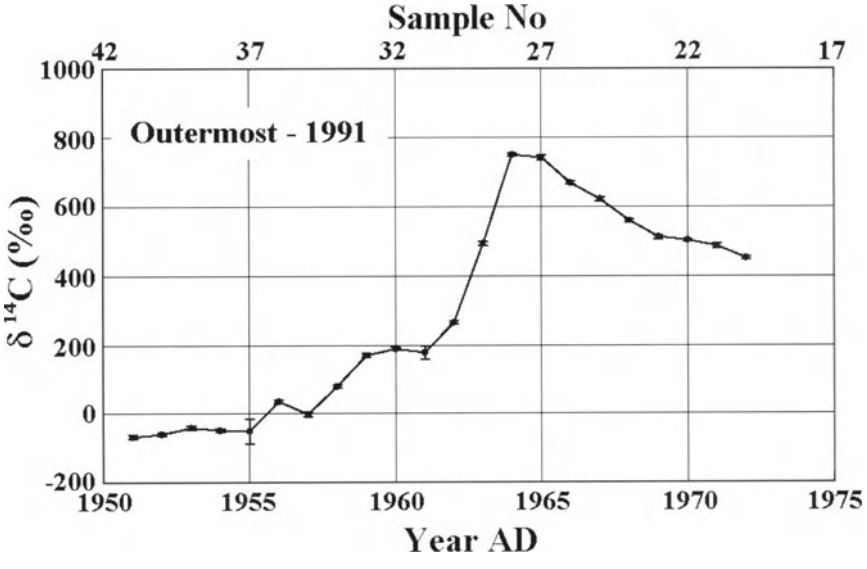

Fig. 17.5.1. H-bomb effect in radiocarbon contents in cedar tree grown in Yaku Island (30°18'N, 130°30'E), which was cut down in 1994 (according to Kato et al., 2001).

Comparison of Eq. 17.5.5-17.5.7 with these results and with experimental data of Wilkom and Erlenkenser (1968), Kolesnikov et al. (1970) on the radiocarbon contents in annual rings of trees before, during and after 1962 (H-bomb testing was started at the end of the 1950s, but the great maximum was in 1962, and after this year H-bomb testing in the atmosphere was stopped) gives

$$9.98\times10^{-3} A\Delta t \approx 0.9, \qquad (17.5.8)$$

which gives for $\Delta t = 1$ year, A = 90.2. It means that in the period of extensive testing of hydrogen H-bombs in the atmosphere in 1962 by USSR and USA, additional

6.83×10^{9} atom ^{14}C.cm^{-2} were produced, in comparison with 7.48×10^{7} atom ^{14}C.cm^{-2} owed to galactic CR. The total additional produced radiocarbon atoms in this year was about 3.5×10^{28} atom ^{14}C; if about 1% of explosion energy was going to neutrons with an energy of about few MeV, we can estimate from this that in 1962 the total TNT equivalent of all H-bomb explosions was about 240 million tons.

17.5.4. H-bomb explosions and parameters of 2-reservoir model of planetary exchange of elements on the Earth

Let us examine now the time dependence of the ^{14}C content in the annual rings of trees after 1962. Let us substitute Eq. 17.5.7 and the result for $A\Delta t$ obtained above (Eq. 17.5.8) in Eq. 17.5.5. Then by comparing with experimental data of Wilkom and Erlenkenser (1968) and Kolesnikov et al. (1970) we find that

$$\lambda_1 = \lambda + \lambda_{AF} + \lambda_{FA} = 0.147 \text{ year}^{-1}. \tag{17.5.9}$$

Taking into account Eq. 17.4.19 and that $\lambda = 1.21\times10^{-4}$ year^{-1} we obtain from Eq. 17.5.9:

$$\lambda_{AF} = 0.145 \text{ year}^{-1}, \quad \lambda_{FA} = 1.66\times10^{-3} \text{ year}^{-1}. \tag{17.5.10}$$

For the characteristic times of elements exchange we obtain

$$T_{AF} = \lambda_{AF}^{-1} = 6.89 \text{ years}, \quad T_{FA} = \lambda_{FA}^{-1} = 602 \text{ years}. \tag{17.5.11}$$

17.5.5. Expected time variation of radiocarbon contents in atmosphere and in ocean owing to H-bomb explosions

On the basis of Eq. 17.5.6 we can estimate the expected time of maximum and value of maximum of radiocarbon contents in the reservoir F owed to hydrogen bomb explosions:

$$t_{\max F} = t_o + \lambda_1^{-1} \ln\left[(\lambda + \lambda_1)/\lambda\right], \tag{17.5.12}$$

$$N_{F\max} = N_{Fst}\left[1 + A\Delta t\lambda_1^2\left(\lambda_1^2 - \lambda^2\right)^{-1}\left(1 - \left(\lambda(\lambda+\lambda_1)^{-1}\right)^{\lambda/\lambda_1}\right)\right], \tag{17.5.13}$$

where $\lambda_1 = \lambda + \lambda_{AF} + \lambda_{FA}$. By using Eq. 17.5.11, we obtain from Eq. 17.5.12 and Eq. 17.5.13 that

$$t_{\max F} = t_o + 48.3 \text{ years} = 2010.3 \text{ years}, \tag{17.5.14}$$

$$N_{F\max} = N_{Fst}\left(1 + 5.31\times10^{-3} A\Delta t\right) = N_{Fst}(1 + 0.479), \tag{17.5.15}$$

The results, described by Eq. 17.5.14 and Eq. 17.5.15, show that the influence of hydrogen bomb explosions in 1962 on the reservoir F until now is very large and will be important for a long time also after the maximum in 2010.3 because it will decrease very slowly, according to Eq. 17.5.6 as $\propto \exp(-\lambda(t-t_o))$ caused by radiocarbon decay.

Expected time variations of radiocarbon contents in the reservoirs A and F due to hydrogen bomb explosions in 1962, and described by Eq. 17.5.5 and Eq. 17.5.6 (with taking into account Eq. 17.5.10) are shown in Fig. 17.5.2.

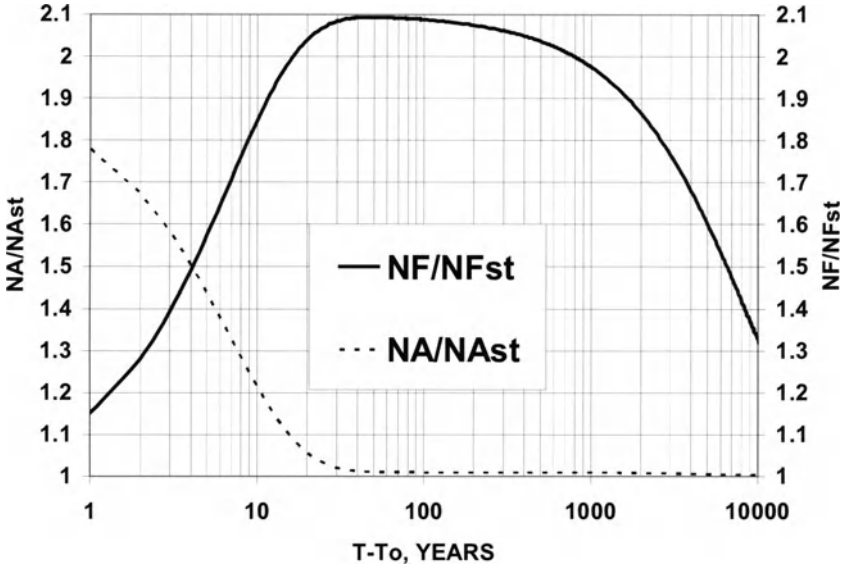

Fig. 17.5.2. Expected radiocarbon contents time variation caused by H-bomb explosions in T_0 = 1962 in the reservoir A (atmosphere, left scale) and in the reservoir F (mostly deep ocean, right scale).

From Fig. 17.5.2 it can be seen that now, about 40 years after the H-bomb explosions in 1962, the effect in the atmosphere is negligible, but in the reservoir F (mostly the deep ocean) the effect is significant (the radiocarbon contents increased by about two times in comparison with the stationary level). Let us note that in the reservoir F the effect from the H-bomb explosions in 1962 will remain considerable for more than 1000 years.

17.6. The reflection of CR cyclic modulation in radiocarbon content in the framework of the 2-reservoir model of elements planetary exchange on the Earth

17.6.1. General solution for the planetary reservoir A

Let us suppose that CR intensity is modulated in the form of several cycles (27 days, 1 year, 11 years, 22 years, and others) according to Eq. 17.3.27 from $t=-\infty$ to the present time t. After taking into account the vertical and planetary mixing of elements, the planetary radiocarbon production rate should be described by Eq. 17.3.28. Let us substitute Eq. 17.3.28 in the general solution described by Eq. 17.4.18 for radiocarbon

contents in the atmosphere, taking into account the planetary exchange of elements. After integrating we obtain:

$$N_A(t) = N_{Ast}\left(1 + \sum_n A_n \beta_n \cos(\omega_n(t - \gamma_n))\right), \tag{17.6.1}$$

where

$$\beta_n = \frac{2\lambda\lambda_1}{\omega_n T_p(\lambda + \lambda_{FA})}\left(\frac{(\lambda + \lambda_{FA})^2 + \omega_n^2}{(\lambda^2 + \omega_n^2)(\lambda_1^2 + \omega_n^2)}\right)^{1/2} \times \begin{cases} \sin(\omega_n T_p/2) & \text{if } \omega_n T_p \le \pi, \\ 1 & \text{if } \omega_n T_p > \pi, \end{cases} \tag{17.6.2}$$

$$\gamma_n = \frac{T_p}{2} + \omega_n^{-1} \arctan\left(\frac{\omega_n(\omega_n^2 + \lambda(\lambda + \lambda_{FA}) + \lambda_{FA}\lambda_1)}{\omega_n^2(\lambda + \lambda_{AF}) + \lambda\lambda_1(\lambda + \lambda_{FA})}\right), \tag{17.6.3}$$

with $\lambda_1 = \lambda + \lambda_{AF} + \lambda_{FA}$.

17.6.2. Very long-term and very short-term cyclic modulation of radiocarbon content in the atmosphere

Let us consider very long term variation in the production rate characterized with $\omega_n << \lambda$ (and in this case also $\omega_n << T_p^{-1}$, and $\omega_n << \lambda_1$). Then β_n and γ_n will not depend on ω_n and we obtain

$$\beta_n \approx 1, \quad \text{and} \quad \gamma_n \approx \frac{T_p}{2} + \frac{\lambda(\lambda + \lambda_{FA}) + \lambda_{FA}\lambda_1}{\lambda\lambda_1(\lambda + \lambda_{FA})} \approx \frac{T_p}{2} + 7710 \text{ years}, \tag{17.6.4}$$

where we have used values of $\lambda_1, \lambda_{AF}, \lambda_{FA}$ determined by Eq. 17.5.9 and Eq. 17.5.10. This result shows that in this case the cyclic variations in content after mixing and exchange processes will have about the same relative amplitude as in production rate. The relative delay in phase is also very small compared to the period T_n of production rate modulation ($T_n = 2\pi/\omega_n >> \ln 2/\lambda = 5730$ years).

In the opposite case of very short-term variations when $\omega_n >> \lambda_1$ (and in this case $\omega_n >> \lambda$ also), we obtain

$$\beta_n \approx \frac{2\lambda\lambda_1}{\omega_n^2 T_p(\lambda + \lambda_{FA})} \times \begin{cases} \sin(\omega_n T_p/2) & \text{if } \omega_n T_p \le \pi, \\ 1 & \text{if } \omega_n T_p > \pi, \end{cases} \tag{17.6.5}$$

$$\gamma_n = \frac{T_p}{2} + \omega_n^{-1} \arctan\left(\frac{\omega_n}{(\lambda + \lambda_{AF})}\right). \tag{17.6.6}$$

Because $\sin(\omega_n T_p/2) \le 1$, value $\beta_n << 1$. On the other hand, $\omega_n/(\lambda + \lambda_{AF}) >> 1$, but $\arctan(\omega_n/(\lambda + \lambda_{AF})) \le \pi/2$, so in this case $T_p/2 \le \gamma_n \le T_p/2 + \pi/2\omega_n$.

17.6.3. Amplitude reduction and time lag in cyclic variation of radiocarbon content in the atmosphere as a function of CR modulation frequency

In Table 17.6.1 are listed the values of β_n and γ_n for different values of $T_n = 2\pi/\omega_n$, expected according to Eq. 17.6.2 and 17.6.3 (including solar activity cycle with $T_n = 11$ years and solar magnetic cycle with $T_n = 22$ years). We assumed that $T_p \approx 1.5$ years and used parameters of elements exchange from Eq. 17.5.9 and 17.5.10.

Table 17.6.1. Expected values of β_n and γ_n as a function of T_n.

T_n years	β_n	γ_n
0.1	8.06×10^{-8}	0.775
1	3.40×10^{-4}	0.996
2	9.55×10^{-4}	1.236
11	1.64×10^{-2}	3.065
22	3.08×10^{-2}	4.607
10^2	6.24×10^{-2}	7.60
10^3	7.05×10^{-2}	48.6
10^4	0.201	1666
10^5	0.888	7070

Table 17.6.1 shows that the planetary mixing and exchange of elements significantly reduces the amplitude of cyclic variations: 27 day CR variation (period about 0.1 year) in radiocarbon will be reduced by a factor of 1.24×10^7, annual variation by 2941, 2 year variation by 1047, 11 year (solar activity cycle) CR modulation by 61, and 22 year (solar magnetic cycle) modulation by 32.4. The possible very long change in radiocarbon production rate caused by variations of geomagnetic field and by modulation of galactic CR in the Heliosphere will be reduced much less: for 10^2 years period by about a factor of 16, for 10^3 years period by 14.2, for 10^4 years period by 5.0, and for 10^5 years period by 1.13. It is necessary to take into account the expected amplitude of radiocarbon planetary production rate that is not the same as that observed by ground neutron monitors, but much bigger (owing to the large difference in coupling functions). For 11 year variation according to Table 17.6.1 the expected time delay relative to production rate will be about 3 years.

17.6.4. Reflection of CR cyclic modulation in radiocarbon content in reservoir F

Let us consider the situation in reservoir *F*. For this case we substitute Eq. 17.3.28 in the general solution described by Eq. 17.4.19 for radiocarbon content in the reservoir *F*, taking into account the planetary exchange of elements. After integrating we obtain:

$$N_F(t) = N_{F\mathrm{st}}\left(1 + \sum_n A_n \eta_n \cos(\omega_n(t - \varphi_n))\right), \tag{17.6.7}$$

where

$$\beta_n = \frac{2\lambda\lambda_1\left(\eta_{n1}^2 + \eta_{n2}^2\right)^{1/2}}{\omega_n T_p(\lambda + \lambda_{FA})\left(\lambda^2 + \omega_n^2\right)\left(\lambda_1^2 + \omega_n^2\right)} \times \begin{cases} \sin(\omega_n T_p/2) & \text{if } \omega_n T_p \le \pi, \\ 1 & \text{if } \omega_n T_p > \pi, \end{cases} \tag{17.6.8}$$

$$\varphi_n = \frac{T_p}{2} + \omega_n^{-1} \arctan(\eta_{n2}/\eta_{n1}). \tag{17.6.9}$$

In Eq. 17.6.8–17.6.9 $\lambda_1 = \lambda + \lambda_{AF} + \lambda_{FA}$ and

$$\eta_{n1} = \lambda\left(\lambda_1^2 + \omega_n^2\right) - \lambda_1\left(\lambda^2 + \omega_n^2\right); \quad \eta_{n2} = \omega_n\left(\lambda_1^2 - \lambda^2\right). \tag{17.6.10}$$

17.7. The reflection of CR burst from local supernova explosion in radiocarbon content in the framework of the 2-reservoir model of elements exchange

Let us suppose that a local supernova explosion occurred at time t_{sn} at a distance r_{sn} from the Sun and that the diffusion coefficient for CR particles in the local interstellar space is κ. Before the supernova explosion we assume a stationary solution with

$$N_A(t) = N_{A\mathrm{st}} \text{ and } N_F(t) = N_{F\mathrm{st}} \text{ at } t < t_{sn}, \tag{17.7.1}$$

described by Eq. 17.4.15 and Eq. 17.4.16. Let us assume that $r_{sn}^2/\kappa >> T_p$ (e.g., if $\kappa \approx 10^{29}$ cm^2/sec, we have $r_{sn}^2/\kappa \ge 80$ years $>> T_p$ for $r_{sn} \ge 10$ pc). In this case the CR burst from the local supernova explosion will be reflected in the radiocarbon production rate after vertical and planetary mixing by Eq. 17.3.34. After introducing Eq. 17.3.34 in the general solution Eq. 17.4.20 for the radiocarbon content in the atmosphere (reservoir *A*) and in Eq. 17.4.21 (reservoir *F*) we obtain for $t \ge t_{sn}$:

$$N_A(t) = \frac{\lambda_{FA}}{\lambda_{AF} + \lambda_{FA}} \exp(-\lambda t)\left[\int_{t_{sn}}^{t} [1 + A_{sn} f(\tau)] \exp(\lambda\tau) d\tau + Q_{av}/\lambda\right]$$

$$+ \frac{\lambda_{AF}}{\lambda_{AF} + \lambda_{FA}} \exp(-\lambda_1 t)\left[\int_{t_{sn}}^{t} [1 + A_{sn} f(\tau)] \exp(\lambda_1\tau) d\tau + Q_{av}/\lambda_1\right], \tag{17.7.2}$$

$$N_F(t)=\frac{\lambda_{AF}}{\lambda_{AF}+\lambda_{FA}}\exp(-\lambda t)\left[\int_{t_{sn}}^{t}[1+A_{sn}f(\tau)]\exp(\lambda\tau)d\tau+Q_{av}/\lambda\right]$$

$$-\frac{\lambda_{AF}}{\lambda_{AF}+\lambda_{FA}}\exp(-\lambda_1 t)\left[\int_{t_{sn}}^{t}[1+A_{sn}f(\tau)]\exp(\lambda_1\tau)d\tau+Q_{av}/\lambda_1\right], \qquad (17.7.3)$$

where

$$f(\tau)=(2\pi\kappa(\tau-t_{sn}))^{-3/2}\exp\left(-r_{sn}^2/4\kappa(\tau-t_{sn})\right). \qquad (17.7.4)$$

As a first approximation let us insert $\delta(\tau-t_{sn})$ instead of the function $f(\tau)$ described by Eq. 17.7.4; then we obtain:

$$N_A(t)=N_{Ast}\left[1+A_{sn}\alpha_1\exp(-\lambda(t-t_{sn}))\left(1+\frac{\lambda_{AF}}{\lambda_{FA}}\exp(-(\lambda_{AF}+\lambda_{FA})(t-t_{sn}))\right)\right], \qquad (17.7.5)$$

$$N_F(t)=N_{Fst}[1+A_{sn}\alpha_2\exp(-\lambda(t-t_{sn}))(1-\exp(-(\lambda_{AF}+\lambda_{FA})(t-t_{sn})))], \qquad (17.7.6)$$

where

$$\alpha_1=\frac{\lambda\lambda_{FA}\lambda_1}{(\lambda_{AF}+\lambda_{FA})(\lambda_1+\lambda_{FA})},\quad \alpha_2=\frac{\lambda\lambda_1}{\lambda_{AF}+\lambda_{FA}}. \qquad (17.7.7)$$

17.8. Radiocarbon content in dated samples and planetary elements exchange in the framework of the 5-reservoir model

17.8.1. The basic equations for the 5-reservoir model

In accordance with the analysis carried out in Kocharov et al. (1972) and Dorman (1977f,g), the most reliable model of the radiocarbon exchange on the Earth is the 5-reservoir model proposed by Craig (1957). It includes: **reservoir *A*** – the atmosphere with radiocarbon production by CR and by vertical and planetary mixing as was considered in Sections 17.1–17.3; **reservoir *B*** – the biosphere which is located mostly at the bottom of atmosphere and where the radiocarbon production rate is negligible; **reservoir *H*** – the humus which is also located at the bottom of atmosphere and where the radiocarbon production rate is also negligible; **reservoir *M*** – mixed oceanic level (the highest 80–100 m of oceans); and **reservoir *O*** – deep oceanic layer (deeper than 80–100 m). If we take into account planetary elements exchange with corresponding probabilities λ_{ik} from reservoir i to reservoir k, and that radiocarbon is produced only in reservoir A, we obtain the following set of equations that determines the time dependence of the radiocarbon content in the above mentioned five planetary reservoirs:

$$dN_A(t)/dt = Q_p(t) - (\lambda + \lambda_{AM} + \lambda_{AB})N_A(t) + \lambda_{HA}N_H(t) + \lambda_{MA}N_M(t), \quad (17.8.1)$$

$$dN_B(t)/dt = -(\lambda + \lambda_{BH})N_B(t) + \lambda_{AB}N_A(t), \quad (17.8.2)$$

$$dN_H(t)/dt = -(\lambda + \lambda_{HA})N_H(t) + \lambda_{BH}N_B(t), \quad (17.8.3)$$

$$dN_M(t)/dt = -(\lambda + \lambda_{MO} + \lambda_{MA})N_M(t) + \lambda_{AM}N_A(t), \quad (17.8.4)$$

$$dN_O(t)/dt = -(\lambda + \lambda_{OM})N_O(t) + \lambda_{MO}N_M(t). \quad (17.8.5)$$

17.8.2. The solution for the total radiocarbon content on the Earth

Let us sum up Eq. 17.8.1–17.8.5. We then obtain

$$dN_p(t)/dt = Q_p(t) - \lambda N_p(t), \quad (17.8.6)$$

where

$$N_p(t) = N_A(t) + N_B(t) + N_H(t) + N_M(t) + N_O(t) \quad (17.8.7)$$

is the total planetary radiocarbon content on the Earth. Let us suppose that $N_p(t=0) = N_{pst}$, then the solution of Eq. 17.8.6 will be

$$N_p(t) = \exp(-\lambda t)\left[\int_0^t Q_p(\tau)\exp(\lambda\tau)d\tau + Q_p/\lambda\right], \quad (17.8.8)$$

where Q_p is the average value of radiocarbon production rate. The stationary solution of Eq. 17.8.6 at $dN_p(t)/dt = 0$ will be

$$N_{pst} = Q_p/\lambda. \quad (17.8.9)$$

By using for Q_p the value $Q_p = 2.495$ atom ^{14}C.cm^{-2}.sec^{-1} obtained in Section 17.3 for average planetary radiocarbon production rate, taking into account vertical and planetary mixing, and averaging over many solar cycles, we obtain for N_{pst}:

$$N_{pst} = 6.186\times10^{11} \text{ atom } ^{14}\text{C.cm}^{-2}, , \quad (17.8.10)$$

the same value as for the two-reservoir model of planetary elements mixing on the Earth, according to Eq. 17.4.12.

17.8.3. The steady state solution for the 5-reservoir model and estimation of the probabilities of the planetary exchange of elements

Let us suppose that in Eq. 17.8.1–17.8.5 all $d/dt = 0$ and $Q_p(t) = Q_p = \text{const}$, then we obtain the stationary solution:

$$N_{A\text{st}} = D^{-1}Q_p(\lambda + \lambda_{BH})(\lambda + \lambda_{HA})[\lambda(\lambda + \lambda_{MA} + \lambda_{OM}) + \lambda_{OM}(\lambda + \lambda_{MA})], \quad (17.8.11)$$

$$N_{B\text{st}} = D^{-1}Q_p\lambda_{AB}(\lambda + \lambda_{HA})[\lambda(\lambda + \lambda_{MA} + \lambda_{OM}) + \lambda_{OM}(\lambda + \lambda_{MA})], \quad (17.8.12)$$

$$N_{H\text{st}} = D^{-1}Q_p\lambda_{AB}\lambda_{BH}(\lambda + \lambda_{HA})[\lambda(\lambda + \lambda_{MA} + \lambda_{OM}) + \lambda_{OM}(\lambda + \lambda_{MA})], \quad (17.8.13)$$

$$N_{M\text{st}} = D^{-1}Q_p\lambda_{AM}(\lambda + \lambda_{BH})(\lambda + \lambda_{HA})(\lambda + \lambda_{OM}), \quad (17.8.14)$$

$$N_{O\text{st}} = D^{-1}Q_p\lambda_{AM}\lambda_{MO}(\lambda + \lambda_{BH})(\lambda + \lambda_{HA}), \quad (17.8.15)$$

where

$$D = [(\lambda + \lambda_{AB} + \lambda_{AM})(\lambda + \lambda_{BH})(\lambda + \lambda_{HA}) - \lambda_{AB}\lambda_{BH}\lambda_{HA}][\lambda_{OM}(\lambda + \lambda_{MA}) + \lambda(\lambda + \lambda_{MA} + \lambda_{OM})] - \lambda_{AM}\lambda_{MA}(\lambda + \lambda_{BH})(\lambda + \lambda_{HA})(\lambda + \lambda_{OM}). \quad (17.8.16)$$

Let us take into account the results of average radiocarbon content measurements in the planetary reservoirs (in units $\text{atom}^{14}\text{C.cm}^{-2}$) described in Craig (1957) and in Kocharov et al.(1972):

$$N_{A\text{st}} = 7.5\times10^9, \quad N_{B\text{st}} = 3.8\times10^9, \quad N_{H\text{st}} = 12.4\times10^9,$$
$$N_{M\text{st}} = 8.8\times10^9, \quad N_{O\text{st}} = 5.86\times10^{11}\ \text{atom}^{14}\text{C.cm}^{-2}. \quad (17.8.17)$$

In Eq. 17.8.17 we changed only the value of $N_{O\text{st}}$ in accordance with Eq. 17.8.10 because experimentally $N_{O\text{st}}$ was determined with the largest relative errors. Now we can consider the problem of estimation of the probabilities of the planetary exchange of elements on the basis of Eq. 17.8.11–17.8.17. According to Craig (1957) and Kocharov et al. (1972) more exact determinations are

$$\lambda_{AB} \approx 3.33\times10^{-2}\ \text{year}^{-1} \quad (17.8.18)$$

(corresponding to $T_{AB} \approx 30$ years) and

$$\lambda_{AM} \approx 0.143\ \text{year}^{-1} \quad (17.8.19)$$

(corresponding to $T_{AM} \approx 7$ years, in accordance with Eq. 17.5.11 of determining T_{AF} from the H–bomb test data in the frame of the two-reservoir planetary exchange model). From these experimental data we determine also

$$\lambda_{OM} \approx 1.667 \times 10^{-3} \text{ year}^{-1} \tag{17.8.20}$$

($T_{OM} \approx 600$ years), which corresponds approximately to λ_{FA} and T_{FA} according to Eq. 17.5.11. From Eq. 17.8.11 and 17.8.12 it follows that the ratio

$$\beta_{AB} = N_{A\text{st}}/N_{B\text{st}} = (\lambda + \lambda_{BH})/\lambda_{AB} = 1.97\,, \tag{17.8.21}$$

from which we determine

$$\lambda_{BH} = \beta_{AB}\lambda_{AB} - \lambda = 6.55 \times 10^{-2} \text{ year}^{-1}. \tag{17.8.22}$$

This corresponds to $T_{BH} = 15.3$ years. Similarly, from Eq. 17.8.12 and 17.8.13 follows that the ratio

$$\beta_{BH} = N_{B\text{st}}/N_{H\text{st}} = (\lambda + \lambda_{HA})/\lambda_{BH} = 0.306\,, \tag{17.8.23}$$

and we find

$$\lambda_{HA} = \beta_{BH}\lambda_{BH} - \lambda = 1.922 \times 10^{-2} \text{ year}^{-1}\,, \tag{17.8.24}$$

corresponding to $T_{HA} = 50.2$ years. From Eq. 17.8.14 and 17.8.15 we find

$$\beta_{MO} = N_{M\text{st}}/N_{O\text{st}} = (\lambda + \lambda_{OM})/\lambda_{MO} = 1.502 \times 10^{-2}\,, \tag{17.8.25}$$

from which follows

$$\lambda_{MO} = (\lambda + \lambda_{OM})/\beta_{MO} = 0.119 \text{ year}^{-1}\,, \tag{17.8.26}$$

and $T_{MO} = 8.4$ years. From Eq. 17.8.11 and 17.8.15 we determine

$$\lambda_{MA} = [\beta_{AO}\lambda_{AM}\lambda_{MO} - \lambda(\lambda + \lambda_{MO} + \lambda_{OM})]/(\lambda + \lambda_{OM}) = 0.1136 \text{ year}^{-1}\,, \tag{17.8.27}$$

which corresponds $T_{MA} = 8.8$ years. In Eq. 17.8.27

$$\beta_{AO} = N_{A\text{st}}/N_{O\text{st}} = 1.28 \times 10^{-2}\,. \tag{17.8.28}$$

So the values of exchange probabilities for the 5-reservoir model in the first approximation will be (in units year^{-1}):

$$\begin{aligned}&\lambda_{AB}=0.0333,\ \lambda_{AM}=0.143,\ \lambda_{BH}=0.0655,\ \lambda_{HA}=0.01922,\\&\lambda_{MA}=0.1136,\ \lambda_{MO}=0.119,\ \lambda_{OM}=1.667\times10^{-3}\ \text{year}^{-1},\end{aligned}\tag{17.8.29}$$

and corresponding characteristic times of elements exchange (in years):

$$\begin{aligned}&T_{AB}=30,\ T_{AM}=7.0,\ T_{BH}=15.3,\ T_{HA}=50.2,\\&T_{MA}=8.8,\ T_{MO}=8.4,\ T_{OM}=600\ \text{years}.\end{aligned}\tag{17.8.30}$$

17.8.4. Non-stationary solution for the radiocarbon 5-reservoir model

To obtain the non-stationary solution for the 5-reservoir model, described by the set of Eq. 17.8.1–17.8.5, let us consider the characteristic equation for this set:

$$\begin{vmatrix}\lambda_{AB}+\lambda_{AM}+x & 0 & -\lambda_{HA} & -\lambda_{MA} & 0\\ -\lambda_{AB} & \lambda_{BH}+x & 0 & 0 & 0\\ 0 & -\lambda_{BH} & \lambda_{HA}+x & 0 & 0\\ -\lambda_{AM} & 0 & 0 & \lambda_{MA}+\lambda_{MO}+x & -\lambda_{OM}\\ 0 & 0 & 0 & -\lambda_{MO} & \lambda_{OM}+x\end{vmatrix}=0,\tag{17.8.31}$$

where $x=\lambda+S$. This equation can be rewritten in the form

$$x\left(x^4+ax^3+bx^2+cx+d\right)=0,\tag{17.8.32}$$

where:

$$a=\lambda_{AB}+\lambda_{AM}+\lambda_{BH}+\lambda_{HA}+\lambda_{MA}+\lambda_{MO}+\lambda_{OM},\tag{17.8.33}$$

$$\begin{aligned}b=&(\lambda_{AB}+\lambda_{AM})(\lambda_{BH}+\lambda_{HA}+\lambda_{MO}+\lambda_{OM})+\lambda_{MA}(\lambda_{AB}+\lambda_{MO})\\&+(\lambda_{BH}+\lambda_{HA})(\lambda_{MA}+\lambda_{MO}+\lambda_{OM})+\lambda_{BH}\lambda_{HA},\end{aligned}\tag{17.8.34}$$

$$\begin{aligned}c=&\lambda_{MA}\lambda_{MO}(\lambda_{AB}+\lambda_{AM}+\lambda_{BH}+\lambda_{HA})+\lambda_{AM}(\lambda_{BH}\lambda_{HA}-\lambda_{MA}\lambda_{OM})\\&+(\lambda_{MO}+\lambda_{OM})[\lambda_{BH}(\lambda_{AB}+\lambda_{AM}+\lambda_{HA})+\lambda_{HA}(\lambda_{AM}+\lambda_{BH})]\\&+\lambda_{MA}[\lambda_{AB}(\lambda_{BH}+\lambda_{HA})+\lambda_{BH}\lambda_{HA}],\end{aligned}\tag{17.8.35}$$

$$\begin{aligned}d=&\lambda_{MA}\lambda_{MO}[(\lambda_{AB}+\lambda_{AM})(\lambda_{BH}+\lambda_{HA})+\lambda_{BH}\lambda_{HA}]\\&+\lambda_{AB}\lambda_{BH}\lambda_{HA}(\lambda_{MO}+\lambda_{OM})-\lambda_{AM}\lambda_{MA}\lambda_{OM}(\lambda_{BH}+\lambda_{HA}).\end{aligned}\tag{17.8.36}$$

The first root of Eq. 17.8.32 will be

$$x_1 = 0 \quad \text{or} \quad S_1 = -\lambda\,. \tag{17.8.37}$$

The other 4 roots can be found by the substitution $x = y - a/4$, which reduces our fourth power equation to the incomplete form

$$y^4 + \left(b - \frac{3a^2}{8}\right)y^2 + \left(\frac{a^3}{8} - \frac{ab}{2} + c\right)y + \left(-\frac{3a^4}{256} + \frac{a^2 b}{16} - \frac{ac}{4} + d\right) = 0\,. \tag{17.8.38}$$

According to the Descartes–Euler method, the roots of Eq. 17.8.38 will be (Korn and Korn, M1968):

$$y_{2,3,4,5} = \pm\sqrt{z_1} \pm \sqrt{z_2} \pm \sqrt{z_3}\,, \tag{17.8.39}$$

where the signs must be chosen so that

$$\left(\pm\sqrt{z_1}\right)\left(\pm\sqrt{z_2}\right)\left(\pm\sqrt{z_3}\right) = -a^3/64 + ab/16 - c/8, \tag{17.8.40}$$

and z_1, z_2, z_3 are the roots of the cubic equation

$$z^3 + \left(b/2 - 3a^2/16\right)z^2 + \frac{1}{16}\left(\left(b - 3a^2/8\right)^2 - \left(-3a^4/64 + a^2 b/4 - ac + 4d\right)\right)z$$
$$- \frac{1}{64}\left(a^3/8 - ab/2 + c\right)^2 = 0. \tag{17.8.41}$$

The roots of this equation are:

$$\begin{aligned} z_1 &= A_1^{1/3} + A_2^{1/3} - \frac{1}{6}\left(b - 3a^2/8\right), \\ z_{2,3} &= -\frac{1}{2}\left(A_1^{1/3} + A_2^{1/3}\right) - \frac{1}{6}\left(b - 3a^2/8\right) \pm i\left(\sqrt{3}/2\right)\left(A_1^{1/3} - A_2^{1/3}\right), \end{aligned} \tag{17.8.42}$$

where

$$A_{1,2} = k \pm \left[-12^{-3} \times \left(-\frac{3a^4}{256} + \frac{a^2 b}{16} - \frac{ac}{4} + d + \frac{\left(b - 3a^2/8\right)^2}{12}\right)^3 + k^2\right]^{1/2}, \tag{17.8.43}$$

and

$$k = \frac{1}{1728}\left(b - 3a^2/8\right)^3 - \frac{1}{48}\left(b - 3a^2/8\right)\left(-3a^4/256 + a^2 b/16 - ac/4 + d\right)$$
$$+ \frac{1}{128}\left(a^3/8 - ab/2 + c\right)^2. \tag{17.8.44}$$

These expressions determine the four other roots S_2, S_3, S_4, S_5 of the characteristic Eq. 17.8.31 and on this basis the standard procedure (Korn and Korn, M1968) yields the non-stationary solution for the 5-reservoir model:

$$N_A(t)=\sum_{k=1}^{5} C_{Ak}\exp(S_k t),\ N_B(t)=\sum_{k=1}^{5} C_{Bk}\exp(S_k t),\ N_H(t)=\sum_{k=1}^{5} C_{Hk}\exp(S_k t),$$
$$N_M(t)=\sum_{k=1}^{5} C_{Mk}\exp(S_k t),\ N_O(t)=\sum_{k=1}^{5} C_{Ok}\exp(S_k t), \qquad (17.8.45)$$

where the constants $C_{Ak}, C_{Bk}, C_{Hk}, C_{Mk}, C_{Ok}$ are determined by initial conditions (for more details see in Dorman, 1976, 1977a-g).

17.9. A short review on the research of CR variations and related phenomena in the past by radiocarbon method

17.9.1. Radiocarbon data

The journal *Radiocarbon*, published since 1959, contains a lot of data on radiocarbon measurements in different kinds of samples as well as results of investigations of CR variations and related phenomena in the past made by the radiocarbon method. Many results on CR research by the radiocarbon method were published also in the Proceedings of International CR Conferences (in about each ICRC were rapporteur or invited papers that reviewed the results obtained by the radiocarbon method). A sufficiently high accuracy (from 0.5–0.3% up to 0.1%) has been reached by the conventional method of measuring ^{14}C in annual rings of trees and by measuring the radiocarbon H-disintegrations with a proportional counter. Now high precision data have become available from several laboratories for more than 10,000 calendar years (Suess, 1980; Stuiver et al., 1986; Stuiver and Becker, 1993; Stuiver and Reimer, 1993). These data were used to obtain extremely interesting and important results on CR temporal variations in the past and related phenomena (long time variations of the geomagnetic field, solar activity cycles, local supernova explosions, etc.).

17.9.2. The radiocarbon method and CR variations in the past, caused by long time variations of geomagnetic field

According to Damon et al. (1978), a substantial part of the observed long-term variations of the radiocarbon content with amplitude about 12% for the last 10,000 years may be explained by the changes of the Earth's magnetic dipole. According to archaeo-magnetic and paleo-magnetic data (McElhinny and Senanayake, 1982; Burlatskaya, 1987) the dominant periodicity in planetary geomagnetic field variation is 8,000-9,000 years. On the other hand, in Section 17.4 it was shown that the variation of radiocarbon production rate with characteristic period of $\approx 10^4$ years, taking into account the planetary mixing and exchange processes on the Earth will be reflected in radiocarbon contents with the same period, but with ≈ 0.2 from amplitude in CR (see Table 17.6.1); This means that we expect a relative change of $\approx 5\times 12\%$ in radiocarbon production

rate. It was shown in Section 17.3.2 using the planetary coupling function method that 10% of increase in radiocarbon production rate corresponds on the average to $\approx 17\%$ decrease in the Earth's dipole magnetic moment $\mu(t)$. Therefore for the last 10,000 years we expect from radiocarbon data a change in $\mu(t)$ of $1.7 \times 60\% \approx 100\%$, i.e. about 2 times. Dergachev et al. (1977), Dergachev (1987), Dergachev and Akhmetkereev (1990) summarized the results obtained using the radiocarbon method to determine the variations of the Earth's dipole magnetic moment during the last 12,000 years (see Fig. 17.9.1).

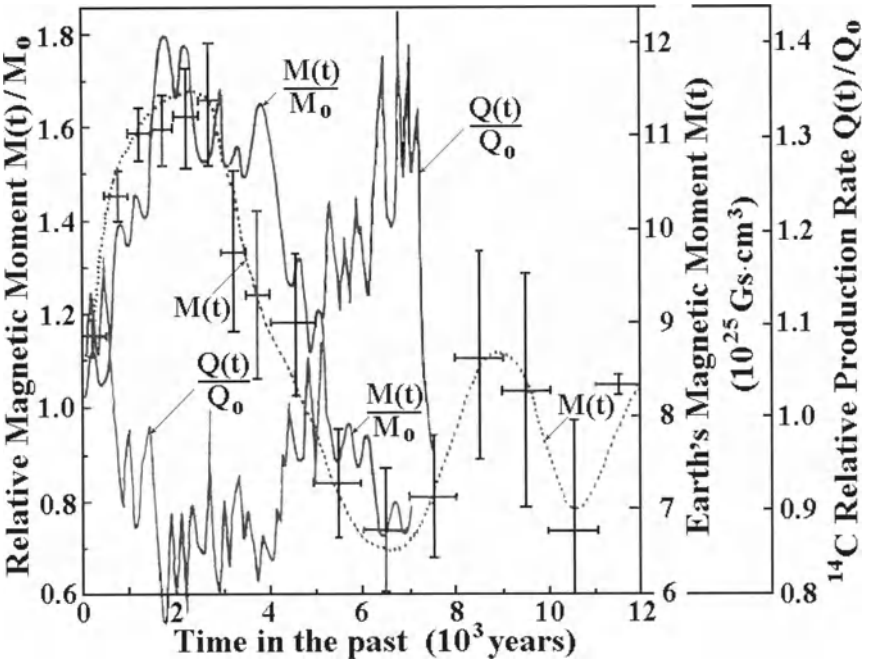

Fig. 17.9.1. Variation of radiocarbon production rate $Q(t)/Q_o$, calculated using the Earth's magnetic moment change $M(t)/M_o$ according radiocarbon data, and global changes of the dipole moment $M(t)$ according to archae-magnetic data of McElhinny and Senanayake (1982). Comparison made according to Dergachev (1987).

The results obtained are in good agreement with the archae-magnetic and paleo-magnetic data above mentioned, indicating that during this period there was a minimum of $\mu(t)/\mu_o \approx 0.8$ and a maximum $\mu(t)/\mu_o \approx 1.6$ (a change of two times, as we expect according to the coupling function method in the frame of the 2-reservoir model of planetary elements mixing and exchange). Geomagnetic variations in radiocarbon content in annual tree rings and in stalactites in comparison with archaic-magnetic and pale-magnetic data as well as with data of ^{10}Be contents in different ice columns was investigated for the last 30,000 years in Kocharov et al. (1990). To exclude time variations that are not connected with changing of geomagnetic field ^{10}Be data from near polar ice columns (where cut off rigidity is about zero) were used (see Fig. 17.9.2).

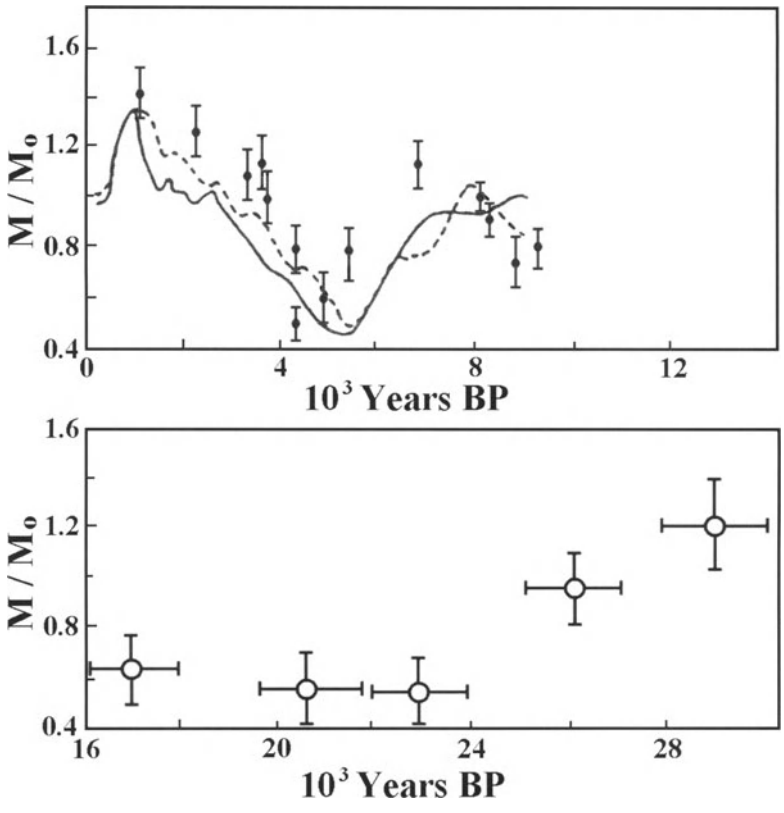

Fig. 17.9.2. Geomagnetic variations over the last 30,000 years: solid line – derived from ^{14}C tree rings data; dashed line – archaeo-magnetic determinations; full circles – derived from ^{10}Be data, empty circles – from ice column ^{10}Be data at station Vostok in Antarctica and ^{14}C data from stalactites. According to Kocharov et al. (1990a).

Data shown in Fig. 17.9.2 confirm the above described results and show that about 22,000 years ago there was a second minimum of $\mu(t)/\mu_o \approx 0.6 \pm 0.15$ and $\approx 30{,}000$ years ago there was a maximum $\mu(t)/\mu_o \approx 1.2 \pm 0.2$ (unfortunately these results cannot be compared with archaeo-magnetic and paleo-magnetic data because these data for the period 15–30 thousand years ago have too large uncertainties, up to ±50%).

17.9.3. The radiocarbon method and grand solar activity minima

As we described above, radiocarbon is produced mainly by the secondary neutrons of CR in the upper atmosphere. Hence, the production rate of the radiocarbon is determined by the flux of incoming CR, and is controlled by solar activity. The radiocarbon (^{14}C) produced forms carbon dioxide ($^{14}CO_2$) immediately, and circulates within the global carbon cycle together with $^{12}CO_2$ and $^{13}CO_2$. A number of carbon dioxide is absorbed into trees to form tree rings. Thus, a record of the variation of the radiocarbon abundance caused by changes of solar activity is stored in the tree rings. Accordingly it became possible to trace the history of solar activity by measuring the

detailed radiocarbon content of long-lived trees. Suess (1965) showed that tree rings contain quantitative information on CR modulation by solar activity in the past. The results of detail investigation of Stuiver et al. (1998) are shown in Fig. 17.9.3 (it is an example of ^{14}C data which reveals the variation of solar activity in the last millennium).

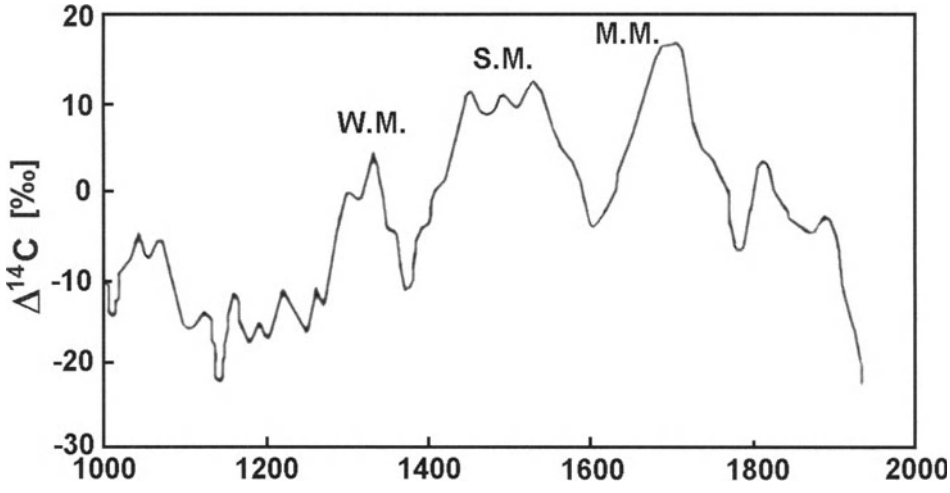

Fig. 17.9.3. Radiocarbon content in tree rings in the last millennium (decadal). Letters W.M., S.M., and M.M. near three peaks denote Wolf, Spoerer and Maunder Minimum, respectively. According to Stuiver et al. (1998).

The three large peaks in Fig. 17.9.3 show the times of the grand minima, called Wolf, Spoerer and Maunder minima, respectively. The Maunder Minimum (1645-1715 AD), one of the grand minima in the last millennium, is well known to have had almost no sunspots. This period seems to coincide with the so-called Little Ice Age, that is, a period of cold climate in 17th century and around (see Chapter 14, Section 14.4). The duration of the Maunder Minimum is defined as the years when the sunspot number was almost nil (Eddy, 1976). The rare appearance of aurora and higher production of cosmogenic nuclides such as ^{14}C and ^{10}Be confirm the reality of this event.

Kocharov et al. (1995) and Stuiver and Braziunas (1993) measured the ^{14}C contents in annual tree rings during the Maunder Minimum. Although both data sets indicate an increase of ^{14}C content, corresponding to a solar activity minimum, they differ in several points. In order to clarify the cause of the disagreement and to what extent the variation is due to solar activity, Masuda et al. (2003) have made measurements of the radiocarbon content in annual tree rings using a Japanese cedar tree. The wood samples were taken from a block of the trunk of a Japanese cedar (Cryptomeria japonica) tree. This wood was obtained from the Murou-ji temple area in Nara, Japan (geographical location 34°32' N, 136°02' E and 400m above sea level). The block was obtained as a trunk section of 1.1 m in diameter and 30 cm thick. The calendar year corresponding to each tree ring was determined by counting the number of annual rings from the outermost, which corresponds to 1998. The estimated age of the tree is 392 years. Annual samples of tree rings, corresponding to the period of the Maunder Minimum and around (1629–1739), were separated. As a first step, it was measured the ^{14}C

content for every single year for a part of this period (1693-1731). The cellulose component was extracted from the wood sample by dissolving resins in a benzene - ethyl alcohol mixture and by bleaching in a $NaClO_2$/HCl solution to remove lignin. Then the cellulose was combusted with CuO in vacuum and converted to CO_2, which was successively purified with cold traps (-90°C and -130°C). The CO_2 samples sealed in Pyrex glass tubes were sent to the AMS ^{14}C Laboratory of the ETH and converted to graphite as targets for the ion source of accelerator mass spectrometers (AMS). Standard reference samples (NIST SRM4990C, oxalic acid) and blank samples for determination of the background (commercial oxalic acid from Wako Pure Chemical Industries) were also converted to graphite in the same way. The ^{14}C content in terms of the ratio of $^{14}C/^{12}C$ was measured in the single-year samples using the AMS of ETH/PSI, Switzerland (Bonani et al., 1986). The measurement scheme followed the normal procedure of the AMS facility. The accuracy achieved was about 0.31 % for most samples. The isotope ratio $^{13}C/^{12}C$ was measured simultaneously and used to correct the ^{14}C content for isotope fractionation. The measured ^{14}C content expressed as $\Delta^{14}C$ are plotted versus the calendar year of the tree rings in Fig. 17.9.4, together with the data by Kocharov et al. (1995) and Stuiver and Braziunas (1993).

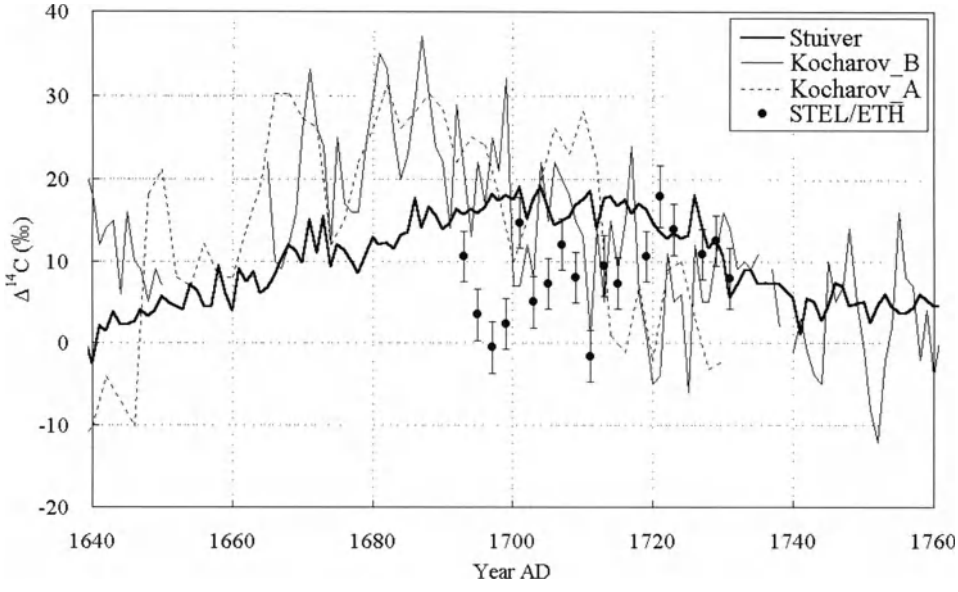

Fig. 17.9.4. Preliminary results of the measurement of radiocarbon contents in tree rings for the Maunder Minimum. Contents of radiocarbon shown as STEL/ETH of Masuda et al. (2003) are compared with Kocharov et al. (1995) and Stuiver and Braziunas (1993) results. According to Masuda et al. (2003).

From Fig. 17.9.4 can be seen that the obtained by Masuda et al. (2003) contents are in agreement with the data of Stuiver and Braziunas (1993) in the latter part of the measured period (1719-1731) but lower before 1715. On the other hand, the Masuda et al. (2003) data coincide well with the data of Kocharov et al. (1995) except for the early part of the measured period (1693-1699). Kocharov et al. (1995) published two series of

$\Delta^{14}C$ data for the Maunder Minimum, which are shown in the Fig. 19.9.4 as Kocharov-A and Kocharov-B. The measurement was done by the liquid scintillation method and the measurement error was claimed to be 0.3 %. The sample in Series A comprised bi-annual rings of pine trees from the South Urals and in Series Kocharov-B annual rings of pine trees from the West Ukraine. They reveal a similar tendency in that the $\Delta^{14}C$ content increased during 1670–1710, which corresponds to the main period of the Maunder Minimum (1645–1715). Stuiver and Braziunas (1993) reported a variation of $\Delta^{14}C$ content in annual tree rings from Washington (Pacific Northwest coast), USA, for the time span 1510–1945. The measurement was carried out using gas proportional counters and the measurement error is about 0.2 %. The data of Stuiver and Braziunas (1993) shows a broad peak in the $\Delta^{14}C$ content around 1710, which is a few decades later than that of Kocharov et al. (1995). Peristykh and Damon (1998) analyzed the data and concluded that the 11-year cycle was present before and after the Maunder Minimum but was totally suspended during the Maunder Minimum, while the 22-year periodicity existed throughout. The maximum $\Delta^{14}C$ content in the peak of the Maunder Minimum in the data of Kocharov et al. (1995) is much larger than that of Stuiver and Braziunas (1993). As shown above, the $\Delta^{14}C$ data sets for the Maunder Minimum are not in agreement with each other. One possibility for the difference might be regional effects on $\Delta^{14}C$ circulation.

17.9.4. The radiocarbon method and solar activity cycles

Attolini et al. (1987b, 1990) on the basis of radiocarbon data for 1180–1500 found a periodicity of 11.4 ± 0.2 years. By analyzing the data on radiocarbon contents in tree rings from 1564 to 1952 Galli et al. (1987a) show existing 11 year and 22 year variations and some unstable periodicities in the intervals 40–70 years and about 130 years. Galli et al. (1987b) and Kocharov et al. (1995) found that in the period of the Maunder minimum (1645–1715) the radiocarbon contents in dated samples are significantly higher than before. They also found that the 11 year variations (connected with solar activity cycle) are rather suppressed, whilst the 22 year variations (connected with solar magnetic cycle) are clearly expressed, in good agreement with the result obtained earlier by Kocharov et al. (1985). A periodicity of ≈ 130 years in the variations of radiocarbon and ^{10}Be data, as well as in occurrence frequency of auroras was obtained also by Attolini et al. (1987a) from the analyses of data for several thousand years. Cini Castagnoli et al. (1990) found the largest amplitude for the 137.7 year periodicity (all other found periodicities have amplitudes about 5 times smaller; among them 10.8, 22.03 and 28.05 years which exist also in sunspot numbers). Stuiver and Braziunas (1989), on the basis of 9600 years data of radiocarbon contents in annual tree rings found periodicities with periods about 420, 200, and 140 years; among them was found the fundamental oscillatory mode with frequency $\omega_n \approx 2.4\times10^{-3}$ year^{-1} (period about 417 years). The 137.7 year periodicity found by Cini Castagnoli et al. (1990) corresponds to the frequency $3\omega_n$. Dergachev and Akhmetkereev (1990) analyzed radiocarbon data for about 11,000 years and found periodicities ≈ 200, ≈ 400 and ≈ 600 years as well as a periodicity ≈ 2400 years with amplitude $0.7 \div 0.8\%$ (see Fig. 17.9.5 and Fig. 17.9.6).

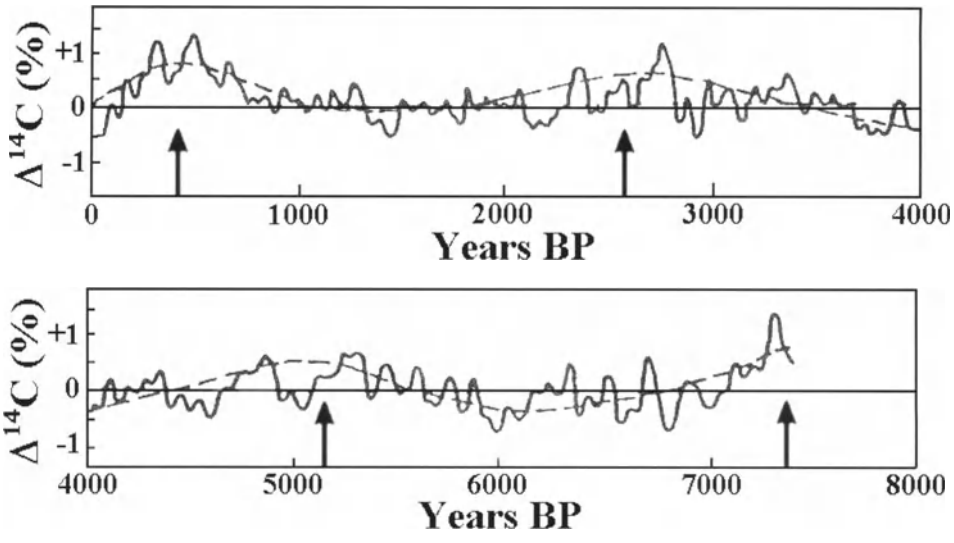

Fig. 17.9.5. ^{14}C contents in tree rings after removal of the long-term trend. According to Dergachev and Akhmetkereev (1990).

According to Dergachev (1993) the radiocarbon data show also the existence of periodicities with periods ≈1.5, ≈3.8, ≈6.1, ≈8.2, ≈10.5 and ≈12.6 thousand years; some of them can be connected with solar activity cycles. In Dergachev (1995a,b) were found periodicities in radiocarbon data ≈210 and ≈2000 years (the periodicities ≈500 and ≈2500 years were found in ^{10}Be data for about 40,000 years by Cini Castagnoli et al., 1993). According to Dergachev (1995a), the cycle ≈210 years may be connected with existence of extremely low solar activity periods as the well known Maunder, Spoerer and Wolf minima with intervals between them of about two hundred years. Dergachev and Chistjakov (1993) determined by radiocarbon data the structure of the ≈2000 years cycle: the mean interval between two extremes is 2400 ± 200 years, the time from the maximum of the active phase to the minimum of the depressed phase is 600-800 years, the duration of quiet phase is 1100 ± 300 years (the present level of solar activity corresponds to the quiet phase of ≈2000 years solar cycle).

Sakurai et al. (1999) and Matsumoto et al. (2001) measured the time variations of the radiocarbon contents in old cedar's tree rings for the last 2500 years, focusing on periodicities such as the 11 year cycle. The sample of tree rings is a cedar tree buried before 2500 years ago by a volcanic eruption of Mt. Choukai in Japan (the sample has about 2 m diameter and 1.5 m length; the accuracy of radiocarbon measurements about 0.15%). It was found that the average amplitude of 11-year variation in radiocarbon content is about 0.27%, what is in good agreement with the one obtained for the 11 year cycle during the 18^{th}–19^{th} centuries 0.14% for Pacific trees and 0.48% for Russian trees according to Kocharov (1995). Sakurai et al. (2003) continued the radiocarbon measurements in the old cedar's single-year tree rings and found that about 2500 years ago solar cycle variation in radiocarbon was characterized by the period about 11.5 years and amplitude 0.39%.

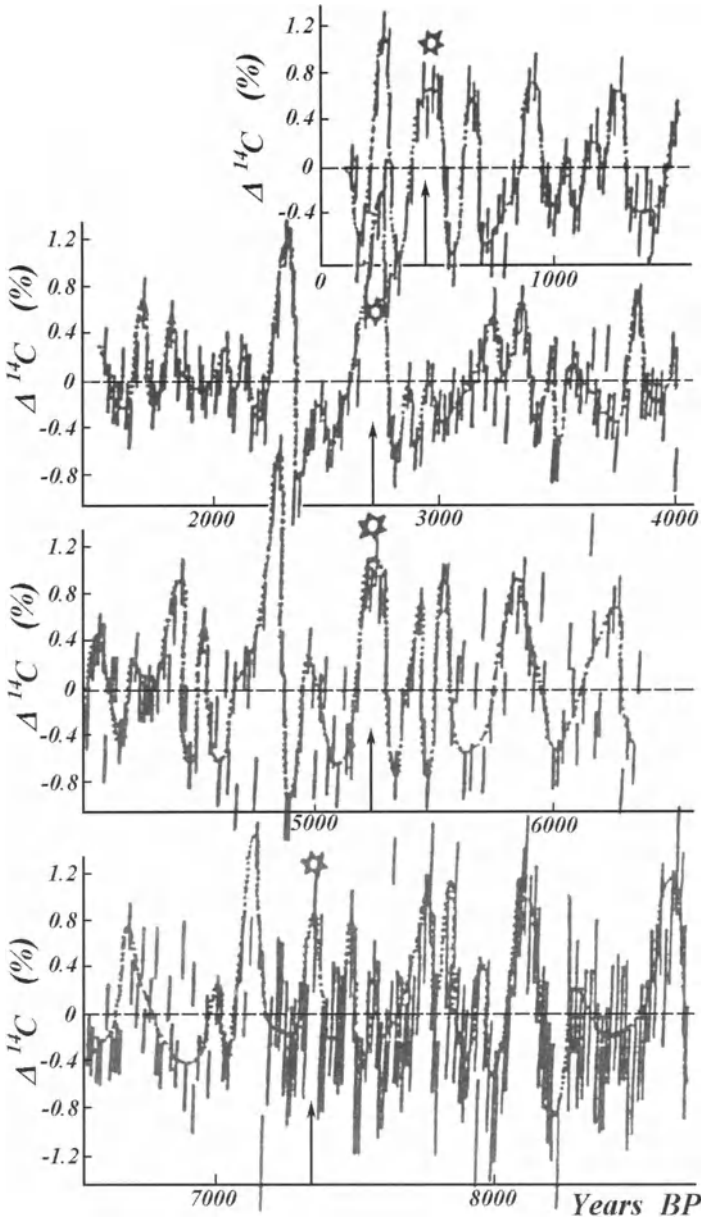

Fig. 17.9.6. ^{14}C contents in tree rings (stars point out the maximums of super-secular CR variations). According to Dergachev and Akhmetkereev (1990)

Kato et al. (2001) analyzed the radiocarbon content variations during the Spoerer minimum (1414–1534 AD) with an accuracy of about 0.3% by using the trunk of a cedar tree grown in Yaku Island (southern Japan) that was cut down in 1994. Preliminary results for the first part of the Spoerer minimum are presented on the Fig. 17.9.7 in comparison with results obtained by Stuiver et al. (1998).

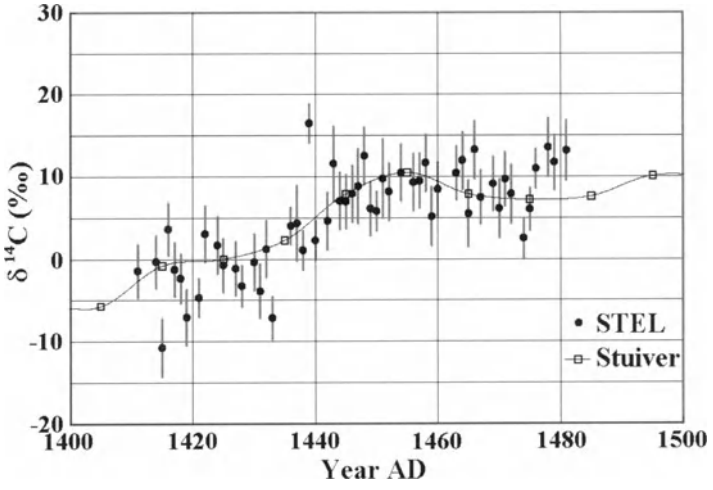

Fig. 17.9.7. Radiocarbon content variations during the Spoerer minimum (1414–1534 AD) by using a cedar tree grown in Yaku Island. Preliminary results of Kato et al. (2001) for the first part of the Spoerer minimum in comparison with results obtained by Stuiver et al. (1998).

This investigation was continued by Miyahara et al. (2003). In previous studies, a weakened 11-year period and the existence of a 22-year period during the Maunder Minimum has been suggested by Kocharov et al. (1995) and by Peristykh and Damon (1998). To determine if this characteristic is common among the grand minima, Miyahara et al. (2003) survey the radiocarbon contents of tree rings from the Spoerer Minimum. For this study, a 704-year-old Japanese cedar tree, obtained from Yaku Island (30.18° N, 130.30° E), was used (the same as by Kato et al., 2001). The ^{14}C content of each tree ring was measured using the accelerator mass spectrometer (AMS) at Nagoya University. For the measurement, cellulose is extracted from each tree ring and converted to graphite as the target material of the ion source of the machine. The preliminary procedure was as follows: the tree rings were separated annually, and milled into small pieces. Each of the samples was then washed with a benzene - ethyl alcohol mixture to remove resins etc. The extracts were subsequently bleached by a $NaClO_2$/HCl solution at 80 to remove lignin. They were then boiled and rinsed in distilled water. The resultant celluloses were combusted with CuO to obtain CO_2 gas. After purification, the CO_2 gas was de-oxidized to graphite using H_2 gas (according to Kitagawa et al., 1993). Fig. 17.9.8 shows the radiocarbon content of tree rings from 1410 to 1550 AD. The solid curve is the same decadal data of Stuiver et al. (1998) as in Fig. 17.9.3 and Fig. 17.9.7.

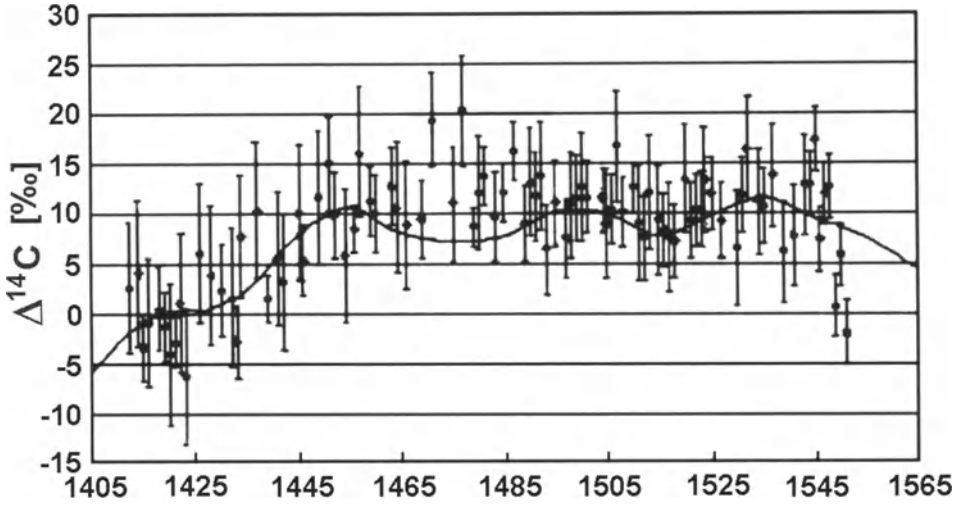

Fig. 17.9.8. The same as Fig. 17.9.7, but extended for the full Spoerer Minimum. According to Miyahara et al. (2003).

Results of Miyahara et al. (2003) are consistent with the curve in Fig. 17.9.3 but reveal short term variations, which are not seen in the decadal data. The time series of data shown in Fig. 17.9.8 was investigate by Fourier analysis (see Fig. 17.9.9).

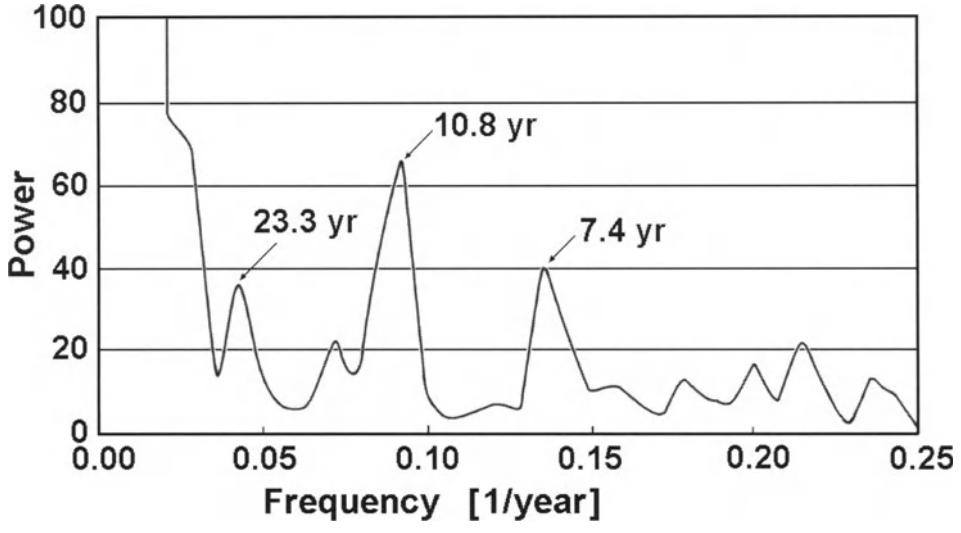

Fig. 17.9.9. The power spectrum of radiocarbon annual contents data for the Spoerer Minimum (shows peaks in the periodicity at 7, 11 and 22 years). According to Miyahara et al. (2003).

The confidence levels of the 11-year and 22-year periodicities, which can be assumed to be manifestations of solar activity, were 95% and 70%, respectively. Next, Miyahara et al. (2003) surveyed the variation of strength of these two cycles during the

Spoerer Minimum. By using a band-pass filter, two cycles were extracted from the time series of the data in Fig. 17.9.7 and shown in Fig. 17.9.10.

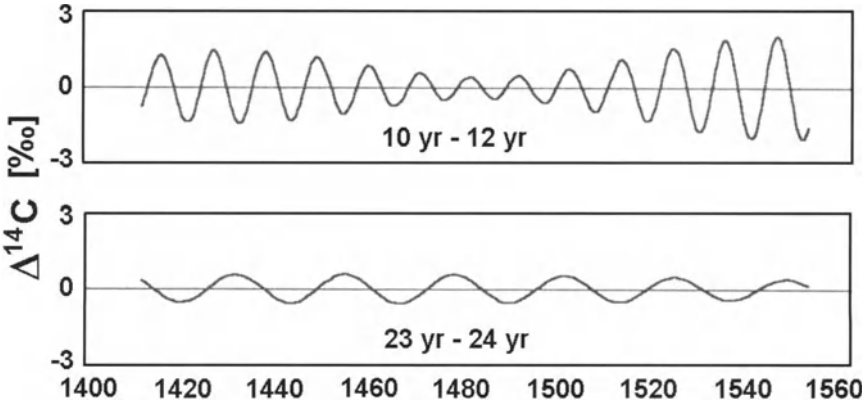

Fig. 17.9.10. Variation of the amplitude of 11-year and 22-year periodicities of annual radiocarbon contents. According to Miyahara et al. (2003).

Fig. 17.9.10 shows that there is an obvious difference between the two types of radiocarbon periodicities during Spoerer Minimum and in vicinities: the 11-year cycle is weaker during 1460-1500 AD, while the 22-year cycle maintains steady amplitude.

Sonett and Smith (1999) on the basis of radiocarbon data found a periodicity of 17.5 ± 0.5 years, which is close to the Saros cycle – the retrograde 18.5 year period of rotation of the Moon's nodal plane (Kaula, M1968).

Let us note that according to the Section 17.6, periodicities in radiocarbon production rate will be transformed to periodicities in radiocarbon content with the same frequency but with reduced amplitude and different time lag in phase. Therefore to determine the amplitude of cyclic variations in radiocarbon production rate and CR intensity on the basis of experimental data of radiocarbon contents in dated samples it is necessary to multiply the obtained amplitude by factors of 5 and 14 for periods 10^4 and 10^3 years; up to factors 32 and 61 for periods 22 and 11 years according to Table 17.6.1 (see above, Section 17.6).

From this point of view the results of Cini Castagnoli et al. (1997) concerning the comparison of 3-year averaged radiocarbon and thermo-luminescence[1] (TL) data for about 2600 years are very important. The TL data were obtained from the core GT89-3 (180 m water depth at Ionian sea) sampled at consecutive intervals of 2 mm, corresponding to a time step of 3.096 years (it was shown that in this area of Ionian sea

[1] According to Cini Castagnoli et al. (1997), when crystalline minerals are exposed by CR ionizing radiation in their natural environment, free electrons and holes are produced. A small fraction of the former becomes trapped as defects in the crystals. These trapped charges are then released and recombine giving rise to the TL signal during the heating of the samples. Let us note that TL data gave very important information, independent from radiocarbon information, on CR time variations in the past, mostly free from planetary mixing and exchange processes.

the sedimentation rate $s = 0.0645 \pm 0.0007$ cm.year^{-1}). Results are shown in Fig. 17.9.11 and Fig. 17.9.12.

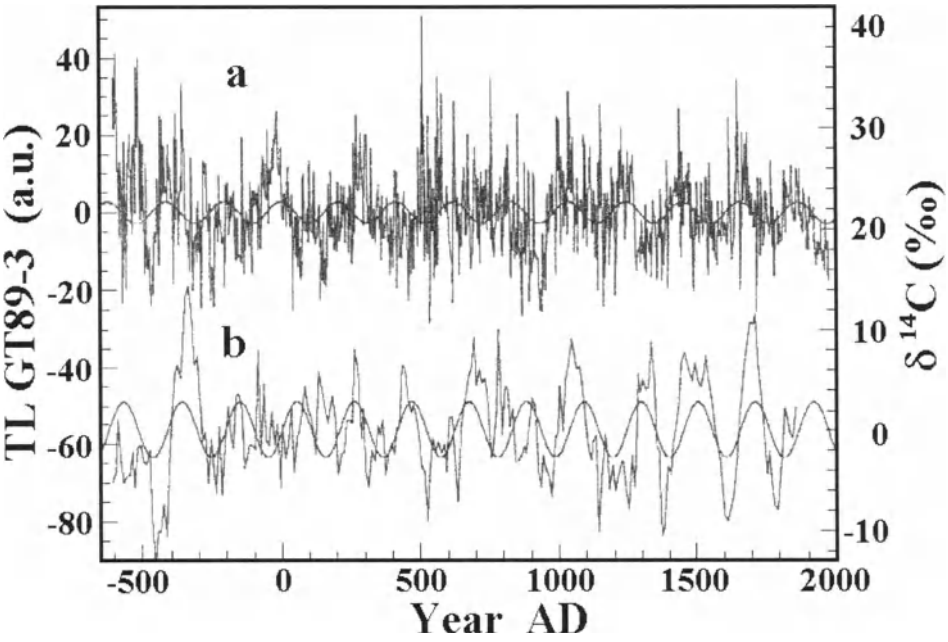

Fig. 17.9.11. (a) Thermo-luminescence (TL) data for about 2600 years, obtained from the core GT89-3 (180 m water depth at Ionian sea) according to Cini Castagnoli et al. (1997); (b) radiocarbon decadal tree ring records according to Stuiver and Braziunas (1988).

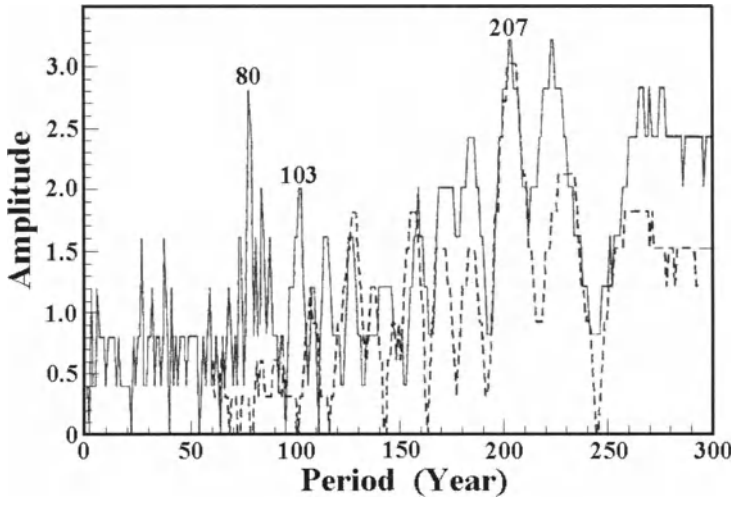

Fig. 17.9.12. Amplitudes of the least square fit sinusoids to the superposed data, obtained for radiocarbon record (dash line) and for TL data (solid line). According to Cini Castagnoli et al. (1997).

Cini Castagnoli et al. (1997) came to the conclusion that the 207 years harmonic has an amplitude about 3.6%, and the second harmonic with period about 103 years has an amplitude 2.4%.

17.9.5. Radiocarbon and ^{10}Be data related to possible local supernova explosions in the past

Using the data from several laboratories on radiocarbon content in annual tree rings and in stalactites for about 40,000 years (averaged for groups of 10 and 100 years) as well as ^{10}Be data from Greenland and Antarctic stations for about 150,000 years, Kocharov et al. (1990) analyzed four events of long-term (several thousand years) gradual CR intensity increase. The first event starts about 40 thousand years ago, the first maximum with increase of production rate of ^{10}Be and radiocarbon (CR intensity of particles with rigidity ≥ 0.5 GV) of $\approx 50\%$ was reached after 2 thousand years. Then during the next 2,000 years the level of intensity decreased by $\approx 20\%$ and then about 34 thousand years ago a second maximum reached with amplitude $\approx 100\%$, and then recovered during ≈ 4 thousand years to the same level as before the event. These results were confirmed by Cini Castagnoli et al. (1995) on the basis of ^{10}Be data in the Mediterranean sea sediments. It is important that during this event there was no significant enhancement in ^{18}O contents, so that the results cannot be explained by changies in atmospheric circulation processes (the enhancement in ^{18}O contents, connected with the last ice age, occurred about 10,000 years after this event). To explain the first event Kocharov et al. (1990) supposed that it was caused by a supernova explosion at a distance 45–65 pc, with full energy of about $5\times\left(10^{49}-10^{50}\right)$ erg, and that the diffusion coefficient for CR propagation in the local interstellar space $\kappa(E)=\kappa_o\left(E/E_o\right)^{\alpha}$ where $\alpha\approx 0.3$, E_o is the rest energy of CR particles, and $\kappa_o=(0.5-1.0)\times 10^{29}$ cm^2/sec. The remnant of this supernova can be Loop 1 with the following characteristics: distance from the Sun about 50 pc, age about 3×10^4 years (Nishimura et al., 1979). More detailed interpretation of this event was made by Kocharov et al. (1991): it was assumed that the first maximum (see Fig. 17.9.13) was caused by CR generated during supernova explosion, but the second maximum of CR increasing 4 thousand years after the first increasing was caused by the Heliosphere capturing by the strong shock wave from supernova propagated with an average velocity $\approx 8\times 10^8$ cm/sec.

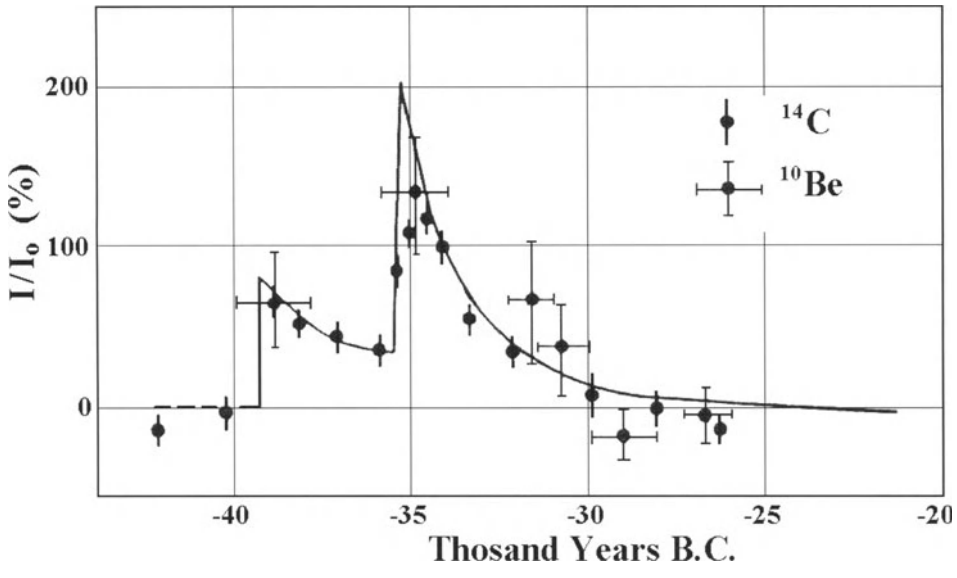

Fig. 17.9.13. The comparison of calculations for double-shock acceleration model (thick curve, see text) with CR intensity variation on the Earth, reconstructed from ^{14}C and ^{10}Be data for the period 42–25 thousand years ago. According to Kocharov et al., (1991).

The other three increases of ^{10}Be contents were observed ≈ 60, ≈ 95 and ≈ 140 thousand years ago, but during these events significant enhancements in ^{18}O contents were also observed in the same cores of ice which were used for measurements of ^{10}Be contents. Enhancements in ^{18}O show that during these three ^{10}Be increases there were considerable changes in atmospheric circulation processes; therefore events observed ≈ 60, ≈ 95 and ≈ 140 thousand years ago can be caused not by local supernova explosions but by changes of atmospheric circulation processes. In any case, for these three events it is necessary to make additional detailed analysis taking into account atmospheric circulation processes. We cannot now exclude the possibility that some of these increases are caused by local supernova explosions.

Important evidence on a nearby supernova explosion in the last 5 million years at a distance ≤ 30 pc from the Sun was obtained by Fields (2001) on the basis of measurements of ^{60}Fe ($T_{1/2} = 1.5 \times 10^6$ years) content in a deep ocean ferromagnetic crust (the observed signal appears to be two orders of magnitude above background level).

17.10. Summary and perspectives of radiocarbon method

Let us summarize the main results considered above in this Chapter:

1. The method of polar and local radiocarbon coupling functions allowed us to connect the CR spectrum and cut off rigidity variations with changes of radiocarbon production rate, taking into account vertical mixing of elements in the Earth's atmosphere. On the basis of Lingenfelter's (1963) calculations we determined analytical approximations of polar and local radiocarbon coupling functions.

2. Introduction and calculation of planetary radiocarbon coupling functions allowed us to take into account the planetary mixing of elements in Earth's atmosphere and determine the connection between time variations of the planetary radiocarbon production rate with change of CR primary spectrum and the Earth's magnetic dipole moment.
3. Consideration of the 2-reservoir model of planetary elements exchange on the Earth, taking into account data on H-bomb explosions in the atmosphere, allowed us to determine the probabilities of element exchange and determine on the basis of radiocarbon content in the dated samples the planetary radiocarbon production rate in atmosphere as well as CR intensity variations in the past. In the framework of this model it was determined how different types of CR time variations are manifested in radiocarbon content.
4. In the first approximation the probabilities of element exchange in the frame of 5-reservoir model were estimated, obtaining the steady state solution and the parameters for the non-stationary solution were calculated.
5. On the basis of the method of radiocarbon coupling functions in the frame of the planetary mixing and exchange of elements model, we considered and analyzed the radiocarbon and ^{10}Be data for CR variations in the past, that are connected with long term variations of the Earth's magnetic field, solar activity cycles, and possible supernova explosions not far from the Sun.
6. Further development of the radiocarbon method, in combination with data on other cosmogenic nuclides, will give important new results on CR variations in the past caused by the global meteorological changes and exchange processes in the Earth's atmosphere, by variations in the geomagnetic field, by solar activity cycles, by possible local supernova explosions.
7. The described results of radiocarbon research formatted a basis for many important applications of radiocarbon method (see below, Chapter 18, Sections 18.6 and 18.7).

Chapter 18

Potential and Realized Applications of Cosmic Ray Research in Science and Technology

18.1. Possible CR applications in Meteorology and in Service of great airports

18.1.1. The matter of the problem

The subject of the problem which we consider in this Section is the possible application of general spectrographic method based on CR data of different CR components (e.g. neutron monitor, multi-directional muon telescopes on the ground and underground, detector of slow muons) for continuous registration of time variation of vertical distribution of air temperature up to 35–40 km, as well as possible using in meteorological service of great airports and space shot centers, in the work of the International Meteorological Service. In Chapter 15 we considered in detail the inverse problem to the theory of CR meteorological effects: how to determine continuously the vertical air temperature profile by using only CR data or by using CR data and ground temperature (which is easy to measure continuously). It was shown that for this purpose one can use standard NM (for excluding variations of extra-terrestrial origin) and multi-directional muon telescopes on the ground and underground, detector of slow muons (that have different densities of temperature coefficients). In Section 15.5 we described in detail the generalized spectrographic method, specially developed for solving this inverse problem, and gave formulas for a practically continuous passive location of vertical profile of air temperature up to 35–40 km on the basis of CR data (see the sketch of the method in Fig. 18.1.1). Let us note that now for excluding variations of extra-terrestrial origin one can use CR data from other Observatories that are available in real time scale from the Internet. In our opinion, together with the traditional method of balloon sounding, this CR method of passive location of atmospheric conditions up to 35–40 km can be essentially useful in meteorological service of large airports that have frequent plane flights, and in meteorological service of space launch centers. It is not excluded that in the near future this method can be used widely also in the International Meteorological Service for giving more exact forecast of weather (in addition to the traditional methods).

18.1.2. Generalized spectrographic method and using CR data of different CR components

As was shown in Section 15.5, the on-line use of CR data of several secondary CR components with different temperature and barometric coefficients can provide continuous information not only on the vertical air temperature distribution, but also on the air mass in the vertical cm^2 column over detector. The difference between this value and the simultaneously measured dynamic air pressure by the standard barometer will

give the value of Bernoulli effect and then it is very easy to determine from the Bernoulli formula (see Section 6.2 and Section 16.4) the effective wind velocity over the CR detectors.

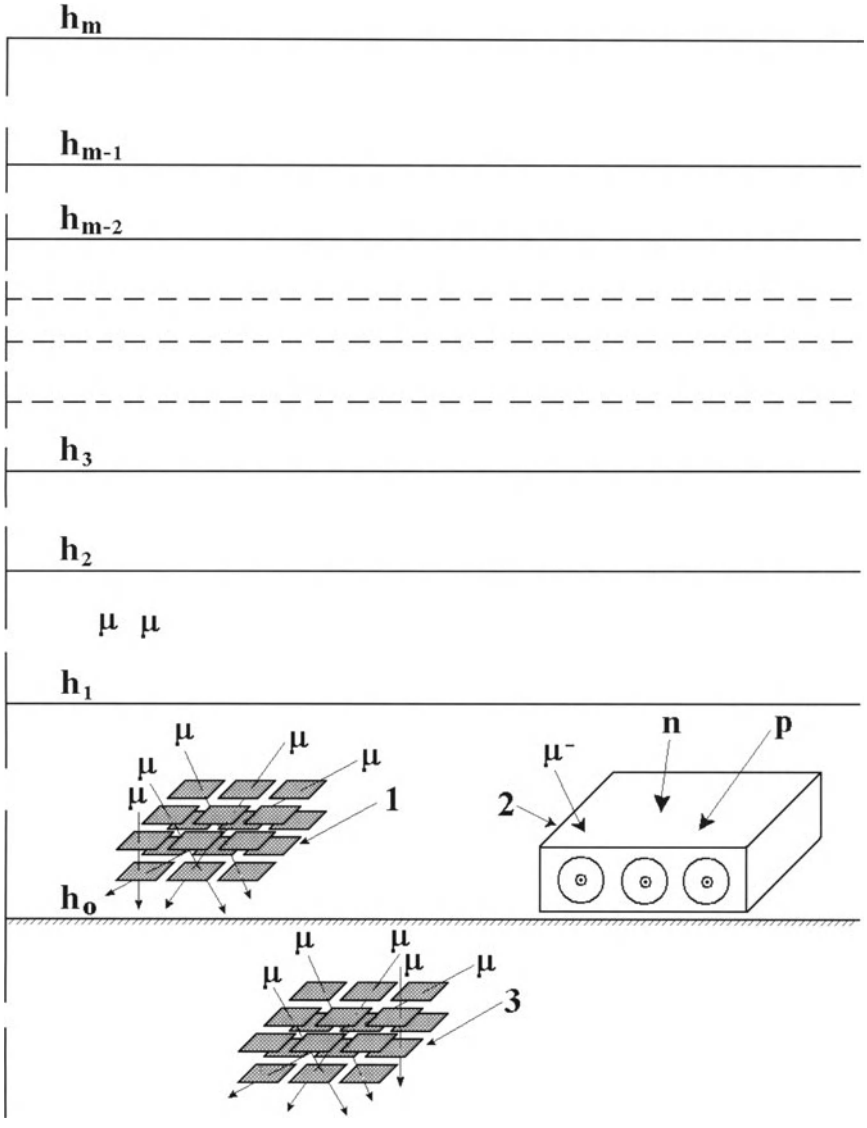

Fig. 18.1.1. Sketch of the general spectrographic method for continuous determination of the vertical distribution of air temperature: 1 and 3 – scintillation multi-directional telescopes on the ground and underground detecting mostly muons at different zenith and azimuthally angles; 2 – neutron monitor which detects mostly neutrons, but also a small part of protons and small energy negative muons which generate lead mesoatoms (nucleus of mesoatoms captured negative muons with generation of secondary neutrons – this part of counting rate is affected by air temperature, see Section 5.5). Also shown are isobaric levels (the total number m of levels must be equal or smaller of the number of secondary CR components with different temperature coefficients).

18.2. Possible CR applications in Hydrology and Agriculture

18.2.1. Using small CR detectors for automatic continuous measurements of snow mass in vertical column over detector and determining of total snow mass reserve in river basins (for hydrology) and on the fields (for agriculture)

In Section 6.1 we considered in detail the snow effect in total neutron component and in different multiplicities. This effect was investigated for exact correction of CR data for meteorological effects to obtain information on magnetospheric and extraterrestrial CR variations. On the other hand, the CR snow effect can be applied in hydrology and agriculture. For determining of expected level of spring flood in river, one needs a very important piece of information on total snow mass in all territory of the river basin. For this aim it can be very effective to carry out automatic measurements in many places of river basin (especially in places which are difficult of access) of snow mass in the vertical cm^2 column over small neutron monitor based on ^3He counters (in units g/cm^2; it is important that the result will not be dependent on the density of snow). Let us note that the increase of snow mass by 1 g/cm^2 will give a decrease in CR intensity of about 0.5%. From this it follows that in order to obtain an accuracy of $\pm$ 1 g/cm^2 for 4 hours' observation the small NM should have an effective area of only 0.25 m^2. The snow mass can be measured also by CR detectors based on muon or electron-photon component (double coincidence of two gas filled counters or two scintillators) with an expected effect of about 0.1% per 1 g/cm^2. In this case to obtain an accuracy of $\pm$ 1 g/cm^2 for 4 hours' observation the effective area of detector can be about 0.25 m^2. The values of snow masses at different places can be obtained by CR detectors automatically by the preliminary calibration of all detectors and after on-line correction of measured CR intensity on barometric effect (according to data of measured simultaneously air pressure), and correction on magnetospheric and extraterrestrial CR variations (on the basis of on-line CR intensity registration on the worldwide network of CR Observatories, available now from Internet on the real time scale). The information from many places will be transmitted to a central computer, which will produce final continuous information on the distribution of snow mass reserves in the river basins and total snow mass reserves on agriculture fields (see in more details in Fridman et al (M1990).

18.2.2. Possible CR applications for Agriculture: using neutron counters for automatic continuous measurements of water content in soil by albedo neutrons generated underground by CR

For agriculture it is important to have continuous information on the water content in soil. This can be obtained by using albedo neutrons generated underground by CR; the flux of albedo neutrons depends very strongly on the effective Z and average density of underground matter. Special experiments made in Kazakhstan by Kolomeets and Fridman (M1981), Aitbaev et al. (1985), Fridman et al (M1990) show that neutron counters without lead are very sensitive to the content of water in soil (see also below, in Section 18.5.2).

18.2.3. Possible use of underwater CR detectors for automatic continuous measurements of level of river, lake, sea, and ocean

Small underwater muon telescopes placed on the bottom or at some altitude above the bottom can be used for exact automatic measurements of time variations of the level of river, lake, sea, and ocean. The CR intensity data obtained by these detectors can very easily be corrected on-line for barometric effect (according to data of simultaneously measured air pressure), and corrected for magnetospheric and extraterrestrial CR variations (on the basis of on-line CR intensity registration on the worldwide network of CR Observatories, available from Internet on the real time scale). From Section 2.4 it can be seen that expected effect in CR intensity is about 0.1% decreasing for the level of water increasing by 1 cm. This means that very simple CR detector based on double coincidence of two gas filled counters or two scintillators with small area of 0.25 m^2 will give an accuracy of ± 1 cm for 4 hours data collection.

18.2.4. Possible use of underground muon telescopes for automatic monitoring of the condition of different types of weirs

One of serious problem in hydrology is the washing out of different types of earthen weirs. For continuous and automatic monitoring of the condition of earthen weirs (dykes, dam-flow and others), simple muon telescope on double coincidences of gas filled counters or plastic scintillators can be used. It is important to make corrections for the barometric effect (which can be done easily using simultaneous measurements of air pressure by a barometer); small corrections on magnetospheric and extraterrestrial CR variations can also be made automatically on the basis of on-line CR intensity registration on the world wide network of CR Observatories, available now from Internet on the real time scale. The choice of the effective area of muon telescope will be dependent on the ground depth where the telescope is supposed to be placed, accepted aperture and necessary accuracy. For example, to have an accuracy of about ± 1 g/cm^2 for 4 hours' observation on the depth 10 m w.e. the effective area of vertical cubic muon telescope must be about 1 m^2, but if daily data are enough, this accuracy can be reached with a very small muon telescope of about 0.2 m^2. Obtained data will be transmitted to the central computer, which performs automatically all the necessary corrections and makes comparison with control values; if the difference is higher than a predefined dangerous condition for the weirs, an alert and signals on the urgent situation will automatically be given.

18.3. Possible CR applications in research of atmospheric electric field phenomenon

As was shown in Section 8.6, the measurements of the CR total neutron component and different multiplicities by the standard NM-IQSY simultaneously with measurements of atmospheric electric field by an specialized EFS-1000 (Electric Field Sensor) give important information on the integral value of the electric field between the level of observations and charged clouds. Let us note that more complete and exact information on atmospheric electric field phenomenon can be obtained by the special CR detector based on separate registration of intensity of positive and negative hard and soft muons (see Section 2.5 on separate measurements of positive and negative muons and

Sections 8.3 and 8.4 on the theory on atmospheric electric field effects in these CR components).

18.4. CR applications in Geology and Geophysical Prospecting

18.4.1. Peculiarities of secondary CR transport through the ground

In Section 2.4 we considered properties of secondary CR underwater and underground. We mentioned that in the first approximation the absorption of muons in water and in different rocks underground are determined mostly by the depth of matter in g/cm^2. Here we will consider peculiarities of secondary CR transport through the ground, which are important for CR research applications in Geology and Geophysical prospecting. For the solution of the problems of Geology and Geophysical prospecting by CR it is important to know how the absorption coefficient depends on the chemical composition of ground. This investigation was made by Blokh et al. (1965) on the basis of results reviewed in Dobrotin (M1954) on muon absorption in air, aluminum, lead, and in other materials as a function of muon energy. With increasing of effective Z of rock's nucleus the absorption coefficient decreases according to Fig. 18.4.1, which shows the change of absorption (in %) *vs* the difference $Z_i - Z_k$ of two types of rocks.

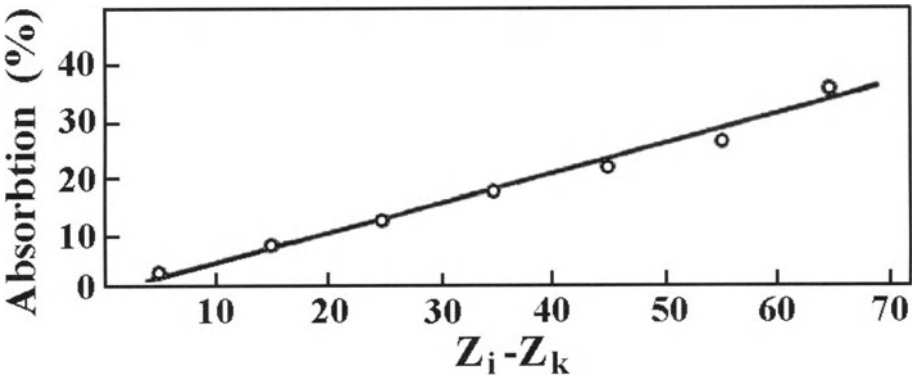

Fig. 18.4.1. The relative change of CR absorption (in %) underground as a function of the difference $Z_i - Z_k$ of two types of rocks. According to Blokh et al. (1965).

For example, for serpentine rock (usually containing sulfide ore) in comparison with background rock $Z_i - Z_k \approx 14$, which gives a decrease of CR absorption by about 7% (at the same thickness of stratum in g/cm^2). This difference in absorption can be used for approximate determination of type of rocks above the CR detector.

The other peculiarity is the difference in muon absorption in water and in rocks. According to Clay and Van Gemert (1939), the absorption in rocks is on average 1.19 times smaller than in water (at the same thickness in g/cm^2). This observation gives an important possibility for searching underground water layers among rocks by CR measurements.

18.4.2. Use of multi-directional muon telescopes inside tunnels, caves, streaks in mines

Bondarenko et al. (1960), Blokh et al. (1963, 1964, 1965, 1967) developed and widely checked the method that use underground multi-directional muon telescopes inside tunnels, caves, streaks in mines for investigation of geological structure, as well as for search and prospecting of useful minerals, water, and ores. Mostly used were vertical muon telescopes on triple coincidences of Geiger counters with aperture 110^{o} and effective area about 0.1 m^2 . The calibration curve for this telescope from 10 m w.e. (on the top of ground at sea level) up to 1,000 m w.e. is shown in Fig 18.4.2.

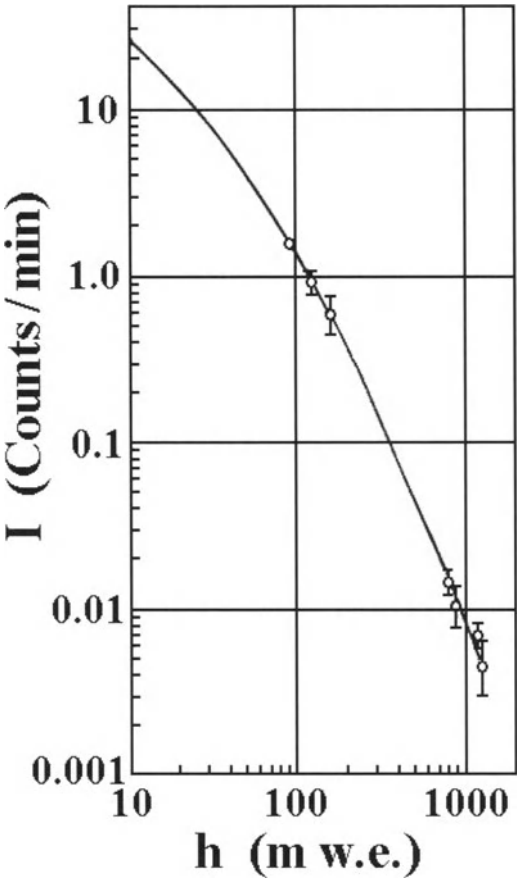

Fig 18.4.2. The calibration curve for muon underground vertical telescope with aperture 110°.

In Blokh et al. (1965) it was shown that by this muon telescope it is very easy to determine the position of karsts zones and holes in rocks, and investigate geological scans (on examples of Kungur cave and mine 'Novaja' of Krivorozhje iron ore basin in Ukraina). These determinations are very important for worked mines: karsts zones and holes in rocks are frequently filled by water and friable material what are dangerous at mine exploitation. The values of average rock density obtained by muon telescope are

important in combination with gravity and seismic prospecting of useful minerals and ores. Small scintillation telescope with an effective area 12 cm^2 was also developed for measurements of average density of rocks in borehole. In Table 18.4.1 are shown results of investigations with this telescope in five boreholes of the 'Medvedovsky' oil and gas field in Krasnodar territory (North Caucus) on the depths from 8 to 30 m.

Table 18.4.1. Results of measurements by scintillation telescope inside of boreholes on different depths. According to Blokh et al. (1965).

Number of borehole	Depth, m	*N*, pulses	*T*, min	*I*, pulses/min	Average density, $g.cm^{-3}$ (relative error, %)
62	10	90	45	2.00 ± 0.21	2.00 ± 0.21 (± 10.5%)
	20	115	120	0.96 ± 0.09	1.85 ± 0.173 (± 9.4%)
	30	436	773	0.56 ± 0.027	1.80 ± 0.087 (± 4.8%)
71	8	306	60	2.55 ± 0.15	1.94 ± 0.114 (± 5.9%)
106	12	108	60	1.80 ± 0.117	1.83 ± 0.119 (± 6.5%)
110	10	182	75	2.43 ± 0.18	1.65 ± 0.122 (± 7.3%)
	20	238	270	0.88 ± 0.057	1.95 ± 0.126 (± 6.5%)
	26	54	90	0.60 ± 0.106	1.98 ± 0.35 (± 17.7%)
161	10	406	180	2.25 ± 0.111	1.79 ± 0.088 (± 5.0%)
	20	222	234	0.95 ± 0.06	1.86 ± 0.117 (± 6.3%)
	30	496	770	0.57 ± 0.025	1.79 ± 0.078 (± 4.4%)

From Table 18.4.1 it can be seen that at the depth 10 m the time of exposition *T* changes from 45 min (with relative error in determination of average rocks density about ±10%) up to 180 min (with relative error ±5%), on depth 20 m from 90 min (with relative error ±10%) up to 270 min (with relative error ±6%), and on the depth 30 m 770 min (with relative error ±4.4%; to obtain accuracy ±3% the time of exposition *T* must be increased up to 35 hours).

Ore body frequently has a difference in density of about 30% in comparison with background rocks (so called anomaly of the ore body, in %). For localization by CR of this type of ore body with probability $P = 99.7\%$ it is necessary to detect $N_{min} = 400$ pulses (relative error ±5%), and with probability $P = 68\%$ $N_{min} = 50$ pulses (relative error ±14%). In Fig. 18.4.3 are shown the expected dependencies of N_{min} from the anomaly of ore body for the probabilities of ore body detection $P = 99.7\%$ and $P = 68\%$.

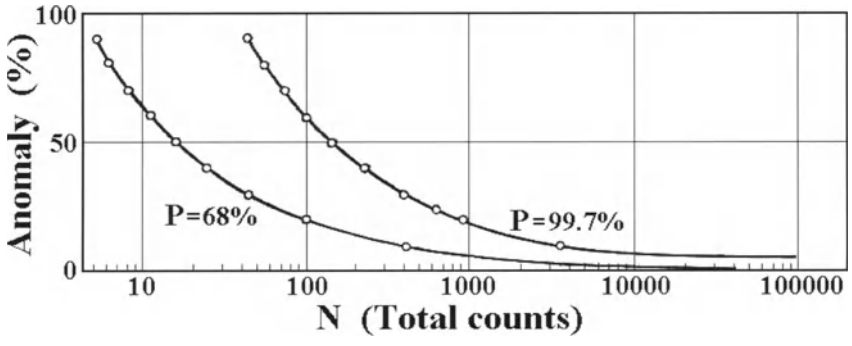

Fig. 18.4.3. The expected dependencies of total counts *N* from the anomaly of ore body for the probabilities of ore body detection $P = 99.7\%$ and $P = 68\%$. According to Blokh et al. (1967).

Blokh et al. (1967) investigated by muon telescopes on Geiger counters with different apertures chalcopyrite basin in the Middle Ural. Here the chalcopyrite ore body have a length about 4800 m; the effective density of the ore body (relative to background rocks) is from +1.3 up to +1.7 g.cm^{-3} (average anomaly 45–50%). The CR intensity measurements were made at depths of 300–350 m. Results are shown in Fig. 18.4.4 together with geological cross-section and expected CR intensity change, calculated on the basis of the geological cross-section.

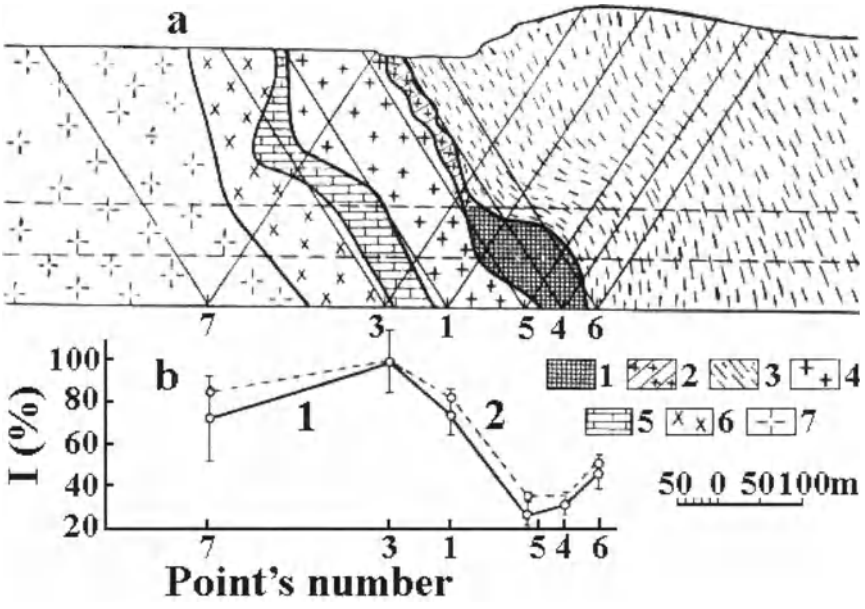

Fig. 18.4.4. Investigation by underground muon telescope of the chalcopyrite basin in the Middle Ural: ***a*** – the geological cross-section (1 – the chalcopyrite ore-vein, **2–7** different background rocks); ***b*** – comparison of measured CR intensity (full curve **1**) with expected CR intensity (dashed curve **2**, calculated on the basis of the geological cross-section). According to Blokh et al. (1967).

In this case (see Fig. 18.4.4) according to CR data the lateral dimension of the chalcopyrite ore-vein was estimated as 145 m in comparison with value 120 m derived from geological cross-section (the obtained difference can be explained by the fact that really sufficient part of chalcopyrite was scattered in the vicinity of ore-vein, in the background rocks).

Blokh et al. (1967) checked the method also in the poly-metallic basin in the Middle Asia at depths 25 and 44 m by two underground muon telescopes on Geiger counters with apertures 55^{o} and 65^{o}. This was a more complicated case (the density inside ore-body changes from 2.4 g.cm^{-3} to 5.1 g.cm^{-3} with density of background rocks being about 2.6 g.cm^{-3}), but in this case the ore body was also choused by CR measurements with probability 98%. The investigations of iron ore basin in the Middle Asia by two underground muon telescopes on Geiger counters with apertures 55^{o} and 65^{o} enabled finding several magnetite-ore bodies above horizontal gallery (Blokh et al., 1967).

18.4.3. Possible use of special neutron monitor for underground searches

In several CR expeditions where we used standard NM-IQSY and NM without lead, we observed very strange phenomenon, the so called CR shore effect: when the ship with our apparatus entered a port or crossed narrow canals, the intensity of total neutron intensity, and especially the counting rate of multiple neutrons in the NM without lead increased considerably, from few to several tens of percents (Dorman et al., 1979, 1984a,b, 1985; Aleksanyan et al, 1979a,b; Bednazhevsky et al, 1979). It is important to note that simultaneous measurements with the standard NM-IQSY (with lead as generator of secondary neutrons) show practically no variations in counting rate. We interpreted these results by the hypothesis that NM without lead is very sensitive to the environment surrounding the NM because a significant fraction of counting rates of total neutron intensity and different multiplicities is caused by neutrons and other secondary particles generated by CR not inside the monitor (as in the case of standard NM-IQSY or standard NM-IGY), but outside the NM body, in the environment. In the papers mentioned above it was shown that NM without lead reflects well the situation in environment up to distances of several tens of meters. The relative sensitivity to the environment in the case of ground in comparison with water (and especially in the case of more heavy atoms as iron) increases with increasing of neutron multiplicity. In 1991 we planed in the framework of 'Israel Cosmic Ray Center and Foundation of International Cosmic Ray Service' Project (Dorman, M1991) to develop a special detector on the basis of NM without lead, but protected mostly from direct CR arriving from above (by using combination of cadmium and some other materials on the top of NM). In this case the sensitivity of NM without lead to the environment and its contents is expected to increase several times. According to the Project it was planed to check this special detector in many applications (geology and geophysical prospecting, archeology, security service and so on). This Project was accepted by the Ministry of Science of Israel (the Minister Prof. Yuval Ne'eman) at the end of 1991, but after the 1992 general elections in Israel this acceptance was cancelled. Nevertheless, a few years later, the main part of the Project was realized, thanks to the great help of Prof. Yuval Ne'eman: founding in 1997–1998 of Israel Cosmic Ray Center (ICRC), including Israel-Italian Emilio Segre' Observatory on Mt. Hermon, World Data Center C1 for CR (archive of this former WDC was transferred from Sweden), and in 2002 the founding of the National Space Weather Center (in the frame of ICRC). We hope that our plan to develop a special NM detector with high sensitivity to the environment will be realized in the near future. We think that this type of detector after special calibration experiments can be widely used for quickly searching water, holes with gas, oil, different types of ore in mountains or underground (at a depth of up to a few tens of meters) by registration of the neutron intensity and multiple neutrons generated by CR out of NM, in the environment. The time exposition will depend on the effective surface of detector and type of searched environment (from few hours to few minutes). Simultaneously it is necessary to measure also the intensity of natural radiation (CR + radioactivity of soil and radioactive emanations in the atmosphere; this information will be very important for geophysical prospecting and can be used for preparing a map of natural radiation distribution, see Section 18.8 below). Let us note that for using the special neutron detector in expedition conditions to search quickly a wide area, the neutron detector must

be placed on a special platform without heavy elements (e.g. made mostly from wood or plastic), which can be conveyed by track or helicopter to a distance of several meters from the detector. In this case the special NM will continue to work while being moved for continuous investigation of the environmental conditions on the ground and underground. In Fig. 18.4.5 we gave a sketch of the possible expedition measurements by car and/or by helicopter for search over ground surface and over mountains for ore, water, oil, holes or other objects underground at a depth of up to several tens of meters.

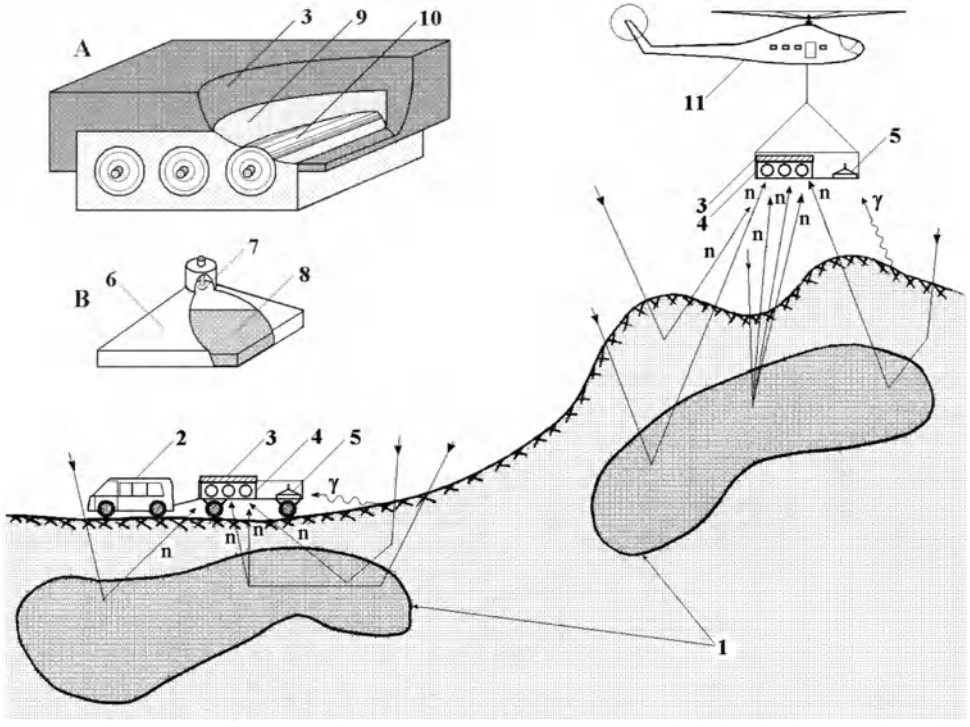

Fig. 18.4.5. Sketch of possible use for geophysical prospecting special NM (without lead and mostly protected on the top from directly arriving CR, is shown in more detail in the upper left corner, ***A***) and scintillation detector (also for using in navigation according to description in Section 18.8, is shown in upper left corner, ***B***), conveyed by truck (2) or helicopter (11). Denotes: 1 – ore of metals or minerals, petroleum, water or other matter with density or/and Z different from soil; 2 – expedition truck; 3 – protector of special NM from direct arriving CR, 4 - special without lead NM, 5 scintillation detector, 6 – reflector of scintillation detector, 7 – photo-multiplier, 8 – scintillator, 9 – polyethylene, 10 – neutron counters filled with ^{3}He or $^{10}BF_3$ 11 - expedition helicopter.

18.4.4. Use of special NM without lead for quick determination of the quality of ore

The special NM without lead covered on the top by a thick sheet of cadmium and other materials for protecting mostly from direct CR can be effectively used for quickly determining the quality of ore in rocks on transporter or in tracks. It will be based on the rough estimation of the relative contents of heavy elements as iron, copper, silver, gold,

molybdenum, wolfram, lead, uranium and so on in comparison with background elements by the method of multiple albedo neutrons generated by CR in ore on a transporter or in tracks.

18.4.5. Use of special NM without lead for search in old mines or in acting mines

The special NM without lead described above, which is very sensitive to the environment, can be effectively used in old and working mines (as well as in planning new mines) for the search of places underground with rocks containing ore of good quality by the method of multiple albedo neutrons generated by CR. It can significantly increase the effectiveness of acting mines, and allow restoring old mines.

18.5. CR applications in Environmental Science

18.5.1. Using cosmogenic isotope data for estimation parameters of planetary mixing and exchange of chemical elements

In Chapter 17 we considered in detail the radiocarbon method. In Section 17.5 we mentioned H-bomb explosions in atmosphere carried out by the USA and USSR in 1962, generation of radiocarbon and estimation of parameters of the element mixing and exchange model; influence on global environment. In this Section radiocarbon data for 1962 and several years after 1962 are used for determining parameters of chemical elements planetary mixing and exchange. In principle these important environmental parameters may not be constant: they can change with long term climate change.

On other hand it was shown in Chapter 17 that radiocarbon content in the atmosphere, in the ocean, in dated samples (tree year rings, old wines, etc) depends not only on CR intensity, but also on parameters planetary mixing and exchange of chemical elements. Let us consider the cases in which CR intensity can be determined independently by other methods (it means that one can determine independently the production rate of radiocarbon in the atmosphere):

1) from ^{10}Be and other cosmogenic isotopes data (see Chapter 10),

2) from data on the Earth's magnetic field (which gives the possibility of calculating the long term change of cut off rigidity ΔR_C, and then expected change of CR intensity according to the second member in the right hand of Eq. 3.1.3; for more details see in Dorman, M2005).

3) from data on sunspot numbers in the past (giving the possibility to determine parameters of convection-diffusion and drift modulations derived from investigations of hysteresis effects in connection of solar activity cycle variation with galactic CR modulation, and then to determine the expected CR intensity long term variation; for more details see Dorman, M2005).

After determination of the expected radiocarbon production rate in the atmosphere in the past by ^{10}Be data or by calculation on the basis of geomagnetic data and sunspot data by using information on convection-diffusion and drift CR global modulations we compare with observed long-term variations of radiocarbon contents according to ring trees annual data. This comparison can be made in the framework of the two-reservoir

model of elements planetary mixing and exchange (described in Section 17.4), or in the framework of the five-reservoir model (described in Section 17.8). From this comparison we can estimate parameters of planetary elements mixing and exchange and their long term variations caused by the global climate change in the past. These types of investigations (which can be made in near future) will be very important for understanding the deep causes leading to the global climate change on our planet (see also Chapter 14 and in Jockel, 2000).

18.5.2. CR applications for treating pollution of the Earth atmosphere, water, snow, and soils

Fridman et al. (1995) tried to use CR for treating pollution of the Earth atmosphere, water, and soils on the basis of CR neutron absorption. The physical essence of the method is in the determination of ingredient concentrations according to the characteristic emission of atoms and nuclei excited by the CR protons, neutrons and gamma rays. The physical process involved for pollution determining can be described by the reactions:

$$A+p \rightarrow A'+p'+\gamma,\ A+n \rightarrow A'+n'+\gamma,\ A+p \rightarrow A'+n+\gamma, \text{ and so on,} \qquad (18.5.1)$$

where $A(A')$ and $p(p')$, $n(n')$, $p(n)$ and so on are the atomic nuclei of the impurity and CR proton or neutron before (after) an interaction (Kogan et al., M1976; Boos et al., 1983). To determine the impurity concentration the dominating characteristic lines corresponding to the lower excitation level of pollution atoms and nuclei are considered. In general these lines are from background atoms excited by the CR protons ($E_k \geq 5$ MeV), neutrons and gamma rays. The volume of matter what can be investigated by this method is determined by the free path of gamma rays from exited atoms. For example, the carbon characteristic line 4.44 MeV can be measured in dry air with density 1.29×10^{-3} g.cm^{-3} at sea level from distances $L \leq 250$ m. Fig. 18.5.1 shows the characteristic emission spectrum at nuclear level in the energy range 0–5 MeV.

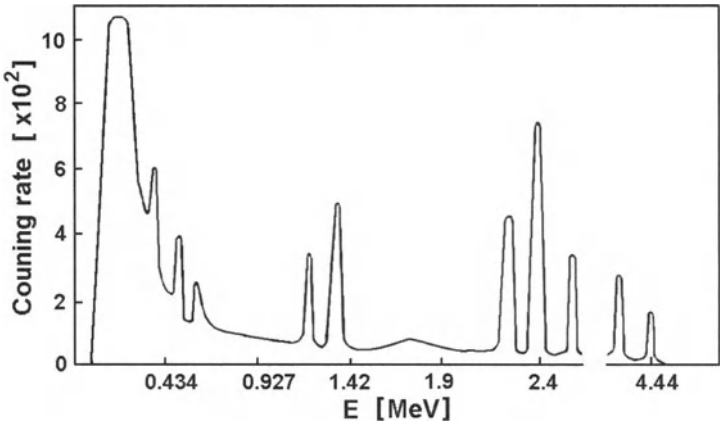

Fig. 18.5.1. Characteristic emission spectrum of elements at the nuclear level. According to Fridman et al. (1995).

Fridman et al. (1995) show that for developed detector the exposure time of ~ 10 hours is enable to observe statistically significant nuclear lines of ^{40}K, uranium and ferrous groups as well as carbon lines. The obtained results demonstrate the possibility of ingredients concentration measurements in the atmosphere, water and soils up to 10^{-5} g/cm^3 within a reasonable exposure time. Model calculations and experimental data indicate that there is an unambiguous relation between moisture contents in soils, snow and ice at corresponding depths (Kodama et al., 1975; Kolomeets and Fridman, M1981). Fig. 18.5.2 shows the time dependence of moisture content in snow at the mountains of Zailiisky Alatau.

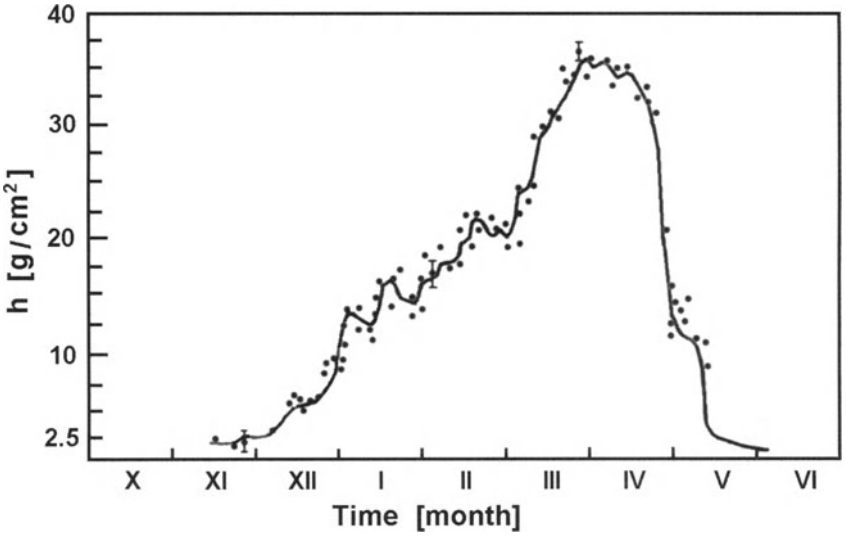

Fig. 18.5.2. Dynamics of the moisture content reserve change in the snow. The points refer to control measurements; the solid curve – on the basis of CR data. According to Fridman et al. (1995).

The moisture content dependence on the slow neutron flux reduction can be described by the following peculiarities. In the snow layers of ~ 20 g/cm^2 thickness the main role play neutrons slowing down by the interactions with hydrogen nuclei due to the thermal neutron absorption. Father it was considered nuclear reactions of energetic neutrons with nuclei of the ice and snow substance, an intermediate energy neutrons generation and the slowing down and absorption of these neutrons. On the basis of this consideration Fridman et al. (1995) developed an automatic remote system of moisture and pollution content measurements in soils at the depths of 0–5 m and moisture content reserve as well as pollution in the snow in the interval of 0–500 g/cm^2. These automatic measurements in many different sites may be very important for Ecology as well as for Agriculture (see above, in Section 18.2.2). Let us mention also the paper of Cecchini et al. (1995) on the developing of a compact scintillation NaI(Tl) detector, long term stable and reliable, to monitor the environmental gamma radiation in the energy range 0.28-2.8 MeV, due to very low energy secondary cosmic radiation and radioactivity, airborne and from environment matter.

18.6. CR applications in Archeology

18.6.1. Using multi-directional muon telescope inside pyramids or other historical objects for search for some peculiarities in the structure

It is well known that many years ago muon telescopes were used to search for some holes in pyramids; by this method mysterious rooms with very important historical artifacts were discovered. For more detailed investigations of the structure of pyramids or other historical objects one can also use multi-directional muon telescopes based on gas filled counters or on scintillators. For these CR applications we can use the same methods that were developed for using CR inside tunnels, caves, streaks in mines and so on for determining of mass in different directions for research of the geological structure and search of water, holes, and some types of ore (see Section 18.4).

18.6.2. The well known improvement of the radiocarbon method for the dating of important historical samples

In the well known use of the radiocarbon method for dating important historical samples (see review in Michels, M1973; Gillespie, M1984; Faure, M1986; Taylor, M1987; Aitken, M1990; Bowman, M1990; Geyh and Schleicher, M1990; Taylor et al., M1994) it is usually suggested that CR intensity and radiocarbon production rate is constant and equal to the present value. But in reality, as was shown in Chapters 10 and 17, CR intensity in the past varied. Moreover, we can calculate the expected CR intensity and radiocarbon production rate on the basis of geomagnetic data and data on solar activity in the past as it was considered in Section 18.5.1 (for more details see Dorman, M2005). This information will significantly increase the accuracy of dating historical samples by radiocarbon method.

18.6.3. Possible use of special neutron monitor without lead for searching some historical samples in soil

The method described above in Section 18.4.3 on the possible using for geophysical prospecting special NM (without lead and mostly protected on the top from direct arriving CR), may be used also for searching some historical samples in soil (at depths of not more than a few tens of meters), content of elements different from soil: light elements (such as wood) or heavy elements (such as iron, silver, gold, platinum) by the method of multiple neutrons generated by CR in soil and in historical artifacts. This method is based on the experimental investigations of the dependence of multiple neutron generation in different materials: it was shown that the generation rate is proportional to the square of Z.

18.7. Possible Forensic applications

18.7.1. Using radiocarbon method for dating of samples important for criminal investigations

Radiocarbon method, described in detail in Chapter 17, can be used for dating of samples important for criminal investigation. The radiocarbon contents in some criminal

sample $N_s(t_o)$ measured at time t_o in this sample, but dated (exposed) at some unknown time t, will be reflected in the radiocarbon contents $N_A(t)$ in the atmosphere at time t according to relation

$$N_A(t) = N_s(t_o)\exp(\lambda(t - t_o)), \tag{18.7.1}$$

where λ is the decay constant of radiocarbon, and corresponds to $T_{1/2} = 5730$ years. In radiocarbon application method for archeology, it is usually supposed that CR intensity is about constant, so the radiocarbon production rate will be about the same as in the present time and in this case (see Eq. 17.4.15 in Chapter 17):

$$N_A(t) = N_{A\text{st}} = Q_{av}(\lambda + \lambda_{FA})(\lambda(\lambda + \lambda_{AF} + \lambda_{FA}))^{-1}, \tag{18.7.2}$$

where Q_{av} is the average for many years production rate of radiocarbon, λ_{AF} and λ_{FA} are the probabilities per one year of radiocarbon exchange from reservoir A (atmosphere) to the other planetary reservoir F and inverse, from F to A, respectively. From Eq. 18.7.1 and Eq. 18.7.2 follows

$$\begin{aligned} t - t_o &= \lambda^{-1}\ln(N_{A\text{st}}/N_s(t_o)) \\ &= \lambda^{-1}\ln\left\{\left[Q_{av}(\lambda + \lambda_{FA})(\lambda(\lambda + \lambda_{AF} + \lambda_{FA}))^{-1}\right]/N_s(t_o)\right\}. \end{aligned} \tag{18.7.3}$$

The accuracy of the results obtained can be increased if the real long term CR intensity variation by using data of CR observations by the network of NM is accounted for. These data from 1952 up to the present time are available from WDC in Boulder or from the Internet. For discovery of historical criminal acts in the past from 1750 up to 1970 one can use information on CR intensity derived from data on long term variations of cut off rigidity (determined from data on geomagnetic field change), and from data on the long term CR modulation (derived from data on solar activity by using information on convection-diffusion and drift modulation parameters derived from comparison of theoretically expected CR long-term variation with observed for several solar 11 year cycles in 1953–2001). Let us note that for discovery of historical criminal act many years ago by radiocarbon method very useful are ^{10}Be data what gave directly information on CR intensity long term variation in the past up to several thousand years. So let us suppose that the production rate of radiocarbon $Q_p(\tau)$ is known exactly. In this case, by measurements of radiocarbon contents in the crime object can be determined the time when this object was exposed by CR in the framework of the two-reservoir model (see Section 17.4) or in the framework of the five-reservoir model (see Section 17.8). Let us consider, for example, the two-reservoir model. In the framework of this model the time variation of contents in the atmosphere $N_A(t)$ will be described by (see Section 17.4, Eq. 17.4.18):

$$N_A(t)=\frac{\lambda_{FA}\exp(-\lambda t)}{\lambda_{AF}+\lambda_{FA}}\left[\int_0^t\exp(\lambda\tau)Q_p(\tau)d\tau+\frac{Q_{av}}{\lambda}\right]$$
$$+\frac{\lambda_{AF}\exp(-\lambda_1 t)}{\lambda_{AF}+\lambda_{FA}}\left[\int_0^t\exp(\lambda_1\tau)Q_p(\tau)d\tau+\frac{Q_{av}}{\lambda_1}\right], \qquad (18.7.4)$$

where we denote $\lambda_1=\lambda+\lambda_{AF}+\lambda_{FA}$. By substituting Eq. 18.7.4 in Eq. 18.7.1 we obtain

$$N_s(t_o)\exp(\lambda(t-t_o))=\frac{\lambda_{FA}\exp(-\lambda t)}{\lambda_{AF}+\lambda_{FA}}\left[\int_0^t\exp(\lambda\tau)Q_p(\tau)d\tau+\frac{Q_{av}}{\lambda}\right]$$
$$+\frac{\lambda_{AF}\exp(-\lambda_1 t)}{\lambda_{AF}+\lambda_{FA}}\left[\int_0^t\exp(\lambda_1\tau)Q_p(\tau)d\tau+\frac{Q_{av}}{\lambda_1}\right]. \qquad (18.7.5)$$

The solution of Eq. 18.7.5 will give the exact value of the unknown $t-t_o$ taking into account not only the decay of radiocarbon (as described by Eq. 18.7.3), but also the long term variations of CR intensity.

18.7.2. Use of special neutron monitor without lead in forensic science

We described this type of detector above in Section 18.4.3, where it was shown to be useful for geophysical prospecting to search underground water, petroleum, minerals, different types of ores (see Fig. 18.4.5). The same detector (mainly protected from direct CR by cadmium and other materials on the top) can also be used for seeking criminal evidence in soil (at a depth of not more than a few meters) with elemental content different from soil: light elements (such as people's bodies) or heavy elements (such as a dagger, rifle, revolver, pistol, and so on) by the method of multiple neutrons generated by the neutron component of CR, arriving underground and in nuclear interactions with soil and atoms of criminal things single and multiple albedo neutrons. It is important to note that the density or/and average Z of soil and sought objects will be different.

18.7.3. Possible application of special neutron monitor without lead for searching cemeteries

The same detector, described in Section 18.4.3 (see Fig. 18.4.5) and mentioned in the previous Section 18.7.2 may be useful for searching for criminal, secret, or forgotten cemeteries by the method of multiple albedo neutrons generated by CR underground in soil and in people's bodies (the search is based on the difference in the density and average Z of soil and people's bodies).

18.8. Possible CR applications for Navigation

In Dorman (M1991) the use of the well known altitude dependence of natural radiation intensity (CR + radiation from soil radioactivity) was supposed for the roughly estimation of the real distance to the ground for any flight object (rocket, airplane, helicopter and others). There are well known terrible catastrophes caused by mistakes in

determining of this distance by standard sensors. So, any additional independent method for the determination of this distance will be useful. Our rough estimation shows that to obtain enough accuracy for a collected time of about 1 sec one may use CR detector (plastic scintillator) with effective area about 0.5–1.0 m^2. It is necessary to make preliminary expedition measurements over the investigated area (e.g., in vicinity of airport, in some mountain region, and so on) with scintillation detector on helicopter on different distances from the ground (e.g., as it was shown in Section 18.4, in Fig. 18.4.5), and to obtain a 3-D map of the distribution of natural radiation intensity (CR + radiation from environment radioactivity) from the ground up to few hundred meters (as illustration, Fig. 18.8.1 shows a cross-section of such a 3-D map).

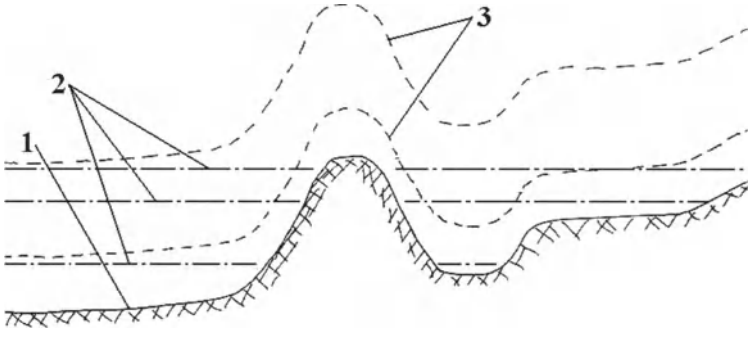

Fig.18.8.1. Illustration of the natural radiation method of automatic continuous measurements of the real distance from the flight object to the ground: *1* – the ground surface; *2* – surfaces of equal barometric pressure; *3* – surfaces of equal intensity of natural radiation (CR intensity + fluxes from radioactivity environment). According to Dorman (M1991).

Corrections for CR intensity time variations are relatively small and may be very easily taken into account by real time data from stationary CR detector on the ground (or by real time CR data from Internet what are available now from many CR Observatories).

18.9. CR data applications for the Physics of the Earth's magnetosphere

18.9.1. Use of CR spectrographic method for continuous determination of magnetosphere equatorial ring current's properties

In Sections 3.11 and 3.12 it was shown that by the spectrographic method can determine independently spectrum of primary CR variation $\Delta D(R,t)/D_o(R)$ and variation of cut off rigidity $\Delta R_c(t)$. Continuous information on $\Delta R_c(t)$ at different latitudes is very important for the Physics of the Earth's magnetosphere: by using data on magnetic field variation on the Earth's surface (or/and on the low orbit satellites) and data on $\Delta R_c(t)$ one can determine the effective radius of equatorial ring current, and its

value as well as its time variations. So CR data can be used for continuous monitoring of the equatorial ring current of the Earth's magnetosphere (this problem will be considered in detail in Dorman, M2005).

18.9.2. Using CR latitude surveys data for testing magnetosphere models

On the basis of magnetosphere models for quiet and magnetically disturbed periods (e.g. Tsyganenko, 1989; Tsyganenko and Stern, 1996) by trajectory calculations in many investigations were determined the planetary distribution of CR cut off rigidities (Shea et al., 1976; Villoresi et al., 2000; Dorman et al., 2000). The obtained planetary distribution of CR cut off rigidities can be checked by CR latitude surveys data and on the basis of this comparison the considered model of the magnetosphere can be accepted, corrected, or rejected as not real (e.g. Dorman et al., 1982, 2000; Villoresi et al., 2000; Iucci et al., 2000). Details of this problem will be considered in Dorman M2005).

18.10. CR data application for the Physics of the Heliosphere

CR data for several 11 year solar cycles were used for the analyzing of the hysteresis connection between CR intensity long term variations and solar activity. As a result, in 1967 for the first time the real dimension of the Heliosphere was estimated: about 100 AU (Dorman and Dorman, 1967a,b). In the latter years these investigations were continued and the relative roles in the Heliosphere convection-diffusion and drift modulations, the change with solar activity dimension of the Heliosphere, CR diffusion coefficient, and CR intensity out the Heliosphere were determined (Dorman, 2001b; Dorman et al., 2001b,c). Important information for the physics of the Heliosphere also gave investigations of CR anisotropy by ground based neutron monitors and by muon telescopes on the ground and underground (Ahluwalia and Dorman, 1995a,b, 1997; Dorman and Ahluwalia, 1995; see review in Dorman, 2000). Nonlinear effects of CR in the interplanetary space (CR pressure and kinetic stream instability effects, formation of the boundary of the Heliosphere, terminal shock wave, and 'buffer layer') are also important for the physics of the Heliosphere (see review in Dorman, 1995, 1999c). These problems of CR role in the Physics of the Heliosphere and CR using for Heliosphere research are out of the scope of this book; details of these problems will be considered in the next book (Dorman, M2005).

18.11. CR research and climate change: possible applications

In Chapter 14 we considered the problem of CR influence on cloud coverage, on the amount of rain, on the ground temperature, and on global climate change. On the basis of this research Stozhkov et al. (1999, 2001) suggested using the phenomenon of CR influence on climate change: by producing artificial CR in the definite places to influence on the natural climate change in the useful direction. For this purpose a small electron accelerator on an airplane or on a helicopter can be used. From results of Chapter 14 follows that increasing of ionization by artificial CR on low altitudes (up to few km) will lead to increasing of cloudiness and raining, and lowering the ground temperature; the same on higher altitudes can lead to increase of ground temperature. It is important that using of ^{14}C and ^{10}Be data for determining of CR intensity variation in

the past can help in estimation of long term climate change during many thousand years ago; the obtained results can be checked by ^{18}O data on the average temperature of the World Ocean. For shorter period (few hundred years) for exact determination of long term CR intensity variation in the past in dependence of particle rigidity can be used solar activity data (Dorman, 2003a) and data on the long term variation of CR cut off rigidity distribution on the Earth in dependence on the latitude and longitude (Shea and Smart, 2003a,b; Smart and Shea, 2003; Flückiger et al., 2003). This information can be used then for determination of long term variation in air ionization by CR on different altitudes and latitudes, owed by CR long term change in cloudiness planetary distribution in dependence of altitude, and finally – on the part of long term climate change owed by CR (see in detail Chapter 14). Let us note that for this aim will be important also investigations on the connection between CR and atmospheric electric field phenomenon, between CR and thunderstorm discharges (see Chapters 8 and 11).

18.12. CR research applications for space weather monitoring and forecasting

This problem is an example of how fundamental research in Cosmic Ray Astrophysics and Geophysics can be applied to a very important modern practical problem: monitoring and prediction of space weather by CR, using on-line CR data. This activity covers space phenomena dangerous for satellite electronics and astronauts health in the space, for crew and passenger's health in commercial jets in the atmosphere, and in some rare cases for technology and people on the ground (see Fig. 18.12.1).

This problem is very wide and will be considered in detail in the next book Dorman (M2005); here we will give only very short description of the problem and some main references. In Chapter 1 (see Section 1.2.10) we mentioned that in 1993 it was suggested to create the International Cosmic Ray Service (ICRS) for continuous monitoring of space weather and for forecasting of dangerous space phenomena by using on-line CR data (Dorman, 1993; Dorman et al., 1993a-c).

There are two types of space phenomena for which monitoring and forecasting are very important: 1) big space radiation storms caused by solar CR accelerated to energy up to 15–20 GeV during great solar flares and diffusion propagated through the solar corona and interplanetary space (1a), by energetic particles up to energy 10–30 MeV accelerated and propagated by coronal mass ejection and interplanetary shock waves (1b), and 2) great space magnetic storms produced geomagnetic storms accompanied as a rule by CR Forbush-decreases. The continuous on-line CR ground observations by NM and MT on the world network may be useful for monitoring and forecasting of great space radiation storms (caused by solar CR) and great space magnetic storms (space weather effects on human health we consider shortly below in Section 18.16).

It is well known that in periods of great FEP (Flare Energetic Particle) events, fluxes can be so high that memories of computers and other electronic components in space may be harmed, satellites and spacecraft became destroyed. Let us note that each year insurance companies paid a lot of money for these failures and satellite loose. In Fig. 18.12.2 is shown information from insurance companies on the premiums what they paid for satellite losses and failures (at least about half was caused by space weather effects; the problem on satellite malfunctions, as one of important applications of CR research, we consider shortly in Section 18.17).

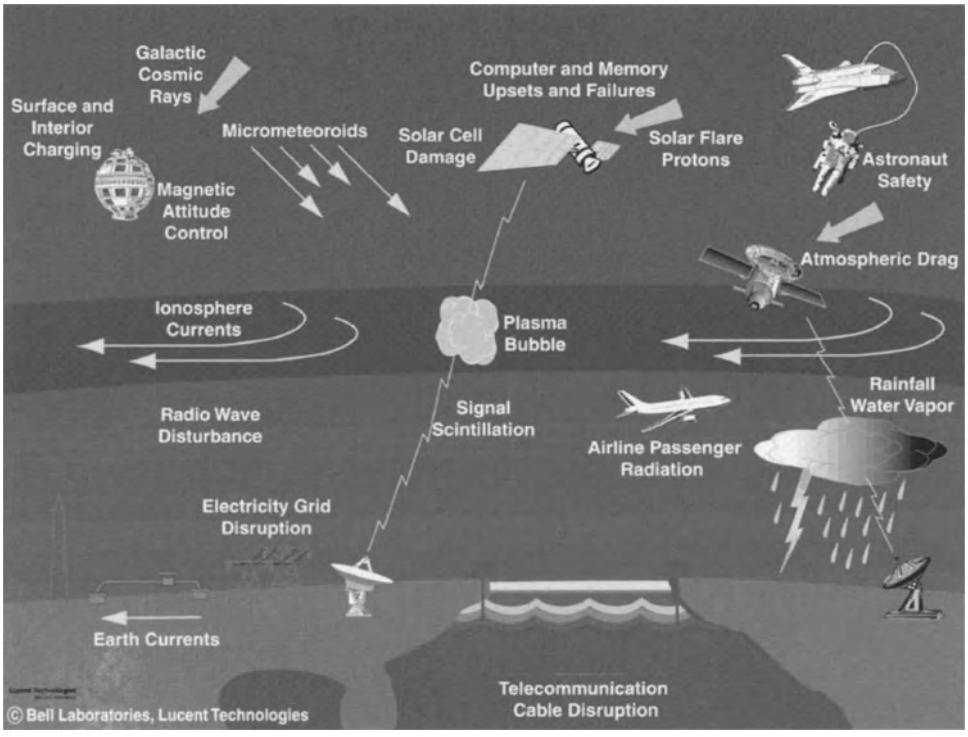

Fig. 18.12.1. Space weather effects (from Bell Laboratories website in Internet).

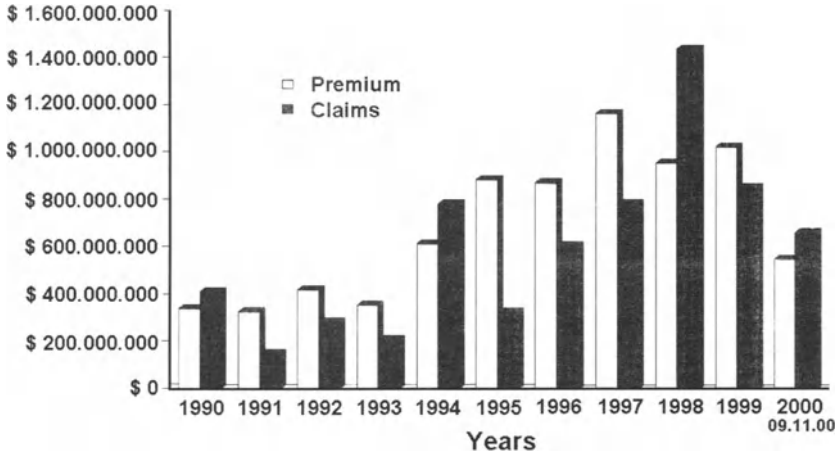

Fig. 18.12.2. Market premiums of insurance companies for satellite losses and failures in 1990–2000. From J.H. Allen (private communication).

Let us note that if in near future exact forecasting will be not organized, very great problems may arise. For example, an event similar to that of February 23, 1956 occurs,

practically all satellites in space may be destroyed: the price of this will be many billions of dollars; satellite based communication will disappear; astronauts will be exposed to a lethal dose of radiation (the same may be for passengers and crew of airplanes); other big problems may also arise. To avoid these it is necessary first to organize an international service for continuous monitoring and forecasting of these dangerous space phenomena. The second step required is to develop procedures for what to do for satellites and planes in case of dangerous situations in space (for example, in these periods is necessary to switch off some systems to protect the electronic components, to decrease the altitude of plains, and so on).

The problem is how to forecast exactly these dangerous phenomena. We show that an exact forecast can be made by using high energy particles (about 5–10 GeV/nucleon and higher) whose transport from the Sun is characterized by much bigger diffusion coefficient than for small and middle energy particles, which are especially dangerous owing to their high flux. Therefore high energy particles came from the Sun much sooner (8–20 minutes after acceleration and escaping into solar wind) than the main part of smaller energy particles that cause the dangerous situation for electronics and people health (about 30–60 minutes later). In Israel Cosmic Ray Center and Emilio Segre' Observatory we developed principles and obtained experience of automatically working program FEP-Search-1 min, FEP-Search-2 min, FEP-Search-5 min (see Section 4.8). The second step is to determine automatically the flare energetic particle spectrum, and then the diffusion coefficient in the interplanetary space, time of ejection and energy spectrum of FEP in source. These steps allow forecasting of expected FEP flux and radiation hazard for apparatus in space, satellites in the magnetosphere, jets and various objects in the atmosphere, and on the ground.

Also in recent years there were theoretical and experimental developments in the use of high energy CR data for forecasting of major geomagnetic storms accompanied by Forbush effects (which affect communications, navigation systems, satellites and high level technology systems in space, in the atmosphere, and on the ground).

Many aspects of these problems are considered in Dorman and Miroshnichenko (M1968), Dorman (M1991, 1993, 1999a,b; 2001a,b; 2002, 2003b,c), Villoresi et al. (1994a,b; 1995), Belov et al. (1995, 2002, 2003a,b), Badhwar and O'Neill (1996), Ahluwalia et al. (1996), Dorman and Pustil'nik (1995, 1999), Beaujean et al. (1999), Friedberg et al. (1999), Dorman et al. (1993a,b,c; 1995a,b; 2001a, 2003a-e, 2004), Munakata et al. (2000), Kudela et al. (2000), Daglis (M2001), Belov (2002), Belov and Eroshenko (2002), Struminsky (2002), Dorman and Zukerman (2003), Stassinopoulos et al. (2003), Smart and Shea (2003a), Mortazavi et al. (2003), Zhou et al. (2003).

18.13. Application of regular CR measurements by radio balloons for environment monitoring of radioactive clouds from nuclear explosions or nuclear plant failures

In Section 2.13 we considered important results obtained using regular CR measurements by radio balloons in investigations of secondary CR and precipitation phenomenon (the used apparatus was described in Section 4.6.3). According to Stozhkov et al. (2001), regular radio balloon measurements of charged particle fluxes in the troposphere and stratosphere provides the prompt control of radiation conditions and allows to detect radioactive clouds from nuclear explosions or nuclear plant failures. In

Fig. 18.13.1 and 18.13.2 the observations of radioactive clouds in the northern polar atmosphere (Murmansk region) in 1970 and over Moscow in 1993 are shown as an examples.

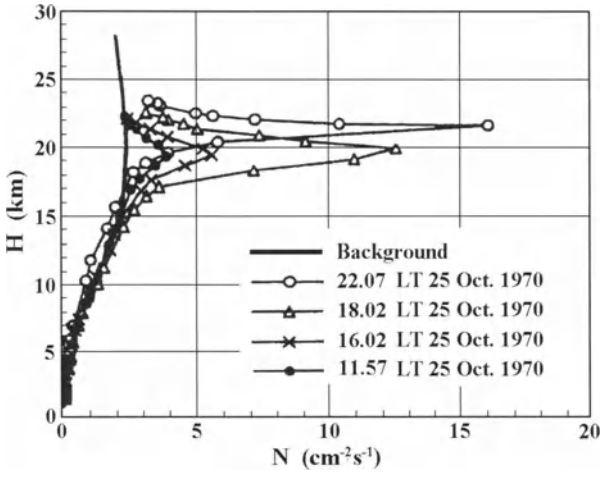

Fig. 18.13.1. Charged particle fluxes in the northern polar atmosphere (Murmansk region) detected by single counters of radio balloons. At $H > 15$ km the excess of flux over the CR background (solid line) is owed to radioactive cloud particles produced by the nuclear explosion in China on 14 October 1970. In the insert the legend on the date and balloon start times are given. According to Stozhkov et al. (2001).

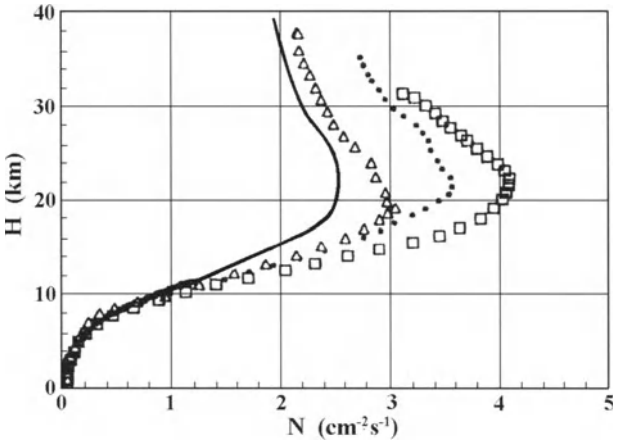

Fig. 18.13.2. The counting rate of single counter vs. altitude in the atmosphere over Moscow on 12-14 April 1993: solid line - background from galactic CR; black points - charged particle flux measurements at 13 April, launching time 08.30 LT; triangles – at 13 April, 14.30 LT; squares - at 14 April, 08.30 LT. According to Stozhkov et al. (2001).

The excesses of particles over the CR background recorded by single counter were due to the radioactivity particles (in these cases the telescope data showed normal counting rate from CR only). A powerful ground nuclear explosion was produced near lake Lobnor in China at the 14th of October 1970. In the atmosphere radioactive cloud

was observed near Murmansk by radio balloon measurements at October 25-26 (see Fig. 18.13.1). Near Alma Ata radioactive cloud from China nuclear explosion was observed by radio balloon measurements on November 5–6 of 1970, and near Moscow on November 11–12 1970. In Murmansk region it was observed in the altitude range $H \approx$ 15–25 km and charged particle flux increased 7–8 times in comparison with the CR background. At the first registration the radioactive cloud had the shape of a disk with vertical size of nearly 4 km and horizontal size along the wind direction of ≈ 1100 km. The maximal activity was ≈ 10^{-3} Bq/cm^3 as measured at H ≈ 18–22 km. After 26 October the radioactive cloud passed away from the Murmansk region.

In Fig. 18.13.2 are shown results of observations by radio balloons the radioactive cloud in the atmosphere over Moscow at 12–14 April 1993. In this case, the cloud was seen at H ≈ l0–30 km and had an horizontal extension of nearly 1000 km and maximum activity ~10^{-4} Bq/cm^3. The origin of this radioactive cloud was not known exactly, but according to Bazilevskaya, et al. (1994) on 6 April the failure at the big plant in Siberia (Seversk town near Tomsk) occurred.

According to Stozhkov et al. (2001), a denser cloud was observed over Moscow on 27th October 1999, the maximum activity being 7×10^{-3} Bq/cm^3 at $H > 15$ km. The horizontal extension of the cloud was about 200 km. The source of this radioactive cloud is also unknown.

18.14. Possible application of CR research to the problem of great earthquakes forecasting

In this problem CR are used as the instrument for determining possible extraterrestrial and internal sources that initiate great earthquakes (or so called Strong Destructive Earthquakes – SDE).

18.14.1. CR research on extraterrestrial causes of great earthquakes: neutron bursts from the Earth's crust at new and full Moon

Attempts to search for extraterrestrial causes for the initiation of great Strong Destructive Earthquakes (SDE) were made by many authors, among them: Yu Zhen-dong (1985), Sobolev et al. (1988), Sitinski (1987, 1989), Volodichev et al. (1991, 1993, 1995; 1997a,b,c, 1999, 2001a,b,c), Gokhberg et al. (1998), Shatashvili et al. (1999), Despotashvili et al. (1999a,b).

Some potential sources are very exotic: e. g., Yu Zhen-dong (1985) connects some of the SDE with the great fluxes of CR in the far regions of the Galaxy during the explosions of Novae stars.

On the other hand, the possible influence of gravitational tidal forces on the Earth's crust caused by the Moon looks more realistic. According to Volodichev et al. (1997a,b,c; 1999) the correlation discovered of the radiation splashes from the Earth's crust of low energy neutrons with periods of passing of maximum tidal waves in the Earth's crust (at new Moon and full Moon), can be understood if we take into account the following: when the angle between the lines joining the Earth with the Sun and the Earth with the Moon is a minimum, the total gravitation influence on the Earth from these space bodies is high, and deformations in the Earth's crust become a maximum. It leads to an increase in neutron concentration in the surface stratum of the Earth's crust

and the atmosphere because of two processes: mechanical emission, i.e., liberation of different atomic and nuclear particles during cracking rocks of the Earth's crust because of deformation, and strengthening of the stream of radioactive gases (mostly, an isotope of radon), which leads to increasing of energetic alpha-particles' flux entering the nuclear interactions with the elements of the Earth's crust and the atmosphere with small energy neutron generation.

The second mechanism of small energy neutrons generation was supported by investigation of Volodichev et al. (1999): it was found that in days of the new Moon and full Moon, when increase (up to dozen times) of radioactive gas emission was observed by measurements of alpha-particle fluxes in the different seismic active regions of Pamir Mountains. The active role of the tidal waves, influencing the Earth's crust, in formation of neutron splashes may be demonstrated by means of a measurement carried out in 1997 at Pamir (the Dgerino area at a height of 1100 m above sea level, 30 km to the North of Dushanbe). In the period 16–24 July 1997 the small energy neutron flux passed through a maximum value every day. The neutron flux reached the highest value on the 20-th July at 05.37 ± 3 min UT. At that day about two hours earlier, at 03.20 UT the Moon passed the phase of fool Moon. Little later, in period 17.22–19.09 UT of 21 July 1997 a large multi-pulse splash of neutron radiation (which exceeded the background value by about one hundred times in its maximum) was observed (see Fig. 18.14.1).

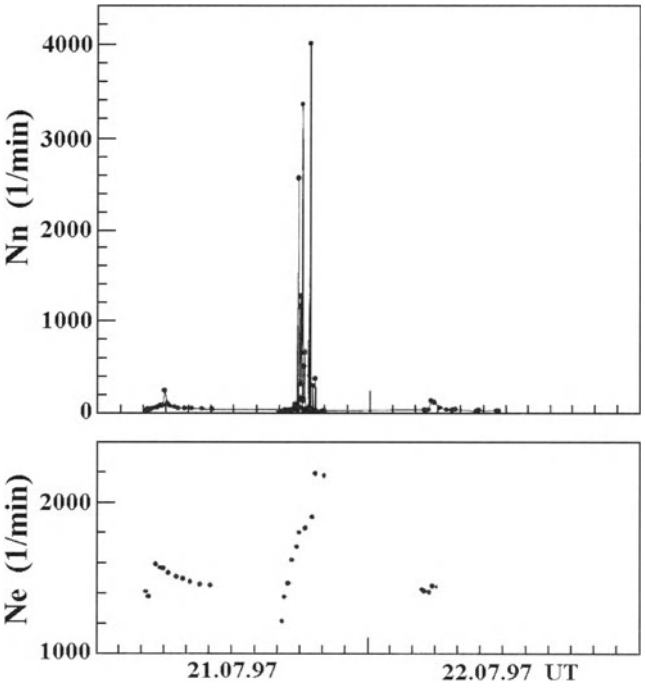

Fig. 18.14.1. Counting rate variations in July 21–22, 1997 of low energy neutrons (the top panel) and electrons (the bottom panel) from the Earth's crust at Pamir Mountains. According to Volodichev et al. (1999).

The other example (the event in December 1999) is shown in Fig. 18.14.2.

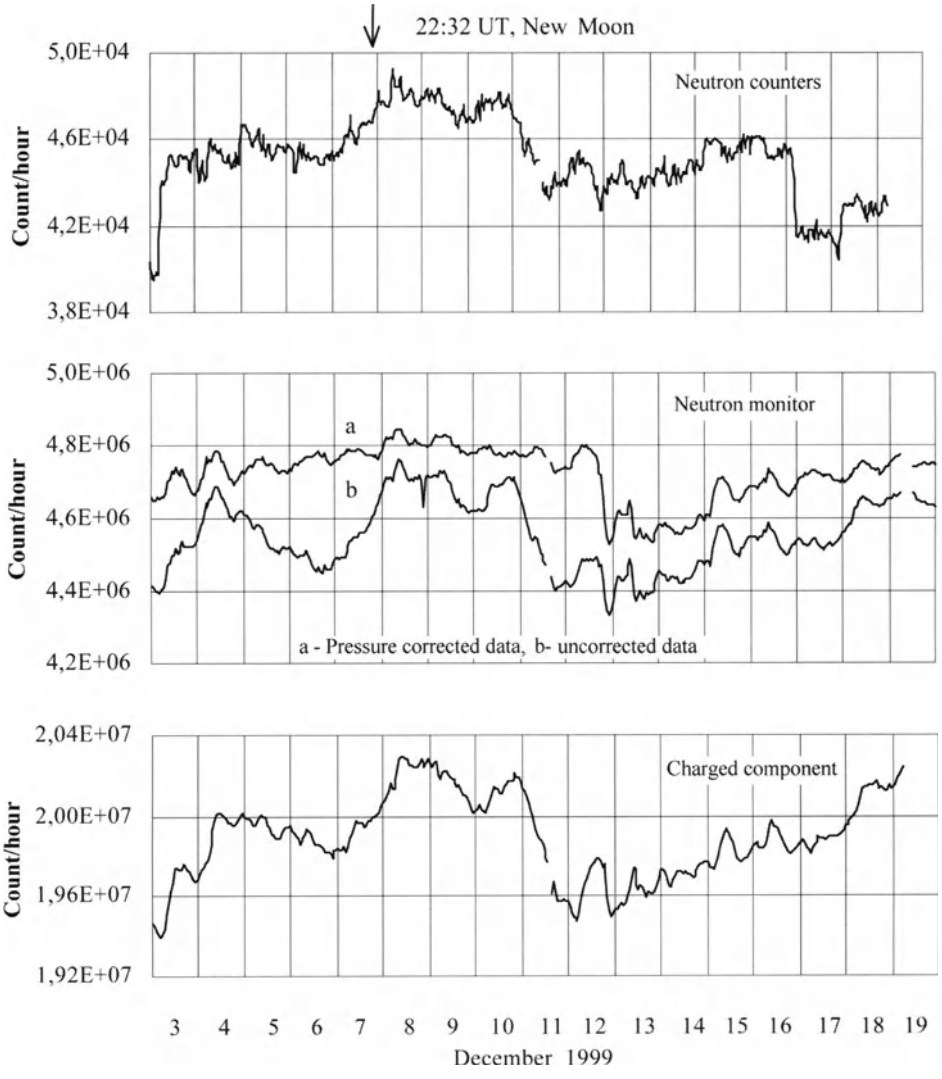

Fig. 18.14.2. The neutrons and charged particles fluxes at the North Tien Shan in December 1999. According to Volodichev et al. (2001b).

The results of analysis of earthquakes catalogues for 1964–1992 (Volodichev et al., 1999) demonstrate that the Moon's bi-weekly modulation appeared exactly in the large series of earthquakes at the region of Pacific seismic ring. It was found that in 1964–1992 a total of 37 series of earthquakes, with ≥ 30 earthquakes of magnitude $m \geq 4$ in each series were observed. Among them 16 series were situated to the North of 40°N or to the South of 10°S and all of them started on new Moon ± 3 days or on full Moon ± 3 days. Volodichev et al. (1999) suggested that neutron splashes can be used as precursors of seismic activity and great earthquakes. From Fig. 18.14.1 and 18.14.2 it can be seen

that the neutron flux as well as flux of charged particles from the Earth's crust starts to increase significantly before the moments of extreme tidal forces.

18.14.2. CR research on extraterrestrial causes of great earthquakes: crossing of the neutral current sheet of IMF by the Earth and CR daily variations

The other possible extraterrestrial phenomenon influencing the Earth's crust is considered in Shatashvili et al. (1999), Despotashvili et al. (1999a,b): the crossing by the Earth of the neutral current sheet of the IMF (interplanetary magnetic field). It is shown that from all extraterrestrial phenomena connected directly or indirectly with strong destructive earthquakes (SDE), the process of the Earth's passage through the neutral current sheet of IMF is the most powerful for its stimulation. To prove this statement the results of the analysis of multiple histograms, the distribution of the Earth's passage through the neutral IMF sheets relative to the cases of SDE with the magnitude ≥ 6.0 (Dunbar et al, 1992) are analyzed according to the data of 1958–1988. For each 5 years Cree diagrams were determined, in which the moments of SDE were taken as zero days and found the number of neutral current sheet crossing in this day, and in days before (up to –10 days) and after (up to +10 days). An example of such a Cree diagram is shown in Fig. 18.14.3.

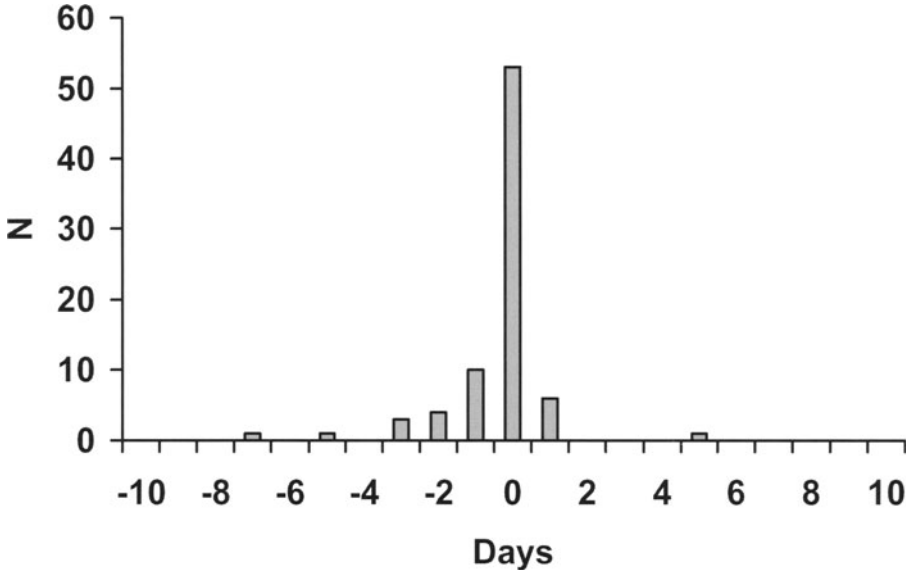

Fig. 18.14.3. Cree histogram obtained on the basis of data on SDE and neutral current sheet passing by the Earth for 5 years period 1965–1969. On the ordinate axes plotted numbers N of the Earth's passage through the neutral IMF sheet; 0 on the abscissa corresponds to the day of great earthquakes (SDE), negative –1, –2, etc. are the days before SDE, and positive numbers after SDE. According to Despotashvili et al. (1999a).

From Fig. 18.14.3 it can be seen that most of neutral current sheet passes was in days –1 and 0, i.e. in one day before and on the day of SDE (about 80% of all passes for days from –10 to +10). This percentage corresponds to the middle of interval 1965–1969, i.e. to 1967. These values were found for each 5 years interval of all used data for 1957–1988; they are plotted in Fig. 18.14.4 in comparison with yearly sunspot numbers.

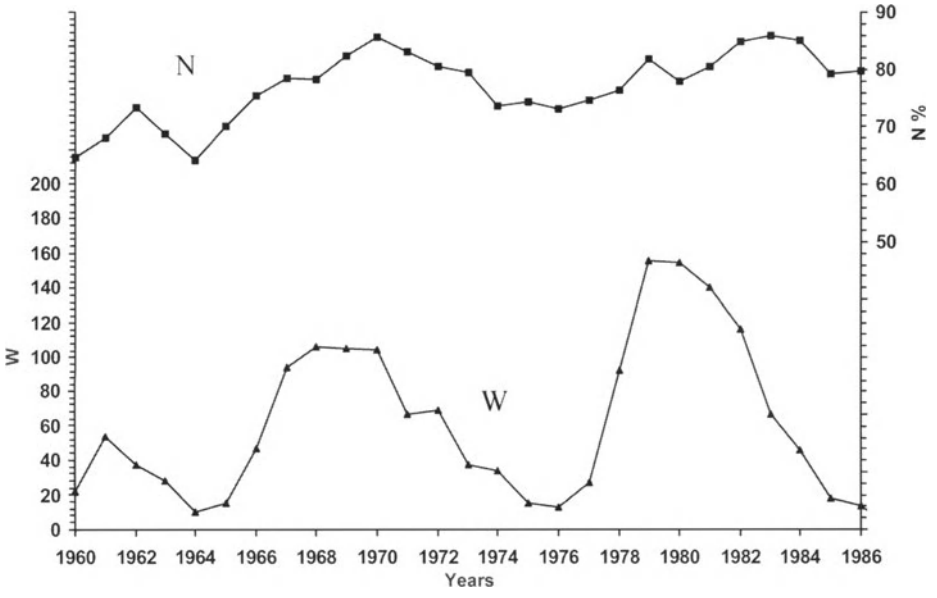

Fig. 18.14.4. The diagrams of cyclic variations of the experimental values of N (in %, right scale) of the passages through the neutral current sheet of IMF near SDE moments (in days –1 and 0, see Fig. 18.14.3), by moving average method (with the period of averaging 5 years) on the basis of data 1957–1988, and yearly average values of numbers of sunspots W in the period of 1960–1986. According to Despotashvili et al. (1999a).

The analysis of Fig. 18.14.3 and Fig. 18.14.4 shows:

1. SDEs, in almost in 75% of the cases, take place a day before or on the day of the Earth's passage through the neutral current sheet of IMF.
2. According to the analysis of planetary observation data during about 3 solar cycles, the is a tendency for 11-year cycle variation of SDEs as observed at the Earth's passage through the neutral current sheet of IMF.
3. Because the time of the Earth's passage through the neutral current sheet of IMF is not difficult to predict, described results can be used for approximately forecasting of SDEs.

Fig. 18.14.5 shows Cree diagrams of the amplitude of the first harmonic of solar-diurnal CR variations according to the data of Kiel and Tokyo neutron monitors and Nagoya meson telescope for 1978 with connection of SDE events (as 0 days). Tentative analysis of Fig. 18.14.5 shows that in the region of relatively high CR energies (Tokyo and Nagoya stations) there are weak tendency of the amplitude of the first harmonic of solar-diurnal CR variation to increase a day before SDE.

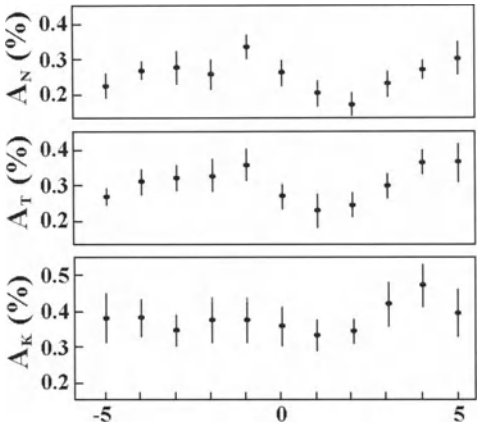

Fig. 18.14.5. Averaged Cree diagrams of the amplitude of the first harmonic of solar diurnal CR variations according to the data of Kiel (A_K) and Tokyo (A_T) neutron monitors and Nagoya meson telescope (A_N). The days of initiation of SDE are taken as zero days. According to Despotashvili et al. (1999a).

18.14.3. CR research on internal causes of great earthquakes

Many authors tried to use CR research for search for internal sources of strong earthquakes. Let us mention the work of Asatrian et al. (1991), showing that during the terrible Spitak earthquake the intensity of CR increased by about 100% in the stratosphere over Yerevan starting 30 minutes before this SDE (this increasing was not connected with solar flare effects).

Galperin et al. (1992), Pustovetov and Malyshev (1993), Galper et al. (1987, 1995, 1997,1999a,b), Galper and Voronov (1997) on satellites Salyut–7, Mir, Meteor–3, Intercosmos-Bulgaria–1300, Oreol–3 and others observed many bursts of high-energy charged particles, precipitating from the Earth's radiation belts. The duration of bursts ranges from few seconds to several minutes. Galper et al. (1995, 1997,1999a,b), Galper and Voronov (1997) showed using space-borne detectors (described in Voronov et al., 1991) that a significant part of precipitating particle bursts are connected with seismic activity; they occur several hours (2–4) before the main earthquake phase. Moreover, the spatial parameters of the radiation belt precipitations correlate with coordinates of the earthquake epicenter: L-shell parameter of the precipitations practically coincides with L-shell of earthquake epicenter. Hence, these precipitation events may be considered as short-term earthquake predictors.

The explanation of this phenomenon, given in Galper et al. (1995), is based on the suggestion of Molchanov (1991) that several hours before the main seismic shock ultra low frequency (ULF) electromagnetic waves are generated in the future earthquake epicenter; these ULF electromagnetic waves go upward through the atmosphere practically without losses. At the altitudes about 100 km and higher these waves are trapped in channel by L-shell (corresponding exactly to L-shell of future earthquake epicenter), and propagate farther along the strength lines of the geomagnetic field, reach the inner boundary of radiation belts and interact resonantly with trapped charged particles – protons and electrons in energy range several tens of MeV (the oscillation frequency of these trapped particles between mirror points coincides with frequency of ULF electromagnetic waves). This resonant interaction changes the particle pitch angles

what leads to decrease of mirror point altitude for some part of trapped particles, and to their precipitation. The described mechanism was simulated for real geomagnetic field by using four order Runge–Kutta method for calculations of particle trajectories. The problem is that the position of future earthquake epicenter is unknown. To determine the position of future earthquake epicenter Galper et al. (1999b) made simulation calculations for differences in geographic longitudes between the site of precipitation and future earthquake epicenter $\Delta\lambda$ from 0° to 360° by the step 20°. For each step it is necessary to made comparison with experimental data on time variations of precipitation particle fluxes and determine χ^2-parameter for each $\Delta\lambda$: the minimum of χ^2 will determine the expected $\Delta\lambda$ and by known longitude of precipitation measurements – to determine the longitude of precipitation burst formation (longitude of future earthquake epicenter). The described procedure is illustrated in Fig. 18.14.6 and Fig. 18.14.7 in application to experimental data of precipitation particle fluxes from radiation belts at 06.13 UT 31 March, 1994 ($L \approx 1.15$; $B \approx 0.23$ Gs) according to measurements on space station Mir.

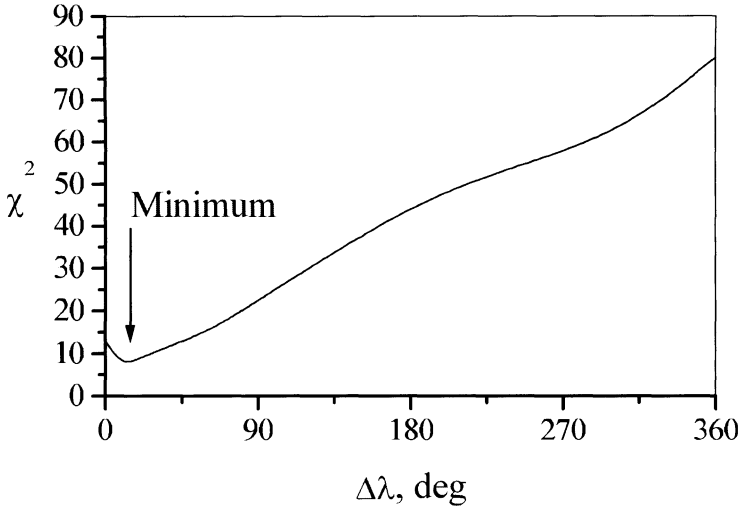

Fig. 18.14.6. The dependence of χ^2 on $\Delta\lambda$ for the event at 06.13 UT 31 March, 1994 ($L \approx 1.15$; $B \approx 0.23$ Gs). According to Galper et al. (1999b).

From Fig. 18.14.6 it is seen that χ^2-parameter has pronounced minimum in the range of $\Delta\lambda \approx 0$–20°. So knowing Mir space stations location during the event observation one can determine the range of geographical longitudes of precipitation burst formation: $\lambda \approx 280$–300°. In Fig. 18.14.7 is shown the comparison of experimental data of counting rate according to measurements on space station Mir with simulation at minimal value of χ^2 for this event (for $\lambda = 290°$ – the middle of the determined range of precipitation burst formation geographical longitudes). Enough good agreement between experimental and theoretical results should be stressed. Because the geomagnetic situation in this day was quite, Galper et al. (1999b) come to the conclusion that

observed on the space station Mir precipitation burst at 06.13 UT 31 March, 1994 at $L \approx 1.15$ can be considered as a precursor of the strong earthquake which is expected a few hours later at about the same geographical longitude: the real great earthquake took place about two hours later at about the same L-shell and same longitude (at 08.34 UT 31 March, 1994 at $L \approx 1.12$, $\lambda = 291°$).

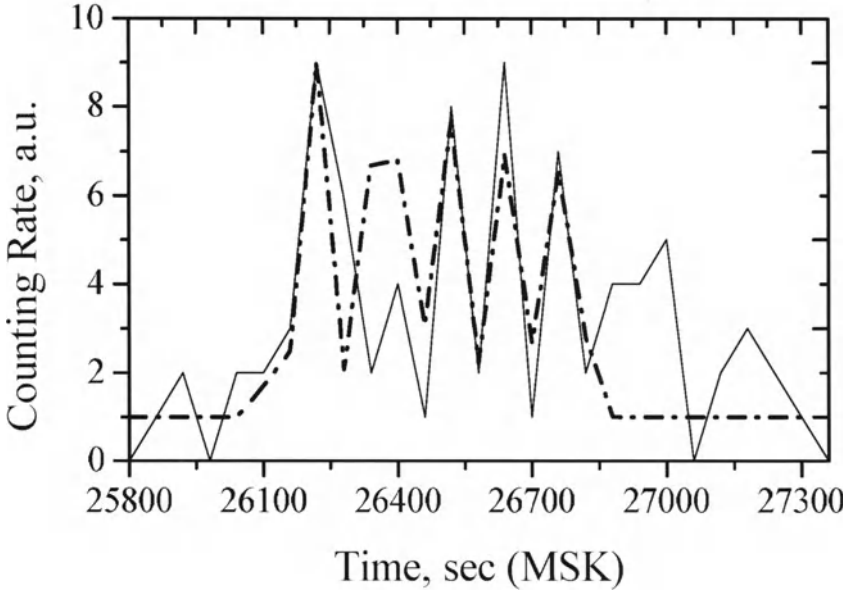

Fig. 18.14.7. The comparison of experimental data of counting rate according to measurements on the space station Mir (solid line) with simulation at minimal value of χ^2 (dashed line) for the event at 06.13 UT 31 March, 1994 ($L \approx 1.15$; $B \approx 0.23$ Gs). On the abscissa is shown Moscow time (in seconds). According to Galper et al. (1999b).

18.15. Experience in the research of CR in the Earth's atmosphere and underground: applications to CR interactions with the Sun, planets, and other solar system bodies

The huge experience of CR investigations in the Earth's atmosphere and underground (for about 70–80 years) can be applied to the research of expected galactic and solar CR behavior in the atmosphere of the Sun, in atmospheres and bodies of Mercury, Venus, Mars, Jupiter, Saturn, Neptune, Pluto, and their satellites, as well as with asteroids and meteorites in interplanetary space. We started to investigate this problem many years ago (Dorman and Yanke, 1979a,b,c; Dorman et al., 1979a,b). Only in the laster years this problem became relevant, in connection with wide space investigations of the Sun's and planets' atmospheres, asteroids and meteorites. Here we will only mention this very interesting and broad problem. Details will be considered in the next book (Dorman, M2005).

18.16. CR research applications to Human Health and Medicine, to the Problem of Car and Train Accidents

18.16.1. Short historical review

In the last decades many investigations have been carried out on the influence of 'space weather' parameters through the action of natural geomagnetic field, upon the morbidity in different diseases, so-called "biogeomagnetics" (e.g. review Roederer, 1995; Ptitsyna et al., 1998 and refs. therein). The idea of geomagnetic variations having any effects on living systems is viewed with great skepticism by physicists because magnitudes involved are very small in comparison to local intracellular electric and magnetic fields (e.g. Adair, 1991; Bennet, 1994). However emerging bodies of empirical findings support the possibility that the association has a real biophysical basis. The most significant empirical results seem to be those on cardiovascular and on nervous system diseases. Laboratory results on sensitivity of human blood system to solar and geomagnetic activity support these findings.

In the last decades some evidence has been accumulated also on the association between geomagnetic disturbances and increases accident frequency in work at different plants and in car and train traffic (Reiter, 1955; Srivastava and Saxena, 1980; Ptitsyna et al., 1995, 1998). These studies were based on the hypothesis that a significant part of traffic accidents could be caused by the incorrect or retarded reaction of drivers to the traffic circumstances; the capability to react correctly being influenced by the environmental magnetic and electric fields.

One of the most important problems in biogeomagnetics is the definition of the characteristics of geomagnetic activity that are more related to health effects. Apart from usual geomagnetic indices some parameters of interplanetary medium perturbations could be used for characterizing the geomagnetic activity level and also short-term cosmic ray intensity variations, related to interplanetary disturbances, may provide alternative indications. In Villoresi et al. (1994a, b; 1998), Ptitsyna et al. (1995, 1998), Dorman et al. (1999) it was shown that CR Forbush-decreases could be considered as sensitive indicators of association between geomagnetic field disturbances and such health parameters, as incidence of myocardial infarction, brain stroke, and also vehicular traffic accidents.

Here we will show that the most remarkable and statistically significant effects have been observed during days of geomagnetic perturbations defined by the days of the declining phase of Forbush decreases in CR intensity. Here we will consider also the possible influence of the long term CR intensity variation (controlled by solar activity cycle) on the different types of human diseases and traffic accidents.

18.16.2. Frequency of myocardial infarcts, brain strokes, and car accident road traumas in connection with CR Forbush-decreases

On the basis of great statistical data on many millions of medical events in Moscow and in St. Petersburg, it was found that there is a significant influence of geomagnetic storms accompanied with CR Forbush decreases on the frequency of myocardial infarcts, brain strokes, and car accident road traumas (Villoresi et al., 1994a,b; 1995). It was found that among all characteristics of geomagnetic activity, Forbush decreases are

better related to hazardous effects of solar variability driven disturbances of the geomagnetic field (Ptitsyna et al., 1998). Results are shown in Fig. 18.6.1-18.6.3.

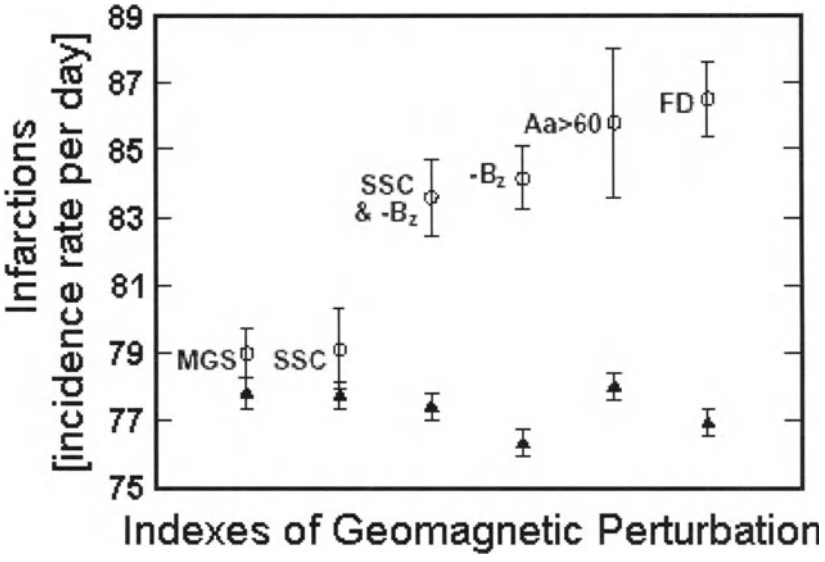

Fig. 18.16.1. Average daily numbers of myocardial infarctions in Moscow during geomagnetic quiet and perturbed days according to different indices of activity and in days of CR Forbush decreases (FD). According to Ptitsyna et al. (1998).

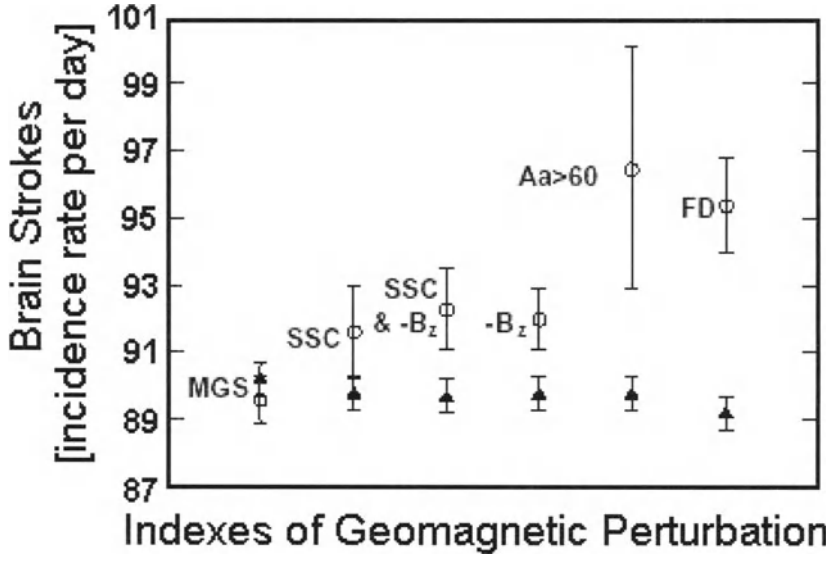

Fig. 18.16.2. Average daily numbers of brain strokes in Moscow during geomagnetic quiet and perturbed days according to different indices of activity and in days of CR Forbush decreases (FD). According to Ptitsyna et al. (1998).

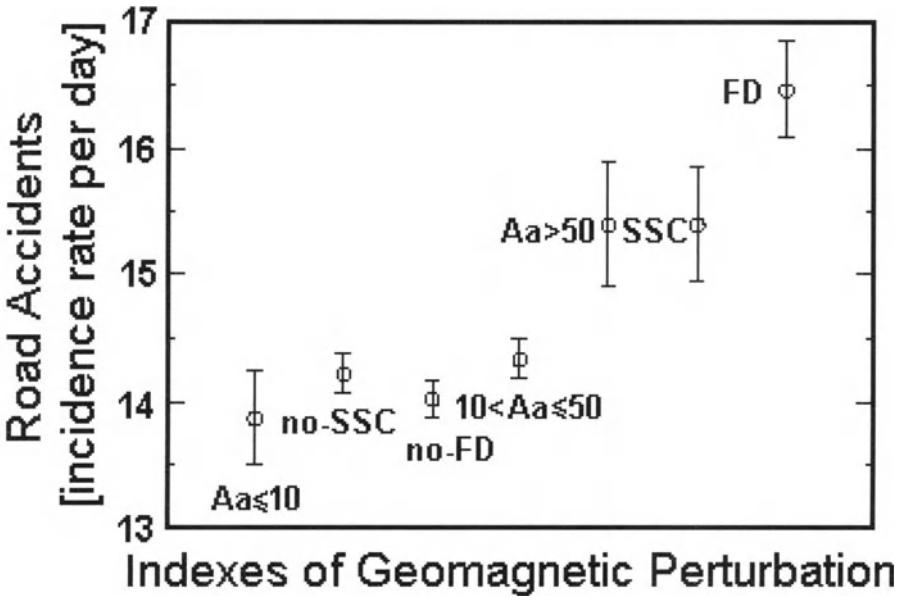

Fig. 18.16.3. Average daily numbers of road accidents in St. Petersburg during geomagnetic quiet and perturbed days according to different indices of activity and in days of CR Forbush decreases (FD). According to Ptitsyna et al. (1998).

Fig. 18.16.1-18.6.3 show the correlation between cardiovascular diseases, car accidents and different characteristics of geomagnetic activity: planetary index AA, major geomagnetic storms (MGS), sudden commencements of geomagnetic storms (SSC), occurrence of downward vertical component of the interplanetary magnetic field Bz and also decreasing phase of Forbush-decreases (FD). The most remarkable and statistically significant effects have been observed during days of geomagnetic perturbations defined as the days of the declining phase of Forbush decreases in CR intensity. During these days the average numbers of traffic accidents, infarctions, and brain strokes increase by (17.4 ± 3.1)%, (10.5 ± 1.2)%, and (7.0 ± 1.7)%, respectively.

18.16.3. In what days of CR Forbush decrease there is sufficient influence on people health and car road accidents?

In Fig. 18.16.4 we show the effect on infarction myocardial and car accident rates during the time development of Forbush decreases in CR intensity. For the Fig. 18.16.4 all CR Forbush decreases are divided into two groups, according to the time duration T of the CR intensity decreasing phase. Then the average incidence of infarctions and traffic accidents was computed beginning from one day before the Forbush decrease's onset until 5 days after. For the first group ($\Delta T < 1$ day) the average daily incidence of infarctions and traffic incidence increases only in the first day of CR Forbush decrease; no effect is observed during the recovery phase (that usually lasts for several days). Also for the second group (1 day $< \Delta T < 2$ days) the increase in incidence rates is observed only during the 2 days period of the decreasing phase of CR Forbush decrease. So, we came to conclusion that the influence of CR Forbush decrease on human health is

sufficient only in days of CR intensity decreasing (it means, not more than one-two days), but not in the CR intensity recovery period which may prolong many days.

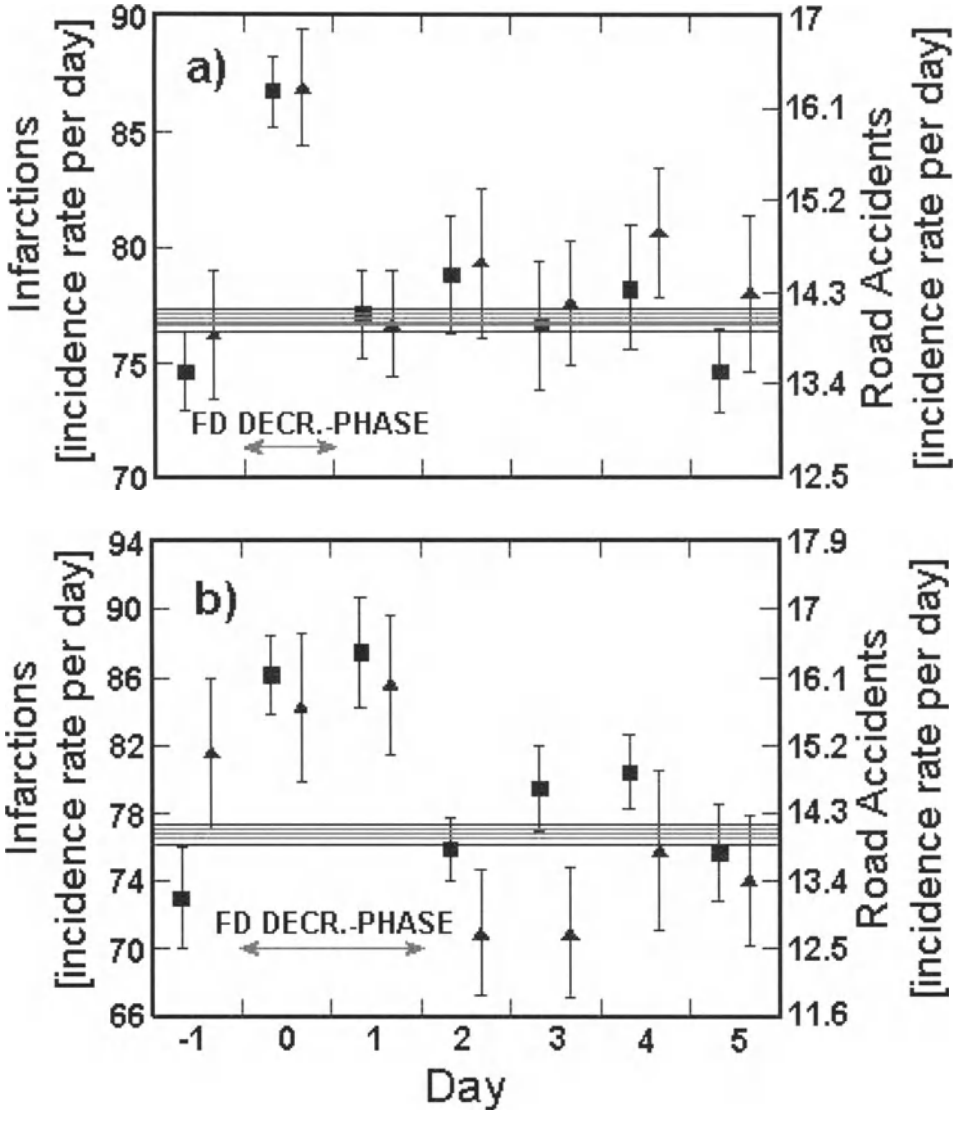

Fig 18.16.4. Infarction (full squares) and road accidents (full triangles) incidence during the time development of CR Forbush decrease (FD): **a**) CR decrease phase $\Delta T < 1$ day; **b**) CR decrease phase 1 day $< \Delta T < 2$ days.

18.16.4. The train accidents in connection with CR Forbush decreases

In the research of Dorman et al. (2001a) were used daily and monthly averaged data of malfunctions and accidents in Siberian Railways (Russia) for the period 1 January, 1986

up to 30 November, 1993 (about 8 years data). The data were divided on two types by Siberian Railway experts: the first related to technological factors (total number 4661), and the second related to personnel errors, caused by man-related factors (total number 2754). For studying the possible association with short term perturbations in geomagnetic field (daily scale) we considered as magnetically perturbed days the first three days of the decrease phase of Forbush decreases (FD) in the cosmic ray intensity (daily amplitude >2.5% at high latitude neutron monitor station Mt. Washington). During the analyzed period such days were 141. Average frequency of train malfunctions computed during magnetically quiet days (two days before the FD onset day) and disturbed days (FD onset day and two days after) are presented in Table 18.16.1.

Table 18.16.1. Train malfunctions average daily incidences from day –2 to day +2 relative to the CR Forbush decrease (FD) onset time (day 0).

Day	-2	-1	0	+1	+2
F_m	0.98±0.17	0.96±0.17	1.11±0.18	1.26±0.18	1.15±0.16

The comparison of the average frequency of malfunctions between the first three days of FD (days 0, +1 and +2) and two days before FD (days -2 and -1) shows an increase of malfunctions of ~(20±10)% during FD days. This is in good agreement with Villoresi et al. (1994a,b; 1998), Ptitsyna et al. (1995, 1998) in which it was found that during FD days the average numbers of traffic accidents, infarctions, and brain strokes increased by (17.4±3.1)%, (10.5±1.2)% and (7.0±1.7)% respectively (see above, section 18.16.2).

18.16.5. The problem of the long-term variations of the train accident frequency in comparison with solar activity and CR intensity variations

For this investigation in Dorman et al. (2001a) were used monthly averaged data of malfunctions and accidents in Siberian Railways (Russia) for the same period (January 1986 up to November 1993). The data were divided on two types by Siberian Railway experts: the first related to technological factors (the number per month F_t), and the second related to personnel errors caused by man-related factors (the number per month F_m). For studying possible long-term effects related to space weather we used data on Wolf number, neutron monitor cosmic ray intensity, tilt angle of interplanetary plasma sheet T and geomagnetic index SSC (number of geomagnetic storms with sudden commencement). In Fig. 18.16.5 we show the frequency of the train malfunctions in the Russian Siberian Railway (F_m is the 11-month moving average of the monthly daily frequency of man-related malfunctions and F_t is the same for technological malfunctions), and 11-month moving average of Wolf sunspot numbers.

In Fig. 18.16.5 can be seen an increase in frequency of train malfunctions and accidents observed in the period 1986-1987 simultaneously with an increase in solar activity. However, at the same time the Russian 'perestroika' introduced big stress factors, rapid changes and disorganization in almost all social and economical fields. For instance, traffic accidents data in St. Petersburg (1987-1989), used by Ptitsyna et al.

(1995), cannot be included in the present analysis because they show an increase in this period due mostly to the considerable increase in number of cars. To avoid this 'perestroika effect' we excluded the years 1986-1987 from the analysis of long-term effects.

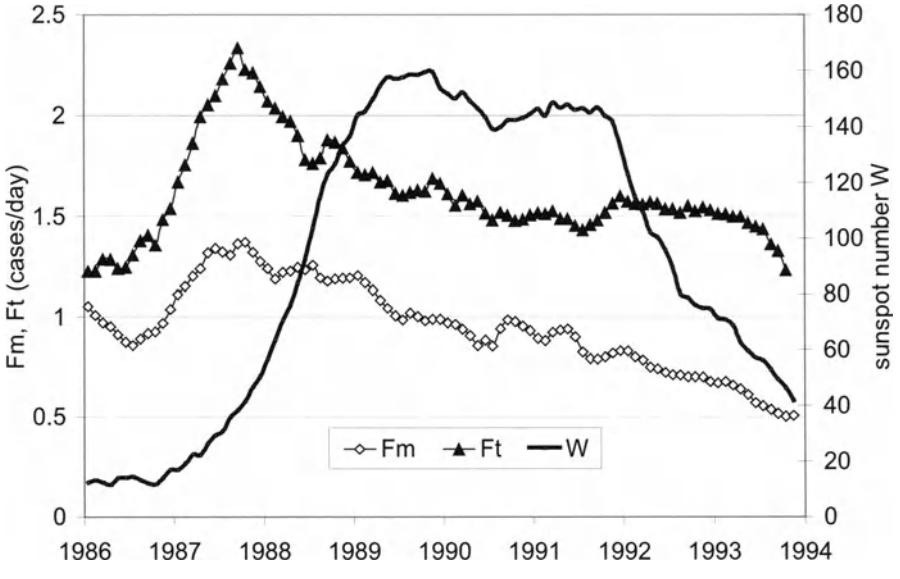

Fig. 18.16.5. Daily occurrences of train malfunctions (F_m , man-related; F_t , technological) and Wolf number W. According to Dorman et al. (2001a).

We also tried to eliminate, at least partly, malfunctions caused by other social reasons common for both original data sets. For this purpose we correlated the original data sets; the obtained result is the following:

$$F_m = 0.6778F_t - 0.1424\,, \tag{18.16.1}$$

To diminish the contribution of social factors we assumed that they affect both types of malfunctions in the same way. The corrected data of man-related malfunctions will be:

$$F_m(\text{corr}) = F_m - \left(0.6778F_t - 0.1424\right). \tag{18.16.2}$$

In Fig. 18.16.6 we show $F_m(\text{corr})$ together with the neutron monitor CR intensity data at Climax.

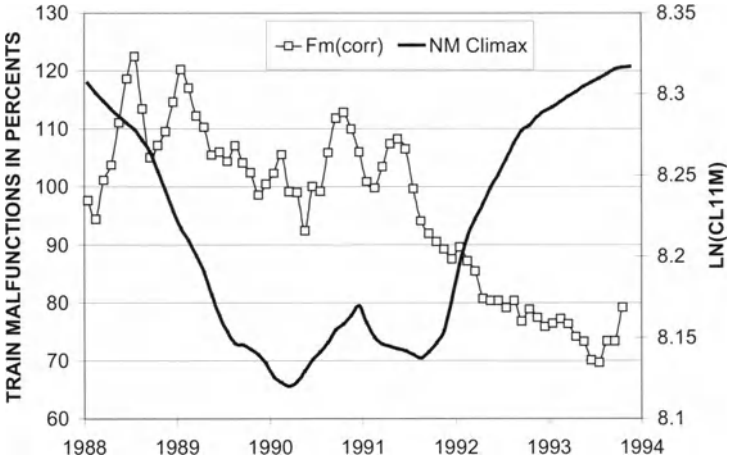

Fig. 18.16.6. Time behavior of 'corrected' man-related train malfunctions F_m(corr) (in % of the average value of total period) and logarithm of Climax neutron monitor counting rate (NM Climax). According to Dorman et al. (2001a).

18.16.6. Long-term variations of the myocardial infarctions, brain strokes, and train accident frequency in connection with sunspot number, CR intensity, tilt angle and number of geomagnetic storms

Table 18.16.2 presents results of correlation analysis done on three data sets of train malfunctions (technical, man-related and man-related corrected for social factors), infarctions and brain strokes with different parameters of space weather: Wolf number (W), cosmic ray intensity as measured by Climax and Rome neutron monitors (NM), current sheet tilt angle (T) and number of geomagnetic storms characterized by sudden commencement (SSC).

Table 18.16.2. Regression (b) and correlation (r) coefficients between cardiovascular pathologies, train accidents and space weather parameters.

Data		W	NM Climax	NM Rome	T	SSC
Myocard. Infarct. 1979-81	b	-0.013	-21.6	-61.7	-0.111	1.130
	r	-0.16	-0.65	-0.72	-0.69	0.54
Brain Stroke 1979-81	b	-0.031	-16.8	-46.7	-0.050	0.954
	r	-0.28	-0.64	-0.69	-0.39	0.58
F_t 1988-93	b		0.47	1.25	0.001	0.001
	r	0	0.20	0.25	0.06	0.02
F_m 1988-93	b	0.002	-0.625	-1.01	0.006	0.051
	r	0.43	-0.21	-0.16	0.39	0.28
F_m(corr) 1988-93	b	0.0024	-0.922	-1.64	0.0060	0.050
	r	0.68	-0.49	-0.42	0.67	0.44

From Table 18.16.2 it is seen that there is good inverse correlation between number of infarctions and brain strokes and NM intensity, as it is also shown in Fig. 18.16.7.

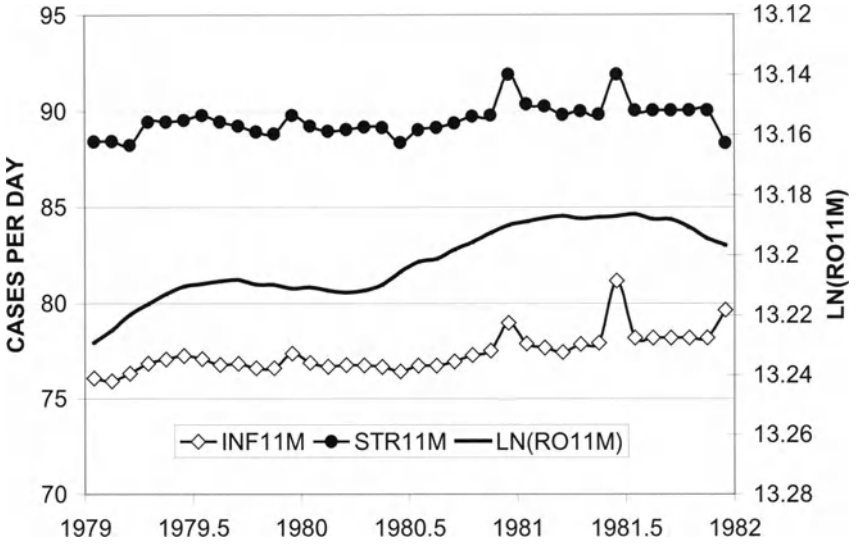

Fig. 18.16.7. Time behavior of infarctions (INF11M) and brain stroke (STR11M) incidences together with CR NM intensity (note the inverse scale) at Rome (denoted as LN(RO11M))for the period 1979-1981.

For the same data a good correlation is also observed with tilt angle T and SSC, while there is no correlation with W. The lack of correlation with W indicates that in this short time period W and NM are not correlated, as it is shown in Fig. 18.16.8 in which the correlation between the two data sets is characterized by very low correlation coefficient r = +0.2.

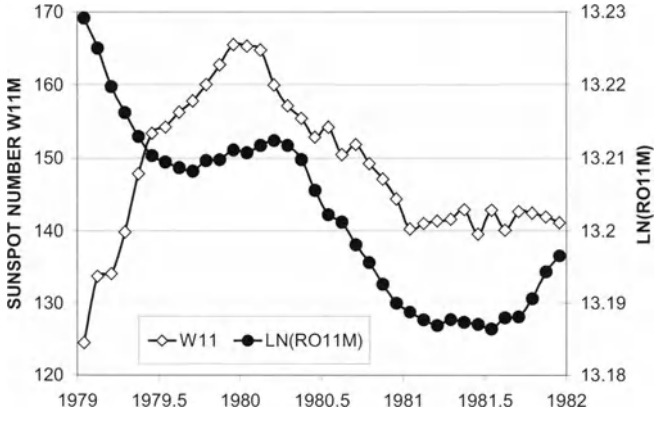

Fig. 18.16.8. Time behavior of sunspot number W and CR NM intensity at Rome for the period 1979-1981.

From Table 18.16.2 also can be seen that for the long term variation of myocardial infarctions and brain strokes for the period 1979-1981 the best negative correlations are with CR intensity, and the best positive correlations are with tilt angle and number of geomagnetic storms. For the long term variation of train accident frequency for the period 1988-1993 we see from Table 18.16.2 that for technological accidents F_t there are no correlation with any of considered parameters (as it is expected). From other hand, for corrected man-made train accidents F_m(corr) there are significant negative correlation with CR intensity and positive correlations with tilt angle, number of geomagnetic storms, and sunspot number.

18.16.7. Discussion of obtained results and possible causes of the human diseases connection with CR intensity and other space weather parameters

It is found that the main cardiovascular diseases, as myocardial infarction and brain strokes, as well as train malfunctions of man-related origin can be influenced by space weather parameters, both in short (during Forbush decrease events) and long-term scale (solar activity cycle).

These results on man-related train accidents give additional support to the idea that the capability of operators to react correctly to the environmental circumstances can be influenced by space weather parameters.

In short-time scale the CR intensity seems to be the best indicator of such correlation; this is true not only when the days of Forbush decrease occurrences are considered, but also when the correlation is done with the neutron monitor intensity. Also the current sheet tilt angle and the number of SSC give high levels of correlation.

Regarding long-term variations, Wolf sunspot number seems to be the best indicator of space weather influence, at least in relation to man-related train accidents, but also CR intensity, tilt angle, and SSC can be considered as reliable indicators.

The described results (some of them obtained with high statistical power, other at the limits of statistics) indicate the possibility of some influence of space weather on the analyzed health and safety-related parameters. To draw more definite conclusions it is necessary to increase the statistics; i.e. to obtain results for several solar cycles. Anyway, the results obtained up to now suggest the necessity of forecasting the solar activity and the related interplanetary perturbations, not only to protect technology and satellites, but also to bring benefits connected to health and safety on the Earth.

What are the biophysical and medical manifestations of these effects? Monitoring of cardiovascular function among cosmonauts of 'MIR' space station revealed a reduction of heart rate variability during geomagnetic storms; the reduction in heart rate variability has been associated with 550% increase in the risk of coronary artery diseases (Baevsky et al., 1997). The increase of car accident frequency during CR Forbush decreases can be explained by retarded reactions of the drivers in these days. Retarded reaction in connection with naturally occurring magnetic field disturbances was observed by many authors (see, e.g., Reiter, 1955; Konig and Ankermuller, 1960; Friedman et al., 1967; Konig, 1974; Srivastava and Saxena, 1980; Becker and Marino, M1982). More details on the problems considered here, as well as how to use on-line CR data for forecasting space phenomena dangerous for people health, will be considered in Dorman (M2005).

18.17. Application of CR research to the problem of satellite malfunctions

18.17.1. Importance of the problem

In Section 18.12 we mentioned on the problem of space weather influence on the work of satellites and their importance (see above, Fig. 18.12.2). Here we will present preliminary results of a Project INTAS–00810, which is aimed to improve the methods of safeguarding satellites in the Earth magnetosphere from the negative effects of space weather mostly by using of CR observations (Dorman, 1999a,b; 2002, 2003b; Belov and Eroshenko, 2002; Dorman for INTAS–00810 Team, 2002; Belov et al., 2003a,b). Satellites usually spend several years in space, so they are exposed to the short and long-term effects of space weather. There is a body of evidence on the existence of spacecraft anomalies, which are caused by the space environment. However till now thorough statistical analysis of spacecraft anomalies in dependence of different parameters of space weather have not been done. For the purposes of such analysis malfunction data on 'Kosmos' satellite series (circular orbit at altitude about 800 km, 74° inclination) in the period 1971-1997 were combined in one database together with similar information on other spacecrafts. Since these data refer to a unique series of satellites of the same type, the classification and the further comparison of anomalies with space environment parameters may be thought as more reliable.

A comparative analysis of distribution each of these parameters relatively satellite malfunction was carried out for the total number of malfunctions (about 6000 events), and separately for the high (~5000 events) and low (about 800 events) altitude orbit satellite as well. It was found no relation between low and high altitude satellite malfunctions. The majority of malfunctions of "Kosmos" satellites occurred at the same time with failures on the other low altitude orbit spacecrafts, and they seemed to be related with space weather parameters. Daily number of the satellite malfunctions averaged by epoch method around the SSC and proton event onsets for high (>1000 km) and low (<1000 km) altitude orbits revealed a big difference in a behavior. The mean value of spacecraft failed in certain days, is correlated with the geomagnetic and CR activity indices.

18.17.2. Data cleaning and formation of database

Analysis of possible reasons for every case of orbital satellite malfunction was performed. Excluding of malfunctions due to construction errors, errors of operating personnel, low-quality ground spacecraft presetting before launch, low-quality ground service etc. was done. About 50% of the total number of anomalies was identified as not related to man or technological factors. It was supposed that the data free from these malfunctions might be related to space weather and were taken for correlation analysis. We used following parameters for correlation analysis:

1) parameters of solar activity (sunspot numbers, 2800 MHz (10.7 cm) solar flux F10.7);

2) parameters of geomagnetic activity (Ap, AE and Dst – indices);

3) galactic cosmic ray activity index, determined by NM data;

4) proton (>10 MeV and >60 MeV) and electron (>2 MeV) fluxes;

5) parameters of spacecraft mission reliability: normalized (relative) frequency of anomalies R = M/Nt, where M- all anomalies registered in an certain time interval, t- time interval, and N- number of satellites in operation (this normalized parameter R defines number of malfunctions M in one day per one satellite);

6) average statistical satellite lifetime Tav = (T1 + T2 + ...+Tn)/n before the satellite loss.

18.17.3. Situations in October 1989 and April-May 1991 as examples of very high frequency of satellite malfunctions

In Fig. 18.17.1 are shown situation with satellite malfunctions and behaviors of some related parameters in October 1989.

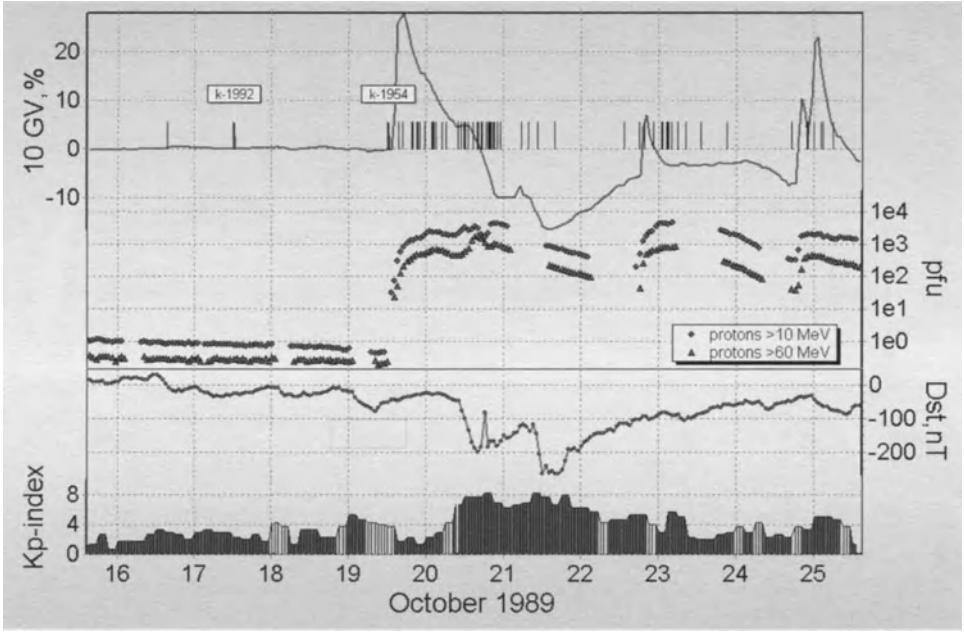

Fig. 18.17.1. Satellite malfunctions and other parameters in October 1989. Upper panel – CR activity near the Earth: variations of 10 GV CR density; solar proton (> 10 MeV and >60 MeV) and electron (> 2 MeV) fluxes. Lower panel – geomagnetic activity: Kp- and Dst-indices. Vertical lines on the upper panel correspond to the malfunction moments. 'Kosmos' satellites are marked. According to Dorman for INTAS-00810 Team (2002).

In Fig. 18.17.1 we see that during 17-25 October 1989 we have 69 satellite malfunctions as whole, but the only 2 of them were on low altitudes (both on 'Kosmos' satellites). In this period we see several proton enhancements, 3 GLEs (19, 22 and 24 October), big Forbush-effects, strong geomagnetic storms, including severe (Kp = 8+) storm on 20-21 October.

In Fig. 18.17.2 is shown the situation in April-May 1991. It can be seen a majority of satellite malfunctions coincides with period of the strong geomagnetic storm accompanied with a great Forbush decrease according to NM world-wide network (CR intensity at 10 GV). In this period was also a great FEP enhancement of several order increasing of high-energy electron flux.

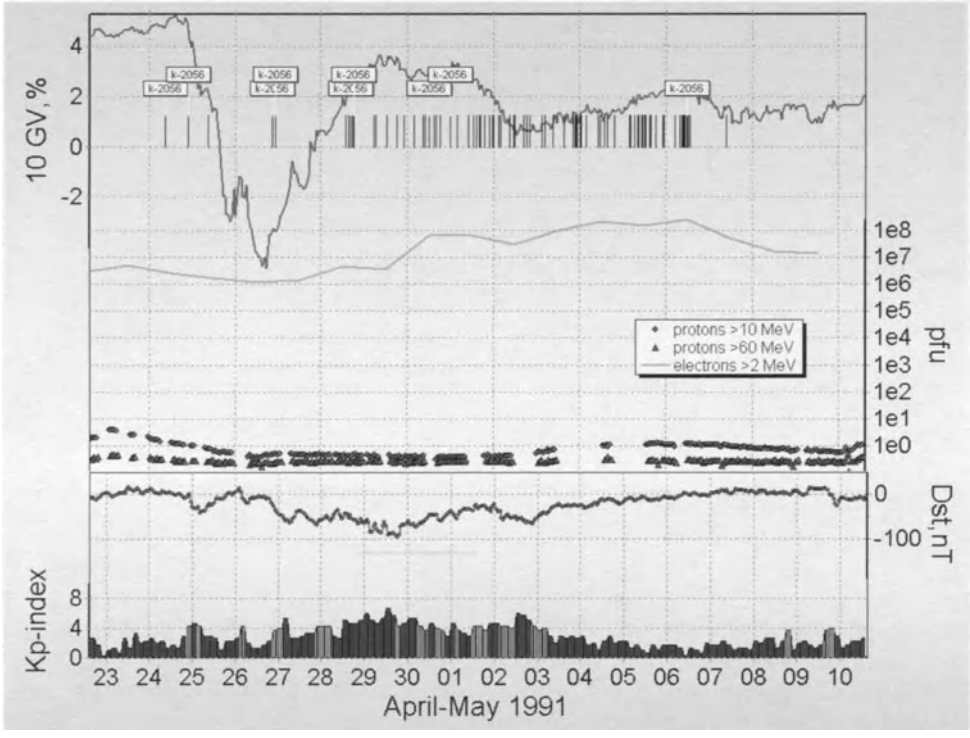

Fig. 18.17.2. Satellite malfunctions in April-May 1991. Upper panel – CR activity near the Earth: variations of 10 GV CR density; solar proton (> 10 MeV and >60 MeV) and electron (> 2 MeV) fluxes. Lower panel – geomagnetic activity: Kp- and Dst-indices. Vertical lines on the upper panel correspond to the malfunction moments. 'Kosmos' satellites are marked. According to Dorman for INTAS-00810 Team (2002).

18.17.4. Comparison of malfunctions in high (> 1000 km) and low (< 1000 km) altitude satellites

In Fig. 18.17.3 are shown daily numbers of satellite malfunctions for high (> 1000 km) altitudes and low (< 1000 km) altitudes.

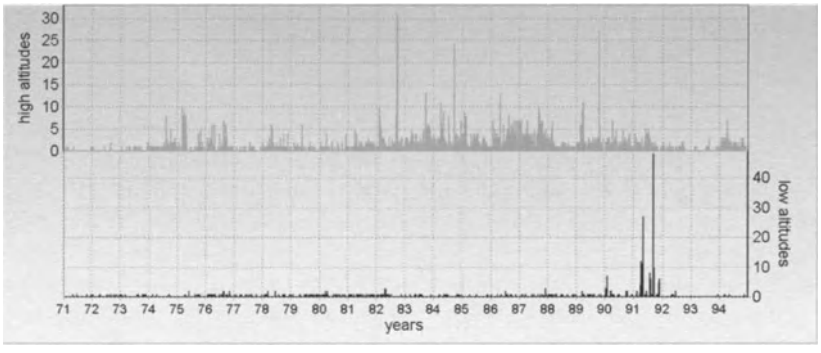

Fig. 18.17.3. Daily numbers of satellite malfunctions for high (> 1000 km) and low (< 1000 km) altitudes. According to Dorman for INTAS-00810 Team (2002). According to Dorman for INTAS-00810 Team (2002).

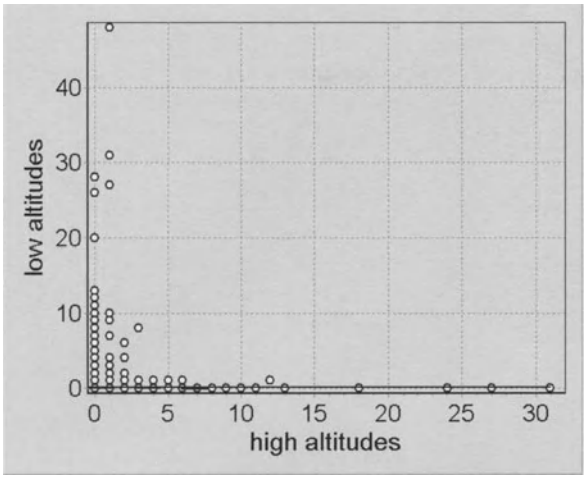

In Fig. 18.17.4 is shown an important fact, that there are no real relation between low- and high-altitude satellite malfunctions (correlation coefficient smaller than 0.01).

Fig. 18.17.4. Daily numbers of low satellite malfunctions versus the same for high altitudes. According to Dorman for INTAS-00810 Team (2002).

18.17.5. Peculiarities of 'Kosmos' satellite malfunctions

Let us consider in more details data on soviet Kosmos satellites. These satellites were 49 single-type low Earth (LEO) orbit satellites with orbit inclination of 74°, circular orbit at about 800 km. During 1971-1997 were registered 459 cases of anomalous performance. During the studied period at least two of Kosmos satellites were present simultaneously in the magnetosphere. On the average, about 9 anomalies that may be related to space weather were observed in each satellite, though for certain satellites this number was much bigger. Kosmos data were 7% of the total data in our data-base, but in the low-altitude subset, Kosmos anomalies came to 25%. Moreover, majority of days with low-altitude anomalies were provided by Kosmos data. In Fig. 18.17.5 is shown the long-term variation of the relative frequency of anomalies (per day and per one satellite) in Kosmos satellites during more than two solar cycles.

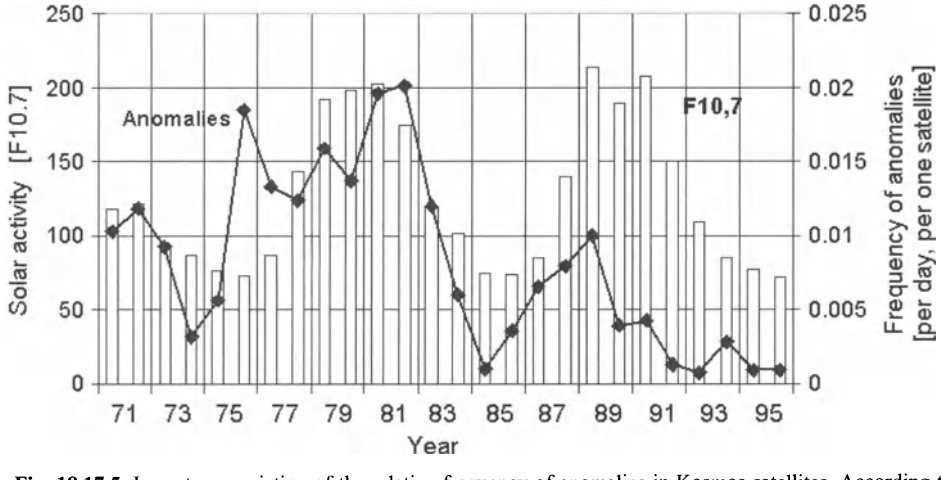

Fig. 18.17.5. Long-term variation of the relative frequency of anomalies in Kosmos satellites. According to Dorman for INTAS-00810 Team (2002).

The dependence of Kosmos anomalies relative frequency from the level of geomagnetic activity (index AE) is shown in Fig. 6. It can be seen that with increasing of geomagnetic activity the frequency of Kosmos anomalies increases in many times (from smaller than 0.01 up to 0.3 anomalies per day and per one satellite).

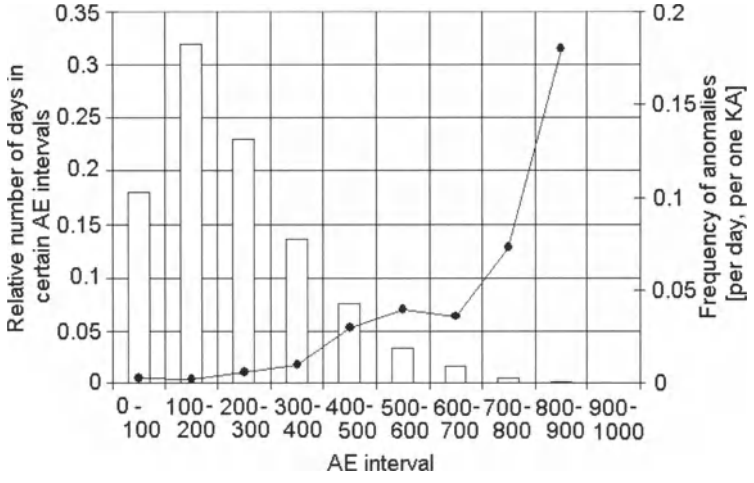

Fig. 18.17.6. The dependence of Kosmos anomalies frequency from the level of AE index geomagnetic activity according to data for 1970-1997. According to Dorman for INTAS-00810 Team (2002).

18.17.6. Seasonal variations of the number of satellite malfunctions

The analysis of the total number of satellite malfunctions (about 6000 events) showed well pronounced half-year variation with maxima in spring and autumn (see Fig. 18.17.7). The shape and phase of the half-year wave in the malfunction number looks similar to the seasonal wave in Ap-index of the geomagnetic activity (see Fig. 18.17.8), but the percentage amplitude is bigger.

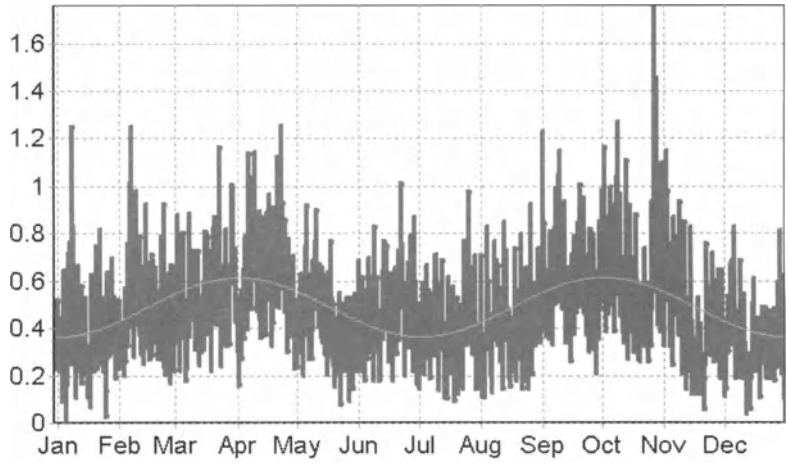

Fig. 18.17.7. Seasonal variations of the satellite malfunctions. According to Dorman for INTAS-00810 Team (2002).

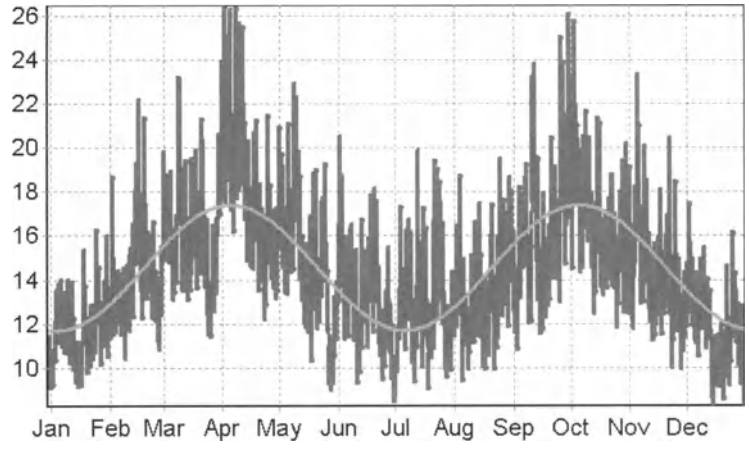

Fig. 18.17.8. Seasonal variations of the Ap index of geomagnetic activity. According to Dorman for INTAS-00810 Team (2002).

18.17.7. Clusterization of satellite malfunctions

The observation data show that malfunctions of high- altitude as well as low-altitude satellites are not independently, but their distribution in time show that mainly they occurred by groups with length of few days (see Fig. 18.17.9).

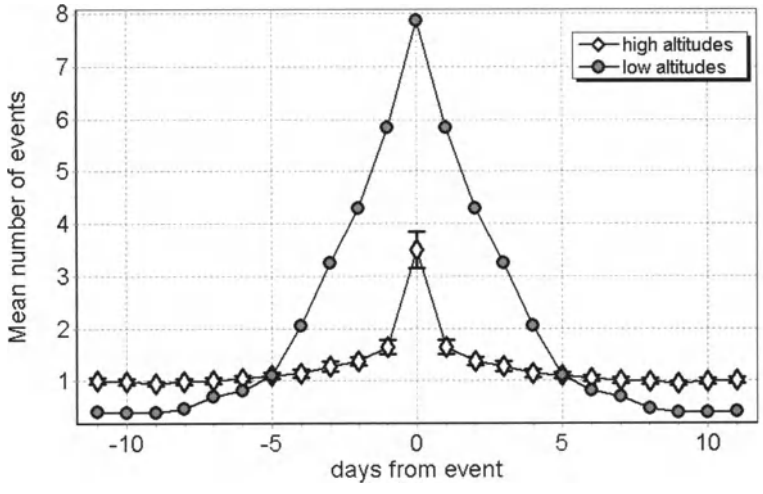

Fig. 18.17.9. The mean distribution of the satellite malfunctions (events) relative to day of each malfunction for low (< 1000 km) and high (> 1000 km) altitude satellites separately. According to Dorman for INTAS-00810 Team (2002).

The Fig. 18.17.9 demonstrates the clusterization of malfunctions. It means that the satellites malfunctions occur often by series. It is true as for high altitudes so for low altitudes, but the clusterization is more pronounced for low altitude malfunctions: on low altitudes the series are more abundant and more prolonged.

18.17.8. On the connection of satellite malfunctions with Cosmic Ray Activity index; possible using of this index for forecasting

The connection with Cosmic Ray Activity (CRA) index (Belov et al., 1999) is shown in Fig. 18.17.10 for high-altitude satellites (for low-altitude satellites in the frame of statistical errors we did not find any connection with CRA).

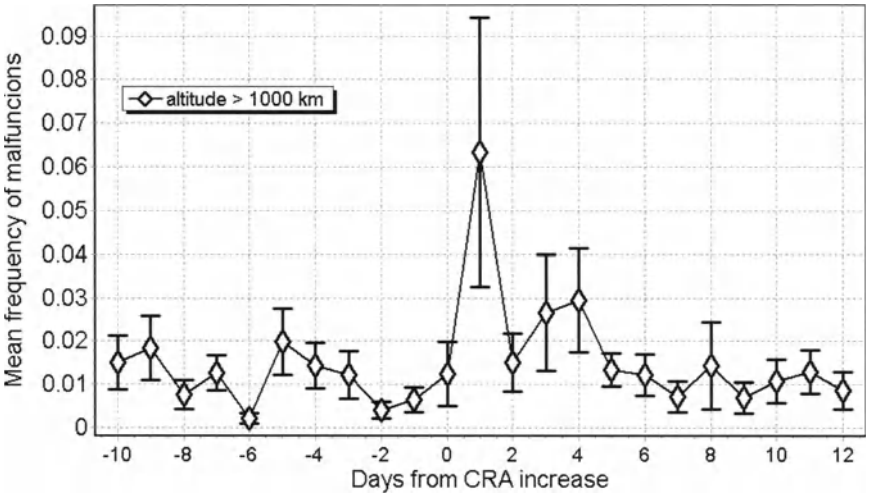

Fig. 18.17.10. The connection of malfunctions frequency for high-altitude satellites with Cosmic Ray Activity (CRA) index. According to Dorman for INTAS-00810 Team (2002).

From Fig. 18.17.10 can be seen an important feature: the increasing about 6 times of malfunction frequency occurred about one day after CRA increasing. This increasing of high-altitude satellite malfunction frequency about one day after Cosmic Ray Activity (CRA) index increasing can be used for forecasting.

18.17.9. Influence of proton and electron fluxes on the satellite malfunction frequency in dependence of the type of satellite orbit; CR effects and peculiarities for forecasting

The satellite characteristics were added from different Internet sources. We have ~300 satellites and ~6000 anomalies in our database. All satellites were divided in the groups regarding of their orbit altitude and inclination. In Fig. 18.17.11 each orbit is presented by corresponded sign. Sometimes, one point represents numerous satellites of the very close orbits, for example, a majority (>100) geostationary satellites and 49 "Kosmos" spacecrafts. We can use any altitudinal boundary within the wide range (1500-15000 km) for altitude separation. Inclination boundary (58°) was chosen to separate "shuttles", which are too specific to be analyzed with the other satellites. In result, four groups were obtained, with essentially different physical conditions on the orbits: HL (high altitude - low inclination), LH (low altitude-high inclination), HH (high altitude - high inclination) and LL (low altitude - low inclination). HH group with all GEO satellites is the most abundant.

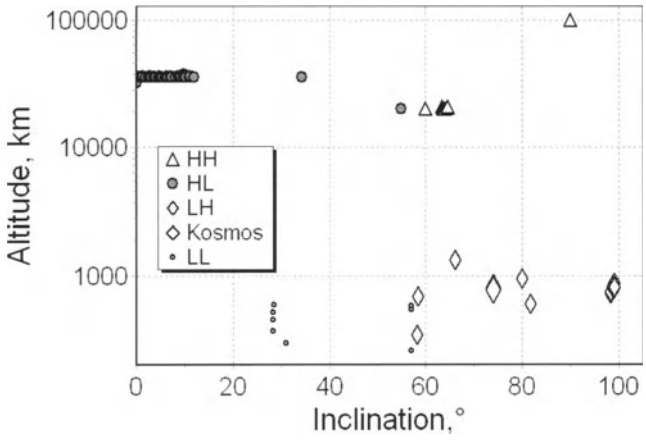

Fig. 18.17.11. Altitude-inclination distribution of the satellite orbits. According to Belov et al. (2003a).

Satellite malfunctions are very irregularly distributed along the time. In some days tens malfunctions at several satellites are recorded. One of the famous periods, with a high frequency of malfunctions, was 19-26 October 1989 (see above, Fig. 18.17.1), when the magnetic storms, including the severe one on 20-22 October, were observed. However the satellite malfunctions in this period correlate better to 3 huge proton enhancements, observed also as Ground Level Events (19-20, 22-23 and 24-25 October). The absolute majority of anomalies were recorded in HH (high altitude - high inclination) group, just at the orbits with maximal effect of solar cosmic rays. Another sample of high frequency satellite malfunctions was presented in Fig. 18.17.1 (the period of 28 April – 6 May, 1991). In these days there was a severe magnetic storm, no proton enhancements but big fluxes of relativistic electrons. The malfunctions were entirely absent in HH group, which played the main role in preceding example (Fig. 18.17.1). Only a few malfunctions were in GEO group and huge majority of anomalies happened at low altitudes. These two examples illustrate both a relation satellite malfunctions to the CR events, and essential difference between various satellite groups. In fact, there is no correlation between variations of the satellite anomaly frequency at high and low altitudes not only in these examples, but over the whole database (see Section 18.17.4).

We compared variations of daily frequency of the satellite anomalies with the different characteristics of solar, interplanetary, geomagnetic and cosmic ray activity. In proton enhancements the frequency of anomalies arises significantly at the high altitudes during two first days, with the greater is proton flux the bigger is an increase of anomalies (see Fig. 18.17.12). This effect is especially big in the HH group of satellites. The electron flux variations are more important for HL (GEO) and LH groups. Fig. 18.17.13 is obtained by the epoch method with a day of every malfunction as 0-day. Mean fluencies of the relativistic electrons is maximal in the malfunction day. It is important, that electron fluency arises significantly some days before the malfunction. Such a behavior is characteristic not only for electrons, but for geomagnetic activity and some other indices as well. This peculiarity we used in elaboration of the satellite malfunction frequency models and forecasting methods.

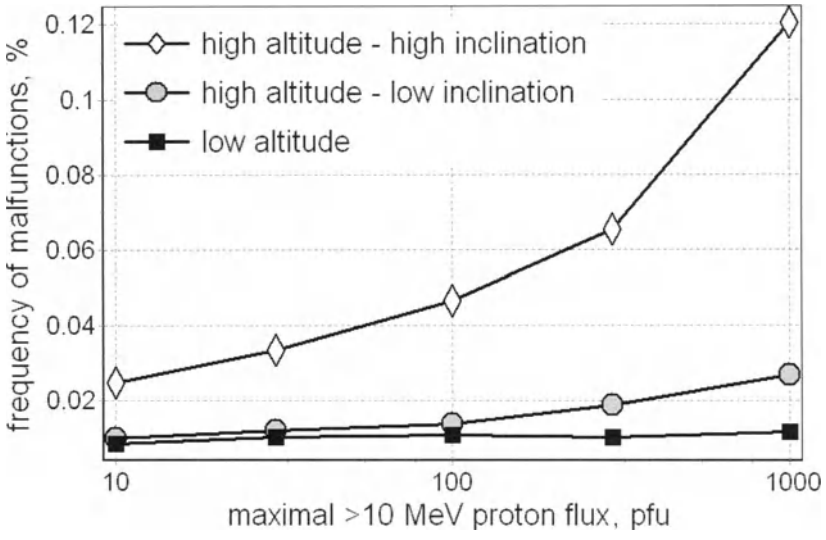

Fig. 18.17.12. Mean anomaly frequency in 2 first days of proton enhancement at different orbits in dependence on maximal proton flux of E >10 MeV. According to Belov et al. (2003a).

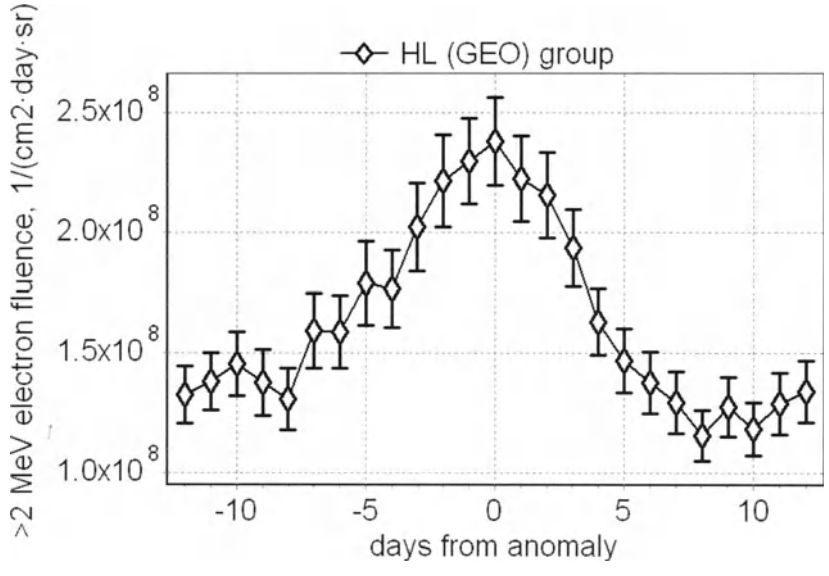

Fig. 18.17.13. Electron fluencies vs. the satellite malfunctions in 1987-1994 by the epoch method derived (0-day is the satellite anomaly day). According to Belov et al. (2003a).

Fig. 18.17.14 demonstrates a difference in CR effect on malfunctions at different orbits. Proton fluencies are much higher in HH group than in other groups. LH group is sooner electron-dependent, and HL group may be considered as mixed one.

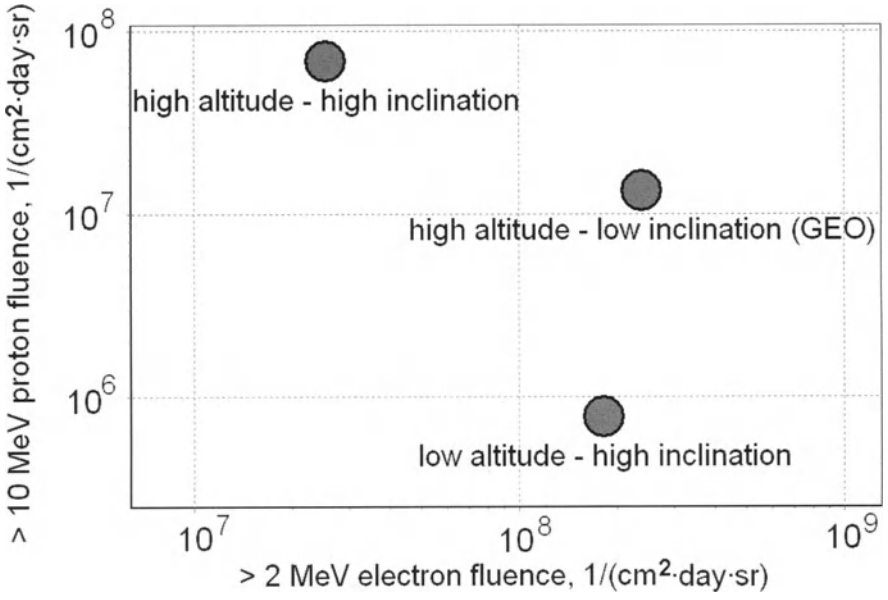

Fig. 18.17.14. Mean proton and electron fluencies in the anomaly satellite day for different types of satellite orbits according to data for 1987-1994. According to Belov et al. (2003a).

Belov et al. (2003a) checked a relation between different space weather parameters (more than 30 in total) and their combinations and satellite anomalies at different orbits in 1987-1994. We used the parameters for anomaly day and for several preceding days and simplest linear regression (with power law dependence for the proton and electron indices). Some peculiarities of models, simulated frequency of the satellite malfunctions by means of 5-8 different indices, are presented in Table 18.17.1. Index sequence and letters' size in the names reflect a contribution of this index to the model.

Table 18.17.1. Models of the satellite malfunction frequency. According to Belov et al. (2003a).

Group of satellites	HL	HH	LH
Parameters of model	**e2** p100, p60d sf, Ap, V_{sw} B_z, da10	p60d, p100 Eak SSN365, $B_z$nsum	**e2** CRA AE, sf, Ap B_z, V_{sw}

Explanations to the Table 18.17.1: e2 and p100 – >2 MeV electron and >100 MeV proton fluencies (data of GOES satellites); p60d – daily flux of >60 MeV protons (data of IMP8 satellites); Ap and AE –indices of geomagnetic activity, Eak – estimation of energy incoming to the magnetosphere supposed by Akasofu (1981); V_{sw} – solar wind velocity; B_z – daily mean B_z-component of IMF, $B_z$nsum – sum of

negative values B_z- component; SSN365 – yearly running averaged sunspot number; CRA and da10 - cosmic ray activity indices (Belov et al. 1999), obtained from neutron monitor network data. Seasonal factor sf (semi-annual variation with maxima close to equinoxes) was used as one of the independent parameters.

The models describe a relation of the satellite malfunction frequency to the space weather parameters by the complex way and they differ significantly for satellite groups. They combine the geomagnetic activity indices, CR, solar wind and some other parameters. However, CR give the main contribution for all groups. Characteristics of the obtained models allow them to be used for the satellite malfunction forecasting.

Conclusion and Problems

In this monograph I have tried to describe CR as an **object of research** (**primary and secondary CR**), as well as the theoretical and experimental basis of CR as a **research instrument** for Geophysics and Space Physics (Part 1, Chapters 1–4), the detail description on the **influence of the changing atmosphere on CR** (Part 2, Chapters 5–9), and inversely, on the **influence of the changing CR on the atmosphere and atmospheric processes** (Part 3, Chapters 10–14), and on many realized and potential **applications of CR research** in different branches of Science and Technology (Part 4, Chapters 15–18).

In 1969 as Rapporteur at the 11-th International Cosmic Ray Conference in Budapest, I formulated a list of unsolved problems in the geophysical aspect of CR research. Many of these problems have been solved during the last 35 years (their solutions are reflected in this monograph), but several have not been solved up to now. Here I try to formulate the extended list of **some known unsolved problems**, which seems to be important to solve in the near future for the developing of CR research in atmosphere and underground, as well as in space. From my opinion, the described here CR research in the atmosphere and underground developed now so deep and so detailed that it became necessary in additional to traditional integral multiplicities to introduce and to calculate partial integral multiplicities for different CR secondary components generated by different primary particles (protons, alpha-particles, nuclei with different Z > 2, electrons, gamma-quanta, neutrons), and then on the basis of these results to calculate more exactly partial meteorological coefficients, traditional integral multiplicities and coupling functions, and finally – full meteorological coefficients, variational coefficients and accepting vectors. The following list of Problems is not full; I think that any thoughtful reader will be available to formulate many actual Problems to each Chapter of this book which need to be solve and really can be solved according to the current level of Science. The clearly formulation of actual Problems is important not only for education (many Problems can be considered as subject of Diploma Work in College or in University or as subject for Ph.D. Thesis), but also for acceleration of the progress in CR research and in connected branches of Science and Technology.

Problem 1. Partial integral multiplicity $m_{\mu p}\left(E_o,\theta_o,\varphi_o,E_\mu,\theta_\mu,\varphi_\mu,h_o,g,T(h),e(h),\mathbf{E}(h)\right)$ for muons with energy E_μ detected on a mass level h_o at zenith angle θ_μ and azimuth angle φ_μ **generated by primary proton** with the total energy out of atmosphere E_o arrived on the boundary of atmosphere at zenith angle θ_o and azimuth angle φ_o should be calculated on the basis of an up-to-date model of the meson nucleon cascade developing in the real atmosphere in dependence on the level of observations h_o, gravitational acceleration g, and vertical distributions in atmosphere of temperature $T(h)$, humidity $e(h)$ and electric field $\mathbf{E}(h)$. In these calculations it will be necessary to take into account the scattering and attenuation of secondary particles. The same should be calculated for **secondary pions** $m_{\pi p}$, **secondary protons** m_{pp}, **secondary neutrons** m_{np}, **secondary electrons** m_{ep}, and **secondary gamma rays** $m_{\gamma p}$.

Problem 2. The partial integral multiplicities should be calculated for the same secondary CR components as in Problem 1, but **generated by primary alpha-particles**: $m_{\mu\alpha}$, $m_{\pi\alpha}$, $m_{p\alpha}$, $m_{n\alpha}$, $m_{e\alpha}$, and $m_{\gamma\alpha}$.

Problem 3. The same as in Problem 1 but **generated by primary nuclei Z > 2**: $m_{\mu Z}$, $m_{\pi Z}$, m_{pZ}, m_{nZ}, m_{eZ}, and $m_{\gamma Z}$.

Problem 4. The same as in Problem 1 but **generated by primary electrons**: m_{ee} and $m_{\gamma e}$.

Problem 5. The same as in Problem 1 but **generated by primary gamma rays**: $m_{e\gamma}$ and $m_{\gamma\gamma}$.

Problem 6. The same as in Problem 1 but **generated by primary neutrons** (important for investigations of solar neutron events): $m_{\mu n}$, $m_{\pi n}$, m_{pn}, m_{nn}, m_{en}, and $m_{\gamma n}$.

Problem 7. On the basis of solving Problems 1–3 taking into account contents of primary **galactic CR** should be calculated traditional (total) **integral multiplicity for muons.** On the basis of obtained results should be calculated expected energy spectrum of muons, their altitude and cutoff rigidity dependences, and angle distribution, and compared with experimental data. The **integral multiplicity for muons** should be calculated also for different contents of **solar CR** and compared with available experimental data on observed altitude and cutoff rigidity dependences of solar CR effects in muon component.

Problem 8. The same as in Problem 7 but for total **integral multiplicity for secondary pions.**

Problem 9. The same as in Problem 7 but for total **integral multiplicity for secondary protons.**

Problem 10. The same as in Problem 7 but for total **integral multiplicity for secondary neutrons.**

Problem 11. On the basis of solving Problems 1–5 taking into account contents of primary **galactic CR** should be calculated traditional (total) **integral multiplicity for secondary electrons.** On the basis of obtained results should be calculated expected energy spectrum of secondary electrons, their altitude and cutoff rigidity dependences, and angle distribution, and compared with experimental data. The integral multiplicity for secondary electrons should be calculated also for different contents of **solar CR** and compared with available experimental data on observed altitude and cutoff rigidity dependences of solar CR effects in the secondary electrons.

Problem 12. The same as in Problem 11 but for total **integral multiplicity for secondary gamma rays.**

Problem 13. On the basis of solution of Problem 7 should be calculated **partial integral multiplicities, total integral multiplicities, and coupling functions for ground and underground muon telescopes** of different geometry in dependence of the level of observation. The same should be calculated for detectors of **soft muons**.

Problem 14. On the basis of solution of Problems 7-10 should be calculated **partial integral multiplicities, total integral multiplicities, and coupling functions for total neutron intensity and multiple neutrons for standard neutron monitors of IGY type and IQSY type as well as for NM without lead and for bore neutron counters** for different levels of observations.

Problem 15. On the basis of solution of Problems 7-12 should be calculated **partial integral multiplicities, total integral multiplicities, and coupling functions for electron-photon detectors** of different geometry in dependence of the level of observation.

Problem 16. On the basis of solution of Problems 7-12 should be calculated **partial integral multiplicities, total integral multiplicities, and coupling functions for** standard detectors (single counter and vertical telescope) for **regular measurements on radio-balloons at different altitudes up to 35-40 km.**

Problem 17. On the basis of solutions of Problems 1-5 should be calculated **partial integral multiplicities, total integral multiplicities, and coupling functions for EAS arrays equipped by electron-photon, muon, and neutron detectors** of different geometry in dependence of the level of observation; the calculations should be carried out for EAS generated by different primary particles at different zenith angle: protons, alpha-particles, nuclei with $Z > 2$, electrons, gamma-quanta (see above, Problems 1–5).

Problem 18. On the basis of solution of Problem 13 should be calculated the **partial and total meteorological coefficients** (barometric, temperature, humidity, gravitational, and electric field) **for muon detectors** of different geometry **on the ground** at different altitudes **and underground** at different depths as well as **for detectors of soft muons.**

Problem 19. On the basis of solution of Problem 14 should be calculated the **partial and total meteorological coefficients** (barometric, temperature, humidity, gravitational, and electric field) **for total neutron intensity and multiple neutrons for standard neutron monitors of IGY type and IQSY type as well as for NM without lead and for bore neutron counters** for different levels of observations.

Problem 20. On the basis of solution of Problem 15 should be calculated the **partial and total meteorological coefficients** (barometric, temperature, humidity, gravitational, and electric field) **for electron-photon detectors** of different geometry at different altitudes.

Problem 21. On the basis of solution of Problem 16 should be calculated the **partial and total meteorological coefficients** (barometric, temperature, humidity, gravitational, and electric field) **for EAS arrays equipped by electron-photon, muon, and neutron detectors** of different geometry in dependence on the level of observation.

Problem 22. On the basis of the solution of Problem 6 **partial integral multiplicities and coupling (response) functions for detecting solar neutrons arrived to the boundary of atmosphere at different zenith angles by neutron telescopes, neutron monitors of IGY and IQSY types, by muon and electron-photon detectors of different geometry at different altitudes** should be calculated**.** At these calculations is necessary to take into account the scattering and attenuation of primary solar neutrons as well as secondary particles generated by these neutrons (refraction effect).

Problem 23. Special functions for spectrographic method (Sect. 3.11 and 3.12) should be **recalculated** on the basis of the obtained new solutions for coupling functions for different secondary CR components underground and in atmosphere at different h_O.

Problem 24. Variational coefficients for muon telescopes and neutron monitors at different R_C for the method of ring CR Observatories (see Section 3.13) should be **recalculated** on the basis of obtained more exact new solutions for coupling functions.

Problem 25. Acceptance vectors for muon telescopes underground and in atmosphere at different h_O, and for neutron super-monitors of IQSY type at different h_O and R_C for global-spectrographic method (see Section 3.14) should be **recalculated** on the basis of obtained more exact new solutions for coupling functions.

Problem 26. On the basis of the obtained solutions for integral multiplicities of secondary neutrons and other secondary components should be recalculated **integral multiplicities and coupling functions** for generation by CR in the Earth's atmosphere **radiocarbon and other cosmogenic atoms.**

The solution of these and other problems, as well as extension of the theoretical and experimental basis of CR research in atmosphere and underground, and wider use of many CR research applications in different branches of Science and Technology, will considerably support the further development of the subject of the present monograph (some features of this will be considered also in Dorman, M2005).

References

References for Monographs and Books

Abagyan L.P, N.O. Bazazyants, I.I. Bondarenko, and M.N. Nikolaev, *Group Contacts for Calculating the Nuclear Reactors*. Atomizdat, Moscow, M1964.

Aitken M.J., *Science-based Dating in Archaeology*, Longman, England, M1990.

Alania M.V. and L.I. Dorman, *Cosmic Ray Distribution in the Interplanetary Space.* METSNIEREBA, Tbilisi, M1981.

Alania M.V., L.I. Dorman, R.G. Aslamazashvili, R.T. Gushchina, and T.V. Dzhapiashvili, *Galactic Cosmic Ray Modulation by Solar Wind.* METSNIEREBA, Tbilisi, M1987.

Bahcall J.N., *Neutrino Astrophysics,* Cambridge Univ. Press, Cambridge, M1989.

Baldin A.M., V.I. Goldansky, V.M. Maximenko, and I.L. Rosental, *Kinematics of nuclear reactions.* Atomizdat, Moscow, M1968.

Barashenkov V.S. and V.D. Tokayev, *Interactions of High-Energy Particles and Atomic Nuclei with Nuclei.* Atomizdat, Moscow, M1972.

Becker R.O. and A.A. Marino, *Electromagnetism and Life*. State University of New York Press, M1982

Bekurz K. and K. Wirtz, *Neutron Physics*, Atomizdat, Moscow, M1968.

Belenky S., *Avalanches Processes in Cosmic Rays*, Gostekhteorizdat, Moscow, M1948.

Berezinsky V.S., S.V. Bulanov, V.L. Ginzburg, V.A. Dogiel, and V.S. Ptuskin (ed. V.L. Ginzburg), *Astrophysics of Cosmic Rays*, Physmatgiz, Moscow, M1990. (English translation: North Holland, Amsterdam, M1990).

Bowman S.G.E., *Radiocarbon Dating*. British Museum Publications, London, M1990.

Carmichael H., *IQSY Insruction Manuel*, No. 7: Cosmic Rays, IQSY Secretariat, London, M1964.

Chalmers J.A., *Atmospheric Electricity* (in Russian), Gidrometeoizdat, Leningrad, M1961.

Chalmers J.A., *Atmospheric Electricity*, Pergamon Press, M1967.

Chipperfield M., *The TOMCAT offline chemical transport model*, M1996.

Daglis I.A. (ed.), *Space Storms and Space Weather Hazards*, Kluwer Ac. Publ., M2001.

Dobrotin N.A., *Cosmic Rays*, Gostechteorizdat, Moscow, M1954.

Dorman Irena V., *Cosmic Rays (Historical Outlook),* NAUKA, Moscow, M1981.

Dorman Irena V., *Cosmic Rays, Accelerators, and New Particles,* NAUKA, Moscow, M1989.

Dorman L.I., *Cosmic Ray Variations*. Gostekhteorizdat, Moscow, M1957. (English translation: US Department of Defense, Ohio Air-Force Base, 1958).

Dorman L.I., *Geophysical and Astrophysical Aspects of Cosmic Rays.* North-Holland, Amsterdam, in series "Progress in Physics of Cosmic Ray and Elementary Particles", ed. J.G. Wilson and S.A. Wouthuysen, Vol. 7, pp. 1-324, M1963a.

Dorman L.I., *Cosmic Ray Variations and Space Research.* NAUKA, Moscow, M1963b.

Dorman L.I., *Meteorological Effects of Cosmic Rays.* NAUKA, Moscow, M1972a.

Dorman L.I., *Acceleration Processes in Space*, VINITI, Moscow, M1972b.

Dorman L.I., *Cosmic Rays: Variations and Space Exploration.* North-Holland, Amsterdam, M1974.

Dorman L.I., *Experimental and Theoretical Principles of Cosmic Ray Astrophysics.* FIZMATGIZ, Moscow, M1975a.

Dorman L.I., *Variations of Galactic Cosmic Rays.* Moscow State University Press, Moscow, M1975b.

Dorman L.I., *Israel Cosmic Ray Center and Foundation of International Cosmic Ray Service*, Project to the Ministry of Science of Israel, Tel Aviv (M1991).

Dorman L.I., *Cosmic Rays in the Magnetosphere and in the Space,* Kluwer Ac. Publishers, M2005 (in press).

Dorman L.I., R.T. Gushchina, D.F. Smart and M.A. Shea, *Effective Cut-Off Rigidities of Cosmic Rays.* NAUKA, Moscow (in Russian and in English), M1972.

Dorman L.I. and E.V. Kolomeets, *Solar Diurnal and Semidiurnal Cosmic Ray Variations from Maxima to Minima of Solar Activity*. NAUKA, Moscow, M1968.

Dorman L.I. and I.D. Kozin, *Cosmic Radiation in the Upper Atmosphere.* FIZMATGIZ, Moscow, M1983.

Dorman L.I., I.Ya. Libin, and Ya.L. Blokh, *Scintillation Method of Cosmic Ray Investigations,* NAUKA, Moscow, M1979.

Dorman L.I. and L.I. Miroshnichenko, *Solar Cosmic Rays*, FIZMATGIZ, Moscow, M1968.

Dorman L.I., I.A. Pimenov and V.S. Satsuk, *Mathematical Service of Geophysical Investigations on the Example of Cosmic Ray Variations.* NAUKA, Moscow, M1978.

Dorman L.I., V.S. Smirnov and M.I. Tyasto, *Cosmic Rays in the Earth's Magnetic Field.* FIZMATGIZ, Moscow, M1971.
Faure G., *Principles of Isotope Geology*. Wiley, New York, M1986.
Forbush S.E. and L. Lange, *Cosmic Ray Results*, Washington, M1948.
Forbush S.E. and L. Lange, *Cosmic Ray Results*, Washington, M1957.
Fridman Sh.D., A.N. Pegoev, E.V. Kolomeets, V.V. Oskomov, and V.V. Obelentsev, *Monitoring of Water Conteins in Snow, Soil and Icecaps by Natural Penetrating Radiation*, Gidrometeoizdat, Leningrad, M1990.
Gaisser T.K., *Cosmic Rays and Particle Physics*, Cambrige Univercity Press, M1990.
Geant4 Collaboration, *Geant4 Physics Reference Manual*, CERN, M2003.
Geyh M.A. and H. Schleicher, *Absolute Age Determination : Physical and Chemical Dating Methods and their Application,* Springer-Verlag, NY, M1990.
Gillespie R., *Radiocarbon User's Handbook*. Oxford-Oxonian Rewley Press, M1984.
Ginzburg V.L. and Syrovatsky S.I., *The Origin of Cosmic Rays*, Pergamon Press, Oxford-London, M1964.
Grieder P.K.F., *Cosmic rays on Earth*, Elsevier, Nitherlands, M2002.
Hayakawa S., *Cosmic Ray Physics,* John Wiley & Sons, New York-London-Sydney-Toronto, M1969
Hayakava S., *Cosmic Ray Physics*, Part I, Mir, Moscow, M1973.
Ivanov-Kholodny G.S. and G.M. Nikolsky, *Sun and the Ionosphere,* Physmatgiz, Moscow, M1969.
Janossy, L., *Cosmic Rays*, Clarendon Press, Oxford, M1950.
Kaula W.M., *Introduction to Planetary Physics*, Wiley, New York, M1968.
Khristiansen G.B., *Cosmic Rays of Superhigh Energies*, Moscow State University Press, Moscow, M1975.
Kogan R.M., I.M. Nazarov, and Sh.D. Fridman, *Foundations of Gamma Spectrometry of Natural Media*, Moscow, Atomizdat, M1976.
Kolomeets E.V. and Sh.D. Fridman, *The Method of the Moisture Content Reserv Determination in the Snow and Soils by Cosmic Rays*, Leningrad, Gidrometeoizdat, M1981.
Korn G. and T. Korn, *Handbook of Mathematics*, Nauka, Moscow, M1968.
Krymsky G.F., *Cosmic Ray Modulation in the Interplanetary Space*, Nauka, Moscow, M1969.
Kuzmin A.I., *Variations of High Energy Cosmic Rays*, Nauka, Moscow, M1964.
Kuzmin A.I., *Variations of Cosmic Rays and Solar Activity*, Nauka, Moscow, M1968.
Landau L.D. and E.M. Lifshitz, *Electrodynamics of Continuous Media*, Pergamon Press, Oxford, M1960.
MacGorman D.R. and W.D. Rust, *The Electrical Nature of Storms*, Oxford University Press, New York, M1998.
McElhinny M.W. and P.L. McFadden, *Paleomagnetism*, Academic Press, M2000.
Merrill R.T., M.W. McElhinny, and P.L. McFadden, *The Magnetic Field of the Earth: Paleomagnetism, the Core and the Deep Mantle*, Academic Press, San Diego, CA, M1997.
Merrill R.T. and M.W. McElhinny, *The Earth's Magnetic Field*, Academic Press, London, M1983.
Mesjaz G.A. and Ju. D. Korolev, *Physics of Impuls Discharge in Gases*, Nauka, Moscow, M1991.
Michels J.W., *Dating methods in archaeology*, Seminar Press, NY, M1973.
Millikan R.A., *Electrons (+ and -), Protons, Photons, Neutrons and Cosmic Rays*, Chicago, M1935.
Miroshnichenko L.I., *Solar Cosmic Rays*, Kluwer Ac. Publishers, M2001.
Mukhin K.N. *Introduction to Nuclear Physics*, Gosatomizdat, Moscow, M1963.
Murzin V.S., *Introduction to Cosmic Ray Physics*, Moscow University Press, Moscow, M1988
Myssowsky L.V., *Cosmic Rays*, Gosizdat, Moscow-Leningrad, M1929.
Parker E.N., *Interplanetary Dynamical Processes*, John Wiley and Suns, New York-London, M1963.
Raiser Yu.P., *Physics of Gas Discharge*, Nauka, Moscow , M1987.
Rogers, J.E.T., *Agriculture and Prices in England*, Volume I-VIII, Oxford, Clarendon Press, M1887; Reprinted by Kraus Reprint Ltd, Vaduz in 1963.
Rosen S. (ed.), *Selected Papers on Cosmic Ray Origin Theories*, New York, M1969.
Rossi B., *Cosmic Rays*, Atomizdat, Moscow, M1966.
Rossi B. and K. Greisen, *Interaction of Cosmic Rays with Matter*, MIR, Moscow, M1948.
Schlickeiser R., *Cosmic Ray Astrophysics*, Springer, Berlin, M2001
Sekido Y. and H Elliot (Eds.), *Early History of Cosmic Ray Studies*, Dordrecht, D. Reidel Publ. Co., M1985.
Shafer Yu.G. and G.V. Shafer, *Data on Precesion Observations of Cosmic Ray Intensity*, Nauka, Moscow, M1985.
Simpson J.A., *Neutron Monitor*, Chicago Univ. Press, Chicago, M1955.
Smith A., *An Inquiry into the Nature and Causes of the Wealth of Nations*, W. Strahan & T. Cadell, London, M1776.
Stecker F.W., *Cosmic Gamma Rays*, Mono Book Co, Baltimore, M1971.
Taylor R.E., *Radiocarbon Dating. An archaeological perspective*, Academic Press, Orlando, USA, M1987.

Taylor R.E, A. Long, and R. Kra (eds), *Radiocarbon after Four Decades. An Interdisciplinary Perspective.* Springer - Verlag, NY, M1994.
Uman M.A., *Lightning*, Dover, New York, M1984.
Uman M.A., *The Lightning Discharge*, Acad. Press, Orlando, M1987.
Veksler V.I., L.V. Groshev, and B.M. Isaev, *Ionization Methods of Radiation Investigations*, Gostekhizdat, Moscow, M1959.
Velinov P., G. Nestorov, and L. Dorman, *Cosmic Ray Influence on the Ionosphere and Radio Wave Propagation*, Bulgarian Ac. Sci. Press, Sofia, M1974
Volland H., *Atmospheric Electrodynamics*, Springer, Berlin, M1984.
Walt M., *Introduction to Geomagnetically Trapped Radiation*, Cambridge Press, M1994
Yasue S., S. Mori, S. Sakakibara, and K. Nagashima, *Coupling Coefficients of Cosmic Ray Daily Variations for Neutron Monitor Stations*, Nagoya University, Japan, M1982.
Zombeck, M., *Handbook of Space Astronomy and Astrophysics,* Cambridge University Press, M1982.

References for Chapter 1 and Preface for Part 1

Adams N. "A temporary increase in the neutron component of CR", *Philos. Mag.*, **41**, 503-505 (1950).
Agrawal V., T.K. Gaisser, P. Lipari, and T. Stanev "Atmospheric neutrino flux above 1 GeV", *Phys.Rev.*, **D53**, 1314 -1323, (1996).
Aizu H., Y. Fujimoto, S. Hasegawa, M. Koshiba, I. Mito, J. Nishimura, K. Yokoi, and M. Schein "Heavy Nuclei in the Primary Cosmic Radiation at Prince Albert, Canada. II", *Phys. Rev.*, **121,** 1206-1218 (1961).
Alcaraz J., D. Alvisi, B. Alpat et al. "Search for antihelium in cosmic rays", *Phys. Lett.*, **B461**, 387-396 (1999).
Alfven H. "On the solar origin of cosmic radiation, I", *Phys. Rev.*, **75,** 1732-1735 (1949).
Alfven H. "On the solar origin of cosmic radiation, II", *Phys. Rev.*, **77**, 375-379 (1950).
Anders E. and N. Grevesse "Abundances of the elements: Meteoritic and Solar", *Geochimica et Cosmochimica Acta*, **53**, No. 1, 197-214 (1989).
Anderson C.D. "The apparent existence of easily deflectable positives", *Science*, **76**, 238 (1932).
Anderson C.D. "The positive electron", *Phys. Rev.*, **43**, 491-494 (1933a).
Anderson C.D. "Cosmic ray positive and negative electrons", *Phys. Rev.*, **44**, 406-416 (1933b).
Apanasenko A.V., V.A. Beresovskaya, M. Fujii et al. "All particle spectrum observed by RUNJOB", *Proc. 27th Intern. Cosmic Ray Conf.,* Hamburg, **5**, 1622-1625 (2001).
Asakimori K., T.H. Burnett, M.L. Cherry et al. "Cosmic-ray proton and helium spectra: results from the JACEE experiment", *Astrophys. J.*, **502**, 278-283 (1998).
Asaoka Y., J. F. Ormes, K. Abel et al. "Precise measurements of cosmic-ray antiproton spectrum following the solar field reversal", *Proc. 27th Intern. Cosmic Ray Conf.*, Hamburg, **5**, 1699-1702 (2001).
Axford W.I., E. Leer, and G. Skadron "The acceleration of cosmic rays by shock waves", *Proc. 15th Intern. Cosmic Ray Conf.,* Plovdiv, **11**, 132-137 (1977).
Baade W. and F. Zwicky "Remarks on super-novae and cosmic rays", *Phys. Rev.*, **46,** 76-77 (1934a).
Baade W. and F. Zwicky "Cosmic rays from super-novae", *Proc. Nat. Acad. Sci. USA*, **20**, 259-263 (1934b).
Badhwar G.D., R.L. Golden, J.L.Lacy, J.E. Zipse, R.R. Daniel, and S.A. Stephens "Relative abundance of antiprotons and antihelium in the primary cosmic radiation ", Nature, 274, 137-139 (1978).
Barnothy J. and M. Forro "Cosmic rays from Nova Herculis", *Nature*, **135**, 618-619 (1935a).
Barnothy J. and M. Forro "Diurnal of cosmic ray intensity and Nova Herculis", *Nature*, **136**, 680-681 (1935b).
Basini G., R.Bellotti, M.T. Brunetti et al. "The Flux of Cosmic Ray Antiprotons from 3.7 to 24 GeV", *Proc. 26th Intern. Cosmic Ray Conf.*, Salt Lake City, **3**, 77-80 (1999).
Bell A.R. "The acceleration of cosmic rays in shock fronts, I", *Mon. Not. Roy. Astron. Soc.*, **182**, 147-156 (1978a).
Bell A.R. "The acceleration of cosmic rays in shock fronts, II", *Mon. Not. Roy. Astron. Soc.*, **182**, 443-455 (1978b).
Bergström L., J. Edsjö, P. Gondolo, and P. Ullio "Clumpy neutralino dark matter", *Phys. Rev.*, **D59**, 043506, 11 pages (1999a).
Bergström L., J. Edsjö, and P. Ullio "Cosmic Antiprotons as a Probe for Supersymmetric Dark Matter?", *Astrophys. J.*, **526**, 215-235 (1999b).
Bieber J.W., R.A. Burger, R. Engel, T.K Gaisser, S Roesler, T. Stanev " Antiprotons at Solar Maximum", *Phys. Rev. Lett.*, **83**, 674-677 (1999a).
Bieber J.W., R.A. Burger, R. Engel, T.K. Gaisser, and T. Stanev "Antiprotons as Probes of Solar Modulation", *Proc. 26th Intern. Cosmic Ray Conf.*, Salt Lake City, **7**, 17-20 (1999b).
Bieber, J.W. and P. Evenson "Spaceship Earth – an optimized network of neutron monitors", *Proc. 24th Intern. Cosmic Ray Conf*, Rome, **4**, 1316-1319 (1995).

Binns W.R., T.L. Garrard, P.S. Gibner, M.H. Israel, M.P. Kertzman, J. Klarmann, B.J. Newport, E.C. Stone, and C.J. Waddington "Abundances of ultraheavy elements in the cosmic radiation: results from HEAO 3", *Astrophys. J.*, **346**, No.2, 997-1009 (1989)

Blanford R.D. and J.R. Ostriker "Particle acceleration by astrophysical shocks ", *Astrophys. J.*, **221**, L29-L32 (1978).

Blokh Ya.L., Dorman L.I., Kaminer N.S., and Kapustin I.N. "Cosmic ray neutron spectrograph on the basis of registration channels with different tau using", *Geomagnetism and Aeronomy*, **11**, No. 5, 891-892 (1971).

Blokh Ya.L., E.S. Glokova, L.I. Dorman and O.I. Inozemtseva "Electromagnetic conditions in interplanetary space in the period from August 29 to September 10, 1957 determined by cosmic ray variation data", *Proc. 6th Intern. Cosmic Ray Conf.*, Moscow, **4**, 172-177 (1959).

Boezio M., P. Carlson, T. Francke et al. "The Cosmic-Ray Antiproton Flux between 0.62 and 3.19 G eV Measured Near Solar Minimum Activity", *Astrophys. J.*, **487**, 415-423 (1997).

Boezio M., M. Ambriola, S. Bartalucci et al. "High-Energy cosmic-ray antiprotons with the CAPRICE98 experiment", *Proc. 27th Intern. Cosmic Ray Conf.*, Hamburg, **5**, 1695-1698 (2001).

Bogomolov E.A., N.D. Lubyanaya, V.A. Romanov, S.V. Stepanov and M.S. Shulakova "A stratospheric magnetic spectrometer investigation of the singly charged component spectra and composition of the primary and secondary cosmic radiation" *Proc. 16th Intern. Cosmic Ray Conf*, Kyoto, **1**, 330-335 (1979).

Bogomolov E.A., G.I. Vasilyev, S.Yu. Krut'kov, N.D. Lubyanaya, V.A. Romanov, S.V. Stepanov, and M.S. Shulakova "Galactic antiproton spectrum in the 0.2-5 GeV range", *Proc. 20th Intern. Cosmic Ray Conf.*, Moscow, **2**, 72-75 (1987).

Bogomolov E.A., G.I. Vasilyev, S.V. Krut'kov, N.D. Lubyanaya, V.A. Romanov, S.V. Stepanov, M.S. Shulakova "New antiproton studies in the 2-5 GeV range", *Proc. 21th Intern. Cosmic Ray Conf.*, Adelaide, **3**, 288-290 (1990).

Bogomolov E.A., G.I. Vasilyev, S.Yu. Krut'kov, S.V. Stepanov and M.S.Shulakova "The deuterium cosmic ray intensity from balloon measurement in energy range 0.8–1.8 GeV/nucl.", *Proc. 24th Intern. Cosmic Ray Conf*, Rome, **2**, 598-601 (1995).

Bowen I.S., R.A. Millikan, and H.V. Neher "The influence of the Earth's magnetic field on cosmic rays intensities up to the top of the atmosphere", *Phys. Rev.*, **52**, 80-88 (1937).

Bowen I.S., R.A. Millikan, and H.V. Neher "New light on the nature and origin of the incoming cosmic rays", *Phys. Rev.*, **53**, 861-885 (1938).

Buffington A., S.M.Schindler, and C.R. Pennypacker "A measurement of the cosmic-ray antiproton flux and a search for antihelium", *Astrophys. J.*, **248**, 1179-1193 (1981).

Chapman S.B. "Cosmic rays and magnetic storms", *Nature*, **140**, No3540, 423-424. (1937).

Chardonnet P., J. Orloff, and P Salati "The production of anti-matter in our galaxy", *Phys. Lett.*, **B409**, 313-320 (1997).

Clay J. "Ultraradiation (penetrating radiation), III. Annual variation and variation with the geographical latitude", *Proc. Roy. Acad. Amsterdam*, **33**, 711 (1930).

Clay J. "The Earth-magnetic effect and the corpuscular nature of ultra-radiation", *Proc. Roy. Acad. Amsterdam*, **35**, 1282 (1932).

Clay J. "Results of the Dutch cosmic ray expedition 1933", *Physica.* **1**, No. 5, 363-382. (1934).

Compton A.H. "Progress of cosmic ray survey", *Phys. Rev.*, **41**, 681- 682 (1932).

Compton A.H. "A geographic study of cosmic rays", *Phys. Rev.*, **43**, 387-403 (1933).

Compton A.H. "Recent developments in cosmic rays", *Rev. Sci. Instr.*, **7**, 71-81 (1936).

Compton A.H. and R.N. Turner "Cosmic rays on the Pacific Ocean", *Phys. Rev.*, **52**, 799-814 (1937).

Compton A.H., R.D. Bennet, and J.C. Stearns "Diurnal variation of cosmic rays", *Phys. Rev.*, **41**, 119-126 (1932).

Compton A.H., E. Wollan, and R.D. Bennet "A precision recording cosmic ray meter", *Rev. Sci. Instr.*, **5**, 415-422 (1934).

Connell J.J. "Galactic Cosmic-Ray Confinement Time: ULYSSES High Energy Telescope Measurements of the Secondary Radionuclide ^{10}Be", *Astrophys. J.*, **501**, No. 1, L59-L62 (1998).

Coulomb C.A. "Troisieme memoire sur l'electricité et le magnetisme", *Memoires de l'Academie des Sciences*, Paris, 612-638 (1785).

Coutu S., A.S. Beach, J.J. Beatty et al. "Positron measurements with the HEAT-pbar instrument", *Proc. 27th Intern. Cosmic Ray Conf.*, Hamburg, **5**, 1687-1690 (2001).

De Nolfo G.A., L.M. Barbier, M. Bremerich et al. "A measurement of the $^{10}\mathrm{Be}/^{9}\mathrm{Be}$ ratio above 1.0 GeV/nucleon: Results from the 1998 flight of ISOMAX", *Proc. 27th Intern. Cosmic Ray Conf.*, Hamburg, **5**, 1659-1662 (2001).

De Nolfo G.A., N.E. Yanasak, W.R. Binns et al. "New measurements of the Li, Be, and B isotopes as a test of cosmic ray transport models", *Proc. 28th Intern. Cosmic Ray Conf.*, Tsukuba, **4**, 1777-1780 (2003).

Dirac P.A.M. "A theory of electrons and protons", *Proc. Roy. Soc. London*, **A126**, 360-365 (1930).
Dirac P.A.M. "Quantized singularities in the electromagnetic field", *Proc. Roy. Soc.,* London, **A133**, 60-72 (1931).
Dorman L.I. "Two-meson theory of cosmic ray hard component temperature effect", *Special Report 1951-3*, Science-Research Institute of Terrestrial Magnetism, Troitsk, Moscow region (1951a).
Dorman L.I. "Instruction for calculation of temperature corrections to hard component of cosmic ray intensity data", *Special Report, 1951-4*, Science-Research Institute of Terrestrial Magnetism, Troitsk, Moscow region (1951b).
Dorman L.I. "To the theory of cosmic ray meteorological effects", *Doklady Academy of Sciences of USSR* (Moscow), **94**, No. 3, 433-436 (1954a).
Dorman L.I. "On the temperature effect of the cosmic ray hard component", *Doklady Academy of Sciences of USSR* (Moscow), **95**, No.1, 49-52 (1954b).
Dorman L.I. "On the nature of cosmic ray variations", *Ph. D. Thesis*, Physical Lebedev Institute Academy of Sciences of USSR, Moscow, pp. 327 (1955).
Dorman L.I. "Information on solar corpuscular streams obtained from investigation of cosmic ray variations", In the book "*Physics of solar corpuscular streams*", Academy of Sciences of USSR Press, Moscow, pp. 112-128 (1957).
Dorman L.I. "To the theory of meteorological effects of cosmic ray neutron component", *Proc.of Yakutsk Filial of Academy of Sciences*, Series of Physics, Academy of Sciences of USSR Press, Moscow, No. 2, 68-72 (1958a).
Dorman L.I. "To the theory of meteorological effects of cosmic ray soft and general components", *Proc.of Yakutsk Filial of Academy of Sciences*, Series of Physics, Academy of Sciences of USSR Press, Moscow, No. 2, 59-67 (1958b).
Dorman L.I. "The generation and propagation of solar cosmic rays", *Nuovo Cimento*, Vol. 8, Suppl. No. 2, (Proc. of 5th Intern.Cosmic Ray Conf., Varenna, 1957), 391-402 (1958c).
Dorman L.I. "On the energetic spectrum and lengthy of cosmic ray intensity increase on the Earth caused by shock wave and albedo from magnetized front of corpuscular stream", *Proc. of 6th Intern. Cosmic Ray Conf.*, Moscow, Vol. 4, 132-139 (1959a).
Dorman L.I. "To the theory of cosmic ray modulation by solar wind", *Proc. of 6th Intern. Cosmic Ray Conf.*, Moscow, Vol. 4, 328-334 (1959b).
Dorman L.I. "The origin of cosmic ray variations", *D. Sci. Thesis*, Physical Lebedev Institute Academy of Sciences of USSR, Moscow (1962).
Dorman L.I. "Theory of cosmic ray variations", *Cosmic Rays* (Moscow, NAUKA), **13**, 5-66 (1972).
Dorman L.I. "Geophysical effects and second components of cosmic rays in the atmosphere", *Cosmic Rays* (Moscow, NAUKA), **14**, 5-28 (1974).
Dorman L.I. "Cosmic rays in the atmosphere and magnetosphere of the Earth and in the interplanetary space (invited review)", In "*Geomagnetism and High Layers of the Atmosphere*", Moscow, NAUKA, 7-82 (1975).
Dorman L.I. "The nature of the observed cosmic ray spectrum, I. Classification and the features of particle propagation in space", *Proc. 15th Intern. Cosmic Ray Conf.*, Plovdiv, **1**, 405-410 (1977a).
Dorman L.I. "The nature of the observed cosmic ray spectrum, II. Intervals (1) and (2) ($3\cdot10^{11}$-10^{20}eV) ", *Proc. 15th Intern. Cosmic Ray Conf.*, Plovdiv, **1**, 411-415 (1977b).
Dorman L.I. "The nature of the observed cosmic ray spectrum, III. Intervals (3)-(5) (10^4-$3\cdot10^{11}$eV)", *Proc. 15th Intern. Cosmic Ray Conf.*, Plovdiv, **1**, 416-421 (1977c).
Dorman L.I. "The mode of energy gain by particles in the statistical acceleration mechanism including the angular distribution of particles and the relativistic composition of velocities", *Proc. 16th Intern. Cosmic Ray Conf.*, Kyoto, **2**, 50-54 (1979a).
Dorman L.I. "Generation of energy spectrum by statistical mechanism of particle acceleration", *Proc. 16th Intern. Cosmic Ray Conf.*, Kyoto, **2**, 55-60 (1979b).
Dorman L.I. "Cosmic ray interaction with magnetosphere and ionosphere (invited paper)", In the book: *"Problems of Solar- Terrestrial Relations"*, Ashkhabad, 108-131 (1981).
Dorman L.I. "On the formation of energy spectrum and character of particle energy gain in the statistical mechanism of acceleration", *Cosmic Rays* (Moscow, NAUKA), **23**, 5-13 (1983).
Dorman L.I. "Geomagnetic and atmospheric effects in primary and secondary cosmic rays; cosmogeneous nuclei (rapporteur paper)", *Proc. 20th Intern. Cosmic Ray Conf.*, Moscow, **8**, 186-237 (1987a).
Dorman L.I. "Cosmic ray intensity variations (ground observations, methods of investigations, theory). In *Problems of Cosmic Ray Physics*, Moscow, Nauka, 45-82 (1987b).
Dorman L.I. "Cosmic rays: composition, spectrum, anisotropy and origin", In *Results of Science and Technology*, Seria Astronomy, **33**, 3-120 (1988).

Dorman L.I. "On the Cosmic Ray World Service", *Izvestia Academy of Science of USSR*, Seria Phys., **57**, No. 7, 149-152 (1993).

Dorman I.V. and L.I. Dorman "Solar wind properties obtained from the study of the 11-year cosmic ray cycle", *J. Geophys. Res.*, **72**, No. 5, 1513-1520 (1967a).

Dorman I.V. and L.I. Dorman "Propagation of energetic particles through interplanetary space according to the data of 11-year cosmic ray variations", *J. Atmosph. & Terr. Phys.*, **29**, No.4, 429-449 (1967b).

Dorman I.V.and L.I. Dorman "S.N.Vernov and development of investigation of cosmic ray variations in the Soviet Union", *Izvestia Academy of Sciences of USSR*, Series Phys., **47**, No.9, 1678-1683 (1983).

Dorman L.I. and E.L. Feinberg "On the nature of cosmic ray variations", *Proc. 4th Intern.Cosmic Ray Conf.*, Guanajhato, Mexico, 395-432 (1955).

Dorman L.I. and G.I. Freidman "The cosmic ray burst of February 23, 1956 and its interpretation", *Proc.of Yakutsk Filial of Academy of Sciences,* Series of Physics, Academy of Sciences of USSR Press, Moscow, No. 2, 129-169 (1958).

Dorman L.I. and G.I. Freidman "On the possibility of charged particle acceleration by shock waves in the magnetized plasma", *Proc. All-Union Conf. on Magnetohydrodinamics and Plasma Physics*, Latvia SSR Academy of Sciences Press, Riga, 77-81 (1959).

Dorman L.I, Iucci N., Villoresi G. "The use of cosmic rays for continuos monitoring and prediction of some dangerous phenomena for the Earth's civilization", *Astrophysics and Space Science*, **208**, 55-68 (1993a).

Dorman L.I., Iucci N. and Villoresi G. "Possible monitoring of space processes by cosmic rays", *Proc. 23th Intern. Cosmic Ray Conf.*, Calgary, **3**, 695-698 (1993b).

Dorman L.I., Iucci N. and Villoresi G. "Space dangerous phenomena and their possible prediction by cosmic rays", *Proc. 23th Intern. Cosmic Ray Conf.*, Calgary, **3**, 699-702 (1993c).

Dorman L.I. and M.E. Kats "Cosmic ray kinetics in space", *Space Science Review*, **20**, 529-575 (1977).

Dorman L.I. and I.Ya. Libin "Cosmic ray scintillations and dynamic processes in space", *Space Sci. Rev.*, **39**, 91-152 (1984).

Dorman L.I., L.A. Pustil'nik, A. Sternlieb, I.G. Zukerman, A.V. Belov, E.A. Eroshenko, V.G. Yanke, H. Mavromichalaki, C. Sarlanis, G. Souvatzoglou, S. Tatsis, N. Iucci, G. Villoresi, Yu. Fedorov, B.A. Shakhov, and M. Murat "Monitoring and Forecasting of Great Solar Proton Events Using the Neutron Monitor Network in Real Time", *IEEE Plasma Sciences*, in press (2004).

Dorman L.I. and D. Venkatesan "Solar Cosmic Rays", *Space Sci. Review*, **64**, 183-362 (1993).

Duperier A. "The meson intensity at the surface of the Earth and the temperature at the production level", *Proc. Phys. Soc.*, **62A**, No. 11, 684-696 (1949).

Duperier A. "On the positive temperature effect of the upper atmosphere and the process of meson production", *J. Atm. Terr. Physics*, **1**, No. 5-6, 296-310 (1951)

Elster J. and H. Geitel "Weitere Versuche uber die Elektrizitats zerstrehung in abgeschlossenen Luftmengen", *Phys. Ztschr.*, **2**, 560 (1900).

Evenson P. "A Search for Antihelium in Primary Cosmic Radiation", *Astrophys. J.*, **176**, 797-808 (1972).

Feinberg E.L. "On the nature of cosmic ray barometric and temperature effects", *DAN SSSR*, **53**, No. 5, 421-424 (1946).

Fermi E. "On the origin of the cosmic radiation", *Phys. Rev.*, **75**, 1169-1174 (1949).

Forbush S.E. "On cosmic ray effects associated with magnetic storms", *Terr. Magn. Atmosph. Electr.*, **43**, 203-218 (1938).

Forbush S.E. "On the 27-day and 13.5-day waves in cosmic ray intensity and their relation to corresponding waves in terrestrial-magnetic activity", *Assoc. Terr. Magn. Electr. Bull*, **11**, 438 (1940).

Forbush S.E. "Solar influences on cosmic rays", *Proc. Nat. Acad. Sci. USA*, **43**, No. 1, 28-41 (1957).

Forro M. "Temperature effect of cosmic radiation at 100 m-water equivalent depth", *Phys. Rev.*, **72**, 868-869 (1947).

Fuke H., T. Maeno, S. Orito et al. "Search for Cosmic-Ray Antideuteron with the BESS Spectrometer", *Proc. 28th Intern. Cosmic Ray Conf.*, Tsukuba, **4**, 1797-1800 (2003).

Gaisser T.K., M. Honda, P. Lipari, and T. Stanev "Primary spectrum to 1 TeV and beyond", *Proc. 27th Intern. Cosmic Ray Conf.*, Hamburg, **5**, 1643-1647 (2001).

Garcia-Munoz M., G.M. Mason, and J.A. Simpson "Cosmic Ray Age", *Astrophys. J.*, **217**, 859-877 (1977).

Ginzburg V.L. "Cosmic ray origin and radio-astronomy", *UFN*, **51**, No. 3, 343-392 (1953a).

Ginzburg V.L. "Supernova and Nova stars as sources of cosmic and radio radiations", *DAN SSSR*, **92**, No. 6, 1133-1136 (1953b).

Garcia-Munoz M., G.M. Mason, and J.A. Simpson "The age of the galactic cosmic rays derived from the abundance of ^{10}Be", *Astrophys. J.*, **217**, No. 3, 859-877 (1977).

Garcia-Munoz, M., J.A. Simpson, and J.P. Wefel "The propagation lifetime of galactic cosmic rays determined from the measurement of the beryllium isotopes", *Proc. 17th Intern. Cosmic Ray Conf.*, Paris, **2**, 72-75 (1981).

Golden R.L., S. Horan, B.G. Mauger, G.D. Badhwar,J.L. Lacy, S.A. Stephens, R.R. Daniel and J.E. Zipse "Evidence for the existence of cosmic-ray antiprotons", *Phys. Rev. Lett.*, **43**, 1196-1199 (1979).

Golden R.L., B.G. Mauger, S. Nunn and S. Horan "Energy dependence of the $\bar{P}/P$ ratio in cosmic rays", *Astrophys. Lett.*, **24**, No.2, 75-83 (1984).

Golden R.L., S.J. Stochaj, S.A. Stephens et al. "Search for Antihelium in the Cosmic Rays", *Astrophys. J.*, **479**, 992-996 (1997).

Hams T., K. Abe, K. Anraku et al. "Measurement of electron spectrum to high energies with the BESS-1999 experiment", *Proc. 28th Intern. Cosmic Ray Conf.*, Tsukuba, **4**, 1813-1816 (2003).

Hess V.F. "Uber Beobachtungen der durchdringenden Strahlung bei sieben Freiballonfahrten, *Phys. Ztschr.*, **13**, 1084-1091. (1912).

Hess V.F. and A. Demmelmair "World-wide effect in cosmic ray intensity, as observed during a recent geomagnetic storm", *Nature*, **140**, 316-317. (1937).

Hess V.F. and H.T. Graziadei "On the diurnal variation of the cosmic radiation", *Terr. Magn.*, **41**, No. 1, 9-14. (1936).

Hess V. and R. Steinmaurer "Cosmic rays from Nova Herculis?", *Nature*, **135**, 617-618 (1935).

Hoffman G. "Probleme der Ultrastrhlung", *Phys. Ztschr.*, **33**, No. 17, 633-662. (1932).

Johnson T.H. "Preliminary report of angular distribution measurements of cosmic radiation in equatorial latitudes", *Phys. Rev.*, **44**, 856-858 (1933).

Johnson T.H. "Cosmic ray intensity and geomagnetic effects", *Rev. Mod. Phys.*, **10**, 193-244 (1938).

Johnson T.H. and D.V. Read "Unidirectional measurements of the cosmic ray latitude effects", *Phys. Rev.*, **51**, 557- 564 (1937).

Kolhörster W. "Intensitates und Richtungsmessungen der durchdringenden Strahlung", *Berlin. Ber.*, **24**, 366 - 377 (1923).

Kolhörster W. "Hohenstrahlung and Nova Herculis", *Phys. Ztschr.*, **93**, No. 5-6, 429-431. (1935).

Krymsky, G.F. "A regular mechanism for the acceleration of charged particles on the front of a shock wave", *DAN SSSR*, 243, 1306–1308 (1977).

Kyker G.C. and A.R. Liboff "Absolute cosmic ray ionization measurements in a 900-liter chamber", *J. Geophys. Res.*, **A83**, No. 12, 5539-5549 (1978).

Lamanna G., B. Alpat, R. Battiston, B. Bertucci, W.J. Burger, G. Esposito, E. Fiandrini, and P. Zuccon "Measurement of deuteron spectra in Low Earth Orbit with the Alpha Magnetic Spectrometer", *Proc. 27th Intern. Cosmic Ray Conf.,* Hamburg, **5**, 1614-1617 (2001).

Lindholm F. and G. Hoffmann "Registriebeobachtungen der Hessshen Ultra-γ-Strahlung auf Muottas Muralgi (2456 m)", *Gerlach Beitz. Ztschr. Geophys.*, **20**, 12 (1928).

Link J.T., L.M. Barbier, W.R. Binns et al. "Measurements of the Ultra-Heavy Galactic Cosmic-Ray Abundances between Z = 30 and Z = 40 with the TIGER Instrument", *Proc. 28th Intern. Cosmic Ray Conf.*, Tsukuba, **4**, 1781-1784 (2003).

Lukasiak A., F.B. McDonald, and W.R. Webber "Voyager measurements of the isotopic composition of Li, Be and B nuclei", *Proc. 25th Intern. Cosmic Ray Conf.*, Durban, **3**, 389-392, 1997.

Maeda K. and M. Wada "Atmospheric temperature effect upon the cosmic ray intensity at sea level", *J. Sci. Res. Inst.* (Tokyo), **48**, 71-79 (1954).

McDonald F.B. "Integration of neutron monitor data with spacecraft observations; a historical perspective", *Space Sci. Rev.*, **93**, 263-284 (2000).

Menn W., L.M. Barbier, E.R. Christian et al. "Measurement of the absolute proton and helium flux at the top of the atmosphere using IMAX", *Proc. 25th Intern. Cosmic Ray Conf.*, Durban, **3**, 409-412 (1997).

Messerschmidt W. "Über Schwankungsmessungen der Ultrastrahlung, II", *Ztschr. Phys.*, **85**, 332-335 (1933).

Messerschmidt W. "Ionizationsmessungen zum Zusammenhang zwischen Ultrastrahlung und Nova Herculis", *Phys. Ztschr.*, **95**, No1-2, 42-45. (1935).

Mewaldt R.A. "Isotope abundances of solar coronal material derived from solar energetic particle measurements ", *Proc. Cosm. Abund. of Matt.*, AIP No. 183, 124 (1989).

Mewaldt R.A. "The abundances of isotopes in the cosmic radiation ", *AIP Conf. Proc.*, **183,** No. 1, 124-146 (1989).

Meyer J.P. "Solar-stellar outer atmospheres and energetic particles, and galactic cosmic rays", *Astrophys. J. Suppl.*, **57,** No. 1, 173-204 (1985).

Meyer J.P., L.O.C. Drury and D.C. Ellison "Galactic cosmic rays from supernova remnants .1. A cosmic-ray composition controlled by volatility and mass-to-charge ratio", *Astrophys. J.*, **487**, No. 1, 182-196 (1997).

Millikan R.A. "On the question of the constancy of the cosmic radiation and the relation of these rays to meteorology", *Phys. Rev.*, **36**, 1595-1603 (1930).

Millikan R.A. and G.H. Cameron "High frequency rays of cosmic origin", *Phys. Rev.*, **28**, 851-868 (1926).

Millikan R.A. and G.H. Cameron "High altitude tests on the geographical directional and spectral distribution of cosmic rays", *Phys. Rev.*, **31**, 163-173 (1928a).

Millikan R.A. and G.H. Cameron "The origin of the cosmic rays", *Phys. Rev.*, **32**, 533-557 (1928b).

Mitchell J.W., L.M. Barbier, E.R. Christian et.al. "Measurement of 0.25-3.2 GeV Antiprotons in the Cosmic Radiation", *Phys. Rev. Lett.*, **76**, 3057-3060 (1996).

Molnar A. and M. Simon "Test of the Diffusion Halo and the Leaky Box Model by means of secondary radioactive cosmic ray nuclei with different lifetimes" *Proc. 27th Intern. Cosmic Ray Conf.,* Hamburg, **5**, 1860-1863 (2001).

Monk A.T. and A.H. Compton "Recurrence phenomena in cosmic ray intensity", *Rev. Mod. Phys.*, **11**, 173-179 (1939).

Moraal H., A. Belov, and J.M. Clem "Design and co-ordination of multi-station international neutron monitors networks", *Space Sci. Rev.*, **93**, 285-303 (2000).

Moskalenko I. and A.W. Strong "Diffuse Galactic γ-rays: Constraining Cosmic-Ray Origin and Propagation", *Astrophys. and Space Science*, **272**, 247-254 (2000).

Myssowsky L. and L. Tuwim "Unregelmassige Intensitatsschwankungen der Hohenstrahlung geringer in Seehohe", *Ztschr. Phys.*, **39**, No 2-3, 146-150. (1926).

Nozaki M., M. Sasaki , T. Saeki et al. "A search for antihelium down to 10^{-6} relative to helium", *Proc. 26th Intern. Cosmic Ray Conf.,* Salt Lake City, **3**, 85-88 (1999).

Olbert S. "Atmospheric effects on cosmic ray intensity near sea level", *Phys. Rev.*, **92**, 454-461 (1953).

Orito S., T. Maeno, H. Matsunaga et al. "Precision Measurement of Cosmic-Ray Antiproton Spectrum", *Phys. Rev. Lett.*, **84**, 1078-1081 (2000).

Ormes J.F., A.A. Moiseev, T. Saeki et at. "Antihelium in Cosmic Rays: A New Upper Limit and Its Significance", *Astrophys. J.*, **482**, 187-190 (1997).

Richtmyer R.D. and E. Teller "On the origin of cosmic rays", *Phys. Rev.*, **75**, 1729-1731 (1948).

Roka E. "Über einen indikerten Einfluss der Sonnenäktivität auf die intensität der kosmischen Strahlung", *Ztschr. Naturforsch.*, **5A**, 517 (1950).

Saeki T., K. Anraku, S Orito et al. "A new limit on the flux of cosmic antihelium", *Phys. Lett.*, **B422**, 319-324 (1998).

Sasaki M., M. Nozaki, T. Saeki et al. "A search for antihelium with the BESS spectrometer", *Proc. 27th Intern. Cosmic Ray Conf.,* Hamburg, **5**, 1711-1714 (2001).

Schein M., W.P. Jesse, and E.O. Wollan "The nature of the primary cosmic radiation and the origin of the mesotron", *Phys. Rev.*, **59**, 615-618 (1941).

Seo E.S. and V.S. Ptuskin "Stochastic reacceleration of cosmic rays in the interstellar medium", *Astrophys. J.*, **431**, 705-714 (1994)

Seo E.S., F.B. McDonald, N. Lal and W.R. Webber "Study of cosmic-ray H and He isotopes at 23 AU", *Astrophys. J.*, **432**, 656-664 (1994)

Simon M., A. Molnar and S. Roesler "A new calculation of the interstellar secondary cosmic-ray antiprotons", *Astrophys. J.*, **499**, 250-257 (1998).

Simpson J.A. "The cosmic radiation: reviewing the present and future" (The Victor Hess memorial lecture), *Proc. 25th Intern. Cosmic Ray Conf.*, **8**, 4-23 (1997).

Simpson J.A., W.H. Fonger, and S.B. Treiman "Cosmic radiation intensity-time variations and their origin. I. Neutron intensity variation method and meteorological factors", *Phys. Rev.*, **90**, 934-950 (1953).

Smoot G.F., A. Buffington, and C.D. Orth "Search for cosmic-ray antimatter", *Phys. Rev. Lett.*, **35**, 258-261 (1975).

Steinke E. "Wasserversenkmessungen der durchdrinkenden Hessschen Strahlung", *Ztschr. Phys.*, **58**, 183-193 (1929).

Steinmaurer R. and H.T. Graziadei "Ergebnisse der Registrierung der kosmischen Ultrastrahlung auf dem Hafelekar (2300 m) bei Innsbruck, II Teil. Meteorologische und Solare Einflüsse auf die Ultrastrahlung", *Sitzungs ber. Akad. Wiss. Wien*, **22**, No. 21/22, 672-685 (1933).

Stephens S.A. "Deuterium and He-3 in cosmic rays", *Adv. Space Res.*, **9**, No. 12, 145-148 (1989).

Stochaj S.J. "Direct measurements of cosmic rays", In Invited, Rapporteur, and Highlight papers of 27th ICRC, Hamburg, 136-146 (2001).

Stoker P.H. "Relativistic Solar Proton Events", *Space Sci. Rev.* **73**, 327-385 (1994).

Treiman S.B. "Effect of equatorial ring current on cosmic ray intensity", *Phys. Rev.*, **89**, 130-133 (1953).

Ullio P. "Signatures of exotic physics in antiproton cosmic ray measurements", *Astro-Phys./*9904086, 7 pages (1999).

Vannuccini E. on behalf of the CAPRICE98 collaboration "Measurement of the Deuterium Flux in the Kinetic Energy Range 12-22 GeV/n with the CAPRICE98 Experiment", *Proc. 28th Intern. Cosmic Ray Conf.*, Tsukuba, **4**, 1801-1804 (2003)

Vernov S.N. "Cosmic ray latitude effect in the stratosphere", *Izvestia of Academy of Science of USSR*, Ser. Phys., No. 5/6, 738-740 (1938).

Vernov S.N. "Analysis of cosmic ray latitude effect in the stratosphere", *DAN SSSR (Reports of Academy of Science of USSR)*, **23**, No. 2, 141-143 (1939).

Waddington C.J. "Propagation of elements just heavier than Nickel", In *Acceleration and Transport of Energetic Particles Observed in the Heliosphere*, ed R.A. Mewaldt et al., AIP Conf. Proc., **528**, 441-444 (2000).

Waddington C.J. "Discrimination between possible cosmic ray sources", *Proc. 27th Intern. Cosmic Ray Conf.*, Hamburg, **5**, 1784-1787 (2001).

Wang J.Z., E.S. Seo, K. Anraku, et al. "Measurement of cosmic-ray hydrogen and helium and their isotopic composition with the BESS experiment", *Astrophys. J.*, **564**, No.1, 244-259 (2002).

Webber W.R, R.L. Golden, S.J. Stochaj, J.F. Ormes and R.E. Strittmatter "A measurement of the cosmic ray ^{2}H and ^{3}He spectra and ^{2}H/^{4}He and ^{3}He/^{4}He ratios in 1989", *Astrophys. J.*, **380**, No. 1, 230-234 (1991).

Wiedenbeck M.E. and D.E. Greiner "A cosmic-ray age based on the abundance of Be-10 ", *Astrophys. J.*, **239**, L139-L142 (1980).

Wilson C.T.R. "On the leakage of electricity through dust-free air", *Proc. Cambr. Phil. Soc.*, **11**, 32 (1900).

Wilson C.T.R. "On the ionization of atmospheric air", *Proc. Roy. Soc.*, London, **68**, 151-161 (1901).

Yamamoto A., K. Abe, K. Anraku, et al. "BESS and its future prospect for polar long duration flights", *Adv. Space Res.*, **30**, No. 5, 1253-1262 (2002).

Yanasak N., W.R. Binns, A.C. Cummings, E.R. Christian, J.S. George, P.L. Hink, J.Klarmann, R.A. Leske, M. Lijowski, R.A.Mewaldt, E.C. Stone, T.T. von Rosenvinge, and M.E.Wiedenbeck. "Implications for cosmic ray propagation from ACE measurements of radioactive clock isotope abundances", *Proc. 26th Intern. Cosmic Ray Conf.*, Salt-Lake City, **3**, 9-12 (1999).

Yanasak N.E., M.E. Wiedenbeck, R.A. Mewaldt et al. "Measurement of the Secondary Radionuclides ^{10}Be, ^{26}Al, ^{36}Cl, ^{54}Mn, and ^{14}C and Implications for the Galactic Cosmic-Ray Age", *Astrophys. J*, **563**, 768-792 (2001)

Yoshida S. and M. Wada "Storm-time increase of cosmic ray intensity", *Nature*, **183**, No. 4658, 381-383 (1959).

References for Chapter 2

Aglietta M., B. Alpat, E.D. Alyea, et al. "Neutrino-induced and atmospheric single-muon fluxes measured over 5 decades of intensity by LVD at Gran-Sasso-Laboratory", Astropart. Phys., 3 (4), 311-320 (1995).

Agrawal V., T.K. Gaisser, P. Lipari, and T. Stanev "Atmospheric neutrino flux above 1 GeV", *Phys.Rev.*, **D53**, 1314 -1323, (1996).

Akhmedov E.Kh. and O.V. Bychuk "Resonant spin-flavor precession of neutrinos and the solar neutrino problem", *Zh. Éksp. Teor. Fiz.* **95**, 442-457 (1989).

Ambrosio M., R. Antolini, G. Auriemma, et al. "Vertical muon intensity measured with MACRO at the Gran Sasso laboratory ", *Phys. Rev.*, **D52**, 3793-3802 (1995).

Andreev Yu.M., V.I. Gurentsov, and I.M. Kogai "Muon intensity from the Baksan underground scintillation telescope", *Proc. 20th Intern. Cosmic Ray Conf.*, Moscow, **6**, 200-203 (1987).

Appleton I.C., M.T. Hogue, and B.C. Rastin "A study of the muon momentum spectrum and positive-negative ratio at sea-level", *Nucl. Phys.*, **B26**, No. 2, 365-389 (1971).

Bahcall J.N., M.H. Pinsonneault, and S. Basu "Solar Models: Current Epoch and Time Dependences, Neutrinos, and Helioseismological Properties", *Astrophys. J.*, **555**, 990-1012 (2001).

Bahcall J.N. and W.N. Press "Solar-cycle modulation of event rates in the chlorine solar neutrino experiment", *Astrophys. J.*, **370**, 730-742 (1991).

Battistoni G. "A 3-D calculation of the atmospheric neutrino fluxes", *Astropart. Phys.*, **12**, 315-333 (2000).

Battistoni G., A. Ferrari, T. Montaroli, and P. Sala "Improvements in the FLUKA calculations of the atmospheric neutrino fluxes", *Proc. 27th Intern. Cosmic Ray Conf.*, Hamburg, **3**, 1166 (2001).

Baxendale J.M., C.J. Hume, and M.J. Thompson "Precise measurement of sea level muon charge ratio", *J. Phys.*, **G1**, No. 7, 781-788 (1975).

Bazilevskaya G.A., D.Sc. Thesis, Physical Lebedev Institute, Moscow (1985).

Bazilevskaya G.A., D.N. Korolkov, M.B. Krainev, A.K. Svirzhevskaya, and N.S. Svirzhevsky "On the angular distribution of cosmic ray intensity in the Earth's atmosphere", *Proc. 25th Intern. Cosmic Ray Conf.*, Durban, **7**, 321-324 (1997).

Bazilevskaya G.A. and V.S. Makhmutov "The electron precipitation into the atmosphere according to cosmic ray experiment in the stratosphere", *Izvestia Academy of Sciences USSR*, Series Phys., **63**, No. 8, 1670-1674 (1999).

Bazilevskaya G.A., A.M. Mukhamedzhanov, S.I. Nikolsky, Yu.I. Stozhkov, and T.N. Carakhchy'an "Cosmic rays and the neutrino flux in the Davis' experiment", *Sov. J. Nucl. Phys.*, **39**, 543-550 (1984).

Berezinsky V. "Solar neutrino as highlight of Astroparticle Physics", *Proc. 25th Intern. Cosmic Ray Conf.*, Durban, **8**, 59-79 (1997).

Berger Ch., M. Fröhlich, H. Mönch, et al. "Experimental study of muon bundles observed in the Fréjus detector", *Phys. Rev.*, **D40,** No. 7, 2163-2171 (1989).

Bleeker J.A.M., J.J. Burger, A. Scheepmaker, B.N. Swanenburg, and Y. Tanaka "A balloon observation of high energy electrons", *Proc. 9th Intern. Cosmic Ray Conf*, London, **1**, 327-329 (1965).

Bollinger L.M., *Bull. Amer. Phys. Soc.*, **25**, No. 3, 16 (1950).

Bower C.R., A.S. Beach, J.J. Beatty, et al. "The HEAT-pbar Cosmic Ray Antiproton Experiment", *Proc. 26th Intern. Cosmic Ray Conf.*, Salt Lake Sity, **5**, 13-16 (1999).

Briesmeister J.F. "MNCP – A general Monte Carlo N-particle transport code version 4A", *LA-12625-M*, pp. 693, Los Alamos Nat. Lab., Los Alamos, N.M. (1993).

Brun B. et al. "GEANT3 User's guide", *Rep. DD/EE/84-1*, pp 584, Eur. Org. for Nucl. Res., Geneva (1987).

Bucik R., A. Dmitriev, K. Kudela, and S. Ryumin "Gamma-radiation of the Earth's atmosphere from the CORONAS-I data", *Proc. 26th Intern. Cosmic Ray Conf.,* Salt-Lake City, 7, 433-436 (1999).

Bykov A.A., V.Yu. Popov, A.I. Rez, V.B. Semikoz, and D.D. Sokoloff "Aperiodic spin-flavor conversions and electron-antineutrino from the Sun with random magnetic field", *Proc. of EU-Conference New Trends in Neutrino Physics*, Ringberg Castle, Germany, 24-29 May 1998, World Scientific Publishing Company, 201-210 (1998).

Castagnoli G.C. and D. Lal "Solar modulation effects in terrestrial production of carbon 14", *Radiocarbon*, **22**, 133-158 (1980).

Clay J., C.G. Hooft, L.J. Dey, and J.T. Wiersma "An experimental test of the Super Nova hypothesis. Intensity of Cosmic rays in the Earth Crust", *Physica*, **4**, No. 2, 121-137 (1937).

Clay J. and A. Van Gemert "Decrease of the intensity of cosmic rays in the earth down to 1380 m waterequivalent", *Physica,* **6**, No. 6, 497-510 (1939a).

Clay J. and A.G.M. Van Gemert "Absorption of the hard cosmic rays in different materials", *Physica,* **6**, No. 7, 649-655 (1939b).

Cleveland B.T., T. Daily, R.Jr. Davis, J.R. Distel, K. Lande, C.K. Lee, P.S. Wildenhain, J. Ullman "Measurement of the solar electron neutrino flux with the Homestake chlorine detector ", *Astrophys. J.*, **496**, No1, pt.1, 505-526 (1998).

Cousins J.E., W.F. Nash, and A.J. Pointon "The Effect of the Angular Variation of the Intensity on Scattering Distribution of μ-Mesons Underground at a Depth of 40 m w.e.", *Il Nuovo Cimento,* 6, 1113-1121 (1957).

Crouch M. "An improved world survey expression for cosmic ray vertical intensity vs. depth in standard rock", *Proc. 20th Intern. Cosmic Ray Conf.,* Moscow, **6**, 165-168 (1987).

Daniel R.R. and S.A. Stephens "Cosmic ray produced electrons and gamma rays in the atmosphere", *Rev. Geophys. Space Sci.*, **12**, No. 2, 233-258 (1974).

Davis R. Jr. "A half-century with solar neutrinos", *Nobel Lecture in Physics*, 1-21 (2002).

Davis R Jr, A.K. Mann, L. Wolfenstein "Solar neutrinos", *Annu. Rev. Nucl. Part. Sci.*, **39**, 467-506 (1989).

De Nolfo G.A., S.W. Barwick, J.J. Beatty et al. "Secondary and re-entrant albedo electrons in the atmosphere", *Proc. 25th Intern. Cosmic Ray Conf.*, Durbin, **2**, 373-376 (1997).

Desorgher L., E.O. Flückiger, M.R. Moser, and R.Bütikofer "Geant4 Simulation of the Propagation of Cosmic Rays through the Earth's Atmosphere", *Proc. 28th Intern. Cosmic Ray Conf.*, Tsukuba, **7,** 4277-4280 (2003).

Dorman L.I. "Solar-Neutrino Variations: A Manifestation of Nonzero Neutrino Mass and Magnetic Moment, and Mixing", *Physics of Atomic Nuclei*, **63**, No. 6, 984–988 (2000a).

Dorman L.I. "The Asymmetry of Solar-Neutrino Fluxes" *Physics of Atomic Nuclei*, **63**, No. 6, 989–992 (2000b).

Dorman L.I., V.L. Dorman, and A.W. Wolfendale "North-South asymmetry in solar neutrino fluxes and in correlation coefficients", *Proc. 23th Intern. Cosmic Ray Conf.*, Calgary, **4**, 873-876 (1993).

Dorman L.I., V.L. Dorman, and A.W. Wolfendale "The solar cycle variations of solar neutrino flux and heliolatitude anisotropy", *Proc. 24th Intern. Cosmic Ray Conf.*, Rome, **4**, 1239-1242 (1995).

Dorman L.I. and A.W. Wolfendale "The correlation of the solar neutrino rate with solar activity", *J. Phys. G: Nucl. Part. Phys.*, **17**, 769-778 (1991a).

Dorman L.I. and A.W. Wolfendale "Solar neutrino rate and solar activity", *Geophys. Astrophys. Fluid Dynamics,* **62**, 173-182 (1991b).

Dorman L.I. and A.W. Wolfendale "Relationship between the solar neutrino counting rate in the Homestake experiment, solar activity, cosmic ray intensity and the Earth's heliolatitude", *Proc.22th Intern. Cosmic Ray Conf.*, Dublin, **3**, 736-739 (1991c).

Dorman L.I. and A.W. Wolfendale "The solar neutrino problem: connection with elementary particle physics and the physics of the solar interior", *Proc.22th Intern. Cosmic Ray Conf.*, Dublin, **3**, 740-743 (1991d).

DuVernois M.A., A.S. Beach, J.J. Beatty et al. "Splash and reentrant albedo observations of electrons and positrons at a 4.2 GV vertical magnetic cutoff", *Proc. 27th Intern. Cosmic Ray Conf.*, Hamburg, **10**, 4003-4006 (2001a).

DuVernois M.A., J.J. Beatty, C. Bower et al. "Absolute rigidity spectra of protons and helium from 16 to 250 GV", *Proc. 27th Intern. Cosmic Ray Conf.*, Hamburg, **5**, 1618-1621 (2001b).

Ehmert A. "Die Absorptionkurve der harten component der kosmichen ultrasrahlung", *Zs. Phys.*, **106**, No. 11-12, 751-772 (1937).

Engel R., T.K. Gaisser, and T. Stanev "The flux of atmospheric muons", *Proc. 27th Intern. Cosmic Ray Conf.*, Hamburg, **3**, 1029-1032 (2001).

Follet D.H. and I.D. Crawskaw "Cosmic ray measurements under thirty meters of clay", *Proc. Roy. Soc.*, **A155**, 546-558 (1936).

Gaisser T.K. and T. Stanev "Cosmic Rays", *Phys. Rev.*, **D54**, No. 1, 122-127 (1996).

Gavryusev V., J. Provost, E. Gavryuseva, and G. Berthomieu "The Spectrum of Gravity Modes as a Function of the Solar Structure - Model with a Mixed Core", *Sol. Phys.*, **133**, 139-161 (1991).

George E.P. "Observations of cosmic rays underground and their interpretation", in *Progress in Cosmic Ray Physics*, ed. By J.G. Wilson, North Holland Publ. Co., Amsterdam, **1**, 395-454 (1952).

Golenkov A.E., A.K. Svirzhevskaya, N.S. Svirzhevsky, and Yu.I. Stozhkov "Cosmic ray latitude survey in the stratosphere during the 1987 solar minimum", *Proc. 21-st Intern. Cosmic Ray Conf.*, Adelaida, **7**, 14-17 (1990).

Gonzales W.D., B.T. Tsurutani, P.S. McIntosh, and A.L. Clua de Gonzalez "Coronal hole-active region-current sheet (CHARCS) association with intense interplanetary and geomagnetic activity", *Geophys. Res. Lett.*, **23**, No. 19, 2577-2580 (1996).

Hansen P., M. Ambriola, S. Bartalucci, et al. "A new measurement of muon spectra in the atmosphere", *Proc. 27th Intern. Cosmic Ray Conf.*, Hamburg, **3**, 921-924 (2001).

Hebbeker T. and C.Timmermans, Preprint hep-ph/0102042 (2001).

Hirata K.S., T. Kajita, M. Koshiba et al. "Observation of a neutrino burst from the supernova SN1987A", *Phys. Rev. Lett.*, **58**, No. 14, 1490-1493 (1987).

Hirata K.S., T. Kajita, M. Koshiba et al. "Experimental-study of the atmospheric neutrino flux", *Phys. Lett.*, **B 205,** No. 2-3, 416-420 (1988).

Hirata K.S., T. Kajita, K. Kifune et al. "Observation of ^{8}B-solar neutrinos in the Kamiokande-II detector", *Phys. Rev. Lett.*, **63,** No. 1, 16-19 (1989).

Honda M., T. Kajita, K. Kasahara, and S. Midorikawa "Calculation of the flux of atmospheric neutrinos", *Phys. Rev.* **D52**, 4985-5005 (1995).

Hovestadt D. and P. Meyer "The geomagnetic cut-off at Ft. Churchill and the primary cosmic ray electron spectrum from 10 MeV to 12 GeV in 1968", *Acta Phys. Acad. Scient. Hungaricae,* **29**, suppl. 2, 525-531 (1970).

Israel M.H. "Cosmic-Ray Electrons between 12 MeV and 1 GeV in 1967", *J. Geophys. Res.*, **74**, No. 19, 4701-4713 (1969).

Kajita T. "Muons and neutrinos", *Proc. 27th Intern. Cosmic Ray Conf.*, Hamburg, Vol. Invited, Rapporteur, and Highlight Papers, 194-205 (2001).

Kasahara K., E. Mochizuki, S. Torii, et al. "Atmospheric gamma-ray observations with BETS for calibrating atmospheric neutrino flux calculations", *Proc. 27th Intern. Cosmic Ray Conf.*, Hamburg, **3**, 966-969 (2001).

Kolhörster W. "Intensitates und Richtungsmessungen der durchdringenden Strahlung", *Berl. Ber.*, **24**, 366-377 (1923).

Kolhörster W. "The Hardest Cosmic Rays and the Electric Charge of the Earth", *Nature*, **132**, No. 3332, 407-407 (1933).

Koshiba M. "Observational Neutrino Astrophysics", *Phys. Rep.*, **220**, No. 5-6, 229-381 (1992).

Koshiba M. "Birth of Neutrino Astrophysics", *Nobel Lecture in Physics*, 1-15 (2002).

Letaw J.R., G.H. Share, R.L. Kinzer, R. Silberberg, and E.L. Chupp "Satellite observation of atmospheric nuclear gamma radiation", *J. Geophys. Res.*, **94**, 1211-1221 (1989).

Ling J.C. "A semiempirical model for atmospheric gamma rays from 0.3 to 10 MeV at a geomagnetic latitude of 40°", *J. Geophys. Res.*, **80**, 3241-3252 (1975).

Lingenfelter R.E. "Production of carbon 14 by cosmic ray neutrons", *Reviews of Geophysics*, **1**, No. 1, 35-55 (1963)

Mahoney W.A., J.C. Ling, and A.S. Jacobson "HEAO 3 measurements of the atmospheric positron annihilation line", *J. Geophys. Res.*, **86**, 11098-11104 (1981).

Makhmutov V.S., G.A. Bazilevskaya, A.I. Podgorny, Yu.I. Stozhkov, and N.S. Svirzhevsky "The precipitation of electrons into the Earth's atmosphere during 1994", *Proc. 24th Intern. Cosmic Ray Conf.*, Rome, **4**, 1114-1117 (1995).

Makhmutov V.S., G.A. Bazilevskaya, and M.B. Krainev "Characteristics of energetic electron precipitation into the Earth's polar atmosphere and geomagnetic conditions", *Adv. Space. Res.*, 2001a (in press).

Makhmutov V.S., G.A. Bazilevskaya, M. B. Krainev, and M. Storini "Long-term cosmic ray experiment in the atmosphere: energetic electron precipitation events during 20-23 solar activity cycles", *Proc. 27th Intern. Cosmic Ray Conf.*, Hamburg, **10**, 4196-4199 (2001b).

Makhmutov V.S., G.A. Bazilevskaya, M.B. Krainev, Y.I. Stozhkov, A.K. Svirzhevskaya, N.S. Svirzhevsky, S.Y. Malin "Semiannual variation in the number of energetic electron precipitation events recorded in the polar atmosphere", *Proc. 28th Intern. Cosmic Ray Conf*, Tsukuba, **7**, 4233-4236 (2003).

Masarik J. and J. Beer "Simulation of particle fluxes and cosmogenic nuclide production in the Earth's atmosphere", *J. Geophys. Res.*, **104**, No. D10, 12099-12111 (1999).

Massetti S. "Is there a North-South asymmetry in the Homestake neutrino data connected with solar activity?", *Proc. 24th Intern. Cosmic Ray Conf.*, Rome, **4**, 1251-1254 (1995).

Massetti S., M. Storini, and N. Iucci "Summary of correlative analyses between Homestake neutrino data and related to solar activity", *Proc. 24th Intern. Cosmic Ray Conf*, Rome, **4**, 1243- 1247 (1995).

Menon M., P.V. Ramanamurthy, B.V. Sreekantan, and S. Miyake "Cosmic Ray Intensity at Great Depth and Neutrino experiments", *Nuovo Cimento*, **30**, No. 5, 5766-5777 (1963).

Mikheyev S.P. and A.Yu. Smirnov "Resonance enhancement of oscillations in matter and solar neutrino spectroscopy", *Sov. J. Nucl. Phys.* **42**, No. 6, 1441-1448 (1985).

Mikheyev S.P. and A.Yu. Smirnov "Resonant amplification of ν oscillations in matter and solar-neutrino spectroscopy", *Nuovo Cimento*, **9C**, Ser.1, No 1, 17-26 (1986).

Millikan R.A. "High Frequency Rays of Cosmic Origin", *Nature*, **116**, No.2927, 823-826 (1925).

Millikan R.A. and G.H. Cameron "High Frequency Rays of Cosmic Origin III. Measurements in Snow-Fed Lakes at High Altitudes", *Phys. Rev.*, **28**, No. 5, 851-868 (1926).

Millikan R.A. and G.H. Cameron "New Precision in Cosmic Ray Measurements; Yielding Extension of Spectrum and Indications of Bands", *Phys. Rev.*, **31**, No. 6, 921-930 (1928).

Millikan R.A. and G.H. Cameron "A More Accurate and More Extended Cosmic-ray Ionization-Depth Curve, and the Present Evidence for Atom-Building", *Phys. Rev.*, **37**, No. 3, 235 -252 (1931).

Motoki M., T. Sanuki, S. Orito, et al. "Precise measurement of atmospheric muon fluxes at sea level", *Proc. 27th Intern. Cosmic Ray Conf.*, Hamburg, **3**, 927-930 (2001).

Myssowsky L. and L. Tuwim "Versuche uber die Absorption der Hohenstrahlung im Wasser", *Ztschr. Phys.*, **35**, No. 4, 299-305 (1925).

Nandi B.C. and M. Sinha "Charge ratio of muons at sea level in range 5-600 GeV/c", *Nucl. Phys.*, **B40**, No. 1, 289-297 (1972)

Oakley D.S., H.B. Snodgrass, R.K. Ulrich, and T.L. VanDeKop "On the correlation of solar surface magnetic flux with solar neutrino capture rate", *Astrophys. J. Lett.*, **437**, L63-L66 (1994).

Oakley D.S. and H.B. Snodgrass "Correlation Studies of Solar Magnetic with Solar Neutrino Flux", *Bull. Am. Phys. Soc.*, **40**, No. 7, 1511 (1995).

Oakley D.S. and H.B. Snodgrass, *Technical Progress Report No. 65*, University of Colorado Nuclear Physics Laboratory (1996).

Oakley D.S. and H.B. Snodgrass "Interactions between solar neutrinos and solar magnetic fields ", *Astropart. Phys.*, **7**, No. 4, 297-306 (1997).

Ramaty R., B. Kozlovsky, and R.E. Lingenfelter "Nuclear Gamma Rays from Energetic Particle Interactions", *Astrophys. J. Suppl.*, **40**, 487-495 (1979).

Randell C.A. and W.E. Hazen "The ratio of electrons to mesons 1100 feet underground", *Phys. Rev.*, **81**, No. 1, 144-145 (1951).

Rastin B.C. "A study of the muon charge ratio at sea level within the momentum range 4 to 2000 GeV/c", *J. Phys.*, **G10**, No. 11, 1629-1638 (1984).

Raychaudhuri P. "Time variations in Kamiokande solar neutrino data", *Mod. Phys. Lett.*, **A6**, No.22, 2003-2007 (1991).

Reedy R.C. "Nuclide production by primary-ray protons", *J. Geophys. Res.*, **92**, Suppl., E697-E702, 1987.

Reedy R.C. and J. Masarik "Cosmogenic-nuclide depth profiles in the lunar surface", *Lunar Planet. Sci*, **25**, 1119-1120 (1994).

Reeves G.D. "Relativistic electrons and magnetic storms: 1992-1995", *Geoph. Res. Lett.*, **25**, No. 11, 1817-1820 (1998).

Regener E. "Spectrum of cosmic rays", *Nature*, **127**, 233-234 (1931).

Rivin Yu.R. "Temporal variations in the flux of high-energy solar neutrinos based on data from the detector in South Dakota", *Astron. Reports*, **37**, 202-208 (1993).

Rivin Yu.R. and V.N. Obridko "Cyclic variation of the high-energy solar neutrino flux", *Astron. Reports*, **41**, 76-84 (1997).

Rockstroh J. and W.R. Webber "A measurement of the spectrum of cosmic ray electrons between 20 MeV and 3 GeV in 1968 – Further evidence for extensive time variations of this component", *J. Geophys. Res.*, **74**, No. 21, 5041-5053 (1969).

Sanuki T., Y. Yamamoto, M. Motoki, et al. "Atmospheric muons at various altitudes", *Proc. 27th Intern. Cosmic Ray Conf.,* Hamburg, **3**, 950-953 (2001).

Schmoker J.W. and J.A. Earl "Magnetic-Cloud-Chamber Observations of Low Energy Cosmic-Ray Electrons", *Phys. Rev.*, **138**, No. 1B, B300-B302 (1965)

Share G.H., R.J. Murphy, and E. Rieger "Atmospheric gamma-ray lines produced by cosmic rays and solar energetic particles", *Proc 26th Intern. Cosmic Ray Conf,* Salt-Lake City, **7**, 329-332 (1999).

Shea M.A., D.F. Smart, and L.C. Gentile "Estimating cosmic ray vertical cutoff rigidities as a function of the McIlwain L-parameter for different epochs of the geomagnetic field", *Phys. of the Earth and Planet. Interiors*, **48**, 200-205 (1987).

Snodgrass H.B. and D.S. Oakley "Comment on "Absence of Correlation between the Solar Neutrino Flux and the Sunspot Number", *Phys. Rev. Letters*, **83**, No. 9, 1894 (1999)

Sreekantan B.V., S. Naranan, and P.V. Ramanamurthy "On the angular distribution of penetrating cosmic-ray particles at a depth 103 mwe below ground", *Proc. Indian Academy of Sciences*, Ser. A, **43**, No. 2, 113-129 (1956).

Stephens S.A. "Atmospheric electron spectrum over Hyderabad and a study of re-entrant albedo electrons", *Acta Phys. Acad. Scient. Hungaricae*, **29**, suppl. 2, 727-732 (1970)

Stozhkov Y.I., N.S. Svirzhevsky, and V.S. Makhmutov "Cosmic ray measurements in the atmosphere", *Preprint No. 8*, FIAN, Moscow, 1-21, 2001.

Sturrock P.A., G. Walther and M.S. Wheatland "Apparent Latitudinal Modulation of the Solar Neutrino Flux", *Astrophys. J.*, **507**, 978-983 (1998).

Tsuji S., K. Himei, T. Katayama, et al. "Atmospheric muon measurements I: Vertical measurements", *Proc. 27th Intern. Cosmic Ray Conf.,* Hamburg, **3**, 931-934 (2001).

Vannuccini E., Grimani C., Papini P., and Stephens S.A. "The Secondary Proton Spectrum at Small Atmospheric Depths", *Proc. 28th Intern. Cosmic Ray Conf.*, Tsukuba, **7**, 4287-4290 (2003)

Verma S.D. "Measurement of the charged splash and re-entrant albedo of the cosmic radiation", *J. Geophys. Res.*, **72**, No.3, 915-925 (1967).

Verma S.D. and S.P. Bhatnagar "Observation of Energy Spectrum of Electron Albedo in Low Latitude Region at Hyderabad, India", *Proc. 19th Intern. Cosmic Ray Conf.*, La Jolla, **5**, 316-319 (1985).

Walther G. "On the Solar-Cycle Modulation of the Homestake Solar Neutrino Capture Rate and the Shuffle Test ", *Astrophys. J.* **513**, 990-996 (1999).

Willett J.B. and W.A. Mahoney "High spectral resolution measurement of gamma ray lines from the earth's atmosphere", *J. Geophys. Res.*, **97**, 131- 139(1992).

Wilson V.C. "Cosmic-Ray Intensities at Great Depths", *Phys. Rev.*, **53**, No. 5, 337-343 (1938a).

Wilson V.C. "On the Nature of the Penetrating Cosmic Rays", *Phys. Rev.*, **53**, No. 11, 908-909 (1938b).

Wolfenstein L. " Neutrino oscillations in matter", *Phys. Rev.* **D17**, 2369-2374 (1978).

Zanini A., C. Ongaro, E. Durisi, L. Visca, S. DeAgostini, F. Fasolo, M. Pelliccioni, and O. Saavedra "Differential Neutron Flux in Atmosphere at Various Geophysical Conditions", *Proc. 28th Intern. Cosmic Ray Conf.,* Tsukuba, **7**, 4291-4294 (2003)

References for Chapter 3

Ahluwalia H.S. and S.S. Xue "Atmospheric attenuation length for relativistic solar protons", *Geophys. Res. Letters*, **20**, No. 10, 995-998 (1993).

Akopyan M.R., G.A. Bazilevskaya, L.P. Borovkov, et al. "Large solar proton events during the beginning of 22nd cycle", *Izvestia Ac. of Sci. USSR*, Ser. Phys., **55**, No. 10, 1881-1884 (1991).

Alanko K., I.G. Usoskin, K. Mursula, and G.A. Kovaltsov "Effective energy of neutron monitors", *Proc. 28th Intern. Cosmic Ray Conf.*, Tsukuba, **7**, 3901-3904 (2003).

Aleksanyan T.M., V.M. Bednazhevsky, Ya.L. Blokh, L.I. Dorman, and F.A. Starkov "Coupling coefficients of the neutron component for the stars of various multiplicities inferred from the measurements on board

research vessel 'Academician Kurchatov'", *Proc. 16th Intern. Cosmic Ray Conf.*, Kyoto, **4**, 315-320 (1979a).

Aleksanyan T.M., Ya.L. Blokh, L.I. Dorman, and F.A. Starkov "Examination of the differences in the coupling coefficients and barometric coefficients of 3NM-64 neutron supermonitor and lead-free monitor", *Proc 16th Intern. Cosmic Ray Conf.*, Kyoto, **4**, 321-324, 1979b.

Aleksanyan T.M., L.I. Dorman, V.G. Yanke and V.K. Korotkov "Coupling functions for lead and lead-free neutron monitors from the latitudinal measurements performed in 1982 in the survey by research vessel 'Academician Kurchatov'", *Proc. 19th Intern. Cosmic Ray Conf., La Jolla,* **5**, 300-303 (1985).

Baisultanova L.M., A.V. Belov, L.I. Dorman, E.A. Eroshenko, E.G. Klepach, V.A. Oleneva, and V.G. Yanke "North-South cosmic ray asymmetry in 1974, and development of global-spectrographic method", In *Solar Activity and Solar-Terrestrial Relations*, Leningrad, 153-158 (1987).

Belov A.V., L.I. Dorman, and V.G. Yanke "The simplest versions of the global-spectrographical method", *Proc. 18th Intern. Cosmic Ray Conf.*, Bangalore, **10**, 144-147 (1983).

Belov A.V. and E.A. Eroshenko "Proton spectra of the four remarkable GLE in the 22nd solar cycle", *Radiation Measurements*, **26**, No. 3, 461-466 (1996).

Belov A.V. and A.B. Struminsky "Neutron monitor sensitivity to primary protons below 3 GeV derived from data of ground level events", *Proc. 25th Intern. Cosmic Ray Conf.*, Durban, Vol. 1, 201-204 (1997)

Bishara A.A. and L.I. Dorman "Spectrum of 11-year cosmic ray variation in the high energy region and great-scale structure of solar wind", *Geomagnetism and Aeronomy*, **13**, No. 5, 782-787 (1973a).

Bishara A.A. and L.I. Dorman "Estimation of cosmic ray variation spectrum in the high energy region by underground observations", *Izvestia Academy of Sciences USSR*, Series Phys., **37**, No. 6, 1293-1297 (1973b).

Bishara A.A. and L.I. Dorman "High-energy spectra of the 11-year, 27-day and solar-diurnal cosmic ray variations and Forbush-decreases according to the underground observation data", *Proc. 13th Intern. Cosmic Ray Conf.*, Denver, **2**, 1218-1224 (1973c).

Bishara A.A. and L.I. Dorman "Spectrum of cosmic ray Forbush-decreases in the high energy region", *Geomagnetism and Aeronomy*, **14**, No. 2, 357-360 (1974a).

Bishara A.A. and L.I. Dorman "Spectrum of cosmic ray solar-diurnal variation in the high energy region", *Geomagnetism and Aeronomy*, **14**, No. 4, 573-579 (1974b).

Bishara A.A. and L.I. Dorman "Some problems of cosmic ray variation investigation by underground observation data", *Cosmic Rays* (Moscow, NAUKA), **15**, 198-202 (1975).

Blokh Ya.L., L.I. Dorman, and F.A. Starkov "Determination of the effective cut-off rigidities taking account of the particle arrival angles", *Proc 15th Intern. Cosmic Ray Conf.*, Plovdiv, **4**, 250-253 (1977).

Blokh Ya.L., L.I. Dorman, I.Ya. Libin et al. "Difference coupling coefficients for the IZMIRAN scintillation supertelescope", *Proc. 16th Intern. Cosmic Ray Conf.*, Kyoto, **4**, 408-412 (1979).

Burger R.A., M.S. Potgieter, and B. Heber "Rigidity dependence of cosmic ray proton latitudinal gradients measured by the Ulysses spacecraft: Implications for the diffusion tensor ", *J. Geophys. Res-Space.*, **105,** No. A12, 27447-27455(2000).

Chirkov N.P., A.M. Altukhov, G.F. Krymsky, P.A. Krivoshapkin, A.I. Kuzmin., and G.V. Skripin "Cosmic ray distribution and acceptance vectors of detectors, III.", *Geomagnetism and Aeronomia*, 7, No. 4, 620-631 (1967).

Clem J.M. and L.I. Dorman "Neutron monitor response functions", *Space Science Rev.*, **93**, 335-359 (2000).

Debrunner H. and E. Flückiger "Calculation of the multiplicity yield function on the NM-64 neutron monitor", *Proc. 12th Intern. Cosmic Ray Conf.*, Hobart, **3**, 911-916 (1971a).

Debrunner H. and E. Flückiger "Calculation of multiplicity yield function of IGY neutron monitor", *Helv. Phys. Acta*, **44** , No. 2, 241-251 (1971b).

Debrunner H., J.A. Lockwood, and E. Flückiger "Specific yield function S(P) for a neutron monitor at sea level", *Preprint for 8th Europ. Cosmic Ray Symp.*, Rome, 1-13 (1982).

Dorman L.I. "Influence of meteorological factors on the cosmic ray latitude effect and the process of meson generation", *J. of Experim. and Theoret. Phys. (JETP),* Moscow, **26**, No. 5, 504-505 (1954).

Dorman L.I. "Method of differential cosmic ray coupling coefficients", *Geomagnetism and Aeronomy*, **16**, No. 6, 980-985 (1976a).

Dorman L.I. "Differential coupling coefficients and differential meteorological coefficients for cosmic ray underground observations", *Geomagnetism and Aeronomy*, **16**, No. 6, 1107-1110 (1976b).

Dorman L.I. "Method of different coupling coefficients for research of cosmic ray variations of magnetospheric and out-terrestrial origin", In *Symposium of KAPG on Solar-Terrestrial Physics* (Tbilisi, September 1976), Moscow, NAUKA, Part 1, 74-76 (1976c).

Dorman L.I. "The difference coupling coefficients for the study of cosmic ray variations. I. Ground observation", *Proc. 15th Intern. Cosmic Ray Conf.*, Plovdiv, **4**, 417-422 (1977a).

Dorman L.I. "The difference coupling coefficients for the study of cosmic ray variations. II. Underground measurements", *Proc. 15th Intern. Cosmic Ray Conf.*, Plovdiv, **4**, 423-428 (1977b).

Dorman L.I. "Spectrographic method for separately studying the geomagnetic and extraterrestrial variations for the complex spectrum of the extraterrestrial cosmic ray variation. I. The case of four detectors at one point", *Proc. 16th Intern. Cosmic Ray Conf.*, Kyoto, **4**, 388-392 (1979a).

Dorman L.I. "Spectrographic method for separately studying the geomagnetic and extraterrestrial variations for the complex spectrum of the extraterrestrial cosmic ray variation. II. The case of detection at several points", *Proc. 16th Intern. Cosmic Ray Conf.*, Kyoto, **4**, 401-406 (1979b).

Dorman L.I. "Spectrographical method of cosmic ray variations research", In *Dynamic of Current Sheets and Physics of Solar Activity*, Riga, ZINATNE, 179-185 (1982a).

Dorman L.I. "Spectrographical method with taking into account interference of cosmic ray effects of various classes ", *Izvestia Academy of Sciences of USSR*, Series Phys., **46**, No.9, 1720-1722 (1982b).

Dorman L.I. and Kh.M. Khamirzov "Modification of the spectrographic method", *Cosmic Rays* (NAUKA, Moscow), **24**, 32-48 (1987).

Dorman L.I. and V.K. Korotkov "Energy response of neutron monitor multiplicity", *Geomagnetism and Aeronomy*, **21**, No. 5, 788-791 (1981).

Dorman L.I. and V.K. Korotkov "Relevance of the parameters of multiplicity distribution in neutron monitor to cosmic ray energy spectrum at observation level", *Proc. 18th Intern. Cosmic Ray Conf.*, Bangalore, **9**, 437-440 (1983).

Dorman L.I., M.Yu. Medvedev and V.S. Smirnov "Cosmic ray particle trajectories in the Earths magnetic field presented with high degree of accuracy", *Geomagnetism and Aeronomy*, **6**, No. 1, 19-26 (1966).

Dorman L.I. and N.I. Pakhomov "The dependence of the integral generation multiplicity of neutron component at various depths in the atmosphere on zenith angle on primary particle incidence", *Proc. 16th Intern. Cosmic Ray Conf.*, Kyoto, **4**, 416-420 (1979).

Dorman L.I. and N.I. Pakhomov "Geomagnetic field effect on cosmic rays in the Earth's atmosphere", *Proc. 18th Intern. Cosmic Ray Conf.*, Bangalore, **3**, 516-519 (1983a).

Dorman L.I. and N.I. Pakhomov "Geomagnetic field influence on cosmic rays in the Earth's atmosphere", *Geomagnetism and Aeronomy*, **23**., No. 5, 710-714 (1983b).

Dorman L.I. and L.E. Rishe "Calculations of the integral generation multiplicity, coupling coefficients and partial barometric coefficients for the cosmic ray neutron component observations at various altitudes using the method of discontinues Markov processes including non-ordinary of nuclear-meson cascade", *Proc. 13th Intern. Cosmic Ray Conf.*, Denver, **2**, 835-842 (1973).

Dorman L.I. and L.E. Rishe "Calculations of cosmic ray neutron component integral multiplicity, coupling coefficients and partial barometric coefficients by the method of nonorderly Markov processes", *Geomagnetism and Aeronomy*, **14**, No. 3, 417-423 (1974).

Dorman L.I. and G.Sh. Shkhalakhov "Spectrographical method of cosmic ray variation investigation with taking into account penumbra", *Geomagnetism and Aeronomy*, **15**, No. 3, 405-411 (1975a).

Dorman L.I. and G.Sh. Shkhalakhov "Spectrographical method of cosmic ray variation investigation with taking into account underground observations", *Geomagnetism and Aeronomy*, **15**, No. 4, 605-610 (1975b).

Dorman L.I. and G.Sh. Shkhalakhov "The spectrograph method for studying the cosmic ray variations taking account of the penumbra structure", *Proc. 15th Intern. Cosmic Ray Conf.*, Plovdiv, **4**, 255-260 (1977a).

Dorman L.I. and G.Sh. Shkhalakhov "Extension of the spectrum of the extraterrestrial cosmic ray variation to the high-energy range using the spectrographical method on the basis of underground measurements of cosmic rays", *Proc. 15th Intern. Cosmic Ray Conf.*, Plovdiv, **4**, 261-266 (1977b).

Dorman L.I. and V.S. Smirnov "On the calculations of cosmic ray asymptotic directions for soviet cosmic ray stations", *Izvestia Academy of Sciences of USSR*, Series Phys., **30**, No. 11, 1837-1838 (1966).

Dorman L.I. and V.S. Smirnov "Cosmic ray asymptotical directions for soviet station network", *Cosmic Rays* (NAUKA, Moscow), Vol. 8, 128-151 (1967).

Dorman L.I., G. Villoresi, N. Iucci, M. Parisi, N.G. Ptitsyna "Cosmic ray survey to Antarctica and coupling functions for neutron component in solar minimum (1996-1997), 3. Geomagnetic effects and coupling functions", *Proc. 26th Intern. Cosmic Ray Conf.*, Salt Lake City, **7**, 382-385 (1999).

Dorman L.I., G. Villoresi, N. Iucci, M. Parisi, M.I. Tyasto, O.A. Danilova, and N.G. Ptitsyna "Cosmic ray survey to Antarctica and coupling functions for neutron component near solar minimum (1996-1997), 3, Geomagnetic effects and coupling functions", *J. Geophys. Res.* **105**, No. A9, 21,047-21,058 (2000).

Dorman L.I. and V.G. Yanke "The coupling functions of NM-64 neutron supermonitor", *Proc. 17th Intern. Cosmic Ray Conf.*, Paris, **4**, 326-329 (1981).

Dorman L.I., V.G. Yanke and V.K. Korotkov "Energy sensitivity of supermonitors to the multiple neutrons and the coupling functions", *Proc. 17th Intern. Cosmic Ray Conf.*, Paris, **4**, 330-333 (1981).

Dorman L.I., A.V. Zaikin, and V.G. Yanke "Precision of the spectrographical method", *Proc. 18th Intern.*

Cosmic Ray Conf., Bangalore, **10**, 140-143 (1983).
Dostrovsky L., P. Rabinowitz, and R. Bivins "Monte Carlo calculations of high-energy nuclear interactions. I. Systematics of nuclear evaporation", *Phys. Rev.*, **111**, No. 6, 1659-1676 (1958).
Efimov Yu.E., L.G. Kocharov, G.A. Kovaltsov, and I.G. Usoskin "Detection of solar neutrons by the neutron monitor network", *Proc. 23th Intern. Cosmic Ray Conf.*, Calgary, **3**, 159-162 (1993).
Gaisser T.K. "Calculations of muon response functions", *Proc. of Intern. Cosmic Ray Sympos. "High Energy Cosmic Ray Modulation"*, Tokyo, 33-38 (1976).
George E.P. "Observations of cosmic rays underground and their interpretation", in *Progress in Cosmic Ray Physics*, ed. By J.G. Wilson, North Holland Publ. Co., Amsterdam, **1**, 395-454 (1952).
Gleeson L.J. and W.I. Axford "Solar modulation of galactic cosmic rays", *Astrophys. J.*, **154,** Part 1, No. 3, 1011-1026 (1968).
Grigorov N.L. and V.S. Murzin "Interaction of primary cosmic rays of different energy with matter", *Izvestia Ac. of Sci. of USSR,* Ser. Phys., **19**, No. 1, 21-38 (1953).
Grigorov N.L., V.S. Murzin, and I.D. Rapoport "Study of the 10^{11}-10^{12} eV particle interactions with iron nuclei", *JETP*, **36**, No. 4, 1069-1079 (1959).
Hess W.N., R.E. Confield, and R.E. Lingenfelter "Cosmic ray neutron demography", *J. Geophys. Res.*, **66**, 665-667 (1961).
Iucci N., Villoresi G., Dorman L.I., Parisi M. "Cosmic ray survey to Antarctica and coupling functions for neutron component near solar minimum (1996-1997), 2, Determination of meteorological effects ", *J. Geophys. Res.*, **105**, No. A9 , 21,035-21,046 (2000).
Johnson T.H. and D.V. Read "Unidirectional measurements of the cosmic ray latitude effects", *Phys. Rev.*, **51**, 557- 564 (1937).
Krymsky G.F., A.I. Kuzmin. N.P. Chirkov, P.A. Krivoshapkin, G.V. Skripin, and A.M. Altukhov "Cosmic ray distribution and acceptance vectors of detectors, I.", *Geomagnetism and Aeronomia*, **6**, No. 6, 991-996 (1966a).
Krymsky G.F., A.I. Kuzmin. G.V. Skripin, P.A. Krivoshapkin, and A.M. Altukhov "Calculations of coupling coefficients for the compleks of azimuthal cosmic ray detectors", in *Research in Geomagnetism and Aeronomy*, NAUKA, Moscow, 124-138 (1966b).
Krymsky G.F., A.I. Kuzmin. N.P. Chirkov, P.A. Krivoshapkin, G.V. Skripin, and A.M. Altukhov "Cosmic ray distribution and acceptance vectors of detectors, II. Methods of investigation of cosmic ray distribution", *Geomagnetism and Aeronomia*, **7**, No. 1, 11-15 (1967a).
Krymsky G.F., A.M. Altukhov, P.A. Krivoshapkin, A.I. Kuzmin, G.V. Skripin, and N.P. Chirkov "Cosmic ray distribution and acceptance vectors of detectors, IV", *Geomagnetism and Aeronomia*, **7**, No. 5, 794-798 (1967b).
Krymsky G.F., A.M. Altukhov, P.A. Krivoshapkin, A.I. Kuzmin, and N.P. Chirkov "Using of matrixes for cosmic ray distribution investigation", *Izvestia Acad. of Sci. of USSR*, Seria Phys., **31**, No. 8, 1381-1383 (1967c).
Lingenfelter R.E. "Production of carbon 14 by cosmic ray neutrons", *Reviews of Geophysics*, **1**, No. 1, 35-55 (1963a).
Lingenfelter R.E. "The cosmic-ray neutron leakage flux", *J. Geophys. Res.*, **68**, No. 20, 5633-5639 (1963b).
Luzov A.A., Yu.G. Matyukhin, and V.E. Sdobnov "Calculations of energy sensitivity of NM-64 neutron monitor", *Studies in Geomagnetism, Aeronomy, and Solar Physics*, Nauka, Moscow, No. 20, 356-362 (1971).
McCracken K.G., V.R. Rao, and M.A. Shea "The trajectories of cosmic rays in a high degree simulation of the geomagnetic field", in *Technical report*, No. 77, Massachusetts Institute of Technology, USA (1962).
McCracken K.G., V.R. Rao, B.C. Fowler, M.A. Shea, and D.F. Smart "Cosmic ray tables (asymptotic directions, variational coefficients and cut-off rigidities", in *IQSY Instruction Manuel*, No. 10, London (1965).
Metropolis N., R. Bivins, M. Storm, A. Turkevich, and G. Friedlander "Monte Carlo Calculations on Intranuclear cascades, I. Low-Energy Studies" *Phys. Rev.*, **110**, No. 1, 185-203 (1958a).
Metropolis N., R. Bivins, M. Strom, J.M. Miller, G. Friedlander, and A. Turkevich "Monte Carlo calculations on intranuclear cascades. II. High-energy studies and pion processes", *Phys. Rev.*, **110**, No.1, 204-219 (1958b).
Moraal H., M.S. Potgieter, P.H. Stoker, and A.J. Van der Walt "Neutron monitor latitude survey of cosmic ray intensity during the 1986/1987 solar minimum", *J. Geophys. Res.,* **94**, No. A2, 1459-1464 (1989).
Nagashima K. "Three-dimensional cosmic ray anisotropy in interplanetary space", *Rep. Ionosphere Space Res. Japan*, **25**, 189-211 (1971).
Nagashima K., S. Sakakibara, K. Murakami, et al. "Response and yield functions of neutron monitor, galactic cosmic-ray spectrum and its solar modulation, derived from all the available world-wide surveys", *Nuovo Cimento*, **12**, No. 2, 173-209 (1989).

Newkirk L.L. "Calculation of low-energy neutron flux in the atmosphere by the S_n method ", *J.Geophys.Res.*, **68**, 1825-1839 (1963).

Nobles R.A., R.A Alber, E.B Hughes, L.L. Newkirk, and M Walt "Neutron multiplicity monitor observations during1965", *J. Geophys. Res*, **72**, No. 15, 3817-3828 (1967).

Pakhomov N.I. and V.E. Sdobnov "Calculations of the neutron supermonitor parameters", in *Studies on Geomagn., Aeron., and Solar Phys.*, Nauka, Moscow, **42**, 185-189 (1977).

Pearce R.M. and A.G. Fowler "Calculated spectral sensitivity of IGY and IQSY neutron monitors", *J. Geophys. Res.*, **69**, No. 21, 4451-4455 (1964).

Pyle K.R. "Neutron monitor sensitivity to solar modulation changes: altitude vs. cutoff rigidity", *Proc. 25th Intern. Cosmic Ray Conf.*, Durban, **2**, 197-200 (1997).

Rao U.R. and V. Sarabhai "Yime variations of directional cosmic ray intensity of low latitudes. 1. Comparison daily variation of the intensity of cosmic rays incident from east and west", *Proc. Phys. Soc.*, **263A**, No. 1312, 101-117 (1961).

Skripin G.V. "The complex of azimuthal telescopes and investigation of space-energetic characteristics of cosmic ray anisotropy", *Ph.D. Thesis*, Yakutsk (1965).

Usoskin I.G., K. Alanko, K. Mursula and G.A. Kovaltsov "Heliospheric modulation strength during the neutron monitor era", *Solar Phys.*, **207**, 389-399 (2002).

Vernov S.N., N.L. Grigorov, G.T. Zatsepin, and A.E. Chudakov "The research of nucleons interactions with light nucleus at energies 10^9-10^{12} eV", *Izvestia Ac. of Sci. of USSR*, Ser. Phys., **19**, No. 5, 493-501 (1955).

Villoresi G., L.I. Dorman, N. Iucci, and N.G. Ptitsyna "Cosmic ray survey to Antarctica and coupling functions for neutron component near solar minimum (1996-1997), 1, Methodology and data quality assurance", *J. Geophys. Res.*, **105**, No. A9, 21,025-21,034 (2000).

Viskov V.V., L.I. Dorman, and V.G. Yanke "Calculations of integral multiplicities and coupling coefficients", *Izvestia Academy of Sciences USSR*, Series Phys., **38**, No. 9, 1978-1981 (1974).

Vzorov I.K., *Report No R12442*, Joint Inst. Nucl. Res., Dubna (1969).

Webber W.R. and J.J. Quenby "On the deviation of cosmic ray yield functions", *Philos. Mag.*, **4**, No. 41, 654-664 (1959).

Yanchukovsky A.L., A.A. Luzov, and A.A. Sergeev "Spectrografic complex to study variation of the cosmic ray intensity", *Studies in Geomagnetism, Aeronomy, and Solar Physics*, Nauka, Moscow, No. 20, 389-395 (1971).

References for Chapter 4

Abrosimov A.T. "Producing of great plastic scintillators on the basis of polystirol", *Cosmic Rays* (NAUKA, Moscow), No 5, 171-177 (1963).

Abrosimov A.T., Ya.L. Blokh, and A.A. Pomanskij "Liquid scintillation detectors of great dimensions", *Cosmic Rays* (NAUKA, Moscow), No 7, 260-279 (1965).

Achenbach C.P. and J.H. Cobb "A new airborne detector for atmospheric muons", *Proc. 27th Intern. Cosmic Ray Conf.*, Hamburg, **3**, 1313-1316 (2001).

Aita Y., T. Aoki, Y. Arai et al. "The ASHRA Detector", *Proc. 28th Intern. Cosmic Ray Conf.*, Tsukuba, **2**, 1061-1064 (2003).

Alania M.V., T.S. Bakradze, D.P. Bochikashvili et al. "The Tbilisi experimental cosmic ray array and the on-line system for automation of the collection and processing of observation data", *Proc. 15th Intern. Cosmic Ray Conf.*, Plovdiv, **9**, 228-231 (1977).

Alent'ev A.N., Ya.L. Blokh, L.I. Dorman, and A.A. Chaikin "Calculation and experimental determination of parameters of a big scintillation counters ", In *Cosmic Ray Variations and Space Research*, Moscow, NAUKA, 274-280 (1986).

Alent'ev A.N., A.A. Chaikin, Ya.L. Blokh, and L.I. Dorman "Theoretical and experimental study of a large temporal scintillation counter of ionizing radiation", *Proc. 18th Intern. Cosmic Ray Conf.*, Bangalore, **9**, 433-436 (1983).

Ambriola M.L., G. Barbiellini, S. Bartalucci, et al. "CAPRICE98: a balloon borne magnetic spectrometer to study cosmic ray at different atmospheric depths" *Proc. 26th Intern. Cosmic Ray Conf.*, Salt Lake Sity, **5**, 17-20 (1999).

Ambriola M., R. Bellotti, F. Cafagna et al. "PAMELA space mission: The transition radiation detector", *Proc. 28th Intern. Cosmic Ray Conf.*, Tsukuba, **4**, 2121-2124 (2003).

Amenomori M., S. Ayabe, S.W. Cui, et al. "Performance of the Tibet-III Air-Shower Array", *Proc. 27th Intern. Cosmic Ray Conf.*, Hamburg, **2**, 573-576 (2001).

Aoki T., Y. Arai, K. Arisaka, et al."The Telescope Array Project", *Proc. 27th Intern. Cosmic Ray Conf.*, Hamburg, **2**, 915-918 (2001).

Asatrian G.A., V.Kh. Babayan, A.R. Arseniev, and Yu.I. Stozhkov "The radiosonde for the neutron component of cosmic rays measurements in the atmosphere", *Proc. 24th Intern. Cosmic Ray Conf.*, Rome, **4**, 1304-1307 (1995).

Ashton F., R.B. Coats, and D.A. Simpson "Liquid scintillation counters", *Proc. 9th Intern. Cosmic Ray Conf.*, London, **2**, 1079-1081 (1965).

Bachelet F., P. Balata, E. Dyring, and N. Iucci "On the multiplicity effect in a standard cosmic-ray neutron monitor", *Nuovo Cimento*, Ser. X, **31**, 1126-1130 (1964).

Bachelet F., N. Iucci, and G. Villoresi "The Cosmic Ray Spectral Modulation above 2 GV during the Descending Phase of Solar Cycle Number 19. I: A Comprehensive Treatment of the Neutron Monitor Data from the Worldwide Station Network and Latitude Surveys", *Nuovo Cimento B*, **7**, 17-33 (1972).

Badhwar G.D. "The radiation environment in low-Earth orbit", *Radiation Research*, **148**, No.5, S3-S10 (1997).

Bakatanov V.N., Ya.L. Blokh, L.I. Dorman et al. "Scintillation supertelescope", *Cosmic Rays* (Moscow, NAUKA), **15**, 137-140 (1975).

Baradzei L.T., Yu.I. Logachev, and P.P. Shishkov "Investigations of cosmic ray variations on altitudes 9-12 km", *Cosmic Rays* (NAUKA, Moscow), No 3. 137-142 (1961).

Bartely W.C, K.G. McCracken, and U.R. Rao "Pioneer VI detector to measure degree of anisotropy of cosmic radiation in energy range 7.5-90 MeV/nucleon", *Rev. Scient. Instrum.* **38**, No 2, 266-272 (1967).

Barton C. and A. Crispin "The development of scintillation counters based on medicinal paraffin", *Proc. Intern. Cosmic Ray Conf.*, London, **2**, 1097-1098 (1965).

Bashindzhagyan G., J. Adams, P. Bashindzhagyan, et al. "Polar balloon experiment for astrophysics research (Polar BEAR)", *Proc. 27th Intern. Cosmic Ray Conf.*, Hamburg, **6**, 2147-2150 (2001).

Bauleo P., C. Bonifazi, A. Filevich, and A. Reguera "TANGO Array I: An air shower experiment in Buenos Aires", *Proc. 27th Intern. Cosmic Ray Conf.*, Hamburg, **2**, 577-580 (2001).

Bazilevskaya G.A. and A. K. Svirzhevskaya "On the stratospheric measurements of cosmic rays", *Space Sci. Rev.*, **85**, 431-521 (1998).

Beatty J.J., S. Beach, S. Coutu, et al. "Cosmic Ray Energetics And Mass (CREAM): A Detector for Cosmic Ray near the Knee", *Proc. 26th Intern. Cosmic Ray Conf.*, Salt Lake City, **5**, 61-64 (1999).

Belomestnikh V.A. and Yu.G. Shafer "Cosmic ray intensity variations in the stratosphere and methods of their registrations and investigations", *Proc. of YaFAN* (Ac. of Sci. USSR Press, Moscow), Ser. Phys., No. 2, 47-56 (1958).

Belov A. and E. Eroshenko "Cosmic Ray Observations for Space Weather", *The Proceedings for the 22-nd ISTC Japan Workshop on Space Weather Forecast*, Japan, 2002, Vol. 1, 74-94 (2002).

Belov A.V., E.A. Eroshenko, V.G. Yanke, K.F. Yudakhin, and G. Villoresi "Isotropic and anisotropic cosmic ray variations in March-June 1991", *Adv. Space Res.*, **16**, 249-254 (1995).

Belov A.V. and K.F. Yudakhin "The cosmic ray data database", *Proc. 24th Intern. Cosmic Ray Conf.*, Rome, **4**, 1324-1325 (1995).

Bercovitch M. "A simple semi-cubical plastic-scintillator meson mega-telescope", Deep River Laboratory, Canada, Preprint (1962).

Bertou X. (for the Pierre Auger Collaboration) "Calibration and Monitoring of the Pierre Auger Surface Detectors", *Proc. 28th Intern. Cosmic Ray Conf.*, Tsukuba, **2**, 813-816 (2003)

Bieber J.W. and P. Evenson "Spaceship Earth – an Optimized Network of Neutron Monitors", *Proc. 24th Intern. Cosmic Ray Conf.*, Rome, **4**, 1078-1081 (1995).

Bieber J.W., P.E. Evenson, J.E. Humble, and M.L. Duldig "Cosmic Ray Spectra Deduced from Neutron Monitor Surveys", *Proc. 25th Intern. Cosmic Ray Conf.*, Durban, **2**, 45-48 (1997).

Binns W.R., J.H. Adams, L.M. Barbier et al." The Heavy Nuclei eXplorer (HNX) Mission", *Proc. 27th Intern. Cosmic Ray Conf.*, Hamburg, **6**, 2181-2184 (2001).

Blau B., S.M. Harrison, H. Hofer et al. "The Superconducting Magnet System of the Alpha Magnetic Spectrometer AMS-02", *Proc. 28th Intern. Cosmic Ray Conf.*, Tsukuba, **4**, 2153-2156 (2003).

Blokh Ya.L., L.I. Dorman, N.S. Kaminer, and I.N. Kapustin "Cosmic ray neutron spectrograph on the basis of registration channels with different dead times using", *Geomagnetism and Aeronomy*, **11**, No. 5, 891-892 (1971).

Blokh Ya.L., L.I. Dorman, V.K. Koiava et al. "Great neutron counters for super-monitors", *Cosmic Rays* (Moscow, NAUKA), **13**, 181-182 (1972).

Blokh Ya.L., L.I. Dorman, and I.Ya. Libin "Zenith angle directive diagrams for scintillation telescopes of various geometry", *Cosmic Rays* (Moscow, NAUKA), **14**, 141-156 (1974).

Blokh Ya.L., L.I. Dorman, and I.Ya. Libin "Choosing of optimally dimensions of scintillation supertelescope", *Cosmic Rays* (Moscow, NAUKA), **15**, 123-125 (1975a).

Blokh Ya.L., L.I. Dorman, and I.Ya. Libin "Azimuth and zenith angle direction diagrams for scintillation telescopes of arbitrary geometry", *Cosmic Rays* (Moscow, NAUKA), **15**, 141-149 (1975b).

Blokh Ya.L., L.I. Dorman, and I.Ya. Libin, and E.T. Franzus "Some problems of determination apparatus origin "variations" for muon telescopes", *Cosmic Rays* (Moscow, NAUKA), **14**, 93-112 (1974).

Blokh Ya.L., L.I. Dorman, and I.Ya. Libin et al. "Investigation of cosmic ray intensity variations by underground telescope on great plastic scintillators", *Cosmic Rays* (Moscow, NAUKA), **17**, 76-79 (1976).

Blokh Ya.L., L.I. Dorman, and I.Ya. Libin et al. "Taking into account accident coincidences for scintillation supertelescope", *Cosmic Rays* (Moscow, NAUKA), **17**, 45-50 (1976).

Blokh Ya.L., L.I. Dorman, and F.A. Starkov "Some problems of neutron supermonitor methodical research", *Cosmic Rays* (Moscow, NAUKA), **21**, 85-93 (1980).

Blokh Ya.L., I.Ya. Libin, L.I. Dorman et al. "The device for controlling the amplifiers-discriminators", *Proc. 15th Intern. Cosmic Ray Conf.*, Plovdiv, **9**, 118-120 (1977).

Bollinger L.M., G.E. Thomas, and R.J. Ginther "Neutron detection with glass scintillators", *Nucl. Lnstrum. and Methods* **17**, No 1, 97-116 (1962).

Borog V.V., A.Yu. Burinsky, A.V. Gvozdev et al. "Large aperture muon hodoscope for studies in solar-terrestrial physics", *Proc. 24th Intern. Cosmic Ray Conf.*, Rome, **4**, 1291-1294 (1995).

Borog V.V., A.Yu. Burinsky, V.V. Dronov, and A.V. Gvozdev "Angular and temporary cosmic ray muon flux characteristics measured with large aperture scintillator hodoscope", *Proc. 25th Intern. Cosmic Ray Conf.*, Durban, **2**, 449-452 (1997).

Bortnik S.G. and L.V. Granitskij "Expeditionar monitor for registration of cosmic ray neutron component", *Results of Observations and Investigations in the Period of IQSY*, NAUKA, Moscow, No. 4, 13-16 (1967a).

Bortnik S.G. and L.V. Granitskij "A simple formatter-amplifier for mechanical counter MES-54", *Results of Observations and Investigations in the Period of IQSY*, NAUKA, Moscow, No. 4, 26-28 (1967b).

Bortnik S.G., L.V. Granitskij, and V.N. Medvedev "Decoded instrument for data transforming in the form available for calculator mashine", *Results of Observations and Investigations in the Period of IQSY*, NAUKA, Moscow, No 5 (1968)

Bortnik S.G., L.V. Granitskij, A.F. Neermolov, and V.E. Nosov "Diskriminator of neutron monitor on tunnel diods", *Results of Observations and Investigations in the Period of IQSY*, NAUKA, Moscow, No 3 (1967).

Budnev N., D. Chernov, V. Galkin, et al. "Tunka EAS Cherenkov Array – status 2001", *Proc. 27th Intern. Cosmic Ray Conf.*, Hamburg, **2**, 581-584 (2001).

Buénerd M. "The AMS-02 RICH Imager Prototype In-Beam Tests with 20 GeV/c per Nucleon Ions", *Proc. 28th Intern. Cosmic Ray Conf.*, Tsukuba, **4**, 2157-2160 (2003).

Burger J. and S. Gentile "The AMS-02 TRD for the International Space Station", *Proc. 28th Intern. Cosmic Ray Conf.*, Tsukuba, **4**, 2161-2164 (2003).

Bütikofer R., E.O. Flückiger, L. Desorgher, M.R. Moser, Y. Muraki, Y. Matsubara, T. Sako, H. Tsuchiya, and T. Sakai "SONTEL-Measurements at Gornergrat and Environmental Radioactivity", *Proc. 28th Intern. Cosmic Ray Conf.*, Tsukuba, **7**, 4189-4192 (2003).

Capell M. and E. Cortina "AMS-02 Electronics", *Proc. 28th Intern. Cosmic Ray Conf.*, Tsukuba, **4**, 2173-2176 (2003).

Carrel O. and M. Martin "Observation of time correlations in cosmic-rays", *Phys. Lett.*, **B325**, No. 3-4, 526-530 (1994).

Casadei D. "The AMS-02 Time of Flight System. Final Design", *Proc. 28th Intern. Cosmic Ray Conf.*, Tsukuba, **4**, 2169-2172 (2003).

Casaus J. "Cosmic-ray Astrophysics with AMS–02", *Proc. 28th Intern. Cosmic Ray Conf.*, Tsukuba, **4**, 2149-2152 (2003).

Casolino M., V. Bidoli, A. Canestro et al. "Launch in orbit of NINA detector for cosmic ray nuclei study", *Proc. 26th Intern. Cosmic Ray Conf.*, Salt Lake Sity, **5**, 108-111 (1999).

Casolino M.and V. Mikhailov "Solar Particle Events Observation Capabilities of PAMELA Experiment", *Proc. 28th Intern. Cosmic Ray Conf.*, Tsukuba, **6**, 3477-3480 (2003).

Catalano O., A. Petrolini, A. Santangelo, and L. Scarsi "The EUSO Instrument onboard the International Space Station", *Proc. 28th Intern. Cosmic Ray Conf.*, Tsukuba, **2**, 1081-1084 (2003).

Charakhchyan A.N. "Radiozond for measurements of cosmic radiation intensity in the stratosphere", *Cosmic Rays* (Nauka, Moscow), No. 3, 134-136 (1961).

Chasson R.L., M. Iona, V.Y. Kisselbach, and P. Baker "Results from the new Denver multidirectional meson telescope", *Proc. 9th Intern. Cosmic Ray Conf.*, London, **1**, 282-284 (1965).

Chilingarian A., K. Avakyan, E. Mnatzakanyan, Y. Muraki, Y. Matsubara, T. Sako, and K. Watanabe "A New Solar Neutron Telescope at Mt. Aragats", *Proc. 28th Intern. Cosmic Ray Conf.*, Tsukuba, **6**, 3445-3448 (2003).

Christl M.J., C.M. Benson, F.A. Berry, et al. "The Scintillating Optical Fiber Calorimeter Instrument Performance (SOFCAL)", *Proc. 26th Intern. Cosmic Ray Conf.*, Salt Lake Sity, **5**, 5-8 (1999).

Chubenko A.P., A.L. Shepetov, V.P. Antonova, S.V. Kryukov, R.A. Mukhamedshin, V.V. Oskomov, V.V. Piscal, T.Kh. Sadykov, N.N. Sobolevsky, L.I. Vildanova, and A.P. Zhukov "Multiplicity spectrum of NM64 neutron supermonitor and hadron energy spectrum at mountain level", *Proc. 28th Intern. Cosmic Ray Conf.*, Tsukuba, **2**, 789-792 (2003).

Chudakov A.E., N.M. Nesterova, V.I. Zatsepin, and E.I. Tukish "Cherenkov radiation of cosmic ray EAS", *Proc. 6th Intern. Cosmic Ray Conf.*, Moscow, **2**, 46-55 (1959).

Clark G.W., F. Scherb, W.B. Smith "Preparation of large plastic scintillators", *Rev. Scient. Instrum.* **28**, 433 (1957).

Clem J.M. "Atmospheric Yield Functions and the Response to Secondary Particles of Neutron Monitors", *Proc. 26th Intern. Cosmic Ray Conf.*, Salt Lake Sity, 7, 317-320 (1999).

Clem J.M. and L.I. Dorman "Neutron monitor response functions", *Space Science Rev.* **93**, 335-359 (2000).

Clem J.M., J.W Bieber, P.Evenson, D.Hall, J.E Humble, and M. Duldig "Contribution of obliquely incident particles to neutron monitor rate", *J.Geophys.Res.*, **102**, No. A12, 26919-26926 (1997).

Cocconi G., V. Cocconi Tongiorgi, and M. Widgoff "Cascades of nuclear disintegration induced by the cosmic radiation", *Phys. Rev.* **79**, No 5, 768-780 (1950).

Conversi M. "Experiments on cosmic-ray mesons and protons at several altitudes and latitudes", *Phys. Rev.*, **79**, No. 5, 749–767 (1950).

Cordaro E.G. "Antarctic Laboratory for Cosmic Rays: 1991-1995", *Proc. 24th Intern. Cosmic Ray Conf.*, Rome, **4**, 1320-1323 (1995).

Coxell H., M.A. Pomerantz, and S.P. Agarwal "Survey of cosmic-ray intensity in the lower atmosphere", *J. Geophys. Res.*, **71**, No 1, 143-154 (1966).

Cronin J.W. "The Pierre Auger Observatory", *Proc. 27th Intern. Cosmic Ray Conf.*, Hamburg, Vol. Invited, Rapporteur, and Highlight Papers, 234-239 (2001).

Davis A.J., W. Menn, L.M. Barbier, et al. "Interpretation of the Helium Isotope Ratios Measured by IMAX", *Proc. 24th Intern. Cosmic Ray Conf.*, Rome, **2**, 622-625 (1995).

Dementyev A. and N. Sobolevsky, "SHIELD – Universal Monte Carlo Hadron Transport Code Scope and Application", *Proceedings of the Third Workshop on Simulating of Accelerator Radiation Environment (SARE-3)*, Tsukuba, KEK Proceedings **97-5**, 21-31 (1997)

Dorman L.I. "The possibility of designing the worldwide network of cosmic ray spectrographs on the basis of the existing network of cosmic ray stations and using the method of the difference coupling coefficients", *Proc. 15th Intern. Cosmic Ray Conf.*, Plovdiv, **4**, 392-394 (1977).

Dorman L.I. "Solar Energetic Particle Events and Geomagnetic Storms Influence on People's Health and Technology; Principles of Monitoring and Forecasting of Space Dangerous Phenomena by Using On-Line Cosmic Ray Data", in *Proc. 22nd ISTC Japan Workshop on Space Weather Forecast in Russia/CIS* (ed. Y. Muraki), Nagoya University, **2**, 133-151 (2002).

Dorman L.I. "Principles of cosmic ray using for space weather monitoring and forecasting", *Proc. 28th Intern. Cosmic Ray Conf.*, Tsukuba, **7**, 4269-4272 (2003).

Dorman L.I., S.G. Fedchenko, L.V. Granitskij, and G.A. Rische "Coupling and barometer coefficients for measurements of cosmic ray variations at altitudes of 260-400 mb", *Acta Phys. Acad. Sci. Hung.*, **29** Suppl. 2, 233-236 (1970).

Dorman L.I., N. Iucci, M. Murat, M. Parisi, L.A. Pustil'nik, A. Sternlieb, G. Villoresi, and I.G. Zukerman "Dangerous FEP events: real-time data of ground and satellite CR measurements using for monitoring of beginning and forecasting of expected particle fluxes in atmosphere and in space", *Proc. 28th Intern. Cosmic Ray Conf.*, Tsukuba, **6**, 3411-3414 (2003).

Dorman L.I. and Kh.M. Khamirzov "Spectrographical method of cosmic ray variation investigation by inclined muon telescopes with using differential coupling coefficients", *Geomagnetism and Aeronomy*, **17**, No. 1, 20-25 (1977).

Dorman L.I., Kh.M. Khamirzov et al. "Complex muon-neutron detectors for cosmic ray variations investigation, I. Block-scheme, electronics, geometry", In *Research on Solar-Terrestrial Physics Problems*, Moscow, NAUKA, 83-88 (1977).

Dorman L.I., Kh.M. Khamirzov, A.A. Shadov, and G.Sh. Shkhalakhov "Elbrus spectrograph complex and cosmic ray variations research by spectrographical method", *Izvestia Academy of Sciences USSR*, Series Phys., **42**, No. 7, 1507-1510 (1978).

Dorman L.I., Kh.M. Khamirzov, G.Sh. Shkhalakhov et al. "The Elbrus spectrographical array for studying the cosmic ray variations of the galactic and extragalactic origin", *Proc. 15th Intern. Cosmic Ray Conf.*, Plovdiv, **3**, 274-278 (1977).

Dorman L.I. and V.K. Korotkov "Multiple measurements in a neutron monitor with automatic compensation for the coincidence effect", *Proc. 21th Intern. Cosmic Ray Conf.*, Adelaide, **7**, 204-206 (1990).

Dorman L.I., I.Ya. Libin, A.Z. Chechenov, and A.Z. Ghappuev "Telescope of cosmic ray Elbrus spectrograph", In *Research on Solar-Terrestrial Physics Problems*, Moscow, NAUKA, 79-82 (1977).

Dorman L.I., I.Ya. Libin, V.G. Yanke et al. "Complex muon-neutron detectors for cosmic ray variations investigation, II. Calculations of directionality diagrams, meteorological effects and coupling coefficients", In *Research on Solar-Terrestrial Physics Problems,* Moscow, NAUKA, 89-94 (1977).

Dorman L.I., L.A. Pustil'nik, A. Sternlieb et al. "Monitoring and Forecasting of Great Solar Proton Events Using the Neutron Monitor Network in Real Time", *IEEE Plasma Sciences*, in press (2004).

Dorman L.I. and D. Venkatesan "Solar Cosmic Rays", *Space Sci. Review*, **64**, 183-362 (1993).

Dorman L.I., G. Villoresi, N. Iucci, M. Parisi, M.I. Tyasto, O.A. Danilova, and N.G. Ptitsyna "Cosmic ray survey to Antarctica and coupling functions for neutron component near solar minimum (1996-1997), 3, Geomagnetic effects and coupling functions", *J. Geophys. Res.* **105**, No. A9, 21,047-21,058 (2000).

Dragun G.S., L.V. Kurnosova, V.I. Logachev, LA. Razorenov, I.A. Sirotkin, and M.I. Fradkin "Apparaturos for investigation of cosmic nuclear component on space rockets and satellites", In *Iskusstvennye sputniki Zemli*, NAUKA, Moscow, No 9, 86-110 (1961).

Duggal S.P. "Relativistic solar cosmic rays", *Rev. Geophys. Space Phys.*, **17**, 1021-1058 (1979).

Duldig M.L. "Muon observations", *Space Sci. Rev.*, **93**, 207-226 (2000).

Duldig M.L. and J. E. Humble "A mobile neutron monitor to intercalibrate the worldwide network", *Proc. 27th Intern. Cosmic Ray Conf.*, Hamburg, **10**, 4083-4086 (2001)

Engel J., T.K. Gaisser, P. Lipari, and T. Stanev "Nucleus-nucleus collisions and interpretation of cosmic ray cascades", *Phys. Rev.*, **D46**, No.11, 5013-5025 (1992).

Engelmann G., L. Koch, and G.P. Meyer "Use of semiconductor telescopes in charge and energy spectrometry of cosmic rays", *Proc. 9th Intern. Cosmic Ray Conf.*, London, **1**, 419-422 (1965).

Enqvist T., L. Ding, A.-M. Elo et al. "Underground Multimuon Experiment in Pyhäsalmi Mine", *Proc. 28th Intern. Cosmic Ray Conf.*, Tsukuba, **2**, 997-1000 (2003).

Erlykin A.D., N.M. Nesterova, S.I. Nikolsky, et al. "An installation for the study of the extensive showers and nuclear interaction of the cosmic radiation pafticles of the energies 10^{12} - 10^{16} eV", *Cosmic Rays* (NAUKA, Moscow), No. 10, 104-115 (1969).

Fassó A., A. Ferrary, A. Ranft, and P.R. Sala "CERN Divisional Report CERN/TIS-RP/97-05", *Proc. of the 2nd Workshop on Simulating Accelerator Radiation Environment,* SARE-2, CERN-Geneva, October 9–11 1995, 158-170 (1997).

Fazio G.G. and E.M. Hafner "The OSO-1 high-energy gamma-ray experiment", *J. Geophys. Res.*, **72**, No 9, 2452-2455 (1967).

Fieldhouse P., E.B. Hughes, and P.L. Marsden "Multiple neutron production in an IGY neutron monitor", *J. Phys. Soc. Japan*, **17**, Suppl. A-II, 518-519 (1962).

Furani G., F. Bacciorelli, V. Bidoli et al. "Measurement of Nuclear Mass Distribution of Primary and Recoil Heavy Ions inside MIR Space Station with SilEye Silicon Detector", *Proc. 26th Intern. Cosmic Ray Conf.*, Salt Lake Sity, **5**, 128-131 (1999).

Geiger K.W. "Evaporation neutrons from cosmic ray nuclear interactions in various elements", *Can. J. Phys.*, **34**, 288-303 (1956).

Gentile S. "The Alpha Magnetic Spectrometer on the International Space Station", *Proc. 28th Intern. Cosmic Ray Conf.*, Tsukuba, **4**, 2145-2148 (2003).

Ginzburg V.L., L.V. Kurnosova, and M.I. Fradkin "Investigation of charged particle intensity during flights of 2-nd and 3-rd ship-satellites" In *Iskusstvennye sputniki Zemli*, NAUKA, Moscow, No 10, 22-33 (1961).

Glasstetter R., T. Antoni, W.D. Apel et al. "Shower Reconstruction Performance of KASCADE-Grande", *Proc. 28th Intern. Cosmic Ray Conf.*, **2**, 781-784 (2003).

Granitskij L.V. and S.G. Bortnik "Apparaturus for cosmic ray intensity registration in stratosphere", *Results of Observations and Investigations in the Period of IQSY*, NAUKA, Moscow, No 5 (1968).

Granitskij L.V. and S.G. Bortnik "Decoding instrument to study the second cosmic rays in the atmosphere and stratosphere", *Studies in Geomagnetism, Aeronomy, and Solar Physics*, SibIZMIRAN, Eastern-Siberian book issie, No. 2, 356- 359 (1971).

Granitskij L.V., S.G. Bortnik, L. K. Zhuravleva, and A.F. Neermolov "The instrument to study neutrons and charged particles in the atmosphere and stratosphere", *Studies in Geomagnetism, Aeronomy, and Solar Physics*, SibIZMIRAN, Eastern-Siberian book issie, No. 2, 346- 350 (1971).

Granitskij L.V. and V.N. Medvedev "Metodics of mashine processing of data observations on airplanes", *Results of Observations and Investigations in the Period of IQSY*, NAUKA, Moscow, No. 4 (1968). '

Granitskij L.V. and **A.V.** Sergeev "On the using counters with ^{3}He dor detection of cosmic ray neutron component", In *Results of Observations and Investigations in IQSY Period*, NAUKA, Moscow, No 1, 151-154 (1966).

Grigorov N.L., G.P. Kakhidze, V.E. Nesterov, I.D. Rapoport, I.A. Savenko, A.V. Smirnov, A.F. Titenkova, and P.P. Shishkov "Spectrometer of primary cosmic ray particles of high energy for satellite of type "Proton", *Space Research* (Moscow), **5**. No 3, 383-394 (1967).

Hamaguchi T., Y.S. Honda, M. Katsumata et al. "Wide Area Small Air Shower Detection System Linked by Internet", *Proc. 28th Intern. Cosmic Ray Conf.*, Tsukuba, **2**, 785-788 (2003).

Hatton C.J. "The Neutron Monitor", in *Progress in Elementary Particle and Cosmic Ray Physics* , Ed. J.G. Wilson and S.A. Wouthuysen, North Holland Publishing Co., Amsterdam, **10**, 3-97 (1971).

Hatton C.J. and H. Carmichael "Experimental investigation of the NM-64 neutron monitor", *Can. J. Phys.*, **42**, No 12, 2443-2472 (1964).

Higashi S., T. Kitamura, S. Miyamoto, Y. Mishima, T. Takahashi, and Y. Watase "Cosmic ray intensities under sea-water at depths down to 1500 meters", *Progr. Theoret. Physics*, **34**, No 6, 1042-1043 (1965).

Hill D.A. and N.A. Porter "Photography of Cherenkov light from extensive air showers in the atmosphere", *Nature*, **191**, No 4789, 690-690 (1961).

Hughes E.B. "Neutron production by the cosmic radiation at sea level", *Ph. D. Thesis*, University of Leeds, Leeds, England (1961).

Hughes E.B. and P.L. Marsden "Response of a standard IGY neutron monitor", *J. Geophys. Res.*, **71**, No 5, 1435-1444 (1966).

Hughes E.B., P.L. Marsden, G. Brooke, M.A. Meyer, and A.W. Wolfendale "Neutron production by cosmic ray protons in lead", *Proc. Phys. Soc.*, London, **A83**, 239-251 (1964).

Hughes E.B., P.L. Marsden, M.A. Meyer, and A.W. Wolfendale "Neutron production in lead by cosmic ray protons", *J. Phys. Soc. Japan*, **17**, Suppl. A-II, 516-517 (1962).

Jelley J.V. "Cherenkov radiation from extensive air showers", In *Progress in Elementary Particle and Cosmic Ray Physics*, Eds. J.G. Wilson and SA. Wouthuysen, North-Holland Publishing Company, Amsterdam, Vol. 9, 41-159 (1967).

Jones S.L., G.H. Ludwig, D.E. Stilwell, J.H. Trainor, and S.H. Way "OGO-E cosmic radiation-nuclear abundance experiment", *IEEE Trans. Nucl. Sci.*, **14**, No 1, 56-63 (1967).

Kaminer N.S. "Cosmic ray intensity registration by plastic scintillators", *Cosmic Rays* (NAUKA, Moscow), No 3, 122-133 (1961).

Kitamura T., S. Ohara, T. Konishi, et al. "Chaos in cosmic ray air showers", *Astroparticle Phys.*, **6**, No. 3-4, 279-291 (1997).

Kopylov Yu.M. "On the possibility of increasing of effectivness of neutron component intensity registration by using scintillation method" In *Investigations in Geomagnetizm and Aeronomy*, NAUKA, Moscow, 139-142 (1966).

Kozlov V., L. Ksenofontov, K. Kudela, S. Starodubtsev, A. Turpanov, I. Usoskin, and V. Yanke "REal-time COsmic Ray Database (RECORD)", *Proc. 28th Intern. Cosmic Ray Conf.*, Tsukuba, **6**, 3473-3476 (2003).

Krasil'nikov D.D. "The encreasing of barometric effect with increasing of EAS energy", *JETP*, **35**, No. 1, 295-296 (1958).

Krasil'nikov D.D. "On the properties of EAS according to observations near sea level", *Proc. 6th Intern. Cosmic Ray Conf.*, Moscow, **2**, 205-211 (1959a).

Krasil'nikov D.D. "Daily variation of cosmic ray intensity with energy $2x10^{14} - 2x10^{15}$ eV", *Proc. 6th Intern. Cosmic Ray Conf.*, Moscow, **4**, 280-281 (1959b).

Krasil'nikov D.D. "Apparaturus for registration time variations of EAS frequency with detectors from Geiger-Muller counters", *Proc. YaFAN*, Ser. Phys., No 3. NAUKA, Moscow, 22-39 (1960).

Krüger H., H. Moraal, J.W. Bieber, J.M. Clem, P.A. Evenson, K.R. Pyle, M.L. Duldig, and J.E. Humble "First results of a mobile neutron monitor to intercalibrate the worldwide network", *Proc. 28th Intern. Cosmic Ray Conf.*, Tsukuba, **6**, 3441-3444 (2003).

Krymsky G.F., A.I. Kuzmin. N.P. Chirkov, P.A. Krivoshapkin, G.V. Skripin, and A.M. Altukhov "Cosmic ray distribution and acceptance vectors of detectors, I.", *Geomagnetism and Aeronomia*, **6**, No. 6, 991-996 (1966).

Krymsky G.F., A.I. Kuzmin. N.P. Chirkov, P.A. Krivoshapkin, G.V. Skripin, and A.M. Altukhov "Cosmic ray distribution and acceptance vectors of detectors, II. Methods of investigation of cosmic ray distribution", *Geomagnetism and Aeronomia*, **7**, No. 1, 11-15 (1967a).

Krymsky G.F., A.M. Altukhov, P.A. Krivoshapkin, A.I. Kuzmin, G.V. Skripin, and N.P. Chirkov "Cosmic ray distribution and acceptance vectors of detectors, IV", *Geomagnetism and Aeronomia*, **7**, No. 5, 794-798 (1967b).

Kurnosova L.V., L.A. Razorenov, and M.I. Fradkin "Heavy nuclei in primary cosmic radiation", In *Iskusstvennye sputniki Zemli*, NAUKA, Moscow, No 2, 70-74 (1958).

Kurnosova L.V., V.I. Logachev, L.A. Razorenov, and M.I. Fradkin "Cosmic ray investigation during the flight of the second space rocket on the Moon", In *Iskusstvennye sputniki Zemli*, NAUKA, Moscow, No 5, 30-37 (1960).

Kurnosova L.V., L.A. Razorenov, and M.I. Fradkin "Short-term incresings of cosmic ray nuclear component connected with solar activity", In *Iskusstvennye sputniki Zemli*, NAUKA, Moscow, No 6, 132-138 (1961a).

Kurnosova L.V., L.A. Razorenov, and M.I. Frankin "Investigation of cosmic ray nuclear component on the 3-rd space rocket", In *Iskusstvennye sputniki Zemli*, NAUKA, Moscow, No 8. 87-89 (1961b).

Lazutin L.L. and E.T. Franzus "Radiozond for cosmic ray intensity measurements in the stratosphere", *Izv. Ac. Sci. USSR*, Ser. Phys., **28**, No. 12, 2085-2086 (1964).

Libin I.Ya., Blokh Ya.L., Dorman L.I et al., 1978. "Development of the scintillation supertelescope", Cosmic Rays (Moscow, NAUKA), Vol. 18, pp. 76-87.

Lin Z., J.W. Bieber, and P. Evenson "Electron trajectories in a model magnetosphere: Simulation and observation under active conditions", *J. Geophys. Res.*, **100**, No. A12, 23543-23550 (1995).

Lindgren S. "Directional response of cosmic ray telescopes", Arkiv. Geofys. **5**, No 1, 23-29 (1966).

Lindner J.W. "Experimental techniques employed in space physics", In *Space Physics*, John Wiley & Sons Inc., New York-London-Sydney, 82-106 (1964).

Link J.T., L.M. Barbier, W.R. Binns, et al. "Measuring the abundances of ultra-heavy galactic cosmic rays through ultra long duration ballooning", *Proc. 27th Intern. Cosmic Ray Conf.*, Hamburg, **6**, 2143-2146 (2001)

Linsley J. "Call for project and ideas in High Energy Astrophysics", *Preprint*, Leeds (1979).

Lovell J.L., M.L. Duldig, and , J.E. Humble "An extended analysis of the September 1989 cosmic ray ground level enhancement", *J. Geophys. Res.*, **103**, 23733-23742 (1998).

Maduev V.D., I.A. Savenko, and M.V. Tel'tsov "Differential magnetic analizator of electrons and protons of small energy", *Geomagnetizm and Aeronomya*, **5**, No 5, 950-951 (1965).

Matsubara Y., Y. Muraki, A. Okada et "New experiment on the observation of solar neutrons at Chakaltaya", *Proc. 24th Intern. Cosmic Ray Conf.*, Rome, **4**, 1312-1315 (1995)

Matsumoto H., H. Koshiishi, T. Goka, M. Fujii, and N. Hasebe "Heavy Ion Telescope onboard the "TSUBASA" Satellite", *Proc. 28th Intern. Cosmic Ray Conf.*, Tsukuba, **6**, 3469-3472 (2003).

Mazur P.O. (for the Pierre Auger Collaboration) "The surface detectors of the Pierre Auger Observatory", *Proc. 28th Intern. Cosmic Ray Conf.*, **2**, 1037-1040 (2003)

McCracken K.G., V.R. Rao, B.C. Fowler, M.A. Shea, and D.F. Smart "Cosmic ray tables (asymptotic directions, variational coefficients and cut-off rigidities", in *IQSY Instruction Manuel*, No. 10, London (1965).

McCullough J.F. for the Milagro Collaboration "Status of the Milagro Gamma Ray Observatory", *Proc. 26th Intern. Cosmic Ray Conf.*, Salt Lake City, **2**, 369-372 (1999).

McDonald F.B. "Integration of neutron monitor data with spacecraft observations", *Space Science Rev.*, **93**, 263-284 (2000).

Meyer B. "Korrelierte Neutronen in Simpson-Pile", *P. Dr. Thesis*, Ludwig-Maximilians-Universitat (1961).

Meyer M.A., A.W. Wolfendale, E.B. Hughes, and P.L. Marsden "The production of neutrons by fast cosmic ray muons", *Proc. Phys. Soc.*, London, **83**, 253-258 (1964).

Matsubara Y., Y. Muraki, S. Sakakibara et al. "A new solar neutron telescope in Hawaii", *Proc. 25th Intern. Cosmic Ray Conf.*, Durban, **1**, 37-40 (1997).

Moraal H., A. Belov, and J.M. Clem "Design and coordination of multi-station innternational neutron monitor networks", *Space Sci. Rev.*, **93**, 285-303 (2000).

Moraal H., M.S. Potgieter, P.H. Stoker, and A.J. Van der Walt "Neutron Monitor Latitude Survey of the Cosmic Ray Intensity During the 1986/87 Solar Minimum", *J. Geophys. Res.*, **94**, 1459-1464 (1989).

Munakata K., J.W. Bieber, S.-I. Yasue, et al. "Precursors of geomagnetic storms observed by the muon detector network", *J. Geophys. Res.*, **105**, No. A12, 27457-27468 (2000).

Muraki Y., Y. Matsubara, I. Imaida, T. Koi et al. "Solar flare and neutron telescope", *Nuclear Physics B-Proceedings Supplements,* **60B**, 3-11 (1998).

Nagashima K. "Three-dimensional cosmic ray anisotropy in interplanetary space", *Rep. Ionosphere Space Res. Japan*, **25**, 189-211 (1971).

Nobles R.A., R.A. Alber, E.B. Hughes, L.L. Newkirk, and M. Walt "Neutron multiplicity monitor observations during 1965", *J. Geophys. Res.*, **72**, No 15, 3817-3828 (1967).

Ochi N., T. Wada, T. Konishi, et al. "LAAS Network Observation of Air Showers", *Proc. 26th Intern. Cosmic Ray Conf.*, Salt Lake City, **2**, 419-422 (1999).

28th International Cosmic Ray Conference 1005

Ochi N., A. Iyono, T. Konishi et al. "The status and future prospect of the LAAS project", *Proc. 28th Intern. Cosmic Ray Conf.*, Tsukuba, **2**, 1005-1008 (2003).

Ohashi Y., A. Okada, T. Aoki, et al. "New narrow angle muon telescope at Mt. Norikura", *Proc. 25th Intern. Cosmic Ray Conf.*, Durban, **1**, 441-444 (1997).

Palmeira R.A.R. and K.G. McCracken "Observation of a short-lived cosmic-ray solar flare increase with a high-counting-rate meson detector", *Phys. Rev. Letters*, **5**, No 1, 15-16 (1960).

Palmeira R.A.R. and R. Williams "Rapid decrease of cosmic-ray intensity", *Nuovo Cimento*, **8**, 352-355 (1958).

Phillips J. and N.R. Parsons "Some experiments with a mobile neutron monitor", *J. Phys. Soc. Japan*, **17**, Suppl. A-II, 519-523 (1962).

Piccardi S. for the PAMELA Collaboration "The PAMELA experiment", *Proc. 26th Intern. Cosmic Ray Conf.*, Salt Lake City, **5**, 96-99 (1999).

Pyle R. "The Haleakala cosmic ray neutron monitor station: intercalibration with the Huancayo station", *Proc. 23rd Intern. Cosmic Ray Conf.*, Calgary, **3**, 609-612 (1993).

Pyle R. "Public access to neutron monitor datasets", *Space Sci. Rev.*, **93**, 381-400 (2000).

Pyle R., P. Evenson, J.W. Bieber, J.M. Clem, J.E. Humble, and M.L. Duldig "The Use of ^{3}He Tubes in a Neutron Monitor Latitude Survey", *Proc. 26th Intern. Cosmic Ray Conf.*, Salt Lake City, **7**, 386-389 (1999).

Raubenheimer B.C. and P.H. Stoker "Various aspects of the attenuation coefficient of a neutron monitor", *J. Geophys. Res.*, **79,** No.34., 5069-5076 (1974).

Reinecke J.P.L., H. Moraal, M.S. Potgieter, F.B. McDonald, and W.R. Webber "Different crossovers?", *Proc. 25th Intern. Cosmic Ray Conf.*, Durban, **2**, 49-52 (1997).

Rielage K., M. Christl, J. Adams et al. "An engineering prototype of the Imaging Calorimeter for ACCESS (ICA)", *Proc. 27th Intern. Cosmic Ray Conf.*, Hamburg, **6**, 2239-2242 (2001)

Rossi B. "The programm of EAS investigations in the MIT", *Proc. 6th Intern. Cosmic Ray Conf.*, Moscow, **2**, 17-30 (1959).

Rozman M. and S.F. Kilin "Luminiscense of plastic scintillators", *UFN*, **69**, No 3, 459-482 (1959).

Sako T., Y. Muraki, and N. Hirano "Application of CPLD for the Mexico Solar Neutron Telescope", *Proc. 28th Intern. Cosmic Ray Conf.*, Tsukuba, **6**, 3449-3452 (2003).

Sako T., Y. Muraki, N. Hirano, and H. Tsuchiya "Super Solar Neutron Telescope for the Next Solar Maximum", *Proc. 28th Intern. Cosmic Ray Conf.*, Tsukuba, **6**, 3437-3440 (2003).

Sandström A.E. "Cosmic ray soft component measurements during a flight from Scandinavia across the North pole and around Asia and Europe", *Nuovo Cimento,* **8**, Suppl. No 2, 263-276 (1958).

Sandström A.E., E. Dyring, L. Ekström, and B. Östman "Cosmic ray meson monitors with plastic scintillators", *Arkiv Fys.* **29,** No 26, 329-341 (1965).

Savenko I.A, P.I. Shavrin, V.E. Nesterov, and N.F. Pisarenko "Cosmic ray equator according to data of the 2-nd soviet space-ship", In *Iskusstvennye sputniki Zemli*, NAUKA, Moscow, No 10, 45-47 (1961).

Savenko I.A., O.I. Savun, P.I. Shavrin, and B.M. Yakovlev "Kombined proton spectrometer for space research", *Geomagnetizm and Aeronomya*, **5**, No 3, 546-549 (1965a).

Savenko I.A., O.I. Savun, and A.V. Yurovskij "Instrument for registration protons with energy E = 3 - 14 MeV, α–particles, and nuclei with $Z > 2$", *Geomagnetizm and Aeronomya*, **5**, No 3, 550-553 (1965b).

Scarsi L. for the OA collaboration "The OWL - AIRWATCH Experiment: Overview", *Proc. 26th Intern. Cosmic Ray Conf.*, Salt Lake City, **2**, 384-387 (1999).

Seo E.S., J.F. Ormes, R.E. Streitmatter, S.J. Stochaj, W.V. Jones, S.A. Stephens, and T.Bowen "Measurement of cosmic-ray proton and helium spectra during the 1987 solar minimum", *Astrophys. J.*, **378**, 763-772 (1991).

Seo E.S., H.S. Ahn, P.S. Allison et al. "CREAM for high energy composition measurements", *Proc. 28th Intern. Cosmic Ray Conf.*, Tsukuba, **4**, 2101-2104 (2003).

Shafer Yu.G. and A.V. Yarygin "Cosmic ray measurements on geophysical rockets", in *Iskusstvennye sputniki Zemli*, No 4. NAUKA, Moscow, 184-189 (1960a).

Shafer Yu.G. and A.V. Yarygin "Investigations of primary cosmic radiation by the Earth's satellite", *Proc. YaFAN*, Ser. Phys., NAUKA, Moscow, No 3, 5-14 (1960b).

Shea M.A. and D.F. Smart "Fifty years of cosmic radiation data", *Space Sci. Rev.*, **93**, 229-262 (2000).

Shibata S., Y. Munakata, R. Tatsuoka et al. "Calibration of neutron monitor using an accelerator", *Proc. 25th Intern. Cosmic Ray Conf.*, Durban, **1**, 45-48 (1997).

Shibata S., Y. Munakata, R. Tatsuoka et al. "Calibration of Neutron Monitor using Accelerator Neutron Beam", *Proc. 26th Intern. Cosmic Ray Conf.*, Salt Lake Sity, **7**, 313-316 (1999).

Shibata S., Y. Munakata, R. Tatsuoka et al. "Detection efficiency of a neutron monitor calibrated by an accelerator neutron beam", *Nucl Instrum. Meth.*, **A463**, 326 (2001).

Simon M. "Status of the PAMELA experiment on-board of the Resurs DK-1 Spacecraft", *Proc. 28th Intern. Cosmic Ray Conf.*, Tsukuba, **4**, 2117-2120 (2003).

Simpson J.A. "The latitude dependence of neutron densities in the atmosphere as a function of altitude", *Phys. Rev.* **73**, No 11, 1389-1391 (1948).

Smith F.G., W.A. Porter, and J.V. Jelley "The detection of radio pulses of wavelength 6.8 m, in coincidence with extensive air showers, in the energy region 10^{16}-10^{17} eV", *Proc. 9th Intern. Cosmic Ray Conf.*, London, **2**, 701-705 (1965).

Sparvoli R. "Isotope discrimination with the experiment NINA", *Proc. 25th Intern. Cosmic Ray Conf.*, Durban, **2**, 181-184 (1997).

Stoker P.H. "Relativistic Solar Proton Events", *Space Sci. Rev.*, **73**, 327-385 (1994).

Stoker P.H., L.I. Dorman, and J.M. Clem "Neutron monitor design improvements", *Space Science Rev.*, **93**, 361-380 (2000).

Stoker P.H. and Moraal H. "Neutron Monitor Latitude Surveys at Aircraft Altitudes", *Astrophys. Space Sci.* **230**, 365- 373 (1995).

Stozhkov Yu.I. "Cosmic ray modulation by the solar activity and general magnetic field of the Sun", *Thesis of Doctor of Sciences Degree*, Moscow, Lebedev Physical Institute, pp.244 (1980).

Strong A.W. and I.V. Moskalenko "Propagation of cosmic-ray nucleons in the Galaxy ", *Astrophys. J.*, **509**, No. 1, Part 1, 212-228 (1998).

Strong A.W. and I.V. Moskalenko "Models for galactic cosmic-ray propagation", *Adv. Space Res.*, **27**, No. 4, 717-726 (2001).

Szadkowski Z., A.V. Dorofeev, J. Darling et al. "The surface detector trigger for the Auger Observatory", *Proc. 28th Intern. Cosmic Ray Conf.*, Tsukuba, **2**, 805-808 (2003).

Takahashi Y. "Maximum-Energy Auger Air Shower Satellite (MASS) for Observing Cosmic Rays in the Energy Region 10^{19}–10^{22} eV", *Proc. 24th Intern. Cosmic Ray Conf.*, Rome, **3**, 595-598 (1995).

Takashima T., T. Kashiwagi, S. Okuno, K. Mori, and H. Onabe "The Development of the High Energy Particle Detector onboad the SELENE spacecraft", *Proc. 28th Intern. Cosmic Ray Conf.*, Tsukuba, **6**, 3465-3468 (2003).

Teshima M., P. Lipari, and A. Santangelo "EUSO (The Extreme Universe Space Observatory) – Scientific Objectives", *Proc. 28th Intern. Cosmic Ray Conf.*, Tsukuba, **2**, 1069-1072 (2003).

Tsuchiya H., T. Hoshida, Y. Muraki et al. "Arrival of solar neutrons from large zenith angle", *Proc. 27th Intern. Cosmic Ray Conf.*, Hamburg, **9**, 3056-3059 (2001a).

Tsuchiya H., Y. Muraki, K. Masuda et al. "Detection efficiency of a new type of solar neutron detector calibrated by an accelerator neutron beam", *Nucl. Instrum. Meth.*, **A463**, 183-186 (2001b).

Usoskin I.G., G.A. Kovaltsov, H. Kananen, and P.Tanskanen "The World Neutron Monitor Network as a Tool for the Study of Solar Neutrons", *Ann. Geophysicae*, **15**, 375-386 (1997).

Vacci A. "The telescope NINA to investigate nuclear fluxes in the near-Earth space", *Proc. 25th Intern. Cosmic Ray Conf.*, Durban, **2**, 177-180 (1997).

Valdes-Galicia J. F., A. Hurtado, O. Musalem et al. "A New Solar Neutron Telescope in Mexico", *Proc. 28th Intern. Cosmic Ray Conf.*, Tsukuba, **6**, 3433-3436 (2003).

Veprik Ya.M., L.V. Kurnosova, L.A. Razorenov, K.D. Tolstov, M.I. Fradkin, and V.S. Chukin "The experience of photo-emulsion development on the board of the ship-satellite", In *Iskusstvennye sputniki Zemli*, NAUKA, Moscow, No 11, 35-41 (1961).

Vemov S.N. and A.E. Chudakov "Investigations of cosmic rays and the Earth's corpuscular radiation by rockets and satellites", *UFN*, **70**, No 4, 585-619 (1960).

Vernov S.N., T.A. Egorov, N.N. Efimov, et al. "The project of a great EAS installation in Yakutsk", *Izvestia Ac. of Sci. of USSR*, Ser. Phys., **29**, No9, 1690-1692 (1965).

Vernov S.N., N.L. Grigorov, Yu.I. Logachev, and A.E. Chudakov "Cosmic radiation measurements on the Earth's satellite", *DAN SSSR*, **120**, No 6, 1231-1233 (1958).

Vernov S.N., G.B. Khristiansen, A.T. Abrosimov, et al. "Description of modernized complex apparatus for EAS investigation", *Izvestia Ac. of Sci. of USSR*, Ser. Phys., **28**, No 12, 2087-2092 (1964).

Vernov S.N., Yu.I. Logachev, A.E. Chudakov, and Yu.G. Shafer "Investigation of cosmic radiation variations", *UFN*, **63**, No 1, 149-162 (1957).

Vernov S.N., I.A. Savenko, P.I. Shavrin, V.E. Nesterov, and N.F. Pisarenko "Outer Earth's radiation belt on the altitude 320 km", In *Iskusstvennye sputniki Zemli*, NAUKA, Moscow, No 10, 34-39 (1961a).

Vernov S.N., I.A. Savenko, P.I. Shavrin, and N.F. Pisarenko "Discovery of the inner radiation belt on the altitude 320 km in the region of South-Atlantic magnetic anomaly", In *Iskusstvennye sputniki Zemli*, NAUKA, Moscow, No 10, 40-44 (1961b).

Vernov S.N., P.V. Vakulov, E.V. Gorchakov, Yu.I. Logachev, and A.E. Chudakov "Investigation of soft cosmic ray component out of the atmosphere", In *Iskusstvennye sputniki Zemli*, NAUKA, Moscow, No 2. 61-69 (1958).

Vishnyakov V.V., Tan Syao-vej, and A.A. Tyapkin "Low-voltage galogen counters (mechanism of discharge)", *UFN*, **72**, No 1, 133-152 (1960).

Voitovetskij V.K. and N.S. Tolmacheva "Litium-silicat scintillation glasses for detection of slow neutrons", *Atomic Energy* (Moscow), **6,** No 4, 472-474 (1959).

Wefel J.P. (for the ATIC collaboration) "The ATIC experiment: first balloon flight", *Proc. 27th Intern. Cosmic Ray Conf.*, Hamburg, **6**, 2111-2114 (2001).

Wefel J.P. and T.L. Wilson "The ACCESS Mission: ISS Accommodation Study", *Proc. 26th Intern. Cosmic Ray Conf.*, Salt Lake City, **5**, 84-87 (1999).

Winckler J.R. "Balloon Study of High-Altitude Radiations during the International Geophysical Year", *J. Geophys. Res.*, **65**, No. 5, 1331-1361 (1960).

Winn M.M. "Cosmic-ray astronomy", *New Scientist*, **30**, No 490, 24-26 (1966).

Yamamoto A., J. Mitchell, K. Abe, et al. "BESS-polar long duration flights in Antarctica", *Proc. 27th Intern. Cosmic Ray Conf.*, Hamburg, **6**, 2135-2138 (2001)

Yamashita M., L.D. Stephens, and H.W. Patterson "Cosmic-ray produced neutrons at ground level: neutron production rate and flux distribution", *J. Geophys. Res.* **71,** No 16, 3817-3834 (1966).

Yasue S., S. Mori, S. Sakakibara, and K. Nagashima "Coupling coefficients of cosmic ray daily variations for NM stations", *Report of Cosmic Ray Research Laboratory*, **7**, Nagoya, Japan (1982)

References for Chapter 5 and Preface for Part 2

Babadzhanov I. "Multiplicity of neutron generation in muon capture", *Proc. of All-Union Conference on Cosmic Ray Phys.*, Tashkent, 1968, Vol. 1, No. 2, FIAN USSR, Moscow, 17-20 (1969).

Cocconi G. and M. Widgoff "Cascades of Nuclear Disintegrations Induced by the Cosmic Radiation", *Phys. Rev.*, **79**, No. 5, 768-780 (1950).

Cocconi G., and V. Tongiorgi "Nuclear disintegrations induced by μ-mesons", *Phys. Rev.*, **84**, No. 1, 29-36 (1951).

Dorman L.I. "Two-meson theory of cosmic ray hard component temperature effect", *Special Report 1951-3*, Science-Research Institute of Terrestrial Magnetism, Troitsk, Moscow region (1951a).

Dorman L.I. "Instruction for calculation of temperature corrections to hard component intensity data", *Special Report, 1951-4*, Science-Research Institute of Terrestrial Magnetism, Troitsk, Moscow region (1951b).

Dorman L.I. "To the theory of cosmic ray meteorological effects", *Doklady Academy of Sciences of USSR* (Moscow), **94**, No. 3, 433-436 (1954a).

Dorman L.I. "On the temperature effect of the cosmic ray hard component", *Doklady Academy of Sciences of USSR* (Moscow), **95**, No.1, 49-52 (1954b).

Dorman L.I. "On the nature of cosmic ray variations", *Ph. D. Thesis*, Physical Lebedev Institute Academy of Sciences of USSR, Moscow, pp. 327 (1955).

Dorman L.I. "To the theory of meteorological effects of cosmic ray neutron component", *Proc.of Yakutsk Filial of Academy of Sciences*, Series of Physics, Academy of Sciences of USSR Press, Moscow, No. 2, 68-72 (1958a).

Dorman L.I. "To the theory of meteorological effects of cosmic ray soft and general components", *Proc. of Yakutsk Filial of Academy of Sciences*, Series of Physics, Academy of Sciences of USSR Press, Moscow, No. 2, 59-67 (1958b).

Dorman L.I. "Theory of cosmic ray variations", *Cosmic Rays* (Moscow, NAUKA), **13**, 5-66 (1972).

Dorman L.I. "Geophysical effects and second components of cosmic rays in the atmosphere", *Cosmic Rays* (Moscow, NAUKA), **14**, 5-28 (1974).

Grigorov N.L. and V.S. Murzin "Interaction of primary cosmic rays of different energy with matter", *Izvestia Ac. of Sci. of USSR,* Ser. Phys., **19**, No. 1, 21-38 (1953).

Hughes E.B., P.L. Marsden, G. Brooke, M.A. Meyer, and A.W. Wolfendale "Neutron production by cosmic ray protons in lead", *Proc. Phys. Soc.,* London **A83**, 239-251 (1964).

Hughes E.B. and P.L. Marsden "Response of standard IGY neutron monitor", *J. Geophys. Res.*, **71**, No. 5, 1435-1444 (1966).

Kaminer N.S. "On the changing of meteorological coefficients of the hard cosmic ray component", *Proc. 6th Intern. Cosmic Ray Conf*, Moscow, **4**, 42-46 (1960).

Maeda K. and M. Wada "Atmospheric temperature effect upon the cosmic ray intensity at sea level", *J. Sci. Res. Inst.* (Tokyo), **48**, 71-79 (1954).

Meyer M.A., A.W. Wolfendale, E.B. Hughes, and P.L. Marsden "The production of neutrons by fast cosmic ray muons", *Proc. Phys. Soc.*, London, **83**, 253-258 (1964).

Olbert S. "Atmospheric effects on cosmic ray intensity near sea level", *Phys. Rev.*, **92**, 454-461 (1953).

Uotila, U.A. "Determination of the shape of the geoid", In Proc. of Symposium: *Size and Shape of the Earth*, Ohio State University, Columbus, Ohio, Nov. 13-15, 1956, Inst. of Geodesy, Photogrammetry and Cartography, Publ. No. 7 (1957).

Vernov S.N., N.L. Grigorov, G.T. Zatsepin, and A.E. Chudakov "The research of nucleons interactions with light nucleus at energies 10^9-10^{12} eV", *Izvestia Ac. of Sci. of USSR*, Ser. Phys., **19**, No. 5, 493-501 (1955).

References for Chapter 6

Adams N. and H.J. Braddick. "Time and other variations in the intensity of cosmic ray neutrons", *Z. Naturforsch.*, **6a**, No. 11, 592-598 (1949).

Agrawal S.P., S.K. Ray and U.R. Rao. "Multiplicity measurements at Ahmedabad", *Acta Phys. Acad. Sci. Hung.*, **29**, Suppl. 2, 597-600 (1970).

Ahluwalia H.S. and S.S. Xue. "Mean attenuation length for solar protons of 29 September 1989", *Proc. 23th Intern. Cosmic Ray Conf*, Calgary, **3**, 757-760 (1993).

Alania M.V., O.G. Rogava, and L.Kh. Shatashvili. "Barometric effect of cosmic ray neutron component", *Proceedings of the 5th Every Year Winter Cosmophysical School*, Apatity, 298-300 (1968).

Alania M.V., O.G. Rogava, and L.Kh. Shatashvili. "Investigation of the barometric effect of the cosmic ray neutron component", *Acta Phys. Acad. Sci. Hung.*, **29**, Suppl. 2, 605-609 (1970).

Alexeenko V.V., A.B. Chernyaev, A.E. Chudakov, et al. "29 September 1989 GLE (Ground Level Enhancement) at Baksan Air Shower Array (BASA)", *Proc. 23rd Intern. Cosmic Ray Conf.*, Calgary, **3**, 163-166 (1993).

Alexeyev E.N., V.V. Alexeenko, E.V. Gorchakov, A.F. Litvinenko, S.I. Mokhrov, N.S. Khaerdinov, A.B. Chernyaev, and A.E. Chudakov "Preliminary analysis of solar flare event of 29 September 1989 by the data of array 'Carpet' of the Baksan Neutrino Observatory", *Izvestiya AN USSR*, Ser.Phys., **55**, No.10, 1874-1876 (1991).

Bachelet F., P. Balata, E. Dyring, and N. Iucci. "Attenuation coefficients of the cosmic ray nucleonic component in the lower atmosphere", *Nuovo Cimento*, **35**, No. 1, 23-35 (1965a).

Bachelet F., P. Balata, and N. Iucci. "L'effetto di attenuazione della componente nucleonica dei raggi cosmici nella bassa atmosphera", *Atti 14-mo Convegno Annuale Assoc. Geofis. Ital.*, Roma, 215-222 (1965b).

Bachelet F., P. Balata, and N. Iucci. "Some properties of the radiation recorded by the IGY cosmic-ray neutron monitors in the lower atmosphere", *Nuovo Cimento*, **A40**, No. 1, 250-260 (1965c).

Bachelet F., E. Dyring, N. Iucci, and G. Villoresi. "Synoptic study of the attenuation coefficients for the cosmic ray neutron monitors of the IGY network from 1957 to 1965", *Nuovo Cimento*, **52B**, No. 1, 106-123 (1967)

Bachelet F., E. Dyring, N. Iucci, and G. Villoresi. "Time changes of the attenuation coefficients for the cosmic ray neutron monitors ", *Canad. J. Phys*, **46**, No. 10, Part 4, S1041-S1043 (1967),

Baker C.P., D.L. Hall, J.E. Humble, and M.L. Duldig. "Atmospheric correction analysis for the Mawson muon telescopes", *Proc. 23th Intern. Cosmic Ray Conf.*, Calgary, **3**, 753-756 (1993).

Bercowitch M. "Atmospheric effects on cosmic ray monitors", *Proc. 10th Intern. Cosmic Ray Conf.*, Calgary, Part A, 269-344 (1967).

Blomster K.A. and P.J. Tanskanen. "The influence of snow and water on the different multiplicities as observed in a neutron monitor NM-64 in Oulu", *Acta Phys. Acad. Sci. Hung.*, **29**, Suppl. 2, 627-630 (1970).

Boliev M.M., S.N. Karpov, V.B. Petkov, A.V. Radchenkov, and A.N. Zaichenko "Meteorological effects of a single cosmic ray component by the data of Baksan air shower array Andyrchy", *Proc. 28th Intern. Cosmic Ray Conf.*, Tsukuba, **7,** 4193-4196 (2003).

Bridge H.S. and R.H. Rediker "Ionization chamber measurements of the absorption of the N-component of cosmic rays in lead", *Phys. Rev.*, **88,** No.2, 206-224 (1952).

Broxon J.V. "Barometric and temperature coefficients of frequency of small cosmic-ray bursts and of burst-corrected cosmic-ray ionization", *Phys. Rev.*, **81,** No.4, 555-564 (1951).

Butikofer R. and E.O. Fluckiger "Pressure correction of GLE measurements in turbulent winds", *Proc. 26th Intern. Cosmic Ray Conf.*, Salt Lake City, **6**, 395-398 (1999).

Carmichael H. "Studies of bursts at see level", *Phys. Rev.*, **74,** No.11, 1667-1688 (1948).

Carmichael H., M. Bercovitch, J.F. Steljes, and M. Magidin. "Latitude survey in North America", *Proc. 9th Intern. Cosmic Ray Conf.*, London, **1**, 553-556 (1965).

Carmichael H., M. Bercovitch, M.A. Shea, M. Magidin, and R.W. Peterson. "Attenuation of neutron monitor radiation in the atmosphere ", *Canad. J. Phys*, **46**, No. 10, Part 4, S1006-S1013 (1968).

Carmichael H., M.A. Shea, and R.W. Peterson. "Cosmic ray latitude survey in Western USA and Hawaii in Summer 1966, III", *Canad. J. Phys.*, **47**, 2057-2066 (1969).

Carmichael H. and R.W. Peterson. "Dependence of the neutron monitor attenuation coefficient on atmospheric depth and on geomagnetic cutoff in 1966 and in 1970", *Proc. 12th Intern. Cosmic Ray Conf*, Hobart (Australia), **3**, 887-892 (1971).

Chasson R.L. "Cosmic ray intensity fluctuations at sea level", *Phys. Rev.*, **96**, No. 4, 1116-1123 (1954).

Coxell H., M.A. Pomerantz, and S.P. Agarwal. "Survey of cosmic ray intensity in the lower atmosphere", *J. Geophys. Res.*, **71**, No. 1, 143-154 (1966).

Cristy R.F. and S Kusaka "Burst production by mesotrons", *Phys. Rev.*, **59,** No.5, 414-421 (1941).

Daudin A. and J. Daudin "Effets atmosphériques sur les gerbes d'Auger", *J. Atmos. Terr. Phys.*, **3**, 245-257 (1953).

Dawton D.I. and H. Elliot. "Time variations of the soft component of the cosmic radiation. *J. Atmosph. Terrestr. Phys.*, **3**, No. 6, 295-300 (1953).

Dorman, L.I., N. Iucci, L. Pustilnik, G. Villoresi, I.G. Zukerman "Determination of neutron monitor barometric effect on the basis of the altitude cosmic ray intensity dependence as measured by the Israel-Italian mobile laboratory", *Proc. of 26th Intern. Cosmic Ray Conf,* Salt Lake City, **7**, pp. 371-373 (1999a).

Dorman, L.I., N. Iucci, M. Parisi, G. Villoresi, I.G. Zukerman "Determination of barometric coefficients for total neutron intensity and neutron multiplicities on the base of Emilio Segre' Observatory data corrected for primary variations according to Rome neutron monitor data", *Proc. of 26th Intern. Cosmic Ray Conf,* Salt Lake City, **7**, pp. 374-377 (1999b).

Dorman L.I., N. Iucci, H. Mavromichalaki, L.A. Pustil'nik, A. Sternlieb, G. Villoresi, and I.G. Zukerman. "Cosmic ray snow effect in different multiplicities according to Emilio Segre' Observatory NM hourly data", *Proc. 27th Intern. Cosmic Ray Conf*, Hamburg, **10**, 4079-4082 (2001a).

Dorman L.I., N. Iucci, A. Sternlieb, G. Villoresi, and I.G. Zukerman. "Barometric coefficients for different neutron multiplicities according to ESO NM data (Israel) and data of University "Roma Tre" NM (Italy)", *Proc. 27th Intern. Cosmic Ray Conf*, Hamburg, **10**, 4075-4078 (2001b).

Dorman L.I. and N.S. Kaminer. "Meteorological effects of cosmic rays", *Izvestia Academy of Sciences of USSR, Series Phys.*, **33**, No. 11, pp. 1926-1929 (1969).

Dorman L.I. and V.A. Kovalenko. "To the methodic of barometric pressure corrections introduction in cosmic ray intensity data", *Geomagnetism and Aeronomy*, **6**, No. 5, 922-923 (1966).

Dorman L.I., I.A. Pimenov, and M.G. Seregina "To the problem on methodic of neutron component barometric coefficient determination", *Izvestia Academy of Sciences USSR*, Series Phys., **38**, No. 9, 1957-1960 (1974).

Dorman L.I., I.A. Pimenov, and M.G. Seregina "Method of determination of cosmic ray neutron component barometric coefficient", In *Ionosphere and Solar-Terrestrial Relations*, Alma-Ata, 121-126 (1978).

Dorman L.I., O.G. Rogava, and L.Kh. Shatashvili. "Planetary distribution of cosmic ray neutron component barometric coefficients during IQSY", *Geomagnetism and Aeronomy*, **8**, No. 1, 166-167 (1968).

Dubinsky J., P. Chaloupka, and T. Kawalski "Wind influence on cosmic ray neutron intensity", *Mat.-fys. časop.*, **10**, No. 1, 57-62 (1960).

Duggal S.P. "Relativistic solar cosmic rays", *Rev. Geophys. Space Phys.*, **17**, 1021-1058 (1979).

Dutt J.C. and T. Tambyaphillai. "Atmospheric effects on the cosmic ray intensity of a depth of 60 m w.e. underground at London", *J. Atmos. and Terr. Phys.*, **27**, No. 3, 349-358 (1965).

Dyring E., S. Lindgren, and S. Martinelle. "Solar cycle variation in the attenuation length of the cosmic ray nucleon component", *Arkiv Geofys.*, **5**, No. 1, 87-90 (1966).

Dyring E. and B. Sporre. "On the multiplicity effect in an IGY neutron monitor", *Proc. 9th Intern. Cosmic Ray Conf*, London, **1**, 478-480 (1965).

Dyring E. and B. Sporre. "Multiplicity measurements on the Uppsala IGY-neutron monitor", *Arkiv geofys.*, **5**, No.1, 79-85 (1966).

Escobar I.V., N. Nerurkar, and R. Weil "Sidereal Anisotropy of High Energy Cosmic Rays - II", *Planet. Space Sci.*, **2**, 187-192 (1960).

Falkoner R.E., *Trans. Amer. Geophys. Union*, **28**, 385 (1947).

Fenton A.G., R.M. Jacklin, and R.B. Taylor. "Cosmic Ray observations at 42 m w.e. underground at Hobart, Tasmania", *Nuovo cimento*, **22**, No. 2, 285-295 (1961).

Forman M.A. "Solar-cycle variation in the mass absorption coefficients for the Climax and Chicago neutron monitors, 1953-1965", *J. Geophys. Res.*, **72**, No. 21, 5572-5575 (1967).

Forman M.A. "The relation between latitude and solar-cycle variations in the neutron monitor mass absorption coefficient", *Canad. J. Phys*, **46**, No. 10, Part 4, S1087-S1089 (1968).

George E.P. and P.T. Trent "Penetrating bursts of cosmic radiation", *Proc. Phys. Soc.* **64**, No. 8, 733-745 (1951)

Granitskij L.V., L.I. Dorman, S.G. Bortnik, G.A. Novikova, and I.M. Raikhbaum "Study of cosmic ray neutron component on the atmosphere depth 260-315 mb", *Izvestia Academy of Sci. of USSR*, Series Phys., **31**, No.8, 1322-1323 (1967).

Griffiths W.K., C.V. Harman, C.J. Hatton, and P. Ryder "Studies of the barometric coefficients of IGY and NM-64 neutron monitors", *Proc. 9th Intern. Cosmic Ray Conf.*, London, **1**, 475-477 (1965)

Griffiths W.K., C.J. Hatton, P. Ryder and C.V. Harman "The variation of the barometric coefficient of the Leeds neutron monitor during the solar cycle 1954-1965", J. Geophys. Res., 71, No. 7, 1895-1898 (1966).

Iucci N., G. Villoresi, L.I.Dorman, and M Parisi "Cosmic ray survey to Antarctica and coupling functions for neutron component near solar minimum (1996-1997), 2, Determination of meteorological effects", *J. Geophys. Res.* **105** , No. A9 , pp. 21,035-21,046, 2000.

Kaminer N.S. "On the barometric effect of neutron component in periods of cosmic ray bursts", *Geomagnetism and Aeronomy*, **7**, No. 5, 806-809 (1967).

Kamphouse J.L. "Correlation of neutron monitor pressure coefficient and the solar cycle", *J. Geophys. Res.*, **68**, No. 19, 5608-5610 (1963).

Kapustin I.N., V.A. Radkevich, and V.T. Ustinovich "Multiplicity measurements", *Acta Phys. Acad. Sci. Hung.*, **29**, Suppl. 2, 631-633 (1970).

Karpov S.N., V.V. Alexeenko, Z.M. Karpova, N.S. Khaerdinov, and V.B. Petkov "A Search for the 200 GeV Muon Intensity Bursts during Powerful Solar Flares of 23rd Solar Cycle", *Proc. 28th Intern. Cosmic Ray Conf.*, Tsukuba, **6**, 3407-3410 (2003).

Kawasaki S. "On the anomalous time variation in cosmic ray neutron intensity caused by atmospere pressure deviation due to high wind", *Scient. Papers Inst. Phys. and Chem. Res.*, **60**, No. 2, 3 (1966).

Kent D.W. and M.A. Pomerantz "Longterm variation of the atmospheric attenuation length of the nucleonic component of cosmic rays", *Trans. Amer. Geophys. Union*, **47**, No. 1, 157 (1966).

Kisselbach V.G. and R.L. Chasson. "Barometric correction anomaly and nucleonic component time variations during IQSY", *Proc. 9th Intern. Cosmic Ray Conf*, London, **1**, 471-474 (1965).

Kodama M. and A. Inoue "Differential rigidity response of different multiplicities in the NM-64 neutron monitor", *Acta Phys. Acad. Sci. Hung.*, **29**, Suppl. 2, 577-581 (1970).

Kodama M. and Y. Ishida. " Multiplicity measurements of cosmic ray neutron monitors in low latitude", *Rept. Ionosphere and Space Res.*, Japan, **21**, No. 1-2, 55-58 (1967).

Kodama M. and T. Ohuchi "Latitude survey of neutron multiplicity using a ship-borne NM-64 neutron monitor", *Proc. 10th Intern. Cosmic Ray Conf.* Calgary, *Canad. J. Phys.*, **46**, S1090-S1093 (1968).

Krasilnikov D.D. and S.I. Nikolsky "Spectrum and meteorological effects of ionization bursts", *Trudy YaFAN, Ser. Phys.*, **1**, 48-54 (1955).

Krivoshapkin P.A., V.P. Mamrukova, G.V. Skripin, and G.V. Shafer. Variations of the burst frequency registered with the ionization chamber in Yakutsk, *Proc. 25th Intern. Cosmic Ray Conf*, Durban, **2**, 205-207 (1997).

Lapointe S.M. and D.C. Rose. "A statistical analysis of the barometer coefficients for cosmic ray intensities", *Canad. J. Phys.*, **40**, No. 6, 687-697 (1962).

Lockwood J.A. and A.R. Calawa "On the barometric pressure coefficient for cosmic ray neutrons", *J. Atmos. and Terr. Phys.*, **11**, 23-31 (1957).

MacAnuff J.W., *Ph. D. Thesis*, London (1951). See in George, 1952 (References to Chapter 2).

Mathews T. "Characteristics of Forbush decreases in cosmic ray intensity observed underground", *Philos. Mag.*, **8**, No. 87, 387-400 (1963).

McCracken K.G. "The cosmic ray flare effect, 1. Some new methods of analyses", *J. Geophys. Res.*, **67**, No. 2, 423-434 (1962).

McCracken K.G. and D.H. Johns. "The attenuation length of the high energy nucleonic component of the cosmic radiation near sea level", *Nuovo cimento*, **13**, No. 1, 96-107 (1959).

McCracken K.G. and R.A.R. Palmeira. "Comparison of solar cosmic ray injections including July 17, 1959 and May 4, 1960", *J. Geophys. Res.*, **65**, No. 9, 2673-2684 (1960).

Nagashima K., K. Fujimoto, and I. Morishita "Interplanetary magnetic field collimated cosmic ray flow across magnetic shock from inside of Forbush decrease, observed as local-time-dependent precursory decrease on the ground", *J. Geophys. Res.*, **99**, No. 21, 419-421 (1994).

Niemi S. "On the variations of the mean recorded multiplicity in the super neutron monitor 9-NM-64 at Oulu, Finland, for the period November 5 1965 to April 30 1967", *Canad. J. Phys.*, **46**, No. 14, 1645-1646 (1968)

Nobles R.A., L. Newkirk, M. Walt, and E.B. Hughes. "Neutron multiplicity monitor observations of secondary cosmic radiation at sea level 3800 meter elevation in 1965", *Trans. Amer. Geophys. Union*, **41**, No. 1, 127 (1966).

Poirier J. and C. D'Andrea "Ground level muons in coincidence with the solar flare of 15 April 2001", *J. Geophys. Res.*, **107**, No. A11, SSH-14, 1-9 (2002).

Raubenheimer B.C. and P.H. Stoker. "Attenuation coefficients of various cosmic ray components in the lower atmosphere", *Proc. 12th Intern. Cosmic Ray Conf.*, Hobart (Australia), **3**, 893-899 (1971).

Rogava O.G. and L.Kh. Shatashvili "Cyclic variations of the barometric coefficient of the neutron component of cosmic rays", *Geomagnetism and Aeronomy*, **31**, 343-345 (1991).

Ryan J.M. "Detection of 6 November 1997 Ground Level Event by Milagrito", *Proc. 26th Intern. Cosmic Ray Conf.* Salt Lake City, **6**, 378-381 (1999).

Sandor T., A. Somogyi, and F. Telbisz. "On the methods generally used to compensate the atmospheric effects of the muon component of the cosmic radiation", *Nuovo cimento*, **23**, No. 6, 1080-1088 (1962).

Sergeev A.V. and A.A. Luzov. "Barometric coefficient for neutron component", *Cosmic Rays*, Moscow, No. 3, 163-165 (1961)

Shamos M.A. and A.R. Liboff. "A new measurement of the intensity of cosmic ray ionization at sea level", *J. Geophys. Res.*, **71**, No. 19, 4651-4660 (1966).

Shatashvili L. Kh. and O.G. Rogava. "The cyclic variations of the barometric coefficient of the cosmic ray neutron intensity", *Proc. 24th Intern. Cosmic Ray Conf.*, Rome, **4**, 1176-1179 (1995).

Simpson J.A. and W.C. Fagot "Properties of the low energy nucleonic component at large atmospheric depth" *Phys. Rev.*, **90**, No.6, 1068-1072 (1953).

Simpson J.A., W.H. Fonger, and S.B. Treiman. "Cosmic radiation intensity-time variations and their origin, 1. Neutron intensity variation method and meteorological factors", *Phys. Rev.*, **90**, 934-950 (1953).

Simpson N.G. and D.V. Slade. "Fast neutron attenuation coefficient in the atmosphere", *Proc. 12th Intern. Cosmic Ray Conf.*, Hobart (Australia), **3**, 881-886 (1971).

Singh P., J.A. Lockwood, and H. Razdan "Altitude dependence of the barometric coefficient of cosmic ray neutron monitors", *J. Geophys. Res.*, **75**, No. 22, 4354-4356 (1970).

Stinchcomb T.G. "Experiments on large cosmic-ray bursts under thick absorbers at 11500 feet elevation", *Phys.Rev.*, **83**, No. 2, 422-431 (1951).

Tongiorgi V. "On the mechanism of production of the neutron component of the cosmic radiation", *Phys. Rev.*, **76**, No. 4, 517-526 (1949).

Yanchukovsky V.L. "Modulation effect of barometric coefficient of neutron component of secondary cosmic rays", *Proc. 24th Intern. Cosmic Ray Conf.*, Rome, **4**, 1145-1147 (1995).

Yanchukovsky V.L. and G.Y. Philimonov "Barometric effect of cosmic rays as a function of several variables", *Proc. 25th Intern. Cosmic Ray Conf.*, Durban, **2**, 445-448 (1997).

Zier M. and R. Knuts. "Zur Bestimmung der atmospharishen Korrekturgrosen fur Intensitatsmessungen der kosmischen Stahlung", Z. Meteorol., 15, No. 10-12, 350-352 (1961).

References for Chapter 7

Bachelet F., P. Balata, and N. Iucci. "Some properties of the radiation recorded by the IGY cosmic-ray neutron monitors in the lower atmosphere", *Proc. 9th Intern. Cosmic Ray Conf.*, London, **1**, 481-482 (1965).

Bachelet F. and A.M. Conforto "Atmospheric effects on the cosmic ray total intensity at sea level", *Nuovo Cimento*, **4**, No. 6, 1479-1495 (1956).

Belov A.V., L.I. Dorman, R.T. Gushchina, and V.G. Yanke "Temporal and latitude dependence of the temperature effect for neutron component of cosmic rays", *Proc. 24th Intern. Cosmic Ray Conf.*, Rome, **4**, 1141-1144 (1995).

Belov A.V., R.T. Gushchina, and V.G. Yanke "The temperature effect of cosmic ray neutron component", *Geomagnetism and Aeronomy*, **37**, No. 2, 100-106 (1997).

Bercovitch M. and B.C. Robertson "Meteorological factors affecting the counting rate of neutron monitors", *Proc. 9th Intern. Cosmic Ray Conf*, London, **1**, 489-491 (1965).

Berdichevskaya T.M., B.F. Shvartsman, and L.D. Fuks "The temperature effect in season and daily variations of cosmic ray meson intensity on the Cape Shmidt", *Problems of Arctic*, No. 4, 51-64 (1957).

Blackett P.H. "On the instability of the barytron and the temperature effect of cosmic rays", *Phys. Rev.*, **54**, 973-974 (1938)

Blokh Ya.L., L.I. Dorman and M.M. Dubrovin "Cosmic ray meteorological effects underground", *Cosmic Rays* (Moscow), No.3, 166-169 (1961).

Blokh Ya.L., S.N. Vernov, L.I. Dorman, and M.M. Dubrovin "Preliminary results of investigations of cosmic ray variations underground", *Cosmic Rays*, Moscow, No. 1, 37-47 (1959).

Carmichael H., M. Bercovitch, and J.F. Steljes "A comparison of several methods of correcting cosmic ray meson intensity for atmosphere temperature variations", *Proc. 8th Intern. Cosmic Ray Conf.*, Jaipur, **2**, 350-355 (1963)

Carmichael H., M. Bercovitch, and J.F. Steljes "Application of Canadian radiosonde data to the correction of cosmic ray intensity", *Trans. Amer. Geophys. Union*, **46**, No. 1, 97 (1965a).

Carmichael H., M. Bercovitch, and J.F. Steljes "Introduction of meteorological corrections into meson monitor data", *Proc. 9th Intern. Cosmic Ray Conf.*, London, **1**, 492-494 (1965b)

Chasson R.L., V.I. Kisselbach, and T.C. Sharma "Atmospheric water vapor and attenuation of the cosmic-ray nucleonic component", *J. Geophys. Res.*, **71**, No. 21, 5183-5184 (1966).

Dorman L.I. "On the theory of cosmic ray meteorological effects" *Reports of Academy of Sciences of USSR (DAN SSSR),* Moscow, **94**, No. 3, 433-436 (1954a).

Dorman L.I. "On the temperature effect of the hard component of cosmic rays" *Reports of Academy of Sciences of USSR (DAN SSSR),* Moscow, **95**, No. 1, 49-52 (1954b).

Dorman L.I., A.I. Kuzmin, G.V. Tyanutova, E.L. Feinberg, and Yu.G. Shafer "Variations of cosmic ray intensity and the role of meteorological factors", *Zh. Exper. Theor. Phys. (JETP),* **26**, No. 5, 537-544 (1954).

Dorman L.I., A.A. Lagutin, and G.V. Chernyaev "Temperature effect of neutron component", *Proc. 21th Intern. Cosmic Ray Conf.*, Adelaide, **7**, 81-84 (1990).

Dorman L.I. and V.G. Yanke "To the theory of cosmic ray meteorological effects, I", *Izvestia Ac. of Sci. USSR*, Series Phys., **35**, No. 12, 2556-2570 (1971a).

Dorman L.I. and V.G. Yanke "To the theory of cosmic ray meteorological effects, II", *Izvestia Ac. of Sci. USSR*, Series Phys., **35**, No. 12, 2571-2582 (1971b).

Duperier A. "The meson intensity at the surface of the Earth and the temperature at the production level", *Proc. Phys. Soc.*, **62A**, No. 11, 684-696 (1949).

Duperier A. "On the positive temperature effect of the upper atmosphere and the process of meson production", *J. Atm. Terr. Physics*, **1**, No. 5-6, 296-310 (1951)

Ehmert A. "On the correction of muon intensity on atmosphere temperature", *Proc. 6th Intern. Cosmic Ray Conf.*, Moscow, **4**, 22-26 (1960).

Farley F.J.M. and J.R. Storey, "Time Variations of Extensive Air Showers", *Proc. Phys. Soc., Section **B**,* **70**, 840-844 (1957).

French W.R. and R.L. Chasson "Atmospheric effects on the hard component of cosmic radiation near sea level", *J. Atmosph. Terrestr. Phys.*, **14**, No. 1-2, 1-18 (1959),

Glokova E.S. "Some results of investigations of variations of cosmic ray hard component", *Izv. Ac. of Sci. of USSR*, Serie Phys., **20**, No. 1, 47-54 (1956).

Glokova E.S. "Annual variations of cosmic ray intensity and temperature corrections", *Proc. of Yakutsk Branch of Academy of Sciences of USSR*, Series Physics, No. 3, 84-91 (1960a).

Glokova E.S. "Annual variations of cosmic ray intensity and temperature corrections", *Proc. 6th Intern. Cosmic Ray Conf.*, Moscow, **4**, 32-33 (1960b)

Glokova E.S. "Daily variation of cosmic ray hard component in the minimum of solar activity", *Proc. 6th Intern. Cosmic Ray Conf*, Moscow, **4**, 250-257 (1960c).

Glokova E.S. "To the problem on the sidereal-daily effect in cosmic rays in 1954", *Cosmic Rays*, Moscow, No. 4, 225-228 (1961).

Glokova E.S., L.I. Dorman, N.S. Kaminer, and G.V. Tyanutova "Intensity variations of the cosmic ray hard component during the cycle of solar activity", *Preprint NIZMIR*, Moscow (1955).

Glokova E.S., N.A. Mishina, N.S. Kaminer "Cyclic and season variations of the cosmic ray intensity daily wave", *Proc. of Yakutsk Branch of Academy of Sciences of USSR*, Series Physics, No. 2, 93-106 (1958).

Harman C.V. and C.H. Hatton "Contributions to the counting rate and the temperature dependence of neutron monitors", Canad. J. Phys., 46, No. 10, Part 4, 1052-1056 (1968).

Kaminer N.S. "Influence of small chromospheres flares on the cosmic ray hard component intensity", *Proc. of Yakutsk Branch of Academy of Sciences of USSR*, Series Physics, No. 3, 92-98 (1960).

Kaminer N.S., S.F. Ilgach, and T.S. Khadakhanova "The temperature effect of cosmic ray neutron component", *Geomagnetism and Aeronomy*, **4**, No. 4, 653-658 (1964a).

Kaminer N.S., S.F. Ilgach, and T.S. Khadakhanova "The temperature effect of cosmic ray neutron component in the period of high solar activity", *Geomagnetism and Aeronomy*, **4**, No. 5, 946-947 (1964b).

Kaminer N.S., S.F. Ilgach, and T.S. Khadakhanova "Non-regular variations of intensity of cosmic ray neutron component caused by the temperature effect", *Geomagnetism and Aeronomy*, **4**, No. 6, 1116-1117 (1964c).

Kaminer N.S., S.F. Ilgach, and T.S. Khadakhanova "Temperature effect of the cosmic ray neutron component", *Proc. 9th Intern. Cosmic Ray Conf.*, London, **1**, 486-488 (1965).

Kaminer N.S. and T.S. Khadakhanova "Annual variations of cosmic ray neutron component and the temperature effect", *Geomagnetism and Aeronomy*, **6**, No. 5, 921-922 (1966).

Krasil'nikov D.D. "Daily effect of the cosmic ray hard component intensity in cloudy and clear days", *Proc. of Yakutsk Branch of Academy of Sciences of USSR*, Ser. Phys., No. 1, 19-22 (1955).

Kuzmin A.I. "On the contribution of the meteorological variations of the Earth's atmosphere in the daily variations of cosmic ray intensity", *Zh. Exper. & Theor. Phys. (JETP)*, **28**, No. 5, 614-616 (1955a).

Kuzmin A.I. "On the daily variations of cosmic ray hard component global intensity according to Yakutsk station data", *Proc. of Yakutsk Branch of Academy of Sciences of USSR*, Ser. Phys., No. 1, 11-18 (1955b).

Kuzmin A.I. and A.A. Danilov "On the cosmic ray meteorological effects underground on the depth smaller than 100 *m* w.e.", *Proc. Yakutsk Branch of Academy of Sciences USSR*, Series Physics, N. 3, 58-64 (1960).

Kuzmin A.I., G.F. Krimskij, G.V. Skripin, N.P. Chirkov, G.V. Shafer, and Yu.G. Shafer "Some results of cosmic ray variation investigations by Yakutsk's group", *Investigations in Geomagnetism and Aeronomy*, Moscow, 115-125 (1963).

Kuzmin A.I. and G.V. Skripin "On the cosmic ray intensity decreasing during geomagnetic storms", *Proc. of Yakutsk Branch of Academy of Sciences of USSR*, Series Physics, No. 3, 121- 139 (1960).

Kuzmin A.I. and G.V. Skripin "Cosmic ray variations underground in 1957-1959", *Proc. of Yakutsk Branch of Academy of Sciences of USSR*, Series Physics, No. 4, 66-82 (1962).

Maeda K. and M. Wada "Atmospheric temperature effect upon the cosmic ray intensity at sea level", *J. Scient. Res. Inst. (Tokyo)*, **48**, 71-79 (1954)

Manzano J.R., J.G. Anderson, J.M. Cardoso, H. Ghielmetti, J.G. Roederer, and O.R. Santochi "Determination of the temperature coefficient for nuclear component at –23° geomagnetic latitude", *Abstracts of 6th Intern. Cosmic Ray Conf.*, Moscow, 178-179 (1959).

Mathews P.M. "Atmospheric effects on cosmic ray intensity at sea level", *Canad. J. Phys.*, **37**, No. 2, 85-101 (1959),

Messerschmidt W. "Geophysikalische Probleme bei Dauermessungen der kosmischen Strahlung", *Leopoldina*, No. 4-5, 190-196 (1961).

Sandor T, A. Somogyi and F. Teblisz "On the methods generally used to compensate the atmospheric effects of the muon component of the cosmic radiation", *Nuovo Cimento*, **23**, No. 6, 1080-1088 (1962).

Tanskanen P.J. "On the variation of cosmic ray meson intensity at sea level in connection with atmospheric disturbances (Ph. D. Thesis)", Sar. A., 6, No. 185, 1-96 (1965).

Trefall H. "On the positive temperature effect in the cosmic radiation and the $\pi \rightarrow \mu$ decay", *Physica*, **23**, No. 1, 65-72 (1957).

Wada M. "Atmospheric effects on the intensity of cosmic-ray mesons, II. The temperature effects", *Scient. Papers Inst. Phys. and Chem. Res.*, **55**, No. 1, (1961)

Wada M. and S. Kudo "The relation between cosmic-ray intensities and heights of isobar levels, II. On the positive temperature effect", *J. Sci. Res. Inst.*, Japan, **48**, 245-259 (1954).

Wang C.P. and A.H. Lee "Cosmic-ray muons and the atmospheric coefficients near geomagnetic equator", *J. Geophys. Res.*, **72**, No. 23, 6107-6109 (1967).

References for Chapter 8

Aglietta M., B. Alessandro, P. Antonioni et al. "Gamma-rays and ionizing component during thunderstorms at Gran Sasso", *Proc. 26th Intern. Cosmic ray Conference*, Salt Lake City, **7**, 351-354 (1999).

Alexeenko V.V., A.E. Chudakov, V.G. Sborshikov, and V.A. Tizengauzen "Short perturbations of cosmic ray intensity and electric field in atmosphere", *Proc. 19th Intern. Cosmic Ray Conf.*, La Jolla, **5,** 352-355 (1985).

Alexeenko V.V., A.B. Chernyaev, A.E. Chudakov, N.S. Khaerdinov, S. Kh. Ozrokov, and V.G. Sborshikov "Short perturbations of cosmic ray intensity and electric field in atmosphere", *Proc. 20th Intern. Cosmic Ray Conf.*, Moscow, **4,** 272-275 (1987).

Alexeenko V.V., N.S. Khaerdinov, A.S. Lidvansky, and V.B. Petkov "Electric field disturbances in the summer-time atmosphere and associated variations of CR intensity", *Proc. 27th Intern. Cosmic Ray Conf.*, Hamburg, **10,** 4161-4164 (2001).

Alexeenko V.V., N.S. Khaerdinov, A.S. Lidvansky, and V.B. Petkov "Transient variations of secondary cosmic rays due to atmospheric electric field and evidence for pre-lightning particle acceleration", *Phys. Lett.*, **A301**, No. 3-4, 299-306 (2002).

Attolini M.R., S. Cecchini, M. Galli, and J. Guidi "Cosmic-ray microvariations during thunderstorm perturbations", *Lettere al Nuovo Cimento*, **1**, 716-720 (1971)

Brunetti M., S. Cecchini, M. Galli, G. Giovannini, and A. Pagliarin "Gamma-ray bursts of atmospheric origin in the MeV energy range ", *Geophys. Res. Letter*, **27**, 1599-1602 (2000).

Cattani D., S. Cecchini, M. Galli, G. Giovannini, and A. Pagliarin "On the Acceleration of the Secondary Cosmic Ray Component in Low Atmosphere by Thunderstorms", *Proc. 28th Intern. Cosmic Ray Conf.*, Tsukuba, **7,** 4183 (2003).

Cecchini S., M. Galli, G. Giovannini, A. Pagliarin, and F. Sporetti "The sea-land transistion of the environmental radiation during the expeditions Italy – Antarctica – Italy", *Proc. 25th Intern. Cosmic Ray Conf.*, Durban, **2,** 417-420 (1997).

Clay J., H.F. Jongen, and A.J.J. Aarts "High energy electrons produced in thunderstorm", *Physica*, **18**, No. 11, 801-808 (1952)

Dorman L.I. "To the theory of cosmic ray meteorological effects", *Doklady Academy of Sciences of USSR* (Moscow), **94**, No. 3, 433-436 (1954).

Dorman L.I. "Geomagnetic and atmospheric effects in primary and secondary cosmic rays; cosmogeneous nuclei", *Proc. 20th Intern. Cosmic Ray Conf.*, Moscow, **8**, 186-237 (1987).

Dorman L.I. and I.V. Dorman "Cosmic-ray atmospheric electric field effects", *Canadian J. of Physics*, **73**, 440-443 (1995a).

Dorman L.I. and I.V. Dorman "On the theory of atmospheric electric field effect in cosmic ray muon component", *Proc. 24th Intern. Cosmic Ray Conf.*, Rome, **4**, 1160-1163 (1995b).

Dorman L.I. and I.V. Dorman "Formation of lead mesoatoms in neutron monitor by soft negative muons and expected atmospheric electric field effect in the cosmic ray neutron component", *Proc. 26th Intern. Cosmic Ray Conf.*, Salt Lake City, **7**, 309-312 (1999a).

Dorman L.I. and I.V. Dorman "Formation of lead mesoatoms in neutron monitor by soft negative muons and expected atmospheric electric field effect in the cosmic ray neutron component", In *Solar Wind Nine* (Ed. S.R. Habbal et al.), *AIP Conf. Proc.*, **471**, 791-794 (1999b).

Dorman L.I., I.V. Dorman, N. Iucci, M. Parisi, and G. Villoresi "On the possibility of atmospheric electric field effect in cosmic ray neutron component", *Proc. 24th Intern. Cosmic Ray Conf.*, Rome, **4**, 1164-1167 (1995).

Dorman L.I., I.V. Dorman, G. Villoresi, N. Iucci, and M. Parisi "Expected time-variations of neutron monitor counting rate caused by CR particle energy change in the periods of thunderstorms", *Proc. 25- th Intern. Cosmic Ray Conf.*, Durban (South Africa), **7**, 349-352 (1997).

Dorman L.I., I.V. Dorman, N. Iucci, M. Parisi, G. Villoresi, and I.G. Zukerman "Emilio Segre' Observatory and expected time-variations in neutron monitor total and multiplicities counting rates caused by cosmic ray particle energy change in the periods of thunderstorms", *Proc. 26th Intern. Cosmic Ray Conf.*, Salt Lake City, **7**, 425-428 (1999).

Dorman L.I., I.V. Dorman, N. Iucci, Yu. Ne'eman, L.A. Pustil'nik, A. Sternlieb, G. Villoresi, and I.G. Zukerman "Atmospheric Electric Field Effect in Different Neutron Multiplicities According to Emilio Segre' Observatory One Minute Data", *Proc. 27th Intern. Cosmic Ray Conf.*, Hamburg, **10**, 4019-4022 (2001a).

Dorman L.I., I.V. Dorman, N. Iucci, M. Parisi, Yu. Ne'eman, L.A. Pustil'nik, F. Signoretti, A. Sternlieb, G. Villoresi, and I.G. Zukerman " Thunderstorm's atmospheric electric field effects in the intensity of cosmic ray muons and in neutron monitor data", *J. Geophys. Res.,* **108**, No. A5, 1181-1188 (2003).

Dorman L.I., N. Iucci, A. Sternlieb, G. Villoresi, and I.G. Zukerman "Barometric coefficients for different neutron multiplicities according to ESO NM data (Israel) and data of University "Roma Tre" NM (Italy)", *Proc. 27th Intern. Cosmic Ray Conf.*, Hamburg, **10**, 4075-4078 (2001b).

Dorman L.I., N. Iucci, H. Mavromichalaki, L.A. Pustil'nik, A. Sternlieb, G. Villoresi, and I.G. Zukerman "Cosmic ray snow effect in different multiplicities according to Emilio Segre' Observatory NM hourly data", *Proc. 27th Intern. Cosmic Ray Conf.*, Hamburg, **10**, 4079-4082 (2001c).

Dorman L.I., A.A. Lagutin, and G.V. Chernyaev "Sensitivity of cosmic ray muon component to electric field in atmosphere", *Proc. 21th Intern. Cosmic Ray Conf.*, Adelaide, **7**, 92-95 (1990).

Eack K.B., W.H. Beasley, W.D. Rust, T.C. Marshall, and M. Stolzenburg "X-ray pulses observed above a mesoscale convective system, *Geophys. Res. Lett.*, **23**, 2915-2918 (1996a).

Eack K.B., W.H. Beasley, W.D. Rust, T.C. Marshall, and M. Stolzenburg, Initial results from simultaneous observation of X rays and electric fields in a thunderstorm, *J. Geophys. Res.*, **101**, 29637-29640 (1996b).

Gurevich A.V. and K.P. Zybin "Lightning initiation by simultaneous effect of runaway breakdown and cosmic ray showers", *UFN,* **A254**, 79-87 (2000).

Gurevich A.V., K.P. Zybin, and R. Russel-Dupre "Runaway electron mechanism of air breakdown and preconditioning during thunderstorms", *Physics Letters,* **A165**, 463-468 (1992).

Gurevich A.V., K.P. Zybin, and R.A. Russel-Dupre "Lightning initiation by simultaneous effect of runaway breakdown and cosmic ray showers", *Physics Letters,* **A254**, 79-87 (1999).

Khaerdinov N.S., A.S. Lidvansky, V.B. Petkov, Yu.P. Surovetsky, and A.F. Yanin "Estimate of Distance to Lightning Events Associated with Cosmic Ray Enhancements during Thunderstorms", *Proc. 28th Intern. Cosmic Ray Conf.*, Tsukuba, **7**, 4165-4168 (2003a).

Khaerdinov N.S., A.S. Lidvansky, V.B. Petkov, and Yu.P. Surovetsky "Effect of Disturbed Electric Field of the Atmosphere on Cosmic Rays: 1. Soft Component", *Proc. 28th Intern. Cosmic Ray Conf.*, Tsukuba, **7**, 4169-4172 (2003b).

Khaerdinov N.S., A.S. Lidvansky, and V.B. Petkov "Effect of Disturbed Electric Field of the Atmosphere on Cosmic Rays: 2. Hard Component", *Proc. 28th Intern. Cosmic Ray Conf.*, Tsukuba, **7**, 4173-4176 (2003c).

Khaerdinov N.S., A.S. Lidvansky, V.B. Petkov, and Yu.P. Surovetsky "Effect of Lightning on the Intensity of the Soft Component of Cosmic Rays", *Proc. 28th Intern. Cosmic Ray Conf.*, Tsukuba, **7**, 4185-4188 (2003d).

McCarthy M. and G.K. Parks "Further observations of X-rays inside thunderstorms", Geophys. Res. Lett., 12, No.6, 393-396 (1985)

Muraki Y., Y. Miyamoto, T. Takami et al. "Acceleration below Thunder Clouds at Mount Norikura", *Proc. 28th Intern. Cosmic Ray Conf.*, Tsukuba, **7**, 4177-4180 (2003).

Nobles R.A., L. Newkirk, M. Walt, and E.B. Hughes "Neutron Multiplicity Monitor Observations during 1965", *J. Geophys. Res.*, **72**, 3817-3827 (1967).

Parks G.K., B.H. Mauk, R. Spiger, J. Chin "X-ray enhancements detected during thunderstorm and lightning activities", *Geophys. Res. Letter*, **8**, 1176-1179 (1981).

Shaw G.E. "Background cosmic count increase associated with thunderstorm", *J. Geophys. Res.*, **72**, 4623-4626 (1967).

Shonland B.F.J. "Thunderstorms and penetrating radiation", *Proc. Royal Soc., London,* **A130**, 37-63 (1930).

Shonland B.F.J. and J.P.T. Vilfoen "On a penetrating radiation from thunderclouds", *Proc. Royal Soc., London,* **A140**, 314-334, 1933.

Suszynsky D.M. and R. Roussel-Dupre "Ground-based search for X rays generated by thunderstorms and lightning", *J. Geophys. Res.*, **101**, 23505-23516 (1996).

Takami T., Y. Muraki, Y. Matsubara et al. "Particle acceleration in thunderstorms", *Proc. 27th Intern. Cosmic ray Conference*, Hamburg, **10**, 4027-4030 (2001).

Vernetto S. for the EAS-TOP Collaboration "The EAS counting rate during thunderstorms", *Proc. 27th Intern. Cosmic ray Conference*, Hamburg, **10**, 4165-4168 (2001).

Wilson C.T. "The acceleration of β–particles in strong electric fields such as those of thunderclouds", *Proc. Cambridge Phil. Soc.*, **22**, 534-538 (1925).

References for Chapter 9

Belov A.V. and L.I. Dorman "On the dependence of cosmic ray barometric effect from the primary cosmic ray variation spectrum", *Geomagnetism and Aeronomy*, **20**, No. 1, 21-24 (1980).

Blokh Ya.L., L.I. Dorman, I.Ya. Libin, and V.G. Yanke "Calculations of meteorological coefficients for scintillation supertelescope", *Geomagnetism and Aeronomy*, **15**, No. 6, 1084-1086 (1975).

Brooke G., P.J. Hayman, Y. Kamiya, and A.W. Wolfendale "The interrelation of the primary and sea level spectra of cosmic rays", *Proc. Phys. Soc.*, **83**, No. 5, 853-869 (1964).

Brooke G., M.A. Meyer, and A.W. Wolfendale "The energy spectrum of cosmic ray pions near sea level in the range 0.7-150 GeV", *Proc. Phys. Soc.*, **83**, No. 5, 871-877 (1964).

Cini Castagnoli G. and M.A. Dodero "Temperature effect of the muon component underground and pion attenuation length", *Il Nuovo cimento*, **B51**, No. 2, 525-534 (1967).

Cranshow T.E. and A.M. Hillas "A model for the interpretation of air shower data", *Proc. 6th Intern. Cosmic Ray Conf.*, Moscow, **2**, 210-213 (1960).

Dorman L.I. "Two-meson theory of cosmic ray hard component temperature effect", *Special Report, Sci.-Res. Institute of Terrestrial Magnetism (NIIZM)*, Troitsk, Moscow region, (1951).

Dorman L.I. "Instructions for calculation of temperature corrections to hard component intensity data", *Special Report, Sci.-Res. Institute of Terrestrial Magnetism (NIIZM),* Troitsk, Moscow region (1952).

Dorman L.I. "On the temperature effect of the cosmic ray hard component", *Doklady Academy of Sciences of USSR* (Moscow), **94**, No.1, 49-52 (1954a).

Dorman L.I. "To the theory of cosmic ray meteorological effects", *Doklady Academy of Sciences of USSR* (Moscow), **94**, No. 3, 433-436 (1954b).

Dorman L.I. "Influence of meteorological factors on the cosmic ray latitude effect and the process of meson generation", *J. Experim. and Theoret. Phys. (JETP),* Moscow, **26**, No.5, 504-505 (1954c).

Dorman L.I. "On the nature of cosmic ray variations", *Ph. D. Thesis*, Physical Lebedev Institute Academy of Sciences of USSR, Moscow, pp. 328 (1955).

Dorman L.I. "Determination of cosmic ray barometrical effect by partial barometric coefficient", *Cosmic Rays* (NAUKA, Moscow), Vol. 8, 247-250 (1966).

Dorman L.I. "The cosmic ray barometric effect with taking into account of energetic spectrum and cut-off rigidity (the method of partial barometric coefficients)", *Acta Phys. Sci. Hung.*, **29**, Suppl. 2, 715-719 (1970).

Dorman L.I. and E.L. Feinberg "On the nature of cosmic ray variations", *Proc. of 4th Intern.Cosmic Ray Conf.*, Guanajhato, Mexico, 395-432 (1955).

Dorman L.I., A.I. Kuzmin, G.V. Tyanutova, E.L. Feinberg, and Yu.G. Shafer "Variations of cosmic ray intensity and role of meteorological factors", *J. of Experim. and Theoret. Phys. (JETP),* Moscow, **26**, No.5, 537-544 (1954).

Dorman L.I., A.A. Lagutin and G.V. Chernyaev "Temperature effect of neutron component", *Proc. 21th Intern. Cosmic Ray Conf.*, Adelaide, **7,** 81-84 (1990).

Dorman L.I. and A.V. Sergeev "Estimations of integral multiplicity partial barometric coefficient for secondary cosmic radiation neutron component", *Proc. of 6th All-Union Winter School on Cosmophysics*, Apatity, **2**, 79-80 (1969).

Dorman L.I. and A.V. Sergeev "Differential and integral barometric coefficients of neutron component", *Research in Geomagnetism, Aeronomy and Physics of the Sun*, Moscow, NAUKA, **20**, 320-328 (1971).

Dorman L.I. and L.E. Rishe "Calculations of the integral generation multiplicity, coupling coefficients and partial barometric coefficients for the cosmic ray neutron component observations at various altitudesusing the method of discontinues Markov processes including non-ordinary of nuclear-meson cascade", *Proc. of 13th Intern. Cosmic Ray Conf.,* Denver, **2**, 835-842 (1973).

Dorman L.I. and L.E. Rishe "Calculations of cosmic ray neutron component integral multiplicity, coupling coefficients and partial barometric coefficients by the method of non-ordinary Markov processes", *Geomagnetism & Aeronomy*, **14**, No. 3, 417-423 (1974).

Dorman L.I., O.G. Rogava and L.Kh. Shatashvili "Partial barometric coefficients of cosmic ray neutron component intensity", Proc. of the Institute of Geophysics Georgian Academy of Sciences, Tbilisi, METSNIEREBA, Vol. 35, pp. 20-27 (1976).

Dorman L.I. and V.V. Viskov "Estimation of coupling coefficients for muon component in three-dimensional model of elementary act", *Cosmic Rays* (NAUKA, Moscow), No. 7, 178-196 (1965).

Dorman L.I. and V.G. Yanke "To the theory of cosmic ray meteorological effects, I", *Izvestia Academy of Sciences USSR*, Series Phys., **35**, No. 12, 2556-2570 (1971a).

Dorman L.I. and V.G. Yanke "To the theory of cosmic ray meteorological effects, II", *Izvestia Academy of Sciences USSR*, Series Phys., **35**, No. 12, 2571-2582 (1971b).

Harman C.V. "Meteorological effects in neutron monitor data", *Ph. D. Thesis*, Univ. Leeds, Leeds (1967).

Hatton C.J. and W.K. Griffiths "Barometric coefficients of multiplicities in neutron monitors", *J. Geophys. Res.*, **73**, No. 23, 7503-7509 (1968).

Hayman P. and A. Wolfendale "The momentum spectrum of cosmic ray muons near sea level on the momentum range 5-1000 GeV/c", *Proc. Phys. Soc.*, **80**, No.3, 710-728 (1962).

Hughes E.B. and P.L. Marsden "Response of a standard IGY neutron monitor", *J. Geophys. Res.*, **71**, No. 5, 1435-1444 (1966).

Iucci N., G. Villoresi, L.I. Dorman, and M. Parisi " Cosmic Ray Survey to Antarctica and Coupling Functions for Neutron Component Near Solar Minimum (1996-1997) 2. Meteorological Effects and Correction of Survey Data", *Proc. 26th Intern. Cosmic Ray Conf.*, Salt Lake City, **7**, 321-324 (1999).

Iucci N., G. Villoresi, L.I. Dorman, and M. Parisi "Cosmic ray survey to Antarctica and coupling functions for neutron component near solar minimum (1996-1997), 2, Determination of meteorological effects ", *J. Geophys. Res.* **105** , No. A9, 21,035-21,046 (2000).

Kawasaki S., I. Kondo, and M. Wada "On the standard cosmic ray neutron monitor", *J. Scient. Res. Inst.*, **51**, 107-137 (1957).

Murthy G.T., K. Sivaprasad, M.V Srinivasa Rao, S.C. Tonwar, R.H. Valcha, and P.R. Viswanath "Calculations of average characteristics of EAS components and Monte Carlo calculations of their fluctuations using different models of nuclear interactions, 1. Methodology – lateral structure and transition curve of electrons", *Canad. J. Phys.*, **46**, No. 10, Part 2, S147-S153 (1968).

Pullar J.D. and E.G. Dymond "The penetrating component of cosmic radiation in the upper atmosphere", *Philos. Mag.*, **44**, No. 353, 565-577 (1953).

Rossi B. "Electrons and photons in cosmic rays", *Rev. Mod. Phys.*, **21**, No. 1, 104-112 (1949).

Viskov V.V., L.I. Dorman, and T.M. Krupitskaya "The theory of meteorological effects of muon component accounting data on elementary act", *Cosmic Rays,* No. 8, Moscow, 242-247 (1967).

Volkova L.V. "Temperature effect and mechanism of high energy muon generation in the atmosphere", Nuclear Physics, 12, No. 2, 347-359 (1970).

Wainio K.M., Preprint Air Force Cambridge Research Labs Rept., AFCRL-67-0149 (1967).

References for Chapter 10 and Preface for Part 3

Alanko K., I.G. Usoskin, K. Mursula, and G.A. Kovaltsov "Effective energy of neutron monitors", *Proc. 28th Intern. Cosmic Ray Conf.*, Tsukuba, **7**, 3901-3904 (2003).

Arnold J.R, M. Honda and D. Lal "Record of Cosmic-Ray Intensity in the Meteorites", *J. Geophys. Res.*, **66**, No.10, 3519-3531 (1961).

Bard E., G.M. Raisbeck, F. Yiou, and J. Jouzeel "Solar modulation of cosmogenic nuclide production over the last millennium: comparison between ^{14}C and ^{10}Be records", *Earth and Planetary Science Letters*, **150**, 453-462 (1997).

Beer J., A. Blinov, G. Bonani, et al. "Use of ^{10}Be in polar ice to trace the 11-year cycle of solar activity", *Nature*, **347**, 164-167 (1990).

Beer J., S. Tobias, and N. Weiss "An active sun throughout the Maunder Minimum", *Solar Phys.*, **181**, No. 1, 237-249 (1998).

Beer J., M.V. Vonmoos, R. Muscheler, K.G. McCracken, and W. Mende "Heliospheric Modulation over the past 10,000 Years as derived from Cosmogenic Nuclides", *Proc. 28th Intern. Cosmic Ray Conf.*, Tsukuba, **7**, 4147-4150 (2003).

Begeman F., J. Geiss, and D.C. Hess "Radiation age of a meteorite from cosmic-ray produced He^3 and H^3", *Phys. Rev.*, **107**, No. 2, 540-542 (1957).

Biswas M.M., C. Mayer-Böricke, and W. Gentner "Cosmic ray produced ^{22}Na and ^{26}Al activities in chondrites", in *Earth Science and Meteoritics*, North-Holland Publ. Co., Amsterdam, 207-218 (1963).

Bleichrodt J.F. "Mean tropospheric residence time of cosmic-ray-produced Beryllium-7 at north temperate latitudes", *J. Geophys. Res.*, **83**, No. NC6, 3058-3062 (1978).

Blinov A. "The dependence of cosmogenic isotope production rate on solar activity and geomagnetic field variations", in *Secular Solar and Geomagnetic Variations in the last 10,000 years*, edited by F.R. Stephenson and A.W. Wolfendale, Kluwer Acad., Norwell, Mass., 329-340 (1988).

Bodemann R., H.J. Lange, I. Leya, et al. "Production of residual nuclei by proton-induced reactions on C, N, O, Mg, Al and Si", *Nucl. Instr. Meth.*, **B82**, No. 1, 9-31 (1993).

Brown E.T., T.W. Trull, P. Jean-Baptiste et al. "Determinaton of cosmogenic production rates of ^{10}Be, ^{3}He, and ^{3}H in water", *Nuclear Instruments and Methods in Nuclear Research*, **B172**, 873-883 (2000).

Craig H.D. and D. Lal "The production rate of natural tritium", *Tellus*, **13**, 85-105 (1961).

Dibb J.E. "Atmospheric deposition of Beryllium-7 in the Chesapeake bay region", *J. Geophys. Res.*, **94**, No. D2, 2262-2265 (1989).

Dorman L.I. "Radiocarbon coupling coefficients and the functions of cosmic ray "response" in ^{14}C, I. The local and polar coupling coefficients in the Earth's atmosphere", *Proc. 15th Intern. Cosmic Ray Conf.*, Plovdiv, **4**, 369-373 (1977a).

Dorman L.I. "Radiocarbon coupling coefficients and the functions of cosmic ray "response" in ^{14}C, II. The atmospheric mixing and the planetary coupling coefficients, the magnetic and barometric coefficients", *Proc. 15th Intern. Cosmic Ray Conf.*, Plovdiv, **4**, 374-377 (1977b).

Dorman L.I. "Radiocarbon coupling coefficients and the functions of cosmic ray "response" in ^{14}C, III. The functions of the "response" in the planetary rate of radiocarbon production including the mixing in the atmosphere", *Proc. 15th Intern. Cosmic Ray Conf.*, Plovdiv, **4**, 378-382 (1977c).

Dorman L.I. "Radiocarbon coupling coefficients and the functions of cosmic ray "response" in ^{14}C, IV. The two-basin model of radiocarbon exchange on the Earth, estimation of the basis constants", *Proc. 15th Intern. Cosmic Ray Conf.*, Plovdiv, **4**, 383-386 (1977d).

Dorman L.I. "Radiocarbon coupling coefficients and the functions of cosmic ray "response" in ^{14}C, V. The two-basin model and the functions of the "response" in ^{14}C", *Proc. 15th Intern. Cosmic Ray Conf.*, Plovdiv, **4**, 387-391 (1977e).

Dorman L.I. "Five-basin model of the radiocarbon dynamics on the Earth including the temporal variations in the rate of production by cosmic rays. I. Set on equations, stationary case, estimates of the basic constants", *Proc. 15th Intern. Cosmic Ray Conf.*, Plovdiv, **4**, 395-399 (1977f).

Dorman L.I. "Five-basin model of the radiocarbon dynamics on the Earth including the temporal variations in the rate of production by cosmic rays. II. Nonstationary solution", *Proc. 15th Intern. Cosmic Ray Conf.*, Plovdiv, **4**, 400-404 (1977g).

Dorman L.I. "Peculiarities of cosmic ray research by radio-carbon method", *Proc. 6th All-Union Meeting on the Problem "Astrophysics Phenomena and Radio-Carbon"* (Tbilisi, 1976), Tbilisi, METSNIEREBA, 49-96 (1978).

Dorman L.I. "Cosmic Ray Nonlinear Processes in Gamma-Ray Sources", *Astronomy and Astrophysics*, Suppl. Ser., **120**, No. 4, 427-435 (1996).

Dorman L. I. "Cosmic rays and cosmogenic nuclides, 1. In space, inside bodies, in atmospheres", In *Towards the Millennium in Astrophysics*, ed. M.M. Shapiro, R. Silberberg and J.P. Wefel, World Sci. Publ. Co., Singapore, New Jersey, London, Hong Kong, 303-322 (1998a).

Dorman L. I. "Cosmic rays and cosmogenic nuclides, 2. Radiocarbon method and elements global mixing and exchange on the Earth", In *Towards the Millennium in Astrophysics*, M.M. Shapiro, R. Silberberg and J.P. Wefel, World Sci. Publ. Co., Singapore, New Jersey, London, Hong Kong, 323-352 (1998b).

Dunai T.J. "Scaling factors for production rates of in situ produced cosmogenic nuclides: a critical reevaluation ", *Earth Planet. Sci. Lett.*, **176**, 157-169 (2000).

Ebeoglu D.B., K.M. Wainio, K. More, and O.L. Tiffany "Monte Carlo calculations of radionuclide production in iron targets bombarded with 400-MeV protons", *J. Geophys. Res.*, **71**, No. 5, 1445-1451 (1966).

Eberhardt P. and J. Geiss "Meteorite classes and radiation ages" In *Isotopic and Cosmic Chemistry*, North-Holland Publ.Co., Amsterdam, 452-470 (1963).

Eberhardt P., J. Geiss, and H. Lutz "Neutrons in meteorites", in *Earth Science and Meteoritics*, North-Holland Publ. Co., Amsterdam, 143-168 (1963).

Eberhardt P., O. Eugster, and J. Geiss "Radiation Ages of Aubrites", *J. Geophys. Res.*, **70**, No. 18, 4427-4434 (1965).

Feely H.W., R.J. Larsen, and C.G. Sanderson "Factors that cause seasonal variations in Beryllium-7 concentrations in surface air", *J. Environ. Radioactivity*, **9**, No. 3, 223-249 (1989).

Hess W.N., E.H. Canfield, and R.E. Lingenfelter "Cosmic ray demography", *J. Geophys. Res.* **66**, 665-677 (1961).

Haigh J.D. "The impact of solar variability on climate", *Science*, **272**, No. 5264, 981-984 (1996).

Honda M. and J.R. Arnold "Effects of cosmic rays on meteorites", *Science*, **143**, No. 3603, 203-212 (1964).

Hoyt D.V. and K.H. Schatten "Group Sunspot Numbers: A new solar activity reconstruction", *Solar Phys.*, **181**, No. 2, 491-512 (1998).

Kruger S.T. and D. Heymann "Cosmic-ray-produced Hydrogen 3 and Helium 3 in Stony Meteorites", *J. Geophys. Res.*, **73**, No.14, 4784-4787 (1968).

Lal D. "^{10}Be in polar ice data reflect changes in cosmic ray flux or polar meteorology", *Geophys. Res. Lettrs*, **14**, No. 8, 785-788 (1987).

Lal D. "Theoretically expected variations in the terrestrial cosmic ray production of isotopes", in *Solar-Terrestrial Relationships*, edited by G.C. Castagnoli and D. Lal, Soc. Italiana di Fisica-Bologna-Italy, Bologna, 216-233 (1988).

Lal D. "Cosmic ray labeling of erosion surfaces - In situ nuclide production rates and erosion models", *Earth Planet. Sci. Lett.*, **104**, 424-439 (1991).

Lal, D. and B. Peters "Cosmic ray produced isotopes and their application to problems in geophysics", In *Progress in Elementary Particle and Cosmic Ray Physics* (eds. J.G. Wilson and S.A. Wouthysen), North-HollandPubl. Co., Amsterdam, **6**, 1-74 (1962).

Lal D. and B. Peters "Cosmic ray produced radioactivity on the Earth", in *Handbuch der Physik*, **XLVI/2**, 551-612, Springer Verlag, New York (1967).

Lal D. and V.S. Venkavaradan "Activation of cosmic dust by cosmic-ray particles", *Earth and Planetary Science Letters*, **3**, No. 4, 299-310 (1968).

Lal D., R.S. Rajan, and V.S. Venkatavaradan "Nuclear effects of solar and galactic cosmic ray particles in near-surface regions of meteorite", *Geochim. Cosmochim. Acta,* **31**, No. 10, 1859-1869 (1967).

Lavrukhina A.K. and T.A. Ibraev "Determination of preatmospheric size of meteorites on the basis of the effects of nuclear reactions induced by cosmic rays", *Izvestia Ac. of Sci. of USSR,* Ser. Phys., **30**, No. 11, 1794-1798 (1966).

Light E.S., M. Merker, H.J. Vershell, R.B. Mendel, and S.A. Korff "Time-dependent worldwide distribution of atmospheric neutrons and of their products, 2. Calculations", *J. Geophys. Res.,* **78**, 2741-2762 (1973).

Lingenfelter R.E. "Production of carbon-14 by cosmic ray neutrons", *Rev. Geophys. J.*, **1**, No. 1, 35-55 (1963).

Martell E.A. and H.E. Moore "Tropospheric aerosol residence times: a critical review", *J. Rech. Atmos.*, **8**, No. 3-4, 903-910 (1974).

Masarik J. and J. Beer "Monte Carlo simulation of particle fluxes and cosmogenic nuclide production in Earth's atmosphere", *Proc. 25th Intern. Cosmic Ray Conf.*, Durbin, **2**, 461-464 (1997).

Masarik J. and J. Beer "Simulation of particle fluxes and cosmogenic nuclide production in the Earth's atmosphere", *J. Geophys. Res.,* **104**, No. D10, 12099-12111 (1999).

Masarik J. and R.C. Ready "Terrestrial cosmogenic-nuclide production systematic calculated from numerical simulations", *Earth Planet. Sci. Lett.,* **136**, 381-395 (1995).

Matsunami T. and K. Megumi "Variation of ^{7}Be concentrations in surface air and in deposition with the solar activity", *Radioisotopes*, **43**, 334-340 (1994).

McCracken K.G. "Variations in the production of ^{10}Be due to the 11 year modulation of the cosmic radiation, and variations in the vector geomagnetic dipole", *Proc. 27th Intern. Cosmic Ray Conf.*, Hamburg, **10**, 4129-4132 (2001).

McCracken K.G. "The Accuracy of Cosmogenic 10Be as a Quantitative Measurement of the GCR", *Proc. 28th Intern. Cosmic Ray Conf.*, Tsukuba, **7**, 4127-4130 (2003).

McCracken K.G., J. Beer, and F.B. McDonald "Properties of the Long Term Heliospheric Modulation -Tests to be met by Modulation Theory", *Proc. 28th Intern. Cosmic Ray Conf.*, Tsukuba, **7**, 4123-4126 (2003).

McCracken K.G., D.F. Smart, M.A. Shea, and G.A.M. Dreschhoff "400 years of large fluence solar proton events", *Proc. 27th Intern. Cosmic Ray Conf.*, Hamburg, **8**, 3209-3212 (2001).

Nagashima K., S. Sakakibara, K. Murakami, et al. "Response and yield functions of neutron monitor, galactic cosmic-ray spectrum and its solar modulation, derived from all the available world-wide surveys", *Nuovo Cimento*, **C12**, No. 2, 173-209 (1989).

Newkirk L.L. "Calculation of low-energy neutron flux in the atmosphere by the Sn method", *J. Geophys. Res.* **68**, 1825-1839 (1963).

Nishiizumi K., R.C. Finkel, J. Klein, and C.P. Kohl "Cosmogenic production of ^{7}Be and ^{10}Be in water targets", *J. Geophys. Res.* **101**, 22225-22232 (1996).

O'Brien K. "Secular variations in the production of cosmogenic isotopes in the Earth's atmosphere", *J. Geophys. Res.* **84**, 423-431 (1979).

Oeschger H., J. Houtermann, H. Loosli, and M. Wahlen. "The constancy of cosmic radiation from isotope studies in meteorites and on the Earth", in *Radiocarbon Variations and Absolute Chronology*, edited by I.U. Olsen, John Wiley, New York (1969).

Pomerantz M.A. and S.P. Agrawal "Spatial distribution of cosmic-ray intensity and geomagnetic theory", *Philos. Mag.*, **7**, No. 81, 1503-1511 (1962).

Raisbeck G.M. and F. Yiou "Influence of solar activity on cosmogenic ^{7}Be in the atmosphere", *Proc. 16th Intern. Cosmic Ray Conf.*, Kyoto, **2**, 285-287 (1979).

Rehfeld S. and M. Heimann "Three dimensional atmospheric transport simulation of the radioactive tracers ^{210}Pb, ^{7}Be, ^{10}Be, and ^{90}Sr", *J. Geophys. Res.*, **100**, No. D12, 26141-26161 (1995).

Reiter E.R. "Stratospheric-tropospheric exchange processes", *Rev. Geophys. Space Phys.*, 13, 459-474 (1975).
Rowe M.W., D.D. Bogard, and P.K. Kuroda "Mass yield spectrum of cosmic-ray-produced xenon", *J. Geophys. Res.*, **71**, No. 19, 4679-4684 (1966).
Sakurai H., T. Aoki, T. Gandou, W. Kato, S. Gunji, and F. Tokanai "Daily Variation of Cosmogenic Nuclide Be-7 Concentration in the Atmosphere and Solar Activities", *Proc. 28th Intern. Cosmic Ray Conf.*, Tsukuba, **7**, 4221-4224 (2003).
Sakurai H., T. Masuda, K. Endo, et al. "Continuous ubservation of Be-7 in the atmosphere for 5 years", *Proc. 25th Intern. Cosmic Ray Conf.*, Durban, **2**, 473-476 (1997).
Sakurai H., Y. Shouji, T. Maeda et al. "A relation between daily variation of Be-7 concentration in atmosphere and sunspot numbers", *Proc. 27th Intern. Cosmic Ray Conf.*, Hamburg, **10**, 4138-4138 (2001).
Shapiro M.A. "Turbulent mixing within tropopause folds as a mechanism for exchange of chemical constituents between the stratosphere and troposphere", *J. Atmos. Sci.*, **37**, No. 5, 994-1004 (1980).
Shea M.A. and D.F. Smart "A summary of major solar proton events", *Solar Physics*, **127**, 297-320 (1990).
Singer S.F. "The Specific Ionization of the Cosmic Radiation above the Atmosphere", *Phys. Rev.*, **76**, No. 5, 701-702 (1949).
Singer S.F. and F.A. Paneth "Meteorites and cosmic rays", *Nature,* **170**, 728-729 (1952).
Steig E.J., P.J. Polissar, M. Stuiver, et al. "Large amplitude solar modulation cycles of ^{10}Be in Antarctica: implications for atmospheric mixing and interpretation of the ice core record", *Geophys. Res. Lett.*, **23**, 523-526 (1996).
Viezee W. and H.B. Singh "The distribution of Beryllium-7 in the troposphere: implications on stratospheric-tropospheric air exchange", *Geophys. Res. Lett.*, 7, No.10, 805-808 (1980).
Wasson J.T. "Radioactivity in Interplanetary Dust ", *Icarus*, **2**, No. 1, 54-88 (1963).
Yokoyama Y. and H. Mabuchi "Les nuclides radioactifs induits par le rayonnement cosmique solaire dans les chondrites", *C.R. Acad. Sci.* **264**, No. 8, B655-B657 (1967).
Yoshimori M., H. Hirayama, and S. Mori "Production of ^{7}Be Nuclei in the Earth's Upper Atmosphere from Galactic Cosmic Rays and Solar Energetic Particles", *Proc. 28th Intern. Cosmic Ray Conf.*, Tsukuba, **7**, 4273-4276 (2003a).
Yoshimori M., H. Hirayama, S. Mori, and K. Sasaki "Seasonal Variations in ^{7}Be Radioactivity Measured at Ground Level", *Proc. 28th Intern. Cosmic Ray Conf.*, Tsukuba, **7**, 4217-4220 (2003b).

References for Chapter 11

Amatuni A.Z., E.A Mamidzshanjan, S.G. Matinjan, S.I. Nikolsky, E.I. Tukish, and E.L. Feinberg "Project ANI and the perspective of the experimental study of super high energy particle interactions", In the book *Problems of Comic Ray Physics*, Nauka, Moscow, 251-266 (1987).
Babich L.P., T.V. Loiko, and V.A. Tsukerman "High-voltage nanosecond discharge in a dense gas at a high overvoltage with runaway electrons", *UFN*, **160**, No. 7, 49-82 (1990).
Baker M.B. and J.G. Dash "Mechanism of charge transfer between colliding ice particles in thunderstorms", *J. Geophys. Res.*, **99**, 10621-10626 (1994).
Bazilevskaya G.A. and A.K. Svirzhevskaya "On the stratospheric measurements of cosmic rays", *Space Sci. Rev.*, **85**, No.3-4, 431-521 (1988).
Beasley W., M.A. Uman, and P.L. Jr. Ruslen "Electric field, preceding cloud-to-ground lightning flashes", *J. Geophys. Res.*, **87**, No. C7, 4883-4902 (1982).
Beasley W.H., K.B. Eack, H.E. Morris, W.D. Rust, and D.R. Macgorman "Electric-field changes of lightning observed in thunderstorms", *Geophys. Res. Lett.*, **27**, No. 2, 189-192 (2000).
Christian H.J., R.J. Blakeslee, D.J. Bossipio et al. "Global frequency and distribution of lightning as observed by the optical transient detector", *Proc. 11th Intern. Conf. on Atmospheric Electricity*, Alabama, USA, 726-729 (1999).
Chubenko A.P., V.P. Antonova, S.Yu. Kryukov, V.V. Piskal, M.O. Ptitsyn, A.L. Shepetov, L.I. Vildanova, K.P. Zybin, and A.V. Gurevich "Intensive X-ray emission bursts during thunderstorms", *Physics Letters,* **A275**, 90-100 (2000).
Daniel R.R. and S.A. Stephens "Cosmic ray produced electrons and gamma rays in the atmosphere", *Rev. Geophys. Space Sci.*, **12**, No. 2, 233-258 (1974).
Eack K.B. "Balloon-borne X-ray spectrometer for detection of X rays produced by thunderstorms", *Rev. Sci. Instrum.*, **67**, 2005-2009 (1996).
Eack K.B., W.H. Beasley, W.D. Rust, T.C. Marshall, and M. Stolzenburg "Initial results from simultaneous observation of X rays and electric fields in a thunderstorm", *J. Geophys. Res.*, **101**, 29637-29640 (1996a).
Eack K.B., W.H. Beasley, W.D. Rust, T.C. Marshall, and M. Stolzenburg "X ray pulses observed above a mesoscale convective system", *Geophys. Res. Lett.*, **23**, No.21, 2915-2918 (1996b).

Eack K.B., D.M. Suszynsky, W.H. Beasley, R. Roussel-Dupre, E. Symbalisty "Gamma-ray emissions observed in a thunderstorm anvil", *Geophys. Res. Lett.*, **27**, No. 2, 185-188 (2000).

Ermakov V.I. "Lightning iniciation by galactic cosmic rays", *Proc. 9th Intern. Conf. Atmosper. Electr.*, St. Petersburg, **2**, 485-488 (1992).

Ermakov V.I., G.A. Bazilevskaya, P.E. Pokrevsky, and Y.I. Stozhkov "Ion balance equation in the atmosphere", *J. Geophys. Res. D.*, **102**, No. 19, 23413-23419 (1997).

Ermakov V.I. and Y.I. Stozhkov "New mechanism of thundercloud and lightning production", *Proc. 11th Intern. Conf. Atmosper. Electr.*, Alabama, USA, 242-245 (1999).

Ermakov V.I. and Y.I. Stozhkov "Mechanism of thundercloud electricity production", Preprint FIAN, No. 25, pp. 28 (2002)

Ermakov V.I. and Y.I. Stozhkov "Cosmic rays in the mechanism of thundercloud production", *Proc. 28th Intern. Cosmic Ray Conf.*, Tsukuba, **7**, 4157-4160 (2003).

Fulks J. and P. Meyer "Cosmic ray electrons in the atmosphere", *J. Geophys.*, **40**, 751- 759(1974).

Fullekrug M. "Global lightning triangulation", *Proc. 11th Intern. Conf. on Atmospheric Electricity*, Alabama, USA, 709-711 (1999).

Gish O.H. and G.R. Wait "Thunderstorms and Earth's General Electrification", *J. Geophys. Res.*, **55**, No. 4, 473-484 (1950).

Gurevich A.V. "On the number of accelerated particles in the ionized gas at different acceleration mechanisms", *JETP*, **38**, No. 5, 1597-1607 (1960).

Gurevich A.V., H.C. Carlson, Yu.V. Medvedev, and K.P. Zybin "Kinetic theory of runaway breakdown in inhomogeneous and thundercloud electric field", *Physics Letters*, **A282**, 180-185 (2001).

Gurevich A.V. and G.M. Milikh "Generation of X-rays due to multiple runaway breackdown inside thunderclouds", *Physics Letters*, **A262**, 457-463 (1999).

Gurevich A.V.and K.P. Zybin "Runaway breakdown and electric discharges in thunderstorms ", *UFN*, **171**, No. 11, 1177-1199 (2001).

Gurevich A.V., K.P. Zybin, and R. Russel-Dupre "Runaway electron mechanism of air breakdown and preconditioning during thunderstorms", *Physics Letters*, **A165**, 463-468 (1992).

Gurevich A.V., K.P. Zybin, and R.A. Russel-Dupre " Lightning initiation by simultaneous effect of runaway breakdown and cosmic ray showers ", *Physics Letters*, **A254**, 79-87 (1999).

McCarthy M. and G.K. Parks. "Further observations of X-rays inside thunderstorms ", *Geophys. Res. Lett.*, **12**, No.6, 393-396 (1985)

Marshall T., M. McCarthy and W. Rust "Electric field magnitudes and lightning initiation in thunderstorms", *J. Geophys. Res.*, **100**, 7097-7104 (1996a).

Marshall T., W. Rust and H. Stolzenberg "Electrical structure and updraft speeds in thunderstorms over the southern Great Plains", *J. Geophys. Res.*, **100**, 1001-1016 (1996b).

Orville R.E. and G.R. Huffines "Lightning ground flash measurements over contiguous United States: a ten year summary 1989-1998", *Proc. 11th Int. Conf. Atmosph. Electr.*, Alabama, 412 (1999).

Orville R.E. and G.R. Huffines "Lightning ground flash measurements over contiguous United States: 1995-97", *Mon. Weather Rev.*, **127**, 2693-2703 (1999).

Orville R.E. and G.R. Huffines "Cloud-to-ground lightning in the United States: NLDN results in the first decade, 1989-1998", *Mon. Weather Rev.*, **129**, 1179-1193 (2001).

Roble R.G. "On solar-terrestrial relationships in the atmospheric electricity", *J. Geophys. Res.*, **D90**, No. 4, 6000-6012 (1985).

Rodger C.J. "Red sprites, upward lightning, and VLF perturbations", *Rev. Geophysics*, **37**, No. 3, 317-336 (1999).

Rusanov A.I. and V.L. Kuzmin "Electric field influence on the surface tension of polar liquid", *Kolloidny Journal*, **39**, No. 2, 388-390 (1977).

Sentman D.D. and E.M. Wescott "Red sprites and blue jets: high-altitude optical emissions linked to lightning", *EOS*, **77**, No. 1, 1-24 (1982).

Stergis C.G., G.C. Rein, and T. Kangas "Electric field measurements above thunderstorms", *J. Atmosph. and Terr. Phys.*, **11**, 83-90 (1957).

Stozhkov Yu. I. "The role of cosmic rays in atmospheric processes", *J. Phys. G: Nucl. Part. Phys.*, **28**, 1-11 (2002).

Stozhkov Yu. I., V.I. Ermakov, and P.E. Pokrevsky "Cosmic rays and atmospheric processes", *Izvestia Academy of Sci.*, Ser. Phys., **65**, No. 3, 406-410 (2001).

Suszynsky D.M., R. Roussel-Dupre, and G. Shaw "Ground-based search for X rays generated by thunderstorms and lightning", *J. Geophys. Res.*, **101**, 23505-23516 (1996).

Uman M.A. "Natural and artificially lightning and test standards", *Proceedings of the IEEE*, **76**, No. 12, 5-26 (1988).

Vaughan O.H. and B. Vonnegut "Recent observations of lightning discharges from the top of a thundercloud into the clear air above", *J. Geophys. Res.*, **94**, No. D11, 13179-13182 (1989).

Wilson C.T. "The acceleration of β–particles in strong electric fields such as those of thunderclouds", *Proc. Cambridge Phil. Soc.*, **22**, 534-538 (1925a).

Wilson C.T.R. "The Electric Field of a Thundercloud and Some of its Effects", *Proc. Roy. Soc.*, London, **37**, 32D (1925b).

References for Chapter 12

Adams G.W. and A.J. Masley "Production rates and electron densities in the lower ionosphere due to solar cosmic rays", *J. Atmosph. Terr. Phys.*, **77**, No 3, 289-298 (1965).

Ahluwalia H.S. and L.I. Dorman "Transverse cosmic ray gradients in the heliosphere and the solar diurnal anisotropy", *J. Geophys. Res.*, **102**, No. A8, 17433-17443 (1997).

Bailey D.K. "Disturbances in the lower ionosphere observed at VHE following the solar flare of 23 February 1956, with particular reference to auroral-zone absorption", *J. Geophys. Res.*, **62**, 431-463 (1957).

Bailey D.K. "Abnormal ionization in the lower ionosphere associated with cosmic ray flux enhancements", *Proc. IRE*, **47**, No. 2, 255-256 (1959).

Bates D.R. "Recombination of small ions in the troposphere and lower stratosphere", *Planet. Space Sci.*, **30**, No. 12, 1275-1282 (1982).

Bazilevskaya G.A. and A.K. Svirzhevskaya "On the stratospheric measurements of cosmic rays", *Space Sci. Rev.*, **85**, No. 3-4, 431-521 (1998).

Bazilevskaya G.A., M.B. Krainev, and V.S. Makhmutov "Effects of cosmic rays on the Earth's environment", *J. Atmosph. Solar-Terr. Phys.*, **62**, No. 17-18, 1577-1586 (2000).

Belrose J.S., M.H. Defenport, and R. Weekes "Some unusual radio observations made on 23 February 1956", *J. Atmosph. Terr. Phys.*, **8**, No 4-5, 281-286 (1956).

Clem J.M. and L.I. Dorman "Neutron monitor response functions", *Space Science Rev.*, **93**, 335-359 (2000).

Cooper J.F., T.G. Guzik, J.P. Wefel, K.R. Pyle, and I.G. Richardson "Polar cap intensity structure during the 22 July 1982 flare: correlation to interplanetary fluxes and anisotropies". *Proc. 24th Intern. Cosmic Ray Conf.*, Rome, **4**, 1133-1136 (1995).

Davis L.R. and K.W. Ogilvie "Rocket observations of solar protons during the November 1960 events", *J. Geophys. Res.*, **67**, No. 5, 1711-1716 (1962)

Dorman L.I. "Analytical approach to the problem of the rate of ion production by cosmic rays and precipitating particles in the low-energy range", *Proc. 15th Intern. Cosmic Ray Conf.*, Plovdiv, **4**, 411-416 (1977a).

Dorman L.I. "The ionospheric coupling coefficients and the spectrographical method for studying the extraterrestrial cosmic ray variations and the changes in the geomagnetic cut-off rigidities on the basis of the data of the ionospheric and riometric observations", *Proc. 15th Intern. Cosmic Ray Conf.*, Plovdiv, **4**, 405-410 (1977b).

Dorman L.I. "Methods of cosmic ray variation research by difference ionospheric and radio-carbonic coupling coefficients", *Izvestia Academy of Sciences USSR*, Series Phys., **42**, No. 5, 1092-1097 (1978).

Dorman L.I. "Cosmic ray long-term variation: even-odd cycle effect, role of drifts, and the onset of cycle 23", *Adv. Space Res.*, **27**, No. 3, 601-606 (2001).

Dorman I.V. and Dorman L.I. "Analytical approach to direct and inverse problems in the problem of cosmic ray influence on the lower ionosphere ", *Izvestia Academy of Sciences USSR*, Series Phys., **37**, No. 6, 1327-1331 (1973a).

Dorman I.V. and Dorman L.I. "Analytical solution to the direct and inverse problems for the solar cosmic ray effect on lower ionosphere", Proc. of 13th Intern. Cosmic Ray Conf., Denver, Vol. 2, pp. 1108-1115 (1973b).

Dorman L.I., I.V. Dorman, N. Iucci, M. Parisi, and G. Villoresi "Hysteresis between solar activity and cosmic rays during cycle 22: the role of drifts, and the modulation region", *Adv. Space Res.*, **27**, No. 3, 589-594 (2001a).

Dorman L.I., N. Iucci, and G. Villoresi "Time lag between cosmic rays and solar activity; solar minimum of 1994-1996 and residual modulation", *Adv. Space Res.*, **27**, No. 3, 595-600 (2001b).

Dorman L.I. and I.D Kozin "Determination of the variations in the integral energy spectrum of cosmic rays on the basis of radio wave propagation data", *Proc. 15th Intern. Cosmic Ray Conf.*, Plovdiv, **4**, 434-438 (1977).

Dorman L.I. and T.M. Krupitskaya "On the possibility of determination of solar cosmic ray energy spectrum and geomagnetic cut-off rigidity by ionospheric data", *Geomagnetism and Aeronomy*, **12**, No. 2, 180-183 (1972).

Dorman L.I. and Krupitskaya T.M., 1975. "Calculations of expected ratio of solar cosmic ray ion generation speeds on different altitudes", Cosmic Rays (Moscow, NAUKA), Vol. 15, pp. 30-33.

Dorman L.I., T.M. Krupitskaya, and M.I. Tyasto "Influence of cut-off rigidity changes on the speed of electron generation by cosmic rays in the atmosphere", *Cosmic Rays* (Moscow, NAUKA), Vol. 13, 98-102 (1972).

Dorman L.I., Sergeev A.V., Luzov A.A., Matyukhin Yu.G., Mamrukova V.P. and Yanchukovsky A.L. "Spectrographical method of cosmic ray intensity variations", *Izvestia Academy of Sciences of USSR*, Series Phys., **32**, No. 11, 1896-1903 (1968).

Ellison M.A. and J.H. Reid "A long-wave anomaly associated with the arrival of cosmic ray particles of solar origin on 23 February 1956", *J. Atmosph. Terr. Phys.*, **8**, No 4-5, 290-293 (1958).

Elsasser W., E.P. Nay, and J.R. Winckler "Cosmic-ray intensity and geomagnetism", *Nature*, **178**, 1226-1227 (1956).

Ermakov V.I., G.A. Bazilevskaya, P.E. Pokrevsky, and Yu. I. Stozhkov "Cosmic rays and ion production in the atmosphere". *Proc. 25th Intern. Cosmic Ray Conf.*, Durbin, **7**, 317-320 (1997a).

Ermakov V.I., G.A. Bazilevskaya, P.E. Pokrevsky, and Yu. I. Stozhkov "Ion balance equation in the atmosphere", *J. Geophys. Res.*, **102**, No. D19, 23413–23419 (1997b).

Ermakov V.I., G.A. Kokin, A.V. Komotskov, and M.G. Sorokin "Results of measurements of the concentration of negative ions in the polar stratosphere ", *Geomagnetism and Aeronomia*, **32**, No. 3, 47-54 (1992).

Ermakov V.I. and A.V. Komotskov "Charged particle measurements in the equatorial, middle, and polar latitudes", *Proc. Central Aerological Observatory* (Trudy ZAO), Moscow, Gidrometizdat, **179**, 73-81 (1992).

Forbush S.E. and B.F. Burke "Absorption of cosmic radio noise at 22.2 MHz following solar flare on February 23, 1956", *J. Geophys. Res.*, **61**, No. 3, 573-575 (1956).

Heaps M.G. "Parametrization of the cosmic ray ion-pair production rate above 18 km", *Planet. Space Sci.*, **26**, No. 6, 513-517 (1978).

Heck D., J. Knapp, J.N. Capdevielle, G. Schatz, and T. Thouw "CORSIKA: A Monte Carlo Code to Simulate Extensive Air Showers", Forschungszentrum Karlsruhe, FZKA 6019 (1998).

Hensen A. and J.C.H. Van Der Hage "Parametrization of cosmic radiation at sea level", *J. Geophys. Res.*, **99**, No. D5, 10693-10695 (1994).

Kallenrode M.B. and E.W. Cliver "Roggue SEP events: Observational aspects", *Proc. 27th Intern. Cosmic Ray Conf*, Hamburg, **8**, 3314-3317 (2001a).

Kallenrode M.B. and E.W. Cliver "Roggue SEP events: Modelling", *Proc. 27th Intern. Cosmic Ray Conf*, Hamburg, **8**, 3318-3321 (2001b).

Lied F. "Ionosperic absorption observed on the 23-rd February 1956 at Kjeller and Tromso", *J. Atmosph. Terr. Phys.*, **10**, No. 1, 48-48 (1957).

Little C.G. and H. Leinbach "Some measurements of high-latitude ionospheric absorption using extraterrestrial radio waves", *Proc. IRE*, **46**, 334-348 (1958).

Little C.G. and H. Leinbach "The riometer – a device for the continuous measurements of ionospheric absorption", *Proc. IRE*, **47**, 315-320 (1959).

Marsh N. and H. Svensmark "Solar Influence on Earth's Climate", *Space Sci. Rev.*, **107**, No. 1-2, 317-325 (2003).

Minnes C.M., G.H. Bazzard, and H.C. Bevan "Ionospheric changes associated with the solar event of 23 February 1956", *J. Atmosph. Terr. Phys.*, **9**, 233-234 (1957).

Neher H.V. "Cosmic ray knee in 1958", *J. Geophys. Res.*, **66**, No. 12, 4007-4012 (1961).

Neher H.V. "Cosmic ray particles that changed from 1954 to 1965", *J. Geophys. Res.*, **72**, No. 5, 1527-1539 (1967).

Neher H.V. "Cosmic rays at high latitudes and altitudes covering four solar maxima", *J. Geophys. Res.*, **76**, No. 7, 1637-1651 (1971).

Pierce J.A. "VIF phase shifts associated with the disturbance of February 23, 1956", *J. Geophys. Res.*, **61**, 475-483, 1956.

Porter H.S., C.H. Jackman, and A.E.S. Green "Efficiencies for production of atomic nitrogen and oxygen by relativistic proton impact in air", *J. Chem. Phys.*, **65**, No. 1, 154-167 (1976).

Quack M., M.B. Kallenrode, König M., et al. "Ground level events and consequences for stratospheric chemistry", *Proc. 27th Intern. Cosmic Ray Conf*, Hamburg, **10**, 4023-4026 (2001).

Reid G.C. "A study of enhanced ionization produced by solar protons during a polar cap absorption event", *J. Geophys. Res.*, **66**, No. 12, 4071-4085 (1961).

Rosen J.M. and D.J. Hofmann "Balloonborne measurements of electrical conductivity, mobility, and the recombination coefficient", *J. Geophys. Res.*, **86**, No. C8, 7406–7410 (1981).

Shapley A.H. and R.W. Knecht "Ionospheric effect of the great solar-cosmic ray event of February 23, 1956", *Report on URSI-IRE Meeting*, Washington, D.C. (1957).

Usoskin I.G., K. Alanko, K. Mursula, and G.A. Kovaltsov "Heliospheric modulation strength during the neutron monitor era", *Solar Phys.*, **207**, No. 2, 389-399 (2002a).

Usoskin I.G., K. Mursula, S. Solanki, M. Schüssler, and G.A. Kovaltsov "Physical reconstruction of cosmic ray intensity since 1610", *J. Geophys. Res.*, **107**, No. A11, SSH 13-1, doi:10.1029/2002JA009343 (2002b).

Usoskin I.G., O.G. Gladysheva, and G.A. Kovaltsov "Cosmic ray induced ionization in the atmosphere: spatial and temporal changes", *J. Atmosph. Solar-Terr. Phys.*, in press (2004).

Yu, F. "Altitude variations of cosmic ray induced production of aerosols: Implications for global cloudiness and climate", *J. Geophys. Res.*, **107,** No. A7, SIA 8-1, doi:10.1029/2001JA000248 (2002).

References for Chapter 13

Atkin A.C.Z. "Energetic particle-induced enhancements of stratospheric nitric acid", *Geophys. Res. Lett.*, **21**, No.10, 859-862 (1994).

Attolini M., S.Cecchini, M. Galli and T. Nanni "On the persistence of the 22-y solar cycle", *Solar Phys.*, **125,** No. 2, 389-398 (1990).

Carrington R.C. "Description of a singular appearance seen on the Sun on September 1, 1859", *Mon. Not. Royal Astron. Soc.*, **20**, 13-15 (1860).

Crutzen P.J., I.S.A. Isaksen, and G.C. Reid "Solar proton events: stratospheric sources of nitric oxide", *Science*, **189**, No.4201, 457- 459 (1975).

Dorman I.V., L.I. Dorman and D. Venkatesan "Solar cosmic ray event frequency distribution in dependence of fluence and of solar activity level", *Proc. 23th Intern. Cosmic Ray Conf.*, Calgary, **4**, 79-82 (1993).

Dorman L.I. and L.A. Pustil'nik "Solar cosmic ray events: statistical characteristics for the diagnostic of acceleration, excaping and propagation processes", *Proc. 24th Intern. Cosmic Ray Conf.*, Rome, **4**, 86-89 (1995).

Dorman L.I. and L.A. Pustil'nik "Statistical characteristics of FEP events and their connection with acceleration, escaping and propagation mechanisms", *Proc. 26th Intern. Cosmic Ray Conf.*, Salt Lake City, **6**, 407-410 (1999).

Dreschhoff G.A.M. and E.J. Zeller "Evidence of individual solar proton events in Antarctic snow", *Solar Physics*, **127**, 337-346 (1990).

Dreschhoff G.A.M. and E.J. Zeller "415-year Greenland ice core record of solar proton events dated by volcanic eruptive events", *TER-QUA Symposium Series*, 2, Inst. Tertiary-Quaternary Studies, 1-24 (1994).

Dreschhoff G.A.M. and E.J. Zeller "The solar signal in a 415-year nitrate record from a polar ice core", *Proc. 24th Intern. Cosmic Ray Conf.*, Rome, **4**, 1196-1199 (1995).

Gladysheva O.G. and G.E. Kocharov "Solar protons from August 1972 flare and nitrate abundance in Antarctic snow", *Proc. 24th Intern. Cosmic Ray Conf.*, Rome, **4**, 1126-1128 (1995).

Gladysheva O.G., I. Iwasaka, G.E. Kocharov, and Y. Muraki "Unique possibility to obtain upper limit of total energy induced by solar flare protons", *Proc. 24th Intern. Cosmic Ray Conf.*, Rome, **4**, 1129-1132 (1995).

Heath D.F., A.J. Krüger, and P.J. Crutzen "Solar proton event: influence on stratospheric ozone", *Science*, **197**, 886-889 (1977).

Jackman C.H., A.R. Douglass, R.B. Rood, R.D. McPeters, and P.E. Meade "Effect of solar proton events on the middle atmosphere during the past two solar cycles as computed using a two-dimensional model", *J. Geophys. Res.*, **95**, No. D6, 7417-7428 (1990).

Jackman C.H., E.L. Fleming, and F.M. Vitt "Influence of extremely large solar proton events in a changing stratosphere", *J. Geoph. Res.*, **105**, No.D6, 11659-11670 (2000).

Jackman C.H., R.D. McPeters, G.J. Labow, E.L. Fleming, C.J. Praderas, and J.M. Russell "Northern Hemisphere atmospheric effects due to the July 2000 solar proton event", *Geophys. Res. Lett.*, **28**, No. 15, 2883-2886 (2001).

Kinnersley J.S. "The climatology of the stratospheric `THIN AIR' model." *Quarterly Journal of the Royal Meteorological Society,* **122**, No.529, 219-252 (1996).

Krivsky L.and K. Pejml, *Publ. 75*, Ondrejov, Czech Republic (1988)

Marcucci M.F., S. Orsini, M. Candidi, and M. Storini "On a possible relationship between atmospheric ozone dynamics and global auroral activity", *Proc. 24th Intern. Cosmic Ray Conf.*, Rome, **4**, 1156-1159 (1995).

Martin I.M., T. Toroshelidze, W.E. Alves, et al. "Stratospheric cosmic ray and ozone variations during last three solar cycles", *Proc. 25th Intern. Cosmic Ray Conf.*, Durban, **2**, 453-456 (1997).

McCracken K.G., G.A.M. Dreschhoff, D.F. Smart, and M.A. Shea "The Gleissberg periodicity in large fluence solar proton events", *Proc. 27th Intern. Cosmic Ray Conf.*, Hamburg, **8**, 3205-3208 (2001a).

McCracken K.G., D.F. Smart, M.A. Shea, and G.A.M. Dreschhoff "400 years of large fluence solar proton events", *Proc. 27th Intern. Cosmic Ray Conf.*, Hamburg, **8**, 3209-3212 (2001b).

McCracken K.G., G.A.M. Dreschhoff, E.J. Zeller, D.F. Smart, and M.A. Shea "Solar cosmic ray events for the period 1561-1994, 1. Identification in polar ice, 1561-1950", *J. Geophys. Res.*, **106**, No. A10, 21585-21598 (2001c).

McCracken K.G., G.A.M. Dreschhoff, D.F. Smart, and M.A. Shea "Solar cosmic ray events for the period 1561-1994, 2. The Gleissberg periodicity", *J. Geophys. Res.*, **106**, No. A10, 21599-21609 (2001d).

Nachkebia N., M. Despotashvili, and J. Kharchilava "Interplanetary Magnetic Field Disturbances Affect on the Ozone Profiles", *Proc. 28th Intern. Cosmic Ray Conf.*, Tsukuba, **7**, 4237-4240 (2003).

Nevanlinna H. and E. Kataja "An extension of the geomagnetic activity index series AA for 2 solar cycles (1844-1898)", *Geophys. Res. Lett.*, **20**, No.23, 2703-2706 (1993).

Nevanlinna H., A. Ketola, L. Hakkinen, A. Viljanen, and K. Ivory "Geomagnetic activity during solar cycle 9 (1844-1856)", *Geophys. Res. Lett.*, **20**, No. 8, 743-746 (1993).

Quack M., M.B. Kallenrode, König M., et al. "Ground level events and consequences for stratospheric chemistry", *Proc. 27th Intern. Cosmic Ray Conf.*, Hamburg, **10**, 4023-4026 (2001).

Porter H.S., C.H. Lackman, and A.E.S. Green "Efficiencies for production of atomic nitrogen and oxygen by relativistic proton impact in air", *J. Chem. Phys.*, **65**, No. 1, 154-167 (1976).

Russell C.T., and R.L. McPherro "Semiannual variation of geomagnetic activity ", *J. Geophys. Res.*, **78**, No. 1, 92-108 (1973).

Shea M.A., D.F. Smart, G.A.M. Dreschhoff, and K.G. McCracken "The Seasonal Dependency of the NO(Y) Impulsive Precipitation Events in Arctic Polar Ice", *Proc. 28th Intern. Cosmic Ray Conf.*, Tsukuba, **7**, 4225-4228 (2003).

Smart D.F. and M.A. Shea "A comparison of the magnitude of the 29 Sept. 1989 high energy event with solar cycle 17, 18 and 19 events", *Proc. 22th Intern. Cosmic Ray Conf.*, Dublin, **3**, 101-104 (1991).

Solomon S., D.W. Rush, J.-C. Goard, G.C Reid, and P.J. Crutzen "The effect of particle precipitation events on the neutral and ion chemistry of the middle atmosphere, 2. Odd hydrogen", *Planet. Space Sci.*, **29**, No. 8, 885-892 (1981).

Swinson D.B. and M.A. Shea "The September 29, 1989 ground level event observd at high rigidity", *Geophys. Res. Letters*, **17**, No. 8, 1073-1075 (1990).

Vitt F.M., T.P. Armstrong, T.E. Cravens, G.A.M. Dreschhoff, C.H. Jackman, and C.M. Laird "Computed contributions to odd nitrogen concentrations in the Earth's polar middle atmosphere by energetic charged particles", *J. Atm. Solar-Terr. Phys.*, **62**, 669-683 (2000).

Zeller E.J. and G.A.M. Dreschhoff "Anomalues nitrate concentrations in polar ice – do they result from solar particle injections into the polar atmosphere?", *Geophys. Res. Lett.*, **22** (18), 2521-2524 (1995).

Zeller E.J., G.A.M. Dreschhoff, and C.M. Laird "Nitrate flux on the Ross Ice Shelf, Antarctica and its relation to solar cosmic rays", *Geophys. Res. Lett.*, **13**, 1264-1267 (1986).

References for Chapter 14

Ahluwalia H.S. "Three activity cycle periodicity in galactic cosmic rays", *Proc. 25th Intern. Cosmic Ray Conf.*, Durban, **2**, 109-112 (1997).

Anderson R.Y. "Possible connection between surface winds, solar activity and the earths magnetic field", *Nature*, **358**, No. 6381, 51-53 (1992).

Ardanuy P.E., L.L. Stowe, A. Gruber, and M. Weiss "Shortwave, longwave and net cloud-radiative forcing as determined from NIMBUS-7 observations", *J. Geophys. Res.*, **96**, 18537-18549 (1991).

Barraclough D.R. "Spherical harmonic analyses of geomagnetic field for 8 epochs between 1600 and 1910", *Geophys. J., R. Astro. Soc.*, **36**, No. 3, 497-513 (1974).

Barraclough D.R. "Spherical harmonic models of the geomagnetic field", *Geomagnetic Bulletin of the Institute of Geological Sciences,* HMSO, London, **8**, 1-62 (1978).

Beer J., S. Tobias, and N. Weiss "An active Sun throughout the Maunder minimum", *Solar Phys.*, **181**, 237-249 (1998).

Beer J., G.M. Raisbeck, and F. Yiou "Time variations of ^{10}Be and solar activity", in C.P. Sonett, M.S. Giampapa, and M.S. Matthews (eds.) *The Sun in time*, University of Arizona Press, 343-359 (1991).

Constable C.G., C.L. Johnson, and S.P. Lund "Global geomagnetic field models for the past 3000 years: transient or permanent flux lobes?", *Phil. Trans., R. Soc.*, London, **A358**, No. 1768, 991-1008 (2000).

Dickinson R.E. "Solar variability and the lower atmosphere", *Bull. Am. Met. Soc.*, **56**, 1240-1248 (1975).

Dorman L.I. "Determination of cosmic ray intensity variations in the last 400 years on the basis of solar activity data with taking into account convection-diffusion and drift mechanisms: applications to

radiocarbon and climate change data", *2nd World Space Congress and 34th COSPAR*, Houston, October 2002, *Adv. Space Res.* (2003), submitted for publication.

Dorman L.I. and I.V. Dorman "Cosmic rays, thunderstorm clouds, and possible influence on climate, 1. Formation of lead mesoatoms in neutron monitor by soft negative muons and expected atmospheric electric field effect in the cosmic ray neutron component", *2nd World Space Congress and 34th COSPAR*, Houston, October 2002, *Adv. Space Res.* (2003), submitted for publication.

Dorman L.I., I.V. Dorman, N. Iucci, Yu. Ne'eman, M.A. Parisi, L.A. Pustil'nik, F. Signoretti, A. Sternlieb, G. Villoresi, and I.G. Zukerman "Cosmic rays, thunderstorm clouds, and possible influence on climate, 2. Atmospheric electric field effect in different neutron multiplicities according to Emilio Segre' Observatory one minute data", *2nd World Space Congress and 34th COSPAR*, Houston, October 2002, *Adv. Space Res.* (2003), submitted for publication.

Dorman L.I., I.Ya. Libin, M.M. Mikalayunas, and K.F. Yudakhin "On the connection between cosmophysical and geophysical parameters in 19-20 cycles of solar activity", *Geomagnetism and Aeronomy*, **27**, No. 2, 303-305 (1987).

Dorman L.I., I.Ya. Libin, and M.M. Mikalajunas "About the possibility of the influence of cosmic factors on weather, spectral analysis: cosmic factors and intensity of storms", *The Regional Hidrometeorology* (Vilnius), **12**, 119-134 (1988a).

Dorman L.I., I.Ya. Libin, and M.M. Mikalajunas "About the possible influence of the cosmic factors on the weather. Solar activity and sea storms: instantaneous power spectra", *The Regional Hidrometeorology* (Vilnius), **12**, 135-143 (1988b).

Dorman L.I., L.A. Pustil'nik, and G. Yom Din "Possible manifestation of solar activity and cosmic ray intensity influence on climate change in England in middle ages (through wheat market dynamics): I. Data source and conceptual model", *2nd World Space Congress and 34th COSPAR*, Houston, October 2002, *Adv. Space Res.* (2003a), submitted for publication.

Dorman L.I., L.A. Pustil'nik, and G. Yom Din "Possible manifestation of solar activity and cosmic ray intensity influence on climate change in England in middle ages (through wheat market dynamics): II. Data analysis and discussion of results", *2nd World Space Congress and 34th COSPAR*, Houston, October 2002, *Adv. Space Res.* (2003b), submitted for publication.

Eddy J.A. "The Maunder Minimum", *Science*, **192**, 1189-1202 (1976).

Ely J.T.A. and T.C. Huang "Geomagnetic activity and local modulations of cosmic ray circa 1 GeV", *Geophys. Res. Lett.*, **14**, No. 1, 72-75 (1987)

Ely J.T.A., J.J. Lord, and F.D. Lind "GCR, the Cirrus hole, global warming and record floods", *Proc. 24th Intern. Cosmic Ray Conf.*, Rome, **4**, 1137-1140 (1995).

Farrar P.D. "Are cosmic rays influencing oceanic cloud coverage or is it only El Niño", *Clim. Change*, **47**, 7-15 (2000).

Fastrup B., E. Pedersen, E. Lillestol et al. (Collaboration CLOUD)"A study of the link between cosmic rays and clouds with a cloud chamber at the CERN PS", *Proposal CLOUD*, CERN/SPSC 2000-021 (2000).

Ferraro R.R., F. Weng, N.C. Grody, and A. Basist "An eight-year (1987-1994) time series of rainfall, clouds, water vapor, snow cover, and sea ice derived from SSM/I measurements", *Bull. Am. Met. Soc.*, **77**, 891-905 (1996).

Flückiger E.O., R. Bütikofer, L. Desorgher, and M.R. Moser "Global cosmic ray cutoff rigidities over the past 2000 years", *Proc. 28th Intern. Cosmic Ray Conf.*, Tsukuba, **7**, 4229-4232 (2003).

Friis-Christiansen E. and K. Lassen "Length of the solar cycle: an indicator of solar activity closely associated with climate", *Science*, **254**, 698-700 (1991).

Hartmann D.L. "Radiative effects of clouds on the Earth's climate in aerosol-cloud-climate interactions", in P.V. Hobbs (ed) *Aerosol-Cloud-Climate Interactions*, Academic Press, 151- (1993).

Herschel W. "Observations tending to investigate the Nature of the Sun, in order to find the Causes or Symptoms of its variable Emission of Light and Heat; with Remarks on the Use that may possibly be drawn from Solar Observations", *Philosophical Transactions of the Royal Society*, London, **91**, Part1, 265-318 (1801).

Haigh J.D. "The impact of solar variability on climate", *Science*, **272**, 981-984 (1996).

Jevons W.S. "Commercial crises and sun-spots",*Nature*, **19**, 33-37 (1878).

JevonsW. S. "The solar commercial cycle", *Nature*, **26**, 226-228 (1882).

Jones P.D., K.R. Briffa, T.P. Barnett, and S.F.B. Tett "High resolution palaeoclimatic records for the last millennium: interpretation, integration and comparison with general circulation model control run temperatures", *The Holocene*, **8**, 455-471 (1998).

King J.W. "Sun-weather relationships", *Astronautics and Aeronautics*, **13**, No. 4, 10-19 (1975).

Kristjánsson J.E., J. Kristiansen, and E. Kaas "Solar activity, cosmic rays, clouds and climate - an update", *Adv. Space Res.*, **32**, accepted for publication (2003).

Labitzke K. and H. van Loon "Some recent studies of probable connections between solar and atmospheric variability", *Ann. Geophys.*, **11**, 1084-1094 (1993).

Lassen K. and E. Friis-Christiansen "Variability of the solar cycle length during the past five centuries and the apparent association with terrestrial climate", *J. Atmos. Solar-Terr. Phys.*, **57**, 835-845 (1995).

Lean J., J. Beer, and R. Breadley "Reconstruction of solar irradiance since 1610: implications for climate change", *Geophys. Res. Lett.*, **22**, 3195-3198 (1995).

Lean J., A. Skumanich, and O. White "Estimating the Sun's radiative output during the Maunder minimum", *Geophys. Res. Lett.*, **19**, 1591-1594 (1992).

Lockwood M., R. Stamper, and M.N. Wild "A doubling of the Sun's coronal magnetic field during the past 100 years , *Nature*, **399**, No. 6735, 437-439 (1999)

Lockwood J.A., W.R. Webber, and L. Hsieh "Solar flare proton rigidity spectra deduced from cosmic ray neutron monitor observations", *J. Geophys. Res.*, **79**, No. 28, 4149-4155 (1974).

Mann M.E., R.S. Bradley, and M.K. Hughes "Global-scale temperature patterns and climate forcing over the past six centuries", *Nature*, **392**, 779-787 (1998).

Markson R. "Solar modulation of atmospheric electrification and possible implications for the Sun-weather relationship", *Nature*, **273**, 103-109 (1978).

Marsh N.D. and H. Swensmark "Low cloud properties influenced by cosmic rays", *Phys. Rev. Lett.*, **85**, 5004-5007 (2000a).

Marsh N. and H. Swensmark "Cosmic rays, clouds, and climate", *Space Sci. Rev.*, **94**, No. 1-2, 215-230 (2000b).

Martin I.M., A.A. Gusev, G.I. Pugacheva, A. Turtelli, and Y.V. Mineev "About the origin of high-energy electrons in the inner radiation belt", *J. Atmos. and Terr. Phys.*, **57**, No. 2, 201-204 (1995)

Ney E.R. "Cosmic radiation and weather", *Natur*e, **183**, 451-452 (1959).

Ohring G. and P.F. Clapp "The effect of changes in cloud amount on the net radiation on the top of the atmosphere", *J. Atmospheric Sci.*, **37**, 447-454 (1980).

Price C. "Evidence for a link between global lightning activity and upper tropospheric water vapour", Nature, 406, 290-293 (2000).

Proctor R.A. "Sun-Spots and Financial Panics", Scribners Monthly, 20, No. 2, 170-178 (1880).

Pudovkin M.I. and O.M. Raspopov "The mechanism of action of solar activity on the state of the lower atmosphere and meteorological parameters (a review)", *Geomagn. and Aeronomy*, **32**, 593-608 (1992).

Pudovkin M. and S. Veretenenko "Cloudiness decreases associated with Forbush-decreases of galactic cosmic rays",*J. Atmos. Solar-Terr. Phys.*, **57**, 1349-1355 (1995).

Pudovkin M. and S. Veretenenko "Variations of the cosmic rays as one of the possible links between the solar activity and the lower atmosphere. *Adv. Space Res.*, **17** (11), 161-164 (1996).

Pugacheva G.I., A.A. Gusev, I.M. Martin et al. "The influence of geomagnetic disturbances on the meteorological parameters in the BMA region", *Proc. 24th Intern. Cosmic Ray Conf.*, Rome, **4**, 1110-1113 (1995).

Pulkkinen T.I., H. Nevanlinna, P.J. Pulkkinen, and M. Lockwood "The Sun-Earth connection in time scales from years to decades and centuries", *Space Sci. Rev.*, **95**, 625-637 (2001).

Pustil'nik L., G. Yom Din, and L. Dorman "Manifestations of Influence of Solar Activity and Cosmic Ray Intensity on the Wheat Price in the Medieval England (1259–1703 Years)", *Proc. 28th Intern. Cosmic Ray Conf.*, Tsukuba, **7**, 4131-4134 (2003).

Ramanathan V., R.D. Cess, E.F. Harrison, P. Minnis, B.R. Barkstrom, E. Ahmad, and D. Hartmann "Cloud-radiative forcing and climate: results from the Earth Radiation Budget Experiment", *Science*, **243**, No. 4887, 57-63 (1989).

Rossow W.B. and B. Cairns "Monitoring changes of clouds", *J. Climate*, **31**, 305-347 (1995).

Rossow W.B. and R. Shiffer "ISCCP cloud data products", *Bull. Am. Met. Soc.*, **72**, 2-20 (1991).

Sabaka T.J., R.A. Langel, R.T. Baldwin, and J.A. Conrad "The geomagnetic field 1900-1995, including the large-scale field from magnetospheric sources, and the NASA candidate models for the 1995 revision of the IGRF ", *J. Geomag. Geoelect.*, **49**, No. 2-3, 157-206 (1997).

Sakurai K. "The Long-Term Variation of Galactic Cosmic Ray Flux and Its Possible Connection with the Current Trend of the Global Warming", *Proc. 28th Intern. Cosmic Ray Conf.*, Tsukuba, **7**, 4209-4212 (2003).

Schlegel K., G. Diendorfer, S. Them, and M. Schmidt "Thunderstorms, lightning and solar activity – Middle Europe", *J. Atmos. Solar-Terr. Phys.*, **63**, 1705-1713 (2001).

Shea M.A. and D.F. Smart " The effects of recent secular variations of the geomagnetic field on vertical cutoff rigidity calculations", *Proc. 15th Intern. Cosmic Ray Conf.*, Plovdiv, **4**, 204-209 (1977).

Shea M.A. and D.F. Smart "The influence of the changing geomagnetic field on cosmic ray measurements", *J. Geomag. Geoelectr.*, **42**, No. 9, 1107-1121 (1990).

Shea M.A. and D.F. Smart "Secular changes in the geomagnetic cutoff rigidities and their effect on cosmic ray measurements", *Proc. 25th Intern. Cosmic Ray Conf.*, Durban, **2**, 393-396 (1997).

Shea M.A. and D.F. Smart "Preliminary Study of the 400-Year Geomagnetic Cutoff Rigidity Changes, Cosmic Rays and Possible Climate Changes", *Proc. 28th Intern. Cosmic Ray Conf.*, Tsukuba, **7**, 4205-4208 (2003).

Shea M.A. and D.F. Smart "Cosmic rays, geomagnetic field and climate change", Report on 2nd World Space Congress and 34th COSPAR, *Adv. Space Res.* (2003), submitted for publication.

Shindell D., D. Rind, N. Balabhandran, J. Lean, and P. Lonengran "Solar cycle variability, ozone, and climate", *Science*, **284**, 305-308 (1999).

Smart D.F. and M.A. Shea "Geomagnetic Cutoff Rigidity Calculations at 50-Year Intervals Between 1600 and 2000", *Proc. 28th Intern. Cosmic Ray Conf.*, Tsukuba, 7, 4201-4204 (2003a).

Smart D.F. and M.A. Shea, Report on 2nd World Space Congress and 34th COSPAR, Houston, October 2002, *Adv. Space Res.* (2003b), submitted for publication.

Stozhkov Yu. I. "The role of cosmic rays in atmospheric processes", *J. Phys. G: Nucl. Part. Phys.*, **28**, 1-11 (2002).

Stozhkov Yu.I., P.E. Pokrevsky, I.M. Martin et al. "Cosmic ray fluxes and precipitations", *Proc. 24th Intern. Cosmic Ray Conf.*, Rome, **4**, 1122-1125 (1995a).

Stozhkov Yu.I., J. Zullo, I.M. Martin et al. "Rainfalls during great Forbush-decreases", *Nuovo Cimento*, **C18**, 335-341 (1995b).

Stozhkov Yu.I., P.E. Pokrevsky, J. Jr. Zullo et al. "Influence of charged particle fluxes on precipitation", *Geomagn. and Aeronomy*, **36**, 211-216 (1996).

Stozhkov Yu.I., P.E. Pokrevsky, and V.P. Okhlopkov "Long-term negative trend in cosmic ray flux", *J. Geophys. Res.*, **105**, No. A1, 9-17 (2000).

Stozhkov Yu.I., V.I. Ermakov, and P.E. Pokrevsky "Cosmic rays and atmospheric processes", *Izvestia Academy of Sci.*, Ser. Phys., **65**, No. 3, 406-410 (2001).

Stowe L.L., C.G. Wellemayer, T.F. Eck, H.Y.M. Yeh, and the Nimbus-7 Team "Nimbus-7 global cloud climatology, Part 1: Algorithms and validation", *J. Climate*, **1**, 445-470 (1988).

Sun B. and R.S. Bradley "Solar influences on cosmic rays and cloud formation: A reassessment", J. Geophys. Res., 107, No. D24, AAC5, 1-12 (2002).

Swensmark H. "Influence of cosmic rays on the Earth's climate", *Phys. Rev. Lett.*, **81**, 5027-5030 (1998).

Swensmark H. "Cosmic rays and Earth's climate", *Space Sci. Rev.*, **93**, 175-185, 2000.

Swensmark H. and E. Friis-Christiansen "Variation of cosmic ray flux and global cloud coverage – a missing link in solar-climate relationships", *J. Atmos. Solar-Terr. Phys.*, **59**, 1225-1232 (1997).

Tinsley B.A. "Solar wind modulation of the global electric circuit and the apparent effects of cloud microphysics, latent heat release, and tropospheric dynamics", *J. Geomagn. Geoelectr.*, **48**, 165-175 (1996).

Tinsley B.A. "Influence of solar wind on the global electric circuit, and inferred effects on cloud microphysics, temperature, and dynamics in the troposphere", *Space Sci. Rev.*, **94**, No. 1-2, 231-258 (2000).

Tinsley B.A. and G.W. Deen "Apparent tropospheric response to MeV-GeV particle flux variations: a connection via electrofreezing of supercooled water in high-level clouds?", *J. Geophys. Res.*, **96**, No. D12, 22283-22296 (1991).

Veretenenko S.V. and M.I.Pudovkin "Effects of Forbush-decreases in cloudiness variations", *Geomanetism and Aeronomy*, **34**, 38-44 (1994).

Weng F. and N.C. Grody "Retrieval of cloud liquid water using the special sensor microwave imager (SSM/I)", *J. Geophys. Res.*, **99**, 25535-25551 (1994).

References for Chapter 15 and Preface for Part 4

Belov A.V., Ya.L. Blokh, L.I. Dorman and S.I. Rogovaya "Method of determining of altitudinal atmosphere temperature profile", *Patent SU 1429070 A1*, Prioritet at April 18, 1986.

Belov A.V., Ya.L. Blokh, L.I. Dorman and S.I. Rogovaya "The temperature diagnostics of the atmosphere allowing for the temperature of the near-surface layer", *Proc. 20th Intern. Cosmic Ray Conf.*, Moscow, **4**, 263-265 (1987).

Belov A.V., Ya.L. Blokh, L.I. Dorman and S.I. Rogovaya "Variations of atmospheric temperature profile inferred from the data on cosmic ray ionizing component", *Proc. 21th Intern. Cosmic Ray Conf.*, Adelaide, 7, 85-87 (1990).

Dorman L.I. "Generalization of the spectrographic method and by cosmic-ray sounding of meteorological conditions", *Geomagnetism and Aeronomy* (USA), **17**, No. 3, 264-267 (1977a).

Dorman L.I. "The continuous passive location of the variations in the vertical distribution of the atmospheric temperature and the air column mass over the observation level by means of cosmic rays", *Proc. 15th Intern. Cosmic Ray Conf.,* Plovdiv, **4**, 281-286 (1977b).

Dorman L.I. "Generalization of the spectrographic method to isolate and separately study the cosmic ray variations of the atmospheric, geomagnetic and extraterrestrial origin", *Proc. 15th Intern. Cosmic Ray Conf.*, Plovdiv, **4**, 364-368 (1977c).

Dorman L.I. "Generalized spectrographic method for separately studying the geomagnetic, atmospheric and extraterrestrial variations for the complex spectrum of the extraterrestrial cosmic ray variation", *Proc. 16th Intern. Cosmic Ray Conf.*, Kyoto, **4**, 394-399 (1979).

Dorman L.I. and Yu.Ya. Krestyannikov "Determination of the atmospheric variations of cosmic rays from the data of observations with the Sayan's spectrographic array", *Proc. 15th Intern. Cosmic Ray Conf.*, Plovdiv, **4**, 287-290 (1977a).

Dorman L.I. and Yu.Ya. Krest'yannikov " Spectrographic method of determining the temperature variations of cosmic-rays", *Geomagnetism and Aeronomy* (USA), **17**, No. 3, 268-270 (1977b).

Dorman L.I. and Yu.Ya. Krestyannikov "Mass-average temperature and spectrographical method of cosmic ray variations investigation ", *Geomagnetism and Aeronomy*, **17**, No. 4, 622-626 (1977c).

Dorman L.I. and Yu.Ya. Krest'yannikov "Using of meson telescope observation data without correction on the temperature effect", In *Cosmic Ray Variations and Space Research*, Moscow, NAUKA, 244-249 (1986).

Kuz'min A.I., P.A. Krivoshapkin, G.F. Krymsky, and G.V. Skripin "Study of temperature variations of upper atmosphere by data of cosmic ray underground measurements", In *Cosmic Rays and Problems of Cosmophysics*, Nauka, Novosibirsk, 239-245 (1965).

MacAnuff J.W., *Ph.D. Thesis*, London (1951). See in George, 1952 (References to Chapter 2).

Methodical Instructions for Meteorological Sounding Balloon Measurements, Central Aerological Observatory, Dolgoprudny, Moscow region (1955).

Miyazaki Y. and M. Wada "Simulation of cosmic ray variation due to temperature effect", *Acta phys. Acad. Sci. hung.*, **29**, Suppl. 2, 591-595 (1970).

References for Chapter 16

Aleksanyan, T.M., V.M. Bednazhevsky, Ya.L. Blokh, L.I. Dorman, and F.A. Starkov "Coupling coefficients of the neutron component for the stars of various multiplicities inferred from the measurements on board research vessel "Academician Kurchatov", *Proc. of 16th Intern. Cosmic Ray Conf.,* Kyoto, **4,** 315-320 (1979a).

Aleksanyan, T.M., Ya.L. Blokh, L.I. Dorman, and F.A. Starkov "Examination of the differences in the coupling coefficients and barometric coefficients of 3NM-64 neutron supermonitor and lead-free monitor", *Proc. of 16th Intern. Cosmic Ray Conf.,* Kyoto, **4,** 321-324 (1979b).

Aleksanyan, T.M., L.I. Dorman, V.G. Yanke and V.K. Korotkov "Coupling functions for lead and lead-free neutron monitors from the latitudinal measurements performed in 1982 in the survey by research vessel "Academician Kurchatov", *Proc. of 19th Intern. Cosmic Ray Conf.,* La Jolla, **5,** 300-303 (1985).

Allkofer O.C., R.D. Andresen, E. Bagge, W.D. Dau, and H. Funk "Der Einfluss des Erdmagnetfeldes auf die kosmische Strahlung, I, Untersuchungen der Nukleonenkomponente der kosmische Strahlung waehrend der atlantischen Espedition IQSY 1965 auf dem Forschungsschif "Meteor", in *"Meteor" Forschungsergebnisse,* Reihe B, Heft 3, Gebruder Borntraeger, Berlin (1969).

Avdeev E.A., V.N. Alexandrov, V.M. Bednaghevsky, Ya.L. Blokh, V.V. Viskov, L.I. Dorman, S.F. Ilgach, and I.N. Kapustin "Investigation of cosmic ray geomagnetic effects by expedition measurements on the scientific ship "Academician Kurchatov", *Cosmic Rays* (Moscow, NAUKA), **14**, 34-50 (1974).

Avdeev E.A., V.M. Bednaghevsky, Ya.L. Blokh, V.V. Viskov, L.I. Dorman, and A.A. Manshilina "Experimental and theoretical investigations of coupling coefficients and integral multiplicities", *Izvestia Academy of Sciences USSR*, Series Phys., **36**, No. 11, 2451-2459 (1972).

Avdeev E.A., V.M. Bednaghevsky, Ya.L. Blokh, V.V. Viskov, L.I. Dorman, and A.A. Manshilina "Studies of the coupling coefficients of the cosmic ray neutron component for the period of 1967-1971", *Proc. 13th Intern. Cosmic Ray Conf.*, Denver, **2**, 843-850 (1973).

Bachelet F., P. Balata , E. Dyring, and N. Iucci "The intercalibration of the cosmic ray neutron monitors at 9 European sea level stations and the deduction of a daily latitude effect in 1963", *Nuovo Cim*, **36**, 762-772 (1965).

Bachelet, F., N. Iucci, G.Villoresi, and B. Sporre "The cosmic ray spectrum modulation above 2 GV during the descending phase of solar cycle number 19. I: A comprehensive treatment of the neutron monitor data from the worldwide station network and latitude surveys", *Nuovo Cim*, **7B**, No. 1, 17-33 (1972a).

Bachelet, F., N. Iucci, G.Villoresi, and N.L. Zangrilli "The cosmic ray spectrum modulation above 2 GV. IV:

The influence on the attenuation coefficient of the nucleonic component", *Nuovo Cim*, **11B**, No. 1, 1-12 (1972b).

Bachelet, F., N. Iucci, M. Parisi, and G. Villoresi "The cosmic ray spectrum modulation above 2 GV during the descending phase of solar cycle number 19, V: The influence on the coupling functions of the nucleonic component", *Nuovo Cim.*, **18B**, No. 2, 258-264 (1973).

Belov, A.V., L.I. Dorman and V.G. Yanke "The simplest versions of the global-spectrographical method", *Proc. of 18th Intern. Cosmic Ray Conf.,* Bangalore, **10,** 144-147 (1983).

Belov, A.V., L.I. Dorman, R.T. Gushchina, and V.G. Yanke "Temporal and latitudinal dependence of the temperature effect for neutron component of cosmic rays", *Proc. of 24th Intern. Cosmic Ray Conf.,* Rome, **4,** 1141-1144 (1995).

Bieber, J.W., M. Duldig, P. Evenson, D. Hall, J. Humble "Neutron monitor survey of the Southern ocean", *Proc. of 24th Intern. Cosmic Ray Conf.,* Rome, **4,** 1078-1081 (1995).

Bieber, J.W., P. Evenson, J.E. Humble, and M.L. Duldig "Cosmic ray spectra deduced from neutron monitor surveys", *Proc. of 25th Intern. Cosmic Ray Conf.,* Durban, **2,** 45-48 (1997).

Blokh Ya.L., L.I. Dorman, I.V. Dorman, V.M. Bednaghevsky, V.V. Viskov and A.A. Manshilina "Research of cosmic ray latitude effects", *Izvestia Academy of Sciences USSR,* Series Phys., **38**, No. 9, 1970-1973 (1974).

Carmichael, H. and M. Bercovitch "V. Analysis of IQSY cosmic ray survey measurement", *Canad. J. Phys.*, **47**, No. 19, 2051-2055 (1969).

Clem, J.M., J.W. Bieber, M. Duldig, P. Evenson, D. Evenson, D. Hall, and J. Humble "Contribution of obliquity incident particles to neutron counting rate", *J. Geophys. Res.*, **102**, 26919-26926 (1997).

Danilova O.A., L.I. Dorman, N. Iucci, M. Parisi, N.G. Ptitsyna, M.I. Tyasto, and G. Villoresi "Latitude survey in December 1996-March 1997, 1. Cut-off rigidities for different azimuth and zenith angles ", *Proc. 27th Intern. Cosmic Ray Conf.*, Hamburg, **10**, 4039-4042 (2001).

Dorman L.I. "Influence of meteorological factors on the cosmic ray latitude effect and the process of meson generation", *J. of Experim. and Theoret. Phys. (JETP),* Moscow, **26**, No. 5, 504-505 (1954).

Dorman, L.I. "Geophysical effects and properties of the various components of the cosmic radiation in the atmosphere", *Proc. of 11th Intern. Cosmic Ray Conf., Volume of Invited Papers and Rapporteur Talks,* Budapest, 381-444 (1969).

Dorman L.I. "Cosmic rays in the atmosphere and magnetosphere of the Earth and in the interplanetary space (invited review)", In "*Geomagnetism and High Layers of the Atmosphere*", Moscow, NAUKA, 7-82 (1975).

Dorman L.I. "Geomagnetic and atmospheric effects in primary and secondary cosmic rays; cosmogeneous nuclei (rapporteur paper)", *Proc. 20th Intern. Cosmic Ray Conf.*, Moscow, **8**, 186-237 (1987).

Dorman L.I., Ya.L. Blokh, N.S. Kaminer, I.A. Pimenov and A.B. Rodionov "Inserting of corrections on cosmic ray planetary variations in the data of latitude cosmic ray expeditions", *Geomagnetism and Aeronomy,* **11**, No. 2, 207-210 (1971).

Dorman L.I., O.A. Danilova, N. Iucci,. M. Parisi, N.G. Ptitsina, M.I. Tyasto, G. Villoresi "Latitude survey in December 1996-March 1997, 2. Apparent cut-off rigidities", *Proc. 27th Intern. Cosmic Ray Conf*, Hamburg, **10**, 4043-4046 (2001).

Dorman, L.I., L.V. Granitskij, S.G. Bortnik, G.A. Novikova and I.M. Raikhbaum "Investigations of cosmic ray neutron component on atmospheric depth 260-315 mb", *Izvestia Academy of Sciences of USSR,* Series Phys, **31**, No. 8, 1322-1324 (1967c).

Dorman L.I. and N.S. Kaminer "Meteorological effects of cosmic rays", *Izvestia Academy of Sciences of USSR,* Series Phys., **33**, No. 11, 1926-1929 (1969).

Dorman, L.I., V.A. Kovalenko, and N.P. Milovidova "Latitude distribution and coupling coefficients for cosmic radiation neutron and general ionizing components", *Izvestia Academy of Sciences of USSR,* Series Phys., **31**, No. 8, 1387-1390 (1967a).

Dorman L.I., V.A. Kovalenko, and N.P. Milovidova "The latitude distribution, integral multiplicities and coupling coefficients for the neutron, total ionizing and hard components of cosmic rays", *Nuovo Cimento*, Ser. X, **50**, 27-39 (1967b).

Dorman L.I., V.A. Kovalenko, N.P. Milovidova and S.B. Chernov "The cosmic ray intensity distribution on the territory of USSR and the coupling coefficients", *Acta Phys. Sci. Hung.*, **29**, Suppl. 2, 359-365 (1970).

Dorman, L.I., A.A. Lagutin, and G.V. Chernyaev "Temperature effect of neutron component", *Proc. 21th Intern. Cosmic Ray Conf.,* Adelaide, *7,* 81-84 (1990).

Dorman, L.I., Yu.I. Okulov, N.S. Kaminer, and A.A. Manshilina "Determination of coupling coefficients of the cosmic ray neutron component on the base of ship "*Zarya*" data", *Izvestia Academy of Sciences of USSR,* Series Phys., **30**, No. 11, 1873-1874 (1966).

Dorman L.I., G. Villoresi, N. Iucci, M. Parisi, and N.G. Ptitsyna "Cosmic ray survey to Antarctica and coupling functions for neutron component in solar minimum (1996-1997), 3. Geomagnetic effects and

coupling functions", *Proc. 26th Intern. Cosmic Ray Conf.*, Salt Lake City, **7**, 382-385 (1999).

Dorman L.I., G. Villoresi, N. Iucci, M. Parisi, M.I. Tyasto, O.A. Danilova, and N.G. Ptitsyna "Cosmic ray survey to Antarctica and coupling functions for neutron component near solar minimum (1996-1997), 3, Geomagnetic effects and coupling functions", *J. Geophys. Res.*, **105**, No. A9, 21047-21058 (2000).

Dubinsky J., P. Chaloupka and T. Kowalski "The influence of wind fluxes on cosmic ray intensity", *Mat. Fyz. Casop.*, **10**, 57-62 (1960).

Gushchina R.T., L.I. Dorman, and N.S. Kaminer "Atmospherically dynamic effects in cosmic ray intensity", *Cosmic Rays* (NAUKA, Moscow), **11**, 78-81 (1969).

Iucci N., G. Villoresi, L.I. Dorman, and M. Parisi "Cosmic ray survey to Antarctica and coupling functions for neutron component near solar minimum (1996-1997), 2. Meteorological effects and correction of survey data", *Proc. 26th Intern. Cosmic Ray Conf.*, Salt Lake City, **7**, 321-324 (1999)

Iucci N., G. Villoresi, L.I. Dorman, and M. Parisi "Cosmic ray survey to Antarctica and coupling functions for neutron component near solar minimum (1996-1997), 2, Determination of meteorological effects", *J. Geophys. Res.*, **105**, No. A9, 21,035-21,046 (2000).

Kawasaki, S. "On the anomalous barometric coefficient of cosmic-ray neutron monitor at Mt. Norikura", *Sci. Papers of Inst. Phys. and Chem. Res.*, **66**, No 2, 25-32 (1972).

Keith J.E., R.W. Peterson, R.L. Tjonaman, and J.R. Wang "Cosmic-ray neutron monitor functions, Gross transformation, and nucleonic component mean free paths", *J. Geophys. Res.*, **73**, 353-360 (1968).

Kodama M. "Geomagnetic and solar modulation effects of sea-level cosmic ray intensity. Summary of cosmic ray latitude surveys aboard the expedition ship SOYA during 1956-1962", *Japanese Antarctic Research Expedition Scientific Reports Aeronomy,* Series A, No. 5 (1968).

Lockwood J.A. and A.R. Calawa "On the barometric pressure coefficients for comic ray neutrons", *J. Atmospheric Terrest. Phys.*, **11**, 23-31 (1957).

Lockwood, J.A., and W.R. Webber "Differential response and specific yield functions of cosmic-rays neutron monitors", *J. Geophys. Res.*, **72**, 3395-3402 (1967).

Moraal, H., M.S. Potgieter, and P.H. Stoker, and A.J. Van der Walt "Neutron monitor latitude survey of cosmic ray intensity during the 1986/1987 solar minimum", *J. Geophys. Res.*, **94**, No. A2, 1459-1464 (1989).

Nagashima, K., S. Sakakibara, and K. Kurakami "Response and yield functions of neutron monitor, galactic cosmic ray spectrum and its solar modulation, derived from all the available word-wide surveys", *Nuovo Cim. C,* Serie 1, **12C**, 173-209 (1989).

Potgieter M.S., B.C. Raubenheimer, P.H. Stoker, and A.J. Van der Walt "Modulation of cosmic rays during solar minimum. 2. Cosmic ray latitude distribution at sea-level during 1976", *S. Africa J. Phys.*, **3,** 77-89 (1980a).

Potgieter, M.S., H. Moraal, B.C. Raubenheimer, and Van der Walt "Modulation of cosmic rays during solar minimum. 3. Comparison of the latitude distributions for the periods of solar minimum during 1954, 1965, 1976", *S. Africa J. Phys.*, **3,** 90-97 (1980b).

Stoker, P.H. "Cosmic ray latitude distribution at neutron monitor and aircraft altitudes", *Proc. 23th Intern. Cosmic Ray Conf.*, Calgary, **3**, 785-788 (1993).

Stoker, P.H. "Neutron monitor latitude surveys, response functions and 22-year modulation", *Proc. 24th Intern. Cosmic Ray Conf., Rome,* **4**, 1082-1085 (1995).

Stoker, P.H., and H. Moraal "Neutron monitor latitude surveys at aircraft altitudes", *Astrophysics and Space Science,* **230**, 365-373 (1995).

Stoker, P.H., J. Clem, J.W. Bieber and P. Evenson "Apparent" geomagnetic cutoffs and cosmic ray anomaly in the Cape Town region", *Proc. 25th Intern. Cosmic Ray Conf.*, Durban (South Africa), **2**, 385-387 (1997).

Tsyganenko N.A. "A magnetospheric magnetic field model with a warped tail current sheat", *Planet. Space Sci.*, **37**, No. 1, 5-20 (1989).

Uotila U.A. "Determination of the shape of the geoid", In Proc. of Symposium: *Size and Shape of the Earth*, Ohio State University, Columbus, Ohio, Nov. 13-15, 1956, Inst. of Geodesy, Photogrammetry and Cartography, Publ. No. 7 (1957).

Villoresi G., N. Iucci, M.I. Tyasto, L.I. Dorman, F. Re, F. Signoretti, N. Zangrilli, S. Cecchini, M. Parisi, C. Signorini, O.A. Danilova, and N.G. Ptitsyna "Latitude survey of the cosmic ray nucleonic component (Italy-Antarctic-Italy, 1996-1997)", *Proc 25th Intern. Cosmic Ray Conf.*, Durban (South Africa), **2**, 421-424 (1997).

Villoresi G., L.I. Dorman, N. Iucci, M.I. Tyasto, O.A. Danilova, and N.G. Ptitsyna "Cosmic ray survey to Antarctica and coupling functions for neutron component near solar minimum (1996-1997), 1. The latitude survey", *Proc. 26th Intern. Cosmic Ray Conf.*, Salt Lake City, **7**, 378-381 (1999).

Villoresi G., L.I. Dorman, N. Iucci, and N.G. Ptitsyna "Cosmic ray survey to Antarctica and coupling functions for neutron component near solar minimum (1996-1997), 1, Methodology and data quality assurance", *J. Geophys. Res.*, **105**, No. A9 , 21,025-21,034 (2000).

References for Chapter 17

Anderson E.C. "The production and distribution of natural radiocarbon", *Ann. Rev. Nuclear Sci.*, **2**. 63-78 (1953).

Anderson E.C. and W.F. Libby "World-wide distribution of natural radiocarbon", *Phys. Rev,* **81**, 64-69 (1951).

Aoki T., H. Sakurai, and W. Kato "Altitude distribution of C-14 concentration by Geant-4", *Proc. 28th Intern. Cosmic Ray Conf.,* Tsukuba, **7**, 4151-4154 (2003).

Attolini M.R., S. Cecchini, M. Galli, and T. Nanni "The Gleissberg and 130 year periodicity in the cosmogenic isotopes in the past: the Sun as a quasi-periodic system", *Proc. 20th Intern. Cosmic Ray Conf.*, Moscow, **4**, 323-326 (1987a).

Attolini M.R., S. Cecchini, C. Cini Castagnoli, M. Galli, and T. Nanni "The 11 year cycles in solar activity before Maunder minimum", *Proc. 20th Intern. Cosmic Ray Conf.,* Moscow, **4**, 324-327 (1987b).

Attolini M.R., S. Cecchini, H. Galli, T. Nanni "Solar variations in radiocarbon", *Proc. 21th Intern. Cosmic Ray Conf.*, Adelaide, **7**, 132-135 (1990).

Bonani G., H.J. Hofmann, E. Morenzoni, M. Nessi, M. Suter, and W. Wolfli, "The ETH/SIN Dating Facility: A Status-Report", *Radiocarbon*, **28**, No. 2A, 246-255 (1986).

Burlatskaya S.P. "Pecular features of geomagnetic field variations on archeomagnetic data ", *Physics of the Earth* (in Russian), No. 5, 81-86 (1987).

Cini Castagnoli G., G. Bonino, A. Provenzale, and M. Serio "Long-term solar cycles in the TL profile of the GT14 core and in tree ring radiocarbon data", *Proc. 21th Intern. Cosmic Ray Conf.*, Adelaide, **7**, 152-154 (1990).

Cini Castagnoli G., G. Bonino, E. Callegari, C. Taricco, and Zhu Guang-mey "Thermoluminescence in sea sediments during the cosmogenic isotopes enhancement 35000 yr BP", *Proc. 23th Intern. Cosmic Ray Conf.*, Calgary, **3**, 834- 837, (1993).

Cini Castagnoli G., G. Bonino, B. Lehman, and C. Taricco "Cosmogenic isotopes, geomagnetic and geochemical signals in a Mediterranean sea sediment at 35000 yr BP", *Proc. 24th Intern. Cosmic Ray Conf.*, Rome, **4**, 1204-1207, (1995).

Cini Castagnoli G., G. Bonino, P. Della Monica, and C. Taricco "Common long term periodicities in cosmogenic and climatic records over the last 3000 years", *Proc. 25th INTERN. COSMIC RAY CONF*, Durban, **2**, 469-472 (1997).

Craig H. "Isotopic standards for carbon and oxygen and correction factors for mass-spectrometric analysis of carbon dioxide", *Geochim. Cosmochim. Acta,* **12**, 133-149 (1957).

Craig H.D "The natural distribution of radiocarbon and the exchange time of carbon dioxide between atmosphere and sea", *Tellus,* **9**, 1-17 (1957).

Damon P.E., J.C. Lerman, and A. Long "Temporal Fluctuations of Atmospheric ^{14}C: Causal Factors and Implications", *Ann. Rev. Earth Planet. Sci.,* **6**, 457-494 (1978).

Dergachev V.A. "Variation of cosmogenic radiocarbon concentration and character of geomagnetic field changes in the past", *Proc. 20th Intern. Cosmic Ray Conf., Moscow*, **4**, 292-295 (1987).

Dergachev V.A. "Cosmogenic radiocarbon, climate and powerful manifestation of solar activity in the past", *Proc. 23th Intern. Cosmic Ray Conf.*, Calgary, **3**, 857-860 (1993).

Dergachev V.A. "Medium- and long-term cyclic variations of cosmic rays in the past", *Proc. 24th Intern. Cosmic Ray Conf.*, Rome, **4**, 1200-1203 (1995a).

Dergachev V.A. "Large-scale cyclic variations of cosmogenic radiocarbon concentration", *Izvestia Russian Ac. of Sci.,* Ser. Phys., **59**, No. 4, 91-96 (1995b)

Dergachev V.A. and S.Kh. Akhmetkereev "On the nature of supersecular variations of radiocarbon in the Earth's atmosphere", *Proc. 21st Intern. Cosmic Ray Conf.*, Adelaide, **7**, 128-131 (1990).

Dergachev V.A. and V.F. Chistjakov "210 and 2400 year solar cycles and fluctuations of the climate", In *Solar Cycle*, Ioffe Phys.-Techn. Inst., St.Petersburg, 112-130 (1993).

Dergachev V.A. and V.F. Chistjakov "210 and 2400 year solar cycles and fluctuations of the climate", In Solar Cycle, St.Petersburg, Ioffe Phys.-Techn. Inst., 112-130 (1993).

Dergachev V.A., G.E. Kocharov, and N. Tuichiev "Investigation of variations of Earth's magnetic field intensity by means of radiocarbon data", *Proc. 15th Intern. Cosmic Ray Conf.*, Plovdiv, **4**, 353-357 (1977).

Dorman L.I. "Geophysical effects and properties of the various components of the cosmic radiation in the atmosphere (Rapporteur Talk)", *Proc. 11th Intern. Cosmic Ray Conf.*, Budapest, Volume of Invited Papers and Rapporteur Talks, 381-444 (1969).

Dorman L.I. "Cosmic ray variations and radiocarbon method", In the book *Radiocarbon*, Vilnus, 13-21 (1971).

Dorman L.I. "On the possibility of various type cosmic ray variations investigation by data on relative content of ^{14}C in the annual tree cycles", In the book *Dendroclimatechronology and Radiocarbon*, Kaunas, 312-316 (1972).

Dorman L.I. "Radiocarbon coupling coefficients and the functions of cosmic ray "response" in ^{14}C, I. The local and polar coupling coefficients in the Earth's atmosphere", *Proc. 15th Intern. Cosmic Ray Conf.*, Plovdiv, **4**, 369-373 (1977a).

Dorman L.I. "Radiocarbon coupling coefficients and the functions of cosmic ray "response" in ^{14}C, II. The atmospheric mixing and the planetary coupling coefficients, the magnetic and barometric coefficients", *Proc. 15th Intern. Cosmic Ray Conf.*, Plovdiv, **4**, 374-377 (1977b).

Dorman L.I. "Radiocarbon coupling coefficients and the functions of cosmic ray "response" in ^{14}C, III. The functions of the "response" in the planetary rate of radiocarbon production including the mixing in the atmosphere", *Proc. 15th Intern. Cosmic Ray Conf.*, Plovdiv, **4**, 378-382 (1977c).

Dorman L.I. "Radiocarbon coupling coefficients and the functions of cosmic ray "response" in ^{14}C, IV. The two-basin model of radiocarbon exchange on the Earth, estimation of the basis constants", *Proc. 15th Intern. Cosmic Ray Conf.*, Plovdiv, **4**, 383-386 (1977d).

Dorman L.I. "Radiocarbon coupling coefficients and the functions of cosmic ray "response" in ^{14}C, V. The two-basin model and the functions of the "response" in ^{14}C", *Proc. 15th Intern. Cosmic Ray Conf.*, Plovdiv, **4**, 387-391 (1977e).

Dorman L.I. "Five-basin model of the radiocarbon dynamics on the Earth including the temporal variations in the rate of production by cosmic rays. I. Set on equations, stationary case, estimates of the basic constants", *Proc. 15th Intern. Cosmic Ray Conf.*, Plovdiv, **4**, 395-399 (1977f).

Dorman L.I. "Five-basin model of the radiocarbon dynamics on the Earth including the temporal variations in the rate of production by cosmic rays. II. Nonstationary solution", *Proc. 15th Intern. Cosmic Ray Conf.*, Plovdiv, **4**, 400-404 (1977g).

Dorman L.I. "Peculiarities of cosmic ray research by radio-carbon method", *Proc. 6th All-Union Meeting on the Problem "Astrophysics Phenomena and Radio-Carbon"* (Tbilisi, 1976), Tbilisi, METSNIEREBA, 49-96 (1978).

Dorman L.I. "Methods of cosmic ray variation research by difference ionospheric and radio-carbonic coupling coefficients", *Izvestia Academy of Sciences USSR*, Series Phys., **42**, No. 5, 1092-1097 (1978).

Dorman Lev I. "Cosmic rays and cosmogenic nuclides, 1. In space, inside bodies, and in atmospheres", In *Towards the Millennium in Astrophysics*, ed. M.M. Shapiro, R. Silberberg and J.P. Wefel, World Sci. Publ. Co., Singapore, New Jersey, London, Hong Kong, 303-322 (1998a).

Dorman Lev I. "Cosmic rays and cosmogenic nuclides, 2. Radiocarbon method and elements global mixing and exchange on the Earth", In *Towards the Millennium in Astrophysics*, M.M. Shapiro, R. Silberberg and J.P. Wefel, World Sci. Publ. Co., Singapore, New Jersey, London, Hong Kong, 323-352 (1998b).

Eddy J.A. "The Maunder Minimum", *Science*, **192**, 1189-1202 (1976).

Fields D. "Deep-ocean iron-60 as a possible signature of a nearby supernova", *Proc. 27th Intern. Cosmic Ray Conf.*, Hamburg, **10**, 4212-4212 (2001).

Galli M., G. Cini Castagnoli, M.R. Attolini, et al. "400 year radiocarbon record: 11 year and more longer cycles", *Proc. 20th Intern. Cosmic Ray Conf.*, Moscow, **4**, 280-283 (1987a).

Galli M., G. Cini Castagnoli, M.R. Attolini, et al. "The 20 year cycle of solar activity in C14 and Be10 (before and during Maunder minimum)", *Proc. 20th Intern. Cosmic Ray Conf.*, Moscow, **4**, 284-287 (1987b).

Kato M., Kh.A. Arslanov, H. Kitagawa et al. "Radiocarbon abundances in tree rings from the Spoerer minimum", *Proc. 27th Intern. Cosmic Ray Conf.*, 10, 4035-4038 (2001).

Kitagawa H., T. Masuzawa, T. Makamura and E. Matsumoto "A batch preparation method for graphite targets with low background for AMS C-14 measurements", *Radiocarbon*, **35**, No. 2, 295-300 (1993).

Kocharov G.E., R.Y. Metskvarishvili, and S.L. Tsereteli "High precise measurements of cosmogenic radiocarbon abundance by complex of scintillation equipments", *Proc. 19th Intern. Cosmic Ray Conf.*, La Jolla, **5**, 410- 413 (1985).

Kocharov G.E., A.V. Blinov, A.N. Konstantinov, and V.A. Levchenko "Cosmogenic isotopes and geomagnetic field in the past", *Proc. 21st Intern. Cosmic Ray Conf.*, Adelaide, **7**, 116-119 (1990a).

Kocharov G.E., A.N. Konstantinov, and V.A. Levchenko "Cosmogenic ^{10}Be: cosmic ray over the last 150,000 years", *Proc. 21st Intern. Cosmic Ray Conf.,* Adelaide, **7**, 120-123 (1990b).

Kocharov G.E, A.N. Konstantinov, V.A. Levchenko, E.G. Berezhko, and G.F. Krymsky "Cosmic rays near the Earth from the supernova explosion", *Proc. 22nd Intern. Cosmic Ray Conf.,* Dublin, **2**, 388-391 (1991).

Kocharov G.E., V.M. Ostryakov, A.N. Peristykh, and V.A. Vasil'ev "Radiocarbon content variations and Maunder minimum of solar activity", *Solar Physics*, **159**, 381-391 (1995).

Kolesnikov N.V., I.A. Gorshkov, and Yu.F. Biryulin "Shift of the radiocarbon concentration maximum in annual rings of trees accompanying the jamp-like increase of radiocarbon content in the stratosphere", *Proc. All-Union Meeting on Astrophysical Events and Radiocarbon,* Tbilisi, 27-29 (1970).

Kouts H.J. and L.C.L. Yuan "The production rate of cosmic-ray neutrons and C^{14}", *Phys. Rev.,* **86**, 128-129 (1952).

Landenburg R. "The absorption rate of cosmic-ray neutrons producing C^{14} in the atmosphere", *Phys. Rev.,* **86**, 128-128 (1952).

Libby W.F. "Atmospheric helium three and radiocarbon from cosmic radiation", *Phys. Rev.*, **69**, 671-672, (1946).

Lingenfelter R.E. "Production of carbon 14 by cosmic ray neutrons", *Rev. of Geophysics*, **1**, No. 1, 35-55, (1963).

Matsumoto M., H. Sakurai, Y. Sawaki, et al. "Measurements of time variation of cosmogenic C-14 from 2500-year-old tree rings", *Proc. 27th Intern. Cosmic Ray Conf.*, Hamburg, **10**, 4133-4136 (2001).

McElhinny M.W. and W.E. Senanayake "Variations in the geomagnetic dipole. I. The past 50000 years ", *J. Geomagn. and Geoelectr.*, **34**, 39-51 (1982).

Masuda K., H. Furuzawa, H. Miyahara et al. "Radiocarbon Content in Japanese Cedar during the Maunder Minimum", *Proc. 28th Intern. Cosmic Ray Conf.,* Tsukuba, **7**, 4143-4146 (2003).

Miyahara H., K. Masuda, H. Furuzawa1 et al. "Variation of the Radiocarbon Content of Tree Rings during the Spoerer Minimum", *Proc. 28th Intern. Cosmic Ray Conf.,* Tsukuba, **7**, 4139-4142 (2003).

Montgomery **C.G.** and D.D. Montgomery "The intensity of neutrons of thermal energy in the atmosphere at sea level, *Phys. Rev.,* **56**, 10-12 (1939).

Muraki Y., G. Kocharov, T. Nishiyama, et al. "The new Nagoya radiocarbon laboratory", *Radiocarbon*, **40**, 177-182 (1998).

Nishimura J., M. Fujii, and T. Taira "Electron spectrum at the high energy side", *Proc. 16th Intern. Cosmic Ray Conf.*, Kyoto, **1**, 488-493 (1979).

Peristykh A.N. and P.E. Damon "Modulation of atmospheric C-14 concentration by the solar wind and irradiance components of the Hale and Schwabe solar cycles", *Solar Physics*, **177**, No. 1-2, 343-355 (1998).

Pfotzer G. "Calculation of the equilibrium amount of beta-active carbon in the atmosphere from data on cosmic neutrons", *Z. Naturforsch.*, **7a**, 145-149 (1952).

Sakurai H., K. Endo, A. Suzuki, et al. "High accurate C-14 measurement of an old tree rings in the past 2500 years", *Proc. 26th Intern. Cosmic Ray Conf.*, Salt-Lake City, **7**, 421-424 (1999)

Sakurai H., W. Kato, T. Gandou et al. "Measurements of C-14 concentration for 22 single-year tree rings of an old cedar ca. 2500 years ago", *Proc. 28th Intern. Cosmic Ray Conf.,* Tsukuba, **7**, 4135-4138 (2003).

Sonett C.P. and L.A. Smith "Cosmic ray anomaly and lunar Saros cycle", *Proc. 26th Intern. Cosmic Ray Conf.,* Salt Leik City, **7**, 448-451 (1999).

Stuiver M. and B. Becker "High-precision decadal calibration of the radiocarbon time scale, AD 1950-6000 BC" *Radiocarbon*, **35**, No. 1, 35-65 (1993).

Stuiver M. and T.F. Braziunas "The solar component of the atmospheric ^{14}C record", In *Secular, Solar and Geomagnetic Variations in the Last 10,000 Years* (ed. F.R. Stephenson and A.W. Wolfendale), Dordrecht, Kluwer Ac. Press, 245-266 (1988).

Stuiver M. and T.F. Braziunas "Atmospheric C-14 and century-scale solar oscillations", *Nature*, **338**, 405- 408 (1989).

Stuiver M. and T.F. Braziunas "Sun, ocean climate and atmospheric $^{14}CO_2$: an evaluation of causal relationships", *The Holocene*, **3**, 289-305 (1993).

Stuiver M. and P.J. Reimer "Extended C-14 data-base and revised Calib 3.0 C-14 AGE calibration program", *Radiocarbon*, **35**, No. 1, 215-230 (1993).

Stuiver M., G.W. Pearson, and T. Braziunas "Radiocarbon age calibration of marine samples back to 9000 Cal Yr BP", *Radiocarbon*, **28**, 980-1021 (1986).

Stuiver M., P.J. Reimer, and T.F. Braziunas "High-precession radiocarbon age calibration for terrestrial and marine samples", *Radiocarbon*, **40**, 1127-1151 (1998).

Suess H.E. "Secular Variations of the Cosmic-Ray-Produced Carbon 14 in the Atmosphere and Their Interpretation", *J. Geophys. Res.*, **70**, No. 23, 5937-5952 (1965).

Suess H.E. "The radiocarbon record in tree rings of the last 8000 years" *Radiocarbon*, **22**, 200-209 (1980).

Van der Plicht J., H.A.J. Meijer, B. van Geel, and H. Renssen "PE-02: Climate Change", *Scientific Report 1995-1997*, Netherlands, 1998.

Wilkom H. and H. Erlenkenser "University of Kiel radiocarbon measurements, III" *Radiocarbon*, **10**, No. 2, 328-332 (1968).

References for Chapter 18.

Adair R.K. "Constraints on biological effects of weak extremely low frequency electromagnetic fields", *Phys. Rev.*, **A43**, No. 2, 1039-1048 (1991).

Ahluwalia H.S., G.R. Gisler, and L.I. Dorman "Milagro: an ideal detector for monitoring space weather?", In *Solar Drivers of Interplanetary and Terrestral Disturbances*, ASP Conference Series, **95**, 518-525 (1996).

Aitbaev F.B., A.A. Vorobjev, A.Kh. Lyakhova, V.V. Oskomov, E.V. Kolomeets, A.N. Pegoev, Sh.D. Fridman, and N.V. Slunyaeva "Experimental determination of the neutron flux dependence from water contain in snow and from humidity of soil", *Proc. of Institute of Applied Geophysics*, Moscow, 60-66, (1985).

Akasofu S.I. "Energy coupling between the solar wind and the magnetosphere", *Space Sci. Rev.*, **28**, No. 2, 121-190 (1981).

Aleksanyan T.M., Ya.L. Blokh, L.I. Dorman, I.V. Dorman, I.Ya. Libin and A.N. Khodzhaev "Shore effect in cosmic rays", *Proc. 16th Intern. Cosmic Ray Conf.*, Kyoto, **4**, 365-367 (1979a).

Aleksanyan T.M., Ya.L. Blokh, L.I. Dorman and F.A. Starkov "Examination of the differences in the coupling coefficients and barometric coefficients of 3 NM-64 neutron supermonitor and lead-free monitor", *Proc. 16th Intern. Cosmic Ray Conf.*, Kyoto, **4**, 321-324 (1979b).

Aleksanyan T.M., V.M. Bednazhevsky, Ya.L. Blokh, L.I. Dorman, N.S. Kaminer, and F.A. Starkov "Experimental verification of the theoretical calculations of geomagnetic cutoff rigidities on the basis of the results of cosmic ray measurements on board r/v "Academician Kurchatov", *Proc. 17th Intern. Cosmic Ray Conf.*, Paris, **4**, 225-228 (1981).

Asatrian G.A., Gr.A. Asatrian, V.Kh. Babayan, Yu.I. Stozhkov, and G.Zh. Oganian "Increasing of cosmic ray ionizing component intensity during Spitak earthquake 1988", *Izvestia Academy of Sciences of the USSR*, Phys. Series, **55**, No. 10, 1979-1981 (1991).

Badhwar G.D. and P.M. O'Neill "Galactic cosmic radiation model and its applications", *Adv. Space Res.*, **17**, No. 2, 7-17 (1996).

Baevsky R.M., V.M. Petrov, G. Cornélissen et al. "Meta-analyzed heart rate variability, exposure to geomagnetic storms, and the risk of ischemic heart disease", *Scripta medica*, **70**, 199–204 (1997).

Beaujean R., J. Kopp, and G. Reitz "Radiation exposure in civil aircraft", *Radiat. Prot. Dosimetry*, **85**, 1-4 (1999).

Belov A.V. "The connection of cosmic ray variations with interplanetary and geomagnetic disturbances: diagnostics and prognosis", *The Proceedings of Conf. on the Physics of Solar-Terrestrial Links*, Irkutsk, 24-29 September 2001, in *Solar-Terrestrial Physics* (Irkutsk), No. 2 (115), 68-73 (2002).

Belov A.V., L.I. Dorman, E.A. Eroshenko, N. Iucci, G. Villoresi, and V.G. Yanke "Search for predictors of Forbush-decreases", *Proc. 24th Intern. Cosmic Ray Conf.*, Rome, **4**, 888-891 (1995).

Belov A., L. Dorman, E. Eroshenko, L. Gromova, N. Iucci, D. Ivanus, M. Parisi, N. Ptitsyna, M. Tyasto, E. Vernova, G. Villoresi, and V. Yanke "The relation between malfunctions of satellites at different orbits and cosmic ray variations", *Proc. 28th Intern. Cosmic Ray Conf.*, Tsukuba, **7**, 4213-4216 (2003a).

Belov A., L. Dorman, N. Iucci, O. Kryakunova, N. Ptitsyna "The relation of high- and low-orbit satellite anomalies to different geophysical parameters", *Proc. of Rhodos ESPRIT Workshop*, in press (2003b).

Belov A. and E. Eroshenko "Cosmic Ray Observations for Space Weather", *The Proceedings for the 22-nd ISTC Japan Workshop on Space Weather Forecast*, Japan, 2002, Vol. 1, 74-94 (2002).

Belov A.V., E.A. Eroshenko, V.A. Oleneva, Kh.I. Dalgatova, and V.G. Yanke "Prognosis properties of cosmic ray pitch-angle distribution before great geomagnetic storms according to data of neutron monitors", *The Proceedings of Conf. on the Physics of Solar-Terrestrial Links*, Irkutsk, 24-29 September 2001, in *Solar-Terrestrial Physics* (Irkutsk), No. 2 (115), 83-85 (2002).

Belov A.V., E.A. Eroshenko, and V.G. Yanke "Indices of cosmic ray activity as reflection of situation in interplanetary medium", *Workshop on Space Weather*, ESA, ESTEC, 325-328 (1999).

Bennet W.R. "Cancer and power lines", *Phys. Today*, **47**, No. 4, 23-29 (1994).

Blokh Ya.L., V.M. Bondarenko, and A.G. Tarkhov "Underground registration of cosmic rays intended on the solution of some geological problems", *Geomagnetism and Aeronomy*, **3**, No. 2, 390-392 (1963).

Blokh Ya.L., V.M. Bondarenko, N.D. Kovalenko, and A.G. Tarkhov "On the cosmic ray use in the aim of underground geophysical prospecting", *Applied Geophysics* (Moscow), **38**, 142-157 (1964).

Blokh Ya.L., V.M. Bondarenko, and A.G. Tarkhov "Using of cosmic rays for solving of geological-geophysical problems", *Cosmic Rays* (NAUKA, Moscow), **7**, 208-225 (1965).

Blokh Ya.L., V.M. Bondarenko, and A.G. Tarkhov "Using of cosmic rays for solving some geological problems", *Cosmic Rays* (NAUKA, Moscow), **8**, 209-213 (1967).

Boos E.Y., E.V. Kolomeets, and Sh.D. Fridman "The Method of the Pollution Level Determination of the Earth's Atmosphery", *Patent No. 1427983*, USSR (1983).

Bondarenko V.M., Ya.L. Blokh, A.G. Tarkhov, and N.D. Kovalenko "Method of underground geophysical investigations", Patent No. 148162 with prioritet at 29 December, 1960.

Cecchini S., A.C. Ramusino, F. Frontera, M. Galli, I. Longo, M. Ricciotti, and R. Sacchetti "A real time compact monitor for environmental radiation: cosmic rays and radioactivity", *Proc. 24th Intern. Cosmic Ray Conf.*, Rome, **4**, 1329 (1995).

Clay J. and A.G.M. Van Gemert "Absorption of the hard cosmic rays in different materials", *Physica,* **6**, No. 7, 649-655 (1939).

Despotashvili M.A., N.G. Khazaradze, N.A.Nachkebia, L.Kh. Shatashvili, and D.I. Sikharulidze "Anomalous solar-diurnal variation of Cosmic Ray Neutron and Hard components intensity, cosmic phenomena and the problem of Earthquakes", *Proc. 26th Intern. Cosmic Ray Conf.*, Salt Lake City, **7**, 440-443 (1999a).

Despotashvili M.A., N.A. Nachkebia, and L.Kh. Shatashvili "Unusual changes of solar diurnal variations of cosmic ray neutron and hard components intensity", *Proc. 26th Intern. Cosmic Ray Conf.*, Salt Lake City, **7**, 284-287 (1999b).

Dorman L.I. "On the Cosmic Ray World Service", *Izvestia Academy of Science of USSR*, Seria Phys., **57**, No. 7, 149-152 (1993).

Dorman L.I. "On the prediction of great flare energetic particle events to save electronics on spacecrafts", *Proc. 26th Intern. Cosmic Ray Conf.*, Salt Lake City, **6**, 382-385 (1999a).

Dorman L.I. "How to Save Microelectronics Code on Satellites, Rockets and Balloons from Great Solar Energetic Particle Events", *Proc. 14th European Space Agency Symposium,* Potsdam, Germany, 207-210 (1999b).

Dorman L.I. "Expected Gamma-Ray Fluxes from Interactions of Flare Energetic Particles with Solar Wind Matter", in *Gamma-Ray Astrophysics, 2001* (ed. S. Ritz et al.), AIP Conf. Proc., Vol. 587, 628-632 (2001a).

Dorman L.I. "Possible Using of Gamma Ray Measurements for Monitoring and Prediction of Radiation Hazard", in *15th ESA Symposium on European Rocket and Balloon Programmes and Related Research*, Biarritz 28-31 May 2001, 457-462 (2001b).

Dorman L.I. "Cosmic ray long-term variation: even-odd cycle effect, role of drifts, and the onset of cycle 23", *Adv. Space Res.*, **27**, No. 3, 601-606 (2001c).

Dorman L.I. "Solar Energetic Particle Events and Geomagnetic Storms Influence on People's Health and Technology; Principles of Monitoring and Forecasting of Space Dangerous Phenomena by Using On-Line Cosmic Ray Data", in *Proc. 22nd ISTC Japan Workshop on Space Weather Forecast in Russia/CIS* (ed. Y. Muraki), Nagoya University, **2**, 133-151 (2002).

Dorman L.I. "Determination of cosmic ray intensity variations in the last 400 years on the basis of solar activity data with taking into account convection-diffusion and drift mechanisms: applications to radiocarbon and climate change data", *2nd World Space Congress and 34th COSPAR*, Houston, October 2002, *Adv. Space Res.* (2003a), submitted for publication.

Dorman L.I. "Cosmic rays and Space Weather", in *The Early Universe and the Cosmic Microwave Background: Theory and Observations* (ed. N.G. Sanchez and Yu.I. Parijskij), NATO Science Series, **130**, 517-557 (2003b).

Dorman L.I. "Principles of cosmic ray using for space weather monitoring and forecasting", *Proc. 28th Intern. Cosmic Ray Conf.*, Tsukuba, **7**, 4269-4272 (2003c).

Dorman L.I., T.M. Aleksanyan et al. "Experimental examination of theoretical calculations of geomagnetic cutoff rigidity", *Geomagnetism and Aeronomy*, **22**, No. 5, 858-861 (1982).

Dorman L.I., A.V. Belov, E.A. Eroshenko, L.A. Pustil'nik, A. Sternlieb, V.G. Yanke, and I.G. Zukerman "Possible cosmic ray using for forecasting of major geomagnetic storms, accompanied by Forbush-effects", *Proc. 28th Intern. Cosmic Ray Conf.*, Tsukuba, **6**, 3553-3556 (2003).

Dorman I.V. and L.I. Dorman "Solar wind properties obtained from the study of the 11-year cosmic ray cycle", *J. Geophys. Res.*, **72**, No. 5, 1513-1520 (1967a).

Dorman I.V. and L.I. Dorman "Propagation of energetic particles through interplanetary space according to the data of 11-year cosmic ray variations", *J. Atmosph. and Terr. Phys.*, **29**, No.4, 429-449 (1967b).

Dorman I.V., L.I. Dorman, V.K. Korotkov, and I.Ya. Libin " Neutron multiplication in lead-free monitors and its possible applications ", *Izvestia Academy of Sciences of USSR*, Series Phys., **48**, No. 11, 2123-2125 (1984a).

Dorman I.V., L.I. Dorman, V.K. Korotkov, and I.Ya. Libin "Influence of environment chemical contents on the without lead neutron monitor data", *Geomagnetism and Aeronomy*, **24**, No. 5, 823-825 (1984b).

Dorman I.V., L.I. Dorman, and I.Ya. Libin "Sensitivity of single and multiple cosmic ray neutrons to the surrounding medium in a lead-free monitor", *Proc. 19th Intern. Cosmic Ray Conf.*, La Jolla, **5**, 490-493 (1985).

Dorman L.I., I.V. Dorman, I.Ya. Libin, and A.N. Khodzhaev "Coupling coefficients and latitude effect of the cosmic ray neutron component inferred from the expedition measurements with a lead-free monitor", *Proc. 16th Intern. Cosmic Ray Conf.*, Kyoto, **4**, 325-328 (1979).

Dorman L.I, Iucci N., Villoresi G. "The use of cosmic rays for continuos monitoring and prediction of some dangerous phenomena for the Earth's civilization", *Astrophysics and Space Science*, **208**, 55-68 (1993a).

Dorman L.I., Iucci N. and Villoresi G. "Possible monitoring of space processes by cosmic rays", *Proc. 23th Intern. Cosmic Ray Conf.*, Calgary, **3**, 695-698 (1993b).

Dorman L.I., Iucci N. and Villoresi G. "Space dangerous phenomena and their possible prediction by cosmic rays", *Proc. 23th Intern. Cosmic Ray Conf.*, Calgary, **3**, 699-702 (1993c).

Dorman L.I., Iucci N., Villoresi G. "The nature of cosmic ray Forbush-decrease and precursory effects", Proc. 24th Intern. Cosmic Ray Conf., Rome, Vol. 4, pp. 892-895 (1995a).

Dorman L.I., N.Iucci, N.G.Ptitsyna, G.Villoresi "Cosmic ray Forbush-decrease as indicators of space dangerous phenomenon and possible use of cosmic ray data for their prediction", *Proc. 26th Intern. Cosmic Ray Conf.*, Salt Lake City, **6**, 476-479 (1999).

Dorman, L. I. ; Villoresi, G. ; Iucci, N. ; Parisi, M. ; Tyasto, M. I., Danilova, O. A. ; Ptitsyna, N. G., "Cosmic ray survey to Antarctica and coupling functions for neutron component near solar minimum (1996-1997), 3, Geomagnetic effects and coupling functions", *J. Geophys. Res.*, **105**, No. A9, p. 21,047-21,058 (2000).

Dorman L.I., N. Iucci, N.G. Ptitsyna, G. Villoresi "Cosmic rays as indicators of space weather influence on the incidence of myocardial infarction, brain stroke, car and train accidents", *Proc. 27th Intern. Cosmic Ray Conf*, Hamburg, **9**, 3511-3514 (2001a).

Dorman L.I., I.V. Dorman, N. Iucci, M. Parisi, and G. Villoresi "Hysteresis between solar activity and cosmic rays during cycle 22: the role of drifts, and the modulation region", *Adv. Space Res.*, **27**, No. 3, 589-594 (2001b).

Dorman L.I., N. Iucci, and G. Villoresi "Time lag between cosmic rays and solar activity; solar minimum of 1994-1996 and residual modulation", *Adv. Space Res.*, **27**, No. 3, 595-600 (2001c).

Dorman L.I. for INTAS-00810 Team "Different space weather effects in malfunctions of the high and low orbital satellites", Report on 34 COSPAR Sci. Assambley, Houston (2002); *Adv. Space Res.*, submitted for publication.

Dorman L.I., N. Iucci, M. Murat, M. Parisi, L.A. Pustil'nik, A. Sternlieb, G. Villoresi, and I.G. Zukerman "Dangerous FEP events: real-time data of ground and satellite CR measurements using for monitoring of beginning and forecasting of expected particle fluxes in atmosphere and in space", *Proc. 28th Intern. Cosmic Ray Conf.*, Tsukuba, **6**, 3411-3414 (2003a).

Dorman L.I. and L.A. Pustil'nik "Solar cosmic ray events: statistical characteristics for the diagnostic of acceleration, excaping and propagation processes", *Proc. 24th Intern. Cosmic Ray Conf.*, Rome, **4**, 86-89 (1995).

Dorman L.I. and L.A. Pustil'nik "Statistical characteristics of FEP events and their connection with acceleration, escaping and propagation mechanisms", *Proc. 26th Intern. Cosmic Ray Conf.*, Salt Lake City, **6**, 407-410 (1999).

Dorman Lev, Lev Pustil'nik, Abraham Sternlieb, and Igor Zukerman "Using Ground-Level Cosmic Ray Observations for Automatically Generating Predictions of Hazardous Energetic Particle Levels", *Adv. Space Res.*, **31**, No. 4, 847-852 (2003).

Dorman L.I., L.A. Pustil'nik, A. Sternlieb, I.G. Zukerman, A.V. Belov, E.A. Eroshenko, V.G. Yanke, H. Mavromichalaki, C. Sarlanis, G. Souvatzoglou, S. Tatsis, N. Iucci, G. Villoresi, Yu. Fedorov, B.A. Shakhov, and M. Murat "Monitoring and Forecasting of Great Solar Proton Events Using the Neutron Monitor Network in Real Time", *IEEE Plasma Sciences*, in press (2004).

Dorman L.I., G. Villoresi, A.V. Belov, E.A. Eroshenko, N. Iucci, V.G. Yanke, K.F. Yudakhin, B. Bavassano, N.G. Ptitsyna, and M.I. Tyasto "Cosmic-ray forecasting features for big Forbush-decreases", *Nuclear Physics B*, **49A**, 136-144 (1995b).

Dorman L.I. and V.G. Yanke "Cosmic rays in the Mercurian atmosphere", *Proc. 16th Intern. Cosmic Ray Conf.*, Kyoto, **3**, 180 (1979a).

Dorman L.I. and V.G. Yanke "The expected meteorological effects in cosmic rays as measured on the Martian surface", *Proc. 16th Intern. Cosmic Ray Conf.*, Kyoto, **3**, 192 (1979b).

Dorman L.I. and V.G. Yanke "Cosmic rays in the Jovian atmosphere", *Proc. 16th Intern. Cosmic Ray Conf.,* Kyoto, **3**, 193 (1979c).

Dorman L.I., V.G. Yanke, A.B. Kaichermazov, and A.S. Kumakhov "Secondary components of cosmic rays in the Martian atmosphere; integral multiplicities of generation and coupling coefficients for measurements on the Martian surface", *Proc. 16th Intern. Cosmic Ray Conf.,* Kyoto, **3**, 187-191 (1979a).

Dorman L.I., V.G. Yanke, and O.Kh. Unezhiv "Secondary cosmic ray components in the Venusian and Jovian atmospheres", *Proc. 16th Intern. Cosmic Ray Conf.,* Kyoto, **3**, 181-185 (1979b).

Dorman L.I. and I.G. Zukerman "Initial concept for forecasting the flux and energy spectrum of energetic particles using ground-level cosmic ray observations", *Adv. Space Res.*, **31**, No. 4, 925-932 (2003).

Dunbar A., A. Lockrige, and S. Whiteside "Catalog of significant Earthquakes 2150. B.C-191", World Center A., Boulder USA (1992).

Flückiger E.O., R. Bütikofer, L. Desorgher, and M.R. Moser "Global cosmic ray cutoff rigidities over the past 2000 years", *Proc. 28th Intern. Cosmic Ray Conf.*, Tsukuba, **7,** 4229-4232 (2003).

Fridman Sh.D., E.V. Kolomeets, V.V. Oskomov, and A.A. Vorobjev "An Application of Cosmic Rays for Solving Some Ecology and Hydrology Problems", *Proc. 24th Intern. Cosmic Ray Conf.*, Rome, **4**, 1326-1328 (1995).

Friedberg W., K Copeland, F.E.Duke et al. "Guideleness and technical information provided by the Federal Aviation Administration to promote radiation safety for air carrier crew members", *Radiat. Prot. Dosimetry*, **86**, No. 4, 323-327 (1999).

Friedman, H., R.O. Becker and C.H. Bachman "Effect of magnetic fields on reaction time performance", *Nature*, **213**, No. 5079, 949-950 (1967).

Galper A.M., S.V. Koldashov, and S.A. Voronov "High-energy particle-flux variations as earthquake predictors", *Adv. Space Res.*, **15**, No. 11, 131-134 (1995).

Galper A.M., S.V. Koldashov, L.V. Maslennikov, V.V. Mikhailov, N.I. Shevtz, and S.A. Voronov "Energy Spectra of Stationary and Unstable Electron Radiation Belts", *Proc. 25th Intern. Cosmic Ray Conf.*, Durban, **2**, 333-336 (1997a).

Galper A.M., S.V. Koldashov, L.V. Maslennikov, A.M. Murashov, N.I. Shevtz, and S.A. Voronov "High Energy Charged Particle Waves on the Low Boundary of the Radiation Belt", *Proc. 25th Intern. Cosmic Ray Conf.*, Durban, **2**, 349-352 (1997b).

Galper A.M., S.V. Koldashev, A.M. Murashev, and S.A. Voronov "The fluctuations of high-energy charged particle fluxes in the near-Earth space and the earthquake prediction", *Proc. 26th Intern. Cosmic Ray Conf.*, Salt Lake City, **7**, 444-447 (1999).

Galperin Yu.I., V.A. Gladyshev, N.V. Dzshordzshio, V.I. Larkina, and M.M. Mogilevsky "Precipitation of energetic trapped particles in magnetosphere over epicenter of reading earthquake", *Kosmicheskie Issledovanija.*, **30**, No. 1, 89-106 (1992).

Gokhberg M.V., A.V. Kustov, V.A. Liperovsky, R.K. Liperovskaja, E.P. Kharin, S.L. Shalimov "On disturbances in F-layer of ionosphere before strong earthquakes", *Izvestia of Academy of Sciences of USSR*, Series Physics of Earth, No. 4, 12-20 (1988).

Iucci N., G. Villoresi, L.I. Dorman, and M. Parisi "Cosmic ray survey to Antarctica and coupling functions for neutron component near solar minimum (1996-1997), 2. Determination of meteorological effects", *J. Geophys. Res.*, **105**, No. A9, 21,035-21,046 (2000).

Jockel P. "Cosmogenic ^{14}CO as tracer for atmospheric chemistry and transport", *Dissertation Dr. of Natural Sciences*, Heidelberg – Mainz, Germany, pp. 347 (2000).

Kodama M., S. Kawasaki, and M. Wada "Cosmic ray snow gauge", *J. Appl. Rad. Isotopes*, **26**, No. 12, 774-775 (1975).

Kogan R.M., I.M. Nazarov, and Sh.D. Fridman "Gamma spectrometry of natural environments and formations", *Israel Prog. for Sci. Trans.* No. 5778 (1969).

Konig H.H. "Behavioral changes in human subjects associated with ELF electric fields", in *ELF and VLF Electromagnetic Field Effects* (M.A. Persinger, Ed.), New York, Plenum, 81-133 (1974).

Konig, H.H. and F. Ankermuller "Uber den Einfluss besonders niederfrequenter elektrischer Vorgange in der Atmosphare auf den Menschen", *Naturwissenschaften*, **47**, 486-490 (1960).

Kudela K., M. Storini, M.Y. Hoper, and A. Belov "Cosmic rays in relation to space weather", *Space Sci. Rev.*, **93**, 153-174 (2000).

Molchanov O.A. "Propagation of electromagnetic fields from seismic sources into the upper ionosphere", *Geomagnetism and Aeronomy*, **31**, 111-119 (1991).

Mortazavi S.M.J., J.R. Cameron, and A. Niroomand-rad "Is the Adaptive Response an Efficient Protection Against the Detrimental Effects of Space Radiation", *Proc. 28th Intern. Cosmic Ray Conf.*, Tsukuba, **4**, 2299-2302 (2003).

Munakata K., J.W. Bieber, S.-I. Yasue, et al. "Precursors of geomagnetic storms observed by the muon detector network", *J. Geophys. Res.*, **105**, No. A12, 27,457-27,468 (2000).

Ptitsyna N.G., G. Villoresi, M.I. Tyasto, N. Iucci, and L.I. Dorman "Possible effect of geomagnetic disturbances on the incidence of traffic accidents (St. Petersburg 1987-1989)", *Phys. Med.*, **11**, No. 3, 93-101 (1995).

Ptitsyna N.G., G. Villoresi, L.I. Dorman, N. Iucci, and M. I. Tyasto "Natural and man-made low-frequency magnetic fields as a potential health hazard", *UFN (Uspekhi Fisicheskikh Nauk)*, **168**, No 7, 767-791 (1998).

Pustovetov V.P. and A.B. Malyshev "Space-time correlation of earthquakes and variation of high energy particle flux in the inner radiation belt", *Kosmicheskie Issledovanija.*, **31**, No. 5, 84-90 (1993).

Reiter R. "Bio-meteorologie auf physikalisher Basis", *Phys. Blaetter*, **11**, 453-464 (1955)

Roederer J.G. "Are magnetic storms hazardous to your health?", *EOS Transactions* (American Geophysical Union), **76**, No. 44, 441, 444-445 (1995).

Shatashvili L.Kh., D.I. Sikharulidze, N.G. Khazaradze, and N.G. Tutberidse "Anomal daily variations of neutron and muon cosmic ray components during periods of the Earth's crossing of neutral sheet of interplanetary magnetic field", *Izvestia of Russian Academy of Sciences*, Physical Series, **63 , No.** 8, 1645-1648 (1999).

Shea M.A. and D.F. Smart "Cosmic rays, geomagnetic field and climate change", *2nd World Space Congress and 34th COSPAR*, Houston, October 2002, *Adv. Space Res.* (2003a), submitted for publication.

Shea M.A. and D.F. Smart "Preliminary Study of the 400-Year Geomagnetic Cutoff Rigidity Changes, Cosmic Rays and Possible Climate Changes", *Proc. 28th Intern. Cosmic Ray Conf.*, Tsukuba, **7,** 4205-4208 (2003b).

Shea M.A., D.F. Smart, and H. Carmichael "Summary of cutoff rigidities calculated with the International Geomagnetic Reference Field for various epochs", *Rep. AFGL-TR-76-0115*, Environ. Res. Pap. 651, Air Force Geophys. Lab., Bedford, Mass. (1976).

Sitinski A.D. "On the relationship of the Earth's seismicity with processes in the interplanetary space and in atmosphere", *Docladi Akademii Nauk SSSR*, **295**, No. 2, 338-341 (1987).

Sitinski A.D. "On the relationship of earthquakes with solar activity", *Izvestija Akademii nauk SSSR*, Ser. Fisika Zemli, **55**, № 2, 13-30 (1989).

Smart D.F. and M.A. Shea "Evaluation of Magnetic Shielding of Interplanetary Spacecraft from Cosmic Radiation", *Proc. 28th Intern. Cosmic Ray Conf.*, Tsukuba, **6**, 3481-3484 (2003a).

Smart D.F. and M.A. Shea "Geomagnetic cutoff rigidity calculations at 50-year intervals between 1600 and 2000", *Proc. 28th Intern. Cosmic Ray Conf.*, Tsukuba, **7,** 4201-4204 (2003b).

Sobolev G.A., I.P. Shestopalov, and E.P. Kharin "Geoeffective solar flares and seismic activity of the Earth", *Fizika Zemli*, No. 7, 85-90 (1998).

Srivastava B.J. and S. Saxena "Geomagnetic-biological correlations: some new results", *Indian J. of Radio and Space Phys.*, **9**, No. 4, 121-126 (1980).

Stassinopoulos E.G., C.A. Stauffer, and G.J. Brucker "A systematic global mapping of the radiation field at aviation altitudes", *Space Weather*, **1**, No. 1, 1005, 1-9 (2003).

Stozhkov Y.I., N.S. Svirzhevsky, and V.S. Makhmutov "Cosmic ray measurements in the atmosphere", *Preprint No. 8*, FIAN, Moscow, 1-21 (2001).

Struminsky A. "Forbush precursory increase and shock associated particles on October 20, 1989", *Anales Geophysicae*, **20**, No. 8, 1247-1252 (2002).

Tsyganenko N.A. "A magnetospheric magnetic field model with a warped tail current sheat", *Planet. Space Sci.*, **37**, No. 1, 5-20 (1989).

Tsyganenko N.A. and D.P. Stern "Modeling the global magnetic field of the large-scale Birkeland current system", *J. Geophys. Res.*, **101**, No. A12, 27187-27198 (1996).

Villoresi G., T.K. Breus, L.I. Dorman, N. Iucci,and S.I. Rapoport "The influence of geophysical and social effects on the incidences of clinically important pathologies (Moscow 1979-1981)", *Physica Medica*, **10**, No 3, 79-91 (1994a).

Villoresi G., Y.A. Kopytenko, N.G. Ptitsyna, M.I. Tyasto, E.A. Kopytenko, N. Iucci, and P.M. Voronov "The influence of geomagnetic storms and manmade magnetic field disturbances on the incidence of myocardial infarction in St. Petersburg (Russia)", *Phys. Med.*, **10**, No. 4, 107-117 (1994b).

Villoresi G., L.I. Dorman, N.G. Ptitsyna, N. Iucci, and M.I. Tyasto "Forbush-decreases as indicators of health-hazardous geomagnetic storms", *Proc. 24th Intern. Cosmic Ray Conf.*, Rome, **4**, 1106-1109 (1995).

Villoresi G., L.I. Dorman, N. Iucci, and N.G. Ptitsyna "Cosmic ray survey to Antarctica and coupling functions for neutron component near solar minimum (1996-1997), 1, Methodology and data quality assurance", *J. Geophys. Res.*, **105**, No. A9, 21,025-21,034 (2000).

Volodichev N.N., B.M. Kuzhevskij, O.Yu. Nechaev et al. "Unusual Burst of Thermal Neutron Intensity at Height of 4200m above Sea Level during July 22, 1990 Solar Eclipse", *Astron. Tsirk. Akad. Nauk SSSR*, No.1547, 25-26 (1991).

Volodichev N.N., B.M. Kuzhevskij, O.Yu. Nechaev et al. "Neutron Intensity Burst during Penumbral July 26, 1991 Lunar Eclipse", *Kosmicheskie Issledovanija*, **31**, No. 4, 120-122 (1993).

Volodichev N.N., B.M. Kuzhevsky, O.Yu. Nechaev, and P.I.Shavrin "The effect of neutron intensity increase formation during new-Moon and full-Moon periods", *Proc. 24th Intern. Cosmic Ray Conf.*, Rome, **4**, 1151-1154 (1995).

Volodichev N.N., B.M. Kuzhevskij, O.Yu. Nechaev et al. "Phenomenon of Neutron Intensity Bursts during New and Full Moons, *Kosmicheskie Issledovanija*, **35**, No. 2, 135-143 (1997a).

Volodichev N.N., B.M. Kuzshevskij, O.Yu. Nechaev, M.M. Panasjuk, and P.I. Shavrin "The phenomenon of neutron intensity bursts appearing in periods of new and full Moon", *Kosmicheskie Issledovanija*, **35**, No. 2, 144-154 (1997b).

Volodichev N.N., B.M. Kuzhevskij, O.Yu. Nechaev, M.I. Panasyuk, A.N. Podorolsky, and P.I. Shavrin "Neutron Flux from Earth Surface at Newmoon and Fullmoon", *Proc. 25th Intern. Cosmic Ray Conf.*, Durban, **2**, 441-444 (1997c).

Volodichev N.N., I. Kushevski, O. Nechaev, and M.I. Panasyuk "Lunar periodicity of the neutron radiation burst and seismic activity on the Earth", *Proc. 26th Intern. Cosmic Ray Conf.*, Salt Lake City, **7**, 437-439 (1999).

Volodichev N.N., B.M. Kuzhevskij, O.Yu. Nechaev et al. "The Astrogeophysical Reasons of Bursts Intensity Neutron Radiation and Seismic Activity on the Earth", *Preprint of Skobeltsin INP Lomonosov MSU*, No. 5/645, pp. 16 (2001a).

Volodichev N.N., A.N. Podorolsky, B.W. Levin, and V.A. Podorolsky "Correlation of appearing of great series of rarthquakes with times of new and full Moon phases", *Vulcanologiya and Seismologiya*, 7, 60-67 (2001b).

Volodichev N.N., V.A. Zakharov, B.M. Kuzhevskij, O.Yu. Nechaev, A.N. Podorolsky, A.P. Chubenko, A.L. Sh'epetov, and V.P. Antonova "The flows of neutrons of space radiation and from terrestrial crust", Proc. 27th *Intern. Cosmic Ray Conf.*, Hamburg, **10**, 4204-4207 (2001c).

Vorobjev A.A., E.V. Kolomeets, V.V. Oskomov, R.G.-E. Pfeffer, and Sh.D. Fridman "Block for conjunction of water contain in snow detector based on measurements of CR neutrons with automatical meteorological station", *Proc. of Institute of Applied Geophysics*, Moscow, 72-78 (1985).

Voronov S.A., A.M. Galper, V.G. Kirillov-Ugriymov, S.V. Koldashov, V.V. Mikhailov, A.V. Popov, and V.Yu. Chesnokov "Registration of sporadic increase of high energy particle flux near the Brazilian anomaly region", *Proc. 20th Intern. Cosmic Ray Conf.*, Moscow, **4**, 451-452 (1987).

Voronov S.A., A.M. Galper, S.V. Koldashev, V.V. Mikhailov, P.Yu. Naumov, A.V. Popov, and V.Yu. Chesnokov "Magnetic spectrometer of charged particles Marija-2" *Pribori i Tehnika Experimenta (PTE)*, No. 2, 59-61 (1991).

Yu Zhen-dong "Strong Earthquakes, Novae and Cosmic Ray Environment", *Proc. 19th Intern. Cosmic Ray Conf.*, La Jolla, **5**, 529-532 (1985).

Zhou D., D. O'Sullivan, E. Semones et al. "Dose Equivalent, Absorbed Dose and Charge Spectrum Measurements Made in the International Space Station Orbit", *Proc. 28th Intern. Cosmic Ray Conf.*, Tsukuba, **4**, 2263-2266 (2003).

Object Index

Author Index

Astrophysics and Space Science Library

Volume 300: ***Scientific Detectors for Astronomy,*** edited by Paola Amico, James W. Beletic, Jenna E. Beletic
Hardbound, ISBN 1-4020-1788-X, February 2004

Volume 299: ***Open Issues in Local Star Fomation,*** edited by Jacques Lépine, Jane Gregorio-Hetem
Hardbound, ISBN 1-4020-1755-3, December 2003

Volume 298: ***Stellar Astrophysics - A Tribute to Helmut A. Abt,*** edited by K.S. Cheng, Kam Ching Leung, T.P. Li
Hardbound, ISBN 1-4020-1683-2, November 2003

Volume 297: ***Radiation Hazard in Space,*** by Leonty I. Miroshnichenko
Hardbound, ISBN 1-4020-1538-0, September 2003

Volume 296: ***Organizations and Strategies in Astronomy, volume 4,*** edited by André Heck
Hardbound, ISBN 1-4020-1526-7, October 2003

Volume 295: ***Integrable Problems of Celestial Mechanics in Spaces of Constant Curvature,*** by T.G. Vozmischeva
Hardbound, ISBN 1-4020-1521-6, October 2003

Volume 294: ***An Introduction to Plasma Astrophysics and Magnetohydrodynamics,*** by Marcel Goossens
Hardbound, ISBN 1-4020-1429-5, August 2003
Paperback, ISBN 1-4020-1433-3, August 2003

Volume 293: ***Physics of the Solar System,*** by Bruno Bertotti, Paolo Farinella, David Vokrouhlický
Hardbound, ISBN 1-4020-1428-7, August 2003
Paperback, ISBN 1-4020-1509-7, August 2003

Volume 292: ***Whatever Shines Should Be Observed,*** by Susan M.P. McKenna-Lawlor
Hardbound, ISBN 1-4020-1424-4, September 2003

Volume 291: ***Dynamical Systems and Cosmology,*** by Alan Coley
Hardbound, ISBN 1-4020-1403-1, November 2003

Volume 290: ***Astronomy Communication,*** edited by André Heck, Claus Madsen
Hardbound, ISBN 1-4020-1345-0, July 2003

Volume 287/8/9: ***The Future of Small Telescopes in the New Millennium,*** edited by Terry D. Oswalt
Hardbound Set only of 3 volumes, ISBN 1-4020-0951-8, July 2003

Volume 286: ***Searching the Heavens and the Earth: The History of Jesuit Observatories,*** by Agustín Udías
Hardbound, ISBN 1-4020-1189-X, October 2003

Volume 285: ***Information Handling in Astronomy - Historical Vistas,*** edited by André Heck
Hardbound, ISBN 1-4020-1178-4, March 2003

Volume 284: ***Light Pollution: The Global View,*** edited by Hugo E. Schwarz
Hardbound, ISBN 1-4020-1174-1, April 2003

Volume 283: ***Mass-Losing Pulsating Stars and Their Circumstellar Matter,*** edited by Y. Nakada, M. Honma, M. Seki
Hardbound, ISBN 1-4020-1162-8, March 2003

Volume 282: ***Radio Recombination Lines,*** by M.A. Gordon, R.L. Sorochenko
Hardbound, ISBN 1-4020-1016-8, November 2002

Volume 281: ***The IGM/Galaxy Connection,*** edited by Jessica L. Rosenberg, Mary E. Putman
Hardbound, ISBN 1-4020-1289-6, April 2003

Volume 280: ***Organizations and Strategies in Astronomy III,*** edited by André Heck
Hardbound, ISBN 1-4020-0812-0, September 2002

Volume 279: ***Plasma Astrophysics , Second Edition,*** by Arnold O. Benz
Hardbound, ISBN 1-4020-0695-0, July 2002

Volume 278: ***Exploring the Secrets of the Aurora,*** by Syun-Ichi Akasofu
Hardbound, ISBN 1-4020-0685-3, August 2002

Volume 277: ***The Sun and Space Weather,*** by Arnold Hanslmeier
Hardbound, ISBN 1-4020-0684-5, July 2002

Volume 276: ***Modern Theoretical and Observational Cosmology,*** edited by Manolis Plionis, Spiros Cotsakis
Hardbound, ISBN 1-4020-0808-2, September 2002

Volume 275: ***History of Oriental Astronomy,*** edited by S.M. Razaullah Ansari
Hardbound, ISBN 1-4020-0657-8, December 2002

Volume 274: ***New Quests in Stellar Astrophysics: The Link Between Stars and Cosmology,*** edited by Miguel Chávez, Alessandro Bressan, Alberto Buzzoni,Divakara Mayya
Hardbound, ISBN 1-4020-0644-6, June 2002

Volume 273: ***Lunar Gravimetry,*** by Rune Floberghagen
Hardbound, ISBN 1-4020-0544-X, May 2002

Volume 272:***Merging Processes in Galaxy Clusters,*** edited by L. Feretti, I.M. Gioia, G. Giovannini
Hardbound, ISBN 1-4020-0531-8, May 2002

Volume 271: ***Astronomy-inspired Atomic and Molecular Physics,*** by A.R.P. Rau
Hardbound, ISBN 1-4020-0467-2, March 2002

Volume 270: ***Dayside and Polar Cap Aurora,*** by Per Even Sandholt, Herbert C. Carlson, Alv Egeland
Hardbound, ISBN 1-4020-0447-8, July 2002

Volume 269: ***Mechanics of Turbulence of Multicomponent Gases,*** by Mikhail Ya. Marov, Aleksander V. Kolesnichenko
Hardbound, ISBN 1-4020-0103-7, December 2001

Volume 268: ***Multielement System Design in Astronomy and Radio Science,*** by Lazarus E. Kopilovich, Leonid G. Sodin
Hardbound, ISBN 1-4020-0069-3, November 2001

Volume 267: ***The Nature of Unidentified Galactic High-Energy Gamma-Ray Sources,*** edited by Alberto Carramiñana, Olaf Reimer, David J. Thompson
Hardbound, ISBN 1-4020-0010-3, October 2001

Volume 266: ***Organizations and Strategies in Astronomy II,*** edited by André Heck
Hardbound, ISBN 0-7923-7172-0, October 2001

Volume 265: ***Post-AGB Objects as a Phase of Stellar Evolution,*** edited by R. Szczerba, S.K. Górny
Hardbound, ISBN 0-7923-7145-3, July 2001

Volume 264: ***The Influence of Binaries on Stellar Population Studies,*** edited by Dany Vanbeveren
Hardbound, ISBN 0-7923-7104-6, July 2001

Volume 262: ***Whistler Phenomena - Short Impulse Propagation,*** by Csaba Ferencz, Orsolya E. Ferencz, Dániel Hamar, János Lichtenberger
Hardbound, ISBN 0-7923-6995-5, June 2001

Volume 261: ***Collisional Processes in the Solar System,*** edited by Mikhail Ya. Marov, Hans Rickman
Hardbound, ISBN 0-7923-6946-7, May 2001

Volume 260: ***Solar Cosmic Rays,*** by Leonty I. Miroshnichenko
Hardbound, ISBN 0-7923-6928-9, May 2001

Volume 259: ***The Dynamic Sun,*** edited by Arnold Hanslmeier, Mauro Messerotti, Astrid Veronig
Hardbound, ISBN 0-7923-6915-7, May 2001

Volume 258: ***Electrohydrodynamics in Dusty and Dirty Plasmas- Gravito-Electrodynamics and EHD,*** by Hiroshi Kikuchi
Hardbound, ISBN 0-7923-6822-3, June 2001

Volume 257: ***Stellar Pulsation - Nonlinear Studies,*** edited by Mine Takeuti, Dimitar D. Sasselov
Hardbound, ISBN 0-7923-6818-5, March 2001

Volume 256: ***Organizations and Strategies in Astronomy,*** edited by André Heck
Hardbound, ISBN 0-7923-6671-9, November 2000

Volume 255: ***The Evolution of the Milky Way- Stars versus Clusters,*** edited by Francesca Matteucci, Franco Giovannelli
Hardbound, ISBN 0-7923-6679-4, January 2001

Volume 254: ***Stellar Astrophysics***, edited by K.S. Cheng, Hoi Fung Chau, Kwing Lam Chan, Kam Ching Leung
Hardbound, ISBN 0-7923-6659-X, November 2000

Volume 253: ***The Chemical Evolution of the Galaxy***, by Francesca Matteucci
Paperback, ISBN 1-4020-1652-2, October 2003
Hardbound, ISBN 0-7923-6552-6, June 2001

Volume 252: ***Optical Detectors for Astronomy II***, edited by Paola Amico, James W. Beletic
Hardbound, ISBN 0-7923-6536-4, December 2000

Volume 251: ***Cosmic Plasma Physics***, by Boris V. Somov
Hardbound, ISBN 0-7923-6512-7, September 2000

Volume 250: ***Information Handling in Astronomy***, edited by André Heck
Hardbound, ISBN 0-7923-6494-5, October 2000

Volume 249: ***The Neutral Upper Atmosphere***, by S.N. Ghosh
Hardbound, ISBN 0-7923-6434-1, July 2002

Volume 247: ***Large Scale Structure Formation***, edited by Reza Mansouri, Robert Brandenberger
Hardbound, ISBN 0-7923-6411-2, August 2000

Volume 246: ***The Legacy of J.C. Kapteyn***, edited by Piet C. van der Kruit, Klaas van Berkel
Paperback, ISBN 1-4020-0374-9, November 2001
Hardbound, ISBN 0-7923-6393-0, August 2000

Volume 245: ***Waves in Dusty Space Plasmas,*** by Frank Verheest
Paperback, ISBN 1-4020-0373-0, November 2001
Hardbound, ISBN 0-7923-6232-2, April 2000

Volume 244: ***The Universe***, edited by Naresh Dadhich, Ajit Kembhavi
Hardbound, ISBN 0-7923-6210-1, August 2000

Volume 243: ***Solar Polarization***, edited by K.N. Nagendra, Jan Olof Stenflo
Hardbound, ISBN 0-7923-5814-7, July 1999

Volume 242: ***Cosmic Perspectives in Space Physics***, by Sukumar Biswas
Hardbound, ISBN 0-7923-5813-9, June 2000

Volume 241: ***Millimeter-Wave Astronomy: Molecular Chemistry & Physics in Space,*** edited by W.F. Wall, Alberto Carramiñana, Luis Carrasco, P.F. Goldsmith
Hardbound, ISBN 0-7923-5581-4, May 1999

Volume 240: ***Numerical Astrophysics,*** edited by Shoken M. Miyama, Kohji Tomisaka,Tomoyuki Hanawa
Hardbound, ISBN 0-7923-5566-0, March 1999

Volume 239: ***Motions in the Solar Atmosphere,*** edited by Arnold Hanslmeier, Mauro Messerotti
Hardbound, ISBN 0-7923-5507-5, February 1999

Volume 238: ***Substorms-4,*** edited by S. Kokubun, Y. Kamide
Hardbound, ISBN 0-7923-5465-6, March 1999

Volume 237: ***Post-Hipparcos Cosmic Candles,*** edited by André Heck, Filippina Caputo
Hardbound, ISBN 0-7923-5348-X, December 1998

Volume 236: ***Laboratory Astrophysics and Space Research,*** edited by P. Ehrenfreund, C. Krafft, H. Kochan, Valerio Pirronello
Hardbound, ISBN 0-7923-5338-2, December 1998

Missing volume numbers have not yet been published.
For further information about this book series we refer you to the following web site:
http://www.wkap.nl/prod/s/ASSL

To contact the Publishing Editor for new book proposals:
Dr. Harry (J.J.) Blom: harry.blom@wkap.nl